



ATLAS NOTE

ATL-COM-PHYS-2016-1696

14th October 2017



Draft version 1.4

Measurements of $t\bar{t}$ differential cross-sections in the all-hadronic channel with the ATLAS detector using highly boosted top quarks in pp collisions at $\sqrt{s} = 13$ TeV with the full 2015+2016 dataset

Peter Berta^a, Ye Chen^c, Kyle Cormier^b, Riccardo Di Sipio^b, Robin Hayes^b, Petr Jačka^f, Roman Lysák^f, Jiří Kvita^d, Rupert Leitner^a, Cassandra Miller^b, Shima Shimizu Noda^c, Jan Palicka^d, Marino Romano^e, Pekka Sinervo^b, Francesco Spanó^g, Federica Fabbri^e, Yuji Yamazaki^c

^a*Charles University in Prague*, ^b*University of Toronto*, ^c*Kobe University*, ^d*Palacky University*, ^e*University of Bologna*, ^f*Acad. of Sciences of the Czech Rep.*, ^g*Royal Holloway, University of London*

Abstract

This note documents the measurement by the ATLAS experiment of the top quark pair production differential cross-sections as a function of the top quark and $t\bar{t}$ system kinematic observables. The study is performed using the full dataset from pp collisions at $\sqrt{s} = 13$ TeV collected by the ATLAS detector in 2015 and 2016, corresponding to an integrated luminosity of 36.1 fb^{-1} . The $t\bar{t}$ events are selected in the all-hadronic channel using highly-boosted top quarks. A measurement is made of the fiducial phase-space total particle-level cross-section and differential cross-sections. Measurements of fiducial phase-space parton-level differential cross-sections are also presented. These are compared with several Standard Model predictions for $t\bar{t}$ production. Due to the large $t\bar{t}$ cross-section at the LHC, such measurements allow a detailed study of the properties of the top-quark production and decay, enabling precision tests of perturbative QCD.

23 **Contents**

24	1 Introduction	6
25	2 Samples	8
26	2.1 Data samples	8
27	2.2 Monte Carlo samples	8
28	3 Objects selection	10
29	4 Event selection	12
30	5 Background determination and event reconstruction	21
31	5.1 Backgrounds with $t\bar{t}$ pairs containing final state leptons	21
32	5.2 Backgrounds from single top-quark production	21
33	5.3 Backgrounds from $t\bar{t} + W/Z/H$	21
34	5.4 Multijet background estimation	22
35	5.5 $t\bar{t}$ system reconstruction and event variables	25
36	6 Measurement of particle-level fiducial cross-sections	31
37	6.1 Fiducial phase space	31
38	6.2 Unfolding procedure	31
39	7 Measurement of parton-level cross-sections	43
40	7.1 Parton-level phase space	43
41	7.2 Unfolding Procedure	43
42	8 Systematic uncertainties	51
43	8.1 Object reconstruction and calibration	51
44	8.2 Signal modelling	51
45	8.3 Integrated Luminosity	52
46	8.4 Background modelling	52
47	9 Results	54
48	9.1 Measured differential cross-sections at particle level and comparison with predictions	54
49	9.2 Particle-level fiducial phase-space total cross-section	62
50	9.3 Measured differential cross-section at parton level and comparison with predictions	64
51	10 Conclusion	70
52	Appendix	71
53	A Monte Carlo datasets	72
54	A.1 $t\bar{t}$ modelling	72
55	A.2 Background modelling	73
56	B Hadronic trigger efficiencies	74
57	B.1 Data sets	74

Not reviewed, for internal circulation only

58	B.2 Triggers	74
59	B.3 Event selection	74
60	B.4 Results	75
61	C Second-leading jet selection optimization	80
62	C.1 Second leading large- R jet p_T threshold	80
63	D Validation regions	82
64	E Resolution of observables	95
65	F Particle-level uncertainties after unfolding	100
66	F.1 Fractional uncertainties	100
67	F.2 Statistical uncertainty of modelling systematics	106
68	F.3 Tables of systematic uncertainties	113
69	F.3.1 Summary tables	113
70	F.3.2 Full breakdown tables	128
71	G Parton-Level cross-sections and systematic uncertainties	156
72	G.1 Fractional uncertainties	156
73	G.2 Tables of differential cross-sections	164
74	G.3 Summary tables	174
75	G.4 Full breakdown tables	188
76	H Uncertainties at detector level	219
77	H.1 Detector fractional uncertainties	219
78	H.2 Tables of detector systematic uncertainties	220
79	I Particle-level unfolding validation	235
80	I.1 Closure test	235
81	I.2 Stress test	237
82	I.3 An additional closure test using smeared MC distributions	242
83	I.4 Pull test	247
84	I.5 Stress test of τ_{32} variable	252
85	J Stress tests at parton-level	256
86	J.1 Parton-level phase-space stress tests	256
87	J.1.1 Parton-level phase-space selection	257
88	J.1.2 Stress test results in parton level phase-space	257
89	J.1.3 Stress test results with single bump in the distributions	261
90	K Stress test for full parton-level phase space	265
91	K.1 Reweighted distributions	265
92	K.2 Stress test results at full phase space	269
93	K.3 Stress test of individual steps of unfolding	269
94	L The ABCD background estimation method	283
95	L.1 General principles	283

96	L.2 ABCD method using 9 regions	284
97	L.3 Correlation factor between N_t and N_b	285
98	L.4 Data \oplus MC statistical uncertainties	286
99	M Comparison of the old ABCD9 and Monte Carlo QCD multijet background estimates	292
100	N Comparison of Monte Carlo Generators	293
101	O ABCD method using 16 regions	298
102	O.1 Classification of events into 16 regions	298
103	O.2 Correlations between parameters	298
104	O.2.1 Measurement of the effect of correlations on the ABCD multijet background estimate	300
105	O.3 Effect of correlations in 9 regions	301
106	O.3.1 Transformation from 16 to 9 regions	301
108	O.3.2 Theoretical description of impact of correlation	302
109	O.3.3 Measured effect of correlations	302
110	O.4 ABCD estimates from the 16 regions	304
111	O.5 Results from MC dijet samples	307
112	O.5.1 Measured effect of correlations on simple ABCD estimates	307
113	O.5.2 Effect of correlations in 9 regions	307
114	O.5.3 Comparison of ABCD estimates	307
115	O.6 The ABCD Method with Matrix Operations	309
116	P Optimization of B-Tagging Working Points	313
117	Q Optimization of Signal Scale Factor	314
118	R Comparison against different Powheg +Pythia8 tunings	323
119	R.1 Initial- and final-state radiation	323
120	R.1.1 Parton level comparison	329
121	R.2 Parton distribution functions	333
122	S Checks on data yield dependence on data-taking periods	339
123	S.1 Data yield vs data set periods	339
124	T Comparsion of Powheg +Pythia8 with Powheg +Herwig7	343
125	T.1 Comparison with τ_{32} at each step in the RECO level	348
126	T.2 Comparison with τ_{32} at each step in the particle level	350
127	U 2D distributions	353
128	V Statistical correlations among variable using bootstrapping methods	360
129	W Evaluation of covariance matrices	365
130	W.1 Particle level covariances and correlations	368
131	W.2 Parton level covariances and correlations	395
132	X Studies to investigate global χ^2 calculation	419

133	X.1	Determination of covariance matrices	419
134	X.1.1	Calculation of post-unfolding covariance matrix	419
135	X.1.2	Calculation of hybrid pre-unfolding covariance matrix	421
136	X.2	Limitations of the approaches studied	421
137	X.2.1	Limitations in data statistical covariance matrix	421
138	X.2.2	Limits of pre-unfolding and hybrid post-unfolding schemes	422
139	X.2.3	Difference between post-unfolding and pre-unfolding calculations	422
140	X.2.4	Correlations of systematic uncertainties across variables	423
141	X.2.5	Number of degrees of freedom	424
142	X.3	Alternate Approach: Combining p -values using the Brown/Kost method	424
143	X.4	Conclusions	428

144 Version Changes

- 145 • Version 1.4 Incorporated Appendix X describing the global χ^2 studies.
- 146 • Version 1.3.3 Continued investigation of tau32 and mass discrepancies. Added studies where
147 PowHEG+HERWIG7 is used as nominal model instead of PowHEG+PYTHIA8.
- 148 • Version 1.3.2 Further addressing top wg approval comments. Reco plots include modelling sys-
149 tematics.
- 150 • Version 1.3.1 Addressing top wg approval comments. First batch of comments implemented: nor-
151 malized SR plots with overflow, Sherpa 2.2.1, stress tests extended to all observables
- 152 • Version 1.3.0 Changes arising from pre-approval all implemented, with updated unfolding results
153 for parton-level and updated conclusions. Frozen version for approval presentation.
- 154 • Version 1.2.0 First set of improvements from pre-approval comments implemented, progress to-
155 wards full approval ongoing.
- 156 • Version 1.1.1 Updated yield table and descriptions in text to reflect up to date uncertainty estimates.
- 157 • Version 1.1 Updated for consistency and clarity for Top Cross-Section Subgroup pre-approval.
158 Several additional pieces will be ready shortly. Where possible expected updates are mentioned in
159 the note explicitly.
- 160 • Version 1.00 Updated with full nominal MC results, improved background calculation, updated
161 modelling systematics and various cross-checks to analysis. This was prepared for the Top Cross-
162 Section Subgroup pre-approval presentation.
- 163 • Version 0.26 Updated to be clear about current status and future plans as compared to results from
164 the CONF note. Updated trigger descriptions and monte carlo descriptions, added some more
165 explanation of parton level analysis. Added more information to dataset appendix.
- 166 • Version 0.25 Added in fiducial phase-space cross-section; updated MC descriptions; corrected MC
167 scale factor to 0.77.
- 168 • Version 0.24 Updated to be consistent with 0.70 b-tagging working point and the use of the ABCD16
169 multijet background estimates.

- Version 0.23 Added Appendix M comparing different *b*-tagging working points.
- Version 0.2 First parton-level results, without modelling uncertainties and comparing to POWHEG+PYTHIA6. This version still has the cutflow from 14.7 fb-1 analysis, and missing correlation figures in Appendix. The ABCD background study has been updated, but analysis is still using ABCD9 technique. The 77working-point for b-tagging is used.
- Version 0.1 First version cloned from the CONF note INT note, but with 36 fb-1 of data.

1. Introduction

This note describes the measurements of the top quark pair differential cross-section as a function of kinematic and event-wise observables using highly boosted top quarks. The large top-quark pair production cross-section at the LHC allows detailed studies of the characteristics of $t\bar{t}$ production, providing a unique opportunity to test the Standard Model (SM) at the TeV scale. Furthermore, effects beyond the SM can appear as modifications of $t\bar{t}$ differential distributions with respect to the SM predictions [1] that may not be detectable with an inclusive cross-section measurement. A precise measurement of the boosted $t\bar{t}$ differential cross-section therefore has the potential to enhance the sensitivity to possible effects beyond the SM, as well as to clarify the ability of the most up-to-date theoretical calculations to describe this process.

The ATLAS [2–5] and CMS [6, 7] experiments have published measurements of the $t\bar{t}$ differential cross-sections at a centre-of-mass energy $\sqrt{s} = 7$ TeV and $\sqrt{s} = 8$ TeV in pp collisions, both in the full phase space using parton-level variables and in fiducial phase-space regions using observables constructed from final-state particles (particle level). This analysis focuses on the all-hadronic channel with at least one top quark with $p_T > 500$ GeV and the other sufficiently boosted that differential cross-section measurements of the top quark pair can be accurately made. The event selection and background estimation follows the approach used in [8], but with updated top-tagging techniques and b-tagging methods. The results presented here represent a natural extension of the previous ATLAS measurements of the $t\bar{t}$ differential cross-sections at the higher center-of-mass energy of $\sqrt{s} = 13$ TeV and complement measurements made at the same centre-of-mass energies in other channels. These measurements are based on the full data-set collected by the ATLAS detector in 2015 and 2016 from pp collisions at $\sqrt{s} = 13$ TeV and available for analysis. The dataset corresponds to an integrated luminosity of 36.1 fb^{-1} . This measurement is an extension of an analysis reported using half of the data sample [9].

In the SM, the top quark decays almost exclusively into a W boson and a b -quark. The signature of a $t\bar{t}$ decay is therefore determined by the W boson decay modes. This analysis makes use of the all-hadronic $t\bar{t}$ decay mode, where both W bosons decay into a quark-antiquark pair. Only top quarks with high transverse-momentum (p_T) are selected so that the decay products of each top quark are collimated due to its Lorentz boost and can be reconstructed as a single large-radius jet.

This paper presents a set of measurements of the $t\bar{t}$ production cross-section as a function of different properties of the reconstructed top quarks and of the $t\bar{t}$ system. The results, unfolded to a fiducial particle-level phase space, are compared to the predictions of Monte Carlo (MC) generators. The goal of unfolding to a fiducial particle-level phase space and of using variables directly related to detector observables is to allow precision tests of QCD calculations, avoiding large model-dependent extrapolation corrections to the parton-level top-quark and to a phase space region outside the detector acceptance. Measurements are

210 also made by unfolding the data to the parton-level differential cross-sections for additional comparisons
 211 against theoretical predictions.

212 In addition to the variables measured at $\sqrt{s} = 7$ TeV and $\sqrt{s} = 8$ TeV, a set of new measurements is
 213 presented. The differential cross-sections measured here are similar to those studied in dijet measurements
 214 at large jet transverse momentum [10, 11] and are sensitive to effects of initial- and final-state radiation,
 215 to the different parton distribution functions (PDF), and to non-resonant processes including particles
 216 beyond the SM [12]. The rapidities of the two top quarks in the laboratory frame are denoted by $y^{t,1}$
 217 and $y^{t,2}$, while their rapidities in the $t\bar{t}$ centre-of-mass frame are $y^* = 1/2(y^{t,1} - y^{t,2})$ and $-y^*$. These
 218 define the production angle $\chi^{t\bar{t}} = \exp^{2|y^*|}$, a variable of particular interest as many processes not included
 219 in the Standard Model are predicted to peak at low values of $\chi^{t\bar{t}}$ [10]. The longitudinal motion of the
 220 $t\bar{t}$ system in the laboratory frame is described by the rapidity boost $y_B^{t\bar{t}} = 1/2(y^{t,1} + y^{t,2})$ and is sensitive
 221 to PDFs. Measurements are made of the absolute value of the azimuthal angle between the two top
 222 quarks, $\Delta\phi^{t\bar{t}}$; the absolute value of the out-of-plane momentum, $|p_{out}^{t\bar{t}}|$ (i.e. the projection of top-quark
 223 three-momentum onto the direction perpendicular to a plane defined by the other top quark and the beam
 224 axis (z) in the laboratory frame [11]); the longitudinal boost of the $t\bar{t}$ system in the laboratory frame, $y_B^{t\bar{t}}$
 225 [10]; the production angle between the two top quarks, $\chi^{t\bar{t}}$ [10] and the cosine of the production angle in
 226 the Collins-Soper¹ reference frame, $\cos\theta^*$; and the scalar sum of the transverse momenta of the two top
 227 quarks, $H_T^{t\bar{t}}$ [13, 14]. All of these are sensitive to the modelling of the $t\bar{t}$ production process.

228 The paper is organized as follows: Sect. 2 describes the data and simulation samples used in the measure-
 229 ments. The reconstruction of physics objects and the event selection is explained in Sect. 3 and Sect. 4, re-
 230 spectively. Section 5 describes the kinematic reconstruction of the $t\bar{t}$ pairs and discusses the background
 231 processes affecting these measurements. The measurements of the fiducial phase-space cross-sections,
 232 including the definition of the fiducial phase-space, are described in Sect. 6. The measurements of the
 233 parton-level differential cross sections are discussed in Sect. 7. Statistical and systematic uncertainties
 234 are discussed in Sect. 8. The results are presented in Sect. 9, where the comparison with theoretical
 235 predictions is also discussed. Finally, a summary is presented in Sect. 10.

¹ The Collins-Soper frame is the rest frame of the $t\bar{t}$ pair, wherein the two top quarks have equal and opposite momenta; thus, each makes the same angle θ^* with the beam direction.

2. Samples

2.1. Data samples

The data used for this analysis were recorded with the ATLAS detector at a centre-of-mass energy of 13 TeV in 2015 and 2016. The data correspond to an integrated luminosity of 36.1 fb^{-1} . Only data taken under stable beam conditions and with fully operational relevant subdetectors (e.g. operational IBL) are considered, using the standard good-run lists (V79 is used for the 2015 data and V83 is used for the 2016 data).

Events are required to have satisfied an un-prescaled inclusive high- p_T jet trigger. Due to changing run conditions and trigger keys the trigger requirements differ for data taking in different years. The trigger requirements are:

HLT_j420_a10r_L1J100 for 2016.

Both triggers were found to be fully efficient at the p_T thresholds used in this analysis, as shown in Appendix B.

2.2. Monte Carlo samples

The signal and background processes are modelled using Monte Carlo (MC) generators. Multiple overlaid proton-proton collisions are simulated with the soft QCD processes of Pythia 8.186 [15] using tune A2 [16] and the MSTW2008LO parton distribution functions (PDF)[17]. The detector response is simulated in GEANT4 [18]. The data and MC events are reconstructed with the same software algorithms. Changing detector and beam conditions are taken into account by assigning each MC event a pseudo run number which corresponds to a physics run matching the simulated pile-up and detector conditions. Pseudo run numbers are assigned in such a way that the Monte Carlo weight associated with a given data taking period is approximately proportional to the recorded luminosity during that period. Events are required to pass the trigger requirements for the period associated with the assigned pseudo run number.

A full list of MC samples used in this analysis as well as methodology used to generate high- p_T events efficiently is given in Appendix A.

The POWHEG-BOX v2 [19] generator using the NNPDF30 NLO PDF set and interfaced with the PYTHIA8 parton shower and hadronization model employing the NNPDF 23 LO PDF sets [20] with the corresponding A14 tune [21] is used for the generation of the $t\bar{t}$ process for the detector and particle level results. The $t\bar{t}$ samples are normalized to the NNLO+NNLL cross-section $\sigma_{t\bar{t}} = 831.76^{+46.45}_{-50.85} \text{ pb}$ [22] and the top quark mass is set to 172.5 GeV.

Simulation of the $t\bar{t}$ process with Powheg + Pythia8 using alternate tunes, Powheg + Herwig7, and aMC@NLO + Pythia8 are used for the determination of systematic uncertainties as described in Section 8.2.

Final comparisons of unfolded results to $t\bar{t}$ predictions also include comparisons to a sample generated with Sherpa version 2.2.1 interfaced with the NNPDF 30 NNLO PDF set.

The Powheg + Pythia6 generator is used to model the production and decay of single top-quarks (the Wt process only). An independent sample for electroweak t -channel single top-quark production is not

- available. Single top s -channel production is considered negligible due to its small cross section. For the single top process, the CT10 PDF set is used for the matrix element calculation, the top quarks are decayed using MADSPIN [23], the parton shower, fragmentation, and the underlying event are simulated using PYTHIA 6.428 [24] with the CTEQ6L1 PDF sets and the corresponding Perugia 2012 tune (P2012) [25]. The single-top cross sections are normalized to their NLO predictions [26].
- The associated production of $t\bar{t}$ pairs with W^\pm , Z and Higgs bosons are modelled using the aMC@NLO Monte Carlo generator [27] coupled to the PYTHIA8 shower and hadronization model using the same PDF sets and tunes as the $t\bar{t}$ sample. The cross-sections for these processes are 0.603 pb, 0.586 pb and 0.231 pb for $t\bar{t} + W^\pm$, $t\bar{t} + Z$ and $t\bar{t} + H$, respectively (computed by the MADGRAPH5_aMC@NLO MC generator). The EvtGEN v1.2.0 program [28] is used for modelling the properties of the bottom and charm hadron decays.
- Multijet background rates and shapes are estimated using data-driven methods, similar to those employed in Ref. [8]. In Appendix M data driven predictions are compared to Multijet processes simulated using POWHEG +PYTHIA8 generator.

286 3. Objects selection

287 The analysis described in this note makes use of jets, electrons and muons. Two types of anti- k_t jets are
 288 considered here, so-called *small-R* jets with a radius parameter of $R = 0.4$ and *large-R* jets with a radius
 289 parameter of $R = 1.0$. The events are selected and reconstructed with the AnalysisTop software (v. 2.4.29)
 290 of the ATLAS top group.

291 The jets are reconstructed from topological calorimeter clusters using the anti- k_t algorithm with radius
 292 parameters of $R = 0.4$ and 1.0 . The jets are calibrated using the LCW technique, which takes into account
 293 the detector response in η and p_T and applies local corrections [29]. Small- R jets with $|\eta| < 2.5$ and
 294 $p_T > 25$ GeV are selected. To reduce pileup-effects, an additional cut on the *jet-vertex tagger* (JVT)
 295 value is applied. The JVT is a multi-variate quantity that combined information from several track-based
 296 variables and identifies jets coming from the primary event vertex. This JVT cut is only applied to jets
 297 with $p_T < 50$ GeV and $|\eta| < 2.4$. The jet object which is closest to an electron candidate (described
 298 below) within a radius of $\Delta R < 0.2$ is removed.

299 To identify small- R jets containing b -hadrons, a multivariate discriminant (MV2c10) is used which com-
 300 bines information about secondary vertices and impact parameters. Small- R jets are considered b -tagged
 301 if the value of the MVA discriminant is larger than a certain threshold, defined by requiring that a certain
 302 efficiency for tagging be achieved. In this analysis, the 70% working point is chosen. The corresponding
 303 rejection factors for charm quarks and light jets are 12 and 380, respectively [30]. This working point was
 304 selected after optimizing the overall uncertainty in the detector-level background-subtracted event yield,
 305 as described in Appendix P.

306 All large- R jets are required to fulfill $|\eta| < 2.0$ and $p_T > 300$ GeV. A trimming algorithm [31] with
 307 parameters $R_{\text{sub}} = 0.2$ and $f_{\text{cut}} = 0.05$ is applied to suppress QCD radiation and mitigate pileup-effects.
 308 A simple top-tagging algorithm [32] is applied that makes p_T dependent requirements on the calibrated
 309 calorimeter jet mass and on the N-subjettiness ratio τ_{32} . The jet mass requirement varies from > 100 GeV
 310 at the low end of our pT range to > 132 GeV at $p_T \sim 1.7$ TeV. In the same range the τ_{32} requirement
 311 ranges from < 0.71 to < 0.54 . The p_T -dependent cut is tuned to give an efficiency of 50%, is constant as
 312 a function of p_T , with corresponding reduction in rejection with increasing p_T . The 50% “tight” working
 313 point is used instead of the looser 80% working point as it results in a larger expected signal to background
 314 ratio in the signal region.

315 A large- R jet is considered b -matched if a b -tagged small- R jet is within $\Delta R \equiv \sqrt{\Delta\eta^2 + \Delta\phi^2} < 1.0$ of the
 316 large- R jet. The b -jet closest to the leading large- R jet axis is identified first, then a second loop over the
 317 remaining b -tagged jets is performed to identify the b -jet closest to the second-leading large- R jet axis.

318 We define electron candidates by requiring a track reconstructed in the inner detector be matched to energy
 319 deposits in the electromagnetic calorimeter. These clusters have to have a $E_T > 25$ GeV, $|\eta| < 2.47$ and
 320 have to be outside the calorimeter crack region: $1.37 \leq |\eta| \leq 1.52$. Only electrons passing the tight
 321 likelihood-based requirements [33] are considered in this analysis. Calorimeter and track-based isolation
 322 criteria are applied. These are p_T and η dependent and ensure an efficiency of 90% for electrons with
 323 p_T of 25 GeV and 99% efficiency for electrons at 60 GeV. These efficiencies were measured in $Z \rightarrow ee$
 324 events. To reduce the impact of non-prompt leptons, we remove electrons within $\Delta R < 0.4$ of a small- R
 325 jet.

326 We reconstruct muon candidates by requiring a track which fulfills certain quality criteria in the inner
 327 detector and in the muon spectrometer [34]. Only muons with $p_T > 25$ GeV and $|\eta| < 2.5$ are considered

328 in the analysis that fulfill the medium ID criteria. Similar isolation criteria as for electrons are used. To
329 reduce the impact of non-prompt leptons, we reject muons within $\Delta R < 0.4$ of a small- R jet.

[Not reviewed, for internal circulation only]

330 4. Event selection

331 The event selection is designed to maximize signal while minimizing background contamination. Each
 332 event must have a reconstructed primary vertex with five or more associated tracks. The events are
 333 required to contain exactly zero reconstructed lepton candidates with $p_T > 25$ GeV to reject SM $t\bar{t}$ events
 334 arising from the semileptonic decay of at least one of the top quarks. We require at least two (large- R)
 335 anti- k_t $R = 1.0$ jets with $p_T > 350$ GeV and $|\eta| < 2.0$, at least one of which has $p_T > 500$ GeV. The event
 336 must also contain at least two (small- R) anti- k_t $R = 0.4$ jets with $p_T > 25$ GeV and $|\eta| < 2.5$.

337 These requirements define what we call the “preselection.”

338 For the signal sample selection, as the two leading large- R jets represent the two top quark candidates,
 339 their mass is required to be within 50 GeV of the top-quark mass. This reduces the background from
 340 QCD multijet events where two jets have been created with jet masses in excess of 222.5 GeV. Finally,
 341 to define the signal region as a function of tags, we require both large- R jets to be top-tagged and to be
 342 b -matched.

343 The event selection is summarized in Table 1. The event yields are displayed in Table 2 for data, sim-
 344 ulated signal, and backgrounds (the background determination is described in Sects. 5.1 through 5.4).
 345 Figures 1–7 show, for some key distributions, the comparison between data and predictions normalized to
 346 the integrated luminosity of the data sample. The selection produces a relatively clean $t\bar{t}$ sample, the total
 347 background being at the 25–35% level. Although there is a difference in the total number of expected and
 348 observed events in the signal region, the shapes of the distributions are generally well described by the
 349 predictions as shown in Figures 11–14. Comparison between data and predictions in control regions can
 350 be seen in Appendix D which show good agreement between the prediction and data in regions domi-
 351 nated by background. For detector-level plots the systematic uncertainties related to modelling are defined
 352 as the difference in the predicted yield between the given systematic variation of the MC sample and the
 353 nominal MC sample. For technical reasons this definition differs slightly from the definition of systematic
 354 uncertainties associated with modelling used in the final results which is described in Section 8.2.

355 Figures 4(a) and 4(b) show a shift in the large- R jet masses in data as compared to the prediction. Although
 356 the peaked nature of this distribution makes the difference between MC and data appear significant, the
 357 overall shift is of the order 2 GeV and covered by the large- R jet systematic uncertainties described in
 358 Section 8.

359 The second-leading jet p_T requirement was studied and optimized to obtain high yield without significant
 360 compromise to the proportion of fully-contained top-quark jets. The optimization of the second-leading
 361 large- R jet p_T cut is described in Appendix C.1.

Not reviewed, for internal circulation only

Cut	Event pre-selection
Hadronic trigger	HLT_j360_a10r_L1J100 OR HLT_j420_a10r_L1J100
Primary vertex	≥ 5 tracks with $p_T > 0.4$ GeV
Exactly no isolated lepton	Muons: $p_T > 25$ GeV, $ \eta < 2.5$ Electrons: $p_T > 25$ GeV $ \eta < 2.47$, excluding $1.37 < \eta < 1.52$
Jets $R = 0.4$	≥ 2 jets $p_T > 25$ GeV, $ \eta < 2.5$
Jets $R = 1.0$	≥ 2 jets $p_T > 350$ GeV, $ \eta < 2.0$ ≥ 1 jets $p_T > 500$ GeV, $ \eta < 2.0$
Cut	Event selection
b-matching	$ m_{J,1} - m_{\text{top}} < 50$ GeV $ m_{J,2} - m_{\text{top}} < 50$ GeV
Top-tagging	leading and subleading large- R jets are both b-matched leading and subleading large- R jets are both top-tagged

Table 1: Summary of all requirements included in the event pre-selection and selection.

$t\bar{t}$ (all-hadronic)	3 250	\pm	470
$t\bar{t}$ (non-all-hadronic)	200	\pm	40
Single top-quark	24	\pm	12
$t\bar{t} + W/Z/H$	33	\pm	10
Multijet events	810	\pm	50
Prediction	4 320	\pm	530
Data (36.1 fb^{-1})	3 541		

Table 2: Event yields after the selection. The signal model, denoted $t\bar{t}$ in the table, is generated using PowHEG+PYTHIA8, as is the non all-hadronic top-quark pair production process. The background estimates include systematic uncertainties on the detector-level variables used for the event selection. The multijet background uncertainty includes both the uncertainty on the data-driven method as well as the systematic uncertainties arising from the MC-based signal subtraction in the control regions used to make the data-driven estimate (see subsection 5.4). Neither modelling uncertainties nor uncertainties on the inclusive $t\bar{t}$ cross-section are included in the systematic uncertainties. The full prediction uncertainty takes into account correlated uncertainties, and is somewhat larger than the sum in quadrature of the individual components.

Not reviewed, for internal circulation only

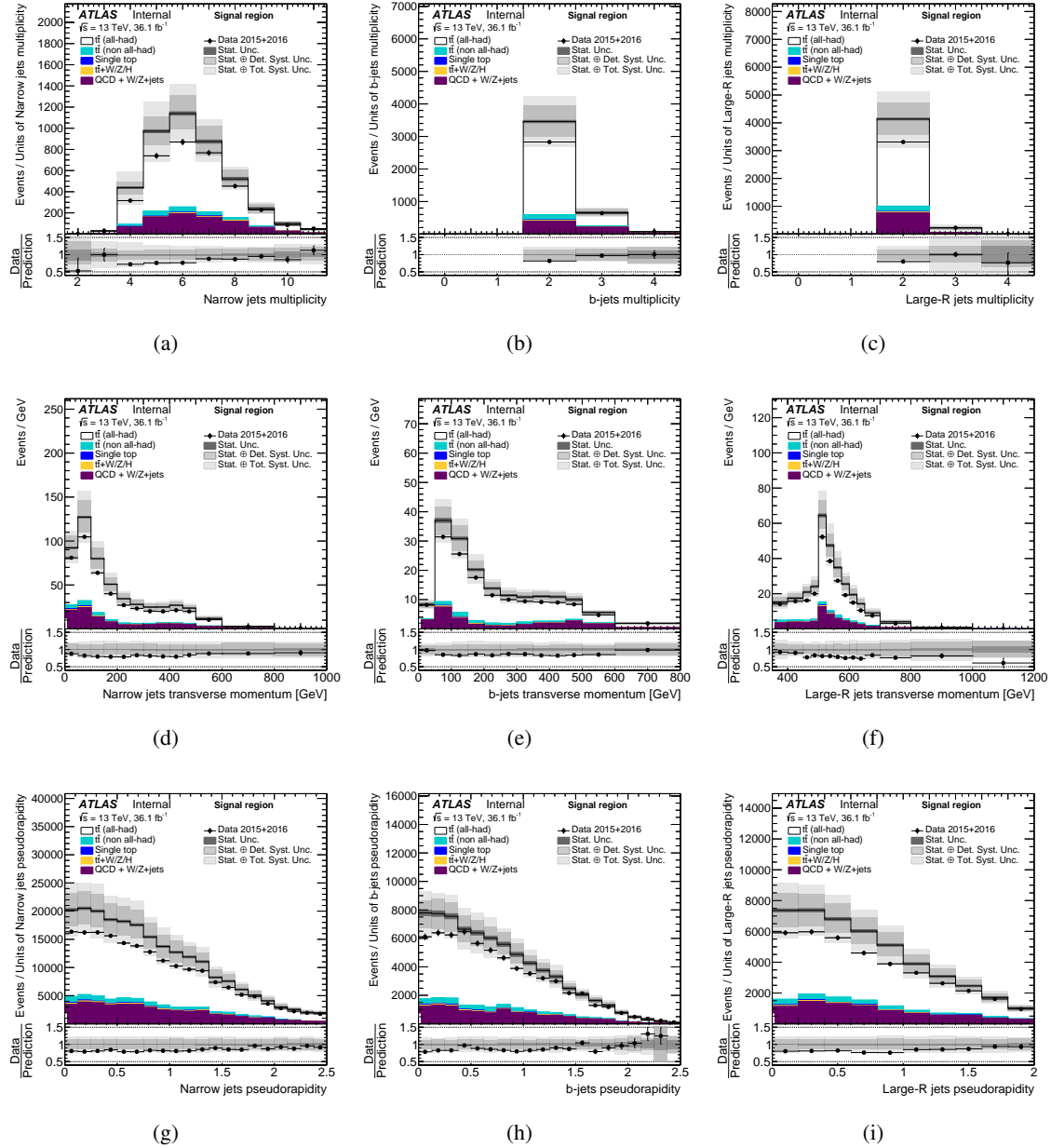


Figure 1: Kinematic distributions of jets in the signal region (S): (a) multiplicity, (d) transverse momentum and (g) rapidity of anti- k_t R=0.4 jets, (b) multiplicity, (e) transverse momentum and (h) rapidity of anti- k_t R=0.4 b -tagged jets, (c) multiplicity, (f) transverse momentum and (i) rapidity of anti- k_t R=1.0 jets. Data distributions are compared to predictions using Powheg+Pythia8 as the $t\bar{t}$ signal model. The hashed area indicates the combined statistical and systematic uncertainties on the total prediction. The light gray band shows systematic uncertainties related to the modelling of the $t\bar{t}$ system.

Not reviewed, for internal circulation only

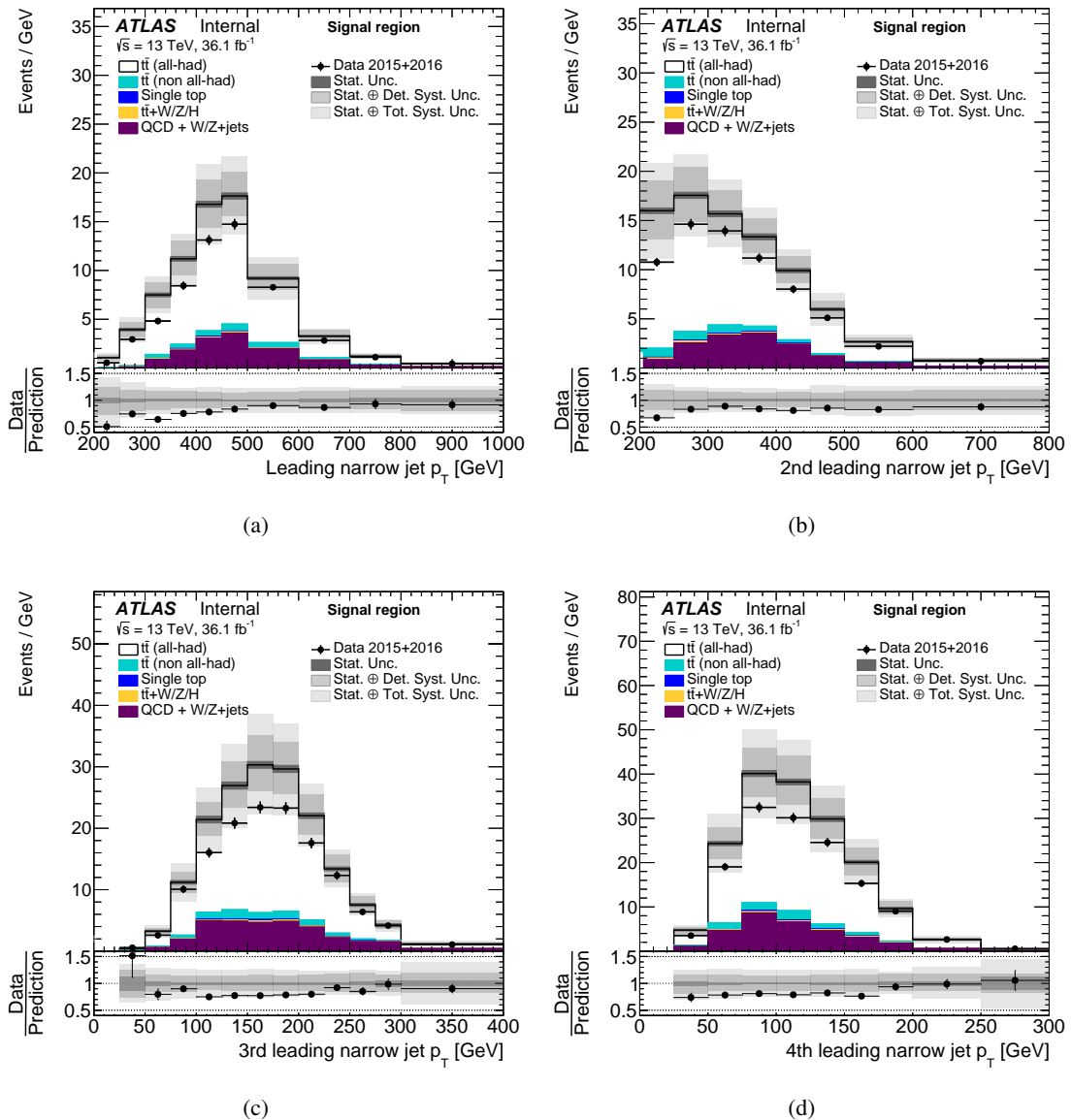


Figure 2: Kinematic distributions of the four leading small- R jets in the signal region (S): (a) leading jet transverse momentum, (b) second-leading jet transverse momentum, (c) third-leading jet transverse momentum and (d) fourth-leading jet transverse momentum. Data distributions are compared to predictions using PowHEG+PYTHIA8 as the $t\bar{t}$ signal model. The hashed area indicates the combined statistical and systematic uncertainties on the total prediction. The light gray band shows systematic uncertainties related to the modelling of the $t\bar{t}$ system.

Not reviewed, for internal circulation only

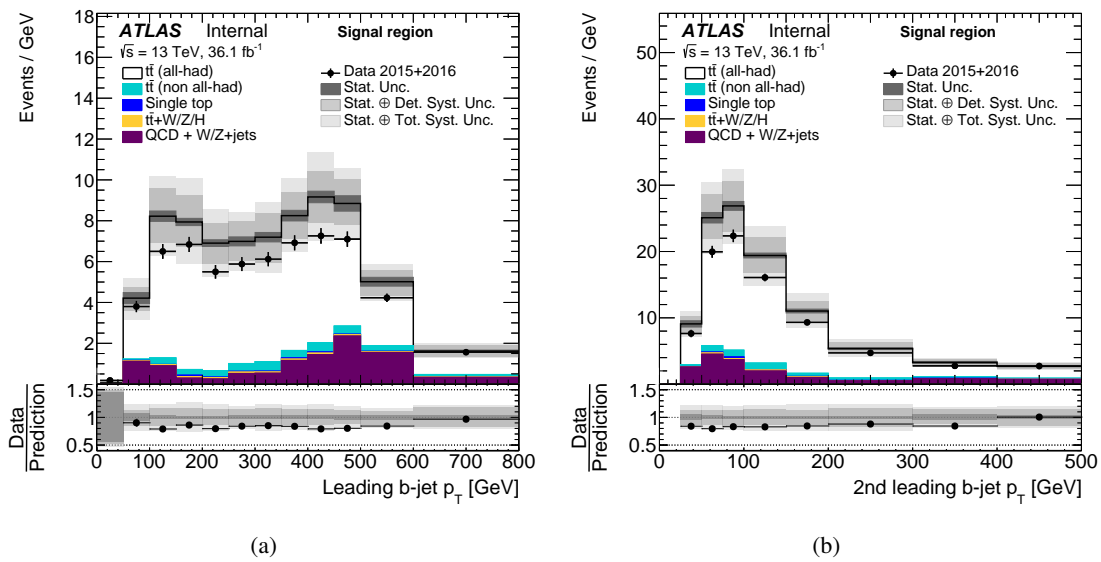


Figure 3: Kinematic distributions of b -tagged jets in the signal region (S): (a) leading b -tagged and (b) second-leading b -tagged jet transverse momenta. Data distributions are compared to predictions using PowHEG+PYTHIA8 as the $t\bar{t}$ signal model. The hashed area indicates the combined statistical and systematic uncertainties on the total prediction. The light gray band shows systematic uncertainties related to the modelling of the $t\bar{t}$ system.

Not reviewed, for internal circulation only

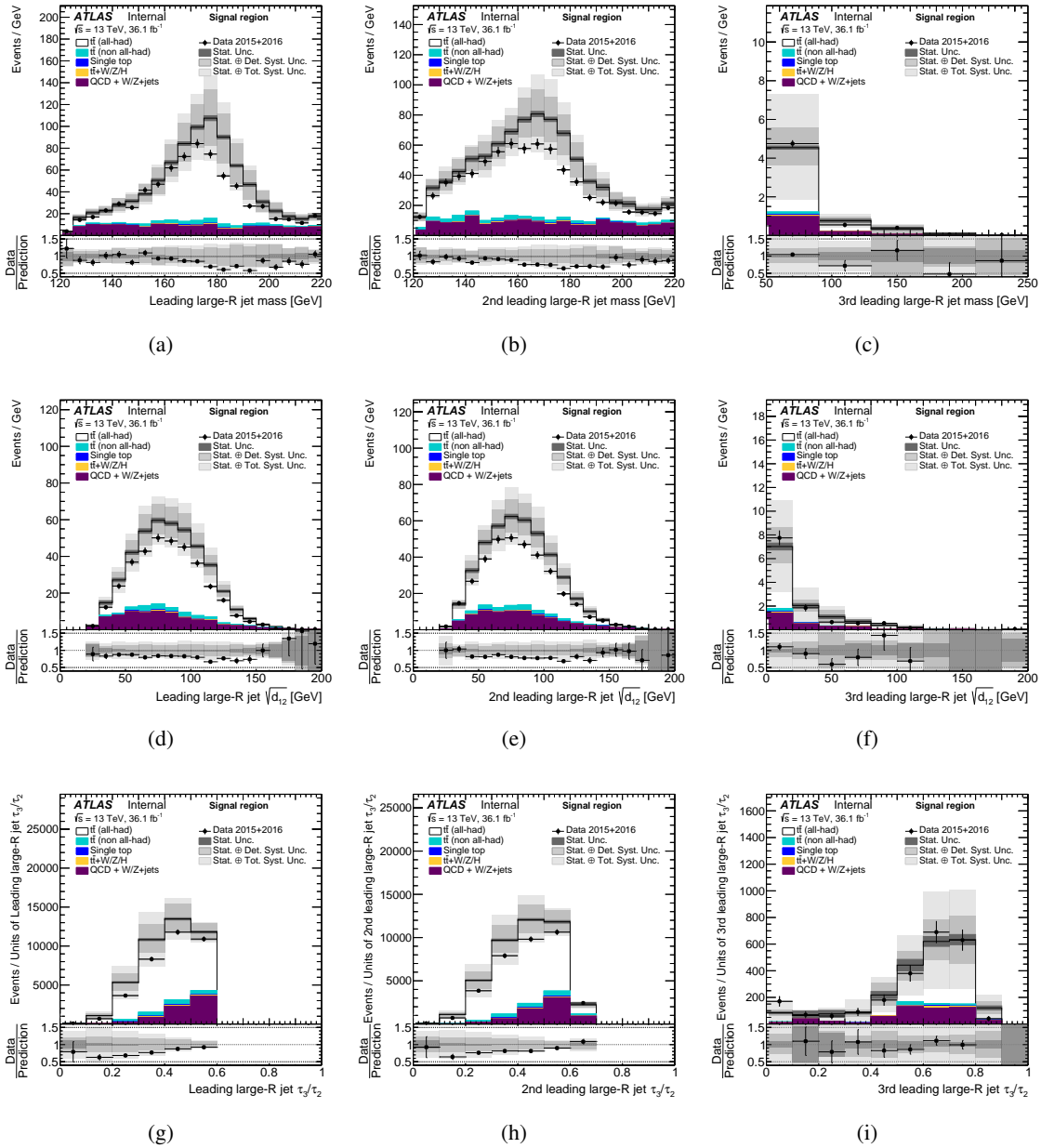


Figure 4: Kinematic distributions of large- R jets in the signal region (S): (a) mass, (d) splitting scale and (g) N-subjettiness of the leading anti- k_t R=1.0 trimmed jet, (b) mass, (e) splitting scale and (h) N-subjettiness of the second leading large- R jet and (c) mass, (f) splitting scale and (i) N-subjettiness of the third leading large- R jet. Data distributions are compared to predictions using POWHEG+PYTHIA8 as the $t\bar{t}$ signal model. The hashed area indicates the combined statistical and systematic uncertainties on the total prediction. The light gray band shows systematic uncertainties related to the modelling of the $t\bar{t}$ system.

Not reviewed, for internal circulation only

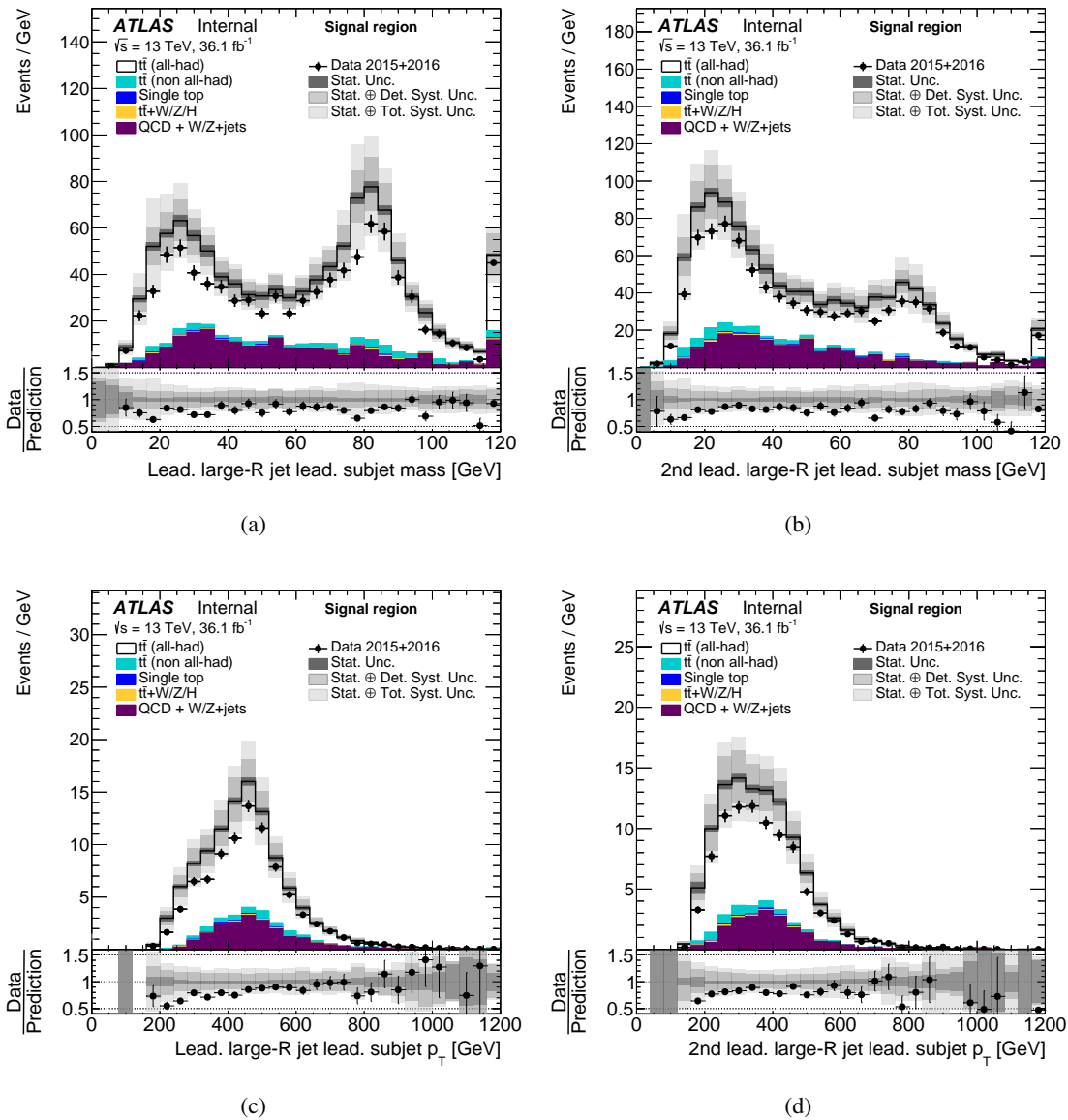


Figure 5: Kinematic distributions of the leading small- R jet embedded in a large- R jet in the signal region (S): (a) mass and (c) transverse momentum of the leading small- R jet embedded in the leading large- R jet, and (b) mass and (d) transverse momentum of the leading small- R jet embedded in the second-leading large- R jet. Data distributions are compared to predictions using PowHEG+PYTHIA8 as the $t\bar{t}$ signal model. The hashed area indicates the combined statistical and systematic uncertainties on the total prediction. The light gray band shows systematic uncertainties related to the modelling of the $t\bar{t}$ system.

Not reviewed, for internal circulation only

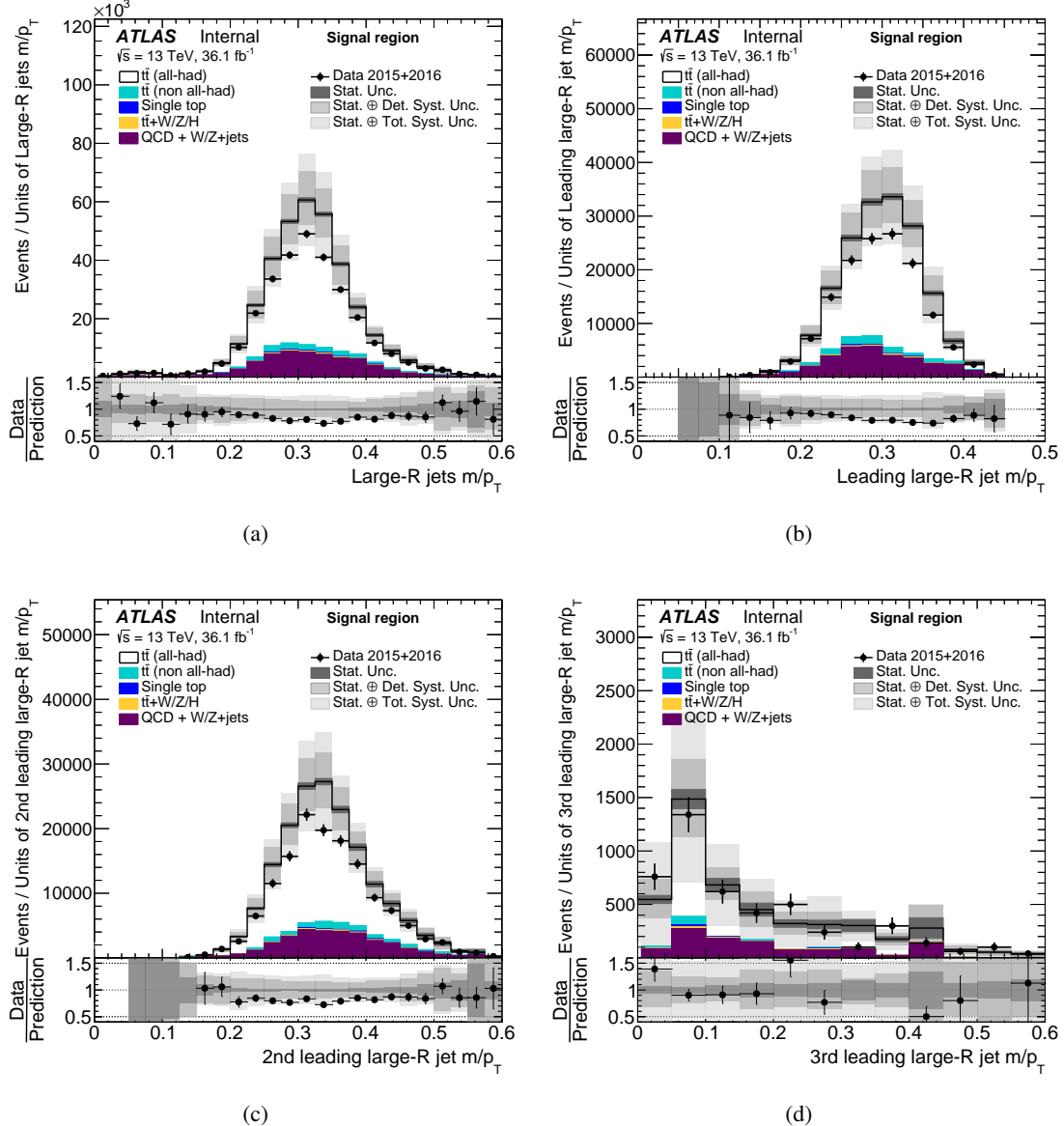


Figure 6: Kinematic distributions of mass-over-transverse-momentum of (a) all large- R jets, (b) the leading large- R jet, (c) the second-leading large- R jet and (d) the third-leading large- R jet. Data distributions are compared to predictions using Powheg+Pythia8 as the $t\bar{t}$ signal model. The hashed area indicates the combined statistical and systematic uncertainties on the total prediction. The light gray band shows systematic uncertainties related to the modelling of the $t\bar{t}$ system.

Not reviewed, for internal circulation only

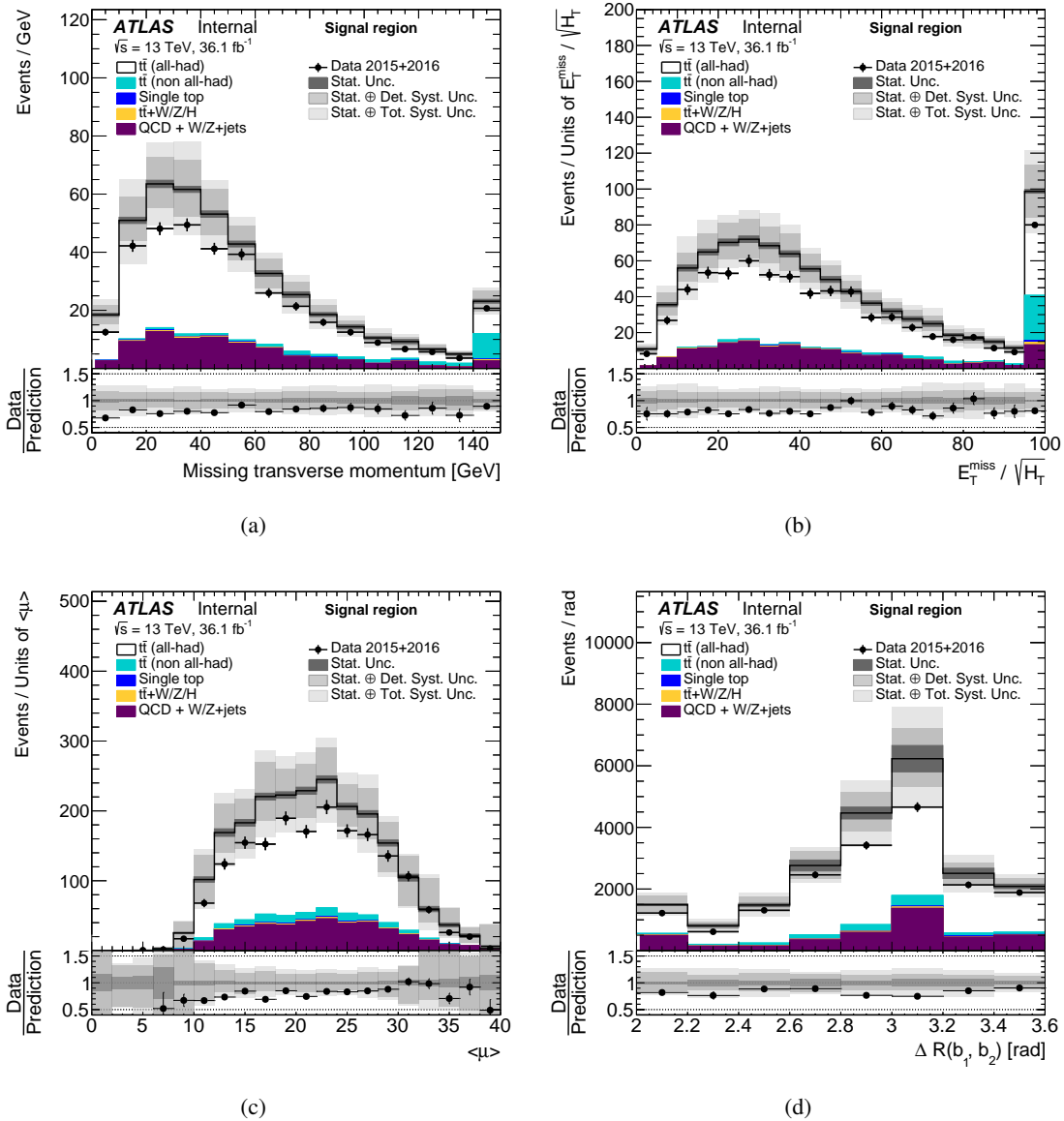


Figure 7: Event-wise variables in the signal region (S): (a) E_T^{miss} , (b) E_T^{miss} significance, (c) average number of interactions per bunch crossing ($\langle \mu \rangle$), and (d) ΔR between two b -tagged jets matched to large- R jets. Data distributions are compared to predictions using PowHEG+PyTHIA8 as the $t\bar{t}$ signal model. The hashed area indicates the combined statistical and systematic uncertainties on the total prediction. The light gray band shows systematic uncertainties related to the modelling of the $t\bar{t}$ system. N.B. The average number of interactions per bunch in the data has been prescaled by the factor of 1/1.09 and pileup reweighting has been done to propagate any pileup-dependent effects into the MC event selection.

362 5. Background determination and event reconstruction

363 After the event preselection and selection described in Sect.4, we estimate the rate of various sources of
 364 backgrounds.

365 The signal region corresponds to events with two top quark tags and two b -matches. Angular correlations
 366 among large- R and b -tagged jets are present only in events containing at least one real top quark,
 367 i.e. $t\bar{t}$ semi-leptonic events, single top, and $t\bar{t}+W/Z/H$ events. The contributions of these Standard Model
 368 processes to the signal region are taken from Monte Carlo simulation normalized to the more accurate
 369 total cross-section calculations (i.e. NNLO+NNLL for $t\bar{t}$). The estimated background yields from these
 370 processes are subtracted before the estimation of the primary background source, multijet events, is per-
 371 formed using a data-driven approach.

372 5.1. Backgrounds with $t\bar{t}$ pairs containing final state leptons

373 Production of $t\bar{t}$ pairs which decay into final states with one or more leptons are considered as a back-
 374 ground in the analysis. These events are simulated in MC and represent the second largest background,
 375 after multijet production with an expected yield in the signal region of 204 ± 44 events. As with the signal,
 376 the $t\bar{t}$ non all-hadronic yield is obtained by normalizing the $t\bar{t}$ MC simulations to the full NNLO+NNLL
 377 cross-section.

378 5.2. Backgrounds from single top-quark production

379 We use the MC generated samples for the Wt single top quark process to estimate the number of single
 380 top-quarks that are in the signal region and related control regions. The estimated rate is 24 ± 13 events
 381 in the sample in the signal region.

382 We do not directly include in this calculation the t -channel single top quark process because the necessary
 383 MC samples are not available. A private MC sample of this process was created and processed with a
 384 RIVET calculation to estimate the yield of events from this process. We find this additional contribution to
 385 be somewhat less than the Wt yield, though with large uncertainties due to the uncertainty in the rejection
 386 factor from the top-tagging algorithm and from the fraction of this background that is already included in
 387 the multijet background estimate. We do not explicitly subtract this component as a background. Rather,
 388 we assign an additional systematic uncertainty on the single top quark yield that is 50% of the Wt channel
 389 yield.

390 5.3. Backgrounds from $t\bar{t}+W/Z/H$

391 We use the MC-generated samples for associated production of $t\bar{t}+W/Z/H$ to estimate the backgrounds
 392 from these processes. The estimated rate is 33 ± 10 events in the signal region, where we have included
 393 the uncertainty on the production cross-sections.

394 5.4. Multijet background estimation

395 Multijet final states are expected to be the largest background in the all-hadronic $t\bar{t}$ sample. We have used
 396 Monte Carlo inclusive jet samples to better understand this background, as documented in Appendix M.
 397 However, the systematic uncertainties associated with this Monte Carlo background calculation are large.
 398 A data-driven technique is used to estimate the rate and distributions associated with this background.

399 For this purpose, events satisfying the preselection requirements are classified in sixteen regions according
 400 to the number of top tagged large- R jets and the number of b -matched large- R jets. As noted earlier, a
 401 large- R jet is said to be b -matched if there is at least one b -tagged jet within $\Delta R < 1.0$ of the axis of the
 402 nearest large- R jet axis.

403 The multijet background in the signal region is estimated using a sideband method. To perform the side-
 404 band calculation the expected contribution from events containing real top quarks is first subtracted from
 405 each region using the MC calculations for the non-all-hadronic $t\bar{t}$ process, single top-quark production
 406 and $t\bar{t} + W/Z/H$ production. The expected proportion of $t\bar{t}$ events for each region shown in Table 3 is
 407 calculated by dividing the number of $t\bar{t}$ events from all final states as calculated in MC by the event yield
 408 observed in data. The method takes into account the possibility of correlations between all parameters
 409 used to define 16 regions (top-tagging and b -matching) and is described in more detail in Appendix O. A
 410 similar approach using a 9-region calculation is detailed in Appendix L.

	1t1b	J (7.57%)	K (21.3%)	L (41.6%)	S
2nd large- R jet	0t1b	B (2.19%)	D (5.76%)	H (13.4%)	N (47.2%)
	1t0b	E (0.723%)	F (2.39%)	G (6.44%)	M (30.2%)
	0t0b	A (0.228%)	C (0.763%)	I (2.23%)	O (10.7%)
	0t0b		1t0b	0t1b	1t1b

Table 3: The labels and expected proportion of $t\bar{t}$ events for the classes of events used for the data-driven background prediction arising from multijet events. A b -match is defined as $\Delta R(J, b) < 1.0$, where J represents a large- R jet and b represents a b -tagged jet.

For a given observable, the background distribution in the signal region is taken from formula in Eq. 1:

$$S_i = \frac{J_i \times O_i}{A_i} \cdot \frac{D_i \times A_i}{B_i \times C_i} \cdot \frac{G_i \times A_i}{E_i \times I_i} \cdot \frac{F_i \times A_i}{E_i \times C_i} \cdot \frac{H_i \times A_i}{B_i \times I_i} = \frac{J_i \times O_i \times H_i \times F_i \times D_i \times G_i \times A_i^3}{(B_i \times E_i \times C_i \times I_i)^2} \quad (1)$$

411 Here, X_i is the number of events in region X falling in the i^{th} bin of the distribution for the given observ-
 412 able. The procedure is thus carried out for each bin independently. The sum of the bin-by-bin background
 413 calculation is not necessarily equal to the expected background calculated using the total number of events
 414 in the regions. The method is a product of a simple ABCD estimate $\frac{J_i \times O_i}{A_i}$ and four factors correcting four
 415 possible correlations between tagging variables.

416 Regions N and L (1 top-tag, 2 b -matches) are used as validation regions. Kinematic distribution of final
 417 state objects measured in the validation regions are shown in Appendix D.

418 The distributions concerning b -tagged jet observables have been treated in a slightly different way. The
 419 use of b -matching in defining the ABCD regions introduces correlations with b -jet observables. These

420 correlations can violate assumptions of the ABCD method if the choice of the regions is not done care-
 421 fully. Events with 2 b -matches must also have at least 2 b -tagged jets, so in these cases observables such
 422 as the second leading b -jet transverse momentum or $\Delta R(t_2, b)$ are well defined. On the other hand, events
 423 with 0 or 1 b -matches can arise from events having less than 2 b -jets. In these cases, the background
 424 calculation makes use of regions where the leading jet is top-tagged ($S' = NM/O$) or where the second-
 425 leading jet is top-tagged ($S' = LK/J$). The b -jet multiplicity, p_T and rapidity distributions are taken from
 426 regions where both jets are b -matched ($S' = LN/H$).

427 Finally, a few control observables suffer from low statistics in some kinematic bins. To overcome this dif-
 428 ficulties, the multijet background is calculated using a different combination of control regions, namely:

- 429 • Leading jet τ_{32} (Fig. 4(g)): $S' = KM'/F$ where $M' = FO/C$
- 430 • 2nd leading jet τ_{32} (Fig. 4(h)): $S' = K'M/F$, where $K' = JF/E$
- 431 • ΔR_{bb} (Fig. 7(d)): $S' = L'N'/H$ where $L' = JH/B$ and $N' = OH/I$

432 The total number of events found in various regions can be also predicted by this ABCD technique, and
 433 have been found to be consistent within the statistical uncertainty of the samples with the observed rates.
 434 We refer the reader to Appendices L and O for more details on the assumptions and cross-checks made
 435 to validate this calculation.

436 The effectiveness of top-tagging and b -matching has been further investigated to highlight the separation
 437 between signal and background and its impact on the signal selection. Figure 8(a) shows that requiring
 438 b -tagged jets to be matched angularly to the two leading large- R jets removes the signal component due
 439 to the decay of W bosons alone, as can be seen from the suppression of the W boson mass peak around 80
 440 GeV. Similarly, data events with no b -matches do not show any particular structure around the top mass.
 441 The requirement of b -matching selects jets with a mass around the top mass.

442 Conversely, we can probe the effect of top-tagging in events with two b -matches. Figure 9 shows that
 443 the shape of events with no top-tags is steeply decreasing. On the other hand, the request of two top-tags
 444 selects jets with a characteristic mass around 170 GeV.

Not reviewed, for internal circulation only

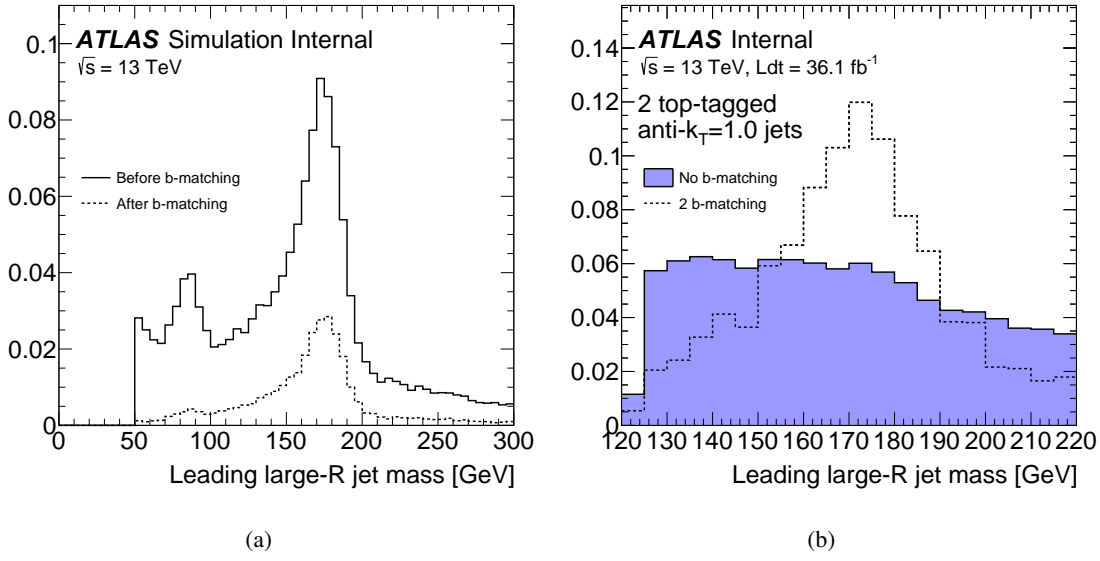


Figure 8: Leading large- R jet mass distribution is shown in (a) before and after the requirement of b -tagged jets matched angularly to the two leading large- R jets. Figure (b) shows the mass distributions for events with no b -matches and compares it to the distribution for events with 2 b -matches. The distributions are normalized to unit area to facilitate the shape comparison.

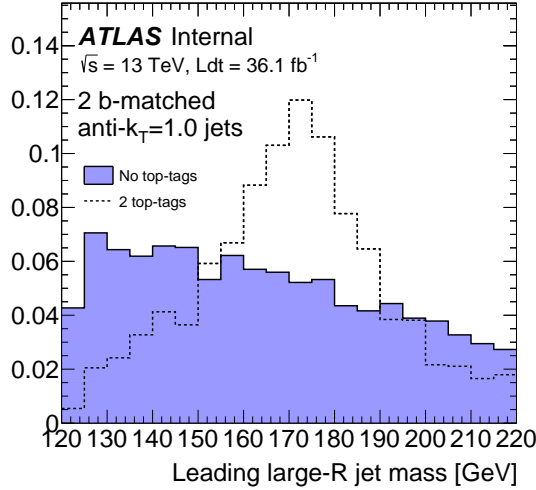


Figure 9: Leading large- R jet mass distribution for events with two b -matched large- R jets and with no top-tags (filled histogram) and two top-tags (dashed histogram). The distributions are normalized to unit area to facilitate the shape comparison.

445 5.5. $t\bar{t}$ system reconstruction and event variables

446 After the event selection, the $t\bar{t}$ system is obtained by the sum of the four-vectors of the two leading large-
 447 R jets, interpreted as top-quark candidates. In the following, the indices 1 and 2 refer, respectively, to the
 448 leading and sub-leading top-quark, ordered by decreasing transverse momentum.

449 First, a set of baseline observables are presented: transverse momentum (p_T^t) and absolute value of the
 450 rapidity ($|y^t|$) of the leading and second leading top-quark candidate and the transverse momentum ($p_T^{t\bar{t}}$),
 451 absolute value of the rapidity ($|y^{t\bar{t}}|$) and invariant mass ($m^{t\bar{t}}$) of the $t\bar{t}$ system in Fig. 11. These observables
 452 have been previously measured by the ATLAS experiment using the 7 TeV and 8 TeV datasets [3–5].

453 The following additional observables are measured:

- 454
- The absolute value of the azimuthal angle between the two top-quarks ($\Delta\phi^{t\bar{t}}$);
 - the absolute value of the out-of-plane momentum ($|p_{out}^{t\bar{t}}|$), *i.e.* the projection of top-quark three-momentum onto the direction perpendicular to a plane defined by the other top-quark and the beam axis (\hat{z}) in the laboratory frame [11]:

$$|p_{out}^{t\bar{t}}| = \left| \vec{p}^{t,1} \cdot \frac{\vec{p}^{t,2} \times \hat{z}}{|\vec{p}^{t,2} \times \hat{z}|} \right|; \quad (2)$$

- 455
- the longitudinal boost of the $t\bar{t}$ system in the laboratory frame ($y_B^{t\bar{t}} = \frac{1}{2} [y^{t,1} + y^{t,2}]$) [10];
 - 456 • the production angle between the two top-quarks ($\chi^{t\bar{t}} = e^{2|y^\star|}$) [10]. Where $y^\star = \frac{1}{2} (y^{t,1} - y^{t,2})$ and
 457 $-y^\star$ are the rapidities of the two top-quarks in the $t\bar{t}$ centre-of-mass frame.
 - 458 • the cosine of the production angle θ^\star in the Collins-Soper² reference frame ($\cos \theta^\star$); and
 - 459 • the scalar sum of the transverse momenta of the two top-quarks ($H_T^{t\bar{t}}$) [13, 14]

460 The observables $\Delta\phi^{t\bar{t}}$ and $|p_{out}^{t\bar{t}}|$ are sensitive to a p_T imbalance in the transverse plane, *i.e.* to the emission
 461 of radiation associated with the production of the top-quark pair. They are employed to emphasize the
 462 central production region [11]. The angle between the two top-quarks has been found to be sensitive to
 463 non-resonant contributions due to hypothetical new particles exchanged in the t -channel [10]. In particu-
 464 lar, many signals due to processes not included in the Standard Model are predicted to peak at low values
 465 of $\chi^{t\bar{t}}$ [10]. Observables depending on the transverse momentum of the decay products of the top quark
 466 have been found to be sensitive to higher-order corrections [13, 14].

467 These observables are shown in Figs. 11–13 at detector level.

468 Finally, as a cross-check, other observables of the reconstructed event have been studied as shown in
 469 Fig. 14. The same observables measured in the validation region (N+L) are shown in Appendix D.

470 The parton level analysis includes two further measurements. These are the top p_T and rapidity distribu-
 471 tions filled by choosing a top quark at random from each event, as opposed to filling the distributions based
 472 on the p_T ordering of the top quarks. This choice is designed to allow for comparisons with theoretical
 473 calculations to NNLO as done by Czakon et. al. [35]. However, the current parton level unfolding scheme
 474 as discussed in 7 does not allow for a direct comparison due to the fact that we unfold to a restricted parton-
 475 level phase space. The possibility of including a similar theoretical comparison is under investigation.

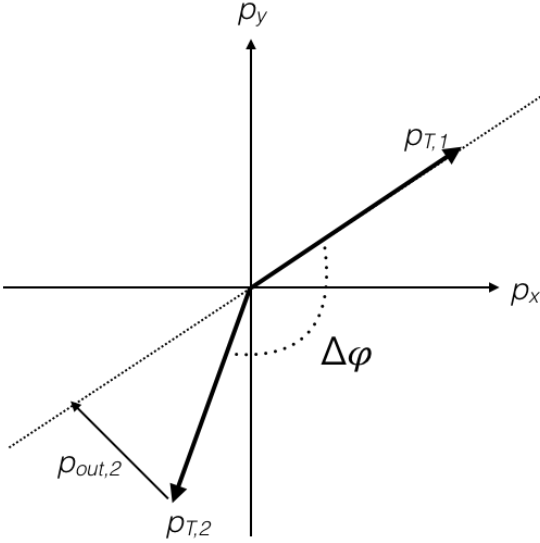


Figure 10: Diagram to illustrate the physical meaning of the variable $|p_{out}^{t\bar{t}}|$ defined in Eq. 2

Not reviewed, for internal circulation only

⁴⁷⁶ Table 4 presents the number of events during the different selection steps for data, $t\bar{t}$ signal, and the various
⁴⁷⁷ backgrounds.

Cuts	Preselection	Trigger	2J450	1J500	m(J1)	m(J2)	2 TopTags	2 b-matches
Data	87981640.00	78661720.00 (0.89)	54756660.00 (0.70)	22702684.00 (0.41)	3251154.00 (0.14)	629576.00 (0.19)	629576.00 (1.00)	3541.00 (0.006)
Signal	222892.23	209432.06 (0.94)	147963.20 (0.71)	74162.17 (0.50)	34869.92 (0.47)	18831.47 (0.54)	18831.47 (1.00)	3249.14 (0.173)
ttbarNonAllHadronic	67347.81	63088.98 (0.94)	41139.98 (0.65)	25995.77 (0.63)	9032.08 (0.35)	2663.61 (0.29)	2663.61 (1.00)	204.03 (0.077)
SingleTop	24092.60	22704.38 (0.94)	16829.76 (0.74)	10048.01 (0.60)	2281.27 (0.23)	520.05 (0.23)	520.05 (1.00)	23.70 (0.046)
ttbar+W/Z/H	2880.95	2644.03 (0.92)	1903.05 (0.72)	1161.33 (0.61)	522.89 (0.45)	238.41 (0.46)	238.41 (1.00)	33.13 (0.139)
MultijetDataDriven	-	-	-	-	-	-	-	811.09
S/B (MC)	-	-	-	-	-	-	-	3.03

Table 4: Numbers of selected events for the different steps of the analysis presented for data, $t\bar{t}$ signal and backgrounds. The fractions of the sample removed by the given requirement are shown in the bracket figures. The signal-over-background ratio is taken as the ratio of the predicted signal events in MC to the total predicted background and is shown only for the last selection cut.

² The Collins-Soper frame is the rest frame of the $t\bar{t}$ pair, wherein the two top-quarks have equal and opposite momenta; thus, each makes the same angle θ^* with the beam direction.

Not reviewed, for internal circulation only

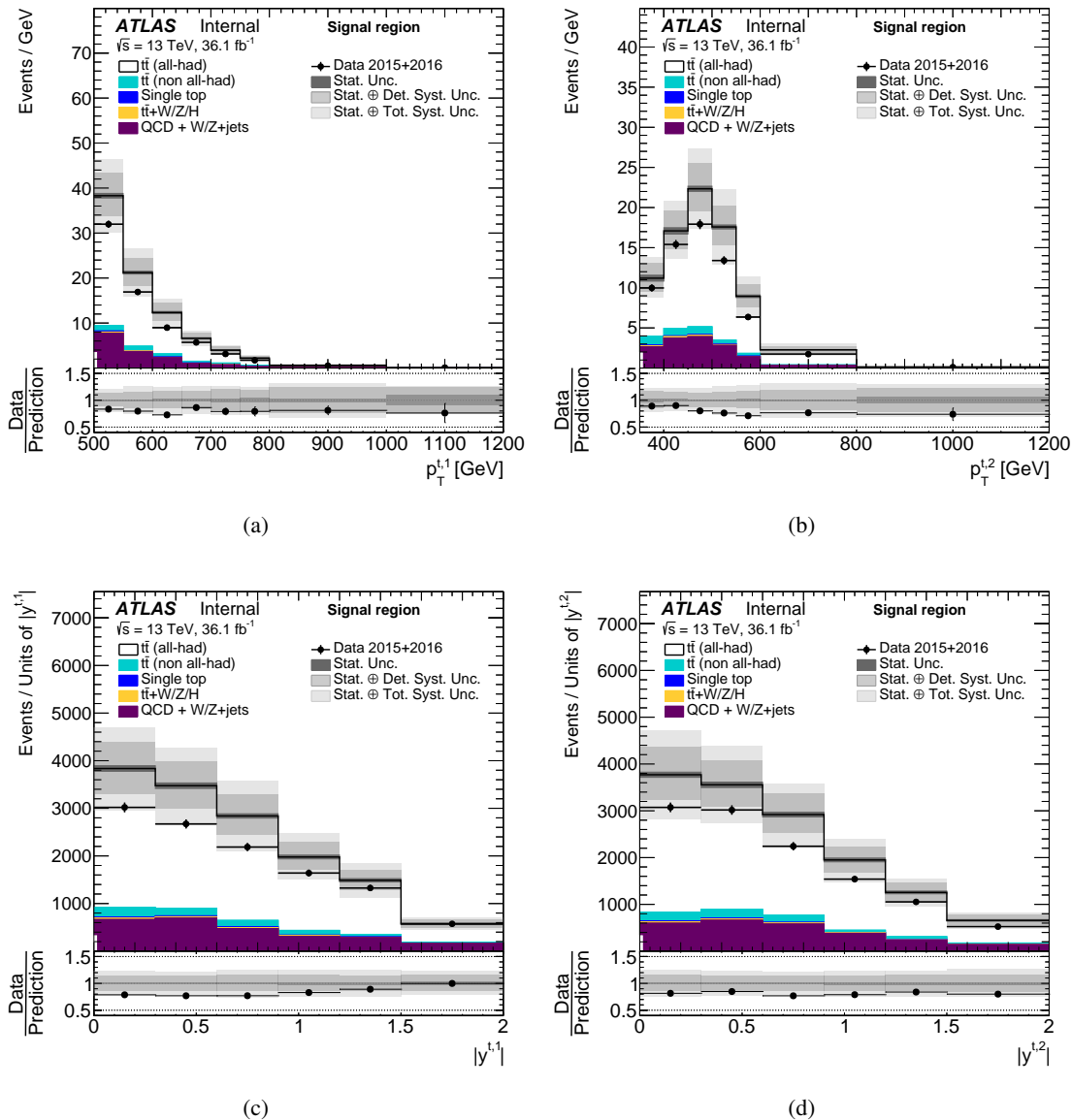


Figure 11: Kinematic distributions of top-quark candidates in the signal region (S): (a) transverse momentum and (c) absolute value of the rapidity of the leading top-quark; and (b) transverse momentum and (d) absolute value of the rapidity of the second leading top-quark. Data distributions are compared to predictions using PowHEG+PYTHIA8 as the $t\bar{t}$ signal model. The hashed area indicates the combined statistical and systematic uncertainties on the total prediction. The light gray band shows systematic uncertainties related to the modelling of the $t\bar{t}$ system.

Not reviewed, for internal circulation only

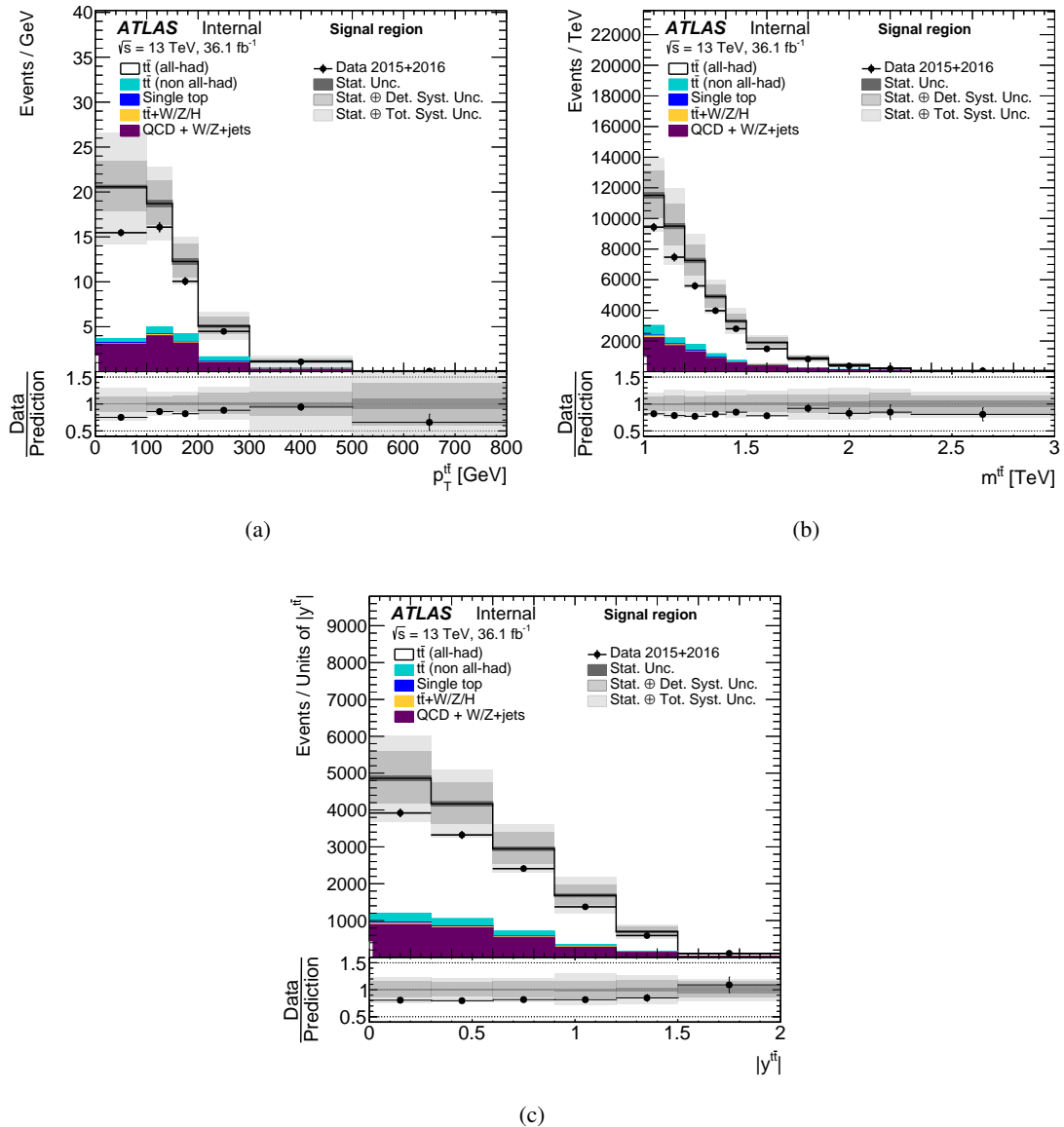


Figure 12: Kinematic distributions of $t\bar{t}$ system in the signal region (S): (a) transverse momentum, (b) invariant mass and (c) absolute value of the rapidity of the $t\bar{t}$ system. Data distributions are compared to predictions using PowHEG+PYTHIA8 as the $t\bar{t}$ signal model. The hashed area indicates the combined statistical and systematic uncertainties on the total prediction. The light gray band shows systematic uncertainties related to the modelling of the $t\bar{t}$ system.

Not reviewed, for internal circulation only

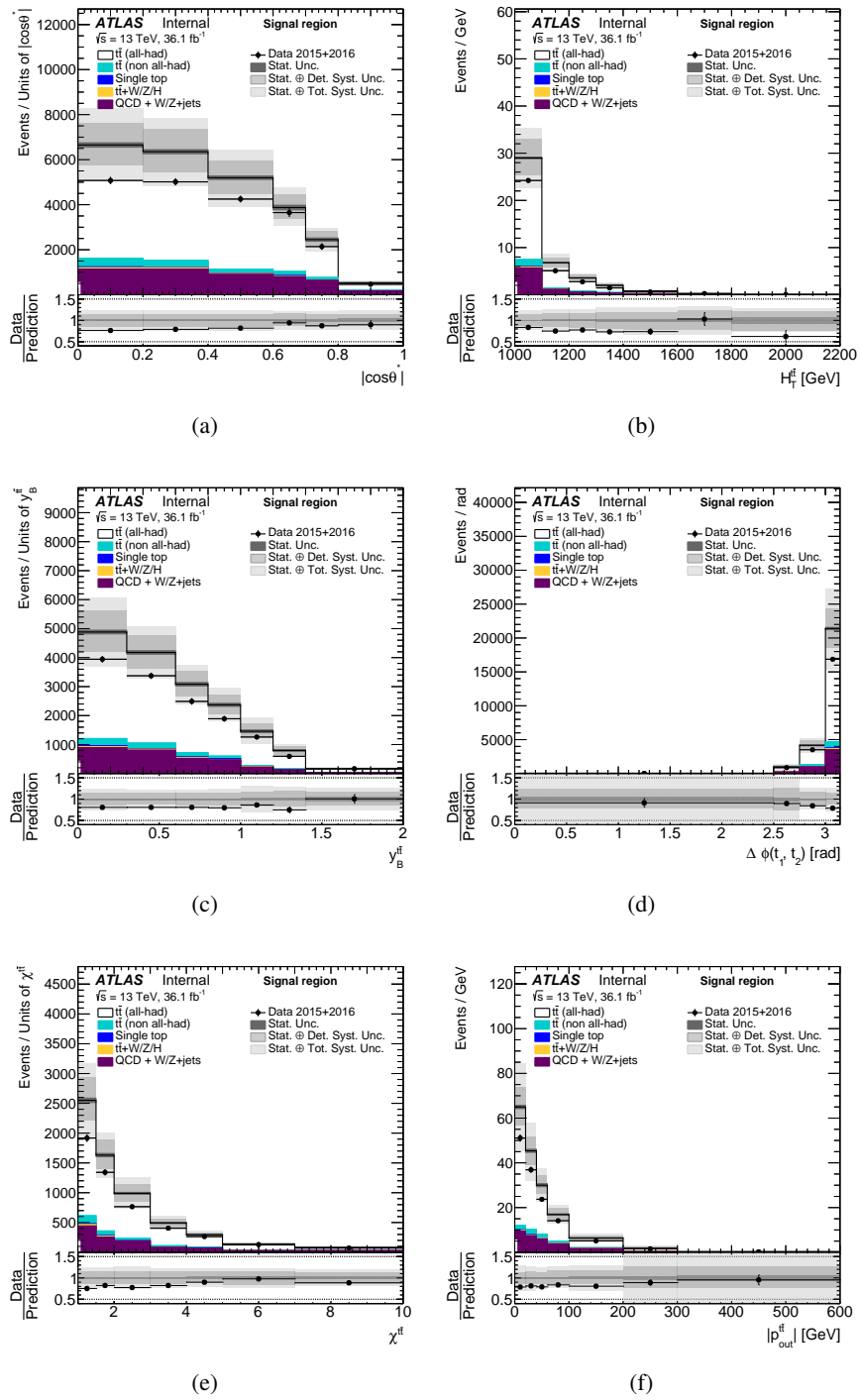


Figure 13: Kinematic distributions of $t\bar{t}$ system in the signal region (S): (a) production angle in the Collins-Soper reference frame, (b) scalar sum of the two top-quarks' transverse momenta, (c) longitudinal boost $y_B^{t\bar{t}}$, (d) azimuthal angle between the two top-quarks $\Delta\phi^{t\bar{t}}$, (e) production angle $\chi^{t\bar{t}}$ and (f) absolute value of the out-of-plane momentum $p_{t\bar{t} \text{out}}^0$. Data distributions are compared to predictions using PowHEG+PYTHIA8 as the $t\bar{t}$ signal model. The hashed area indicates the combined statistical and systematic uncertainties on the total prediction. The light gray band shows systematic uncertainties related to the modelling of the $t\bar{t}$ system.

Not reviewed, for internal circulation only

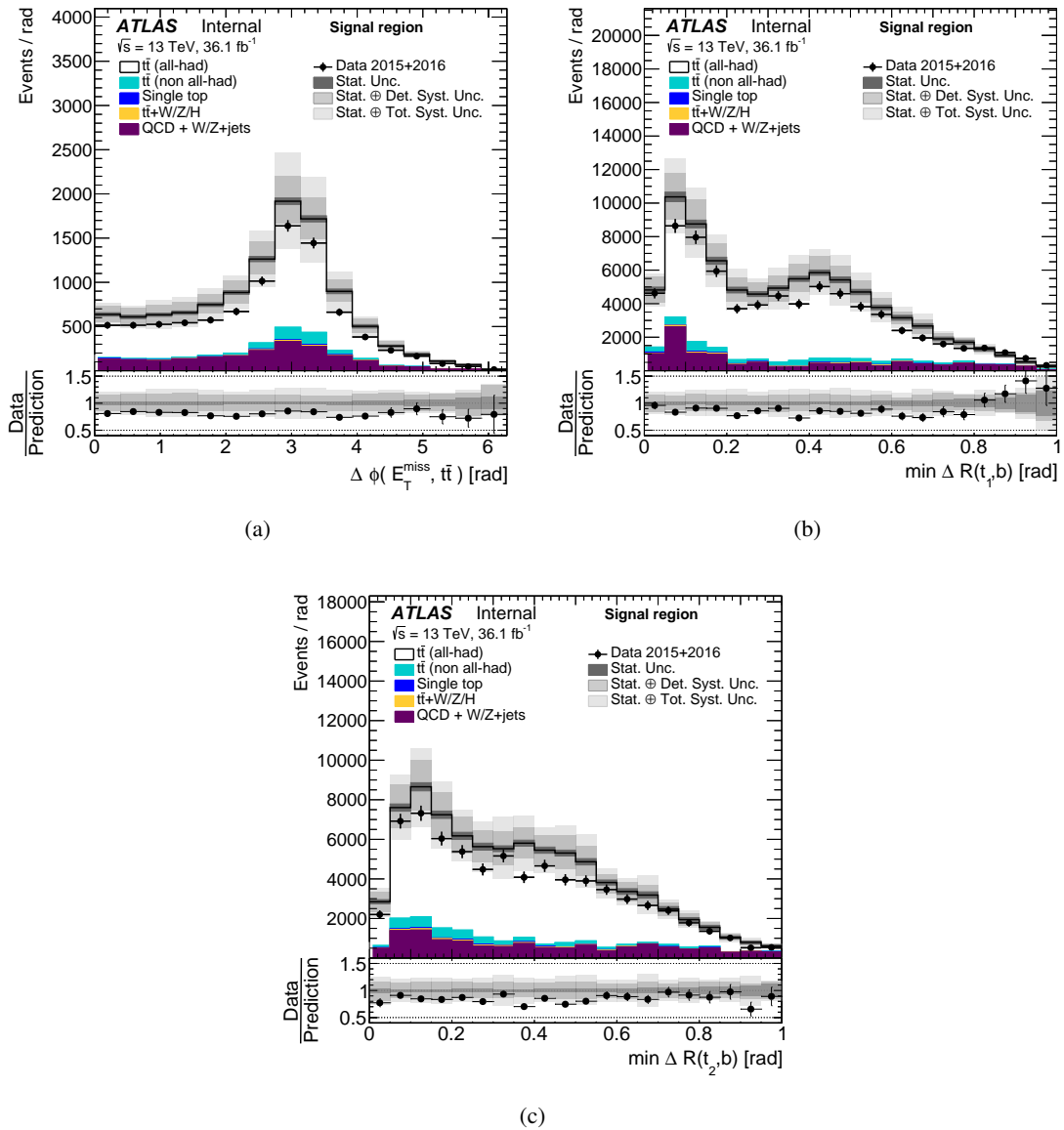


Figure 14: Event-wise observables in the signal region (S): (a) $\Delta\phi$ between E_T^{miss} and the $t\bar{t}$ system, (b) minimum ΔR between the leading top candidate and a b -tagged jet, (c) minimum ΔR between the second leading top candidate and a b -tagged jet. Data distributions are compared to predictions using PowHEG+PYTHIA8 as the $t\bar{t}$ signal model. The multijet background estimate in the latter two subfigures has not been calculated correctly. The hashed area indicates the combined statistical and systematic uncertainties on the total prediction. The light gray band shows systematic uncertainties related to the modelling of the $t\bar{t}$ system.

478 6. Measurement of particle-level fiducial cross-sections

479 The underlying differential cross-sections are obtained from the detector-level events using an unfolding
 480 technique that corrects for detector effects. The iterative Bayesian method [36] as implemented in
 481 RooUnfold [37] is used.

482 6.1. Fiducial phase space

483 The fiducial phase-space definition models the kinematic requirements used to select the final state. These
 484 requirements, defined on particle-level objects, are

- 485 • at least 2 anti- k_t , $R = 1.0$ jets with $p_T > 350$ GeV,
- 486 • at least 1 anti- k_t , $R = 1.0$ jet with $p_T > 500$ GeV,
- 487 • at least 2 anti- k_t , $R = 0.4$ jets with $p_T > 25$ GeV,
- 488 • the masses of both $R = 1.0$ jets be within 50 GeV of the top-quark mass,
- 489 • the two leading $R = 1.0$ jets be associated with a b -hadron in the final state using a ghost-matching
 490 technique as described in Ref. [38], and
- 491 • no electrons or muons with $p_T > 25$ GeV be in the event.

492 Particle-level leptons are required not to come from a hadron decay in the MC truth record. The four
 493 momenta of the leptons is defined by adding the four-momentum of all stable photons within $\delta R = 1.0$ of
 494 the lepton to its bare four-momentum. Particle-level jets are clustered from all stable particles excluding
 495 the selected leptons and their associated photons.

496 We select MC events that meet these requirements, and then use that sample to derive the acceptance
 497 corrections and other information needed for the unfolding procedure.

498 6.2. Unfolding procedure

499 The unfolding starts from the detector-level event distribution (N_{reco}), from which the backgrounds (N_{bg})
 500 are then subtracted.

501 Next, an acceptance correction f_{acc} is applied which corrects for two types of events. The acceptance cor-
 502 rection takes into account events that are generated outside the fiducial phase-space but pass the detector-
 503 level selection ("false-positives") as well as events which are not well-reconstructed as defined by a set of
 504 matching criteria. Events which are not well-reconstructed are folded back in by the efficiency correction
 505 applied after the unfolding step.

506 The matching criteria require that for an event to be considered well-reconstructed the detector- and
 507 particle-level objects interpreted as top-quarks must be angularly matched and have the same rank when
 508 ordered by transverse momentum. The angular matching requires that each detector-level top quark
 509 candidate is matched to a particle-level top quark with an angular separation $\Delta R < 1.0$. The angular
 510 matching is found to be fully efficient; angular separation between detector- and particle-level large- R
 511 jets is shown in Figure 15. On the other hand, it is observed that in about 13% of the cases the p_T -
 512 ordering of the two leading jets at detector- and particle-level is inverted. This effect is found to be almost

constant as a function of rapidity distributions and of the leading-top transverse momentum, but presents a certain degree of dependency on other observables, as shown in Figs.16–18. In particular, about 40% of the events are not matched correctly and thus rejected when the transverse momentum of the $t\bar{t}$ system is less than 50 GeV.

Next, the unfolding step uses a migration matrix (\mathcal{M}) derived from simulated $t\bar{t}$ events which maps the binned generated particle-level events to the binned detector-level events. The probability for particle-level events to remain in the same bin is therefore represented by the elements on the diagonal, and the off-diagonal elements describe the fraction of particle-level events that migrate into other bins. Therefore, the elements of each row add up to unity. The binning is chosen such that the fraction of events in the diagonal bins is always greater than 50%. A finer optimization has been performed in order to ensure that the shape of rapidly-falling distribution can be clearly measured (e.g. top-quark rapidity, $t\bar{t}$ rapidity, $p_{out}^{t\bar{t}}$ and $\cos \theta^*$) while still retaining a total uncertainty of about 30%. The unfolding is performed using four iterations to balance the goodness of fit and the statistical uncertainty. The effect of varying the number of iterations by one was tested and proved to be negligible.

Finally, the efficiency correction ϵ_{eff} corrects for two types of events. The efficiency correction takes into account events which pass the particle-level selection but are not reconstructed at the detector level ("false-negatives") and the poorly reconstructed events removed by the acceptance correction. Given the similarity between the particle- and detector-level phase space definitions efficiency corrections are dominated by top-tagging and b-tagging efficiencies. Observables correlated with b-jet p_T show drops in efficiency due to the drop in b-tagging efficiency at higher jet p_T [39]. Top-tagging efficiencies are optimized to provide nearly constant efficiency as a function of p_T .

Figures 19–24 show the acceptance and efficiency corrections as a function of kinematic observables. The blue and red bands indicate the statistical uncertainty on the signal Monte Carlo in each bin.

The unfolding procedure for an observable X at particle level is summarized by the expression

$$\frac{d\sigma^{\text{fid}}}{dX^i} \equiv \frac{1}{\mathcal{L} \cdot \Delta X^i} \cdot \frac{1}{\epsilon_{\text{eff}}^i} \cdot \sum_j \mathcal{M}_{ij}^{-1} \cdot f_{\text{acc}}^j \cdot (N_{\text{reco}}^j - N_{\text{bg}}^j), \quad (3)$$

where the index j iterates over bins of X at detector level while the i index labels bins at particle level; ΔX^i is the bin width while \mathcal{L} is the integrated luminosity and the Bayesian unfolding is symbolized by \mathcal{M}_{ij}^{-1} .

The integrated cross-section is obtained by integrating the unfolded cross-section over the kinematic bins, and its value is used to compute the normalized differential cross-section $1/\sigma^{\text{fid}} \cdot d\sigma^{\text{fid}}/dX^i$.

Tests have been performed to verify that the unfolding procedure is able to recover the particle-level distribution for input distributions that vary from the observed distributions or nominal predictions. These tests are document in Appendix I.

Not reviewed, for internal circulation only

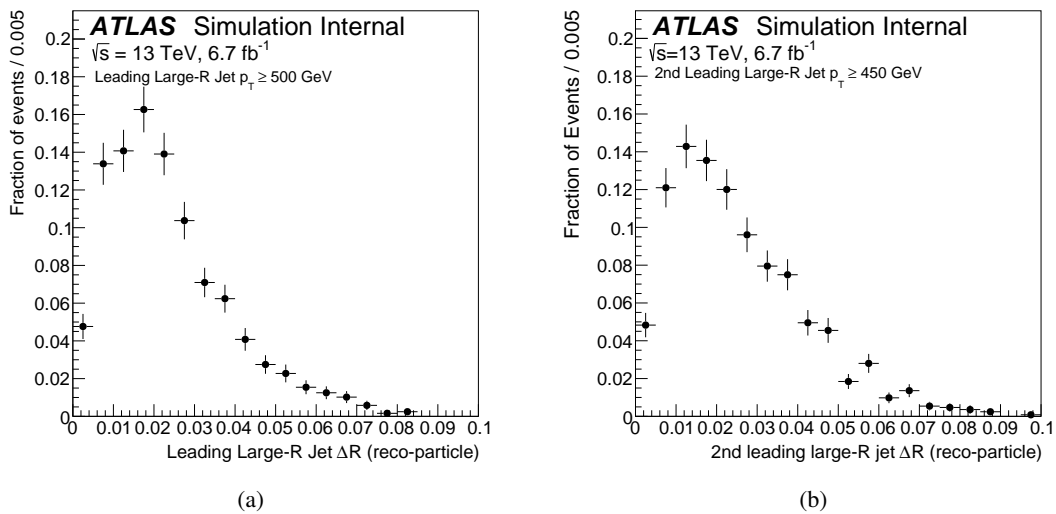


Figure 15: Angular separation between detector- and particle-level for (a) leading and (b) second-leading large- R jets.

Not reviewed, for internal circulation only

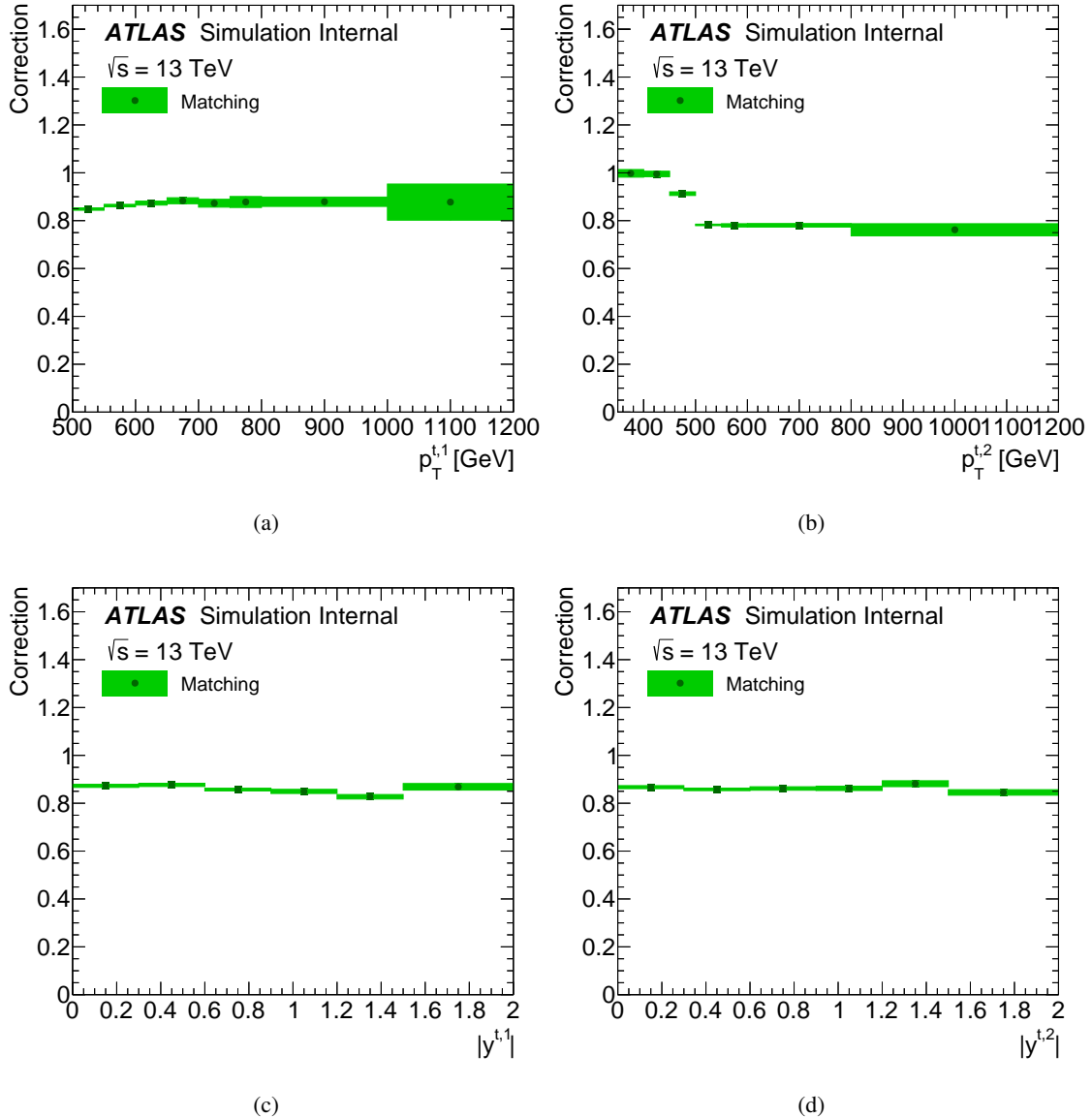


Figure 16: Fiducial phase-space matching correction as a function of (a) transverse momentum and (c) absolute value of the rapidity of the leading top-quark, and (b) transverse momentum and (d) absolute value of the rapidity of the second-leading top-quark. The green bands indicate the statistical uncertainty on the signal Monte Carlo in each bin. The PowHEG+PYTHIA8 generator is used as the nominal prediction to correct for detector effects. Uncertainties are estimated using standard binomial statistics.

Not reviewed, for internal circulation only

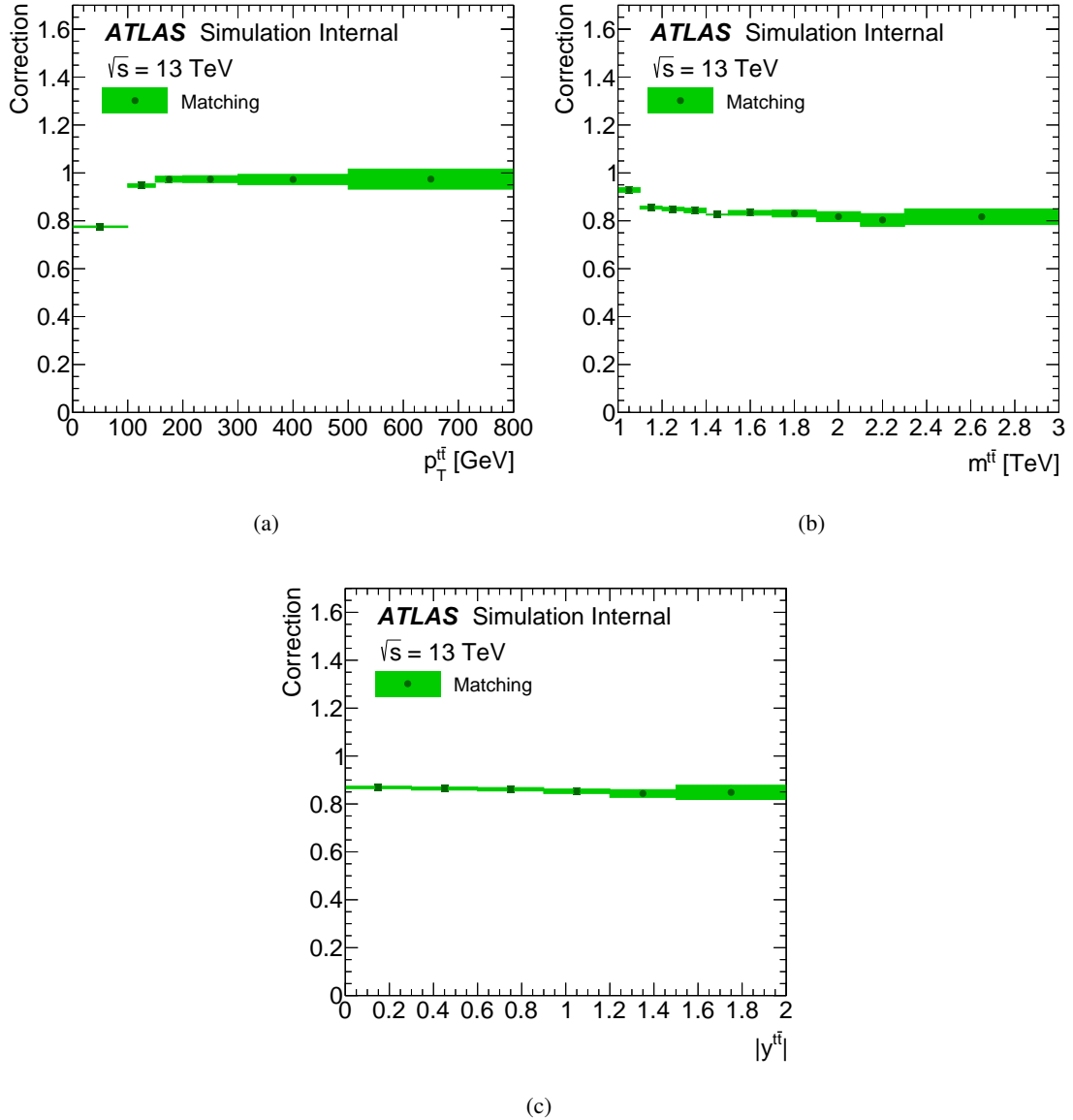


Figure 17: Fiducial phase-space matching correction of (a) transverse momentum, (b) invariant mass and (c) absolute value of the rapidity of the $t\bar{t}$ system. The green bands indicate the statistical uncertainty on the signal Monte Carlo in each bin. The PowHEG+PYTHIA8 generator is used as the nominal prediction to correct for detector effects. Uncertainties are estimated using standard binomial statistics.

Not reviewed, for internal circulation only

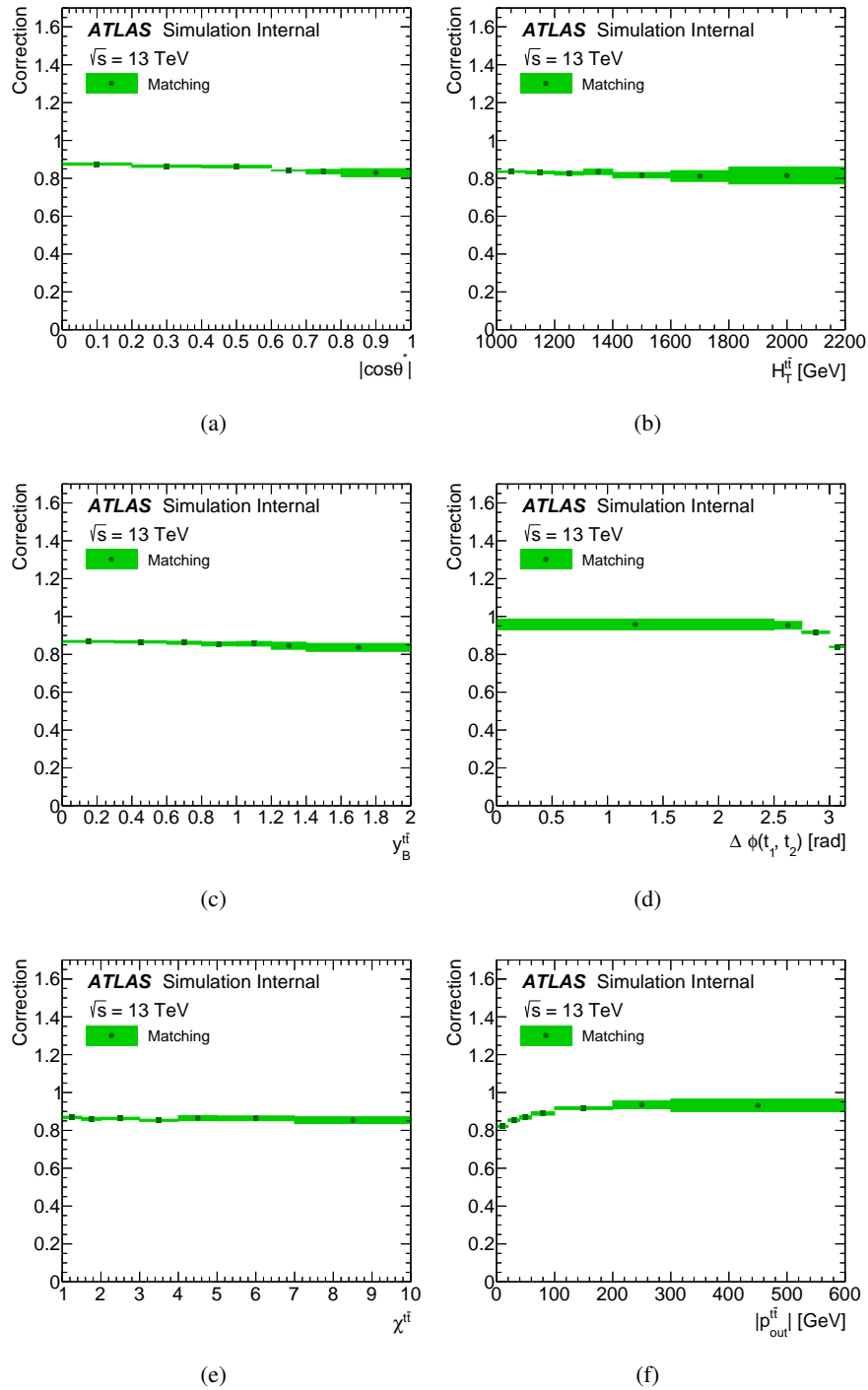


Figure 18: Fiducial phase-space matching correction of (a) production angle in the Collins-Soper reference frame, (b) scalar sum of the two top-quarks' transverse momenta, (c) longitudinal boost $y_B^{t\bar{t}}$, (d) azimuthal angle between the two top-quarks $\Delta\phi_{t\bar{t}}$, (e) production angle $\chi^{t\bar{t}}$ and (f) absolute value of the out-of-plane momentum $p_{out}^{t\bar{t}}$. The green bands indicate the statistical uncertainty on the signal Monte Carlo in each bin. The PowHEG+PYTHIA8 generator is used as the nominal prediction to correct for detector effects. Uncertainties are estimated using standard binomial statistics.

Not reviewed, for internal circulation only

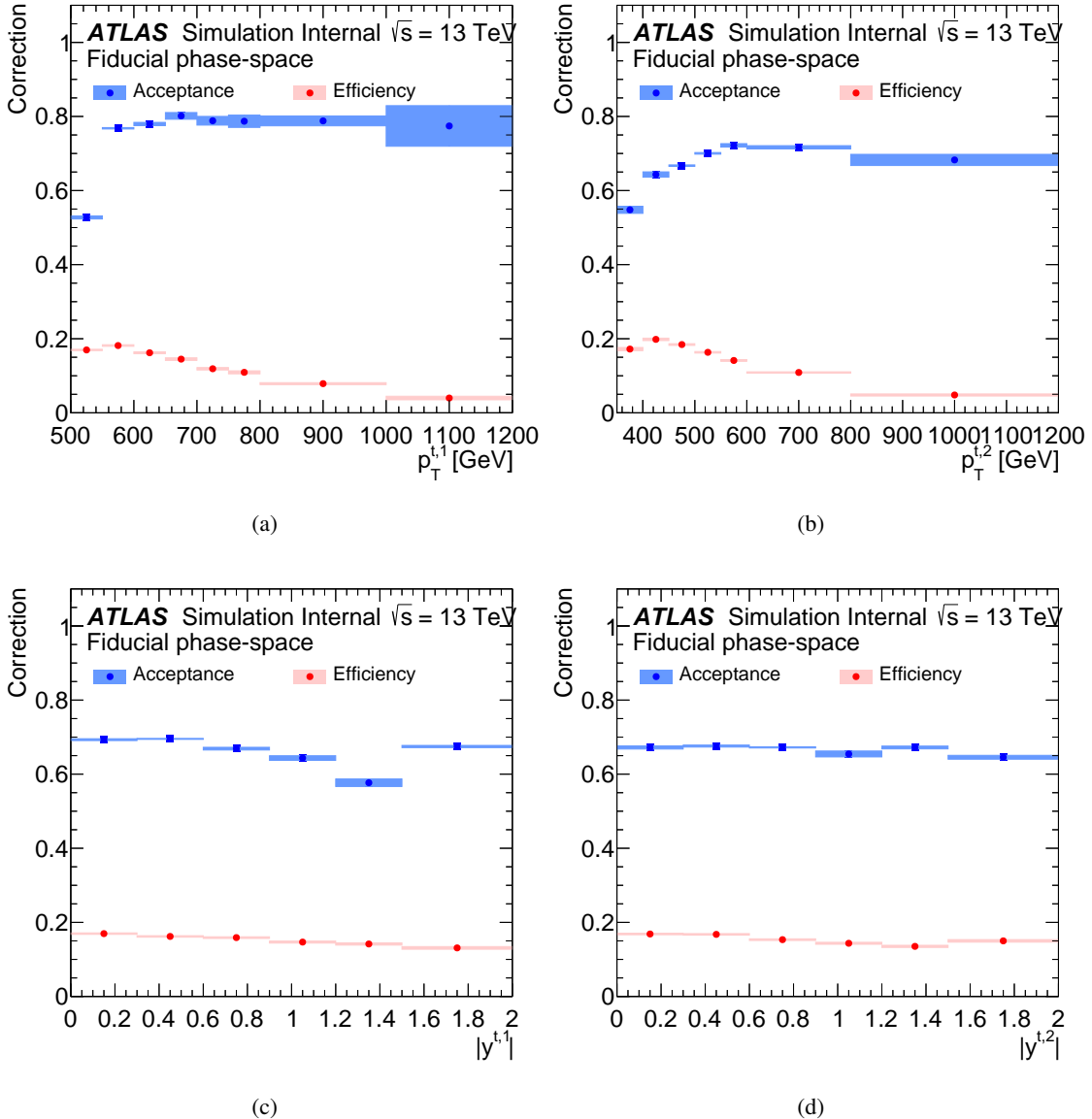


Figure 19: Fiducial phase-space acceptance and efficiency corrections as a function of (a) transverse momentum and (c) absolute value of the rapidity of the leading top-quark, and (b) transverse momentum and (d) absolute value of the rapidity of the second-leading top-quark. The blue and red bands indicate the statistical uncertainty on the signal Monte Carlo in each bin. The PowHEG+PYTHIA8 generator is used as the nominal prediction to correct for detector effects. Uncertainties are estimated using standard binomial statistics.

Not reviewed, for internal circulation only

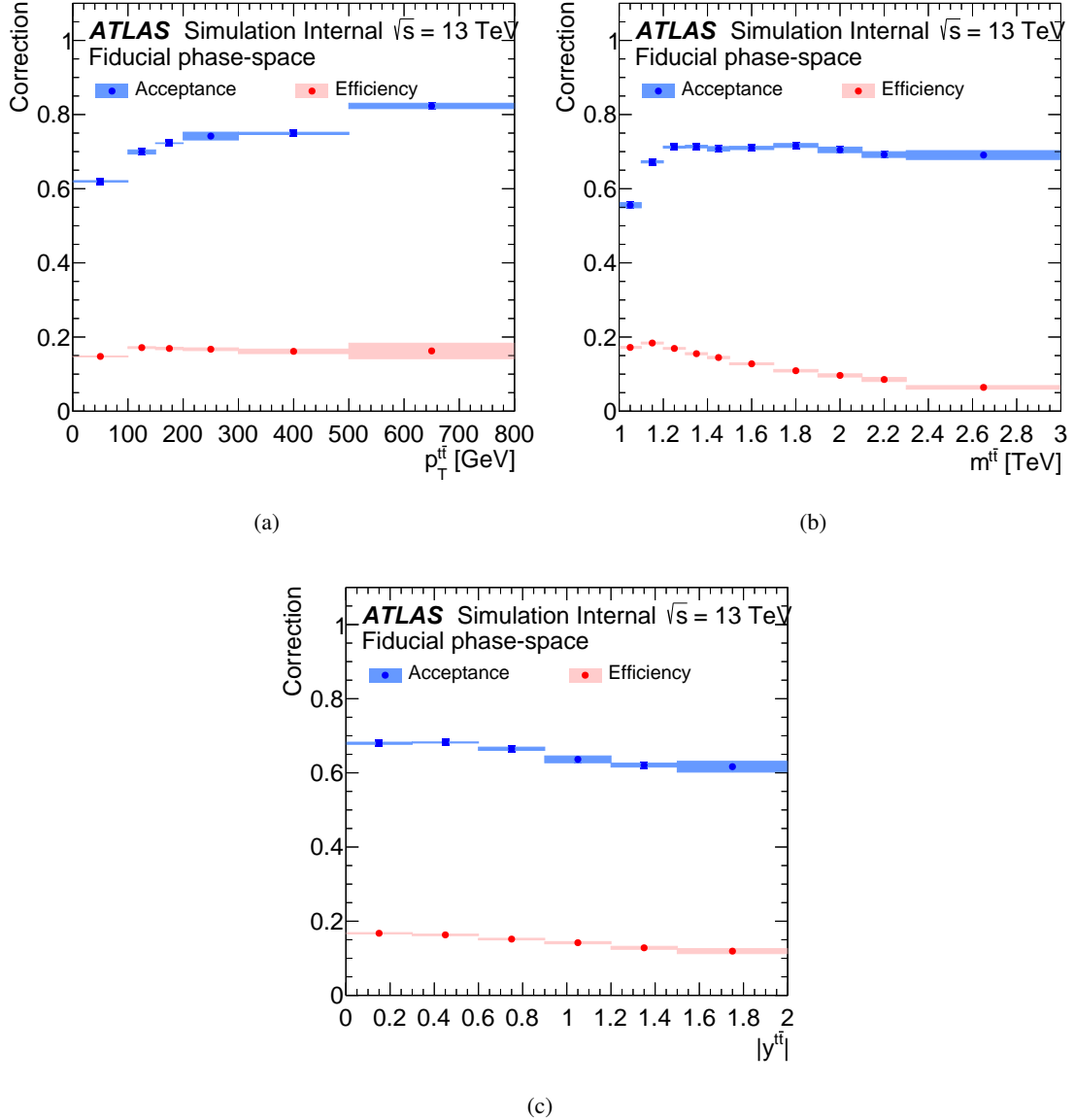


Figure 20: Fiducial phase-space acceptance and efficiency corrections as a function of (a) transverse momentum, (b) invariant mass and (c) absolute value of the rapidity of the $t\bar{t}$ system. The blue and red bands indicate the statistical uncertainty on the signal Monte Carlo in each bin. Uncertainties are estimated using standard binomial statistics.

Not reviewed, for internal circulation only

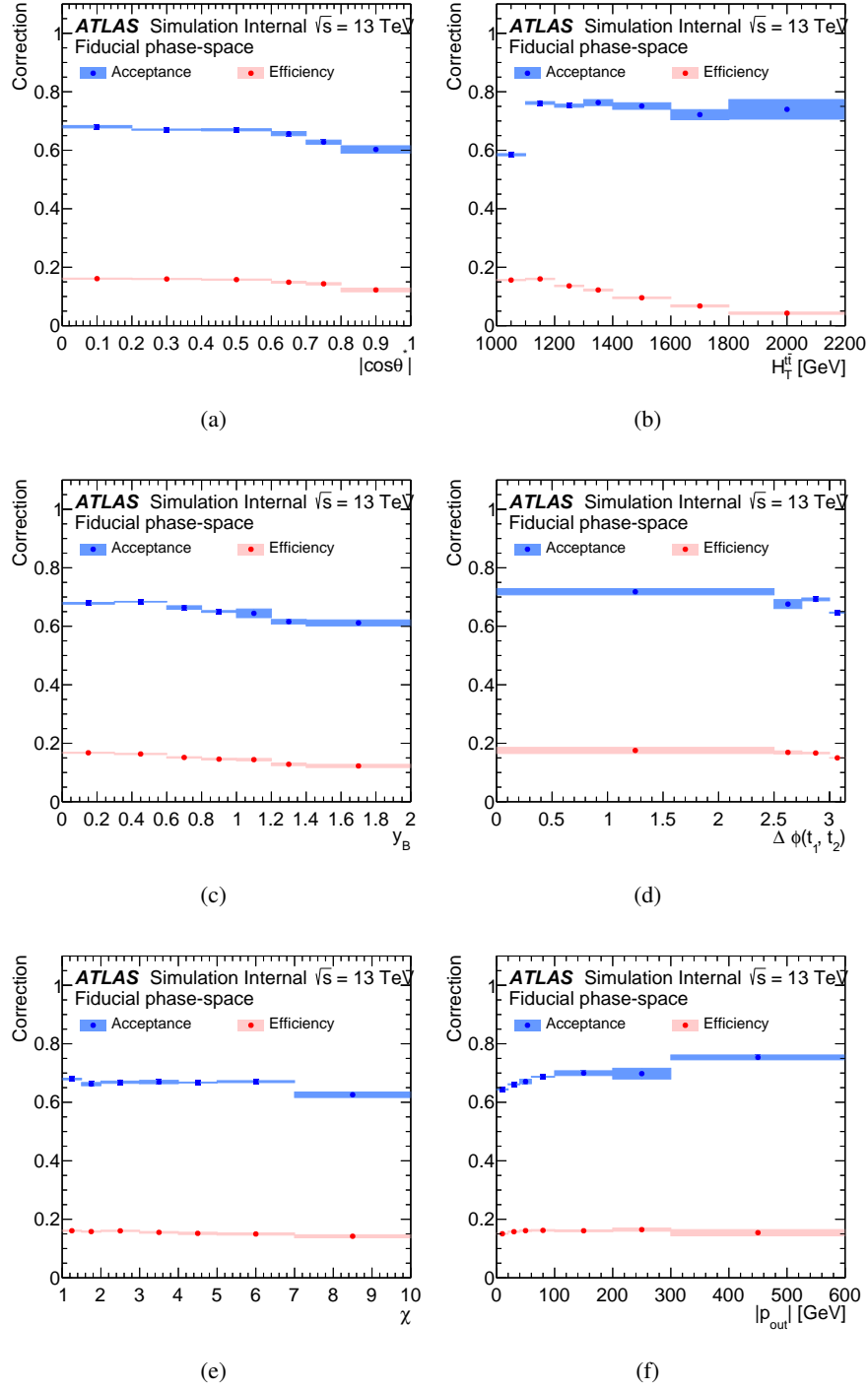


Figure 21: Fiducial phase-space acceptance and efficiency corrections as a function of (a) production angle in the Collins-Soper reference frame, (b) scalar sum of the two top-quarks transverse momenta, (c) longitudinal boost y_B^t , (d) azimuthal angle between the two top-quarks $\Delta\phi_{t\bar{t}}$, (e) production angle $\chi^{t\bar{t}}$ and (f) absolute value of the out-of-plane momentum $p_{out}^{t\bar{t}}$. The blue and red bands indicate the statistical uncertainty on the signal Monte Carlo in each bin. Uncertainties are estimated using standard binomial statistics.

Not reviewed, for internal circulation only

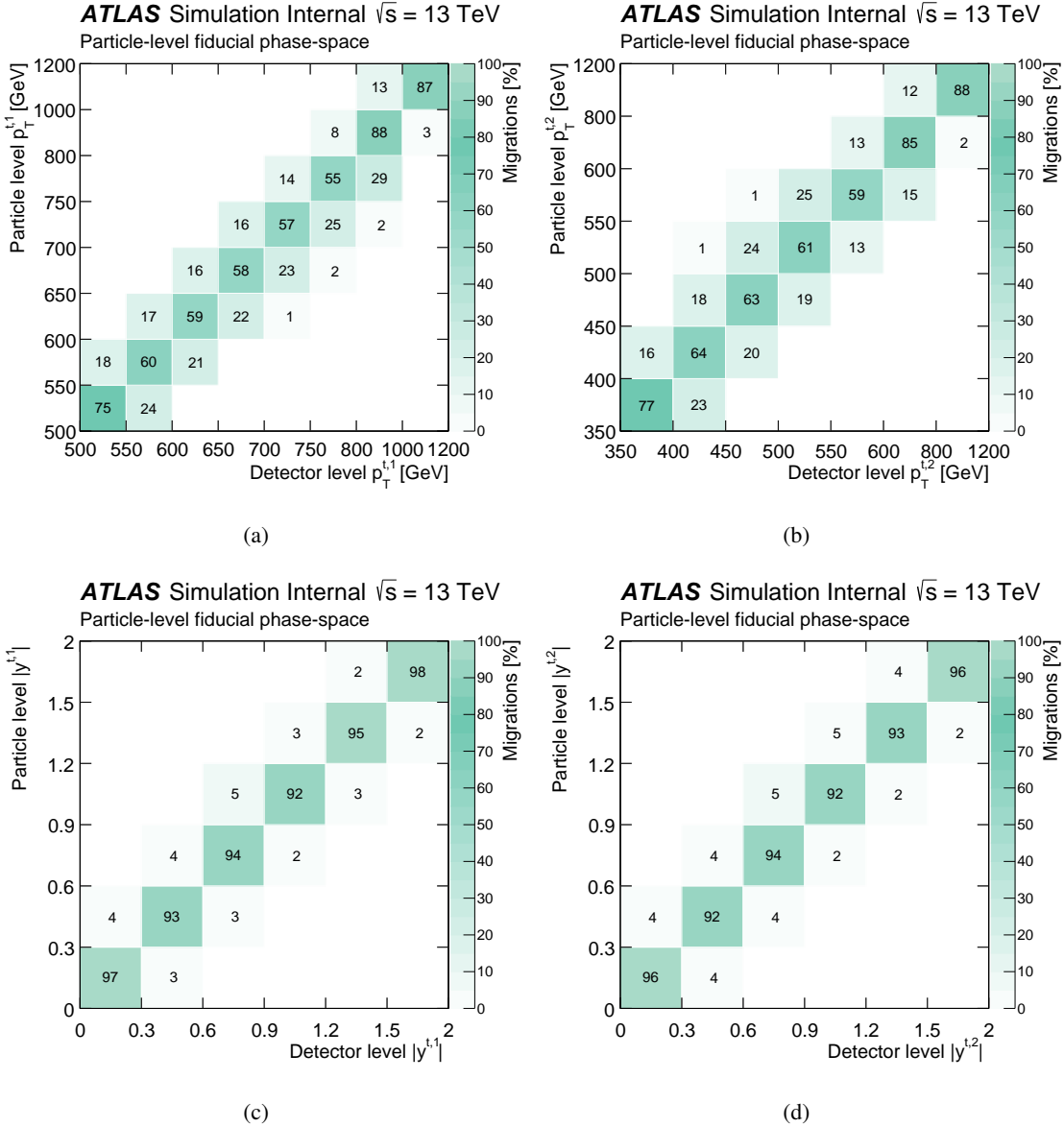


Figure 22: Fiducial phase-space migration matrices of (a) transverse momentum and (c) absolute value of the rapidity of the leading top-quark, and (b) transverse momentum and (d) absolute value of the rapidity of the second-leading top-quark.

Not reviewed, for internal circulation only

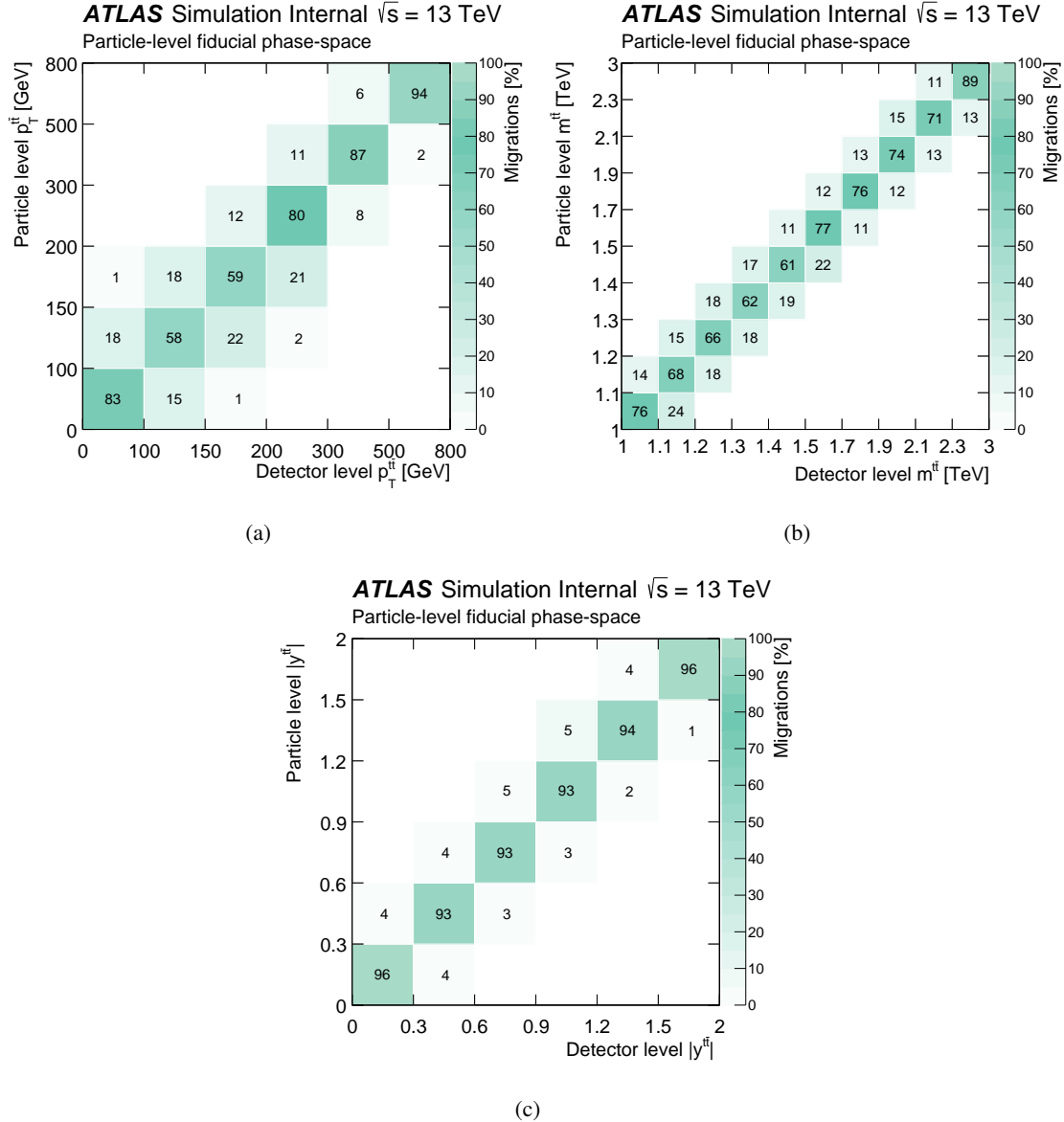


Figure 23: Fiducial phase-space migration matrices of (a) transverse momentum, (b) invariant mass and (c) absolute value of the rapidity of the $t\bar{t}$ system.

Not reviewed, for internal circulation only

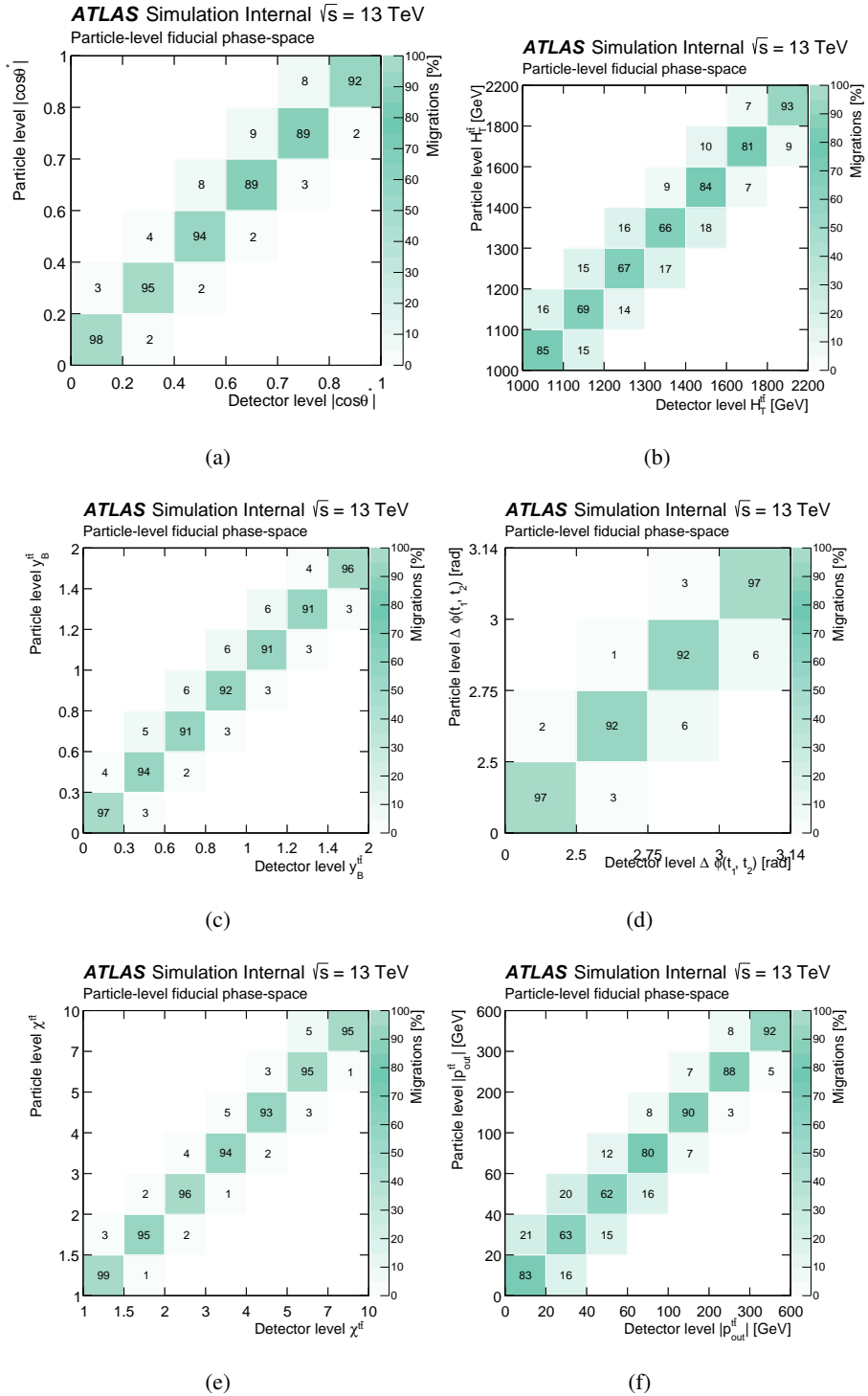


Figure 24: Fiducial phase-space migration matrices of (a) production angle in the Collins-Soper reference frame, (b) scalar sum of the two top-quarks' transverse momenta, (c) longitudinal boost $y_B^{t\bar{t}}$, (d) azimuthal angle between the two top-quarks $\Delta\phi_{t\bar{t}}$, (e) production angle $\chi^{t\bar{t}}$ and (f) absolute value of the out-of-plane momentum $p_{\text{out}}^{t\bar{t}}$.

544 7. Measurement of parton-level cross-sections

545 The parton-level differential cross-sections are obtained directly from the detector-level distributions by
 546 removing detector level effects using the Bayes unfolding method.

547 7.1. Parton-level phase space

548 The top/antitop quark at parton-level is defined as the top/antitop quark after FSR (taking the last top/antitop
 549 quark from MC decay chain).

550 The parton-level results are considered in the phase space defined by kinematic requirements applied on
 551 produced $t\bar{t}$ pairs. The requirements are

- 552 • at least one quark from $t\bar{t}$ pair has $p_T > 500$ GeV,
- 553 • both top and antitop quark have $p_T > 350$ GeV.

554 No other selections are applied. η range of top quarks is not limited.

555 The original analysis goal was to unfold to the full phase space. However, the stress test results showed

556 that the extrapolation to the full phase space introduced significant uncertainties into the unfolded results.

557 Based on the stress test studies, documented in Appendix J for the fiducial phase space unfolding, the
 558 parton-level fiducial space definition was chosen.

559 7.2. Unfolding Procedure

560 The unfolding starts from the detector-level event distribution (N_{reco}), from which the backgrounds (N_{bg})
 561 are first subtracted. An acceptance correction f_{acc} is then applied to correct for events that pass the
 562 detector-level selection but fall outside the measured range of a given observable at parton-level.

563 The parton-level analysis applies matching as part of the acceptance and efficiency corrections identical
 564 to those applied in the particle-level unfolding and described in Section 6.2. The angular matching re-
 565 quires that each detector-level top quark candidate is matched to a parton-level top quark with an angular
 566 separation $\Delta R < 1.0$. The order matching requires that the angularly matched top quarks have the same
 567 p_T ordering at parton- and detector-level.

568 The unfolding step uses a migration matrix (\mathcal{M}) derived from simulated $t\bar{t}$ events that maps the binned
 569 generated parton-level events to the binned detector-level events. The iterative Bayesian method [36] as
 570 implemented in RooUnfold [37] is used with four iterations. Finally, the efficiency correction ϵ_{eff} corrects
 571 for events which fall within the measured observable range at parton-level but are not reconstructed at
 572 the detector level. Figures 25, 26 and 27 show the acceptance and efficiency corrections. The migration
 573 matrices are shown in Figures 28, 29 and 30.

The unfolding procedure for an observable X at parton-level is summarized by the expression

$$\frac{d\sigma^{\text{parton}}}{dX^i} \equiv \frac{1}{\mathcal{L} \cdot \Delta X^i} \cdot \frac{1}{\epsilon_{\text{eff}}^{i,\text{parton}}} \cdot \sum_j \mathcal{M}_{ij}^{-1,\text{parton}} \cdot f_{\text{acc}}^{j,\text{parton}} \cdot (N_{\text{reco}}^j - N_{\text{bg}}^j), \quad (4)$$

574 where the index j iterates over bins of X at detector level while the i index labels bins at parton-level;
575 ΔX^i is the bin width while \mathcal{L} is the integrated luminosity and the Bayesian unfolding is symbolized by
576 $\mathcal{M}_{ij}^{-1,parton}$. The efficiencies and acceptance corrections are computed for the detector-level to parton-level
577 requirements.

578 Parton-level binning is chosen to be harmonized with the particle-level binning in most cases. However,
579 some observables make use of different binning choices between parton- and particle-level to ensure
580 diagonality of the migration matrix or to smooth out bin-to-bin fluctuations in the uncertainty.

581 Tests have been performed to verify that the unfolding procedure is able to recover the parton-level dis-
582 tribution for input distributions that vary from the observed distributions or nominal predictions. These
583 tests are documented in Appendix J and show that the unfolding procedure results are unbiased so long as
584 the features of the input distributions are consistent with the measurement resolution of the variable.

Not reviewed, for internal circulation only

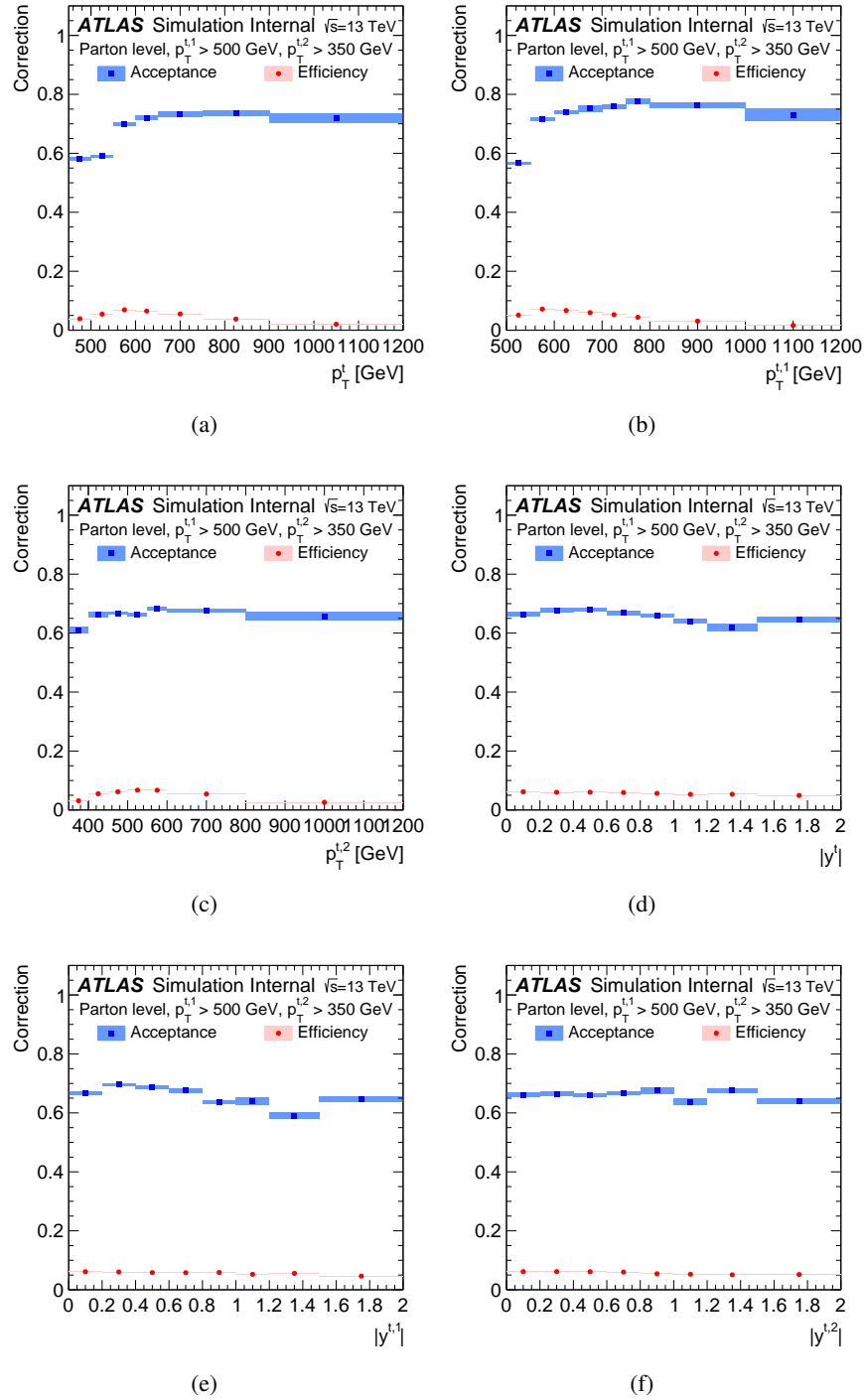


Figure 25: The parton-level efficiency and acceptance corrections as a function of (a) the transverse momentum of a randomly chosen top quark from each event, (b) the leading top p_T , (c) subleading top p_T , (d) absolute value of the rapidity of a randomly chosen top quark from each event, (b) the leading top $|y|$, and (c) subleading top $|y|$.

Not reviewed, for internal circulation only

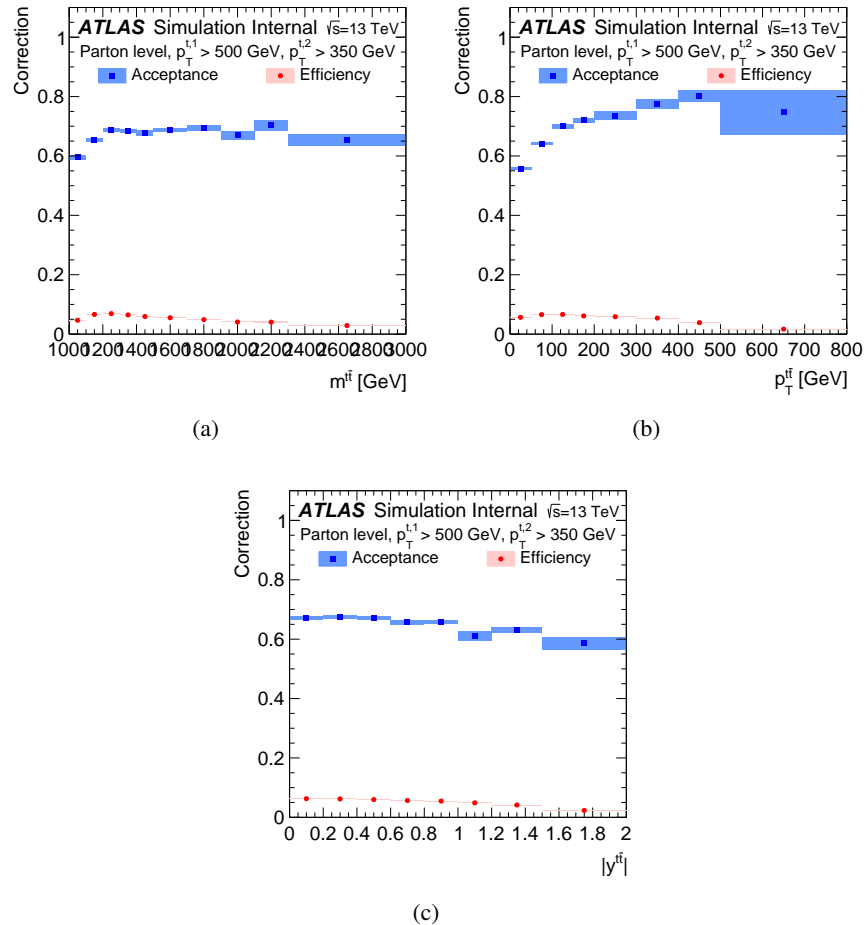


Figure 26: The parton-level efficiency and acceptance corrections as a function of (a) the $t\bar{t}$ mass, (b) the $t\bar{t}$ p_T , and (c) the absolute value of $t\bar{t}$ rapidity.

Not reviewed, for internal circulation only

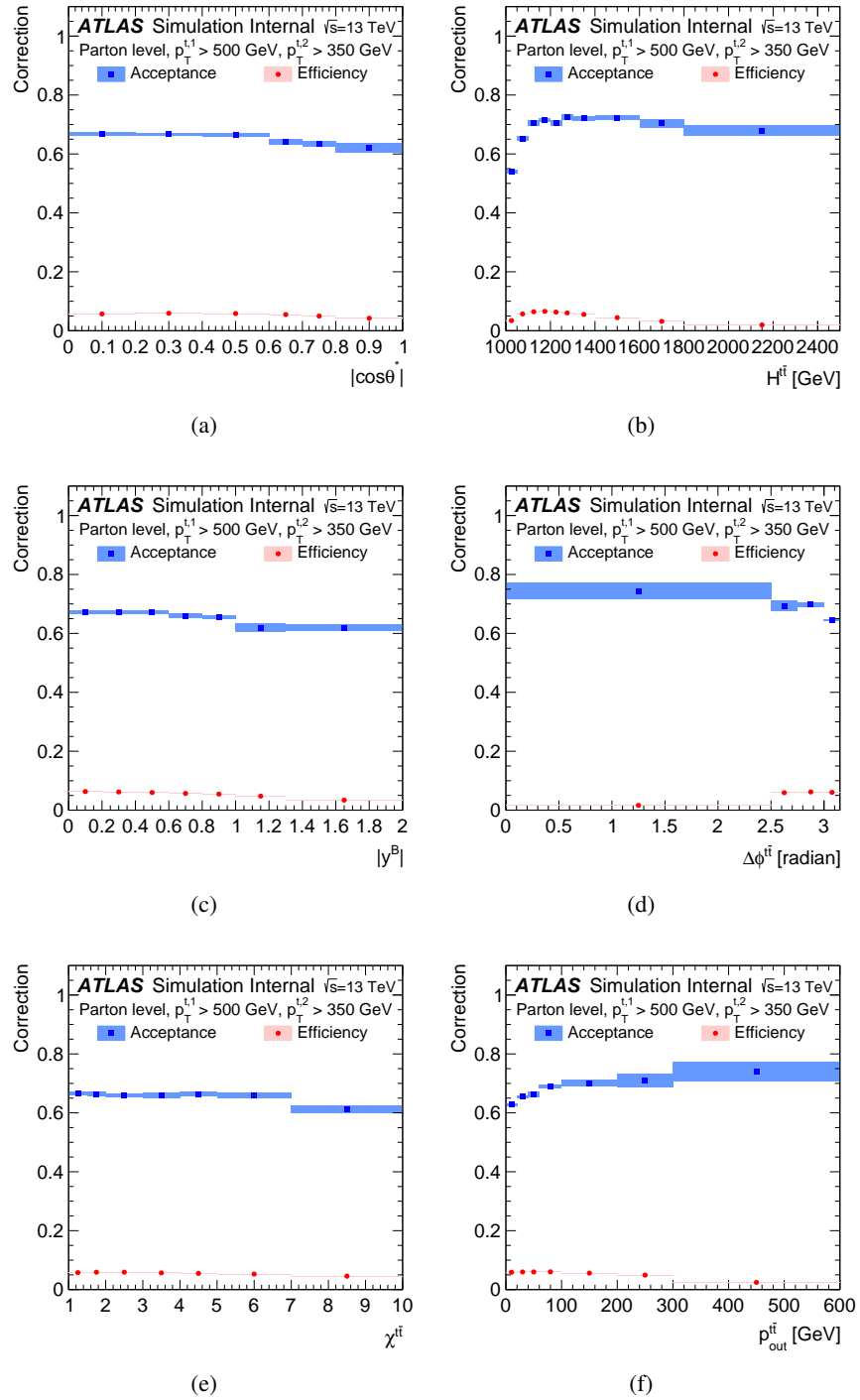


Figure 27: The parton-level efficiency and acceptance corrections as a function of (a) the $|\cos \theta^*|$, (b) the $H^{\bar{t}\bar{t}}$, (c) the $|y^B|$, (d) the $\Delta\phi^{\bar{t}\bar{t}}$, (e) the $\chi^{\bar{t}}$, and (f) the $p_{out}^{\bar{t}\bar{t}}$.

Not reviewed, for internal circulation only

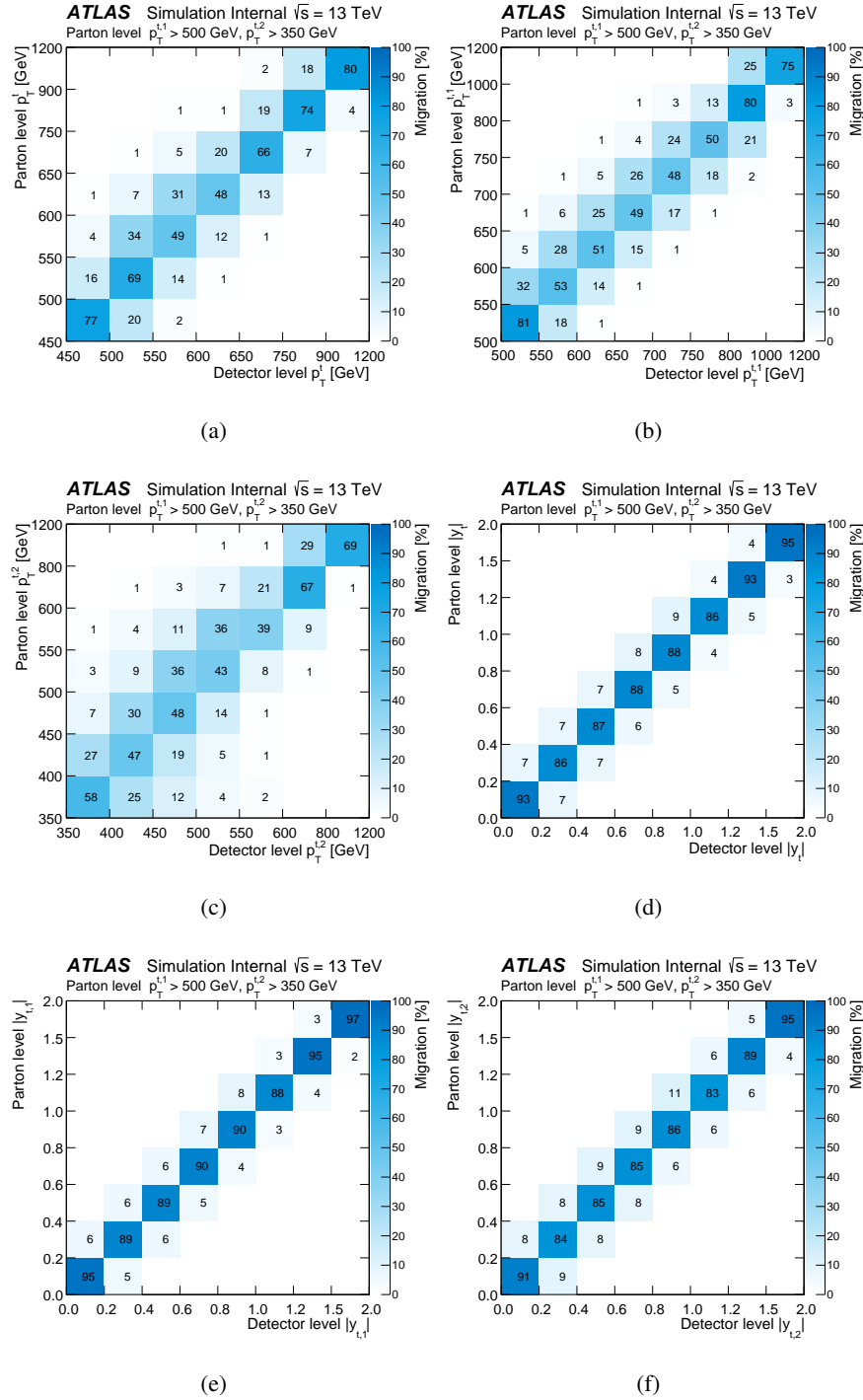


Figure 28: The parton-level migration matrices for (a) the transverse momentum of a randomly chosen top quark from each event, (b) the leading top p_T , (c) subleading top p_T , (d) absolute value of the rapidity of a randomly chosen top quark from each event, (b) the leading top $|y|$, and (c) subleading top $|y|$.

Not reviewed, for internal circulation only

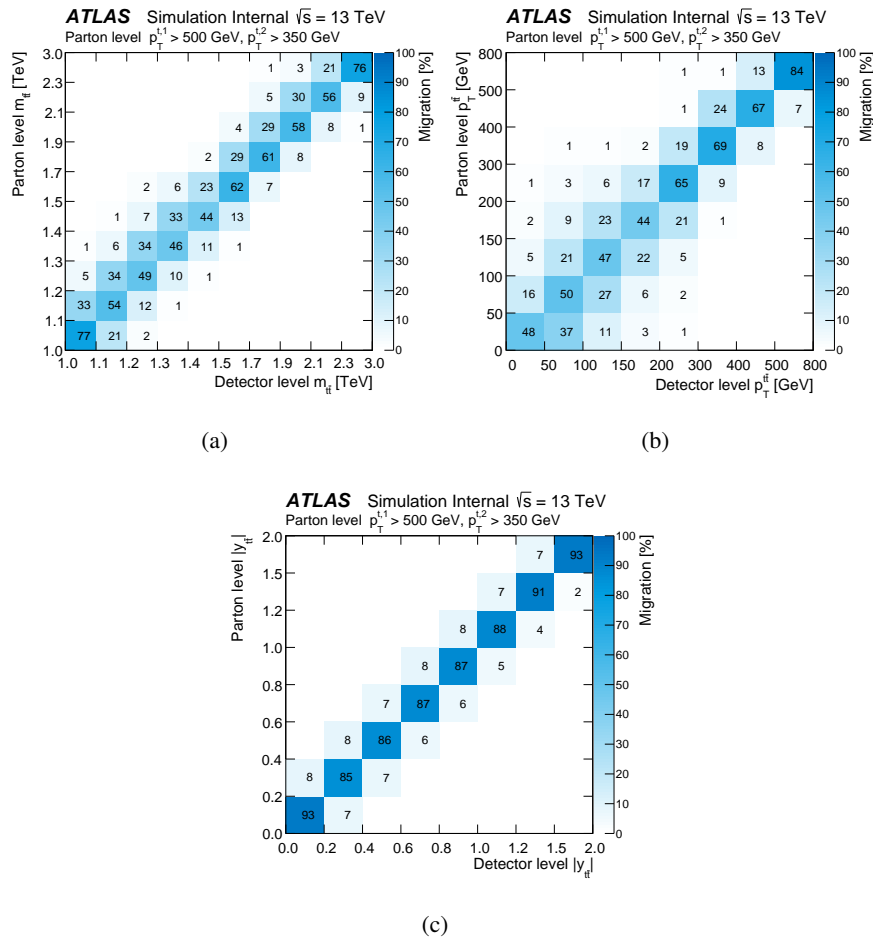


Figure 29: The parton-level migration matrices for (a) the $t\bar{t}$ mass, (b) the $t\bar{t} p_T$, and (c) the absolute value of $t\bar{t}$ rapidity.

Not reviewed, for internal circulation only

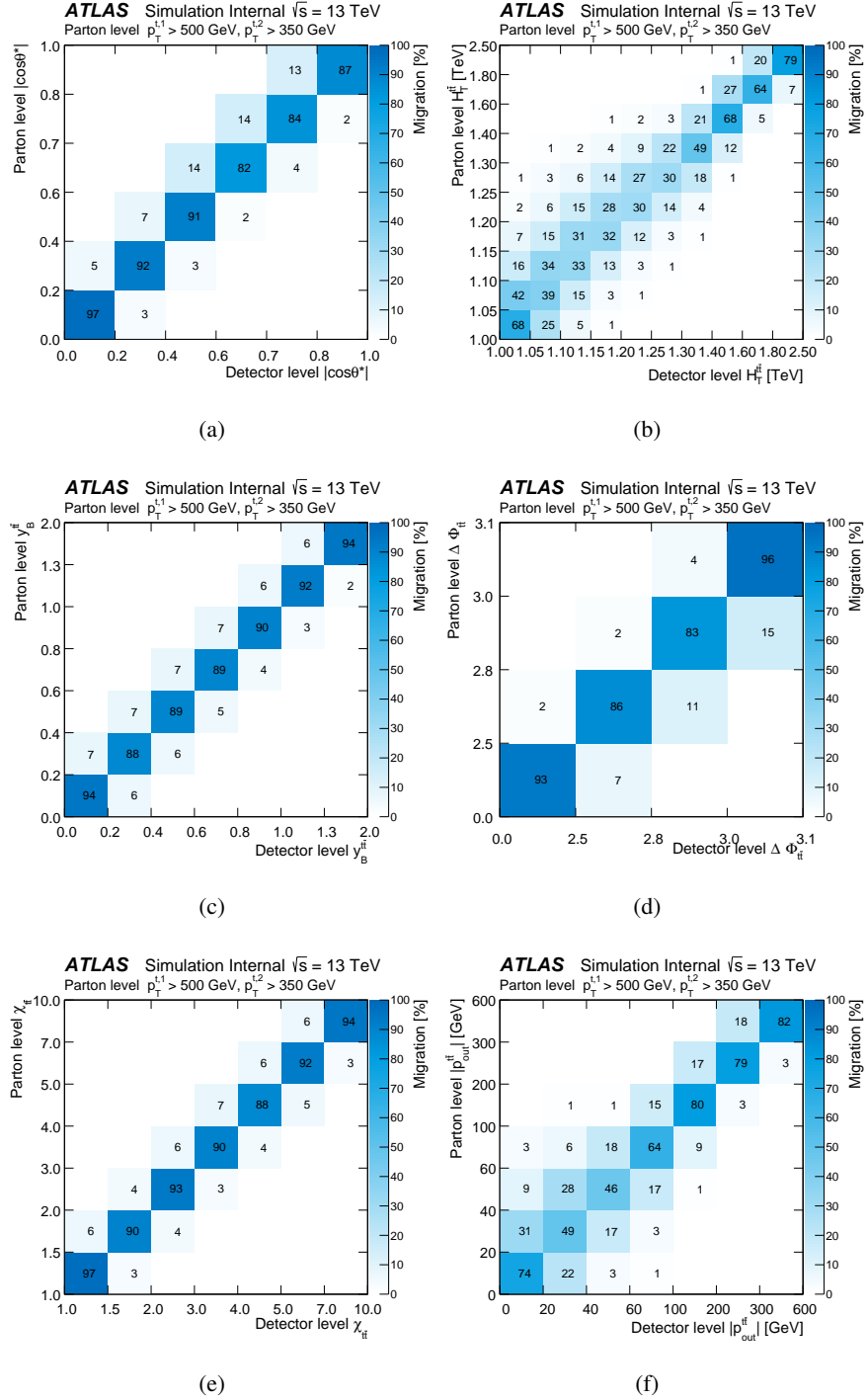


Figure 30: The parton-level migration matrices for (a) the $|\cos \theta^*|$, (b) the $H^{t\bar{t}}$, (c) the $|y_B^t|$, (d) the $\Delta\phi^{t\bar{t}}$, (e) the $\chi^{t\bar{t}}$, and (f) the p_{out}^t .

585 8. Systematic uncertainties

586 This section describes the estimation of systematic uncertainties related to object reconstruction and cal-
 587 ibration, MC generator modelling and background estimation. A summary of all the systematic uncer-
 588 tainties at particle level, grouped in broad categories, is presented in Tab. 5.

589 To evaluate the impact of each uncertainty after the unfolding, the reconstructed distribution expected
 590 from simulation is varied. Corrections based on the nominal PowHEG signal sample are used to correct
 591 for detector effects and the unfolded distribution is compared to the known particle-level and parton-level
 592 distributions. All detector- and background-related systematic uncertainties have been evaluated using
 593 the same MC sample, while alternative MC samples have been employed to assess modelling systematic
 594 uncertainties (e.g. different parton showers or hard-scattering). In these cases, nominal corrections are still
 595 used to unfold the detector-level spectra, but the comparison is performed with respect to the particle-level
 596 and parton-level spectra of the corresponding alternative generator. Then, the relative uncertainty from
 597 the simulation is assigned to the unfolded data.

598 The covariance matrices for the normalized unfolded spectra due to the statistical and systematic uncer-
 599 tainties are obtained by evaluating the covariance between the kinematic bins using pseudo-experiments.
 600 Systematic variations are included in the pseudo-experiments before unfolding to take into account cor-
 601 relations as reported in Section 9.

602 8.1. Object reconstruction and calibration

603 The jet energy scale uncertainty is derived using a combination of simulations, test beam data and *in*
 604 *situ* measurements [29, 40–42]. Additional contributions from the jet flavour composition, calorimeter
 605 response to different jet flavours, and pile-up are taken into account. Uncertainties in the jet energy
 606 resolution are obtained with an *in situ* measurement of the jet response asymmetry in dijet events [43].

607 The efficiency to tag jets containing b -hadrons is corrected in simulation events by applying b -tagging
 608 scale factors, extracted in $t\bar{t}$ and dijet samples, in order to account for the residual difference between data
 609 and simulation. Scale factors are also applied for jets originating from light quarks that are mis-identified
 610 as b -jets. The associated systematic uncertainties are computed by varying the scale factors within their
 611 uncertainties [30, 44–46].

612 The lepton energy scale and resolution are varied within their uncertainties [34, 47–49].

613 We have incorporated the large- R jet systematic uncertainties developed for the 2015 + 2016 data analyses
 614 for Moriond 2017. The list of systematic variations considered in the large- R jet systematics is described
 615 in Appendix F.

616 8.2. Signal modelling

617 The uncertainties of the signal modelling affect the kinematic properties of simulated $t\bar{t}$ events and recon-
 618 struction efficiencies.

619 To assess the impact of different parton-shower and hadronization models events simulated with the
 620 PowHEG + HERWIG7 generators using the same PDF set as the nominal PowHEG + PYTHIA8 sample are un-
 621 folded using the migration matrix and correction factors derived from the PowHEG + PYTHIA8 sample. The

622 difference between the unfolded distribution and the known particle-level distribution of the POWHEG + HERWIG7
 623 sample is assigned as the relative uncertainty for the fiducial phase-space distributions.

624 In order to evaluate the uncertainty related to the modelling of the ISR/FSR, $t\bar{t}$ MC samples with modified
 625 ISR/FSR modelling are used. The MC samples used for the evaluation of this uncertainty are generated
 626 using the POWHEG generator interfaced to PYTHIA8 with the same PDF sets. The modification of the
 627 ISR/FSR samples is done with two samples to simulate the effects of more and less radiation being
 628 produced than predicted by the nominal sample. The modifications are described in appendix A. Using
 629 these samples the uncertainty related to the ISR/FSR is assessed using the same method as described for
 630 the parton-shower and hadronization modelling uncertainty above.

631 To assess the uncertainty related to the generator matrix-element calculation events simulated with MAD-
 632 GRAPH5_aMC@NLO + PYTHIA8 are unfolded using the migration matrix and correction factors derived
 633 from the POWHEG + PYTHIA8 sample. The MC@NLO + PYTHIA8 sample suffers from a known mismodel-
 634 ling of several observables (in our case $p_T^{t\bar{t}}$, p_{out} and $\delta\phi$). However, the mismodelling does not cause an
 635 intolerable inflation of the associated systematic uncertainty. The systematic uncertainty is assessed using
 636 the same method as for the parton shower and hadronization systematic described above.

637 The impact of the uncertainty related to the PDF is assessed by means of nominal POWHEG + PYTHIA8
 638 sample. An envelope of spectra is evaluated by reweighting the central prediction of the PDF4LHC PDF
 639 set[50], using the full set of 30 eigenvectors at 68% CL.

640 We have assumed that the uncertainty arising from the variations in the top-quark mass are negligible.

641 8.3. Integrated Luminosity

642 The preliminary uncertainty on the combined 2015 + 2016 integrated luminosity is 3.2%. It is derived,
 643 following a methodology similar to that detailed in [51], from a preliminary calibration of the luminosity
 644 scale using $x - y$ beam-separation scans performed in August 2015 and May 2016.

645 This uncertainty is incorporated in the uncertainty of the estimate of the $t\bar{t}$ signal yield, the estimate of the
 646 non-hadronic $t\bar{t}$ yield and the single-top background estimate. It is then propagated to the multijet back-
 647 ground estimate given that the data yields are corrected by the expected $t\bar{t}$ and single-top contamination
 648 in the control regions.

649 8.4. Background modelling

650 The systematic uncertainty in the single-top background is determined by incorporating the uncertainty
 651 in the Wt single-top production cross section, on the integrated luminosity and on all of the systematic
 652 uncertainties that enter into the object reconstruction and event selection. To account for the missing
 653 t -channel process, we have included an uncertainty in the unfolded differential cross-section determined
 654 by doubling the Wt rate.

655 An uncertainty on the background rate of $t\bar{t} + W^\pm/Z/H$ production arises from the production cross-
 656 section uncertainty. We use the uncertainties summarized in Ref. [52], assuming that the $t\bar{t} + W^\pm/Z$
 657 cross-section uncertainties are fully correlated. This results in a 15% systematic uncertainty on this
 658 background source. Systematic uncertainties affecting the background but not signal are modeled by
 659 using the ABCD16 method to determine how each systematic affects the background normalization and

$d\sigma / d\sigma_{\text{fid}}$ [pb/pb]	$2.917 \cdot 10^{-1}$
Total Uncertainty [%]	± 24.4
Statistics [%]	± 2.3
Systematics [%]	± 24.3
Luminosity [%]	± 2.01
Large- R jets JES [%]	± 5.91
Large- R jets JMS [%]	± 1.44
Large- R jets top-tagging [%]	± 12.5
Flavor tagging [%]	± 8.29
Narrow jets [%]	$\begin{array}{c} +0.33 \\ -0.21 \end{array}$
Pile-up [%]	± 0.55
Background [%]	± 0.89
(MOD) Monte Carlo sample statistics [%]	± 0.90
(MOD) ISR/FSR + scale [%]	± 1.13
(MOD) Alternative hard-scattering model [%]	∓ 11.2
(MOD) Alternative parton-shower model [%]	∓ 13.7

Table 5: Uncertainties in the fiducial phase-space absolute inclusive cross-sections calculated as a percentage of the cross-section.

660 shape. The uncertainty on the subtraction of the $t\bar{t}$ all-hadronic signal in the control regions comes from
 661 the uncertainty on the MC $t\bar{t}$ cross-section as well as the systematic uncertainty arising from b -matching.
 662 The other sources of systematic uncertainty are propagated in a correlated way to both signal and all
 663 background contributions. These are then added together using pseudo-experiments to determine the
 664 overall uncertainty on the observed distributions.

665 The uncertainty on the multijet background comes from the statistical uncertainties in the control regions,
 666 the uncertainties in the tagging efficiency correlations (measured using the control regions) and the un-
 667 certainties on the subtraction of the single-top and $t\bar{t}$ contamination, as described in Appendix L.4. These
 668 first two uncertainties are determined by the number of events in the smallest control regions. The third
 669 class of uncertainties is taken into account by applying the detector-level systematic uncertainties and
 670 uncertainties on the integrated luminosity to the data-driven estimate.

671 9. Results

672 9.1. Measured differential cross-sections at particle level and comparison with predictions

673 Comparisons between unfolded data distributions and several SM predictions are presented for the dif-
 674 ferent observables discussed in Sect. 5. Events are selected by requiring no isolated lepton, two large- R
 675 jets with high transverse momentum and at least two narrow jets tagged as originating from a b -quark.
 676 Normalized differential cross-sections are shown along with absolute ones in order to remove systematic
 677 uncertainties on the normalization.

678 Results are compared to the SM prediction using the nominal PowHEG + PYTHIA8 MC samples as well
 679 as the MC samples used to determine signal modelling uncertainties, namely PowHEG + HERWIG7, MAD-
 680 GRAPH5_aMC@NLO+PYTHIA8 and the PowHEG + PYTHIA8 samples using modified IFSR settings. Results
 681 are also compared to a SHERPA sample. All samples are normalized to the full NNLO+NNLL pre-
 682 ditions.

683 A covariance matrix is constructed for each differential cross-section including the effect of all uncertain-
 684 ties to allow quantitative comparisons with theoretical predictions. This covariance matrix is derived by
 685 summing two covariance matrices following the same approach used in [53, 54]. The description of the
 686 procedure is reported in Appendix W.

The agreement between the measured differential cross-sections and a variety of MC predictions is quantified by calculating χ^2 values employing the calculated covariance matrix and by inferring the corresponding p -values (probabilities that the χ^2 is less than or equal to the observed value assuming that the measured and predicted distributions are statistically equivalent) from the χ^2 and the number of degrees of freedom (NDF). The χ^2 values are obtained using

$$\chi^2 = V_{N_b}^T \cdot \text{Cov}_{N_b}^{-1} \cdot V_{N_b},$$

687 where V_{N_b} is the vector of differences between measured differential cross-section values and predictions,
 688 and $\text{Cov}_{N_b}^{-1}$ is the inverse of the covariance matrix.

The normalisation constraint used to derive the normalized differential cross-sections lowers the NDF that is the rank of the $N_b \times N_b$ covariance matrix by one unit, where N_b is the number of bins of the unfolded distribution. The χ^2 for the normalized differential cross-sections is

$$\chi^2 = V_{N_b-1}^T \cdot \text{Cov}_{N_b-1}^{-1} \cdot V_{N_b-1},$$

689 where V_{N_b-1} is the vector of differences between measurement and prediction obtained by discarding one
 690 of the N_b elements and Cov_{N_b-1} is the $(N_b - 1) \times (N_b - 1)$ sub-matrix derived from the covariance matrix
 691 discarding the corresponding row and column.

692 The set of Figures 31–36 presents the normalized $t\bar{t}$ fiducial phase-space differential cross-sections as
 693 a function of the different observables. In particular, Figures 31–32 show the distributions of the leading
 694 and sub-leading top-quarks transverse momentum and the absolute value of the rapidity; Figures 33–34
 695 present the $t\bar{t}$ system invariant mass, transverse momentum, and absolute value of the rapidity, while the
 696 additional observables related to the $t\bar{t}$ system are shown in Figures 35–35.

697 The tables 6 and 7, provide the χ^2 and p -values resulting from the comparisons of the differential cross-
 698 sections with predictions for particle-level results.

Observable	PWG+PY8		MG5_AMC@NLO+Py8		PWG+H7		PWG+PY8 (more IFSR)		PWG+PY8 (less IFSR)		SHERPA 2.2.1	
	χ^2/NDF	$p\text{-value}$										
$p_{T,i}^{t,1}$	7.6/8	0.48	8.9/8	0.35	6.1/8	0.63	9.7/8	0.29	7.5/8	0.49	9.8/8	0.28
$ y^{t,1} $	16.7/6	0.01	27.3/6	<0.01	12.6/6	0.05	21.9/6	<0.01	15.1/6	0.02	12.1/6	0.06
$p_T^{t,2}$	10.7/7	0.15	6.6/7	0.47	10.4/7	0.17	15.9/7	0.03	6.2/7	0.52	8.5/7	0.29
$ y^{t,2} $	5.7/6	0.45	7.8/6	0.25	3.5/6	0.74	6.3/6	0.40	4.2/6	0.65	5.3/6	0.51
$m^{t\bar{t}}$	8.6/10	0.57	11.9/10	0.29	5.6/10	0.85	11.0/10	0.36	7.9/10	0.64	15.0/10	0.13
$p_{T\bar{t}}^{t\bar{t}}$	8.8/6	0.19	26.8/6	<0.01	10.2/6	0.12	17.3/6	<0.01	2.7/6	0.84	3.4/6	0.76
$ y^{t\bar{t}} $	5.6/6	0.47	8.2/6	0.23	3.7/6	0.72	5.5/6	0.48	5.3/6	0.50	3.4/6	0.76
$\chi^{t\bar{t}}$	16.2/7	0.02	16.1/7	0.02	13.1/7	0.07	21.3/7	<0.01	9.8/7	0.20	22.7/7	<0.01
$y_B^{t\bar{t}}$	8.4/7	0.30	11.0/7	0.14	5.6/7	0.59	9.1/7	0.25	7.7/7	0.36	6.0/7	0.54
$ p_{out}^{t\bar{t}} $	5.8/7	0.56	59.6/7	<0.01	5.3/7	0.63	11.9/7	0.10	5.2/7	0.64	8.9/7	0.26
$\Delta\phi^{t\bar{t}}$	5.1/4	0.28	49.2/4	<0.01	6.2/4	0.19	13.2/4	0.01	1.4/4	0.84	3.6/4	0.47
$H_T^{t\bar{t}}$	8.8/7	0.27	9.8/7	0.20	6.0/7	0.54	10.3/7	0.17	7.6/7	0.37	6.0/7	0.54
$\cos\theta^*$	11.7/6	0.07	14.4/6	0.03	9.3/6	0.16	16.6/6	0.01	6.8/6	0.34	21.6/6	<0.01

Not reviewed, for internal circulation only

Table 6: Comparison between the absolute particle-level fiducial differential cross-sections and the predictions from several MC generators. For each variable and prediction, a χ^2 and a p -value are calculated using the covariance matrix described in the text, which includes all sources of uncertainty. The number of degrees of freedom (NDF) is equal to N_b , where N_b is the number of bins in the distribution. The description of the calculation is available in Appendix W.

Observable	PWG+PY8		MG5_AMC@NLO+Py8		PWG+H7		PWG+PY8 (more IFSR)		PWG+PY8 (less IFSR)		SHERPA 2.2.1	
	χ^2/NDF	$p\text{-value}$										
$p_{T,i}^{t,1}$	7.7/7	0.36	8.2/7	0.32	8.0/7	0.33	9.1/7	0.24	8.7/7	0.27	9.3/7	0.23
$ y^{t,1} $	7.5/5	0.18	12.2/5	0.03	6.8/5	0.24	8.8/5	0.12	8.1/5	0.15	4.0/5	0.55
$p_T^{t,2}$	8.6/6	0.20	2.6/6	0.86	9.9/6	0.13	12.2/6	0.06	5.0/6	0.54	5.0/6	0.55
$ y^{t,2} $	3.7/5	0.59	4.6/5	0.46	3.1/5	0.68	3.5/5	0.63	3.2/5	0.67	2.9/5	0.72
$m^{t\bar{t}}$	4.5/9	0.88	4.7/9	0.86	4.0/9	0.91	5.3/9	0.81	5.2/9	0.82	10.0/9	0.35
$p_{T\bar{t}}^{t\bar{t}}$	7.8/5	0.17	20.9/5	<0.01	12.6/5	0.03	15.0/5	0.01	1.9/5	0.86	1.9/5	0.87
$ y^{t\bar{t}} $	1.1/5	0.95	2.2/5	0.83	0.9/5	0.97	0.8/5	0.98	1.8/5	0.88	1.7/5	0.89
$\chi^{t\bar{t}}$	14.2/6	0.03	12.7/6	0.05	13.6/6	0.03	16.9/6	<0.01	10.1/6	0.12	18.5/6	<0.01
$y_B^{t\bar{t}}$	2.5/6	0.87	3.3/6	0.77	2.2/6	0.90	2.6/6	0.86	2.8/6	0.84	3.0/6	0.81
$ p_{out}^{t\bar{t}} $	1.9/6	0.93	53.1/6	<0.01	3.1/6	0.80	4.2/6	0.64	4.8/6	0.57	5.9/6	0.44
$\Delta\phi^{t\bar{t}}$	0.9/3	0.84	16.3/3	<0.01	2.0/3	0.58	3.0/3	0.40	0.6/3	0.89	3.4/3	0.33
$H_T^{t\bar{t}}$	4.8/6	0.57	5.2/6	0.52	4.5/6	0.61	5.0/6	0.54	5.0/6	0.55	3.1/6	0.80
$\cos\theta^*$	9.9/5	0.08	10.5/5	0.06	9.3/5	0.10	12.8/5	0.03	6.5/5	0.26	18.7/5	<0.01

Table 7: Comparison between the normalized particle-level fiducial differential cross-sections and the predictions from several MC generators. For each variable and prediction, a χ^2 and a p -value are calculated using the covariance matrix described in the text, which includes all sources of uncertainty. The number of degrees of freedom (NDF) is equal to $N_b - 1$, where N_b is the number of bins in the distribution. The description of the calculation is available in Appendix W.

699 Subsections W.1 and W.2 give the covariance and correlation matrices for all the differential cross section
700 results.

Not reviewed, for internal circulation only

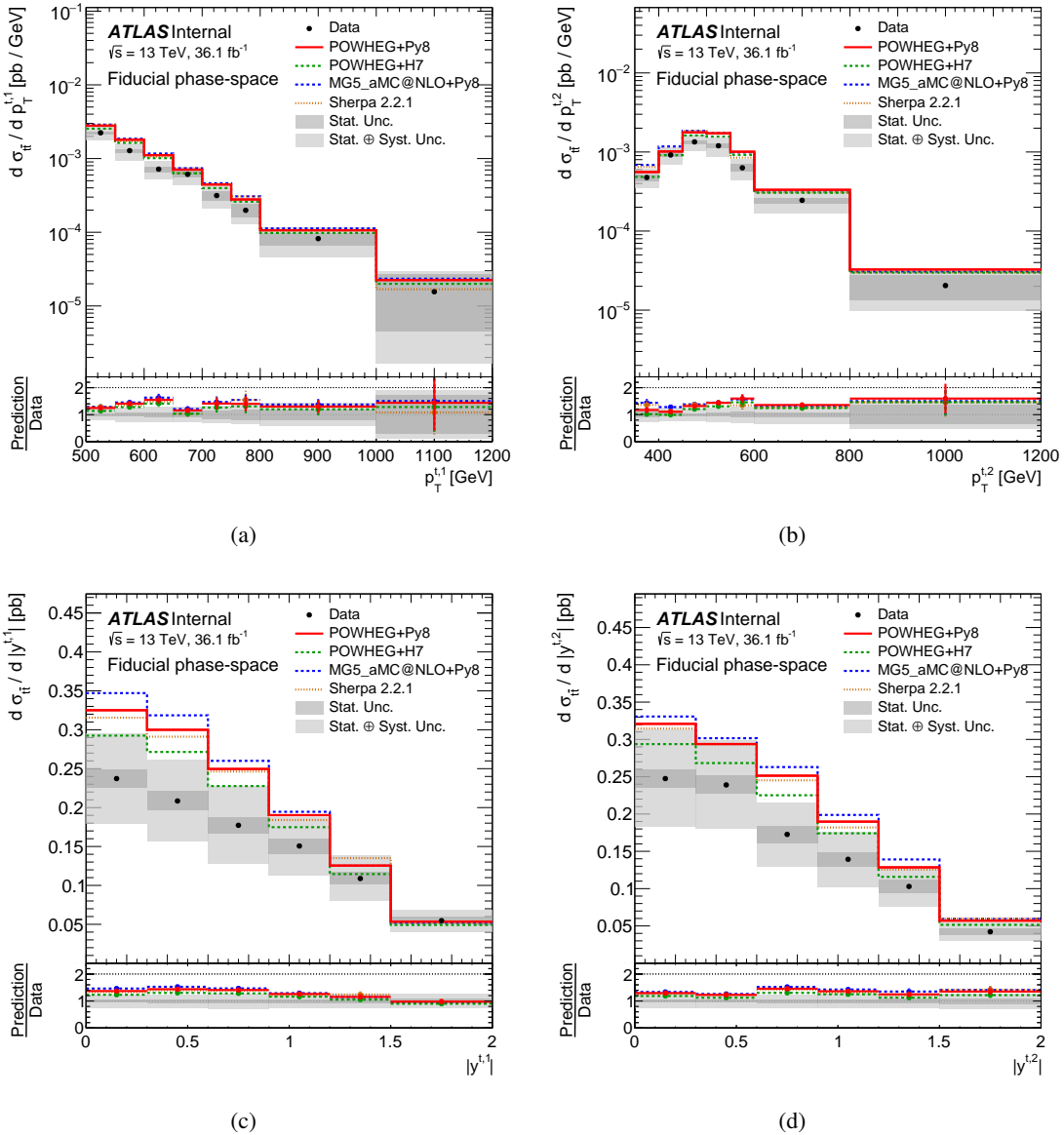


Figure 31: Fiducial phase-space absolute differential cross-sections as a function of (a) transverse momentum and (c) absolute value of the rapidity of the leading top-quark, and (b) transverse momentum and (d) absolute value of the rapidity of the second-leading top-quark. The gray bands indicate the total uncertainty on the data in each bin. The Powheg+Pythia8 generator is used as the nominal prediction to correct for detector effects.

Not reviewed, for internal circulation only

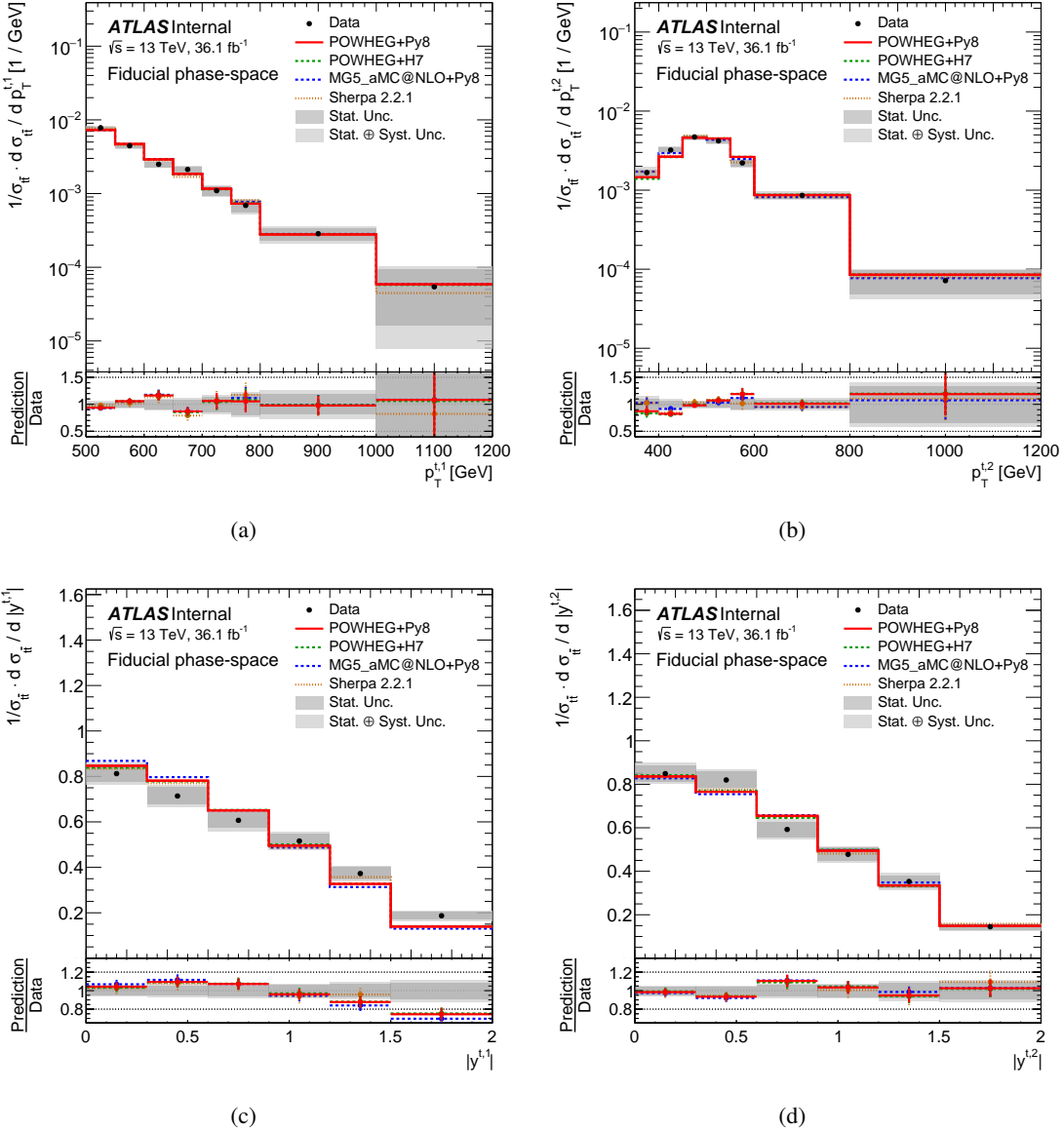


Figure 32: Fiducial phase-space normalized differential cross-sections as a function of (a) transverse momentum and (c) absolute value of the rapidity of the leading top-quark, and (b) transverse momentum and (d) absolute value of the rapidity of the second-leading top-quark. The gray bands indicate the total uncertainty on the data in each bin. The Powheg+Pythia8 generator is used as the nominal prediction to correct for detector effects.

Not reviewed, for internal circulation only

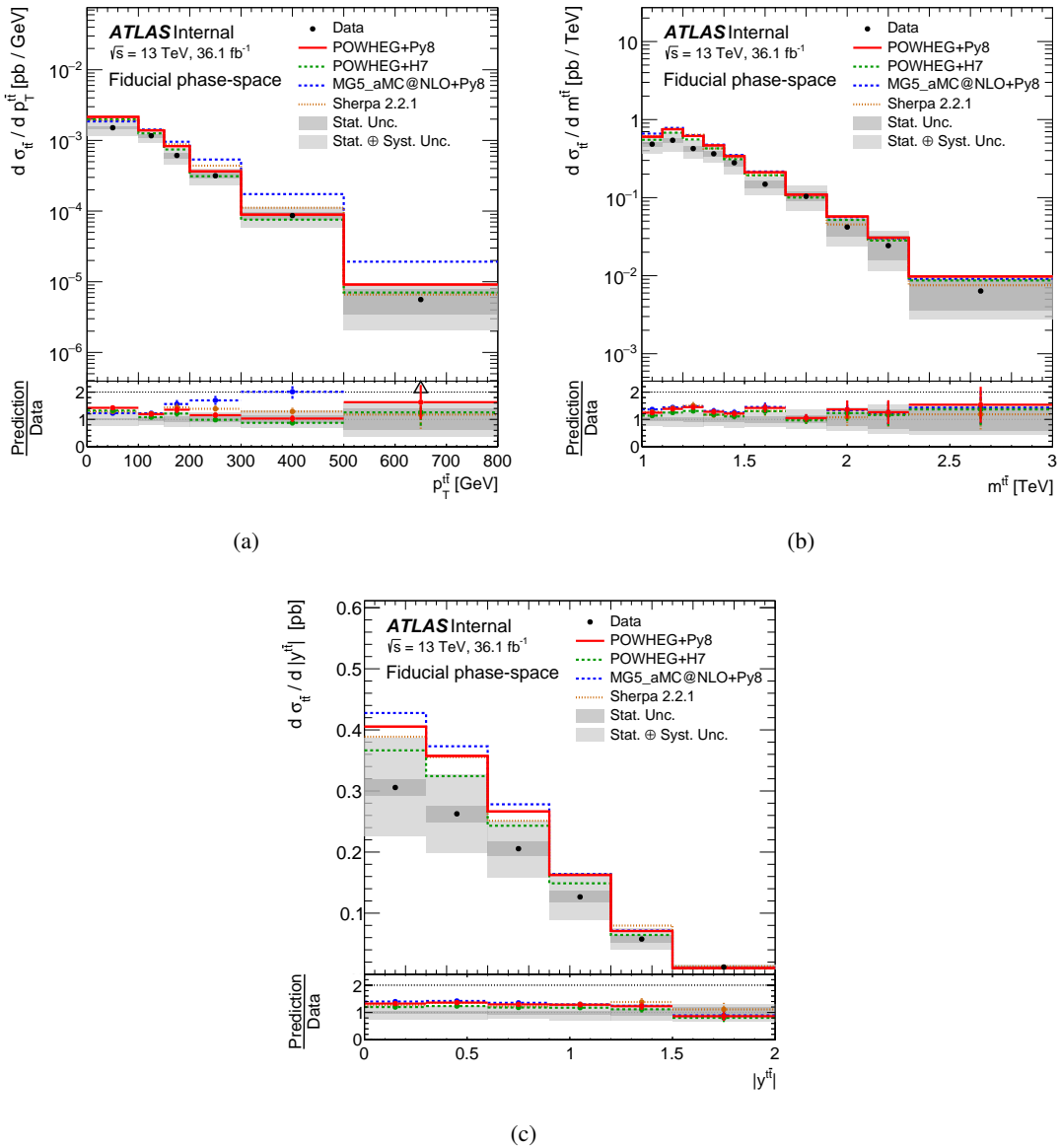


Figure 33: Fiducial phase-space absolute differential cross-sections as a function of (a) transverse momentum, (b) invariant mass and (c) absolute value of the rapidity of the $t\bar{t}$ system. The gray bands indicate the total uncertainty on the data in each bin. The Powheg+Pythia8 generator is used as the nominal prediction to correct for detector effects.

Not reviewed, for internal circulation only

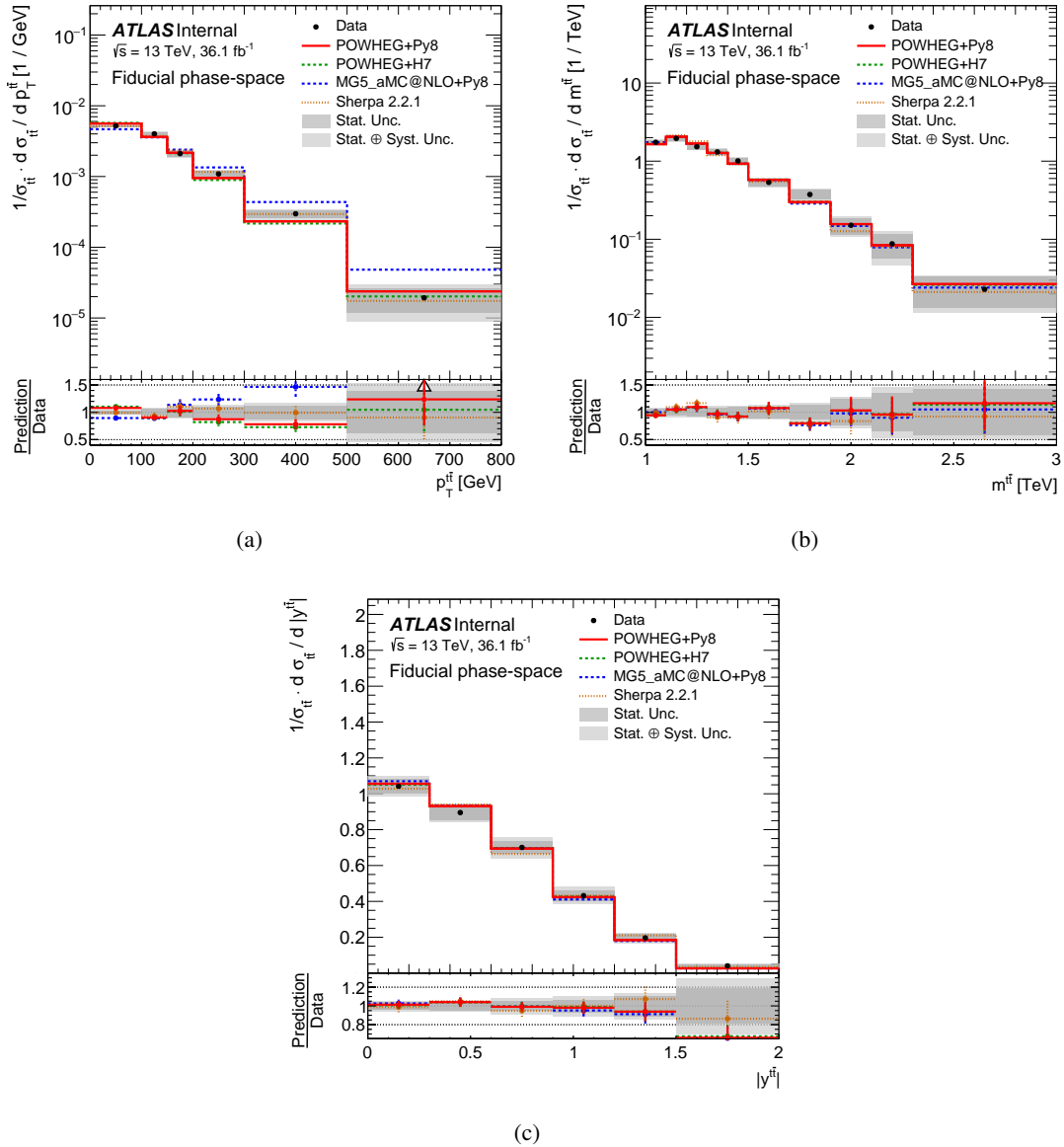


Figure 34: Fiducial phase-space normalized differential cross-sections as a function of (a) transverse momentum, (b) invariant mass and (c) absolute value of the rapidity of the $t\bar{t}$ system. The gray bands indicate the total uncertainty on the data in each bin. The Powheg+Pythia8 generator is used as the nominal prediction to correct for detector effects.

Not reviewed, for internal circulation only

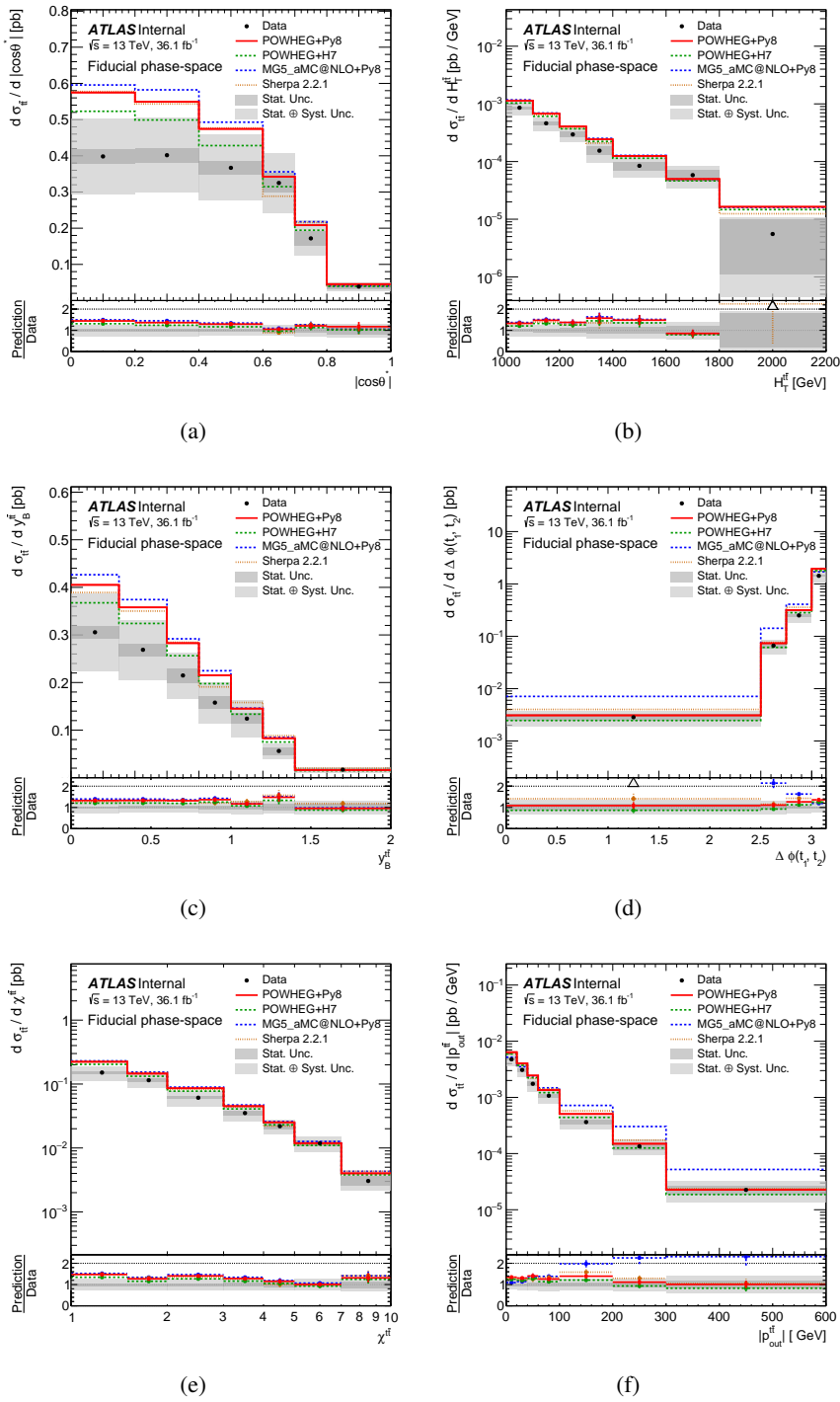


Figure 35: Particle-level fiducial phase-space absolute differential cross-sections as a function of (a) production angle in the Collins-Soper reference frame, (b) scalar sum of the two top-quarks' transverse momenta, (c) longitudinal boost $y_B^{t\bar{t}}$, (d) azimuthal angle between the two top-quarks $\Delta\phi_{t\bar{t}}$, (e) production angle $\chi^{t\bar{t}}$ and (f) absolute value of the out-of-plane momentum $p_{out}^{t\bar{t}}$. The gray bands indicate the total uncertainty on the data in each bin. The Powheg+Pythia8 generator is used as the nominal prediction to correct for detector effects.

Not reviewed, for internal circulation only

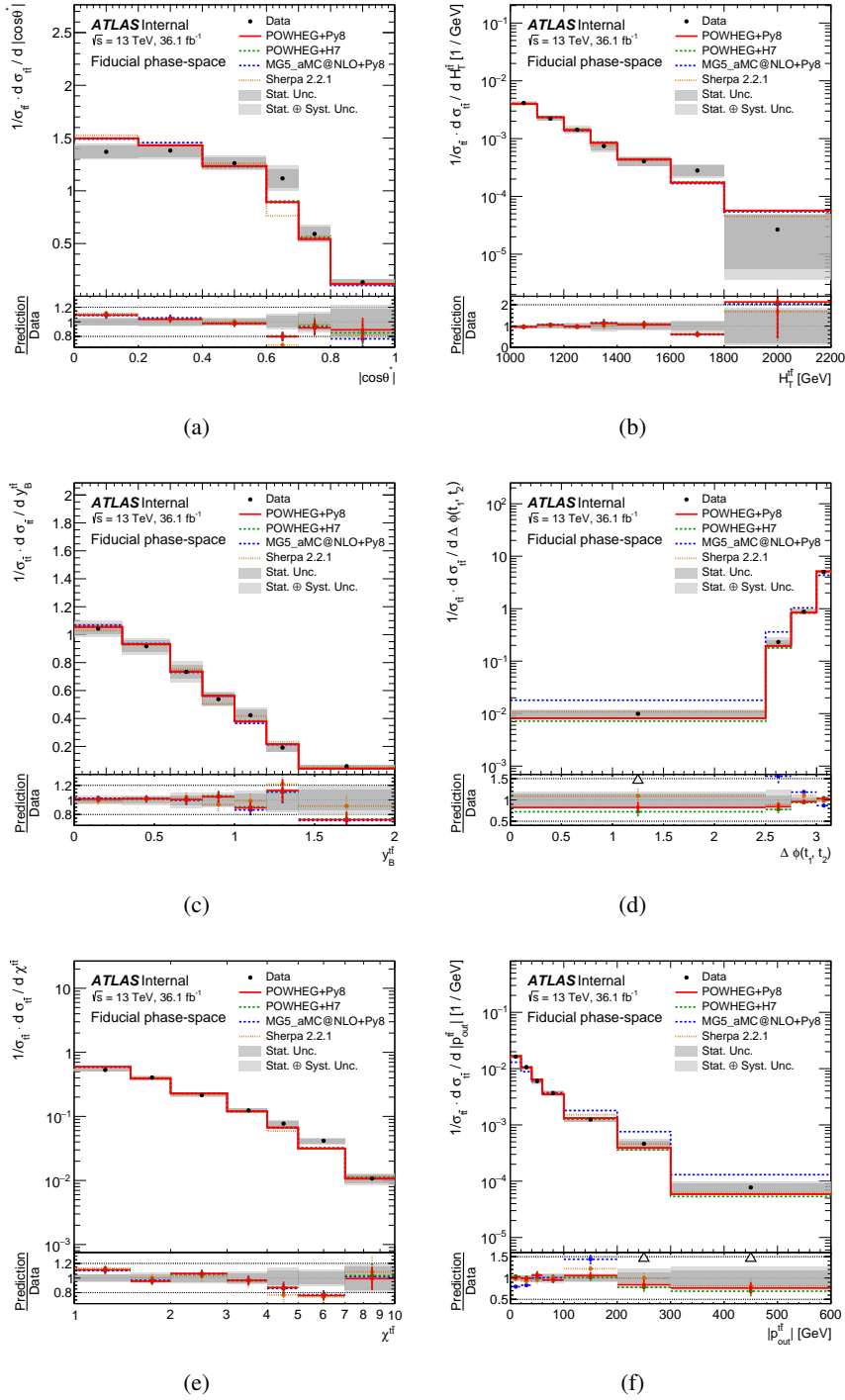


Figure 36: Particle-level fiducial phase-space normalized differential cross-sections as a function of (a) production angle in the Collins-Soper reference frame, (b) scalar sum of the two top-quarks' transverse momenta, (c) longitudinal boost $y_B^{t^f}$, (d) azimuthal angle between the two top-quarks $\Delta\phi_{t^f}$, (e) production angle χ_{t^f} and (f) absolute value of the out-of-plane momentum $p_{out}^{t^f}$. The gray bands indicate the total uncertainty on the data in each bin. The Powheg+Pythia8 generator is used as the nominal prediction to correct for detector effects.

701 9.2. Particle-level fiducial phase-space total cross-section

702 It is of interest to calculate the total cross section in the phase-space region defined in this analysis, as this
 703 tests the predictions of various Monte Carlo calculations, and affects searches in this region for non-SM
 704 contributions.

705 We implement the calculation using the unfolding software, essentially creating a single-bin histogram
 706 and then unfolding that histogram so that all systematic uncertainties are taken into account. The result
 707 of this calculation is shown in Fig.37. The inclusive fiducial cross-section is

$$\sigma_{fid} = 292 \pm 7 \text{ (stat)} \pm 76 \text{ (syst)} \text{ fb.} \quad (5)$$

708 To verify this calculation, we also measured this cross-section using the standard counting experiment
 709 method:

$$\sigma_{fid} = \frac{f_{acc}}{\mathcal{L} \cdot \epsilon_{eff}} \cdot (N_{reco} - N_{bg}) \quad (6)$$

$$= \frac{0.6687}{(36.1) \cdot (0.1569)} \cdot (3541 - 1071) \quad (7)$$

$$= 292 \text{ fb.} \quad (8)$$

701 As noted in Sect. 6, a correction, f_{acc} , has to be made to take into account the fraction of observed events
 702 that do not come from the fiducial phase-space. The efficiency factor ϵ_{eff} is dominated by the combined
 703 efficiencies of requiring two top-tags (at a 50% working point each) and two b -matches (at a 70% working
 704 point each). Although a less-refined estimate than the results from the unfolding procedure, it is a simple
 705 cross-check that the unfolding machinery is working correctly.

706 The measured fiducial phase-space cross-section can be compared with the cross-section predicted of
 707 384 fb by the PowHeg +PYTHIA8 calculation after normalizing the full phase space cross-section to the
 708 NNLO+NNLL prediction.

Not reviewed, for internal circulation only

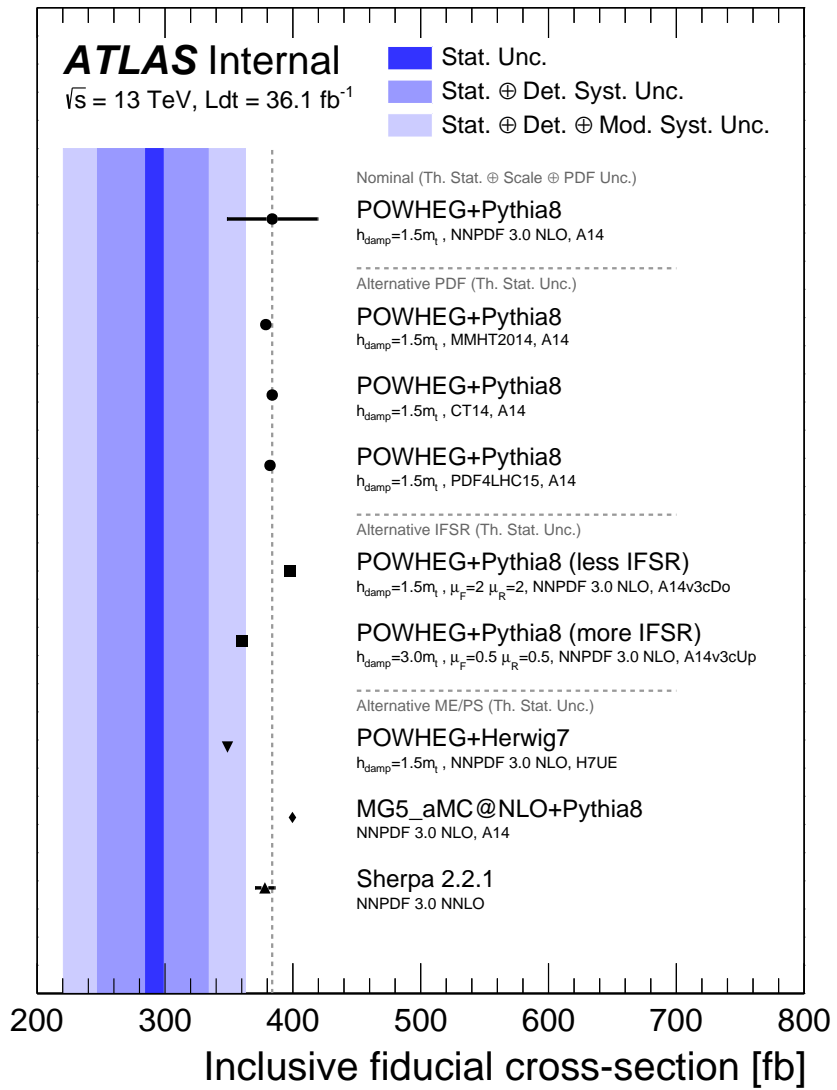


Figure 37: Inclusive particle-level fiducial phase-space cross-section. The grey bands indicate the statistical, and detector and modelling systematic uncertainty on the data in each bin. The Powheg+Pythia8 generator is used as the nominal prediction to correct for detector effects. The uncertainty associated with the Powheg+Pythia8 signal model is the sum in quadrature of scale and PDF uncertainties. The scale uncertainty is obtained as the envelope of all possible variations of the factorization μ_F and renormalization μ_R scale variations in the range 0.5–2.0. The PDF uncertainty is obtained using the PDF4LHC prescription with 30 eigenvectors.

718 9.3. Measured differential cross-section at parton level and comparison with predictions

719 The unfolded parton-level differential cross-section distributions are compared to Standard Model predictions.
720 The results are shown in Fig. 38, 39 for the transverse momentum and rapidity of the top quark,
721 where the top quark is chosen at random on an event-by-event basis, the transverse momentum and rapidity
722 of the leading and subleading top quark, for the invariant mass, rapidity and p_T of the $t\bar{t}$ system, and
723 for the $H^{t\bar{t}}, \chi^{t\bar{t}}, \Delta\phi(t_1, t_2), p_{out}^{t\bar{t}}$ and $\cos\theta^*$ variables.

724 Figure 40, 41 show similar comparison for normalized unfolded distributions. Systematic uncertainties
725 are significantly smaller for normalized distributions.

726 The systematic uncertainties are shown in Appendix G. The covariance and correlation matrices are
727 shown in Appendix W.2 .

728 The tables 8 and 9, provide the χ^2 and p -values resulting from the comparisons of the differential cross-
729 sections with predictions for parton-level results.

Not reviewed, for internal circulation only

Observable	PWG+PY8		MG5_AMC@NLO+Py8		PWG+H7		PWG+PY8 (more IFSR)		PWG+PY8 (less IFSR)		SHERPA 2.2.1	
	χ^2/NDF	$p\text{-value}$										
p_T^t	5.2/7	0.63	4.8/7	0.68	5.4/7	0.61	4.5/7	0.72	6.2/7	0.52	6.2/7	0.51
$ y' $	12.2/8	0.14	8.9/8	0.35	10.3/8	0.24	10.7/8	0.22	13.3/8	0.10	13.1/8	0.11
$p_T^{t,1}$	10.6/8	0.23	11.5/8	0.18	10.2/8	0.25	10.6/8	0.23	11.6/8	0.17	15.9/8	0.04
$ y'^1 $	19.8/8	0.01	22.5/8	<0.01	17.6/8	0.02	18.0/8	0.02	21.0/8	<0.01	17.0/8	0.03
$p_T^{t,2}$	9.8/7	0.20	4.3/7	0.75	10.2/7	0.18	7.2/7	0.40	13.4/7	0.06	12.0/7	0.10
$ y'^2 $	8.6/8	0.37	8.4/8	0.40	7.6/8	0.47	7.5/8	0.48	8.9/8	0.35	13.5/8	0.10
$m^{\tilde{t}t}$	9.4/10	0.49	7.2/10	0.70	8.5/10	0.58	7.5/10	0.68	11.4/10	0.33	11.6/10	0.31
$p_{T\perp}^{\tilde{t}t}$	10.7/8	0.22	11.4/8	0.18	11.8/8	0.16	7.6/8	0.47	15.1/8	0.06	55.3/8	<0.01
$y^{\tilde{t}t}$	6.9/8	0.54	8.0/8	0.43	6.7/8	0.57	6.8/8	0.56	7.4/8	0.49	11.3/8	0.18
$\chi^{\tilde{t}t}$	14.3/7	0.05	8.3/7	0.31	12.9/7	0.07	10.7/7	0.15	17.0/7	0.02	16.7/7	0.02
$y_B^{\tilde{t}t}$	6.7/7	0.46	7.3/7	0.40	6.2/7	0.51	6.8/7	0.45	7.2/7	0.40	8.2/7	0.31
$ p_{out}^{\tilde{t}t} $	5.7/7	0.57	35.1/7	<0.01	3.9/7	0.79	5.4/7	0.61	8.3/7	0.31	12.9/7	0.08
$\Delta\Phi^{\tilde{t}t}$	2.6/4	0.62	31.2/4	<0.01	3.0/4	0.56	0.6/4	0.96	5.8/4	0.22	4.0/4	0.40
$H_T^{\tilde{t}t}$	14.6/10	0.15	11.6/10	0.31	13.7/10	0.19	11.3/10	0.33	16.4/10	0.09	19.4/10	0.04
$\cos\theta^*$	10.4/6	0.11	5.3/6	0.50	9.5/6	0.15	8.3/6	0.22	12.2/6	0.06	16.5/6	0.01

Table 8: Comparison between the absolute parton-level differential cross-sections and the predictions from several MC generators. For each variable and prediction, a χ^2 and a p -value are calculated using the covariance matrix described in the text, which includes all sources of uncertainty. The number of degrees of freedom (NDF) is equal to N_b , where N_b is the number of bins in the distribution. The description of the calculation is available in Appendix W.

Observable	PWG+PY8		MG5_AMC@NLO+Py8		PWG+H7		PWG+PY8 (more IFSR)		PWG+PY8 (less IFSR)		SHERPA 2.2.1	
	χ^2/NDF	$p\text{-value}$										
p_T^t	3.7/6	0.72	4.5/6	0.61	4.0/6	0.67	3.9/6	0.69	4.0/6	0.68	4.3/6	0.64
$ y' $	4.3/7	0.75	4.1/7	0.77	4.0/7	0.78	4.4/7	0.73	4.3/7	0.74	5.3/7	0.62
$p_T^{t,1}$	5.9/7	0.55	7.0/7	0.43	5.9/7	0.55	6.4/7	0.50	6.2/7	0.52	7.6/7	0.37
$ y'^1 $	5.5/7	0.60	8.3/7	0.31	5.1/7	0.65	5.9/7	0.55	5.5/7	0.60	4.7/7	0.70
$p_T^{t,2}$	5.7/6	0.46	2.8/6	0.83	6.1/6	0.41	4.6/6	0.60	7.4/6	0.29	7.0/6	0.32
$ y'^2 $	4.4/7	0.73	5.1/7	0.65	4.2/7	0.76	4.4/7	0.73	4.3/7	0.74	5.9/7	0.55
$m^{\tilde{t}t}$	4.0/9	0.91	3.7/9	0.93	3.9/9	0.92	3.9/9	0.92	4.3/9	0.89	4.6/9	0.86
$p_{T\perp}^{\tilde{t}t}$	5.1/7	0.65	7.0/7	0.42	6.2/7	0.52	3.7/7	0.81	6.8/7	0.45	30.1/7	<0.01
$y^{\tilde{t}t}$	1.8/7	0.97	2.9/7	0.90	2.0/7	0.96	2.0/7	0.96	1.9/7	0.97	4.2/7	0.76
$\chi^{\tilde{t}t}$	7.9/6	0.24	5.0/6	0.55	7.3/6	0.29	6.4/6	0.38	9.0/6	0.17	7.6/6	0.27
$y_B^{\tilde{t}t}$	1.0/6	0.99	1.4/6	0.96	1.0/6	0.98	1.1/6	0.98	1.0/6	0.99	1.0/6	0.99
$ p_{out}^{\tilde{t}t} $	1.7/6	0.94	16.9/6	<0.01	1.2/6	0.98	1.9/6	0.93	2.7/6	0.84	3.9/6	0.69
$\Delta\Phi^{\tilde{t}t}$	0.5/3	0.93	13.1/3	<0.01	0.7/3	0.87	0.1/3	1.00	1.1/3	0.78	0.2/3	0.98
$H_T^{\tilde{t}t}$	5.2/9	0.81	5.7/9	0.77	7.4/9	0.60	6.9/9	0.64	5.6/9	0.78	5.9/9	0.75
$\cos\theta^*$	5.5/5	0.35	3.2/5	0.66	5.3/5	0.38	5.0/5	0.42	6.2/5	0.29	7.8/5	0.17

Table 9: Comparison between the normalized parton-level differential cross-sections and the predictions from several MC generators. For each variable and prediction, a χ^2 and a p -value are calculated using the covariance matrix described in the text, which includes all sources of uncertainty. The number of degrees of freedom (NDF) is equal to $N_b - 1$, where N_b is the number of bins in the distribution. The description of the calculation is available in Appendix W.

Not reviewed, for internal circulation only

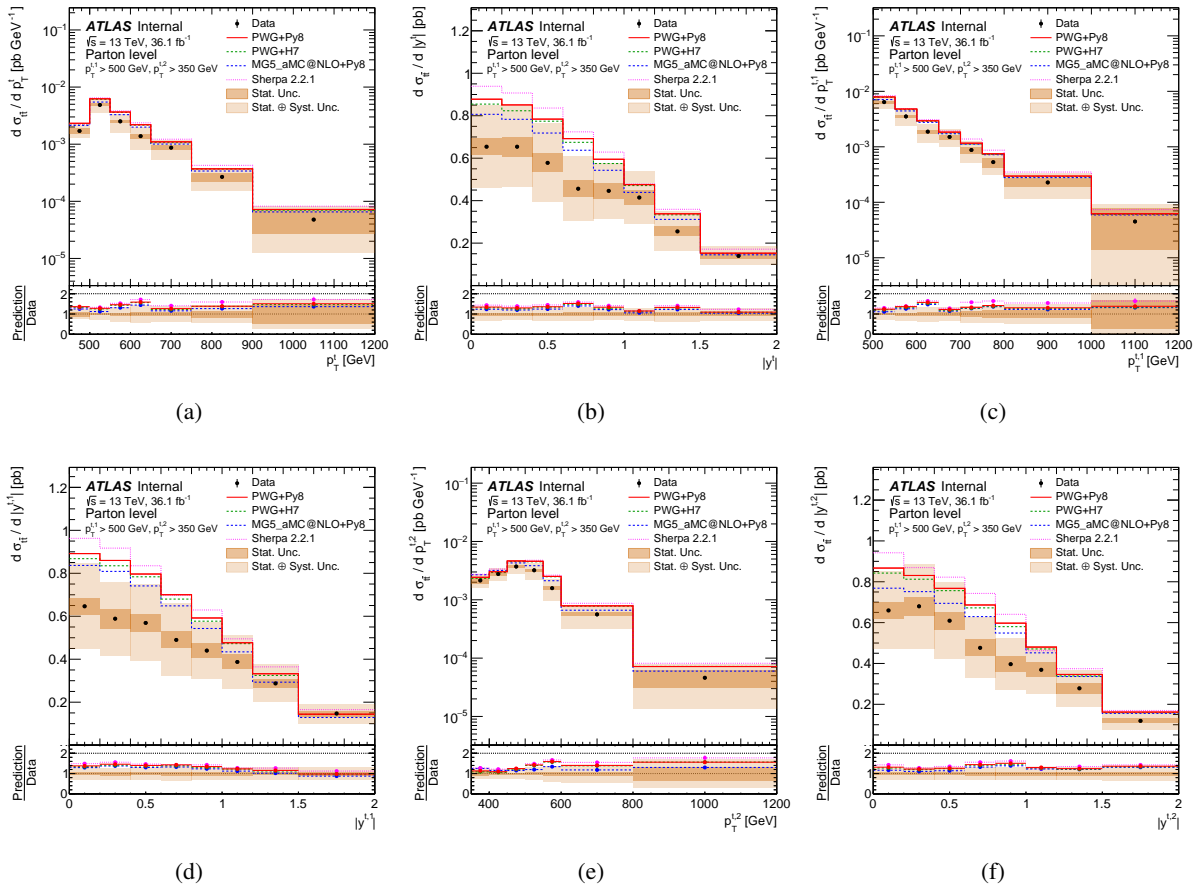


Figure 38: The unfolded parton-level absolute differential cross-sections are shown for (a) the transverse momentum of the top quark, (b) the absolute value of the rapidity of the top quark, (c) the transverse momentum of the leading top quark, (d) the absolute value of the rapidity of the leading top quark, (e) the transverse momentum of the subleading top quark, and (f) the the absolute value of the rapidity of the subleading top quark.

Not reviewed, for internal circulation only

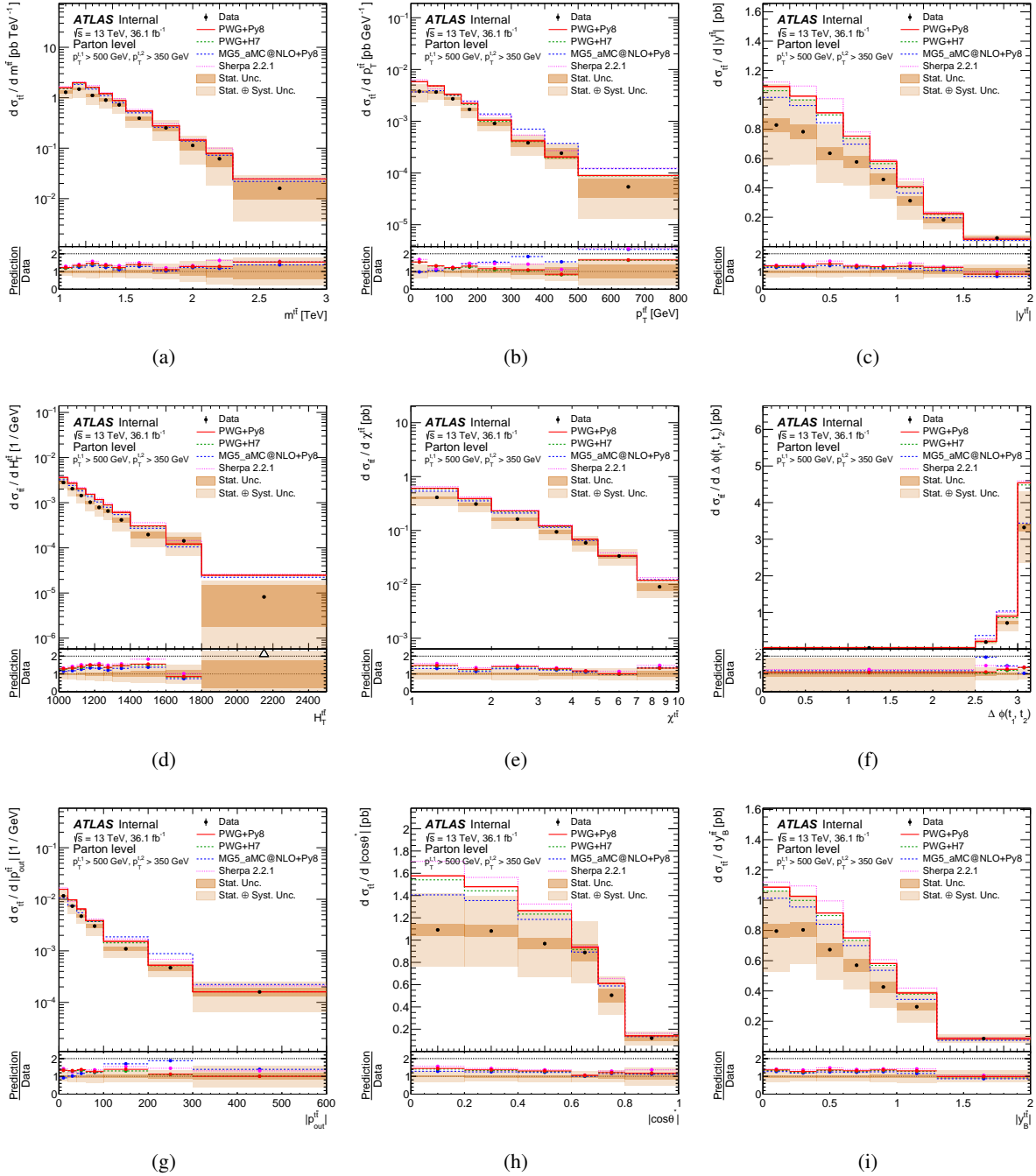


Figure 39: The unfolded parton-level absolute differential cross-sections are shown for (a) the $t\bar{t}$ invariant mass, (b) the $t\bar{t}$ p_T , (c) the absolute value of $t\bar{t}$ rapidity, (d) the $H^{t\bar{t}}$, (e) $\chi^{t\bar{t}}$, and (f) the $\Delta\phi(t_1, t_2)$, (g) the $p_{t\bar{t}}^{\text{out}}$, (h) the $\cos\theta^*$, and (i) the $y_B^{t\bar{t}}$.

Not reviewed, for internal circulation only

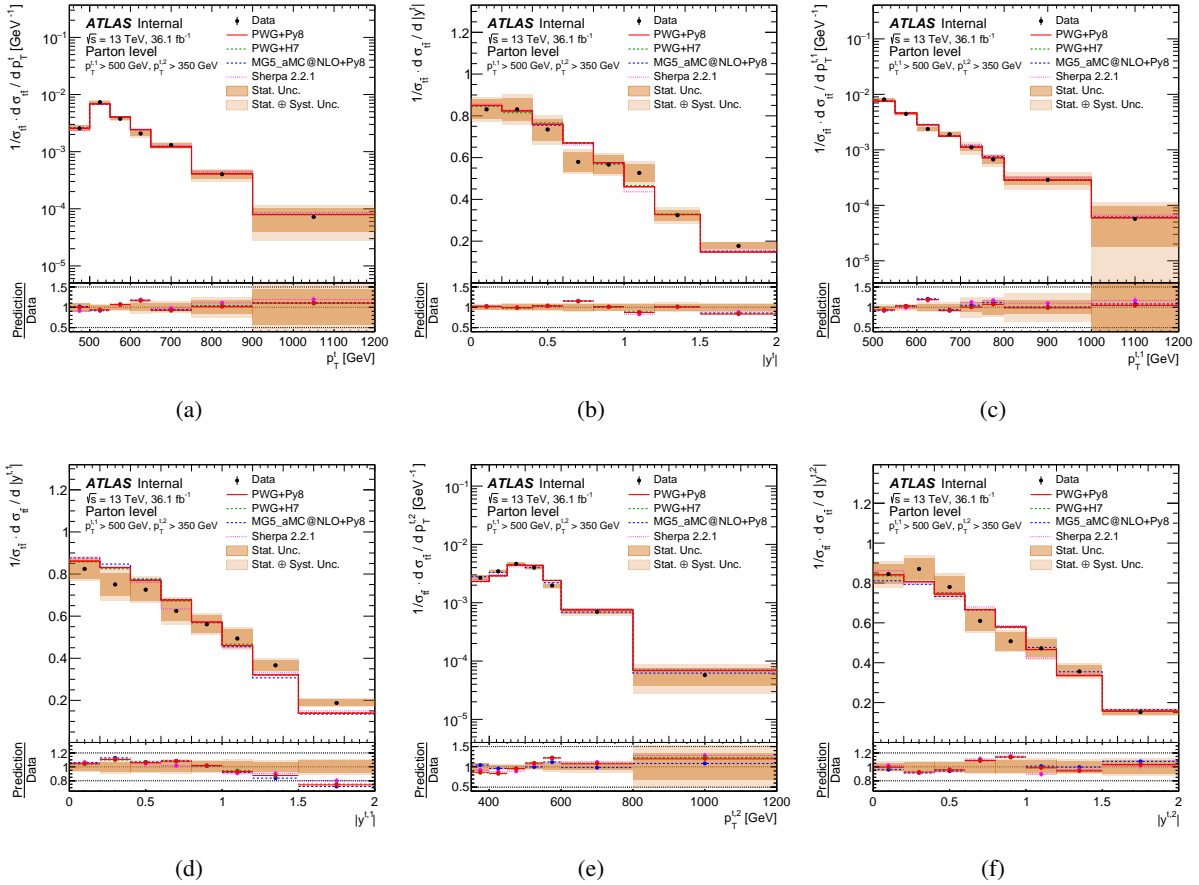


Figure 40: The unfolded parton-level relative differential cross-sections are shown for (a) the transverse momentum of the top quark, (b) the absolute value of the rapidity of the top quark, (c) the transverse momentum of the leading top quark, (d) the absolute value of the rapidity of the leading top quark, (e) the transverse momentum of the subleading top quark, and (f) the absolute value of the rapidity of the subleading top quark.

Not reviewed, for internal circulation only

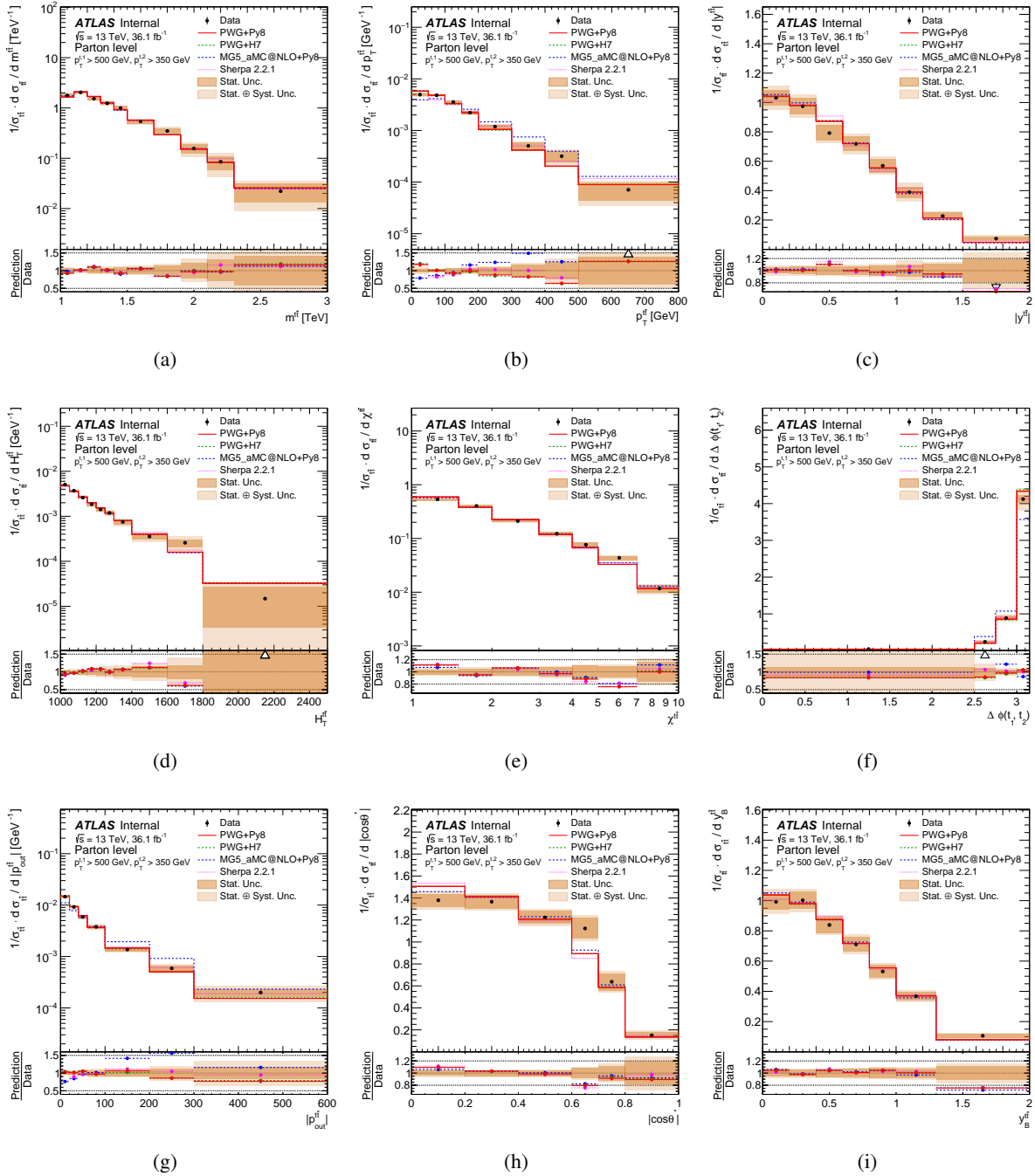


Figure 41: The unfolded parton-level relative differential cross-sections are shown for (a) the $t\bar{t}$ invariant mass, (b) the $t\bar{t}$ p_T , (c) the absolute value of $t\bar{t}$ rapidity, (d) the $H^{t\bar{t}}$, (e) $\chi^{t\bar{t}}$, and (f) the $\Delta\phi(t_1, t_2)$, (g) the $p_{\text{out}}^{t\bar{t}}$, (h) the $\cos\theta^*$, and (i) the $y_B^{t\bar{t}}$.

730 10. Conclusion

731 Kinematic distributions of the top quarks in $t\bar{t}$ events, selected in the boosted all-hadronic channel, are
 732 measured at the particle-level and parton-level in a fiducial phase-space using data from 13 TeV proton–
 733 proton collisions collected by the ATLAS detector at the Large Hadron Collider, corresponding to an
 734 integrated luminosity of 36.1 fb^{-1} . The sample of 3541 events has an observed signal-to-background
 735 ratio of approximately 2.3.

736 Absolute and normalized differential cross-sections are measured as a function of the leading and sub-
 737 leading top-quark transverse momentum and rapidity, and as a function of the mass, transverse mo-
 738 mentum, and rapidity of the $t\bar{t}$ system. In addition, a set of observables describing the hard-scattering
 739 interaction ($\cos \theta^*, \chi^{t\bar{t}}, y_B^{t\bar{t}}$) and sensitive to the emission of radiation along with the $t\bar{t}$ pair ($\Delta\phi^{t\bar{t}}, |p_{out}^{t\bar{t}}|$,
 740 $H_T^{t\bar{t}}$) are presented. Differential cross-sections at the parton-level are also shown for the same set of vari-
 741 ables. The differential-cross sections for the transverse momentum and absolute rapidity of a top-quark
 742 chosen at random from the event are also shown at the parton-level. The measurements are all made by
 743 unfolding the data to a phase-space that reflects the boosted region, requiring at least one top quark with
 744 $p_T > 500 \text{ GeV}$ and a second with $p_T > 350 \text{ GeV}$.

745 The measurements presented here exhibit, for most distributions and in large part of the phase space, a
 746 precision of the order of 20% or better and are in agreement with several Standard Model predictions.
 747 A key observation is that the total cross-section for top quarks with $p_T > 500 \text{ GeV}$ is $292 \pm 72 \text{ fb}$, or
 748 $(24 \pm 26)\%$ lower than predicted by the PowHEG + PYTHIA8 MC generator. This confirms earlier studies
 749 that have shown similar results. Although the observed cross-section is only one-standard deviation from
 750 the MC prediction, it is limited by the uncertainties in the MC modelling itself.

751 The normalized differential cross-sections at both the particle-level and parton-level are in good agree-
 752 ment with several MC predictions. In particular, there is excellent agreement in the differential cross-
 753 section as a function of the transverse momentum and rapidity of the top quarks. The largest discrepancy
 754 is in the description of several $t\bar{t}$ kinematic observables by the aMC@NLO + PYTHIA8 setup.

755 These results provide confirmation that the Standard Model provides an accurate description of top quark
 756 production in this very boosted regime. They also demonstrate that final states with full-hadronic top
 757 quark decays can be effectively separated from the intrinsically large backgrounds from multijet pro-
 758 duction, and therefore can be used for other Standard Model measurements as well as searches for new
 759 phenomena beyond the Standard Model.

760 **Appendix**

[Not reviewed, for internal circulation only]

761 A. Monte Carlo datasets

762 Monte Carlo simulations are used within the analysis for modelling the signal and backgrounds as well as
 763 assessing uncertainties associated with signal modelling. The Monte Carlo samples used in this analysis
 764 are listed in Table 10.

765 A.1. $t\bar{t}$ modelling

766 Standard ATLAS top simulations were used in the conference note results [9]. However, they have been
 767 found to provide limited statistics for the signal in the phase-space of interest for this analysis. This is due
 768 to the fact that the boosted regime represents a small fraction of the overall $t\bar{t}$ cross-section. This results
 769 in large statistical uncertainties and imprecise determination of systematic uncertainties associated with
 770 signal modelling. In order to provide sufficient statistics for this analysis two methods of enhancing event
 771 generation statistics in the relevant phase-space have been explored.

772 For Monte Carlo samples produced using the PowHEG generator the Born-suppression factor technique
 773 has been studied. This technique consists of biasing the probability of generating an event in a given
 774 region of phase space by the multiplicative factor $\frac{p_T^2}{p_T^2 + b_f^2}$ where p_T is transverse momentum of the Born-

775 level configuration and b_f is the Born-suppression factor. Events weight are multiplied by the factor $\frac{p_T^2 + b_f^2}{p_T^2}$
 776 such that, in the limit of large statistics, the weighted distribution of events agrees with those produced
 777 when no Born-suppression factor is applied. This provides a larger number of events in regions of high
 778 transverse momentum, and so long as the distribution of event weights is sufficiently narrow improves
 779 statistical uncertainties. All $t\bar{t}$ samples used in this analysis which employ PowHEG for the matrix element
 780 calculation use a Born-suppression factor of 500 GeV. Previous samples with a Born-suppression factor
 781 of 2000 GeV were found to have a wide distribution in event weights such that a small number of large-
 782 weight events spoiled the statistical precision in some bins.

783 The initial PowHEG samples produced with a born-suppression factor suffer from a bug such that all
 784 events are required to include at least one charm quark coming from a top decay. These samples have
 785 been supplemented with additional samples using identical settings except requiring no charm quarks
 786 from top decays. Each set of samples has its own DSID and the number of events produced for each
 787 sample is proportional to the total cross-section for that decay channel.

788 For MC samples using the MC@NLO generator the Born-suppression technique is not available and a
 789 cut on the leading top p_T at Born-level of 300 GeV has been studied. This effectively generates events in
 790 the high-pt regime but the sample must be appropriately combined with a similar sample using no p_T cut
 791 to ensure that events with low top p_T at Born-level but with high top p_T at particle or detector level are
 792 properly accounted for.

793 Based on these studies we have requested production of a set of MC samples to use for our signal,
 794 signal modelling systematics and for comparisons to unfolded results which use the most modern MC
 795 programs with recommended ATLAS top group settings which also apply the described techniques to
 796 reduce statistical uncertainties. These samples have now all been produced and are incorporated in the
 797 analysis, details on the datasets can be found in Table 10.

798 All parameters besides the parameters of interest for a given variation are kept the same between samples
 799 or as similar as possible. For the sample producing more radiation the PowHEG h_{damp} parameter is scaled

800 up by a factor of two, the renormalization and factorization scales are scaled down by a factor of two and
 801 a modified tune for more radiation is used. For the sample producing less variation the Powheg h_{damp}
 802 parameter is unchanged, the renormalization and factorization scales are scaled up by a factor of two and
 803 a modified tune suitable for less radiation is used.

804 The samples, as well as improving the statistical uncertainties match with the latest recommended ATLAS
 805 top modelling recommendations. In particular the h_{damp} parameter, which regulates high p_T radiation, is
 806 being changed from the mass of the top to $1.5 \times$ the mass of the top to more accurately match ATLAS
 807 data.

808 A.2. Background modelling

809 The MC samples for background processes are summarized in Table 10.

Dataset ID	Simulation	Monte Carlo Generator	Tune	σ (pb)	Comment
410506	FullSim	POWHEG+PYTHIA8+EVTGEN	A14 NNPDF23LO	832	$t\bar{t}$ all-hadronic with born-suppression, missing charmless decays
410532	FullSim	POWHEG+PYTHIA8+EVTGEN	A14 NNPDF23LO	832	$t\bar{t}$ all-hadronic with born-suppression charmless decays only
410521	FullSim	POWHEG+PYTHIA8+EVTGEN	A14v3cUp NNPDF23LO	832	Increased IFSR $t\bar{t}$ all-hadronic with born suppression factor, missing charmless decays
410534	FullSim	POWHEG+PYTHIA8+EVTGEN	A14v3cUp NNPDF23LO	832	Increased IFSR $t\bar{t}$ all-hadronic with born suppression factor, charmless decays only
410522	FullSim	POWHEG+PYTHIA8+EVTGEN	A14v3cDown NNPDF23LO	832	Decreased IFSR $t\bar{t}$ all-hadronic with born-suppression factor, missing charmless decays
410535	FullSim	POWHEG+PYTHIA8+EVTGEN	A14v3cDown NNPDF23LO	832	Decreased IFSR $t\bar{t}$ all-hadronic with born-suppression factor, charmless decays only
410530	FullSim	POWHEG+HERWIG7+EVTGEN	H7UE NNPDF23LO	832	$t\bar{t}$ all-hadronic alternative shower and hadronization model, with born-suppression factor, missing charmless decays
410537	FullSim	POWHEG+HERWIG7+EVTGEN	H7UE NNPDF23LO	832	$t\bar{t}$ all-hadronic alternative shower and hadronization model, with born-suppression factor, charmless decays only
410227	FullSim	MC@NLO+PYTHIA8+EVTGEN	A14 NNPDF23LO	832	$t\bar{t}$ all-hadronic alternative matrix element model inclusive sample.
410368	FullSim	MC@NLO+PYTHIA8+EVTGEN	A14 NNPDF23LO	832	$t\bar{t}$ all-hadronic alternative matrix element model with born pT cut.
410249	FullSim	SHERPA +EVTGEN	NNPDF3.0 NNLO	832	$t\bar{t}$ all-hadronic model, used in final comparison only.
410501	FullSim	POWHEG+PYTHIA8+EVTGEN	A14 NNPDF23LO	832	$t\bar{t}$ non-hadronic
410013	FullSim	POWHEG+PYTHIA6+EVTGEN	CT10 and Perugia2012	72	Wt inclusive single top
410014	FullSim	POWHEG+PYTHIA6+EVTGEN	CT10 and Perugia2012	72	Wt inclusive single anti-top
410155	FullSim	MC@NLO+PYTHIA8+EVTGEN	A14 NNPDF23LO	0.603	ttW inclusive sample
410157	FullSim	MC@NLO+PYTHIA8+EVTGEN	A14 NNPDF23LO	0.586	ttZ sample with Z decaying to qq
343365	FullSim	MC@NLO+PYTHIA8+EVTGEN	A14 NNPDF23LO	0.508	ttH dileptonic sample
343366	FullSim	MC@NLO+PYTHIA8+EVTGEN	A14 NNPDF23LO	0.508	ttH semileptonic sample
343367	FullSim	MC@NLO+PYTHIA8+EVTGEN	A14 NNPDF23LO	0.508	ttH all hadronic sample
426007	FullSim	POWHEG+PYTHIA8+EVTGEN	A14 NNPDF23LO	26410	multijet sample

Table 10: The Monte Carlo datasets used in this analysis.

810 B. Hadronic trigger efficiencies

811 B.1. Data sets

812 The triggers used in the simulation and data collection were studied by measurement of their efficiencies
 813 as a function of the leading jet p_T on pp collision data and two Monte Carlo simulations. The data
 814 was acquired during the LHC 2016 run at $\sqrt{s} = 13$ TeV and corresponded to an integrated luminosity
 815 of 0.5 fb^{-1} . The two Monte Carlo samples were both created with the TOPQ1 derivations with a pre-
 816 selection requiring at least one jet with $p_T > 300$ GeV. The $t\bar{t}$ (all-hadronic) samples were simulated using
 817 PowHEG+PYTHIA, while the samples of dijets were simulated using PYTHIA8 361024, 361025, and 361026.
 818 The data was accessed through the TOPQ4 derivation with the same pre-selection requirements.

819 The first Monte Carlo sample, the $t\bar{t}$ (all-hadronic), simulates a collision with subsequent W boson decay
 820 via the fully-hadronic channel for both top quarks. The second, consisting of a sample of dijets, simulates
 821 a $q\bar{q}$ annihilation or gg fusion collision that proceeds via QCD to a shower of quarks and gluons.

822 B.2. Triggers

823 At high p_T the hadronic decay products of the top quarks tend to be collimated in the direction of the
 824 parent quark. Consequently, jets in this boosted kinematic regime are often best clustered by algorithms
 825 that allow for large jet radii. These algorithms cluster the products into two large- R jets, one from the
 826 top quark and one from the antitop quark, as opposed to many narrow resolved jets. Because the boosted
 827 topology prevails over the resolved one in the events of interest, we measured the p_T turn-on of the triggers
 828 for large- R jets. Each of these triggers are intended to fire for events having at least one large- R jet with a
 829 p_T greater than the threshold value. The large- R jet triggers studied as well as the H_T and multijet triggers
 830 studied are shown in Table 11.

Trigger Class	Trigger
large- R jet	HLT_j360_a10r_L1J100
	HLT_j400_a10r_L1J100
	HLT_j420_a10r_L1J100
	HLT_j460_a10r_L1J100
HT	HLT_ht1000_L1J100
Multijet	HLT_j400

Table 11: All of the triggers included in the trigger efficiency study.

831 B.3. Event selection

832 The event selection is based on the expected characteristics of the desired final-state event topology. The
 833 standard event selection is discussed in Section 4. For this study, the event selection was slightly altered
 834 and is summarized in Table 12. The p_T cuts were relaxed to require only that two large- R jets have
 835 $p_T > 300$ GeV. There was additionally no mass-cut or b -tagging requirement applied in this study. This
 836 allowed the turn-on of each trigger to be seen clearly.

Cut	Event pre-selection
Hadronic trigger	<code>HLT_j360_a10r_L1J100 HLT_j400_a10r_L1J100</code> <code>HLT_j420_a10r_L1J100 HLT_j460_a10r_L1J100</code> <code>HLT_ht1000_L1J100 HLT_j400</code>
Primary vertex	≥ 5 tracks with $p_T > 0.4 \text{ GeV}$
Exactly no isolated lepton	Muons: $p_T > 25 \text{ GeV}$, $ \eta < 2.5$ Electrons: $p_T > 25 \text{ GeV}$ $ \eta < 2.47$, excluding $1.37 < \eta < 1.52$
Jets $R = 0.4$	≥ 2 jets $p_T > 25 \text{ GeV}$, $ \eta < 2.5$
Jets $R = 1.0$	≥ 2 jets $p_T > 300 \text{ GeV}$, $ \eta < 2.0$

Table 12: Summary of all requirements included in the event selection for trigger studies.

B.4. Results

Trigger efficiency is calculated by dividing two histograms. The first measure of efficiency is Trigger/NoTrigger, where Trigger is the histogram filled with Monte Carlo events selected by the trigger of interest. The denominator, NoTrigger, is a histogram filled with Monte Carlo events without requiring a trigger to have fired. All plots of Trigger/NoTrigger are shown in Figure 42. The second measure of trigger efficiency is Trigger/Baseline, where the baseline histogram is filled with data events for which the loosest unprescaled trigger fired. In this study, the loosest trigger is the trigger with the lowest p_T cut, `HLT_j360_a10r_L1J100`. All plots showing Trigger/Baseline as a function of p_T are in Figure 43, and all plots showing Trigger/Baseline for the large- R jets as a function of p_T and η are in Figure 44.

For the large- R jet triggers, the Trigger/NoTrigger plots show a distinctive sigmoid shape common to all four triggers. The plots feature a turn-on region in which efficiency rises rapidly, followed by a plateau at 100% efficiency which is achieved around 65-75 GeV after the trigger becomes active. The two simulated data sets show fairly good agreement in the turn-on region, with the triggers plateauing at 100% for both MC samples. The plots show that the `HLT_j360_a10r_L1J100` trigger accepts the most events due to its lower p_T threshold, reaching maximum efficiency near 425 GeV.

The HT and multijet triggers also have a turn-on region after which they reach 100% efficiency. Their turn-on is slower, however, and full efficiency is not achieved until a jet p_T of 600-700 GeV. The agreement between the two Monte Carlo simulations is also not as good as it was for the large- R jet triggers, especially for `HLT_j400`. This is expected given the different topologies for the two MC samples, though the detailed behaviour was not anticipated.

The Trigger/Baseline plots have similar features and allow for a comparison between trigger efficiencies in simulations and data. The agreement is excellent for the large- R jet triggers, especially in the plateau region where the efficiency is 100%. This is also the case for `HLT_ht1000_L1J100`. The `HLT_j400` efficiency has some discrepancy between data and Monte Carlo dijet samples in the turn-on region. Once again, the agreement is excellent once the trigger is fully efficient. For the Trigger/Baseline plots as a function of p_T and η , the agreement is still good between the data and dijet Monte Carlo samples and the efficiency is only weakly dependent on eta.

In conclusion, the trigger efficiency plots show that the large- R jet triggers will have a behaviour that is appropriate for this analysis. In particular, `HLT_j360_a10r_L1J100` will be most beneficial as the

866 principal trigger. It achieves 100% efficiency by 425 GeV, so it is fully efficient in the p_T region of
867 interest. The other large- R jet triggers achieve 100% efficiency at higher p_T , typically 6-75 GeV above
868 the nominal threshold, so they will still prove useful if the luminosity becomes high enough that the
869 HLT_j360_a10r_L1J100 trigger must be prescaled. In that case, we recommend retaining a lower p_T
870 prescaled trigger to be able to verify the turn-on behaviour from the data sample.

[Not reviewed, for internal circulation only]

Not reviewed, for internal circulation only

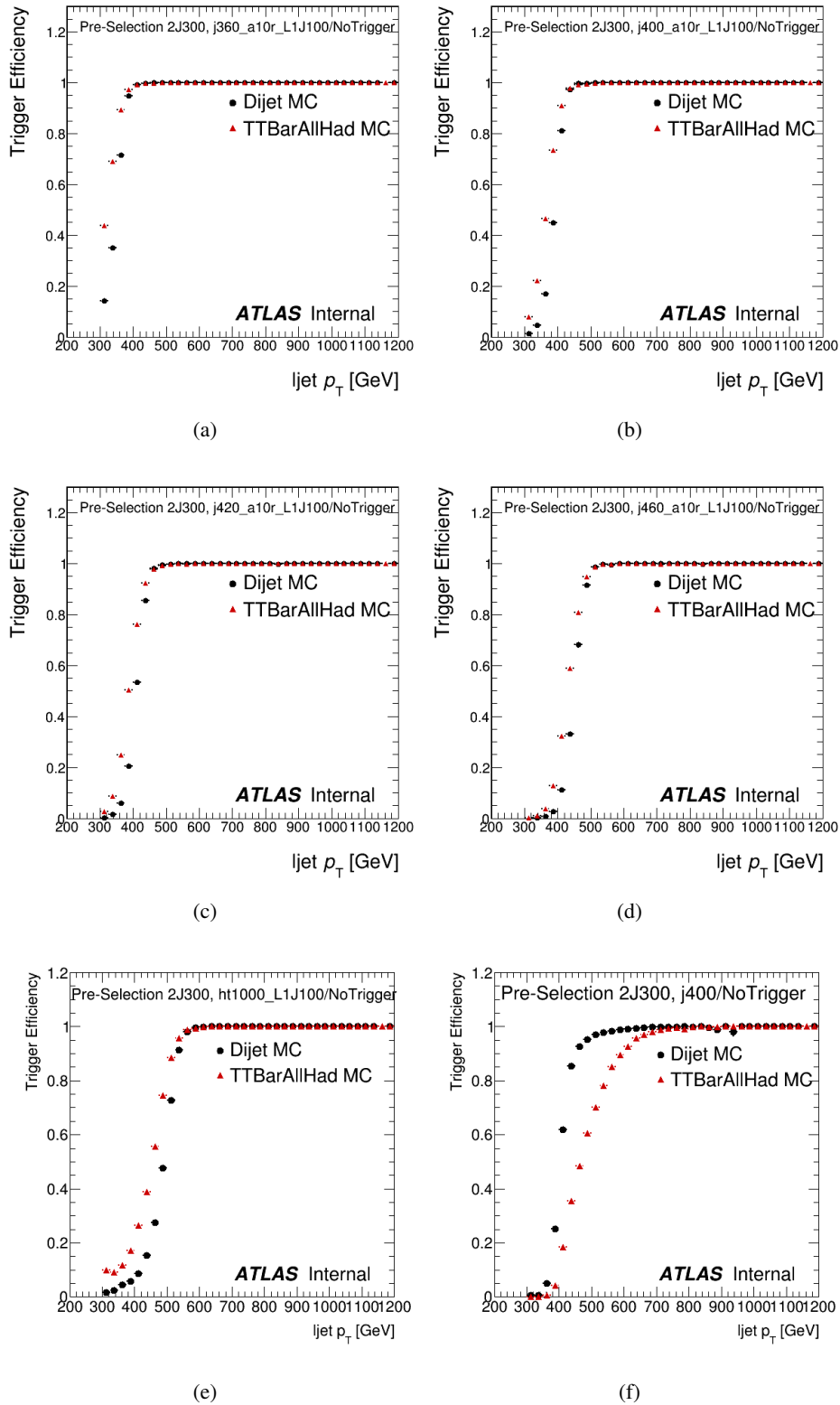


Figure 42: The Trigger/NoTrigger plots for: (a) - (d) the large- R jet triggers, (e) the HT trigger, and (f) the multijet trigger in two Monte Carlo samples.

Not reviewed, for internal circulation only

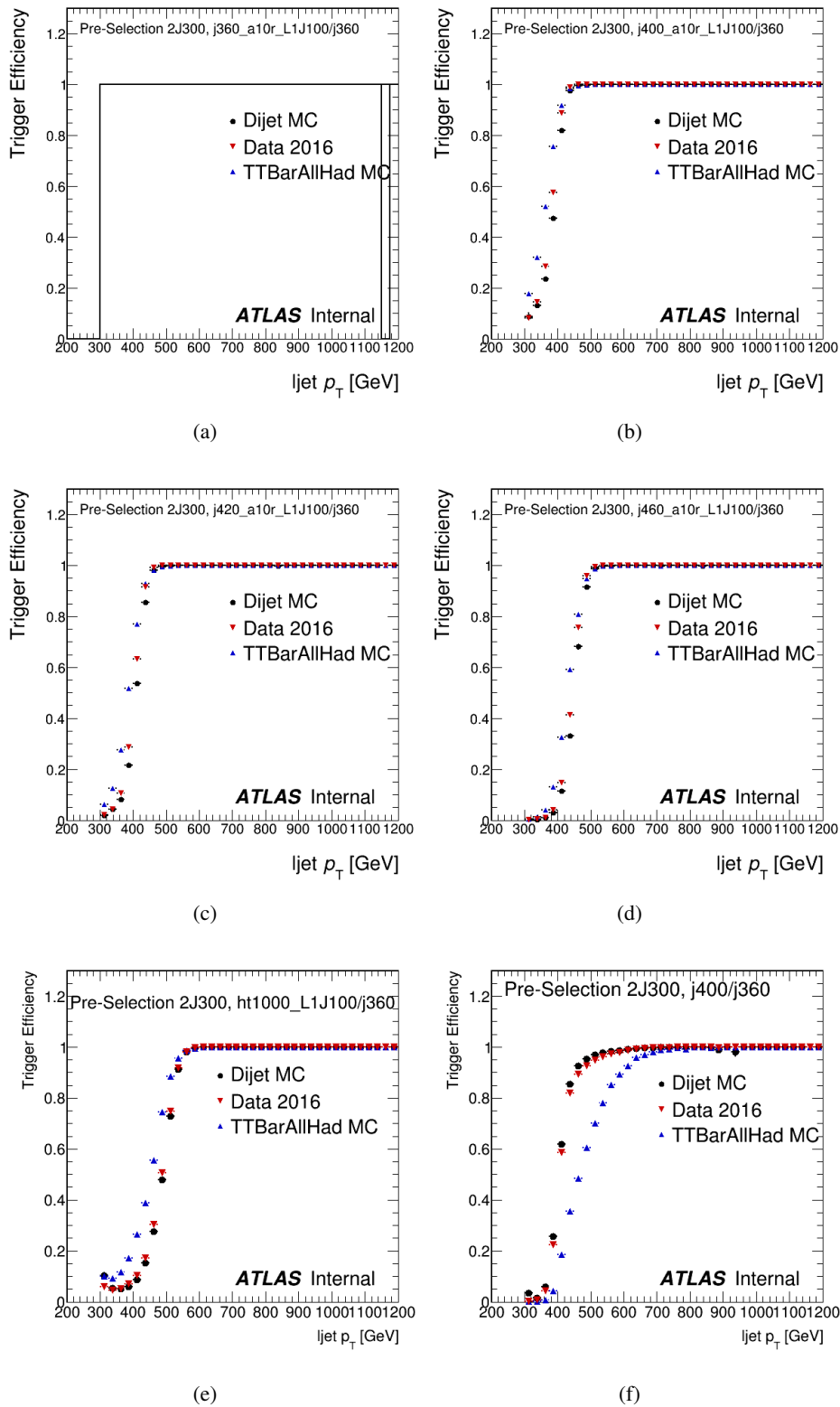


Figure 43: The Trigger/Baseline plots for the (a) - (d) large- R jet triggers, (e) the HT trigger, and (f) the multijet trigger observed in 13 TeV data.

Not reviewed, for internal circulation only

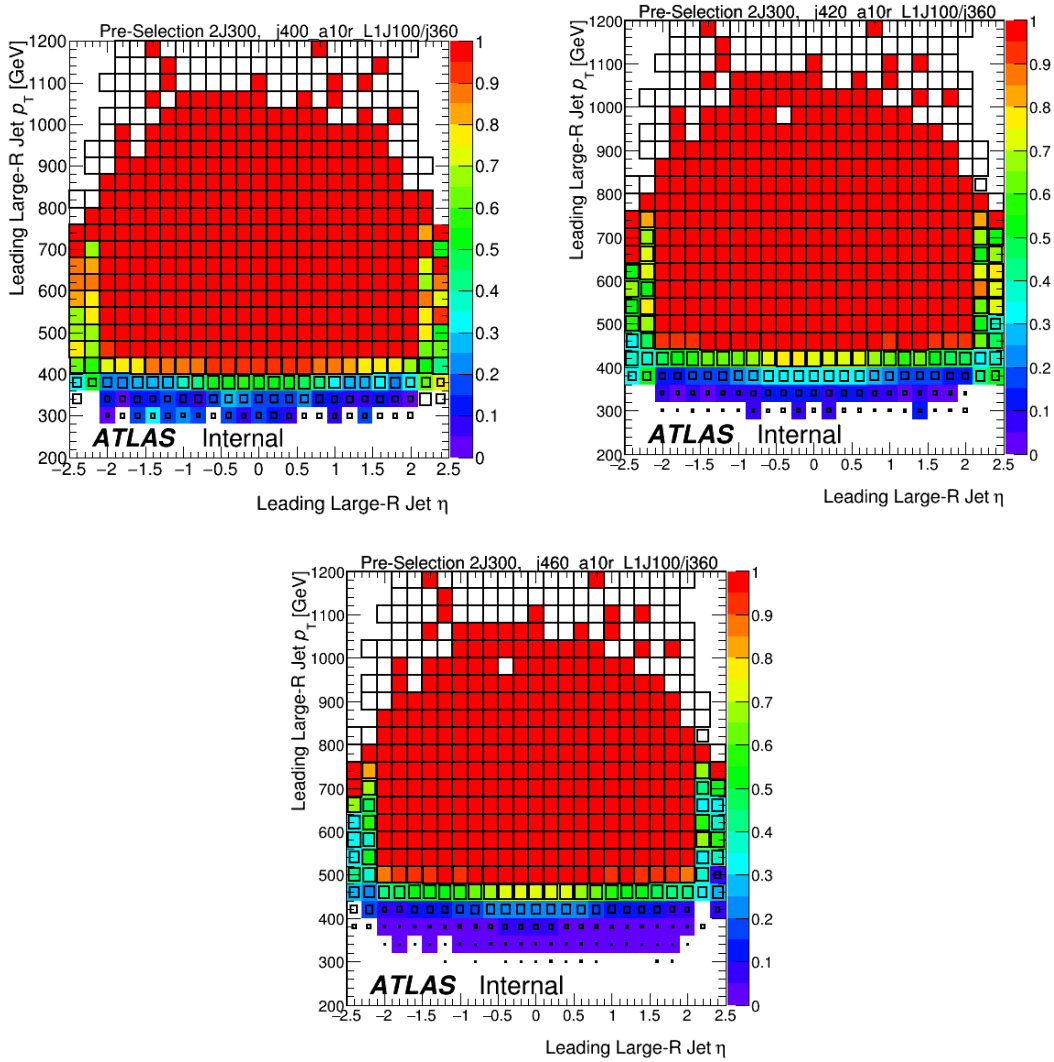


Figure 44: The Trigger/Baseline plots for the large- R jet triggers as a function of p_T and η observed in 13 TeV data. The efficiency of the data is represented by the colour scale, and the efficiency of the trigger is shown in varying box size.

871 C. Second-leading jet selection optimization

872 C.1. Second leading large- R jet p_T threshold

873 The optimization of the second-leading large- R jet p_T cut is based on the mass distribution of the leading
 874 embedded narrow-jet, *i.e.* a narrow jet that is angularly matched to the large- R jet. The shape of this ob-
 875 servable is remarkably different between signal and background, giving a unique handle to the underlying
 876 physics of the hadronic decay of top quarks.

877 Two possibilities has been considered: a tight cut ($p_T^{t,2} > 450$ GeV) and a loose cut ($p_T^{t,2} > 350$ GeV). In
 878 the tight-cut scenario, shown in Figure 45, the leading sub-jet mass presents a clear peak corresponding
 879 to a boosted W boson for both the leading and sub-leading large- R jets. In the loose-cut scenario, shown
 880 in Figure 46, the leading sub-jet mass presents a clear peak corresponding to a boosted W boson only
 881 for the leading large- R jet, and a broad excess around the W mass for the second-leading large- R jet. By
 882 loosening the cut, a significant increase of statistics is observed, estimated to be around 40% under the W
 883 boson peak. Data events increase from 558 to 829 for 8.3 fb^{-1} . However, the tighter-cut scenario selects
 884 events with a higher boost, resulting in a better S/B ratio of 4.4, compared to 3.8 obtained in the loose-cut
 885 scenario.

886 The choice to use the looser p_T cut was driven by two main considerations. Firstly, keeping the subleading
 887 top momentum cut as low as possible while still being consistent with the boosted topology allows for
 888 the most inclusive cross-section measurement. Secondly, the large asymmetric cut between the leading
 889 and subleading top minimizes ordering migrations where the leading top at particle or parton level is the
 890 subleading top at detector level.

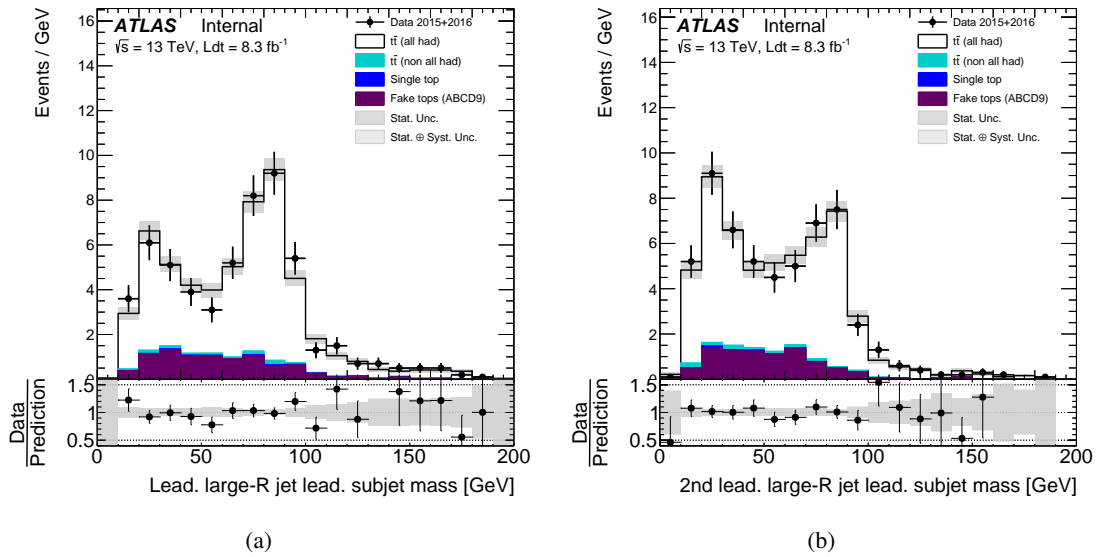


Figure 45: Jet mass distribution of the leading sub-jet mass of the 45(a) leading and 45(b) sub-leading large- R jet,
 where the second leading large- R jet has a $p_T > 450$ GeV (tight cut).

Not reviewed, for internal circulation only

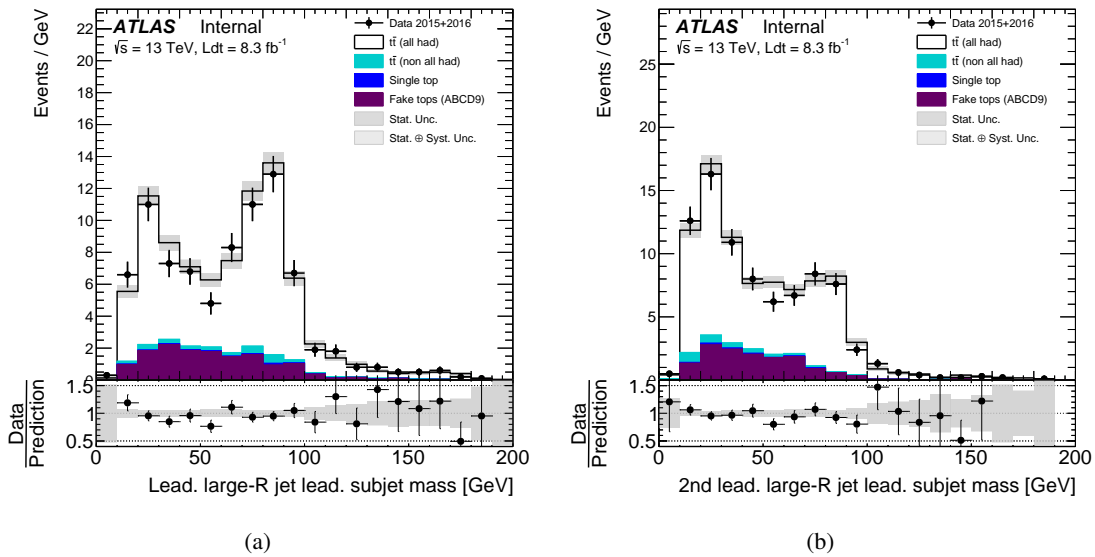


Figure 46: Jet mass distribution of the leading sub-jet mass of the 45(a) leading and 45(b) sub-leading large- R jet, where the second leading large- R jet has a $p_T > 350 \text{ GeV}$ (loose cut).

891 D. Validation regions

892 The validity of the signal prediction and background estimation is tested in a region of the phase-space
 893 where the two leading large- R jets are matched to b -tagged narrow jets, but only one large- R jet is tagged
 894 as originated from the decay of a high- p_T top quark. In these regions the S/B ratio is lower than in the
 895 signal region, with a purity around 40% in both cases. Figures 47–51 and 52–56 show a number of control
 896 plots and observables measured in region N and L respectively.

897 Finally, Fig. 57 shows the same observables for the combined regions $S + N$ and $S + L$, i.e. where either
 898 jet is top-tagged. No scale factor is applied to the signal model in these cases.

899 The overall agreement between data and prediction is generally good. This demonstrates that the combin-
 900 ation of the signal Monte Carlo calculation and the background estimation are behaving as expected. A
 901 slope can be clearly seen in the τ_{32} for control regions $S + N$ and $S + L$, hinting at a mis-modelling in the
 902 signal which is likely to affect the estimation of the selection efficiency. To further investigate this mis-
 903 modelling, the correlation between the leading and 2nd-leading jets τ_{32} for the 58(b) POWHEG+PYTHIA8
 904 and 58(c) POWHEG+HERWIG7 generators is measured after the b-matching requirement is applied. The
 905 Pearson correlation parameters are very small, in the order of 0.01–0.02 for the two generators under
 906 consideration. The average of the 2nd-leading jet τ_{32} as a function of the leading jet τ_{32} is shown in figure
 907 58(d), where the uncertainty represents the RMS of the y-axis distribution in each x-bin.

Not reviewed, for internal circulation only

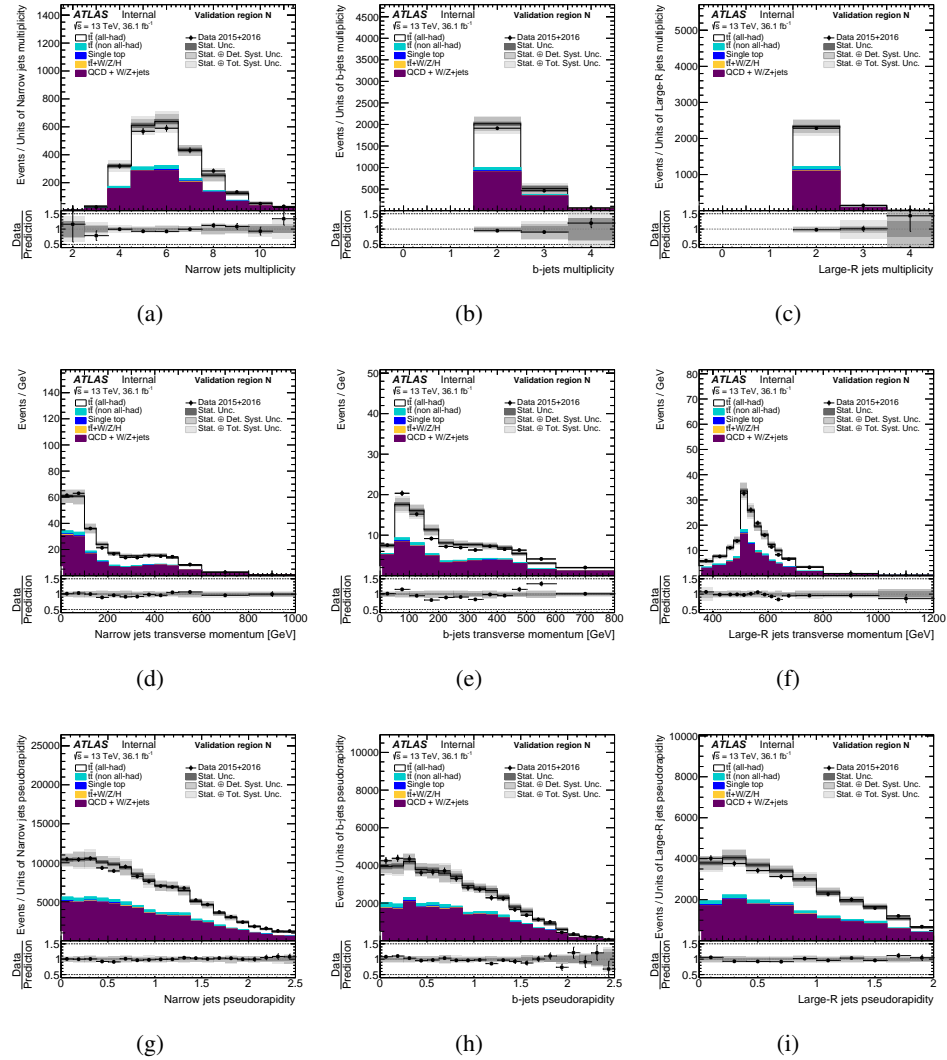
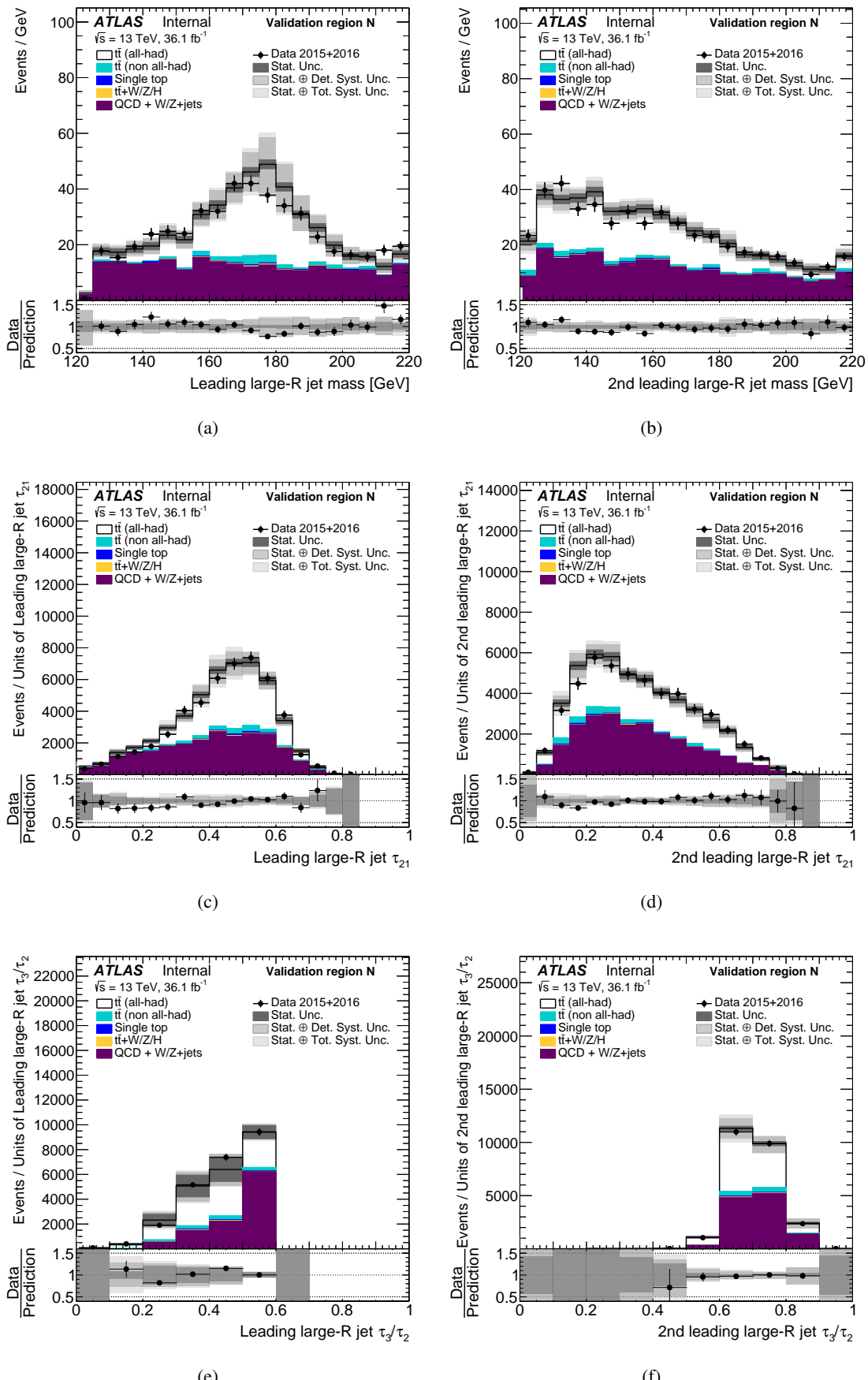


Figure 47: Kinematic distributions of narrow jets in the validation region N : (a) multiplicity, (d) transverse momentum and (g) rapidity of anti- k_t $R=0.4$ jets, (b) multiplicity, (e) transverse momentum and (h) rapidity of anti- k_t $R=0.4$ b -tagged jets, (c) multiplicity, (f) transverse momentum and (i) rapidity of anti- k_t $R=1.0$ jets. Data distributions are compared to predictions using Powheg+Pythia8 with $h_{\text{damp}} = 1.5m_t$ as the $t\bar{t}$ signal model. The colour bands indicate the statistical uncertainty.

Not reviewed, for internal circulation only



14th October 2017 – 15:48

84

Figure 48: Kinematic distributions of large- R jets in the validation region N : (a) mass, (c) and (e) N-subjettiness of the leading anti- k_t $R=1.0$ trimmed jet, (b) mass, (d) and (f) N-subjettiness of the second leading anti- k_t $R=1.0$ trimmed jet. Data distributions are compared to predictions using PowHEG+PYTHIA8 with $h_{\text{damp}} = 1.5m_t$ as the $t\bar{t}$ signal model. The hashed area indicates the combined statistical and systematic uncertainties on the total prediction, excluding systematic uncertainties related to the modelling of the $t\bar{t}$ system.

Not reviewed, for internal circulation only

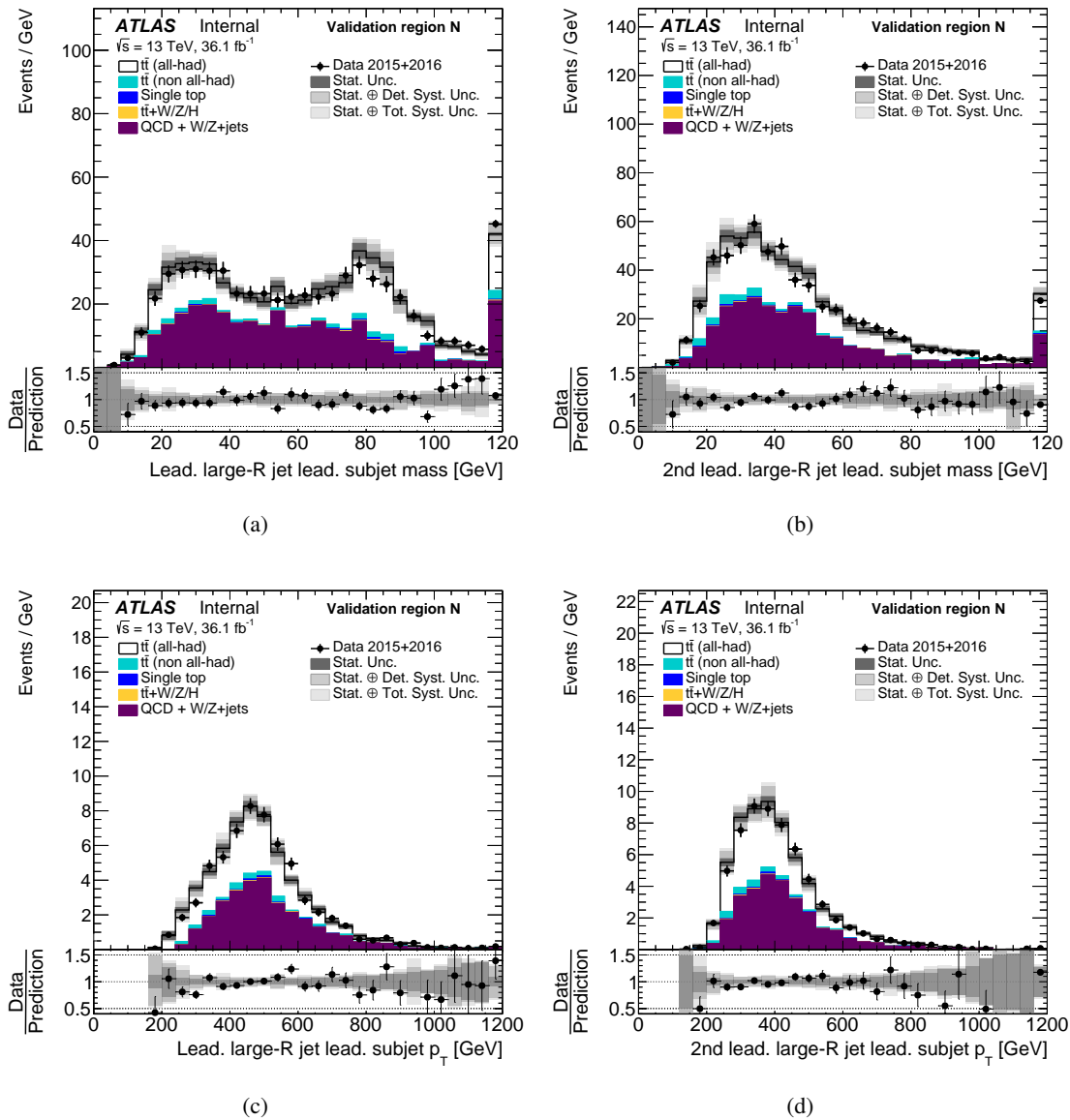


Figure 49: Kinematic distributions of the leading small- R jet embedded in a large- R jet in the validation region N : (a) mass and (c) transverse momentum of the leading small- R jet embedded in the leading large- R jet, and (b) mass and (d) transverse momentum of the leading small- R jet embedded in the second-leading large- R jet. Data distributions are compared to predictions using PowHEG+PYTHIA8 with $h_{\text{damp}} = 1.5m_t$ as the $t\bar{t}$ signal model. The hashed area indicates the combined statistical and systematic uncertainties on the total prediction, excluding systematic uncertainties related to the modelling of the $t\bar{t}$ system.

Not reviewed, for internal circulation only

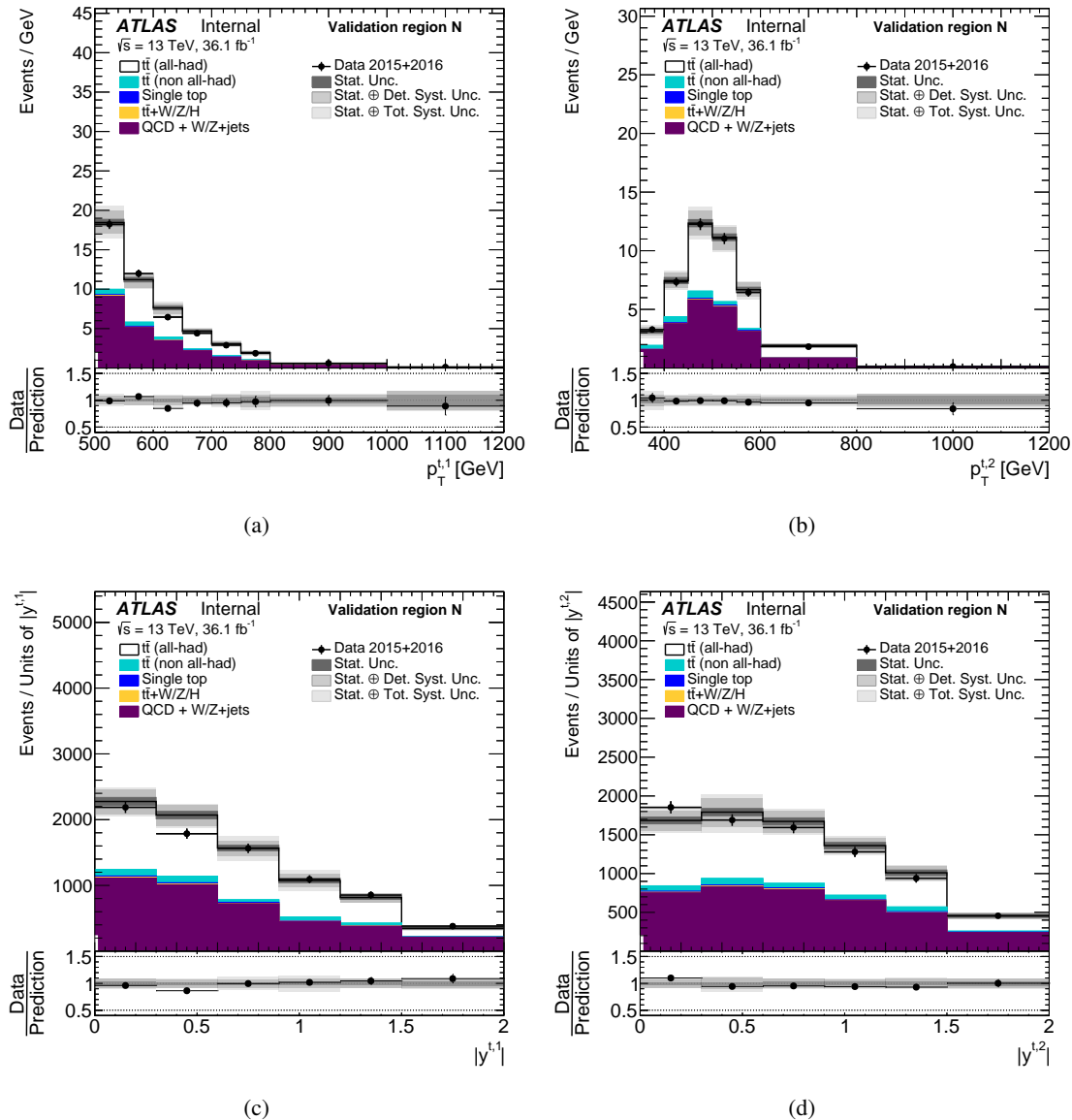


Figure 50: Kinematic distributions of top quark candidates in the validation region N : (a) transverse momentum and (c) absolute value of the rapidity of the leading top, and (b) transverse momentum and (d) absolute value of the rapidity of the second leading top. Data distributions are compared to predictions using PowHEG+PYTHIA8 with $h_{\text{damp}} = 1.5m_t$ as the $t\bar{t}$ signal model. The hashed area indicates the combined statistical and systematic uncertainties on the total prediction, excluding systematic uncertainties related to the modelling of the $t\bar{t}$ system.

Not reviewed, for internal circulation only

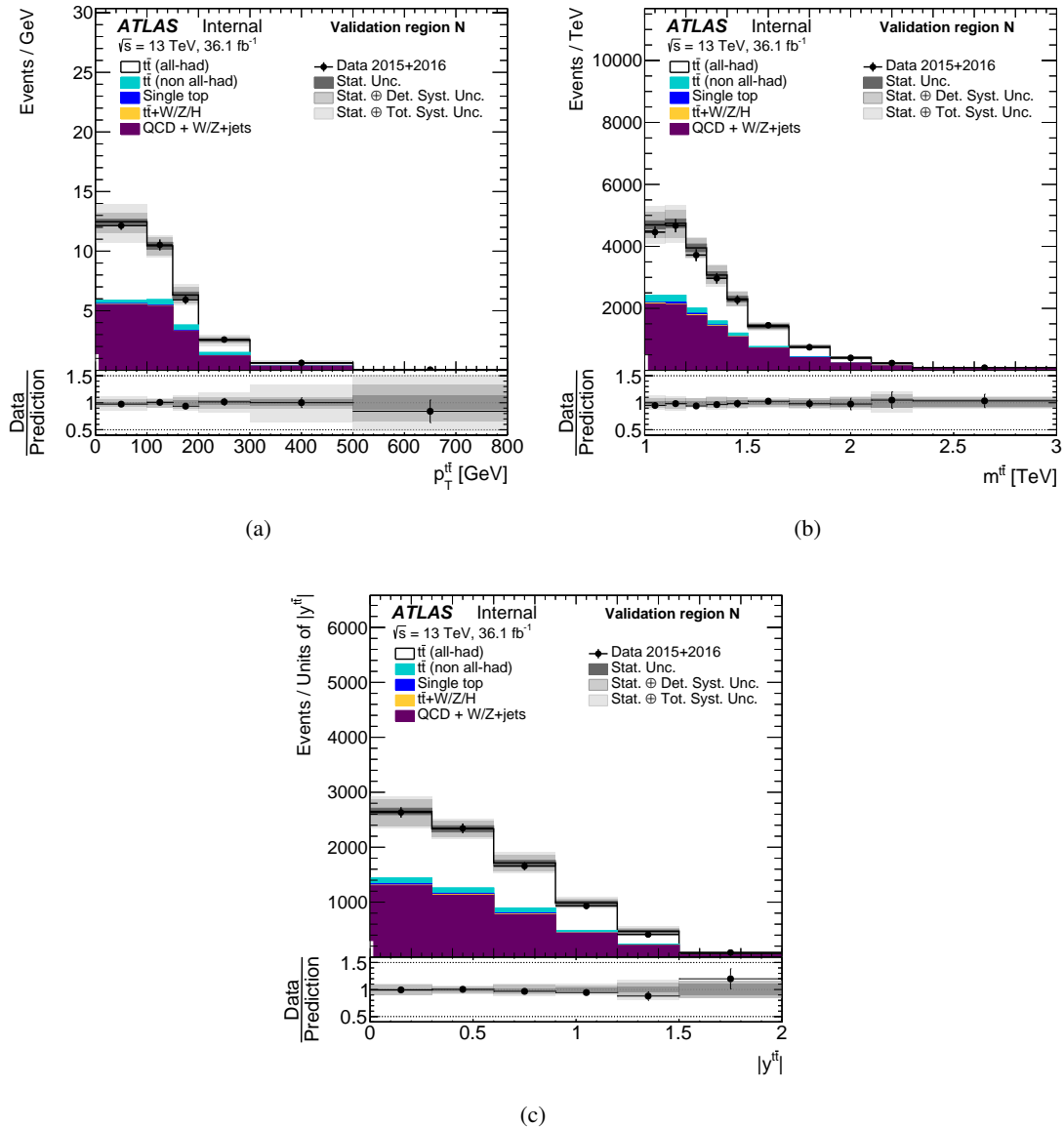


Figure 51: Kinematic distributions of $t\bar{t}$ system in the validation region N : (a) transverse momentum, (b) invariant mass and (c) absolute value of the rapidity of the $t\bar{t}$ system. Data distributions are compared to predictions using Powheg+Pythia8 with $h_{\text{damp}} = 1.5m_t$ as the $t\bar{t}$ signal model. The hashed area indicates the combined statistical and systematic uncertainties on the total prediction, excluding systematic uncertainties related to the modelling of the $t\bar{t}$ system.

Not reviewed, for internal circulation only

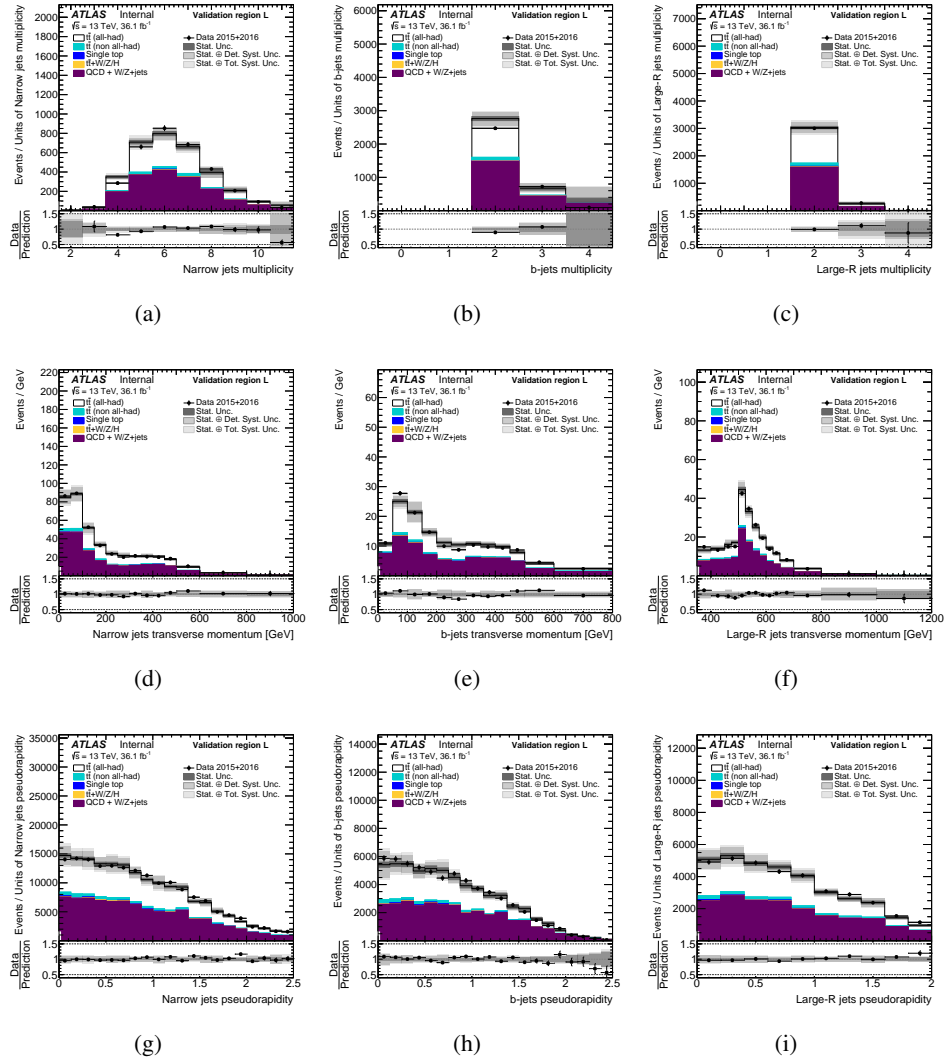
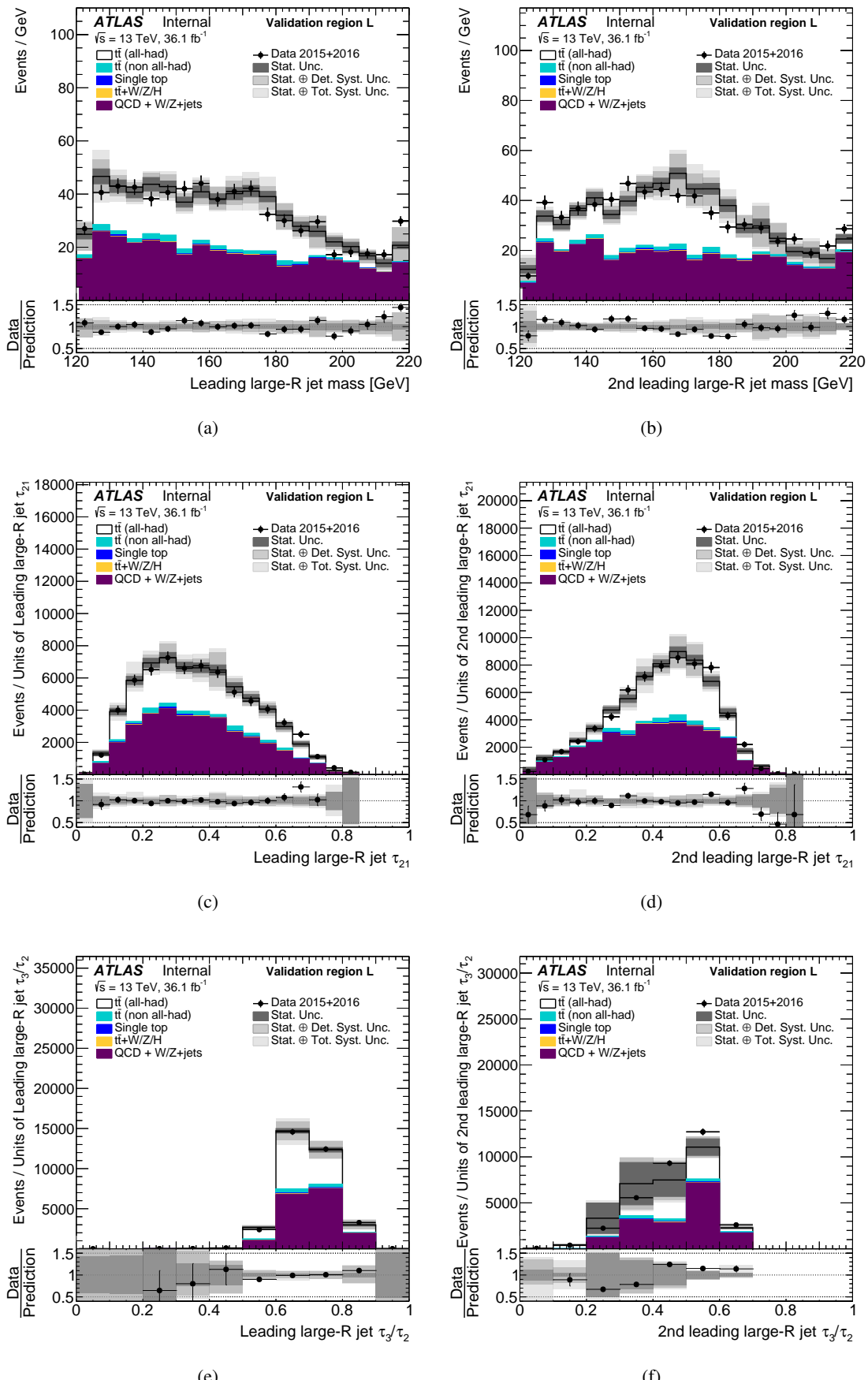


Figure 52: Kinematic distributions of narrow jets in the validation region L : (a) multiplicity, (d) transverse momentum and (g) rapidity of anti- k_t $R=0.4$ jets, (b) multiplicity, (e) transverse momentum and (h) rapidity of anti- k_t $R=0.4$ b -tagged jets, (c) multiplicity, (f) transverse momentum and (i) rapidity of anti- k_t $R=1.0$ jets. Data distributions are compared to predictions using Powheg+Pythia8 with $h_{\text{damp}} = 1.5m_t$ as the $t\bar{t}$ signal model. The hashed area indicates the combined statistical and systematic uncertainties on the total prediction, excluding systematic uncertainties related to the modelling of the $t\bar{t}$ system.

Not reviewed, for internal circulation only



14th October 2017 – 15:48

89

Figure 53: Kinematic distributions of large- R jets in the validation region L : (a) mass, (c) and (e) N-subjettiness of the leading anti- k_t $R=1.0$ trimmed jet, (b) mass, (d) and (f) N-subjettiness of the second leading anti- k_t $R=1.0$ trimmed jet. Data distributions are compared to predictions using PowHEG+PYTHIA8 with $h_{\text{damp}} = 1.5m_t$ as the $t\bar{t}$ signal model. The hashed area indicates the combined statistical and systematic uncertainties on the total prediction, excluding systematic uncertainties related to the modelling of the $t\bar{t}$ system.

Not reviewed, for internal circulation only

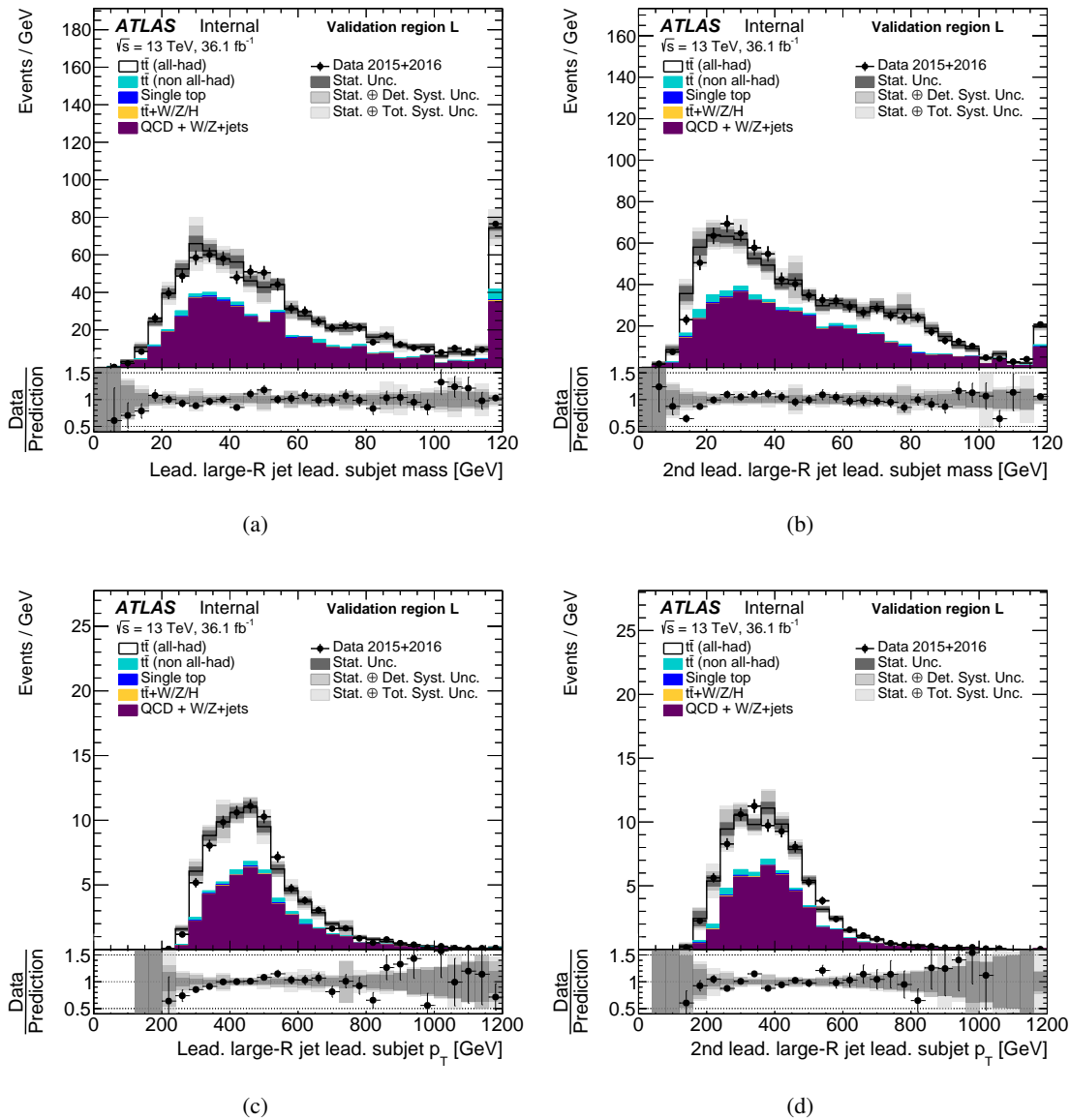


Figure 54: Kinematic distributions of the leading small- R jet embedded in a large- R jet in the validation region L : (a) mass and (c) transverse momentum of the leading small- R jet embedded in the leading large- R jet, and (b) mass and (d) transverse momentum of the leading small- R jet embedded in the second-leading large- R jet. Data distributions are compared to predictions using PowHEG+PYTHIA8 with $h_{\text{damp}} = 1.5m_t$ as the $t\bar{t}$ signal model. The hashed area indicates the combined statistical and systematic uncertainties on the total prediction, excluding systematic uncertainties related to the modelling of the $t\bar{t}$ system.

Not reviewed, for internal circulation only

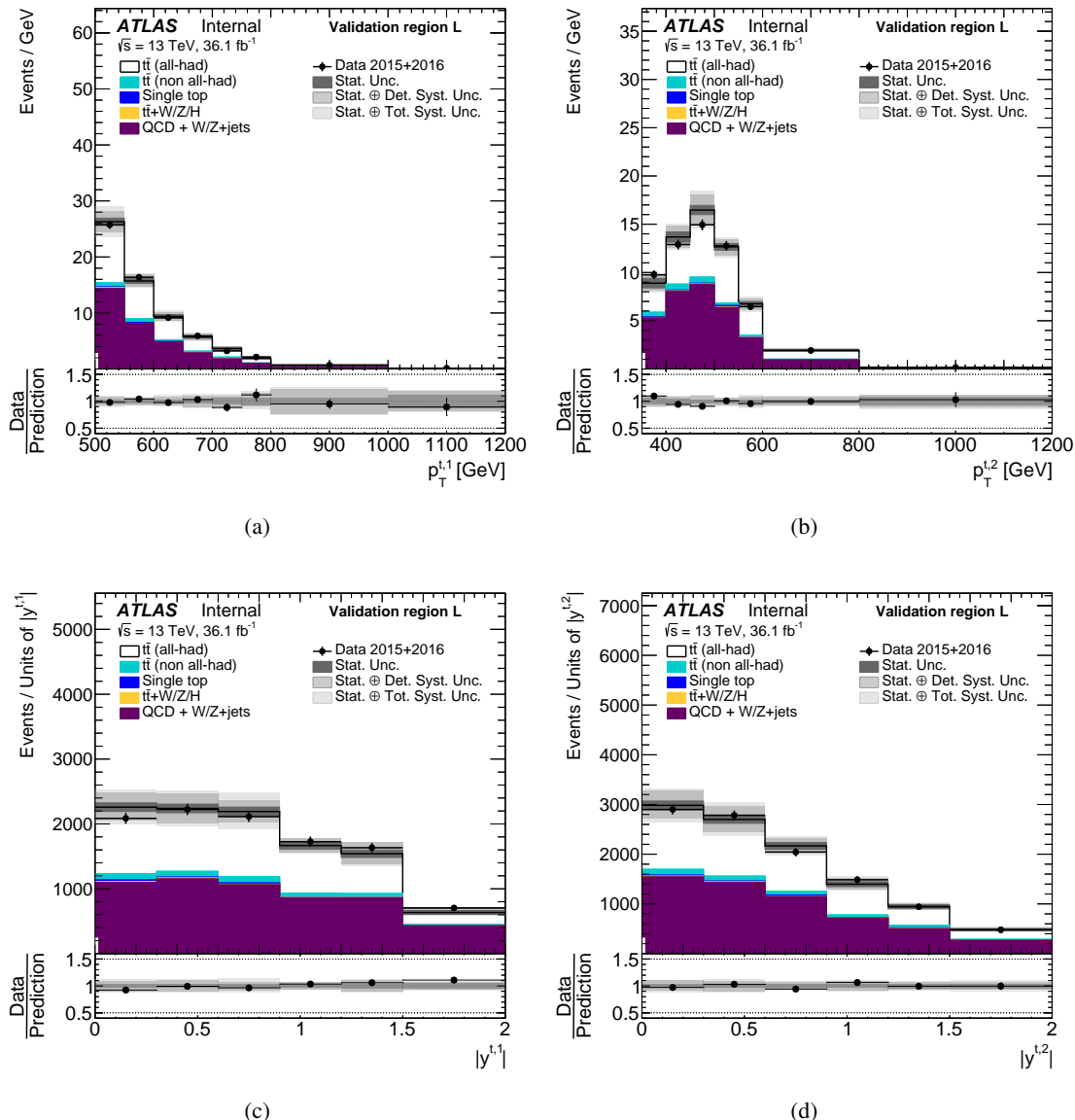


Figure 55: Kinematic distributions of top quark candidates in the validation region L : (a) transverse momentum and (c) absolute value of the rapidity of the leading top, and (b) transverse momentum and (d) absolute value of the rapidity of the second leading top. Data distributions are compared to predictions using PowHEG+PYTHIA8 with $h_{\text{damp}} = 1.5m_t$ as the $t\bar{t}$ signal model. The hashed area indicates the combined statistical and systematic uncertainties on the total prediction, excluding systematic uncertainties related to the modelling of the $t\bar{t}$ system.

Not reviewed, for internal circulation only

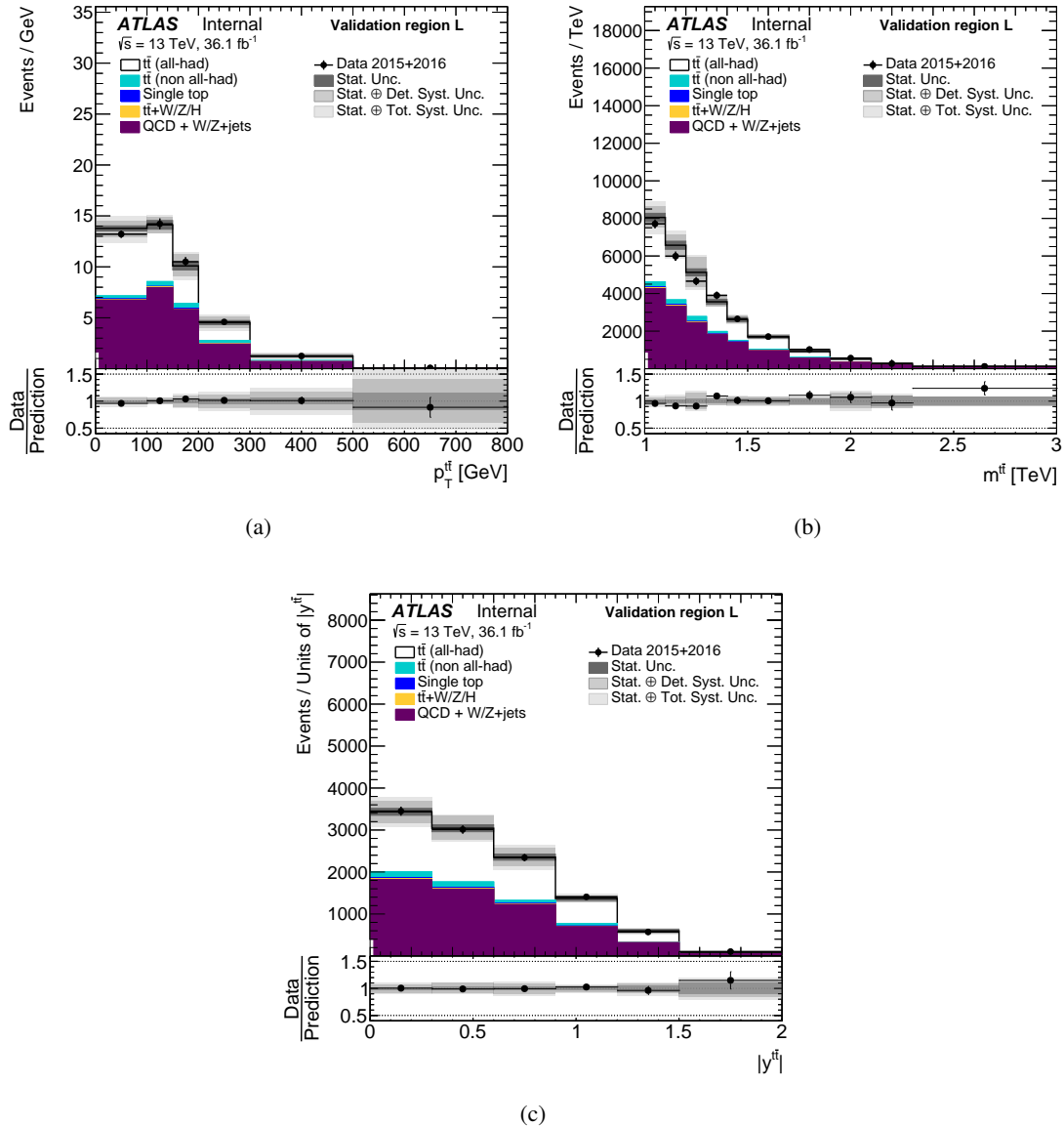


Figure 56: Kinematic distributions of $t\bar{t}$ system in the validation region L: (a) transverse momentum, (b) invariant mass and (c) absolute value of the rapidity of the $t\bar{t}$ system. Data distributions are compared to predictions using PowHEG+PYTHIA8 with $h_{\text{damp}} = 1.5m_t$ as the $t\bar{t}$ signal model. The hashed area indicates the combined statistical and systematic uncertainties on the total prediction, excluding systematic uncertainties related to the modelling of the $t\bar{t}$ system.

Not reviewed, for internal circulation only

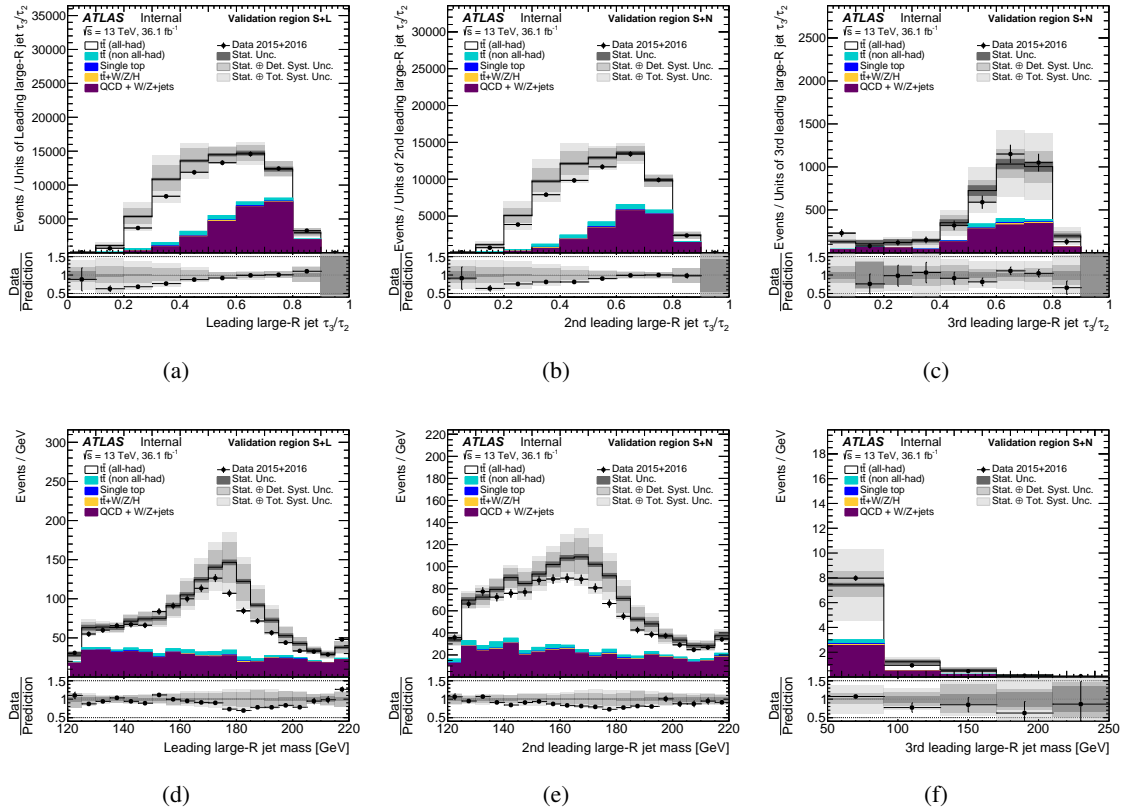


Figure 57: Kinematic distributions of top quark candidates in the validation regions S+N and S+L: (a) N-subjettiness and (d) mass of the leading, (b) N-subjettiness and (e) mass of the sub-leading and (c) N-subjettiness and (f) mass of the 3rd-leading anti- k_t R=1.0 trimmed jet in combined regions where either jet is top-tagged. Data distributions are compared to predictions using PowHEG+PYTHIA8 with $h_{\text{damp}} = 1.5m_t$ as the $t\bar{t}$ signal model. The hashed area indicates the combined statistical and systematic uncertainties on the total prediction. The light grey band shows systematic uncertainties related to the modelling of the $t\bar{t}$ system.

Not reviewed, for internal circulation only

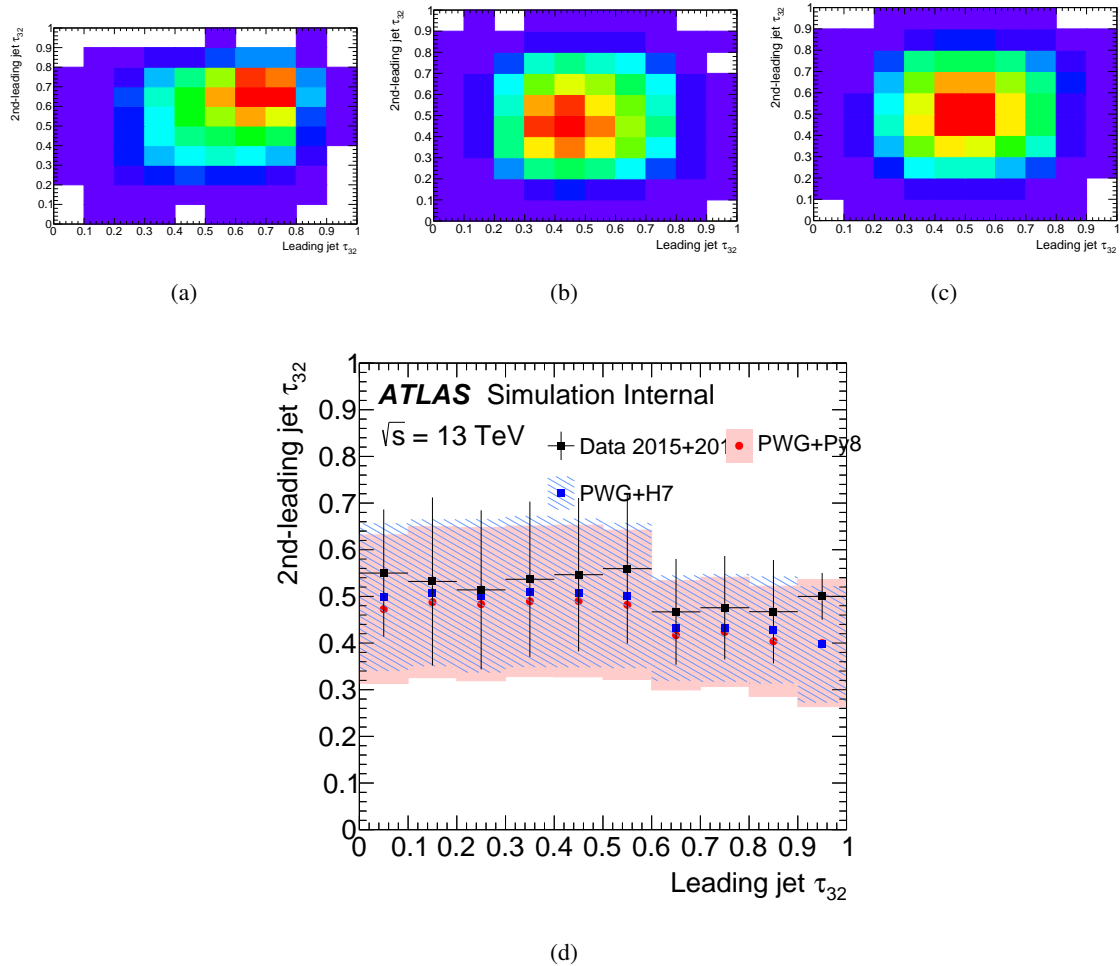


Figure 58: Correlation between the leading and 2nd-leading jets τ_{32} for (a) data 2015+2016 and for the (b) Powheg+Pythia8 and (c) Powheg+Herwig7 generators. The Pearson correlation parameters are very small, in the order of 0.01–0.02 for all the samples under consideration. The average of the 2nd-leading jet τ_{32} as a function of the leading jet τ_{32} is shown in figure (d), where the uncertainty represents the RMS of the y-axis distribution in each x-bin.

908 E. Resolution of observables

909 The resolution of the unfolded variables defined as $1 - \langle x_{reco}/x_{particle} \rangle$ is measured in the Monte Carlo
 910 simulation for regions S, L, N and H. Figures 59–61 show a comparison among these regions as a function
 911 of their particle-level for region S only. The points represent the mean of the distribution for a give range
 912 in the particle-level distribution. The painted bands indicate the RMS of the distribution in the same range.
 913 The resolution is consistent among the four regions within the RMS of the distributions in each bin, with
 914 a bias generally close to zero. The leading top transverse momentum shows a small systematic offset of
 915 about 1%. Some trends are observed at low $t\bar{t}$ transverse momentum, $p_{out}^{t\bar{t}}$ and $H_T^{t\bar{t}}$.

916 Fig. 62 shows the mass resolution of the leading and second leading large- R jets. The normalized inclusive
 917 distribution is compared to the resolution obtained for events with an average number of interactions
 918 per bunch-crossing $\langle\mu\rangle < 20$ or $\langle\mu\rangle > 20$. The distributions show a bias of about 3% in the leading jet and
 919 about 1% for the second leading jet, independent on the $\langle\mu\rangle$ range.

Not reviewed, for internal circulation only

Not reviewed, for internal circulation only

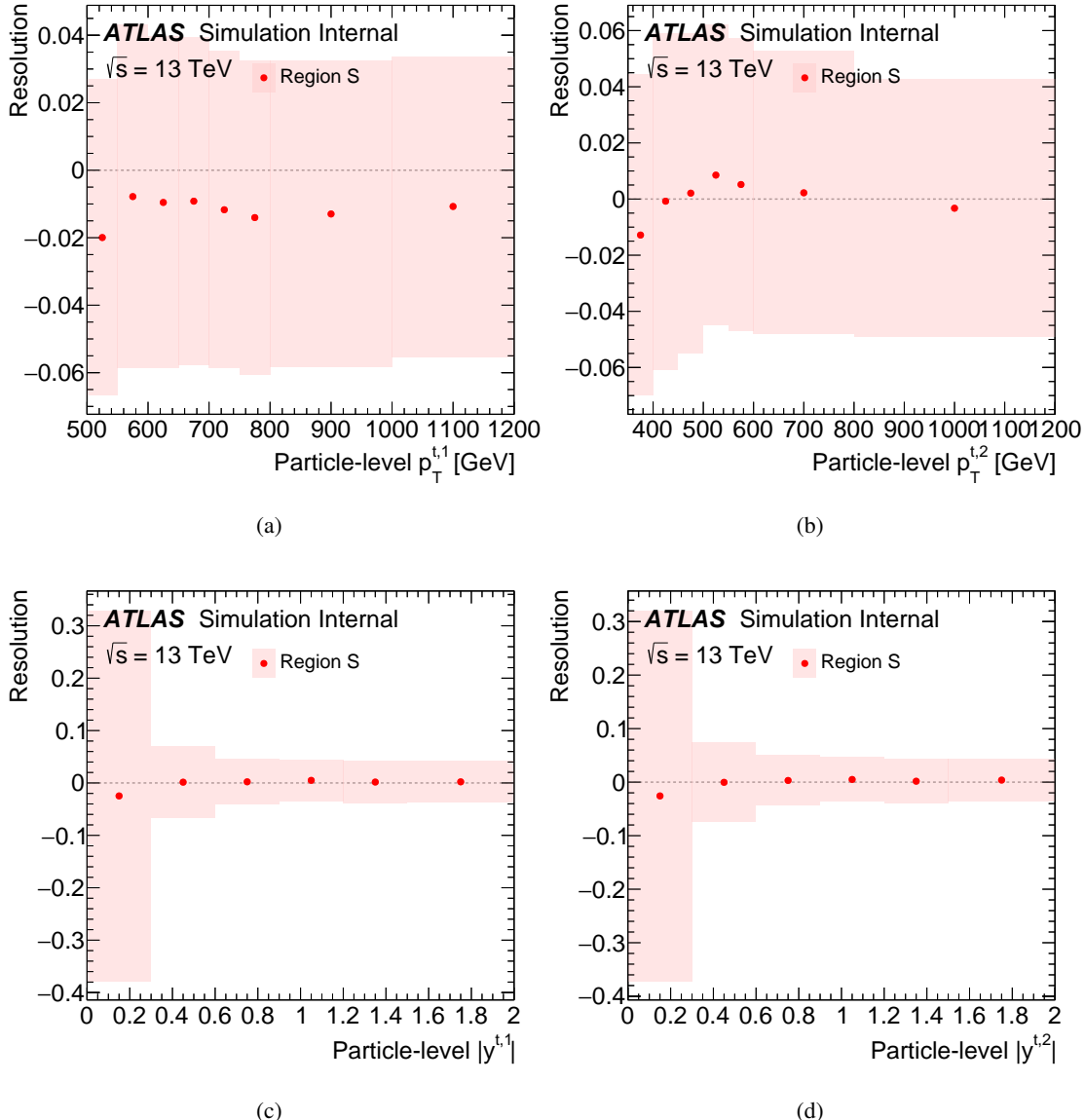


Figure 59: Fiducial phase-space resolution of (a) transverse momentum and (c) absolute value of the rapidity of the leading top-quark, and (b) transverse momentum and (d) absolute value of the rapidity of the second-leading top-quark. The points represent the mean of the distribution for a given range in the x-axis. The painted bands indicate the RMS of the distribution in each bin. The POWHEG+PYTHIA8 generator is used as the nominal prediction to correct for detector effects.

Not reviewed, for internal circulation only

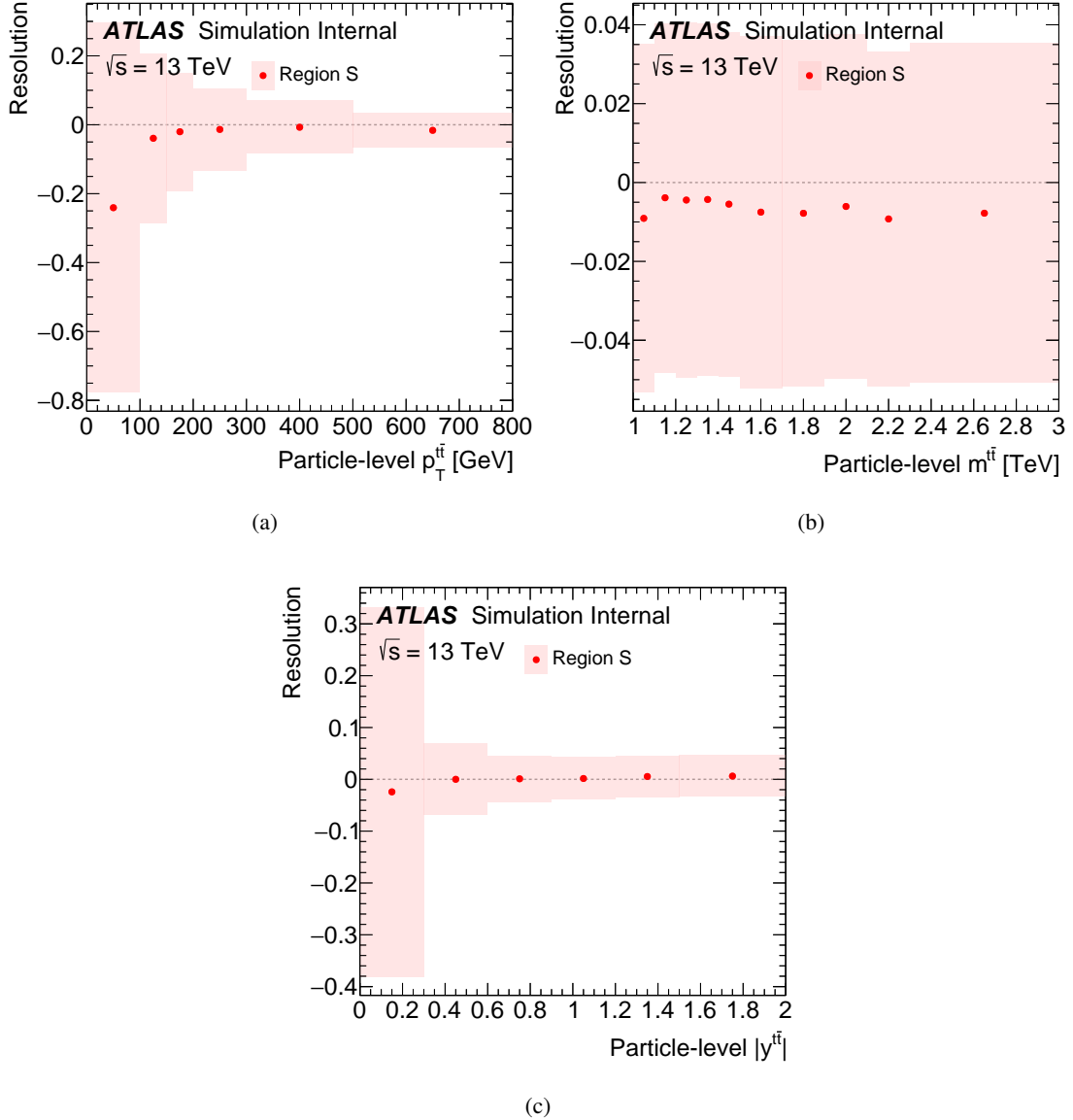


Figure 60: Fiducial phase-space resolution of (a) transverse momentum, (b) invariant mass and (c) absolute value of the rapidity of the $t\bar{t}$ system. The points represent the mean of the distribution for a give range in the x-axis. The painted bands indicate the RMS of the distribution in each bin. The PowHEG+PYTHIA8 generator is used as the nominal prediction to correct for detector effects.

Not reviewed, for internal circulation only

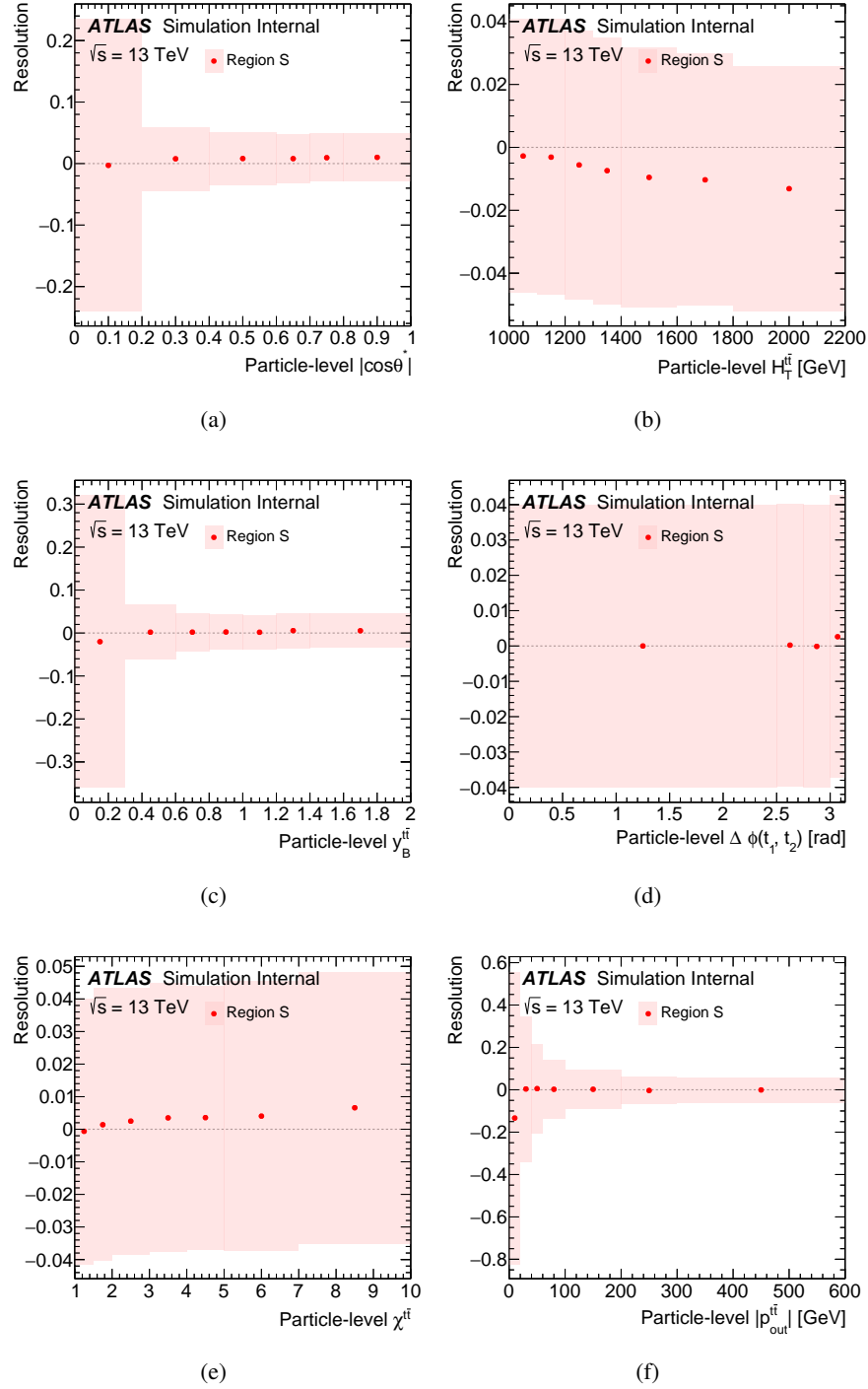


Figure 61: Fiducial phase-space resolution of (a) production angle in the Collins-Soper reference frame, (b) scalar sum of the two top-quarks' transverse momenta, (c) longitudinal boost $y_B^{t\bar{t}}$, (d) azimuthal angle between the two top-quarks $\Delta\phi_{t\bar{t}}$, (e) production angle $\chi^{t\bar{t}}$ and (f) absolute value of the out-of-plane momentum $p_{out}^{t\bar{t}}$. The points represent the mean of the distribution for a given range in the x-axis. The painted bands indicate the RMS of the distribution in each bin. The PowHEG+PYTHIA8 generator is used as the nominal prediction to correct for detector effects.

Not reviewed, for internal circulation only

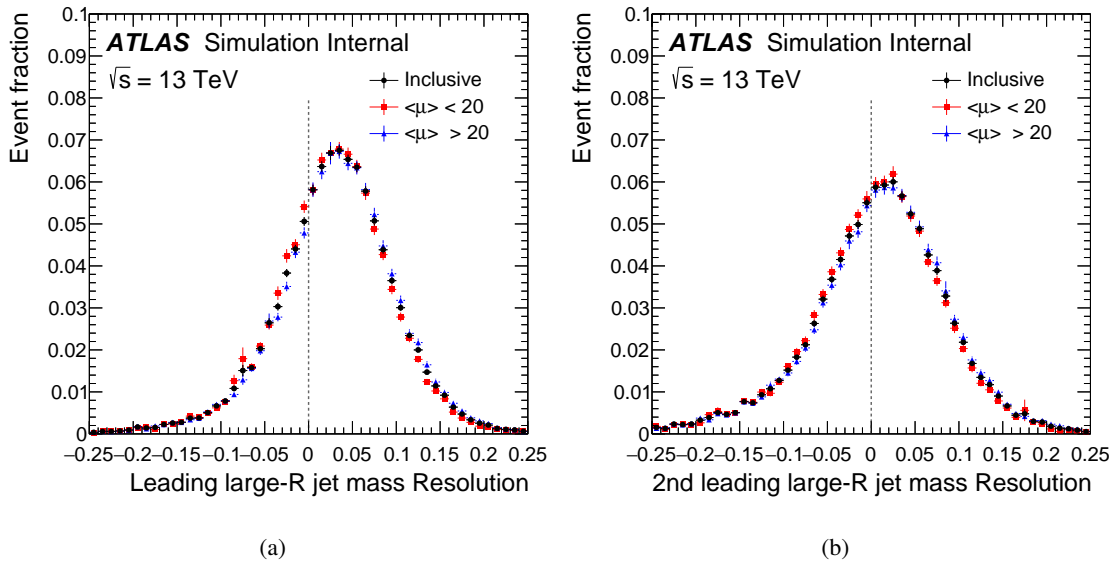


Figure 62: Mass resolution of the (a) leading and (b) second leading large- R jets. The distributions are normalized to unit area to facilitate the shape comparison.

920 F. Particle-level uncertainties after unfolding

921 F.1. Fractional uncertainties

922 To show visually the impact of the systematics for each observable, we grouped the systematics in broad
 923 groups and plotted their relative impact compared to the nominal prediction. The groups are defined as
 924 follows:

925 **Large- R Jet Energy Scale and Tagging** Baseline mass and pT calibration, modelling mass and pT cal-
 926 ibration, tracking mass and pT calibration, total statistics mass and pT calibration, sub-jettiness
 927 ratio τ_3/τ_2 calibration, modelling sub-jettiness ratio τ_3/τ_2 calibration, tracking sub-jettiness ratio
 928 τ_3/τ_2 calibration and total statistics sub-jettiness ratio τ_3/τ_2 calibration;

929 **Narrow Jet Energy Scale (21NPs)** b-Tagged jet energy scale, η intercalibration model, flavor composi-
 930 tion, flavor response, effective detector, effective mixed, effective model, effective statistical jet
 931 energy resolution, punch-through, single particle high- p_T , pile-up offset ρ topology and pile-up
 932 offset p_T ;

933 **Pileup** E_T^{miss} soft jet scale, E_T^{miss} soft jet resolution, jet reconstruction efficiency, jet vertex fraction, pile-
 934 up offset μ and pile-up offset N_{PV} ;

935 **Flavour tagging** b -tagging efficiency, c -tagging efficiency and light-flavor tagging efficiency;

936 **Leptons** Lepton trigger efficiency, lepton reconstruction efficiency, lepton identification efficiency, muon
 937 (ID) momentum resolution, muon momentum scale, muon (MS) momentum resolution, electron
 938 energy scale, and electron energy resolution;

939 **Background** Multijet background shape and statistics, single top cross-section and t -channel treatment;

940 **MC Modelling** MC sample statistics, hard scattering, hadronization, initial- and final-state radiation,
 941 parton distribution functions (PDF4LHC15).

942 Other smaller uncertainties (e.g., the background uncertainty) are not shown separately, but are included
 943 in the total uncertainty.

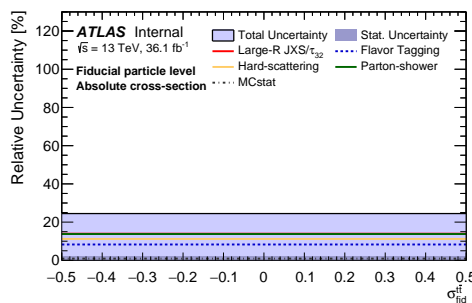


Figure 63: Fractional uncertainties for the absolute inclusive differential cross-sections in the fiducial phase-space.

Not reviewed, for internal circulation only

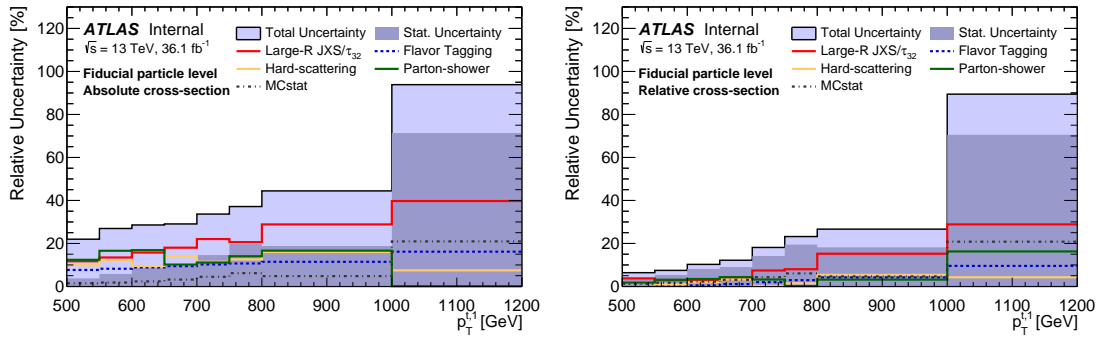


Figure 64: Fractional uncertainties for the absolute (left) and relative (right) differential cross-sections as a function of the leading top-quark transverse momentum in the fiducial phase-space.

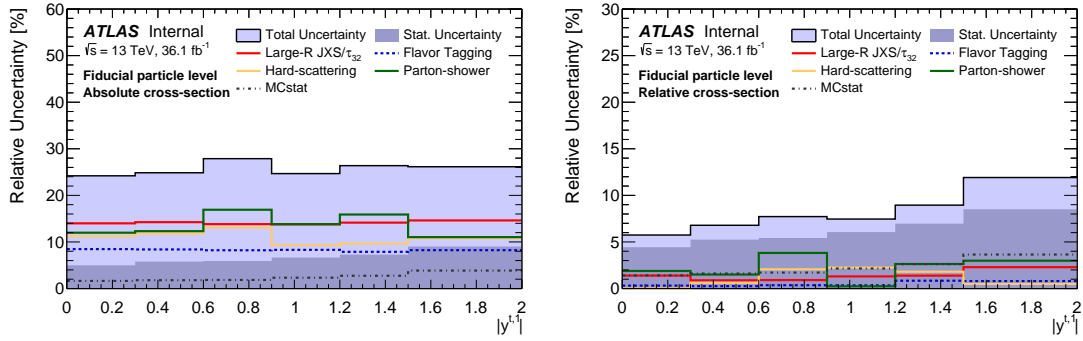


Figure 65: Fractional uncertainties for the absolute (left) and relative (right) differential cross-sections as a function of the leading top-quark rapidity in the fiducial phase-space.

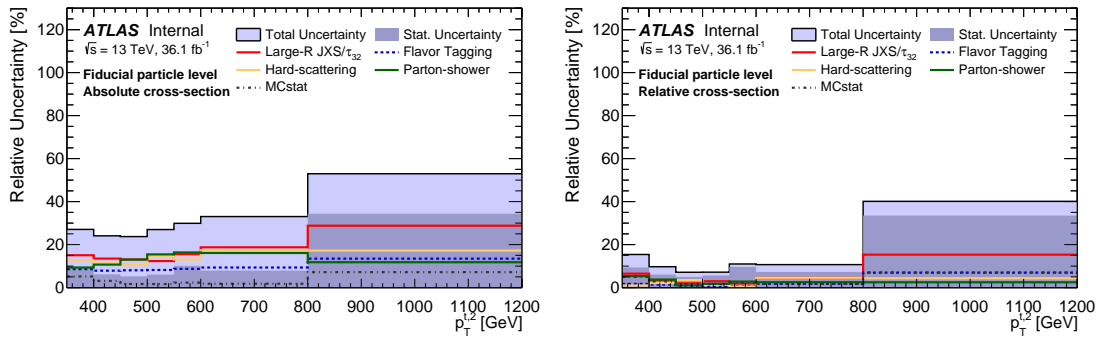


Figure 66: Fractional uncertainties for the absolute (left) and relative (right) differential cross-sections as a function of the 2nd leading top-quark transverse momentum in the fiducial phase-space.

Not reviewed, for internal circulation only

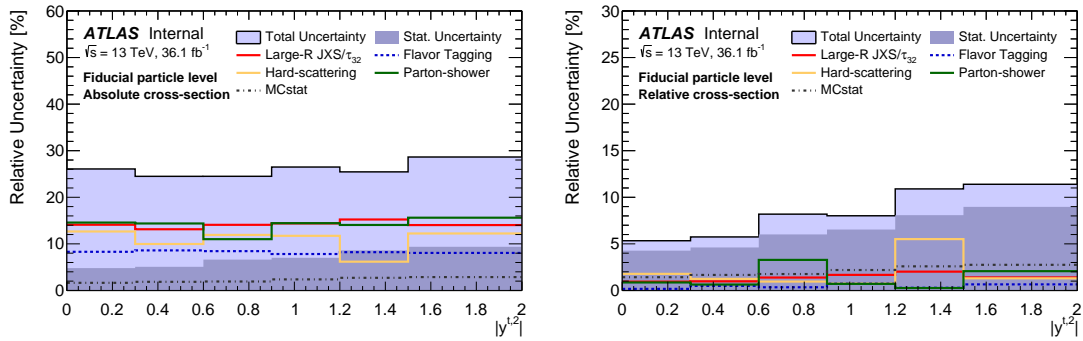


Figure 67: Fractional uncertainties for the absolute (left) and relative (right) differential cross-sections as a function of the 2nd leading top-quark rapidity in the fiducial phase-space.

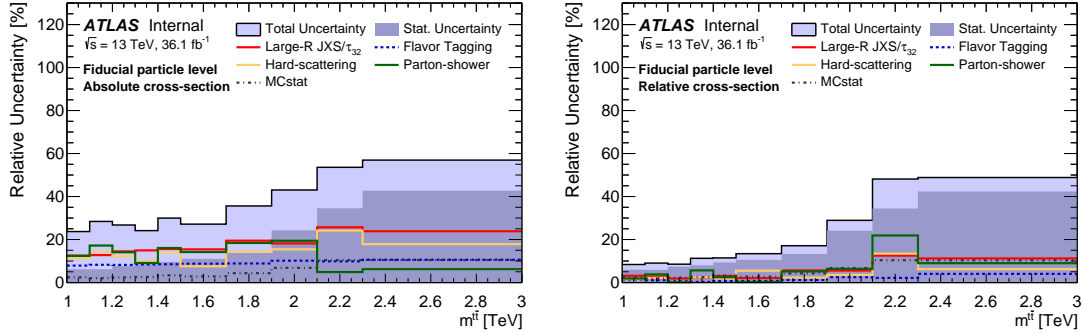


Figure 68: Fractional uncertainties for the absolute (left) and relative (right) differential cross-sections as a function of the top-antitop invariant mass in the fiducial phase-space.

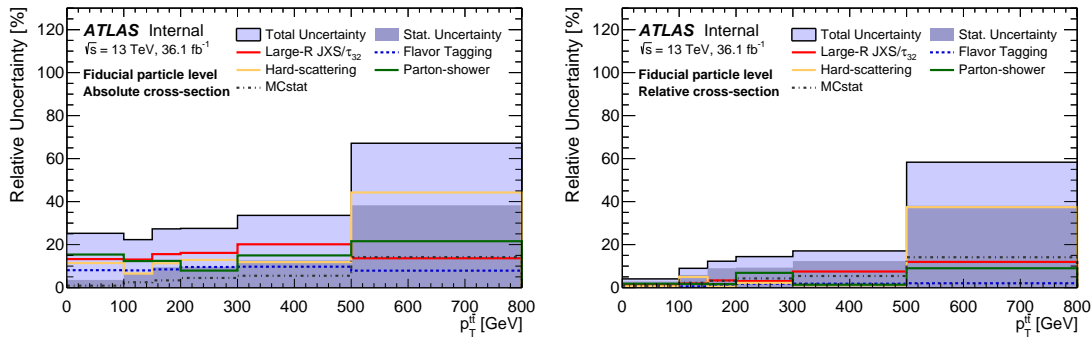


Figure 69: Fractional uncertainties for the absolute (left) and relative (right) differential cross-sections as a function of the top-antitop transverse momentum in the fiducial phase-space.

Not reviewed, for internal circulation only

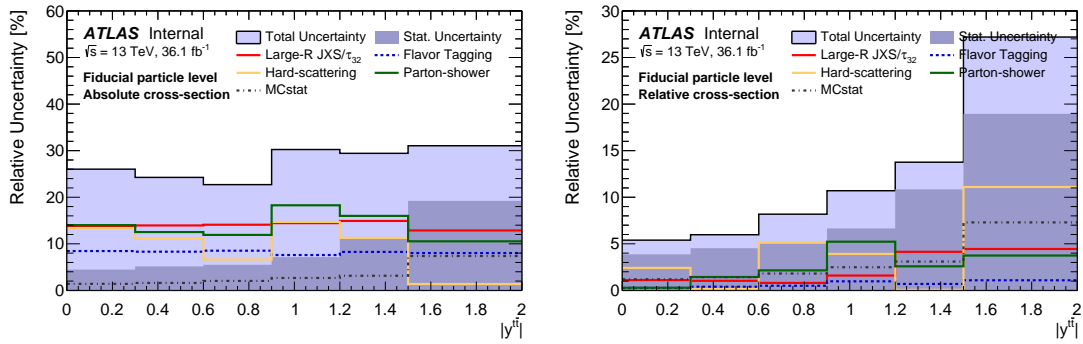


Figure 70: Fractional uncertainties for the absolute (left) and relative (right) differential cross-sections as a function of the top-antitop rapidity in the fiducial phase-space.

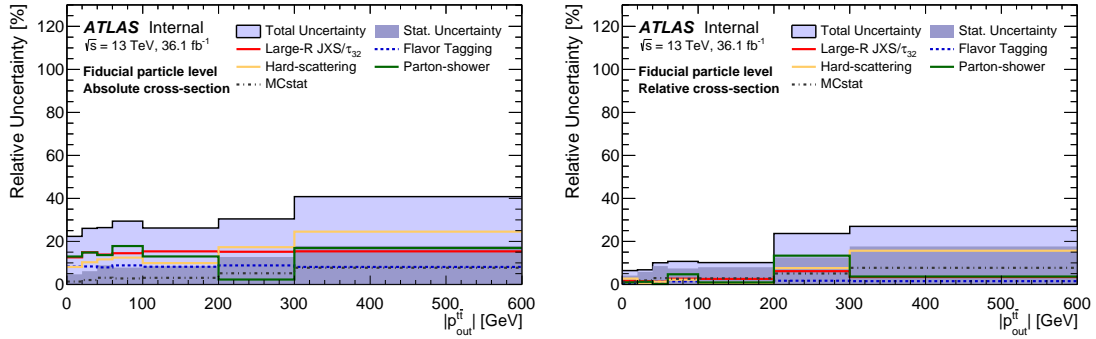


Figure 71: Fractional uncertainties for the absolute (left) and relative (right) differential cross-sections as a function of the top-antitop out-of-plane momentum $|p_{out}^{t\bar{t}}|$ in the fiducial phase-space.

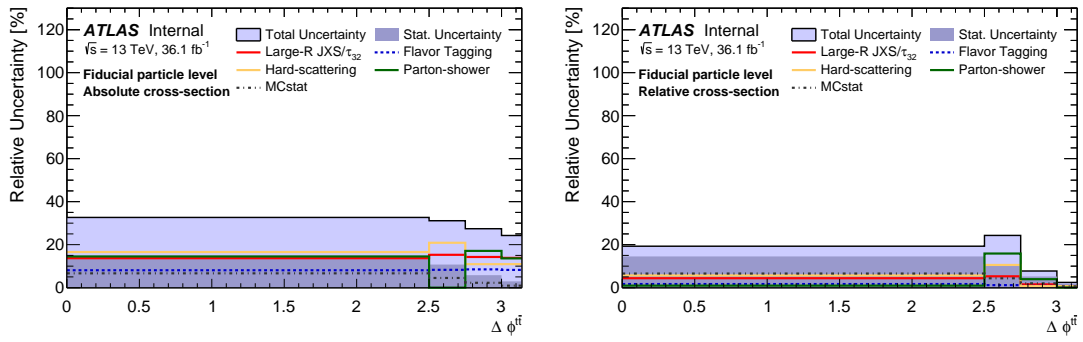


Figure 72: Fractional uncertainties for the absolute (left) and relative (right) differential cross-sections as a function of the top-antitop aperture $\Delta\phi^{t\bar{t}}$ in the fiducial phase-space.

Not reviewed, for internal circulation only

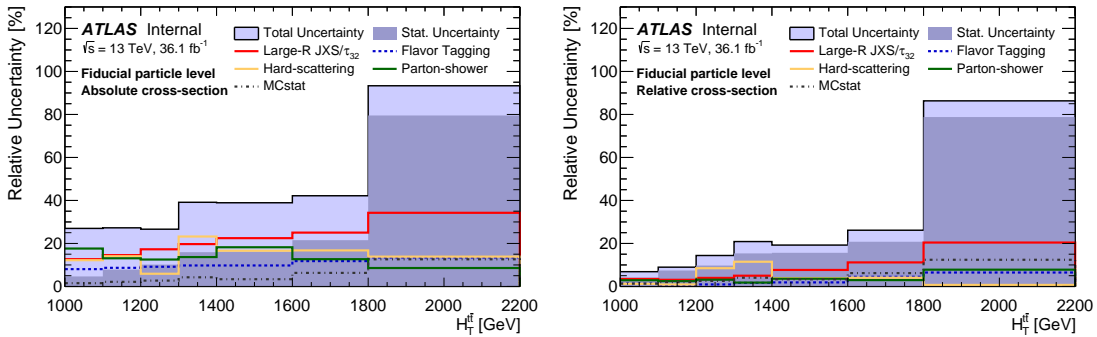


Figure 73: Fractional uncertainties for the absolute (left) and relative (right) differential cross-sections as a function of the scalar sum of the top quark and antiquark transverse momenta $H_T^{t\bar{t}}$ in the fiducial phase-space.

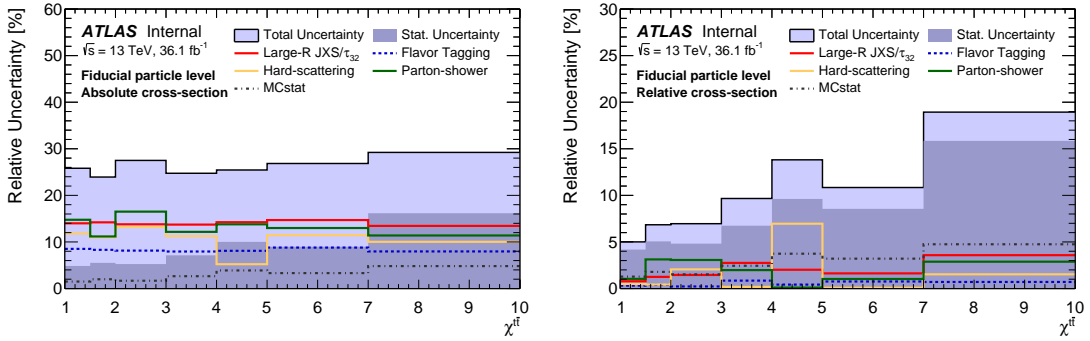


Figure 74: Fractional uncertainties for the absolute (left) and relative (right) differential cross-sections as a function of the top-quark and antiquark system $\chi^{t\bar{t}}$ in the fiducial phase-space.

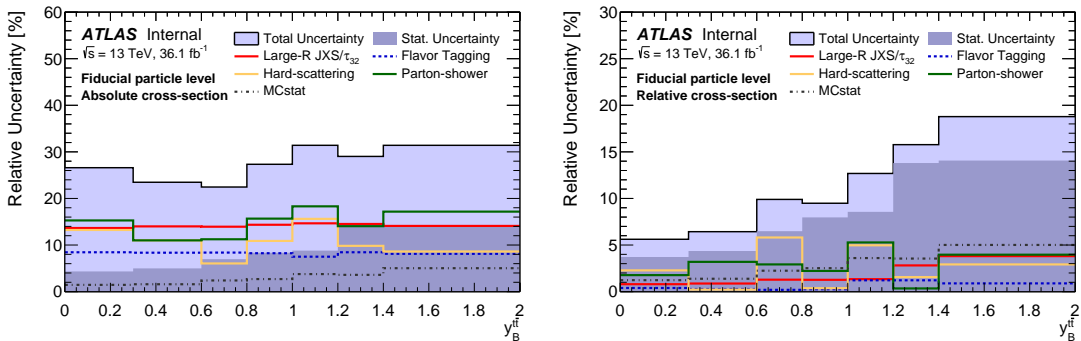


Figure 75: Fractional uncertainties for the absolute (left) and relative (right) differential cross-sections as a function of the top-quark and antiquark system longitudinal boost $y_B^{t\bar{t}}$ in the fiducial phase-space.

Not reviewed, for internal circulation only

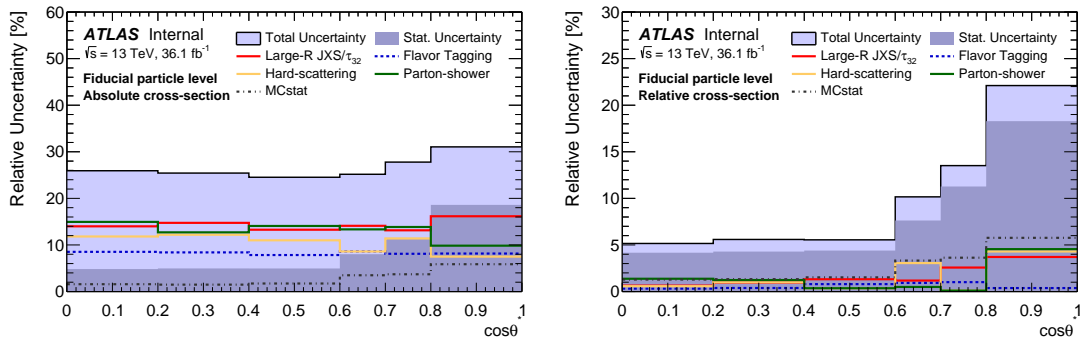


Figure 76: Fractional uncertainties for the absolute (left) and relative (right) differential cross-sections as a function of the top-quark and antiquark system $\cos\theta^*$ in the fiducial phase-space.

944 F.2. Statistical uncertainty of modelling systematics

945 The statistical uncertainty of the samples used to assess modelling systematic uncertainties is estimated
 946 using pseudo-experiments and compared to the statistical uncertainty of the nominal sample. Fig 77–89
 947 shows this comparison for the fiducial phase-space differential cross-sections.

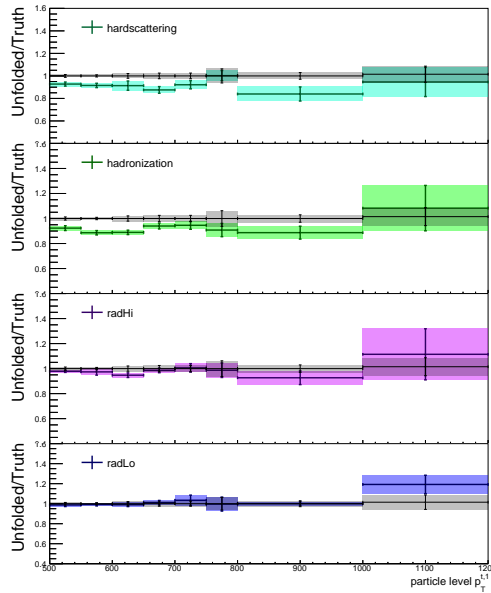


Figure 77: Statistical uncertainties of the samples used to assess modelling systematics for the absolute differential cross-sections as a function of the leading top-quark transverse momentum in the fiducial phase-space.

Not reviewed, for internal circulation only

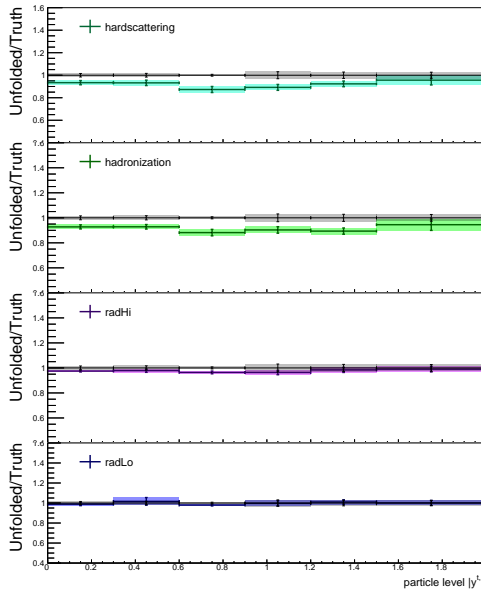


Figure 78: Statistical uncertainties of the samples used to assess modelling systematics for the absolute differential cross-sections as a function of the leading top-quark rapidity in the fiducial phase-space.

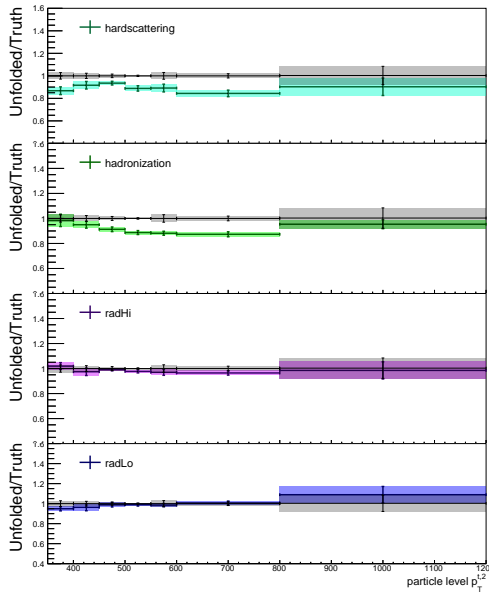


Figure 79: Statistical uncertainties of the samples used to assess modelling systematics for the absolute differential cross-sections as a function of the 2nd leading top-quark transverse momentum in the fiducial phase-space.

Not reviewed, for internal circulation only

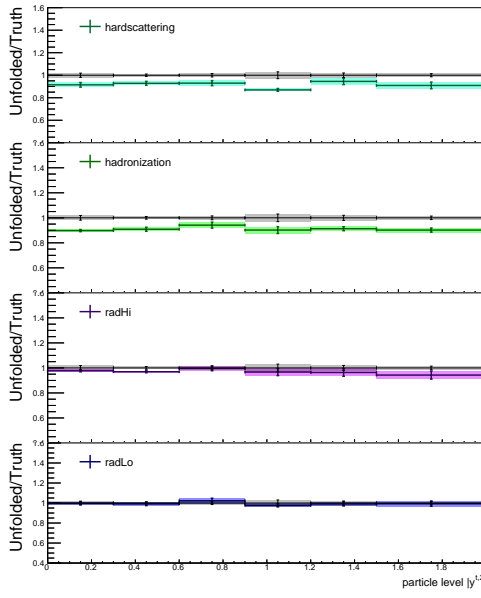


Figure 80: Statistical uncertainties of the samples used to assess modelling systematics for the absolute differential cross-sections as a function of the 2nd leading top-quark rapidity in the fiducial phase-space.

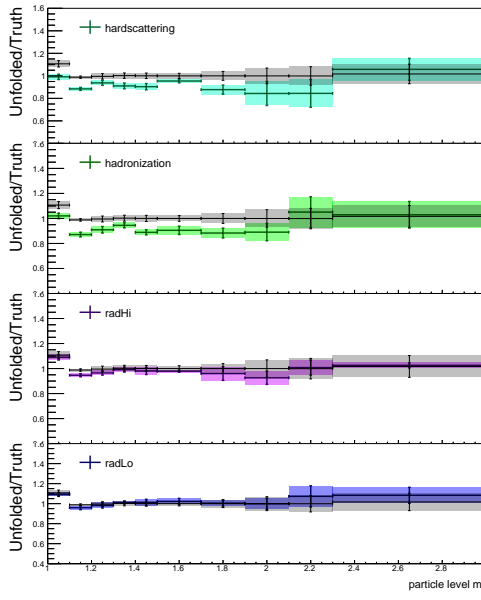


Figure 81: Statistical uncertainties of the samples used to assess modelling systematics for the absolute differential cross-sections as a function of the top-antitop invariant mass in the fiducial phase-space.

Not reviewed, for internal circulation only

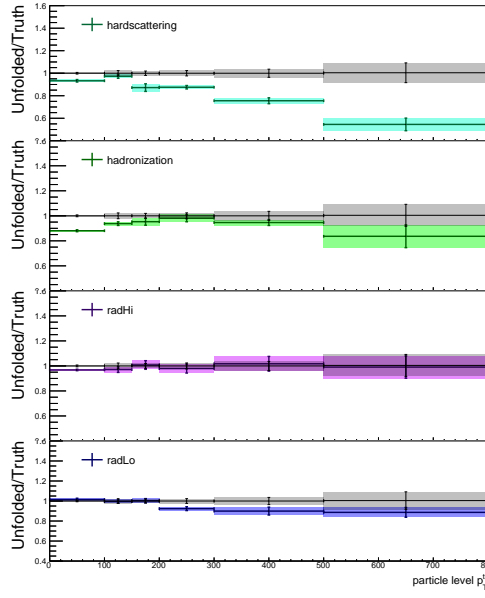


Figure 82: Statistical uncertainties of the samples used to assess modelling systematics for the absolute differential cross-sections as a function of the top-antitop transverse momentum in the fiducial phase-space.

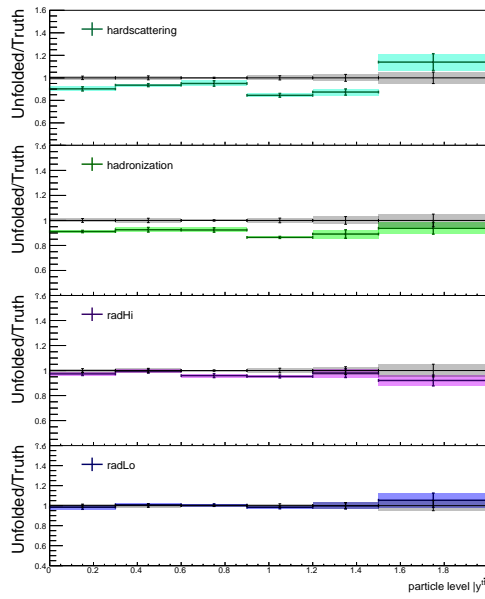


Figure 83: Statistical uncertainties of the samples used to assess modelling systematics for the absolute differential cross-sections as a function of the top-antitop rapidity in the fiducial phase-space.

Not reviewed, for internal circulation only

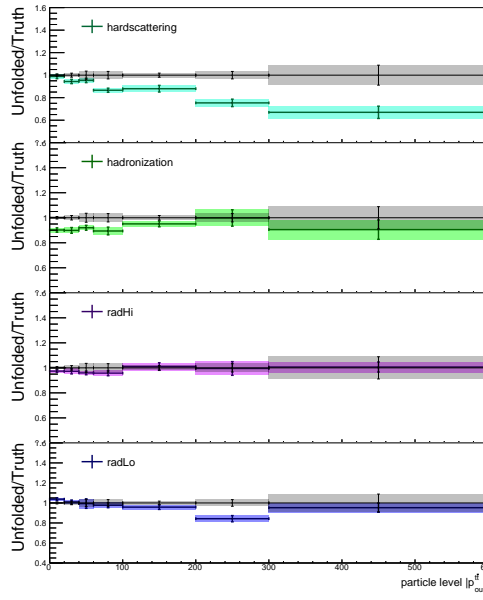


Figure 84: Statistical uncertainties of the samples used to assess modelling systematics for the absolute differential cross-sections as a function of the top-antitop out-of-plane momentum $|p_{out}^t|$ in the fiducial phase-space.

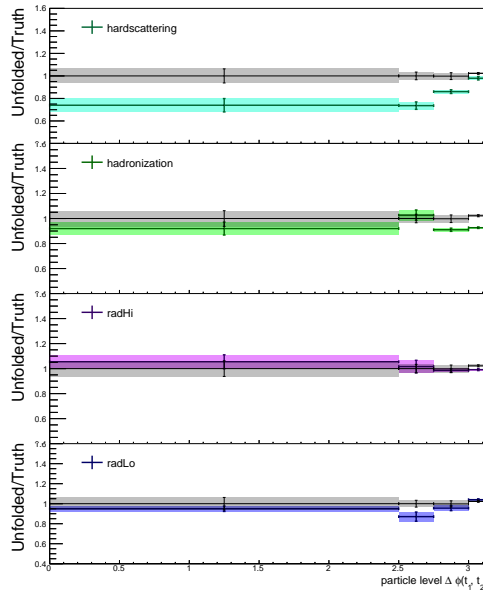


Figure 85: Statistical uncertainties of the samples used to assess modelling systematics for the absolute differential cross-sections as a function of the top-antitop aperture $\Delta\phi^{t\bar{t}}$ in the fiducial phase-space.

Not reviewed, for internal circulation only

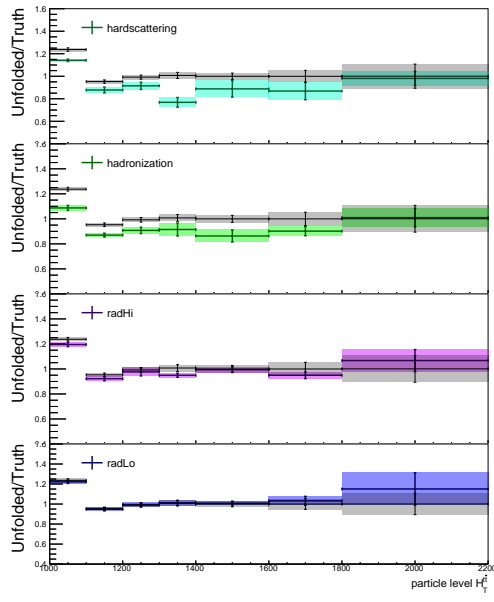


Figure 86: Statistical uncertainties of the samples used to assess modelling systematics for the absolute differential cross-sections as a function of the scalar sum of the top quark and antiquark transverse momenta $H_T^{t\bar{t}}$ in the fiducial phase-space.

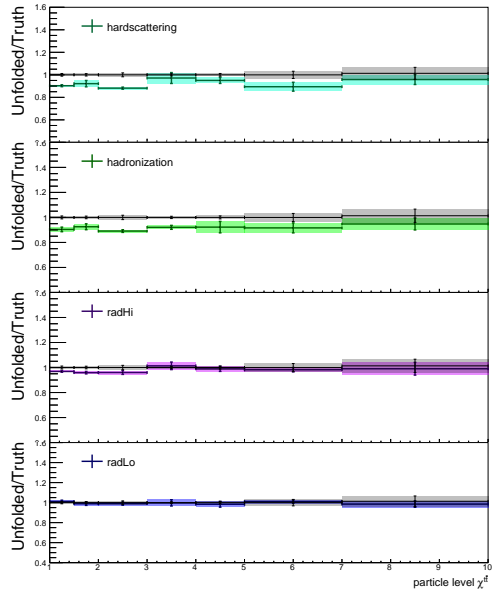


Figure 87: Statistical uncertainties of the samples used to assess modelling systematics for the absolute differential cross-sections as a function of the top-antitop $\chi_{\tilde{t}\tilde{t}}$ in the fiducial phase-space.

Not reviewed, for internal circulation only

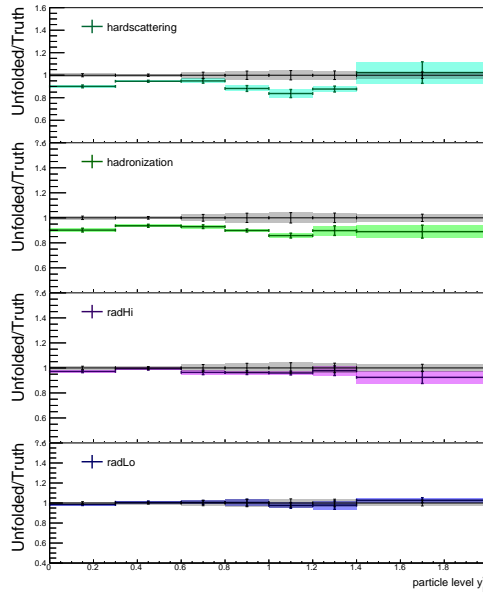


Figure 88: Statistical uncertainties of the samples used to assess modelling systematics for the absolute differential cross-sections as a function of the top-antitop longitudinal boost $y_B^{t\bar{t}}$ in the fiducial phase-space.

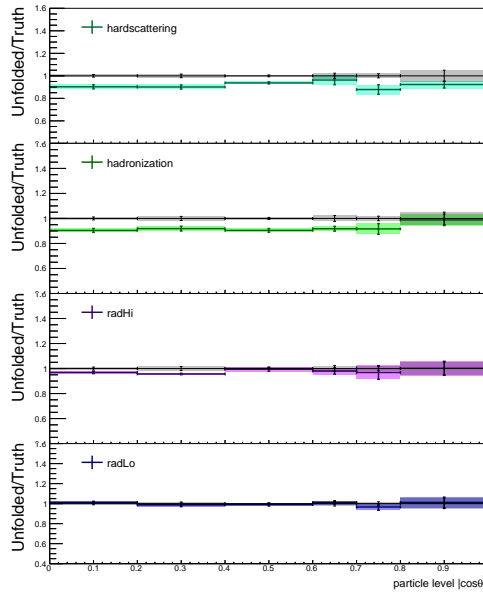


Figure 89: Statistical uncertainties of the samples used to assess modelling systematics for the absolute differential cross-sections as a function of the top-antitop $\cos \theta^*$ in the fiducial phase-space.

⁹⁴⁸ **F.3. Tables of systematic uncertainties**

⁹⁴⁹ **F.3.1. Summary tables**

$d\sigma / d\sigma_{fid}$ [pb/pb]	$2.917 \cdot 10^{-1}$
Total Uncertainty [%]	± 24.4
Statistics [%]	± 2.3
Systematics [%]	± 24.3
Luminosity [%]	± 2.01
Large- R jets JES [%]	± 5.91
Large- R jets JMS [%]	± 1.44
Large- R jets top-tagging [%]	± 12.5
Flavor tagging [%]	± 8.29
Narrow jets [%]	$^{+0.33}_{-0.21}$
Pile-up [%]	± 0.55
Background [%]	± 0.89
(MOD) Monte Carlo sample statistics [%]	± 0.90
(MOD) ISR/FSR + scale [%]	± 1.13
(MOD) Alternative hard-scattering model [%]	∓ 11.2
(MOD) Alternative parton-shower model [%]	∓ 13.7

Table 13: Summary of systematic uncertainties in the fiducial phase-space absolute inclusive cross-sections calculated as a percentage of the cross-section. Dashes are used when the estimated relative systematic uncertainty is below 0.1%.

Not reviewed, for internal circulation only

$d\sigma / dp_T^{t,\dagger}$ [pb/GeV]	$2.236 \cdot 10^{-3}$	$1.280 \cdot 10^{-3}$	$7.177 \cdot 10^{-4}$	$6.111 \cdot 10^{-4}$	$3.146 \cdot 10^{-4}$	$1.985 \cdot 10^{-4}$	$8.196 \cdot 10^{-5}$	$1.560 \cdot 10^{-5}$
Total Uncertainty [%]	± 21.9	± 26.9	± 28.6	± 29.1	± 33.6	± 37.1	± 44.4	± 93.8
Statistics [%]	± 3.7	± 5.8	± 8.6	± 9.4	$\pm 14.$	$\pm 19.$	$\pm 18.$	$\pm 71.$
Systematics [%]	± 21.5	± 26.1	± 26.9	± 27.1	± 29.6	± 30.4	± 39.7	± 50.2
Luminosity [%]	± 1.97	± 2.04	± 2.02	± 2.08	± 2.11	± 2.05	± 1.94	± 2.18
Large- R jets JES [%]	± 5.04	± 5.37	± 6.81	± 8.54	± 8.62	± 6.00	± 21.2	± 6.19
Large- R jets JMS [%]	± 0.95	± 2.49	± 2.98	± 0.41	± 1.69	± 2.01	± 0.66	± 11.3
Large- R jets top-tagging [%]	± 10.5	± 12.1	± 13.8	± 16.4	± 20.1	± 19.8	± 22.1	± 35.6
Flavor tagging [%]	± 7.67	± 8.23	± 8.84	± 9.43	± 10.2	± 10.6	± 11.4	± 16.1
Narrow jets [%]	± 0.21	± 0.51	± 0.47	± 0.40	± 0.39	± 0.29	± 0.68	± 0.51
Pile-up [%]	± 0.15	± 0.12	± 0.27	± 0.85	± 0.89	± 0.30	± 1.38	± 12.9
Background [%]	± 1.83	± 2.02	± 2.71	± 2.87	± 4.21	± 5.29	± 4.85	± 27.4
(MOD) Monte Carlo sample statistics [%]	± 1.46	± 1.81	± 2.34	± 3.19	± 4.47	± 6.17	± 4.80	± 20.9
(MOD) ISR/FSR + scale [%]	± 2.34	± 1.62	± 3.79	± 0.75	± 3.64	± 2.06	± 6.77	± 20.5
(MOD) Alternative hard-scattering model [%]	∓ 9.88	∓ 12.1	∓ 9.52	∓ 14.1	∓ 11.5	∓ 12.5	∓ 16.0	∓ 7.47
(MOD) Alternative parton-shower model [%]	± 12.3	± 16.5	± 16.8	± 10.1	± 11.1	± 14.0	± 16.6	± 0.11

Table 14: Summary of systematic uncertainties in the fiducial phase-space absolute differential cross-sections for the leading top-quark transverse momentum calculated as a percentage of the cross-section in each bin. Dashes are used when the estimated relative systematic uncertainty for that bin is below 0.1%.

$1/\sigma \cdot d\sigma / dp_T^{t,\dagger}$	$7.781 \cdot 10^{-3}$	$4.452 \cdot 10^{-3}$	$2.497 \cdot 10^{-3}$	$2.126 \cdot 10^{-3}$	$1.095 \cdot 10^{-3}$	$6.908 \cdot 10^{-4}$	$2.852 \cdot 10^{-4}$	$5.426 \cdot 10^{-5}$
Total Uncertainty [%]	± 6.40	± 7.46	± 10.2	± 12.2	± 18.0	± 23.1	± 26.6	± 89.3
Statistics [%]	± 3.6	± 5.3	± 8.1	± 9.0	$\pm 14.$	$\pm 19.$	$\pm 18.$	$\pm 70.$
Systematics [%]	± 4.80	± 4.48	± 5.12	± 7.06	± 9.62	± 9.70	± 18.1	± 42.9
Luminosity [%]	-	-	-	-	-	-	-	± 0.16
Large- R jets JES [%]	± 2.26	± 1.96	± 0.92	± 1.98	± 3.20	± 4.63	± 14.8	± 11.6
Large- R jets JMS [%]	± 0.73	± 1.29	± 1.62	± 1.06	± 1.66	± 1.88	± 1.55	± 13.9
Large- R jets top-tagging [%]	± 3.65	± 0.81	± 0.78	± 2.15	± 6.44	± 4.90	± 9.59	± 22.4
Flavor tagging [%]	± 2.69	± 2.23	± 1.15	± 3.45	± 6.44	± 2.15	± 7.23	± 22.4
Narrow jets [%]	± 1.46	± 0.73	± 0.48	± 1.08	± 1.97	± 2.92	± 4.19	± 9.54
Pile-up [%]	± 0.14	± 0.20	± 0.12	± 0.59	± 0.61	± 0.18	± 0.33	± 0.44
Background [%]	± 1.80	± 2.02	± 2.70	± 2.86	± 4.21	± 5.29	± 4.83	± 27.4
(MOD) Monte Carlo sample statistics [%]	± 1.27	± 1.70	± 2.23	± 3.07	± 4.32	± 6.06	± 4.69	± 20.8
(MOD) ISR/FSR + scale [%]	± 0.11	± 0.44	± 0.23	± 1.95	± 4.53	± 2.87	± 5.98	± 21.6
(MOD) Alternative hard-scattering model [%]	± 1.55	± 0.96	± 1.95	∓ 3.27	∓ 0.27	∓ 1.48	∓ 5.38	± 4.26
(MOD) Alternative parton-shower model [%]	± 1.76	± 3.11	± 3.46	± 4.34	± 3.22	± 0.16	± 3.18	± 16.2

Table 15: Summary of systematic uncertainties in the fiducial phase-space relative differential cross-sections for the leading top-quark transverse momentum calculated as a percentage of the cross-section in each bin. Dashes are used when the estimated relative systematic uncertainty for that bin is below 0.1%.

$d\sigma / d y^{t,1} $ [pb/Unit $ y^{t,1} $]	$2.372 \cdot 10^{-1}$	$2.085 \cdot 10^{-1}$	$1.772 \cdot 10^{-1}$	$1.507 \cdot 10^{-1}$	$1.089 \cdot 10^{-1}$	$5.463 \cdot 10^{-2}$
Total Uncertainty [%]	± 24.1	± 24.8	± 27.9	± 24.6	± 26.4	± 26.1
Statistics [%]	± 4.9	± 5.7	± 5.8	± 6.6	± 7.2	± 9.0
Systematics [%]	± 23.5	± 23.9	± 27.0	± 23.5	± 25.0	± 23.8
Luminosity [%]	± 2.01	± 1.97	± 2.01	± 2.04	± 1.97	± 1.99
Large- R jets JES [%]	± 5.40	± 6.53	± 5.70	± 5.50	± 6.50	± 6.64
Large- R jets JMS [%]	± 1.43	± 1.48	± 1.68	± 2.23	± 1.16	± 2.04
Large- R jets top-tagging [%]	± 12.8	± 12.6	± 12.4	± 12.4	± 12.4	± 12.8
Flavor tagging [%]	± 8.46	± 8.38	± 8.21	± 8.29	± 7.87	± 8.22
Narrow jets [%]	$+0.31$ -0.13	± 0.33	$+0.47$ -0.24	± 0.26 -0.16	$+0.27$ -0.20	$+0.41$ -0.69
Pile-up [%]	$+0.92$ -0.52	$+0.60$ -0.87	$+0.29$ -0.45	± 0.47	$+1.13$ -1.59	$+0.28$ -0.58
Background [%]	± 1.94	± 2.40	± 1.92	± 2.12	± 2.58	± 4.61
(MOD) Monte Carlo sample statistics [%]	± 1.62	± 1.78	± 1.84	± 2.32	± 2.73	± 3.85
(MOD) ISR/FSR + scale [%]	± 2.32	-0.59 $+1.29$	± 2.97	± 2.60	∓ 0.30	± 1.30
(MOD) Alternative hard-scattering model [%]	∓ 11.2	∓ 11.7	∓ 13.0	∓ 9.25	∓ 9.64	∓ 10.8
(MOD) Alternative parton-shower model [%]	∓ 11.9	∓ 12.3	∓ 16.9	∓ 13.8	∓ 15.8	∓ 11.0

Table 16: Summary of systematic uncertainties in the fiducial phase-space absolute differential cross-sections for the leading top-quark absolute value of the rapidity calculated as a percentage of the cross-section in each bin. Dashes are used when the estimated relative systematic uncertainty for that bin is below 0.1%.

$1/\sigma \cdot d\sigma / d y^{t,1} $	$8.123 \cdot 10^{-1}$	$7.139 \cdot 10^{-1}$	$6.067 \cdot 10^{-1}$	$5.158 \cdot 10^{-1}$	$3.728 \cdot 10^{-1}$	$1.871 \cdot 10^{-1}$
Total Uncertainty [%]	± 5.74	± 6.79	± 7.71	± 7.45	± 8.95	± 11.9
Statistics [%]	± 4.4	± 5.2	± 5.4	± 6.0	± 6.9	± 8.5
Systematics [%]	± 2.76	± 3.20	± 4.86	± 3.13	± 4.25	± 5.91
Luminosity [%]	-	-	-	-	-	-
Large- R jets JES [%]	± 0.60	± 0.70	$+0.43$ -0.31	± 0.61	± 0.88	± 0.94
Large- R jets JMS [%]	$+0.54$ -0.74	± 0.41	$+0.58$ -0.93	± 0.89	± 0.91	± 1.70
Large- R jets top-tagging [%]	± 1.06	± 0.32	± 0.29	± 0.71	± 0.53	± 1.19
Flavor tagging [%]	± 0.31	± 0.24	± 0.35	± 0.33	± 0.83	± 0.79
Narrow jets [%]	-	± 0.13	$+0.14$	$+0.16$	± 0.12	± 0.47
Pile-up [%]	± 0.34	- 0.33	- 0.28	$+0.67$ -0.11	$+0.55$ -1.06	$+0.83$ -1.15
Background [%]	± 1.92	± 2.39	± 1.92	± 2.11	± 2.56	± 4.61
(MOD) Monte Carlo sample statistics [%]	± 1.41	± 1.60	± 1.71	± 2.15	± 2.61	± 3.64
(MOD) ISR/FSR + scale [%]	$+0.48$ -1.21	± 2.44	± 1.86	± 1.57	± 1.46	$+0.94$ -0.18
(MOD) Alternative hard-scattering model [%]	-	∓ 0.61	∓ 2.06	∓ 2.24	∓ 1.80	∓ 0.49
(MOD) Alternative parton-shower model [%]	± 1.88	± 1.50	∓ 3.81	∓ 0.23	∓ 2.63	± 2.98

Table 17: Summary of systematic uncertainties in the fiducial phase-space relative differential cross-sections for the leading top-quark absolute value of the rapidity calculated as a percentage of the cross-section in each bin. Dashes are used when the estimated relative systematic uncertainty for that bin is below 0.1%.

$d\sigma / dp_T^{t,2}$ [pb/GeV]	$4.757 \cdot 10^{-4}$	$9.169 \cdot 10^{-4}$	$1.341 \cdot 10^{-3}$	$1.199 \cdot 10^{-3}$	$6.307 \cdot 10^{-4}$	$2.449 \cdot 10^{-4}$	$2.045 \cdot 10^{-5}$
Total Uncertainty [%]	± 27.0	± 24.1	± 23.6	± 26.9	± 29.9	± 33.0	± 52.9
Statistics [%]	± 9.6	± 6.1	± 5.2	± 6.0	$\pm 10.$	± 7.9	$\pm 34.$
Systematics [%]	± 23.8	± 22.8	± 23.0	± 26.1	± 27.9	± 31.9	± 38.6
Luminosity [%]	± 2.10	± 1.99	± 2.02	± 2.00	± 1.99	± 1.97	± 1.93
Large- R jets JES [%]	± 5.80	± 6.97	± 5.96	± 4.76	± 5.99	± 7.28	± 15.2
Large- R jets JMS [%]	± 7.12 $^{+1.51}_{-1.03}$		± 1.62	± 1.12	± 1.40	± 0.38	± 3.40
Large- R jets top-tagging [%]	± 13.5 $^{+11.4}_{-10.1}$		± 11.5	± 11.2	± 14.2	± 17.2	± 24.1
Flavor tagging [%]	± 8.58	± 7.86	± 8.05	± 8.20	± 8.71	± 9.34	± 13.4
Narrow jets [%]	± 0.40	± 0.33	± 0.34	± 0.35	± 0.35	± 0.22	± 0.96
Pile-up [%]	± 0.67 $^{+0.58}_{-0.73}$	± 0.34	± 0.23	± 0.13	± 0.25	± 0.93 $^{+0.03}_{-1.52}$	± 4.03
Background [%]	± 6.78	± 3.65	± 1.98	± 1.77	± 2.57	± 1.82	± 9.09
(MOD) Monte Carlo sample statistics [%]	± 5.17	± 3.13	± 1.67	± 1.65	± 2.31	± 1.80	± 7.19
(MOD) ISR/FSR + scale [%]	± 2.63	± 3.82	± 0.85 $^{+0.85}_{-1.97}$	± 2.27	± 3.06	± 1.98	± 3.60
(MOD) Alternative hard-scattering model [%]	∓ 12.6	∓ 11.6	∓ 10.4	∓ 14.5	∓ 13.0	∓ 17.4	∓ 17.2
(MOD) Alternative parton-shower model [%]	∓ 9.34	∓ 10.7	∓ 13.0	∓ 15.4	∓ 16.3	∓ 16.1	∓ 11.7

Table 18: Summary of systematic uncertainties in the fiducial phase-space absolute differential cross-sections for the 2nd leading top-quark transverse momentum calculated as a percentage of the cross-section in each bin. Dashes are used when the estimated relative systematic uncertainty for that bin is below 0.1%.

$1/\sigma \cdot d\sigma / dp_T^{t,2}$	$1.667 \cdot 10^{-3}$	$3.214 \cdot 10^{-3}$	$4.701 \cdot 10^{-3}$	$4.201 \cdot 10^{-3}$	$2.211 \cdot 10^{-3}$	$8.583 \cdot 10^{-4}$	$7.168 \cdot 10^{-5}$
Total Uncertainty [%]	± 15.4	± 9.71	± 7.13	± 7.17	± 10.9	± 10.7	± 40.1
Statistics [%]	± 9.3	± 6.0	± 4.9	± 5.6	± 9.6	± 7.3	$\pm 33.$
Systematics [%]	± 8.89	± 5.98	± 4.46	± 3.78	± 3.96	± 7.38	± 18.8
Luminosity [%]	-	-	-	-	-	-	-
Large- R jets JES [%]	± 1.65	± 1.97 $^{+1.45}_{-1.45}$	± 0.93	± 2.17	± 1.26	± 1.39 $^{+1.39}_{-1.83}$	± 10.2
Large- R jets JMS [%]	± 5.95	± 2.33	± 0.40	± 0.38	± 0.33 $^{+0.33}_{-0.49}$	± 1.48	± 2.38
Large- R jets top-tagging [%]	± 2.71 $^{+2.71}_{-0.46}$	± 1.32 $^{+1.32}_{-2.22}$	± 1.41 $^{+1.41}_{-2.05}$	± 1.97	± 0.80 $^{+0.80}_{-1.31}$	± 3.92 $^{+9.02}_{-13.0}$	-
Flavor tagging [%]	± 1.73	± 1.42	± 0.90	± 0.72	± 0.57	± 1.77	± 6.95
Narrow jets [%]	± 0.29	± 0.19	± 0.11	-	-	± 0.11	± 0.72
Pile-up [%]	± 0.49 $^{+0.32}_{-0.17}$	± 0.14 $^{+0.22}_{-0.31}$	-	± 0.44	± 1.87 $^{+1.87}_{-0.65}$	± 0.27 $^{+0.27}_{-0.94}$	± 3.35 $^{+3.35}_{-0.93}$
Background [%]	± 6.77	± 3.64	± 1.97	± 1.75	± 2.57	± 1.81	± 9.07
(MOD) Monte Carlo sample statistics [%]	± 4.95	± 2.88	± 1.59	± 1.55	± 2.24	± 1.74	± 7.02
(MOD) ISR/FSR + scale [%]	± 2.77 $^{+2.77}_{-0.83}$	± 1.77	± 1.25	± 0.31	± 0.99	± 1.48	± 5.81
(MOD) Alternative hard-scattering model [%]	± 0.97	± 2.11	± 3.49	± 1.23	± 0.45	± 4.56	± 4.33
(MOD) Alternative parton-shower model [%]	± 5.33	± 3.75	± 1.03	± 1.76	± 2.82	± 2.52	± 2.47

Table 19: Summary of systematic uncertainties in the fiducial phase-space relative differential cross-sections for the 2nd leading top-quark transverse momentum calculated as a percentage of the cross-section in each bin. Dashes are used when the estimated relative systematic uncertainty for that bin is below 0.1%.

$d\sigma / d y^{t,2} $ [pb/ Unit $ y^{t,2} $]	$2.475 \cdot 10^{-1}$	$2.390 \cdot 10^{-1}$	$1.727 \cdot 10^{-1}$	$1.393 \cdot 10^{-1}$	$1.029 \cdot 10^{-1}$	$4.222 \cdot 10^{-2}$
Total Uncertainty [%]	± 26.0	± 24.4	± 24.4	± 26.4	± 25.4	± 28.6
Statistics [%]	± 4.7	± 5.0	± 6.6	± 7.0	± 8.6	± 9.3
Systematics [%]	± 25.5	± 23.8	± 23.4	± 25.2	± 23.6	± 26.6
Luminosity [%]	± 2.04	± 2.03	± 1.99	± 1.94	± 2.02	± 1.97
Large- R jets JES [%]	± 5.74	± 5.56	± 6.09	± 6.04	$^{+7.65}_{-5.83}$	± 6.12
Large- R jets JMS [%]	± 2.14	± 1.38	$^{+0.60}_{-0.83}$	± 2.18	± 1.31	± 1.79
Large- R jets top-tagging [%]	± 12.7	± 11.8	± 12.6	$^{+14.5}_{-11.1}$	± 13.5	± 12.4
Flavor tagging [%]	± 8.29	± 8.59	± 8.43	± 7.81	± 8.21	± 8.05
Narrow jets [%]	$^{+0.29}_{-0.22}$	$^{+0.45}_{-0.33}$	$^{+0.33}_{-0.22}$	$^{+0.32}_{-0.14}$	± 0.23	$^{+0.43}_{-0.19}$
Pile-up [%]	± 0.71	± 0.23	$^{+0.35}_{-0.79}$	$^{+0.33}_{-0.23}$	$^{+1.12}_{-0.14}$	$^{+1.03}_{-1.83}$
Background [%]	± 1.68	± 2.17	± 2.51	± 2.42	± 2.85	± 3.46
(MOD) Monte Carlo sample statistics [%]	± 1.63	± 1.84	± 1.91	± 2.37	± 2.71	± 2.86
(MOD) ISR/FSR + scale [%]	± 1.07	± 1.87	± 1.73	± 3.54	± 2.20	± 4.21
(MOD) Alternative hard-scattering model [%]	∓ 12.6	∓ 9.97	∓ 11.9	∓ 11.7	∓ 6.17	∓ 12.2
(MOD) Alternative parton-shower model [%]	∓ 14.5	∓ 14.3	∓ 11.0	∓ 14.4	∓ 14.0	∓ 15.6

Table 20: Summary of systematic uncertainties in the fiducial phase-space absolute differential cross-sections for the leading top-quark absolute value of the rapidity calculated as a percentage of the cross-section in each bin. Dashes are used when the estimated relative systematic uncertainty for that bin is below 0.1%.

$1/\sigma \cdot d\sigma / d y^{t,2} $	$8.490 \cdot 10^{-1}$	$8.198 \cdot 10^{-1}$	$5.924 \cdot 10^{-1}$	$4.778 \cdot 10^{-1}$	$3.530 \cdot 10^{-1}$	$1.448 \cdot 10^{-1}$
Total Uncertainty [%]	± 5.33	± 5.74	± 8.18	± 8.01	± 10.9	± 11.3
Statistics [%]	± 4.2	± 4.6	± 6.0	± 6.5	± 8.0	± 8.9
Systematics [%]	± 2.33	± 2.05	± 4.64	± 3.29	± 6.22	± 5.45
Luminosity [%]	-	-	-	-	-	-
Large- R jets JES [%]	± 0.37	$^{+0.53}_{-0.28}$	± 0.78	$^{+0.33}_{-0.24}$	± 1.30	± 0.44
Large- R jets JMS [%]	$^{+0.63}_{-1.04}$	± 0.39	± 0.91	± 1.01	± 1.04	$^{+1.42}_{-0.77}$
Large- R jets top-tagging [%]	$^{+0.20}_{-0.14}$	$^{+0.53}_{-0.99}$	± 0.69	± 1.29	$^{+0.61}_{-1.46}$	± 0.71
Flavor tagging [%]	$^{+0.19}_{-0.14}$	± 0.48	± 0.33	± 0.78	$^{+0.24}_{-0.32}$	± 0.65
Narrow jets [%]	-	± 0.15	± 0.11	± 0.11	± 0.14	± 0.14
Pile-up [%]	$^{+0.10}_{-0.23}$	$^{+0.58}_{-0.32}$	± 0.29	± 0.29	± 0.56	$^{+0.46}_{-1.34}$
Background [%]	± 1.66	± 2.17	± 2.49	± 2.42	± 2.83	± 3.46
(MOD) Monte Carlo sample statistics [%]	± 1.42	± 1.66	± 1.76	± 2.19	± 2.58	± 2.75
(MOD) ISR/FSR + scale [%]	± 0.19	± 0.74	± 2.78	± 2.42	± 1.19	$^{+0.60}_{-3.23}$
(MOD) Alternative hard-scattering model [%]	∓ 1.77	∓ 1.24	∓ 0.95	∓ 0.73	± 5.51	∓ 1.30
(MOD) Alternative parton-shower model [%]	∓ 0.85	∓ 0.63	∓ 3.27	∓ 0.70	∓ 0.26	∓ 2.06

Table 21: Summary of systematic uncertainties in the fiducial phase-space relative differential cross-sections for the leading top-quark absolute value of the rapidity calculated as a percentage of the cross-section in each bin. Dashes are used when the estimated relative systematic uncertainty for that bin is below 0.1%.

$d\sigma / dm^H$ [pb/GeV]	$4.842 \cdot 10^{-1}$	$5.433 \cdot 10^{-1}$	$4.257 \cdot 10^{-1}$	$3.648 \cdot 10^{-1}$	$2.799 \cdot 10^{-1}$	$1.488 \cdot 10^{-1}$	$1.040 \cdot 10^{-1}$	$4.202 \cdot 10^{-2}$	$2.430 \cdot 10^{-2}$	$6.364 \cdot 10^{-3}$
Total Uncertainty [%]	± 23.6	± 28.4	± 26.7	± 24.1	± 29.9	± 27.1	± 35.6	± 43.0	± 53.5	± 56.9
Statistics [%]	± 6.1	± 6.1	± 7.6	± 8.4	± 9.6	$\pm 11.$	$\pm 13.$	$\pm 24.$	$\pm 34.$	$\pm 42.$
Systematics [%]	± 22.4	± 27.5	± 25.3	± 22.2	± 27.9	± 24.4	± 32.1	± 33.9	± 38.1	± 33.2
Luminosity [%]	± 2.00	± 1.99	± 2.00	± 2.03	± 1.99	± 1.92	± 1.96	± 1.99	± 2.15	± 1.93
Large- R jets JES [%]	± 7.46	± 4.47	± 6.24	± 5.67	± 8.30	± 6.23	± 8.42	± 9.24	± 10.8	± 12.8
Large- R jets JMS [%]	± 1.17	± 1.43	± 1.38	± 2.76	± 1.50	± 1.29	± 1.13	± 5.66	± 2.89	
Large- R jets top-tagging [%]	± 10.6	± 12.1	± 12.9	± 13.5	± 13.1	± 14.4	± 16.6	± 18.6	± 24.1	± 23.9
Flavor tagging [%]	± 7.87	± 8.25	± 8.18	± 8.41	± 8.48	± 8.77	± 8.86	± 10.1	± 9.84	± 10.6
Narrow jets [%]	± 0.28	± 0.32	± 0.26	± 0.31	± 0.45	± 0.36	± 0.24	± 0.30	± 0.43	± 0.65
Pile-up [%]	± 1.36	± 0.51	-	± 0.34	± 0.17	± 0.09	± 0.56	± 1.48	± 3.49	± 1.57
Background [%]	± 3.23	± 2.53	± 2.88	± 2.91	± 3.26	± 3.28	± 4.87	± 7.96	± 10.5	± 13.9
(MOD) Monte Carlo sample statistics [%]	± 2.44	± 2.00	± 2.39	± 2.59	± 3.33	± 2.85	± 4.34	± 6.82	± 10.4	± 10.4
(MOD) ISR/FSR + scale [%]	± 0.34	± 2.14	± 4.25	± 2.44	± 1.03	± 0.43	± 2.47	± 3.52	± 7.65	± 6.39
(MOD) Alternative hard-scattering model [%]	± 11.0	± 14.2	± 12.2	± 10.2	± 13.9	± 7.54	± 14.3	± 15.4	± 24.1	± 17.8
(MOD) Alternative parton-shower model [%]	± 12.3	± 17.2	± 14.0	± 9.10	± 16.0	± 14.1	± 18.3	± 19.4	± 4.87	± 6.21

Table 22: Summary of systematic uncertainties in the fiducial phase-space absolute differential cross-sections for the top quark-antiquark system invariant mass calculated as a percentage of the cross-section in each bin. Dashes are used when the estimated relative systematic uncertainty for that bin is below 0.1%.

$1/\sigma \cdot d\sigma / dm^H$	$1.741 \cdot 10^0$	$1.954 \cdot 10^0$	$1.531 \cdot 10^0$	$1.312 \cdot 10^0$	$1.007 \cdot 10^0$	$5.350 \cdot 10^{-1}$	$3.740 \cdot 10^{-1}$	$1.511 \cdot 10^{-1}$	$8.740 \cdot 10^{-2}$	$2.289 \cdot 10^{-2}$
Total Uncertainty [%]	± 8.38	± 9.03	± 8.52	± 11.2	± 11.4	± 13.4	± 17.1	± 28.9	± 48.1	± 48.8
Statistics [%]	± 5.9	± 5.8	± 7.3	± 8.0	± 9.3	$\pm 10.$	$\pm 13.$	$\pm 24.$	$\pm 34.$	$\pm 42.$
Systematics [%]	± 4.40	± 6.09	± 2.38	± 6.91	± 4.85	± 7.15	± 8.68	± 12.1	± 30.2	± 17.2
Luminosity [%]	-	-	-	-	-	-	-	-	± 0.15	-
Large- R jets JES [%]	± 1.60	± 2.91	± 1.75	± 1.37	± 1.80	± 1.31	± 2.35	± 4.43	± 4.56	± 7.12
Large- R jets JMS [%]	± 0.27	± 0.71	± 0.58	± 1.51	± 1.48	± 1.42	± 1.00	± 3.43	± 1.45	± 5.79
Large- R jets top-tagging [%]	± 2.54	± 0.99	± 0.45	± 0.38	± 0.63	± 1.14	± 3.87	± 4.28	± 7.23	± 9.03
Flavor tagging [%]	± 1.15	± 1.04	± 0.57	± 0.26	± 0.66	± 0.72	± 1.19	± 2.49	± 2.15	± 4.01
Narrow jets [%]	± 0.17	± 0.11	± 0.14	± 0.15	± 0.14	± 0.20	± 0.30	± 0.15	± 0.18	± 0.49
Pile-up [%]	± 0.66	-	± 0.62	± 0.91	± 0.88	± 0.18	± 0.13	± 0.92	± 2.92	± 1.01
Background [%]	± 3.18	± 2.47	± 2.83	± 2.85	± 3.20	± 3.23	± 4.79	± 7.81	± 10.3	± 13.7
(MOD) Monte Carlo sample statistics [%]	± 2.28	± 1.92	± 2.25	± 2.49	± 3.21	± 2.73	± 4.25	± 6.74	± 10.3	± 10.3
(MOD) ISR/FSR + scale [%]	± 1.34	± 0.86	± 3.00	± 1.16	± 2.03	± 1.77	± 3.81	± 2.57	± 6.73	± 3.21
(MOD) Alternative hard-scattering model [%]	± 1.47	± 2.16	± 0.11	± 2.41	± 1.84	± 5.50	± 2.28	± 3.51	± 13.4	± 6.23
(MOD) Alternative parton-shower model [%]	± 1.83	± 3.77	± 0.13	± 5.64	± 2.44	± 0.23	± 5.15	± 6.35	± 21.8	± 8.99

Table 23: Summary of systematic uncertainties in the fiducial phase-space relative differential cross-sections for the top quark-antiquark system invariant mass calculated as a percentage of the cross-section in each bin. Dashes are used when the estimated relative systematic uncertainty for that bin is below 0.1%.

$d\sigma / dp_T^{ff}$ [pb/GeV]	$1.512 \cdot 10^{-3}$	$1.165 \cdot 10^{-3}$	$6.129 \cdot 10^{-4}$	$3.162 \cdot 10^{-4}$	$8.644 \cdot 10^{-5}$	$5.602 \cdot 10^{-6}$
Total Uncertainty [%]	± 25.2	± 22.2	± 27.2	± 27.5	± 33.5	± 67.1
Statistics [%]	± 3.5	± 6.2	± 9.4	± 9.6	$\pm 12.$	$\pm 38.$
Systematics [%]	± 24.9	± 21.1	± 24.9	± 25.0	± 30.0	± 52.5
Luminosity [%]	± 1.99	± 1.97	± 1.98	± 2.21	± 2.08	± 1.90
Large- R jets JES [%]	± 5.41	± 6.12	$+4.75$ -6.58	$+8.79$ -6.55	± 10.4	± 8.62
Large- R jets JMS [%]	± 0.93	± 2.60	$+2.15$ -3.20	± 2.37	$+2.88$ -2.14	$+5.00$ -3.42
Large- R jets top-tagging [%]	± 12.0	± 11.1	± 14.2	± 13.9	$+20.1$ -13.1	$+1.89$ -14.4
Flavor tagging [%]	± 8.09	± 8.00	± 8.46	± 9.56	± 9.73	± 7.88
Narrow jets [%]	$+0.22$ -0.14	$+0.40$ -0.25	$+0.48$ -0.34	$+0.35$ -0.21	± 0.95	$+1.26$ -0.91
Pile-up [%]	± 0.72	-0.13	$+0.70$	$+1.40$	$+0.36$	± 1.73
Background [%]	± 1.04	± 2.92	± 5.02	± 4.18	± 5.88	± 9.48
(MOD) Monte Carlo sample statistics [%]	± 0.89	± 2.49	± 3.36	± 4.48	± 5.51	± 14.2
(MOD) ISR/FSR + scale [%]	± 1.84	± 1.58	± 3.18	± 5.53	$+0.52$ -4.87	± 6.62
(MOD) Alternative hard-scattering model [%]	∓ 11.4	∓ 6.51	∓ 11.2	∓ 12.8	∓ 11.8	∓ 44.2
(MOD) Alternative parton-shower model [%]	∓ 15.3	∓ 12.3	∓ 12.4	∓ 7.91	∓ 14.9	∓ 21.5

Table 24: Summary of systematic uncertainties in the fiducial phase-space absolute differential cross-sections for the top quark-antiquark system transverse momentum calculated as a percentage of the cross-section in each bin. Dashes are used when the estimated relative systematic uncertainty for that bin is below 0.1%.

$1/\sigma \cdot d\sigma / dp_T^{ff}$	$5.202 \cdot 10^{-3}$	$4.008 \cdot 10^{-3}$	$2.108 \cdot 10^{-3}$	$1.088 \cdot 10^{-3}$	$2.973 \cdot 10^{-4}$	$1.927 \cdot 10^{-5}$
Total Uncertainty [%]	± 4.05	± 8.96	± 12.2	± 14.4	± 17.0	± 58.3
Statistics [%]	± 2.8	± 5.8	± 9.0	± 9.2	$\pm 12.$	$\pm 38.$
Systematics [%]	± 2.59	± 5.67	± 5.83	± 9.27	± 8.67	± 40.8
Luminosity [%]	-	-	-	± 0.20	-	± 0.11
Large- R jets JES [%]	± 1.07	± 0.67	± 2.13	$+3.14$ -1.62	± 5.47	$+2.73$ -4.02
Large- R jets JMS [%]	± 0.79	± 1.21	$+1.21$ -2.10	± 1.04	$+1.81$ -1.08	$+5.69$ -4.13
Large- R jets top-tagging [%]	$+0.69$ -0.28	$+0.67$ -1.82	$+0.94$ -2.73	± 1.51	$+6.98$ -1.42	± 10.3
Flavor tagging [%]	$+0.47$ -0.32	± 0.56	± 0.82	± 1.81	± 1.81	± 2.02
Narrow jets [%]	± 0.10	-	$+0.23$ -0.13	$+0.20$ -0.46	± 0.71	± 0.90
Pile-up [%]	$+0.14$ -0.22	$+0.85$ -0.55	-	± 0.84 -0.85	$+0.88$ -1.54	± 1.16
Background [%]	± 1.01	± 2.92	± 5.01	± 4.16	± 5.85	± 9.49
(MOD) Monte Carlo sample statistics [%]	± 0.85	± 2.26	± 3.15	± 4.26	± 5.38	± 14.1
(MOD) ISR/FSR + scale [%]	∓ 0.73	-	± 4.30	± 4.45	$+1.62$ -3.79	± 5.56
(MOD) Alternative hard-scattering model [%]	∓ 0.57	∓ 4.93	∓ 0.42	∓ 2.21	∓ 1.06	∓ 37.4
(MOD) Alternative parton-shower model [%]	∓ 1.80	∓ 1.72	∓ 1.62	∓ 6.86	∓ 1.33	∓ 8.99

Table 25: Summary of systematic uncertainties in the fiducial phase-space relative differential cross-sections for the top quark-antiquark system transverse momentum calculated as a percentage of the cross-section in each bin. Dashes are used when the estimated relative systematic uncertainty for that bin is below 0.1%.

$d\sigma / d y'' $ [pb/ Unit $ y'' $]	$3.057 \cdot 10^{-1}$	$2.626 \cdot 10^{-1}$	$2.055 \cdot 10^{-1}$	$1.266 \cdot 10^{-1}$	$5.760 \cdot 10^{-2}$	$1.178 \cdot 10^{-2}$
Total Uncertainty [%]	± 25.9	± 24.2	± 22.6	± 30.2	± 29.4	± 31.0
Statistics [%]	± 4.4	± 5.1	± 5.5	± 7.1	$\pm 11.$	$\pm 19.$
Systematics [%]	± 25.5	± 23.5	± 21.8	± 29.1	± 26.8	± 21.0
Luminosity [%]	± 2.04	± 2.00	± 2.02	± 1.98	± 1.96	± 2.00
Large- R jets JES [%]	± 5.56	± 5.83	± 6.47	± 5.88	± 6.47	± 7.71
Large- R jets JMS [%]	± 2.15	± 0.70	± 1.40	± 2.74	± 1.19	± 3.06
Large- R jets top-tagging [%]	± 12.2	± 12.6	± 12.4	± 12.9	± 13.2	± 11.4 -8.21
Flavor tagging [%]	± 8.45	± 8.31	± 8.52	± 7.59	± 8.26	± 8.02
Narrow jets [%]	$+0.43$ -0.18	$+0.30$ -0.21	± 0.30	$+0.19$ -0.25	$+0.46$ -0.30	± 0.93
Pile-up [%]	$+0.43$ -0.84	± 0.47	± 0.79	$+0.78$ -0.22	$+0.53$ -2.01	± 2.62
Background [%]	± 1.67	± 1.91	± 2.06	± 2.27	± 3.96	± 9.65
(MOD) Monte Carlo sample statistics [%]	± 1.40	± 1.60	± 2.03	± 2.66	± 3.14	± 7.37
(MOD) ISR/FSR + scale [%]	± 2.52	± 1.30	± 2.53	± 3.83	$+0.40$ -1.47	∓ 5.45
(MOD) Alternative hard-scattering model [%]	∓ 13.3	∓ 11.1	∓ 6.63	∓ 14.7	∓ 11.2	∓ 1.37
(MOD) Alternative parton-shower model [%]	∓ 14.0	∓ 12.5	∓ 11.9	∓ 18.2	∓ 15.9	∓ 10.5

Table 26: Summary of systematic uncertainties in the fiducial phase-space absolute differential cross-sections for the top quark-antiquark system absolute value of the rapidity calculated as a percentage of the cross-section in each bin. Dashes are used when the estimated relative systematic uncertainty for that bin is below 0.1%.

$1/\sigma \cdot d\sigma / d y'' $	$1.042 \cdot 10^0$	$8.953 \cdot 10^{-1}$	$7.008 \cdot 10^{-1}$	$4.317 \cdot 10^{-1}$	$1.964 \cdot 10^{-1}$	$4.017 \cdot 10^{-2}$
Total Uncertainty [%]	± 5.39	± 5.97	± 8.18	± 10.7	± 13.8	± 27.1
Statistics [%]	± 3.8	± 4.5	± 5.0	± 6.6	$\pm 10.$	$\pm 18.$
Systematics [%]	± 3.14	± 3.09	± 5.86	± 7.67	± 6.82	± 15.2
Luminosity [%]	-	-	-	-	-	-
Large- R jets JES [%]	$+0.55$ -0.25	± 0.47	$+0.72$ -0.55	± 0.33	$+0.63$ -0.48	± 2.76 -1.51
Large- R jets JMS [%]	$+0.57$ -1.03	± 0.87	± 0.18	± 1.48	± 2.50	± 2.55
Large- R jets top-tagging [%]	± 0.58	$+0.17$ -0.29	± 0.44	$+0.21$ -0.60	± 3.25	± 4.07 -1.59
Flavor tagging [%]	± 0.26	± 0.39	± 0.49	± 0.97	± 0.69	± 1.08
Narrow jets [%]	± 0.11	-	± 0.14	± 0.16	± 0.21	± 0.67
Pile-up [%]	± 0.31	$+0.73$	$+0.28$ -0.21	± 0.38	± 1.49	± 2.10
Background [%]	± 1.65	± 1.90	± 2.02	± 2.28	± 3.95	± 9.65
(MOD) Monte Carlo sample statistics [%]	± 1.19	± 1.42	± 1.80	± 2.48	± 3.09	± 7.29
(MOD) ISR/FSR + scale [%]	-	± 2.34	-1.52 $+0.89$	± 2.84	$+1.44$ -0.31	∓ 5.58
(MOD) Alternative hard-scattering model [%]	∓ 2.41	± 0.14	± 5.18	∓ 3.91	-	± 11.1
(MOD) Alternative parton-shower model [%]	∓ 0.29	± 1.43	± 2.15	∓ 5.22	∓ 2.58	± 3.74

Table 27: Summary of systematic uncertainties in the fiducial phase-space relative differential cross-sections for the top quark-antiquark system absolute value of the rapidity calculated as a percentage of the cross-section in each bin. Dashes are used when the estimated relative systematic uncertainty for that bin is below 0.1%.

$d\sigma / d p_{out}^{t\bar{t}} $ [pb/GeV]	$4.754 \cdot 10^{-3}$	$3.087 \cdot 10^{-3}$	$1.746 \cdot 10^{-3}$	$1.070 \cdot 10^{-3}$	$3.638 \cdot 10^{-4}$	$1.345 \cdot 10^{-4}$	$2.254 \cdot 10^{-5}$
Total Uncertainty [%]	± 22.3	± 26.0	± 26.4	± 29.4	± 26.1	± 30.4	± 40.8
Statistics [%]	± 4.6	± 6.1	± 8.8	± 7.8	± 8.4	$\pm 12.$	$\pm 17.$
Systematics [%]	± 21.7	± 25.1	± 24.4	± 28.0	± 24.3	± 26.7	± 34.8
Luminosity [%]	± 2.00	± 2.05	± 2.05	± 2.03	± 1.93	± 1.97	± 1.74
Large- R jets JES [%]	± 4.69	± 6.53	± 5.33	± 7.11	± 8.02	± 8.26	± 9.71
Large- R jets JMS [%]	± 1.83	± 1.45	± 1.41	± 2.09	± 1.93	± 4.32	± 1.71
Large- R jets top-tagging [%]	± 11.4	± 13.3	± 12.7	± 12.4	± 13.7	± 13.4	± 12.7
Flavor tagging [%]	± 8.27	± 8.34	± 7.90	± 8.83	± 8.20	± 8.82	± 8.11
Narrow jets [%]	$+0.26$	$+0.31$	$+0.35$	$+0.38$	± 0.38	± 0.82	$+0.93$
Pile-up [%]	-0.15	-	-0.24	-0.63	-	$+0.14$	-0.45
Background [%]	± 1.43	± 2.11	± 3.30	± 3.40	± 3.87	± 4.76	± 8.38
(MOD) Monte Carlo sample statistics [%]	± 1.31	± 2.02	± 3.08	± 2.75	± 3.05	± 5.17	± 7.73
(MOD) ISR/FSR + scale [%]	-0.85	± 1.16	± 3.02	± 3.00	± 2.30	± 0.44	∓ 2.19
(MOD) Alternative hard-scattering model [%]	∓ 8.09	∓ 10.2	∓ 11.6	∓ 12.4	∓ 9.90	∓ 17.3	∓ 24.5
(MOD) Alternative parton-shower model [%]	∓ 12.9	∓ 14.8	∓ 13.6	∓ 17.8	∓ 12.9	∓ 2.26	∓ 16.9

Table 28: Summary of systematic uncertainties in the fiducial phase-space absolute differential cross-sections for the top quark-antiquark system out-of-plane momentum $|p_{out}^{t\bar{t}}|$, calculated as a percentage of the cross-section in each bin. Dashes are used when the estimated relative systematic uncertainty for that bin is below 0.1%.

$1/\sigma \cdot d\sigma / d p_{out}^{t\bar{t}} $	$1.633 \cdot 10^{-2}$	$1.060 \cdot 10^{-2}$	$5.997 \cdot 10^{-3}$	$3.677 \cdot 10^{-3}$	$1.250 \cdot 10^{-3}$	$4.619 \cdot 10^{-4}$	$7.743 \cdot 10^{-5}$
Total Uncertainty [%]	± 6.42	± 6.78	± 10.0	± 10.7	± 10.1	± 23.6	± 27.0
Statistics [%]	± 4.0	± 5.8	± 8.4	± 7.4	± 7.9	$\pm 12.$	$\pm 17.$
Systematics [%]	± 4.57	± 2.05	± 3.09	± 6.44	± 4.52	± 18.8	± 16.9
Luminosity [%]	-	-	-	-	-	-	± 0.25
Large- R jets JES [%]	± 1.25	± 0.79	± 1.05	± 0.69	± 2.07	± 2.21	± 3.91
Large- R jets JMS [%]	$+0.49$	± 0.42	± 0.91	± 0.78	± 0.72	± 4.96	± 1.27
Large- R jets top-tagging [%]	-0.37	± 1.48	± 0.61	-1.52	± 1.26	± 1.78	± 0.77
Flavor tagging [%]	± 0.70	-1.01	-0.49	± 1.75	± 1.26	± 1.78	± 1.50
Narrow jets [%]	-0.29	± 0.41	± 1.27	± 1.40	± 0.54	± 1.70	± 0.60
Pile-up [%]	± 0.11	± 0.14	-	± 0.25	± 0.15	± 0.46	± 0.60
Background [%]	± 1.41	± 2.11	± 3.31	± 3.38	± 3.86	± 4.76	± 8.37
(MOD) Monte Carlo sample statistics [%]	± 1.24	± 1.87	± 2.91	± 2.57	± 2.82	± 5.06	± 7.70
(MOD) ISR/FSR + scale [%]	± 3.06	± 0.20	± 2.00	± 1.97	± 3.36	± 1.50	± 1.14
(MOD) Alternative hard-scattering model [%]	± 2.69	± 0.24	± 1.25	∓ 2.17	± 0.67	∓ 7.58	± 15.6
(MOD) Alternative parton-shower model [%]	± 0.94	∓ 1.21	± 0.17	∓ 4.70	± 0.91	± 13.3	∓ 3.64

Table 29: Summary of systematic uncertainties in the fiducial phase-space relative differential cross-sections for the top quark-antiquark system out-of-plane momentum $|p_{out}^{t\bar{t}}|$, calculated as a percentage of the cross-section in each bin. Dashes are used when the estimated relative systematic uncertainty for that bin is below 0.1%.

$d\sigma / d\Delta\phi^{t\bar{t}}$ [pb/ Unit $\Delta\phi^{t\bar{t}}$]	$2.844 \cdot 10^{-3}$	$6.634 \cdot 10^{-2}$	$2.506 \cdot 10^{-1}$	$1.430 \cdot 10^0$
Total Uncertainty [%]	± 32.6	± 31.1	± 27.4	± 24.2
Statistics [%]	$\pm 14.$	$\pm 10.$	± 5.7	± 2.9
Systematics [%]	± 27.8	± 28.3	± 26.5	± 24.0
Luminosity [%]	± 1.88	± 1.89	± 2.00	± 2.02
Large- R jets JES [%]	± 6.00	± 9.43	± 6.44	± 5.52
Large- R jets JMS [%]	$^{+1.06}_{-0.56}$	± 1.91	± 1.80	± 1.65
Large- R jets top-tagging [%]	± 12.2	$^{+13.9}_{-9.73}$	± 12.6	± 12.6
Flavor tagging [%]	± 8.09	± 8.28	± 8.50	± 8.25
Narrow jets [%]	± 1.56	± 0.41	$^{+0.33}_{-0.48}$	$^{+0.30}_{-0.14}$
Pile-up [%]	$^{+1.36}_{-0.51}$	± 0.51	$^{+0.54}_{-0.35}$	± 0.55
Background [%]	± 5.75	± 5.49	± 2.76	± 1.02
(MOD) Monte Carlo sample statistics [%]	± 6.65	± 4.50	± 2.26	± 0.91
(MOD) ISR/FSR + scale [%]	± 4.35	$^{+2.55}_{-9.34}$	$^{+0.19}_{-2.93}$	± 1.38
(MOD) Alternative hard-scattering model [%]	∓ 16.5	∓ 20.8	∓ 10.9	∓ 10.9
(MOD) Alternative parton-shower model [%]	∓ 14.5	-	∓ 17.0	∓ 13.6

Table 30: Summary of systematic uncertainties in the fiducial phase-space absolute differential cross-sections for the top quark-antiquark system aperture angle $\Delta\phi^{t\bar{t}}$, calculated as a percentage of the cross-section in each bin. Dashes are used when the estimated relative systematic uncertainty for that bin is below 0.1%.

Not reviewed, for internal circulation only

$1/\sigma \cdot d\sigma / d\Delta\phi^{t\bar{t}}$	$9.926 \cdot 10^{-3}$	$2.315 \cdot 10^{-1}$	$8.744 \cdot 10^{-1}$	$4.991 \cdot 10^0$
Total Uncertainty [%]	± 19.2	± 24.2	± 7.74	± 2.43
Statistics [%]	$\pm 14.$	$\pm 10.$	± 5.2	± 1.7
Systematics [%]	± 9.26	± 20.8	± 4.63	± 1.27
Luminosity [%]	± 0.12	± 0.11	-	-
Large- R jets JES [%]	± 3.00	$+4.15$ -3.06	$+0.55$ -0.88	± 0.43
Large- R jets JMS [%]	± 2.15	± 2.95	± 0.81	± 0.21
Large- R jets top-tagging [%]	± 2.34	± 2.42	± 1.06	± 0.24
Flavor tagging [%]	± 1.67	± 1.17	± 0.84	± 0.34
Narrow jets [%]	± 1.31 $+0.80$ -0.10	$+0.32$ -0.24 $+0.12$	$+0.11$ -0.27 -	-
Pile-up [%]				-
Background [%]	± 5.65	± 5.41	± 2.70	± 0.98
(MOD) Monte Carlo sample statistics [%]	± 6.56	± 4.35	± 2.00	± 0.60
(MOD) ISR/FSR + scale [%]	± 5.13	$+3.31$ -8.21	$+0.94$ -1.71	-0.64 $+1.00$
(MOD) Alternative hard-scattering model [%]	∓ 5.68	∓ 10.5	± 0.69	± 0.67
(MOD) Alternative parton-shower model [%]	∓ 0.94	± 15.8	∓ 3.93	± 0.10

Table 31: Summary of systematic uncertainties in the fiducial phase-space relative differential cross-sections for the top quark-antiquark system aperture angle $\Delta\phi^{t\bar{t}}$, calculated as a percentage of the cross-section in each bin. Dashes are used when the estimated relative systematic uncertainty for that bin is below 0.1%.

$d\sigma / dH_T^{\bar{t}t}$ [pb/GeV]	$8.573 \cdot 10^{-4}$	$4.603 \cdot 10^{-4}$	$2.953 \cdot 10^{-4}$	$1.543 \cdot 10^{-4}$	$8.434 \cdot 10^{-5}$	$5.814 \cdot 10^{-5}$	$5.542 \cdot 10^{-6}$
Total Uncertainty [%]	± 26.9	± 27.2	± 26.6	± 39.1	± 38.9	± 42.1	± 93.2
Statistics [%]	± 4.6	± 7.8	$\pm 10.$	$\pm 15.$	$\pm 16.$	$\pm 21.$	$\pm 79.$
Systematics [%]	± 26.4	± 25.9	± 24.2	± 35.2	± 35.0	± 35.2	± 43.2
Luminosity [%]	± 2.04	± 1.99	± 2.06	± 2.00	± 1.88	± 2.00	± 1.83
Large- R jets JES [%]	± 5.58	± 5.45	± 7.32 $^{+3.81}_{-3.82}$	± 8.15 $^{-11.3}_{+1.3}$	± 10.6	± 15.7 $^{-9.00}_{+0.00}$	± 17.4
Large- R jets JMS [%]	± 1.52	± 1.12	± 1.12 $^{-2.52}_{+2.52}$	± 0.79	± 1.96	± 0.90	± 10.8
Large- R jets top-tagging [%]	± 11.2	± 13.4	± 16.1	± 16.9	± 19.6	± 21.6	± 27.3
Flavor tagging [%]	± 8.04	± 8.65	± 9.15	± 9.75	± 9.75	± 11.7	± 13.4
Narrow jets [%]	± 0.41 $^{+0.18}_{-0.18}$	± 0.45 $^{-0.26}_{+0.26}$	± 0.32	± 0.21	± 0.32 $^{-0.44}_{+0.44}$	± 0.58 $^{+0.85}_{-0.85}$	± 0.85 $^{-10.3}_{+10.3}$
Pile-up [%]	± 0.26	± 0.99	± 0.33 $^{-1.09}_{+1.09}$	± 0.75 $^{-0.23}_{+0.23}$	± 0.14	± 1.68 $^{-0.40}_{+0.40}$	± 4.85 $^{-12.5}_{+12.5}$
Background [%]	± 1.91	± 2.26	± 2.63	± 4.06	± 3.91	± 5.84	± 19.0
(MOD) Monte Carlo sample statistics [%]	± 1.51	± 2.14	± 2.70	± 4.25	± 3.36	± 6.30	± 12.6
(MOD) ISR/FSR + scale [%]	± 2.28	± 1.48	± 0.40 $^{-1.24}_{+1.24}$	± 4.31 $^{-1.05}_{+1.05}$	± 1.75 $^{-0.05}_{+0.05}$	± 3.19 $^{+2.03}_{-2.03}$	± 12.5
(MOD) Alternative hard-scattering model [%]	∓ 12.2	∓ 14.0	∓ 5.90	∓ 23.2	∓ 16.6	∓ 16.7	∓ 13.8
(MOD) Alternative parton-shower model [%]	∓ 17.6	∓ 13.0	∓ 12.5	∓ 13.6	∓ 18.2	∓ 12.6	∓ 8.57

Table 32: Summary of systematic uncertainties in the fiducial phase-space absolute differential cross-sections for the scalar sum of the top-quark and antiquark transverse momenta $H_T^{\bar{t}t}$, calculated as a percentage of the cross-section in each bin. Dashes are used when the estimated relative systematic uncertainty for that bin is below 0.1%.

$1/\sigma \cdot d\sigma / dH_T^{\bar{t}t}$	$4.133 \cdot 10^{-3}$	$2.219 \cdot 10^{-3}$	$1.424 \cdot 10^{-3}$	$7.439 \cdot 10^{-4}$	$4.066 \cdot 10^{-4}$	$2.803 \cdot 10^{-4}$	$2.672 \cdot 10^{-5}$
Total Uncertainty [%]	± 6.86	± 8.96	± 14.3	± 20.9	± 19.2	± 26.1	± 86.3
Statistics [%]	± 4.1	± 7.4	± 9.7	$\pm 15.$	$\pm 15.$	$\pm 20.$	$\pm 78.$
Systematics [%]	± 5.03	± 4.13	± 9.97	± 12.9	± 10.0	± 13.5	± 27.9
Luminosity [%]	-	-	-	-	± 0.12	-	± 0.17
Large- R jets JES [%]	± 1.03 -1.82	± 2.22	± 3.20 -5.43	± 2.32 $+0.67$	± 4.75	± 9.89 -6.58	± 9.33 -14.2
Large- R jets JMS [%]	± 0.42	± 0.51	± 0.79 $^{+1.63}_{-1.63}$	± 1.20	± 2.93	± 2.01	± 9.83
Large- R jets top-tagging [%]	± 3.11	± 2.06	± 0.77 -1.90	± 3.17 -3.78	± 6.42	± 7.20 $+11.5$	± 15.1
Flavor tagging [%]	± 1.39	± 0.61	± 0.93	± 1.65	± 1.88	± 4.49	± 6.47
Narrow jets [%]	-	± 0.11	± 0.17	± 0.19	± 0.15	± 0.53	± 0.70
Pile-up [%]	± 0.30 -0.47	± 0.42	± 0.55	± 0.40	± 0.71	± 2.24 -0.97	± 9.74 -4.33
Background [%]	± 1.74	± 2.09	± 2.42	± 3.74	± 3.62	± 5.39	± 17.5
(MOD) Monte Carlo sample statistics [%]	± 1.28	± 2.01	± 2.59	± 4.04	± 3.31	± 6.20	± 12.4
(MOD) ISR/FSR + scale [%]	± 1.07	∓ 0.27	± 1.62 -0.22	± 3.15 $+0.22$	± 2.99 $+3.29$	± 2.01 $+4.04$	± 13.9
(MOD) Alternative hard-scattering model [%]	± 1.21	∓ 0.92	∓ 8.48	∓ 11.4	∓ 3.86	∓ 4.04	∓ 0.70
(MOD) Alternative parton-shower model [%]	∓ 2.88	∓ 2.45	∓ 3.13	∓ 1.79	∓ 3.58	∓ 2.94	∓ 7.79

Table 33: Summary of systematic uncertainties in the fiducial phase-space relative differential cross-sections for the scalar sum of the top-quark and antiquark transverse momenta $H_T^{\bar{t}t}$, calculated as a percentage of the cross-section in each bin. Dashes are used when the estimated relative systematic uncertainty for that bin is below 0.1%.

$d\sigma / dy_B^{\ell\bar{\ell}}$ [pb/ Unit $y_B^{\ell\bar{\ell}}$]	$3.056 \cdot 10^{-1}$	$2.688 \cdot 10^{-1}$	$2.148 \cdot 10^{-1}$	$1.577 \cdot 10^{-1}$	$1.241 \cdot 10^{-1}$	$5.617 \cdot 10^{-2}$	$1.686 \cdot 10^{-2}$
Total Uncertainty [%]	± 26.6	± 23.4	± 22.4	± 27.3	± 31.4	± 28.9	± 31.4
Statistics [%]	± 4.3	± 4.9	± 6.9	± 8.3	± 8.8	$\pm 13.$	$\pm 14.$
Systematics [%]	± 26.1	± 22.8	± 21.0	± 25.6	± 29.7	± 24.8	± 26.7
Luminosity [%]	± 2.04	± 2.00	± 2.03	± 1.96	± 1.99	± 1.96	± 2.00
Large- R jets JES [%]	± 5.58	± 5.88	± 6.40	± 5.66	$^{+7.65}_{-5.64}$	± 5.93	± 7.80
Large- R jets JMS [%]	± 1.89	± 0.76	± 2.31	± 1.84	± 1.67	$^{+1.50}_{-1.03}$	± 2.35
Large- R jets top-tagging [%]	± 12.2	± 12.6	± 12.1	± 13.1	± 12.9	± 13.1	± 11.4
Flavor tagging [%]	± 8.44	± 8.34	± 8.38	± 8.23	± 7.49	± 8.44	± 8.11
Narrow jets [%]	$^{+0.44}_{-0.29}$	$^{+0.28}_{-0.17}$	± 0.37	$^{+0.10}_{-0.19}$	± 0.35	$^{+0.36}_{-0.68}$	± 0.60
Pile-up [%]	$^{+0.26}_{-0.60}$	$^{+0.16}_{-0.29}$	± 0.93	± 0.63	± 1.52	$^{+1.47}_{-1.47}$	± 1.81
Background [%]	± 1.70	± 1.92	± 2.32	± 3.18	± 2.79	± 4.14	± 6.35
(MOD) Monte Carlo sample statistics [%]	± 1.44	± 1.57	± 2.39	± 2.68	± 3.76	± 3.59	± 5.02
(MOD) ISR/FSR + scale [%]	± 2.52	± 1.13	± 2.13	± 2.61	± 3.37	$^{+0.59}_{-2.74}$	$^{+1.18}_{-6.45}$
(MOD) Alternative hard-scattering model [%]	∓ 13.2	∓ 11.0	∓ 6.04	∓ 10.8	∓ 15.6	∓ 9.82	∓ 8.61
(MOD) Alternative parton-shower model [%]	∓ 15.2	∓ 10.9	∓ 11.2	∓ 15.6	∓ 18.3	∓ 14.0	∓ 17.1

Table 34: Summary of systematic uncertainties in the fiducial phase-space absolute differential cross-sections for the top quark-antiquark system longitudinal boost $y_B^{\ell\bar{\ell}}$, calculated as a percentage of the cross-section in each bin. Dashes are used when the estimated relative systematic uncertainty for that bin is below 0.1%.

$1/\sigma \cdot d\sigma / dy_B^{\ell\bar{\ell}}$	$1.043 \cdot 10^0$	$9.174 \cdot 10^{-1}$	$7.333 \cdot 10^{-1}$	$5.382 \cdot 10^{-1}$	$4.236 \cdot 10^{-1}$	$1.917 \cdot 10^{-1}$	$5.753 \cdot 10^{-2}$
Total Uncertainty [%]	± 5.61	± 6.42	± 9.89	± 9.48	± 12.6	± 15.7	± 18.8
Statistics [%]	± 3.7	± 4.3	± 6.4	± 7.9	± 8.5	$\pm 13.$	$\pm 14.$
Systematics [%]	± 3.66	± 4.10	± 6.75	± 3.19	± 8.16	± 5.35	± 9.41
Luminosity [%]	-	-	-	-	-	-	-
Large- R jets JES [%]	± 0.38	± 0.42	$^{+0.38}_{-0.87}$	± 0.49	$^{+1.40}_{-0.85}$	± 0.66	± 2.00
Large- R jets JMS [%]	$^{+0.36}_{-0.88}$	± 0.70	± 0.98	$^{+1.15}_{-0.11}$	± 0.52	± 1.86	± 2.33
Large- R jets top-tagging [%]	$^{+0.30}_{-0.10}$	$^{+0.32}_{-0.18}$	$^{+0.60}_{-0.22}$	$^{+0.32}_{-0.87}$	± 0.45	± 1.99	± 2.21
Flavor tagging [%]	± 0.39	± 0.28	± 0.18	± 0.24	± 1.21	± 1.21	± 0.88
Narrow jets [%]	± 0.11	-	$^{+0.15}_{-0.21}$	-	± 0.17	$^{+0.17}_{-0.17}$	± 0.44
Pile-up [%]	± 0.31	± 0.25	$^{+0.46}_{-0.30}$	$^{+1.15}_{-0.52}$	$^{+1.10}_{-0.81}$	$^{+0.11}_{-0.94}$	± 1.29
Background [%]	± 1.68	± 1.91	± 2.30	± 3.16	± 2.80	± 4.13	± 6.35
(MOD) Monte Carlo sample statistics [%]	± 1.22	± 1.37	± 2.24	± 2.51	± 3.60	± 3.54	± 5.00
(MOD) ISR/FSR + scale [%]	± 1.37	± 2.18	∓ 1.12	$^{+1.59}_{+0.65}$	± 2.22	± 1.61	$^{+2.38}_{-5.47}$
(MOD) Alternative hard-scattering model [%]	∓ 2.27	∓ 0.21	∓ 5.80	∓ 0.36	∓ 4.97	∓ 1.55	∓ 2.91
(MOD) Alternative parton-shower model [%]	∓ 1.76	∓ 3.19	∓ 2.91	∓ 2.22	∓ 5.27	∓ 0.34	∓ 3.96

Table 35: Summary of systematic uncertainties in the fiducial phase-space relative differential cross-sections for the top quark-antiquark system longitudinal boost $y_B^{\ell\bar{\ell}}$, calculated as a percentage of the cross-section in each bin. Dashes are used when the estimated relative systematic uncertainty for that bin is below 0.1%.

$d\sigma / d\chi''$ [pb/Unit χ'']	$1.512 \cdot 10^{-1}$	$1.148 \cdot 10^{-1}$	$6.104 \cdot 10^{-2}$	$3.515 \cdot 10^{-2}$	$2.190 \cdot 10^{-2}$	$1.183 \cdot 10^{-2}$	$3.050 \cdot 10^{-3}$
Total Uncertainty [%]	± 25.8	± 23.9	± 27.5	± 24.7	± 25.4	± 26.8	± 29.1
Statistics [%]	± 4.8	± 5.5	± 5.2	± 7.1	$\pm 10.$	± 8.9	$\pm 16.$
Systematics [%]	± 25.2	± 23.1	± 26.9	± 23.4	± 22.6	± 24.9	± 22.8
Luminosity [%]	± 1.99	± 2.01	± 1.96	± 2.03	± 1.97	± 2.08	± 1.93
Large- R jets JES [%]	± 5.96	± 5.85	± 5.65	± 6.07	± 6.33	± 6.42	± 4.70
Large- R jets JMS [%]	± 1.90	$+0.59$ -0.87	$+1.26$ -1.72	$+2.25$ -1.50	± 1.64	± 1.63	± 2.96
Large- R jets top-tagging [%]	± 12.4	± 12.9	± 12.4	$+14.4$ -9.82	± 12.6	± 13.0	$+14.4$ -10.0
Flavor tagging [%]	± 8.51	± 8.30	± 8.14	± 7.94	± 8.09	± 8.79	± 7.96
Narrow jets [%]	$+0.34$ -0.21	$+0.41$ -0.13	± 0.33	$+0.21$ -0.13	$+0.38$ -0.20	$+0.39$ -0.63	$+0.36$ -0.75
Pile-up [%]	± 1.01	± 1.02	$+0.30$ -0.20	$+0.48$ -0.35	± 1.63	± 1.06	$+0.87$ -2.84
Background [%]	± 1.79	± 2.02	± 2.04	± 2.43	± 4.72	± 3.26	± 6.88
(MOD) Monte Carlo sample statistics [%]	± 1.49	± 1.98	± 1.67	± 2.64	± 3.87	± 3.30	± 4.81
(MOD) ISR/FSR + scale [%]	± 1.35	± 2.56	± 2.81	$+3.48$ -0.34	$+0.25$ -3.26	-0.23 $+2.74$	± 3.27
(MOD) Alternative hard-scattering model [%]	∓ 11.8	∓ 10.9	∓ 13.2	∓ 11.2	∓ 5.21	∓ 11.4	∓ 10.0
(MOD) Alternative parton-shower model [%]	∓ 14.7	∓ 11.1	∓ 16.5	∓ 12.1	∓ 13.7	∓ 12.9	∓ 11.3

Table 36: Summary of systematic uncertainties in the fiducial phase-space absolute differential cross-sections for the top quark-antiquark system $\chi''t\bar{t}$, calculated as a percentage of the cross-section in each bin. Dashes are used when the estimated relative systematic uncertainty for that bin is below 0.1%.

$1/\sigma \cdot d\sigma / d\chi''$	$5.327 \cdot 10^{-1}$	$4.043 \cdot 10^{-1}$	$2.150 \cdot 10^{-1}$	$1.238 \cdot 10^{-1}$	$7.713 \cdot 10^{-2}$	$4.168 \cdot 10^{-2}$	$1.074 \cdot 10^{-2}$
Total Uncertainty [%]	± 5.00	± 6.84	± 6.96	± 9.66	± 13.8	± 10.8	± 18.9
Statistics [%]	± 4.1	± 5.0	± 4.8	± 6.7	± 9.6	± 8.5	$\pm 15.$
Systematics [%]	± 1.66	± 3.75	± 4.33	± 6.00	± 7.89	± 4.86	± 6.13
Luminosity [%]	-	-	-	-	-	-	-
Large- R jets JES [%]	± 0.35	± 0.38	± 0.62	± 0.55	± 0.82	± 1.38	± 1.61
Large- R jets JMS [%]	± 0.65	± 0.89	± 0.61	± 1.35	± 1.27	± 0.61	$+3.09$ -1.67
Large- R jets top-tagging [%]	$+0.19$ -0.28	± 0.79	± 1.16	± 2.32	± 1.32	$+0.74$ -0.41	± 2.06
Flavor tagging [%]	± 0.31	± 0.39	$+0.25$ -0.18	± 0.84	± 0.42	± 0.75	± 0.70
Narrow jets [%]	-	± 0.14	-0.13	± 0.12	± 0.13	$+0.34$ -0.46	$+0.17$ -0.11
Pile-up [%]	$+0.39$ -0.58	± 0.50	± 0.27	$+1.27$ -0.89	± 2.15	$+0.64$ -0.47	$+1.31$ -2.37
Background [%]	± 1.78	± 2.01	± 2.03	± 2.42	± 4.70	± 3.23	± 6.87
(MOD) Monte Carlo sample statistics [%]	± 1.27	± 1.78	± 1.52	± 2.44	± 3.73	± 3.20	± 4.75
(MOD) ISR/FSR + scale [%]	-0.20 $+0.86$	± 1.43	± 1.68	± 4.69 -2.11	$+1.42$ -3.95	$+0.13$ -2.13	
(MOD) Alternative hard-scattering model [%]	∓ 0.49	± 0.43	∓ 2.05	± 0.17	± 6.95	-	± 1.52
(MOD) Alternative parton-shower model [%]	∓ 1.03	± 3.12	∓ 3.06	± 1.97	± 0.10	± 1.02	± 2.88

Table 37: Summary of systematic uncertainties in the fiducial phase-space relative differential cross-sections for the top quark-antiquark system $\chi''t\bar{t}$, calculated as a percentage of the cross-section in each bin. Dashes are used when the estimated relative systematic uncertainty for that bin is below 0.1%.

$d\sigma / d\cos\theta^*$ [pb/ Unit $\cos\theta^*$]	$3.983 \cdot 10^{-1}$	$4.017 \cdot 10^{-1}$	$3.668 \cdot 10^{-1}$	$3.250 \cdot 10^{-1}$	$1.719 \cdot 10^{-1}$	$3.876 \cdot 10^{-2}$
Total Uncertainty [%]	± 25.9	± 25.4	± 24.4	± 25.1	± 27.8	± 31.0
Statistics [%]	± 4.8	± 4.9	± 4.9	± 8.0	$\pm 11.$	$\pm 18.$
Systematics [%]	± 25.4	± 24.8	± 23.9	± 23.3	± 24.6	± 22.9
Luminosity [%]	± 2.01	± 1.98	± 1.97	± 2.05	± 2.01	± 1.99
Large- R jets JES [%]	± 5.88	± 6.06	± 5.83	± 5.80	$+4.89$	$+6.41$
Large- R jets JMS [%]	± 1.71	$+1.10$	$+1.50$	± 1.74	-6.46	-4.34
Large- R jets top-tagging [%]	± 12.6	± 13.3	± 11.8	± 12.7	± 2.17	± 3.53
Flavor tagging [%]	± 8.52	± 8.39	± 7.83	± 8.61	± 8.09	± 8.15
Narrow jets [%]	$+0.37$	-0.21	± 0.28	$+0.36$	-0.12	$+0.43$
Pile-up [%]	± 1.01	± 0.57	± 0.35	± 1.27	-0.20	± 0.21
Background [%]	± 1.79	± 1.95	± 1.76	± 3.43	± 2.57	± 1.37
(MOD) Monte Carlo sample statistics [%]	± 1.56	± 1.47	± 1.72	± 3.49	± 3.70	± 5.86
(MOD) ISR/FSR + scale [%]	± 1.41	± 2.88	± 1.43	-0.62	± 3.65	± 1.72
(MOD) Alternative hard-scattering model [%]	∓ 11.8	∓ 12.1	∓ 10.9	∓ 8.59	∓ 11.3	∓ 7.49
(MOD) Alternative parton-shower model [%]	∓ 14.9	∓ 12.7	∓ 14.0	∓ 13.3	∓ 13.8	∓ 9.84

Table 38: Summary of systematic uncertainties in the fiducial phase-space absolute differential cross-sections for the top quark-antiquark system $\cos\theta^*$, calculated as a percentage of the cross-section in each bin. Dashes are used when the estimated relative systematic uncertainty for that bin is below 0.1%.

$1/\sigma \cdot d\sigma / d\cos\theta^*$	$1.370 \cdot 10^0$	$1.381 \cdot 10^0$	$1.261 \cdot 10^0$	$1.118 \cdot 10^0$	$5.910 \cdot 10^{-1}$	$1.333 \cdot 10^{-1}$
Total Uncertainty [%]	± 5.16	± 5.58	± 5.54	± 10.1	± 13.4	± 22.0
Statistics [%]	± 4.1	± 4.2	± 4.3	± 7.6	$\pm 11.$	$\pm 18.$
Systematics [%]	± 2.10	± 2.70	$+3.17$ -1.49	± 4.75	± 4.59	± 8.11
Luminosity [%]	-	-	-	-	-	-
Large- R jets JES [%]	$+0.45$ -0.19	$+0.19$ -0.34	± 0.29	± 0.65	± 1.57	$+1.80$ -1.03
Large- R jets JMS [%]	± 0.46	± 0.50	± 0.92	$+0.74$ -0.48	± 1.69	± 2.48
Large- R jets top-tagging [%]	$+0.19$ -0.29	$+0.65$ -0.87	$+1.21$ -0.47	± 0.75	$+1.44$ -0.76	$+3.16$ -1.36
Flavor tagging [%]	± 0.31	± 0.38	± 0.79	± 0.92	± 1.00	± 0.37
Narrow jets [%]	-	-	± 0.11	± 0.30	± 0.12	$+0.22$ -0.30
Pile-up [%]	$+0.40$ -0.54	-	$+0.64$ -0.20	± 1.80	± 2.04	± 0.85
Background [%]	± 1.77	± 1.94	± 1.76	± 3.40	± 4.61	± 7.43
(MOD) Monte Carlo sample statistics [%]	± 1.28	± 1.32	± 1.52	± 3.32	± 3.63	± 5.76
(MOD) ISR/FSR + scale [%]	-0.29 $+1.01$	± 1.78	$+2.50$ -0.35	± 2.61	± 2.54	∓ 0.64
(MOD) Alternative hard-scattering model [%]	∓ 0.57	∓ 0.99	± 0.35	± 3.05	∓ 0.10	± 4.29
(MOD) Alternative parton-shower model [%]	∓ 1.37	∓ 1.23	∓ 0.35	± 0.49	∓ 0.10	± 4.54

Table 39: Summary of systematic uncertainties in the fiducial phase-space relative differential cross-sections for the top quark-antiquark system $\cos\theta^*$, calculated as a percentage of the cross-section in each bin. Dashes are used when the estimated relative systematic uncertainty for that bin is below 0.1%.

950 **F.3.2. Full breakdown tables**

[Not reviewed, for internal circulation only]

Bins [pb]	-0.50-0.50
dr / dc_{fid} [pb/pb]	$2.917 \cdot 10^{-1}$
Total Uncertainty [%]	± 24.4
Statistics [%]	± 2.3
Systematics [%]	± 24.3
(JES) b -Tagged jet energy scale [%]	-
(JES) Effective detector NP set 1 [%]	-
(JES) Effective detector NP set 2 [%]	-
(JES) Effective detector NP set 3 [%]	-
(JES) Effective detector NP set 4 [%]	-
(JES) Effective detector NP set 5 [%]	-
(JES) Effective detector NP set 6 [%]	-
(JES) Effective detector NP set 7 [%]	-
(JES) Effective detector NP set 8 restTerm [%]	-
(JES) η intercalibration model [%]	-
(JES) η intercalibration total stat [%]	-
(JES) Flavor composition [%]	$+0.24$
(JES) Flavor response [%]	-0.16
(JES) Pile-up offset μ [%]	-
(JES) Pile-up offset N_{V}/N [%]	-
(JES) Pile-up offset p_T topology [%]	$+0.19$
(JES) Punch-through [%]	-0.10
(JES) Single particle high- p_T [%]	-
(LJES) Large- R jet Baseline mass [%]	$+0.30$
(LJES) Large- R jet Baseline p_T [%]	-0.49
(LJES) Large- R jet Baseline r_{d2} [%]	± 2.27
(LJES) Large- R jet Modelling mass [%]	∓ 7.76
(LJES) Large- R jet Modelling p_T [%]	± 2.25
(LJES) Large- R jet Modelling r_{d2} [%]	∓ 9.84
(LJES) Large- R jet Tracking mass [%]	± 0.13
(LJES) Large- R jet Tracking p_T [%]	± 4.96
(LJES) Large- R jet Tracking r_{d2} [%]	± 0.39
(LJES) Large- R jet TotalStat mass [%]	-
(LJES) Large- R jet TotalStat p_T [%]	± 0.28
(LJES) Large- R jet TotalStat r_{d2} [%]	± 0.16
(LJES) Large- R jet top-quark mass resolution [%]	∓ 1.30
(FTAG) b -Quark tagging efficiency (eigenvector 0) [%]	∓ 5.29
(FTAG) b -Quark tagging efficiency (eigenvector 1) [%]	∓ 4.90
(FTAG) b -Quark tagging efficiency (eigenvector 2) [%]	∓ 0.75
(FTAG) b -Quark tagging efficiency (eigenvector 3) [%]	∓ 0.51
(FTAG) b -Quark tagging efficiency (eigenvector 4) [%]	∓ 0.24
(FTAG) c -Quark tagging efficiency (eigenvector 0) [%]	∓ 2.06
(FTAG) c -Quark tagging efficiency (eigenvector 1) [%]	∓ 1.29
(FTAG) c -Quark tagging efficiency (eigenvector 2) [%]	∓ 0.59
(FTAG) c -Quark tagging efficiency (eigenvector 3) [%]	∓ 0.13
(FTAG) Light-jet tagging efficiency (eigenvector 0) [%]	∓ 0.44
(FTAG) Light-jet tagging efficiency (eigenvector 1) [%]	-
(FTAG) Light-jet tagging efficiency (eigenvector 2) [%]	± 0.12
(FTAG) Light-jet tagging efficiency (eigenvector 3) [%]	-
(FTAG) Light-jet tagging efficiency (eigenvector 4) [%]	-
(FTAG) Light-jet tagging efficiency (eigenvector 5) [%]	-
(FTAG) Light-jet tagging efficiency (eigenvector 6) [%]	-
(FTAG) Light-jet tagging efficiency (eigenvector 7) [%]	-
(FTAG) Light-jet tagging efficiency (eigenvector 8) [%]	∓ 0.24
(FTAG) Light-jet tagging efficiency (eigenvector 9) [%]	∓ 0.24
(FTAG) Light-jet tagging efficiency (eigenvector 10) [%]	-
(FTAG) Light-jet tagging efficiency (eigenvector 11) [%]	-
(FTAG) Light-jet tagging efficiency (eigenvector 12) [%]	-
(FTAG) Light-jet tagging efficiency (eigenvector 13) [%]	-
(FTAG) b -Quark tagging extrapolation [%]	± 3.02
(FTAG) b -Quark tagging extrapolation from c -Quark [%]	-
(PDF) PDF4LHC15 eigenvector 01 [%]	-
(PDF) PDF4LHC15 eigenvector 02 [%]	± 0.55
(PDF) PDF4LHC15 eigenvector 03 [%]	-
(PDF) PDF4LHC15 eigenvector 04 [%]	± 0.20
(PDF) PDF4LHC15 eigenvector 05 [%]	± 2.19
(PDF) PDF4LHC15 eigenvector 06 [%]	± 0.26
(PDF) PDF4LHC15 eigenvector 07 [%]	-
(PDF) PDF4LHC15 eigenvector 08 [%]	± 0.35
(PDF) PDF4LHC15 eigenvector 09 [%]	± 0.19
(PDF) PDF4LHC15 eigenvector 10 [%]	-
(PDF) PDF4LHC15 eigenvector 11 [%]	± 0.33
(PDF) PDF4LHC15 eigenvector 12 [%]	± 0.29
(PDF) PDF4LHC15 eigenvector 13 [%]	-
(PDF) PDF4LHC15 eigenvector 14 [%]	-
(PDF) PDF4LHC15 eigenvector 15 [%]	± 0.16
(PDF) PDF4LHC15 eigenvector 16 [%]	-
(PDF) PDF4LHC15 eigenvector 17 [%]	± 0.36
(PDF) PDF4LHC15 eigenvector 18 [%]	-
(PDF) PDF4LHC15 eigenvector 19 [%]	± 0.73
(PDF) PDF4LHC15 eigenvector 20 [%]	± 0.12
(PDF) PDF4LHC15 eigenvector 21 [%]	-
(PDF) PDF4LHC15 eigenvector 22 [%]	± 0.83
(PDF) PDF4LHC15 eigenvector 23 [%]	-
(PDF) PDF4LHC15 eigenvector 24 [%]	-
(PDF) PDF4LHC15 eigenvector 25 [%]	-
(PDF) PDF4LHC15 eigenvector 26 [%]	-
(PDF) PDF4LHC15 eigenvector 27 [%]	± 0.25
(PDF) PDF4LHC15 eigenvector 28 [%]	± 0.11
(PDF) PDF4LHC15 eigenvector 29 [%]	-
(PDF) PDF4LHC15 eigenvector 30 [%]	-
(LEP) Electron energy resolution [%]	-
(LEP) Electron energy scale [%]	-
(LEP) Muon energy scale [%]	-
(LEP) Muon (MS) momentum resolution [%]	-
(LEP) Muon (ID) momentum resolution [%]	-
(LEP) Muon sagitta resolution bias [%]	-
(LEP) Muon sagitta ρ [%]	-
(MET/PU) jet^{miss} Soft jet resolution para [%]	-
(MET/PU) jet^{miss} Soft jet resolution perp [%]	-
(MET/PU) jet^{miss} Soft jet scale [%]	-
(MET/PU) Jet vertex tagging [%]	-
Luminosity [%]	± 2.01
(BKG) Single top Wt cross-section [%]	-
(BKG) Single top t -channel treatment [%]	± 0.21
(BKG) $t\bar{t} + W$ cross-section [%]	-
(BKG) $t\bar{t} + Z$ cross-section [%]	-
(BKG) $t\bar{t} + H$ cross-section [%]	-
(BKG) Multijet background statistics [%]	± 0.86
(MOD) Monte Carlo sample statistics [%]	± 0.90
(MOD) ISR/FSR + scale [%]	± 1.13
(MOD) Alternative hard-scattering model [%]	± 11.2
(MOD) Alternative parton-shower model [%]	± 13.7

Table 40: The individual systematic uncertainties in the fiducial phase-space absolute inclusive cross-sections calculated as a percentage of the cross-section. Dashes are used when the estimated relative systematic uncertainty is below 0.1%.

Not reviewed, for internal circulation only

Bins [GeV]	500–550	550–600	600–650	650–700	700–750	750–800	800–1000	1000–1200
$d\sigma / dp_T^2$ [pb/GeV]	$2.336 \cdot 10^{-3}$	$1.280 \cdot 10^{-3}$	$7.177 \cdot 10^{-4}$	$6.111 \cdot 10^{-4}$	$3.146 \cdot 10^{-4}$	$1.985 \cdot 10^{-4}$	$8.196 \cdot 10^{-5}$	$1.560 \cdot 10^{-5}$
Total Uncertainty [%]	± 21.9	± 26.9	± 28.6	± 29.1	± 33.6	± 37.1	± 44.4	± 93.8
Statistics [%]	± 3.7	± 5.8	± 8.6	± 9.4	$\pm 14.$	$\pm 19.$	$\pm 18.$	$\pm 71.$
Systematics [%]	± 21.5	± 26.1	± 26.9	± 27.1	± 29.6	± 30.4	± 39.7	± 50.2
(JES) b -Tagged jet energy scale [%]	-	-	-	-	-	-	-	-
(JES) Effective detector NP set 1 [%]	-	-	-	-	± 0.12	± 0.12	± 0.30	-
(JES) Effective detector NP set 2 [%]	-	-	-	± 0.22	± 0.35	-	-	-
(JES) Effective detector NP set 3 [%]	-	-	-	-	-	-	-	-
(JES) Effective detector NP set 4 [%]	-	-	-	-	-	-	-	-
(JES) Effective detector NP set 5 [%]	-	-	-	-	-	-	-	-
(JES) Effective detector NP set 6 [%]	-	-	-	-	-	-	-	-
(JES) Effective detector NP set 7 [%]	-	-	-	-	-	-	-	-
(JES) Effective detector NP set 8 restTerm [%]	-	-	-	-	-	-	-	-
(JES) η intercalibration model [%]	-	-	-	-	-	-	-	-
(JES) η intercalibration total stat [%]	-	-	-	-	-	-	-	-
(JES) Flavor composition [%]	± 0.15	± 0.39	± 0.34	± 0.30	± 0.22	± 0.41	± 0.15	± 0.42
(JES) Flavor response [%]	-	-	-	± 0.28	± 0.31	-	-	± 0.14
(JES) Pile-up offset μ [%]	-	-	-	-	-	-	-	-
(JES) Pile-up offset N_{Vtx} [%]	-	-	-	-	± 0.33	-	± 0.12	-
(JES) Pile-up offset p topology [%]	-	± 0.25	± 0.25	± 0.19	± 0.22	± 0.46	± 0.18	± 0.37
(JES) Puschtschug [%]	-	-	-	± 0.34	± 0.46	-	-	-
(JES) Single particle high- p_T [%]	-	-	-	-	-	-	-	-
(LJES) Large- R jet Baseline mass [%]	± 0.25	± 0.31	± 0.39	± 0.28	± 0.78	± 1.23	± 0.33	± 8.14
(LJES) Large- R jet Baseline ρ_T [%]	± 2.18	± 0.99	± 0.20	± 4.23	± 5.46	± 7.06	± 15.4	± 9.32
(LJES) Large- R jet Baseline τ_{23} [%]	± 1.4	-	-	± 5	± 1.5	± 1.5	-	-
(LJES) Large- R jet Modeling mass [%]	± 6.55	± 7.46	± 8.24	± 10.1	± 12.8	± 10.8	± 14.1	± 22.1
(LJES) Large- R jet Modeling τ_{23} [%]	± 0.67	± 0.28	± 1.74	± 0.50	± 0.86	± 1.63	± 0.50	± 7.16
(LJES) Large- R jet Modeling ρ_T [%]	± 2.60	± 2.38	± 2.05	± 1.29	± 1.19	± 2.75	± 1.64	± 21
(LJES) Large- R jet Tracking mass [%]	± 8.23	± 9.79	± 11.1	± 12.8	± 15.5	± 15.6	± 19.4	± 26.6
(LJES) Large- R jet Tracking ρ_T [%]	-	± 0.26	± 0.92	± 0.19	± 1.05	± 0.03	-	± 8.29
(LJES) Large- R jet Tracking τ_{23} [%]	± 3.92	± 4.81	± 6.17	± 4.66	± 5.56	± 3.95	± 4.45	± 10
(LJES) Large- R jet Tracking TotalStat [%]	± 0.33	± 0.32	± 0.40	± 0.28	± 0.39	± 0.39	± 0.23	± 5.16
(LJES) Large- R jet TotalStat ρ_T [%]	-	± 0.30	± 0.46	± 0.26	± 0.45	± 0.31	± 0.13	± 3.97
(LJES) Large- R jet TotalStat τ_{23} [%]	± 0.15	± 0.14	± 0.11	± 0.22	-	± 0.18	± 0.29	± 31
(LJES) Large- R jet top-quark mass resolution [%]	± 0.60	± 2.43	± 2.09	± 0.26	± 0.84	± 0.31	± 0.13	± 1.69
(FTAG) Q tagging efficiency (eigenvector 0) [%]	± 5.05	± 5.28	± 5.46	± 5.66	± 6.00	± 5.87	± 5.95	± 7.25
(FTAG) Q tagging efficiency (eigenvector 1) [%]	± 4.70	± 4.86	± 5.15	± 5.31	± 5.59	± 5.46	± 5.29	± 6.46
(FTAG) Q tagging efficiency (eigenvector 2) [%]	± 0.62	± 0.75	± 0.87	± 0.92	± 1.08	± 1.15	± 1.25	± 1.67
(FTAG) Q tagging efficiency (eigenvector 3) [%]	± 0.40	± 0.50	± 0.61	± 0.63	± 0.76	± 0.88	± 1.04	± 1.66
(FTAG) Q tagging efficiency (eigenvector 4) [%]	± 0.20	± 0.23	± 0.28	± 0.30	± 0.34	± 0.49	± 0.43	± 0.62
(FTAG) Q tagging efficiency (eigenvector 0) [%]	± 1.99	± 2.16	± 2.05	± 2.33	± 2.38	± 2.17	± 2.45	± 4.06
(FTAG) Q tagging efficiency (eigenvector 1) [%]	± 1.16	± 1.41	± 1.40	± 1.31	± 1.41	± 1.90	± 1.28	± 0.85
(FTAG) Q tagging efficiency (eigenvector 2) [%]	± 0.31	± 0.65	± 0.66	± 0.63	± 0.71	± 0.55	± 0.54	± 0.65
(FTAG) Q tagging efficiency (eigenvector 3) [%]	± 0.39	± 0.46	± 0.47	± 0.52	± 0.62	± 0.64	± 0.62	± 0.94
(FTAG) Light-jet tagging efficiency (eigenvector 0) [%]	± 0.33	-	± 0.14	± 0.67	± 0.64	-	-	± 1.69
(FTAG) Light-jet tagging efficiency (eigenvector 1) [%]	-	-	± 0.10	-	-	± 0.15	-	± 0.77
(FTAG) Light-jet tagging efficiency (eigenvector 2) [%]	± 0.13	-	± 0.12	± 0.22	± 0.23	± 0.11	-	± 0.84
(FTAG) Light-jet tagging efficiency (eigenvector 3) [%]	-	-	± 0.15	± 0.11	± 0.14	± 0.16	± 0.10	-
(FTAG) Light-jet tagging efficiency (eigenvector 4) [%]	± 0.12	-	-	-	± 0.35	-	-	± 1.07
(FTAG) Light-jet tagging efficiency (eigenvector 5) [%]	-	-	-	-	± 0.12	-	-	± 0.42
(FTAG) Light-jet tagging efficiency (eigenvector 6) [%]	-	-	-	-	± 0.10	-	-	± 0.32
(FTAG) Light-jet tagging efficiency (eigenvector 7) [%]	-	-	-	-	± 0.10	± 0.17	-	± 0.26
(FTAG) Light-jet tagging efficiency (eigenvector 8) [%]	± 0.24	± 0.23	± 0.24	± 0.20	± 0.25	± 0.49	± 0.31	± 0.17
(FTAG) Light-jet tagging efficiency (eigenvector 9) [%]	± 0.24	± 0.25	± 0.23	± 0.20	± 0.29	± 0.44	± 0.21	± 0.19
(FTAG) Light-jet tagging efficiency (eigenvector 10) [%]	-	-	-	-	-	-	-	± 0.10
(FTAG) Light-jet tagging efficiency (eigenvector 11) [%]	-	-	-	-	-	-	-	± 0.10
(FTAG) Light-jet tagging efficiency (eigenvector 12) [%]	-	-	-	-	-	-	-	-
(FTAG) Light-jet tagging efficiency (eigenvector 13) [%]	-	-	-	-	-	-	-	-
(FTAG) Q Quark tagging extrapolation [%]	± 2.13	± 2.85	± 3.79	± 4.34	± 5.13	± 6.21	± 7.55	± 12.2
(FTAG) Q Quark tagging extrapolation from c-Quark [%]	-	-	-	-	-	± 0.14	± 0.39	± 0.45
(PDF) PDF4LHC15 eigenvector 0 [%]	-	-	-	-	-	-	-	± 0.10
(PDF) PDF4LHC15 eigenvector 1 [%]	± 0.48	± 0.57	± 0.63	± 0.66	± 0.61	± 0.79	± 0.35	± 0.73
(PDF) PDF4LHC15 eigenvector 03 [%]	-	± 0.12	± 0.13	± 0.15	± 0.15	± 0.17	± 0.24	± 0.50
(PDF) PDF4LHC15 eigenvector 04 [%]	± 0.22	± 0.19	± 0.17	± 0.20	± 0.17	± 0.22	± 0.16	± 0.32
(PDF) PDF4LHC15 eigenvector 05 [%]	± 1.94	± 2.22	± 2.39	± 2.58	± 2.71	± 2.85	± 2.97	± 3.56
(PDF) PDF4LHC15 eigenvector 06 [%]	± 0.22	± 0.27	± 0.26	± 0.34	± 0.37	± 0.43	± 0.38	± 0.93
(PDF) PDF4LHC15 eigenvector 07 [%]	-	-	-	-	-	-	-	± 0.10
(PDF) PDF4LHC15 eigenvector 08 [%]	± 0.26	± 0.36	± 0.42	± 0.48	± 0.56	± 0.63	± 0.68	± 0.95
(PDF) PDF4LHC15 eigenvector 09 [%]	± 0.18	± 0.19	± 0.20	± 0.23	± 0.24	± 0.24	± 0.23	± 0.35
(PDF) PDF4LHC15 eigenvector 10 [%]	-	± 0.10	± 0.12	± 0.14	± 0.18	± 0.19	± 0.20	± 0.32
(PDF) PDF4LHC15 eigenvector 11 [%]	± 0.29	± 0.34	± 0.36	± 0.39	± 0.42	± 0.44	± 0.43	± 0.54
(PDF) PDF4LHC15 eigenvector 12 [%]	± 0.23	± 0.29	± 0.33	± 0.39	± 0.45	± 0.43	± 0.48	± 0.71
(PDF) PDF4LHC15 eigenvector 13 [%]	-	-	-	-	-	-	-	± 0.13
(PDF) PDF4LHC15 eigenvector 14 [%]	-	-	-	-	-	-	-	-
(PDF) PDF4LHC15 eigenvector 15 [%]	± 0.10	± 0.14	± 0.20	± 0.23	± 0.30	± 0.33	± 0.48	± 0.71
(PDF) PDF4LHC15 eigenvector 16 [%]	-	-	-	-	-	-	-	± 0.11
(PDF) PDF4LHC15 eigenvector 17 [%]	± 0.35	± 0.36	± 0.37	± 0.39	± 0.41	± 0.41	± 0.37	± 0.52
(PDF) PDF4LHC15 eigenvector 18 [%]	-	-	-	-	-	± 0.10	± 0.12	± 0.16
(PDF) PDF4LHC15 eigenvector 19 [%]	± 0.67	± 0.74	± 0.77	± 0.82	± 0.85	± 0.84	± 0.80	± 0.86
(PDF) PDF4LHC15 eigenvector 20 [%]	-	± 0.12	± 0.14	± 0.18	± 0.17	± 0.21	± 0.27	± 0.36
(PDF) PDF4LHC15 eigenvector 21 [%]	-	-	-	-	-	-	± 0.15	-
(PDF) PDF4LHC15 eigenvector 22 [%]	± 0.56	± 0.84	± 1.01	± 1.23	± 1.40	± 1.63	± 1.89	± 2.90
(PDF) PDF4LHC15 eigenvector 23 [%]	-	-	-	-	-	-	-	± 0.17
(PDF) PDF4LHC15 eigenvector 24 [%]	-	-	-	-	-	-	-	-
(PDF) PDF4LHC15 eigenvector 25 [%]	-	-	-	-	-	-	-	± 0.22
(PDF) PDF4LHC15 eigenvector 26 [%]	-	-	-	-	-	-	-	± 0.13
(PDF) PDF4LHC15 eigenvector 27 [%]	± 0.20	± 0.26	± 0.30	± 0.34	± 0.36	± 0.42	± 0.47	± 0.46
(PDF) PDF4LHC15 eigenvector 30 [%]	-	-	-	-	-	-	-	± 0.13
(LEP) Electron energy resolution [%]	-	-	-	-	-	-	-	-
(LEP) Electron energy scale [%]	-	-	-	-	-	-	-	-
(LEP) Muon (MS) momentum resolution [%]	-	-	-	-	-	-	-	-
(LEP) Muon (ID) momentum resolution [%]	-	-	-	-	-	-	-	-
(LEP) Muon sagitta resolution bias [%]	-	-	-	-	-	-	-	-
(LEP) Muon sagitta ρ [%]	-	-	-	-	-	-	-	-
(MET/PU) $E_{\text{miss}}^{\text{soft}}$ Soft jet resolution para [%]	-	-	-	-	-	-	-	-
(MET/PU) $E_{\text{miss}}^{\text{soft}}$ Soft jet resolution perp [%]	-	-	-	-	-	-	-	-
(MET/PU) $E_{\text{miss}}^{\text{soft}}$ Soft jet scale [%]	-	-	-	-	-	-	-	-
(MET/PU) vertex tagging [%]	± 0.12	-	± 0.14	± 0.10	-	-	-	± 0.29
(BKG) Singl-top cross-section [%]</td								

Not reviewed, for internal circulation only

Bins [GeV]	500–550	550–600	600–650	650–700	700–750	750–800	800–1000	1000–1200
$1/\sigma \cdot d\sigma / dp_T^3$	$7.781 \cdot 10^{-3}$	$4.452 \cdot 10^{-3}$	$2.497 \cdot 10^{-3}$	$2.126 \cdot 10^{-3}$	$1.095 \cdot 10^{-3}$	$6.908 \cdot 10^{-4}$	$2.852 \cdot 10^{-4}$	$5.426 \cdot 10^{-5}$
Total Uncertainty [%]	± 6.40	± 7.46	± 10.2	± 12.2	± 18.0	± 23.1	± 26.6	± 89.3
Statistics [%]	± 3.6	± 5.3	± 8.1	± 9.0	$\pm 14.$	$\pm 19.$	$\pm 18.$	$\pm 70.$
Systematics [%]	± 4.80	± 4.48	± 5.12	± 7.06	± 9.62	± 9.70	± 18.1	± 42.9
(JES) b -Tagged jet energy scale [%]	-	-	-	-	-	-	-	-
(JES) Effective detector NP set 1 [%]	-	-	-	-	± 0.23	± 0.28	-	± 0.20
(JES) Effective detector NP set 2 [%]	-	-	-	-	± 0.17	-	-	-
(JES) Effective detector NP set 3 [%]	-	-	-	-	-	-	-	-
(JES) Effective detector NP set 4 [%]	-	-	-	-	-	-	-	-
(JES) Effective detector NP set 5 [%]	-	-	-	-	-	-	-	-
(JES) Effective detector NP set 6 [%]	-	-	-	-	-	-	-	-
(JES) Effective detector NP set 7 [%]	-	-	-	-	-	-	-	-
(JES) Effective detector NP set 8 restTerm [%]	-	-	-	-	-	-	-	-
(JES) η intercalibration model [%]	-	-	-	± 0.16	-	-	-	-
(JES) η intercalibration total stat [%]	-	-	-	± 17	-	-	-	-
(JES) Flavor composition [%]	-	± 0.14	-	± 0.24	± 0.24	-	± 0.17	± 0.36
(JES) Flavor response [%]	-	-	-	± 0.22	± 0.25	-	-	-
(JES) Pile-up offset μ [%]	-	-	-	-	-	-	-	-
(JES) Pile-up offset N_{Vtx} [%]	-	-	-	-	± 0.31	-	± 0.14	-
(JES) Pile-up offset p_T topology [%]	-	-	-	-	-	-	± 0.16	± 0.29
(JES) Puschtschug [%]	-	-	-	-	-	-	-	-
(JES) Single particle high- p_T [%]	-	-	-	-	-	-	-	-
(LIES) Large- R jet Baseline mass [%]	-	-	-	± 0.49	± 0.40	± 0.85	± 0.71	± 7.73
(LIES) Large- R jet Baseline p_T [%]	-0.73	± 1.85	± 0.08	± 1.25	± 2.03	± 0.14	± 1.71	± 6.74
(LIES) Large- R jet Baseline τ_{23} [%]	± 2.25	± 0.36	± 0.75	± 1.65	± 4.34	± 1.45	± 5.58	± 13.5
(LIES) Large- R jet Modeling mass [%]	± 0.30	± 0.48	± 1.34	± 0.27	± 1.23	± 1.23	± 0.42	± 6.76
(LIES) Large- R jet Modeling p_T [%]	± 0.53	± 0.23	± 0.27	± 0.09	± 0.51	± 0.52	± 0.61	± 2.01
(LIES) Large- R jet Modeling τ_{23} [%]	± 2.36	± 0.69	± 0.85	± 1.38	± 4.75	± 1.86	± 7.29	± 15.9
(LIES) Large- R jet Tracking mass [%]	± 0.23	± 0.17	± 0.13	± 0.13	± 0.95	± 0.47	± 0.13	± 8.04
(LIES) Large- R jet Tracking p_T [%]	± 1.24	± 0.79	± 0.92	± 1.70	± 1.18	± 4.47	± 4.83	± 9.35
(LIES) Large- R jet Tracking τ_{23} [%]	± 2.31	± 0.31	± 0.38	± 0.21	± 0.20	± 0.26	± 0.21	± 0.39
(LIES) Large- R jet TotalStat p_T [%]	-	-	-	± 0.11	-	± 0.15	± 0.67	± 0.7
(LIES) Large- R jet TotalStat τ_{23} [%]	± 0.21	± 0.11	-	± 0.27	± 0.12	± 0.12	± 0.32	± 1.31
(LIES) Large- R jet top-quark mass resolution [%]	± 0.62	± 1.22	± 0.88	± 0.96	± 0.38	± 0.91	± 1.36	± 0.53
(FTAG) Quark tagging efficiency (eigenvector 0) [%]	± 0.32	± 0.11	-	± 0.27	± 0.60	± 0.47	± 0.56	± 1.85
(FTAG) Quark tagging efficiency (eigenvector 1) [%]	± 0.29	± 0.13	± 0.15	± 0.32	± 0.59	± 0.47	± 0.29	± 1.47
(FTAG) Quark tagging efficiency (eigenvector 2) [%]	± 0.18	-	-	± 0.11	± 0.26	± 0.34	± 0.43	± 0.86
(FTAG) Quark tagging efficiency (eigenvector 3) [%]	± 0.17	-	-	-	± 0.19	± 0.30	± 0.48	± 1.09
(FTAG) Quark tagging efficiency (eigenvector 4) [%]	-	-	-	-	-	± 0.12	± 0.17	± 0.36
(FTAG) Quark tagging efficiency (eigenvector 5) [%]	-	-	-	-	-	-	-	± 0.55
(FTAG) Quark tagging efficiency (eigenvector 6) [%]	-	-	± 0.19	± 0.27	± 0.23	± 0.13	± 0.23	± 0.62
(FTAG) Quark tagging efficiency (eigenvector 7) [%]	± 0.14	± 0.12	± 0.10	-	-	-	-	± 0.12
(FTAG) Quark tagging efficiency (eigenvector 8) [%]	-	-	-	-	-	-	-	± 0.47
(FTAG) Quark tagging efficiency (eigenvector 9) [%]	-	-	-	-	-	-	-	± 0.30
(FTAG) Quark tagging efficiency (eigenvector 10) [%]	-	-	-	-	-	-	-	-
(FTAG) Quark tagging efficiency (eigenvector 11) [%]	-	-	-	-	-	-	-	-
(FTAG) Quark tagging efficiency (eigenvector 12) [%]	-	-	-	-	-	-	-	-
(FTAG) Quark tagging efficiency (eigenvector 13) [%]	-	-	-	-	-	-	-	-
(FTAG) Quark tagging extrapolation [%]	± 1.35	± 0.64	± 0.29	± 0.84	± 1.64	± 2.71	± 4.06	± 8.79
(FTAG) Quark tagging extrapolation from c -Quark [%]	-	-	-	-	-	-	-	-
(PDF) PDF4LHC15 eigenvector 01 [%]	-	-	-	-	-	± 0.15	± 0.40	± 0.46
(PDF) PDF4LHC15 eigenvector 02 [%]	-	-	-	± 0.10	-	± 0.23	± 0.29	± 0.16
(PDF) PDF4LHC15 eigenvector 03 [%]	-	-	-	-	-	± 0.15	± 0.15	± 0.41
(PDF) PDF4LHC15 eigenvector 04 [%]	-	-	-	-	-	-	-	± 0.11
(PDF) PDF4LHC15 eigenvector 05 [%]	± 0.30	-	± 0.15	± 0.35	± 0.49	± 0.62	± 0.74	± 1.35
(PDF) PDF4LHC15 eigenvector 06 [%]	-	-	-	-	-	± 0.15	± 0.11	± 0.66
(PDF) PDF4LHC15 eigenvector 07 [%]	-	-	-	-	-	-	-	-
(PDF) PDF4LHC15 eigenvector 08 [%]	± 0.11	-	-	± 0.11	± 0.19	± 0.26	± 0.31	± 0.58
(PDF) PDF4LHC15 eigenvector 09 [%]	-	-	-	-	-	-	-	± 0.15
(PDF) PDF4LHC15 eigenvector 10 [%]	-	-	-	-	-	-	± 0.10	± 0.22
(PDF) PDF4LHC15 eigenvector 11 [%]	-	-	-	-	-	-	-	± 0.19
(PDF) PDF4LHC15 eigenvector 12 [%]	-	-	-	-	-	-	-	± 0.19
(PDF) PDF4LHC15 eigenvector 13 [%]	-	-	-	-	± 0.14	± 0.13	± 0.17	± 0.41
(PDF) PDF4LHC15 eigenvector 14 [%]	-	-	-	-	-	-	-	-
(PDF) PDF4LHC15 eigenvector 15 [%]	-	-	-	-	± 0.14	± 0.16	± 0.31	± 0.54
(PDF) PDF4LHC15 eigenvector 16 [%]	-	-	-	-	-	-	-	± 0.15
(PDF) PDF4LHC15 eigenvector 17 [%]	-	-	-	-	-	-	-	± 0.11
(PDF) PDF4LHC15 eigenvector 18 [%]	-	-	-	-	-	-	-	± 0.12
(PDF) PDF4LHC15 eigenvector 19 [%]	-	-	-	-	± 0.11	± 0.10	-	± 0.12
(PDF) PDF4LHC15 eigenvector 20 [%]	-	-	-	-	-	-	± 0.14	± 0.24
(PDF) PDF4LHC15 eigenvector 21 [%]	± 0.31	-	± 0.13	± 0.35	± 0.52	± 0.75	± 1.01	± 2.01
(PDF) PDF4LHC15 eigenvector 23 [%]	-	-	-	-	-	-	-	± 0.22
(PDF) PDF4LHC15 eigenvector 24 [%]	-	-	-	-	-	-	-	-
(PDF) PDF4LHC15 eigenvector 25 [%]	-	-	-	-	-	-	-	-
(PDF) PDF4LHC15 eigenvector 26 [%]	-	-	-	-	-	-	± 0.12	± 0.18
(PDF) PDF4LHC15 eigenvector 27 [%]	-	-	-	-	± 0.10	± 0.15	± 0.20	± 0.19
(PDF) PDF4LHC15 eigenvector 28 [%]	± 0.12	-	-	± 0.15	± 0.22	± 0.32	± 0.50	± 0.90
(PDF) PDF4LHC15 eigenvector 29 [%]	-	-	-	± 0.07	-	-	-	-
(PDF) PDF4LHC15 eigenvector 30 [%]	-	-	-	-	-	-	-	± 0.10
(LEP) Electromagnetic energy resolution [%]	-	-	-	-	-	-	-	± 0.19
(LEP) Electron energy scale [%]	-	-	-	-	-	-	± 0.53	± 0.27
(LEP) Muon energy scale [%]	-	-	-	-	-	-	-	-
(LEP) Muon (MS) momentum resolution [%]	-	-	-	-	-	-	-	-
(LEP) Muon (ID) momentum resolution [%]	-	-	-	-	-	-	-	-
(LEP) Muon sagitta resolution [%]	-	-	-	-	-	-	-	-
(LEP) Muon sagitta resolution bias [%]	-	-	-	-	-	-	-	-
(MET/PU) $E_{\text{miss}}^{\text{soft}}$ Soft jet resolution para [%]	-	-	-	-	-	-	-	-
(MET/PU) $E_{\text{miss}}^{\text{soft}}$ Soft jet resolution perp [%]	-	-	-	-	-	-	-	-
(MET/PU) $E_{\text{miss}}^{\text{soft}}$ Soft jet scale [%]	-	-	-	-	-	-	-	-
(MET/PU) jet vertex tagging [%]	-	-	-	-	± 0.12	-	-	± 0.21
(BKG) Singl-top W cross-section [%]	-	-	-	-	-	-	-	-
(BKG) Single top W -channel treatment [%]	-	-	± 0.12	-	± 0.14	± 0.20	± 0.23	± 0.91
(BKG) it+ W cross-section [%]	-	-	-	-	-	-	-	-
(BKG) it+ Z cross-section [%]	-	-	-	-	-	-	-	-
(BKG) it+ H cross-section [%]	-	-	-	-	-	-	-	-
(MOD) Monte Carlo sample statistics [%]	± 1.80	± 2.01	± 2.70	± 2.86	± 4.21	± 5.29	± 4.82	± 27.3
(MOD) ISR/FSR + scale [%]	± 1.27	± 1.70	± 2.23	± 3.07	± 4.32	± 6.06	± 4.69	± 20.8
(MOD) Alternative hard-scattering model [%]	± 1.55	± 0.96	± 1.95	± 3.27	± 0.27	± 1.48	± 5.38	± 4.26
(MOD) Alternative parton-shower model [%]	± 1.76	± 3.11	± 3.46	± 4.34	± 3.22	± 0.16	± 3.18	± 16.2

Table 42: The individual systematic uncertainties in the fiducial phase-space relative differential cross-sections for the leading top-quark transverse momentum calculated as a percentage of the cross-section in each bin. Dashes are used when the estimated relative systematic uncertainty for that bin is below 0.1%.

Bins [Unit GeV^{-1}]	0-0.30	0.30-0.60	0.60-0.90	0.90-1.20	1.20-1.50	1.50-2
$d\sigma / d\eta^{\pm} [\text{pb}/\text{Unit } \eta^{\pm}]$	$2.72 \cdot 10^{-3}$	$2.08 \cdot 10^{-3}$	$1.77 \cdot 10^{-3}$	$1.50 \cdot 10^{-3}$	$1.08 \cdot 10^{-3}$	$5.46 \cdot 10^{-4}$
Total Uncertainty [%]	± 24.1	± 24.8	± 27.9	± 24.6	± 26.1	± 26.1
Stat. [%]	± 4.9	± 5.7	± 5.8	± 6.6	± 7.2	± 9.0
Systematics [%]	± 23.5	± 23.9	± 23.0	± 23.5	± 25.0	± 23.8
(JES) b-Tagged jet energy scale [%]	-	-	-	-	-	-
(JES) Effective detector NP set 1 [%]	-	± 0.12	± 0.13	-	-	± 0.22
(JES) Effective detector NP set 2 [%]	-	-	-	-	-	-
(JES) Effective detector NP set 3 [%]	-	-	-	-	-	-
(JES) Effective detector NP set 4 [%]	-	-	-	-	-	-
(JES) Effective detector NP set 5 [%]	-	-	-	-	-	-
(JES) Effective detector NP set 6 [%]	-	-	-	-	-	-
(JES) Effective detector NP set 7 [%]	-	-	-	-	-	-
(JES) Effective detector NP set 8 resTerm [%]	-	-	-	-	-	-
(JES) η intercalibration model [%]	-	-	-	-	-	-
(JES) η intercalibration offset [%]	-	-	-	-	-	-
(JES) Flavor composition [%]	± 0.23	± 0.25	± 0.35	± 0.15	± 0.16	± 0.20
(JES) Flavor response [%]	-	-	± 0.17	-	-	± 0.22
(JES) Pile-up offset η [%]	-	-	-	-	-	-
(JES) Pile-up offset p_T [%]	-	-	-	-	-	± 0.25
(JES) Pile-up offset η topology [%]	± 0.10	± 0.17	± 0.2	-	± 0.14	± 0.15
(JES) Pile-up offset p_T topology [%]	-	± 0.12	± 0.13	-	-	± 0.23
(JES) Single particle high- p_T [%]	-	-	-	-	-	-
(JES) Large- R jet Baseline mass [%]	± 2.8	± 0.56	± 0.47	± 0.62	± 0.15	± 0.24
(JES) Large- R jet Baseline p_T [%]	± 2.9	± 0.35	± 0.31	± 0.19	± 0.26	± 0.33
(JES) Large- R jet Modeling mass [%]	± 0.02	± 0.75	± 0.75	± 0.69	± 0.26	± 0.34
(JES) Large- R jet Modeling mass p_T [%]	± 0.07	± 0.40	± 0.44	± 0.72	± 0.33	± 1.07
(JES) Large- R jet Modeling p_T [%]	± 0.95	± 2.51	± 2.66	± 2.12	± 1.11	± 2.26
(JES) Large- R jet τ_2/τ_1 [%]	± 0.09	± 0.44	± 0.44	± 0.74	± 0.24	± 0.92
(JES) Large- R jet Tracking p_T [%]	± 0.26	± 0.42	± 0.32	-	± 0.19	-
(JES) Large- R jet Tracking η_2/η_1 [%]	± 4.62	± 5.33	± 4.72	± 4.56	± 5.52	± 5.78
(JES) Large- R jet Tracking η_2/η_1 p_T [%]	± 0.04	± 0.28	± 0.28	± 0.28	± 0.25	± 0.39
(JES) Light-jet baseline mass [%]	± 0.08	± 0.21	± 0.21	-	-	-
(JES) Light-jet baseline p_T [%]	± 0.23	± 0.12	± 0.16	-	± 0.12	± 0.35
(JES) Light-jet baseline τ_{21} [%]	± 0.23	-	-	-	-	-
(JES) Light-jet jet-quark extrapolation [%]	± 1.00	± 1.18	± 1.18	± 1.07	± 1.07	± 1.04
(ITAG) b-Quark tagging efficiency (eigencenter 0) [%]	± 5.31	± 5.37	± 2.26	± 5.28	± 18	± 5.20
(ITAG) b-Quark tagging efficiency (eigencenter 1) [%]	± 4.95	± 4.97	± 4.94	± 4.46	± 4.66	± 4.82
(ITAG) b-Quark tagging efficiency (eigencenter 2) [%]	± 0.78	± 0.78	± 0.78	± 0.70	± 0.68	± 0.64
(ITAG) b-Quark tagging efficiency (eigencenter 3) [%]	± 0.28	± 0.40				
(ITAG) b-Quark tagging efficiency (eigencenter 4) [%]	± 0.25	± 0.24	± 0.24	± 0.23	± 0.23	± 0.21
(ITAG) c-Quark tagging efficiency (eigencenter 0) [%]	± 2.18	± 1.98	± 1.83	± 2.38	± 1.75	± 2.44
(ITAG) c-Quark tagging efficiency (eigencenter 1) [%]	± 1.18	± 1.25	± 1.25	± 1.34	± 1.02	± 1.69
(ITAG) c-Quark tagging efficiency (eigencenter 2) [%]	± 0.69	± 0.67	± 0.66	± 0.65	± 0.55	± 0.62
(ITAG) c-Quark tagging efficiency (eigencenter 3) [%]	± 0.47	± 0.46	± 0.43	± 0.44	± 0.35	± 0.50
(ITAG) Light-jet tagging efficiency (eigencenter 0) [%]	± 0.21	± 0.10	± 0.21	± 0.22	± 0.69	± 0.55
(ITAG) Light-jet tagging efficiency (eigencenter 1) [%]	-	-	± 0.10	-	-	-
(ITAG) Light-jet tagging efficiency (eigencenter 2) [%]	-	-	± 0.15	± 0.11	± 0.27	± 0.21
(ITAG) Light-jet tagging efficiency (eigencenter 3) [%]	-	-	± 0.13	± 0.10	± 0.13	± 0.16
(ITAG) Light-jet tagging efficiency (eigencenter 4) [%]	-	-	-	-	± 0.37	± 0.22
(ITAG) Light-jet tagging efficiency (eigencenter 5) [%]	-	-	-	-	-	-
(ITAG) Light-jet tagging efficiency (eigencenter 6) [%]	-	-	-	-	-	-
(ITAG) Light-jet tagging efficiency (eigencenter 7) [%]	-	-	-	-	± 0.14	-
(ITAG) Light-jet tagging efficiency (eigencenter 8) [%]	-	-	-	-	± 0.11	-
(ITAG) Light-jet tagging efficiency (eigencenter 9) [%]	± 0.27	± 0.23	± 0.22	± 0.23	± 0.26	± 0.15
(ITAG) Light-jet tagging efficiency (eigencenter 10) [%]	-	± 0.74	± 0.71	± 0.76	± 0.17	± 0.77
(ITAG) Light-jet tagging efficiency (eigencenter 11) [%]	-	-	-	-	-	-
(ITAG) Light-jet tagging efficiency (eigencenter 12) [%]	-	-	-	-	-	-
(ITAG) Light-jet tagging efficiency (eigencenter 13) [%]	± 0.25	± 0.25	± 0.27	± 0.27	± 0.40	± 0.57
(ITAG) Light-jet tagging efficiency (eigencenter 14) [%]	-	-	-	-	± 0.12	± 0.24
(ITAG) Light-jet tagging efficiency (eigencenter 15) [%]	± 0.21	± 0.17	± 0.13	-	± 0.11	± 0.24
(ITAG) Light-jet tagging efficiency (eigencenter 16) [%]	-	-	-	-	± 0.16	± 0.10
(ITAG) Light-jet tagging efficiency (eigencenter 17) [%]	± 0.34	± 0.33	± 0.32	± 0.33	± 0.44	± 0.71
(ITAG) Light-jet tagging efficiency (eigencenter 18) [%]	-	-	-	-	± 0.16	± 0.34
(ITAG) Light-jet tagging efficiency (eigencenter 19) [%]	± 0.67	± 0.73	± 0.86	± 0.88	± 0.79	-
(ITAG) Light-jet tagging efficiency (eigencenter 20) [%]	-	-	± 0.10	± 0.25	± 0.37	± 0.48
(ITAG) Light-jet tagging efficiency (eigencenter 21) [%]	-	-	-	-	± 0.17	± 0.41
(ITAG) Light-jet tagging efficiency (eigencenter 22) [%]	± 0.18	± 0.30	± 0.56	± 1.03	± 2.03	± 4.23
(ITAG) Light-jet tagging efficiency (eigencenter 23) [%]	-	-	-	-	-	-
(ITAG) Light-jet tagging efficiency (eigencenter 24) [%]	± 0.10	-	-	-	-	± 0.14
(ITAG) Light-jet tagging efficiency (eigencenter 25) [%]	-	-	-	-	-	-
(ITAG) Light-jet tagging efficiency (eigencenter 26) [%]	-	-	-	-	± 0.10	± 0.18
(ITAG) Light-jet tagging efficiency (eigencenter 27) [%]	± 0.23	± 0.23	± 0.25	± 0.27	± 0.32	± 0.35
(ITAG) Light-jet tagging efficiency (eigencenter 28) [%]	± 0.20	-	± 0.10	± 0.39	± 0.70	± 0.79
(ITAG) Light-jet tagging efficiency (eigencenter 29) [%]	-	-	-	-	-	-
(ITAG) Light-jet tagging efficiency (eigencenter 30) [%]	-	-	-	-	-	-
(ITAG) Light-jet tagging efficiency (eigencenter 31) [%]	-	-	-	-	-	-
(ITAG) Muon (MS) momentum resolution [%]	-	-	-	-	-	-
(ITAG) Muon (MS) momentum bias [%]	-	-	-	-	-	-
(ITAG) Muon (MS) sagitta resolution bias [%]	-	-	-	-	-	-
(ITAG) Muon (MS) ρ resolution [%]	-	-	-	-	-	-
(METTPU) ρ^{jet} Soft jet resolution per %	-	-	-	-	-	-
(METTPU) ρ^{miss} Soft jet resolution per %	-	-	-	-	-	-
(METTPU) Jet vertex resolution [%]	-	-	-	-	-	-
(METTPU) Jet vertex tagging [%]	-	-	-	-	± 0.10	± 0.15
Luminosity [%]	± 0.03	± 1.97	± 2.01	± 2.04	± 1.97	± 1.99
BRG $t \bar{t}$ cross-section [%]	± 0.28	± 0.20	± 0.12	± 0.25	± 0.23	-
BRG $b \bar{b}$ cross-section [%]	-	-	-	-	-	-
BRG $t \bar{t} + Z$ cross-section [%]	-	-	-	-	-	-
(BRG) Multijet background statistics [%]	± 1.92	± 2.39	± 1.92	± 2.11	± 2.56	± 4.61
(MOD) Monte Carlo sample statistics [%]	± 1.62	± 1.78	± 1.84	± 2.32	± 2.73	± 3.85
(MOD) ISR-FSR + scale [%]	± 2.75	± 1.79	± 2.97	± 2.60	± 3.30	± 4.30
(MOD) Alternative hadron shower model [%]	± 1.12	± 1.11	± 1.0	± 0.54	± 0.64	± 0.88
(MOD) Alternative parton-shower model [%]	± 11.9	± 12.3	± 16.9	± 13.8	± 15.8	± 11.0

Table 43: The individual systematic uncertainties in the fiducial phase-space absolute differential cross-sections for the leading top-quark absolute value of the rapidity calculated as a percentage of the cross-section in each bin. Dashes are used when the estimated relative systematic uncertainty for that bin is below 0.1%.

Not reviewed, for internal circulation only

Bin [Unit [fb^{-1}]]	0-0.30	0.30-0.60	0.60-0.90	0.90-1.20	1.20-1.50	1.50-2
$b\bar{b}$ d [†] d [†] [fb]	$8.123 \cdot 10^{-3}$	$7.139 \cdot 10^{-3}$	$6.067 \cdot 10^{-3}$	$5.158 \cdot 10^{-3}$	$4.725 \cdot 10^{-3}$	$4.371 \cdot 10^{-3}$
Total Uncertainty [%]	± 5.74	± 6.79	± 7.71	± 7.45	± 8.95	± 11.9
Stat. [%]	± 4.4	± 5.2	± 5.4	± 6.0	± 6.9	± 8.5
Systematics [%]	± 2.76	± 3.20	± 4.86	± 3.13	± 2.25	± 5.91
(JES) b-Tagged jet energy scale [%]	-	-	-	-	-	-
(JES) Effective detector NP set 1 [%]	-	-	-	-	-	± 0.16
(JES) Effective detector NP set 2 [%]	-	-	-	-	-	-
(JES) Effective detector NP set 3 [%]	-	-	-	-	-	-
(JES) Effective detector NP set 4 [%]	-	-	-	-	-	-
(JES) Effective detector NP set 5 [%]	-	-	-	-	-	-
(JES) Effective detector NP set 6 [%]	-	-	-	-	-	-
(JES) Effective detector NP set 7 [%]	-	-	-	-	-	-
(JES) Effective detector NP set 8 resTerm [%]	-	-	-	-	-	-
(JES) η intercalibration model [%]	-	-	-	-	-	-
(JES) Jet energy scale offset [%]	-	-	-	-	-	-
(JES) Single particle high- p_T [%]	-	-	-	-	-	-
(JES) Large- R jet Baseline mass [%]	-	± 0.25	± 0.4	± 0.36	± 0.20	± 0.60
(JES) Large- R jet Baseline p_T [%]	-	± 0.56	± 0.11	± 0.28	± 0.05	± 0.48
(JES) Large- R jet Modeling mass [%]	± 0.02	± 0.11	± 0.09	± 0.36	± 0.51	± 0.96
(JES) Large- R jet Modeling p_T [%]	-	± 0.33	± 0.28	± 0.37	± 0.62	± 1.53
(JES) Large- R jet Tracking p_T [%]	± 0.31	± 0.35	± 0.23	± 0.37	± 0.60	± 0.11
(JES) Large- R jet Tracking τ_{23} [%]	± 0.08	± 0.28	± 0.28	± 0.59	-	± 0.65
(JES) Large- R jet Tracking p_T [%]	± 0.28	± 0.13	± 0.56	± 0.39	± 0.35	± 0.15
(JES) Large- R jet Tracking τ_{23} [%]	± 0.45	± 0.47	± 0.38	± 0.48	± 0.55	± 0.80
(JES) Large- R jet Tracking τ_{23} [%]	± 0.17	± 0.75	-	± 0.36	± 0.16	± 0.32
(JES) Large- R jet TotalsR p_T [%]	-	± 0.12	± 0.12	-	-	-
(JES) Large- R jet TotalsR τ_{23} [%]	-	± 0.18	-	-	-	-
(JES) Large- R jet TotalsR p_T [%]	-	-	-	-	-	± 0.17
(JES) Large- R jet Quark-quark resolution [%]	± 0.34	± 0.17	± 0.14	± 0.70	± 0.27	± 0.30
(PTAG) b-Quark tagging efficiency (eigenvector 0) [%]	-	-	-	-	± 0.11	-
(PTAG) b-Quark tagging efficiency (eigenvector 1) [%]	-	-	-	-	± 0.24	-
(PTAG) b-Quark tagging efficiency (eigenvector 2) [%]	-	-	-	-	-	± 0.11
(PTAG) b-Quark tagging efficiency (eigenvector 3) [%]	-	-	-	-	-	± 0.10
(PTAG) b-Quark tagging efficiency (eigenvector 4) [%]	-	-	-	-	-	-
(PTAG) b-Quark tagging efficiency (eigenvector 0) [%]	-	± 0.15	-	± 0.23	± 0.30	± 0.36
(PTAG) b-Quark tagging efficiency (eigenvector 1) [%]	-	± 0.17	-	± 0.18	-	± 0.38
(PTAG) b-Quark tagging efficiency (eigenvector 2) [%]	-	-	-	-	-	-
(PTAG) b-Quark tagging efficiency (eigenvector 3) [%]	-	-	-	-	-	-
(PTAG) Light-jet tagging efficiency (eigenvector 0) [%]	-	± 0.15	-	-	± 0.42	± 0.30
(PTAG) Light-jet tagging efficiency (eigenvector 1) [%]	-	-	-	-	-	-
(PTAG) Light-jet tagging efficiency (eigenvector 2) [%]	-	-	-	-	-	-
(PTAG) Light-jet tagging efficiency (eigenvector 3) [%]	-	-	-	-	-	-
(PTAG) Light-jet tagging efficiency (eigenvector 4) [%]	-	-	-	-	-	-
(PTAG) Light-jet tagging efficiency (eigenvector 5) [%]	-	-	-	-	-	-
(PTAG) Light-jet tagging efficiency (eigenvector 6) [%]	-	-	-	-	-	-
(PTAG) Light-jet tagging efficiency (eigenvector 7) [%]	-	-	-	-	± 0.16	-
(PTAG) Light-jet tagging efficiency (eigenvector 8) [%]	-	-	-	-	-	-
(PTAG) Light-jet tagging efficiency (eigenvector 9) [%]	-	-	-	-	-	-
(PTAG) Light-jet tagging efficiency (eigenvector 10) [%]	-	-	-	-	-	-
(PTAG) Light-jet tagging efficiency (eigenvector 11) [%]	-	-	-	-	-	-
(PTAG) Light-jet tagging efficiency (eigenvector 12) [%]	-	-	-	-	-	-
(PTAG) Light-jet tagging efficiency (eigenvector 13) [%]	-	-	-	-	-	-
(PTAG) b-Quark tagging resolution [%]	± 0.17	± 0.10	-	± 0.10	± 0.28	± 0.40
(POD) PDF4LHC15 eigenvector 0 [%]	± 0.23	± 0.16	-	± 0.15	± 0.41	± 0.43
(POD) PDF4LHC15 eigenvector 2 [%]	± 0.20	± 0.18	± 0.15	-	± 0.32	± 0.99
(POD) PDF4LHC15 eigenvector 0 [%]	-	-	± 0.16	-	± 0.18	± 0.49
(POD) PDF4LHC15 eigenvector 0 [%]	-	-	-	± 0.19	-	± 0.60
(POD) PDF4LHC15 eigenvector 0 [%]	± 0.22	± 0.17	± 0.10	-	± 0.30	± 1.05
(POD) PDF4LHC15 eigenvector 0 [%]	± 0.33	± 0.24	± 0.12	-	± 0.51	± 1.27
(POD) PDF4LHC15 eigenvector 0 [%]	-	-	-	-	-	± 0.10
(POD) PDF4LHC15 eigenvector 10 [%]	± 0.20	± 0.17	-	-	± 0.32	± 0.72
(POD) PDF4LHC15 eigenvector 10 [%]	± 0.11	-	-	-	± 0.19	± 0.27
(POD) PDF4LHC15 eigenvector 10 [%]	-	-	-	-	± 0.12	± 0.41
(POD) PDF4LHC15 eigenvector 12 [%]	-	-	-	-	± 0.10	± 0.28
(POD) PDF4LHC15 eigenvector 13 [%]	-	-	-	-	-	± 0.18
(POD) PDF4LHC15 eigenvector 14 [%]	-	-	-	-	-	± 0.15
(POD) PDF4LHC15 eigenvector 15 [%]	-	-	-	-	-	-
(POD) PDF4LHC15 eigenvector 16 [%]	-	-	-	-	± 0.13	± 0.13
(POD) PDF4LHC15 eigenvector 17 [%]	-	-	-	-	-	± 0.33
(POD) PDF4LHC15 eigenvector 18 [%]	-	-	-	-	-	± 0.10
(POD) PDF4LHC15 eigenvector 19 [%]	-	-	-	-	-	± 0.27
(POD) PDF4LHC15 eigenvector 20 [%]	± 0.16	± 0.11	-	± 0.11	± 0.23	± 0.34
(POD) PDF4LHC15 eigenvector 21 [%]	-	-	-	-	-	± 0.34
(POD) PDF4LHC15 eigenvector 22 [%]	± 0.75	± 0.62	± 0.37	-	± 1.08	± 3.26
(POD) PDF4LHC15 eigenvector 23 [%]	-	-	-	-	-	-
(POD) PDF4LHC15 eigenvector 24 [%]	-	-	-	-	-	± 0.18
(POD) PDF4LHC15 eigenvector 25 [%]	-	-	-	-	-	-
(POD) PDF4LHC15 eigenvector 26 [%]	-	-	-	-	± 0.18	± 0.14
(POD) PDF4LHC15 eigenvector 27 [%]	-	-	-	-	-	-
(POD) PDF4LHC15 eigenvector 28 [%]	± 0.35	± 0.24	-	± 0.24	± 0.55	± 0.64
(POD) PDF4LHC15 eigenvector 29 [%]	-	-	-	-	-	-
(POD) PDF4LHC15 eigenvector 30 [%]	-	-	-	-	-	-
(LEP) Electron energy scale [%]	-	-	-	-	± 0.11	-
(LEP) Muon energy scale [%]	-	-	-	-	-	-
(LEP) Muon (MS) momentum resolution [%]	-	-	-	-	-	-
(LEP) Muon (ID) momentum resolution [%]	-	-	-	-	-	-
(LEP) Muon track resolution bias [%]	-	-	-	-	-	-
(LEP) Muon sagitta [%]	-	-	-	-	-	-
(METTP) $E^{\mu\mu}_{\text{miss}}$ Soft jet resolution per [%]	-	-	-	-	-	-
(METTP) $E^{\mu\mu}_{\text{miss}}$ Soft jet resolution per [%]	-	-	-	-	-	-
(METTP) Jet energy scale [%]	-	-	-	-	-	-
(METTP) Jet vertex tagging [%]	-	-	-	-	-	-
Luminosity [%]	-	-	-	-	-	-
(BKGG) $t\bar{t}$ + Z cross-section [%]	-	-	-	-	-	-
(BKGG) Single top v -channel invariant [%]	-	-	-	-	-	± 0.23
(BKGG) $t\bar{t}$ + W cross-section [%]	-	-	-	-	-	-
(MOD) Alternative parton-shower model [%]	± 1.88	± 1.50	± 3.81	± 0.23	± 2.63	± 2.98

Table 44: The individual systematic uncertainties in the fiducial phase-space relative differential cross-sections for the leading top-quark absolute value of the rapidity calculated as a percentage of the cross-section in each bin. Dashes are used when the estimated relative systematic uncertainty for that bin is below 0.1%.

Not reviewed, for internal circulation only

Bins (GeV)	350-400	400-450	450-500	500-550	550-600	600-600	800-1200
$d\sigma/dp_T$ [pb/GeV]	$4.757 \cdot 10^{-9}$	$9.169 \cdot 10^{-9}$	$1.341 \cdot 10^{-8}$	$1.199 \cdot 10^{-8}$	$6.307 \cdot 10^{-9}$	$2.449 \cdot 10^{-9}$	$2.045 \cdot 10^{-9}$
Total Uncertainty [%]	± 27.0	± 24.1	± 23.6	± 26.9	± 29.9	± 33.0	± 52.9
JES [$\pm\%$]	± 1.8	± 1.1	± 1.2	± 1.0	± 1.1	± 1.1	± 1.4
Systematics [%]	± 23.8	± 22.8	± 23.0	± 26.1	± 27.9	± 31.9	± 38.6
JES b-Tagged jet energy scale [%]	-	-	-	-	-	-	-
(JES) b-Tagging efficiency [%]	-	± 10	-	-	-	-	± 33
(JES) Effective detector NP set 1 [%]	-	-	-	-	-	-	-
(JES) Effective detector NP set 2 [%]	-	-	-	-	-	-	-
(JES) Effective detector NP set 3 [%]	-	-	-	-	-	-	-
(JES) Effective detector NP set 4 [%]	-	-	-	-	-	-	-
(JES) Effective detector NP set 5 [%]	-	-	-	-	-	-	-
(JES) Effective detector NP set 6 [%]	-	-	-	-	-	-	-
(JES) Effective detector NP set 7 [%]	-	-	-	-	-	-	-
(JES) Effective detector NP set 8 recTerm [%]	-	-	-	-	-	-	-
(JES) η intercalibration model [%]	-	-	-	-	-	-	-
(JES) Flavor composition star [%]	-	-	-	-	-	-	-
(JES) Flavor composition [%]	± 0.21	± 0.24	± 0.28	± 0.21	± 0.21	± 0.12	± 0.11
(JES) Flavor response [%]	± 0.27	± 0.21	± 0.24	± 0.21	-	-	± 0.15
(JES) Hadronic energy [%]	-	-	-	-	-	-	-
(JES) Pile-up offset N_{PU} [%]	-	-	-	-	-	-	-
(JES) Pile-up offset p_T [%]	± 0.12	-	± 0.16	-	± 0.11	± 0.13	± 0.15
(JES) Punch-through [%]	-	-	± 0.12	-	-	-	-
(JES) Single particle high- p_T [%]	-	-	-	-	-	-	-
(JES) Single particle low- p_T [%]	± 1.25	± 0.29	± 0.30	-	± 0.18	± 0.11	± 0.61
(JES) Large- η jet Baseline p_T [%]	± 3.54	± 3.94	± 2.81	± 2.81	± 2.68	± 3.04	± 11.6
(JES) Large- η jet Baseline r_{jet} [%]	± 0.48	± 0.20	± 0.17	± 0.17	± 0.07	± 0.15	± 15.5
(JES) Large- η jet Modeling p_T [%]	± 18.8	-	± 15.5	-	± 14.6	-	± 55
(JES) Large- η jet Modeling r_{jet} [%]	± 1.82	± 1.35	± 2.85	± 2.29	± 2.27	± 1.39	± 1.08
(JES) Large- η jet Modeling r_{jet}^2 [%]	± 1.5	± 1.35	± 1.00	± 0.97	± 1.12	± 1.15	± 1.84
(JES) Large- η jet Modeling r_{jet}^3 [%]	± 1.5	± 1.39	± 0.20	± 0.20	± 0.27	± 0.27	± 0.71
(JES) Large- η jet Tracking p_T [%]	± 4.19	± 5.37	± 4.85	± 4.12	± 5.43	± 6.47	± 9.55
(JES) Large- η jet Tracking r_{jet} [%]	± 0.36	± 0.24	± 0.55	± 0.43	± 0.47	± 0.42	± 0.23
(JES) Large- η jet Tracking r_{jet}^2 [%]	± 0.36	± 0.24	± 0.55	± 0.43	± 0.47	± 0.42	± 0.23
(JES) Large- η jet TotalStar p_T [%]	± 0.74	± 0.24	± 0.55	± 0.43	± 0.47	± 0.42	± 0.23
(JES) Large- η jet TotalStar r_{jet} [%]	± 0.52	-	± 0.21	-	± 0.31	± 0.52	-
(JES) Large- η jet TotalStar r_{jet}^2 [%]	± 0.52	-	± 0.21	-	± 0.31	± 0.52	-
(JES) Large- η jet TotalStar r_{jet}^3 [%]	± 0.52	-	± 0.21	-	± 0.31	± 0.52	-
(JES) Large- η jet TotalStar r_{jet}^4 [%]	± 0.52	-	± 0.21	-	± 0.31	± 0.52	-
(JES) Large- η jet TotalStar r_{jet}^5 [%]	± 0.52	-	± 0.21	-	± 0.31	± 0.52	-
(JES) Large- η jet TotalStar r_{jet}^6 [%]	± 0.52	-	± 0.21	-	± 0.31	± 0.52	-
(JES) Large- η jet TotalStar r_{jet}^7 [%]	± 0.52	-	± 0.21	-	± 0.31	± 0.52	-
(JES) Large- η jet TotalStar r_{jet}^8 [%]	± 0.52	-	± 0.21	-	± 0.31	± 0.52	-
(JES) Large- η jet TotalStar r_{jet}^9 [%]	± 0.52	-	± 0.21	-	± 0.31	± 0.52	-
(JES) Large- η jet TotalStar r_{jet}^{10} [%]	± 0.52	-	± 0.21	-	± 0.31	± 0.52	-
(JES) Large- η jet TotalStar r_{jet}^{11} [%]	± 0.52	-	± 0.21	-	± 0.31	± 0.52	-
(JES) Large- η jet TotalStar r_{jet}^{12} [%]	± 0.52	-	± 0.21	-	± 0.31	± 0.52	-
(JES) Large- η jet TotalStar r_{jet}^{13} [%]	± 0.52	-	± 0.21	-	± 0.31	± 0.52	-
(JES) Quark tagging extrapolation [%]	± 1.98	± 2.17	± 2.60	± 2.93	± 3.86	± 5.15	± 10.1
(FTAG) c-Quark tagging extrapolation [%]	± 1.98	± 2.17	± 2.60	± 2.93	± 3.86	± 5.15	± 10.1
(FTAG) PDF4LHC13c c-Quark mass [%]	± 0.21	± 0.17	-	-	± 0.11	± 0.28	± 0.80
(FTAG) PDF4LHC13c c-Quark resolution [%]	± 0.50	± 0.51	± 0.53	± 0.57	± 0.59	± 0.64	± 0.74
(FTAG) PDF4LHC13c s-Quark mass [%]	-	-	-	-	± 0.13	± 0.15	± 0.25
(FTAG) PDF4LHC13c s-Quark resolution [%]	± 0.43	± 0.31	± 0.23	± 0.17	-	-	± 0.13
(FTAG) PDF4LHC13c s-Quark resolution 0 [%]	± 2.01	± 2.05	± 2.09	± 2.18	± 2.35	± 2.55	± 2.97
(FTAG) PDF4LHC13c s-Quark resolution 1 [%]	± 0.39	± 0.37	± 0.28	± 0.22	± 0.19	± 0.12	± 0.19
(FTAG) PDF4LHC13c s-Quark resolution 2 [%]	-	-	-	-	-	-	± 0.11
(FTAG) PDF4LHC13c s-Quark resolution 3 [%]	-	-	-	-	-	-	± 0.11
(FTAG) PDF4LHC13c s-Quark resolution 4 [%]	-	-	-	-	-	-	± 0.11
(FTAG) PDF4LHC13c s-Quark resolution 5 [%]	-	-	-	-	-	-	± 0.11
(FTAG) PDF4LHC13c s-Quark resolution 6 [%]	-	-	-	-	-	-	± 0.11
(FTAG) PDF4LHC13c s-Quark resolution 7 [%]	-	-	-	-	-	-	± 0.11
(FTAG) PDF4LHC13c s-Quark resolution 8 [%]	-	-	-	-	-	-	± 0.11
(FTAG) PDF4LHC13c s-Quark resolution 9 [%]	-	-	-	-	-	-	± 0.11
(FTAG) PDF4LHC13c s-Quark resolution 10 [%]	-	-	-	-	-	-	± 0.11
(FTAG) PDF4LHC13c s-Quark resolution 11 [%]	± 0.33	± 0.34	± 0.33	± 0.32	± 0.35	± 0.35	± 0.40
(FTAG) PDF4LHC13c s-Quark resolution 12 [%]	± 0.18	± 0.24	± 0.26	± 0.25	± 0.35	± 0.43	± 0.58
(FTAG) PDF4LHC13c s-Quark resolution 13 [%]	-	-	-	-	-	-	-
(FTAG) PDF4LHC13c s-Quark resolution 14 [%]	-	-	-	-	-	-	-
(FTAG) PDF4LHC13c s-Quark resolution 15 [%]	-	-	-	-	-	-	-
(FTAG) PDF4LHC13c s-Quark resolution 16 [%]	-	-	-	-	-	-	-
(FTAG) PDF4LHC13c s-Quark resolution 17 [%]	± 0.44	± 0.41	± 0.36	± 0.34	± 0.33	± 0.31	± 0.28
(FTAG) PDF4LHC13c s-Quark resolution 18 [%]	± 0.71	± 0.77	± 0.71	± 0.69	± 0.74	± 0.75	± 0.76
(FTAG) PDF4LHC13c s-Quark resolution 19 [%]	-	-	-	-	-	-	-
(FTAG) PDF4LHC13c s-Quark resolution 20 [%]	-	-	-	-	-	-	-
(FTAG) PDF4LHC13c s-Quark resolution 21 [%]	-	-	-	-	-	-	-
(FTAG) PDF4LHC13c s-Quark resolution 22 [%]	± 0.65	± 0.64	± 0.72	± 0.82	± 0.99	± 1.28	± 1.98
(FTAG) PDF4LHC13c s-Quark resolution 23 [%]	-	-	-	-	-	-	-
(FTAG) PDF4LHC13c s-Quark resolution 24 [%]	-	-	-	-	-	-	-
(FTAG) PDF4LHC13c s-Quark resolution 25 [%]	-	-	-	-	-	-	-
(FTAG) PDF4LHC13c s-Quark resolution 26 [%]	-	-	-	-	-	-	-
(FTAG) PDF4LHC13c s-Quark resolution 27 [%]	-	± 0.14	± 0.22	± 0.29	± 0.35	± 0.45	± 0.59
(FTAG) PDF4LHC13c s-Quark resolution 28 [%]	-	-	-	± 0.12	± 0.23	± 0.40	± 0.81
(FTAG) PDF4LHC13c s-Quark resolution 29 [%]	-	-	-	-	-	-	-
(FTAG) PDF4LHC13c s-Quark resolution 30 [%]	-	-	-	-	-	-	-
(LEP) Electron energy resolution [%]	-	-	-	-	-	-	-
(LEP) Electron energy scale [%]	-	-	-	-	-	-	-
(LEP) Muon energy scale [%]	-	-	-	-	-	-	-
(LEP) Muon energy resolution [%]	-	-	-	-	-	-	-
(LEP) Muon momentum resolution [%]	-	-	-	-	-	-	-
(LEP) Muon pT resolution [%]	-	-	-	-	-	-	-
(LEP) Muon rapidity resolution [%]	-	-	-	-	-	-	-
(METFPU E_T^{miss}) Soft jet scale peep [%]	-	-	-	-	-	-	-
(METFPU E_T^{miss}) Soft jet scale peep 2 [%]	-	-	-	-	-	-	-
Luminosity [%]	± 2.10	± 1.99	± 2.02	± 2.00	± 1.99	± 1.97	± 1.93
(BKGR) Single top W cross-section [%]	-	-	-	-	-	-	-
(BKGR) Single top Z cross-section [%]	± 0.21	± 0.29	± 0.18	± 0.27	-	± 0.15	± 0.13
(BKGR) t+Z cross-section [%]	-	-	-	-	-	-	-
(BKGR) t+W cross-section [%]	-	-	-	-	-	-	-
(BKGR) Multi-jet background statistics [%]	± 6.78	± 3.64	± 1.97	± 1.75	± 2.57	± 1.81	± 9.08
(MOD) Monte Carlo statistics [%]	± 5.17	± 3.13	± 1.67	± 1.65	± 2.31	± 1.80	± 7.19
(MOD) Alternative hard-scattering model [%]	± 2.18	± 1.82	± 1.25	± 1.20	± 1.37	± 1.16	± 1.60
(MOD) Alternative parton-shower model [%]	± 12.6	± 11.6	± 10.4	± 14.5	± 13.0	± 17.4	± 17.2
(MOD) Alternative parton-shower model [%]	± 9.34	± 10.7	± 13.0	± 15.4	± 16.3	± 16.1	± 11.7

Bins (GeV)	350-400	400-450	450-500	500-550	550-600	600-600	800-1200
$1/\sigma \cdot d\sigma / d p_T^2$	$1.667 \cdot 10^{-3}$	$3.214 \cdot 10^{-3}$	$4.701 \cdot 10^{-3}$	$4.291 \cdot 10^{-3}$	$2.211 \cdot 10^{-3}$	$8.583 \cdot 10^{-4}$	$7.168 \cdot 10^{-4}$
Total Uncertainty [%]	± 15.4	± 9.71	± 7.13	± 7.17	± 6.09	± 6.07	± 6.01
JES [$\pm \sigma$]	± 3.3	± 3.0	± 3.0	± 3.0	± 3.0	± 3.7	± 3.5
Systematics [%]	± 8.89	± 5.98	± 4.46	± 3.78	± 3.96	± 7.38	± 18.8
JES b-Tagged jet energy scale [%]	-	-	-	-	-	-	-
(JES) b-Tagged jet energy scale [%)	± 0.16	-	-	-	-	-	± 0.44
(JES) Effective detector NP set 1 [%]	-	-	-	-	-	-	-
(JES) Effective detector NP set 2 [%]	-	-	-	-	-	-	-
(JES) Effective detector NP set 3 [%]	-	-	-	-	-	-	-
(JES) Effective detector NP set 4 [%]	-	-	-	-	-	-	-
(JES) Effective detector NP set 5 [%]	-	-	-	-	-	-	-
(JES) Effective detector NP set 6 [%]	-	-	-	-	-	-	-
(JES) Effective detector NP set 7 [%]	-	-	-	-	-	-	-
(JES) Effective detector NP set 8 recTerm [%]	-	-	-	-	-	-	-
(JES) η intercalibration model [%]	-	-	-	-	-	-	-
(JES) JES factor for the total star [%]	-	-	-	-	-	-	-
(JES) Flavor composition [%]	± 0.20	-	-	-	-	-	± 0.10
(JES) Flavor response [%]	-	-	-	-	-	-	± 0.12
(JES) Pile-up offset [%]	-	-	-	-	-	-	-
(JES) Pile-up offset N_{PU} [%]	-	-	-	-	-	-	-
(JES) Pile-up offset p_T [%]	-	-	-	-	-	-	-
(JES) Pile-up offset jet energy [%]	± 0.12	-	-	-	-	-	± 0.08
(JES) Pile-up offset jet multiplicity [%]	-	-	-	-	-	-	-
(JES) Punch-through [%]	-	-	-	-	-	-	-
(JES) Single particle high- p_T [%]	-	-	-	-	-	-	-
(JES) Single particle low- p_T [%]	± 1.0	± 0.43	-	± 0.36	-	± 0.32	± 0.38
(LBRS) Large- η jet Baseline p_T [%]	± 1.2	± 1.8	± 2.48	± 1.84	± 1.78	± 0.45	± 9.28
(LBRS) Large- η jet Baseline r_{jet} [%]	± 1.0	± 1.5	± 1.25	± 1.22	± 1.15	± 0.45	± 5.01
(LBRS) Large- η jet Baseline r_{jet}^2 [%]	± 1.1	± 1.7	± 1.27	± 1.29	± 1.05	± 0.69	± 12.4
(LBRS) Large- η jet Modeling p_T [%]	± 0.15	± 0.76	± 0.27	± 0.29	± 0.40	± 0.04	± 0.71
(LBRS) Large- η jet Modeling r_{jet} [%]	± 0.22	± 1.21	± 1.40	± 1.29	± 0.52	± 0.12	± 8.07
(LBRS) Large- η jet Tracking p_T [%]	± 0.08	± 0.29	± 0.07	± 0.07	± 0.14	± 0.01	± 0.60
(LBRS) Large- η jet Tracking r_{jet} [%]	± 0.11	± 0.14	± 0.16	± 0.13	-	-	± 0.15
(LBRS) Large- η jet TotalStar p_T [%]	± 0.11	± 0.52	-	-	-	-	-
(LBRS) Large- η jet TotalStar r_{jet} [%]	± 0.42	± 0.22	± 0.23	± 0.44	-	± 0.31	-
(LBRS) Large- η jet TotalStar r_{jet}^2 [%]	-	-	-	± 0.13	-	± 0.17	-
(LBRS) Large- η jet Quark mass resolution [%]	± 5.40	± 2.11	± 0.28	± 0.10	± 0.18	± 1.38	± 8.81
(FTAG) c-Quark tagging efficiency [generator 0] [%]	± 0.43	-	± 0.15	± 0.17	-	-	-
(FTAG) c-Quark tagging efficiency [generator 1] [%]	± 0.43	-	± 0.13	± 0.15	± 0.14	± 0.10	± 0.54
(FTAG) c-Quark tagging efficiency [generator 2] [%]	± 0.22	± 0.16	-	-	-	± 0.10	± 0.60
(FTAG) c-Quark tagging efficiency [generator 3] [%]	± 0.27	± 0.13	-	-	-	± 0.17	± 0.73
(FTAG) c-Quark tagging efficiency [generator 4] [%]	± 0.11	± 0.09	-	-	-	-	± 0.27
(FTAG) c-Quark tagging efficiency [generator 0] [%]	± 0.15	± 0.24	± 0.02	± 0.01	± 0.27	± 0.29	± 0.56
(FTAG) c-Quark tagging efficiency [generator 1] [%]	± 0.11	± 0.24	± 0.15	± 0.15	± 0.12	± 0.12	± 0.46
(FTAG) c-Quark tagging efficiency [generator 2] [%]	± 0.25	± 0.23	-	± 0.10	-	-	± 0.23
(FTAG) Light jet tagging efficiency [generator 0] [%]	± 0.11	± 0.24	-	-	-	-	± 0.12
(FTAG) Light jet tagging efficiency [generator 1] [%]	-	-	-	-	-	-	± 0.17
(FTAG) Light jet tagging efficiency [generator 2] [%]	-	± 0.14	-	-	-	-	± 0.13
(FTAG) Light jet tagging efficiency [generator 3] [%]	-	-	-	-	-	-	± 0.22
(FTAG) Light jet tagging efficiency [generator 4] [%]	± 0.15	± 0.20	-	-	-	-	± 0.12
(FTAG) Light jet tagging efficiency [generator 5] [%]	-	-	-	-	-	-	± 0.13
(FTAG) Light jet tagging efficiency [generator 6] [%]	-	-	-	-	-	-	± 0.22
(FTAG) Light jet tagging efficiency [generator 7] [%]	± 0.22	± 0.22	-	-	-	-	± 0.19
(FTAG) Light jet tagging efficiency [generator 11] [%]	-	-	-	-	-	-	-
(FTAG) Light jet tagging efficiency [generator 12] [%]	-	-	-	-	-	-	-
(FTAG) Light jet tagging efficiency [generator 13] [%]	-	-	-	-	-	-	-
(FTAG) c-Quark tagging extrapolation [%]	± 1.45	± 1.26	± 0.83	± 0.50	± 0.42	± 1.71	± 6.70
(FTAG) c-Quark tagging extrapolation from c-Quark [%]	-	-	-	-	-	-	-
(PDF) PDF4LHC13c e-Quark 0 [%]	± 0.15	± 0.12	-	± 0.16	± 0.33	± 0.85	-
(PDF) PDF4LHC13c e-Quark 1 [%]	-	-	-	-	-	-	± 0.19
(PDF) PDF4LHC13c e-Quark 2 [%]	-	-	± 0.12	-	-	-	± 0.18
(PDF) PDF4LHC13c e-Quark 3 [%]	± 0.20	-	-	-	± 0.14	± 0.21	± 0.77
(PDF) PDF4LHC13c e-Quark 4 [%]	± 0.14	-	-	-	± 0.21	± 0.41	± 0.83
(PDF) PDF4LHC13c e-Quark 5 [%]	± 0.11	-	-	-	± 0.16	-	-
(PDF) PDF4LHC13c e-Quark 6 [%]	-	-	-	-	-	-	-
(PDF) PDF4LHC13c e-Quark 7 [%]	-	-	-	-	-	-	-
(PDF) PDF4LHC13c e-Quark 8 [%]	-	-	-	-	-	-	-
(PDF) PDF4LHC13c e-Quark 9 [%]	-	-	-	-	-	-	-
(PDF) PDF4LHC13c e-Quark 10 [%]	-	-	-	-	-	-	± 0.19
(PDF) PDF4LHC13c e-Quark 11 [%]	-	-	-	-	-	-	-
(PDF) PDF4LHC13c e-Quark 12 [%]	-	-	-	-	-	-	-
(PDF) PDF4LHC13c e-Quark 13 [%]	-	-	-	-	-	-	-
(PDF) PDF4LHC13c e-Quark 14 [%]	-	-	-	-	-	-	-
(PDF) PDF4LHC13c e-Quark 15 [%]	-	-	-	-	± 0.12	± 0.26	± 0.61
(PDF) PDF4LHC13c e-Quark 16 [%]	-	-	-	-	-	-	± 0.19
(PDF) PDF4LHC13c e-Quark 17 [%]	-	-	-	-	-	-	-
(PDF) PDF4LHC13c e-Quark 18 [%]	-	-	-	-	-	-	-
(PDF) PDF4LHC13c e-Quark 19 [%]	-	-	-	-	-	-	-
(PDF) PDF4LHC13c e-Quark 20 [%]	-	-	-	-	-	-	-
(PDF) PDF4LHC13c e-Quark 21 [%]	± 0.12	± 0.13	-	± 0.21	± 0.50	± 1.19	-
(PDF) PDF4LHC13c e-Quark 22 [%]	-	-	-	-	-	-	-
(PDF) PDF4LHC13c e-Quark 23 [%]	-	-	-	-	-	-	-
(PDF) PDF4LHC13c e-Quark 24 [%]	-	-	-	-	-	-	-
(PDF) PDF4LHC13c e-Quark 25 [%]	-	-	-	-	-	-	-
(PDF) PDF4LHC13c e-Quark 26 [%]	-	-	-	-	-	-	-
(PDF) PDF4LHC13c e-Quark 27 [%]	± 0.14	-	-	± 0.12	± 0.22	± 0.36	-
(PDF) PDF4LHC13c e-Quark 28 [%]	-	-	-	-	± 0.14	± 0.31	± 0.73
(PDF) PDF4LHC13c e-Quark 29 [%]	-	-	-	-	-	-	-
(PDF) PDF4LHC13c e-Quark 30 [%]	-	-	-	-	-	-	-
(LEP) Electron energy resolution [%]	-	-	-	-	-	-	-
(LEP) Electron energy scale [%]	-	-	-	-	-	± 0.12	-
(LEP) Muon energy resolution [%]	-	-	-	-	-	-	-
(LEP) Muon (MS) momentum resolution [%]	-	-	-	-	-	-	-
(LEP) Muon (ID) momentum resolution [%]	-	-	-	-	-	-	-
(LEP) Muon sagitta ρ [%]	-	-	-	-	-	-	-
(LEP) Muon transverse resolution η [%]	-	-	-	-	-	-	-
(METFPU E_T^{miss}) Soft jet scale [%]	-	-	-	-	-	-	-
(METFPU E_T^{miss}) Soft jet scale peep [%]	-	-	-	-	-	-	-
Luminosity [%]	-	-	-	-	-	-	-
(BKG) Single top W cross-section [%]	-	-	-	-	-	-	-
(BKG) Single top Z cross-section [%]	-	-	-	-	-	-	-
(BKG) n-tW cross-section [%]	-	-	-	-	-	-	-
(BKG) Multi-jet background statistics [%]	± 6.77	± 3.63	± 1.97	± 1.74	± 2.56	± 1.81	± 9.07
(MOD) Monte Carlo sample statistics [%]	± 4.95	± 2.88	± 1.59	± 1.55	± 2.24	± 1.74	± 7.02
(MOD) Alternative hard-scattering model [%]	± 1.1	± 1.7	± 1.25	± 0.99	± 1.1	± 0.81	± 4.11
(MOD) Alternative parton-shower model [%]	± 0.97	± 2.11	± 3.49	± 1.23	± 0.45	± 4.56	± 4.33
(MOD) Alternative parton-shower model [%]	± 5.33	± 3.75	± 1.03	± 1.76	± 2.82	± 2.52	± 2.47

Table 46: The individual systematic uncertainties in the fiducial phase-space relative differential cross-sections for the 2nd leading top-quark transverse momentum calculated as a percentage of the cross-section in each bin. Dashes are used when the estimated relative systematic uncertainty for that bin is below 0.1%.

Not reviewed, for internal circulation only

Bin [Unit μb^{-1}]	0...30	0.30...0.60	0.60...0.90	0.90...1.20	1.20...1.50	1.50...2
$d\sigma / d\eta^{\pm} [\text{pb} / \text{Unit } \eta^{\pm}]$	$2.45 \cdot 10^{-3}$	$2.390 \cdot 10^{-3}$	$1.727 \cdot 10^{-3}$	$1.393 \cdot 10^{-3}$	$1.029 \cdot 10^{-3}$	$4.222 \cdot 10^{-4}$
Total Uncertainty [%]	± 26.0	± 24.4	± 24.4	± 26.4	± 25.8	± 28.6
Stat. [%]	± 4.7	± 5.0	± 6.6	± 7.0	± 8.6	± 9.3
Systematics [%]	± 25.5	± 23.8	± 23.4	± 23.2	± 23.6	± 26.6
(JES) b-Tagged jet energy scale [%]	-	-	-	-	-	-
(JES) Effective detector NP set 1 [%]	-	-	-	-	-	-
(JES) Effective detector NP set 2 [%]	-	-	-	-	-	-
(JES) Effective detector NP set 3 [%]	-	-	-	-	-	-
(JES) Effective detector NP set 4 [%]	-	-	-	-	-	-
(JES) Effective detector NP set 5 [%]	-	-	-	-	-	-
(JES) Effective detector NP set 6 [%]	-	-	-	-	-	-
(JES) Effective detector NP set 7 [%]	-	-	-	-	-	-
(JES) Effective detector NP set 8 resTerm [%]	-	-	-	-	-	-
(JES) η intercalibration model [%]	-	-	-	-	-	-
(JES) η intercalibration offset [%]	-	-	-	-	-	-
(JES) Flavor composition [%]	± 0.2	± 0.31	± 0.18	± 0.27	± 0.15	± 0.28
(JES) Flavor response [%]	± 0.15	± 0.21	-	-	± 0.21	± 0.12
(JES) Pile-up offset η [%]	-	-	-	-	-	-
(JES) Pile-up offset p_T [%]	-	-	-	-	-	-
(JES) Pile-up offset τ_2 [%]	-	-	-	-	-	-
(JES) Single particle high- p_T [%]	-	-	-	-	-	-
(JES) Large- R jet Baseline mass [%]	± 0.84	± 0.31	± 0.2	± 0.18	± 0.4	± 0.19
(JES) Large- R jet Baseline p_T [%]	± 0.95	± 0.33	± 0.44	± 0.18	± 0.21	± 0.17
(JES) Large- R jet Modeling mass [%]	± 0.70	± 0.28	± 0.91	± 0.18	± 0.11	± 0.63
(JES) Large- R jet Modeling p_T [%]	± 0.75	± 0.28	± 0.16	-	± 0.90	± 0.29
(JES) Large- R jet Modeling τ_2 [%]	± 0.73	± 0.21	± 0.24	± 0.17	± 0.16	± 0.27
(JES) Large- R jet Modeling τ_2 p_T [%]	± 0.74	± 0.28	± 0.19	± 0.16	± 0.10	± 0.68
(JES) Large- R jet Tracking p_T [%]	± 0.82	± 0.22	± 0.20	-	± 0.48	-
(JES) Large- R jet Tracking τ_2 [%]	± 0.84	± 0.68	± 0.98	± 0.04	± 5.68	± 5.27
(JES) Large- R jet Tracking τ_2 p_T [%]	± 0.84	± 0.42	± 0.37	± 0.29	± 0.25	± 0.54
(JES) Large- R jet TotalsR τ_2 [%]	± 0.83	± 0.27	± 0.31	± 0.34	± 0.19	± 0.24
(JES) Large- R jet TotalsR p_T [%]	± 0.73	± 0.23	± 0.14	± 0.16	± 0.17	± 0.16
(JES) Large- R jet TotalsR τ_2 p_T [%]	± 0.77	± 0.17	± 0.19	± 0.17	± 0.16	± 0.16
(FTAG) ℓ -Quark tagging efficiency (eigencenter 0) [%]	± 5.31	± 5.38	± 3.39	± 5.10	± 2.20	± 5.13
(FTAG) ℓ -Quark tagging efficiency (eigencenter 1) [%]	± 4.91	± 5.01	± 5.04	± 4.61	± 4.87	± 4.79
(FTAG) ℓ -Quark tagging efficiency (eigencenter 2) [%]	± 0.77	± 0.79	± 0.80	± 0.67	± 0.68	± 0.70
(FTAG) ℓ -Quark tagging efficiency (eigencenter 3) [%]	± 0.73	± 0.73	± 0.73	± 0.69	± 0.69	± 0.61
(FTAG) ℓ -Quark tagging efficiency (eigencenter 4) [%]	± 0.24	± 0.24	± 0.25	± 0.23	± 0.24	± 0.20
(FTAG) ℓ -Quark tagging efficiency (eigencenter 5) [%]	± 2.00	± 2.34	± 1.92	± 1.67	± 2.21	± 2.46
(FTAG) ℓ -Quark tagging efficiency (eigencenter 6) [%]	± 0.70	± 1.56	± 1.70	± 1.17	± 1.35	± 1.25
(FTAG) ℓ -Quark tagging efficiency (eigencenter 7) [%]	± 0.22	± 0.26	± 0.26	± 0.22	± 0.22	± 0.22
(FTAG) ℓ -Quark tagging efficiency (eigencenter 8) [%]	± 0.24	± 0.23	± 0.21	± 0.21	± 0.21	± 0.21
(FTAG) ℓ -Quark tagging efficiency (eigencenter 9) [%]	± 0.24	± 0.23	± 0.24	± 0.39	± 0.46	± 0.36
(FTAG) Light-jet tagging efficiency (eigencenter 0) [%]	± 0.23	± 0.16	± 0.14	± 0.68	± 0.17	± 0.28
(FTAG) Light-jet tagging efficiency (eigencenter 1) [%]	-	-	-	-	± 0.10	-
(FTAG) Light-jet tagging efficiency (eigencenter 2) [%]	-	± 0.10	-	± 0.27	± 0.17	± 0.16
(FTAG) Light-jet tagging efficiency (eigencenter 3) [%]	± 0.10	± 0.12	-	-	± 0.12	-
(FTAG) Light-jet tagging efficiency (eigencenter 4) [%]	-	-	-	± 0.26	-	-
(FTAG) Light-jet tagging efficiency (eigencenter 5) [%]	-	-	-	-	-	-
(FTAG) Light-jet tagging efficiency (eigencenter 6) [%]	-	-	-	-	-	-
(FTAG) Light-jet tagging efficiency (eigencenter 7) [%]	-	-	-	-	-	-
(FTAG) Light-jet tagging efficiency (eigencenter 8) [%]	± 0.24	± 0.26	± 0.21	± 0.26	± 0.28	± 0.21
(FTAG) Light-jet tagging efficiency (eigencenter 9) [%]	± 0.24	± 0.27	± 0.21	± 0.21	± 0.23	± 0.19
(FTAG) Light-jet tagging efficiency (eigencenter 10) [%]	-	-	-	-	-	-
(FTAG) Light-jet tagging efficiency (eigencenter 11) [%]	-	-	-	-	-	-
(FTAG) Light-jet tagging efficiency (eigencenter 12) [%]	-	-	-	-	-	-
(FTAG) Light-jet tagging efficiency (eigencenter 13) [%]	-	-	-	-	-	-
(FTAG) Light-jet tagging efficiency (eigencenter 14) [%]	-	-	-	-	-	-
(FTAG) Light-jet tagging efficiency (eigencenter 15) [%]	± 0.19	± 0.18	± 0.14	± 0.10	-	± 0.19
(FTAG) Light-jet tagging efficiency (eigencenter 16) [%]	-	-	-	± 0.11	± 0.12	-
(FTAG) Light-jet tagging efficiency (eigencenter 17) [%]	± 0.34	± 0.33	± 0.31	± 0.35	± 0.41	± 0.65
(FTAG) Light-jet tagging efficiency (eigencenter 18) [%]	-	-	-	-	± 0.12	± 0.13
(FTAG) Light-jet tagging efficiency (eigencenter 19) [%]	± 0.68	± 0.76	± 0.81	± 0.89	± 0.81	± 0.18
(FTAG) Light-jet tagging efficiency (eigencenter 20) [%]	-	-	± 0.12	± 0.22	± 0.36	± 0.45
(FTAG) Light-jet tagging efficiency (eigencenter 21) [%]	-	-	-	-	± 0.13	± 0.35
(FTAG) Light-jet tagging efficiency (eigencenter 22) [%]	± 0.23	± 0.33	± 0.50	± 1.09	± 1.80	± 3.70
(FTAG) Light-jet tagging efficiency (eigencenter 23) [%]	-	-	-	-	-	-
(FTAG) Light-jet tagging efficiency (eigencenter 24) [%]	-	-	-	-	-	± 0.12
(FTAG) Light-jet tagging efficiency (eigencenter 25) [%]	-	-	-	-	-	-
(FTAG) Light-jet tagging efficiency (eigencenter 26) [%]	± 0.22	± 0.24	± 0.26	± 0.27	± 0.31	± 0.33
(FTAG) Light-jet tagging efficiency (eigencenter 28) [%]	± 0.16	-	± 0.11	± 0.36	± 0.64	± 0.76
(FTAG) Light-jet tagging efficiency (eigencenter 30) [%]	-	-	-	-	-	-
(FTAG) Light-jet tagging efficiency (eigencenter 31) [%]	-	-	-	-	-	-
(FTAG) Light-jet tagging efficiency (eigencenter 32) [%]	-	-	-	-	-	-
(FTAG) Light-jet tagging efficiency (eigencenter 33) [%]	-	-	-	-	-	-
(FTAG) Light-jet tagging efficiency (eigencenter 34) [%]	-	-	-	-	-	-
(FTAG) Light-jet tagging efficiency (eigencenter 35) [%]	-	-	-	-	-	-
(FTAG) Light-jet tagging efficiency (eigencenter 36) [%]	-	-	-	-	-	-
(FTAG) Light-jet tagging efficiency (eigencenter 37) [%]	-	-	-	-	-	-
(FTAG) Light-jet tagging efficiency (eigencenter 38) [%]	-	-	-	-	-	-
(FTAG) Light-jet tagging efficiency (eigencenter 39) [%]	-	-	-	-	-	-
(FTAG) Light-jet tagging efficiency (eigencenter 40) [%]	-	-	-	-	-	-
(FTAG) Light-jet tagging efficiency (eigencenter 41) [%]	-	-	-	-	-	-
(FTAG) Light-jet tagging efficiency (eigencenter 42) [%]	-	-	-	-	-	-
(FTAG) Light-jet tagging efficiency (eigencenter 43) [%]	-	-	-	-	-	-
(FTAG) Light-jet tagging efficiency (eigencenter 44) [%]	-	-	-	-	-	-
(FTAG) Light-jet tagging efficiency (eigencenter 45) [%]	-	-	-	-	-	-
(FTAG) Light-jet tagging efficiency (eigencenter 46) [%]	-	-	-	-	-	-
(FTAG) Light-jet tagging efficiency (eigencenter 47) [%]	-	-	-	-	-	-
(FTAG) Light-jet tagging efficiency (eigencenter 48) [%]	-	-	-	-	-	-
(FTAG) Light-jet tagging efficiency (eigencenter 49) [%]	-	-	-	-	-	-
(FTAG) Light-jet tagging efficiency (eigencenter 50) [%]	-	-	-	-	-	-
(FTAG) Light-jet tagging efficiency (eigencenter 51) [%]	-	-	-	-	-	-
(FTAG) Light-jet tagging efficiency (eigencenter 52) [%]	-	-	-	-	-	-
(FTAG) Light-jet tagging efficiency (eigencenter 53) [%]	-	-	-	-	-	-
(FTAG) Light-jet tagging efficiency (eigencenter 54) [%]	-	-	-	-	-	-
(FTAG) Light-jet tagging efficiency (eigencenter 55) [%]	-	-	-	-	-	-
(FTAG) Light-jet tagging efficiency (eigencenter 56) [%]	-	-	-	-	-	-
(FTAG) Light-jet tagging efficiency (eigencenter 57) [%]	-	-	-	-	-	-
(FTAG) Light-jet tagging efficiency (eigencenter 58) [%]	-	-	-	-	-	-
(FTAG) Light-jet tagging efficiency (eigencenter 59) [%]	-	-	-	-	-	-
(FTAG) Light-jet tagging efficiency (eigencenter 60) [%]	-	-	-	-	-	-
(FTAG) Light-jet tagging efficiency (eigencenter 61) [%]	-	-	-	-	-	-
(FTAG) Light-jet tagging efficiency (eigencenter 62) [%]	-	-	-	-	-	-
(FTAG) Light-jet tagging efficiency (eigencenter 63) [%]	-	-	-	-	-	-
(FTAG) Light-jet tagging efficiency (eigencenter 64) [%]	-	-	-	-	-	-
(FTAG) Light-jet tagging efficiency (eigencenter 65) [%]	-	-	-	-	-	-
(FTAG) Light-jet tagging efficiency (eigencenter 66) [%]	-	-	-	-	-	-
(FTAG) Light-jet tagging efficiency (eigencenter 67) [%]	-	-	-	-	-	-
(FTAG) Light-jet tagging efficiency (eigencenter 68) [%]	-	-	-	-	-	-
(FTAG) Light-jet tagging efficiency (eigencenter 69) [%]	-	-	-	-	-	-
(FTAG) Light-jet tagging efficiency (eigencenter 70) [%]	-	-	-	-	-	-
(FTAG) Light-jet tagging efficiency (eigencenter 71) [%]	-	-	-	-	-	-
(FTAG) Light-jet tagging efficiency (eigencenter 72) [%]	-	-	-	-	-	-
(FTAG) Light-jet tagging efficiency (eigencenter 73) [%]	-	-	-	-	-	-
(FTAG) Light-jet tagging efficiency (eigencenter 74) [%]	-	-	-	-	-	-
(FTAG) Light-jet tagging efficiency (eigencenter 75) [%]	-	-	-	-	-	-
(FTAG) Light-jet tagging efficiency (eigencenter 76) [%]	-	-	-	-	-	-
(FTAG) Light-jet tagging efficiency (eigencenter 77) [%]	-	-	-	-	-	-
(FTAG) Light-jet tagging efficiency (eigencenter 78) [%]	-	-	-	-	-	-
(FTAG) Light-jet tagging efficiency (eigencenter 79) [%]	-	-	-	-	-	-
(FTAG) Light-jet tagging efficiency (eigencenter 80) [%]	-	-	-	-	-	-
(FTAG) Light-jet tagging efficiency (eigencenter 81) [%]	-	-	-	-	-	-
(FTAG) Light-jet tagging efficiency (eigencenter 82) [%]	-	-	-	-	-	-
(FTAG) Light-jet tagging efficiency (eigencenter 83) [%]	-	-	-	-	-	-
(FTAG) Light-jet tagging efficiency (eigencenter 84) [%]	-	-	-	-	-	-
(FTAG) Light-jet tagging efficiency (eigencenter 85) [%]	-	-	-	-	-	-
(FTAG) Light-jet tagging efficiency (eigencenter 86) [%]	-	-	-	-	-	-
(FTAG) Light-jet tagging efficiency (eigencenter 87) [%]	-	-	-	-	-	-
(FTAG) Light-jet tagging efficiency (eigencenter 88) [%]	-	-	-	-	-	-
(FTAG) Light-jet tagging efficiency (eigencenter 89) [%]	-	-	-	-	-	-
(FTAG) Light-jet tagging efficiency (eigencenter 90) [%]	-	-	-	-	-	-
(FTAG) Light-jet tagging efficiency (eigencenter 91) [%]	-	-	-	-	-	-
(FTAG) Light-jet tagging efficiency (eigencenter 92) [%]	-	-	-	-	-	-
(FTAG) Light-jet tagging efficiency (eigencenter 93) [%]	-	-	-	-	-	-
(FTAG) Light-jet tagging efficiency (eigencenter 94) [%]	-	-	-	-	-	-
(FTAG) Light-jet tagging efficiency (eigencenter 95) [%]	-	-	-	-	-	-
(FTAG) Light-jet tagging efficiency (eigencenter 96) [%]	-	-	-	-	-	-
(FTAG) Light-jet tagging efficiency (eigencenter 97) [%]	-	-	-	-	-	-
(FTAG) Light-jet tagging efficiency (eigencenter 98) [%]	-	-	-	-	-	-
(FTAG) Light-jet tagging efficiency (eigencenter 99) [%]	-	-	-	-	-	-
(FTAG) Light-jet tagging efficiency (eigencenter 100) [%]	-	-	-	-	-	-
(LEP) Muon (MS) momentum resolution [%]	-	-	-	-	-	-
(LEP) Muon (MS) energy resolution [%]	-	-	-	-	-	-
(LEP) Muon sagitta resolution bias [%]	-	-	-	-	-	-
(LEP) Muon (MS) energy resolution [%]	-	-	-	-	-	-
(METTPU) ρ^{jet} Soft jet resolution per %	-	-	-			

Bin [Unit [μb^{-1}]]	0-0.30	0.30-0.60	0.60-0.90	0.90-1.20	1.20-1.50	1.50-2
$b\bar{b}$ \rightarrow $d\bar{d}\pi^+\pi^-$	$8.490 \cdot 10^{-3}$	$8.198 \cdot 10^{-3}$	$8.924 \cdot 10^{-3}$	$4.778 \cdot 10^{-3}$	$3.530 \cdot 10^{-3}$	$1.448 \cdot 10^{-3}$
Total Uncertainty (%)	± 5.33	± 5.74	± 4.8	± 8.01	± 10.9	± 11.3
Stat. (%)	± 4.2	± 4.6	± 6.0	± 6.5	± 8.0	± 8.9
Systematics (%)	± 22.3	± 21.05	± 14.64	± 3.29	± 5.23	± 5.45
(JES) b-Tagged jet energy scale [%]	-	-	-	-	-	-
(JES) Effective detector NP set 1 [%]	-	-	-	-	-	-
(JES) Effective detector NP set 2 [%]	-	-	-	-	-	-
(JES) Effective detector NP set 3 [%]	-	-	-	-	-	-
(JES) Effective detector NP set 4 [%]	-	-	-	-	-	-
(JES) Effective detector NP set 5 [%]	-	-	-	-	-	-
(JES) Effective detector NP set 6 [%]	-	-	-	-	-	-
(JES) Effective detector NP set 7 [%]	-	-	-	-	-	-
(JES) Effective detector NP set 8 resTerm [%]	-	-	-	-	-	-
(JES) η intercalibration model [%]	-	-	-	-	-	-
(JES) Jet energy scale offset [%]	-	-	-	-	-	-
(JES) Flavor composition [%]	-	-	-	-	-	-
(JES) Pile-up response [%]	-	-	-	-	-	-
(JES) Pile-up offset μ [%]	-	-	-	-	-	-
(JES) Pile-up offset ρ [%]	-	-	-	-	-	-
(JES) Pile-up offset τ topology [%]	-	-	-	-	-	-
(JES) Single particle high- p_T [%]	-	-	-	-	-	-
(JES) Large- R jet Baseline mass [%]	± 0.94	-	± 0.16	± 0.11	± 0.43	± 0.11
(JES) Large- R jet Baseline p_T [%]	± 0.90	± 0.22	± 0.72	± 0.26	± 0.85	± 0.10
(JES) Large- R jet Modeling mass [%]	± 0.95	± 0.26	± 0.41	± 0.54	± 0.27	± 0.04
(JES) Large- R jet Modeling p_T [%]	± 0.98	± 0.24	± 0.17	± 0.34	± 0.60	± 0.03
(JES) Large- R jet Modeling τ_2 [%]	-	± 0.11	± 0.24	-	± 0.68	± 0.18
(JES) Large- R jet Modeling τ_3 [%]	-	± 0.14	± 0.21	± 0.17	± 0.70	± 0.26
(JES) Large- R jet Tracking τ_2 [%]	± 0.97	± 0.27	± 0.17	± 0.19	± 0.44	± 0.21
(JES) Large- R jet Tracking p_T [%]	± 0.29	± 0.12	± 0.17	± 0.15	± 0.02	± 0.20
(JES) Large- R jet Tracking τ_2 [%]	-	± 0.14	-	± 0.16	-	± 0.17
(JES) Large- R jet Tracking τ_3 [%]	-	-	-	-	-	-
(JES) Large- R jet Totalsat p_T [%]	-	-	-	-	-	± 0.16
(JES) Large- R jet Totalsat τ_2 [%]	-	-	-	-	-	-
(JES) Large- R jet Totalsat τ_3 [%]	-	-	-	-	-	-
(ITAG) Q-Qbar tagger resolution [8] %	± 0.40	± 0.14	± 0.84	± 0.87	± 0.58	± 0.35
(ITAG) Q-Qbar tagger efficiency (eigenvector 0) (%)	-	-	± 0.11	± 0.18	-	± 0.15
(ITAG) Q-Qbar tagger efficiency (eigenvector 1) (%)	-	-	± 0.11	± 0.14	± 0.29	± 0.10
(ITAG) Q-Qbar tagger efficiency (eigenvector 2) (%)	-	-	-	-	-	-
(ITAG) Q-Qbar tagger efficiency (eigenvector 3) (%)	-	-	-	-	-	-
(ITAG) Q-Qbar tagger efficiency (eigenvector 4) (%)	-	-	-	-	-	-
(ITAG) Q-Qbar tagger efficiency (eigenvector 0) (%)	-	± 0.28	± 0.11	± 0.40	± 0.20	± 0.39
(ITAG) Q-Qbar tagger efficiency (eigenvector 1) (%)	-	± 0.27	-	± 0.13	-	-
(ITAG) Q-Qbar tagger efficiency (eigenvector 2) (%)	-	± 0.15	-	-	-	± 0.14
(ITAG) Q-Qbar tagger efficiency (eigenvector 3) (%)	-	-	-	-	-	-
(ITAG) Light-jet tagging efficiency (eigenvector 0) [%]	-	± 0.10	± 0.11	± 0.41	-	-
(ITAG) Light-jet tagging efficiency (eigenvector 1) [%]	-	-	-	-	-	-
(ITAG) Light-jet tagging efficiency (eigenvector 2) [%]	-	-	-	± 0.14	-	-
(ITAG) Light-jet tagging efficiency (eigenvector 3) [%]	-	-	-	± 0.18	-	-
(ITAG) Light-jet tagging efficiency (eigenvector 4) [%]	-	-	-	-	-	-
(ITAG) Light-jet tagging efficiency (eigenvector 5) [%]	-	-	-	-	-	-
(ITAG) Light-jet tagging efficiency (eigenvector 6) [%]	-	-	-	-	-	-
(ITAG) Light-jet tagging efficiency (eigenvector 7) [%]	-	-	-	-	-	-
(ITAG) Light-jet tagging efficiency (eigenvector 8) [%]	-	-	-	-	-	-
(ITAG) Light-jet tagging efficiency (eigenvector 9) [%]	-	-	-	-	-	-
(ITAG) Light-jet tagging efficiency (eigenvector 10) [%]	-	-	-	-	-	-
(ITAG) Light-jet tagging efficiency (eigenvector 11) [%]	-	-	-	-	-	-
(ITAG) Light-jet tagging efficiency (eigenvector 12) [%]	-	-	-	-	-	-
(ITAG) Light-jet tagging efficiency (eigenvector 13) [%]	-	-	-	-	-	-
(ITAG) Q-Qbar tagger resolution [%]	-	± 0.15	± 0.12	± 0.22	± 0.10	± 0.43
(POD) PDF4LHC15 eigenvector 0 [%]	-	-	-	-	-	-
(POD) PDF4LHC15 eigenvector 0 [%]	± 0.17	± 0.12	-	± 0.20	± 0.38	± 0.49
(POD) PDF4LHC15 eigenvector 0 [%]	± 0.15	-	-	± 0.10	± 0.20	± 0.45
(POD) PDF4LHC15 eigenvector 0 [%]	-	-	-	± 0.10	-	± 0.72
(POD) PDF4LHC15 eigenvector 0 [%]	± 0.16	-	-	± 0.11	± 0.33	± 0.95
(POD) PDF4LHC15 eigenvector 0 [%]	± 0.21	± 0.14	-	± 0.19	± 0.48	± 1.15
(POD) PDF4LHC15 eigenvector 0 [%]	± 0.14	± 0.10	-	± 0.13	± 0.31	± 0.67
(POD) PDF4LHC15 eigenvector 0 [%]	-	-	-	-	± 0.15	-
(POD) PDF4LHC15 eigenvector 0 [%]	-	-	-	-	± 0.16	± 0.27
(POD) PDF4LHC15 eigenvector 0 [%]	-	-	-	-	± 0.10	± 0.37
(POD) PDF4LHC15 eigenvector 0 [%]	-	-	-	-	± 0.24	-
(POD) PDF4LHC15 eigenvector 13 [%]	-	-	-	-	-	± 0.17
(POD) PDF4LHC15 eigenvector 14 [%]	-	-	-	-	-	± 0.12
(POD) PDF4LHC15 eigenvector 15 [%]	-	-	-	-	-	-
(POD) PDF4LHC15 eigenvector 16 [%]	-	-	-	-	-	-
(POD) PDF4LHC15 eigenvector 17 [%]	-	-	-	-	-	-
(POD) PDF4LHC15 eigenvector 18 [%]	-	-	-	-	-	± 0.30
(POD) PDF4LHC15 eigenvector 19 [%]	-	-	-	-	-	± 0.39
(POD) PDF4LHC15 eigenvector 20 [%]	± 0.12	-	-	± 0.11	± 0.24	± 0.33
(POD) PDF4LHC15 eigenvector 21 [%]	-	-	-	-	-	± 0.31
(POD) PDF4LHC15 eigenvector 22 [%]	± 0.47	± 0.37	± 0.14	± 0.38	± 1.09	± 2.97
(POD) PDF4LHC15 eigenvector 23 [%]	-	-	-	-	-	-
(POD) PDF4LHC15 eigenvector 24 [%]	-	-	-	-	-	± 0.18
(POD) PDF4LHC15 eigenvector 25 [%]	-	-	-	-	-	-
(POD) PDF4LHC15 eigenvector 26 [%]	-	-	-	-	-	-
(POD) PDF4LHC15 eigenvector 27 [%]	-	-	-	-	-	-
(POD) PDF4LHC15 eigenvector 28 [%]	± 0.26	± 0.19	-	± 0.26	± 0.53	± 0.66
(POD) PDF4LHC15 eigenvector 29 [%]	-	-	-	-	-	-
(POD) PDF4LHC15 eigenvector 30 [%]	-	-	-	-	-	-
(LEP) Electron energy scale [%]	-	-	-	-	-	-
(LEP) Electron energy scale [%]	-	-	-	-	-	-
(LEP) Muon (ID) momentum resolution [%]	-	-	-	-	-	-
(LEP) Muon (ID) momentum resolution [%]	-	-	-	-	-	-
(LEP) Muon (ID) sagitta resolution bias [%]	-	-	-	-	-	-
(LEP) Muon (ID) sagitta resolution bias [%]	-	-	-	-	-	-
(METTP) $E_{\text{miss}}^{\text{soft}}$ Soft jet resolution para [%]	-	-	-	-	-	-
(METTP) $E_{\text{miss}}^{\text{soft}}$ Soft jet resolution perp [%]	-	-	-	-	-	-
(METTP) Jet vertex tagging [%]	-	-	-	-	-	-
(METTP) Jet vertex tagging [%]	-	-	-	-	-	-
(BKGG) Top W cross-section [%]	-	-	-	-	-	-
(BKGG) Single t-channel treatment [%]	-	-	-	-	± 0.23	± 0.19
(MOD) G + Z cross-section [%]	-	-	-	-	-	-
(MOD) Multijet cross-section [%]	-	-	-	-	-	-
(MOD) Monte Carlo sample statistics [%]	± 1.66	± 2.17	± 2.49	± 2.42	± 2.82	± 3.45
(MOD) ISR/FSR + scale [%]	± 1.42	± 1.66	± 1.76	± 2.19	± 2.58	± 2.75
(MOD) ISR/FSR + smearing model [%]	± 1.77	± 2.24	± 0.98	± 2.42	± 1.10	± 0.60
(MOD) Alternative parton-shower model [%]	± 0.85	± 0.63	± 3.27	± 0.70	± 0.26	± 2.06

Table 48: The individual systematic uncertainties in the fiducial phase-space relative differential cross-sections for the leading top-quark absolute value of the rapidity calculated as a percentage of the cross-section in each bin. Dashes are used when the estimated relative systematic uncertainty for that bin is below 0.1%.

Table 49: The individual systematic uncertainties in the fiducial phase-space absolute differential cross-sections for the top quark-antiquark system invariant mass calculated as a percentage of the cross-section in each bin. Dashes are used when the estimated relative systematic uncertainty for that bin is below 0.1%.

Table 50: The individual systematic uncertainties in the fiducial phase-space relative differential cross-sections for the top quark-antiquark system invariant mass calculated as a percentage of the cross-section in each bin. Dashes are used when the estimated relative systematic uncertainty for that bin is below 0.1%.

Bins (GeV)	0-100	100-150	150-200	200-300	300-500	500-800
$d\sigma / d p_T$ [pb/GeV]	$1.512 \cdot 10^{-3}$	$1.165 \cdot 10^{-3}$	$6.129 \cdot 10^{-4}$	$3.162 \cdot 10^{-4}$	$8.644 \cdot 10^{-5}$	$5.602 \cdot 10^{-5}$
Total Uncertainty [%]	± 25.2	± 22.2	± 27.2	± 27.5	± 33.5	± 67.1
Stat. [%]	± 3.3	± 6.2	± 9.4	± 9.6	± 1.2	± 8.8
Systematics [%]	± 24.9	± 21.1	± 24.9	± 23.0	± 30.0	± 87.5
(JES) b-Tagged jet energy scale [%]	-	-	-	± 0.0	± 0.47	-
(JES) Effective detector NP set 1 [%]	-	-	-	± 0.19	± 0.27	± 0.28
(JES) Effective detector NP set 2 [%]	-	-	-	± 0.29	± 0.37	± 0.29
(JES) Effective detector NP set 3 [%]	-	-	-	-	-	-
(JES) Effective detector NP set 4 [%]	-	-	-	-	-	-
(JES) Effective detector NP set 5 [%]	-	-	-	-	-	-
(JES) Effective detector NP set 6 [%]	-	-	-	-	-	-
(JES) Effective detector NP set 7 [%]	-	-	-	-	-	-
(JES) Effective detector NP set 8 resTerm [%]	-	-	-	-	-	-
(JES) η intercalibration model [%]	-	-	-	-	± 0.41	-
(JES) η intercalibration total stat [%]	-	-	-	± 0.16	-	-
(JES) Flavor composition [%]	± 0.17	± 0.29	± 0.39	± 0.28	± 0.67	± 0.73
(JES) Flavor response [%]	-	-	-	± 0.20	± 0.20	± 0.48
(JES) Pile-up offset μ_T [%]	-	-	-	-	± 0.14	± 0.25
(JES) Pile-up offset μ_T [%]	-	-	-	-	± 0.25	± 0.37
(JES) Pile-up offset μ_T + topology [%]	-	-	± 0.23	± 0.27	± 0.19	± 0.30
(JES) Pile-up offset μ_T + topology [%]	-	-	± 0.12	-	-	± 0.12
(JES) Single particle $h_{\gamma pT}$ [%]	-	-	-	-	-	-
(JES) Large- R jet Baseline mass [%]	± 0.01	± 0.22	-	± 0.25	± 1.25	± 0.96
(JES) Large- R jet Baseline p_T [%]	± 0.09	± 0.35	± 0.49	± 0.65	± 7.34	± 5.08
(JES) Large- R jet Modeling mass [%]	± 0.02	± 0.05	± 0.08	± 0.09	± 0.09	± 0.03
(JES) Large- R jet Modeling p_T [%]	± 0.40	± 1.10	± 0.60	± 0.29	± 11.57	± 3.11
(JES) Large- R jet Modeling $r_{\gamma T}$ [%]	± 2.44	± 1.87	± 1.57	± 1.62	± 2.30	± 2.13
(JES) Large- R jet Modeling $r_{\gamma T}$ + topology [%]	-	± 0.27	± 0.29	-	± 0.68	± 1.13
(JES) Large- R jet Tracking $r_{\gamma T}$ [%]	± 4.65	± 5.17	± 4.38	± 6.17	± 8.42	± 6.50
(JES) Large- R jet Tracking $r_{\gamma T}$ + topology [%]	± 0.35	± 0.12	± 0.11	-	± 0.38	± 0.23
(JES) Large- R jet Totalstat p_T [%]	± 0.26	± 0.30	± 0.36	± 0.27	± 0.23	± 2.10
(JES) Large- R jet Totalstat $r_{\gamma T}$ [%]	± 0.11	± 0.28	-	± 0.35	± 0.26	± 0.54
(JES) Large- R jet tag quark-antiquark resolution [%]	± 0.01	± 2.57	± 1.79	± 2.16	± 19.19	± 0.69
(FTAG) b-Quark tagging efficiency (eigencenter 0) [%]	± 5.14	± 3.21	± 5.52	± 5.88	± 3.87	± 4.88
(FTAG) b-Quark tagging efficiency (eigencenter 2) [%]	± 0.76	± 4.82	± 5.11	± 5.26	± 5.41	± 4.50
(FTAG) b-Quark tagging efficiency (eigencenter 4) [%]	± 0.24	± 0.23	± 0.22	± 0.24	± 0.26	± 0.25
(FTAG) c-Quark tagging efficiency (eigencenter 0) [%]	± 1.96	± 1.84	± 1.61	± 3.20	± 3.15	± 1.48
(FTAG) c-Quark tagging efficiency (eigencenter 2) [%]	± 1.14	± 1.06	± 1.27	± 2.34	± 2.10	± 1.03
(FTAG) c-Quark tagging efficiency (eigencenter 3) [%]	± 2.35	± 0.55	± 0.50	± 1.09	± 1.09	± 1.03
(FTAG) Light-jet tagging efficiency (eigencenter 0) [%]	± 0.19	± 0.35	± 0.26	± 0.39	± 0.52	± 0.49
(FTAG) Light-jet tagging efficiency (eigencenter 2) [%]	± 0.10	± 0.14	-	± 0.11	-	± 0.11
(FTAG) Light-jet tagging efficiency (eigencenter 3) [%]	-	± 0.17	-	± 0.15	± 0.38	-
(FTAG) Light-jet tagging efficiency (eigencenter 6) [%]	-	-	-	-	± 0.14	-
(FTAG) Light-jet tagging efficiency (eigencenter 7) [%]	-	-	-	-	± 20	-
(FTAG) Light-jet tagging efficiency (eigencenter 9) [%]	-	-	± 0.37	± 0.48	± 0.45	± 0.60
(FTAG) Light-jet tagging efficiency (eigencenter 11) [%]	-	-	± 0.30	± 0.31	± 0.49	± 0.67
(FTAG) Light-jet tagging efficiency (eigencenter 12) [%]	-	-	-	-	-	-
(FTAG) Light-jet tagging efficiency (eigencenter 13) [%]	-	-	-	-	-	-
(POF) α_s Quark tag extrapolation [%]	± 3.08	± 2.73	± 2.79	± 3.27	± 3.66	± 3.23
(POF) α_s Quark tag extrapolation from ϵ -Quark [%]	-	-	-	-	-	-
(POF) PDF4LHC15 eigencenter 0 [%]	± 0.16	± 0.17	± 0.24	± 0.28	± 0.36	± 0.57
(POF) PDF4LHC15 eigencenter 2 [%]	± 0.50	± 0.60	± 0.60	± 0.64	± 0.86	-
(POF) PDF4LHC15 eigencenter 0 [%]	-	± 0.10	± 0.12	± 0.15	± 0.20	-
(POF) PDF4LHC15 eigencenter 1 [%]	-	± 0.11	± 0.11	± 0.16	± 0.20	± 0.60
(POF) PDF4LHC15 eigencenter 0 [%]	± 2.06	± 2.24	± 2.30	± 2.46	± 2.68	± 2.91
(POF) PDF4LHC15 eigencenter 0 [%]	-	± 0.48	± 0.53	± 0.54	± 0.66	± 0.79
(POF) PDF4LHC15 eigencenter 07 [%]	-	-	-	-	-	-
(POF) PDF4LHC15 eigencenter 16 [%]	± 0.33	± 0.35	± 0.37	± 0.41	± 0.46	± 0.44
(POF) PDF4LHC15 eigencenter 0 [%]	± 0.14	± 0.24	± 0.25	± 0.27	± 0.30	± 0.36
(POF) PDF4LHC15 eigencenter 10 [%]	-	-	± 0.10	± 0.12	± 0.13	± 0.27
(POF) PDF4LHC15 eigencenter 11 [%]	± 0.28	± 0.39	± 0.40	± 0.42	± 0.42	± 0.40
(POF) PDF4LHC15 eigencenter 12 [%]	± 0.29	± 0.30	± 0.29	± 0.29	± 0.23	-
(POF) PDF4LHC15 eigencenter 13 [%]	-	-	-	-	± 0.10	± 0.18
(POF) PDF4LHC15 eigencenter 14 [%]	-	-	-	-	-	-
(POF) PDF4LHC15 eigencenter 15 [%]	-	-	-	-	-	-
(POF) PDF4LHC15 eigencenter 17 [%]	± 0.28	± 0.45	± 0.47	± 0.49	± 0.51	± 0.53
(POF) PDF4LHC15 eigencenter 18 [%]	-	± 0.11	± 0.11	± 0.15	± 0.15	-
(POF) PDF4LHC15 eigencenter 19 [%]	± 0.63	± 0.87	± 0.86	± 0.83	± 0.83	± 0.71
(POF) PDF4LHC15 eigencenter 20 [%]	± 0.18	-	-	-	-	± 0.13
(POF) PDF4LHC15 eigencenter 21 [%]	-	-	-	-	-	± 0.16
(POF) PDF4LHC15 eigencenter 22 [%]	-	± 0.72	± 0.81	± 0.90	± 1.13	± 1.64
(POF) PDF4LHC15 eigencenter 24 [%]	-	-	-	-	-	± 0.26
(POF) PDF4LHC15 eigencenter 25 [%]	-	-	-	-	-	-
(POF) PDF4LHC15 eigencenter 26 [%]	-	-	-	-	-	-
(POF) PDF4LHC15 eigencenter 27 [%]	± 0.34	± 0.16	± 0.14	± 0.14	± 0.13	-
(POF) PDF4LHC15 eigencenter 28 [%]	± 0.15	-	-	± 0.10	-	± 0.41
(POF) PDF4LHC15 eigencenter 29 [%]	-	-	-	-	-	-
(POF) PDF4LHC15 eigencenter 30 [%]	-	-	-	-	-	-
(LEP) Electron energy resolution [%]	-	-	-	-	± 0.33	-
(LEP) Electron energy scale [%]	-	-	-	-	± 0.33	-
(LEP) Muon (MS) momentum resolution [%]	-	-	-	-	-	-
(LEP) Muon (ID) momentum resolution [%]	-	-	-	-	-	-
(LEP) Muon sagitta resolution bias [%]	-	-	-	-	-	-
(LEP) Muon χ^2 resolution [%]	-	-	-	-	-	-
(METTP) $\ell^\pm \ell^\mp$ Soft jet resolution para [%]	-	-	-	-	-	-
(METTP) $\ell^\pm \ell^\mp$ Soft jet resolution perp [%]	-	-	-	-	-	-
(METTP) Jet energy scale [%]	-	-	-	-	-	-
(METTP) Jet vertex tagging [%]	-	-	-	± 0.11	± 0.12	± 0.23
Luminosity [%]	± 1.99	± 1.97	± 1.98	± 2.21	± 2.08	± 1.90
(BKG) Single top t -channel reweight [%]	± 0.25	-	± 0.10	± 0.34	± 0.60	± 0.79
(BKG) $t\bar{t}$ cross-section [%]	-	-	-	-	-	± 0.14
(BKG) $t\bar{t}$ cross-section τ -channel reweight [%]	-	-	-	-	± 0.11	-
(BKG) $t\bar{t}$ cross-section t -channel reweight [%]	-	-	-	-	-	-
(MOD) Multi-jet background statistics [%]	± 1.00	± 2.92	± 5.02	± 4.16	± 5.84	± 9.44
(MOD) Monte Carlo sample statistics [%]	± 0.89	± 2.49	± 3.36	± 4.48	± 5.51	± 14.2
(MOD) ISR-FSR + scale [%]	± 1.84	± 1.58	± 1.18	± 5.53	± 4.87	± 6.62
(MOD) Alternative hadron shower model [%]	± 1.14	± 0.51	± 1.05	± 1.83	± 3.42	-
(MOD) Alternative parton-shower model [%]	± 15.3	± 12.3	± 12.4	± 7.91	± 14.9	± 21.5

Table 51: The individual systematic uncertainties in the fiducial phase-space absolute differential cross-sections for the top quark-antiquark system transverse momentum calculated as a percent of the cross-section in each bin. Dashes are used when the estimated relative systematic uncertainty for that bin is below 0.1%.

Binn	0-100	100-150	150-200	200-300	300-500	500-800
$10^6 \text{ d}t / \text{d}p_T$	5.20.10 $^{-3}$	4.08.10 $^{-3}$	2.10.10 $^{-3}$	1.08.10 $^{-3}$	7.93.10 $^{-4}$	1.97.10 $^{-4}$
Total Uncertainty [%]	+4.05	+8.96	+12.2	+14.4	+17.0	+18.3
Statistics [%]	+2.8	+5.8	+9.0	+9.2	+12.	+12.
Syst. [stat.] [%]	+2.59	+5.67	+5.83	+9.27	+8.67	+8.08
JES b-tagged jet energy scale [%]	-	-	-	-	-	-
(JES) Effective detector NP set 1 [%]	-	-	-	-	+0.38	-
(JES) Effective detector NP set 2 [%]	-	-	-	-	+0.21	-
(JES) Effective detector NP set 3 [%]	-	-	-	-	+0.25	-
(JES) Effective detector NP set 4 [%]	-	-	-	-	+0.21	-
(JES) Effective detector NP set 5 [%]	-	-	-	-	+0.21	-
(JES) Effective detector NP set 6 [%]	-	-	-	-	+0.21	-
(JES) Effective detector NP set 7 [%]	-	-	-	-	+0.21	-
(JES) Effective detector NP set 8 & Term [%]	-	-	-	-	+0.21	-
JES y intercalibration model [%]	-	-	-	-	+0.38	-
JES y intercalibration total stat [%]	-	-	-	-	+0.38	-
JES Pile-up offset [μm] [%]	-	-	-	+0.14	+0.62	-
(JES) Flavour response [%]	-	-	-	-	+3.9	+0.41
(JES) Pile-up offset μ [%]	-	-	-	-	+0.10	+0.10
(JES) Pile-up offset N_{Vtx} [%]	-	-	-	-	+0.11	+0.34
(JES) Pile-up offset p_T [%]	-	-	-	-	+0.24	+0.24
(JES) Pile-up offset ρ topology [%]	-	-	-	-	+0.40	+0.24
(JES) Pile-up offset η [%]	-	-	-	-	+2.0	-
(JES) Pile-up offset ϕ [%]	-	-	-	-	+0.17	-
(JES) Pile-up offset p_T topology [%]	-	-	-	-	+0.26	-
(LHER6) Large R ₀ & Baseline mass [%]	-0.16	+0.14	+0.71	+0.15	+0.98	+2.26
(LHER6) Large R ₀ & Baseline p_T [%]	+1.01	+0.62	+1.52	+2.38	+5.05	+1.01
(LHER6) Large R ₀ & Baseline η [%]	+0.14	+0.22	+0.22	+0.15	+0.99	+0.13
(LHER6) Large R ₀ & Baseline ϕ [%]	+0.48	+0.48	+0.48	+0.48	+0.48	+0.06
(LHER6) Large R ₀ & Modelling p_T [%]	+0.23	+0.04	+0.84	+0.30	+1.91	+0.39
(LHER6) Large R ₀ & Modelling η [%]	+0.25	+0.57	+1.81	+0.85	+7.25	+8.19
(LHER6) Large R ₀ & Modelling ϕ [%]	+0.29	+0.32	+0.81	+0.55	+4.66	+4.66
(LHER6) Large R ₀ & Tracking mass [%]	+0.29	+0.19	+0.18	+0.15	+1.46	+1.46
(LHER6) Large R ₀ & Tracking p_T [%]	+0.16	+0.18	+0.18	+0.15	+0.17	+0.35
(LHER6) Large R ₀ & Total mass [%]	-	-	-	+0.27	+0.31	+0.31
(LHER6) Large R ₀ & Total p_T [%]	-	-	-	+0.23	+0.23	+0.23
(LHER6) Large R ₀ & Total η [%]	-	-	-	+0.27	+0.17	+0.17
(LHER6) Large R ₀ & top-quark mass resolution [%]	+0.57	+0.97	+0.46	+0.84	+0.60	+1.85
(FTAG) Q tag tagging efficiency (eigenvector 0) [%]	+0.15	-	-	+0.21	+0.59	+0.56
(FTAG) Q tag tagging efficiency (eigenvector 1) [%]	-	-	-	+0.20	+0.34	+0.49
(FTAG) Q tag tagging efficiency (eigenvector 2) [%]	-	-	-	-	-	-
(FTAG) Q tag tagging efficiency (eigenvector 3) [%]	-	-	-	-	-	-
(FTAG) Q tag tagging efficiency (eigenvector 4) [%]	+0.12	+0.39	+0.46	+0.12	+1.24	+0.50
(FTAG) Q tag tagging efficiency (eigenvector 5) [%]	+0.24	+0.29	+0.36	+1.03	+9.85	+0.50
(FTAG) Q tag tagging efficiency (eigenvector 6) [%]	+0.18	-0.17	+0.29	+0.53	+0.50	+0.86
(FTAG) Q tag tagging efficiency (eigenvector 7) [%]	+0.14	+0.11	+0.23	+0.36	+0.36	+0.72
(FTAG) Q tag tagging efficiency (eigenvector 8) [%]	-	-	-	+0.13	+0.26	+0.26
(FTAG) Light-jet tagging efficiency (eigenvector 1) [%]	-	-	-	+0.13	-	+0.14
(FTAG) Light-jet tagging efficiency (eigenvector 2) [%]	-	-	-	-	+0.11	-
(FTAG) Light-jet tagging efficiency (eigenvector 3) [%]	-	-	-	-	+0.11	-
(FTAG) Light-jet tagging efficiency (eigenvector 4) [%]	-	-	-	-	+0.30	-
(FTAG) Light-jet tagging efficiency (eigenvector 5) [%]	-	-	-	-	+0.14	-
(FTAG) Light-jet tagging efficiency (eigenvector 6) [%]	-	-	-	-	+0.17	-
(FTAG) Light-jet tagging efficiency (eigenvector 7) [%]	-	-	-	-	+0.23	+0.20
(FTAG) Light-jet tagging efficiency (eigenvector 8) [%]	-	-	-	+0.23	+0.20	+0.05
(FTAG) Light-jet tagging efficiency (eigenvector 9) [%]	-	-	-	+0.26	+0.24	+0.62
(FTAG) Light-jet tagging efficiency (eigenvector 10) [%]	-	-	-	-	+0.14	-
(FTAG) Light-jet tagging efficiency (eigenvector 11) [%]	-	-	-	-	+0.17	-
(FTAG) Light-jet tagging efficiency (eigenvector 12) [%]	-	-	-	-	+0.17	-
(FTAG) Light-jet tagging efficiency (eigenvector 13) [%]	-	-	-	-	+0.17	-
(FTAG) Light-jet tagging efficiency (eigenvector 14) [%]	-	-	-	-	+0.30	+0.24
(FTAG) Light-jet tagging efficiency (eigenvector 15) [%]	-	-	-	-	+0.23	+0.62
(FTAG) Light-jet tagging extrapolation from C-quark [%]	+0.23	+0.10	+0.17	+0.21	+0.29	+0.51
(PDF) PDF4LHC15 eigenerote 01 [%]	-	-	-	-	-	-
(PDF) PDF4LHC15 eigenerote 02 [%]	-	-	-	-	-	-
(PDF) PDF4LHC15 eigenerote 03 [%]	-	-	-	-	-	-
(PDF) PDF4LHC15 eigenerote 04 [%]	+0.21	+0.11	+0.14	+0.18	+0.20	+0.34
(PDF) PDF4LHC15 eigenerote 05 [%]	+0.15	-	-	+0.25	+0.47	+0.62
(PDF) PDF4LHC15 eigenerote 06 [%]	+0.27	+0.14	+0.19	+0.20	+0.32	+0.45
(PDF) PDF4LHC15 eigenerote 07 [%]	-	-	-	-	-	-
(PDF) PDF4LHC15 eigenerote 08 [%]	-	-	-	-	-	+0.10
(PDF) PDF4LHC15 eigenerote 09 [%]	-	-	-	-	-	+0.15
(PDF) PDF4LHC15 eigenerote 10 [%]	-	-	-	-	-	+0.17
(PDF) PDF4LHC15 eigenerote 11 [%]	+0.14	-0.04	-0.10	-	-	-
(PDF) PDF4LHC15 eigenerote 12 [%]	-	-	-	-	-	+0.29
(PDF) PDF4LHC15 eigenerote 13 [%]	-	-	-	-	-	+0.11
(PDF) PDF4LHC15 eigenerote 14 [%]	-	-	-	-	-	+0.11
(PDF) PDF4LHC15 eigenerote 15 [%]	+0.12	-	-	-	-	-
(PDF) PDF4LHC15 eigenerote 16 [%]	-	-	-	-	-	+0.11
(PDF) PDF4LHC15 eigenerote 17 [%]	+0.11	-	-	-	+0.11	+0.13
(PDF) PDF4LHC15 eigenerote 18 [%]	-	-	-	-	-	-
(PDF) PDF4LHC15 eigenerote 19 [%]	+0.14	-0.04	-0.10	-	-	-
(PDF) PDF4LHC15 eigenerote 20 [%]	-	-	-	-	-	-
(PDF) PDF4LHC15 eigenerote 21 [%]	-	-	-	-	-	-
(PDF) PDF4LHC15 eigenerote 22 [%]	+0.11	-	-	+0.28	+0.50	+0.79
(PDF) PDF4LHC15 eigenerote 23 [%]	-	-	-	-	-	-
(PDF) PDF4LHC15 eigenerote 24 [%]	-	-	-	-	+0.12	+0.30
(PDF) PDF4LHC15 eigenerote 25 [%]	-	-	-	-	-	-
(PDF) PDF4LHC15 eigenerote 26 [%]	-	-	-	-	-	-
(PDF) PDF4LHC15 eigenerote 27 [%]	+0.11	-	-	-	-	+0.16
(PDF) PDF4LHC15 eigenerote 28 [%]	-	-	-	-	+0.16	+0.32
(PDF) PDF4LHC15 eigenerote 29 [%]	-	-	-	-	-	-
(PDF) PDF4LHC15 eigenerote 30 [%]	-	-	-	-	-	-
(LEP) Electron energy resolution [%]	-	-	-	-	+0.52	-
(LEP) Electron energy scale [%]	-	-	-	-	+0.12	-
(LEP) Muon energy scale [%]	-	-	-	-	-	-
(LEP) Muon (MS) momentum resolution [%]	-	-	-	-	-	-
(LEP) Muon (ID) momentum resolution [%]	-	-	-	-	-	-
(LEP) Muon (MC) momentum resolution [%]	-	-	-	-	-	-
(LEP) Muon signal ρ [%]	-	-	-	-	-	-
(METFPU) $E^{miss}_{\text{T}}/\text{Soft jet correction para}$ [%]	-	-	-	-	-	-
(METFPU) $E^{miss}_{\text{T}}/\text{Soft jet correction perp}$ [%]	-	-	-	-	-	-
(METFPU) Jet vertex tagging [%]	-	-	-	-	-	-
Luminosity [%]	-	-	-	-	-	+0.14
Number of top-anti-top cross-section [%]	-	+0.21	+0.10	+0.13	+0.20	+0.10
BKG $\pi \pi \rightarrow W$ cross-section [%]	-	-	-	-	-	+0.00
BKG $\pi \pi \rightarrow Z$ cross-section [%]	-	-	-	-	-	+0.10
BKG $\pi \pi \rightarrow \chi_1 \chi_2$ cross-section [%]	-	-	-	-	-	-
BKG $\pi \pi \rightarrow \chi_1 \chi_2 + \text{jet}$ cross-section [%]	-	-	-	-	-	-
BKG MuH background cross-section [%]	-	+0.22	+0.51	+0.16	+0.84	-
BKG MuH background statistics [%]	+0.85	+2.26	+3.15	+2.46	+5.38	-
(M0D) ISR PSR + FSR [%]	+0.13	-0.04	-0.10	-0.04	+1.25	-
(M0D) Alternative hard-part showering model [%]	+0.57	+0.43	+0.42	+0.22	+2.11	+0.59
(M0D) Alternative hard-part showering model [%]	+1.80	+0.72	+1.62	+0.86	+3.33	+0.59

Table 52: The individual systematic uncertainties in the fiducial phase-space relative differential cross-sections for the top quark-antiquark system transverse momentum calculated as a percentage of the cross-section in each bin. Dashes are used when the estimated relative systematic uncertainty for that bin is below 0.1%.

Bins [Unit [μb^{-1}]]	0-0.30	0.30-0.60	0.60-0.90	0.90-1.20	1.20-1.50	1.50-2
$d\sigma / d\eta^2$ [pb/Unit [η^2]]	$3.057 \cdot 10^{-3}$	$2.626 \cdot 10^{-3}$	$2.025 \cdot 10^{-3}$	$1.266 \cdot 10^{-3}$	$2.760 \cdot 10^{-3}$	$1.178 \cdot 10^{-3}$
Total Uncertainty [%]	± 25.9	± 24.2	± 22.6	± 30.2	± 29.4	± 31.0
Statistical [%]	± 4.4	± 5.1	± 5.5	± 7.1	± 11	± 16
Systematic [%]	± 25.5	± 23.5	± 21.8	± 29.1	± 26.8	± 31.0
(JES) b-Tagged jet energy scale [%]	-	-	-	-	± 0.18	-
(JES) Effective detector NP set 2 [%]	-	-	-	-	-	± 0.14
(JES) Effective detector NP set 3 [%]	-	-	-	-	-	-
(JES) Effective detector NP set 4 [%]	-	-	-	-	-	-
(JES) Effective detector NP set 5 [%]	-	-	-	-	-	-
(JES) Effective detector NP set 6 [%]	-	-	-	-	-	-
(JES) Effective detector NP set 7 [%]	-	-	-	-	-	-
(JES) Effective detector NP set 8 resTerm [%]	-	-	-	-	-	-
(JES) η intercalibration model [%]	-	-	-	-	± 0.10	-
(JES) η intercalibration total stat [%]	-	-	-	-	-	-
(JES) Flavor composition [%]	± 0.35	± 0.23	± 0.21	± 0.20	± 0.21	± 0.62
(JES) Flavor response [%]	± 0.11	± 0.13	-	-	-	-
(JES) Pile-up offset η [%]	-	-	-	-	-	-
(JES) Pile-up offset p_T [%]	-	-	-	-	-	-
(JES) Pile-up offset ρ topology [%]	± 0.24	± 0.18	± 0.16	± 0.10	± 0.22	± 0.62
(JES) Single particle high- p_T [%]	-	-	-	-	-	-
(JES) Large- R jet Baseline mass [%]	± 0.31	± 0.30	± 0.27	± 0.26	± 0.48	± 0.60
(JES) Large- R jet Baseline p_T [%]	± 0.05	± 0.11	± 0.09	± 0.17	± 0.23	± 0.20
(JES) Large- R jet Baseline η [%]	± 0.58	± 0.89	± 0.50	± 0.79	± 0.72	± 0.68
(JES) Large- R jet Modeling mass [%]	± 0.19	± 0.16	± 0.32	± 0.29	± 0.64	± 1.19
(JES) Large- R jet Modeling p_T [%]	± 0.17	± 0.19	± 0.34	± 0.06	± 0.44	± 0.21
(JES) Large- R jet Modeling η [%]	± 0.19	± 0.27	± 0.27	± 0.11	± 0.16	± 0.14
(JES) Large- R jet Tracking p_T [%]	± 0.28	± 0.23	± 0.12	-	-	± 0.34
(JES) Large- R jet Tracking η [%]	± 0.46	± 0.43	± 0.40	± 0.05	± 0.46	± 0.48
(JES) Large- R jet Tracking η_2 [%]	± 0.39	± 0.35	± 0.37	± 0.05	± 0.40	± 0.36
(JES) Large- R jet Totalstat p_T [%]	± 0.19	± 0.12	-	-	-	-
(JES) Large- R jet Totalstat η_2 [%]	± 0.18	± 0.16	± 0.40	± 0.21	± 0.65	± 0.31
(JES) Large- R jet Totalstat η [%]	± 0.18	± 0.16	± 0.17	± 0.15	± 0.15	± 0.25
(JES) Large- R jet Totalstat η_1 [%]	-	-	-	-	-	-
(JES) Large- R jet Totalstat η_3 [%]	-	-	-	-	-	-
(ITAG) b-Quark tagging extrapolation [0 %]	± 5.35	± 5.36	± 5.33	± 4.95	± 2.90	± 5.23
(ITAG) b-Quark tagging efficiency (eigencenter 0) [%]	± 4.98	± 4.95	± 4.96	± 4.54	± 4.83	± 4.73
(ITAG) b-Quark tagging efficiency (eigencenter 2) [%]	± 0.81	± 0.77	± 0.76	± 0.60	± 0.69	± 0.55
(ITAG) b-Quark tagging efficiency (eigencenter 4) [%]	± 0.25	± 0.24	± 0.23	± 0.22	± 0.22	± 0.24
(ITAG) b-Quark tagging efficiency (eigencenter 6) [%]	± 0.21	± 1.73	± 2.48	± 1.78	± 2.62	-
(ITAG) b-Quark tagging efficiency (eigencenter 8) [%]	± 1.35	± 1.28	± 1.30	± 1.00	± 1.46	± 1.25
(ITAG) b-Quark tagging efficiency (eigencenter 10) [%]	± 0.80	± 0.80	± 0.89	± 0.89	± 0.90	± 0.20
(ITAG) b-Quark tagging efficiency (eigencenter 12) [%]	± 0.43	± 0.43	± 0.48	± 0.46	± 0.54	± 0.18
(ITAG) Light-jet tagging efficiency (eigencenter 0) [%]	± 0.15	± 0.16	± 0.29	± 0.69	± 0.33	± 0.20
(ITAG) Light-jet tagging efficiency (eigencenter 2) [%]	-	-	± 0.16	± 0.29	± 0.19	± 0.17
(ITAG) Light-jet tagging efficiency (eigencenter 3) [%]	-	± 0.10	-	± 0.14	± 0.11	-
(ITAG) Light-jet tagging efficiency (eigencenter 4) [%]	-	-	-	± 0.24	-	± 0.15
(ITAG) Light-jet tagging efficiency (eigencenter 6) [%]	-	-	-	-	-	-
(ITAG) Light-jet tagging efficiency (eigencenter 7) [%]	-	-	-	± 0.11	-	-
(ITAG) Light-jet tagging efficiency (eigencenter 9) [%]	± 0.24	± 0.25	± 0.28	± 0.27	± 0.22	± 0.10
(ITAG) Light-jet tagging efficiency (eigencenter 11) [%]	± 0.21	± 0.10	-	± 0.32	± 0.32	± 0.11
(ITAG) Light-jet tagging efficiency (eigencenter 13) [%]	± 0.21	± 0.11	± 0.29	± 0.28	± 0.24	± 0.20
(ITAG) Light-jet tagging efficiency (eigencenter 15) [%]	± 0.21	± 0.10	± 0.37	± 0.81	± 1.34	± 1.70
(ITAG) Light-jet tagging efficiency (eigencenter 17) [%]	± 0.12	± 0.23	± 0.47	± 0.69	± 1.00	± 1.72
(ITAG) Light-jet tagging efficiency (eigencenter 19) [%]	± 0.19	± 0.18	± 0.18	± 0.22	± 0.25	± 0.21
(ITAG) Light-jet tagging efficiency (eigencenter 21) [%]	± 0.31	± 0.29	± 0.60	± 0.64	± 0.60	± 0.31
(ITAG) Light-jet tagging efficiency (eigencenter 23) [%]	± 0.28	± 0.26	± 0.27	± 0.36	± 0.40	± 0.53
(ITAG) Light-jet tagging efficiency (eigencenter 24) [%]	± 0.12	-	-	± 0.14	± 0.22	± 0.18
(ITAG) Light-jet tagging efficiency (eigencenter 25) [%]	± 0.17	± 0.15	± 0.12	± 0.14	± 0.26	± 0.44
(ITAG) Light-jet tagging efficiency (eigencenter 27) [%]	± 0.34	± 0.34	± 0.35	± 0.42	± 0.50	± 0.58
(ITAG) Light-jet tagging efficiency (eigencenter 29) [%]	-	-	-	± 0.32	± 0.54	± 1.06
(POD) PDF4LHC15 eigencenter 0 [%]	± 0.33	± 0.39	± 0.59	± 1.01	± 1.51	± 1.68
(POD) PDF4LHC15 eigencenter 6 [%]	-	-	-	± 0.32	± 0.54	-
(POD) PDF4LHC15 eigencenter 8 [%]	± 0.21	± 0.10	-	± 0.32	± 0.52	± 1.15
(POD) PDF4LHC15 eigencenter 9 [%]	± 0.17	± 0.11	± 0.29	± 0.28	± 0.24	± 0.20
(POD) PDF4LHC15 eigencenter 10 [%]	± 0.19	± 0.18	± 0.18	± 0.22	± 0.25	± 0.21
(POD) PDF4LHC15 eigencenter 11 [%]	± 0.31	± 0.29	± 0.60	± 0.64	± 0.60	± 0.31
(POD) PDF4LHC15 eigencenter 12 [%]	± 0.28	± 0.26	± 0.27	± 0.36	± 0.40	± 0.53
(POD) PDF4LHC15 eigencenter 13 [%]	-	-	-	± 0.14	± 0.22	-
(POD) PDF4LHC15 eigencenter 14 [%]	-	-	-	-	± 0.25	± 0.40
(POD) PDF4LHC15 eigencenter 15 [%]	± 0.17	± 0.15	± 0.12	± 0.14	± 0.26	± 0.44
(POD) PDF4LHC15 eigencenter 16 [%]	± 0.23	± 0.19	± 0.10	± 0.10	-	± 0.21
(POD) PDF4LHC15 eigencenter 17 [%]	± 0.13	-	-	-	-	-
(POD) PDF4LHC15 eigencenter 19 [%]	± 0.17	± 0.22	± 0.32	± 0.39	± 0.39	± 0.31
(POD) PDF4LHC15 eigencenter 20 [%]	± 0.41	-	± 0.51	± 0.84	± 0.88	± 0.84
(POD) PDF4LHC15 eigencenter 21 [%]	-	-	-	-	-	-
(POD) PDF4LHC15 eigencenter 22 [%]	± 0.10	± 0.28	-	± 0.50	± 0.68	± 0.76
(POD) PDF4LHC15 eigencenter 23 [%]	-	-	-	± 0.21	± 0.41	± 0.51
(POD) PDF4LHC15 eigencenter 24 [%]	-	-	-	± 0.26	± 0.49	± 0.65
(POD) PDF4LHC15 eigencenter 25 [%]	-	-	-	-	-	-
(POD) PDF4LHC15 eigencenter 27 [%]	± 0.13	± 0.16	± 0.26	± 0.22	-	-
(POD) PDF4LHC15 eigencenter 28 [%]	± 0.41	-	± 0.51	± 0.84	± 0.88	-
(POD) PDF4LHC15 eigencenter 29 [%]	-	-	-	-	-	-
(POD) PDF4LHC15 eigencenter 30 [%]	-	-	-	-	-	-
(POD) PDF4LHC15 eigencenter 31 [%]	-	-	-	-	-	-
(POD) PDF4LHC15 eigencenter 32 [%]	-	-	-	-	-	-
(POD) PDF4LHC15 eigencenter 33 [%]	-	-	-	-	-	-
(POD) PDF4LHC15 eigencenter 34 [%]	-	-	-	-	-	-
(POD) PDF4LHC15 eigencenter 35 [%]	-	-	-	-	-	-
(POD) PDF4LHC15 eigencenter 36 [%]	-	-	-	-	-	-
(POD) PDF4LHC15 eigencenter 37 [%]	-	-	-	-	-	-
(POD) PDF4LHC15 eigencenter 38 [%]	-	-	-	-	-	-
(POD) PDF4LHC15 eigencenter 39 [%]	-	-	-	-	-	-
(POD) PDF4LHC15 eigencenter 40 [%]	-	-	-	-	-	-
(POD) PDF4LHC15 eigencenter 41 [%]	-	-	-	-	-	-
(POD) PDF4LHC15 eigencenter 42 [%]	-	-	-	-	-	-
(POD) PDF4LHC15 eigencenter 43 [%]	-	-	-	-	-	-
(POD) PDF4LHC15 eigencenter 44 [%]	-	-	-	-	-	-
(POD) PDF4LHC15 eigencenter 45 [%]	-	-	-	-	-	-
(POD) PDF4LHC15 eigencenter 46 [%]	-	-	-	-	-	-
(POD) PDF4LHC15 eigencenter 47 [%]	-	-	-	-	-	-
(POD) PDF4LHC15 eigencenter 48 [%]	-	-	-	-	-	-
(POD) PDF4LHC15 eigencenter 49 [%]	-	-	-	-	-	-
(POD) PDF4LHC15 eigencenter 50 [%]	-	-	-	-	-	-
(POD) PDF4LHC15 eigencenter 51 [%]	-	-	-	-	-	-
(POD) PDF4LHC15 eigencenter 52 [%]	-	-	-	-	-	-
(POD) PDF4LHC15 eigencenter 53 [%]	-	-	-	-	-	-
(POD) PDF4LHC15 eigencenter 54 [%]	-	-	-	-	-	-
(POD) PDF4LHC15 eigencenter 55 [%]	-	-	-	-	-	-
(POD) PDF4LHC15 eigencenter 56 [%]	-	-	-	-	-	-
(POD) PDF4LHC15 eigencenter 57 [%]	-	-	-	-	-	-
(POD) PDF4LHC15 eigencenter 58 [%]	-	-	-	-	-	-
(POD) PDF4LHC15 eigencenter 59 [%]	-	-	-	-	-	-
(POD) PDF4LHC15 eigencenter 60 [%]	-	-	-	-	-	-
(POD) PDF4LHC15 eigencenter 61 [%]	-	-	-	-	-	-
(POD) PDF4LHC15 eigencenter 62 [%]	-	-	-	-	-	-
(POD) PDF4LHC15 eigencenter 63 [%]	-	-	-	-	-	-
(POD) PDF4LHC15 eigencenter 64 [%]	-	-	-	-	-	-
(POD) PDF4LHC15 eigencenter 65 [%]	-	-	-	-	-	-
(POD) PDF4LHC15 eigencenter 66 [%]	-	-	-	-	-	-
(POD) PDF4LHC15 eigencenter 67 [%]	-	-	-	-	-	-
(POD) PDF4LHC15 eigencenter 68 [%]	-	-	-	-	-	-
(POD) PDF4LHC15 eigencenter 69 [%]	-	-	-	-	-	-
(POD) PDF4LHC15 eigencenter 70 [%]	-	-	-	-	-	-
(POD) PDF4LHC15 eigencenter 71 [%]	-	-	-	-	-	-
(POD) PDF4LHC15 eigencenter 72 [%]	-	-	-	-	-	-
(POD) PDF4LHC15 eigencenter 73 [%]	-	-	-	-	-	-
(POD) PDF4LHC15 eigencenter 74 [%]	-	-	-	-	-	-
(POD) PDF4LHC15 eigencenter 75 [%]	-	-	-	-	-	-
(POD) PDF4LHC15 eigencenter 76 [%]	-	-	-	-	-	-
(POD) PDF4LHC15 eigencenter 77 [%]	-	-	-	-	-	-
(POD) PDF4LHC15 eigencenter 78 [%]	-	-	-	-	-	-
(POD) PDF4LHC15 eigencenter 79 [%]	-	-	-	-	-	-
(POD) PDF4LHC15 eigencenter 80 [%]	-	-	-	-	-	-
(POD) PDF4LHC15 eigencenter 81 [%]	-	-	-	-	-	-
(POD) PDF4LHC15 eigencenter 82 [%]	-	-	-	-	-	-
(POD) PDF4LHC15 eigencenter 83 [%]	-					

Not reviewed, for internal circulation only

Bin [Unit [μb^{-1}]]	0...30	30...60	60...90	90...120	120...150	150...2
$1/\sigma \cdot d\sigma/dy^2$	$1.042 \cdot 10^6$	$8.853 \cdot 10^7$	$7.008 \cdot 10^{11}$	$4.317 \cdot 10^{12}$	$1.964 \cdot 10^{13}$	$4.017 \cdot 10^{13}$
Total Uncertainty [%]	± 5.39	± 5.97	± 5.18	± 10.7	± 13.8	± 27.1
Statistics [%]	± 3.8	± 4.5	± 5.0	± 6.6	± 10	± 18
Syst. + stat. [%]	± 21.14	± 23.09	± 25.86	± 27.67	± 35.82	± 45.2
(JES) b-Tagged jet energy scale [%]	-	-	-	-	-	± 0.15
(JES) Effective detector NP set 1 [%]	-	-	-	-	± 0.10	-
(JES) Effective detector NP set 2 [%]	-	-	-	-	-	± 0.18
(JES) Effective detector NP set 3 [%]	-	-	-	-	-	-
(JES) Effective detector NP set 4 [%]	-	-	-	-	-	-
(JES) Effective detector NP set 5 [%]	-	-	-	-	-	-
(JES) Effective detector NP set 6 [%]	-	-	-	-	-	-
(JES) Effective detector NP set 7 [%]	-	-	-	-	-	-
(JES) Effective detector NP set 8 resTerm [%]	-	-	-	-	-	-
(JES) η response model [%]	-	-	-	-	-	-
(JES) η intercalibration uncertainty [%]	-	-	-	-	-	± 0.19
(JES) Flavor composition [%]	-	-	-	± 0.14	-	± 0.38
(JES) Flavor response [%]	-	-	-	-	± 0.10	-
(JES) Pile-up offset τ_0 [%]	-	-	-	-	-	-
(JES) Pile-up offset τ_1 [%]	-	-	-	-	-	-
(JES) Pile-up offset τ_2 [%]	-	-	-	-	-	-
(JES) Pile-up offset τ_3 [%]	-	-	-	-	-	-
(JES) Single particle $\tau_2 p_T$ [%]	-	-	-	-	-	-
(JES) Large- R jet Baseline mass [%]	± 0.40	-	± 0.41	± 0.31	± 0.31	± 0.85
(JES) Large- R jet Baseline τ_2 [%]	± 2.29	-	± 0.26	± 0.14	± 0.14	± 0.56
(JES) Large- R jet Modeling mass [%]	± 0.20	-	± 0.20	± 0.11	± 0.11	± 0.85
(JES) Large- R jet Modeling mass [%]	± 0.20	-	± 0.19	± 0.16	± 0.16	± 0.59
(JES) Large- R jet Modeling p_T [%]	-	-	-	± 0.49	± 0.25	± 0.31
(JES) Large- R jet Modeling p_T [%]	-	-	-	± 0.35	± 0.17	± 0.81
(JES) Large- R jet Modeling τ_2 [%]	± 0.43	-	± 0.16	± 0.35	± 0.11	± 2.65
(JES) Large- R jet Tracking p_T [%]	± 2.35	-	± 0.19	± 0.19	± 0.19	± 2.80
(JES) Large- R jet Tracking τ_2 [%]	± 0.47	-	± 0.28	± 0.42	± 0.21	± 0.47
(JES) Large- R jet Tracking τ_2 [%]	-	-	-	-	± 0.14	± 2.08
(JES) Large- R jet TotalStar τ_2 [%]	-	-	-	-	-	-
(JES) Large- R jet TotalStar τ_2 [%]	-	-	-	± 0.10	-	± 0.13
(JES) Large- R jet TotalStar τ_2 [%]	-	-	-	-	-	± 0.14
(JES) Large- R jet top-quark energy resolution [%]	± 0.50	± 0.81	-	± 1.43	± 2.20	-
(FTAG) c-Quark tagging efficiency (eigenvector 0) [%]	-	-	-	± 0.34	-	± 1.14
(FTAG) c-Quark tagging efficiency (eigenvector 1) [%]	-	-	-	-	± 0.34	-
(FTAG) c-Quark tagging efficiency (eigenvector 2) [%]	-	-	-	-	± 0.35	± 0.17
(FTAG) c-Quark tagging efficiency (eigenvector 3) [%]	-	-	-	-	± 0.14	± 0.19
(FTAG) c-Quark tagging efficiency (eigenvector 4) [%]	-	-	-	-	-	± 0.16
(FTAG) c-Quark tagging efficiency (eigenvector 5) [%]	-	-	-	-	-	-
(FTAG) c-Quark tagging efficiency (eigenvector 6) [%]	-	-	± 0.34	± 0.40	± 0.29	± 0.55
(FTAG) c-Quark tagging efficiency (eigenvector 7) [%]	-	-	-	± 0.25	± 0.30	± 0.19
(FTAG) c-Quark tagging efficiency (eigenvector 8) [%]	-	-	-	-	± 0.27	± 0.11
(FTAG) c-Quark tagging efficiency (eigenvector 9) [%]	-	-	-	-	-	± 0.20
(FTAG) c-Quark tagging efficiency (eigenvector 10) [%]	-	-	-	-	-	± 0.20
(FTAG) Light-jet tagging efficiency (eigenvector 0) [%]	± 0.11	± 0.10	-	± 0.42	-	-
(FTAG) Light-jet tagging efficiency (eigenvector 1) [%]	-	-	-	-	-	-
(FTAG) Light-jet tagging efficiency (eigenvector 2) [%]	-	-	-	-	-	-
(FTAG) Light-jet tagging efficiency (eigenvector 3) [%]	-	-	-	-	-	-
(FTAG) Light-jet tagging efficiency (eigenvector 4) [%]	-	-	-	-	-	-
(FTAG) Light-jet tagging efficiency (eigenvector 5) [%]	-	-	-	-	-	-
(FTAG) Light-jet tagging efficiency (eigenvector 6) [%]	-	-	-	-	-	-
(FTAG) Light-jet tagging efficiency (eigenvector 7) [%]	-	-	-	± 0.13	-	-
(FTAG) Light-jet tagging efficiency (eigenvector 8) [%]	-	-	-	-	-	-
(FTAG) Light-jet tagging efficiency (eigenvector 9) [%]	-	-	-	-	-	-
(FTAG) Light-jet tagging efficiency (eigenvector 10) [%]	-	-	-	-	-	-
(FTAG) Light-jet tagging efficiency (eigenvector 11) [%]	-	-	-	-	-	-
(FTAG) Light-jet tagging efficiency (eigenvector 12) [%]	-	-	-	-	-	-
(FTAG) Light-jet tagging efficiency (eigenvector 13) [%]	-	-	-	-	-	-
(FTAG) b-Quark tagging extrapolation [%]	± 0.17	-	-	± 0.45	± 0.32	± 0.73
(FTAG) c-Quark tagging extrapolation from c-Quark [4]	-	-	-	-	-	-
(POF) c-Quark eigenvector 0 [%]	± 0.29	-	± 0.10	± 0.16	± 0.39	± 0.35
(POF) c-Quark eigenvector 1 [%]	± 0.22	-	± 0.16	-	± 0.46	± 2.13
(POF) c-Quark eigenvector 03 [%]	± 0.11	-	-	± 0.23	± 0.46	± 0.97
(POF) c-Quark eigenvector 04 [%]	-	-	± 0.12	± 0.11	± 0.73	± 1.17
(POF) c-Quark eigenvector 05 [%]	-	-	-	± 0.10	± 0.38	± 0.84
(POF) c-Quark eigenvector 07 [%]	± 0.30	± 0.18	± 0.10	± 0.54	± 0.17	± 1.43
(POF) c-Quark eigenvector 08 [%]	± 0.23	± 0.12	± 0.11	± 0.33	± 0.64	± 1.36
(POF) c-Quark eigenvector 10 [%]	± 0.12	-	-	± 0.16	-	± 0.20
(POF) c-Quark eigenvector 11 [%]	-	-	-	-	± 0.27	± 0.48
(POF) c-Quark eigenvector 12 [%]	-	-	-	-	-	± 0.24
(POF) c-Quark eigenvector 13 [%]	-	-	-	-	-	± 0.22
(POF) c-Quark eigenvector 14 [%]	-	-	-	-	± 0.25	± 0.41
(POF) c-Quark eigenvector 15 [%]	-	-	-	-	± 0.11	± 0.29
(POF) c-Quark eigenvector 16 [%]	-	-	-	-	-	± 0.25
(POF) c-Quark eigenvector 17 [%]	-	-	-	-	± 0.14	± 0.21
(POF) c-Quark eigenvector 18 [%]	-	-	-	± 0.12	± 0.46	± 0.77
(POF) c-Quark eigenvector 19 [%]	-	-	± 0.19	± 0.10	± 0.39	± 0.34
(POF) c-Quark eigenvector 20 [%]	± 0.27	± 0.10	± 0.15	± 0.27	± 0.54	± 0.63
(POF) c-Quark eigenvector 21 [%]	-	-	-	± 0.15	± 0.35	± 0.45
(POF) c-Quark eigenvector 22 [%]	± 0.93	± 0.54	± 0.25	± 1.61	± 3.43	± 4.78
(POF) c-Quark eigenvector 23 [%]	-	-	-	-	-	-
(POF) c-Quark eigenvector 24 [%]	-	-	-	-	± 0.10	± 0.19
(POF) c-Quark eigenvector 25 [%]	-	-	-	-	-	± 0.16
(POF) c-Quark eigenvector 26 [%]	± 0.17	-	± 0.12	± 0.22	± 0.18	-
(POF) c-Quark eigenvector 27 [%]	-	-	-	± 0.12	± 0.12	-
(POF) c-Quark eigenvector 28 [%]	± 0.57	± 0.16	± 0.36	± 0.69	± 0.73	± 0.69
(POF) c-Quark eigenvector 29 [%]	-	-	-	-	-	-
(POF) c-Quark eigenvector 30 [%]	-	-	-	-	-	-
(LEP) Muon energy scale [%]	-	-	-	-	-	-
(LEP) Muon momentum resolution [%]	-	-	-	-	-	-
(LEP) Muon rapidity bias [%]	-	-	-	-	-	-
(LEP) Muon sagitta μ [%]	-	-	-	-	-	-
(MET/P) Soft jet resolution para [%]	-	-	-	-	-	-
(MET/P) Soft jet resolution perp [%]	-	-	-	-	-	-
(MET/P) Soft jet scale [%]	-	-	-	-	-	-
(MET/P) Jet vertex tagger [%]	-	-	-	-	-	-
(LHC) Luminosity [%]	-	-	-	-	-	-
(BKG) Single top W cross-section [%]	-	-	± 0.19	± 0.24	-	± 0.39
(BKG) Single top t-channel treatment [%]	-	-	-	-	-	-
(BKG) n-Zero cross-section [%]	-	-	-	-	-	-
(BKG) n-H cross-section [%]	-	-	-	-	-	-
(BKG) Multi-jet background statistics [%]	± 1.65	± 1.90	± 0.02	± 2.27	± 3.95	± 9.65
(BKG) Multi-jet background systematic [%]	± 1.19	± 1.42	± 0.12	± 2.48	± 3.09	± 7.39
(MOD) ISR/FSR + scale [%]	± 2.34	± 3.52	± 2.84	± 1.44	± 5.58	-
(MOD) Alternative hard-scattering model [%]	± 2.41	± 0.14	± 3.18	± 3.91	± 3.11	± 11.1
(MOD) Alternative parton-shower model [%]	± 0.29	± 1.43	± 2.15	± 5.22	± 2.58	± 3.74

Table 54: The individual systematic uncertainties in the fiducial phase-space relative differential cross-sections for the top quark-antiquark system absolute value of the rapidity calculated as a percentage of the cross-section in each bin. Dashes are used when the estimated relative systematic uncertainty for that bin is below 0.1%.

Not reviewed, for internal circulation only

Bins (GeV)	0-20	20-40	40-60	60-100	100-200	200-300	300-600
$d\sigma/dp_T$ [pb/GeV]	$4.754 \cdot 10^{-3}$	$\pm 0.87 \cdot 10^{-3}$	$\pm 1.76 \cdot 10^{-3}$	$\pm 1.07 \cdot 10^{-2}$	$3.638 \cdot 10^{-3}$	$1.345 \cdot 10^{-2}$	$2.254 \cdot 10^{-2}$
Total Uncertainty [%]	± 2.3	± 2.6	± 3.0	± 2.9	± 2.1	± 2.4	± 0.8
(JES) Scale [1%]	± 1.4	± 1.1	± 8.3	± 5.4	± 3.4	± 1.7	± 1.7
Systematic [%]	± 21.7	± 25.1	± 24.4	± 28.0	± 24.3	± 26.7	± 34.8
JES b-Tagged jet energy scale [%]	-	-	-	-	-	-	-
JES b-Tagged jet energy scale 1 [%]	-	-	-	-	-	-	-
JES Effective detector NP set 1 [%]	-	-	-	-	-	-	-
JES Effective detector NP set 2 [%]	-	-	-	-	-	-	-
JES Effective detector NP set 3 [%]	-	-	-	-	-	-	-
JES Effective detector NP set 4 [%]	-	-	-	-	-	-	-
JES Effective detector NP set 5 [%]	-	-	-	-	-	-	-
JES Effective detector NP set 6 [%]	-	-	-	-	-	-	-
JES Effective detector NP set 8 resTerm [%]	-	-	-	-	-	-	-
JES η intercalibration model [%]	-	-	-	-	-	-	-
JES η intercalibration model 1 [%]	-	-	-	-	-	-	-
JES Flavor composition [%]	± 0.18	± 0.24	± 0.28	± 0.25	± 0.19	± 0.44	± 0.45
JES Flavor response [%]	-	-	± 0.18	± 0.24	± 0.24	± 0.15	± 0.15
JES Pile-up offset $N_{\text{V}}^{\text{jet}}$ [%]	-	-	-	-	± 0.30	-	± 0.36
JES Pile-up offset p_T [%]	-	-	-	-	-	± 0.29	-
JES Pile-up offset η [%]	-	-	-	-	-	± 0.18	-
JES Pile-up offset $N_{\text{V}}^{\text{jet}}$ [%]	-	-	-	-	-	± 0.22	± 0.36
JES Pile-up offset p_T [%]	-	-	-	-	-	± 0.22	± 0.35
JES Pile-up offset η [%]	-	-	-	-	-	-	-
JES Punch-Through [%]	-	-	-	-	-	-	-
JES Single particle high- p_T [%]	-	-	-	-	-	-	-
JLHC Large- η jet Baseline p_T [%]	± 0.42	± 0.24	± 0.67	± 0.20	± 0.18	± 1.88	± 0.29
JLHC Large- η jet Baseline η [%]	± 1.57	± 2.05	± 1.81	± 2.79	± 0.05	± 4.43	± 2.76
JLHC Large- η jet Baseline p_T [%]	± 7.12	± 8.23	± 8.00	± 9.00	± 8.41	± 7.93	± 7.94
JLHC Large- η jet Baseline η [%]	± 0.99	± 1.05	± 0.99	± 0.97	± 1.01	± 2.73	± 1.21
JLHC Large- η jet Modeling p_T [%]	± 1.82	± 2.55	± 2.06	± 2.41	± 1.00	± 3.05	± 1.40
JLHC Large- η jet Modeling η [%]	± 9.05	± 10.5	± 9.60	± 11.55	± 10.00	± 9.97	± 9.97
JLHC Large- η jet Tracking p_T [%]	± 0.33	± 0.47	± 0.47	± 0.43	± 0.43	± 0.41	± 0.42
JLHC Large- η jet Tracking η [%]	± 4.01	± 5.54	± 4.48	± 6.08	± 4.67	± 4.49	± 6.99
JLHC Large- η jet Tracking p_T [%]	± 0.33	± 0.42	± 0.42	± 0.48	± 0.43	± 0.41	± 0.42
JLHC Large- η jet Tracking η [%]	± 0.22	± 0.35	± 0.35	± 0.35	± 0.35	± 0.34	± 0.35
JLHC Large- η jet TotalStar p_T [%]	± 0.13	± 0.15	± 0.11	± 0.11	± 0.11	± 0.11	± 0.09
JLHC Large- η jet Top-quark mass resolution [%]	± 1.59	± 1.15	± 0.88	± 1.83	± 1.71	± 1.60	± 1.36
FTAG (Quark tagging efficiency) 0 [%]	± 5.26	± 5.38	± 5.23	± 5.30	± 5.32	± 4.95	-
FTAG (Quark tagging efficiency) 1 [%]	± 0.80	± 0.79	± 0.79	± 0.79	± 0.79	± 0.76	± 0.56
FTAG (Quark tagging efficiency) 2 [%]	± 0.80	± 0.79	± 0.68	± 0.73	± 0.67	± 0.65	± 0.72
FTAG (Quark tagging efficiency) 3 [%]	± 0.52	± 0.53	± 0.50	± 0.50	± 0.47	± 0.52	± 0.52
FTAG (Quark tagging efficiency) 4 [%]	± 0.51	± 0.51	± 0.51	± 0.51	± 0.51	± 0.51	± 0.23
FTAG (Quark tagging efficiency) 5 [%]	± 0.20	± 0.20	± 0.23	± 0.23	± 0.23	± 0.23	-
FTAG (Quark tagging efficiency) 6 [%]	± 0.20	± 0.20	± 0.20	± 0.20	± 0.20	± 0.20	-
FTAG (Quark tagging efficiency) 7 [%]	± 0.20	± 0.20	± 0.10	± 0.10	± 0.14	-	-
FTAG (Quark tagging efficiency) 8 [%]	± 0.20	± 0.18	± 0.08	± 0.09	± 0.04	± 0.41	± 0.26
FTAG (Quark tagging efficiency) 9 [%]	± 0.19	± 0.06	± 0.01	± 0.00	± 0.00	± 0.17	± 0.14
FTAG (Quark tagging efficiency) 10 [%]	± 0.19	± 0.06	± 0.01	± 0.00	± 0.00	± 0.04	± 0.04
FTAG (Quark tagging efficiency) 11 [%]	± 0.23	± 0.33	± 0.40	± 0.42	± 0.42	± 0.41	± 0.40
FTAG (Quark tagging efficiency) 12 [%]	± 0.28	± 0.29	± 0.31	± 0.33	± 0.29	± 0.25	± 0.10
FTAG (Quark tagging extrapolation) [%]	± 3.08	± 3.08	± 2.88	± 3.09	± 2.87	± 2.98	± 3.00
FTAG (Quark tagging extrapolation) from c+Quark [%]	-	-	-	-	-	-	-
PDF PDF4LHC13C1 egenvector 0 [%]	± 0.26	-	± 0.14	± 0.19	± 0.28	± 0.35	± 0.43
PDF PDF4LHC13C1 egenvector 02 [%]	± 0.42	± 0.58	± 0.63	± 0.64	± 0.64	± 0.54	± 0.88
PDF PDF4LHC13C1 egenvector 04 [%]	-	± 0.19	± 0.11	± 0.11	± 0.11	± 0.11	± 0.13
PDF PDF4LHC13C1 egenvector 06 [%]	-	± 0.20	± 0.32	± 0.40	± 0.42	± 0.42	± 0.74
PDF PDF4LHC13C1 egenvector 08 [%]	± 1.96	± 2.16	± 2.26	± 2.34	± 2.41	± 2.54	± 2.77
PDF PDF4LHC13C1 egenvector 09 [%]	-	± 0.26	± 0.44	± 0.51	± 0.55	± 0.59	± 0.73
PDF PDF4LHC13C1 egenvector 10 [%]	± 0.31	± 0.34	± 0.36	± 0.38	± 0.39	± 0.41	± 0.37
PDF PDF4LHC13C1 egenvector 11 [%]	± 0.11	± 0.19	± 0.23	± 0.23	± 0.23	± 0.23	± 0.35
PDF PDF4LHC13C1 egenvector 12 [%]	± 0.23	± 0.33	± 0.40	± 0.42	± 0.42	± 0.41	± 0.40
PDF PDF4LHC13C1 egenvector 13 [%]	± 0.28	± 0.29	± 0.31	± 0.33	± 0.29	± 0.25	± 0.10
PDF PDF4LHC13C1 egenvector 14 [%]	-	-	-	-	-	-	-
PDF PDF4LHC13C1 egenvector 15 [%]	± 0.31	± 0.14	-	-	-	-	-
PDF PDF4LHC13C1 egenvector 16 [%]	± 0.22	± 0.35	± 0.43	± 0.47	± 0.49	± 0.49	± 0.54
PDF PDF4LHC13C1 egenvector 17 [%]	-	± 0.11	-	± 0.10	± 0.13	± 0.14	± 0.18
PDF PDF4LHC13C1 egenvector 18 [%]	-	-	-	-	-	-	-
PDF PDF4LHC13C1 egenvector 19 [%]	± 0.53	± 0.74	± 0.85	± 0.89	± 0.88	± 0.88	± 0.64
PDF PDF4LHC13C1 egenvector 20 [%]	± 0.22	± 0.12	-	-	-	-	± 0.12
PDF PDF4LHC13C1 egenvector 21 [%]	± 0.68	± 0.77	± 0.85	± 0.92	± 1.01	± 1.10	± 1.48
PDF PDF4LHC13C1 egenvector 23 [%]	-	-	-	-	-	-	± 0.19
PDF PDF4LHC13C1 egenvector 25 [%]	-	-	-	-	-	-	-
PDF PDF4LHC13C1 egenvector 27 [%]	± 0.38	± 0.27	± 0.19	± 0.16	± 0.13	± 0.11	-
PDF PDF4LHC13C1 egenvector 28 [%]	± 0.20	± 0.10	-	-	-	± 0.12	± 0.30
PDF PDF4LHC13C1 egenvector 29 [%]	-	-	-	-	-	-	-
PDF PDF4LHC13C1 egenvector 30 [%]	-	-	-	-	-	-	-
LEP Electron energy resolution [%]	-	-	-	-	-	-	-
LEP Electron energy scale [%]	-	-	-	-	-	-	-
LEP Muon energy resolution [%]	-	-	-	-	-	-	-
LEP Muon energy scale [%]	-	-	-	-	-	-	-
LEP Muon sagittap [%]	-	-	-	-	-	-	-
LEP Muon sagittap resolution cuts [%]	-	-	-	-	-	-	-
METMPU E_T^{miss} Soft jet resolution peep [%]	-	-	-	-	-	-	-
METMPU E_T^{miss} Soft jet scale [%]	-	-	-	-	-	-	-
MetFitter b-Tagging [%]	± 2.00	± 2.05	± 2.05	± 2.03	± 1.93	± 1.97	± 1.74
BKG (Single top W cross-section [%]	± 0.26	± 0.15	-	± 0.35	± 0.27	-	± 0.14
BKG (t-W cross-section [%]	-	-	-	-	-	-	-
BKG (t-Z cross-section [%]	-	-	-	-	-	-	-
BKG (Multi-jet background statistics [%]	± 1.41	± 2.11	± 3.30	± 3.38	± 3.86	± 4.76	± 8.38
(MOD) Multi-jet background statistics [%]	± 1.31	± 2.04	± 3.08	± 2.75	± 3.05	± 5.17	± 7.73
(MOD) Alternative hard-scattering model [%]	± 0.16	± 0.02	± 0.02	± 0.02	± 0.02	± 0.02	± 0.19
(MOD) Alternative parton-shower model [%]	± 0.09	± 0.10	± 0.16	± 0.14	± 0.10	± 0.13	± 0.25
(MOD) Alternative parton-shower model [%]	± 12.9	± 14.8	± 13.6	± 17.8	± 12.9	± 2.26	± 16.9

Table 55: The individual systematic uncertainties in the fiducial phase-space absolute differential cross-sections for the top quark-antiquark system out-of-plane momentum $|p_{\text{out}}^{t\bar{t}}|$, calculated as a percentage of the cross-section in each bin. Dashes are used when the estimated relative systematic uncertainty for that bin is below 0.1%.

Bins [GeV]	0-20	20-40	40-60	60-100	100-200	200-300	300-600
$\hat{t} \nu$ $d\sigma / d\hat{p}_{\text{jet}}^{\text{out}}$	$1.63 \cdot 10^{-3}$	$1.06 \cdot 10^{-2}$	$5.99 \cdot 10^{-3}$	$3.67 \cdot 10^{-3}$	$1.25 \cdot 10^{-2}$	$4.619 \cdot 10^{-3}$	$7.743 \cdot 10^{-3}$
Total Uncertainty [%]	± 6.42	± 6.78	± 5.97	± 10.7	± 10.1	± 23.6	± 27.0
Systematic [%]	± 4.10	± 5.5	± 5.84	± 7.7	± 7.7	± 17	± 17
JES b-Tagged jet energy scale [%]	-	-	-	-	-	-	-
(JES) Effective detector NP set 1 [%]	-	-	-	± 0.11	-	± 0.29	± 0.14
(JES) Effective detector NP set 2 [%]	-	-	-	-	-	-	-
(JES) Effective detector NP set 3 [%]	-	-	-	-	-	-	-
(JES) Effective detector NP set 4 [%]	-	-	-	-	-	-	-
(JES) Effective detector NP set 5 [%]	-	-	-	-	-	-	-
(JES) Effective detector NP set 6 [%]	-	-	-	-	-	-	-
(JES) Effective detector NP set 7 softFerm [%]	-	-	-	-	-	-	-
(JES) η intercalibration model [%]	-	-	-	-	-	-	-
(JES) Flavor composition star [%]	-	-	-	-	-	-	-
(JES) Flavor composition star [%]	-	-	-	-	-	± 0.23	± 0.40
(JES) Flavor response [%]	-	-	-	-	-	-	± 0.13
(JES) Flavor response [%]	-	-	-	-	-	-	± 0.29
(JES) Pile-up offset $N_{\text{V}}^{\text{eff}}$ [%]	-	-	-	-	-	-	± 0.26
(JES) Pile-up offset p_T [%]	-	-	-	-	-	-	-
(JES) Pile-up offset energy [%]	-	-	-	-	± 0.17	± 0.10	± 0.22
(JES) Punch-Through [%]	-	-	-	-	-	-	-
(LHERF) Scale of high- p_T [%]	-	-	-	-	-	-	-
(LHERF) Large- η jet Baseline p_T [%]	± 0.12	± 0.32	± 0.36	± 0.31	± 0.24	± 2.39	± 0.50
(LHERF) Large- η jet Baseline r_{had} [%]	± 0.77	± 0.21	± 0.73	± 0.3	± 1.58	± 2.17	± 1.27
(LHERF) Large- η jet Baseline r_{jet} [%]	± 0.51	± 0.09	± 0.50	± 0.20	± 0.20	± 0.07	± 0.07
(LHERF) Large- η jet Baseline r_{miss} [%]	± 0.41	± 0.20	± 0.40	± 0.11	± 0.32	± 0.12	± 0.79
(LHERF) Large- η jet Modeling p_T [%]	± 0.43	± 0.40	± 0.59	± 0.60	± 0.89	± 1.00	± 2.45
(LHERF) Large- η jet Modeling r_{had} [%]	± 0.65	± 0.21	± 0.51	± 0.16	± 1.01	± 1.4	± 2.7
(LHERF) Large- η jet Modeling r_{jet} [%]	± 0.65	± 0.06	± 0.34	± 0.47	± 0.45	± 2.19	± 0.73
(LHERF) Large- η jet Modeling r_{miss} [%]	± 0.61	± 0.57	± 0.50	± 0.11	± 0.98	± 0.11	± 2.07
(LHERF) Large- η jet Tracking p_T [%]	± 0.61	± 0.21	± 0.51	± 0.10	± 0.57	± 0.11	± 0.99
(LHERF) Large- η jet Tracking r_{had} [%]	-	-	-	-	-	-	-
(LHERF) Large- η jet TotalStar p_T [%]	-	-	-	-	-	± 0.18	± 0.14
(LHERF) Large- η jet TotalStar r_{had} [%]	-	-	-	-	-	± 0.11	± 0.05
(LHERF) Large- η jet top-quark mass resolution [%]	± 0.26	± 0.18	± 0.45	± 0.51	± 0.38	± 2.97	-
(PTAG) c-Quark tagging efficiency (egenvector 0) [%]	-	-	-	-	-	-	± 0.33
(PTAG) c-Quark tagging efficiency (egenvector 1) [%]	-	-	-	± 0.11	± 0.10	-	± 0.17
(PTAG) c-Quark tagging efficiency (egenvector 2) [%]	-	-	-	-	-	-	± 0.34
(PTAG) c-Quark tagging efficiency (egenvector 3) [%]	-	-	-	-	-	-	-
(PTAG) c-Quark tagging efficiency (egenvector 4) [%]	-	-	-	-	-	-	-
(PTAG) c-Quark tagging efficiency (egenvector 5) [%]	-	-	-	-	-	-	-
(PTAG) c-Quark tagging efficiency (egenvector 6) [%]	-	-	-	-	-	-	-
(PTAG) c-Quark tagging efficiency (egenvector 7) [%]	-	-	-	-	-	-	-
(PTAG) c-Quark tagging efficiency (egenvector 8) [%]	-	-	-	-	-	-	-
(PTAG) Light-jet tagging efficiency (egenvector 0) [%]	± 0.15	± 0.22	± 0.23	± 0.22	± 0.39	± 0.47	± 0.47
(PTAG) Light-jet tagging efficiency (egenvector 0) [%]	± 0.11	± 0.15	± 0.46	-	± 0.62	± 0.77	-
(PTAG) Light-jet tagging efficiency (egenvector 1) [%]	-	-	-	-	-	-	-
(PTAG) Light-jet tagging efficiency (egenvector 2) [%]	-	-	-	± 0.14	-	-	-
(PTAG) Light-jet tagging efficiency (egenvector 3) [%]	-	-	-	± 0.10	-	± 0.13	± 0.10
(PTAG) Light-jet tagging efficiency (egenvector 4) [%]	-	-	-	± 0.22	-	± 0.32	± 0.20
(PTAG) Light-jet tagging efficiency (egenvector 5) [%]	-	-	-	-	-	-	-
(PTAG) Light-jet tagging efficiency (egenvector 6) [%]	-	-	-	-	-	-	-
(PTAG) Light-jet tagging efficiency (egenvector 7) [%]	-	-	-	-	-	-	-
(PTAG) Light-jet tagging efficiency (egenvector 8) [%]	-	-	-	-	-	-	-
(PTAG) Light-jet tagging efficiency (egenvector 9) [%]	-	-	-	-	-	-	-
(PTAG) Light-jet tagging efficiency (egenvector 10) [%]	-	-	-	-	-	-	-
(PTAG) Light-jet tagging efficiency (egenvector 11) [%]	-	-	-	-	-	-	-
(PTAG) Light-jet tagging efficiency (egenvector 12) [%]	-	-	-	-	-	-	-
(PTAG) Light-jet tagging efficiency (egenvector 13) [%]	-	-	-	-	-	-	-
(PTAG) c-Quark tagging extrapolation [%]	-	-	-	± 0.13	-	-	± 0.15
(PTAG) c-Quark tagging extrapolation from c-Quark [%]	-	-	-	-	-	-	-
(PDF) PDF4LHC13C egevector 0 [%]	-	-	-	-	-	-	-
(PDF) PDF4LHC13C egevector 1 [%]	± 0.17	-	± 0.24	± 0.28	± 0.37	± 0.45	± 0.52
(PDF) PDF4LHC13C egevector 02 [%]	-	-	-	± 0.12	± 0.13	± 0.13	-
(PDF) PDF4LHC13C egevector 03 [%]	-	-	-	-	-	-	± 0.32
(PDF) PDF4LHC13C egevector 04 [%]	± 0.16	-	± 0.21	± 0.29	± 0.31	± 0.30	± 0.03
(PDF) PDF4LHC13C egevector 05 [%]	± 0.13	-	± 0.16	± 0.24	± 0.31	± 0.44	± 0.68
(PDF) PDF4LHC13C egevector 06 [%]	± 0.21	± 0.12	± 0.29	± 0.37	± 0.41	± 0.44	± 0.59
(PDF) PDF4LHC13C egevector 07 [%]	-	-	-	-	-	-	-
(PDF) PDF4LHC13C egevector 08 [%]	-	-	-	-	-	-	-
(PDF) PDF4LHC13C egevector 09 [%]	-	-	-	-	-	-	-
(PDF) PDF4LHC13C egevector 10 [%]	-	-	-	-	-	-	-
(PDF) PDF4LHC13C egevector 11 [%]	-	-	-	± 0.10	± 0.12	± 0.11	± 0.10
(PDF) PDF4LHC13C egevector 12 [%]	-	-	-	-	-	-	± 0.19
(PDF) PDF4LHC13C egevector 13 [%]	-	-	-	-	-	-	-
(PDF) PDF4LHC13C egevector 14 [%]	-	-	-	-	-	-	-
(PDF) PDF4LHC13C egevector 15 [%]	± 0.10	-	± 0.14	± 0.14	± 0.19	± 0.14	-
(PDF) PDF4LHC13C egevector 16 [%]	-	-	-	-	-	-	± 0.16
(PDF) PDF4LHC13C egevector 17 [%]	-	-	-	± 0.12	± 0.17	± 0.18	± 0.22
(PDF) PDF4LHC13C egevector 18 [%]	-	-	-	-	± 0.12	± 0.13	± 0.17
(PDF) PDF4LHC13C egevector 19 [%]	± 0.13	-	± 0.18	± 0.22	± 0.22	± 0.19	-
(PDF) PDF4LHC13C egevector 20 [%]	-	-	-	-	± 0.11	± 0.12	± 0.12
(PDF) PDF4LHC13C egevector 21 [%]	-	-	-	-	-	-	-
(PDF) PDF4LHC13C egevector 22 [%]	-	-	-	± 0.16	± 0.25	± 0.33	± 0.71
(PDF) PDF4LHC13C egevector 23 [%]	-	-	-	-	-	-	-
(PDF) PDF4LHC13C egevector 24 [%]	-	-	-	-	-	-	-
(PDF) PDF4LHC13C egevector 25 [%]	-	-	-	-	-	-	-
(PDF) PDF4LHC13C egevector 26 [%]	-	-	-	± 0.10	± 0.10	± 0.10	± 0.26
(PDF) PDF4LHC13C egevector 27 [%]	-	-	-	± 0.10	± 0.14	± 0.17	± 0.18
(PDF) PDF4LHC13C egevector 28 [%]	-	-	-	± 0.10	± 0.11	-	± 0.16
(PDF) PDF4LHC13C egevector 29 [%]	-	-	-	-	-	-	-
(PDF) PDF4LHC13C egevector 30 [%]	-	-	-	-	-	-	-
(LEP) Electron energy resolution [%]	-	-	-	-	-	-	-
(LEP) Electron energy scale [%]	-	-	-	-	-	-	-
(LEP) Muon energy resolution [%]	-	-	-	-	-	-	-
(LEP) Muon momentum resolution [%]	-	-	-	-	-	-	-
(LEP) Muon resolution bias [%]	-	-	-	-	-	-	-
(LEP) Muon sagitta ρ [%]	-	-	-	-	-	-	-
(LEP) Muon transverse momentum ratio [%]	-	-	-	-	-	-	-
(METTF) E_T^{miss} Soft jet resolution peep [%]	-	-	-	-	-	-	-
(METTF) E_T^{miss} Soft jet scale [%]	-	-	-	-	-	-	-
(MetFitter) b-Tagging [%]	-	-	-	-	-	-	± 0.18
Luminosity [%]	-	-	-	-	-	-	± 0.25
(BKGR) Single top W cross-section [%]	-	-	-	-	-	-	-
(BKGR) Single top Z cross-section [%]	-	-	-	± 0.21	± 0.14	-	± 0.18
(BKGR) t-W cross-section [%]	-	-	-	-	-	-	-
(BKGR) t-Z cross-section [%]	-	-	-	-	-	-	-
(BKGR) Multi-jet background statistics [%]	± 1.41	± 2.11	± 3.30	± 3.38	± 3.86	± 4.76	± 8.37
(MOD) Multi-jet background statistics [%]	± 1.24	± 1.87	± 2.91	± 2.57	± 2.82	± 5.06	± 7.70
(MOD) Alternative hard-scattering model [%]	± 1.00	± 2.00	± 2.00	± 1.7	± 1.7	± 1.12	± 1.15
(MOD) Alternative parton-shower model [%]	± 2.69	± 0.24	± 1.25	± 2.17	± 0.67	± 2.38	± 15.6
(MOD) Alternative parton-shower model [%]	± 0.94	± 1.21	± 0.17	± 4.70	± 0.91	± 13.3	± 3.64

Not reviewed, for internal circulation only

Bins [Unit $\Delta\phi^{\ell\bar{t}}$]	0-2.50	2.50-2.75	2.75-3	3-3.14
$d\sigma / d\Delta\phi^{\ell\bar{t}}$ [pb/Unit $\Delta\phi^{\ell\bar{t}}$]	$2.844 \cdot 10^{-3}$	$6.634 \cdot 10^{-2}$	$2.506 \cdot 10^{-1}$	$1.430 \cdot 10^0$
Total Uncertainty [%]	± 32.6	± 31.1	± 27.4	± 24.2
Statistics [%]	$\pm 14.$	$\pm 10.$	± 5.7	± 2.9
Systematics [%]	± 27.8	± 28.3	± 26.5	± 24.0
(JES) b -Tagged jet energy scale [%]	-	-	-	-
(JES) Effective detector NP set 1 [%]	± 0.62	± 0.18	-	-
(JES) Effective detector NP set 2 [%]	± 0.10	-	-	-
(JES) Effective detector NP set 3 [%]	-	-	-	-
(JES) Effective detector NP set 4 [%]	-	-	-	-
(JES) Effective detector NP set 5 [%]	-	-	-	-
(JES) Effective detector NP set 6 [%]	-	-	-	-
(JES) Effective detector NP set 7 [%]	-	-	-	-
(JES) Effective detector NP set 8 restTerm [%]	-	-	-	-
(JES) η intercalibration model [%]	-	± 0.12	-	-
(JES) η intercalibration total stat [%]	-	-	-	-
(JES) Flavor composition [%]	± 0.05	± 0.18	± 0.17	± 0.22
(JES) Flavor response [%]	± 0.74	-	-	-
(JES) Pile-up offset μ [%]	± 0.49	± 0.14	-	-
(JES) Pile-up offset ρ [%]	-	-	-	-
(JES) Pile-up offset ρ_{jet} [%]	± 0.26	-	-	-
(JES) Pile-up offset $\rho_{\text{jet}}^{\text{top}}$ [%]	-	± 0.50	-	-
(JES) Pile-up offset ρ_{top} [%]	-	-	-	-
(JES) Punch-through [%]	-	-	-	-
(JES) Single particle high- pr_T [%]	-	-	-	-
(JES) Large- R jet Baseline mass [%]	± 0.19	± 0.61	± 0.24	± 0.33
(JES) Large- R jet Baseline pr_T [%]	± 5.06	± 4.33	± 2.81	± 1.90
(JES) Large- R jet Baseline τ_{12} [%]	± 1.3	± 6.00	± 7.67	± 7.80
(JES) Large- R jet Baseline mass [%]	± 0.29	± 1.20	± 0.49	± 0.58
(JES) Large- R jet Modelling pr_T [%]	± 2.17	± 0.62	± 2.30	± 2.13
(JES) Large- R jet Modelling τ_{12} [%]	± 9.36	± 11.0	± 9.96	± 9.83
(JES) Large- R jet Tracking ρ [%]	± 0.29	± 0.02	± 0.19	-
(JES) Large- R jet Tracking ρ_{τ} [%]	± 0.28	± 7.41	± 5.30	± 4.71
(JES) Large- R jet Tracking τ_{12} [%]	± 0.29	± 0.59	± 0.35	± 0.40
(JES) Large- R jet TotalStat mass [%]	± 0.17	± 0.59	-	-
(JES) Large- R jet TotalStat pr_T [%]	± 0.26	± 0.59	± 0.32	± 0.27
(JES) Large- R jet TotalStat τ_{12} [%]	± 0.34	± 0.49	± 0.32	± 0.15
(JES) Large- R jet top-quark mass resolution [%]	± 0.44	± 0.65	± 1.71	± 1.45
(FTAG) b -Quark tagging efficiency (eigenvector 0) [%]	± 4.94	± 5.28	± 5.33	± 5.29
(FTAG) b -Quark tagging efficiency (eigenvector 1) [%]	± 4.59	± 4.62	± 4.91	± 4.94
(FTAG) b -Quark tagging efficiency (eigenvector 2) [%]	± 0.57	± 0.60	± 0.69	± 0.79
(FTAG) b -Quark tagging efficiency (eigenvector 3) [%]	± 0.38	± 0.45	± 0.48	± 0.53
(FTAG) c -Quark tagging efficiency (eigenvector 4) [%]	± 0.18	± 0.20	± 0.23	± 0.14
(FTAG) c -Quark tagging efficiency (eigenvector 0) [%]	± 0.60	± 2.79	± 2.46	± 1.85
(FTAG) c -Quark tagging efficiency (eigenvector 1) [%]	± 1.92	± 1.62	± 1.77	± 1.09
(FTAG) c -Quark tagging efficiency (eigenvector 2) [%]	± 1.26	± 0.88	± 0.97	± 0.43
(FTAG) c -Quark tagging efficiency (eigenvector 3) [%]	± 0.75	± 0.81	± 0.65	± 0.34
(FTAG) Light-jet tagging efficiency (eigenvector 0) [%]	± 0.48	± 0.47	± 0.26	± 0.22
(FTAG) Light-jet tagging efficiency (eigenvector 1) [%]	-	-	-	-
(FTAG) Light-jet tagging efficiency (eigenvector 2) [%]	± 0.29	± 0.10	± 0.10	± 0.11
(FTAG) Light-jet tagging efficiency (eigenvector 3) [%]	± 0.18	± 0.20	-	-
(FTAG) Light-jet tagging efficiency (eigenvector 4) [%]	± 0.67	-	-	-
(FTAG) Light-jet tagging efficiency (eigenvector 5) [%]	± 0.15	-	-	-
(FTAG) Light-jet tagging efficiency (eigenvector 6) [%]	-	-	-	-
(FTAG) Light-jet tagging efficiency (eigenvector 7) [%]	± 0.20	-	-	-
(FTAG) Light-jet tagging efficiency (eigenvector 8) [%]	± 0.66	± 0.46	± 0.44	-
(FTAG) Light-jet tagging efficiency (eigenvector 9) [%]	± 0.31	± 0.49	± 0.46	-
(FTAG) Light-jet tagging efficiency (eigenvector 10) [%]	-	-	-	-
(FTAG) Light-jet tagging efficiency (eigenvector 11) [%]	-	-	-	-
(FTAG) Light-jet tagging efficiency (eigenvector 12) [%]	-	-	-	-
(FTAG) Light-jet tagging extrapolation [%]	± 2.48	± 2.58	± 2.88	± 3.10
(PDF) b -Quark tagging extrapolation from c -Quark [%]	-	-	-	-
(PDF) PDF4LHC15 eigenvector 01 [%]	± 0.41	± 0.31	± 0.28	± 0.10
(PDF) PDF4LHC15 eigenvector 02 [%]	± 0.69	± 0.58	± 0.65	± 0.52
(PDF) PDF4LHC15 eigenvector 03 [%]	± 1.01	± 0.17	± 0.13	± 0.10
(PDF) PDF4LHC15 eigenvector 04 [%]	± 0.55	± 0.50	± 0.43	± 0.11
(PDF) PDF4LHC15 eigenvector 05 [%]	± 2.50	± 2.45	± 2.36	± 2.11
(PDF) PDF4LHC15 eigenvector 06 [%]	± 0.60	± 0.57	± 0.56	± 0.15
(PDF) PDF4LHC15 eigenvector 07 [%]	-	-	-	-
(PDF) PDF4LHC15 eigenvector 08 [%]	± 0.30	± 0.37	± 0.38	± 0.34
(PDF) PDF4LHC15 eigenvector 09 [%]	± 0.30	± 0.28	± 0.27	± 0.16
(PDF) PDF4LHC15 eigenvector 10 [%]	± 0.12	-	± 0.11	-
(PDF) PDF4LHC15 eigenvector 11 [%]	± 0.34	± 0.40	± 0.43	± 0.30
(PDF) PDF4LHC15 eigenvector 12 [%]	-	± 0.26	± 0.30	± 0.29
(PDF) PDF4LHC15 eigenvector 13 [%]	-	-	-	-
(PDF) PDF4LHC15 eigenvector 14 [%]	-	-	-	-
(PDF) PDF4LHC15 eigenvector 15 [%]	-	-	-	± 0.20
(PDF) PDF4LHC15 eigenvector 16 [%]	-	-	-	-
(PDF) PDF4LHC15 eigenvector 17 [%]	± 0.48	± 0.50	± 0.49	± 0.31
(PDF) PDF4LHC15 eigenvector 18 [%]	± 0.11	± 0.14	± 0.14	-
(PDF) PDF4LHC15 eigenvector 19 [%]	± 0.65	± 0.80	± 0.89	± 0.68
(PDF) PDF4LHC15 eigenvector 20 [%]	-	-	-	± 0.15
(PDF) PDF4LHC15 eigenvector 21 [%]	-	-	-	-
(PDF) PDF4LHC15 eigenvector 22 [%]	± 1.12	± 1.05	± 0.95	± 0.77
(PDF) PDF4LHC15 eigenvector 23 [%]	-	-	-	-
(PDF) PDF4LHC15 eigenvector 24 [%]	± 0.14	-	-	-
(PDF) PDF4LHC15 eigenvector 25 [%]	-	-	-	-
(PDF) PDF4LHC15 eigenvector 26 [%]	-	-	-	-
(PDF) PDF4LHC15 eigenvector 27 [%]	-	± 0.11	± 0.12	± 0.31
(PDF) PDF4LHC15 eigenvector 28 [%]	± 0.21	-	-	± 0.14
(PDF) PDF4LHC15 eigenvector 29 [%]	-	-	-	-
(PDF) PDF4LHC15 eigenvector 30 [%]	-	-	-	-
(LEP) Electron energy resolution [%]	-	-	-	-
(LEP) Electron energy scale [%]	-	-	-	-
(LEP) Electron energy scale [%]	-	-	-	-
(LEP) Muon (MD) momentum resolution [%]	-	-	-	-
(LEP) Muon (ID) momentum resolution [%]	-	-	-	-
(LEP) Muon sagitta resolution bias [%]	-	-	-	-
(LEP) Muon sagitta ρ [%]	-	-	-	-
(MET/PU) $E_{\text{miss}}^{\text{soft}}$ Soft jet resolution para [%]	-	-	-	-
(MET/PU) $E_{\text{miss}}^{\text{soft}}$ Soft jet resolution perp [%]	-	-	-	-
(MET/PU) Soft jet scale [%]	-	-	-	-
(MET/PU) Jet vertex tagging [%]	-	± 0.18	-	-
Luminosity [%]	± 1.88	± 1.89	± 2.00	± 2.02
(BKG) Single top Wt cross-section [%]	-	-	-	-
(BKG) Single top t -channel treatment [%]	± 0.20	-	± 0.27	± 0.21
(BKG) $t\bar{t}W$ cross-section [%]	-	-	-	-
(BKG) $t\bar{t}Z$ cross-section [%]	± 0.10	± 0.11	-	-
(BKG) $t\bar{t}H$ cross-section [%]	-	-	-	-
(BKG) Multijet background statistics [%]	± 5.74	± 5.49	± 2.74	± 1.00
(MOD) Monte Carlo sample statistics [%]	± 6.65	± 4.50	± 2.26	± 0.91
(MOD) ISR/FSR + scale [%]	± 4.35	± 2.55	± 0.19	± 1.38
(MOD) Alternative hard-scattering model [%]	± 16.5	± 20.8	± 10.9	± 10.9
(MOD) Alternative parton-shower model [%]	± 14.5	-	± 17.0	± 13.6

Table 57: The individual systematic uncertainties in the fiducial phase-space absolute differential cross-sections for the top quark-antiquark system aperture angle $\Delta\phi^{\ell\bar{t}}$, calculated as a percentage of the cross-section in each bin. Dashes are used when the estimated relative systematic uncertainty for that bin is below 0.1%.

Not reviewed, for internal circulation only

Bins [Unit $\Delta\phi^t$]	0-2.50	2.50-2.75	2.75-3	3-3.14
$1/\sigma \cdot d\sigma / d\Delta\phi^t$	$9.926 \cdot 10^{-3}$	$2.315 \cdot 10^{-1}$	$8.744 \cdot 10^{-1}$	$4.991 \cdot 10^0$
Total Uncertainty [%]	± 19.2	± 24.2	± 7.74	± 2.43
Statistics [%]	$\pm 14.$	$\pm 10.$	± 5.2	± 1.7
Systematics [%]	± 9.26	± 20.8	± 4.63	± 1.27
(JES) b -Tagged jet energy scale [%]	-	-	-	-
(JES) Effective detector NP set 1 [%]	± 0.56	± 0.12	-	-
(JES) Effective detector NP set 2 [%]	-	-	-	-
(JES) Effective detector NP set 3 [%]	-	-	-	-
(JES) Effective detector NP set 4 [%]	-	-	-	-
(JES) Effective detector NP set 5 [%]	-	-	-	-
(JES) Effective detector NP set 6 [%]	-	-	-	-
(JES) Effective detector NP set 7 [%]	-	-	-	-
(JES) Effective detector NP set 8 restTerm [%]	-	-	-	-
(JES) η intercalibration model [%]	-	-	-	-
(JES) η intercalibration total stat [%]	-	-	-	-
(JES) Flavor composition [%]	± 0.31	-	-	-
(JES) Flavor response [%]	± 0.38	± 0.20	± 0.20	-
(JES) Pile-up offset μ [%]	± 0.36	-	-	-
(JES) Pile-up offset ρ [%]	± 0.23	-	-	-
(JES) Pile-up offset ρ_T [%]	± 0.48	-	-	-
(JES) Pile-up offset $\rho_{T\gamma}$ [%]	-	-	-	-
(JES) Punch-through [%]	± 0.57	± 0.12	-	-
(JES) Single particle high- p_T [%]	-	-	-	-
(LJES) Large- R jet Baseline mass [%]	± 0.50	± 0.61	± 0.23	-
(LJES) Large- R jet Baseline p_T [%]	± 2.59	± 2.08	± 0.66	± 0.33
(LJES) Large- R jet Baseline τ_{12} [%]	± 1.20	± 1.58	± 0.72	± 0.20
(LJES) Large- R jet Tracking mass [%]	± 0.78	± 1.69	± 0.66	± 0.13
(LJES) Large- R jet Modelling p_T [%]	± 0.33	± 2.13	± 0.20	± 0.12
(LJES) Large- R jet Modelling τ_{12} [%]	± 1.99	± 1.82	± 0.70	± 0.14
(LJES) Large- R jet Tracking ρ_T [%]	± 0.53	± 0.09	± 0.27	-
(LJES) Large- R jet Tracking $\rho_{T\gamma}$ [%]	± 1.18	± 2.44	± 0.17	± 0.19
(LJES) Large- R jet Tracking τ_{12} [%]	± 0.13	± 0.18	± 0.52	± 0.29
(LJES) Large- R jet TotalStat mass [%]	± 0.11	± 0.52	-	-
(LJES) Large- R jet TotalStat p_T [%]	-	± 0.27	-	-
(LJES) Large- R jet TotalStat τ_{12} [%]	± 0.21	± 0.15	-	-
(LJES) Large- R jet top-quark mass resolution [%]	± 1.83	± 2.05	± 0.35	-
(FTAG) b -Quark tagging efficiency (eigenvector 0) [%]	± 0.34	-	-	-
(FTAG) b -Quark tagging efficiency (eigenvector 1) [%]	± 0.30	± 0.28	-	-
(FTAG) b -Quark tagging efficiency (eigenvector 2) [%]	± 0.18	± 0.14	-	-
(FTAG) b -Quark tagging efficiency (eigenvector 3) [%]	± 0.13	-	-	-
(FTAG) b -Quark tagging efficiency (eigenvector 4) [%]	-	-	-	-
(FTAG) b -Quark tagging efficiency (eigenvector 0) [%]	± 0.66	± 0.75	± 0.41	± 0.18
(FTAG) c -Quark tagging efficiency (eigenvector 1) [%]	± 0.55	± 0.45	± 0.60	± 0.22
(FTAG) c -Quark tagging efficiency (eigenvector 2) [%]	± 0.68	± 0.30	± 0.39	± 0.15
(FTAG) c -Quark tagging efficiency (eigenvector 3) [%]	± 0.46	± 0.37	± 0.21	-
(FTAG) Light-jet tagging efficiency (eigenvector 0) [%]	± 0.21	± 0.21	-	-
(FTAG) Light-jet tagging efficiency (eigenvector 1) [%]	-	-	-	-
(FTAG) Light-jet tagging efficiency (eigenvector 2) [%]	± 0.17	-	-	-
(FTAG) Light-jet tagging efficiency (eigenvector 3) [%]	-	± 0.11	-	-
(FTAG) Light-jet tagging efficiency (eigenvector 4) [%]	± 0.59	-	-	-
(FTAG) Light-jet tagging efficiency (eigenvector 5) [%]	± 0.15	-	-	-
(FTAG) Light-jet tagging efficiency (eigenvector 6) [%]	± 0.11	-	-	-
(FTAG) Light-jet tagging efficiency (eigenvector 7) [%]	± 0.17	-	-	-
(FTAG) Light-jet tagging efficiency (eigenvector 8) [%]	± 0.41	± 0.21	± 0.19	-
(FTAG) Light-jet tagging efficiency (eigenvector 9) [%]	± 0.56	± 0.24	± 0.21	-
(FTAG) Light-jet tagging efficiency (eigenvector 10) [%]	-	-	-	-
(FTAG) Light-jet tagging efficiency (eigenvector 11) [%]	-	-	-	-
(FTAG) Light-jet tagging efficiency (eigenvector 12) [%]	-	-	-	-
(FTAG) Light-jet tagging efficiency (eigenvector 13) [%]	-	-	-	-
(FTAG) b -Quark tagging extrapolation [%]	± 0.54	± 0.43	± 0.13	-
(FTAG) b -Quark tagging extrapolation from c -Quark [%]	-	-	-	-
(PDF) PDF4LHC15 eigenvector 01 [%]	± 0.44	± 0.34	± 0.30	-
(PDF) PDF4LHC15 eigenvector 02 [%]	± 0.14	-	± 0.10	-
(PDF) PDF4LHC15 eigenvector 03 [%]	± 1.11	-	-	-
(PDF) PDF4LHC15 eigenvector 04 [%]	± 0.37	± 0.32	± 0.25	-
(PDF) PDF4LHC15 eigenvector 05 [%]	± 0.34	± 0.29	± 0.20	-
(PDF) PDF4LHC15 eigenvector 06 [%]	± 0.37	± 0.34	± 0.32	-
(PDF) PDF4LHC15 eigenvector 07 [%]	-	-	-	-
(PDF) PDF4LHC15 eigenvector 08 [%]	-	-	-	-
(PDF) PDF4LHC15 eigenvector 09 [%]	± 0.11	± 0.10	-	-
(PDF) PDF4LHC15 eigenvector 10 [%]	-	-	-	-
(PDF) PDF4LHC15 eigenvector 11 [%]	-	-	± 0.10	-
(PDF) PDF4LHC15 eigenvector 12 [%]	± 0.24	-	-	-
(PDF) PDF4LHC15 eigenvector 13 [%]	-	-	-	-
(PDF) PDF4LHC15 eigenvector 14 [%]	-	-	-	-
(PDF) PDF4LHC15 eigenvector 15 [%]	± 0.12	± 0.11	± 0.15	-
(PDF) PDF4LHC15 eigenvector 16 [%]	-	-	-	-
(PDF) PDF4LHC15 eigenvector 17 [%]	± 0.12	± 0.15	± 0.14	-
(PDF) PDF4LHC15 eigenvector 18 [%]	-	± 0.10	-	-
(PDF) PDF4LHC15 eigenvector 19 [%]	-	-	± 0.18	-
(PDF) PDF4LHC15 eigenvector 20 [%]	-	-	± 0.11	-
(PDF) PDF4LHC15 eigenvector 21 [%]	-	-	-	-
(PDF) PDF4LHC15 eigenvector 22 [%]	± 0.30	± 0.24	± 0.13	-
(PDF) PDF4LHC15 eigenvector 23 [%]	-	-	-	-
(PDF) PDF4LHC15 eigenvector 24 [%]	-	± 0.20	± 0.10	-
(PDF) PDF4LHC15 eigenvector 25 [%]	-	-	-	-
(PDF) PDF4LHC15 eigenvector 26 [%]	-	-	-	-
(PDF) PDF4LHC15 eigenvector 27 [%]	± 0.20	± 0.16	± 0.14	-
(PDF) PDF4LHC15 eigenvector 28 [%]	-	-	± 0.10	-
(PDF) PDF4LHC15 eigenvector 29 [%]	-	-	-	-
(PDF) PDF4LHC15 eigenvector 30 [%]	-	-	-	-
(LEP) Electron energy resolution [%]	-	-	-	-
(LEP) Electron energy scale [%]	-	-	-	-
(LEP) Electron energy scale [%]	-	-	-	-
(LEP) Muon (MD) momentum resolution [%]	-	-	-	-
(LEP) Muon (ID) momentum resolution [%]	-	-	-	-
(LEP) Muon sagitta resolution bias [%]	-	-	-	-
(LEP) Muon sagitta ρ [%]	-	-	-	-
(MET/PU) $E_{\text{miss}}^{\text{jet}}$ Soft jet resolution para [%]	-	-	-	-
(MET/PU) $E_{\text{miss}}^{\text{jet}}$ Soft jet resolution perp [%]	-	± 0.30	-	-
(MET/PU) $E_{\text{miss}}^{\text{jet}}$ Soft jet scale [%]	-	-	-	-
(MET/PU) Jet vertex tagging [%]	-	-	-	-
Luminosity [%]	± 0.12	± 0.11	-	-
(BKG) Single top Wt cross-section [%]	-	-	-	-
(BKG) Single top t -channel treatment [%]	-	± 0.30	-	-
(BKG) $t + b^*$ cross-section [%]	-	-	-	-
(BKG) $t + Z$ cross-section [%]	-	-	-	-
(BKG) $t + H$ cross-section [%]	-	-	-	-
(BKG) Multijet background statistics [%]	± 5.65	± 5.40	± 2.70	± 0.98
(MOD) Monte Carlo sample statistics [%]	± 6.56	± 4.35	± 2.00	± 0.60
(MOD) ISR/FSR + scale [%]	± 5.13	± 3.31	± 0.94	± 0.66
(MOD) Alternative hard-scattering model [%]	± 5.68	± 10.5	± 0.69	± 0.67
(MOD) Alternative proton-shower model [%]	± 0.94	± 15.8	± 3.93	± 0.10

Table 58: The individual systematic uncertainties in the fiducial phase-space relative differential cross-sections for the top quark-antiquark system aperture angle $\Delta\phi^t$, calculated as a percentage of the cross-section in each bin. Dashes are used when the estimated relative systematic uncertainty for that bin is below 0.1%.

Not reviewed, for internal circulation only

Bins (GeV)	1000-1100	1100-1200	1200-1300	1300-1400	1400-1600	1600-1800	1800-2200
$d\sigma/dH_T^{\text{eff}} \text{ [pb/GeV]}$	$8.573 \cdot 10^{-3}$	$\pm 4.63 \cdot 10^{-3}$	$\pm 2.93 \cdot 10^{-3}$	$\pm 1.54 \cdot 10^{-3}$	$8.434 \cdot 10^{-3}$	$5.814 \cdot 10^{-3}$	$5.542 \cdot 10^{-3}$
Total Uncertainty [%]	± 26.9	± 27.2	± 26.6	± 29.1	± 26.9	± 24.1	± 9.2
Systematic [%]	± 4.6	± 4.0	± 3.5	± 3.6	± 3.6	± 2.7	± 2.9
JES b-Tagged jet energy scale [%]	-	-	-	-	-	± 0.17	-
(JES) Effective detector NP set 1 [%]	-	-	-	-	± 0.12	± 0.28	± 0.42
(JES) Effective detector NP set 2 [%]	-	-	-	-	± 0.25	-	± 0.40
(JES) Effective detector NP set 3 [%]	-	-	-	-	-	-	-
(JES) Effective detector NP set 4 [%]	-	-	-	-	-	-	-
(JES) Effective detector NP set 5 [%]	-	-	-	-	-	-	-
(JES) Effective detector NP set 6 [%]	-	-	-	-	-	-	-
(JES) Effective detector NP set 7 [%]	-	-	-	-	-	-	-
(JES) Effective detector NP set 8 [softFerm]	-	-	-	-	-	-	-
(JES) η intercalibration model [%]	-	-	-	-	-	-	-
(JES) Flavor composition star [%]	-	-	-	-	-	-	-
(JES) Flavor composition star [%]	± 0.32	± 0.31	± 0.36	-	± 0.17	± 0.29	± 0.13
(JES) Flavor response [%]	± 0.18	± 0.18	± 0.18	-	-	± 0.11	± 0.15
(JES) Pile-up offset N_{PU} [%]	-	-	-	-	-	-	-
(JES) Pile-up offset p_T [%]	± 0.18	± 0.27	± 0.15	± 0.11	± 0.22	± 0.26	± 0.20
(JES) Punch-Through [%]	-	-	-	-	-	-	-
(JES) Single particle high- p_T [%]	-	-	-	-	-	-	-
(JES) Large- η jet baseline p_T [%]	± 0.15	± 0.40	± 0.41	± 0.29	± 0.13	-	± 3.83
(JES) Large- η jet baseline r_{jet} [%]	± 0.15	± 0.25	± 0.25	± 0.25	± 0.14	-	± 0.5
(JES) Large- η jet Baseline r_{jet} [%]	± 1.85	± 0.52	± 0.66	± 0.66	± 1.14	-	-
(JES) Large- η jet baseline r_{jet} [%]	± 7.12	± 0.07	± 0.87	± 0.08	± 12.1	± 3.53	± 17.5
(JES) Large- η jet Modeling p_T [%]	± 0.15	± 0.27	± 0.27	± 0.29	± 0.34	± 0.32	± 0.26
(JES) Large- η jet Modeling r_{jet} [%]	± 2.60	± 0.90	± 2.35	± 0.89	± 1.15	± 0.73	± 2.9
(JES) Large- η jet Tracking p_T [%]	± 0.31	± 0.15	± 0.17	± 0.15	± 0.11	± 0.11	± 0.05
(JES) Large- η jet Tracking p_T [%]	± 4.56	± 5.14	± 5.75	± 8.25	± 8.06	± 10.4	± 10.8
(JES) Large- η jet Tracking r_{jet} [%]	± 0.30	± 0.32	± 0.31	± 0.48	± 0.33	± 0.33	± 0.22
(JES) Large- η jet Tracking r_{jet} [%]	± 0.43	± 0.32	± 0.51	± 0.48	± 0.43	± 0.43	± 0.10
(JES) Large- η jet TotalStar p_T [%]	-	-	-	-	-	-	-
(JES) Large- η jet TotalStar r_{jet} [%]	± 0.13	± 0.20	± 0.20	± 0.21	± 0.11	± 0.11	± 0.11
(JES) Large- η jet top-quark mass resolution [%]	± 1.42	± 1.00	± 1.72	± 0.14	± 1.60	± 0.80	± 0.78
(FTAG) c-Quark tagging efficiency (egenvector 0) [%]	± 5.18	± 3.35	± 5.59	± 5.75	± 5.32	± 5.89	± 6.26
(FTAG) c-Quark tagging efficiency (egenvector 1) [%]	± 5.18	± 3.35	± 5.59	± 5.75	± 5.32	± 5.89	± 6.26
(FTAG) c-Quark tagging efficiency (egenvector 2) [%]	± 0.70	± 0.80	± 0.96	± 1.10	± 1.02	± 1.27	± 1.35
(FTAG) c-Quark tagging efficiency (egenvector 3) [%]	± 0.46	± 0.56	± 0.71	± 0.78	± 0.77	± 1.14	± 1.27
(FTAG) c-Quark tagging efficiency (egenvector 4) [%]	± 0.31	± 0.41	± 0.51	± 0.51	± 0.51	± 0.71	± 0.71
(FTAG) c-Quark tagging efficiency (egenvector 0) [%]	± 2.19	± 2.40	± 1.53	± 1.48	± 2.26	± 1.73	± 1.91
(FTAG) c-Quark tagging efficiency (egenvector 1) [%]	± 1.40	± 1.46	± 0.90	± 0.90	± 1.52	± 1.04	± 0.95
(FTAG) c-Quark tagging efficiency (egenvector 2) [%]	± 0.42	± 0.35	± 0.50	± 0.40	± 0.43	± 0.43	± 0.15
(FTAG) Light-p jet tagging efficiency (egenvector 0) [%]	± 0.27	± 0.23	± 0.30	± 0.30	± 0.34	± 0.36	-
(FTAG) Light-p jet tagging efficiency (egenvector 1) [%]	± 0.11	± 0.10	± 0.14	± 0.16	-	± 0.15	± 0.44
(FTAG) Light-p jet tagging efficiency (egenvector 2) [%]	-	± 0.12	± 0.19	-	-	± 0.30	-
(FTAG) Light-p jet tagging efficiency (egenvector 3) [%]	-	-	± 0.12	-	-	± 0.13	± 0.27
(FTAG) Light-p jet tagging efficiency (egenvector 4) [%]	-	-	-	-	-	-	± 0.22
(FTAG) Light-p jet tagging efficiency (egenvector 5) [%]	-	-	-	-	-	-	± 0.19
(FTAG) Light-p jet tagging efficiency (egenvector 6) [%]	-	-	-	-	-	-	± 0.18
(FTAG) Light-p jet tagging efficiency (egenvector 7) [%]	± 0.19	-	-	-	-	-	± 0.20
(FTAG) Light-p jet tagging efficiency (egenvector 8) [%]	± 0.19	-	± 0.20	± 0.27	± 0.19	± 0.15	± 0.10
(FTAG) Light-p jet tagging efficiency (egenvector 9) [%]	± 0.11	-	± 0.18	± 0.27	± 0.13	± 0.15	-
(FTAG) Light-p jet tagging efficiency (egenvector 10) [%]	-	-	-	-	-	-	-
(FTAG) Light-p jet tagging efficiency (egenvector 11) [%]	-	-	-	-	-	-	-
(FTAG) Light-p jet tagging efficiency (egenvector 12) [%]	-	-	-	-	-	-	-
(FTAG) Light-p jet tagging efficiency (egenvector 13) [%]	-	-	-	-	-	-	-
(FTAG) c-Quark tagging extrapolation [%]	± 2.58	± 3.46	± 4.43	± 5.21	± 5.71	± 8.27	± 10.1
(FTAG) c-Quark tagging extrapolation from c-Quark [%]	-	-	-	-	-	-	-
(PDF) PDF4LHC15C c-Quark 0 [%]	-	-	± 0.13	± 0.14	± 0.31	± 0.53	± 0.76
(PDF) PDF4LHC15C c-Quark 1 [%]	± 0.52	± 0.63	± 0.58	± 0.68	± 0.74	± 0.77	± 0.77
(PDF) PDF4LHC15C c-Quark 2 [%]	± 0.52	± 0.62	± 0.55	± 0.66	± 0.70	± 0.72	± 0.78
(PDF) PDF4LHC15C c-Quark 3 [%]	± 0.20	± 0.20	± 0.14	± 0.14	± 0.13	± 0.17	-
(PDF) PDF4LHC15C c-Quark 4 [%]	± 0.10	± 0.27	± 0.42	± 0.66	± 2.77	± 2.95	± 3.08
(PDF) PDF4LHC15C c-Quark 5 [%]	± 0.25	± 0.29	± 0.14	± 0.32	± 0.24	± 0.30	± 0.31
(PDF) PDF4LHC15C c-Quark 6 [%]	± 0.31	± 0.42	± 0.46	± 0.52	± 0.62	± 0.71	± 0.79
(PDF) PDF4LHC15C c-Quark 7 [%]	± 0.18	± 0.20	± 0.19	± 0.21	± 0.21	± 0.21	± 0.21
(PDF) PDF4LHC15C c-Quark 8 [%]	± 0.12	± 0.13	± 0.11	± 0.14	± 0.20	± 0.22	± 0.30
(PDF) PDF4LHC15C c-Quark 9 [%]	± 0.32	± 0.37	± 0.34	± 0.38	± 0.41	± 0.41	± 0.43
(PDF) PDF4LHC15C c-Quark 10 [%]	± 0.26	± 0.35	± 0.36	± 0.42	± 0.48	± 0.52	± 0.61
(PDF) PDF4LHC15C c-Quark 11 [%]	-	-	-	-	-	-	-
(PDF) PDF4LHC15C c-Quark 12 [%]	-	-	-	-	-	-	-
(PDF) PDF4LHC15C c-Quark 13 [%]	-	-	-	-	-	-	-
(PDF) PDF4LHC15C c-Quark 14 [%]	-	-	-	-	-	-	-
(PDF) PDF4LHC15C c-Quark 15 [%]	± 0.12	± 0.20	± 0.27	± 0.32	± 0.43	± 0.56	± 0.75
(PDF) PDF4LHC15C c-Quark 16 [%]	± 0.72	± 1.03	± 1.06	± 1.33	± 1.59	± 1.92	± 2.15
(PDF) PDF4LHC15C c-Quark 17 [%]	-	-	-	-	-	-	-
(PDF) PDF4LHC15C c-Quark 18 [%]	-	-	-	-	-	-	-
(PDF) PDF4LHC15C c-Quark 19 [%]	± 0.70	± 0.76	± 0.75	± 0.81	± 0.80	± 0.72	± 0.83
(PDF) PDF4LHC15C c-Quark 20 [%]	± 0.11	± 0.15	± 0.18	± 0.23	± 0.24	± 0.30	± 0.35
(PDF) PDF4LHC15C c-Quark 21 [%]	-	-	-	-	-	-	-
(PDF) PDF4LHC15C c-Quark 22 [%]	± 0.72	± 1.03	± 1.06	± 1.33	± 1.59	± 1.92	± 2.15
(PDF) PDF4LHC15C c-Quark 23 [%]	-	-	-	-	-	-	-
(PDF) PDF4LHC15C c-Quark 24 [%]	-	-	-	-	-	-	-
(PDF) PDF4LHC15C c-Quark 25 [%]	-	-	-	-	-	-	-
(PDF) PDF4LHC15C c-Quark 26 [%]	-	-	-	-	-	-	-
(PDF) PDF4LHC15C c-Quark 27 [%]	± 0.24	± 0.30	± 0.38	± 0.40	± 0.47	± 0.54	± 0.55
(PDF) PDF4LHC15C c-Quark 28 [%]	± 0.17	± 0.28	± 0.38	± 0.49	± 0.67	± 0.91	-
(PDF) PDF4LHC15C c-Quark 29 [%]	-	-	-	-	-	-	-
(PDF) PDF4LHC15C c-Quark 30 [%]	-	-	-	-	-	-	-
(LEP) Electron energy resolution [%]	-	-	-	-	-	-	-
(LEP) Electron energy scale [%]	-	-	-	-	-	-	-
(LEP) Muon energy scale [%]	-	-	-	-	-	-	-
(LEP) Muon energy resolution [%]	-	-	-	-	-	-	-
(LEP) Muon energy resolution (MS) momentum resolution [%]	-	-	-	-	-	-	-
(LEP) Muon energy resolution (ID) momentum resolution [%]	-	-	-	-	-	-	-
(LEP) Muon sagitta ρ [%]	-	-	-	-	-	-	-
(LEP) Muon sagitta ρ resolution [%]	-	-	-	-	-	-	-
(METTFU) E_T^{miss} Soft jet resolution peep [%]	-	-	-	-	-	-	-
(METTFU) E_T^{miss} Soft jet scale [%]	-	-	-	-	-	-	-
(BKG) Single top W cross-section [%]	± 2.04	± 1.99	± 2.06	± 2.00	± 1.88	± 2.00	± 1.83
(BKG) Single top Z cross-section [%]	-	-	-	-	-	-	-
(BKG) t+Z cross-section [%]	-	-	-	-	-	-	-
(BKG) t+W cross-section [%]	-	-	-	-	-	-	-
(BKG) Multi-jet background statistics [%]	± 1.89	± 2.26	± 2.62	± 4.05	± 3.91	± 5.84	± 19.0
(MOD) Monte Carlo scale statistics [%]	± 1.51	± 2.14	± 2.70	± 4.22	± 3.36	± 6.30	± 12.6
(MOD) Alternative hard-scattering model [%]	± 2.20	± 1.81	± 2.14	± 1.77	± 2.07	± 1.71	± 1.25
(MOD) Alternative parton-shower model [%]	± 1.22	± 1.40	± 1.90	± 2.22	± 1.66	± 0.67	± 13.8
(MOD) Alternative parton-shower model [%]	± 17.6	± 13.0	± 12.5	± 13.6	± 18.2	± 12.6	± 8.57

Bins (GeV)	1000-1100	1100-1200	1200-1300	1300-1400	1400-1600	1600-1800	1800-2200
$\nu_T \cdot d\nu/dT$	$4.133 \cdot 10^{-3}$	$2.219 \cdot 10^{-3}$	$1.424 \cdot 10^{-3}$	$7.439 \cdot 10^{-4}$	$4.066 \cdot 10^{-3}$	$2.803 \cdot 10^{-3}$	$2.672 \cdot 10^{-3}$
Total Uncertainty [%]	± 6.86	± 8.96	± 14.3	± 20.9	± 19.2	± 26.1	± 26.3
Systematic [%]	± 4.1	± 7.4	± 9.7	± 11.7	± 15.7	± 27.6	± 27.8
JES b-Tagged jet energy scale [%]	-	-	-	-	-	± 0.17	-
(JES) Effective detector NP set 1 [%]	-	-	-	-	-	± 0.19	± 0.30
(JES) Effective detector NP set 2 [%]	-	-	-	-	-	-	-
(JES) Effective detector NP set 3 [%]	-	-	-	-	-	-	-
(JES) Effective detector NP set 4 [%]	-	-	-	-	-	-	-
(JES) Effective detector NP set 5 [%]	-	-	-	-	-	-	-
(JES) Effective detector NP set 6 [%]	-	-	-	-	-	-	-
(JES) Effective detector NP set 8 softFerm [%]	-	-	-	-	-	-	-
(JES) η intercalibration model [%]	-	-	-	-	-	-	-
(JES) Flavor composition star [%]	-	-	± 0.14	± 0.11	± 0.11	± 0.28	± 0.13
(JES) Flavor response [%]	-	-	-	-	-	-	± 0.14
(JES) Pile-up offset N_{PU} [%]	-	-	-	-	-	± 0.19	± 0.25
(JES) Pile-up offset p_T [%]	-	-	-	-	-	-	± 0.21
(JES) Pile-up offset energy [%]	-	-	-	-	± 0.10	± 0.21	± 0.15
(JES) Punch-Through [%]	-	-	-	-	-	-	-
(JES) Single jet energy high- p_T [%]	-	-	-	-	-	-	-
(LHER) Large- η jet Baseline p_T [%]	± 0.13	± 0.11	± 0.12	± 0.1	± 0.15	± 0.29	± 0.14
(LHER) Large- η jet Baseline r_{jet} [%]	± 0.77	± 2.11	± 2.41	± 2.0	± 2.05	± 2.09	± 2.02
(LHER) Large- η jet Baseline r_{jet}^2 [%]	± 1.78	± 3.66	± 3.71	± 2.0	± 2.55	± 2.63	± 2.62
(LHER) Large- η jet Baseline r_{jet}^3 [%]	± 0.93	± 0.47	± 0.47	± 0.2	± 0.85	± 1.03	± 0.99
(LHER) Large- η jet Modeling p_T [%]	± 0.48	± 0.20	± 0.97	± 1.48	± 0.98	± 2.37	± 0.32
(LHER) Large- η jet Modeling r_{jet} [%]	± 2.53	± 2.1	± 2.2	± 1.85	± 2.15	± 5.72	± 2.12
(LHER) Large- η jet Modeling r_{jet}^2 [%]	± 4.46	± 3.37	± 3.32	± 1.6	± 4.21	± 8.23	± 3.23
(LHER) Large- η jet Modeling r_{jet}^3 [%]	± 0.26	± 0.11	± 0.11	± 0.0	± 0.23	± 0.29	± 0.26
(LHER) Large- η jet Tracking p_T [%]	-	-	-	-	-	-	-
(LHER) Large- η jet Tracking r_{jet} [%]	-	-	-	-	-	-	-
(LHER) Large- η jet Tracking r_{jet}^2 [%]	-	-	-	-	-	-	-
(LHER) Large- η jet Tracking r_{jet}^3 [%]	-	-	-	-	-	-	-
(LHER) Large- η jet top-quark mass resolution [%]	± 0.33	-	± 0.64	± 0.95	± 2.72	± 1.91	± 0.78
(PTAG) c-Quark tagging efficiency (egenvector 0) [%]	± 0.21	-	± 0.21	± 0.36	-	± 0.51	± 0.86
(PTAG) c-Quark tagging efficiency (egenvector 1) [%]	-	-	± 0.23	± 0.39	-	± 0.52	± 0.44
(PTAG) c-Quark tagging efficiency (egenvector 2) [%]	± 0.15	-	± 0.10	± 0.24	± 0.16	± 0.41	± 0.49
(PTAG) c-Quark tagging efficiency (egenvector 3) [%]	± 0.15	-	-	± 0.15	± 0.15	± 0.52	± 0.64
(PTAG) c-Quark tagging efficiency (egenvector 4) [%]	-	-	-	-	-	± 0.11	± 0.22
(PTAG) c-Quark tagging efficiency (egenvector 0) [%]	± 0.12	± 0.30	± 0.54	± 0.58	± 0.20	± 0.38	-
(PTAG) c-Quark tagging efficiency (egenvector 1) [%]	± 0.12	± 0.17	± 0.38	± 0.47	± 0.23	± 0.23	± 0.31
(PTAG) c-Quark tagging efficiency (egenvector 2) [%]	± 0.13	± 0.12	± 0.35	-	-	-	± 0.16
(PTAG) c-Quark tagging efficiency (egenvector 3) [%]	-	-	-	-	-	-	± 0.14
(PTAG) Light-jet tagging efficiency (egenvector 0) [%]	-	-	-	-	-	-	± 0.70
(PTAG) Light-jet tagging efficiency (egenvector 1) [%]	-	-	-	-	-	-	± 0.45
(PTAG) Light-jet tagging efficiency (egenvector 2) [%]	-	-	-	-	-	-	± 0.54
(PTAG) Light-jet tagging efficiency (egenvector 3) [%]	-	-	-	-	-	± 0.19	± 0.10
(PTAG) Light-jet tagging efficiency (egenvector 4) [%]	-	-	-	-	-	± 0.11	± 0.22
(PTAG) Light-jet tagging efficiency (egenvector 5) [%]	-	-	-	-	-	± 0.12	± 0.26
(PTAG) Light-jet tagging efficiency (egenvector 6) [%]	-	-	-	-	-	± 0.12	± 0.22
(PTAG) Light-jet tagging efficiency (egenvector 7) [%]	-	-	-	-	-	± 0.19	± 0.25
(PTAG) Light-jet tagging efficiency (egenvector 8) [%]	-	-	-	-	-	-	± 0.20
(PTAG) Light-jet tagging efficiency (egenvector 9) [%]	-	-	-	-	-	-	-
(PTAG) Light-jet tagging efficiency (egenvector 10) [%]	-	-	-	-	-	-	-
(PTAG) Light-jet tagging efficiency (egenvector 11) [%]	-	-	-	-	-	-	-
(PTAG) Light-jet tagging efficiency (egenvector 12) [%]	-	-	-	-	-	-	-
(PTAG) Light-jet tagging extrapolation [%]	± 1.33	± 0.44	± 0.52	± 1.30	± 1.81	± 4.35	± 6.20
(PTAG) c-Quark tagging extrapolation from c-Quark [%]	-	-	-	-	-	-	-
(PDF) PDF4LHC15C c-Quark 0 [%]	-	-	-	-	± 0.26	± 0.48	± 0.71
(PDF) PDF4LHC15C c-Quark 02 [%]	-	-	-	-	-	± 0.17	± 0.18
(PDF) PDF4LHC15C c-Quark 04 [%]	-	-	-	-	-	± 0.15	± 0.16
(PDF) PDF4LHC15C c-Quark 05 [%]	± 0.22	-	± 0.10	± 0.34	± 0.45	± 0.64	± 0.78
(PDF) PDF4LHC15C c-Quark 07 [%]	-	-	-	-	-	-	± 0.10
(PDF) PDF4LHC15C c-Quark 08 [%]	-	-	-	-	± 0.11	± 0.21	± 0.30
(PDF) PDF4LHC15C c-Quark 10 [%]	-	-	-	-	-	± 0.10	± 0.19
(PDF) PDF4LHC15C c-Quark 11 [%]	-	-	-	-	-	-	-
(PDF) PDF4LHC15C c-Quark 12 [%]	-	-	-	-	-	± 0.14	± 0.19
(PDF) PDF4LHC15C c-Quark 13 [%]	-	-	-	-	-	-	± 0.27
(PDF) PDF4LHC15C c-Quark 14 [%]	-	-	-	-	-	-	-
(PDF) PDF4LHC15C c-Quark 15 [%]	-	-	-	-	± 0.11	± 0.22	± 0.35
(PDF) PDF4LHC15C c-Quark 16 [%]	-	-	-	-	-	-	± 0.18
(PDF) PDF4LHC15C c-Quark 17 [%]	-	-	-	-	-	-	-
(PDF) PDF4LHC15C c-Quark 18 [%]	-	-	-	-	-	-	-
(PDF) PDF4LHC15C c-Quark 19 [%]	-	-	-	-	-	-	-
(PDF) PDF4LHC15C c-Quark 20 [%]	-	-	-	-	-	± 0.14	± 0.19
(PDF) PDF4LHC15C c-Quark 21 [%]	-	-	-	-	-	-	-
(PDF) PDF4LHC15C c-Quark 22 [%]	± 0.25	-	-	± 0.35	± 0.60	± 0.94	± 1.16
(PDF) PDF4LHC15C c-Quark 23 [%]	-	-	-	-	-	-	-
(PDF) PDF4LHC15C c-Quark 24 [%]	-	-	-	-	-	-	-
(PDF) PDF4LHC15C c-Quark 25 [%]	-	-	-	-	-	-	-
(PDF) PDF4LHC15C c-Quark 26 [%]	-	-	-	-	-	-	± 0.20
(PDF) PDF4LHC15C c-Quark 27 [%]	-	-	-	-	± 0.16	± 0.23	± 0.24
(PDF) PDF4LHC15C c-Quark 28 [%]	± 0.12	-	-	± 0.18	± 0.30	± 0.48	± 0.71
(PDF) PDF4LHC15C c-Quark 29 [%]	-	-	-	-	-	-	-
(PDF) PDF4LHC15C c-Quark 30 [%]	-	-	-	-	-	-	-
(LEP) Electron energy resolution [%]	-	-	-	-	± 0.37	-	-
(LEP) Electron energy scale [%]	-	-	-	-	± 0.37	-	± 0.15
(LEP) Muon (MS) momentum resolution [%]	-	-	-	-	-	-	-
(LEP) Muon energy resolution [%]	-	-	-	-	-	-	-
(LEP) Muon sagitt. ρ [%]	-	-	-	-	-	-	-
(LEP) Muon sagitt. ρ [ns]	-	-	-	-	-	-	-
(METTF) E_T^{miss} Soft jet resolution peep [%]	-	-	-	-	-	-	-
(METTF) E_T^{miss} Soft jet scale [%]	-	-	-	-	-	-	-
(MetF) Electron energy tagging [%]	-	-	-	-	-	-	-
Luminosity [%]	-	-	-	-	-	± 0.12	± 0.17
(BKG) Single top W cross-section [%]	-	-	-	-	-	-	± 0.24
(BKG) t-t cross-section [%]	-	-	-	-	-	-	-
(BKG) t-t background statistics [%]	± 1.74	± 2.09	± 2.42	± 3.74	± 3.61	± 5.39	± 17.5
(MOD) Monte-Carlo statistics [%]	± 1.28	± 2.01	± 2.59	± 4.00	± 3.31	± 6.20	± 12.4
(MOD) Alternative hard-scattering model [%]	± 1.07	± 2.27	± 2.43	± 2.91	± 2.09	± 3.0	± 1.19
(MOD) Alternative parton-showers model [%]	± 1.21	± 0.92	± 4.48	± 11.4	± 3.86	± 4.04	± 0.70
(MOD) Alternative parton-showers model [%]	± 2.88	± 2.45	± 3.13	± 1.79	± 3.58	± 2.94	± 7.79

Table 60: The individual systematic uncertainties in the fiducial phase-space relative differential cross-sections for the scalar sum of the top-quark and antiquark transverse momenta H_T^{tt} , calculated as a percentage of the cross-section in each bin. Dashes are used when the estimated relative systematic uncertainty for that bin is below 0.1%.

Run / Unit / Part	0-0.20	0.20-0.50	0.50-0.90	0.90-1.1	1.1-2.0	2.0-3.0	3.0-4.0
# of Events [Units]	10,000	10,000	10,000	10,000	10,000	10,000	10,000
Total Uncertainty [%]	+20.6	+23.4	+22.4	+27.3	+31.4	+28.9	+33.4
Statistics [%]	+4.3	+4.9	+6.0	+8.3	+8.8	+11.5	+16.0
Systematic [%]	+20.1	+22.8	+21.0	+25.6	+29.7	+24.8	+26.7
(HES) J-Lagged jet energy scale [%]	-	-	-	-	-	-	-
(HES) Effective detector NP = 1 [%]	-	-	-0.2	-	-	-	-
(HES) Effective detector NP = 2 [%]	-	-	-0.2	-	-	-	-
(HES) Effective detector NP = 3 [%]	-	-	-0.2	-	-	-	-
(HES) Effective detector NP = 4 [%]	-	-	-0.2	-	-	-	-
(HES) Effective detector NP = 5 [%]	-	-	-0.2	-	-	-	-
(HES) Effective detector NP = 6 [%]	-	-	-0.2	-	-	-	-
(HES) Effective detector NP = 7 [%]	-	-	-0.2	-	-	-	-
(HES) Effective detector NP = 8 [%]	-	-	-0.2	-	-	-	-
(HES) η intercalibration model [%]	-	-	-	-	-	+0.10	-
(HES) η intercalibration model stat [%]	+0.11	+0.12	+0.25	+0.28	+0.21	+0.11	-
(HES) Flavor response [%]	+0.12	-	-	-	-	+0.12	-
(HES) Pile-up offset Nvz [%]	-	-	-	-	-	-	-
(HES) Pile-up offset Nvz [%]	-	-	-	-	-	-	-
(HES) Pile-up offset p_T [%]	+0.25	+0.16	+0.18	+0.14	+0.18	+0.42	-
(HES) Pile-up offset p_T [%]	+0.25	+0.16	+0.18	+0.14	+0.18	+0.42	-
(HES) Punch-through [%]	-	-	-	-	-	-	-
(HES) Single particle high p_T [%]	+0.18	+0.25	+0.26	+0.24	+0.28	+0.20	-
(LHE) Light-jet baseline [%]	+2.15	+2.40	+1.91	+1.90	+2.15	+2.42	+2.50
(LHE) Light-jet baseline [%]	+7.58	+7.91	+7.52	+8.15	+7.85	+8.11	+6.80
(LHE) Light-jet baseline [%]	+19.4	+20.4	+19.6	+20.4	+19.4	+20.4	+19.4
(LHE) Light-jet Modelling pT [%]	+2.18	+2.27	+2.38	+2.18	+2.14	+2.34	+2.34
(LHE) Light-jet Modelling pT [%]	+59.66	+59.90	+59.52	+60.10	+59.33	+60.13	+10.3
(LHE) Light-jet Modelling η [%]	+0.03	+0.03	+0.03	+0.03	+0.03	+0.03	+0.03
(LHE) Light-jet Tracking x [%]	+2.64	+4.85	+5.41	+4.86	+5.68	+4.86	+6.89
(LHE) Light-jet Tracking x [%]	+0.40	+0.33	+0.39	+0.35	+0.34	+0.36	+0.36
(LHE) Light-jet TotalStat [%]	+0.12	+0.23	+0.45	+0.28	+0.12	+0.29	+0.49
(LHE) Light-jet TotalStat [%]	+0.12	+0.16	+0.15	+0.14	+0.14	+0.15	+0.15
(LHE) Light-jet TotalStat [%]	+0.12	+0.16	+0.15	+0.14	+0.14	+0.15	+0.15
(LHE) J-Lagged quark tagging efficiency (evgenie) [%]	+5.40	+5.30	+5.32	+5.27	+4.80	+5.15	+5.31
(FTAG) J-Lagged quark tagging efficiency (evgenie) [%]	+0.10	+0.09	+0.08	+0.08	+0.07	+0.07	+0.05
(FTAG) J-Lagged quark tagging efficiency (evgenie) [%]	+0.10	+0.09	+0.08	+0.08	+0.07	+0.07	+0.05
(FTAG) J-Lagged quark tagging efficiency (evgenie) [%]	+0.06	+0.05	+0.04	+0.04	+0.04	+0.04	+0.03
(FTAG) J-Lagged quark tagging efficiency (evgenie) [%]	+0.06	+0.05	+0.04	+0.04	+0.04	+0.04	+0.03
(FTAG) J-Lagged quark tagging efficiency (evgenie) [%]	+0.11	+0.10	+0.12	+0.12	+0.12	+0.12	+0.12
(FTAG) J-Lagged quark tagging efficiency (evgenie) [%]	+0.02	+0.02	+0.02	+0.02	+0.02	+0.02	+0.01
(FTAG) J-Lagged quark tagging efficiency (evgenie) [%]	+0.11	+1.50	+1.30	+1.31	+1.20	+1.76	+1.76
(FTAG) J-Lagged quark tagging efficiency (evgenie) [%]	+0.11	+1.50	+1.30	+1.31	+1.20	+1.76	+1.76
(FTAG) J-Lagged quark tagging efficiency (evgenie) [%]	+0.11	+0.41	+0.47	+0.47	+0.41	+0.51	+0.52
(FTAG) J-Lagged quark tagging efficiency (evgenie) [%]	+0.10	+0.15	+0.29	+0.39	+0.09	+0.09	+0.09
(FTAG) J-Lagged quark tagging efficiency (evgenie) [%]	+0.10	+0.15	+0.29	+0.39	+0.09	+0.09	+0.09
(FTAG) Light-jet efficiency (evgenie) [%]	+0.16	+0.16	+0.14	+0.19	+0.16	+0.16	+0.16
(FTAG) Light-jet efficiency (evgenie) [%]	+0.16	+0.16	+0.14	+0.19	+0.16	+0.16	+0.16
(FTAG) Light-jet efficiency (evgenie) [%]	+0.10	+0.11	+0.14	+0.14	+0.11	+0.11	+0.11
(FTAG) Light-jet efficiency (evgenie) [%]	+0.10	+0.11	+0.14	+0.14	+0.11	+0.11	+0.11
(FTAG) Light-jet efficiency (evgenie) [%]	+0.11	+0.11	+0.14	+0.14	+0.11	+0.11	+0.11
(FTAG) Light-jet efficiency (evgenie) [%]	+0.11	+0.11	+0.14	+0.14	+0.11	+0.11	+0.11
(FTAG) Light-jet efficiency (evgenie) [%]	+0.11	+0.11	+0.14	+0.14	+0.11	+0.11	+0.11
(FTAG) Light-jet extrapolation from e [%]	+3.21	+3.08	+3.08	+2.88	+2.55	+2.55	+2.48
(FTAG) Light-jet extrapolation from e [%]	+0.23	+0.13	+0.13	+0.16	+0.11	+0.18	+0.18
(PDF) PDF-LHC15C eigenvector 02 [%]	+0.33	+0.39	+0.55	+0.77	+1.12	+1.43	+1.67
(PDF) PDF-LHC15C eigenvector 03 [%]	+0.20	+0.11	+0.14	+0.14	+0.16	+0.26	+0.47
(PDF) PDF-LHC15C eigenvector 05 [%]	+2.17	+2.11	+2.07	+2.18	+2.35	+2.35	+3.02
(PDF) PDF-LHC15C eigenvector 07 [%]	-	-	+0.29	+0.64	+0.86	+1.25	+1.33
(PDF) PDF-LHC15C eigenvector 08 [%]	+0.12	+0.23	+0.43	+0.60	+0.72	+0.89	+1.49
(PDF) PDF-LHC15C eigenvector 09 [%]	+0.19	+0.18	+0.18	+0.23	+0.23	+0.27	+0.31
(PDF) PDF-LHC15C eigenvector 10 [%]	+0.19	+0.18	+0.18	+0.23	+0.23	+0.27	+0.31
(PDF) PDF-LHC15C eigenvector 11 [%]	+0.31	+0.29	+0.28	+0.35	+0.44	+0.44	+0.77
(PDF) PDF-LHC15C eigenvector 12 [%]	+0.28	+0.26	+0.26	+0.32	+0.32	+0.32	+0.53
(PDF) PDF-LHC15C eigenvector 13 [%]	-	-	-	+0.11	+0.15	+0.20	+0.20
(PDF) PDF-LHC15C eigenvector 14 [%]	-	-	-	-	-	+0.13	+0.13
(PDF) PDF-LHC15C eigenvector 15 [%]	+0.17	+0.15	+0.13	+0.11	+0.11	+0.15	+0.23
(PDF) PDF-LHC15C eigenvector 16 [%]	-	-	-	-	-	+0.11	+0.11
(PDF) PDF-LHC15C eigenvector 17 [%]	+0.34	+0.34	+0.34	+0.40	+0.43	+0.43	+0.57
(PDF) PDF-LHC15C eigenvector 18 [%]	+0.85	+0.94	+0.88	+0.69	+0.21	+0.47	+0.47
(PDF) PDF-LHC15C eigenvector 20 [%]	+0.13	+0.13	+0.25	+0.40	+0.55	+0.66	+0.72
(PDF) PDF-LHC15C eigenvector 21 [%]	+0.13	+0.13	+0.25	+0.40	+0.55	+0.66	+0.72
(PDF) PDF-LHC15C eigenvector 22 [%]	+0.28	+0.28	+0.17	+0.14	+0.14	+0.14	+0.14
(PDF) PDF-LHC15C eigenvector 23 [%]	-	-	-	-	-	+0.14	+0.14
(PDF) PDF-LHC15C eigenvector 24 [%]	+0.12	-	-	-	-	-	+0.14
(PDF) PDF-LHC15C eigenvector 25 [%]	-	-	-	-	-	-	+0.14
(PDF) PDF-LHC15C eigenvector 26 [%]	+0.11	+0.11	+0.14	+0.14	+0.14	+0.14	+0.14
(PDF) PDF-LHC15C eigenvector 27 [%]	+0.18	+0.22	+0.31	+0.36	+0.40	+0.40	+0.40
(PDF) PDF-LHC15C eigenvector 28 [%]	+0.40	+0.44	+0.44	+0.74	+0.87	+0.87	+0.87
(LEP) Electron energy resolution [%]	+1.00	+1.00	+1.00	+1.00	+1.00	+1.00	+1.00
(LEP) Electron energy scale [%]	+1.00	+1.00	+1.00	+1.00	+1.00	+1.00	+1.00
(LEP) Muon momentum resolution [%]	+1.00	+1.00	+1.00	+1.00	+1.00	+1.00	+1.00
(LEP) Muon momentum resolution [%]	+1.00	+1.00	+1.00	+1.00	+1.00	+1.00	+1.00
(LEP) Muon $\sin\theta$ resolution [%]	+1.00	+1.00	+1.00	+1.00	+1.00	+1.00	+1.00
(METPU) Soft jet resolution perc [%]	+1.00	+1.00	+1.00	+1.00	+1.00	+1.00	+1.00
(METPU) Soft jet resolution perc [%]	+1.00	+1.00	+1.00	+1.00	+1.00	+1.00	+1.00
(METPU) Soft jet scale [%]	+1.00	+1.00	+1.00	+1.00	+1.00	+1.00	+1.00
Luminosity [%]	+2.04	+2.00	+2.03	+1.96	+1.99	+1.96	+2.00
(BKG) Singlet top cross section [%]	+0.25	+0.13	+0.36	+0.33	+0.18	+0.16	-
(BKG) t-t Cross-section [%]	+0.25	+0.13	+0.36	+0.33	+0.18	+0.16	-
(BKG) t-t Z cross-section [%]	+0.25	+0.13	+0.33	+0.33	+0.17	+0.17	+0.10
(BKG) t-t Z cross-section [%]	+0.25	+0.13	+0.33	+0.33	+0.17	+0.17	+0.10
(MHD) Multi-scale hadronization [%]	+1.68	+1.91	+2.29	+3.16	+2.79	+2.43	+2.00
(MHD) Monte Carlo scale statistics [%]	+1.44	+1.57	+1.79	+2.68	+3.70	+3.59	+5.02
(MHD) Multi-scale hadronization [%]	+2.52	+2.11	+2.23	+2.37	+2.37	+2.37	+2.00
(MHD) Alternative hard-scattering model [%]	+3.12	+11.0	+6.00	+10.8	+15.6	+9.82	+1.00
(MHD) Alternative parton-shower model [%]	+15.2	+10.9	+11.2	+15.6	+18.3	+14.0	+1.00

Table 61: The individual systematic uncertainties in the fiducial phase-space absolute differential cross-sections for the top quark-antiquark system longitudinal boost y_B^{fit} , calculated as a percentage of the cross-section in each bin. Dashes are used when the estimated relative systematic uncertainty for that bin is below 0.1%.

Not reviewed, for internal circulation only

Bins 1 Unit ρ_B^L	0-0.30	0.30-0.60	0.60-0.80	0.80-1	1-1.20	1.20-1.40	1.40-2
$\frac{d\sigma}{dy} \text{ or } \frac{d\sigma}{dy_T}$	$1.045 \cdot 10^{-3}$	$9.174 \cdot 10^{-4}$	$7.331 \cdot 10^{-4}$	$5.582 \cdot 10^{-4}$	$4.236 \cdot 10^{-4}$	$1.017 \cdot 10^{-4}$	$5.753 \cdot 10^{-5}$
Total Uncertainty [%]	± 5.61	± 6.42	± 5.89	± 5.48	± 5.05	± 4.77	± 4.88
JES [14]	± 1.7	± 1.3	± 1.4	± 1.7	± 8.5	± 1.1	± 1.4
Systematics [%]	± 3.66	± 4.10	± 5.75	± 3.19	± 8.16	± 5.35	± 9.41
(JES) b-Tagged jet energy scale [%]	-	-	-	-	-	-	-
(JES) b-Tagged jet energy resolution [%]	-	-	-	-	-	-	± 0.14
(JES) Effective detector NF set 1 [%]	-	-	-	-	-	-	± 0.11
(JES) Effective detector NF set 2 [%]	-	-	-	-	-	-	-
(JES) Effective detector NF set 3 [%]	-	-	-	-	-	-	-
(JES) Effective detector NF set 4 [%]	-	-	-	-	-	-	-
(JES) Effective detector NF set 5 [%]	-	-	-	-	-	-	-
(JES) Effective detector NF set 6 [%]	-	-	-	-	-	-	-
(JES) Effective detector NF set 7 [%] <i>softFermi</i>	-	-	-	-	-	-	-
(JES) η intercalibration model [%]	-	-	-	-	-	-	± 0.11
(JES) Flavor composition [%]	-	-	-	-	-	-	± 0.13
(JES) Flavor response [%]	-	-	-	± 0.10	± 0.21	± 0.14	± 0.16
(JES) Pile-up offset N_{PU} [%]	-	-	-	-	-	-	-
(JES) Pile-up offset p_T [%]	-	-	-	-	-	-	-
(JES) Pile-up offset energy [%]	-	-	-	-	-	-	± 0.25
(JES) Punch-through [%]	-	-	-	-	-	-	-
(JES) Single particle high- p_T [%]	-	-	-	-	-	-	-
(LJES) Large- η Jet Baseline p_T [%]	± 0.9	-	± 0.29	± 0.54	± 0.31	± 0.97	± 1.17
(LJES) Large- η Jet Baseline r_{jet} [%]	± 0.15	± 0.37	± 0.30	± 0.37	± 0.70	± 0.53	± 0.45
(LJES) Large- η Jet Baseline r_{jet}^2 [%]	± 0.21	-	± 0.14	± 0.28	± 0.17	± 1.39	± 0.20
(LJES) Large- η Jet Baseline r_{jet}^3 [%]	± 0.21	± 0.26	± 0.14	± 0.25	± 0.15	± 1.00	-
(LJES) Large- η Jet Modelling p_T [%]	± 0.9	-	± 0.17	± 0.50	± 0.39	± 0.28	± 0.05
(LJES) Large- η Jet Modelling r_{jet} [%]	± 0.19	-	± 0.25	± 0.35	± 0.43	± 1.42	± 1.83
(LJES) Large- η Jet Modelling r_{jet}^2 [%]	± 0.19	-	± 0.25	± 0.32	± 0.30	± 0.37	± 0.37
(LJES) Large- η Jet Modelling r_{jet}^3 [%]	± 0.33	± 0.24	± 0.42	± 0.30	± 0.31	± 0.27	± 1.90
(LJES) Large- η Jet Tracking p_T [%]	-	-	-	± 0.16	± 0.10	-	± 0.03
(LJES) Large- η Jet Tracking r_{jet} [%]	-	-	-	-	-	-	± 0.14
(LJES) Large- η Jet TotalStar p_T [%]	-	-	± 0.10	-	-	± 0.16	-
(LJES) Large- η Jet TotalStar r_{jet} [%]	-	-	-	-	-	-	± 0.13
(LJES) Large- η Jet TotalStar resolution [%]	-	± 0.20	± 0.67	± 0.90	± 0.23	± 0.26	± 1.42
(PTAG) c-Quark tagging efficiency [%]	± 0.11	-	-	-	± 0.26	± 0.14	-
(PTAG) c-Quark tagging efficiency (egregor 0) [%]	± 0.12	-	-	-	-	-	-
(PTAG) c-Quark tagging efficiency (egregor 1) [%]	-	-	-	-	-	-	-
(PTAG) c-Quark tagging efficiency (egregor 2) [%]	-	-	-	-	-	-	-
(PTAG) c-Quark tagging efficiency (egregor 3) [%]	-	-	-	-	-	-	-
(PTAG) c-Quark tagging efficiency (egregor 4) [%]	-	-	-	-	-	-	-
(PTAG) c-Quark tagging efficiency (egregor 5) [%]	-	-	-	-	-	-	-
(PTAG) c-Quark tagging efficiency (egregor 6) [%]	-	-	-	-	-	-	-
(PTAG) c-Quark tagging efficiency (egregor 7) [%]	-	-	-	-	-	-	-
(PTAG) c-Quark tagging efficiency (egregor 8) [%]	-	-	-	-	-	-	-
(PTAG) c-Quark tagging efficiency (egregor 9) [%]	-	-	-	-	-	-	-
(PTAG) c-Quark tagging efficiency (egregor 10) [%]	-	-	-	-	-	-	-
(PTAG) c-Quark tagging efficiency (egregor 11) [%]	-	-	-	-	-	-	-
(PTAG) c-Quark tagging efficiency (egregor 12) [%]	-	-	-	-	-	-	-
(PTAG) c-Quark tagging efficiency (egregor 13) [%]	-	-	-	-	-	-	-
(PTAG) c-Quark tagging extrapolation [%]	± 0.19	-	-	-	± 0.13	± 0.46	± 0.34
(PTAG) c-Quark tagging extrapolation from c-Quark [%]	-	-	-	-	-	-	± 0.54
(PTD) PDF4LHC15 cgenegor 0 [%]	± 0.31	± 0.15	-	± 0.28	± 0.33	± 0.30	± 0.17
(PTD) PDF4LHC15 cgenegor 02 [%]	± 0.27	± 0.21	-	± 0.17	± 0.52	± 0.83	± 1.07
(PTD) PDF4LHC15 cgenegor 03 [%]	± 0.12	-	-	-	± 0.26	± 0.38	± 0.80
(PTD) PDF4LHC15 cgenegor 04 [%]	-	-	-	-	-	-	± 0.02
(PTD) PDF4LHC15 cgenegor 05 [%]	-	-	-	± 0.13	-	± 0.16	± 0.12
(PTD) PDF4LHC15 cgenegor 06 [%]	± 0.37	± 0.25	-	± 0.30	± 0.52	± 0.91	± 1.27
(PTD) PDF4LHC15 cgenegor 07 [%]	-	-	-	-	-	-	± 0.17
(PTD) PDF4LHC15 cgenegor 08 [%]	± 0.27	± 0.16	-	± 0.20	± 0.32	± 0.49	± 1.10
(PTD) PDF4LHC15 cgenegor 09 [%]	-	-	-	± 0.10	± 0.15	± 0.18	± 0.42
(PTD) PDF4LHC15 cgenegor 10 [%]	-	-	-	-	± 0.11	± 0.21	± 0.44
(PTD) PDF4LHC15 cgenegor 11 [%]	-	-	-	-	-	-	± 0.20
(PTD) PDF4LHC15 cgenegor 12 [%]	-	-	-	-	-	-	± 0.14
(PTD) PDF4LHC15 cgenegor 13 [%]	-	-	-	-	-	-	± 0.22
(PTD) PDF4LHC15 cgenegor 14 [%]	-	-	-	-	-	-	± 0.25
(PTD) PDF4LHC15 cgenegor 15 [%]	-	-	-	-	-	-	± 0.17
(PTD) PDF4LHC15 cgenegor 16 [%]	-	-	-	-	-	-	± 0.11
(PTD) PDF4LHC15 cgenegor 17 [%]	-	-	-	-	-	-	± 0.19
(PTD) PDF4LHC15 cgenegor 18 [%]	-	-	-	-	-	-	± 0.68
(PTD) PDF4LHC15 cgenegor 19 [%]	± 0.33	± 0.21	± 0.16	± 0.53	± 0.53	± 0.76	-
(PTD) PDF4LHC15 cgenegor 20 [%]	± 0.32	± 0.15	-	± 0.21	± 0.36	± 0.48	± 0.53
(PTD) PDF4LHC15 cgenegor 21 [%]	-	-	-	-	± 0.18	± 0.29	± 0.43
(PTD) PDF4LHC15 cgenegor 22 [%]	± 0.10	± 0.73	-	± 0.71	± 1.74	± 2.89	± 4.30
(PTD) PDF4LHC15 cgenegor 23 [%]	-	-	-	-	-	-	-
(PTD) PDF4LHC15 cgenegor 24 [%]	-	-	-	-	-	-	-
(PTD) PDF4LHC15 cgenegor 25 [%]	-	-	-	-	-	-	-
(PTD) PDF4LHC15 cgenegor 26 [%]	± 0.20	-	-	± 0.16	± 0.20	± 0.15	-
(PTD) PDF4LHC15 cgenegor 27 [%]	± 0.10	-	-	-	± 0.12	± 0.11	-
(PTD) PDF4LHC15 cgenegor 28 [%]	± 0.66	± 0.26	± 0.19	± 0.48	± 0.62	± 0.62	± 0.59
(PTD) PDF4LHC15 cgenegor 29 [%]	-	-	-	-	-	-	-
(PTD) PDF4LHC15 cgenegor 30 [%]	-	-	-	-	-	-	-
(LEP) Electron energy scale [%]	-	-	-	-	-	-	-
(LEP) Muon energy scale [%]	-	-	-	-	-	-	-
(LEP) Muon resolution bias [%]	-	-	-	-	-	-	-
(MET) Soft pT resolution bias [%]	-	-	-	-	-	-	-
(MET) Soft pT resolution para [%]	-	-	-	-	-	-	-
(MET) Soft pT resolution perp [%]	-	-	-	-	-	-	-
(MET) Soft pT resolution ratio [%]	-	-	-	-	-	-	-
(MET) Jet vertex tagging [%]	-	-	-	-	-	-	-
(BKG) Single top W cross-section [%]	-	-	-	-	-	-	-
(BKG) Single top r-channel treatment [%]	-	-	± 0.15	± 0.12	± 0.24	-	± 0.28
(BKG) In-t+H background statistics [%]	± 1.68	± 1.91	± 2.29	± 3.16	± 2.78	± 4.13	± 6.34
(MOD) NLO Cut-Cat. statistics [%]	± 1.22	± 1.37	± 2.24	± 2.51	± 3.60	± 3.54	± 5.00
(MOD) ISR/FSR + scale [%]	± 1.37	± 2.18	± 1.12	± 1.50	± 2.22	± 1.61	± 1.0
(MOD) Alternative hard-scattering model [%]	± 2.27	± 0.21	± 5.80	± 0.36	± 4.97	± 1.55	± 2.91
(MOD) Alternative parton-shower model [%]	± 1.76	± 1.19	± 2.91	± 2.22	± 2.27	± 0.34	± 3.96

Table 62: The individual systematic uncertainties in the fiducial phase-space relative differential cross-sections for the top quark-antiquark system longitudinal boost $y_B^{t\bar{t}}$ calculated as a percentage of the cross-section in each bin. Dashes are used when the estimated relative systematic uncertainty for that bin is below 0.1%.

Not reviewed, for internal circulation only

Bins [Unit τ^0]	1-1.50	1.50-2	2-3	3-4	4-5	5-7	7-10
$d\sigma/dp_T$ [pb/Unit τ^0]	$1.512 \cdot 10^{-3}$	$1.148 \cdot 10^{-3}$	$6.104 \cdot 10^{-4}$	$3.515 \cdot 10^{-4}$	$2.190 \cdot 10^{-4}$	$1.183 \cdot 10^{-4}$	$3.050 \cdot 10^{-5}$
Total Uncertainty [%]	± 25.8	± 23.9	± 27.5	± 24.7	± 25.4	± 26.8	± 29.1
Systematic [%]	± 4.8	± 5.5	± 5.2	± 5.7	± 5.9	± 4.5	± 4.6
JES b-Tagged jet energy scale [%]	-	-	-	-	-	-	-
(JES) b-Tagging efficiency [%]	-	-	-	-	-	-	-
(JES) Effective detector NP set 1 [%]	-	-	-	-	-	-	-
(JES) Effective detector NP set 2 [%]	-	-	-	-	-	-	-
(JES) Effective detector NP set 3 [%]	-	-	-	-	-	-	-
(JES) Effective detector NP set 4 [%]	-	-	-	-	-	-	-
(JES) Effective detector NP set 5 [%]	-	-	-	-	-	-	-
(JES) Effective detector NP set 6 [%]	-	-	-	-	-	-	-
(JES) Effective detector NP set 7 [%]	-	-	-	-	-	-	-
(JES) Effective detector NP set 8 [softFerm]	-	-	-	-	-	-	-
(JES) η intercalibration model [%]	-	-	-	-	-	-	-
(JES) η intercalibration scale [%]	-	-	-	-	-	-	-
(JES) Flavor composition [%]	± 0.21	± 0.26	± 0.26	-	± 0.26	± 0.33	± 0.30
(JES) Flavor response [%]	-	-	-	-	-	-	-
(JES) p_T scale [%]	-	-	-	-	-	-	-
(JES) Pile-up offset N_{Vtx} [%]	-	-	-	-	-	-	-
(JES) Pile-up offset p_T [%]	± 0.20	± 0.28	± 0.14	± 0.14	± 0.21	± 0.19	± 0.17
(JES) Punch-Through [%]	-	-	-	-	-	-	-
(LHER) Single jet energy at high- p_T [%]	-	-	-	-	-	-	-
(LHER) Single jet energy scale [%]	± 0.27	± 0.26	-	-	± 0.47	± 0.60	± 0.17
(LHER) Large- η jet Baseline p_T [%]	± 2.17	± 2.47	± 2.38	± 2.41	± 2.60	± 2.52	± 1.14
(LHER) Large- η jet Baseline r_{jet} [%]	± 7.64	± 9.06	± 7.87	± 7.93	± 7.91	± 8.27	± 2.25
(LHER) Large- η jet Baseline r_{miss} [%]	± 2.51	± 0.26					
(LHER) Large- η jet Modeling p_T [%]	± 19.39	± 19.66	± 1.32				
(LHER) Large- η jet Modeling r_{miss} [%]	± 2.01	± 2.00	± 0.20				
(LHER) Large- η jet Tracking p_T [%]	± 5.07	± 5.01	± 4.53	± 5.11	± 5.17	± 4.08	-
(LHER) Large- η jet Tracking r_{miss} [%]	± 0.22	± 0.57	± 0.32	± 0.29	± 0.46	± 0.35	± 0.19
(LHER) Large- η jet TotalStar p_T [%]	± 0.21	± 0.25	± 0.31	± 0.31	± 0.14	-	± 0.17
(LHER) Large- η jet top-quark mass resolution [%]	± 1.70	± 0.41	± 1.22	± 1.23	± 1.33	± 1.34	± 0.45
(FTAG) c-Quark tagging efficiency (eigenvector 0) [%]	± 5.38	± 5.22	± 5.20	± 5.23	± 5.14	± 5.49	± 5.25
(FTAG) c-Quark tagging efficiency (eigenvector 1) [%]	± 5.38	± 5.22	± 5.20	± 5.23	± 5.14	± 5.49	± 5.25
(FTAG) c-Quark tagging efficiency (eigenvector 2) [%]	± 0.78	± 0.73	± 0.72	± 0.73	± 0.72	± 0.81	± 0.71
(FTAG) c-Quark tagging efficiency (eigenvector 3) [%]	± 0.54	± 0.51	± 0.49	± 0.49	± 0.57	± 0.50	-
(FTAG) c-Quark tagging efficiency (eigenvector 4) [%]	± 0.54	± 0.51	± 0.52	± 0.52	± 0.57	± 0.54	± 0.24
(FTAG) c-Quark tagging efficiency (eigenvector 5) [%]	± 2.25	± 2.21	± 2.00	± 2.40	± 2.19	± 2.52	± 1.53
(FTAG) c-Quark tagging efficiency (eigenvector 6) [%]	± 1.40	± 1.50	± 1.19	± 1.50	± 1.65	± 1.02	-
(FTAG) c-Quark tagging efficiency (eigenvector 7) [%]	± 0.50	± 0.46	± 0.47	± 0.32	± 0.42	± 0.31	± 0.03
(FTAG) Light-jet tagging efficiency (eigenvector 0) [%]	± 0.15	± 0.50	± 0.21	± 0.20	± 0.44	± 0.31	-
(FTAG) Light-jet tagging efficiency (eigenvector 1) [%]	-	-	-	-	-	-	-
(FTAG) Light-jet tagging efficiency (eigenvector 2) [%]	± 0.10	± 0.18	-	-	-	± 0.16	± 0.16
(FTAG) Light-jet tagging efficiency (eigenvector 3) [%]	-	-	± 0.10	-	-	-	-
(FTAG) Light-jet tagging efficiency (eigenvector 4) [%]	-	-	± 0.17	-	-	± 0.27	-
(FTAG) Light-jet tagging efficiency (eigenvector 5) [%]	-	-	-	-	-	-	-
(FTAG) Light-jet tagging efficiency (eigenvector 6) [%]	-	-	-	-	-	-	-
(FTAG) Light-jet tagging efficiency (eigenvector 7) [%]	-	-	-	-	-	-	-
(FTAG) Light-jet tagging efficiency (eigenvector 8) [%]	± 0.27	± 0.31	-	± 0.30	± 0.24	± 0.15	± 0.21
(FTAG) Light-jet tagging efficiency (eigenvector 9) [%]	± 0.27	± 0.36	-	± 0.36	± 0.23	± 0.21	± 0.26
(FTAG) Light-jet tagging efficiency (eigenvector 10) [%]	-	-	-	-	-	-	-
(FTAG) Light-jet tagging efficiency (eigenvector 11) [%]	-	-	-	-	-	-	-
(FTAG) Light-jet tagging efficiency (eigenvector 12) [%]	-	-	-	-	-	-	-
(FTAG) Light-jet tagging efficiency (eigenvector 13) [%]	-	-	-	-	-	-	-
(FTAG) c-Quark tagging extrapolation [%]	± 3.15	± 3.04	± 2.99	± 2.84	± 2.81	± 2.22	± 2.79
(FTAG) c-Quark tagging extrapolation from c-Quark [%]	-	-	-	-	-	-	-
(PDF) PDF4LHC15 c-Quark 0 [%]	± 0.14	± 0.12	-	± 0.12	± 0.19	± 0.33	± 0.60
(PDF) PDF4LHC15 c-Quark 02 [%]	± 0.42	± 0.45	± 0.54	± 0.63	± 0.76	± 0.83	± 0.95
(PDF) PDF4LHC15 c-Quark 04 [%]	± 0.11	± 0.11	± 0.11	± 0.11	± 0.16	± 0.16	± 0.21
(PDF) PDF4LHC15 c-Quark 04 [%]	± 0.11	± 0.11	± 0.21	± 0.33	± 0.36	± 0.41	± 0.41
(PDF) PDF4LHC15 c-Quark 05 [%]	± 1.83	± 1.90	± 2.11	± 2.41	± 2.70	± 3.00	± 3.50
(PDF) PDF4LHC15 c-Quark 07 [%]	-	-	-	± 0.21	± 0.61	± 0.78	± 1.12
(PDF) PDF4LHC15 c-Quark 08 [%]	± 0.25	± 0.28	± 0.33	± 0.38	± 0.49	± 0.56	± 0.72
(PDF) PDF4LHC15 c-Quark 10 [%]	± 0.12	± 0.14	± 0.19	± 0.22	± 0.25	± 0.32	± 0.40
(PDF) PDF4LHC15 c-Quark 11 [%]	± 0.22	± 0.24	± 0.32	± 0.41	± 0.49	± 0.57	± 0.70
(PDF) PDF4LHC15 c-Quark 12 [%]	± 0.20	± 0.21	± 0.28	± 0.33	± 0.42	± 0.49	± 0.57
(PDF) PDF4LHC15 c-Quark 13 [%]	-	-	-	-	± 0.30	-	± 0.16
(PDF) PDF4LHC15 c-Quark 14 [%]	-	-	-	-	-	-	± 0.11
(PDF) PDF4LHC15 c-Quark 15 [%]	± 0.22	± 0.18	± 0.16	-	± 0.30	-	-
(PDF) PDF4LHC15 c-Quark 16 [%]	-	-	-	-	-	-	-
(PDF) PDF4LHC15 c-Quark 17 [%]	± 0.26	± 0.29	± 0.36	± 0.44	± 0.50	± 0.56	± 0.65
(PDF) PDF4LHC15 c-Quark 18 [%]	-	-	-	-	± 0.34	± 0.38	± 0.28
(PDF) PDF4LHC15 c-Quark 19 [%]	± 0.43	± 0.54	± 0.69	± 0.92	± 1.08	± 1.31	± 1.64
(PDF) PDF4LHC15 c-Quark 20 [%]	± 0.17	± 0.15	± 0.10	-	-	-	± 0.11
(PDF) PDF4LHC15 c-Quark 21 [%]	± 0.59	± 0.61	± 0.78	± 0.88	± 1.21	± 1.36	± 1.76
(PDF) PDF4LHC15 c-Quark 23 [%]	-	-	-	-	-	-	-
(PDF) PDF4LHC15 c-Quark 25 [%]	-	-	-	-	-	-	-
(PDF) PDF4LHC15 c-Quark 26 [%]	-	-	-	-	-	-	-
(PDF) PDF4LHC15 c-Quark 27 [%]	± 0.29	± 0.27	± 0.25	± 0.21	± 0.22	± 0.20	± 0.18
(PDF) PDF4LHC15 c-Quark 28 [%]	± 0.10	-	-	-	± 0.15	± 0.18	± 0.36
(PDF) PDF4LHC15 c-Quark 29 [%]	-	-	-	-	-	-	-
(PDF) PDF4LHC15 c-Quark 30 [%]	-	-	-	-	-	-	-
(LEP) Electron energy resolution [%]	-	-	-	-	-	-	-
(LEP) Electron energy scale [%]	-	-	-	-	-	-	-
(LEP) Muon (MS) momentum resolution [%]	-	-	-	-	-	-	-
(LEP) Muon energy resolution [%]	-	-	-	-	-	-	-
(LEP) Muon sagitt. ρ [%]	-	-	-	-	-	-	-
(LEP) Muon resolution cuts [%]	-	-	-	-	-	-	-
(METTFU) E_T^{miss} Soft jet resolution peep [%]	-	-	-	-	-	-	-
(MetFitter) E_T^{miss} Soft jet scale [%]	-	-	-	-	-	-	-
Luminosity [%]	± 1.99	± 2.01	± 1.96	± 2.03	± 1.97	± 2.08	± 1.93
(BKGR) Single top W cross-section [%]	± 0.20	± 0.23	± 0.12	± 0.13	± 0.39	± 0.42	-
(BKGR) t+Z cross-section [%]	-	-	-	-	-	-	-
(BKGR) Multi-jet background statistics [%]	± 1.78	± 2.01	± 2.03	± 2.42	± 4.70	± 3.23	± 6.88
(MOD) Monte Carlo scale statistics [%]	± 1.49	± 1.98	± 1.67	± 2.64	± 3.87	± 3.30	± 4.81
(MOD) Alternative background [%]	± 1.35	± 2.58	± 2.31	± 2.31	± 2.31	± 2.31	± 1.27
(MOD) Alternative hard-scattering model [%]	± 1.18	± 0.99	± 1.32	± 11.2	± 5.21	± 11.4	± 10.0
(MOD) Alternative parton-shower model [%]	± 14.7	± 11.1	± 16.5	± 12.1	± 13.7	± 12.9	± 11.3

Table 63: The individual systematic uncertainties in the fiducial phase-space absolute differential cross-sections for the top quark-antiquark system $\chi^{\prime\bar{t}}$, calculated as a percentage of the cross-section in each bin. Dashes are used when the estimated relative systematic uncertainty for that bin is below 0.1%.

Bins [Unit χ^2]	1-1.50	1.50-2	2-3	3-4	4-5	5-7	7-10
$\frac{d\sigma}{dt} \cdot \frac{d\sigma}{dp_T}$	$5.327 \cdot 10^{-3}$	$4.043 \cdot 10^{-3}$	$2.150 \cdot 10^{-3}$	$1.238 \cdot 10^{-3}$	$7.713 \cdot 10^{-4}$	$4.168 \cdot 10^{-4}$	$1.074 \cdot 10^{-4}$
Total Uncertainty [%]	± 5.00	± 6.84	± 8.96	± 9.66	± 10.88	± 10.8	± 18.9
(JES) Scale [%]	± 1.1	± 1.0	± 1.5	± 1.8	± 2.0	± 1.5	± 1.5
Systematic [%]	± 1.66	± 3.75	± 4.33	± 6.00	± 7.89	± 4.36	± 13
JES b-Tagged jet energy scale [%]	-	-	-	-	-	-	-
(JES) Effective detector NP set 1 [%]	-	-	-	-	-	-	-
(JES) Effective detector NP set 2 [%]	-	-	-	-	-	-	-
(JES) Effective detector NP set 3 [%]	-	-	-	-	-	-	-
(JES) Effective detector NP set 4 [%]	-	-	-	-	-	-	-
(JES) Effective detector NP set 5 [%]	-	-	-	-	-	-	-
(JES) Effective detector NP set 6 [%]	-	-	-	-	-	-	-
(JES) Effective detector NP set 7 [%] <small>softFerm</small>	-	-	-	-	-	-	-
(JES) η intercalibration model [%]	-	-	-	-	-	-	-
(JES) Flavor composition [%]	-	-	-	-	-	-	-
(JES) Flavor composition stat [%]	-	-	-	-	± 0.11	-	-
(JES) Flavor response [%]	-	-	-	-	-	± 0.19	-
(JES) Flavor response syst [%]	-	-	-	-	-	± 0.19	-
(JES) Pile-up offset N_{PU} [%]	-	-	-	-	-	-	-
(JES) Pile-up offset p_T [%]	-	-	-	-	-	-	-
(JES) Pile-up offset energy [%]	-	-	-	-	-	± 0.18	-
(JES) Punch-Through [%]	-	-	-	-	-	-	-
(JES) Single jet energy high- p_T [%]	-	-	-	-	-	-	-
(LHER) Large- η jet Baseline p_T [%]	± 0.24	-	± 0.28	± 0.72	± 0.39	± 0.29	± 0.70
(LHER) Large- η jet Baseline r_{jet} [%]	± 0.19	± 1.76	± 0.34	± 0.41	± 0.70	± 0.40	± 0.99
(LHER) Large- η jet Baseline r_{miss} [%]	-	-	-	± 0.79	± 0.63	± 0.60	± 0.61
(LHER) Large- η jet Baseline mass [%]	± 0.35	± 0.11	± 0.47	± 0.93	± 1.16	± 0.28	± 1.30
(LHER) Large- η jet Modeling p_T [%]	± 0.24	-	± 0.31	± 0.29	-	± 0.55	± 0.88
(LHER) Large- η jet Modeling r_{jet} [%]	± 0.17	-	± 0.40	± 0.83	± 0.50	± 0.20	± 1.59
(LHER) Large- η jet Modeling r_{miss} [%]	± 0.40	-	± 0.26	± 0.65	± 0.30	± 0.37	± 0.81
(LHER) Large- η jet Tracking p_T [%]	± 0.18	-	± 0.30	± 0.40	± 0.17	± 0.51	± 0.20
(LHER) Large- η jet Tracking r_{jet} [%]	± 0.16	-	± 0.30	± 0.40	± 0.16	± 0.51	± 0.21
(LHER) Large- η jet TotalStar p_T [%]	± 0.10	-	-	± 0.10	-	± 0.11	± 0.13
(LHER) Large- η jet TotalStar r_{jet} [%]	± 0.10	-	-	-	± 0.11	± 0.10	± 0.08
(LHER) Large- η jet top-quark mass resolution [%]	± 0.44	± 0.86	-	-	-	-	± 1.19
(PTAG) -Quark tagging efficiency (eigenvector 0) [%]	± 0.10	-	-	-	± 0.14	± 0.21	-
(PTAG) -Quark tagging efficiency (eigenvector 1) [%]	-	-	-	-	-	± 0.17	-
(PTAG) -Quark tagging efficiency (eigenvector 2) [%]	-	-	-	-	-	-	-
(PTAG) -Quark tagging efficiency (eigenvector 3) [%]	-	-	-	-	-	-	-
(PTAG) -Quark tagging efficiency (eigenvector 4) [%]	-	-	-	-	-	-	-
(PTAG) -Quark tagging efficiency (eigenvector 0) [%]	± 0.15	± 0.14	-	± 0.68	± 0.20	± 0.44	± 0.54
(PTAG) -Quark tagging efficiency (eigenvector 1) [%]	-	± 0.20	± 0.14	± 0.41	-	± 0.34	± 0.27
(PTAG) -Quark tagging efficiency (eigenvector 2) [%]	-	-	-	-	-	± 0.11	± 0.15
(PTAG) -Quark tagging efficiency (eigenvector 3) [%]	-	-	-	-	-	± 0.11	± 0.17
(PTAG) Light jet tagging efficiency (eigenvector 0) [%]	± 0.24	-	-	-	± 0.21	-	-
(PTAG) Light jet tagging efficiency (eigenvector 1) [%]	-	-	-	-	-	-	-
(PTAG) Light jet tagging efficiency (eigenvector 2) [%]	-	-	-	-	-	-	-
(PTAG) Light jet tagging efficiency (eigenvector 3) [%]	-	-	-	-	-	-	-
(PTAG) Light jet tagging efficiency (eigenvector 4) [%]	-	-	-	-	-	-	-
(PTAG) Light jet tagging efficiency (eigenvector 5) [%]	-	-	-	-	-	-	-
(PTAG) Light jet tagging efficiency (eigenvector 6) [%]	-	-	-	-	-	-	-
(PTAG) Light jet tagging efficiency (eigenvector 7) [%]	-	-	-	-	-	-	-
(PTAG) Light jet tagging efficiency (eigenvector 8) [%]	-	-	-	-	-	-	-
(PTAG) Light jet tagging efficiency (eigenvector 9) [%]	-	-	-	-	-	-	-
(PTAG) Light jet tagging efficiency (eigenvector 10) [%]	-	-	-	-	-	-	-
(PTAG) Light jet tagging efficiency (eigenvector 11) [%]	-	-	-	-	-	-	-
(PTAG) Light jet tagging efficiency (eigenvector 12) [%]	-	-	-	-	-	-	-
(PTAG) Light jet tagging efficiency (eigenvector 13) [%]	-	-	-	-	-	-	-
(PTAG) -Quark tagging extrapolation [%]	± 0.12	-	-	-	± 0.17	± 0.21	± 0.19
(PDF) PDF4LHC13s eigenvector 0 [%]	-	-	-	-	-	-	-
(PDF) PDF4LHC13s eigenvector 1 [%]	-	-	-	-	± 0.19	± 0.26	± 0.41
(PDF) PDF4LHC13s eigenvector 02 [%]	-	-	-	-	± 0.14	± 0.28	± 0.34
(PDF) PDF4LHC13s eigenvector 03 [%]	-	-	-	-	-	-	± 0.15
(PDF) PDF4LHC13s eigenvector 04 [%]	-	-	-	-	± 0.17	± 0.20	± 0.25
(PDF) PDF4LHC13s eigenvector 05 [%]	± 0.16	-	± 0.12	± 0.42	± 0.72	± 1.02	± 1.53
(PDF) PDF4LHC13s eigenvector 06 [%]	± 0.11	-	± 0.30	± 0.47	± 0.64	-	± 0.99
(PDF) PDF4LHC13s eigenvector 07 [%]	-	-	-	-	-	-	-
(PDF) PDF4LHC13s eigenvector 08 [%]	-	-	-	-	-	± 0.19	± 0.26
(PDF) PDF4LHC13s eigenvector 09 [%]	-	-	-	-	-	± 0.13	± 0.23
(PDF) PDF4LHC13s eigenvector 10 [%]	-	-	-	-	-	± 0.12	± 0.21
(PDF) PDF4LHC13s eigenvector 11 [%]	-	-	-	-	± 0.13	± 0.22	± 0.30
(PDF) PDF4LHC13s eigenvector 12 [%]	-	-	-	-	± 0.18	± 0.24	± 0.33
(PDF) PDF4LHC13s eigenvector 13 [%]	-	-	-	-	-	-	± 0.12
(PDF) PDF4LHC13s eigenvector 14 [%]	-	-	-	-	-	-	± 0.13
(PDF) PDF4LHC13s eigenvector 15 [%]	-	-	-	-	-	-	± 0.13
(PDF) PDF4LHC13s eigenvector 16 [%]	-	-	-	-	-	-	± 0.13
(PDF) PDF4LHC13s eigenvector 17 [%]	-	-	-	-	± 0.13	± 0.25	± 0.33
(PDF) PDF4LHC13s eigenvector 18 [%]	-	-	-	-	± 0.12	± 0.17	± 0.27
(PDF) PDF4LHC13s eigenvector 19 [%]	± 0.14	-	± 0.11	± 0.33	± 0.50	± 0.72	± 1.06
(PDF) PDF4LHC13s eigenvector 20 [%]	-	-	-	-	-	± 0.10	-
(PDF) PDF4LHC13s eigenvector 21 [%]	-	-	-	-	-	-	-
(PDF) PDF4LHC13s eigenvector 22 [%]	-	-	-	± 0.19	± 0.51	± 0.66	± 1.06
(PDF) PDF4LHC13s eigenvector 23 [%]	-	-	-	-	-	-	-
(PDF) PDF4LHC13s eigenvector 24 [%]	-	-	-	-	-	-	-
(PDF) PDF4LHC13s eigenvector 25 [%]	-	-	-	-	-	-	-
(PDF) PDF4LHC13s eigenvector 26 [%]	-	-	-	-	-	-	-
(PDF) PDF4LHC13s eigenvector 27 [%]	-	-	-	-	-	-	-
(PDF) PDF4LHC13s eigenvector 28 [%]	-	-	-	-	-	-	± 0.26
(PDF) PDF4LHC13s eigenvector 29 [%]	-	-	-	-	-	-	-
(PDF) PDF4LHC13s eigenvector 30 [%]	-	-	-	-	-	-	-
(LEP) Electron energy resolution [%]	-	-	-	-	-	-	-
(LEP) Muon energy scale [%]	-	-	-	-	-	-	-
(LEP) Muon (MS) momentum resolution [%]	-	-	-	-	-	-	-
(LEP) Muon rapidity resolution [%]	-	-	-	-	-	-	-
(LEP) Muon sagitta ρ [%]	-	-	-	-	-	-	-
(LEP) Muon transverse momentum resolution [%]	-	-	-	-	-	-	-
(METFPU) E_T^{miss} Soft jet resolution peep [%]	-	-	-	-	-	-	-
(METFPU) E_T^{miss} Soft jet scale [%]	-	-	-	-	-	-	-
(METFPU) E_T^{miss} Soft jet tagging [%]	-	-	-	-	-	-	-
Luminosity [%]	-	-	-	-	-	-	-
(BKG) Single top W cross-section [%]	-	-	-	-	-	-	-
(BKG) Double top W cross-section [%]	-	-	-	-	-	-	-
(BKG) n-W cross-section [%]	-	-	-	-	-	-	-
(BKG) n-Z cross-section [%]	-	-	-	-	-	-	-
(BKG) Multi-jet background [%]	± 1.78	-	± 2.01	± 2.03	± 2.42	± 4.70	± 3.23
(BKG) Multi-jet background statistics [%]	± 1.27	± 1.78	± 1.52	± 2.44	± 3.73	± 4.70	± 6.87
(MOD) Monte-Carlo statictics [%]	± 2.0	± 1.43	± 1.66	± 1.46	± 1.17	± 3.95	± 1.1
(MOD) Alternative hard-scattering model [%]	± 0.49	± 0.43	± 2.05	± 0.17	± 0.95	-	± 1.52
(MOD) Alternative parton-shower model [%]	± 1.03	± 3.12	± 3.06	± 1.97	± 0.10	± 1.02	± 2.88

Table 64: The individual systematic uncertainties in the fiducial phase-space relative differential cross-sections for the top quark-antiquark system $\chi^{\bar{t}t}$, calculated as a percentage of the cross-section in each bin. Dashes are used when the estimated relative systematic uncertainty for that bin is below 0.1%.

Bins [Unit $\cos\theta^*$]	0...0.20	0.20...0.40	0.40...0.60	0.60...0.70	0.70...0.80	0.80...1
$d\sigma / d\cos\theta^*$ [pb / Unit $\cos\theta^*$]	$3.983 \cdot 10^{-3}$	$4.017 \cdot 10^{-3}$	$3.668 \cdot 10^{-3}$	$3.250 \cdot 10^{-3}$	$1.719 \cdot 10^{-3}$	$3.876 \cdot 10^{-3}$
Total Uncertainty (%)	± 25.9	± 25.4	± 24.4	± 25.1	± 27.8	± 31.0
Stat. (%)	± 4.8	± 4.9	± 4.9	± 8.0	± 11	± 18
Systematics (%)	± 25.4	± 24.8	± 23.9	± 23.3	± 24.6	± 22.9
(JES) b-Tagged jet energy scale [%]	-	-	-	-	-	-
(JES) Effective detector NP set 1 [%]	-	-	-	-	-	-
(JES) Effective detector NP set 2 [%]	-	-	-	-	-	-
(JES) Effective detector NP set 3 [%]	-	-	-	-	-	-
(JES) Effective detector NP set 4 [%]	-	-	-	-	-	-
(JES) Effective detector NP set 5 [%]	-	-	-	-	-	-
(JES) Effective detector NP set 6 [%]	-	-	-	-	-	-
(JES) Effective detector NP set 7 [%]	-	-	-	-	-	-
(JES) Effective detector NP set 8 resTerm [%]	-	-	-	-	-	-
(JES) η intercalibration model [%]	-	-	-	-	-	-
(JES) η intercalibration total stat [%]	-	-	-	-	-	-
(JES) Flavor composition [%]	± 26	± 0.18	± 0.28	± 0.27	± 0.34	± 0.12
(JES) Flavor response [%]	-	-	-	± 0.18	-	-
(JES) Pile-up offset μ [%]	-	-	-	-	-	-
(JES) Pile-up offset ρ [%]	-	-	-	± 0.14	-	-
(JES) Pile-up offset τ [%]	-	-	-	-	-	-
(JES) Pile-up offset τ_2 [%]	-	-	-	-	-	-
(JES) Single particle high- p_T [%]	-	-	-	-	-	-
(JES) Large- R jet Baseline mass [%]	± 27	± 0.54	± 0.64	± 0.59	± 0.24	± 0.61
(JES) Large- R jet Baseline p_T [%]	± 7.7	± 2.42	± 2.73	± 2.35	± 1.72	± 2.75
(JES) Large- R jet Modeling mass [%]	± 7.70	± 0.38	± 0.23	± 0.01	± 0.01	± 0.35
(JES) Large- R jet Modeling p_T [%]	± 7.2	± 0.16	± 0.07	± 0.13	± 1.00	± 0.17
(JES) Large- R jet Tracking p_T [%]	± 7.2	± 2.44	± 2.25	± 1.82	± 1.96	± 2.04
(JES) Large- R jet Tracking τ_2 [%]	± 0.29	± 0.09	± 0.04	± 0.02	± 0.12	± 0.21
(JES) Large- R jet Tracking τ_2 [%]	± 0.29	± 0.09	± 0.04	± 0.02	± 0.12	± 0.21
(JES) Large- R jet Totalstat τ_2 [%]	± 0.29	± 0.09	± 0.07	± 0.02	± 0.12	± 0.20
(JES) Large- R jet Totalstat τ_2 [%]	± 0.29	± 0.20	± 0.14	± 0.02	± 0.12	± 0.17
(ITAG) Q+Quark tagging resolution [%]	± 0.17	-	-	-	-	-
(ITAG) Q+Quark tagging efficiency (eigencenter 0) [%]	± 3.9	± 5.28	± 3.12	± 2.25	± 3.42	± 3.31
(ITAG) Q+Quark tagging efficiency (eigencenter 1) [%]	± 4.97	± 4.89	± 4.79	± 4.95	± 4.95	± 4.87
(ITAG) Q+Quark tagging efficiency (eigencenter 2) [%]	± 0.78	± 0.74	± 0.70	± 0.84	± 0.72	± 0.72
(ITAG) Q+Quark tagging efficiency (eigencenter 3) [%]	± 0.54	± 0.48				
(ITAG) Q+Quark tagging efficiency (eigencenter 4) [%]	± 0.25	± 0.24	± 0.23	± 0.22	± 0.25	± 0.21
(ITAG) Q+Quark tagging efficiency (eigencenter 0) [%]	± 2.22	± 2.37	± 1.44	± 2.79	± 1.24	± 2.82
(ITAG) Q+Quark tagging efficiency (eigencenter 1) [%]	± 1.41	± 1.48	± 0.92	± 1.69	± 0.99	± 1.34
(ITAG) Q+Quark tagging efficiency (eigencenter 2) [%]	± 0.78	± 0.78	± 0.78	± 0.84	± 0.74	± 0.80
(ITAG) Q+Quark tagging efficiency (eigencenter 3) [%]	± 0.50	± 0.50	± 0.36	± 0.41	± 0.25	± 0.35
(ITAG) Light-jet tagging efficiency (eigencenter 0) [%]	± 0.32	± 0.19	± 0.24	± 0.27	± 0.21	± 0.30
(ITAG) Light-jet tagging efficiency (eigencenter 1) [%]	± 0.19	-	-	-	-	-
(ITAG) Light-jet tagging efficiency (eigencenter 2) [%]	± 0.15	± 0.11	-	± 0.11	± 0.13	± 0.18
(ITAG) Light-jet tagging efficiency (eigencenter 3) [%]	± 0.11	± 0.11	-	-	-	± 0.13
(ITAG) Light-jet tagging efficiency (eigencenter 4) [%]	± 0.12	-	-	± 0.20	-	-
(ITAG) Light-jet tagging efficiency (eigencenter 5) [%]	-	-	-	-	-	-
(ITAG) Light-jet tagging efficiency (eigencenter 6) [%]	-	-	-	-	-	-
(ITAG) Light-jet tagging efficiency (eigencenter 7) [%]	-	-	-	-	-	-
(ITAG) Light-jet tagging efficiency (eigencenter 8) [%]	± 0.22	± 0.22	± 0.24	± 0.10	± 0.25	± 0.13
(ITAG) Light-jet tagging efficiency (eigencenter 9) [%]	± 0.30	± 0.22	± 0.21	-	-	-
(ITAG) Light-jet tagging efficiency (eigencenter 10) [%]	-	-	± 0.21	-	± 0.24	-
(ITAG) Light-jet tagging efficiency (eigencenter 11) [%]	-	-	-	-	-	-
(ITAG) Light-jet tagging efficiency (eigencenter 12) [%]	-	-	-	-	-	-
(ITAG) Light-jet tagging efficiency (eigencenter 13) [%]	-	-	-	-	-	-
(ITAG) Q+Quark tagging extrapolation [%]	± 3.16	± 3.06	± 2.83	± 3.12	± 2.84	± 2.76
(ITAG) Q+Quark tagging extrapolation + Quark [%]	-	-	-	-	-	-
(PDF) PDF4LHC15 eigencenter 0 [%]	± 0.13	-	-	± 0.20	± 0.48	± 0.86
(PDF) PDF4LHC15 eigencenter 02 [%]	± 0.42	± 0.49	± 0.59	± 0.77	± 0.90	± 1.16
(PDF) PDF4LHC15 eigencenter 03 [%]	± 0.11	-	± 0.11	± 0.15	± 0.19	± 0.31
(PDF) PDF4LHC15 eigencenter 06 [%]	± 1.83	± 1.96	± 2.20	± 2.77	± 3.29	± 4.11
(PDF) PDF4LHC15 eigencenter 07 [%]	-	-	± 0.12	± 0.34	± 0.99	± 1.54
(PDF) PDF4LHC15 eigencenter 10 [%]	± 0.25	± 0.29	± 0.37	± 0.51	± 0.65	± 0.99
(PDF) PDF4LHC15 eigencenter 16 [%]	± 0.12	± 0.15	± 0.22	± 0.29	± 0.38	± 0.48
(PDF) PDF4LHC15 eigencenter 19 [%]	± 0.42	-	± 0.10	± 0.16	± 0.24	± 0.43
(PDF) PDF4LHC15 eigencenter 20 [%]	± 0.22	± 0.27	± 0.26	± 0.32	± 0.38	± 0.41
(PDF) PDF4LHC15 eigencenter 12 [%]	± 0.20	± 0.23	± 0.31	± 0.44	± 0.54	± 0.79
(PDF) PDF4LHC15 eigencenter 13 [%]	-	-	-	-	-	± 0.21
(PDF) PDF4LHC15 eigencenter 14 [%]	-	-	-	-	-	± 0.17
(PDF) PDF4LHC15 eigencenter 15 [%]	± 0.22	± 0.19	± 0.12	± 0.10	-	± 0.20
(PDF) PDF4LHC15 eigencenter 17 [%]	± 0.26	± 0.31	± 0.41	± 0.51	± 0.62	± 0.74
(PDF) PDF4LHC15 eigencenter 18 [%]	-	-	-	± 0.14	± 0.24	± 0.36
(PDF) PDF4LHC15 eigencenter 19 [%]	± 0.45	± 0.57	± 0.83	± 1.14	± 1.50	± 2.11
(PDF) PDF4LHC15 eigencenter 20 [%]	± 0.17	± 0.14	-	-	-	± 0.12
(PDF) PDF4LHC15 eigencenter 21 [%]	-	-	-	-	-	± 0.20
(PDF) PDF4LHC15 eigencenter 22 [%]	-	-	-	-	-	± 0.28
(PDF) PDF4LHC15 eigencenter 23 [%]	-	-	-	-	-	± 0.21
(PDF) PDF4LHC15 eigencenter 24 [%]	-	-	-	-	-	-
(PDF) PDF4LHC15 eigencenter 25 [%]	-	-	-	-	-	-
(PDF) PDF4LHC15 eigencenter 26 [%]	± 0.29	± 0.27	± 0.23	± 0.22	± 0.19	± 0.22
(PDF) PDF4LHC15 eigencenter 28 [%]	± 0.10	-	± 0.14	± 0.28	± 0.71	-
(PDF) PDF4LHC15 eigencenter 30 [%]	-	-	-	-	-	-
(PDF) PDF4LHC15 eigencenter 31 [%]	-	-	-	-	-	-
(PDF) PDF4LHC15 eigencenter 32 [%]	-	-	-	-	-	-
(PDF) PDF4LHC15 eigencenter 33 [%]	-	-	-	-	-	-
(PDF) PDF4LHC15 eigencenter 34 [%]	-	-	-	-	-	-
(PDF) PDF4LHC15 eigencenter 35 [%]	-	-	-	-	-	-
(PDF) PDF4LHC15 eigencenter 36 [%]	-	-	-	-	-	-
(PDF) PDF4LHC15 eigencenter 37 [%]	-	-	-	-	-	-
(PDF) PDF4LHC15 eigencenter 38 [%]	-	-	-	-	-	-
(PDF) PDF4LHC15 eigencenter 39 [%]	-	-	-	-	-	-
(PDF) PDF4LHC15 eigencenter 40 [%]	-	-	-	-	-	-
(PDF) PDF4LHC15 eigencenter 41 [%]	-	-	-	-	-	-
(PDF) PDF4LHC15 eigencenter 42 [%]	-	-	-	-	-	-
(PDF) PDF4LHC15 eigencenter 43 [%]	-	-	-	-	-	-
(PDF) PDF4LHC15 eigencenter 44 [%]	-	-	-	-	-	-
(PDF) PDF4LHC15 eigencenter 45 [%]	-	-	-	-	-	-
(PDF) PDF4LHC15 eigencenter 46 [%]	-	-	-	-	-	-
(PDF) PDF4LHC15 eigencenter 47 [%]	-	-	-	-	-	-
(PDF) PDF4LHC15 eigencenter 48 [%]	-	-	-	-	-	-
(PDF) PDF4LHC15 eigencenter 49 [%]	-	-	-	-	-	-
(PDF) PDF4LHC15 eigencenter 50 [%]	-	-	-	-	-	-
(PDF) PDF4LHC15 eigencenter 51 [%]	-	-	-	-	-	-
(PDF) PDF4LHC15 eigencenter 52 [%]	-	-	-	-	-	-
(PDF) PDF4LHC15 eigencenter 53 [%]	-	-	-	-	-	-
(PDF) PDF4LHC15 eigencenter 54 [%]	-	-	-	-	-	-
(PDF) PDF4LHC15 eigencenter 55 [%]	-	-	-	-	-	-
(PDF) PDF4LHC15 eigencenter 56 [%]	-	-	-	-	-	-
(PDF) PDF4LHC15 eigencenter 57 [%]	-	-	-	-	-	-
(PDF) PDF4LHC15 eigencenter 58 [%]	-	-	-	-	-	-
(PDF) PDF4LHC15 eigencenter 59 [%]	-	-	-	-	-	-
(PDF) PDF4LHC15 eigencenter 60 [%]	-	-	-	-	-	-
(PDF) PDF4LHC15 eigencenter 61 [%]	-	-	-	-	-	-
(PDF) PDF4LHC15 eigencenter 62 [%]	-	-	-	-	-	-
(PDF) PDF4LHC15 eigencenter 63 [%]	-	-	-	-	-	-
(PDF) PDF4LHC15 eigencenter 64 [%]	-	-	-	-	-	-
(PDF) PDF4LHC15 eigencenter 65 [%]	-	-	-	-	-	-
(PDF) PDF4LHC15 eigencenter 66 [%]	-	-	-	-	-	-
(PDF) PDF4LHC15 eigencenter 67 [%]	-	-	-	-	-	-
(PDF) PDF4LHC15 eigencenter 68 [%]	-	-	-	-	-	-
(PDF) PDF4LHC15 eigencenter 69 [%]	-	-	-	-	-	-
(PDF) PDF4LHC15 eigencenter 70 [%]	-	-	-	-	-	-
(PDF) PDF4LHC15 eigencenter 71 [%]	-	-	-	-	-	-
(PDF) PDF4LHC15 eigencenter 72 [%]	-	-	-	-	-	-
(PDF) PDF4LHC15 eigencenter 73 [%]	-	-	-	-	-	-
(PDF) PDF4LHC15 eigencenter 74 [%]	-	-	-	-	-	-
(PDF) PDF4LHC15 eigencenter 75 [%]	-	-	-	-	-	-
(PDF) PDF4LHC15 eigencenter 76 [%]	-	-	-	-	-	-
(PDF) PDF4LHC15 eigencenter 77 [%]	-	-	-	-	-	-
(PDF) PDF4LHC15 eigencenter 78 [%]	-	-	-	-	-	-
(PDF) PDF4LHC15 eigencenter 79 [%]	-	-	-	-	-	-
(PDF) PDF4LHC15 eigencenter 80 [%]	-	-	-	-	-	-
(PDF) PDF4LHC15 eigencenter 81 [%]	-	-	-	-	-	-
(PDF) PDF4LHC15 eigencenter 82 [%]	-	-	-	-	-	-
(PDF) PDF4LHC15 eigencenter 83 [%]	-	-	-	-	-	-
(PDF) PDF4LHC15 eigencenter 84 [%]	-	-	-	-	-	-
(PDF) PDF4LHC15 eigencenter 85 [%]	-	-	-	-	-	-
(PDF) PDF4LHC15 eigencenter 86 [%]	-	-	-	-	-	-
(PDF) PDF4LHC15 eigencenter 87 [%]	-	-	-	-	-	-
(PDF) PDF4LHC15 eigencenter 88 [%]	-	-	-	-	-	-
(PDF) PDF4LHC15 eigencenter 89 [%]	-	-	-	-	-	-
(PDF) PDF4LHC15 eigencenter 90 [%]	-	-	-	-	-	-
(PDF) PDF4LHC15 eigencenter 91 [%]	-	-	-	-	-	-
(PDF) PDF4LHC15 eigencenter 92 [%]	-	-	-	-	-	-
(PDF) PDF4LHC15 eigencenter 93 [%]	-	-	-	-	-	-
(PDF) PDF4LHC15 eigencenter 94 [%]	-	-	-	-	-	-
(PDF) PDF4LHC15 eigencenter 95 [%]	-	-	-	-	-	-
(PDF) PDF4LHC15 eigencenter 96 [%]	-	-	-	-		

Bins [Unit $\cos^2\theta^*$]	0-0.20	0.20-0.40	0.40-0.60	0.60-0.70	0.70-0.80	0.80-1
$1/\sigma \cdot d\sigma/d\cos^2\theta^*$	$1.370 \cdot 10^0$	$1.381 \cdot 10^0$	$1.261 \cdot 10^0$	$1.118 \cdot 10^0$	$5.910 \cdot 10^{-1}$	$1.333 \cdot 10^{-1}$
Total Uncertainty [%]	± 5.16	± 5.58	± 5.54	± 10.1	± 13.4	± 22.0
Statistics [%]	± 4.1	± 4.2	± 4.3	± 7.6	$\pm 11.$	$\pm 18.$
Syst. stat. [%]	± 2.10	± 2.70	± 3.46	± 4.75	± 4.59	± 8.11
(JES) b-Tagged jet energy scale [%]	-	-	-	± 0.11	-	± 0.14
(JES) Effective detector NP set 1 [%]	-	-	-	-	-	-
(JES) Effective detector NP set 2 [%]	-	-	-	-	-	-
(JES) Effective detector NP set 3 [%]	-	-	-	-	-	-
(JES) Effective detector NP set 4 [%]	-	-	-	-	-	-
(JES) Effective detector NP set 5 [%]	-	-	-	-	-	-
(JES) Effective detector NP set 6 [%]	-	-	-	-	-	-
(JES) Effective detector NP set 7 [%]	-	-	-	-	-	-
(JES) Effective detector NP set 8 [%]	-	-	-	-	-	-
(JES) η intercalibration model [%]	-	-	-	-	-	-
(JES) η intercalibration total stat [%]	-	-	-	-	-	-
(JES) η intercalibration total syst [%]	-	-	-	-	-	-
(JES) Flavor response [%]	-	-	-	± 0.14	-	-
(JES) Pile-up offset x [%]	-	-	-	-	-	-
(JES) Pile-up offset Ay [%]	-	-	-	± 0.13	-	± 0.12
(JES) Pile-up offset Az [%]	-	-	-	-	-	-
(JES) Pile-up offset topology [%]	-	-	-	± 0.13	-	-
(JES) Punch-through [%]	-	-	-	-	-	-
(JES) Single particle high p_T [%]	-	-	-	-	-	-
(JES) Large-R jet baseline p_T [%]	± 0.22	-	± 0.34	± 0.10	± 0.05	± 0.83
(JES) Large-R jet Baseline r_{23} [%]	± 0.16	± 0.14	± 0.14	± 0.43	± 0.67	± 0.67
(JES) Large-R jet Baseline r_{32} [%]	-	± 0.57	± 0.38	± 0.64	± 1.09	± 1.11
(JES) Large-R jet Modelling mass [%]	± 0.29	± 0.41	± 0.64	± 0.61	± 1.48	± 1.54
(JES) Large-R jet Modelling r_{23} [%]	± 0.19	± 0.22	± 0.20	± 0.35	± 0.69	± 0.70
(JES) Large-R jet Modelling r_{32} [%]	± 0.19	± 0.23	± 0.22	± 0.35	± 0.28	± 0.37
(JES) Large-R jet Tracking mass [%]	-	± 0.13	± 0.28	± 0.16	± 0.91	± 0.67
(JES) Large-R jet Tracking p_T [%]	-	-	-	-	-	-
(JES) Large-R jet TotalStat p_T [%]	-	-	-	± 0.12	-	± 0.30
(JES) Large-R jet TotalStat mass [%]	-	-	-	± 0.15	-	-
(JES) Large-R jet TotalStat p_T [%]	± 0.10	-	± 0.14	± 0.23	± 0.19	± 0.18
(JES) Large-R jet TotalStat r_{23} [%]	-	-	-	-	-	-
(JES) Large-R jet TotalStat r_{32} [%]	-	-	-	-	-	-
(PTAG) b-Quark tagging efficiency resolution [%]	± 0.23	± 0.23	± 0.48	± 0.37	± 0.57	± 2.14
(PTAG) b-Quark tagging efficiency (eigenvector 0) [%]	± 0.11	-	± 0.15	-	± 0.14	-
(PTAG) b-Quark tagging efficiency (eigenvector 1) [%]	-	-	± 0.11	-	-	-
(PTAG) b-Quark tagging efficiency (eigenvector 2) [%]	-	-	-	-	-	-
(PTAG) b-Quark tagging efficiency (eigenvector 3) [%]	-	-	-	-	-	-
(PTAG) b-Quark tagging efficiency (eigenvector 4) [%]	-	-	-	-	-	-
(PTAG) b-Quark tagging efficiency (eigenvector 5) [%]	-	-	-	-	-	-
(PTAG) b-Quark tagging efficiency (eigenvector 6) [%]	-	-	-	-	-	-
(PTAG) b-Quark tagging efficiency (eigenvector 7) [%]	-	-	-	-	-	-
(PTAG) b-Quark tagging efficiency (eigenvector 8) [%]	-	-	-	-	-	-
(PTAG) b-Quark tagging efficiency (eigenvector 9) [%]	-	-	-	-	-	-
(PTAG) b-Quark tagging efficiency (eigenvector 10) [%]	-	-	-	-	-	-
(PTAG) b-Quark tagging efficiency (eigenvector 11) [%]	-	-	-	-	-	-
(PTAG) b-Quark tagging efficiency (eigenvector 12) [%]	-	-	-	-	-	-
(PTAG) b-Quark tagging efficiency (eigenvector 13) [%]	-	-	-	-	-	-
(PTAG) b-Quark tagging extrapolation [%]	± 0.14	-	± 0.18	-	± 0.17	± 0.26
(PTAG) b-Quark tagging extrapolation from c-Quark [%]	-	-	-	-	-	-
(PDF) PDF4LHC15 eigenvector 01 [%]	± 0.21	± 0.18	-	± 0.12	± 0.40	± 0.78
(PDF) PDF4LHC15 eigenvector 02 [%]	± 0.18	± 0.12	-	± 0.16	± 0.29	± 0.55
(PDF) PDF4LHC15 eigenvector 03 [%]	-	-	-	-	-	± 0.20
(PDF) PDF4LHC15 eigenvector 04 [%]	± 0.10	-	-	± 0.13	± 0.19	-
(PDF) PDF4LHC15 eigenvector 05 [%]	± 0.54	± 0.40	-	± 0.42	± 0.95	± 1.79
(PDF) PDF4LHC15 eigenvector 06 [%]	± 0.34	± 0.26	-	± 0.24	± 0.61	± 1.17
(PDF) PDF4LHC15 eigenvector 07 [%]	-	-	-	-	-	-
(PDF) PDF4LHC15 eigenvector 08 [%]	± 0.15	± 0.11	-	± 0.10	± 0.24	± 0.59
(PDF) PDF4LHC15 eigenvector 09 [%]	-	-	-	-	± 0.15	± 0.26
(PDF) PDF4LHC15 eigenvector 10 [%]	-	-	-	-	± 0.12	± 0.31
(PDF) PDF4LHC15 eigenvector 11 [%]	± 0.16	± 0.11	-	± 0.13	± 0.26	± 0.49
(PDF) PDF4LHC15 eigenvector 12 [%]	± 0.13	± 0.10	-	± 0.10	± 0.20	± 0.45
(PDF) PDF4LHC15 eigenvector 13 [%]	-	-	-	-	-	± 0.15
(PDF) PDF4LHC15 eigenvector 14 [%]	-	-	-	-	-	± 0.15
(PDF) PDF4LHC15 eigenvector 15 [%]	-	-	-	-	± 0.14	± 0.18
(PDF) PDF4LHC15 eigenvector 16 [%]	-	-	-	-	-	± 0.15
(PDF) PDF4LHC15 eigenvector 17 [%]	± 0.13	-	-	± 0.11	± 0.21	± 0.34
(PDF) PDF4LHC15 eigenvector 18 [%]	-	-	-	-	± 0.16	± 0.28
(PDF) PDF4LHC15 eigenvector 19 [%]	± 0.40	± 0.28	-	± 0.29	± 0.65	± 1.27
(PDF) PDF4LHC15 eigenvector 20 [%]	-	-	-	-	-	-
(PDF) PDF4LHC15 eigenvector 21 [%]	-	-	-	-	-	± 0.13
(PDF) PDF4LHC15 eigenvector 22 [%]	± 0.36	± 0.29	± 0.10	± 0.24	± 0.62	± 1.50
(PDF) PDF4LHC15 eigenvector 23 [%]	-	-	-	-	-	-
(PDF) PDF4LHC15 eigenvector 24 [%]	-	-	-	-	-	-
(PDF) PDF4LHC15 eigenvector 25 [%]	-	-	-	-	-	-
(PDF) PDF4LHC15 eigenvector 26 [%]	-	-	-	-	-	± 0.16
(PDF) PDF4LHC15 eigenvector 27 [%]	-	-	-	-	-	-
(PDF) PDF4LHC15 eigenvector 28 [%]	-	-	-	-	± 0.12	± 0.55
(PDF) PDF4LHC15 eigenvector 29 [%]	-	-	-	-	-	-
(PDF) PDF4LHC15 eigenvector 30 [%]	-	-	-	-	-	-
(LED) Electron energy resolution [%]	-	-	-	-	-	-
(LED) Electron energy scale [%]	-	-	-	-	-	-
(LED) Muon energy scale [%]	-	-	-	-	-	-
(LED) Muon (MS) momentum resolution [%]	-	-	-	-	-	-
(LED) Muon (ID) momentum resolution [%]	-	-	-	-	-	-
(LED) Muon sagitta resolution bias [%]	-	-	-	-	-	-
(LED) Muon tagger resolution bias [%]	-	-	-	-	-	-
(MET/Pt) μ^{jet} Soft jet resolution pT [%]	-	-	-	-	-	-
(MET/Pt) μ^{jet} Soft jet resolution η [%]	-	-	-	-	-	-
(MET/Pt) μ^{jet} Soft jet scale [%]	-	-	-	-	-	-
(MET/Pt) μ^{jet} Soft vertex tagging [%]	-	-	-	-	-	-
Luminosity [%]	-	-	-	-	-	-
(BKG) Single top W cross-section [%]	-	-	-	-	-	-
(BKG) Single top $t\bar{t}$ cross-section treatment [%]	-	-	-	± 0.28	± 0.20	± 0.11
(BKG) t+Z cross-section [%]	-	-	-	-	-	-
(BKG) t+H cross-section [%]	-	-	-	-	-	-
(BKG) Multijet background statistics [%]	± 1.77	± 1.94	± 1.76	± 3.39	± 4.61	± 7.43
(MOD) SR/FSR + scale [%]	± 1.28	± 1.32	± 1.82	± 2.32	± 3.63	± 5.76
(MOD) SR/FSR [%]	± 0.29	± 1.78	± 2.50	± 2.61	± 2.54	± 0.64
(MOD) Alternative hard-scattering model [%]	± 0.57	± 0.99	± 0.35	± 3.05	± 0.10	± 4.29
(MOD) Alternative parton shower model [%]	± 1.37	± 1.23	± 0.35	± 0.49	± 0.10	± 4.54

Table 66: The individual systematic uncertainties in the fiducial phase-space relative differential cross-sections for the top quark-antiquark system $\cos \theta^*$, calculated as a percentage of the cross-section in each bin. Dashes are used when the estimated relative systematic uncertainty for that bin is below 0.1%.

951 **G. Parton-Level cross-sections and systematic uncertainties**

952 **G.1. Fractional uncertainties**

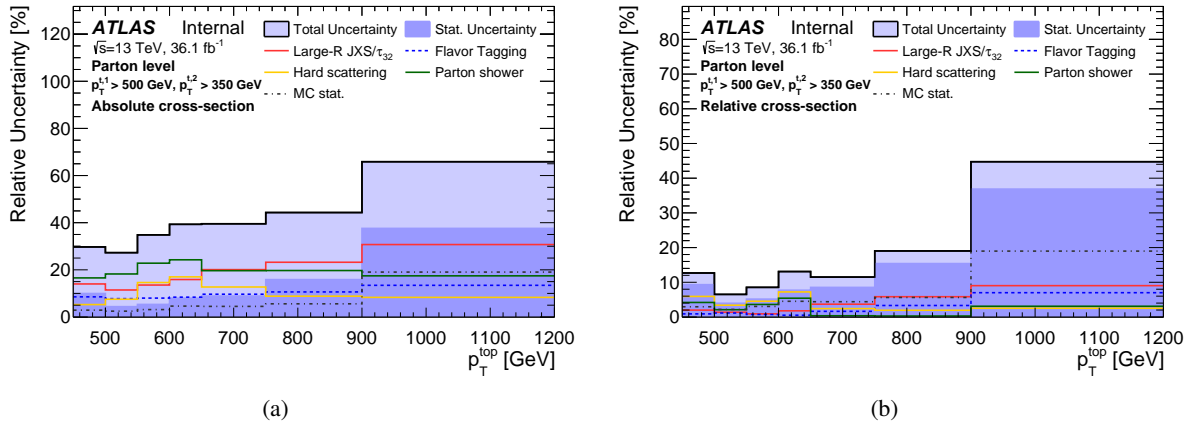


Figure 90: Fractional uncertainties of the absolute ((a)) and the relative ((b)) differential cross-sections as a function of the random top p_T in the parton level phase-space.

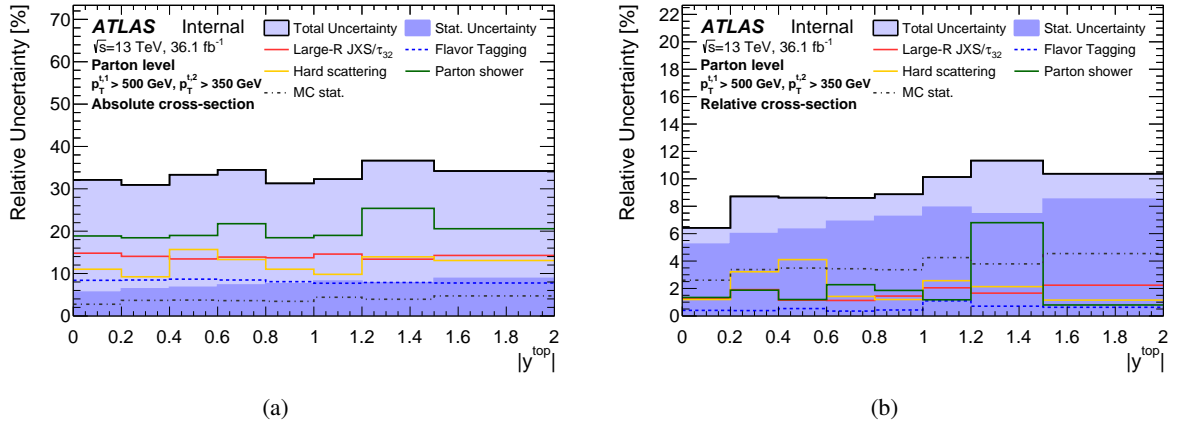


Figure 91: Fractional uncertainties of the absolute ((a)) and the relative ((b)) differential cross-sections as a function of the random top $|y|$ in the parton level phase-space.

Not reviewed, for internal circulation only

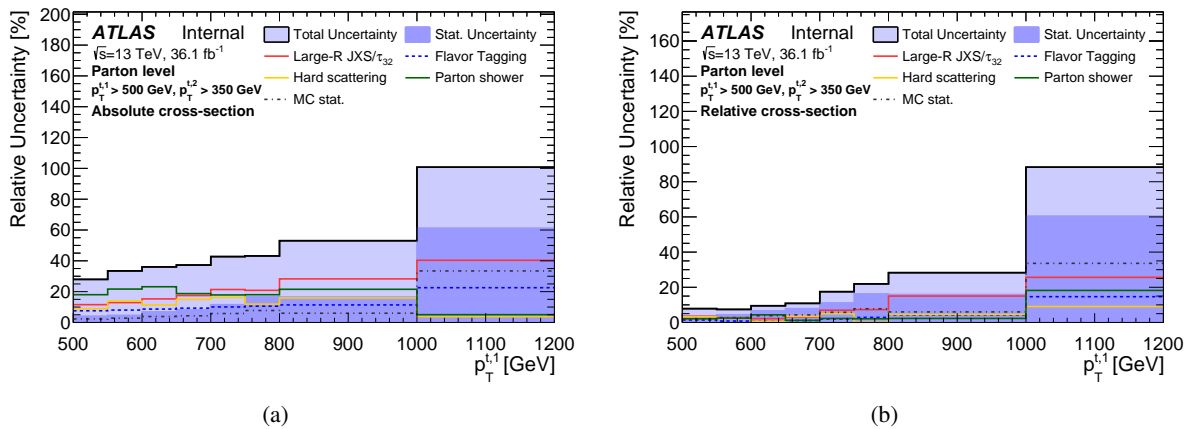


Figure 92: Fractional uncertainties of the absolute ((a)) and the relative ((b)) differential cross-sections as a function of the leading top p_T in the parton level phase-space.

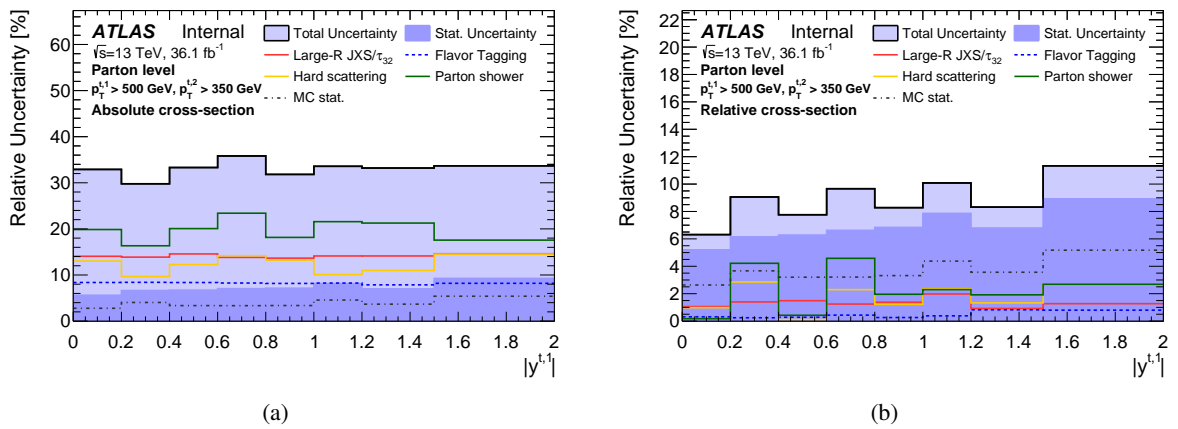


Figure 93: Fractional uncertainties of the absolute ((a)) and the relative ((b)) differential cross-sections as a function of the leading top $|y|$ in the parton level phase-space.

Not reviewed, for internal circulation only

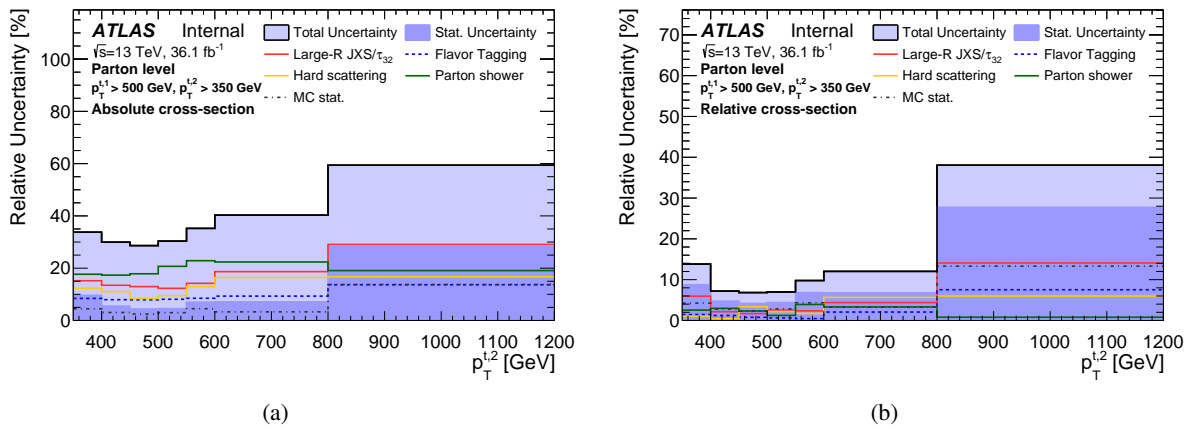


Figure 94: Fractional uncertainties of the absolute ((a)) and the relative ((b)) differential cross-sections as a function of the 2nd leading top p_T in the parton level phase-space.

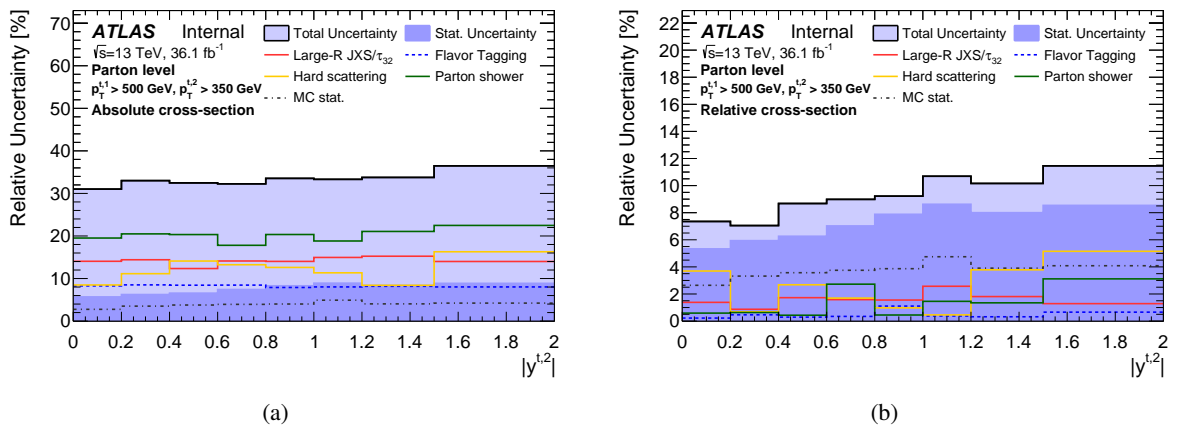


Figure 95: Fractional uncertainties of the absolute ((a)) and the relative ((b)) differential cross-sections as a function of the 2nd leading top $|y|$ in the parton level phase-space.

Not reviewed, for internal circulation only

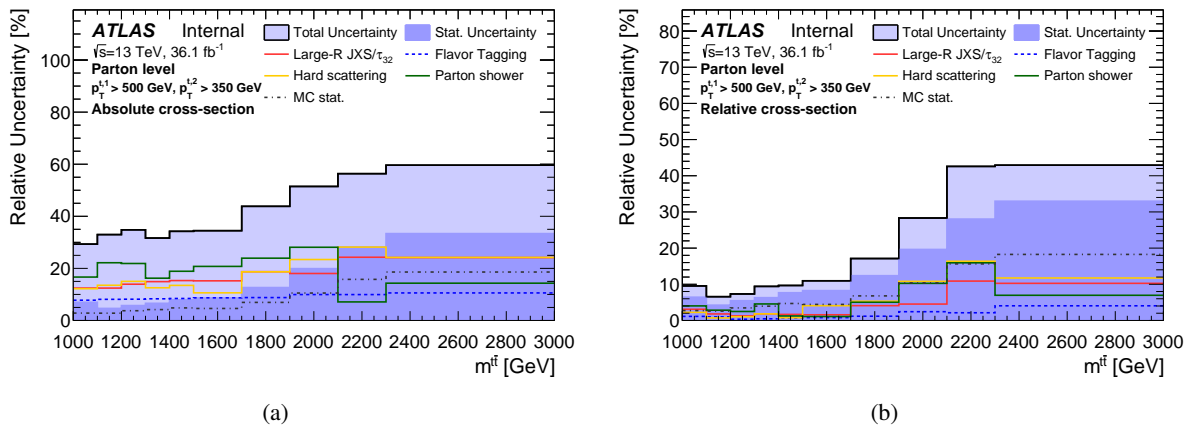


Figure 96: Fractional uncertainties of the absolute ((a)) and the relative ((b)) differential cross-sections as a function of the $t\bar{t}$ mass in the parton level phase-space.

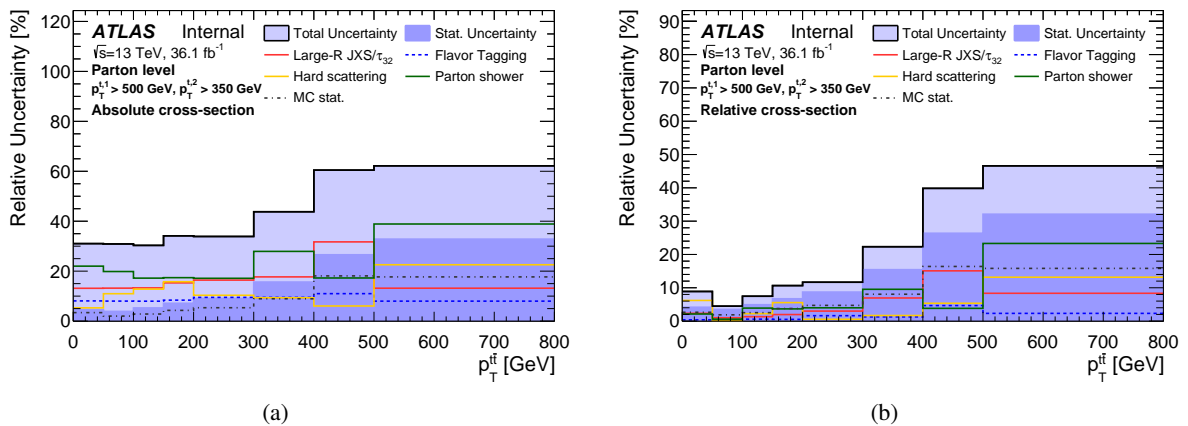


Figure 97: Fractional uncertainties of the absolute ((a)) and the relative ((b)) differential cross-sections as a function of the $t\bar{t}$ p_T in the parton level phase-space.

Not reviewed, for internal circulation only

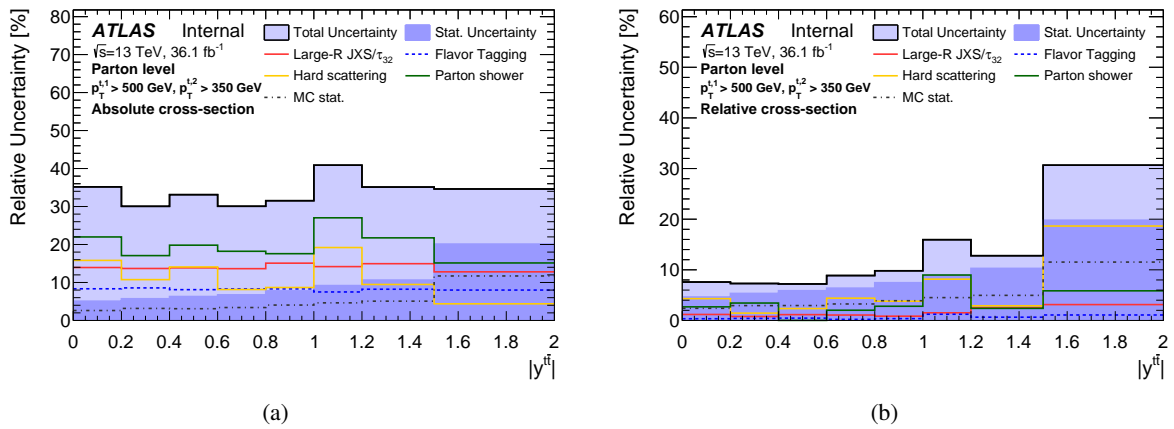


Figure 98: Fractional uncertainties of the absolute ((a)) and the relative ((b)) differential cross-sections as a function of the $t\bar{t}|y|$ in the parton level phase-space.

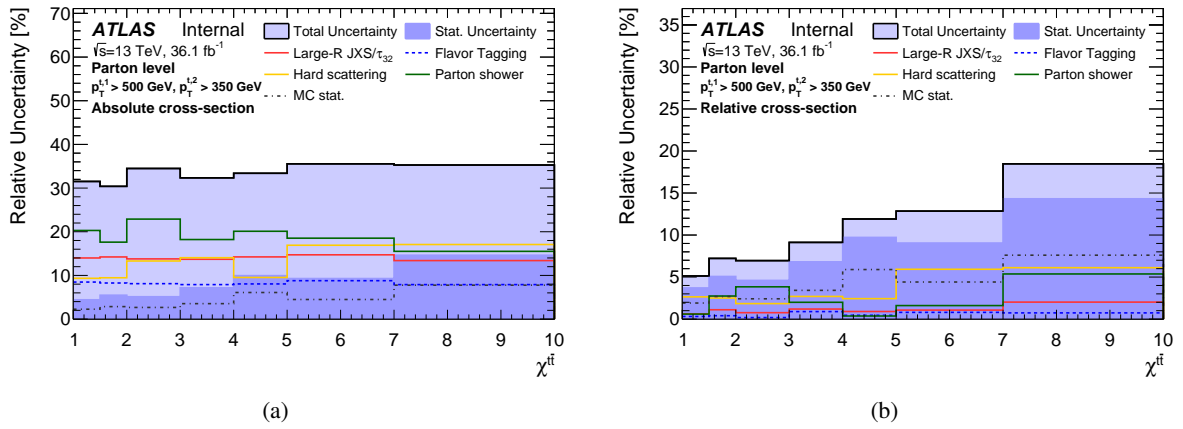


Figure 99: Fractional uncertainties of the absolute ((a)) and the relative ((b)) differential cross-sections as a function of the $|\chi_{t\bar{t}}|$ in the parton level phase-space.

Not reviewed, for internal circulation only

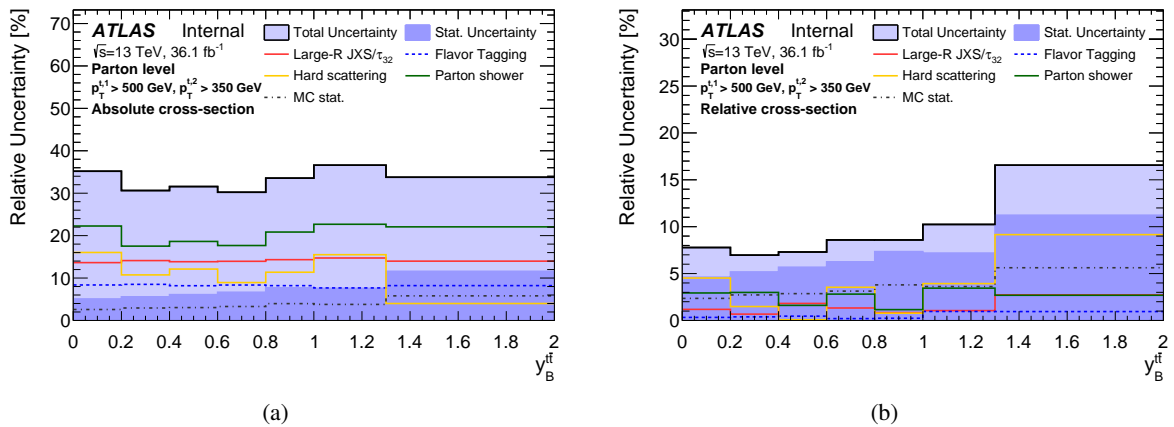


Figure 100: Fractional uncertainties of the absolute ((a)) and the relative ((b)) differential cross-sections as a function of the y_B^t in the parton level phase-space.

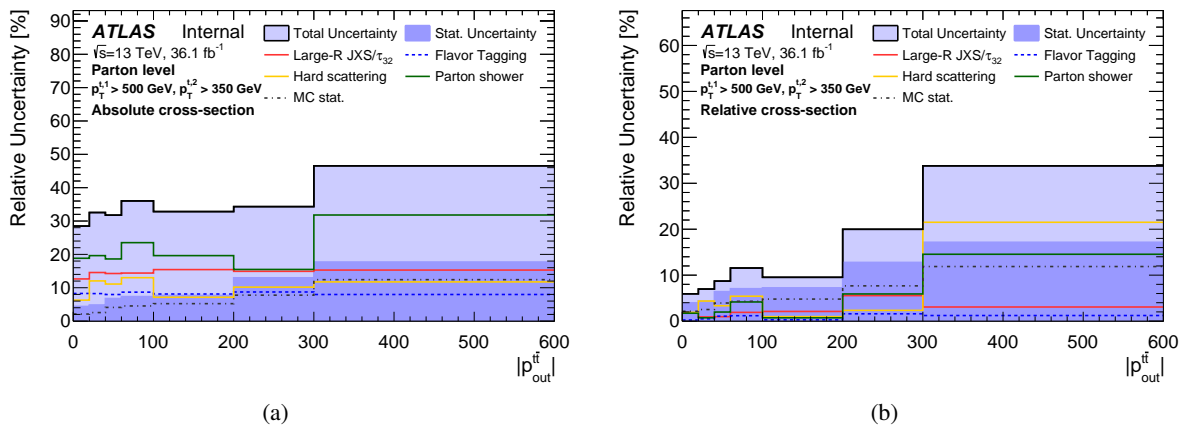


Figure 101: Fractional uncertainties of the absolute ((a)) and the relative ((b)) differential cross-sections as a function of the p_T^t in the parton level phase-space.

Not reviewed, for internal circulation only

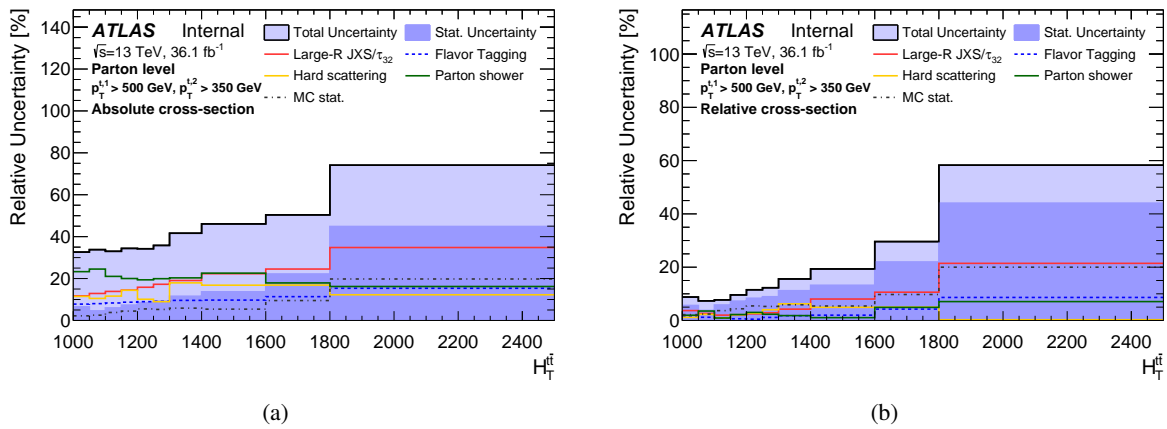


Figure 102: Fractional uncertainties of the absolute ((a)) and the relative ((b)) differential cross-sections as a function of the $H_T^{\ell\bar{\ell}}$ in the parton level phase-space.

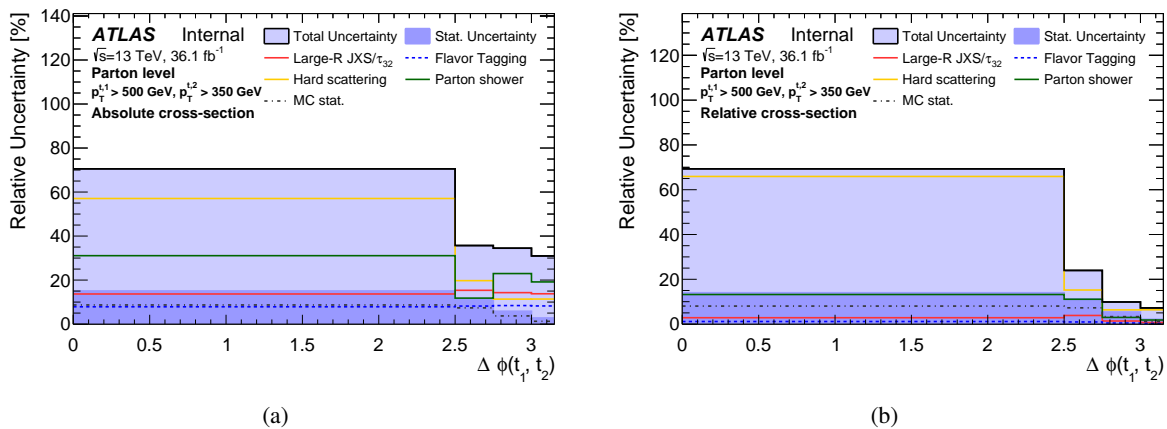


Figure 103: Fractional uncertainties of the absolute ((a)) and the relative ((b)) differential cross-sections as a function of the $|\Delta\phi|_{t_1, t_2}^{\ell\bar{\ell}}$ in the parton level phase-space.

Not reviewed, for internal circulation only

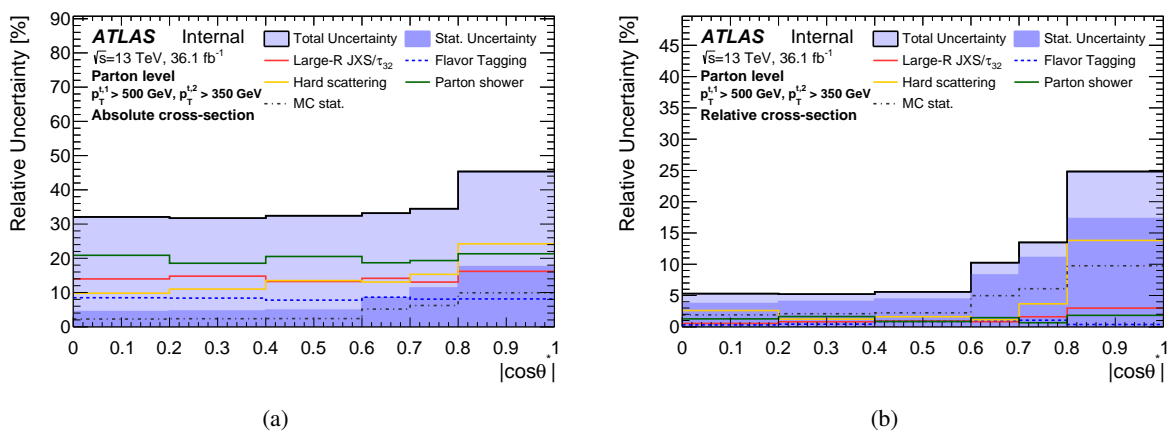


Figure 104: Fractional uncertainties of the absolute ((a)) and the relative ((b)) differential cross-sections as a function of the $|\cos \theta^*|$ in the parton level phase-space.

953 **G.2. Tables of differential cross-sections**

Range [GeV]	Cross section [pb/GeV]	Stat. unc. [%]	Total unc. [%]
[0,1]	0.794	2.23	28.5

Table 67: Table with central value and relative uncertainties for the absolute cross section at parton level phase space.

Range [GeV]	Cross section [pb/GeV]	Stat. unc. [%]	Total unc. [%]
[450,500]	0.00171	9.96	23.6
[500,550]	0.00487	4.38	25.3
[550,600]	0.00251	5.33	34.8
[600,650]	0.00138	7.96	41.1
[650,750]	0.000869	8.88	36.4
[750,900]	0.000268	15.9	38.8
[900,1200]	4.78e-05	37.6	58.9

Table 68: Table with central values and relative uncertainties for the absolute differential cross section at parton level as a function of random top p_T .

Range [GeV]	Cross section [1/GeV]	Stat. unc. [%]	Total unc. [%]
[450,500]	0.00256	9.32	9.64
[500,550]	0.00733	3.95	7.32
[550,600]	0.00378	5.15	9.08
[600,650]	0.00208	7.71	13.6
[650,750]	0.00131	8.53	13.1
[750,900]	0.000403	15.4	20.9
[900,1200]	7.2e-05	36.9	46.6

Table 69: Table with central values and relative uncertainties for the relative differential cross section at parton level as a function of random top p_T .

Not reviewed, for internal circulation only

Range [GeV]	Cross section [pb/GeV]	Stat. unc. [%]	Total unc. [%]
[0,0.2]	0.654	5.59	28.6
[0.2,0.4]	0.654	6.38	28
[0.4,0.6]	0.578	6.74	30.9
[0.6,0.8]	0.456	7.29	31.6
[0.8,1]	0.446	7.59	28.2
[1,1.2]	0.415	8.21	29.5
[1.2,1.5]	0.255	7.78	35.6
[1.5,2]	0.14	8.84	31.4

Table 70: Table with central values and relative uncertainties for the absolute differential cross section at parton level as a function of random top $|y|$.

Range [GeV]	Cross section [1/GeV]	Stat. unc. [%]	Total unc. [%]
[0,0.2]	0.831	5.23	6.35
[0.2,0.4]	0.831	6	8.17
[0.4,0.6]	0.735	6.33	8.6
[0.6,0.8]	0.58	6.9	8.41
[0.8,1]	0.567	7.26	8.48
[1,1.2]	0.527	7.93	10.1
[1.2,1.5]	0.324	7.45	11.2
[1.5,2]	0.177	8.52	10.3

Table 71: Table with central values and relative uncertainties for the relative differential cross section at parton level as a function of random top $|y|$.

Range [GeV]	Cross section [pb/GeV]	Stat. unc. [%]	Total unc. [%]
[500,550]	0.00639	4.08	24.4
[550,600]	0.00352	4.6	31.5
[600,650]	0.00187	6.86	34.1
[650,700]	0.00151	8.16	33.6
[700,750]	0.000875	11.5	38.8
[750,800]	0.00053	16.6	40.3
[800,1000]	0.000228	16.5	48
[1000,1200]	4.5e-05	61.2	115

Table 72: Table with central values and relative uncertainties for the absolute differential cross section at parton level as a function of leading top p_T .

Range [GeV]	Cross section [1/GeV]	Stat. unc. [%]	Total unc. [%]
[500,550]	0.0081	3.56	6.96
[550,600]	0.00446	4.36	7.29
[600,650]	0.00237	6.58	9.6
[650,700]	0.00191	7.85	10.9
[700,750]	0.00111	11.1	17.1
[750,800]	0.000671	16.2	24.7
[800,1000]	0.000288	15.9	28.6
[1000,1200]	5.7e-05	60.5	92.9

Table 73: Table with central values and relative uncertainties for the relative differential cross section at parton level as a function of leading top p_T .

Range [GeV]	Cross section [pb/GeV]	Stat. unc. [%]	Total unc. [%]
[0,0.2]	0.646	5.6	29.8
[0.2,0.4]	0.589	6.63	26.9
[0.4,0.6]	0.569	6.72	29.9
[0.6,0.8]	0.49	7.04	33.4
[0.8,1]	0.44	7.13	28.8
[1,1.2]	0.387	8.15	31.2
[1.2,1.5]	0.287	7	30.2
[1.5,2]	0.147	9.26	30.9

Table 74: Table with central values and relative uncertainties for the absolute differential cross section at parton level as a function of leading top $|y|$.

Range [GeV]	Cross section [1/GeV]	Stat. unc. [%]	Total unc. [%]
[0,0.2]	0.824	5.2	6.23
[0.2,0.4]	0.751	6.15	9.08
[0.4,0.6]	0.726	6.28	7.65
[0.6,0.8]	0.625	6.62	9.51
[0.8,1]	0.561	6.84	8.23
[1,1.2]	0.494	7.86	10.1
[1.2,1.5]	0.367	6.79	8.33
[1.5,2]	0.188	8.93	11.3

Table 75: Table with central values and relative uncertainties for the relative differential cross section at parton level as a function of leading top $|y|$.

Range [GeV]	Cross section [pb/GeV]	Stat. unc. [%]	Total unc. [%]
[350,400]	0.00214	9.6	25
[400,450]	0.00277	5.5	23.7
[450,500]	0.00372	4.41	24.9
[500,550]	0.00321	4.54	30.3
[550,600]	0.00158	7	37.1
[600,800]	0.000562	7.12	41.5
[800,1200]	4.6e-05	28.3	61.6

Table 76: Table with central values and relative uncertainties for the absolute differential cross section at parton level as a function of 2nd leading top p_T .

Range [GeV]	Cross section [1/GeV]	Stat. unc. [%]	Total unc. [%]
[350,400]	0.00267	8.75	8.51
[400,450]	0.00345	4.75	5.96
[450,500]	0.00464	4.16	6.33
[500,550]	0.004	4.39	7.46
[550,600]	0.00197	6.83	11
[600,800]	0.000701	6.77	13.2
[800,1200]	5.74e-05	27.7	41.5

Table 77: Table with central values and relative uncertainties for the relative differential cross section at parton level as a function of 2nd leading top p_T .

Range [GeV]	Cross section [pb/GeV]	Stat. unc. [%]	Total unc. [%]
[0,0.2]	0.66	5.68	28.1
[0.2,0.4]	0.68	6.24	29.8
[0.4,0.6]	0.609	6.57	30.1
[0.6,0.8]	0.476	7.42	29.3
[0.8,1]	0.397	8.3	30.4
[1,1.2]	0.369	8.92	30.3
[1.2,1.5]	0.278	8.38	30.9
[1.5,2]	0.119	8.87	35.2

Table 78: Table with central values and relative uncertainties for the absolute differential cross section at parton level as a function of 2nd leading top $|y|$.

Range [GeV]	Cross section [1/GeV]	Stat. unc. [%]	Total unc. [%]
[0,0.2]	0.844	5.33	7.3
[0.2,0.4]	0.87	5.94	7.01
[0.4,0.6]	0.78	6.26	7.9
[0.6,0.8]	0.61	7.03	8.76
[0.8,1]	0.508	7.88	9.02
[1,1.2]	0.472	8.62	10.6
[1.2,1.5]	0.356	8	10.1
[1.5,2]	0.152	8.54	11.6

Table 79: Table with central values and relative uncertainties for the relative differential cross section at parton level as a function of 2nd leading top $|y|$.

Range [TeV]	Cross section [pb/TeV]	Stat. unc. [%]	Total unc. [%]
[1,1.1]	1.29	6.99	24.4
[1.1,1.2]	1.48	4.63	30.5
[1.2,1.3]	1.11	5.72	33.6
[1.3,1.4]	0.898	6.58	30.6
[1.4,1.5]	0.723	7.95	32.4
[1.5,1.7]	0.392	8.64	33.5
[1.7,1.9]	0.253	12.6	42.5
[1.9,2.1]	0.113	19.9	55.4
[2.1,2.3]	0.0617	28.2	65.4
[2.3,3]	0.016	33.4	66.9

Table 80: Table with central values and relative uncertainties for the absolute differential cross section at parton level as a function of $t\bar{t}$ mass.

Range [TeV]	Cross section [1/TeV]	Stat. unc. [%]	Total unc. [%]
[1,1.1]	1.77	6.43	7.17
[1.1,1.2]	2.04	4.23	6.62
[1.2,1.3]	1.53	5.46	7.52
[1.3,1.4]	1.24	6.3	9.69
[1.4,1.5]	0.996	7.67	10.1
[1.5,1.7]	0.541	8.25	11.4
[1.7,1.9]	0.348	12.4	17.9
[1.9,2.1]	0.156	19.6	29.3
[2.1,2.3]	0.085	28	44.7
[2.3,3]	0.0221	33	48.7

Table 81: Table with central values and relative uncertainties for the relative differential cross section at parton level as a function of $t\bar{t}$ mass.

Range [GeV]	Cross section [pb/GeV]	Stat. unc. [%]	Total unc. [%]
[0,50]	0.00378	4.58	36
[50,100]	0.00366	3.89	27.1
[100,150]	0.00271	5.27	26.1
[150,200]	0.00169	7.14	29.7
[200,300]	0.000906	9.1	28.8
[300,400]	0.000383	15.6	42.2
[400,500]	0.000242	26.6	54.4
[500,800]	5.4e-05	32.8	70.9

Table 82: Table with central values and relative uncertainties for the absolute differential cross section at parton level as a function of $t\bar{t} p_T$.

Range [GeV]	Cross section [1/GeV]	Stat. unc. [%]	Total unc. [%]
[0,50]	0.00496	4.16	9.29
[50,100]	0.00481	3.5	3.86
[100,150]	0.00356	4.91	6.58
[150,200]	0.00222	6.7	9.51
[200,300]	0.00119	8.72	10.2
[300,400]	0.000503	15.4	19.6
[400,500]	0.000317	26.4	36.4
[500,800]	7.09e-05	32.1	43.7

Table 83: Table with central values and relative uncertainties for the relative differential cross section at parton level as a function of $t\bar{t} p_T$.

Range [GeV]	Cross section [pb/GeV]	Stat. unc. [%]	Total unc. [%]
[0,0.2]	0.829	5.08	32.7
[0.2,0.4]	0.783	5.72	27.2
[0.4,0.6]	0.636	6.3	30.2
[0.6,0.8]	0.577	6.74	27.4
[0.8,1]	0.457	7.79	28.3
[1,1.2]	0.313	9.18	41.4
[1.2,1.5]	0.182	10.6	32.5
[1.5,2]	0.0588	20.1	40.1

Table 84: Table with central values and relative uncertainties for the absolute differential cross section at parton level as a function of $t\bar{t} |y|$.

Range [GeV]	Cross section [1/GeV]	Stat. unc. [%]	Total unc. [%]
[0,0.2]	1.03	4.63	7.51
[0.2,0.4]	0.975	5.34	7.34
[0.4,0.6]	0.792	5.88	7.19
[0.6,0.8]	0.719	6.38	8.87
[0.8,1]	0.569	7.46	9.9
[1,1.2]	0.39	8.9	15.8
[1.2,1.5]	0.227	10.3	12.7
[1.5,2]	0.0732	19.8	31.2

Table 85: Table with central values and relative uncertainties for the relative differential cross section at parton level as a function of $t\bar{t}|y|$.

Range [GeV]	Cross section [pb/GeV]	Stat. unc. [%]	Total unc. [%]
[1,1.5]	0.411	4.42	28.5
[1.5,2]	0.31	5.47	27.1
[2,3]	0.163	5.12	32.1
[3,4]	0.0943	7.17	30
[4,5]	0.059	9.95	30.4
[5,7]	0.0337	9.28	33.6
[7,10]	0.00902	14.6	34.3

Table 86: Table with central values and relative uncertainties for the absolute differential cross section at parton level as a function of $|\chi^{t\bar{t}}|$.

Range [GeV]	Cross section [1/GeV]	Stat. unc. [%]	Total unc. [%]
[1,1.5]	0.533	3.71	5.07
[1.5,2]	0.402	5.07	7.02
[2,3]	0.211	4.6	6.92
[3,4]	0.122	6.81	8.84
[4,5]	0.0765	9.72	11.9
[5,7]	0.0437	9.05	12.4
[7,10]	0.0117	14.3	19.1

Table 87: Table with central values and relative uncertainties for the relative differential cross section at parton level as a function of $|\chi^{t\bar{t}}|$.

Range [GeV]	Cross section [pb/GeV]	Stat. unc. [%]	Total unc. [%]
[0,0.2]	0.796	5.07	32.9
[0.2,0.4]	0.804	5.57	27.5
[0.4,0.6]	0.673	6.09	28.4
[0.6,0.8]	0.57	6.65	27.3
[0.8,1]	0.426	7.7	30.5
[1,1.3]	0.295	7.57	34.2
[1.3,2]	0.085	11.6	32.8

Table 88: Table with central values and relative uncertainties for the absolute differential cross section at parton level as a function of $y_B^{\bar{t}t}$.

Range [GeV]	Cross section [1/GeV]	Stat. unc. [%]	Total unc. [%]
[0,0.2]	0.992	4.61	7.72
[0.2,0.4]	1	5.18	7.01
[0.4,0.6]	0.839	5.68	6.84
[0.6,0.8]	0.711	6.25	8.46
[0.8,1]	0.532	7.34	8.61
[1,1.3]	0.368	7.19	10
[1.3,2]	0.106	11.2	16.7

Table 89: Table with central values and relative uncertainties for the relative differential cross section at parton level as a function of $y_B^{\bar{t}t}$.

Range [GeV]	Cross section [pb/GeV]	Stat. unc. [%]	Total unc. [%]
[0,20]	0.0117	4.39	25.9
[20,40]	0.00738	4.83	28.9
[40,60]	0.00471	6.76	28.5
[60,100]	0.00302	7.35	33.9
[100,200]	0.0011	7.69	30.5
[200,300]	0.00047	13	33
[300,600]	0.00016	17.7	59.3

Table 90: Table with central values and relative uncertainties for the absolute differential cross section at parton level as a function of $p_{out}^{\bar{t}t}$.

Range [GeV]	Cross section [1/GeV]	Stat. unc. [%]	Total unc. [%]
[0,20]	0.0146	3.97	5.75
[20,40]	0.00923	4.38	6.62
[40,60]	0.00588	6.4	8.55
[60,100]	0.00378	7.05	11.4
[100,200]	0.00137	7.24	9.59
[200,300]	0.000587	12.8	19.7
[300,600]	0.0002	17.2	35.2

Table 91: Table with central values and relative uncertainties for the relative differential cross section at parton level as a function of $p_{out}^{\bar{t}t}$.

Range [GeV]	Cross section [pb/GeV]	Stat. unc. [%]	Total unc. [%]
[1000,1050]	0.0028	6.49	27.9
[1050,1100]	0.00204	4.58	31.4
[1100,1150]	0.00144	5.99	31.7
[1150,1200]	0.00103	7.33	34
[1200,1250]	0.000788	8.52	34.6
[1250,1300]	0.000655	9.17	35.7
[1300,1400]	0.000416	11.6	42.6
[1400,1600]	0.000197	13.7	43.8
[1600,1800]	0.000143	22.2	51.7
[1800,2500]	8.19e-06	44.9	68.7

Table 92: Table with central values and relative uncertainties for the absolute differential cross section at parton level as a function of $H_T^{\ell\bar{\ell}}$.

Range [GeV]	Cross section [1/GeV]	Stat. unc. [%]	Total unc. [%]
[1000,1050]	0.00506	5.62	6.09
[1050,1100]	0.00369	3.76	7.37
[1100,1150]	0.00261	5.81	8.32
[1150,1200]	0.00186	7.26	10.4
[1200,1250]	0.00143	8.34	13.3
[1250,1300]	0.00118	8.9	13.4
[1300,1400]	0.000752	11.2	16.9
[1400,1600]	0.000356	13.2	19.3
[1600,1800]	0.000258	22	35.1
[1800,2500]	1.48e-05	44	57.7

Table 93: Table with central values and relative uncertainties for the relative differential cross section at parton level as a function of $H_T^{\ell\bar{\ell}}$.

Range [GeV]	Cross section [pb/GeV]	Stat. unc. [%]	Total unc. [%]
[0,2.5]	0.0326	15.1	91.3
[2.5,2.75]	0.191	11.3	35.1
[2.75,3]	0.712	5.85	31.9
[3,3.15]	3.32	2.79	28.5

Table 94: Table with central values and relative uncertainties for the absolute differential cross section at parton level as a function of $|\Delta\phi^{\ell\bar{\ell}}|$.

Range [GeV]	Cross section [1/GeV]	Stat. unc. [%]	Total unc. [%]
[0,2.5]	0.0405	14	69.7
[2.5,2.75]	0.237	11.2	24.2
[2.75,3]	0.884	5.41	9.74
[3,3.15]	4.12	2.16	7.21

Table 95: Table with central values and relative uncertainties for the relative differential cross section at parton level as a function of $|\Delta\phi^{\ell\bar{\ell}}|$.

Range [GeV]	Cross section [pb/GeV]	Stat. unc. [%]	Total unc. [%]
[0,0.2]	1.09	4.43	29
[0.2,0.4]	1.08	4.6	28.1
[0.4,0.6]	0.968	4.86	29.9
[0.6,0.7]	0.889	8.48	30.8
[0.7,0.8]	0.505	11.3	33
[0.8,1]	0.119	17.6	49.7

Table 96: Table with central values and relative uncertainties for the absolute differential cross section at parton level as a function of $|\cos \theta^*|$.

Range [GeV]	Cross section [1/GeV]	Stat. unc. [%]	Total unc. [%]
[0,0.2]	1.38	3.71	5.19
[0.2,0.4]	1.37	4.05	5.13
[0.4,0.6]	1.22	4.41	5.61
[0.6,0.7]	1.12	8.28	10.5
[0.7,0.8]	0.638	11.1	14
[0.8,1]	0.151	17.3	26.3

Table 97: Table with central values and relative uncertainties for the relative differential cross section at parton level as a function of $|\cos \theta^*|$.

954 **G.3. Summary tables**

Bins [GeV]	[450,500]	[500,550]	[550,600]	[600,650]	[650,750]	[750,900]	[900,1200]
Total Uncertainty [%]	+29.21 -30.22	+27.82 -26.76	+35.39 -34.28	+39.93 -38.69	+41.09 -38.00	+45.69 -42.93	+72.44 -59.30
Statistics [%]	± 9.96	± 4.38	± 5.33	± 7.96	± 8.88	± 15.85	± 37.59
Systematics [%]	+27.31 -28.39	+27.36 -26.28	+34.85 -33.72	+38.85 -37.58	+39.87 -36.67	+42.49 -39.50	+58.92 -41.73
Background [%]	+0.69 -0.06	+0.69 -0.95	+0.69 -0.05	+0.69 -0.05	+0.69 -0.06	+0.69 -0.09	+2.20 -
Flavor tagging [%]	+8.60 -8.48	+8.87 -7.70	+8.11 -7.90	+8.51 -8.30	+9.77 -9.55	+10.76 -10.48	+16.11 -10.75
Large-R jet energy scale [%]	+6.86 -5.79	+5.22 -4.62	+5.57 -5.12	+6.72 -6.02	+8.97 -9.51	+10.71 -14.78	+16.71 -10.30
Large-R jet mass scale [%]	+2.72 -2.85	+1.21 -1.21	+1.56 -1.55	+1.94 -2.44	+0.52 -0.91	+3.01 -1.86	+7.19 -7.02
Large-R jet top-tagging [%]	+11.23 -13.08	+10.77 -9.77	+12.97 -11.72	+15.06 -13.71	+19.61 -17.25	+21.81 -16.10	+32.16 -21.09
Leptons [%]	+1.09 -	+1.08 -	+1.09 -	+1.08 -	+1.09 -	+1.09 -	+3.15 -
Luminosity [%]	+2.06 -2.06	+2.00 -2.00	+2.02 -2.01	+1.97 -1.97	+2.06 -2.06	+1.99 -1.99	+2.66 -0.72
MET/PU [%]	+0.02 -0.07	+0.09 -0.13	+0.10 -0.11	+0.07 -0.11	+0.07 -0.03	+0.04 -0.07	+1.12 -
Narrow jets [%]	+1.05 -0.54	+1.05 -0.56	+1.03 -0.56	+1.01 -0.12	+1.01 -0.14	+1.06 -0.70	+4.70 -0.22
(MOD) Monte Carlo sample statistics [%]	± 2.89	± 2.47	± 3.14	± 4.61	± 4.49	± 5.59	± 19.05
(MOD) Alternative hard-scattering model [%]	± 5.26	± 7.53	± 14.61	± 17.02	± 12.72	± 8.82	± 8.31
(MOD) Alternative parton-shower mode [%]	± 16.58	± 18.25	± 22.82	± 24.26	± 19.65	± 19.70	± 17.45
(MOD) ISR/FSR + scale [%]	± 0.44	± 0.56	∓ 1.81	± 0.19	∓ 2.85	∓ 4.10	∓ 3.49

Table 98: Summary of systematic uncertainties in the parton level phase-space absolute differential cross-sections for the random top p_T calculated as a percentage of the cross-section in each bin.

Bins [GeV]	[450,500]	[500,550]	[550,600]	[600,650]	[650,750]	[750,900]	[900,1200]
Total Uncertainty [%]	+12.59 -12.77	+6.50 -6.52	+8.46 -8.61	+12.90 -13.28	+11.04 -11.96	+18.53 -19.53	+45.34 -44.15
Statistics [%]	± 9.32	± 3.95	± 5.15	± 7.71	± 8.53	± 15.39	± 36.86
Systematics [%]	+7.93 -8.23	+4.67 -4.71	+5.99 -6.19	+9.31 -9.83	+5.46 -7.14	+8.65 -10.63	+18.34 -15.17
Background [%]	-	-	-	-	-	-	+1.02
Flavor tagging [%]	+0.78 -1.01	+1.10 -1.18	+0.68 -0.77	+0.44 -0.58	+1.54 -1.71	+3.23 -3.39	+8.79 -5.21
Large-R jet energy scale [%]	+1.07 -0.83	+1.29 -1.30	+0.45 -0.73	+0.87 -1.00	+2.71 -1.67	+3.46 -4.85	+7.30 -1.51
Large-R jet mass scale [%]	+1.33 -0.37	+0.23 -0.45	+0.28 -0.38	+0.61 -0.24	+1.25 -1.30	+2.67 -3.19	+6.20 -5.83
Large-R jet top-tagging [%]	+0.16 -1.57	+0.35 -	+0.23 -0.80	+0.24 -1.90	+0.17 -3.83	+0.17 -3.21	+3.56 -5.97
Leptons [%]	-	-	-	-	-	-	+1.94
Luminosity [%]	+0.03 -0.08	+0.03 -0.03	-0.04 -	-0.06 -	+0.01 -0.08	-0.10 -0.04	+1.29 -
MET/PU [%]	+0.01 -0.07	-	-	-	+0.01 -0.07	-	+1.03 -
Narrow jets [%]	+0.10 -0.40	+0.05 -0.20	+0.16 -0.23	+0.16 -0.26	+0.06 -0.50	+0.22 -0.27	+3.56 -1.91
(MOD) Monte Carlo sample statistics [%]	± 2.94	± 2.18	± 3.04	± 4.52	± 4.39	± 5.62	± 18.98
(MOD) Alternative hard-scattering model [%]	± 5.92	± 3.39	∓ 4.53	∓ 7.22	∓ 2.41	± 1.94	± 2.52
(MOD) Alternative parton-shower mode [%]	± 4.18	± 2.10	∓ 3.62	∓ 5.41	± 0.35	± 0.28	± 3.09
(MOD) ISR/FSR + scale [%]	± 1.67	± 0.58	∓ 0.69	± 1.32	∓ 1.71	∓ 3.01	∓ 2.29

Table 99: Summary of systematic uncertainties in the parton level phase-space relative differential cross-sections for the random top p_T calculated as a percentage of the cross-section in each bin.

Not reviewed, for internal circulation only

Bins [GeV]	[0,0.2]	[0.2,0.4]	[0.4,0.6]	[0.6,0.8]	[0.8,1]	[1,1.2]	[1.2,1.5]	[1.5,2]
Total Uncertainty [%]	+33.08 -31.17	+32.77 -29.09	+33.72 -32.92	+34.20 -34.76	+31.53 -31.04	+32.68 -31.90	+36.93 -36.40	+34.83 -33.57
Statistics [%]	± 5.59	± 6.38	± 6.74	± 7.29	± 7.59	± 8.21	± 7.78	± 8.84
Systematics [%]	+32.48 -30.55	+31.93 -28.15	+32.83 -32.01	+33.22 -33.80	+30.41 -29.90	+31.33 -30.51	+35.89 -35.34	+33.36 -32.04
Background [%]	+0.05 -0.06	+0.06 -0.07	+0.06 -0.05	+0.06 -0.06	+0.06 -0.05	+0.05 -0.05	+0.05 -0.05	+0.05 -0.05
Flavor tagging [%]	+8.49 -8.29	+8.58 -8.35	+8.76 -8.57	+8.55 -8.38	+8.17 -7.98	+7.80 -7.61	+7.95 -7.80	+7.85 -7.67
Large-R jet energy scale [%]	+6.51 -6.08	+8.75 -4.79	+8.86 -5.71	+8.90 -5.61	+6.75 -5.60	+5.81 -5.58	+7.68 -6.79	+5.75 -6.79
Large-R jet mass scale [%]	+1.27 -1.63	+2.62 -2.97	+1.19 -0.68	+1.99 -1.93	+0.74 -1.65	+2.73 -2.74	+1.42 -1.34	+1.82 -0.16
Large-R jet top-tagging [%]	+14.34 -12.28	+14.74 -10.66	+12.56 -11.63	+11.99 -12.96	+12.21 -12.14	+13.68 -12.75	+11.29 -11.62	+13.74 -11.71
Leptons [%]	-0.03 +2.05	- +2.03	- +2.02	- +2.05	- +2.01	- +1.92	- +2.00	- +1.94
Luminosity [%]	+2.05 -2.05	+2.03 -2.03	+2.02 -2.02	+2.05 -2.05	+2.01 -2.01	+1.92 -1.92	+2.00 -2.00	+1.94 -1.94
MET/PU [%]	+0.05 -0.10	+0.11 +0.15	+0.09 -0.05	+0.09 +0.12	+0.03 +0.44	+0.16 +0.32	+0.09 +0.48	+0.09 +0.13
Narrow jets [%]	+0.52 -0.42	+0.27 -0.08	+0.47 -0.52	+0.44 -0.36	+0.32 -0.32	+0.25 -0.22	+0.25 -0.34	+0.47 -0.38
(MOD) Monte Carlo sample statistics [%]	± 2.74	± 3.66	± 3.72	± 3.60	± 3.43	± 4.39	± 3.92	± 4.71
(MOD) Alternative hard-scattering model [%]	± 11.01	± 9.23	± 15.67	± 13.31	± 11.01	± 9.80	± 13.94	± 13.07
(MOD) Alternative parton-shower mode [%]	± 18.86	± 18.44	± 18.98	± 21.76	± 18.45	± 19.00	± 25.38	± 20.57
(MOD) ISR/FSR + scale [%]	± 1.32	∓ 1.33	± 1.88	± 3.18	∓ 0.88	± 2.98	± 1.98	± 1.22

Table 100: Summary of systematic uncertainties in the parton level phase-space absolute differential cross-sections for the random top $|y|$ calculated as a percentage of the cross-section in each bin.

Bins [GeV]	[0,0.2]	[0.2,0.4]	[0.4,0.6]	[0.6,0.8]	[0.8,1]	[1,1.2]	[1.2,1.5]	[1.5,2]
Total Uncertainty [%]	+6.44 -6.41	+8.84 -8.60	+8.63 -8.63	+8.52 -8.71	+8.81 -8.94	+10.09 -10.18	+11.30 -11.36	+10.57 -10.18
Statistics [%]	± 5.23	± 6.00	± 6.33	± 6.90	± 7.26	± 7.93	± 7.45	± 8.52
Systematics [%]	+2.70 -2.64	+5.54 -5.14	+4.72 -4.73	+3.62 -4.05	+3.69 -3.99	+4.57 -4.76	+7.61 -7.70	+4.30 -3.22
Background [%]	-	-	-	-	+0.01	-	-	+0.02
Flavor tagging [%]	+0.42 -0.38	+0.43 -0.34	+0.51 -0.56	+0.33 -0.37	+0.42 -0.43	+1.11 -1.08	+0.70 -0.71	+0.64 -0.62
Large-R jet energy scale [%]	+0.43 -0.68	+0.98 -0.35	+0.22 -0.36	+0.34 -0.50	+0.84 -0.78	+0.37 -0.13	+1.39 -1.31	-
Large-R jet mass scale [%]	+0.60 -0.87	+1.25 -1.60	+1.06 -0.92	+0.68 -0.75	+0.93 -1.38	+1.82 -1.80	+0.57 -0.36	+2.61 -1.20
Large-R jet top-tagging [%]	+1.07 -0.56	+1.51 -0.09	+0.35 -0.57	+0.05 -1.18	+0.09 -0.88	+0.50 -0.92	+0.38 -1.73	+0.66 -0.23
Leptons [%]	-0.03 +0.04	-0.02 +0.02	-0.01 -	-0.02 +0.04	-0.02 -	-0.03 +0.10	-0.03 +0.01	-0.03 +0.08
Luminosity [%]	+0.04 -0.04	+0.02 -0.02	- -	+0.04 -0.04	- +	+0.10 +0.08	+0.01 +0.01	+0.01 +0.07
MET/PU [%]	+0.01 -0.02	+0.04 +0.14	+0.06 +0.14	+0.01 +0.19	+0.04 +0.40	+0.08 +0.32	+0.01 +0.16	+0.02 +0.22
Narrow jets [%]	+0.20 -0.23	+0.22 -0.12	+0.14 -0.32	+0.19 -0.17	+0.40 -0.43	+0.32 -0.11	+0.16 -0.21	+0.22 -0.21
(MOD) Monte Carlo sample statistics [%]	± 2.60	± 3.38	± 3.49	± 3.44	± 3.37	± 4.25	± 3.79	± 4.55
(MOD) Alternative hard-scattering model [%]	∓ 1.19	∓ 3.22	± 4.11	± 1.42	∓ 1.19	∓ 2.57	± 2.13	± 1.15
(MOD) Alternative parton-shower mode [%]	∓ 1.34	∓ 1.87	∓ 1.19	± 2.27	∓ 1.86	∓ 1.17	± 6.80	± 0.79
(MOD) ISR/FSR + scale [%]	± 0.14	∓ 2.53	± 0.68	± 2.04	∓ 2.11	± 1.79	± 0.81	± 0.05

Table 101: Summary of systematic uncertainties in the parton level phase-space relative differential cross-sections for the random top $|y|$ calculated as a percentage of the cross-section in each bin.

Not reviewed, for internal circulation only

Bins [GeV]	[500,550]	[550,600]	[600,650]	[650,700]	[700,750]	[750,800]	[800,1000]	[1000,1200]
Total Uncertainty [%]	+29.38	+33.92	+36.36	+38.12	+44.80	+44.05	+57.21	+115.94
Statistics [%]	-26.51	-33.03	-35.78	-36.39	-40.70	-42.33	-48.90	-85.58
Systematics [%]	±4.08	±4.60	±6.86	±8.16	±11.49	±16.60	±16.47	±61.21
Background [%]	+3.36	+3.36	+3.36	+3.36	+3.36	+3.36	+3.36	+10.72
Flavor tagging [%]	-0.05	-0.06	-0.06	-0.06	-0.07	-0.10	-0.09	-
Large-R jet energy scale [%]	+7.67	+8.14	+8.78	+9.39	+10.19	+10.69	+11.56	+36.87
Large-R jet mass scale [%]	-7.50	-7.93	-8.59	-9.20	-9.94	-10.44	-11.21	-8.24
Large-R jet top-tagging [%]	+5.57	+5.24	+6.39	+8.12	+8.76	+5.84	+20.44	+8.80
Leptons [%]	-4.53	-5.11	-6.58	-6.45	-7.96	-13.05	-15.26	-5.42
Luminosity [%]	+1.01	+2.46	+2.46	+0.78	+1.57	+1.50	+0.22	+24.49
MET/PU [%]	-0.63	-2.14	-3.19	-1.01	-0.61	-0.39	-0.38	-0.80
Narrow jets [%]	+1.38	+11.63	+13.51	+16.05	+20.33	+20.52	+24.80	+15.93
(MOD) Monte Carlo sample statistics [%]	-9.34	-11.59	-13.54	-15.63	-17.96	-15.46	-18.92	-2.37
(MOD) Alternative hard-scattering model [%]	+4.76	+4.76	+4.76	+4.76	+4.76	+4.76	+4.82	+12.54
(MOD) Alternative parton-shower mode [%]	-0.02	-	-	-	-0.07	-	-	-
(MOD) ISR/FSR + scale [%]	+1.96	+2.03	+2.03	+2.07	+2.12	+2.08	+1.96	+7.04
(MOD) ISR/FSR + scale [%]	-0.10	+0.07	+0.11	-	-	+0.04	+0.01	+5.04
(MOD) Alternative parton-shower mode [%]	-0.13	-0.12	-0.15	-0.03	-0.06	-0.08	-0.06	-
Narrow jets [%]	+4.12	+4.14	+4.16	+4.13	+4.12	+4.12	+4.11	+22.27
(MOD) ISR/FSR + scale [%]	-0.17	-0.19	-0.33	-0.79	-0.92	-0.41	-0.24	-5.65
(MOD) Alternative hard-scattering model [%]	±2.28	±2.81	±3.84	±4.32	±5.80	±7.74	±5.99	±33.43
(MOD) Alternative parton-shower mode [%]	±8.90	±13.85	±11.35	±14.96	±16.20	±11.91	±15.89	±3.81
(MOD) ISR/FSR + scale [%]	±18.02	±21.67	±23.18	±18.72	±17.86	±18.02	±21.53	±5.06
(MOD) ISR/FSR + scale [%]	±0.10	±1.70	±0.08	±1.06	±5.62	±7.32	±4.90	±10.44

Table 102: Summary of systematic uncertainties in the parton level phase-space absolute differential cross-sections for the leading top p_T calculated as a percentage of the cross-section in each bin.

Bins [GeV]	[500,550]	[550,600]	[600,650]	[650,700]	[700,750]	[750,800]	[800,1000]	[1000,1200]
Total Uncertainty [%]	+8.31	+7.00	+9.22	+10.44	+17.63	+20.99	+30.35	+95.42
Statistics [%]	-7.42	-7.83	-9.79	-11.27	-17.37	-22.91	-26.26	-81.10
Systematics [%]	±3.56	±4.36	±6.58	±7.85	±11.12	±16.24	±15.90	±60.46
Background [%]	-0.13	-0.12	-0.13	-0.12	-0.12	-0.11	-0.12	+5.21
Flavor tagging [%]	+1.31	+0.68	+0.93	+0.93	+1.81	+2.11	+1.16	+24.85
Large-R jet energy scale [%]	+1.51	-0.94	-0.74	-1.28	+2.15	-3.05	-4.43	-4.45
Large-R jet mass scale [%]	+2.02	+1.70	+0.88	+1.82	+2.93	+0.86	+14.07	+7.79
Large-R jet top-tagging [%]	-1.43	-2.06	-1.78	-1.42	-3.05	-8.02	-10.86	-4.59
Leptons [%]	+0.66	+1.04	+1.32	+0.46	+0.61	+1.02	+1.28	+15.46
Luminosity [%]	-0.68	+0.97	+0.63	+0.67	-0.48	-0.80	+1.36	+1.89
MET/PU [%]	+3.43	+0.97	+0.71	+1.71	+6.51	+5.75	+1.37	+29.26
Narrow jets [%]	-2.54	-2.33	-1.36	-3.53	-6.04	-3.30	-7.11	+16.59
(MOD) Monte Carlo sample statistics [%]	-0.16	-0.16	-0.16	-0.16	-0.17	-0.16	-0.14	-
(MOD) Alternative hard-scattering model [%]	-0.11	-0.08	-0.08	-0.12	+0.04	-	-	+4.87
(MOD) Alternative parton-shower mode [%]	-0.06	-0.07	-0.05	-0.12	-0.13	-0.08	-0.10	+2.41
(MOD) ISR/FSR + scale [%]	+0.08	+0.03	+0.08	+0.02	+0.24	+0.10	+0.34	+12.47
(MOD) Alternative parton-shower mode [%]	-0.30	-0.22	-0.23	-0.46	-0.58	-0.32	-0.37	-5.46
(MOD) ISR/FSR + scale [%]	±2.00	±2.73	±3.81	±4.30	±5.76	±7.78	±5.99	±33.60
(MOD) Alternative hard-scattering model [%]	±3.31	±2.31	±0.53	±3.56	±4.97	±0.11	±4.63	±9.07
(MOD) Alternative parton-shower mode [%]	±2.07	±2.47	±4.34	±1.20	±2.27	±2.08	±2.29	±18.21
(MOD) ISR/FSR + scale [%]	±1.42	±0.21	±1.44	±0.47	±4.13	±5.82	±3.48	±8.77

Table 103: Summary of systematic uncertainties in the parton level phase-space relative differential cross-sections for the leading top p_T calculated as a percentage of the cross-section in each bin.

Not reviewed, for internal circulation only

Bins [GeV]	[0,0.2]	[0.2,0.4]	[0.4,0.6]	[0.6,0.8]	[0.8,1]	[1,1.2]	[1.2,1.5]	[1.5,2]
Total Uncertainty [%]	+33.66	+31.36	+33.84	+35.81	+32.31	+34.13	+33.70	+33.68
Statistics [%]	-32.14	-28.21	-32.78	-35.84	-31.32	-33.02	-32.69	-33.68
Systematics [%]	± 5.60	± 6.63	± 6.72	± 7.04	± 7.13	± 8.15	± 7.00	± 9.26
Background [%]	+0.06	+0.05	+0.06	+0.06	+0.05	+0.06	+0.04	+0.06
Flavor tagging [%]	+8.47	+8.51	+8.47	+8.34	+8.26	+8.35	+7.94	+8.28
Large-R jet energy scale [%]	-8.27	-8.30	-8.26	-8.17	-8.08	-8.14	-7.78	-8.11
Large-R jet mass scale [%]	+5.69	+5.44	+7.72	+6.13	+5.95	+5.21	+6.96	+6.84
Large-R jet top-tagging [%]	-5.89	-4.37	-6.79	-5.27	-5.18	-5.76	-6.03	-6.46
MET/PU [%]	+1.02	+2.35	+1.33	+2.17	+1.36	+3.22	+1.17	+2.17
Narrow jets [%]	-1.31	-2.77	-0.67	-2.37	-1.43	-3.22	-1.10	-1.65
Leptons [%]	+13.75	+14.36	+12.97	+12.14	+12.83	+13.42	+12.89	+12.70
Luminosity [%]	-11.74	-11.06	-12.21	-12.60	-11.95	-11.77	-12.09	-13.03
(MOD) Monte Carlo sample statistics [%]	-	-	-	-	-	-	-	-
(MOD) Alternative hard-scattering model [%]	+2.78	+4.04	+3.36	+3.34	+3.37	+4.56	+3.67	+5.39
(MOD) Alternative parton-shower mode [%]	± 13.03	± 9.66	± 12.26	± 14.18	± 13.24	± 10.09	± 11.00	± 14.53
(MOD) ISR/FSR + scale [%]	± 19.86	± 16.34	± 20.06	± 23.40	± 18.15	± 21.57	± 21.26	± 17.56

Table 104: Summary of systematic uncertainties in the parton level phase-space absolute differential cross-sections for the leading top $|y|$ calculated as a percentage of the cross-section in each bin.

Bins [GeV]	[0,0.2]	[0.2,0.4]	[0.4,0.6]	[0.6,0.8]	[0.8,1]	[1,1.2]	[1.2,1.5]	[1.5,2]
Total Uncertainty [%]	+6.29	+9.04	+7.80	+9.57	+8.28	+10.07	+8.34	+11.44
Statistics [%]	-6.34	-9.08	-7.72	-9.75	-8.28	-10.10	-8.29	-11.23
Systematics [%]	± 5.20	± 6.15	± 6.28	± 6.62	± 6.84	± 7.86	± 6.79	± 8.93
Background [%]	-	-	-	-	-	-	-	-
Flavor tagging [%]	+0.31	+0.23	+0.27	+0.41	+0.25	+0.41	+0.80	+0.78
Large-R jet energy scale [%]	+0.28	+0.57	+1.07	+0.18	+0.21	+0.07	+0.68	+0.23
Large-R jet mass scale [%]	+0.53	-0.70	-0.88	-0.29	-0.42	-0.82	-	-0.50
Large-R jet top-tagging [%]	+0.86	+0.92	+1.16	+0.89	+1.33	+1.89	+0.75	+1.73
Narrow jets [%]	-0.99	-1.29	-1.05	-1.52	-1.31	-1.84	-0.79	-0.35
Leptons [%]	+0.38	+0.77	+0.18	+0.01	+0.26	+0.38	+0.23	+0.18
Luminosity [%]	-0.18	-	-0.16	-0.28	-0.06	-0.13	-0.13	-0.49
(MOD) Monte Carlo sample statistics [%]	± 2.63	± 3.67	± 3.20	± 3.21	± 3.32	± 4.38	± 3.56	± 5.17
(MOD) Alternative hard-scattering model [%]	± 0.98	∓ 2.85	± 0.11	± 2.30	± 1.22	∓ 2.36	∓ 1.33	± 2.69
(MOD) Alternative parton-shower mode [%]	∓ 0.17	± 4.22	∓ 0.42	∓ 4.58	± 1.96	∓ 2.30	∓ 1.92	± 2.69
(MOD) ISR/FSR + scale [%]	± 1.43	± 0.37	∓ 2.30	± 2.98	∓ 0.84	∓ 0.83	∓ 1.16	∓ 1.17

Table 105: Summary of systematic uncertainties in the parton level phase-space relative differential cross-sections for the leading top $|y|$ calculated as a percentage of the cross-section in each bin.

Bins [GeV]	[350,400]	[400,450]	[450,500]	[500,550]	[550,600]	[600,800]	[800,1200]	
Total Uncertainty [%]	+34.87 -32.67	+30.65 -29.27	+28.91 -28.37	+30.88 -29.84	+35.71 -34.75	+41.66 -38.93	+60.37 -58.43	
Statistics [%]	± 9.60	± 5.50	± 4.41	± 4.54	± 7.00	± 7.12	± 28.30	
Systematics [%]	+33.22 -30.91	+29.99 -28.58	+28.47 -27.91	+30.39 -29.34	+34.73 -33.74	+40.92 -38.13	+51.52 -49.24	
Background [%]	+0.28 -0.12	+0.27 -0.09	+0.27 -0.06	+0.26 -0.04	+0.26 -0.04	+0.26 -0.04	+0.85 -	
Flavor tagging [%]	+8.53 +8.35	+8.04 -7.86	+7.98 -7.82	+8.20 -8.00	+8.55 -8.39	+9.05 -9.20	+14.82 -12.81	
Large-R jet energy scale [%]	+8.35 +8.45	+7.41 +7.33	+6.83 +6.55	+5.55 +5.49	+7.15 +7.15	+16.83 +16.97	-	
Large-R jet mass scale [%]	+7.44 +7.40	+6.62 +6.51	+6.81 +6.73	+6.23 +6.24	+1.32 +1.37	-0.37 +0.26	-3.51 -1.09	
Large-R jet top-tagging [%]	+13.57 +10.14	+11.98 +10.93	+11.40 +11.24	+11.67 +10.63	+13.65 +12.48	+18.81 +17.70	+24.90 -24.02	
Leptons [%]	+0.37 -0.05	+0.37 -0.05	+0.37 -0.02	+0.37 -0.02	+0.40 -0.37	+0.37 -0.37	+0.97 -	
Luminosity [%]	+2.11 -2.11	+2.04 -2.04	+2.02 -2.02	+2.01 -2.01	+2.00 -2.00	+1.98 -1.98	+2.31 -1.57	
MET/PU [%]	-0.06 +0.53	-0.18 +0.46	-0.15 +0.48	-0.08 +0.51	-0.11 +0.54	-0.05 +0.37	-	+0.48
Narrow jets [%]	-0.70 -10.17	-0.27 -4.47	-0.23 -5.03	-0.24 -4.45	-0.30 -5.74	-0.25 -9.40	-0.78 -23.04	
(MOD) Monte Carlo sample statistics [%]	± 4.47	± 3.06	± 2.45	± 2.99	± 4.49	± 3.29	± 13.75	
(MOD) Alternative hard-scattering model [%]	± 12.29	± 11.03	± 8.43	± 9.48	± 12.93	± 16.43	± 16.71	
(MOD) Alternative parton-shower mode [%]	± 17.68	± 17.34	± 17.86	± 20.71	± 22.86	± 22.37	± 19.08	
(MOD) ISR/FSR + scale [%]	∓ 4.79	∓ 1.62	∓ 0.84	∓ 0.09	∓ 0.92	± 0.30	± 0.45	

Table 106: Summary of systematic uncertainties in the parton level phase-space absolute differential cross-sections for the 2nd leading top p_T calculated as a percentage of the cross-section in each bin.

Bins [GeV]	[350,400]	[400,450]	[450,500]	[500,550]	[550,600]	[600,800]	[800,1200]
Total Uncertainty [%]	+13.57 -14.08	+7.32 -7.09	+6.75 -6.92	+7.09 -6.86	+9.66 -9.91	+12.03 -12.03	+37.69 -38.42
Statistics [%]	± 8.75	± 4.75	± 4.16	± 4.39	± 6.83	± 6.77	± 27.72
Systematics [%]	+9.46 -10.17	+4.83 -4.47	+4.79 -5.03	+4.80 -4.45	+5.29 -5.74	+9.40 -9.40	+21.79 -23.04
Background [%]	+0.04 -0.08	+0.01 -0.05	- -0.03	- -0.04	+0.02 -0.05	- -0.04	+0.69 -
Flavor tagging [%]	+1.44 -1.47	+1.21 -1.23	+0.76 -0.79	+0.62 -0.61	+0.52 -0.59	+2.11 -2.10	+8.26 -6.80
Large-R jet energy scale [%]	+1.37 -1.99	+1.86 -1.86	+0.63 -0.63	+2.22 -1.92	+1.33 -1.33	+10.34 -10.34	-
Large-R jet mass scale [%]	+5.12 -3.90	+0.84 -0.50	+0.66 -0.60	+0.67 -0.60	+0.66 -0.66	+1.81 -1.81	+2.16 -10.37
Large-R jet top-tagging [%]	+1.84 -0.33	+1.16 -1.19	+0.88 -1.56	+1.41 -1.29	+1.80 -0.54	+3.80 -3.53	+8.17 -10.51
Leptons [%]	-0.04 -0.04	- -0.05	- -0.05	- -0.04	+0.12 -0.03	- -0.03	+0.62 -
Luminosity [%]	+0.08 -0.11	- -0.03	- -0.01	- -0.02	+0.01 -0.03	+0.03 -0.05	+0.45 -
MET/PU [%]	+0.04 -0.07	+0.06 -0.09	+0.03 -0.05	+0.02 -0.04	- -0.01	+0.04 -0.06	+0.40 -
Narrow jets [%]	+0.28 -0.53	+0.12 -0.20	+0.08 -0.16	+0.11 -0.17	+0.13 -0.18	+0.08 -0.25	+1.75 -0.67
(MOD) Monte Carlo sample statistics [%]	± 4.24	± 2.78	± 2.31	± 2.82	± 4.32	± 3.25	± 13.31
(MOD) Alternative hard-scattering model [%]	± 1.00	± 0.43	± 3.37	± 2.18	± 1.72	± 5.67	± 5.98
(MOD) Alternative parton-shower mode [%]	± 2.54	± 2.97	± 2.31	± 1.23	± 3.92	± 3.30	± 0.79
(MOD) ISR/FSR + scale [%]	∓ 3.73	∓ 0.53	± 0.30	± 1.05	± 0.18	± 1.42	± 1.61

Table 107: Summary of systematic uncertainties in the parton level phase-space relative differential cross-sections for the 2nd leading top p_T calculated as a percentage of the cross-section in each bin.

Bins [GeV]	[0,0.2]	[0.2,0.4]	[0.4,0.6]	[0.6,0.8]	[0.8,1]	[1,1.2]	[1.2,1.5]	[1.5,2]
Total Uncertainty [%]	+31.67	+33.92	+32.43	+32.71	+33.98	+34.89	+34.39	+37.34
Statistics [%]	-30.36	-32.10	-32.53	-31.80	-33.09	-31.73	-33.13	-35.64
Systematics [%]	±5.68	±6.24	±6.57	±7.42	±8.30	±8.92	±8.38	±8.87
-29.70	-31.29	-31.64	-30.68	-31.78	-30.05	-31.80	-34.25	
Background [%]	+0.06	+0.06	+0.06	+0.05	+0.06	+0.05	+0.06	+0.04
Flavor tagging [%]	-0.06	-0.06	-0.07	-0.06	-0.06	-0.05	-0.06	-0.04
Large-R jet energy scale [%]	+8.37	+8.61	+8.54	+8.55	+7.98	+8.12	+8.24	+8.11
Large-R jet mass scale [%]	-8.16	-8.41	-8.32	-8.36	-7.81	-7.93	-8.11	-7.94
Large-R jet top-tagging [%]	+6.45	+6.17	+5.00	+5.93	+7.88	+4.73	+7.80	+6.26
Leptons [%]	-5.57	-5.47	-5.12	-6.36	-5.96	-5.37	-5.86	-5.94
Luminosity [%]	+2.53	+1.63	+1.00	+1.03	+1.30	+2.80	+1.48	+1.90
MET/PU [%]	-2.59	-1.86	-1.44	-0.17	-1.70	-2.86	-0.67	-1.72
Narrow jets [%]	+13.01	+14.05	+11.12	+13.31	+12.15	+15.76	+13.80	+13.60
(MOD) Monte Carlo sample statistics [%]	-11.87	-12.09	-11.26	-12.06	-12.01	-11.74	-13.32	-11.34
(MOD) Alternative hard-scattering model [%]	-0.03	-0.12	-	-	-	-	-	-
(MOD) Alternative parton-shower mode [%]	+2.76	+3.51	+3.77	+3.93	+4.01	+4.91	+4.04	+4.22
(MOD) ISR/FSR + scale [%]	+8.48	+11.14	+14.11	+13.24	+12.61	+11.34	+8.41	+16.29
(MOD) ISR/FSR + scale [%]	+19.52	+20.49	+20.33	+17.81	+20.35	+18.82	+21.06	+22.48
(MOD) ISR/FSR + scale [%]	+0.57	+0.80	+2.07	+1.51	+2.45	+1.79	+1.21	+0.54

Table 108: Summary of systematic uncertainties in the parton level phase-space absolute differential cross-sections for the 2nd leading top $|y|$ calculated as a percentage of the cross-section in each bin.

Bins [GeV]	[0,0.2]	[0.2,0.4]	[0.4,0.6]	[0.6,0.8]	[0.8,1]	[1,1.2]	[1.2,1.5]	[1.5,2]
Total Uncertainty [%]	+7.36	+7.07	+8.42	+8.97	+9.28	+10.82	+10.19	+11.54
Statistics [%]	-7.35	-7.03	-8.94	-9.00	-9.16	-10.56	-10.13	-11.38
Systematics [%]	±5.33	±5.94	±6.26	±7.03	±7.88	±8.62	±8.00	±8.54
-4.31	-1.78	-5.29	-4.20	-2.61	-3.82	-4.82	-6.31	
Background [%]	-	-	-0.02	-	-0.01	-	-	+0.02
Flavor tagging [%]	+0.23	+0.47	+0.30	+0.32	+0.08	+0.38	+0.27	+0.66
Large-R jet energy scale [%]	-0.22	-0.46	-0.28	-0.37	-1.13	-0.37	-0.36	-0.66
Large-R jet mass scale [%]	+0.52	+0.53	+0.58	+0.17	+1.74	+0.39	+1.44	+0.34
Large-R jet top-tagging [%]	-0.13	-0.28	-1.43	-1.01	-0.31	-1.40	-0.48	-0.41
Leptons [%]	+1.27	+0.31	+0.43	+1.48	+0.07	+1.59	+1.12	+1.43
Luminosity [%]	-1.32	-0.65	-0.74	-2.26	-0.68	-1.81	-0.66	-0.82
MET/PU [%]	+0.29	+0.78	+0.78	+0.34	+0.18	+2.32	+0.54	+0.76
Narrow jets [%]	-0.30	-0.36	-1.94	-0.23	-1.13	-0.24	-1.51	-
(MOD) Monte Carlo sample statistics [%]	-0.04	-0.10	-	-	-	-	-	-
(MOD) Alternative hard-scattering model [%]	+2.64	+3.32	+3.57	+3.75	+3.87	+4.75	+3.91	+4.09
(MOD) Alternative parton-shower mode [%]	+3.69	+0.69	+2.68	+1.70	+0.98	+0.46	+3.78	+5.15
(MOD) ISR/FSR + scale [%]	+0.59	+0.63	+0.43	+2.72	+0.45	+1.46	+1.35	+3.12
(MOD) ISR/FSR + scale [%]	±0.43	±0.60	±2.92	±1.11	±0.04	±0.87	±0.27	±0.22

Table 109: Summary of systematic uncertainties in the parton level phase-space relative differential cross-sections for the 2nd leading top $|y|$ calculated as a percentage of the cross-section in each bin.

Bins [GeV]	[1000,1100]	[1100,1200]	[1200,1300]	[1300,1400]	[1400,1500]	[1500,1700]	[1700,1900]	[1900,2100]	[2100,2300]	[2300,3000]
Total Uncertainty [%]	+30.16	+33.53	+35.20	+32.20	+34.39	+35.40	+44.60	+53.66	+55.85	+62.64
Statistics [%]	-28.46	-33.43	-34.02	-31.08	-30.07	-30.05	-41.05	-46.46	-50.89	-56.60
Systematics [%]	±6.99	±4.63	±5.72	±6.58	±7.95	±8.64	±12.64	±19.90	±28.23	±33.36
-27.44	-31.99	-33.74	-30.09	-32.78	-32.09	-40.56	-43.82	-46.80	-41.77	
Background [%]	+0.07	+0.05	+0.04	+0.05	+0.05	+0.06	+0.05	+0.03	+0.05	+0.04
Flavor tagging [%]	-0.08	-0.06	-0.05	-0.05	-0.05	-0.05	-0.05	-0.03	-0.06	-0.04
Large-R jet energy scale [%]	+1.70	+0.91	+8.01	+8.07	+8.23	+8.35	+8.67	+9.83	+9.83	+10.37
Large-R jet mass scale [%]	+0.94	+1.51	+1.77	+1.77	+1.50	+1.29	+1.06	+1.31	+1.31	+1.31
Large-R jet top-tagging [%]	-1.17	-1.11	-0.97	-2.20	-1.04	-0.67	-1.92	-2.35	-2.35	-6.55
Leptons [%]	-10.03	-11.19	-11.19	-12.12	-12.73	-12.87	-13.24	-14.74	-12.88	-14.97
Luminosity [%]	+2.07	+2.00	+2.00	+2.03	+2.02	+1.93	+1.93	+1.97	+1.97	+1.93
MET/PU [%]	-2.01	-2.00	-2.00	-2.03	-2.02	-1.94	-1.94	-1.98	-2.15	-1.95
Narrow jets [%]	+0.30	-0.32	+0.38	+0.29	+0.27	+0.14	+0.03	-0.04	+0.16	-
(MOD) Monte Carlo sample statistics [%]	+2.83	+2.79	+3.74	+4.17	+4.82	+4.60	+6.93	+10.53	+15.78	+18.59
(MOD) Alternative hard-scattering model [%]	+12.19	+13.51	+15.01	+12.55	+13.47	+10.61	+18.68	+23.40	+28.17	+24.20
(MOD) Alternative parton-shower mode [%]	+16.66	+22.16	+21.88	+16.23	+18.89	+20.76	+23.92	+28.10	+7.12	+14.31
(MOD) ISR/FSR + scale [%]	±0.28	±2.05	±1.41	±0.61	±1.32	±2.22	±2.58	±5.81	±1.34	±1.51

Table 110: Summary of systematic uncertainties in the parton level phase-space absolute differential cross-sections for the $t\bar{t}$ mass calculated as a percentage of the cross-section in each bin.

Bins [GeV]	[1000,1100]	[1100,1200]	[1200,1300]	[1300,1400]	[1400,1500]	[1500,1700]	[1700,1900]	[1900,2100]	[2100,2300]	[2300,3000]
Total Uncertainty [%]	+9.49	+0.83	+7.43	+9.32	+9.76	+10.00	+17.50	+20.97	+31.01	+43.63
Statistics [%]	±6.43	±4.23	±5.46	±6.30	±7.67	±8.25	±12.38	±19.63	±28.03	±32.97
Systematics [%]	+6.42	+4.40	+3.66	+5.61	+3.33	+5.87	+9.83	+18.77	+25.73	+21.98
Background [%]	+0.02	—	+0.01	+0.01	+0.01	—	—	+0.03	+0.02	+0.04
Flavor tagging [%]	+1.14	+1.03	+0.33	+0.32	+0.38	+0.39	+1.18	+2.38	+2.07	+0.48
Large-R jet energy scale [%]	-1.12	-0.97	-0.34	-0.49	-0.70	-0.79	-1.17	-2.46	-2.18	-4.02
Large-R jet mass scale [%]	+1.66	+1.41	+1.30	+1.30	+1.14	+0.96	+1.48	+4.03	+4.03	+4.81
Large-R jet top-tagging [%]	+0.91	+0.44	+0.40	+0.51	+0.53	+0.57	+1.92	+3.12	+1.40	+5.05
Leptons [%]	-2.66	-1.54	-0.25	-0.52	-0.65	-1.07	-2.69	-0.66	-13.65	-2.95
Luminosity [%]	-0.03	-0.03	-0.03	-0.03	-0.02	+0.06	+0.10	+0.13	+0.13	+0.16
MET/PU [%]	+0.03	+0.02	+0.04	+0.04	—	+0.03	+0.06	-0.05	+0.01	+0.04
Narrow jets [%]	+0.19	-0.02	-0.04	+0.05	+0.14	+0.22	+0.27	+0.17	-0.11	-0.15
(MOD) Monte Carlo sample statistics [%]	±2.74	±2.59	±3.47	±3.95	±4.69	±4.43	±6.79	±10.37	±15.64	±18.26
(MOD) Alternative hard-scattering model [%]	±2.25	±0.70	±1.04	±1.83	±0.76	±4.08	±5.32	±10.81	±16.37	±11.74
(MOD) Alternative parton-shower mode [%]	±4.02	±2.84	±2.48	±4.56	±1.25	±1.08	±5.03	±10.26	±15.94	±6.96
(MOD) ISR/FSR + scale [%]	±0.31	±1.47	±0.82	±1.20	±1.92	±2.83	±2.00	±5.25	±1.94	±0.92

Table 111: Summary of systematic uncertainties in the parton level phase-space relative differential cross-sections for the $t\bar{t}$ mass calculated as a percentage of the cross-section in each bin.

Bins [GeV]	[0,50]	[50,100]	[100,150]	[150,200]	[200,300]	[300,400]	[400,500]	[500,800]
Total Uncertainty [%]	+31.91	+31.51	+30.32	+33.89	+34.94	+45.12	+71.86	+61.45
Statistics [%]	-30.15	-30.28	-30.31	-34.42	-32.83	-42.47	-49.06	-62.92
Systematics [%]	±4.58	±3.89	±5.27	±7.14	±9.10	±15.64	±26.57	±32.83
Background [%]	+0.43	+0.43	+0.43	+0.44	+0.45	+0.45	+0.49	+1.48
Flavor tagging [%]	-0.02	-0.04	-0.07	-0.10	-0.14	-0.16	-0.28	-
Large-R jet energy scale [%]	-7.98	-7.91	-7.88	-8.29	-9.37	-9.41	-10.97	-6.41
Large-R jet mass scale [%]	+5.37	+6.31	+6.10	+5.25	+8.72	+12.00	+8.10	+9.69
Large-R jet top-tagging [%]	-4.51	-5.64	-6.02	-6.49	-6.80	-10.15	-11.30	-7.73
Leptons [%]	-0.67	+1.30	+2.21	+2.20	+2.48	+4.18	+9.50	+4.33
Luminosity [%]	-0.40	-1.38	-2.28	-2.36	-2.49	-3.35	-4.24	-1.32
MET/PU [%]	+1.96	+2.29	+11.58	+13.85	+14.92	+14.53	+41.73	+1.63
Narrow jets [%]	-1.25	-11.09	-11.66	-14.13	-13.55	-11.02	-16.98	-13.48
(MOD) Monte Carlo sample statistics [%]	±3.39	±2.00	±2.83	±4.29	±5.35	±8.93	±18.09	±17.69
(MOD) Alternative hard-scattering model [%]	±5.29	±10.97	±12.81	±15.77	±10.33	±9.33	±6.05	±22.56
(MOD) Alternative parton-shower mode [%]	±22.00	±19.85	±17.20	±17.39	±17.13	±27.91	±17.26	±38.88
(MOD) ISR/FSR + scale [%]	±1.40	±1.80	±0.94	±1.34	±0.72	±0.50	±5.96	±1.72

Table 112: Summary of systematic uncertainties in the parton level phase-space absolute differential cross-sections for the $t\bar{t} p_T$ calculated as a percentage of the cross-section in each bin.

Bins [GeV]	[0,50]	[50,100]	[100,150]	[150,200]	[200,300]	[300,400]	[400,500]	[500,800]
Total Uncertainty [%]	+8.99	+4.54	+7.35	+10.35	+11.86	+22.40	+44.08	+46.37
Statistics [%]	-8.79	-4.42	-7.57	-10.96	-11.46	-22.25	-35.61	-46.85
Systematics [%]	±4.16	±3.50	±4.91	±6.70	±8.72	±15.44	±26.37	±32.09
Background [%]	+0.02	—	—	+0.03	+0.05	+0.05	+0.17	+1.19
Flavor tagging [%]	-0.08	-0.06	-0.04	-0.07	-0.10	-0.12	-0.25	-
Large-R jet energy scale [%]	-0.35	+0.33	+0.51	+0.46	+1.58	+1.14	+4.46	+3.94
Large-R jet mass scale [%]	+2.20	-0.39	+0.93	+0.59	+1.09	+6.36	+3.86	-0.68
Large-R jet top-tagging [%]	-1.90	-0.50	-0.69	-1.74	-1.82	-5.93	-6.33	-2.88
Leptons [%]	+1.07	+0.32	+0.89	+0.88	+1.20	+2.93	+11.10	+6.17
Luminosity [%]	-0.95	-0.37	-1.02	-1.39	-1.17	-3.34	-5.60	-2.83
MET/PU [%]	+0.64	+0.84	+0.40	+0.68	+1.26	+0.95	+17.38	+1.20
Narrow jets [%]	-0.21	-0.58	-1.04	-1.66	-1.42	-0.29	-4.10	-8.51
(MOD) Monte Carlo sample statistics [%]	±2.65	±1.88	±2.53	±3.78	±4.71	±8.06	±16.40	±15.82
(MOD) Alternative hard-scattering model [%]	±6.20	±0.16	±2.23	±5.55	±0.54	±1.67	±5.35	±13.17
(MOD) Alternative parton-shower mode [%]	±2.13	±0.58	±3.90	±3.66	±3.98	±9.54	±3.82	±23.30
(MOD) ISR/FSR + scale [%]	±0.47	±0.87	—	±0.39	±0.18	±1.40	±7.02	±2.55

Table 113: Summary of systematic uncertainties in the parton level phase-space relative differential cross-sections for the $t\bar{t} p_T$ calculated as a percentage of the cross-section in each bin.

Not reviewed, for internal circulation only

Bins [GeV]	[0,0.2]	[0.2,0.4]	[0.4,0.6]	[0.6,0.8]	[0.8,1]	[1,1.2]	[1.2,1.5]	[1.5,2]
Total Uncertainty [%]	+36.18 -34.17	+30.34 -29.76	+33.64 -32.60	+31.34 -28.79	+31.68 -31.38	+41.39 -40.36	+34.07 -36.17	+35.91 -33.32
Statistics [%]	±5.08	±5.72	±6.30	±6.74	±7.79	±9.18	±10.63	±20.11
Systematics [%]	+35.73 -33.69	+29.63 -29.03	+32.90 -31.83	+30.41 -27.78	+30.44 -30.12	+40.09 -39.03	+31.97 -34.20	+27.35 -23.84
Background [%]	+0.05 -0.05	+0.06 -0.06	+0.06 -0.06	+0.06 -0.06	+0.05 -0.05	+0.07 -0.07	+0.06 -0.06	+0.03 -0.03
Flavor tagging [%]	+8.43 -8.25	+8.69 -8.45	+8.20 -8.02	+8.43 -8.24	+8.41 -8.22	+7.58 -7.43	+8.30 -8.14	+8.10 -7.91
Large-R jet energy scale [%]	+6.03 +5.33	+5.32 +5.60	+6.27 +6.18	+6.81 +5.24	+6.02 +6.50	+6.98 +7.41	+6.82 +7.29	+8.44 +7.06
Large-R jet mass scale [%]	+2.26 -2.71	+1.30 +1.27	+0.55 +0.50	+1.88 +1.90	+1.89 +1.64	+2.41 +2.62	+1.29 +0.92	+2.85 +2.88
Large-R jet top-tagging [%]	+13.75 -11.20	+12.76 -12.18	+13.00 -11.99	+13.24 -10.42	+13.85 -13.90	+2.96 -11.49	+11.80 +15.00	+11.46 -8.05
Leptons [%]	-	-	-	+0.14	-	-	+0.01	-
Luminosity [%]	+2.05 +0.06	+2.03 +0.10	+1.98 +0.06	+2.03 +0.05	+2.00 +0.06	+1.99 +0.14	+1.96 +0.07	+2.01 +0.07
MET/PU [%]	+0.10 +0.59	-0.14 +0.29	-0.10 +0.41	-0.09 +0.32	-0.19 +0.33	-0.18 +0.29	-0.10 +0.49	-0.10 +0.48
Narrow jets [%]	-0.41 +2.62	-0.22 +3.17	-0.26 +3.09	-0.21 +3.40	-0.55 +4.05	-0.27 +4.63	-0.28 +5.08	-1.12 +11.71
(MOD) Monte Carlo sample statistics [%]	+15.81	+10.75	+14.09	+8.15	+8.68	+19.20	+9.48	+4.38
(MOD) Alternative hard-scattering model [%]	+21.99	+17.07	+19.82	+18.21	+17.58	+27.02	+21.75	+15.14
(MOD) ISR/FSR + scale [%]	+2.54	+0.82	+1.44	+0.58	+1.67	+1.22	+2.75	+0.65

Table 114: Summary of systematic uncertainties in the parton level phase-space absolute differential cross-sections for the $t\bar{t}|y|$ calculated as a percentage of the cross-section in each bin.

Bins [GeV]	[0,0.2]	[0.2,0.4]	[0.4,0.6]	[0.6,0.8]	[0.8,1]	[1,1.2]	[1.2,1.5]	[1.5,2]
Total Uncertainty [%]	+7.60 -7.57	+7.27 -7.33	+7.19 -7.23	+8.93 -8.81	+9.78 -9.84	+15.93 -15.97	+12.69 -12.88	+30.80 -30.53
Statistics [%]	±4.63	±5.34	±5.88	±6.38	±7.46	±8.90	±10.29	±19.80
Systematics [%]	+5.53 -5.49	+3.97 -4.07	+2.92 -3.01	+5.33 -5.13	+4.98 -5.11	+12.42 -12.46	+5.55 -5.96	+20.58 -20.17
Background [%]	-	-	-	-	-	+0.02	+0.02	+0.03
Flavor tagging [%]	+0.33 -0.35	+0.41 -0.39	+0.44 -0.48	+0.22 -0.22	+0.38 -0.35	+1.24 -1.22	+0.61 -0.68	+1.10 -1.06
Large-R jet energy scale [%]	+0.41 +0.25	+0.38 -0.73	+0.36 -0.37	+0.56 -0.58	+0.34 -0.31	+0.70 -0.92	+0.55 -0.39	+2.61 +1.51
Large-R jet mass scale [%]	+0.94 +0.11	+0.50 -0.56	+1.00 -1.14	+0.43 -0.60	+0.36 -0.52	+1.11 -1.31	+2.24 -2.33	+1.23 +1.98
Large-R jet top-tagging [%]	+0.68 -0.08	+0.15 -	+0.27 -0.09	+1.10 -0.02	+0.07 -0.83	+0.54 -0.13	+0.05 +1.46	+2.43 -0.01
Leptons [%]	-0.02 +0.03	-0.03 +0.02	-0.03 +0.03	-0.01 +0.01	-0.03 +0.02	-0.02 +0.02	-0.02 +0.06	-0.02 -
Luminosity [%]	+0.04 -0.04	-0.02 +0.03	-0.03 +0.01	-0.01 +0.02	-0.02 +0.02	-0.02 +0.07	-0.05 +0.01	-
MET/PU [%]	+0.01 -0.01	+0.03 -0.03	+0.03 -0.01	+0.01 -0.01	+0.02 -0.01	+0.02 -0.07	+0.07 -0.07	-
Narrow jets [%]	+0.26 -0.25	+0.03 -0.05	+0.08 -0.07	+0.11 -0.09	+0.44 -0.48	+0.16 -0.15	+0.20 -0.07	+1.11 -0.99
(MOD) Monte Carlo sample statistics [%]	±2.40	±2.93	±2.94	±3.26	±3.90	±4.51	±4.96	±11.53
(MOD) Alternative hard-scattering model [%]	±4.31	±1.45	±2.35	±4.40	±3.80	±8.16	±2.89	±18.65
(MOD) Alternative parton-shower mode [%]	±2.69	±3.44	±0.01	±2.02	±2.81	±8.97	±2.39	±5.85
(MOD) ISR/FSR + scale [%]	±1.11	±0.68	±0.06	±0.89	±0.21	±0.16	±1.27	±2.17

Table 115: Summary of systematic uncertainties in the parton level phase-space relative differential cross-sections for the $t\bar{t}|y|$ calculated as a percentage of the cross-section in each bin.

Not reviewed, for internal circulation only

Bins [GeV]	[1,1.5]	[1.5,2]	[2,3]	[3,4]	[4,5]	[5,7]	[7,10]
Total Uncertainty [%]	+32.02 -31.01	+31.57 -29.22	+34.18 -34.79	+34.41 -30.28	+33.10 -33.68	+35.96 -35.16	+37.08 -33.48
Statistics [%]	± 4.42	± 5.47	± 5.12	± 7.17	± 9.95	± 9.28	± 14.63
Systematics [%]	+31.64 -30.61	+30.96 -28.56	+33.69 -34.31	+33.47 -29.20	+30.98 -31.59	+34.45 -33.61	+33.18 -29.09
Background [%]	+0.06 -0.06	+0.07 -0.07	+0.05 -0.05	+0.04 -0.05	+0.05 -0.06	+0.03 -0.04	+0.05 -0.05
Flavor tagging [%]	+8.58 -8.37	+8.35 -8.17	+8.21 -8.02	+7.99 -7.80	+8.12 -7.98	+8.89 -8.69	+7.98 -7.81
Large-R jet energy scale [%]	+6.36 -5.38	+6.34 -5.38	+5.62 -5.68	+6.50 -5.66	+6.42 -6.25	+5.83 -7.04	+5.29 -4.01
Large-R jet mass scale [%]	+1.80 -2.10	+0.68 -0.81	+1.29 -1.76	+2.35 -1.26	+1.78 -1.35	+1.66 -1.70	+3.39 -2.50
Large-R jet top-tagging [%]	+12.94 -12.06	+14.08 -11.81	+12.06 -12.89	+14.55 -9.68	+12.17 -13.12	+13.91 -12.29	+14.44 -9.98
Leptons [%]	-	-	-	-	+0.32	-	-
Luminosity [%]	+2.00 -2.00	+2.02 -2.02	+1.97 -1.96	+2.03 -2.03	+1.97 -1.97	+2.10 -2.10	+1.93 -1.93
MET/PU [%]	+0.12 -0.15	+0.07 -0.11	+0.05 -0.09	+0.03 -0.08	+0.13 -0.16	-	+0.07 -0.10
Narrow jets [%]	+0.43 -0.34	+0.42 -0.14	+0.37 -0.37	+0.27 -0.22	+0.42 -0.21	+0.39 -0.65	+0.38 -0.20
(MOD) Monte Carlo sample statistics [%]	± 2.26	± 2.86	± 2.67	± 3.54	± 6.09	± 4.49	± 7.77
(MOD) Alternative hard-scattering model [%]	± 9.34	± 9.46	± 13.30	± 14.06	± 9.53	± 16.91	± 17.08
(MOD) Alternative parton-shower mode [%]	± 20.29	± 17.62	± 22.89	± 18.22	± 20.11	± 18.53	± 15.51
(MOD) ISR/FSR + scale [%]	± 1.06	± 2.53	± 2.06	∓ 1.64	± 2.84	∓ 3.43	± 1.54

Table 116: Summary of systematic uncertainties in the parton level phase-space absolute differential cross-sections for the $|\chi^{t\bar{t}}|$ calculated as a percentage of the cross-section in each bin.

Bins [GeV]	[1,1.5]	[1.5,2]	[2,3]	[3,4]	[4,5]	[5,7]	[7,10]
Total Uncertainty [%]	+5.11 -5.15	+7.26 -7.18	+6.86 -7.05	+9.37 -8.88	+11.85 -11.97	+12.80 -12.90	+18.57 -18.38
Statistics [%]	± 3.71	± 5.07	± 4.60	± 6.81	± 9.72	± 9.05	± 14.31
Systematics [%]	+2.96 -3.02	+4.44 -4.32	+4.48 -4.77	+5.45 -4.56	+3.34 -3.76	+7.90 -8.06	+9.06 -8.67
Background [%]	-	+0.01 -0.02	-	+0.01 -0.01	-	+0.02 -0.01	-
Flavor tagging [%]	+0.32 -0.30	+0.39 -0.42	+0.18 -0.18	+0.90 -0.88	+0.42 -0.49	+0.80 -0.80	+0.68 -0.79
Large-R jet energy scale [%]	+0.30 -0.11	+0.34 -0.52	+0.33 -0.20	+0.39 -0.12	+0.37 -0.12	+0.17 -1.25	+1.17 -0.75
Large-R jet mass scale [%]	+0.47 -0.63	+0.95 -0.98	+0.05 -0.50	+0.78 -0.16	+0.32 -0.07	+0.13 -0.43	+1.49 -1.40
Large-R jet top-tagging [%]	-0.29 -0.29	-0.14 -0.14	+0.01 -0.95	+1.94 -	-	+0.75 -1.31	+1.54 -0.32
Leptons [%]	-	-	-	-	+0.30	-	-0.05
Luminosity [%]	-0.02 -	-0.02 +0.02	-0.02 +0.04	-0.04 +0.03	-0.02 +0.03	-0.04 +0.09	-0.02 +0.08
MET/PU [%]	+0.04 -0.04	-	+0.02 -0.02	+0.02 -0.03	+0.03 -0.03	+0.06 -0.10	+0.08 -0.08
Narrow jets [%]	+0.15 -0.14	+0.23 -0.19	+0.03 -0.12	+0.07 -0.12	+0.13 -0.06	+0.15 -0.44	+0.28 -0.25
(MOD) Monte Carlo sample statistics [%]	± 1.91	± 2.68	± 2.41	± 3.42	± 5.89	± 4.41	± 7.60
(MOD) Alternative hard-scattering model [%]	∓ 2.64	∓ 2.50	± 1.84	± 2.69	∓ 2.43	± 5.93	± 6.11
(MOD) Alternative parton-shower mode [%]	∓ 0.59	± 2.74	∓ 3.84	± 2.00	∓ 0.37	± 1.61	± 5.37
(MOD) ISR/FSR + scale [%]	∓ 0.02	± 1.46	± 0.97	∓ 2.74	± 1.79	∓ 4.61	± 0.48

Table 117: Summary of systematic uncertainties in the parton level phase-space relative differential cross-sections for the $|\chi^{t\bar{t}}|$ calculated as a percentage of the cross-section in each bin.

Not reviewed, for internal circulation only

Bins [GeV]	[0,0.2]	[0.2,0.4]	[0.4,0.6]	[0.6,0.8]	[0.8,1]	[1,1.3]	[1.3,2]
Total Uncertainty [%]	+35.87 -34.49	+31.30 -29.96	+32.35 -30.79	+30.90 -29.54	+33.90 -33.20	+37.08 -36.12	+33.57 -33.95
Statistics [%]	± 5.07	± 5.57	± 6.09	± 6.65	± 7.70	± 7.57	± 11.58
Systematics [%]	+35.42 -34.01	+30.66 -29.29	+31.62 -30.03	+30.00 -28.60	+32.77 -32.05	+36.10 -35.12	+30.97 -31.38
Background [%]	+0.05 -0.05	+0.06 -0.06	+0.06 -0.06	+0.06 -0.06	+0.05 -0.05	+0.07 -0.07	+0.05 -0.05
Flavor tagging [%]	+8.46 -8.27	+8.62 -8.40	+8.28 -8.10	+8.45 -8.25	+8.30 -8.11	+7.74 -7.60	+8.30 -8.13
Large-R jet energy scale [%]	+5.90 -5.56	+5.64 -5.24	+6.49 -5.62	+6.48 -6.35	+5.76 -5.58	+7.02 -5.74	+8.09 -6.48
Large-R jet mass scale [%]	+2.24 -2.61	+1.68 -1.69	+0.82 -0.43	+2.36 -2.44	+1.89 -1.53	+1.75 -1.80	+1.54 -0.69
Large-R jet top-tagging [%]	+13.05 -11.20	+13.59 -12.24	+13.19 -11.71	+12.93 -11.36	+13.41 -12.69	+13.48 -12.81	+10.98 -12.66
Leptons [%]	-	-	+0.11	-	-	-	+0.02
Luminosity [%]	+2.04 -2.03	+2.05 -2.05	+1.98 -1.98	+2.04 -2.04	+1.97 -1.97	+1.98 -1.98	+1.98 -1.98
MET/PU [%]	+0.05 -0.09	+0.11 -0.15	+0.06 -0.10	+0.01 -0.06	+0.09 -0.13	+0.14 -0.17	+0.07 -0.10
Narrow jets [%]	+0.54 -0.40	+0.45 -0.30	+0.31 -0.21	+0.33 -0.41	+0.19 -0.26	+0.33 -0.28	+0.80 -0.52
(MOD) Monte Carlo sample statistics [%]	± 2.58	± 2.94	± 3.04	± 3.29	± 3.97	± 3.78	± 5.80
(MOD) Alternative hard-scattering model [%]	± 16.03	± 10.74	± 12.12	± 8.94	± 11.37	± 15.51	± 4.00
(MOD) Alternative parton-shower mode [%]	± 22.26	± 17.52	± 18.63	± 17.67	± 20.84	± 22.68	± 22.07
(MOD) ISR/FSR + scale [%]	∓ 2.22	± 0.19	± 0.62	∓ 1.50	∓ 1.82	∓ 3.79	± 0.84

Table 118: Summary of systematic uncertainties in the parton level phase-space absolute differential cross-sections for the $y_B^{\bar{t}t}$ calculated as a percentage of the cross-section in each bin.

Bins [GeV]	[0,0.2]	[0.2,0.4]	[0.4,0.6]	[0.6,0.8]	[0.8,1]	[1,1.3]	[1.3,2]
Total Uncertainty [%]	+7.80 -7.76	+6.96 -6.97	+7.26 -7.34	+8.56 -8.62	+8.53 -8.64	+10.22 -10.26	+16.48 -16.63
Statistics [%]	± 4.61	± 5.18	± 5.68	± 6.25	± 7.34	± 7.19	± 11.23
Systematics [%]	+5.83 -5.77	+3.78 -3.79	+3.51 -3.67	+4.94 -5.03	+2.11 -2.54	+6.30 -6.37	+10.68 -10.91
Background [%]	-0.01 -0.01	-0.01 +0.31	-0.01 +0.43	-	-0.01 +0.23	-0.02 +0.95	+0.03 +0.93
Flavor tagging [%]	-0.34 -0.34	-0.38 +0.39	-0.49 +0.43	-0.19 +0.21	-0.24 +0.23	-0.96 +0.95	-0.97 +0.97
Large-R jet energy scale [%]	+0.15 -0.15	+0.49 +0.49	+0.53 +0.53	+0.31 +0.31	+0.36 +0.36	+0.75 +0.75	+1.70 +1.70
Large-R jet mass scale [%]	+0.93 -1.05	+0.13 -0.23	+1.62 -1.72	+1.02 -1.12	+0.28 -0.55	+0.42 -0.63	+1.84 -1.99
Large-R jet top-tagging [%]	+0.83 -0.10	+0.41 -0.36	+0.34 -0.08	+0.64 -0.19	+0.31 -0.82	+0.39 -0.97	+0.10 +0.01
Leptons [%]	-0.02 -0.02	-0.04 +0.02	-	-0.03 +0.02	-0.02 +0.04	-0.02 +0.03	-0.02 +0.03
Luminosity [%]	-0.02 -0.02	-0.04 +0.03	-0.03 +0.03	-0.03 +0.02	-0.04 +0.05	-0.03 +0.02	-0.03 +0.03
MET/PU [%]	+0.02 -0.03	+0.03 -0.04	+0.01 -0.02	+0.05 -0.06	+0.02 -0.02	+0.06 -0.06	- -
Narrow jets [%]	+0.24 -0.24	+0.12 -0.12	+0.13 -0.12	+0.18 -0.25	+0.30 -0.32	+0.14 -0.12	+0.45 -0.37
(MOD) Monte Carlo sample statistics [%]	± 2.36	± 2.72	± 2.86	± 3.13	± 3.79	± 3.62	± 5.62
(MOD) Alternative hard-scattering model [%]	∓ 4.53	± 1.49	∓ 0.08	± 3.54	± 0.77	∓ 3.93	± 9.15
(MOD) Alternative parton-shower mode [%]	± 2.93	∓ 2.99	± 1.61	∓ 2.81	± 1.16	± 3.44	± 2.69
(MOD) ISR/FSR + scale [%]	∓ 1.15	± 1.33	± 1.74	∓ 0.39	∓ 0.71	∓ 2.74	± 2.01

Table 119: Summary of systematic uncertainties in the parton level phase-space relative differential cross-sections for the $y_B^{\bar{t}t}$ calculated as a percentage of the cross-section in each bin.

Not reviewed, for internal circulation only

Bins [GeV]	[0,20]	[20,40]	[40,60]	[60,100]	[100,200]	[200,300]	[300,600]
Total Uncertainty [%]	+29.36 -27.63	+33.82 -31.29	+32.23 -31.30	+34.94 -37.12	+34.02 -31.65	+35.30 -33.35	+47.17 -45.94
Statistics [%]	± 4.39	± 4.83	± 6.76	± 7.35	± 7.69	± 12.97	± 17.71
Systematics [%]	+28.95 -27.19	+33.37 -30.81	+31.25 -30.28	+33.86 -36.10	+32.72 -30.26	+31.89 -29.73	+41.92 -40.53
Background [%]	+0.02 -0.02	+0.04 -0.04	+0.06 -0.06	+0.07 -0.08	+0.09 -0.10	+0.12 -0.13	+0.14 -0.16
Flavor tagging [%]	+8.38 -8.18	+8.33 -8.16	+8.05 -7.88	+8.81 -8.54	+8.21 -8.03	+8.83 -8.61	+8.02 -7.92
Large-R jet energy scale [%]	+5.11 -4.33	+6.57 -5.71	+5.61 -5.94	+6.17 -7.88	+8.11 -4.68	+7.33 -9.19	+9.64 -7.08
Large-R jet mass scale [%]	+1.89 -1.86	+1.46 -1.57	+1.45 -1.21	+1.75 -1.99	+1.89 -2.29	+4.45 -1.73	+1.83 -1.41
Large-R jet top-tagging [%]	+12.44 -10.70	+14.46 -11.77	+13.58 -12.36	+11.31 -13.55	+14.44 -13.21	+13.51 -10.19	+12.91 -12.44
Leptons [%]	-	-	-	+0.15	-	+0.02	-
Luminosity [%]	+2.01 -2.00	+2.05 -2.05	+2.06 -2.06	+2.05 -2.05	+1.93 -1.93	+1.98 -1.98	+1.76 -1.75
MET/PU [%]	+0.04 -0.07	+0.04 -0.13	+0.09 -0.14	+0.03 -0.07	+0.14 -0.18	+0.05 -0.09	+0.26 -0.29
Narrow jets [%]	+0.25 -0.11	+0.38 -0.23	+0.46 -0.37	+0.35 -0.62	+0.43 -0.24	+0.75 -0.76	+1.40 -1.15
(MOD) Monte Carlo sample statistics [%]	± 2.11	± 2.55	± 4.10	± 4.54	± 5.23	± 7.77	± 12.42
(MOD) Alternative hard-scattering model [%]	∓ 6.28	∓ 12.05	∓ 11.11	∓ 13.01	∓ 7.15	∓ 10.18	± 11.75
(MOD) Alternative parton-shower mode [%]	± 18.83	± 19.63	± 18.63	± 23.52	± 19.63	± 15.48	± 31.81
(MOD) ISR/FSR + scale [%]	∓ 0.61	∓ 0.10	∓ 0.14	∓ 1.86	± 2.39	± 8.75	± 2.53

Table 120: Summary of systematic uncertainties in the parton level phase-space absolute differential cross-sections for the $p_{out}^{t\bar{t}}$ calculated as a percentage of the cross-section in each bin.

Bins [GeV]	[0,20]	[20,40]	[40,60]	[60,100]	[100,200]	[200,300]	[300,600]
Total Uncertainty [%]	+6.12 -5.76	+7.08 -6.87	+8.68 -8.74	+11.13 -11.98	+9.69 -9.36	+20.36 -19.61	+33.96 -33.64
Statistics [%]	± 3.97	± 4.38	± 6.40	± 7.05	± 7.24	± 12.77	± 17.16
Systematics [%]	+4.13 -3.58	+4.96 -4.65	+4.34 -4.46	+7.46 -8.67	+4.31 -3.52	+13.87 -12.75	+26.79 -26.39
Background [%]	+0.04 -0.04	+0.02 -0.02	-	+0.02 -0.02	+0.04 -0.04	+0.06 -0.07	+0.08 -0.10
Flavor tagging [%]	+0.24 -0.24	+0.47 -0.52	+1.04 -1.09	+1.25 -1.09	+0.27 -0.28	+1.61 -1.56	+1.15 -1.26
Large-R jet energy scale [%]	+1.45 -1.23	+0.39 -0.12	-1.09 -0.82	+0.10 -2.28	+2.09 -3.76	+1.98 -3.76	+3.64 -1.81
Large-R jet mass scale [%]	+0.57 -0.48	+0.42 -0.48	+0.73 -0.47	+0.57 -1.39	+0.56 -1.02	+5.57 -3.07	+1.47 -1.19
Large-R jet top-tagging [%]	+1.39 -0.66	+1.19 -0.03	+0.38 -0.53	+0.10 -1.76	+1.19 -1.39	+1.84 -0.32	+0.17 -0.60
Leptons [%]	-	-	-	+0.13	-	+0.02	-
Luminosity [%]	-0.02 -	-0.03 +0.04	-0.02 +0.06	-0.03 +0.04	-0.03 +0.07	-0.02 +0.02	-0.05 +0.25
MET/PU [%]	+0.05 -0.17	+0.01 -0.15	+0.01 -0.18	+0.04 -0.50	+0.04 -0.03	+0.06 -0.75	+0.02 -0.99
Narrow jets [%]	-0.17 -0.19	-0.15 +0.17	-0.18 +0.15	-0.50 +0.24	-0.50 +0.16	-0.03 +0.45	-0.75 +1.16
(MOD) Monte Carlo sample statistics [%]	± 2.14	± 2.52	± 3.93	± 4.31	± 4.79	± 7.67	± 11.87
(MOD) Alternative hard-scattering model [%]	± 1.90	∓ 4.36	∓ 3.34	∓ 5.41	± 0.96	∓ 2.33	± 21.51
(MOD) Alternative parton-shower mode [%]	∓ 1.71	∓ 0.72	∓ 1.97	∓ 4.16	∓ 0.71	∓ 5.91	± 14.55
(MOD) ISR/FSR + scale [%]	∓ 1.15	∓ 0.64	∓ 0.66	∓ 2.41	± 1.87	± 8.35	± 2.04

Table 121: Summary of systematic uncertainties in the parton level phase-space relative differential cross-sections for the $p_{out}^{t\bar{t}}$ calculated as a percentage of the cross-section in each bin.

Bins [GeV]	[1000,1050]	[1050,1100]	[1100,1150]	[1150,1200]	[1200,1250]	[1250,1300]	[1300,1400]	[1400,1600]	[1600,1800]	[1800,2500]
Total Uncertainty [%]	+32.53 -32.74	+34.00 -33.93	+32.93 -33.03	+34.14 -34.05	+35.33 -35.12	+37.57 -36.96	+42.54 -40.46	+48.02 -46.46	+53.50 -51.77	+73.76 -64.14
Statistics [%]	+6.49 +31.79	+4.58 +33.60	+5.99 +32.20	+7.33 +33.04	+9.17 +33.84	+9.17 +36.05	+11.55 +10.52	+13.77 +15.67	+22.18 +22.75	+44.85 +55.11
Systematics [%]	-32.02 +0.02	-33.20 +0.05	-32.26 -0.05	-33.57 -0.05	-31.53 -0.05	-32.38 -0.06	-38.60 -31.64	-41.64 -40.65	-56.02 -50.04	
Background [%]	-0.05 +0.09	-0.05 +0.04	-0.05 +0.04	-0.05 +0.04	-0.05 +0.04	-0.06 +0.04	-0.06 +0.04	-0.05 +0.03	-0.08 +0.03	-0.04 +0.04
Flavor tagging [%]	-7.72 +4.84	-7.93 +5.60	-8.25 +6.15	-8.64 +5.66	-8.87 +6.60	-9.04 +7.04	-9.46 +10.60	-9.58 +15.37	-11.17 +17.82	-14.99 +18.00
Large-R jet energy scale [%]	+1.20 +1.03	+1.56 +1.04								
Large-R jet mass scale [%]	-1.33 +1.03	-1.66 +1.04	-1.58 +1.04	-1.27 +1.04	-1.34 +1.04	-1.31 +1.04	-0.50 +0.50	+1.05 +1.05	+1.69 +1.69	+10.50 +17.74
Large-R jet top-tagging [%]	-10.60 +10.43	-11.09 +11.04	-12.69 +12.23	-13.70 +13.92	-13.92 -14.49	-15.33 -15.33	-16.94 -16.94	-19.74 -19.74	-26.31 -26.31	
Leptons [%]	- -	+0.54 +0.54	+0.01 +0.01							
Luminosity [%]	+2.06 +2.06	+2.05 +2.05	+2.02 +1.99	+1.99 +1.99	+2.00 +2.00	+2.05 +2.07	+2.05 +2.07	+1.89 +1.88	+1.98 +1.97	+1.98 +1.97
MET/PU [%]	+0.09 +0.49	+0.10 +0.44	+0.11 +0.47	+0.08 +0.47	+0.04 +0.44	+0.03 +0.28	+0.13 +0.28	+0.03 +0.47	+0.11 +0.38	+0.19 +1.14
Narrow jets [%]	-0.51 +2.21	-0.25 +2.53	-0.11 +3.81	-0.37 +4.47	-0.52 +5.51	-0.37 +5.26	-0.27 +5.87	-0.57 +5.40	-0.14 +9.50	-0.84 +19.79
(MOD) Monte Carlo sample statistics [%]	+11.48 ±2.21	±10.51 ±2.53	±11.61 ±3.81	±14.39 ±4.47	±10.12 ±5.51	±8.97 ±5.26	±17.95 ±5.87	±16.83 ±5.40	±16.87 ±9.50	±12.26 ±19.79
(MOD) Alternative hard-scattering model [%]	+23.30 ±2.30	±24.52 ±2.52	±21.03 ±2.01	±20.01 ±19.39	±19.94 ±19.94	±20.33 ±20.33	±22.58 ±22.58	±17.92 ±17.92	±16.21 ±16.21	
(MOD) ISR/FSR + scale [%]	±1.27 ±1.27	±1.42 ±1.42	±1.62 ±1.62	±0.66 ±0.66	±0.31 ±1.27	±2.06 ±1.14	±2.10 ±1.20	±3.99 ±3.99	±1.59 ±1.59	±2.52 ±2.52

Table 122: Summary of systematic uncertainties in the parton level phase-space absolute differential cross-sections for the $H_T^{\tilde{t}\tilde{t}}$ calculated as a percentage of the cross-section in each bin.

Bins [GeV]	[1000,1050]	[1050,1100]	[1100,1150]	[1150,1200]	[1200,1250]	[1250,1300]	[1300,1400]	[1400,1600]	[1600,1800]	[1800,2500]	
Total Uncertainty [%]	+8.44 -8.43	+7.35 -7.35	+7.48 -7.47	+9.44 -9.43	+11.91 -11.93	+12.78 -12.78	+15.58 -15.58	+19.72 -19.72	+31.00 -31.00	+56.74 -54.82	
Statistics [%]	±5.62 +5.91	±3.76 +5.84	±5.81 +2.93	±7.26 +4.14	±8.34 +4.02	±8.90 +7.51	±11.16 +9.14	±13.21 +13.59	±21.97 +19.59	±44.04 +29.66	
Systematics [%]	-6.86 -6.86	-3.85 -4.03	-4.03 -4.81	-4.95 -4.95	-5.65 -5.65	-9.15 -9.15	-12.46 -12.46	-14.78 -14.78	-35.19 -35.19		
Background [%]	-0.01 +0.10	-0.01 +0.08	-0.01 +0.07	-0.05 +0.07	-0.02 +0.05	-0.02 +0.04	-0.03 +0.04	-0.01 +0.03	+0.02 +0.02	+0.04 +0.04	
Flavor tagging [%]	+1.50 +1.46	+1.12 -1.19	+0.96 -0.98	+0.57 -0.71	+0.53 -0.50	+1.11 -1.16	+1.80 -1.80	+1.96 +4.43	+4.42 +9.31	+8.63 +12.05	
Large-R jet energy scale [%]	+1.40 +1.05	+0.97 +0.40	+1.31 +0.30	+1.79 +0.08	+3.11 +0.71	+2.18 +0.73	+0.98 +0.98	+4.43 +3.55	+9.37 +3.99	+12.05 +3.93	
Large-R jet mass scale [%]	-0.35 +0.29	-0.40 +2.42	-0.37 +0.66	-0.19 +0.01	+1.97 +0.01	-0.67 +0.01	-0.96 +0.01	+2.74 +4.67	+2.89 +7.58	+9.68 +11.92	
Large-R jet top-tagging [%]	-3.55 -2.77	-2.42 -1.94	-1.42 -1.42	-0.37 -0.37	-1.39 -1.39	-2.29 -2.29	-2.74 +4.70	+2.89 +7.58	+11.92 +14.29		
Leptons [%]	-0.04 +0.03	-0.04 +0.02	-0.04 +0.03	-0.04 +0.03	-0.05 +0.01	-0.05 +0.05	-0.07 +0.03	-0.01 +0.14	+0.02 +0.04	+0.04 +0.03	
Luminosity [%]	-0.04 +0.01	-0.03 +0.01	-0.03 +0.02	-0.04 +0.02	-0.02 +0.03	-0.06 +0.06	-0.03 +0.06	-0.14 +0.07	-0.05 +0.05	-0.05 +0.02	
MET/PU [%]	- +	- +	- +	- +	- +	- +	- +	- +	- +	- +	
Narrow jets [%]	+0.12 -0.21	+0.06 -0.07	+0.17 -0.09	+0.09 -0.13	+0.09 -0.21	+0.23 -0.28	+0.38 -0.41	+0.21 -0.30	+0.42 -0.07	+0.69 -0.66	
(MOD) Monte Carlo sample statistics [%]	±2.19 ±2.19	±2.42 ±2.42	±3.69 ±3.69	±4.38 ±4.38	±5.46 ±5.26	±5.88 ±5.88	±5.42 ±5.42	±9.74 ±9.74	±20.00 ±5.00		
(MOD) Alternative hard-scattering model [%]	±1.17 ±1.17	±2.27 ±2.27	±1.01 ±1.01	±2.16 ±2.16	±2.72 ±2.72	±4.03 ±4.03	±6.22 ±6.22	±4.95 ±4.95	±5.00 ±5.00	±0.28 ±0.28	
(MOD) Alternative parton-shower mode [%]	±1.97 ±1.97	±3.54 ±3.54	±0.92 ±0.92	±2.22 ±2.22	±3.02 ±2.32	±2.32 ±1.82	±1.06 ±1.06	±4.90 ±4.90	±7.08 ±7.08		
(MOD) ISR/FSR + scale [%]	±2.22 ±2.22	±0.50 ±0.50	±0.69 ±0.69	±0.29 ±1.27	±1.27 ±1.14	±1.20 ±1.20	±3.08 ±3.08	±0.66 ±0.66	±1.53 ±1.53		

Table 123: Summary of systematic uncertainties in the parton level phase-space relative differential cross-sections for the $H_T^{\tilde{t}\tilde{t}}$ calculated as a percentage of the cross-section in each bin.

Bins [GeV]	[0,2.5]	[2.5,2.75]	[2.75,3]	[3,3.15]
Total Uncertainty [%]	+70.18 -70.93	+37.85 -33.54	+34.25 -34.70	+31.79 -30.15
Statistics [%]	±15.05	±11.31	±5.85	±2.79
Systematics [%]	+67.99 -68.77	+35.36 -30.70	+33.55 -34.00	+31.64 -30.00
Background [%]	+0.14 -0.16	+0.14 -0.15	+0.09 -0.09	+0.04 -0.04
Flavor tagging [%]	+7.90 -7.80	+8.29 -8.08	+8.50 -8.33	+8.34 -8.14
Large-R jet energy scale [%]	+6.51 -5.42	+10.72 -8.66	+6.50 -6.42	+5.78 -5.20
Large-R jet mass scale [%]	+1.04 -0.50	+2.05 -0.80	+1.79 -1.86	+1.60 -1.65
Large-R jet top-tagging [%]	+10.84 -13.62	+14.09 -9.48	+12.26 -12.96	+13.38 -11.67
Leptons [%]	—	—	+0.10	—
Luminosity [%]	+1.89 -1.89	+1.88 -1.88	+2.02 -2.01	+2.03 -2.03
MET/PU [%]	— -0.03	+0.07 —	+0.02 —	+0.01 —
Narrow jets [%]	+1.62 -1.65	+0.45 -0.19	+0.34 -0.48	+0.33 -0.18
(MOD) Monte Carlo sample statistics [%]	±8.68	±7.36	±3.71	±1.26
(MOD) Alternative hard-scattering model [%]	±57.07	±19.74	±11.35	±11.38
(MOD) Alternative parton-shower mode [%]	±31.08	±11.80	±22.96	±19.16
(MOD) ISR/FSR + scale [%]	±1.49	±3.59	±0.78	±0.68

Table 124: Summary of systematic uncertainties in the parton level phase-space absolute differential cross-sections for the $|\Delta\phi^{\tilde{t}\tilde{t}}|$ calculated as a percentage of the cross-section in each bin.

Bins [GeV]	[0,2.5]	[2.5,2.75]	[2.75,3]	[3,3.15]
Total Uncertainty [%]	+69.32 -69.35	+24.22 -23.69	+9.73 -10.01	+7.18 -7.26
Statistics [%]	±13.99	±11.23	±5.41	±2.16
Systematics [%]	+67.41 -67.44	+20.20 -19.56	+7.36 -7.73	+6.73 -6.83
Background [%]	+0.08 -0.10	+0.08 -0.09	+0.03 -0.03	+0.03 -0.03
Flavor tagging [%]	+1.16 -1.14	+0.96 -0.94	+0.43 -0.52	+0.32 -0.30
Large-R jet energy scale [%]	+1.65 -1.48	+3.60 -2.24	+0.65 -0.55	+0.37 -0.20
Large-R jet mass scale [%]	+2.11 -1.81	+2.92 -2.02	+0.59 -0.93	+0.33 -0.36
Large-R jet top-tagging [%]	+0.25 -1.88	+0.57 -0.27	+0.05 -1.52	+0.03 -0.85
Leptons [%]	— -0.02	— -0.03	+0.08 —	— -0.02
Luminosity [%]	+0.12 -0.11	+0.12 -0.12	— -0.01	+0.02 -0.02
MET/PU [%]	+0.07 -0.10	+0.11 -0.10	+0.01 -0.02	— —
Narrow jets [%]	+1.19 -1.36	+0.43 -0.15	+0.06 -0.23	+0.19 -0.12
(MOD) Monte Carlo sample statistics [%]	±8.04	±7.25	±3.34	±1.23
(MOD) Alternative hard-scattering model [%]	±65.92	±15.22	±6.35	±6.38
(MOD) Alternative parton-shower mode [%]	±13.20	±11.08	±2.97	±1.82
(MOD) ISR/FSR + scale [%]	±0.69	±2.81	±1.60	±0.13

Table 125: Summary of systematic uncertainties in the parton level phase-space relative differential cross-sections for the $|\Delta\phi^{\tilde{t}\tilde{t}}|$ calculated as a percentage of the cross-section in each bin.

Not reviewed, for internal circulation only

Bins [GeV]	[0,0.2]	[0.2,0.4]	[0.4,0.6]	[0.6,0.7]	[0.7,0.8]	[0.8,1]
Total Uncertainty [%]	+32.64 -31.55	+32.31 -31.12	+33.27 -31.61	+33.47 -32.88	+34.85 -34.12	+46.90 -43.81
Statistics [%]	± 4.43	± 4.60	± 4.86	± 8.48	± 11.32	± 17.55
Systematics [%]	+32.26 -31.15	+31.89 -30.69	+32.82 -31.14	+31.96 -31.34	+32.37 -31.58	+42.34 -38.89
Background [%]	+0.06 -0.07	+0.06 -0.07	+0.05 -0.05	+0.03 -0.03	+0.05 -0.06	+0.05 -0.06
Flavor tagging [%]	+8.59	+8.46	+7.87	+8.71	+8.16	+8.20
Large-R jet energy scale [%]	-8.37 +6.33	-8.28 +6.29	-7.69 +5.97	-8.56 +6.38	-7.97 +4.84	-8.05 +6.43
Large-R jet mass scale [%]	-5.44 +1.61	-5.87 +1.14	-5.68 +1.60	-5.26 +1.77	-6.55 +2.21	-4.31 +3.56
Large-R jet top-tagging [%]	+1.87 -12.08	+1.47 -12.82	-0.99 -10.80	-1.79 +12.87	-1.86 +12.41	-3.52 +16.80
Leptons [%]	-	-	+0.08	-	-	-
Luminosity [%]	+2.02 -2.02	+1.98 -1.98	+1.98 -1.97	+2.06 -2.06	+2.01 -2.01	+1.99 -1.99
MET/PU [%]	+0.13	+0.05	+0.05	+0.03	-	+0.16
Narrow jets [%]	-0.16 +0.44	-0.09 +0.30	-0.09 +0.48	-0.08 +0.30	-0.05 +0.45	-0.20 +0.15
(MOD) Monte Carlo sample statistics [%]	± 2.26	± 2.36	± 2.39	± 5.15	± 6.22	± 9.92
(MOD) Alternative hard-scattering model [%]	± 9.80	± 11.01	± 13.50	± 13.07	± 15.31	± 24.23
(MOD) Alternative parton-shower mode [%]	± 20.87	± 18.55	± 20.53	± 18.70	± 19.34	± 21.33
(MOD) ISR/FSR + scale [%]	± 2.34	± 1.12	± 1.49	∓ 0.74	± 1.12	∓ 0.29

Table 126: Summary of systematic uncertainties in the parton level phase-space absolute differential cross-sections for the $|\cos \theta^*|$ calculated as a percentage of the cross-section in each bin.

Bins [GeV]	[0,0.2]	[0.2,0.4]	[0.4,0.6]	[0.6,0.7]	[0.7,0.8]	[0.8,1]
Total Uncertainty [%]	+5.30 -5.30	+5.18 -5.25	+5.66 -5.51	+10.23 -10.28	+13.45 -13.53	+24.88 -24.77
Statistics [%]	± 3.71	± 4.05	± 4.41	± 8.28	± 11.07	± 17.30
Systematics [%]	+3.27 -3.28	+2.46 -2.60	+2.75 -2.43	+3.35 -3.50	+4.61 -4.85	+14.99 -14.81
Background [%]	-	-	-	+0.03	+0.01	+0.02
Flavor tagging [%]	+0.31 -0.29	+0.40 -0.43	+0.86 -0.83	+0.95 -1.05	+1.02 -1.07	+0.34 -0.39
Large-R jet energy scale [%]	+0.45 -0.02	+0.22 -0.27	+0.12 -0.23	+0.53 -0.03	-	+1.36 -0.44
Large-R jet mass scale [%]	+0.24 -0.46	+0.24 -0.40	+0.65 -0.52	+0.41 -0.50	+0.71 -0.62	+2.31 -2.35
Large-R jet top-tagging [%]	+0.05 -0.30	+0.60 -0.76	+0.92 -0.43	+0.14 -0.77	+1.24 -0.64	+1.78 -1.36
Leptons [%]	-	-	+0.06	-	-	-
Luminosity [%]	+0.02 -0.02	+0.02 -0.02	+0.02 -0.02	+0.06 -0.06	+0.01 -0.01	-
MET/PU [%]	+0.05 -0.05	+0.02 -0.02	+0.02 -0.02	+0.04 -0.04	+0.06 -0.07	+0.09 -0.09
Narrow jets [%]	+0.14 -0.12	+0.20 -0.22	+0.22 -0.19	+0.15 -0.32	+0.23 -0.20	+0.08 -0.27
(MOD) Monte Carlo sample statistics [%]	± 1.90	± 2.09	± 2.23	± 4.97	± 6.08	± 9.75
(MOD) Alternative hard-scattering model [%]	∓ 2.60	∓ 1.22	± 1.60	± 1.12	± 3.67	± 13.81
(MOD) Alternative parton-shower mode [%]	± 1.26	∓ 1.63	± 0.83	∓ 1.46	∓ 0.65	± 1.82
(MOD) ISR/FSR + scale [%]	± 0.98	∓ 0.25	± 0.10	∓ 2.17	∓ 0.26	∓ 1.63

Table 127: Summary of systematic uncertainties in the parton level phase-space relative differential cross-sections for the $|\cos \theta^*|$ calculated as a percentage of the cross-section in each bin.

955 **G.4. Full breakdown tables**

[Not reviewed, for internal circulation only]

Not reviewed, for internal circulation only

Bins (GeV)	[450,500]	[500,550]	[550,600]	[600,650]	[650,700]	[750,900]	[900,1000]
$d\sigma/dX$ [pb/GeV]	$1.71 \cdot 10^{-3}$	$4.87 \cdot 10^{-3}$	$2.51 \cdot 10^{-3}$	$1.38 \cdot 10^{-3}$	$8.69 \cdot 10^{-4}$	$2.68 \cdot 10^{-3}$	$4.78 \cdot 10^{-3}$
Total Uncertainty [%]	+0.22	+2.26	+1.28	+0.94	+0.69	+0.44	+0.30
Statistics [%]	+0.06	+0.18	+0.33	+0.16	+0.09	+0.05	+0.03
Systematic [%]	+0.71	+1.78	+1.32	+0.85	+0.57	+0.37	+0.22
(FTAG) fTagSF_B , eigen0 [%]	-0.50	+0.50	+0.51	+0.50	+0.50	+0.50	+0.50
(FTAG) fTagSF_B , eigen1 [%]	+0.50	+0.50	+0.52	+0.50	+0.50	+0.50	+0.50
(FTAG) fTagSF_B , eigen2 [%]	+0.50	+0.50	+0.50	+0.50	+0.50	+0.50	+0.50
(FTAG) fTagSF_B , eigen3 [%]	+0.50	+0.50	+0.50	+0.50	+0.50	+0.50	+0.50
(FTAG) fTagSF_B , eigen4 [%]	+0.50	+0.50	+0.50	+0.50	+0.50	+0.50	+0.50
(FTAG) fTagSF_B , eigen5 [%]	+0.50	+0.50	+0.50	+0.50	+0.50	+0.50	+0.50
(FTAG) fTagSF_C , eigen0 [%]	+0.50	+0.50	+0.50	+0.50	+0.50	+0.50	+0.50
(FTAG) fTagSF_C , eigen1 [%]	+0.50	+0.50	+0.50	+0.50	+0.50	+0.50	+0.50
(FTAG) fTagSF_C , eigen2 [%]	+0.50	+0.50	+0.50	+0.50	+0.50	+0.50	+0.50
(FTAG) fTagSF_C , eigen3 [%]	+0.50	+0.50	+0.50	+0.50	+0.50	+0.50	+0.50
(FTAG) fTagSF_C , eigen4 [%]	+0.50	+0.50	+0.50	+0.50	+0.50	+0.50	+0.50
(FTAG) fTagSF_C , eigen5 [%]	+0.50	+0.50	+0.50	+0.50	+0.50	+0.50	+0.50
(FTAG) fTagSF_B , Light, eigen0 [%]	-0.73	+0.73	+0.73	+0.73	+0.73	+0.73	+0.73
(FTAG) fTagSF_B , Light, eigen1 [%]	-0.73	+0.73	+0.73	+0.73	+0.73	+0.73	+0.73
(FTAG) fTagSF_B , Light, eigen2 [%]	-0.73	+0.73	+0.73	+0.73	+0.73	+0.73	+0.73
(FTAG) fTagSF_B , Light, eigen3 [%]	-0.73	+0.73	+0.73	+0.73	+0.73	+0.73	+0.73
(FTAG) fTagSF_B , Light, eigen4 [%]	-0.73	+0.73	+0.73	+0.73	+0.73	+0.73	+0.73
(FTAG) fTagSF_B , Light, eigen5 [%]	-0.73	+0.73	+0.73	+0.73	+0.73	+0.73	+0.73
(FTAG) fTagSF_C , Light, eigen0 [%]	-0.73	+0.73	+0.73	+0.73	+0.73	+0.73	+0.73
(FTAG) fTagSF_C , Light, eigen1 [%]	-0.73	+0.73	+0.73	+0.73	+0.73	+0.73	+0.73
(FTAG) fTagSF_C , Light, eigen2 [%]	-0.73	+0.73	+0.73	+0.73	+0.73	+0.73	+0.73
(FTAG) fTagSF_C , Light, eigen3 [%]	-0.73	+0.73	+0.73	+0.73	+0.73	+0.73	+0.73
(FTAG) fTagSF_C , Light, eigen4 [%]	-0.73	+0.73	+0.73	+0.73	+0.73	+0.73	+0.73
(FTAG) fTagSF_C , Light, eigen5 [%]	-0.73	+0.73	+0.73	+0.73	+0.73	+0.73	+0.73
(FTAG) fTagSF_B , Light, eigen11 [%]	-0.04	+0.04	+0.04	+0.04	+0.04	+0.04	+0.04
(FTAG) fTagSF_B , Light, eigen12 [%]	-0.04	+0.04	+0.04	+0.04	+0.04	+0.04	+0.04
(FTAG) fTagSF_B , Light, eigen13 [%]	-0.04	+0.04	+0.04	+0.04	+0.04	+0.04	+0.04
(FTAG) fTagSF_B , Light, eigen14 [%]	-0.04	+0.04	+0.04	+0.04	+0.04	+0.04	+0.04
(FTAG) fTagSF_B , Light, eigen15 [%]	-0.04	+0.04	+0.04	+0.04	+0.04	+0.04	+0.04
(FTAG) fTagSF_B , extrapolation [%]	-2.70	+2.34	+2.37	+2.82	+2.65	+3.81	+6.52
(FTAG) fTagSF_B , extrapolation, from_charm [%]	-0.01	-0.01	-0.01	-0.01	-0.01	-0.01	-0.01
(MET/Pt) jet [k]	-0.03	+0.09	+0.10	+0.07	+0.01	+0.02	+0.07
Luminosity [%]	+0.07	+0.13	+0.13	+0.13	+0.13	+0.05	+0.09
(BKG) singletop, tchan [%]	-0.49	+0.49	+0.49	+0.49	+0.49	+0.49	+0.49
(BKG) tWW [%]	-0.04	+0.03	+0.04	+0.03	+0.05	+0.04	+0.07
(BKG) tZ [%]	-0.04	+0.03	+0.03	+0.03	+0.03	+0.03	+0.03
(BKG) tH [%]	-0.04	+0.03	+0.03	+0.03	+0.03	+0.03	+0.03
(LIES) LARGERET, Weak, JET, Rrk, Modelling, Tau32WTA [%]	-0.93	+0.93	+0.93	+0.93	+0.93	+0.93	+0.93
(LIES) LARGERET, Weak, JET, Rrk, Baseline, pT [%]	-0.93	+0.93	+0.93	+0.93	+0.93	+0.93	+0.93
(LIES) LARGERET, Weak, JET, Rrk, Baseline, mass [%]	-0.33	+0.33	+0.33	+0.33	+0.33	+0.33	+0.33
(LIES) LARGERET, Weak, JET, Rrk, Baseline, Tau32WTA [%]	-0.74	+0.74	+0.74	+0.74	+0.74	+0.74	+0.74
(JES) JET, 2INP, JET, BIES, Response [%]	-0.02	-0.01	-0.01	-0.01	-0.01	-0.01	-0.01
(JES) JET, 2INP, JET, Pileup, PTerm [%]	-0.02	-0.01	-0.01	-0.01	-0.01	-0.01	-0.01
(JES) JET, 2INP, JET, OffsetNPV [%]	-0.04	+0.04	+0.05	+0.02	-0.01	-0.01	-0.01
(JES) JET, 2INP, JET, Pileup, RhoTopology [%]	-0.20	+0.20	+0.20	+0.20	+0.19	+0.11	+0.16
(JES) JET, 2INP, JET, EffectiveNP, tTerm [%]	-0.04	+0.04	+0.04	+0.03	+0.03	+0.02	+0.03
(LEP) EG, SCALE, Rho, JES [%]	-0.49	+0.49	+0.49	+0.49	+0.49	+0.49	+0.49
(JES) JET, 2INP, JET, EffectiveNP, 3 [%]	-0.02	-0.01	-0.01	-0.01	-0.01	-0.01	-0.01
(JES) JET, 2INP, JET, EffectiveNP, 4 [%]	-0.48	+0.48	+0.48	+0.48	+0.48	+0.48	+0.48
(JES) JET, 2INP, JET, Weak, JET, Rrk, Tracking, mass [%]	-0.20	+0.20	+0.20	+0.20	+0.19	+0.17	+0.21
(JES) JET, 2INP, JET, Pileup, OffsetMu [%]	-0.02	-0.02	-0.02	-0.02	-0.02	-0.01	-0.01
(JES) JET, 2INP, JET, EtaUncalibration, NonClosure [%]	-0.06	-0.10	-0.05	-0.05	-0.04	-0.04	-0.07
(JES) JET, 2INP, JET, EtaUncalibration, TotalStat [%]	-0.16	-0.09	-0.09	-0.09	-0.07	-0.07	-0.06
(JES) JET, 2INP, JET, TotalStat, All [%]	-0.02	-0.02	-0.02	-0.02	-0.02	-0.01	-0.01
(JES) JET, 2INP, JET, Flavor, Baseline [%]	-0.01	-0.01	-0.01	-0.01	-0.01	-0.01	-0.01
(JES) JET, 2INP, JET, Flavor, Composition [%]	-0.33	+0.01	+0.01	+0.01	+0.21	+0.16	+0.11
(JES) JET, 2INP, JET, SingletParticle, HighPt [%]	-0.35	+0.39	+0.39	+0.39	+0.39	+0.39	+0.39
(JES) JET, 2INP, JET, SingleParticle, Modeling, pT [%]	-1.48	+2.74	+2.66	+1.67	+1.67	+1.45	+1.55
(JES) JET, 2INP, JET, TotalStat, All [%]	-2.71	+2.55	+1.83	+2.54	+1.20	+1.79	+1.57
(LEP) MUON, ID [%]	-0.49	+0.49	+0.49	+0.49	+0.49	+0.49	+0.49
(LEP) LARGERET, Weak, JET, Rrk, TotalStat, pT [%]	-	-	-	-	-	-	-
(LEP) MUON, SCALE [%]	-0.49	+0.49	+0.49	+0.49	+0.49	+0.49	+0.49
(LEP) EG, SCALE, ALL [%]	-	-	-	-	-	-	-0.85
(JES) JET, 2INP, JET, EffectiveNP, 7 [%]	-	-	-	-	-	-	+0.50
(JES) LARGERET, Weak, JET, Rrk, Modeling, mass [%]	-0.24	+0.39	+0.09	-	-0.31	+1.32	+1.14
(JES) MUON, MS [%]	-0.49	+0.49	+0.49	+0.49	+0.49	+0.49	+0.49
(JES) MUON, SAIGITA, RHO [%]	-0.49	+0.49	+0.49	+0.49	+0.49	+0.49	+0.49
(JES) JET, 2INP, JET, PunchThrough, MC15 [%]	-0.48	+0.48	+0.48	+0.48	+0.48	+0.48	+0.48
(JES) JET, 2INP, JET, EtaUncalibration, Modelling [%]	-0.03	-0.03	-0.03	-0.03	-0.03	-0.03	-0.44
(JES) JET, 2INP, JET, EffectiveNP, 2 [%]	-0.03	-0.03	-0.03	-0.03	-0.03	-0.03	-0.03
(JES) LARGERET, Weak, JET, Rrk, Tracking, Tau32WTA [%]	-0.92	+0.91	+0.92	+0.93	+0.93	+0.93	+0.92
(JES) LARGERET, Weak, JET, Rrk, Tracking, pT [%]	-0.70	+0.30	+0.32	+0.32	+0.31	+0.45	+0.59
(JES) LARGERET, Weak, JET, Rrk, Tracking, mass [%]	-0.49	+0.49	+0.49	+0.49	+0.49	+0.49	+0.49
(JES) JET, JER, SINGLE, NP [%]	-0.16	+0.22	+0.05	+0.04	+0.25	+0.02	+0.21
(JES) LARGERET, Weak, JET, Top, massRes, mass [%]	2.56	+1.10	+1.51	+1.88	+0.06	+1.86	+6.79
(PDF) PDF4LHC15_nlo_30_eigen01 [%]	0.19	+0.07	+0.06	+0.12	+0.06	+0.08	+0.89
(PDF) PDF4LHC15_nlo_30_eigen02 [%]	0.24	+0.18	+0.17	+0.17	+0.18	+0.14	+1.31
(PDF) PDF4LHC15_nlo_30_eigen03 [%]	0.02	+0.16	+0.09	+0.03	+0.10	+0.09	+1.17
(PDF) PDF4LHC15_nlo_30_eigen04 [%]	0.77	+0.73	+0.13	+0.19	+0.17	+0.22	+1.17
(PDF) PDF4LHC15_nlo_30_eigen05 [%]	0.67	+0.43	+0.40	+0.50	+0.42	+0.41	+1.09
(PDF) PDF4LHC15_nlo_30_eigen06 [%]	0.34	+0.21	+0.19	+0.31	+0.22	+0.22	+1.26
(PDF) PDF4LHC15_nlo_30_eigen07 [%]	0.05	+0.01	+0.02	+0.02	+0.02	+0.02	+0.97
(PDF) PDF4LHC15_nlo_30_eigen08 [%]	0.16	+0.17	+0.16	+0.17	+0.16	+0.11	+1.40
(PDF) PDF4LHC15_nlo_30_eigen09 [%]	0.07	+0.04	+0.05	+0.06	+0.05	+0.06	+1.04
(PDF) PDF4LHC15_nlo_30_eigen10 [%]	0.02	+0.06	+0.06	+0.06	+0.05	+0.02	+1.05
(PDF) PDF4LHC15_nlo_30_eigen11 [%]	0.13	+0.10	+0.09	+0.11	+0.08	+0.06	+1.12
(PDF) PDF4LHC15_nlo_30_eigen12 [%]	0.08	+0.07	+0.07	+0.10	+0.05	+0.03	+1.13
(PDF) PDF4LHC15_nlo_30_eigen13 [%]	0.03	+0.01	+0.01	+0.01	+0.02	+0.02	+0.87
(PDF) PDF4LHC15_nlo_30_eigen14 [%]	0.14	+0.08	+0.08	+0.11	+0.09	+0.09	+0.78
(PDF) PDF4LHC15_nlo_30_eigen15 [%]	0.02	+0.06	+0.06	+0.06	+0.05	+0.06	+0.83
(PDF) PDF4LHC15_nlo_30_eigen16 [%]	0.06	+0.04	+0.04	+0.02	+0.02	+0.01	+0.97
(PDF) PDF4LHC15_nlo_30_eigen17 [%]	0.14	+0.08	+0.08	+0.11	+0.09	+0.09	+0.78
(PDF) PDF4LHC15_nlo_30_eigen18 [%]	0.04	+0.09	+0.07	+0.13	+0.09	+0.08	+0.90
(PDF) PDF4LHC15_nlo_30_eigen19 [%]	0.02	-	-	-	-	-	-0.96
(PDF) PDF4LHC15_nlo_30_eigen20 [%]	0.02	+0.06	+0.06	+0.06	+0.05	+0.06	+0.83
(PDF) PDF4LHC15_nlo_30_eigen21 [%]	0.05	+0.04	+0.04	+0.04	+0.03	+0.02	+0.10
(PDF) PDF4LHC15_nlo_30_eigen22 [%]	0.06	+0.05	+0.52	+0.62	+0.51	+0.46	+0.21
(PDF) PDF4LHC15_nlo_30_eigen23 [%]	0.01	-	-	-	-	-	-0.96
(PDF) PDF4LHC15_nlo_30_eigen24 [%]	0.06	+0.03	+0.03	+0.08	+0.04	+0.07	+1.03
(PDF) PDF4LHC15_nlo_30_eigen25 [%]	0.03	+0.01	+0.01	+0.02	+0.02	+0.02	+0.92
(PDF) PDF4LHC15_nlo_30_eigen26 [%]	0.01	+0.02	+0.02	+0.02	+0.01	+0.01	+0.97
(PDF) PDF4LHC15_nlo_30_eigen27 [%]	-	+0.04	+0.04	+0.03	+0.03	+0.03	+1.14
(PDF) PDF4LHC15_nlo_30_eigen28 [%]	0.08	+0.11	+0.11	+0.12	+0.10	+0.09	+1.18
(PDF) PDF4LHC15_nlo_30_eigen29 [%]	-	-	-	-	-	-	+0.97
(PDF) PDF4LHC15_nlo_30_eigen30 [%]	-	-	-	-	-	-	-0.94
(MOD) Alternative, d-s scattering model [%]	45.26	+7.53	+14.61	+17.02	+12.72	+8.82	+8.31
(MOD) Alternative, shower model [%]	+16.58	+18.25	+22.82	+24.26	+19.65	+19.70	+17.45
(MOD) ISR/FSR + scale [%]	+0.44	+0.56	+1.81	+0.19	+2.85	+4.10	+3.49
(MOD) Monte Carlo sample statistics [%]	+2.89	+2.47	+3.14	+4.61	+4.49	+2.59	+19.05

Table 128: The individual systematic uncertainties in the parton level fiducial phase-space absolute differential cross-sections for the random top p_T calculated as a percentage of the cross-section.

Not reviewed, for internal circulation only

Bins [GeV]	[450,500]	[500,550]	[550,600]	[600,650]	[650,700]	[750,900]	[900,1200]
$1/\sigma d\sigma/dx$ [pb/GeV]	$2.56 \cdot 10^{-3}$	$7.33 \cdot 10^{-3}$	$3.78 \cdot 10^{-3}$	$2.08 \cdot 10^{-3}$	$1.31 \cdot 10^{-3}$	$4.03 \cdot 10^{-3}$	$7.2 \cdot 10^{-3}$
Total Uncertainty [%]	+/-12.77	+/-8.52	+/-6.61	+/-5.28	+/-3.28	+/-1.96	+/-1.53
Statistics [%]	+/-9.32	+/-3.95	+/-2.15	+/-1.71	+/-1.14	+/-0.53	+/-0.26
Systematic [%]	+/-8.23	+/-4.21	+/-3.19	+/-2.83	+/-1.74	+/-1.03	+/-0.51
(FTAG) $\text{fTagSF_B_eigen0}[\%]$	-	-	-	-	-	-	-
(FTAG) $\text{fTagSF_B_eigen1}[\%]$	+/-8.18	+/-8.18	+/-7.71	+/-7.14	+/-7.14	+/-6.63	+/-5.17
(FTAG) $\text{fTagSF_B_eigen2}[\%]$	+/-8.11	+/-8.11	+/-8.21	+/-8.09	+/-8.52	+/-8.26	+/-6.99
(FTAG) $\text{fTagSF_B_eigen3}[\%]$	+/-8.08	+/-8.06	+/-8.08	+/-8.03	+/-8.18	+/-8.28	+/-8.29
(FTAG) $\text{fTagSF_B_eigen4}[\%]$	+/-8.09	+/-8.05	+/-8.10	+/-8.08	+/-8.09	+/-8.17	+/-8.51
(FTAG) $\text{fTagSF_B_eigen5}[\%]$	-	-	-	-	+/-0.02	+/-0.12	+/-0.16
(FTAG) $\text{fTagSF_B_eigen6}[\%]$	-	-	-	-	-	-	-
(FTAG) $\text{fTagSF_C_eigen0}[\%]$	+/-8.11	+/-8.09	+/-8.13	+/-8.33	+/-8.04	+/-8.15	+/-8.06
(FTAG) $\text{fTagSF_C_eigen1}[\%]$	+/-8.11	+/-8.14	+/-8.25	+/-8.06	+/-8.13	+/-8.12	+/-8.03
(FTAG) $\text{fTagSF_C_eigen2}[\%]$	+/-8.20	+/-8.26	+/-8.03	+/-8.09	+/-8.05	+/-8.08	+/-8.05
(FTAG) $\text{fTagSF_C_eigen3}[\%]$	+/-8.08	+/-8.11	+/-8.02	+/-8.09	+/-8.03	+/-8.05	+/-8.05
(FTAG) $\text{fTagSF_Light_eigen0}[\%]$	+/-8.08	+/-8.17	+/-8.13	+/-8.10	+/-8.03	+/-8.04	+/-8.09
(FTAG) $\text{fTagSF_Light_eigen1}[\%]$	+/-8.09	+/-8.11	+/-8.13	+/-8.16	+/-8.03	+/-8.02	+/-8.03
(FTAG) $\text{fTagSF_Light_eigen2}[\%]$	-	-	-	-	-	-	-
(FTAG) $\text{fTagSF_Light_eigen3}[\%]$	-	-	+/-0.07	-	-	+/-0.10	+/-0.05
(FTAG) $\text{fTagSF_Light_eigen4}[\%]$	-	-	+/-0.02	-	-	+/-0.05	+/-0.08
(FTAG) $\text{fTagSF_Light_eigen5}[\%]$	-	-	-	-	-	-	-
(FTAG) $\text{fTagSF_Light_eigen6}[\%]$	-	-	-	-	-	-	-
(FTAG) $\text{fTagSF_Light_eigen7}[\%]$	-	-	-	-	-	-	-
(FTAG) $\text{fTagSF_Light_eigen8}[\%]$	-	-	-	-	-	-	-
(FTAG) $\text{fTagSF_Light_eigen9}[\%]$	-	-	-	-	-	-	-
(FTAG) $\text{fTagSF_Light_eigen10}[\%]$	-	-	-	-	-	-	-
(FTAG) $\text{fTagSF_Light_eigen11}[\%]$	-	-	-	-	-	-	-
(FTAG) $\text{fTagSF_Light_eigen12}[\%]$	-	-	-	-	-	-	-
(FTAG) $\text{fTagSF_Light_eigen13}[\%]$	-	-	-	-	-	-	-
(FTAG) $\text{fTagSF_Light_eigen14}[\%]$	-	-	-	-	-	-	-
(FTAG) $\text{fTagSF_Light_eigen15}[\%]$	-	-	-	-	-	-	-
(FTAG) $\text{fTagSF_extrapolation}[\%]$	+/-0.05	+/-0.06	+/-0.59	+/-0.24	+/-0.41	+/-0.16	+/-0.06
(FTAG) $\text{fTagSF_extrapolation_from_charm}[\%]$	+/-0.60	+/-1.04	+/-0.54	+/-0.32	+/-1.52	+/-3.29	+/-5.21
(MET/Pt) $\text{f1}[\%]$	+/-0.07	-	-	-	+/-0.12	+/-0.05	+/-0.37
Luminosity [%]	+/-0.03	-	+/-0.03	+/-0.02	+/-0.03	+/-0.03	+/-0.03
(BKJ) $\text{singletop_tchan}[\%]$	+/-0.08	+/-0.02	+/-0.04	+/-0.01	+/-0.08	+/-0.04	+/-1.29
(BKJ) $\text{singletop_Wt}[\%]$	-	-	-	-	-	-	+/-0.36
(BKJ) $tW[\%]$	-	-	-	-	-	-	+/-0.44
(BKJ) $tZ[\%]$	-	-	-	-	-	-	+/-0.47
(BKJ) $tH[\%]$	-	-	-	-	-	-	+/-0.46
(LHERF) $\text{fTag-BJET_Weak_JET_Rrk_Modelling_Tau32WTA}[\%]$	-	+/-0.24	-	-	-	-	-
(LHERF) $\text{LARGERIET_Weak_JET_Rrk_Baseline_pT}[\%]$	+/-0.57	-	+/-0.35	+/-0.09	+/-1.22	+/-2.74	+/-5.34
(LHERF) $\text{LARGERIET_Weak_JET_Rrk_Baseline_mass}[\%]$	+/-0.29	+/-0.29	+/-0.17	+/-0.06	+/-0.18	+/-1.25	+/-0.72
(LHERF) $\text{LARGERIET_Weak_JET_Rrk_Baseline_Tau32WTA}[\%]$	+/-0.29	+/-0.08	+/-0.14	+/-0.63	+/-0.16	+/-0.42	+/-1.99
(JES) $\text{JET_2INP_JET_BIAS_Response}[\%]$	-	+/-0.14	-	-	-	-	+/-0.44
(JES) $\text{JET_2INP_JET_Pileup_PTTerm}[\%]$	-	-	-	-	-	-	+/-0.46
(JES) $\text{JET_2INP_JET_Pileup_OffsetNPV}[\%]$	+/-0.07	+/-0.02	+/-0.03	+/-0.08	+/-0.06	+/-0.05	+/-0.01
(JES) $\text{JET_2INP_JET_Pileup_RhoTopology}[\%]$	+/-0.17	+/-0.04	+/-0.03	+/-0.01	+/-0.01	+/-0.02	+/-0.02
(JES) $\text{JET_2INP_JET_EtuIntercalibrationTerm}[\%]$	-	-	-	-	-	-	+/-0.46
(LEP) $\text{EG_SCALE_SUSY_Reconv}[\%]$	-	-	-	-	-	-	+/-0.46
(JES) $\text{JET_2INP_JET_EffectiveNP_3}[\%]$	-	-	-	-	-	-	+/-0.46
(JES) $\text{JET_2INP_JET_EffectiveNP_4}[\%]$	-	-	-	-	-	-	+/-0.45
(JES) $\text{LARGERIET_Weak_JET_Rrk_Tracking_mass}[\%]$	+/-0.14	+/-0.22	+/-0.28	+/-0.06	+/-0.11	+/-1.29	+/-0.49
(JES) $\text{JET_2INP_JET_Pileup_OffSetMu}[\%]$	+/-0.04	+/-0.01	+/-0.03	+/-0.03	+/-0.19	+/-0.11	+/-0.89
(JES) $\text{JET_2INP_JET_TotalStat_mass}[\%]$	+/-0.02	+/-0.01	+/-0.03	+/-0.03	+/-0.12	+/-0.12	+/-0.76
(JES) $\text{JET_2INP_JET_EtuIntercalibration_NonClosure}[\%]$	+/-0.03	+/-0.03	+/-0.02	+/-0.04	+/-0.18	+/-0.02	+/-0.01
(JES) $\text{JET_2INP_JET_EtuIntercalibration_TotalStat}[\%]$	+/-0.03	+/-0.03	+/-0.02	+/-0.04	+/-0.18	+/-0.02	+/-0.00
(JES) $\text{JET_2INP_JET_Flavor_Response}[\%]$	-	-	-	-	-	-	+/-1.60
(JES) $\text{JET_2INP_JET_Flavor_Response_NP}[\%]$	-	-	-	-	-	-	+/-0.54
(JES) $\text{JET_2INP_JET_EffectiveNP_6}[\%]$	-	-	-	-	-	-	+/-0.45
(JES) $\text{JET_2INP_JET_EffectiveNP_5}[\%]$	-	-	-	-	-	-	+/-0.38
(JES) $\text{JET_2INP_JET_Flavor_Composition}[\%]$	+/-0.05	+/-0.03	+/-0.07	+/-0.06	+/-0.11	+/-0.02	+/-0.02
(JES) $\text{JET_2INP_JET_SingleParticle_HighPt}[\%]$	+/-0.19	+/-0.03	+/-0.04	+/-0.04	+/-0.25	+/-0.09	+/-0.05
(JES) $\text{LARGERIET_Weak_JET_Rrk_Modeling_pT}[\%]$	+/-0.90	+/-0.18	+/-0.10	+/-0.86	+/-0.25	+/-0.91	+/-0.54
(JES) $\text{JET_2INP_JET_EffectiveNP_1}[\%]$	+/-0.03	+/-0.26	+/-0.27	+/-0.05	+/-0.25	+/-0.31	+/-0.52
(LEP) $\text{MUON_ID}[\%]$	-	-	-	-	-	-	+/-0.46
(LEP) $\text{MUON_ID_TotalStat_pT}[\%]$	-	-	-	-	-	-	+/-0.75
(LEP) $\text{MUON_SCALE}[\%]$	-	-	-	-	-	-	+/-0.46
(LEP) $\text{EG_SCALE_ALL}[\%]$	-	-	-	-	-	-	+/-0.46
(JES) $\text{JET_2INP_JET_EffectiveNP_7}[\%]$	-	-	-	-	+/-0.01	+/-0.18	+/-0.90
(JES) $\text{LARGERIET_Weak_JET_Rrk_Modeling_mass}[\%]$	-	-	-	-	+/-0.03	+/-0.03	+/-0.12
(LEP) $\text{MUON_MS}[\%]$	-	-	-	-	-	-	+/-0.46
(LEP) $\text{MUON_SAGITTA_RHO}[\%]$	-	-	-	-	-	-	+/-0.46
(JES) $\text{JET_2INP_JET_PunchThrough_MC15}[\%]$	-	-	-	-	-	-	+/-0.46
(JES) $\text{JET_2INP_JET_EtuIntercalibration_Modeling}[\%]$	-	-	-	-	-	-	+/-0.46
(JES) $\text{JET_2INP_JET_EtuIntercalibration_Tau32WTA}[\%]$	-	-	+/-0.03	+/-0.02	+/-0.17	+/-0.01	+/-0.32
(JES) $\text{LARGERIET_Weak_JET_Rrk_Tracking_Tau32WTA}[\%]$	+/-0.16	+/-0.21	+/-0.23	+/-0.23	+/-0.20	+/-1.11	+/-1.06
(JES) $\text{LARGERIET_Weak_JET_Rrk_Tracking_pT}[\%]$	+/-0.25	+/-1.25	+/-0.58	+/-0.87	+/-2.25	+/-2.09	+/-2.98
(JES) $\text{LARGERIET_Weak_JET_Rrk_TotalStat_Tau32WTA}[\%]$	+/-0.05	+/-1.28	+/-0.35	+/-0.30	+/-1.26	+/-0.24	+/-1.93
(JES) $\text{JET_JER_SINGLE_NP}[\%]$	+/-0.03	+/-0.03	+/-0.14	+/-0.15	+/-0.06	+/-0.06	+/-1.91
(JES) $\text{LARGERIET_Weak_JET_Top_massRes_mass}[\%]$	+/-0.19	+/-0.20	+/-0.23	+/-0.60	+/-1.25	+/-3.19	+/-5.58
(PDF) $\text{PDF4LHC15_alo_30_eigen001}[\%]$	+/-0.19	+/-0.07	+/-0.06	+/-0.12	+/-0.06	+/-0.08	+/-0.89
(PDF) $\text{PDF4LHC15_alo_30_eigen002}[\%]$	+/-0.24	+/-0.18	+/-0.17	+/-0.17	+/-0.18	+/-0.14	+/-1.31
(PDF) $\text{PDF4LHC15_alo_30_eigen003}[\%]$	+/-0.24	+/-0.18	+/-0.17	+/-0.17	+/-0.18	+/-0.14	+/-1.31
(PDF) $\text{PDF4LHC15_alo_30_eigen004}[\%]$	+/-0.27	+/-0.13	+/-0.11	+/-0.19	+/-0.17	+/-0.22	+/-1.17
(PDF) $\text{PDF4LHC15_alo_30_eigen005}[\%]$	+/-0.47	+/-0.43	+/-0.40	+/-0.50	+/-0.42	+/-0.41	+/-1.99
(PDF) $\text{PDF4LHC15_alo_30_eigen006}[\%]$	+/-0.34	+/-0.21	+/-0.19	+/-0.31	+/-0.22	+/-0.22	+/-1.26
(PDF) $\text{PDF4LHC15_alo_30_eigen007}[\%]$	+/-0.05	+/-0.01	+/-0.02	+/-0.02	+/-0.02	+/-0.02	+/-0.97
(PDF) $\text{PDF4LHC15_alo_30_eigen008}[\%]$	+/-0.16	+/-0.17	+/-0.16	+/-0.17	+/-0.16	+/-0.11	+/-1.40
(PDF) $\text{PDF4LHC15_alo_30_eigen009}[\%]$	+/-0.07	+/-0.04	+/-0.05	+/-0.06	+/-0.05	+/-0.06	+/-1.04
(PDF) $\text{PDF4LHC15_alo_30_eigen010}[\%]$	+/-0.02	+/-0.06	+/-0.06	+/-0.02	+/-0.05	+/-0.02	+/-1.05
(PDF) $\text{PDF4LHC15_alo_30_eigen011}[\%]$	+/-0.13	+/-0.10	+/-0.09	+/-0.11	+/-0.08	+/-0.06	+/-1.12
(PDF) $\text{PDF4LHC15_alo_30_eigen012}[\%]$	+/-0.08	+/-0.07	+/-0.07	+/-0.10	+/-0.05	+/-0.03	+/-1.13
(PDF) $\text{PDF4LHC15_alo_30_eigen013}[\%]$	+/-0.03	+/-0.02	+/-0.03	+/-0.03	+/-0.07	+/-0.07	+/-0.97
(PDF) $\text{PDF4LHC15_alo_30_eigen014}[\%]$	+/-0.03	+/-0.02	+/-0.02	+/-0.02	+/-0.02	+/-0.01	+/-1.09
(PDF) $\text{PDF4LHC15_alo_30_eigen015}[\%]$	+/-0.03	+/-0.03	+/-0.03	+/-0.02	+/-0.02	+/-0.01	+/-1.09
(PDF) $\text{PDF4LHC15_alo_30_eigen016}[\%]$	-	-	-	+/-0.03	+/-0.01	+/-0.01	+/-0.87
(PDF) $\text{PDF4LHC15_alo_30_eigen017}[\%]$	+/-0.14	+/-0.08	+/-0.08	+/-0.11	+/-0.09	+/-0.09	+/-0.78
(PDF) $\text{PDF4LHC15_alo_30_eigen018}[\%]$	+/-0.14	+/-0.09	+/-0.09	+/-0.07	+/-0.13	+/-0.09	+/-0.90
(PDF) $\text{PDF4LHC15_alo_30_eigen019}[\%]$	+/-0.02	-	-	+/-0.02	+/-0.02	+/-0.02	+/-0.93
(PDF) $\text{PDF4LHC15_alo_30_eigen020}[\%]$	+/-0.02	+/-0.06	+/-0.06	+/-0.06	+/-0.05	+/-0.06	+/-0.83
(PDF) $\text{PDF4LHC15_alo_30_eigen021}[\%]$	+/-0.04	+/-0.04	+/-0.04	+/-0.03	+/-0.03	+/-0.02	+/-1.01
(PDF) $\text{PDF4LHC15_alo_30_eigen022}[\%]$	+/-0.06	+/-0.55	+/-0.52	+/-0.62	+/-0.51	+/-0.46	+/-0.21
(PDF) $\text{PDF4LHC15_alo_30_eigen023}[\%]$	+/-0.01	-	-	-	-	-	+/-0.96
(PDF) $\text{PDF4LHC15_alo_30_eigen024}[\%]$	+/-0.06	+/-0.03	+/-0.03	+/-0.08	+/-0.04	+/-0.07	+/-1.03
(PDF) $\text{PDF4LHC15_alo_30_eigen025}[\%]$	+/-0.03	+/-0.01	+/-0.01	+/-0.02	+/-0.02	+/-0.02	+/-0.92
(PDF) $\text{PDF4LHC15_alo_30_eigen026}[\%]$	+/-0.01	+/-0.02	+/-0.02	+/-0.02	+/-0.01	+/-0.01	+/-0.97
(PDF) $\text{PDF4LHC15_alo_30_eigen027}[\%]$	-	+/-0.04	+/-0.04	+/-0.03	+/-0.03	+/-0.03	+/-1.14
(PDF) $\text{PDF4LHC15_alo_30_eigen028}[\%]$	+/-0.08	+/-0.11	+/-0.11	+/-0.12	+/-0.10	+/-0.09	+/-1.18
(PDF) $\text{PDF4LHC15_alo_30_eigen029}[\%]$	+/-0.03	+/-0.02	+/-0.02	+/-0.02	+/-0.02	+/-0.02	+/-0.97
(PDF) $\text{PDF4LHC15_alo_30_eigen030}[\%]$	-	-	-	+/-0.02	+/-0.02	+/-0.03	+/-0.94
(MOD) Alternative had-scattering model [%]	+/-5.92	+/-3.39	+/-0.53	+/-7.22	+/-2.41	+/-1.94	+/-2.52
(MOD) Alternative parton-shower model [%]	+/-4.18	+/-2.10	+/-3.62	+/-5.41	+/-3.05	+/-2.08	+/-3.09
(MOD) ISR/FSR + scale [%]	+/-1.67	+/-0.58	+/-0.69	+/-1.32	+/-1.71	+/-3.01	+/-2.29
(MOD) Monte Carlo sample statistics [%]	+/-2.94	+/-2.18	+/-3.04	+/-4.52	+/-4.39	+/-5.62	+/-18.98

Table 129: The individual systematic uncertainties in the parton level fiducial phase-space relative differential cross-sections for the random top p_T calculated as a percentage of the cross-section.

Not reviewed, for internal circulation only

Bins [GeV]	[0,0.2]	[0.2,0.4]	[0.4,0.6]	[0.6,0.8]	[0.8,1]	[1,1.2]	[1.2,1.5]	[1.5,2]
$d\sigma/dX$ [pb/GeV]	$6.54 \cdot 10^{-3}$	$6.54 \cdot 10^{-3}$	$5.78 \cdot 10^{-3}$	$4.56 \cdot 10^{-3}$	$4.46 \cdot 10^{-3}$	$4.15 \cdot 10^{-3}$	$2.55 \cdot 10^{-3}$	$1.4 \cdot 10^{-3}$
Total Uncertainty [%]	+31.08	+32.77	+31.72	+34.20	+31.53	+32.68	+36.93	+34.83
Statistics [%]	+5.59	+6.38	+6.74	+7.29	+7.59	+8.21	+7.78	+8.84
Systematics [%]	+3.41	+3.41	+3.43	+3.23	+3.23	+3.33	+3.38	+3.38
(PTAG) $\text{tagSF_B_eigen}1$ [%]	+2.49	+2.15	+2.01	+2.01	+2.01	+2.01	+2.01	+2.01
(PTAG) $\text{tagSF_B_eigen}2$ [%]	+4.95	+5.90	+5.84	+5.41	+4.98	+5.66	+5.63	+5.78
(PTAG) $\text{tagSF_B_eigen}3$ [%]	+0.99	+0.73	+0.73	+0.85	+0.79	+0.95	+0.95	+0.95
(PTAG) $\text{tagSF_B_eigen}4$ [%]	+0.34	+0.34	+0.36	+0.38	+0.35	+0.35	+0.35	+0.35
(PTAG) $\text{tagSF_B_eigen}5$ [%]	+0.04	+0.03	+0.03	+0.05	+0.05	+0.04	+0.04	+0.04
(PTAG) $\text{tagSF_B_eigen}6$ [%]	+0.04	+0.03	+0.03	+0.05	+0.05	+0.04	+0.04	+0.04
(PTAG) $\text{tagSF_C_eigen}1$ [%]	+2.25	+2.45	+2.29	+2.13	+1.78	+2.33	+1.93	+1.95
(PTAG) $\text{tagSF_C_eigen}2$ [%]	+1.25	+1.15	+1.43	+1.50	+1.25	+1.25	+1.18	+1.35
(PTAG) $\text{tagSF_C_eigen}3$ [%]	+0.29	+0.16	+0.27	+0.24	+0.17	+0.06	+0.06	+0.07
(PTAG) $\text{tagSF_Light_eigen}0$ [%]	+0.25	+0.17	+0.14	+0.14	+0.14	+0.07	+0.07	+0.11
(PTAG) $\text{tagSF_Light_eigen}1$ [%]	+0.07	+0.05	+0.05	+0.05	+0.05	+0.05	+0.05	+0.05
(PTAG) $\text{tagSF_Light_eigen}2$ [%]	+0.04	+0.05	+0.05	+0.05	+0.05	+0.05	+0.05	+0.05
(PTAG) $\text{tagSF_Light_eigen}3$ [%]	+0.04	+0.05	+0.05	+0.05	+0.05	+0.05	+0.05	+0.05
(PTAG) $\text{tagSF_Light_eigen}4$ [%]	+0.04	+0.05	+0.05	+0.05	+0.05	+0.05	+0.05	+0.05
(PTAG) $\text{tagSF_Light_eigen}5$ [%]	+0.04	+0.05	+0.05	+0.05	+0.05	+0.05	+0.05	+0.05
(PTAG) $\text{tagSF_Light_eigen}6$ [%]	+0.04	+0.05	+0.05	+0.05	+0.05	+0.05	+0.05	+0.05
(PTAG) $\text{tagSF_Light_eigen}7$ [%]	+0.06	+0.05	+0.05	+0.05	+0.05	+0.05	+0.05	+0.05
(PTAG) $\text{tagSF_Light_eigen}8$ [%]	+0.06	+0.05	+0.05	+0.05	+0.05	+0.05	+0.05	+0.05
(PTAG) $\text{tagSF_Light_eigen}9$ [%]	+0.03	+0.02	+0.03	+0.03	+0.01	+0.01	+0.01	+0.01
(PTAG) $\text{tagSF_Light_eigen}10$ [%]	+0.03	+0.05	+0.05	+0.05	+0.05	+0.05	+0.05	+0.05
(PTAG) $\text{tagSF_Light_eigen}11$ [%]	+0.03	+0.05	+0.05	+0.05	+0.05	+0.05	+0.05	+0.05
(PTAG) $\text{tagSF_Light_eigen}12$ [%]	+0.03	+0.05	+0.05	+0.05	+0.05	+0.05	+0.05	+0.05
(PTAG) $\text{tagSF_Light_eigen}13$ [%]	+0.03	+0.05	+0.05	+0.05	+0.05	+0.05	+0.05	+0.05
(PTAG) $\text{tagSF_Light_eigen}14$ [%]	+0.04	+0.05	+0.05	+0.05	+0.05	+0.05	+0.05	+0.05
(PTAG) $\text{tagSF_Light_eigen}15$ [%]	+0.04	+0.05	+0.05	+0.05	+0.05	+0.05	+0.05	+0.05
(PTAG) $\text{tagSF_extrapolation}$ [%]	+0.16	+0.05	+0.05	+0.05	+0.05	+0.05	+0.05	+0.05
(PTAG) $\text{tagSF_extrapolation_from_charm}$ [%]	-0.01	-0.01	-0.01	-0.01	-0.01	-0.01	-0.01	-0.01
(MET+PU) jvt [%]	+0.03	+0.03	+0.03	+0.03	+0.03	+0.03	+0.03	+0.03
Lambda_top [%]	+0.19	+0.15	+0.15	+0.15	+0.15	+0.13	+0.13	+0.13
(BKG) singletop_Wt [%]	-	-	-	-	-	-	-	-
(BKG) nT [%]	+0.03	+0.04	+0.04	+0.03	+0.03	+0.03	+0.03	+0.05
(BKG) uT [%]	+0.03	+0.03	+0.04	+0.03	+0.03	+0.03	+0.03	+0.03
(BKG) nH [%]	+0.03	+0.03	+0.03	+0.03	+0.03	+0.03	+0.03	+0.03
(LJES) LARGEJET_W JET, Rrk, Modelling, Tau32WTA [%]	+1.30	+1.15	+1.55	+1.99	+2.21	+1.99	+1.92	+1.90
(LJES) LARGEJET_W JET, Rrk, Baseline, pT [%]	+1.96	+1.78	+2.03	+2.28	+2.09	+2.58	+1.88	+2.30
(LJES) LARGEJET_W JET, Rrk, Baseline, mass [%]	+0.91	+0.48	+0.51	+2.14	+2.72	+0.05	+0.91	+0.29
(LJES) LARGEJET_W JET, Rrk, Baseline, Tau32WTA [%]	+2.43	+2.09	+2.59	+2.48	+2.05	+2.05	+2.05	+2.33
(LJES) JET_{2NP} , JET, BES, Response [%]	-	-	-	-	-	-	-	-
(JES) JET_{2NP} , JET, PileUp, PT [%]	+0.02	+0.02	+0.02	+0.02	+0.02	+0.01	+0.01	+0.01
(JES) JET_{2NP} , JET, PileUp, RhoNphi [%]	+0.01	+0.03	+0.09	+0.03	+0.03	+0.03	+0.03	+0.03
(JES) JET_{2NP} , JET, PileUp, RhoNphiNphi [%]	+0.12	+0.01	+0.01	+0.01	+0.01	+0.05	+0.05	+0.05
(JES) JET_{2NP} , JET, EffectiveNP, SeeTerm [%]	+0.13	+0.04	+0.24	+0.15	+0.07	+0.09	+0.15	+0.04
(LEP) MUON_SAGITTA_RESBIAS [%]	-	-	-	-	-	-	-	-
(JES) JET_{2NP} , JET, EffectiveNP, 3 [%]	+0.02	+0.02	+0.02	+0.02	+0.02	+0.01	+0.01	+0.03
(JES) JET_{2NP} , JET, EffectiveNP, 4 [%]	+0.01	+0.01	+0.01	+0.01	+0.01	+0.01	+0.01	+0.01
(LJES) LARGEJET_W JET, Rrk, Tracking, mass [%]	+0.50	+0.35	+0.38	+0.05	+0.12	+0.16	+0.47	+0.17
(JES) JET_{2NP} , JET, Phsing, OffSet [%]	+0.76	+0.03	+0.08	+0.03	+0.03	+0.05	+0.38	+0.89
(JES) JET_{2NP} , JET, EtaCalibration, TotalStat [%]	+0.06	+0.01	+0.01	+0.02	+0.02	+0.02	+0.03	+0.03
(JES) JET_{2NP} , JET, EtaCalibration, NonClosure [%]	+0.08	+0.04	+0.09	+0.02	+0.02	+0.01	+0.02	+0.01
(JES) JET_{2NP} , JET, EtaCalibration, TotalStat [%]	+0.01	-	-	+0.01	+0.01	+0.02	+0.02	+0.04
(JES) JET_{2NP} , RhoCalib [%]	-	-	-	-	-	-	-	-
(JES) JET_{2NP} , JET, Flav, Response [%]	+0.08	+0.01	+0.12	+0.05	+0.05	+0.05	+0.04	+0.04
(JES) JET_{2NP} , JET, EffectiveNP, 5 [%]	+0.10	+0.05	+0.03	+0.03	+0.05	+0.05	+0.09	+0.07
(JES) JET_{2NP} , JET, EffectiveNP, 6 [%]	+0.09	+0.05	+0.05	+0.05	+0.05	+0.05	+0.05	+0.05
(JES) JET_{2NP} , JET, SingleParticle, HighPt [%]	+0.10	+0.02	+0.02	+0.02	+0.02	+0.02	+0.02	+0.02
(JES) JET_{2NP} , JET, EffectiveNP, 1 [%]	+0.11	+0.03	+0.19	+0.05	+0.05	+0.09	+0.09	+0.03
(JEP) MUON_ID [%]	-	-	-	-	-	-	-	-
(JES) JET_{2NP} , JET, Weak, JET, Rrk, Modelling, pT [%]	+0.44	+0.31	+0.16	+0.41	+0.24	+0.22	+0.50	+0.20
(JEP) MUON_SCALE [%]	-0.19	-0.28	-0.26	-0.20	-0.42	-0.17	-0.35	-0.15
(JEP) EG_SCALING_ALL [%]	-	-	-	-	-	-0.01	-	-
(JES) JET_{2NP} , JET, EffectiveNP, 7 [%]	+0.01	+0.01	+0.09	+0.01	+0.01	+0.14	-	-
(JES) JET_{2NP} , JET, Weak, JET, Rrk, Modelling, mass [%]	+0.42	+0.15	+0.11	+0.31	+0.33	+0.33	+0.30	+0.62
(JEP) MUON_MS [%]	+0.98	+1.49	+0.31	+0.99	+0.27	+0.60	+0.60	+1.49
(JEP) MUON_ID [%]	-	-	-	-	-	-	-	-
(JES) JET_{2NP} , JET, Weak, JET, Rrk, TotalStat, Tau32WTA [%]	+0.25	+0.17	+0.15	+0.33	+0.29	+0.30	+0.32	+0.26
(JES) JET_{2NP} , JET, EffectiveNP, 1 [%]	+1.88	+2.08	+0.02	+2.13	+2.18	+2.19	+2.34	+2.81
(JES) JET_{2NP} , JET, EffectiveNP, 2 [%]	+0.11	+0.03	+0.19	+0.16	+0.16	+0.09	+0.09	+0.03
(JES) JET_{2NP} , JET, PunchThrough, MC15 [%]	+0.44	+0.31	+0.16	+0.41	+0.24	+0.22	+0.50	+0.20
(JES) JET_{2NP} , JET, PunchThrough, Modelling [%]	+0.02	+0.03	+0.04	+0.03	+0.03	+0.05	+0.05	+0.03
(PDF) PDF4LHC15_nlo_30_eigen001 [%]	+0.03	+0.03	+0.03	+0.03	+0.03	+0.04	+0.04	+0.04
(PDF) PDF4LHC15_nlo_30_eigen002 [%]	+0.13	+0.16	+0.11	+0.11	+0.19	+0.21	+0.21	+0.30
(PDF) PDF4LHC15_nlo_30_eigen003 [%]	+0.06	+0.07	+0.07	+0.06	+0.07	+0.11	+0.10	+0.05
(PDF) PDF4LHC15_nlo_30_eigen004 [%]	+0.07	+0.06	+0.07	+0.07	+0.07	+0.13	+0.19	+0.39
(PDF) PDF4LHC15_nlo_30_eigen005 [%]	+0.41	+0.48	+0.48	+0.39	+0.47	+0.50	+0.51	+0.55
(PDF) PDF4LHC15_nlo_30_eigen006 [%]	+0.18	+0.22	+0.19	+0.16	+0.23	+0.23	+0.24	+0.38
(PDF) PDF4LHC15_nlo_30_eigen007 [%]	-	-	-	+0.01	+0.01	+0.01	+0.01	+0.08
(PDF) PDF4LHC15_nlo_30_eigen008 [%]	+0.12	+0.15	+0.15	+0.13	+0.18	+0.17	+0.20	+0.18
(PDF) PDF4LHC15_nlo_30_eigen009 [%]	+0.05	+0.05	+0.06	+0.04	+0.06	+0.06	+0.06	+0.06
(PDF) PDF4LHC15_nlo_30_eigen010 [%]	+0.05	+0.06	+0.07	+0.05	+0.05	+0.06	+0.06	+0.09
(PDF) PDF4LHC15_nlo_30_eigen011 [%]	+0.08	+0.09	+0.09	+0.07	+0.10	+0.10	+0.09	+0.13
(PDF) PDF4LHC15_nlo_30_eigen012 [%]	+0.06	+0.06	+0.08	+0.05	+0.05	+0.09	+0.09	+0.03
(PDF) PDF4LHC15_nlo_30_eigen013 [%]	+0.02	+0.03	+0.03	+0.07	+0.03	+0.02	+0.02	+0.03
(PDF) PDF4LHC15_nlo_30_eigen014 [%]	+0.02	+0.02	+0.02	+0.02	+0.02	+0.03	+0.04	+0.06
(PDF) PDF4LHC15_nlo_30_eigen015 [%]	+0.02	+0.02	+0.01	+0.02	+0.03	+0.06	+0.06	+0.05
(PDF) PDF4LHC15_nlo_30_eigen016 [%]	+0.02	+0.03	+0.01	+0.02	+0.01	+0.01	-	-
(PDF) PDF4LHC15_nlo_30_eigen017 [%]	+0.07	+0.10	+0.07	+0.09	+0.10	+0.10	+0.09	+0.13
(PDF) PDF4LHC15_nlo_30_eigen018 [%]	+0.06	+0.07	+0.07	+0.04	+0.08	+0.08	+0.08	+0.05
(PDF) PDF4LHC15_nlo_30_eigen019 [%]	+0.11	+0.14	+0.11	+0.08	+0.08	+0.08	+0.08	+0.14
(PDF) PDF4LHC15_nlo_30_eigen020 [%]	+0.04	+0.04	+0.03	+0.04	+0.06	+0.07	+0.09	+0.07
(PDF) PDF4LHC15_nlo_30_eigen021 [%]	+0.03	+0.04	+0.02	+0.03	+0.03	+0.05	+0.05	+0.05
(PDF) PDF4LHC15_nlo_30_eigen022 [%]	+0.39	+0.44	+0.47	+0.41	+0.57	+0.62	+0.71	+0.82
(PDF) PDF4LHC15_nlo_30_eigen023 [%]	-	-	-	-	-	-	-	-
(PDF) PDF4LHC15_nlo_30_eigen024 [%]	+0.03	+0.03	+0.01	+0.04	+0.04	+0.06	+0.06	+0.04
(PDF) PDF4LHC15_nlo_30_eigen025 [%]	+0.01	+0.01	-	+0.01	+0.02	+0.02	+0.01	+0.07
(PDF) PDF4LHC15_nlo_30_eigen026 [%]	+0.03	+0.04	+0.01	+0.03	+0.03	+0.02	+0.01	-
(PDF) PDF4LHC15_nlo_30_eigen027 [%]	+0.03	+0.03	+0.02	+0.02	+0.05	+0.05	+0.05	+0.05
(PDF) PDF4LHC15_nlo_30_eigen028 [%]	+0.12	+0.14	+0.12	+0.10	+0.14	+0.12	+0.11	+0.09
(PDF) PDF4LHC15_nlo_30_eigen029 [%]	-	-	-	-	-	-	-	-
(PDF) PDF4LHC15_nlo_30_eigen030 [%]	-	-	+0.02	-	-	-	-	+0.04
(MOD) Alternative hard-scattering model [%]	+11.01	+9.23	+15.67	+13.31	+11.01	+9.80	+13.94	+13.07
(MOD) Alternative parton-shower mode [%]	+18.86	+18.44	+18.98	+21.76	+18.45	+19.00	+25.38	+20.57
(MOD) ISR/FSR + scale [%]	+1.32	+1.33	+1.88	+3.18	+0.88	+2.98	+1.98	+1.22
(MOD) Monte Carlo sample statistics [%]	+2.74	+3.66	+3.72	+3.60	+3.43	+4.39	+3.92	+4.71

Table 130: The individual systematic uncertainties in the parton level fiducial phase-space absolute differential cross-sections for the random top $|y|$ calculated as a percentage of the cross-section.

Not reviewed, for internal circulation only

Bins [GeV]	[0,0.2]	[0,2,0.4]	[0,4,0.6]	[0,6,0.8]	[0,8,1]	[1,1,2]	[1,2,1.5]	[1.5,2]
$1/\sigma d\sigma/dX$ [pb/GeV]	$8.31 \cdot 10^{-1}$	$8.31 \cdot 10^{-1}$	$7.35 \cdot 10^{-1}$	$5.8 \cdot 10^{-1}$	$5.67 \cdot 10^{-1}$	$5.27 \cdot 10^{-1}$	$3.24 \cdot 10^{-1}$	$1.77 \cdot 10^{-1}$
Total Uncertainty [%]	+6.44 -4.45	+8.84 -8.43	+8.63 -8.53	+8.52 -8.43	+8.81 -8.74	+10.09 -9.58	+11.30 -10.58	+16.57 -15.18
Statistics [%]	+5.23 +2.70	+6.00 +2.70	+6.33 +2.71	+6.90 +2.71	+7.26 +2.99	+7.93 +2.99	+7.45 +2.76	+8.52 +2.51
Systematics [%]	+2.04 +2.04	+3.14 +3.14	+4.05 +4.05	+3.99 +3.99	+4.26 +4.26	+4.04 +4.04	+4.03 +4.03	+4.21 +4.21
(FTAG) tagSF_B , eigen0 [%]	-	-	-	-	-	-	-	-
(FTAG) tagSF_B , eigen1 [%]	-0.07 +0.15	+0.08 -0.15	+0.15 -0.15	+0.14 -0.14	+0.01 -0.01	-0.03 +0.03	-0.24 +0.24	+0.18 -0.18
(FTAG) tagSF_B , eigen2 [%]	-0.05 +0.12	+0.05 -0.12	+0.15 -0.15	+0.14 -0.14	+0.01 -0.01	-0.03 +0.03	-0.12 +0.12	+0.10 -0.10
(FTAG) tagSF_B , eigen3 [%]	-0.04 +0.11	+0.04 -0.11	+0.13 -0.13	+0.12 -0.12	+0.01 -0.01	-0.03 +0.03	-0.08 +0.08	+0.09 -0.09
(FTAG) tagSF_B , eigen4 [%]	-0.04 +0.11	+0.04 -0.11	+0.13 -0.13	+0.12 -0.12	+0.01 -0.01	-0.03 +0.03	-0.08 +0.08	+0.09 -0.09
(FTAG) tagSF_B , eigen5 [%]	-	-	-	-	-	-	-	-
(FTAG) tagSF_B , eigen6 [%]	-0.13 +0.15	+0.26 -0.15	+0.29 -0.15	+0.11 -0.15	+0.33 -0.03	+0.33 -0.03	+0.20 -0.20	+0.12 -0.12
(FTAG) tagSF_B , eigen7 [%]	-0.07 +0.15	+0.08 -0.15	+0.15 -0.15	+0.14 -0.14	+0.01 -0.01	-0.03 +0.03	-0.20 +0.20	+0.12 -0.12
(FTAG) tagSF_C , eigen1 [%]	-0.05 +0.12	+0.05 -0.12	+0.15 -0.15	+0.14 -0.14	+0.01 -0.01	-0.03 +0.03	-0.12 +0.12	+0.10 -0.10
(FTAG) tagSF_C , eigen2 [%]	-0.05 +0.11	+0.05 -0.11	+0.13 -0.13	+0.12 -0.12	+0.01 -0.01	-0.03 +0.03	-0.12 +0.12	+0.10 -0.10
(FTAG) tagSF_C , eigen3 [%]	-0.05 +0.11	+0.05 -0.11	+0.13 -0.13	+0.12 -0.12	+0.01 -0.01	-0.03 +0.03	-0.12 +0.12	+0.10 -0.10
(FTAG) tagSF_C , eigen4 [%]	-0.05 +0.11	+0.05 -0.11	+0.13 -0.13	+0.12 -0.12	+0.01 -0.01	-0.03 +0.03	-0.12 +0.12	+0.10 -0.10
(FTAG) tagSF_C , eigen5 [%]	-	-	-	-	-	-	-	-
(FTAG) tagSF_C , eigen6 [%]	-0.01 +0.01	+0.05 -0.01	+0.05 -0.01	+0.05 -0.01	+0.03 -0.01	+0.05 -0.01	+0.02 -0.01	+0.02 -0.01
(FTAG) tagSF_C , eigen7 [%]	-0.04 +0.03	+0.03 -0.03	+0.07 -0.07	+0.08 -0.07	+0.04 -0.04	+0.05 -0.04	+0.02 -0.02	+0.02 -0.02
(FTAG) tagSF_C , eigen8 [%]	-0.01 +0.01	+0.01 -0.01	-	-	-	-	-	-
(FTAG) tagSF_C , eigen9 [%]	-0.01 +0.01	+0.01 -0.01	-	-	-	-	-	-
(FTAG) tagSF_C , eigen10 [%]	-0.01 +0.01	+0.01 -0.01	-	-	-	-	-	-
(FTAG) tagSF_C , eigen11 [%]	-0.01 +0.01	+0.02 -0.01	-	-	-	-	-	-
(FTAG) tagSF_C , eigen12 [%]	-0.01 +0.01	+0.02 -0.01	-	-	-	-	-	-
(FTAG) tagSF_C , eigen13 [%]	-0.01 +0.01	+0.02 -0.01	-	-	-	-	-	-
(FTAG) tagSF_C , eigen14 [%]	-0.01 +0.01	+0.02 -0.01	-	-	-	-	-	-
(FTAG) tagSF_C , extrapolation [%]	-0.03 +0.03	+0.10 -0.03	+0.93 -0.03	+0.14 -0.03	+0.03 -0.03	+0.03 -0.03	+0.04 -0.04	+0.04 -0.04
(MET) PU jvt [%]	-0.03 +0.03	+0.04 -0.03	+0.07 -0.03	+0.06 -0.03	+0.05 -0.03	+0.06 -0.03	+0.02 -0.02	+0.02 -0.02
(BKO) singletop_Wt [%]	-	-	-	-	-	-	-	-
(BKO) ntW [%]	-	-	-	-	-	-	-	-
(BKO) ntZ [%]	-	-	-	-	-	-	-	-
(BKO) ntH [%]	-	-	-	-	-	-	-	-
(LJES) LARGERJET_Weak_JET_Rrk_Modelling_Tau32WTA [%]	-0.08 +0.09	+0.09 -0.09	+0.19 -0.09	+0.07 -0.09	+0.08 -0.09	+0.06 -0.09	+0.20 -0.03	+0.03 -0.03
(LJES) LARGERJET_Weak_JET_Rrk_Baseline_gT [%]	+0.03 +0.13	+0.03 -0.13	+0.08 -0.13	+0.02 -0.13	+0.03 -0.13	+0.04 -0.13	+0.04 -0.04	+0.04 -0.04
(LJES) LARGERJET_Weak_JET_Rrk_Baseline_mass [%]	-0.49 +0.15	+1.05 -0.15	+0.92 -0.15	+1.24 -0.15	+0.34 -0.15	+0.59 -0.15	+0.25 -0.15	+0.24 -0.15
(LJES) LARGERJET_Weak_JET_Rrk_Baseline_Tau32WTA [%]	+0.01 +0.01	+0.02 -0.01	+0.02 -0.01	+0.02 -0.01	+0.00 -0.01	+0.02 -0.01	+0.01 -0.01	+0.01 -0.01
(JES) JET_21NP_JET_BIAS_Response [%]	-	-	-	-	-	-	-	-
(JES) JET_21NP_JET_Plug_Response [%]	-	-	-	-	-	-	-	-
(JES) JET_21NP_JET_Plug_OffsetNP [%]	-0.03 +0.06	+0.03 -0.03	+0.05 -0.03	+0.05 -0.03	+0.03 -0.03	+0.03 -0.03	+0.03 -0.03	+0.03 -0.03
(JES) JET_21NP_JET_Plug_RhoTopology [%]	-0.04 +0.04	+0.10 -0.14	-0.14 -0.14	-0.06 -0.03	+0.03 -0.03	+0.18 -0.05	+0.05 -0.05	+0.05 -0.05
(JES) JET_21NP_JET_EffectiveNP_SecTerm [%]	-	-	-	-	-	-	-	-
(LEP) MUON_SAGITTA_RESBIAS [%]	-	-	-	-	-	-	-	-
(JES) JET_21NP_JET_EffectiveNP_3 [%]	-	-0.02	-	-	-	-	-	+0.02
(JES) JET_21NP_JET_EffectiveNP_4 [%]	-	-	-	-	-	-	-	-
(JES) LARGERJET_Weak_JET_Rrk_Tracking_mass [%]	-0.38 +0.22	+0.26 -0.26	-0.08 -0.08	-0.28 -0.08	-0.59 -0.08	-0.29 -0.08	+0.21 -0.03	+0.21 -0.03
(JES) JET_21NP_JET_Plug_OffsetRho [%]	-0.31 +0.06	+0.06 -0.06	+0.05 -0.05	+0.05 -0.05	+0.33 -0.05	+0.31 -0.05	+0.84 -0.05	+0.84 -0.05
(JES) JET_21NP_JET_EffectiveCalibration_TotalStat [%]	-0.06 +0.04	+0.04 -0.04	-0.08 -0.08	+0.02 -0.02	-0.11 -0.02	+0.07 -0.02	-0.08 +0.03	+0.02 +0.03
(JES) JET_21NP_JET_EffectiveCalibration_TotalClosure [%]	-0.05 +0.03	+0.06 -0.03	-0.06 -0.03	+0.04 -0.03	+0.04 -0.03	+0.04 -0.03	+0.04 -0.03	+0.04 -0.03
(JES) JET_21NP_JET_EffectiveCalibration_PtTau [%]	-0.01 +0.01	+0.01 -0.01	-0.01 -0.01	+0.01 -0.01	-0.01 +0.01	-0.01 +0.01	-0.02 +0.02	+0.02 -0.02
(JES) JET_21NP_JET_EffectiveNP_5 [%]	-	-	-	-	-	-	-	-
(JES) JET_21NP_JET_EffectiveNP_6 [%]	-0.04 +0.03	+0.06 -0.03	-0.08 -0.03	-0.04 -0.03	-0.04 +0.01	-0.04 +0.01	-0.03 +0.01	-0.03 +0.01
(JES) JET_21NP_JET_EffectiveNP_7 [%]	-	-	-	-	-	-	-	-
(JES) JET_21NP_JET_EffectiveNP_8 [%]	-0.04 +0.03	+0.06 -0.03	-0.08 -0.03	-0.04 -0.03	-0.04 +0.01	-0.04 +0.01	-0.03 +0.01	-0.03 +0.01
(JES) JET_21NP_JET_EffectiveNP_9 [%]	-0.04 +0.03	+0.06 -0.03	-0.08 -0.03	-0.04 -0.03	-0.04 +0.01	-0.04 +0.01	-0.03 +0.01	-0.03 +0.01
(JES) JET_21NP_JET_EffectiveNP_10 [%]	-0.16 +0.05	+0.06 -0.05	-0.14 -0.05	-0.14 -0.05	-0.18 -0.05	-0.16 -0.05	+0.05 -0.05	+0.05 -0.05
(JES) JET_21NP_JET_EffectiveNP_11 [%]	-0.08 +0.06	+0.09 -0.06	-0.09 -0.06	-0.07 -0.06	-0.07 -0.06	-0.07 -0.06	+0.09 -0.06	+0.09 -0.06
(JES) JET_21NP_JET_EffectiveNP_12 [%]	-0.07 +0.06	+0.08 -0.06	-0.08 -0.06	-0.07 -0.06	-0.07 -0.06	-0.07 -0.06	+0.08 -0.06	+0.08 -0.06
(JES) JET_21NP_JET_EffectiveNP_13 [%]	-0.07 +0.06	+0.08 -0.06	-0.08 -0.06	-0.07 -0.06	-0.07 -0.06	-0.07 -0.06	+0.08 -0.06	+0.08 -0.06
(JES) JET_21NP_JET_EffectiveNP_14 [%]	-0.07 +0.06	+0.08 -0.06	-0.08 -0.06	-0.07 -0.06	-0.07 -0.06	-0.07 -0.06	+0.08 -0.06	+0.08 -0.06
(JES) JET_21NP_JET_EffectiveNP_15 [%]	-0.07 +0.06	+0.08 -0.06	-0.08 -0.06	-0.07 -0.06	-0.07 -0.06	-0.07 -0.06	+0.08 -0.06	+0.08 -0.06
(PDF) PDF4LHC15_nlo_30_eigen01 [%]	-0.03 +0.07	+0.16 -0.07	+0.11 -0.07	+0.11 -0.07	+0.19 -0.07	+0.21 -0.07	+0.20 -0.07	+0.20 -0.07
(PDF) PDF4LHC15_nlo_30_eigen02 [%]	-0.13 +0.07	+0.16 -0.07	+0.11 -0.07	+0.11 -0.07	+0.19 -0.07	+0.21 -0.07	+0.20 -0.07	+0.20 -0.07
(PDF) PDF4LHC15_nlo_30_eigen03 [%]	-0.06 +0.07	+0.07 -0.07	+0.07 -0.07	+0.06 -0.07	+0.06 -0.07	+0.07 -0.07	+0.06 -0.07	+0.06 -0.07
(PDF) PDF4LHC15_nlo_30_eigen04 [%]	-0.07 +0.07	+0.07 -0.07	+0.07 -0.07	+0.07 -0.07	+0.07 -0.07	+0.07 -0.07	+0.07 -0.07	+0.07 -0.07
(PDF) PDF4LHC15_nlo_30_eigen05 [%]	-0.07 +0.07	+0.06 -0.07	+0.07 -0.07	+0.07 -0.07	+0.07 -0.07	+0.07 -0.07	+0.07 -0.07	+0.07 -0.07
(PDF) PDF4LHC15_nlo_30_eigen06 [%]	-0.07 +0.07	+0.06 -0.07	+0.07 -0.07	+0.07 -0.07	+0.07 -0.07	+0.07 -0.07	+0.07 -0.07	+0.07 -0.07
(PDF) PDF4LHC15_nlo_30_eigen07 [%]	-0.07 +0.07	+0.06 -0.07	+0.07 -0.07	+0.07 -0.07	+0.07 -0.07	+0.07 -0.07	+0.07 -0.07	+0.07 -0.07
(PDF) PDF4LHC15_nlo_30_eigen08 [%]	-0.12 +0.15	+0.15 -0.15	+0.13 -0.15	+0.13 -0.15	+0.18 -0.15	+0.17 -0.15	+0.20 -0.15	+0.18 -0.15
(PDF) PDF4LHC15_nlo_30_eigen09 [%]	-0.05 +0.05	+0.05 -0.05	-0.04 -0.05	-0.04 -0.05	-0.08 -0.05	-0.08 -0.05	+0.08 -0.05	+0.08 -0.05
(PDF) PDF4LHC15_nlo_30_eigen10 [%]	-0.05 +0.05	+0.06 -0.05	-0.04 -0.05	-0.04 -0.05	-0.05 -0.05	-0.05 -0.05	+0.06 -0.05	+0.06 -0.05
(PDF) PDF4LHC15_nlo_30_eigen11 [%]	-0.08 +0.08	+0.09 -0.08	-0.09 -0.08	-0.09 -0.08	-0.05 -0.08	-0.05 -0.08	+0.06 -0.08	+0.06 -0.08
(PDF) PDF4LHC15_nlo_30_eigen12 [%]	-0.08 +0.08	+0.09 -0.08	-0.09 -0.08	-0.09 -0.08	-0.05 -0.08	-0.05 -0.08	+0.06 -0.08	+0.06 -0.08
(PDF) PDF4LHC15_nlo_30_eigen13 [%]	-0.08 +0.08	+0.09 -0.08	-0.09 -0.08	-0.09 -0.08	-0.05 -0.08	-0.05 -0.08	+0.06 -0.08	+0.06 -0.08
(PDF) PDF4LHC15_nlo_30_eigen14 [%]	-0.08 +0.08	+0.09 -0.08	-0.09 -0.08	-0.09 -0.08	-0.05 -0.08	-0.05 -0.08	+0.06 -0.08	+0.06 -0.08
(PDF) PDF4LHC15_nlo_30_eigen15 [%]	-0.08 +0.08	+0.09 -0.08	-0.09 -0.08	-0.09 -0.08	-0.05 -0.08	-0.05 -0.08	+0.06 -0.08	+0.06 -0.08
(PDF) PDF4LHC15_nlo_30_eigen16 [%]	-0.08 +0.08	+0.09 -0.08	-0.09 -0.08	-0.09 -0.08	-0.05 -0.08	-0.05 -0.08	+0.06 -0.08	+0.06 -0.08
(PDF) PDF4LHC15_nlo_30_eigen17 [%]	-0.08 +0.08	+0.09 -0.08	-0.09 -0.08	-0.09 -0.08	-0.05 -0.08	-0.05 -0.08	+0.06 -0.08	+0.06 -0.08
(PDF) PDF4LHC15_nlo_30_eigen18 [%]	-0.08 +0.08	+0.09 -0.08	-0.09 -0.08	-0.09 -0.08	-0.05 -0.08	-0.05 -0.08	+0.06 -0.08	+0.06 -0.08
(PDF) PDF4LHC15_nlo_30_eigen19 [%]	-0.08 +0.08	+0.09 -0.08	-0.09 -0.08	-0.09 -0.08	-0.05 -0.08	-0.05 -0.08	+0.06 -0.08	+0.06 -0.08
(PDF) PDF4LHC15_nlo_30_eigen20 [%]	-0.04 +0.04	+0.04 -0.04	+0.04 -0.04	+0.04 -0.04	+0.06 -0.04	+0.06 -0.04	+0.07 -0.04	+0.07 -0.04
(PDF) PDF4LHC15_nlo_30_eigen21 [%]	-0.03 +0.03	+0.03 -0.03	+0.02 -0.03	+0.02 -0.03	+0.05 -0.03	+0.05 -0.03	+0.	

Not reviewed, for internal circulation only

Bins [GeV]	[500,550)	[550,600)	[600,650)	[650,700)	[700,750)	[750,800)	[800,1000)	[1000,1200)
$d\sigma/dp_T$ [fb/GeV]	6.30	3.52	1.87	0.86	0.51	0.29	0.17	0.10
Total Uncertainty [%]	-26.38	-13.92	-8.36	-3.83	-2.04	-1.04	-0.50	-0.21
Statistics [%]	+8.14	+4.60	+3.86	+2.16	+1.49	+0.60	+0.24	+0.11
Systematics [%]	+2.01	+3.14	+3.50	+36.99	+42.91	+40.07	+54.46	+92.62
(FTAG) fTagSF_B_eigen0 [%]	-0.98	-3.15	-5.36	-5.56	-5.87	-5.83	-5.84	-2.68
(FTAG) fTagSF_B_eigen1 [%]	-1.43	-1.78	-2.14	-2.31	-2.48	-2.42	-2.41	-1.94
(FTAG) fTagSF_B_eigen2 [%]	-1.14	-1.59	-1.85	-2.03	-2.15	-2.25	-2.25	-1.36
(FTAG) fTagSF_B_eigen3 [%]	-0.41	-0.72	-0.86	-0.92	-0.95	-1.10	-1.23	-0.59
(FTAG) fTagSF_B_eigen4 [%]	-0.39	-0.48	-0.95	-0.96	-0.73	-0.95	-1.05	-0.77
(FTAG) fTagSF_B_eigen5 [%]	-0.20	+0.23	-0.83	-0.80	-0.84	-0.89	-0.83	-0.41
(FTAG) fTagSF_C_eigen1 [%]	-1.93	-2.05	-1.91	-2.29	-2.46	-2.54	-2.59	-1.71
(FTAG) fTagSF_C_eigen2 [%]	-1.81	-1.72	-1.69	-1.79	-1.87	-1.93	-1.97	-1.59
(FTAG) fTagSF_C_eigen3 [%]	-0.92	-1.32	-1.11	-1.48	-1.23	-1.45	-1.20	-0.45
(FTAG) fTagSF_C_eigen4 [%]	-0.28	-0.39	-0.44	-0.45	-0.45	-0.45	-0.32	-0.12
(FTAG) fTagSF_C_eigen5 [%]	-0.16	-0.17	-0.12	-0.18	-0.27	-0.40	-0.14	-0.04
(FTAG) $\text{fTagSF_Light_eigen0}$ [%]	-0.01	-0.08	-0.10	-0.07	-0.04	-0.11	-0.11	-0.03
(FTAG) $\text{fTagSF_Light_eigen1}$ [%]	-0.01	-0.07	-0.10	-0.07	-0.04	-0.11	-0.11	-0.03
(FTAG) $\text{fTagSF_Light_eigen2}$ [%]	-0.01	-0.05	-0.10	-0.07	-0.04	-0.11	-0.11	-0.03
(FTAG) $\text{fTagSF_Light_eigen3}$ [%]	-0.01	-0.05	-0.10	-0.07	-0.04	-0.11	-0.11	-0.03
(FTAG) $\text{fTagSF_Light_eigen4}$ [%]	-0.07	-0.08	-0.12	-0.13	-0.14	-0.18	-0.11	-0.05
(FTAG) $\text{fTagSF_Light_eigen5}$ [%]	-0.14	-0.02	-0.05	-0.09	-0.15	-0.15	-0.11	-0.05
(FTAG) $\text{fTagSF_Light_eigen6}$ [%]	-	-0.01	-0.03	-0.03	-0.11	-0.08	-0.05	-0.01
(FTAG) $\text{fTagSF_Light_eigen7}$ [%]	-0.02	-0.03	-0.02	-0.08	-0.19	-0.06	-0.07	-0.01
(FTAG) $\text{fTagSF_Light_eigen8}$ [%]	-0.02	-	-0.03	-0.03	-0.11	-0.06	-0.06	-0.01
(FTAG) $\text{fTagSF_Light_eigen9}$ [%]	-0.02	-0.02	-0.03	-0.05	-0.03	-0.05	-0.03	-0.01
(FTAG) $\text{fTagSF_Light_eigen10}$ [%]	-0.01	-0.05	-0.10	-0.05	-0.05	-0.11	-0.11	-0.03
(FTAG) $\text{fTagSF_Light_eigen11}$ [%]	-0.01	-0.05	-0.10	-0.05	-0.04	-0.11	-0.11	-0.03
(FTAG) $\text{fTagSF_Light_eigen12}$ [%]	-0.01	-0.05	-0.10	-0.05	-0.04	-0.11	-0.11	-0.03
(FTAG) $\text{fTagSF_Light_eigen13}$ [%]	-0.01	-0.05	-0.10	-0.05	-0.04	-0.11	-0.11	-0.03
(FTAG) $\text{fTagSF_Light_eigen14}$ [%]	-0.01	-0.05	-0.10	-0.05	-0.04	-0.11	-0.11	-0.03
(FTAG) $\text{fTagSF_Light_eigen15}$ [%]	-0.01	-0.05	-0.10	-0.05	-0.04	-0.11	-0.11	-0.03
(FTAG) $\text{fTagSF_Light_eigen16}$ [%]	-0.01	-0.05	-0.10	-0.05	-0.04	-0.11	-0.11	-0.03
(FTAG) $\text{fTagSF_extrapolation}$ [%]	-2.05	-2.61	-3.58	-4.11	-4.73	-5.09	-5.02	-2.46
(FTAG) $\text{fTagSF_extrapolation_from_charm}$ [%]	-	-	-	-	-	-	-	-
(MET+PU) jet [%]	-0.10	-0.05	-0.11	-0.05	-0.06	-0.06	-0.01	-0.01
(BRG) singletop_chan [%]	-2.18	-2.38	-2.38	-2.38	-2.38	-2.38	-2.38	-1.78
(BRG) singletop_Wt [%]	-2.18	-2.38	-2.38	-2.38	-2.38	-2.38	-2.38	-1.78
(BKG) tW [%]	-0.03	-0.04	-0.05	-0.04	-0.05	-0.06	-0.07	-0.07
(BKG) tH [%]	-0.03	-0.05	-0.08	-0.05	-0.05	-0.08	-0.08	-0.08
(BKG) tHf [%]	-0.02	-0.02	-0.02	-0.02	-0.02	-0.03	-0.03	-0.03
(LJES) $\text{LARGEJET_Weak_JET_Rirk_Modeling_Tau32WTA}$ [%]	-2.31	-2.76	-3.09	-3.24	-3.54	-3.84	-4.13	-2.39
(LJES) $\text{LARGEJET_Weak_JET_Rirk_Baseline_PT}$ [%]	-2.31	-2.76	-3.09	-3.24	-3.54	-3.84	-4.13	-2.39
(LJES) $\text{LARGEJET_Weak_JET_Rirk_Baseline_Tau32WTA}$ [%]	-0.34	-0.38	-1.40	-2.05	-2.59	-3.19	-3.54	-1.02
(LJES) $\text{LARGEJET_Weak_JET_Rirk_Baseline_Tau32WTA}$ [%]	-0.01	-0.01	-0.01	-0.01	-0.01	-0.01	-0.01	-0.01
(JES) $\text{JET_21NP_JET_Response}$ [%]	-0.01	-0.01	-0.01	-0.01	-0.01	-0.01	-0.01	-0.01
(JES) $\text{JET_21NP_JET_Pileup_PTterm}$ [%]	-0.01	-0.01	-0.01	-0.01	-0.01	-0.01	-0.01	-0.01
(JES) $\text{JET_21NP_JET_Pileup_OffSetNP}$ [%]	-0.02	-0.02	-0.02	-0.02	-0.02	-0.02	-0.02	-0.02
(JES) $\text{JET_21NP_JET_Pileup_Scaleability}$ [%]	-0.08	-0.01	-0.05	-0.01	-0.02	-0.11	-0.12	-0.01
(JES) $\text{JET_21NP_JET_Effectivenp_SeeTerm}$ [%]	-0.08	-0.03	-0.06	-0.03	-0.04	-0.07	-0.09	-0.04
(LEP) $\text{MUON_SAGITTA_RESBIAS}$ [%]	-2.38	-2.38	-2.38	-2.38	-2.38	-2.38	-2.38	-1.78
(JES) $\text{JET_21NP_JET_Effectivenp_3}$ [%]	-0.02	-0.02	-0.02	-0.02	-0.02	-0.02	-0.02	-0.02
(JES) $\text{JET_21NP_JET_Effectivenp_4}$ [%]	-0.02	-0.02	-0.02	-0.02	-0.02	-0.02	-0.02	-0.02
(LJES) $\text{LARGEJET_Weak_JET_Rirk_Tracking_mass}$ [%]	-0.08	-0.01	-0.14	-0.01	-0.02	-0.07	-0.07	-0.01
(LJES) $\text{LARGEJET_Weak_JET_Rirk_TotalStat}$ [%]	-0.08	-0.01	-0.11	-0.01	-0.02	-0.07	-0.07	-0.01
(JES) $\text{JET_21NP_JET_Easymcalibration_TotalStat}$ [%]	-0.01	-0.02	-0.04	-0.01	-0.03	-0.08	-0.08	-0.01
(LEP) EG_REJECT [%]	-0.01	-0.02	-0.02	-0.01	-0.02	-0.05	-0.05	-0.01
(JES) $\text{JET_21NP_JET_Flavor_Response}$ [%]	-0.02	-0.02	-0.02	-0.02	-0.02	-0.03	-0.03	-0.02
(JES) $\text{JET_21NP_JET_Effectivenp_5}$ [%]	-0.01	-0.01	-0.01	-0.01	-0.01	-0.02	-0.02	-0.01
(JES) $\text{JET_21NP_JET_Effectivenp_6}$ [%]	-0.01	-0.01	-0.01	-0.01	-0.01	-0.02	-0.02	-0.01
(JES) $\text{JET_21NP_JET_Flavor_Composition}$ [%]	-0.14	-0.01	-0.01	-0.01	-0.01	-0.01	-0.01	-0.01
(JES) $\text{JET_21NP_JET_SingleParticle_HighPt}$ [%]	-0.01	-0.01	-0.01	-0.01	-0.01	-0.01	-0.01	-0.01
(JES) $\text{JET_21NP_JET_Weak_JET_Rirk_Modeling_pT}$ [%]	-2.65	-2.49	-2.05	-2.50	-2.69	-2.86	-2.92	-2.38
(JES) $\text{JET_21NP_JET_Effectivenp_1}$ [%]	-0.02	-0.03	-0.03	-0.26	-0.37	-0.17	-0.06	-0.02
(LEP) MUON_ID [%]	-0.02	-	-	-	-	-	-	-
(LJES) $\text{LARGEJET_Weak_JET_Rirk_TotalStat_pT}$ [%]	-0.30	-0.41	-0.28	-0.30	-0.30	-1.13	-0.10	-0.48
(JES) $\text{JET_21NP_JET_Easymcalibration_Modelling}$ [%]	-0.03	-0.01	-0.02	-0.01	-0.05	-0.08	-0.08	-0.01
(JES) $\text{JET_21NP_JET_Effectivenp_2}$ [%]	-0.02	-0.01	-0.02	-0.01	-0.05	-0.08	-0.08	-0.01
(LJES) $\text{LARGEJET_Weak_JET_Rirk_Tracking_Tau32WTA}$ [%]	-0.05	-0.05	-0.05	-0.05	-0.05	-0.35	-0.02	-0.32
(LJES) $\text{LARGEJET_Weak_JET_Rirk_PT}$ [%]	-0.17	-2.46	-3.96	-2.91	-2.96	-2.96	-1.94	-1.32
(LJES) $\text{LARGEJET_Weak_JET_Rirk_TotalStatWTA}$ [%]	-2.19	-2.49	-2.69	-2.66	-2.61	-2.85	-1.49	-1.11
(JES) $\text{JET_21NP_JET_Weak_JET_Rirk_Modeling_Tau32WTA}$ [%]	-0.01	-0.01	-0.01	-0.01	-0.01	-0.01	-0.01	-0.01
(JES) $\text{JET_21NP_JET_Top_massRes_mass}$ [%]	-0.11	-2.10	-2.38	-0.61	-0.60	-0.41	-0.17	-0.80
(PDF) $\text{PD4LHC15_nlo_30_eigen01}$ [%]	-0.10	-0.09	-0.13	-0.12	-0.08	-0.11	-0.21	-0.34
(PDF) $\text{PD4LHC15_nlo_30_eigen02}$ [%]	-0.21	-0.17	-0.14	-0.17	-0.26	-0.17	-0.20	-0.20
(PDF) $\text{PD4LHC15_nlo_30_eigen04}$ [%]	-0.16	-0.16	-0.19	-0.18	-0.22	-0.23	-0.15	-0.91
(PDF) $\text{PD4LHC15_nlo_30_eigen05}$ [%]	-0.08	-0.15	-0.15	-0.15	-0.19	-0.19	-0.19	-0.63
(PDF) $\text{PD4LHC15_nlo_30_eigen06}$ [%]	-0.25	-0.22	-0.29	-0.27	-0.28	-0.26	-0.30	-0.79
(PDF) $\text{PD4LHC15_nlo_30_eigen07}$ [%]	-0.02	-0.02	-0.03	-0.04	-0.03	-0.02	-0.01	-0.54
(PDF) $\text{PD4LHC15_nlo_30_eigen08}$ [%]	-0.19	-0.16	-0.15	-0.17	-0.17	-0.11	-0.20	-0.50
(PDF) $\text{PD4LHC15_nlo_30_eigen09}$ [%]	-0.05	-0.05	-0.06	-0.06	-0.06	-0.07	-0.08	-0.68
(PDF) $\text{PD4LHC15_nlo_30_eigen10}$ [%]	-0.07	-0.05	-0.07	-0.06	-0.06	-0.07	-0.09	-0.68
(PDF) $\text{PD4LHC15_nlo_30_eigen11}$ [%]	-0.11	-0.09	-0.11	-0.10	-0.09	-0.07	-0.10	-0.70
(PDF) $\text{PD4LHC15_nlo_30_eigen12}$ [%]	-0.08	-0.07	-0.10	-0.06	-0.06	-0.04	-0.07	-0.68
(PDF) $\text{PD4LHC15_nlo_30_eigen13}$ [%]	-0.03	-0.04	-0.05	-0.05	-0.03	-0.08	-0.08	-0.31
(PDF) $\text{PD4LHC15_nlo_30_eigen14}$ [%]	-0.02	-0.02	-0	-0.02	-0.03	-0.03	-	-0.68
(PDF) $\text{PD4LHC15_nlo_30_eigen15}$ [%]	-0.02	-0.02	-0.02	-0.02	-0.02	-0.01	-0.01	-0.57
(PDF) $\text{PD4LHC15_nlo_30_eigen03}$ [%]	-0.01	-0.03	-0.02	-0.02	-0.02	-0.01	-0.01	-0.58
(PDF) $\text{PD4LHC15_nlo_30_eigen24}$ [%]	-0.04	-0.04	-0.07	-0.03	-0.07	-0.06	-0.06	-0.63
(PDF) $\text{PD4LHC15_nlo_30_eigen25}$ [%]	-0.11	-0.08	-0.11	-0.11	-0.10	-0.10	-0.07	-0.40
(PDF) $\text{PD4LHC15_nlo_30_eigen26}$ [%]	-0.02	-0.02	-0.01	-0.01	-0.02	-0.01	-	-0.61
(PDF) $\text{PD4LHC15_nlo_30_eigen27}$ [%]	-0.03	-0.03	-0.02	-0.02	-0.04	-0.02	-0.02	-0.80
(PDF) $\text{PD4LHC15_nlo_30_eigen28}$ [%]	-0.11	-0.10	-0.10	-0.10	-0.12	-0.13	-0.11	-0.41
(PDF) $\text{PD4LHC15_nlo_30_eigen29}$ [%]	-	-	-	-	-	-0.02	-0.01	-0.63
(PDF) $\text{PD4LHC15_nlo_30_eigen30}$ [%]	-	-	-	-	-	-0.02	-0.01	-0.55
(MOD) Alternative hard-scattering model [%]	8.90	+13.85	+11.35	+14.96	+16.20	+11.91	+15.89	+3.81
(MOD) Alternative jet-shower mode [%]	±18.02	+2.167	+23.18	+18.72	+17.86	+18.02	+21.53	+5.06
(MOD) ISR/PSR + scale [%]	±0.10	+1.70	+0.08	+1.06	+5.62	+7.32	+4.90	+10.44
(MOD) Monte Carlo sample statistics [%]	±2.28	+2.81	+3.84	+4.32	+5.80	+7.74	+5.99	+33.43

Table 132: The individual systematic uncertainties in the parton level fiducial phase-space absolute differential cross-sections for the leading top p_T calculated as a percentage of the cross-section.

Bins (GeV)	[500,550]	[550,600]	[600,650]	[650,700]	[700,750]	[750,800]	[800,1000]	[1000,1200]
T_{jet}^2/dT_{jet} (GeV)	$8.1 \cdot 10^{-3}$	$4.46 \cdot 10^{-3}$	$2.37 \cdot 10^{-3}$	$1.91 \cdot 10^{-3}$	$1.1 \cdot 10^{-3}$	$6.71 \cdot 10^{-4}$	$2.83 \cdot 10^{-4}$	$5.7 \cdot 10^{-4}$
Total uncertainty [%]	± 4.8	± 3.8	± 6.7	± 11.27	± 11.27	± 22.0	± 8.32	± 4.10
Statistics [%]	± 3.56	± 4.50	± 5.08	± 5.85	± 4.12	± 2.04	± 15.90	± 4.66
Systematics [%]	± 7.21	± 7.74	± 5.21	± 5.38	± 12.40	± 10.78	± 25.14	± 6.74
(FTAG) fragSF_B_eigen0 [%]	-0.25	-0.08	-0.14	-0.85	-0.67	-0.62	-0.64	-0.25
(FTAG) fragSF_B_eigen1 [%]	-0.23	-0.15	-0.20	-0.21	-0.27	-0.24	-0.35	-0.15
(FTAG) fragSF_B_eigen2 [%]	-0.23	-0.15	-0.13	-0.13	-0.23	-0.22	-0.21	-0.15
(FTAG) fragSF_B_eigen3 [%]	-0.21	-0.13	-0.13	-0.07	-0.20	-0.20	-0.27	-0.01
(FTAG) fragSF_B_eigen4 [%]	-0.22	-0.13	-0.03	-0.05	-0.13	-0.25	-0.41	-0.04
(FTAG) fragSF_B_eigen5 [%]	-	-0.09	-0.04	-0.02	-0.02	-0.07	-0.12	-0.08
(FTAG) fragSF_C_eigen0 [%]	-0.04	-0.09	-0.10	-0.23	-0.39	-0.26	-0.36	-0.04
(FTAG) fragSF_C_eigen1 [%]	-0.09	-0.07	-0.08	-0.14	-0.16	-0.17	-0.19	-0.09
(FTAG) fragSF_C_eigen2 [%]	-0.01	-0.06	-0.02	-0.03	-0.13	-0.13	-0.11	-0.01
(FTAG) fragSF_C_eigen3 [%]	-0.04	-0.03	-0.03	-0.03	-0.03	-0.02	-0.03	-0.04
(FTAG) fragSF_C_eigen4 [%]	-0.14	-0.03	-0.03	-0.03	-0.03	-0.02	-0.03	-0.04
(FTAG) $\text{fragSF_Light_eigen0}$ [%]	-0.14	+0.15	+0.14	+0.25	+0.40	+0.27	+0.19	+0.34
(FTAG) $\text{fragSF_Light_eigen1}$ [%]	-	-0.26	-0.26	-	-	-	-	-0.27
(FTAG) $\text{fragSF_Light_eigen2}$ [%]	-	-	-	-	-	-	-	+1.62
(FTAG) $\text{fragSF_Light_eigen3}$ [%]	-	-	-	-	-	-	-	+2.39
(FTAG) $\text{fragSF_Light_eigen4}$ [%]	-0.12	-	-0.07	-0.03	-0.27	-	+0.13	-0.25
(FTAG) $\text{fragSF_Light_eigen5}$ [%]	-	-0.19	-0.08	+0.21	-	-	-	-5.68
(FTAG) $\text{fragSF_Light_eigen6}$ [%]	-	-	-	-	-	-	-	-2.81
(FTAG) $\text{fragSF_Light_eigen7}$ [%]	-	-	-	-	-	-	-	+2.38
(FTAG) $\text{fragSF_Light_eigen8}$ [%]	-	-	-	-	-	-	-	+2.22
(FTAG) $\text{fragSF_Light_eigen9}$ [%]	-	-	-	-	-	-	-	+2.21
(FTAG) $\text{fragSF_Light_eigen10}$ [%]	-	-	-	-	-	-	-	+2.32
(FTAG) $\text{fragSF_Light_eigen11}$ [%]	-	-	-	-	-	-	-	+2.72
(FTAG) $\text{fragSF_Light_eigen12}$ [%]	-	-	-	-	-	-	-	+2.72
(FTAG) $\text{fragSF_Light_eigen13}$ [%]	-	-	-	-	-	-	-	+2.72
(FTAG) $\text{fragSF_Light_eigen14}$ [%]	-	-	-	-	-	-	-	+2.72
(FTAG) $\text{fragSF_Light_eigen15}$ [%]	-	-	-	-	-	-	-	+2.72
(FTAG) $\text{fragSF_extrapolation}$ [%]	-1.32	-0.76	+0.19	+0.82	+1.54	+2.97	+4.07	+3.03
(FTAG) $\text{fragSF_extrapolation_from_charm}$ [%]	+1.23	+0.65	+0.34	-0.98	-1.72	-2.77	-4.25	-4.45
(MET+PU) $\text{jvt} [\%]$	-0.11	-0.04	-0.04	-0.04	-0.16	-0.11	-0.11	-0.12
(BKG) sigtop_chan [%]	-0.08	-0.08	-0.08	-	-	-	-	+2.32
(BKG) sigtop_Wt [%]	-	-	-	-	-	-	-	+2.32
(BKG) tW [%]	-	-	-	-	-	-	-	-2.33
(BKG) $t\bar{t}Z$ [%]	-	-	-	-	-	-	-	-2.33
(BKG) $t\bar{t}H$ [%]	-	-	-	-	-	-	-	-2.33
(LJES) $\text{LARGEJET_Weak_JET_Rirk_Modelling_Tau32WTA}$ [%]	-2.69	+0.84	-1.60	+0.87	+0.66	+2.45	+5.18	+1.13
(LJES) $\text{LARGEJET_Weak_JET_Rirk_Baseline_PT}$ [%]	-2.03	-1.23	-0.93	+2.21	+2.21	+2.62	+7.18	+0.69
(LJES) $\text{LARGEJET_Weak_JET_Rirk_Baseline_Tau32WTA}$ [%]	+3.13	+1.95	+0.73	+0.28	+0.28	+0.72	+0.92	+2.53
(LJES) $\text{LARGEJET_Weak_JET_Rirk_Baseline_Tau32WTA_TotalStat}$ [%]	-2.12	-0.04	-0.81	-0.23	-0.23	+0.21	+0.21	+0.41
(LJES) $\text{JET_21NP_JET_Rirk_Baseline_Tau32WTA}$ [%]	-2.12	+0.85	+0.92	-1.18	+4.69	+0.82	+0.02	+0.06
(JES) $\text{JET_21NP_JET_Rirk_Response}$ [%]	-	-	-	-	-	-	-	+2.38
(JES) $\text{JET_21NP_JET_Rirk_PfTerm}$ [%]	-	-	-	-	-	-	-	+2.38
(JES) $\text{JET_21NP_JET_Rirk_EgammaTerm}$ [%]	-	-	-	-	-	-	-	+2.25
(JES) $\text{JET_21NP_JET_Rirk_Morphology}$ [%]	-	-	-	-	-	-	-	+0.04
(JES) $\text{JET_21NP_JET_EffectivNP_SeeTerm}$ [%]	-	-	-	-	-	-	-	+2.33
(LEP) $\text{MUON_SAGITTA_RESHIAS}$ [%]	-	-	-	-	-	-	-	+2.32
(JES) $\text{JET_21NP_JET_EffectivNP_3}$ [%]	-	-	-	-	-	-	-	+3.37
(JES) $\text{JET_21NP_JET_EffectivNP_4}$ [%]	-	-	-	-	-	-	-	+2.33
(JES) $\text{JET_21NP_JET_EffectivNP_5}$ [%]	-	-	-	-	-	-	-	+2.32
(JES) $\text{JET_21NP_JET_Flavor_Composition}$ [%]	-	-	-	-	-0.12	-	-	+2.36
(JES) $\text{JET_21NP_JET_Flavor_Offshell}$ [%]	-	-	-	-	-	-	-	+2.31
(JES) $\text{JET_21NP_JET_Weak_JET_Rirk_TotalStat_mass}$ [%]	-	-	-	-	-	-	-0.04	+2.31
(JES) $\text{JET_21NP_JET_Elastercalibration_TotalClosure}$ [%]	-	-	-	-	-	-	-	+2.35
(JES) $\text{JET_21NP_JET_Elastercalibration_TotalStat}$ [%]	-	-	-	-	-	-	-	+2.35
(LEP) EQ_REPLICATOR [%]	-	-	-	-	-	-	+0.20	+2.25
(JES) $\text{JET_21NP_JET_Flavor_Response}$ [%]	-	-	-	-	-	-	-	+2.32
(JES) $\text{JET_21NP_JET_EffectivNP_6}$ [%]	-	-	-	-	-	-	-	+2.32
(JES) $\text{JET_21NP_JET_EffectivNP_5}$ [%]	-	-	-	-	-	-	-	+2.32
(JES) $\text{JET_21NP_JET_Flavor_Composition}$ [%]	-0.02	-0.03	-	-	-	-	+0.05	+2.27
(JES) $\text{JET_21NP_JET_SinglParticle_HighPt}$ [%]	-0.06	-0.10	-0.34	+0.03	+1.28	+0.30	+0.53	+2.32
(JES) $\text{JET_21NP_JET_Weak_JET_Rirk_Modelling_pT}$ [%]	-0.06	-0.13	-0.07	+0.12	+0.43	+0.10	+0.09	+2.33
(JES) $\text{JET_21NP_JET_EffectivNP_1}$ [%]	-0.05	-0.13	-0.07	-0.25	+0.21	+0.05	+0.12	+1.92
(LEP) MUON_ID [%]	-	-	-0.02	-0.25	-0.37	-0.17	-0.06	+4.76
(LEP) MUON_SCALE [%]	-0.06	+0.05	-0.08	-0.04	-0.24	+0.07	-0.35	+2.32
(LEP) MUON_PT [%]	-	-	-	-	-	-	-	+2.17
(JES) $\text{JET_21NP_JET_EffectivNP_7}$ [%]	-0.17	-0.19	-0.28	-0.02	+0.22	+0.26	-0.31	+2.32
(JES) $\text{JET_21NP_JET_Rirk_Modelling_mass}$ [%]	-0.17	-0.19	-0.28	-0.02	+0.03	+0.26	-0.31	+2.32
(LEP) MUON_MS [%]	-	-	-	-	-	-	-	+2.32
(LEP) MUON_SAGITTA_RHO [%]	-	-	-	-	-	-	-	+2.32
(JES) $\text{JET_21NP_JET_Elastercalibration_Modeling}$ [%]	-	-	-	-	-	-	-	+2.32
(JES) $\text{JET_21NP_JET_EffectivNP_2}$ [%]	-	-	-	-	-	-	-	+2.29
(JES) $\text{JET_21NP_JET_Weak_JET_Rirk_Tracking_Tau32WTA}$ [%]	-0.14	+0.12	+0.05	-0.43	-0.10	-0.09	-0.18	+2.33
(JES) $\text{JET_21NP_JET_Weak_JET_Rirk_Modelling_pT}$ [%]	-0.14	-0.02	-0.03	+1.82	+1.12	+3.15	+4.05	+1.05
(JES) $\text{JET_21NP_JET_Weak_JET_Rirk_Baseline_Tau32WTA}$ [%]	-0.05	-0.05	-0.05	+0.09	+0.09	+0.01	+0.01	+2.31
(JES) $\text{JET_21NP_JET_Weak_JET_Rirk_Baseline_Tau32WTA_TotalStat}$ [%]	-0.10	-0.13	-0.08	+0.02	+0.02	+0.00	+0.06	+0.46
(JES) $\text{JET_21NP_JET_Weak_JET_Rirk_Modelling_mass}$ [%]	-0.04	+1.04	+1.32	+0.46	+0.48	+0.08	+0.17	+1.39
(PDF) $\text{PDF4LHC15_nlo_30_eigen001}$ [%]	-0.10	+0.09	+0.13	+0.12	+0.08	+0.11	+0.21	+4.34
(PDF) $\text{PDF4LHC15_nlo_30_eigen002}$ [%]	-0.21	+0.17	+0.14	+0.17	+0.26	+0.17	+0.07	+5.20
(PDF) $\text{PDF4LHC15_nlo_30_eigen003}$ [%]	-0.16	+0.08	-	+0.12	+0.12	+0.08	+0.10	+4.62
(PDF) $\text{PDF4LHC15_nlo_30_eigen004}$ [%]	-0.16	+0.16	+0.19	+0.18	+0.22	+0.23	+0.15	+4.91
(PDF) $\text{PDF4LHC15_nlo_30_eigen005}$ [%]	-0.04	+0.02	+0.05	+0.04	+0.09	+0.09	+0.09	+3.63
(PDF) $\text{PDF4LHC15_nlo_30_eigen006}$ [%]	-0.25	+0.22	+0.29	+0.27	+0.28	+0.26	+0.30	+4.79
(PDF) $\text{PDF4LHC15_nlo_30_eigen007}$ [%]	-0.02	+0.02	+0.03	+0.04	+0.03	+0.02	+0.01	+4.54
(PDF) $\text{PDF4LHC15_nlo_30_eigen008}$ [%]	-0.19	+0.16	+0.15	+0.17	+0.17	+0.11	+0.20	+5.05
(PDF) $\text{PDF4LHC15_nlo_30_eigen009}$ [%]	-0.05	+0.05	+0.06	+0.05	+0.05	+0.06	+0.08	+4.68
(PDF) $\text{PDF4LHC15_nlo_30_eigen010}$ [%]	-0.07	+0.03	+0.01	+0.06	+0.04	+0.04	+0.09	+4.75
(PDF) $\text{PDF4LHC15_nlo_30_eigen011}$ [%]	-0.11	+0.09	+0.11	+0.10	+0.09	+0.07	+0.10	+4.78
(PDF) $\text{PDF4LHC15_nlo_30_eigen012}$ [%]	-0.08	+0.07	+0.10	+0.06	+0.06	+0.04	+0.07	+4.70
(PDF) $\text{PDF4LHC15_nlo_30_eigen013}$ [%]	-0.03	+0.04	-	+0.05	+0.02	+0.03	-	+4.31
(PDF) $\text{PDF4LHC15_nlo_30_eigen014}$ [%]	-0.02	+0.02	-	+0.02	+0.02	+0.03	-	+4.68
(PDF) $\text{PDF4LHC15_nlo_30_eigen015}$ [%]	-0.02	+0.02	-	+0.01	+0.01	+0.01	-	+4.78
(PDF) $\text{PDF4LHC15_nlo_30_eigen016}$ [%]	-	-	+0.03	-	+0.01	+0.04	+0.05	+4.52
(PDF) $\text{PDF4LHC15_nlo_30_eigen017}$ [%]	-0.09	+0.09	+0.11	+0.11	+0.10	+0.10	+0.13	+4.48
(PDF) $\text{PDF4LHC15_nlo_30_eigen018}$ [%]	-0.11	+0.08	+0.11	+0.11	+0.11	+0.10	+0.07	+4.40
(PDF) $\text{PDF4LHC15_nlo_30_eigen019}$ [%]	-	-	+0.01	-	+0.02	-	+0.04	+4.49
(PDF) $\text{PDF4LHC15_nlo_30_eigen020}$ [%]	-0.05	+0.05	+0.06	+0.03	+0.03	+0.06	+0.04	+4.52
(PDF) $\text{PDF4LHC15_nlo_30_eigen021}$ [%]	-0.08	+0.04	+0.03	+0.03	+0.03	+0.03	+0.03	+4.75
(PDF) $\text{PDF4LHC15_nlo_30_eigen022}$ [%]	-0.60	+0.53	+0.57	+0.57	+0.60	+0.54	+0.62	+3.77
(PDF) $\text{PDF4LHC15_nlo_30_eigen023}$ [%]	-	-	+0.02	-	+0.02	-	+0.01	+4.58
(PDF) $\text{PDF4LHC15_nlo_30_eigen024}$ [%]	-0.04	+0.04	+0.07	+0.03	+0.07	+0.09	+0.06	+4.63
(PDF) $\text{PDF4LHC15_nlo_30_eigen025}$ [%]	-0.02	+0.02	+0.03	+0.02	+0.02	+0.02	+0.02	+4.58
(PDF) $\text{PDF4LHC15_nlo_30_eigen026}$ [%]	-0.02	+0.02	+0.01	+0.01	+0.02	+0.01	+0.01	+4.61
(PDF) $\text{PDF4LHC15_nlo_30_eigen027}$ [%]	-0.03	+0.03	+0.02	+0.02	+0.04	+0.02	+0.02	+4.60
(PDF) $\text{PDF4LHC15_nlo_30_eigen028}$ [%]	-0.11	+0.10	+0.10	+0.10	+0.12	+0.13	+0.11	+4.81
(PDF) $\text{PDF4LHC15_nlo_30_eigen029}$ [%]	-	-	-	-	-	+0.02	+0.01	+4.63
(PDF) $\text{PDF4LHC15_nlo_30_eigen030}$ [%]	-	-	+0.02	-	+0.02	-	+0.03	+4.55
(MOD) Alternative hard-scattering model [%]	± 3.31 </							

Not reviewed, for internal circulation only

Bins [GeV]	[0,0.2]	[0,2.0]	[0,4.0]	[0,6.0]	[0,8.1]	[1,1.2]	[1,2,1.5]	[1,5,2]
$d\sigma/dX$ [pb/GeV]	$6.46 \cdot 10^{-1}$	$5.89 \cdot 10^{-1}$	$5.69 \cdot 10^{-1}$	$4.9 \cdot 10^{-1}$	$4.4 \cdot 10^{-1}$	$3.87 \cdot 10^{-1}$	$2.87 \cdot 10^{-1}$	$1.47 \cdot 10^{-1}$
Total Uncertainty [%]	+3.14 -3.14	+28.21 -32.72	+35.84 -31.32	+31.32 -33.02	+32.09 -33.68	+32.09 -33.68	+32.09 -33.68	+32.09 -33.68
Statistics [%]	+5.00 -5.00	+65.63 -63.52	+27.07 -25.04	+17.36 -18.53	+15.45 -16.50	+15.45 -16.50	+15.45 -16.50	+15.45 -16.50
Systematics [%]	+31.07 -31.53	+30.39 -27.12	+33.00 -31.34	+34.95 -31.34	+31.34 -32.83	+32.76 +32.76	+31.93 +31.93	+31.93 +31.93
(FTAG) bTagSE_B_eigen0 (%)	+5.89 -5.89	+5.03 -5.03	+4.82 -4.82	+5.81 -5.81	+5.29 -5.29	+5.59 -5.59	+5.27 -5.27	+5.38 -5.38
(FTAG) bTagSF_B_eigen1 (%)	+5.79 -5.79	+5.79 -5.79	+5.97 -5.97	+5.81 -5.81	+5.79 -5.79	+5.69 -5.69	+5.68 -5.68	+5.84 -5.84
(FTAG) bTagSF_B_eigen2 (%)	+5.78 -5.78	+5.79 -5.79	+5.97 -5.97	+5.81 -5.81	+5.79 -5.79	+5.69 -5.69	+5.68 -5.68	+5.84 -5.84
(FTAG) bTagSF_B_eigen3 (%)	+5.58 -5.58	+5.53 -5.53	+5.53 -5.53	+5.55 -5.55	+5.47 -5.47	+5.47 -5.47	+5.47 -5.47	+5.41 -5.41
(FTAG) bTagSF_B_eigen4 (%)	+5.73 -5.73	+5.28 -5.28	+5.25 -5.25	+5.28 -5.28	+5.24 -5.24	+5.23 -5.23	+5.23 -5.23	+5.21 -5.21
(FTAG) bTagSF_B_eigen5 (%)	+5.05 -5.05	+5.05 -5.05	+5.05 -5.05	+5.05 -5.05	+5.04 -5.04	+5.04 -5.04	+5.04 -5.04	+5.02 -5.02
(FTAG) bTagSF_C_eigen0 (%)	+5.89 -5.89	+5.03 -5.03	+4.82 -4.82	+5.81 -5.81	+5.29 -5.29	+5.59 -5.59	+5.27 -5.27	+5.38 -5.38
(FTAG) bTagSF_C_eigen1 (%)	+5.79 -5.79	+5.79 -5.79	+5.97 -5.97	+5.81 -5.81	+5.79 -5.79	+5.69 -5.69	+5.68 -5.68	+5.84 -5.84
(FTAG) bTagSF_C_eigen2 (%)	+5.78 -5.78	+5.79 -5.79	+5.97 -5.97	+5.81 -5.81	+5.79 -5.79	+5.69 -5.69	+5.68 -5.68	+5.84 -5.84
(FTAG) bTagSF_C_eigen3 (%)	+5.58 -5.58	+5.53 -5.53	+5.53 -5.53	+5.55 -5.55	+5.47 -5.47	+5.47 -5.47	+5.47 -5.47	+5.41 -5.41
(FTAG) bTagSF_C_eigen4 (%)	+5.73 -5.73	+5.28 -5.28	+5.25 -5.25	+5.28 -5.28	+5.24 -5.24	+5.23 -5.23	+5.23 -5.23	+5.21 -5.21
(FTAG) bTagSF_C_eigen5 (%)	+5.05 -5.05	+5.05 -5.05	+5.05 -5.05	+5.05 -5.05	+5.04 -5.04	+5.04 -5.04	+5.04 -5.04	+5.02 -5.02
(FTAG) bTagSF_Light_eigen0 (%)	+5.89 -5.89	+5.03 -5.03	+4.82 -4.82	+5.81 -5.81	+5.29 -5.29	+5.59 -5.59	+5.27 -5.27	+5.38 -5.38
(FTAG) bTagSF_Light_eigen1 (%)	+5.79 -5.79	+5.79 -5.79	+5.97 -5.97	+5.81 -5.81	+5.79 -5.79	+5.69 -5.69	+5.68 -5.68	+5.84 -5.84
(FTAG) bTagSF_Light_eigen2 (%)	+5.78 -5.78	+5.79 -5.79	+5.97 -5.97	+5.81 -5.81	+5.79 -5.79	+5.69 -5.69	+5.68 -5.68	+5.84 -5.84
(FTAG) bTagSF_Light_eigen3 (%)	+5.58 -5.58	+5.53 -5.53	+5.53 -5.53	+5.55 -5.55	+5.47 -5.47	+5.47 -5.47	+5.47 -5.47	+5.41 -5.41
(FTAG) bTagSF_Light_eigen4 (%)	+5.73 -5.73	+5.28 -5.28	+5.25 -5.25	+5.28 -5.28	+5.24 -5.24	+5.23 -5.23	+5.23 -5.23	+5.21 -5.21
(FTAG) bTagSF_Light_eigen5 (%)	+5.05 -5.05	+5.05 -5.05	+5.05 -5.05	+5.05 -5.05	+5.04 -5.04	+5.04 -5.04	+5.04 -5.04	+5.02 -5.02
(FTAG) bTagSF_Light_eigen6 (%)	+5.05 -5.05	+5.05 -5.05	+5.05 -5.05	+5.05 -5.05	+5.04 -5.04	+5.04 -5.04	+5.04 -5.04	+5.02 -5.02
(FTAG) bTagSF_Light_eigen7 (%)	+5.04 -5.04	+5.05 -5.05	+5.05 -5.05	+5.05 -5.05	+5.04 -5.04	+5.04 -5.04	+5.04 -5.04	+5.02 -5.02
(FTAG) bTagSF_Light_eigen8 (%)	+5.04 -5.04	+5.05 -5.05	+5.05 -5.05	+5.05 -5.05	+5.04 -5.04	+5.04 -5.04	+5.04 -5.04	+5.02 -5.02
(FTAG) bTagSF_Light_eigen9 (%)	+5.03 -5.03	+5.02 -5.02	+5.02 -5.02	+5.02 -5.02	+5.01 -5.01	+5.01 -5.01	+5.01 -5.01	+5.00 -5.00
(FTAG) bTagSF_Light_eigen10 (%)	+5.03 -5.03	+5.02 -5.02	+5.02 -5.02	+5.02 -5.02	+5.01 -5.01	+5.01 -5.01	+5.01 -5.01	+5.00 -5.00
(FTAG) bTagSF_Light_eigen11 (%)	+5.04 -5.04	+5.05 -5.05	+5.05 -5.05	+5.05 -5.05	+5.04 -5.04	+5.04 -5.04	+5.04 -5.04	+5.02 -5.02
(FTAG) bTagSF_Light_eigen12 (%)	+5.04 -5.04	+5.05 -5.05	+5.05 -5.05	+5.05 -5.05	+5.04 -5.04	+5.04 -5.04	+5.04 -5.04	+5.02 -5.02
(FTAG) bTagSF_Light_eigen13 (%)	+5.04 -5.04	+5.05 -5.05	+5.05 -5.05	+5.05 -5.05	+5.04 -5.04	+5.04 -5.04	+5.04 -5.04	+5.02 -5.02
(FTAG) bTagSF_Light_eigen14 (%)	+5.04 -5.04	+5.05 -5.05	+5.05 -5.05	+5.05 -5.05	+5.04 -5.04	+5.04 -5.04	+5.04 -5.04	+5.02 -5.02
(FTAG) bTagSF_Light_eigen15 (%)	+5.04 -5.04	+5.05 -5.05	+5.05 -5.05	+5.05 -5.05	+5.04 -5.04	+5.04 -5.04	+5.04 -5.04	+5.02 -5.02
(FTAG) bTagSF_extrapolation (%)	+5.93 -5.93	+5.14 -5.14	+5.36 -5.36	+5.36 -5.36	+5.36 -5.36	+5.36 -5.36	+5.36 -5.36	+5.36 -5.36
(FTAG) bTagSF_extrapolation_from_charm (%)	+5.05 -5.05	+5.05 -5.05	+5.05 -5.05	+5.05 -5.05	+5.05 -5.05	+5.05 -5.05	+5.05 -5.05	+5.05 -5.05
(MET) PU jet [%]	-0.02 -0.02	-0.05 -0.05	-0.03 -0.03	-0.02 -0.02	-0.02 -0.02	-0.02 -0.02	-0.02 -0.02	-0.02 -0.02
Lumi [%]	-0.13 -0.13	-0.07 -0.07	-0.12 -0.12	-0.08 -0.08	-0.12 -0.12	-0.12 -0.12	-0.12 -0.12	-0.01 -0.01
(BKG) singletop_tchan [%]	-2.04 -2.04	-1.95 -1.95	-1.99 -1.99	-2.04 -2.04	-1.99 -1.99	-2.00 -2.00	-1.98 -1.98	-2.00 -2.00
(BKG) singletop_Wt [%]	-	-	-	-	-	-	-	-
(BKG) mW [%]	-	-	-	-	-	-	-	-
(BKG) tZ [%]	-0.01 -0.01	-0.01 -0.01	-0.01 -0.01	-0.01 -0.01	-0.01 -0.01	-0.01 -0.01	-0.01 -0.01	-0.01 -0.01
(BKG) mH [%]	-0.01 -0.01	-0.01 -0.01	-0.01 -0.01	-0.01 -0.01	-0.01 -0.01	-0.01 -0.01	-0.01 -0.01	-0.01 -0.01
(LJES) LARGERJET_Weak_JET_Rtk_Modelling_Tau32WTA [%]	-0.04 -0.04	-0.03 -0.03	-0.03 -0.03	-0.03 -0.03	-0.03 -0.03	-0.03 -0.03	-0.03 -0.03	-0.03 -0.03
(LJES) LARGERJET_Weak_JET_Rtk_Baseline_pT [%]	-0.03 -0.03	+1.23 +1.23	+0.27 +0.27	+0.21 +0.21	+0.15 +0.15	+0.19 +0.19	+0.47 +0.47	+2.33 +2.33
(LJES) LARGERJET_Weak_JET_Rtk_Baseline_Mass [%]	-0.03 -0.03	+1.72 +1.72	+0.27 +0.27	+0.21 +0.21	+0.15 +0.15	+0.21 +0.21	+0.50 +0.50	+2.29 +2.29
(LJES) LARGERJET_Weak_JET_Rtk_Baseline_Tau32WTA [%]	-0.03 -0.03	+0.40 +0.40	+0.27 +0.27	+0.21 +0.21	+0.15 +0.15	+0.21 +0.21	+0.50 +0.50	+2.40 +2.40
(JES) JET_21NP_JET_BHES_Response [%]	+0.03 +0.03	-0.01 -0.01	-0.01 -0.01	-0.01 -0.01	-0.01 -0.01	-0.01 -0.01	-0.01 -0.01	-0.01 -0.01
(JES) JET_21NP_JET_Plus_Pt [%]	+0.01 +0.01	-0.01 -0.01	-0.01 -0.01	-0.01 -0.01	-0.01 -0.01	-0.01 -0.01	-0.01 -0.01	-0.01 -0.01
(JES) JET_21NP_JET_OrekhovN [%]	+0.01 +0.01	-0.01 -0.01	-0.01 -0.01	-0.01 -0.01	-0.01 -0.01	-0.01 -0.01	-0.01 -0.01	-0.01 -0.01
(JES) JET_21NP_JET_Plakor_RhoTopology [%]	+0.22 +0.22	+0.12 +0.12	+0.04 +0.04	+0.02 +0.02	+0.04 +0.04	+0.03 +0.03	+0.03 +0.03	+0.02 +0.02
(JES) JET_21NP_JET_SystTerm [%]	-0.06 -0.06	-0.03 -0.03	-0.20 -0.20	-0.11 -0.11	-0.17 -0.17	+0.06 +0.06	-0.08 -0.08	-0.24 -0.24
(LEP) MUON_SAGITTA_RESBIAS [%]	-	-	-	-	-	-	-	-
(JES) JET_21NP_JET_EffectiveNP_3 [%]	+0.03 +0.03	-0.01 -0.01	-0.01 -0.01	-0.02 -0.02	+0.02 +0.02	+0.02 +0.02	-0.02 -0.02	-0.02 -0.02
(JES) JET_21NP_JET_EffectiveNP_6 [%]	+0.07 +0.07	-0.03 -0.03	-0.03 -0.03	-0.03 -0.03	+0.06 +0.06	+0.06 +0.06	-0.03 -0.03	-0.03 -0.03
(JES) JET_21NP_JET_EffectiveNP_5 [%]	-	-	-0.01 -0.01	-0.01 -0.01	-	-	-	-
(JES) JET_21NP_JET_EffectiveNP_7 [%]	+0.20 +0.20	+0.26 +0.26	+0.28 +0.28	+0.36 +0.36	+0.34 +0.34	+0.15 +0.15	+0.15 +0.15	+0.30 +0.30
(JES) JET_21NP_JET_EffectiveNP_8 [%]	+0.13 +0.13	+0.23 +0.23	+0.23 +0.23	+0.23 +0.23	+0.23 +0.23	+0.13 +0.13	+0.13 +0.13	+0.26 +0.26
(JES) JET_21NP_JET_EffectiveNP_9 [%]	+0.13 +0.13	+0.23 +0.23	+0.23 +0.23	+0.23 +0.23	+0.23 +0.23	+0.13 +0.13	+0.13 +0.13	+0.26 +0.26
(JES) JET_21NP_JET_EffectiveNP_10 [%]	+0.13 +0.13	+0.23 +0.23	+0.23 +0.23	+0.23 +0.23	+0.23 +0.23	+0.13 +0.13	+0.13 +0.13	+0.26 +0.26
(JES) JET_21NP_JET_EffectiveNP_11 [%]	+0.16 +0.16	+0.25 +0.25	+0.10 +0.10	+0.23 +0.23	+0.07 +0.07	+0.07 +0.07	+0.03 +0.03	+0.02 +0.02
(JES) JET_21NP_JET_EffectiveNP_12 [%]	+0.05 +0.05	+0.07 +0.07	+0.08 +0.08	+0.06 +0.06	+0.30 +0.30	+0.12 +0.12	+0.13 +0.13	+0.06 +0.06
(JES) JET_21NP_JET_EffectiveNP_13 [%]	+0.05 +0.05	+0.07 +0.07	+0.08 +0.08	+0.06 +0.06	+0.30 +0.30	+0.12 +0.12	+0.13 +0.13	+0.06 +0.06
(JES) JET_21NP_JET_EffectiveNP_14 [%]	+0.05 +0.05	+0.07 +0.07	+0.08 +0.08	+0.06 +0.06	+0.30 +0.30	+0.12 +0.12	+0.13 +0.13	+0.06 +0.06
(JES) JET_21NP_JET_EffectiveNP_15 [%]	+0.01 +0.01	-	-	-	-	-	-	-
(PDF) PDF4LHC15_nlo_30_eigen003 [%]	+0.06 +0.06	-0.06 -0.06	-0.08 -0.08	-0.06 -0.06	-0.03 -0.03	-0.04 -0.04	-0.07 -0.07	+0.05 +0.05
(PDF) PDF4LHC15_nlo_30_eigen004 [%]	+0.05 +0.05	+0.11 +0.11	+0.06 +0.06	+0.08 +0.08	+0.12 +0.12	+0.21 +0.21	+0.27 +0.27	+0.33 +0.33
(PDF) PDF4LHC15_nlo_30_eigen005 [%]	+0.043 +0.043	+0.54 +0.54	+0.45 +0.45	+0.40 +0.40	+0.48 +0.48	+0.54 +0.54	+0.50 +0.50	+0.55 +0.55
(PDF) PDF4LHC15_nlo_30_eigen006 [%]	+0.018 +0.018	+0.22 +0.22	+0.17 +0.17	+0.17 +0.17	+0.22 +0.22	+0.35 +0.35	+0.26 +0.26	+0.36 +0.36
(PDF) PDF4LHC15_nlo_30_eigen007 [%]	+0.012 +0.012	+0.16 +0.16	+0.14 +0.14	+0.14 +0.14	+0.18 +0.18	+0.20 +0.20	+0.18 +0.18	+0.22 +0.22
(PDF) PDF4LHC15_nlo_30_eigen008 [%]	+0.005 +0.005	+0.06 +0.06	+0.05 +0.05	+0.06 +0.06	+0.07 +0.07	+0.06 +0.06	+0.06 +0.06	+0.05 +0.05
(PDF) PDF4LHC15_nlo_30_eigen010 [%]	+0.005 +0.005	+0.06 +0.06	+0.07 +0.07	+0.06 +0.06	+0.06 +0.06	+0.06 +0.06	+0.06 +0.06	+0.07 +0.07
(PDF) PDF4LHC15_nlo_30_eigen011 [%]	+0.007 +0.007	+0.11 +0.11	+0.02 +0.02	+0.02 +0.02	+0.05 +0.05	+0.06 +0.06	+0.03 +0.03	+0.05 +0.05
(PDF) PDF4LHC15_nlo_30_eigen012 [%]	+0.038 +0.038	+0.49 +0.49	+0.44 +0.44	+0.46 +0.46	+0.59 +0.59	+0.70 +0.70	+0.72 +0.72	+0.86 +0.86
(PDF) PDF4LHC15_nlo_30_eigen023 [%]	-	-	-	-	-	-	-	+0.01 +0.01
(PDF) PDF4LHC15_nlo_30_eigen024 [%]	+0.04 +0.04	-0.03 -0.03	-0.03 -0.03	-0.03 -0.0				

Not reviewed, for internal circulation only

Bins (GeV)	[0,0.2]	[0.2,0.4]	[0.4,0.6]	[0.6,0.8]	[0.8,1]	[1,1.2]	[1.2,1.5]	[1.5,2]	
Lumi/tau_N [pb/GeV]	$8.40 \pm 0.17 \pm 1.51 \pm 0.10 \pm 7.30 \pm 0.11 \pm 6.25 \pm 0.10 \pm 5.00 \pm 0.10 \pm 4.84 \pm 0.10 \pm 3.67 \pm 0.10 \pm 1.88 \pm 0.10$								
Total Uncertainty [%]	± 6.29	± 9.04	± 7.80	± 9.27	± 7.28	± 8.34	± 10.07	± 8.34	± 11.44
Statistics [%]	± 5.20	± 6.15	± 6.28	± 6.62	± 6.84	± 7.86	± 6.79	± 8.93	
Systematics [%]	± 2.35	± 5.51	± 3.34	± 6.13	± 3.28	± 4.32	± 3.28	± 4.93	
(FTAG) TagSF_B_eigen0 [%]	-0.04	-0.04	-0.06	-0.05	+0.09	-	-0.11	+0.08	
(FTAG) TagSF_B_eigen1 [%]	+0.01	-0.01	+0.05	+0.01	-0.06	-0.06	+0.14	+0.08	
(FTAG) TagSF_B_eigen2 [%]	+0.01	+0.01	+0.03	-0.05	+0.02	-0.05	+0.24	+0.03	
(FTAG) TagSF_B_eigen3 [%]	+0.03	+0.03	+0.01	-0.06	-0.03	-0.06	+0.07	-0.11	
(FTAG) TagSF_B_eigen4 [%]	+0.04	+0.01	+0.01	+0.03	-0.05	-0.03	-0.01	+0.01	
(FTAG) TagSF_B_eigen5 [%]	-	-	-	-	-	-0.02	-	-0.03	
(FTAG) TagSF_C_eigen0 [%]	-0.07	-0.08	+0.20	-0.02	+0.04	-0.08	-0.21	-0.28	
(FTAG) TagSF_C_eigen1 [%]	-0.04	-0.06	+0.03	-0.03	-0.07	-0.01	+0.05	+0.32	
(FTAG) TagSF_C_eigen2 [%]	+0.02	-0.11	-0.05	+0.01	+0.06	-0.03	+0.15	+0.10	
(FTAG) TagSF_C_eigen3 [%]	+0.01	-0.01	-0.04	-0.12	-0.04	-0.07	+0.27	+0.26	
(FTAG) TagSF_C_eigen4 [%]	-0.09	-0.01	-0.03	-0.18	+0.04	-0.09	-0.09	+0.09	
(FTAG) TagSF_C_eigen5 [%]	-0.01	-0.01	-0.01	-0.03	-0.05	-0.01	-0.01	-0.01	
(FTAG) TagSF_Light_eigen0 [%]	-0.08	-0.03	+0.20	-0.02	+0.04	-0.08	-0.21	-0.28	
(FTAG) TagSF_Light_eigen1 [%]	-0.04	-0.04	-0.20	-0.03	-0.07	-0.01	+0.05	+0.32	
(FTAG) TagSF_Light_eigen2 [%]	-0.02	-0.11	-0.05	+0.01	+0.06	-0.03	+0.15	+0.10	
(FTAG) TagSF_Light_eigen3 [%]	+0.01	-0.01	-0.04	-0.12	-0.05	-0.07	+0.27	+0.26	
(FTAG) TagSF_Light_eigen4 [%]	-0.08	-0.01	-0.05	+0.04	+0.06	-0.09	+0.04	+0.07	
(FTAG) TagSF_Light_eigen5 [%]	-0.08	+0.02	-0.07	-0.04	-0.08	-0.09	-0.09	+0.17	
(FTAG) TagSF_Light_eigen6 [%]	-0.02	-0.01	-	-0.02	-0.04	-	-0.01	+0.02	
(FTAG) TagSF_Light_eigen7 [%]	-0.01	-0.01	-0.01	-0.03	-	-0.03	-0.11	-0.04	
(FTAG) TagSF_Light_eigen8 [%]	-0.01	-0.02	-0.01	-0.03	-0.02	-0.03	-0.11	-0.08	
(FTAG) TagSF_Light_eigen9 [%]	-	-	-	-0.03	-0.02	-0.02	-0.02	-0	
(FTAG) TagSF_extrapolation [%]	+0.16	-0.08	+0.14	-0.02	+0.05	-0.03	-0.13	-0.40	
(FTAG) TagSF_extrapolation_jvt [%]	-0.18	-0.07	-0.15	-0.07	-0.07	-0.07	-0.28	-0.61	
(FTAG) TagSF_extrapolation_from_charm [%]	-0.01	-0.02	-0.04	-0.05	-0.04	-0.06	-0.11	-0.11	
(MET/Pt) jvt [%]	-0.04	-0.02	-0.04	-0.04	-0.04	-0.06	-0.09	-0.03	
Luminosity [%]	-0.03	-0.06	-0.02	-0.03	-0.03	-0.05	-0.05	-0.03	
(BKG) singletop_1chan [%]	-	-	-	-	-	-	-	-	
(BKG) singletop_Wt [%]	-	-	-	-	-	-	-	-	
(BKG) nW [%]	-	-	-	-	-	-	-	-	
(BKG) nZ [%]	-	-	-	-	-	-	-	-	
(BKG) nH [%]	-	-	-	-	-	-	-	-	
(LJES) LARGERJET_Weak_JET_Rkt_Modelling_Tau32WTA [%]	-0.07	+0.17	+0.04	-0.05	+0.18	+0.26	+0.12	+0.17	
(LJES) LARGERJET_Weak_JET_Rkt_Baseline_PT [%]	-0.12	-0.27	-0.90	-0.03	-0.26	-0.36	-0.32	-0.35	
(LJES) LARGERJET_Weak_JET_Rkt_Baseline_TotalStat [%]	-0.14	+0.56	-0.83	+0.14	+0.19	-0.31	-0.32	-0.49	
(LJES) LARGERJET_Weak_JET_Rkt_Baseline_Tau32WTA [%]	-0.24	-0.58	+0.17	-0.10	+0.04	-0.22	-0.11	-0.32	
(JES) JET_21NP_JET_BHES_Response [%]	-0.02	-	-	-0.02	-	-0.05	-0.01	-0.01	-0.01
(JES) JET_21NP_JET_Plmp_fTTerm [%]	-	-	-	-0.01	-0.01	-0.02	-0.05	-0.01	-0.02
(JES) JET_21NP_JET_Plmp_fTTerm_jvt [%]	-0.02	-0.03	-0.04	-0.03	-0.03	-0.02	-0.04	-0.07	-
(JES) JET_21NP_JET_Plmp_BkgReplay [%]	-0.03	-0.03	+0.03	+0.04	+0.03	-0.01	-0.01	-0.07	-
(JES) JET_21NP_JET_EffectiveNP_SeefTerm [%]	-	-	-	-	-	-	-	-	
(JEP) MUON_SAGITTA_RESBIAS [%]	-	-	-	-	-	-	-	-	
(JES) JET_21NP_JET_EffectiveNP_3 [%]	-	-0.02	-	-	-	-	-	-	
(JES) JET_21NP_JET_EffectiveNP_4 [%]	-	-	-	-	-	-	-	-	
(JES) JET_21NP_JET_EffectiveNP_5 [%]	-0.28	-0.03	+0.34	-0.77	+0.45	-0.09	-0.29	-0.16	
(JES) JET_21NP_JET_EffectiveNP_6 [%]	-0.02	-0.11	-0.33	-0.02	+0.24	-0.21	+0.28	+0.73	
(JES) JET_21NP_JET_EffectiveNP_7 [%]	-0.01	-0.08	-	-0.24	+0.14	-0.02	-	+0.03	
(JES) JET_21NP_JET_EffectiveNP_8 [%]	-0.02	-0.07	-0.07	-0.03	-0.04	-0.07	+0.03	+0.03	
(JES) JET_21NP_JET_EffectiveNP_9 [%]	-0.01	-0.01	-0.01	-0.01	-0.01	-0.05	-0.01	-0.02	
(JES) JET_21NP_JET_EffectiveNP_10 [%]	-0.05	-0.07	-0.09	-0.01	-0.01	-0.08	-0.04	-0.18	
(JES) JET_21NP_JET_EffectiveNP_11 [%]	-0.03	-0.03	-0.12	-0.01	-0.03	-0.17	-0.05	-0.01	
(LEP) MUON_ID [%]	-	-	-	-	-	-	-	-	
(JES) LARGERJET_Weak_JET_Rkt_TotalStat_gT [%]	-0.08	-0.07	+0.11	-0.04	+0.03	-0.07	-0.09	+0.08	
(JEP) MUON_SCALE [%]	-	-	-	-	-	-	-	-	
(JEP) EG_SCALE_ALL [%]	-	-	-	-	-	-	-	-	
(JES) JET_21NP_JET_EffectiveNP_NonClosure [%]	-0.01	-0.01	-0.01	-0.01	-0.01	-0.07	+0.03	+0.03	
(JEP) JET_Recoil [%]	-0.01	-0.01	-0.01	-0.01	-0.01	-0.01	-0.01	-0.01	
(JES) JET_21NP_JET_Flavor_JetResponse [%]	-0.05	-0.07	-0.09	-0.01	-0.01	-0.08	-0.04	-0.18	
(JES) JET_21NP_JET_EffectiveNP_5 [%]	-0.03	-0.03	-0.02	-0.01	-0.01	-0.01	-0.01	-0.01	
(JES) JET_21NP_JET_SingleParticle_HighPt [%]	-0.04	-0.01	+0.04	+0.04	+0.10	-0.09	-0.07	-0.04	
(JES) JET_21NP_JET_EffectiveNP_TotalStat [%]	-0.03	-0.03	-0.03	-0.03	-0.03	-0.03	-0.03	-0.03	
(JES) JET_21NP_JET_EffectiveNP_4 [%]	-0.03	-0.03	-0.03	-0.03	-0.03	-0.03	-0.03	-0.03	
(JES) JET_21NP_JET_EffectiveNP_5 [%]	-0.03	-0.03	-0.03	-0.03	-0.03	-0.03	-0.03	-0.03	
(JES) JET_21NP_JET_EffectiveNP_6 [%]	-0.03	-0.03	-0.03	-0.03	-0.03	-0.03	-0.03	-0.03	
(JES) JET_21NP_JET_EffectiveNP_7 [%]	-0.03	-0.03	-0.03	-0.03	-0.03	-0.03	-0.03	-0.03	
(JES) JET_21NP_JET_EffectiveNP_8 [%]	-0.03	-0.03	-0.03	-0.03	-0.03	-0.03	-0.03	-0.03	
(JES) JET_21NP_JET_EffectiveNP_9 [%]	-0.03	-0.03	-0.03	-0.03	-0.03	-0.03	-0.03	-0.03	
(JES) JET_21NP_JET_EffectiveNP_10 [%]	-0.03	-0.03	-0.03	-0.03	-0.03	-0.03	-0.03	-0.03	
(JES) JET_21NP_JET_EffectiveNP_11 [%]	-0.03	-0.03	-0.03	-0.03	-0.03	-0.03	-0.03	-0.03	
(JES) JET_21NP_JET_EffectiveNP_12 [%]	-0.03	-0.03	-0.03	-0.03	-0.03	-0.03	-0.03	-0.03	
(JES) JET_21NP_JET_EffectiveNP_13 [%]	-0.03	-0.03	-0.03	-0.03	-0.03	-0.03	-0.03	-0.03	
(JES) JET_21NP_JET_EffectiveNP_14 [%]	-	-	-0.01	-	-	-0.02	-0.06	+0.05	
(JES) JET_21NP_JET_EffectiveNP_15 [%]	-0.01	-0.02	-0.02	-0.02	-0.02	-0.07	-0.05	-0.07	
(JES) JET_21NP_JET_EffectiveNP_16 [%]	-0.07	-0.10	-0.08	-0.07	-0.09	-0.12	-0.10	-0.12	
(JES) JET_21NP_JET_EffectiveNP_17 [%]	-0.05	-0.08	-0.05	-0.05	-0.07	-0.11	-0.11	-0.25	
(JES) JET_21NP_JET_EffectiveNP_18 [%]	-0.12	-0.15	-0.12	-0.02	-0.02	-0.12	-0.12	-0.17	
(JES) JET_21NP_JET_EffectiveNP_19 [%]	-0.12	-0.15	-0.12	-0.02	-0.02	-0.12	-0.12	-0.17	
(JES) JET_21NP_JET_EffectiveNP_20 [%]	-0.04	-0.04	-0.03	-0.05	-0.06	-0.06	-0.10	-0.13	
(JES) JET_21NP_JET_EffectiveNP_21 [%]	-0.03	-0.03	-0.02	-0.03	-0.05	-0.06	-0.10	-0.05	
(JES) JET_21NP_JET_EffectiveNP_22 [%]	-0.03	-0.04	-0.04	-0.05	-0.06	-0.06	-0.12	-0.06	
(JES) JET_21NP_JET_EffectiveNP_23 [%]	-0.03	-0.04	-0.04	-0.05	-0.06	-0.06	-0.12	-0.06	
(JES) JET_21NP_JET_EffectiveNP_24 [%]	-0.04	-0.03	-0.03	-0.04	-0.05	-0.05	-0.13	-0.04	
(JES) JET_21NP_JET_EffectiveNP_25 [%]	-0.01	-	-	-0.01	-0.02	-0.02	-0.01	-0.04	
(JES) JET_21NP_JET_EffectiveNP_26 [%]	-0.03	-0.03	-0.02	-0.03	-0.04	-0.03	-0.03	-	
(JES) JET_21NP_JET_EffectiveNP_27 [%]	-0.02	-0.03	-0.04	-0.04	-0.05	-0.05	-0.05	-0.04	
(JES) JET_21NP_JET_EffectiveNP_28 [%]	-0.13	-0.13	-0.12	-0.14	-0.15	-0.13	-0.11	-0.09	
(JES) JET_21NP_JET_EffectiveNP_29 [%]	-	-	-	-	-	-	-	-	
(JES) JET_21NP_JET_EffectiveNP_30 [%]	-	-	-	-0.01	-0.02	-	-0.03	-0.04	
(MOD) Alternative hard-scattering model [%]	0.98	2.85	0.11	2.30	1.22	2.36	1.33	2.69	
(MOD) Alternative parton-shower mode [%]	0.17	4.22	0.42	4.58	1.96	2.30	1.92	2.69	
(MOD) ISR/FSR + scale [%]	1.43	0.37	2.30	2.98	0.84	0.83	1.16	1.17	
(MOD) Monte Carlo sample statistics [%]	2.63	3.67	3.20	3.21	3.32	4.38	3.56	5.17	

Table 135: The individual systematic uncertainties in the parton level fiducial phase-space relative differential cross-sections for the leading top $|y|$ calculated as a percentage of the cross-section.

Not reviewed, for internal circulation only

Bins (GeV)	[350,400]	[400,450]	[450,500]	[500,550]	[550,600]	[600,680]	[800,1200]
$d\sigma/dX$ [pb/GeV]	$2.14 \cdot 10^{-3}$	$2.77 \cdot 10^{-3}$	$3.72 \cdot 10^{-3}$	$3.21 \cdot 10^{-3}$	$1.58 \cdot 10^{-3}$	$5.62 \cdot 10^{-4}$	$4.6 \cdot 10^{-4}$
Total Uncertainty [%]	-29.27	-28.87	-29.84	-34.75	-38.93	-58.43	-37
Statistics [%]	+9.60	+5.50	+4.41	+4.54	+7.12	+28.30	-
Systematic [%]	+2.00	+2.00	+2.00	+2.00	+2.00	+2.00	+2.00
(FTAG) fTagSF_B , eigen0 [%]	-28.59	-27.91	-29.34	-32.24	-38.13	-62.24	-37
(FTAG) fTagSF_B , eigen1 [%]	+3.81	+3.89	+3.24	+3.29	+3.31	+5.46	+5.95
(FTAG) fTagSF_B , eigen2 [%]	+5.37	+5.04	+5.86	+4.83	+5.04	+5.15	+5.94
(FTAG) fTagSF_B , eigen3 [%]	+0.56	+0.69	+0.54	+0.54	+0.69	+1.00	+1.00
(FTAG) fTagSF_B , eigen4 [%]	+0.39	+0.99	+0.49	+0.23	+0.37	+1.92	+1.24
(FTAG) fTagSF_B , eigen5 [%]	+0.13	+0.13	+0.22	+0.24	+0.27	+0.33	+0.37
(FTAG) fTagSF_B , eigen6 [%]	-0.05	-0.05	+0.03	+0.04	+0.06	+0.06	+0.06
(FTAG) fTagSF_C , eigen0 [%]	-2.05	-0.03	-0.04	-0.05	-0.03	-0.06	+0.29
(FTAG) fTagSF_C , eigen1 [%]	+3.73	+3.99	+3.55	+3.55	+3.71	+4.01	+4.25
(FTAG) fTagSF_C , eigen2 [%]	+3.34	+3.22	+3.13	+3.11	+3.14	+3.00	+3.00
(FTAG) fTagSF_C , eigen3 [%]	+0.72	+0.77	+0.74	+0.74	+0.79	+0.15	+0.84
(FTAG) fTagSF_C , eigen4 [%]	+0.18	+0.14	+0.15	+0.15	+0.19	+0.14	+0.29
(FTAG) fTagSF_C , eigen5 [%]	+0.08	+0.07	+0.07	+0.07	+0.07	+0.07	+0.07
(FTAG) fTagSF_C , eigen6 [%]	+0.00	+0.00	+0.00	+0.00	+0.00	+0.00	+0.00
(FTAG) fTagSF_C , eigen7 [%]	-0.05	-0.15	-0.07	-0.08	-0.11	-0.18	+0.32
(FTAG) fTagSF_C , eigen8 [%]	+0.05	+0.19	+0.16	+0.08	+0.03	+0.15	+0.24
(FTAG) fTagSF_C , eigen9 [%]	+0.05	+0.05	+0.07	+0.06	+0.00	+0.01	+0.06
(FTAG) fTagSF_C , eigen10 [%]	+0.00	+0.03	+0.03	+0.03	+0.02	+0.02	+0.02
(FTAG) fTagSF_C , eigen11 [%]	+0.00	+0.04	+0.03	+0.03	+0.03	+0.03	+0.03
(FTAG) fTagSF_C , eigen12 [%]	+0.05	+0.04	+0.03	+0.03	+0.03	+0.10	+0.13
(FTAG) fTagSF_C , eigen13 [%]	+0.05	+0.04	+0.03	+0.03	+0.03	+0.07	+0.09
(FTAG) fTagSF_C , eigen14 [%]	+0.05	+0.06	+0.05	+0.05	+0.03	+0.07	+0.04
(FTAG) fTagSF_C , eigen15 [%]	+0.05	+0.03	+0.03	+0.03	+0.03	+0.07	+0.04
(FTAG) fTagSF_C , extrapolation [%]	+1.84	+1.98	+2.40	+2.79	+3.51	+5.12	+9.61
(FTAG) fTagSF_C , extrapolation from_charm [%]	+0.10	+0.03	+0.03	+0.03	+0.03	+0.03	+0.03
(MET/Pt) jet [%]	+0.00	+0.01	+0.11	+0.04	+0.00	+0.00	+0.38
Luminosity [%]	+2.11	+1.93	+1.93	+1.93	+1.93	+1.93	+1.93
(BKG) singletop, W_1 [%]	+0.14	+0.14	+0.14	+0.14	+0.14	+0.14	+0.14
(BKG) tW [%]	+0.06	+0.04	+0.04	+0.04	+0.04	+0.04	+0.40
(BKG) tZ [%]	+0.06	+0.04	+0.04	+0.04	+0.04	+0.04	+0.45
(BKG) tH [%]	+0.06	+0.04	+0.04	+0.04	+0.04	+0.04	+0.35
(LJES) LARGERET, Weak, JET, Rrk, Modelling, Tau32WTA [%]	+10.69	+9.41	+9.98	+9.28	+10.26	+14.91	+12.63
(LJES) LARGERET, Weak, JET, Rrk, Baseline, pT [%]	+0.03	+0.04	+0.03	+0.03	+0.03	+0.10	+0.13
(LJES) LARGERET, Weak, JET, Rrk, Baseline, mass [%]	+0.03	+0.03	+0.03	+0.03	+0.03	+0.15	+0.15
(LJES) LARGERET, Weak, JET, Rrk, Baseline, Tau32WTA [%]	+2.18	+0.61	+0.23	+0.32	+0.33	+0.12	+0.95
(LJES) LARGERET, Weak, JET, Rrk, Baseline, Response [%]	+0.03	+0.04	+0.03	+0.03	+0.03	+0.03	+0.03
(JES) JET, 2NP, JET, BIES, Response [%]	+0.03	+0.03	+0.03	+0.03	+0.03	+0.03	+0.03
(JES) JET, 2NP, JET, Pileup, PTterm [%]	+0.03	+0.02	+0.02	+0.02	+0.01	+0.01	+0.02
(JES) JET, 2NP, JET, Pileup, OffsetNPV [%]	+0.03	+0.02	+0.02	+0.02	+0.01	+0.01	+0.01
(JES) JET, 2NP, JET, Pileup, rhoTopology [%]	+0.33	+0.20	+0.16	+0.17	+0.20	+0.13	+1.04
(JES) JET, 2NP, JET, EffectiveNP, 2Term [%]	+0.13	+0.18	+0.19	+0.18	+0.18	+0.18	+0.57
(LEP) JET, 2NP, JET, Response [%]	+0.18	+0.18	+0.18	+0.18	+0.18	+0.18	+0.37
(JES) JET, 2NP, JET, EffectiveNP, 3Term [%]	+0.00	-	-	-	-	-	+0.32
(JES) JET, 2NP, JET, EffectiveNP, 4Term [%]	+0.00	-	-	-	-	-	+0.32
(JES) JET, 2NP, JET, Weak, JET, Rrk, TotalStat, mass [%]	+0.84	+0.45	+0.08	-0.07	-0.08	+0.04	+0.38
(JES) JET, 2NP, JET, Pileup, OffsetMu0 [%]	+0.17	+0.26	+0.02	+0.02	+0.02	+0.02	+0.11
(JES) JET, 2NP, JET, TotalStat, mass [%]	+0.15	+0.04	+0.05	+0.02	+0.02	+0.02	+0.39
(JES) JET, 2NP, JET, EtaInterpolation, NonClosure [%]	+0.15	+0.04	+0.05	+0.02	+0.02	+0.02	+0.41
(JES) JET, 2NP, JET, EtaInterpolation, TotalStat [%]	+0.18	+0.04	+0.05	+0.02	+0.02	+0.02	+0.32
(JEP) EG, REJECT, JET, All [%]	+0.05	+0.05	+0.05	+0.05	+0.05	+0.05	+0.32
(JEP) JET, 2NP, JET, Flavor, Response [%]	+0.21	+0.04	+0.03	+0.03	+0.02	+0.02	+0.32
(JEP) JET, 2NP, JET, EffectiveNP, 6Term [%]	+0.07	+0.05	+0.04	+0.04	+0.04	+0.04	+0.32
(JES) JET, 2NP, JET, EffectiveNP, 5Term [%]	+0.02	-	-	-	-	-	+0.38
(JES) JET, 2NP, JET, Flavor, Composition [%]	+0.21	+0.23	+0.28	+0.28	+0.21	+0.13	+0.38
(JES) JET, 2NP, JET, SingleParticle, HighPt [%]	+0.18	+0.18	+0.18	+0.18	+0.18	+0.18	+0.37
(JES) JET, 2NP, JET, Pileup, Modelling, pT [%]	+1.71	+2.32	+2.94	+2.79	+2.40	+1.36	+2.25
(JES) JET, 2NP, JET, EffectiveNP, 1Term [%]	+0.05	+0.05	+0.05	+0.05	+0.05	+0.05	+0.39
(JEP) MUON, ID [%]	+0.05	+0.05	+0.05	+0.05	+0.05	+0.05	+0.10
(JES) JET, 2NP, JET, Flavor, Response [%]	+0.21	+0.04	+0.03	+0.03	+0.02	+0.02	+0.32
(JES) JET, 2NP, JET, Weak, JET, Rrk, TotalStat, pT [%]	+0.03	+0.03	+0.03	+0.03	+0.03	+0.03	+0.38
(JEP) EG, SCALE, All [%]	+0.02	-	-	-	-	-	+0.32
(JES) JET, 2NP, JET, EffectiveNP, 7Term [%]	+0.02	+0.04	+0.02	+0.01	+0.01	+0.01	+0.35
(JES) JET, 2NP, JET, Weak, JET, Rrk, Modeling, mass [%]	+0.91	+1.08	+0.92	+0.92	+0.91	+0.31	+0.39
(JEP) MUON, MS [%]	+0.10	+0.10	+0.10	+0.10	+0.10	+0.10	+0.39
(JEP) MUON, SAGITTA, RHO [%]	+0.18	+0.18	+0.18	+0.18	+0.18	+0.18	+0.37
(JES) JET, 2NP, JET, PunchThrough, MC15 [%]	+0.18	+0.18	+0.18	+0.18	+0.18	+0.18	+0.37
(JES) JET, 2NP, JET, EtaInterpolation, Modelding [%]	+0.03	+0.03	+0.02	+0.02	+0.02	+0.02	+0.40
(JES) JET, 2NP, JET, EffectiveNP, 2Term [%]	+2.93	+0.93	+0.92	+0.93	+0.93	+0.93	+0.37
(JES) JET, 2NP, JET, Weak, JET, Rrk, Tracking, Tau32WTA [%]	+0.98	+0.18	+0.20	+0.20	+0.17	+0.26	+1.30
(JES) JET, 2NP, JET, Weak, JET, Rrk, Tracking, pT [%]	+0.98	+0.18	+0.20	+0.20	+0.17	+0.26	+1.30
(JES) JET, 2NP, JET, Weak, JET, Rrk, TotalStat, Tau32WTA [%]	+0.10	+0.10	+0.10	+0.10	+0.10	+0.10	+0.31
(JES) JET, JER, SINGLE, NP [%]	+0.01	+0.01	+0.14	+0.14	+0.24	+0.03	+0.78
(JES) LARGERET, Weak, JET, Top, massRes, mass [%]	+6.40	+1.24	+0.63	+1.16	+1.25	+0.08	+2.44
(PDF) PDF4LHC15_nlo_30_eigen01 [%]	+0.14	+0.13	+0.12	+0.06	+0.09	+0.09	+0.14
(PDF) PDF4LHC15_nlo_30_eigen02 [%]	+0.25	+0.24	+0.22	+0.16	+0.17	+0.16	+0.59
(PDF) PDF4LHC15_nlo_30_eigen03 [%]	+0.16	+0.23	+0.09	+0.07	+0.07	+0.09	+0.56
(PDF) PDF4LHC15_nlo_30_eigen04 [%]	+0.13	+0.13	+0.20	+0.12	+0.15	+0.20	+0.67
(PDF) PDF4LHC15_nlo_30_eigen05 [%]	+0.77	+0.07	+0.09	+0.08	+0.08	+0.04	+1.02
(PDF) PDF4LHC15_nlo_30_eigen06 [%]	+0.34	+0.34	+0.30	+0.18	+0.21	+0.28	+0.61
(PDF) PDF4LHC15_nlo_30_eigen07 [%]	+0.03	+0.03	+0.03	+0.02	+0.02	+0.02	+0.36
(PDF) PDF4LHC15_nlo_30_eigen08 [%]	+0.28	+0.25	+0.17	+0.16	+0.17	+0.15	+0.62
(PDF) PDF4LHC15_nlo_30_eigen09 [%]	+0.08	+0.08	+0.06	+0.04	+0.05	+0.05	+0.44
(PDF) PDF4LHC15_nlo_30_eigen10 [%]	+0.10	+0.09	+0.02	+0.06	+0.06	+0.04	+0.38
(PDF) PDF4LHC15_nlo_30_eigen11 [%]	+0.15	+0.15	+0.12	+0.08	+0.09	+0.09	+0.45
(PDF) PDF4LHC15_nlo_30_eigen12 [%]	+0.14	+0.12	+0.09	+0.07	+0.06	+0.06	+0.50
(PDF) PDF4LHC15_nlo_30_eigen13 [%]	+0.05	+0.04	+0.02	+0.02	+0.04	+0.06	+0.06
(PDF) PDF4LHC15_nlo_30_eigen14 [%]	+0.01	+0.01	+0.01	+0.02	+0.02	+0.03	+0.42
(PDF) PDF4LHC15_nlo_30_eigen15 [%]	+0.05	+0.03	+0.01	+0.03	+0.02	+0.02	+0.52
(PDF) PDF4LHC15_nlo_30_eigen16 [%]	+0.04	-	-	-	-	-	+0.40
(PDF) PDF4LHC15_nlo_30_eigen17 [%]	+0.12	+0.13	+0.11	+0.07	+0.08	+0.10	+0.23
(PDF) PDF4LHC15_nlo_30_eigen18 [%]	+0.11	+0.14	+0.13	+0.07	+0.08	+0.11	+0.32
(PDF) PDF4LHC15_nlo_30_eigen19 [%]	+0.08	+0.06	+0.03	+0.01	+0.01	+0.02	+0.23
(PDF) PDF4LHC15_nlo_30_eigen20 [%]	+0.08	+0.05	+0.04	+0.04	+0.07	+0.06	+0.24
(PDF) PDF4LHC15_nlo_30_eigen21 [%]	+0.06	+0.06	+0.05	+0.04	+0.04	+0.03	+0.38
(PDF) PDF4LHC15_nlo_30_eigen22 [%]	+0.06	+0.01	+0.01	+0.02	+0.02	+0.01	+0.34
(PDF) PDF4LHC15_nlo_30_eigen23 [%]	+0.01	+0.01	+0.01	-	-	-	+0.37
(PDF) PDF4LHC15_nlo_30_eigen24 [%]	+0.06	+0.03	+0.05	+0.03	+0.04	+0.06	+0.45
(PDF) PDF4LHC15_nlo_30_eigen25 [%]	+0.02	+0.01	+0.02	+0.01	+0.01	+0.01	+0.32
(PDF) PDF4LHC15_nlo_30_eigen26 [%]	+0.06	+0.04	+0.02	+0.02	+0.01	-	+0.34
(PDF) PDF4LHC15_nlo_30_eigen27 [%]	+0.07	+0.05	+0.02	+0.04	+0.03	+0.03	+0.49
(PDF) PDF4LHC15_nlo_30_eigen28 [%]	+0.20	+0.17	+0.12	+0.12	+0.11	+0.09	+0.52
(PDF) PDF4LHC15_nlo_30_eigen29 [%]	+0.01	+0.01	+0.01	-	-	+0.01	+0.35
(PDF) PDF4LHC15_nlo_30_eigen30 [%]	+0.11	+0.11	+0.01	-	-	+0.01	+0.41
(MOD) Alternative hadron-scattering model [%]	+12.29	+11.03	+8.43	+9.48	+12.93	+16.43	+16.71
(MOD) Alternative parton-shower model [%]	+17.68	+17.34	+17.86	+20.71	+22.86	+22.37	+19.08
(MOD) ISR/FSR + scale [%]	+4.79	+1.62	+0.84	+0.09	+0.92	+0.30	+0.45
(MOD) Monte Carlo sample statistics [%]	+4.47	+3.06	+2.45	+2.99	+4.49	+3.29	+13.75

Table 136: The individual systematic uncertainties in the parton level fiducial phase-space absolute differential cross-sections for the 2nd leading top p_T calculated as a percentage of the cross-section.

Not reviewed, for internal circulation only

Bins (GeV)	[350,400]	[400,450]	[450,500]	[500,550]	[550,600]	[600,650]	[600,800]	[800,1200]
$\text{Top} \rightarrow \text{ZX}$ [pb/GeV]	2.67 ± 0.10	3.45 ± 0.10	4.64 ± 0.10	4.19 ± 0.10	1.97 ± 0.09	7.08 ± 0.09	5.74 ± 0.09	1.09 ± 0.08
Total Uncertainty [%]	$+12.5$	$+7.0$	$+6.2$	$+7.0$	$+9.6$	$+12.0$	$+7.0$	$+38.42$
Statistics [%]	$+25.75$	$+16.16$	$+14.49$	$+14.49$	$+16.83$	$+17.77$	$+17.72$	
Systematics [%]	$+9.46$	$+4.83$	$+4.79$	$+4.80$	$+5.29$	$+9.40$	$+21.79$	
(FTAG) ftagSF_B_eigen0 [%]	-	-	-	-	-	-	-	-
(FTAG) ftagSF_B_eigen1 [%]	-0.08	-0.03	-0.15	-0.13	-0.08	-0.02	-0.04	-0.02
(FTAG) ftagSF_B_eigen2 [%]	-0.20	-0.15	-0.05	-0.17	-0.19	-0.11	-0.14	-0.16
(FTAG) ftagSF_C_eigen1 [%]	-0.20	-0.15	-0.05	-0.17	-0.18	-0.11	-0.14	-0.16
(FTAG) ftagSF_C_eigen2 [%]	-0.08	-0.12	-0.03	-0.13	-0.05	-0.02	-0.04	-0.05
(FTAG) ftagSF_C_eigen3 [%]	-0.01	-0.11	-0.02	-0.09	-0.06	-0.03	-0.04	-0.05
(FTAG) ftagSF_Light_eigen0 [%]	-0.08	-0.14	-0.04	-0.05	-0.08	-0.08	-0.04	-0.03
(FTAG) ftagSF_Light_eigen1 [%]	-0.09	-0.14	-0.05	-0.10	-0.10	-0.10	-0.09	-0.09
(FTAG) ftagSF_Light_eigen2 [%]	-0.08	-0.09	-0.04	-0.06	-0.10	-0.10	-0.04	-0.15
(FTAG) ftagSF_Light_eigen3 [%]	-0.01	-0.11	-0.01	-0.08	-0.03	-0.03	-0.07	-0.21
(FTAG) ftagSF_Light_eigen4 [%]	-0.02	-0.12	-0.05	-0.09	-0.05	-0.05	-0.05	-0.09
(FTAG) ftagSF_Light_eigen5 [%]	-0.13	-0.09	-0.09	-0.05	-0.05	-0.02	-0.07	-0.12
(FTAG) ftagSF_Light_eigen6 [%]	-0.02	-0.02	-0.02	-0.02	-0.02	-0.02	-0.01	-0.23
(FTAG) ftagSF_Light_eigen7 [%]	-0.01	-0.06	-0.01	-0.03	-0.03	-0.03	-0.03	-0.20
(FTAG) ftagSF_Light_eigen8 [%]	-0.04	-0.08	-0.02	-0.04	-0.02	-0.02	-0.03	-0.18
(FTAG) ftagSF_Light_eigen9 [%]	-0.03	-0.08	-0.02	-0.02	-0.02	-0.02	-0.03	-0.18
(FTAG) ftagSF_Light_eigen10 [%]	-0.01	-0.08	-0.01	-0.02	-0.02	-0.02	-0.03	-0.18
(FTAG) ftagSF_Light_eigen11 [%]	-	-	-	-	-	-	-0.06	-0.19
(FTAG) ftagSF_Light_eigen12 [%]	-	-	-	-	-	-	-0.06	-0.19
(FTAG) ftagSF_Light_eigen13 [%]	-	-	-	-	-	-	-0.06	-0.17
(FTAG) ftagSF_Light_eigen14 [%]	-	-	-	-	-	-	-0.06	-0.17
(FTAG) ftagSF_Light_eigen15 [%]	-	-	-	-	-	-	-0.06	-0.17
(FTAG) ftagSF_Extrapolation [%]	-1.28	+1.13	+0.22	-0.34	+0.39	+1.14	+0.24	+0.24
(FTAG) ftagSF_Extrapolation_from_charm [%]	+1.29	+1.13	+0.71	+0.31	-0.43	-2.02	-0.73	-0.73
(METPU) jvt [%]	-0.08	-0.06	-0.03	-0.04	-0.05	-0.05	-0.04	-0.04
Luminosity [%]	-0.11	-0.08	-0.01	-0.01	-0.01	-0.01	-0.03	-0.05
(BKG) singletop_tchan [%]	-	-	-	-	-	-	-0.17	-0.17
(BKG) singletop_Wt [%]	-	-	-	-	-	-	-0.01	-0.35
(BKG) tW [%]	-0.03	-	-	-	-0.02	-0.03	-0.03	-0.28
(BKG) tZ [%]	-0.06	-	-	-	-0.05	-0.02	-0.02	-0.38
(BKG) Ht [%]	-0.05	-	-	-	-0.05	-0.02	-0.02	-0.38
(LJES) LARGERET Weak_JET_Rtrk_Modelling_Tau32WTA [%]	-0.05	+1.10	+1.10	-0.54	-3.38	+0.21	-0.21	-0.21
(LJES) LARGERET Weak_JET_Rtrk_Baseline_pt [%]	-0.02	-1.18	-1.56	-1.29	+0.05	+3.80	+8.06	+8.06
(LJES) LARGERET Weak_JET_Rtrk_Baseline_mass [%]	-0.39	-1.45	-0.28	+0.57	+1.98	-0.42	-0.28	-0.28
(LJES) LARGERET Weak_JET_Rtrk_Baseline_Tau32WTA [%]	-1.68	-0.10	-0.29	-0.29	+0.10	+0.18	+0.29	+0.29
(JES) JET_2INP_JET_BJES_Response [%]	-0.08	-0.08	-0.02	-0.02	-0.02	-0.02	-0.01	-0.05
(JES) JET_2INP_JET_Pileup_PtTerm [%]	-0.01	-0.01	-0.01	-0.01	-0.01	-0.01	-0.01	-0.04
(JES) JET_2INP_JET_Pileup_OffsetNPV [%]	-	-	-	-	-	-	-0.20	-0.20
(JES) JET_2INP_JET_Pileup_RhoTopology [%]	-0.11	-0.02	-0.05	-0.04	+0.04	+0.01	-0.05	+0.12
(JES) JET_2INP_JET_EtaCalibration_OffsetTerm [%]	-0.14	-	-	-	-	-	-0.18	-0.18
(LEP) MUON_SAGITTA_RebinMAS [%]	-	-	-	-	-	-	-0.17	-0.17
(JES) JET_2INP_JET_EffectiveNP_3 [%]	-	-	-	-	-	-	-0.16	-0.16
(JES) JET_2INP_JET_EffectiveNP_4 [%]	-	-	-	-	-	-	-0.16	-0.16
(JES) LARGERET_Weak_JET_Rtrk_Tracking_mass [%]	-0.65	+0.26	-0.11	-0.26	-0.27	-0.15	+0.18	+0.18
(JES) JET_2INP_JET_Pileup_OffsetMuT [%]	-0.70	-0.24	+0.03	+0.03	+0.03	-0.05	-0.26	-0.26
(JES) LARGERET_Weak_JET_Rtrk_TotalStat_mass [%]	-0.12	-0.01	+0.01	-0.01	-0.01	-0.01	-0.05	-0.05
(JES) JET_2INP_JET_EtaUncalibration_NonClosure [%]	-0.12	-0.01	-0.01	-0.02	+0.03	-	-0.03	-0.03
(JES) JET_2INP_JET_EtaUncalibration_TotalStat [%]	-0.02	-0.02	-0.02	-0.02	+0.02	-	-0.02	-0.02
(LEP) EG_RESOLUTION_ALL [%]	-0.02	-0.02	+0.08	+0.05	+0.08	-0.08	-0.02	-0.02
(JES) JET_2INP_JET_EffectiveNP_5 [%]	-0.17	-0.02	-0.03	-0.03	-0.03	-0.02	-0.03	-0.03
(JES) JET_2INP_JET_EffectiveNP_6 [%]	-0.02	-0.02	-0.00	-0.01	-0.01	-0.02	-0.02	-0.04
(JES) JET_2INP_JET_EffectiveNP_5 [%]	-	-	-	-	-	-	-0.17	-0.17
(JES) JET_2INP_JET_Flavor_Composition [%]	-	-	-	-	-	-	-0.10	-0.10
(JES) JET_2INP_JET_SingleParticle_HighPt [%]	-	-	-	-	-	-	-0.10	-0.10
(JES) JET_2INP_JET_Modelling_pt [%]	-0.63	-0.03	-0.57	+0.42	+0.04	-0.24	-0.05	-0.05
(JES) JET_2INP_JET_EffectiveNP_1 [%]	-0.29	+0.36	-0.40	-0.33	-0.29	-0.13	-0.32	-0.32
(LEP) MUON_ID [%]	-0.32	-0.21	-	-	-0.02	+0.06	-0.09	+0.18
(LEP) EG_SCALE_Alt [%]	-0.05	-0.05	-0.05	-0.05	-0.05	-0.05	-0.11	-0.11
(LEP) EG_SCALE_Alt [%]	-	-	-	-	-	-	-0.11	-0.11
(JES) JET_2INP_JET_EffectiveNP_7 [%]	-0.15	-0.03	-0.03	-0.02	-0.08	-	-0.33	-0.33
(JES) LARGERET_Weak_JET_Rtrk_Modelling_mass [%]	-0.50	-0.04	-0.03	-0.02	-0.27	-0.59	-0.71	-0.71
(JES) JET_2INP_JET_EffectiveNP_1 [%]	-0.20	-0.31	-0.09	-0.37	-0.54	-0.51	+1.30	+1.30
(LEP) MUON_MS [%]	-	-	-	-	-	-	-0.17	-0.17
(JES) JET_2INP_JET_SAGITTA_rho [%]	-	-	-	-	-	-	-0.17	-0.17
(JES) JET_2INP_JET_PunchThrough_MC15 [%]	-	-	-	-	-	-	-0.17	-0.17
(JES) JET_2INP_JET_EtaUncalibration_Modelling [%]	-0.06	-	-0.02	+0.02	-0.02	-0.03	-0.04	-0.04
(JES) JET_2INP_JET_EffectiveNP_2 [%]	-0.16	-	-0.02	+0.00	-0.02	-0.03	-0.04	-0.04
(JES) JET_2INP_JET_EtaUncalibration_NonClosure [%]	-0.13	-0.01	-0.01	-0.01	-0.04	-0.08	-0.03	-0.03
(JES) JET_2INP_JET_EtaUncalibration_TotalStat [%]	-0.13	-0.01	-0.02	-0.02	-0.03	-0.03	-0.03	-0.03
(LEP) EG_RESOLUTION_ALL [%]	-0.02	-0.02	-0.08	+0.05	-0.08	-	-0.05	-0.05
(JES) JET_2INP_JET_SingleParticle_lowPt [%]	-0.03	-0.03	-0.03	-0.02	-0.02	-0.02	-0.03	-0.03
(JES) JET_2INP_JET_EffectiveNP_8 [%]	-0.26	+0.12	+0.03	+0.09	+0.12	-0.08	-0.07	-0.07
(JES) JET_2INP_JET_Tau32WTA [%]	-0.96	+0.29	+0.90	-0.37	+0.28	+1.62	+0.93	+0.93
(PDF) PDF4LHC15_nlo_30_eigen01 [%]	-0.14	+0.13	+0.12	+0.06	+0.09	+0.09	+0.09	+0.14
(PDF) PDF4LHC15_nlo_30_eigen02 [%]	-0.25	+0.24	+0.22	+0.16	+0.17	+0.16	+0.59	+0.59
(PDF) PDF4LHC15_nlo_30_eigen03 [%]	-0.16	+0.23	+0.09	+0.07	+0.07	+0.09	+0.56	+0.56
(PDF) PDF4LHC15_nlo_30_eigen04 [%]	-0.13	+0.19	+0.20	+0.12	+0.15	+0.20	+0.67	+0.67
(PDF) PDF4LHC15_nlo_30_eigen05 [%]	-0.07	+0.07	+0.09	+0.09	+0.04	+0.04	+1.02	+1.02
(PDF) PDF4LHC15_nlo_30_eigen06 [%]	-0.34	+0.34	+0.30	+0.15	+0.21	+0.28	+0.61	+0.61
(PDF) PDF4LHC15_nlo_30_eigen07 [%]	-0.03	+0.03	+0.03	+0.02	+0.02	+0.02	+0.36	+0.36
(PDF) PDF4LHC15_nlo_30_eigen08 [%]	-0.28	+0.25	+0.17	+0.16	+0.17	+0.15	+0.62	+0.62
(PDF) PDF4LHC15_nlo_30_eigen09 [%]	-0.08	+0.08	+0.06	+0.04	+0.04	+0.05	+0.44	+0.44
(PDF) PDF4LHC15_nlo_30_eigen10 [%]	-0.10	+0.09	+0.02	+0.06	+0.06	+0.04	+0.38	+0.38
(PDF) PDF4LHC15_nlo_30_eigen11 [%]	-0.15	+0.15	+0.12	+0.08	+0.09	+0.09	+0.45	+0.45
(PDF) PDF4LHC15_nlo_30_eigen12 [%]	-0.14	+0.12	+0.09	+0.07	+0.07	+0.06	+0.50	+0.50
(PDF) PDF4LHC15_nlo_30_eigen13 [%]	-0.08	+0.08	+0.08	+0.02	+0.02	+0.04	+0.36	+0.36
(PDF) PDF4LHC15_nlo_30_eigen14 [%]	-0.05	+0.05	+0.05	+0.01	+0.02	+0.02	+0.34	+0.34
(PDF) PDF4LHC15_nlo_30_eigen15 [%]	-0.05	+0.05	+0.01	+0.01	+0.01	+0.02	+0.37	+0.37
(PDF) PDF4LHC15_nlo_30_eigen16 [%]	-0.04	-	-	-	-	-	-0.40	-0.40
(PDF) PDF4LHC15_nlo_30_eigen17 [%]	-0.12	+0.13	+0.11	+0.07	+0.08	+0.10	+0.23	+0.23
(PDF) PDF4LHC15_nlo_30_eigen18 [%]	-0.11	+0.14	+0.13	+0.07	+0.08	+0.11	+0.32	+0.32
(PDF) PDF4LHC15_nlo_30_eigen19 [%]	-0.08	+0.06	+0.03	+0.03	+0.01	-	-0.23	-0.23
(PDF) PDF4LHC15_nlo_30_eigen20 [%]	-0.08	+0.05	+0.04	+0.04	+0.04	+0.07	+0.24	+0.24
(PDF) PDF4LHC15_nlo_30_eigen21 [%]	-0.08	+0.06	+0.05	+0.04	+0.04	+0.03	+0.38	+0.38
(PDF) PDF4LHC15_nlo_30_eigen22 [%]	-0.06	+0.08	+0.01	+0.05	+0.05	+0.52	+0.53	+0.53
(PDF) PDF4LHC15_nlo_30_eigen23 [%]	-0.01	+0.01	+0.01	-	-	-	-0.37	-0.37
(PDF) PDF4LHC15_nlo_30_eigen24 [%]	-0.46	+0.03	+0.05	+0.03	+0.04	+0.06	+0.45	+0.45
(PDF) PDF4LHC15_nlo_30_eigen25 [%]	-0.02	+0.01	+0.02	+0.01	+0.01	+0.01	+0.32	+0.32
(PDF) PDF4LHC15_nlo_30_eigen26 [%]	-0.06	+0.04	+0.02	+0.02	+0.02	+0.01	+0.34	+0.34
(PDF) PDF4LHC15_nlo_30_eigen27 [%]	-0.07	+0.05	+0.02	+0.04	+0.04	+0.03	+0.49	+0.49
(PDF) PDF4LHC15_nlo_30_eigen28 [%]	-0.20	+0.17	+0.12	+0.12	+0.11	+0.09	+0.52	+0.52
(PDF) PDF4LHC15_nlo_30_eigen29 [%]	-0.01	-	-	-	-	-	-0.01	-0.01
(PDF) PDF4LHC15_nlo_30_eigen30 [%]	-0.01	+0.01	+0.01	+0.01	+0.01	+0.02	+0.41	+0.41
(MOD) Alternative hard-scattering model [%]	+1.00	+0.43	+3.37	+2.18	+1.72	+5.67	+5.98	
(MOD) Alternative parton-shower mode [%]	+2.54	+2.97	+2.31	+1.23	+3.92	+3.30	+0.79	+0.79
(MOD) ISRFSR + scale [%]	+3.73	+0.53	+0.30	+1.05	+0.18	+1.42	+1.61	
(MOD) Monte Carlo sample statistics [%]	+4.24	+2.78	+2.31	+2.82	+4.32	+3.25	+13.31	

Table 137: The individual systematic uncertainties in the parton level fiducial phase-space relative differential cross-sections for the 2nd leading top p_T calculated as a percentage of the cross-section.

Not reviewed, for internal circulation only

Bins [GeV]	[0,0.2]	[0.2,0.4]	[0.4,0.6]	[0.6,0.8]	[0.8,1]	[1,1.2]	[1.2,1.5]	[1.5,2]
$d\sigma/dx$ [pb/GeV]	$6.6 \cdot 10^{-4}$	$6.8 \cdot 10^{-4}$	$6.9 \cdot 10^{-4}$	$4.76 \cdot 10^{-4}$	$3.97 \cdot 10^{-4}$	$3.69 \cdot 10^{-4}$	$2.78 \cdot 10^{-4}$	$1.19 \cdot 10^{-4}$
Total Uncertainty [%]	-31.34	-30.36	-32.53	-31.80	-33.09	-31.73	-33.11	-35.64
Statistics [%]	-5.68	+82.30	-45.57	+51.02	+83.20	+72.02	+48.38	+8.87
Systematics [%]	+10.11	+13.26	+11.53	+11.64	+11.71	+13.37	+11.10	+1.02
(FTAG) bTagSF_B_eigen0 (%)	-2.70	-3.20	-3.64	-3.89	-3.73	-3.10	-3.14	-3.00
(FTAG) bTagSF_B_eigen1 (%)	-2.58	-2.88	-3.63	-3.92	-3.79	-3.59	-3.27	-3.29
(FTAG) bTagSF_B_eigen2 (%)	-2.98	-2.94	-3.69	-3.94	-3.92	-3.68	-3.68	-3.96
(FTAG) bTagSF_B_eigen3 (%)	-2.93	-2.97	-3.67	-3.93	-3.92	-3.65	-3.69	-3.71
(FTAG) bTagSF_B_eigen4 (%)	-0.54	-0.52	-0.52	-0.52	-0.52	-0.54	-0.51	-0.50
(FTAG) bTagSF_B_eigen5 (%)	-0.24	-0.23	-0.23	-0.24	-0.23	-0.23	-0.24	-0.21
(FTAG) bTagSF_C_eigen0 (%)	-0.94	-0.95	-0.93	-0.92	-0.93	-0.95	-0.94	-0.94
(FTAG) bTagSF_C_eigen1 (%)	-1.09	-1.08	-1.07	-1.08	-1.07	-1.09	-1.08	-1.08
(FTAG) bTagSF_C_eigen2 (%)	-1.08	-1.08	-1.08	-1.07	-1.07	-1.07	-1.07	-1.05
(FTAG) bTagSF_C_eigen3 (%)	-0.71	-0.70	-0.71	-0.71	-0.71	-0.71	-0.71	-0.71
(FTAG) bTagSF_C_eigen4 (%)	-0.25	-0.25	-0.25	-0.25	-0.25	-0.25	-0.25	-0.25
(FTAG) bTagSF_Light_eigen0 (%)	-0.21	-0.18	-0.18	-0.15	-0.17	-0.17	-0.18	-0.18
(FTAG) bTagSF_Light_eigen1 (%)	-0.03	-0.05	-0.04	-0.03	-0.03	-0.04	-0.03	-0.05
(FTAG) bTagSF_Light_eigen2 (%)	-0.08	-0.07	-0.07	-0.05	-0.05	-0.05	-0.04	-0.05
(FTAG) bTagSF_Light_eigen3 (%)	-0.18	-0.19	-0.11	-0.05	-0.05	-0.14	-0.14	-0.05
(FTAG) bTagSF_Light_eigen4 (%)	-0.13	-0.08	-0.03	-0.03	-0.03	-0.03	-0.03	-0.03
(FTAG) bTagSF_Light_eigen5 (%)	-0.24	-0.23	-0.23	-0.23	-0.23	-0.23	-0.23	-0.23
(FTAG) bTagSF_Light_eigen6 (%)	-0.03	-0.03	-0.03	-0.03	-0.03	-0.03	-0.03	-0.03
(FTAG) bTagSF_Light_eigen7 (%)	-0.07	-0.08	-0.03	-0.05	-0.03	-0.03	-0.03	-0.02
(FTAG) bTagSF_Light_eigen8 (%)	-0.07	-0.08	-0.08	-0.05	-0.11	-0.03	-0.03	-0.02
(FTAG) bTagSF_Light_eigen9 (%)	-0.03	-0.02	-0.01	-0.01	-0.01	-0.03	-0.03	-0.03
(FTAG) bTagSF_Light_eigen10 (%)	-0.03	-0.03	-0.05	-0.08	-0.08	-0.02	-0.02	-0.08
(FTAG) bTagSF_Light_eigen11 (%)	-0.03	-0.03	-0.05	-0.05	-0.05	-0.02	-0.02	-0.05
(FTAG) bTagSF_Light_eigen12 (%)	-0.03	-0.03	-0.05	-0.05	-0.05	-0.02	-0.02	-0.05
(FTAG) bTagSF_Light_eigen13 (%)	-0.03	-0.03	-0.05	-0.05	-0.05	-0.02	-0.02	-0.05
(FTAG) bTagSF_Light_eigen14 (%)	-0.03	-0.03	-0.09	-0.09	-0.09	-0.03	-0.03	-0.03
(FTAG) bTagSF_Light_eigen15 (%)	-0.03	-0.03	-0.09	-0.09	-0.09	-0.03	-0.03	-0.03
(FTAG) bTagSF_Light_eigen16 (%)	-0.03	-0.03	-0.09	-0.09	-0.09	-0.03	-0.03	-0.03
(FTAG) bTagSF_Light_eigen17 (%)	-0.03	-0.03	-0.09	-0.09	-0.09	-0.03	-0.03	-0.03
(FTAG) bTagSF_Light_eigen18 (%)	-0.03	-0.03	-0.09	-0.09	-0.09	-0.03	-0.03	-0.03
(FTAG) bTagSF_Light_eigen19 (%)	-0.03	-0.03	-0.09	-0.09	-0.09	-0.03	-0.03	-0.03
(FTAG) bTagSF_extrapolation (%)	-1.10	-1.04	-1.04	-1.04	-1.04	-1.04	-1.04	-1.04
(FTAG) bTagSF_extrapolation_from_charm (%)	-0.05	-0.05	-0.05	-0.05	-0.05	-0.05	-0.05	-0.05
(METPF) jvt [%]	-0.12	-0.07	-0.10	-0.15	-0.10	-0.10	-0.09	-0.12
Lumi [%]	-2.04	-2.05	-2.03	-1.98	-2.00	-1.97	-2.03	-1.97
(BKG) singletop_tchan [%]	-	-	-	-	-	-	-	-
(BKG) singletop_Wt [%]	-	-	-	-	-	-	-	-
(BKG) nW [%]	-0.04	-0.04	-0.04	-0.04	-0.04	-0.03	-0.03	-0.03
(BKG) tZ [%]	-0.03	-0.03	-0.03	-0.03	-0.03	-0.03	-0.03	-0.03
(BKG) ttH [%]	-0.02	-0.02	-0.05	-0.03	-0.03	-0.03	-0.03	-0.03
(LJES) LARGERJET_Weak_JET_Rtk_Modelling_Tau32WTA [%]	-0.19	-0.19	-0.13	-0.12	-0.12	-0.12	-0.12	-0.19
(LJES) LARGERJET_Weak_JET_Rtk_Baseline_pT [%]	-0.19	-0.19	-0.13	-0.12	-0.12	-0.12	-0.12	-0.19
(LJES) LARGERJET_Weak_JET_Rtk_Baseline_max [%]	-0.24	-0.24	-0.16	-0.16	-0.16	-0.16	-0.16	-0.24
(LJES) LARGERJET_Weak_JET_Rtk_Baseline_Tau32WTA [%]	-0.24	-0.24	-0.16	-0.16	-0.16	-0.16	-0.16	-0.24
(JES) JET_2INP_JET_BJES_Response [%]	-0.01	-0.01	-0.01	-0.01	-0.01	-0.01	-0.01	-0.01
(JES) JET_2INP_JET_Ptup_OffsetNP [%]	-0.06	-0.06	-0.01	-0.01	-0.01	-0.02	-0.02	-0.02
(JES) JET_2INP_JET_OffsetNphi [%]	-0.19	-0.19	-0.13	-0.13	-0.13	-0.13	-0.13	-0.19
(JES) JET_2INP_JET_Ptcor_RhoTopology [%]	-0.14	-0.09	-0.14	-0.12	-0.12	-0.06	-0.06	-0.09
(JES) JET_2INP_JET_EffectiveNP_SystTerm [%]	-	-	-	-	-	-	-	-
(LEP) MUON_SAGITTA_RESBIAS [%]	-	-	-	-	-	-	-	-
(JES) JET_2INP_JET_EffectiveNP_3 [%]	-0.02	-0.02	-0.02	-0.02	-0.02	-0.02	-0.02	-0.02
(JES) JET_2INP_JET_EffectiveNP_4 [%]	-0.01	-0.01	-0.01	-0.01	-0.01	-0.01	-0.01	-0.01
(JES) JET_2INP_JET_Weak_JET_Rtk_Tracking_mass [%]	-0.71	-0.12	-0.10	-0.26	-0.01	-0.44	-0.19	-0.30
(JES) JET_2INP_JET_Ptup_OffsetNphi [%]	-0.03	-0.26	-0.20	-0.45	-0.07	-0.03	-0.59	-0.35
(JES) JET_2INP_JET_EffectiveNP_TotalStat [%]	-0.02	-0.01	-0.01	-0.01	-0.01	-0.01	-0.01	-0.02
(JES) JET_2INP_JET_EffectiveNP_NonClosure [%]	-0.08	-0.11	-0.01	-0.02	-0.02	-0.01	-0.01	-0.03
(JES) JET_2INP_JET_EffectiveNP_TotalStat [%]	-0.01	-0.01	-0.01	-0.01	-0.01	-0.01	-0.01	-0.03
(JES) JET_2INP_JET_EffectiveNP_Rho [%]	-0.12	-0.04	-0.02	-0.07	-0.06	-0.03	-0.02	-0.05
(JES) JET_2INP_JET_Flavor_Response [%]	-0.08	-0.08	-0.02	-0.07	-0.07	-0.03	-0.10	-0.08
(JES) JET_2INP_JET_EffectiveNP_6 [%]	-0.01	-0.01	-0.01	-0.01	-0.01	-0.01	-0.01	-0.01
(JES) JET_2INP_JET_EffectiveNP_5 [%]	-0.29	-0.22	-0.30	-0.30	-0.30	-0.30	-0.30	-0.30
(JES) JET_2INP_JET_Flavor_Composition [%]	-0.29	-0.22	-0.30	-0.30	-0.30	-0.31	-0.31	-0.29
(JES) JET_2INP_JET_SingleParticle_HighPt [%]	-0.13	-0.13	-0.13	-0.13	-0.13	-0.13	-0.13	-0.13
(JES) JET_2INP_JET_Tau32WTA [%]	-0.92	-0.29	-0.35	-0.29	-0.29	-2.12	-1.75	-2.29
(JES) JET_2INP_JET_EffectiveNP_1 [%]	-0.11	-0.02	-0.09	-0.04	-0.04	-0.01	-0.02	-0.08
(LEP) MUON_ID [%]	-0.44	-0.22	-0.22	-0.46	-0.38	-0.11	-0.43	-0.24
(JES) JET_2INP_JET_Weak_JET_Rtk_TotalStat_pT [%]	-0.18	-0.26	-0.26	-0.30	-0.43	-0.21	-0.34	-0.08
(LEP) MUON_SCALE [%]	-	-	-	-	-	-	-	-
(JES) JET_2INP_JET_EffectiveNP_7 [%]	-0.01	-0.09	-0.01	-0.01	-0.01	-0.01	-0.01	-0.01
(JES) JET_2INP_JET_Weak_JET_Rtk_Modelling_mass [%]	-1.04	-0.16	-0.25	-0.51	-0.08	-0.56	-0.97	-0.02
(LEP) MUON_MS [%]	-1.56	-0.57	-0.97	-0.13	-0.13	-0.07	-0.14	-0.74
(LEP) MUON_SAGITTA_RHO [%]	-	-	-	-	-	-	-	-
(JES) JET_2INP_JET_Punchthrough_MC15 [%]	-	-	-	-	-	-	-	-
(JES) JET_2INP_JET_EffectiveNP_Modeling [%]	-0.03	-0.07	-0.01	-0.05	-0.03	-0.03	-0.03	-0.03
(JES) JET_2INP_JET_EffectiveNP_2 [%]	-0.08	-0.03	-0.03	-0.03	-0.03	-0.03	-0.03	-0.03
(JES) JET_2INP_JET_Weak_JET_Rtk_Tracking_Tau32WTA [%]	-0.03	-0.03	-0.03	-0.03	-0.03	-0.03	-0.03	-0.07
(JES) JET_2INP_JET_Weak_JET_Rtk_Tracking_pT [%]	-0.18	-0.28	-0.28	-0.38	-0.38	-0.16	-0.24	-0.31
(JES) JET_2INP_JET_Weak_JET_Rtk_TotalStat_Tau32WTA [%]	-0.17	-0.17	-0.17	-0.17	-0.17	-0.17	-0.17	-0.17
(JES) JET_2INP_JET_Weak_JET_Rtk_TotalStat [%]	-0.29	-0.03	-0.20	-0.09	-0.01	-0.12	-0.03	-0.25
(JES) JET_2INP_JET_Weak_top_msk_JET_top_msk [%]	-1.84	-1.62	-0.90	-0.07	-1.30	-2.76	-0.67	-1.69
(PDF) PDF4LHC15_nlo_30_eigen01 [%]	-0.09	-0.03	-0.07	-0.09	-0.02	-0.06	-0.06	-0.09
(PDF) PDF4LHC15_nlo_30_eigen02 [%]	-0.13	-0.13	-0.13	-0.14	-0.14	-0.14	-0.14	-0.28
(PDF) PDF4LHC15_nlo_30_eigen03 [%]	-0.07	-0.06	-0.07	-0.07	-0.31	-0.09	-0.10	-0.03
(PDF) PDF4LHC15_nlo_30_eigen04 [%]	-0.09	-0.03	-0.13	-0.12	-0.07	-0.19	-0.21	-0.31
(PDF) PDF4LHC15_nlo_30_eigen05 [%]	-0.44	-0.41	-0.45	-0.47	-0.42	-0.50	-0.50	-0.56
(PDF) PDF4LHC15_nlo_30_eigen06 [%]	-0.21	-0.15	-0.20	-0.20	-0.15	-0.20	-0.26	-0.38
(PDF) PDF4LHC15_nlo_30_eigen07 [%]	-0.01	-0.01	-0.01	-0.01	-0.01	-0.01	-0.01	-0.04
(PDF) PDF4LHC15_nlo_30_eigen08 [%]	-0.14	-0.13	-0.14	-0.15	-0.14	-0.16	-0.20	-0.19
(PDF) PDF4LHC15_nlo_30_eigen09 [%]	-0.06	-0.04	-0.06	-0.06	-0.06	-0.06	-0.06	-0.06
(PDF) PDF4LHC15_nlo_30_eigen10 [%]	-0.05	-0.05	-0.05	-0.06	-0.06	-0.05	-0.05	-0.06
(PDF) PDF4LHC15_nlo_30_eigen11 [%]	-0.09	-0.07	-0.08	-0.10	-0.08	-0.08	-0.11	-0.13
(PDF) PDF4LHC15_nlo_30_eigen12 [%]	-0.08	-0.05	-0.07	-0.08	-0.05	-0.07	-0.09	-0.11
(PDF) PDF4LHC15_nlo_30_eigen13 [%]	-0.03	-0.02	-0.02	-0.02	-0.01	-0.01	-0.01	-0.01
(PDF) PDF4LHC15_nlo_30_eigen14 [%]	-0.02	-0.03	-0.02	-0.02	-0.03	-0.03	-0.05	-0.05
(PDF) PDF4LHC15_nlo_30_eigen15 [%]	-0.02	-0.02	-0.02	-0.02	-0.01	-0.02	-0.04	-0.04
(PDF) PDF4LHC15_nlo_30_eigen16 [%]	-0.03	-0.02	-0.02	-0.02	-0.01	-0.02	-0.04	-0.04
(PDF) PDF4LHC15_nlo_30_eigen17 [%]	-0.09	-0.05	-0.09	-0.10	-0.06	-0.10	-0.10	-0.12
(PDF) PDF4LHC15_nlo_30_eigen18 [%]	-0.07	-0.04	-0.07	-0.06	-0.06	-0.07	-0.10	-0.19
(PDF) PDF4LHC15_nlo_30_eigen19 [%]	-0.11	-0.08	-0.08	-0.08	-0.08	-0.08	-0.08	-0.06
(PDF) PDF4LHC15_nlo_30_eigen20 [%]	-0.03	-0.05	-0.04	-0.03	-0.06	-0.05	-0.05	-0.06
(PDF) PDF4LHC15_nlo_30_eigen21 [%]	-0.03	-0.02	-0.02	-0.03	-0.02	-0.03	-0.01	-0.06
(PDF) PDF4LHC15_nlo_30_eigen22 [%]	-0.45	-0.37	-0.48	-0.47	-0.48	-0.55	-0.68	-0.75
(PDF) PDF4LHC15_nlo_30_eigen23 [%]	-	-	-	-	-	-0.01	-0.02	-0.04
(PDF) PDF4LHC15_nlo_30_eigen24 [%]	-0.02	-0.02	-0.04	-0.03	-0.02	-0.05	-0.05	-0.05
(PDF) PDF4LHC15_nlo_30_eigen25 [%]	-0.03	-0.03	-0.02	-0.02	-0.01	-0.03	-0.03	-0.05
(PDF) PDF4LHC15_nlo_30_eigen26 [%]	-0.02	-0.05	-0.03	-0.02	-0.06	-0.04	-0.04	-0.06
(PDF) PDF4LHC15_nlo_30_eigen27 [%]	-0.02	-0.05	-0.03	-0.02	-0.06	-0.04	-0.05	-0.06
(PDF) PDF4LHC15_nlo_30_eigen28 [%]	-0.13	-0.12	-0.12	-0.09	-0.12	-0.12	-0.11	-0.11
(PDF) PDF4LHC15_nlo_30_eigen29 [%]	-	-	-	-	-	-0.01	-	-
(

Bins [GeV]	[0,0.2]	[0,2,0.4]	[0,4,0.6]	[0,6,0.8]	[0,8,1]	[1,1,1.2]	[1,2,1.5]	[1,4,2]
L _{int} × L _{ext} [pb·GeV ⁻¹]	8.4 ^{+10.1} _{-7.36}	8.2 ^{+10.1} _{-7.35}	7.0 ^{+10.1} _{-7.35}	6.1 ^{+10.1} _{-7.35}	5.8 ^{+10.1} _{-7.35}	4.7 ^{+10.1} _{-7.35}	3.5 ^{+10.1} _{-7.35}	1.5 ^{+10.1} _{-7.35}
Total Uncertainty [%]	+1.35	+1.35	+1.35	+1.35	+1.35	+1.35	+1.35	+1.35
Statistics [%]	+3.73	+3.94	+4.26	+4.03	+3.88	+3.62	+3.40	+3.24
Systematics [%]	+4.33	+4.33	+4.34	+4.12	+3.01	+4.49	+4.95	+6.60
(FTAG) TagSF_B_eigen0 [%]	+0.03	+0.03	+0.03	+0.03	+0.03	+0.02	+0.08	+0.16
(FTAG) TagSF_B_eigen1 [%]	+0.04	+0.05	+0.05	+0.05	+0.05	+0.15	+0.05	+0.11
(FTAG) TagSF_C_eigen2 [%]	+0.03	+0.03	+0.03	+0.03	+0.03	+0.05	+0.05	+0.05
(FTAG) TagSF_B_eigen3 [%]	+0.03	+0.03	+0.03	+0.03	+0.03	+0.02	+0.02	+0.05
(FTAG) TagSF_B_eigen4 [%]	+0.02	+0.01	+0.01	+0.01	+0.02	+0.02	+0.02	+0.03
(FTAG) TagSF_B_eigen5 [%]	—	—	—	—	—	—	—	-0.04
(FTAG) TagSF_C_eigen0 [%]	+0.10	-0.22	-0.09	-0.23	+0.81	+0.24	-0.21	-0.40
(FTAG) TagSF_C_eigen1 [%]	+0.03	-0.28	-0.05	-0.15	+0.89	+0.03	-0.08	+0.03
(FTAG) TagSF_C_eigen2 [%]	+0.03	-0.27	-0.05	-0.15	+0.89	+0.03	-0.08	+0.03
(FTAG) TagSF_C_eigen3 [%]	+0.08	-0.13	-0.09	-0.08	-0.13	-0.04	-0.05	-0.11
(FTAG) TagSF_C_eigen4 [%]	+0.04	-0.05	-0.05	-0.02	-0.05	-0.02	-0.02	-0.05
(FTAG) TagSF_Light_eigen0 [%]	+0.01	-0.12	-0.09	-0.13	+0.80	+0.07	-0.09	+0.01
(FTAG) TagSF_Light_eigen1 [%]	+0.01	-0.03	+0.04	-0.04	-0.05	-0.02	+0.05	+0.04
(FTAG) TagSF_Light_eigen2 [%]	+0.01	-0.02	-0.06	-0.08	-0.13	-0.03	-0.03	-0.05
(FTAG) TagSF_Light_eigen3 [%]	+0.01	-0.02	-0.06	-0.08	-0.13	-0.03	-0.03	-0.05
(FTAG) TagSF_Light_eigen4 [%]	+0.01	-0.03	-0.06	-0.08	-0.13	-0.03	-0.03	-0.05
(FTAG) TagSF_Light_eigen5 [%]	+0.01	-0.02	-0.06	-0.08	-0.13	-0.03	-0.03	-0.05
(FTAG) TagSF_Light_eigen6 [%]	+0.01	-0.02	-0.06	-0.08	-0.13	-0.03	-0.03	-0.05
(FTAG) TagSF_Light_eigen7 [%]	+0.01	-0.02	-0.06	-0.08	-0.13	-0.03	-0.03	-0.05
(FTAG) TagSF_Light_eigen8 [%]	+0.01	-0.03	-0.06	-0.08	-0.11	-0.03	-0.04	-0.05
(FTAG) TagSF_Light_eigen9 [%]	+0.01	-0.02	-0.06	-0.08	-0.12	-0.03	-0.03	-0.05
(FTAG) TagSF_Light_eigen10 [%]	+0.01	-0.04	-0.08	-0.03	-0.05	-0.05	-0.05	-0.05
(FTAG) TagSF_Light_eigen11 [%]	+0.01	-0.02	-0.06	-0.08	-0.13	-0.03	-0.03	-0.05
(FTAG) TagSF_Light_eigen12 [%]	+0.01	-0.02	-0.06	-0.08	-0.13	-0.03	-0.03	-0.05
(FTAG) TagSF_Light_eigen13 [%]	+0.01	-0.02	-0.06	-0.08	-0.13	-0.03	-0.03	-0.05
(FTAG) TagSF_Light_eigen14 [%]	+0.01	-0.02	-0.06	-0.08	-0.13	-0.03	-0.03	-0.05
(FTAG) TagSF_Light_eigen15 [%]	+0.01	-0.02	-0.06	-0.08	-0.13	-0.03	-0.03	-0.05
(FTAG) TagSF_extrapolation [%]	+0.04	+0.18	+0.19	+0.19	+0.06	-0.06	+0.16	+0.45
(FTAG) TagSF_extrapolation_from_charm [%]	+0.01	+0.01	+0.01	+0.01	+0.01	+0.01	+0.01	+0.05
(MET/PUD) jet [%]	-0.01	-0.02	-0.02	-0.02	-0.01	-0.01	-0.00	-0.02
Luminosity [fb ⁻¹]	-0.04	-0.04	-0.02	-0.03	-0.01	+0.09	-0.02	+0.04
(BKQ) singletop_tchan [%]	—	—	—	—	—	—	—	—
(BKQ) singletop_W [%]	—	—	—	—	—	—	—	—
(BKQ) nT [%]	—	—	—	—	—	—	—	-0.02
(BKQ) uT [%]	—	—	—	—	—	—	—	—
(LJES) JET_2NP	—	—	—	—	—	—	—	—
(LJES) JET_2NP, JET_Weak, JET_Rtrk, Modelling_Tau32WTA [%]	+0.26	-0.31	+0.66	-0.23	-0.02	+0.29	-1.11	+0.29
(LJES) LARGERJET_Weak, JET_Jet, Baseline, pT [%]	+0.21	-0.17	-1.39	-0.37	-0.26	-1.83	+0.51	+0.12
(LJES) LARGERJET_Weak, JET_Jet, Baseline, mass [%]	+0.25	-0.23	-0.11	-0.29	-0.09	-0.23	+0.24	+0.29
(LJES) LARGERJET_Weak, JET_Jet, Baseline, Tau32WTA [%]	+0.18	-0.12	-0.39	-0.08	-0.11	-0.03	+1.00	+0.68
(LJES) JET_2NP, JET_Weak, JET_Rtrk, Baseline, mass [%]	+0.11	-0.15	-0.55	-0.11	-0.03	-0.03	+0.33	+0.28
(LJES) JET_2NP, JET_Weak, JET_Rtrk, Baseline, Tau32WTA [%]	+0.10	-0.05	-0.05	-0.05	-0.03	-0.03	+0.03	+0.03
(LJES) JET_2NP, JET_Pileup_OffsetMs [%]	—	—	—	—	—	—	—	+0.02
(JES) JET_2NP, JET_Pileup_OffsetNPV [%]	—	—	—	—	—	—	—	—
(JES) JET_2NP, JET_Pileup_RhoTopology [%]	—	—	—	—	—	—	—	+0.02
(JES) JET_2NP, JET_EffectiveNP_SystTerm [%]	—	—	—	—	—	—	—	+0.03
(LEP) MUON_SAGITTA_RESBIAS [%]	—	—	—	-0.01	-0.01	—	—	+0.03
(JES) JET_2NP, JET_EffectiveNP_3 [%]	—	—	—	—	—	—	—	+0.03
(JES) JET_2NP, JET_EffectiveNP_4 [%]	—	—	—	—	—	—	—	+0.03
(LJES) LARGERJET_Weak, JET_Rtrk, Tracking_mass [%]	+0.59	-0.22	-0.14	-0.22	-0.56	+0.07	-0.22	+0.16
(JES) JET_2NP, JET_Pileup_OffsetMs [%]	+0.08	-0.02	-0.05	-0.02	+0.02	+0.01	-0.03	+0.03
(LJES) LARGERJET_Weak, JET_Rtrk, TotalStat, mass [%]	+0.08	+0.03	-0.24	-0.41	-0.12	-0.09	+0.26	+0.31
(JES) JET_2NP, JET_EtaIntercalibration_NonClosure [%]	-0.05	-0.08	-0.02	-0.02	-0.03	-0.03	+0.04	+0.06
(JES) JET_2NP, JET_EtaIntercalibration_TotalStat [%]	-0.02	-0.02	-0.01	-0.01	-0.01	-0.01	-0.02	-0.02
(LEP) MUON_RHO_MS [%]	-0.02	-0.07	-0.01	-0.01	-0.01	-0.01	-0.01	-0.03
(JES) JET_2NP, JET_Flavor_Response [%]	-0.08	-0.02	-0.06	-0.02	-0.02	-0.02	-0.02	+0.03
(JES) JET_2NP, JET_EffectiveNP_6 [%]	+0.02	-0.01	-0.05	-0.03	-0.05	-0.03	-0.04	+0.01
(JES) JET_2NP, JET_EffectiveNP_5 [%]	—	—	—	—	—	—	—	—
(JES) JET_2NP, JET_Flavor_Composition [%]	+0.04	-0.03	+0.05	-0.02	-0.14	-0.15	-0.10	+0.04
(JES) JET_2NP, JET_SingleParticle_HighPt [%]	+0.03	-0.03	-0.05	-0.01	-0.12	-0.13	-0.06	+0.04
(LJES) JET_Weak, JET_Rtrk, Modelling_pT [%]	+0.15	-0.12	-0.23	-0.13	+0.36	-0.32	+0.45	-0.02
(JES) JET_2NP, JET_EffectiveNP_1 [%]	—	—	—	—	—	—	—	-0.01
(LEP) MUON_DD [%]	-0.02	—	—	-0.02	—	—	—	-0.01
(LJES) LARGERJET_Weak, JET_Rtrk, TotalStat, pT [%]	+0.10	-0.01	-0.02	-0.11	+0.07	-0.07	+0.10	—
(LEP) MUON_SCALE [%]	—	—	—	—	—	—	—	—
(JES) JET_2NP, JET_EffectiveNP_7 [%]	+0.02	-0.07	+0.05	-0.01	-0.01	-0.01	-0.01	-0.02
(JES) JET_2NP, JET_Weak, JET_Rtrk, Modelling_mass [%]	+0.20	-0.18	-0.06	-0.17	-0.25	-0.09	+0.63	+0.59
(LEP) MUON_MS [%]	-1.12	-0.13	-0.53	-0.58	-0.07	-0.52	+0.59	+1.19
(LEP) MUON_SAGITTA_RHO [%]	—	—	—	—	—	—	—	—
(JES) JET_2NP, JET_PunchThrough_MCI5 [%]	—	—	—	—	—	—	—	—
(JES) JET_2NP, JET_EtaIntercalibration_Modeling [%]	—	—	—	—	—	—	—	—
(JES) JET_2NP, JET_EffectiveNP_2 [%]	-0.06	-0.05	-0.02	-0.02	+0.18	-0.24	-0.16	+0.05
(LJES) LARGERJET_Weak, JET_Rtrk, Tracking_Tau32WTA [%]	-0.02	-0.04	-0.10	-0.02	-0.18	-0.24	-0.16	+0.05
(LJES) LARGERJET_Weak, JET_Rtrk, pT [%]	+0.11	-0.19	-0.15	-0.03	-0.11	-0.03	-0.11	+0.18
(JES) JET_2NP, JET_EffectiveNP_3 [%]	-0.03	-0.09	-0.41	-0.20	-0.31	-0.39	-0.48	-0.20
(LJES) LARGERJET_Weak, JET_Rtrk, TotalStat, Tau32WTA [%]	-0.03	-0.11	-0.06	-0.06	-0.11	-0.11	-0.11	-0.01
(JES) JET_JER_SINGLE_RJN [%]	+0.17	+0.14	+0.09	+0.03	+0.13	+0.14	+0.14	+0.14
(LJES) LARGERJET_Weak, JET_Top_messRes, mass [%]	+0.53	+0.30	+0.43	+1.26	+0.02	+1.46	+0.66	+0.37
(PDF) PDF4LHC15_nlo_30_eigen001 [%]	+0.09	+0.03	+0.07	+0.09	+0.02	+0.04	+0.09	+0.09
(PDF) PDF4LHC15_nlo_30_eigen002 [%]	+0.09	+0.03	+0.07	+0.09	+0.01	+0.04	+0.09	+0.09
(PDF) PDF4LHC15_nlo_30_eigen003 [%]	+0.07	+0.06	+0.07	+0.07	+0.31	-0.09	+0.10	+0.03
(PDF) PDF4LHC15_nlo_30_eigen004 [%]	+0.09	+0.03	+0.13	+0.12	+0.07	+0.19	+0.21	+0.31
(PDF) PDF4LHC15_nlo_30_eigen005 [%]	+0.44	+0.41	+0.45	+0.47	+0.42	+0.50	+0.50	+0.56
(PDF) PDF4LHC15_nlo_30_eigen006 [%]	+0.21	+0.15	+0.20	+0.20	+0.15	+0.20	+0.26	+0.38
(PDF) PDF4LHC15_nlo_30_eigen007 [%]	+0.08	+0.07	+0.08	+0.08	+0.05	+0.04	+0.04	+0.04
(PDF) PDF4LHC15_nlo_30_eigen008 [%]	+0.14	+0.13	+0.14	+0.13	+0.14	+0.16	+0.20	+0.19
(PDF) PDF4LHC15_nlo_30_eigen009 [%]	+0.07	+0.06	+0.06	+0.06	+0.05	+0.05	+0.06	+0.06
(PDF) PDF4LHC15_nlo_30_eigen010 [%]	+0.05	+0.05	+0.05	+0.05	+0.05	+0.05	+0.06	+0.07
(PDF) PDF4LHC15_nlo_30_eigen011 [%]	+0.09	+0.07	+0.08	+0.10	+0.08	+0.08	+0.11	+0.13
(PDF) PDF4LHC15_nlo_30_eigen012 [%]	+0.08	+0.07	+0.08	+0.08	+0.05	+0.07	+0.09	+0.11
(PDF) PDF4LHC15_nlo_30_eigen013 [%]	+0.03	+0.02	+0.02	+0.09	+0.01	+0.04	+0.03	+0.04
(PDF) PDF4LHC15_nlo_30_eigen014 [%]	+0.02	+0.02	+0.02	+0.02	+0.05	+0.05	+0.05	+0.05
(PDF) PDF4LHC15_nlo_30_eigen015 [%]	+0.03	+0.02	+0.02	+0.02	+0.02	+0.02	+0.02	+0.04
(PDF) PDF4LHC15_nlo_30_eigen016 [%]	+0.09	+0.05	+0.09	+0.10	+0.06	+0.10	+0.10	+0.12
(PDF) PDF4LHC15_nlo_30_eigen017 [%]	+0.07	+0.04	+0.07	+0.06	+0.06	+0.07	+0.10	+0.19
(PDF) PDF4LHC15_nlo_30_eigen018 [%]	+0.07	+0.04	+0.07	+0.06	+0.06	+0.07	+0.10	+0.19
(PDF) PDF4LHC15_nlo_30_eigen019 [%]	+0.11	+0.10	+0.05	+0.08	+0.02	+0.03	+0.10	+0.06
(PDF) PDF4LHC15_nlo_30_eigen020 [%]	+0.03	+0.05	+0.04	+0.10	+0.06	+0.07	+0.05	+0.06
(PDF) PDF4LHC15_nlo_30_eigen021 [%]	+0.03	+0.02	+0.02	+0.02	+0.05	+0.05	+0.04	+0.04
(PDF) PDF4LHC15_nlo_30_eigen022 [%]	+0.45	+0.37	+0.48	+0.47	+0.48	+0.55	+0.68	+0.75
(PDF) PDF4LHC15_nlo_30_eigen023 [%]	—	—	—	—	—	+0.01	+0.02	+0.04
(PDF) PDF4LHC15_nlo_30_eigen024 [%]	+0.02	+0.02	+0.04	+0.03	+0.02	+0.03	+0.05	+0.13
(PDF) PDF4LHC15_nlo_30_eigen025 [%]	+0.01	+0.01	+0.01	+0.01	+0.01	+0.03	—	+0.05
(PDF) PDF4LHC15_nlo_30_eigen026 [%]	+0.03	+0.03	+0.02	+0.01	+0.04	+0.04	—	—
(PDF) PDF4LHC15_nlo_30_eigen027 [%]	+0.02	+0.05	+0.03	+0.02	+0.06	+0.04	+0.04	+0.06
(PDF) PDF4LHC15_nlo_30_eigen028 [%]	+0.13	+0.12	+0.12	+0.09	+0.12	+0.11	+0.09	+0.11
(PDF) PDF4LHC15_nlo_30_eigen029 [%]	—	—	—	—	—	—	—	—
(PDF) PDF4LHC15_nlo_30_eigen030 [%]	—	—	+0.01	—	—	+0.02	—	+0.04
(MOD) Alternative hard-scattering model [%]	+3.69	+0.69	+2.68	+1.70	+0.98	+0.46	+3.78	+5.15
(MOD) Alternative parton-shower mode [%]	+0.59	+0.63	+0.43	+2.72	+0.45	+1.46	+1.35	+3.12
(MOD) ISR/FSR + scale [%]	+0.45	+0.60	+2.92	+1.11	+0.0			

Table 140: The individual systematic uncertainties in the parton level fiducial phase-space absolute differential cross-sections for the $t\bar{t}$ mass calculated as a percentage of the cross-section.

Table 141: The individual systematic uncertainties in the parton level fiducial phase-space relative differential cross-sections for the $t\bar{t}$ mass calculated as a percentage of the cross-section.

Bins [GeV]	[0,50]	[50,100]	[100,150]	[150,200]	[200,300]	[300,400]	[400,500]	[500,600]
$d\tau/dX$ [GeV]	3.78 ± 10 ⁻³	3.66 ± 10 ⁻³	1.69 ± 10 ⁻³	9.06 ± 10 ⁻⁴	3.83 ± 10 ⁻³	2.42 ± 10 ⁻³	5.4 ± 10 ⁻⁴	
Total Uncertainty [%]	+31.91 -29.81	+31.51 -29.78	+30.32 -29.59	+33.80 -31.85	+34.94 -32.85	+45.12 -42.26	+7.86 -6.45	
Statistics [%]	+4.58 -4.58	+5.89 -5.89	+5.27 -5.27	+7.14 -7.14	+9.10 -9.10	+15.64 -15.64	+26.57 -26.57	+32.83 -32.83
Systematics [%]	+2.10 -2.10	+2.39 -2.39	+2.71 -2.71	+3.49 -3.49	+3.69 -3.69	+5.08 -5.08	+10.70 -10.70	+50.88 -50.88
(PDF) fBragg_B_eigen [0]	+5.48 -5.48	+5.21 -5.21	+5.38 -5.38	+5.99 -5.99	+6.03 -6.03	+5.55 -5.55	+5.81 -5.81	
(PDF) fBragg_B_eigen [1%]	+4.85 -4.85	+4.85 -4.85	+4.91 -4.91	+5.15 -5.15	+5.31 -5.31	+5.66 -5.66	+5.34 -5.34	+5.78 -5.78
(PDF) fBragg_B_eigen [2%]	+5.02 -5.02	+5.02 -5.02	+5.07 -5.07	+5.28 -5.28	+5.32 -5.32	+5.55 -5.55	+5.78 -5.78	+5.88 -5.88
(PDF) fBragg_B_eigen [3%]	+5.25 -5.25	+5.24 -5.24	+5.29 -5.29	+5.34 -5.34	+5.35 -5.35	+5.52 -5.52	+5.75 -5.75	+5.85 -5.85
(PDF) fBragg_B_eigen [4%]	+5.45 -5.45	+5.44 -5.44	+5.49 -5.49	+5.56 -5.56	+5.62 -5.62	+5.83 -5.83	+5.88 -5.88	+5.93 -5.93
(PDF) fBragg_B_eigen [5%]	+5.65 -5.65	+5.64 -5.64	+5.69 -5.69	+5.76 -5.76	+5.82 -5.82	+5.98 -5.98	+5.98 -5.98	+6.15 -6.15
(PDF) fBragg_B_eigen [6%]	+5.85 -5.85	+5.84 -5.84	+5.89 -5.89	+5.95 -5.95	+6.02 -6.02	+6.03 -6.03	+6.03 -6.03	+6.03 -6.03
(PDF) fBragg_B_eigen [7%]	+6.05 -6.05	+6.04 -6.04	+6.09 -6.09	+6.15 -6.15	+6.22 -6.22	+6.23 -6.23	+6.23 -6.23	+6.23 -6.23
(PDF) fBragg_B_eigen [8%]	+6.25 -6.25	+6.24 -6.24	+6.29 -6.29	+6.35 -6.35	+6.42 -6.42	+6.43 -6.43	+6.43 -6.43	+6.43 -6.43
(PDF) fBragg_B_eigen [9%]	+6.45 -6.45	+6.44 -6.44	+6.49 -6.49	+6.55 -6.55	+6.62 -6.62	+6.63 -6.63	+6.63 -6.63	+6.63 -6.63
(PDF) fBragg_B_eigen [10%]	+6.65 -6.65	+6.64 -6.64	+6.69 -6.69	+6.75 -6.75	+6.82 -6.82	+6.83 -6.83	+6.83 -6.83	+6.83 -6.83
(PDF) fBragg_B_eigen [11%]	+6.85 -6.85	+6.84 -6.84	+6.89 -6.89	+6.95 -6.95	+7.02 -7.02	+7.03 -7.03	+7.03 -7.03	+7.03 -7.03
(PDF) fBragg_B_eigen [12%]	+7.05 -7.05	+7.04 -7.04	+7.09 -7.09	+7.15 -7.15	+7.22 -7.22	+7.23 -7.23	+7.23 -7.23	+7.23 -7.23
(PDF) fBragg_B_eigen [13%]	+7.25 -7.25	+7.24 -7.24	+7.29 -7.29	+7.35 -7.35	+7.42 -7.42	+7.43 -7.43	+7.43 -7.43	+7.43 -7.43
(PDF) fBragg_B_eigen [14%]	+7.45 -7.45	+7.44 -7.44	+7.49 -7.49	+7.55 -7.55	+7.62 -7.62	+7.63 -7.63	+7.63 -7.63	+7.63 -7.63
(PDF) fBragg_B_eigen [15%]	+7.65 -7.65	+7.64 -7.64	+7.69 -7.69	+7.75 -7.75	+7.82 -7.82	+7.83 -7.83	+7.83 -7.83	+7.83 -7.83
(PDF) fBragg_B_eigen [extrapolation %]	+5.90 -5.90	+5.89 -5.89	+5.94 -5.94	+5.99 -5.99	+6.04 -6.04	+6.05 -6.05	+6.05 -6.05	+6.05 -6.05
(PDF) fBragg_F_extrapolation_from_charm [%]	+3.15 -3.15	+3.14 -3.14	+3.20 -3.20	+3.26 -3.26	+3.32 -3.32	+3.38 -3.38	+3.38 -3.38	+3.38 -3.38
(MET/Pt) jvt [%]	+0.05 -0.05	+0.04 -0.04	+0.05 -0.05	+0.06 -0.06	+0.07 -0.07	+0.08 -0.08	+0.08 -0.08	+0.08 -0.08
Intensity [%]	+0.98 -0.98	+0.97 -0.97	+0.98 -0.98	+0.99 -0.99	+0.99 -0.99	+0.99 -0.99	+0.99 -0.99	+0.99 -0.99
BKGR [0,50]	+1.30 -1.30	+1.29 -1.29	+1.35 -1.35	+1.40 -1.40	+1.46 -1.46	+1.52 -1.52	+1.58 -1.58	+1.64 -1.64
(BKG) singletop_W [%]	+0.30 -0.30	+0.30 -0.30	+0.30 -0.30	+0.30 -0.30	+0.30 -0.30	+0.30 -0.30	+0.30 -0.30	+0.30 -0.30
(BKG) tW [%]	+0.01 -0.01	+0.01 -0.01	+0.01 -0.01	+0.01 -0.01	+0.01 -0.01	+0.01 -0.01	+0.01 -0.01	+0.01 -0.01
(BKG) tH [%]	+0.01 -0.01	+0.01 -0.01	+0.01 -0.01	+0.01 -0.01	+0.01 -0.01	+0.01 -0.01	+0.01 -0.01	+0.01 -0.01
(JES) LARGERET_B, Weak_JET_Rkt, Modeling_Tau32WTA [%]	+8.89 -8.89	+8.71 -8.71	+8.53 -8.53	+8.35 -8.35	+8.17 -8.17	+7.99 -7.99	+7.81 -7.81	+7.63 -7.63
(JES) LARGERET_B, Weak_JET_Rkt, Baseline_T1F [%]	+8.12 -8.12	+8.04 -8.04	+7.86 -7.86	+7.68 -7.68	+7.50 -7.50	+7.32 -7.32	+7.14 -7.14	+6.96 -6.96
(JES) LARGERET_B, Weak_JET_Rkt, Baseline_mass [%]	+8.43 -8.43	+8.25 -8.25	+8.07 -8.07	+7.89 -7.89	+7.71 -7.71	+7.53 -7.53	+7.35 -7.35	+7.17 -7.17
(JES) LARGERET_B, Weak_JET_Rkt, Baseline_Tau32SWTA [%]	+8.21 -8.21	+8.03 -8.03	+7.85 -7.85	+7.67 -7.67	+7.49 -7.49	+7.31 -7.31	+7.13 -7.13	+6.95 -6.95
(JES) JET_21INP_JET_BIAS_Response [%]	+0.01 -0.01	+0.01 -0.01	+0.01 -0.01	+0.01 -0.01	+0.01 -0.01	+0.01 -0.01	+0.01 -0.01	+0.01 -0.01
(JES) JET_21INP_JET_Pileup_PtTerm [%]	+0.01 -0.01	+0.01 -0.01	+0.01 -0.01	+0.01 -0.01	+0.01 -0.01	+0.01 -0.01	+0.01 -0.01	+0.01 -0.01
(JES) JET_21INP_JET_Pileup_OffsetNPV [%]	+0.01 -0.01	+0.01 -0.01	+0.01 -0.01	+0.01 -0.01	+0.01 -0.01	+0.01 -0.01	+0.01 -0.01	+0.01 -0.01
(JES) JET_21INP_JET_Pileup_Random_Region [%]	+0.07 -0.07	+0.08 -0.08	+0.11 -0.11	+0.08 -0.08	+0.18 -0.18	+0.03 -0.03	+0.13 -0.13	+0.13 -0.13
(JES) JET_21INP_JET_Extrapolation_SystTerm [%]	+0.30 -0.30	+0.30 -0.30	+0.30 -0.30	+0.30 -0.30	+0.30 -0.30	+0.30 -0.30	+0.30 -0.30	+0.30 -0.30
(LEP) MUON_SAGITTA_RESBIAS [%]	+0.30 -0.30	+0.30 -0.30	+0.30 -0.30	+0.30 -0.30	+0.30 -0.30	+0.30 -0.30	+0.30 -0.30	+0.30 -0.30
(JES) JET_21INP_JET_ExtrapolateNP_3 [%]	+0.01 -0.01	+0.01 -0.01	+0.01 -0.01	+0.01 -0.01	+0.02 -0.02	+0.02 -0.02	+0.02 -0.02	+0.02 -0.02
(JES) JET_21INP_JET_ExtrapolateNP_4 [%]	+0.01 -0.01	+0.01 -0.01	+0.01 -0.01	+0.01 -0.01	+0.02 -0.02	+0.02 -0.02	+0.02 -0.02	+0.02 -0.02
(JES) JET_21INP_JET_ExtrapolateNP_5 [%]	+0.01 -0.01	+0.01 -0.01	+0.01 -0.01	+0.01 -0.01	+0.02 -0.02	+0.02 -0.02	+0.02 -0.02	+0.02 -0.02
(JES) JET_21INP_JET_ExtrapolateNP_6 [%]	+0.01 -0.01	+0.01 -0.01	+0.01 -0.01	+0.01 -0.01	+0.02 -0.02	+0.02 -0.02	+0.02 -0.02	+0.02 -0.02
(JES) JET_21INP_JET_ExtrapolateNP_7 [%]	+0.01 -0.01	+0.01 -0.01	+0.01 -0.01	+0.01 -0.01	+0.02 -0.02	+0.02 -0.02	+0.02 -0.02	+0.02 -0.02
(JES) JET_21INP_JET_ExtrapolateNP_8 [%]	+0.01 -0.01	+0.01 -0.01	+0.01 -0.01	+0.01 -0.01	+0.02 -0.02	+0.02 -0.02	+0.02 -0.02	+0.02 -0.02
(JES) JET_21INP_JET_ExtrapolateNP_9 [%]	+0.01 -0.01	+0.01 -0.01	+0.01 -0.01	+0.01 -0.01	+0.02 -0.02	+0.02 -0.02	+0.02 -0.02	+0.02 -0.02
(JES) JET_21INP_JET_ExtrapolateNP_10 [%]	+0.01 -0.01	+0.01 -0.01	+0.01 -0.01	+0.01 -0.01	+0.02 -0.02	+0.02 -0.02	+0.02 -0.02	+0.02 -0.02
(JES) JET_21INP_JET_ExtrapolateNP_11 [%]	+0.01 -0.01	+0.01 -0.01	+0.01 -0.01	+0.01 -0.01	+0.02 -0.02	+0.02 -0.02	+0.02 -0.02	+0.02 -0.02
(JES) JET_21INP_JET_ExtrapolateNP_12 [%]	+0.01 -0.01	+0.01 -0.01	+0.01 -0.01	+0.01 -0.01	+0.02 -0.02	+0.02 -0.02	+0.02 -0.02	+0.02 -0.02
(JES) JET_21INP_JET_ExtrapolateNP_13 [%]	+0.01 -0.01	+0.01 -0.01	+0.01 -0.01	+0.01 -0.01	+0.02 -0.02	+0.02 -0.02	+0.02 -0.02	+0.02 -0.02
(JES) JET_21INP_JET_ExtrapolateNP_14 [%]	+0.01 -0.01	+0.01 -0.01	+0.01 -0.01	+0.01 -0.01	+0.02 -0.02	+0.02 -0.02	+0.02 -0.02	+0.02 -0.02
(JES) JET_21INP_JET_ExtrapolateNP_15 [%]	+0.01 -0.01	+0.01 -0.01	+0.01 -0.01	+0.01 -0.01	+0.02 -0.02	+0.02 -0.02	+0.02 -0.02	+0.02 -0.02
(JES) JET_21INP_JET_ExtrapolateNP_16 [%]	+0.01 -0.01	+0.01 -0.01	+0.01 -0.01	+0.01 -0.01	+0.02 -0.02	+0.02 -0.02	+0.02 -0.02	+0.02 -0.02
(JES) JET_21INP_JET_ExtrapolateNP_17 [%]	+0.01 -0.01	+0.01 -0.01	+0.01 -0.01	+0.01 -0.01	+0.02 -0.02	+0.02 -0.02	+0.02 -0.02	+0.02 -0.02
(JES) JET_21INP_JET_ExtrapolateNP_18 [%]	+0.01 -0.01	+0.01 -0.01	+0.01 -0.01	+0.01 -0.01	+0.02 -0.02	+0.02 -0.02	+0.02 -0.02	+0.02 -0.02
(JES) JET_21INP_JET_ExtrapolateNP_19 [%]	+0.01 -0.01	+0.01 -0.01	+0.01 -0.01	+0.01 -0.01	+0.02 -0.02	+0.02 -0.02	+0.02 -0.02	+0.02 -0.02
(JES) JET_21INP_JET_ExtrapolateNP_20 [%]	+0.01 -0.01	+0.01 -0.01	+0.01 -0.01	+0.01 -0.01	+0.02 -0.02	+0.02 -0.02	+0.02 -0.02	+0.02 -0.02
(JES) JET_21INP_JET_ExtrapolateNP_21 [%]	+0.01 -0.01	+0.01 -0.01	+0.01 -0.01	+0.01 -0.01	+0.02 -0.02	+0.02 -0.02	+0.02 -0.02	+0.02 -0.02
(JES) JET_21INP_JET_ExtrapolateNP_22 [%]	+0.01 -0.01	+0.01 -0.01	+0.01 -0.01	+0.01 -0.01	+0.02 -0.02	+0.02 -0.02	+0.02 -0.02	+0.02 -0.02
(JES) JET_21INP_JET_ExtrapolateNP_23 [%]	+0.01 -0.01	+0.01 -0.01	+0.01 -0.01	+0.01 -0.01	+0.02 -0.02	+0.02 -0.02	+0.02 -0.02	+0.02 -0.02
(JES) JET_21INP_JET_ExtrapolateNP_24 [%]	+0.01 -0.01	+0.01 -0.01	+0.01 -0.01	+0.01 -0.01	+0.02 -0.02	+0.02 -0.02	+0.02 -0.02	+0.02 -0.02
(JES) JET_21INP_JET_ExtrapolateNP_25 [%]	+0.01 -0.01	+0.01 -0.01	+0.01 -0.01	+0.01 -0.01	+0.02 -0.02	+0.02 -0.02	+0.02 -0.02	+0.02 -0.02
(JES) JET_21INP_JET_ExtrapolateNP_26 [%]	+0.01 -0.01	+0.01 -0.01	+0.01 -0.01	+0.01 -0.01	+0.02 -0.02	+0.02 -0.02	+0.02 -0.02	+0.02 -0.02
(JES) JET_21INP_JET_ExtrapolateNP_27 [%]	+0.01 -0.01	+0.01 -0.01	+0.01 -0.01	+0.01 -0.01	+0.02 -0.02	+0.02 -0.02	+0.02 -0.02	+0.02 -0.02
(JES) JET_21INP_JET_ExtrapolateNP_28 [%]	+0.01 -0.01	+0.01 -0.01	+0.01 -0.01	+0.01 -0.01	+0.02 -0.02	+0.02 -0.02	+0.02 -0.02	+0.02 -0.02
(JES) JET_21INP_JET_ExtrapolateNP_29 [%]	+0.01 -0.01	+0.01 -0.01	+0.01 -0.01	+0.01 -0.01	+0.02 -0.02	+0.02 -0.02	+0.02 -0.02	+0.02 -0.02
(JES) JET_21INP_JET_ExtrapolateNP_30 [%]	+0.01 -0.01	+0.01 -0.01	+0.01 -0.01	+0.01 -0.01	+0.02 -0.02	+0.02 -0.02	+0.02 -0.02	+0.02 -0.02
(PDF) PDF_HFLIC15_nlo_30_eta001 [%]	+0.02 -0.02	+0.01 -0.01	+0.01 -0.01	+0.01 -0.01	+0.02 -0.02	+0.01 -0.01	+0.02 -0.02	+0.02 -0.02
(PDF) PDF_HFLIC15_nlo_30_eta010 [%]	+0.04 -0.04	+0.04 -0.04	+0.04 -0.04	+0.04 -0.04	+0.05 -0.05	+0.04 -0.04	+0.05 -0.05	+0.05 -0.05
(PDF) PDF_HFLIC15_nlo_30_eta010 [%]	+0.05 -0.05	+0.05 -0.05	+0.05 -0.05	+0.05 -0.05	+0.06 -0.06	+0.05 -0.05	+0.06 -0.06	+0.06 -0.06
(PDF) PDF_HFLIC15_nlo_30_eta010 [%]	+0.04 -0.04	+0.04 -0.04	+0.04 -0.04	+0.04 -0.04	+0.05 -0.05	+0.04 -0.04	+0.05 -0.05	+0.05 -0.05
(PDF) PDF_HFLIC15_nlo_30_eta010 [%]	+0.05 -0.05	+0.05 -0.05	+0.05 -0.05	+0.05 -0.05	+0.06 -0.06	+0.05 -0.05	+0.06 -0.06	+0.06 -0.06
(PDF) PDF_HFLIC15_nlo_30_eta010 [%]	+0.04 -0.04	+0.04 -0.04	+0.04 -0.04	+0.04 -0.04	+0.05 -0.05	+0.04 -0.04	+0.05 -0.05	+0.05 -0.05
(PDF) PDF_HFLIC15_nlo_30_eta010 [%]	+0.05 -0.05	+0.05 -0.05	+0.05 -0.05	+0.05 -0.05	+0.06 -0.06	+0.05 -0.05	+0.06 -0.06	+0.06 -0.06
(PDF) PDF_HFLIC15_nlo_30_eta010 [%]	+0.04 -0.04	+0.04 -0.04	+0.04 -0.04	+0.04 -0.04	+0.05 -0.05	+0.04 -0.04	+0.05 -0.05	+0.05 -0.05
(PDF) PDF_HFLIC15_nlo_30_eta010 [%]	+0.05 -0.05	+0.05 -0.05	+0.05 -0.05	+0.05 -0.05	+0.06 -0.06	+0.05 -0.05	+0.06 -0.06	+0.06 -0.06
(PDF) PDF_HFLIC15_nlo_30_eta010 [%]	+0.04 -0.04	+0.04 -0.04	+0.04 -0.04	+0.04 -0.04	+0.05 -0.05	+0.04 -0.04	+0.05 -0.05	+0.05 -0.05
(PDF) PDF_HFLIC15_nlo_30_eta010 [%]	+0.05 -0.05	+0.05 -0.05	+0.05 -0.05	+0.05 -0.05	+0.06 -0.06	+0.05 -0.05	+0.06 -0.06	+0.06 -0.06
(PDF) PDF_HFLIC15_nlo_30_eta010 [%]	+0.04 -0.04	+0.04 -0.04	+0.04 -0.04	+0.04 -0.04	+0.05 -0.05	+0.04 -0.04	+0.05 -0.05	+0.05 -0.05</td

Table 142: The individual systematic uncertainties in the parton level fiducial phase-space absolute differential cross-sections for the $t\bar{t}$ p_T calculated as a percentage of the cross-section.

Not reviewed, for internal circulation only

Bins (GeV)	[0,50]	[50,100]	[100,150]	[150,200]	[200,300]	[300,400]	[400,500]	[500,800]
$ t\bar{t} - t\bar{t} N$ [pb/GeV]	$4.96 \cdot 10^{-3}$	$4.81 \cdot 10^{-3}$	$3.56 \cdot 10^{-3}$	$2.22 \cdot 10^{-3}$	$1.19 \cdot 10^{-3}$	$5.03 \cdot 10^{-4}$	$3.17 \cdot 10^{-4}$	$7.09 \cdot 10^{-5}$
Total Uncertainty [%]	+8.99	+4.54	+7.35	+10.35	+11.88	+22.40	+44.08	+66.37
Statistics [%]	+4.16	+3.50	+4.91	+6.70	+8.72	+15.44	+26.37	+32.09
Systematics [%]	+7.52	+2.20	+4.84	+4.93	+6.53	+14.08	+31.29	+58.50
(FTAG) TagSF_B_eigen0 %	+0.20	+0.16	+0.07	-0.24	-0.69	-0.81	+0.16	+0.99
(FTAG) TagSF_B_eigen1 %	+0.11	+0.11	+0.09	-0.14	-0.25	-0.25	+0.11	+0.29
(FTAG) TagSF_B_eigen2 %	+0.05	+0.14	+0.07	+0.14	+0.26	+0.63	+0.63	+0.55
(FTAG) TagSF_B_eigen3 %	+0.05	+0.15	+0.07	+0.14	+0.26	+0.63	+0.63	+0.58
(FTAG) TagSF_B_eigen4 %	-	-	-0.02	-	-0.06	+0.03	-0.03	+0.58
(FTAG) TagSF_B_eigen5 %	-	-	-	-	-	-	-	+0.56
(FTAG) TagSF_B_eigen6 %	-	-	-	-	-	-	-	+0.28
(FTAG) TagSF_B_eigen7 %	-	-	-	-	-	-	-	+0.24
(FTAG) TagSF_B_eigen8 %	-	-	+0.03	+0.03	-	-	-	+0.41
(FTAG) TagSF_C_eigen0 %	+0.21	+0.13	+0.27	+0.50	+0.99	+0.90	+3.09	+4.29
(FTAG) TagSF_C_eigen1 %	+0.18	+0.14	+0.28	+0.53	+1.03	+0.97	+3.34	+4.26
(FTAG) TagSF_C_eigen2 %	+0.07	+0.22	+0.31	+0.10	+0.92	-0.01	+1.53	+0.58
(FTAG) TagSF_C_eigen3 %	-	-	-	-	-	-	-	+0.58
(FTAG) TagSF_C_eigen4 %	-	-	-	-	-	-	-	+0.56
(FTAG) TagSF_C_eigen5 %	-	-	-	-	-	-	-	+0.56
(FTAG) $\text{TagSF_Light_eigen0}$ %	+0.11	-0.03	-0.10	-0.07	-0.15	+0.01	-1.12	+1.20
(FTAG) $\text{TagSF_Light_eigen1}$ %	-0.04	-0.05	-0.05	-	-0.09	-0.04	+1.25	+0.24
(FTAG) $\text{TagSF_Light_eigen2}$ %	-0.05	-0.05	-0.05	-0.03	+0.10	+0.10	+1.21	+0.25
(FTAG) $\text{TagSF_Light_eigen3}$ %	-0.05	-0.05	-0.05	-0.03	+0.10	+0.10	+1.21	+0.25
(FTAG) $\text{TagSF_Light_eigen4}$ %	-0.05	-0.05	-0.05	-0.03	+0.10	+0.10	+1.21	+0.25
(FTAG) $\text{TagSF_Light_eigen5}$ %	-0.05	-0.05	-0.05	-0.03	+0.10	+0.10	+1.21	+0.25
(FTAG) $\text{TagSF_Light_eigen6}$ %	-0.05	-0.05	-0.05	-0.03	+0.10	+0.10	+1.21	+0.25
(FTAG) $\text{TagSF_Light_eigen7}$ %	-0.03	-0.05	-0.05	-0.02	-0.02	-0.17	-0.11	+0.29
(FTAG) $\text{TagSF_Light_eigen8}$ %	-0.03	-0.05	-0.05	-0.02	-0.02	-0.17	-0.11	+0.29
(FTAG) $\text{TagSF_Light_eigen9}$ %	-0.04	-0.05	-0.05	-0.02	-0.02	-0.17	-0.11	+0.29
(FTAG) $\text{TagSF_Light_eigen10}$ %	-0.04	-0.05	-0.05	-0.02	-0.02	-0.17	-0.11	+0.29
(FTAG) $\text{TagSF_Light_eigen11}$ %	-0.04	-0.05	-0.05	-0.02	-0.02	-0.17	-0.11	+0.29
(FTAG) $\text{TagSF_Light_eigen12}$ %	-0.04	-0.05	-0.05	-0.02	-0.02	-0.17	-0.11	+0.29
(FTAG) $\text{TagSF_Light_eigen13}$ %	-0.04	-0.05	-0.05	-0.02	-0.02	-0.17	-0.11	+0.29
(FTAG) $\text{TagSF_Light_eigen14}$ %	-0.04	-0.05	-0.05	-0.02	-0.02	-0.17	-0.11	+0.29
(FTAG) $\text{TagSF_Light_eigen15}$ %	-0.04	-0.05	-0.05	-0.02	-0.02	-0.17	-0.11	+0.29
(FTAG) $\text{TagSF_extrapolation}$ [%]	+0.10	-0.11	-0.95	-0.26	+0.93	+0.91	+0.29	+0.58
(FTAG) $\text{TagSF_extrapolation_from_charm}$ [%]	-0.14	+0.08	+0.31	+0.25	-0.22	-0.60	-1.01	+0.43
(METPU) jetv [%]	-0.06	-	-	-0.02	-	-0.06	-0.33	+0.26
Luminosity [%]	-0.04	-0.05	-0.06	-0.03	+0.23	-0.20	-0.04	+0.26
(BFG) $\text{tagSF}_{\text{top}}$, jetch [%]	-	-	-	-	-	-	-	+0.29
(BFG) singlejet , Wt [%]	-	-	-	-	-	-	-	+0.29
(BKG) nW [%]	-0.05	-0.03	-0.01	-	-	+0.02	+0.00	-0.01
(BKG) nZ [%]	-0.04	-0.03	-0.02	-	-	+0.05	-0.03	+0.26
(BKG) nH [%]	-0.04	-0.03	-0.02	-	-	+0.05	-0.03	+0.26
(LJES) LARGEJET , Weak JET, Rrk, Modelling, Tau32WTA [%]	-0.03	-0.20	-0.18	-0.12	+0.09	+0.09	+0.09	+0.25
(LJES) LARGEJET , Weak JET, Rrk, Baseline, PT [%]	-0.03	-0.20	-0.18	-0.12	+0.09	+0.09	+0.09	+0.25
(LJES) LARGEJET , Weak JET, Rrk, Baseline, Tau32WTA [%]	-0.03	-0.20	-0.18	-0.12	+0.09	+0.09	+0.09	+0.25
(LJES) LARGEJET , Weak JET, Baseline, Tau32WTA [%]	-0.03	-0.20	-0.18	-0.12	+0.09	+0.09	+0.09	+0.25
(JES) $\text{JET_21NP_JET_BJES_Response}$ [%]	-0.02	-0.02	-0.01	-0.02	-0.03	-0.07	-0.06	+0.27
(JES) $\text{JET_21NP_JET_Plsq_pTItem}$ [%]	-	-	-	-	-	-	-	+0.29
(JES) $\text{JET_21NP_JET_Plsq_pTItem}$, jetch [%]	-0.04	-0.02	-0.02	-0.05	-0.05	-0.02	-0.02	+0.29
(JES) $\text{JET_21NP_JET_Plsq_RhoTopology}$ [%]	+0.02	+0.02	-0.02	-0.02	-	+0.06	-1.04	+0.63
(JES) $\text{JET_21NP_JET_EffectiveNP_SesTerm}$ [%]	-	-	-	-	-	-	-	+0.29
(JEP) $\text{MUON_SAGITTA_RESBIAS}$ [%]	-	-	-	-	-	-	-	+0.29
(JES) $\text{JET_21NP_JET_EffectiveNP_3}$ [%]	-	-	-	-	-	-	-	+0.28
(JES) $\text{JET_21NP_JET_EffectiveNP_4}$ [%]	-	-	-	-	-	-	-	+0.28
(JES) $\text{JET_21NP_JET_EcalTrk}$, jetch , Tracking mass [%]	-0.02	-0.35	-0.34	-0.02	+0.48	-0.34	+0.13	+0.29
(JES) $\text{JET_21NP_JET_Plsq_OffAxis}$ [%]	+0.22	+0.12	-0.42	-0.73	+0.19	-1.30	+1.38	+0.85
(LJES) LARGEJET , Weak JET, Rrk, TotalStat, mass [%]	-0.02	-0.02	+0.06	+0.08	-0.03	-0.01	-0.09	+0.68
(JES) $\text{JET_21NP_JET_EcalTrcalibration}$, NonClosure [%]	+0.02	-0.16	+0.03	+0.03	+0.21	-0.03	-1.05	+0.75
(JES) $\text{JET_21NP_JET_EcalTrcalibration}$, TotalStat [%]	+0.01	-0.16	-0.02	-0.01	-0.03	-0.01	-0.01	+0.55
(JEP) EQ_ResBias , jetch , pT [%]	-0.02	-0.16	-0.09	-0.09	-0.03	-0.05	-0.09	+0.69
(JES) $\text{JET_21NP_JET_EffectiveNP_1}$ [%]	-0.05	-0.05	-0.02	-0.02	-0.16	-0.08	-1.17	+0.82
(JES) $\text{JET_21NP_JET_Flavor_Response}$ [%]	-0.02	-0.01	-0.04	-0.05	-0.15	-0.05	-0.05	+0.26
(JES) $\text{JET_21NP_JET_EffectiveNP_5}$ [%]	-0.05	-0.06	-0.04	-0.03	-0.15	-0.05	-0.05	+0.27
(JES) $\text{JET_21NP_JET_EffectiveNP_5}$ [%]	-	-	-	-	-	-	-	+0.28
(JES) $\text{JET_21NP_JET_Flavor_Composition}$ [%]	-0.16	-0.08	+0.02	+0.07	-0.01	+0.26	+1.74	+1.25
(JES) $\text{JET_21NP_JET_SingleParticle}$, HighPt [%]	+0.03	-0.02	-0.03	-0.03	-0.13	-0.03	-0.03	+0.53
(JES) $\text{JET_21NP_JET_Weak_JET_Rrk, Modelling, pT}$ [%]	-0.15	-0.10	-0.06	-0.19	+0.02	-0.62	-0.03	+0.59
(JES) $\text{JET_21NP_JET_Weak_JET_Rrk, Modelling, mass}$ [%]	-0.03	-0.05	-0.02	-0.11	-0.01	-0.05	-0.05	+0.55
(JEP) MUON_MS [%]	-	-	-	-	-	-	-	+0.29
(JEP) MUON_SAGITTA_RHO [%]	-	-	-	-	-	-	-	+0.29
(JES) $\text{JET_21NP_JET_Plsq_RhoTopg, MC15}$ [%]	-0.15	-0.04	-0.02	+0.24	+0.34	-0.37	+1.31	+1.14
(JES) $\text{JET_21NP_JET_EffectiveNP_2}$ [%]	-0.01	-0.01	-0.01	-0.01	-0.06	-0.08	-0.02	+0.27
(LJES) LARGEJET , Weak JET, Rrk, Tau32WTA [%]	-0.10	-0.03	+0.06	-0.13	-0.03	-0.02	-0.05	+0.58
(LJES) LARGEJET , Weak JET, Rrk, Tracking, pT [%]	-0.74	-0.19	-0.47	-0.48	+0.01	-0.16	+1.81	+1.81
(LJES) LARGEJET , Weak JET, Rrk, Tau32WTA [%]	-0.08	-0.02	-0.03	-0.12	-0.26	-0.08	-0.08	+0.59
(JES) $\text{JET_21NP_JET_Top_massRes}$, jetch [%]	-0.03	-0.03	-0.03	-0.13	-0.10	-0.30	-0.04	+1.28
(PDF) $\text{PDF4LHC15_nlo_30_eigen01}$ [%]	-0.01	-0.04	-0.07	-0.01	-0.06	-0.08	-0.01	+0.57
(PDF) $\text{PDF4LHC15_nlo_30_eigen02}$ [%]	-0.02	-0.10	-0.03	-0.02	-0.02	-0.03	-0.03	+0.56
(PDF) $\text{PDF4LHC15_nlo_30_eigen03}$ [%]	-0.09	-0.09	-0.09	-0.08	-0.06	-0.13	-0.06	+0.50
(PDF) $\text{PDF4LHC15_nlo_30_eigen04}$ [%]	-0.07	-0.24	-0.17	-0.14	-0.10	-0.24	-0.10	+0.68
(PDF) $\text{PDF4LHC15_nlo_30_eigen05}$ [%]	-0.26	-0.26	-0.25	-0.25	-0.26	-0.26	-0.26	+0.66
(PDF) $\text{PDF4LHC15_nlo_30_eigen06}$ [%]	+0.12	-0.31	-0.22	-0.22	-0.19	-0.26	-0.12	+0.62
(PDF) $\text{PDF4LHC15_nlo_30_eigen07}$ [%]	-0.01	-0.01	-0.01	-0.02	-0.02	-0.03	-0.04	+0.45
(PDF) $\text{PDF4LHC15_nlo_30_eigen08}$ [%]	-0.14	-0.19	-0.19	-0.18	-0.15	-0.19	-0.26	+0.86
(PDF) $\text{PDF4LHC15_nlo_30_eigen09}$ [%]	-0.02	-0.07	-0.05	-0.05	-0.04	-0.07	-0.05	+0.64
(PDF) $\text{PDF4LHC15_nlo_30_eigen10}$ [%]	-0.04	-0.06	-0.06	-0.06	-0.04	-0.04	-0.05	+0.56
(PDF) $\text{PDF4LHC15_nlo_30_eigen11}$ [%]	-0.04	-0.06	-0.12	-0.11	-0.11	-0.12	-0.13	+0.70
(PDF) $\text{PDF4LHC15_nlo_30_eigen12}$ [%]	-0.05	-0.11	-0.11	-0.11	-0.11	-0.16	-0.17	+0.67
(PDF) $\text{PDF4LHC15_nlo_30_eigen13}$ [%]	-0.01	-0.03	-0.03	-0.03	-0.04	-0.05	-0.13	+0.66
(PDF) $\text{PDF4LHC15_nlo_30_eigen14}$ [%]	-0.03	-0.02	-0.02	-0.02	-0.02	-0.02	-0.02	+0.61
(PDF) $\text{PDF4LHC15_nlo_30_eigen15}$ [%]	-0.05	-0.04	-0.02	-0.02	-0.02	-0.04	-0.01	+0.55
(PDF) $\text{PDF4LHC15_nlo_30_eigen16}$ [%]	-0.02	-0.02	-0.02	-0.02	-0.02	-0.02	-0.16	+0.53
(PDF) $\text{PDF4LHC15_nlo_30_eigen17}$ [%]	-0.03	-0.03	-0.03	-0.03	-0.03	-0.03	-0.03	+0.53
(PDF) $\text{PDF4LHC15_nlo_30_eigen18}$ [%]	-0.04	-0.14	-0.11	-0.10	-0.08	-0.13	-0.05	+0.44
(PDF) $\text{PDF4LHC15_nlo_30_eigen19}$ [%]	-0.10	-0.06	-0.03	-0.05	-0.03	-0.05	-0.19	+0.59
(PDF) $\text{PDF4LHC15_nlo_30_eigen20}$ [%]	-0.09	-0.03	-0.06	-0.07	-0.06	-0.06	-0.05	+0.55
(PDF) $\text{PDF4LHC15_nlo_30_eigen21}$ [%]	-0.03	-0.06	-0.06	-0.06	-0.06	-0.06	-0.03	+0.54
(PDF) $\text{PDF4LHC15_nlo_30_eigen22}$ [%]	-0.45	-0.63	-0.58	-0.43	-0.69	-0.57	-0.57	+0.68
(PDF) $\text{PDF4LHC15_nlo_30_eigen23}$ [%]	-0.01	-0.01	-0.01	-	-	-	-0.08	+0.65
(PDF) $\text{PDF4LHC15_nlo_30_eigen24}$ [%]	-0.05	-0.04	-0.02	-0.02	-0.02	-0.02	-0.01	+0.56
(PDF) $\text{PDF4LHC15_nlo_30_eigen25}$ [%]	-0.01	-	-	-	-	-0.04	-	+0.55
(PDF) $\text{PDF4LHC15_nlo_30_eigen26}$ [%]	-0.01	-	-	-	-	-0.01	-0.01	+0.64
(PDF) $\text{PDF4LHC15_nlo_30_eigen27}$ [%]	-0.06	-0.02	-0.06	-0.07	-0.07	-0.07	-0.07	+0.71
(PDF) $\text{PDF4LHC15_nlo_30_eigen28}$ [%]	-0.11	-0.09	-0.12	-0.12	-0.14	-0.14	-0.15	+0.6

Not reviewed, for internal circulation only

Bins (GeV)	[0,0.2]	[0.2,0.4]	[0.4,0.6]	[0.6,0.8]	[0.8,1]	[1,1.2]	[1.2,1.5]	[1.5,2]
$d\sigma/dp_T$ [fb/GeV]	$8.29 \cdot 10^{-4}$	$7.83 \cdot 10^{-4}$	$6.36 \cdot 10^{-4}$	$5.77 \cdot 10^{-4}$	$4.57 \cdot 10^{-4}$	$3.43 \cdot 10^{-4}$	$1.82 \cdot 10^{-4}$	$5.88 \cdot 10^{-5}$
Total Uncertainty [%]	± 38.18	± 30.34	± 35.64	± 31.34	± 31.68	± 41.39	± 34.07	± 35.91
Statistics [%]	± 5.08	± 5.72	± 6.30	± 6.74	± 7.79	± 9.18	± 10.63	± 20.11
Systematics [%]	± 35.73	± 29.63	± 32.90	± 30.41	± 30.44	± 40.09	± 31.97	± 27.35
(FTAG) NagSF_B_eigen0 [%]	-5.29	-5.46	-5.16	-5.38	-5.32	-4.74	-5.14	-5.16
(FTAG) NagSF_B_eigen1 [%]	+2.61	+2.50	+2.48	+2.38	+2.38	+2.52	+2.49	+2.48
(FTAG) NagSF_B_eigen2 [%]	-5.04	-5.13	-5.02	-5.09	-5.09	+4.41	+5.09	+5.23
(FTAG) NagSF_B_eigen3 [%]	-0.82	-0.89	-0.74	-0.75	-0.78	-0.31	-0.71	-0.55
(FTAG) NagSF_B_eigen4 [%]	-0.36	-0.25	-0.31	-0.32	-0.42	-0.44	-0.51	-0.35
(FTAG) NagSF_B_eigen5 [%]	-0.68	-0.05	-0.04	-0.05	-0.04	-0.05	-0.04	-0.04
(FTAG) NagSF_C_eigen0 [%]	-1.96	-2.07	-1.50	-2.31	-2.38	-2.03	-2.63	-1.69
(FTAG) NagSF_C_eigen1 [%]	-1.09	-1.07	-1.08	-1.08	-1.08	-1.22	-1.08	-1.05
(FTAG) NagSF_C_eigen2 [%]	-0.73	-0.29	-0.17	-0.41	-0.34	-0.13	-0.31	-0.03
(FTAG) NagSF_C_eigen3 [%]	-0.33	-0.23	-0.15	-0.15	-0.14	-0.13	-0.15	-0.03
(FTAG) $\text{NagSF_Light_eigen0}$ [%]	-0.29	-0.01	-0.03	-0.09	-0.06	-0.06	-0.07	-0.07
(FTAG) $\text{NagSF_Light_eigen1}$ [%]	-0.09	-0.01	-0.04	-0.01	-0.01	-0.01	-0.01	-0.01
(FTAG) $\text{NagSF_Light_eigen2}$ [%]	-0.05	-0.01	-0.04	-0.01	-0.01	-0.01	-0.01	-0.01
(FTAG) $\text{NagSF_Light_eigen3}$ [%]	-0.05	-0.01	-0.03	-0.01	-0.01	-0.01	-0.01	-0.01
(FTAG) $\text{NagSF_Light_eigen4}$ [%]	-0.07	-0.02	-0.03	-0.03	-0.03	-0.03	-0.03	-0.03
(FTAG) $\text{NagSF_Light_eigen5}$ [%]	-0.04	-0.06	-0.03	-0.01	-0.01	-0.03	-0.03	-0.06
(FTAG) $\text{NagSF_Light_eigen6}$ [%]	-0.02	-0.01	-0.01	-0.01	-0.01	-0.01	-0.01	-0.01
(FTAG) $\text{NagSF_Light_eigen7}$ [%]	-0.05	-0.01	-0.03	-0.04	-0.08	-0.21	-0.05	-0.03
(FTAG) $\text{NagSF_Light_eigen8}$ [%]	-0.09	-0.01	-0.02	-0.03	-0.03	-0.15	-0.03	-0.06
(FTAG) $\text{NagSF_Light_eigen9}$ [%]	-0.03	-0.03	-0.03	-0.03	-0.03	-0.02	-0.03	-0.03
(FTAG) $\text{NagSF_Light_eigen10}$ [%]	-0.04	-0.04	-0.04	-0.03	-0.03	-0.03	-0.03	-0.03
(FTAG) $\text{NagSF_Light_eigen11}$ [%]	-0.04	-0.04	-0.04	-0.03	-0.03	-0.06	-0.06	-0.11
(FTAG) $\text{NagSF_Light_eigen12}$ [%]	-0.04	-0.04	-0.04	-0.03	-0.03	-0.06	-0.06	-0.11
(FTAG) $\text{NagSF_Light_eigen13}$ [%]	-0.04	-0.04	-0.04	-0.03	-0.03	-0.06	-0.06	-0.11
(FTAG) $\text{NagSF_Light_eigen14}$ [%]	-0.04	-0.04	-0.04	-0.03	-0.03	-0.06	-0.06	-0.11
(FTAG) $\text{NagSF_Light_eigen15}$ [%]	-0.04	-0.04	-0.04	-0.03	-0.03	-0.06	-0.06	-0.11
(FTAG) $\text{NagSF_extrapolation}$ [%]	-0.03	-0.04	-0.04	-0.03	-0.03	-0.05	-0.05	-0.11
(FTAG) $\text{NagSF_extrapolation_from_charm}$ [%]	-0.07	-0.07	-0.08	-0.09	-0.09	-0.20	-0.20	-0.27
(METPU) j_ν [%]	-0.01	-0.06	-0.06	-0.05	-0.06	-0.14	-0.07	-0.07
(BKG) $\text{sig2dpt}, W_1$ [%]	-	-	-	-	-	-	-	-
(BKG) nW [%]	-	-	-	-	-	-	-	-
(BKG) nT [%]	-0.03	-0.03	-0.03	-0.03	-0.03	-0.03	-0.03	-0.02
(BKG) nH [%]	-0.02	-0.02	-0.03	-0.03	-0.02	-0.02	-0.02	-0.01
(LJES) $\text{LARGEJET_Weak_JET_Rrk_Modelling_Tau32WTA}$ [%]	-0.49	-0.49	-0.49	-0.49	-0.49	-0.49	-0.49	-0.49
(LJES) $\text{LARGEJET_Weak_JET_Rrk_Baseline_PT}$ [%]	-1.88	-1.88	-1.88	-1.88	-1.88	-1.88	-1.88	-1.88
(LJES) $\text{LARGEJET_Weak_JET_Rrk_Baseline_Tau32WTA}$ [%]	-0.83	-0.83	-0.83	-0.83	-0.83	-0.83	-0.83	-0.83
(LJES) $\text{LARGEJET_Weak_JET_Baseline_Tau32WTA}$ [%]	-0.01	-0.01	-0.01	-0.01	-0.01	-0.01	-0.01	-0.01
(JES) $\text{JET_21NP_JET_Response}$ [%]	-0.01	-0.01	-0.01	-0.01	-0.01	-0.01	-0.01	-0.01
(JES) $\text{JET_21NP_JET_Plung_PTItem}$ [%]	-0.07	-0.07	-0.07	-0.07	-0.07	-0.07	-0.07	-0.06
(JES) $\text{JET_21NP_JET_Plung_Eta}$ [%]	-0.03	-0.03	-0.03	-0.03	-0.03	-0.03	-0.03	-0.03
(JES) $\text{JET_21NP_JET_Plung_PhiTopology}$ [%]	-0.25	-0.14	-0.24	-0.10	-0.09	-0.23	-0.15	-0.83
(JES) $\text{JET_21NP_JET_EffectivNP_SeeTerm}$ [%]	-0.06	-0.10	-0.10	-0.09	-0.11	-0.11	-0.06	+0.30
(LEP) $\text{MUON_SAGITTA_REBIAS}$ [%]	-	-	-	-	-	-	-	-
(JES) $\text{JET_21NP_JET_EffectivNP_3}$ [%]	-0.01	-	-0.01	-0.01	-0.01	-	-0.01	+0.03
(JES) $\text{JET_21NP_JET_EffectivNP_4}$ [%]	-0.01	-	-0.01	-0.01	-0.01	-	-0.02	+0.01
(JES) $\text{JET_21NP_JET_Flavor_Mass}$ [%]	-0.05	-0.27	-	-0.01	-0.01	-0.01	-0.01	+0.04
(JES) $\text{JET_21NP_JET_Flavor_Rebias}$ [%]	-0.05	-0.27	-	-0.01	-0.01	-0.01	-0.01	+0.04
(JES) $\text{JET_21NP_JET_Flavor_Composition}$ [%]	-0.05	-0.04	-0.04	-0.08	-0.08	-0.05	-0.05	-0.09
(JES) $\text{JET_21NP_JET_Ecaltercalibration}$ [%]	-0.08	-0.03	-0.04	-	-0.19	-0.02	-0.02	+0.18
(JES) $\text{JET_21NP_JET_Ecaltercalibration_TotalStat}$ [%]	-0.01	-0.01	-0.02	-	-0.03	-0.03	-0.03	+0.01
(LEP) EG_REBIAS [%]	-0.05	-0.04	-0.04	-0.08	-0.08	-0.05	-0.05	-0.05
(JES) $\text{JET_21NP_JET_Flavor_Response}$ [%]	-0.05	-0.04	-0.04	-0.01	-0.13	-0.03	-0.02	-0.02
(JES) $\text{JET_21NP_JET_EffectivNP_6}$ [%]	-0.05	-0.04	-0.06	-0.08	-0.08	-0.01	-0.07	-0.02
(JES) $\text{JET_21NP_JET_EffectivNP_5}$ [%]	-	-	-	-0.03	-	-0.03	-0.01	-
(JES) $\text{JET_21NP_JET_SingleParticle_HighPt}$ [%]	-0.37	-0.19	-0.35	-0.22	-0.05	-0.26	-0.34	+0.64
(JES) $\text{JET_21NP_JET_Modelling_PT}$ [%]	-2.09	-2.15	-2.03	-2.22	-2.22	-1.95	-2.19	-2.00
(JES) $\text{JET_21NP_JET_Modelling_mass}$ [%]	-0.03	-0.04	-0.10	-0.02	-0.14	-0.02	-0.01	+0.05
(LEP) MUON_ID [%]	-	-	-	-	-	-	-	-
(JES) $\text{JET_21NP_JET_Weak_JET_Rrk_TotalStat_PT}$ [%]	-0.37	-0.33	-0.21	-0.44	-0.40	-0.30	-0.14	+0.30
(JES) $\text{JET_21NP_JET_Modelling}$ [%]	-0.01	-0.24	-0.30	-0.20	-0.21	-0.15	-0.19	-0.17
(JES) $\text{JET_21NP_JET_Ecaltercalibration}$ [%]	-0.02	-0.02	-0.04	-0.02	-0.01	-0.03	-0.03	+0.01
(JES) $\text{JET_21NP_JET_EffectivNP_2}$ [%]	-0.02	-0.02	-0.04	-0.02	-0.02	-0.05	-0.01	+0.08
(JES) $\text{JET_21NP_JET_EffectivNP_7}$ [%]	-0.05	-	-	-	-	-0.01	-0.01	-
(JES) $\text{JET_21NP_JET_Modelling_mass}$ [%]	-0.29	-0.62	-0.16	-0.66	-0.41	-0.09	-0.02	-1.12
(LEP) MUON_MS [%]	-1.76	-	-	-	-	-0.64	-0.64	+1.30
(JES) $\text{JET_21NP_JET_GLE_NP}$ [%]	-0.36	-0.13	-0.09	-0.09	-0.31	-0.01	-0.19	+1.12
(JES) $\text{JET_21NP_JET_Top_massRes_mass}$ [%]	-0.23	-0.23	-0.12	-1.73	-1.64	-0.39	-0.91	+2.51
(PDF) $\text{PDF4LHC15_nlo_30_eigen001}$ [%]	-0.08	-0.04	-0.09	-0.09	-0.04	-0.04	-0.04	-0.01
(PDF) $\text{PDF4LHC15_nlo_30_eigen002}$ [%]	-0.05	-0.09	-0.11	-0.17	-0.29	-0.12	-0.34	+0.53
(PDF) $\text{PDF4LHC15_nlo_30_eigen003}$ [%]	-0.04	-0.03	-0.06	-0.07	-0.32	-0.12	-0.34	+0.33
(PDF) $\text{PDF4LHC15_nlo_30_eigen004}$ [%]	-0.01	-	-	-0.14	-0.26	-0.38	-0.62	+0.83
(PDF) $\text{PDF4LHC15_nlo_30_eigen005}$ [%]	-0.04	-0.03	-0.04	-0.43	-0.48	-0.58	-0.88	+0.92
(PDF) $\text{PDF4LHC15_nlo_30_eigen006}$ [%]	-0.15	-0.11	-0.17	-0.22	-0.34	-0.36	-0.54	+0.73
(PDF) $\text{PDF4LHC15_nlo_30_eigen007}$ [%]	-0.02	-	-	-	-0.05	-0.04	-0.08	+0.06
(PDF) $\text{PDF4LHC15_nlo_30_eigen008}$ [%]	-0.09	-0.11	-0.11	-0.13	-0.18	-0.24	-0.51	+0.39
(PDF) $\text{PDF4LHC15_nlo_30_eigen009}$ [%]	-0.05	-0.04	-0.05	-0.06	-0.07	-0.08	-0.12	+0.09
(PDF) $\text{PDF4LHC15_nlo_30_eigen10}$ [%]	-0.05	-0.05	-0.05	-0.06	-0.04	-0.04	-0.12	+0.40
(PDF) $\text{PDF4LHC15_nlo_30_eigen11}$ [%]	-0.07	-0.06	-0.06	-0.08	-0.09	-0.13	-0.12	+0.26
(PDF) $\text{PDF4LHC15_nlo_30_eigen12}$ [%]	-0.09	-0.06	-0.06	-0.09	-0.09	-0.14	-0.29	+0.33
(PDF) $\text{PDF4LHC15_nlo_30_eigen013}$ [%]	-0.02	-0.04	-0.03	-0.02	-0.04	-0.04	-0.05	+0.20
(PDF) $\text{PDF4LHC15_nlo_30_eigen014}$ [%]	-0.03	-0.01	-0.01	-	-0.04	-0.06	-0.08	+0.10
(PDF) $\text{PDF4LHC15_nlo_30_eigen015}$ [%]	-0.03	-	-	-	-0.06	-0.06	-0.12	+0.16
(PDF) $\text{PDF4LHC15_nlo_30_eigen016}$ [%]	-0.03	-0.03	-0.05	-0.01	-0.03	-0.06	-0.03	+0.06
(PDF) $\text{PDF4LHC15_nlo_30_eigen017}$ [%]	-0.09	-0.05	-0.08	-0.10	-0.17	-0.25	-0.46	+0.26
(PDF) $\text{PDF4LHC15_nlo_30_eigen018}$ [%]	-0.03	-0.03	-0.03	-0.06	-0.12	-0.20	-0.31	+0.54
(PDF) $\text{PDF4LHC15_nlo_30_eigen019}$ [%]	-0.22	-0.15	-0.13	-0.05	-0.07	-0.17	-0.23	+0.22
(PDF) $\text{PDF4LHC15_nlo_30_eigen020}$ [%]	-0.02	-0.03	-0.02	-0.03	-0.05	-0.04	-0.06	+0.04
(PDF) $\text{PDF4LHC15_nlo_30_eigen021}$ [%]	-	-	-0.02	-	-0.03	-0.06	-0.07	+0.08
(PDF) $\text{PDF4LHC15_nlo_30_eigen022}$ [%]	-0.24	-0.29	-0.34	-0.49	-0.71	-0.21	-1.29	+1.01
(PDF) $\text{PDF4LHC15_nlo_30_eigen023}$ [%]	-	-	-	-	-	-0.02	-0.03	-0.03
(PDF) $\text{PDF4LHC15_nlo_30_eigen024}$ [%]	-0.04	-0.03	-0.03	-0.02	-0.04	-0.04	-0.16	+0.27
(PDF) $\text{PDF4LHC15_nlo_30_eigen025}$ [%]	-0.01	-	-	-	-	-0.02	-0.01	+0.15
(PDF) $\text{PDF4LHC15_nlo_30_eigen026}$ [%]	-0.03	-0.04	-0.02	-	-	-0.01	-0.07	+0.05
(PDF) $\text{PDF4LHC15_nlo_30_eigen027}$ [%]	-	-0.04	-0.02	-0.04	-0.07	-0.01	-0.07	+0.08
(PDF) $\text{PDF4LHC15_nlo_30_eigen028}$ [%]	-0.13	-0.13	-0.09	-0.09	-0.08	-0.06	-0.04	+0.17
(PDF) $\text{PDF4LHC15_nlo_30_eigen029}$ [%]	-	-	-	-	-	-	-0.01	-
(PDF) $\text{PDF4LHC15_nlo_30_eigen030}$ [%]	-	-	-	-	-	-	-0.04	-0.01
(MOD) Alternative hard-scattering model [%]	± 15.81	± 10.75	± 14.09	± 8.15	± 8.68	± 19.20	± 9.48	± 4.38
(MOD) Alternative parton-shower mode [%]	\pm							

Not reviewed, for internal circulation only

Bins [GeV]	[0,0.2]	[0.2,0.4]	[0.4,0.6]	[0.6,0.8]	[0.8,1]	[1,1.2]	[1.2,1.5]	[1.5,2]
$1/\sigma \partial/\partial X$ [fb/GeV]	1.03 +2.60 -2.73	$9.75 \cdot 10^{-1}$ +2.27 -2.33	$7.92 \cdot 10^{-1}$ +2.19 -2.23	$7.19 \cdot 10^{-1}$ +2.03 -2.04	$5.69 \cdot 10^{-1}$ +0.78 -0.84	$3.9 \cdot 10^{-1}$ +0.78 -0.84	$2.27 \cdot 10^{-1}$ +0.53 -0.53	$7.32 \cdot 10^{-2}$ +1.69 -1.68
Total Uncertainty [%]	4.63 +4.63 -4.63	+5.34 -5.33 +5.33	+5.88 -5.85 +5.85	+6.38 -6.35 +6.35	+7.46 -7.43 +7.43	+8.90 -8.87 +8.87	+10.29 -10.26 +10.26	+19.80 -19.76 +19.76
Statistics [%]	-	-	-	-	-	-	-	-
Systematics [%]	-	-	-	-	-	-	-	-
(FTAG) VtagSF_B_eigen0 [%]	-0.09 +0.05 -0.05	+0.19 -0.15 +0.15	-0.05 +0.04 -0.04	+0.03 -0.03 +0.03	-0.04 +0.04 -0.04	-0.42 +0.42 -0.42	+0.08 -0.08 +0.08	-0.09 +0.09 -0.09
(FTAG) VtagSF_B_eigen1 [%]	-0.07 +0.05 -0.05	+0.18 -0.14 +0.14	-0.04 +0.04 -0.04	+0.04 -0.03 +0.03	-0.04 +0.04 -0.04	-0.32 +0.32 -0.32	+0.08 -0.08 +0.08	-0.35 +0.35 -0.35
(FTAG) VtagSF_B_eigen2 [%]	-0.05 +0.05 -0.05	+0.18 -0.14 +0.14	-0.04 +0.04 -0.04	+0.03 -0.03 +0.03	-0.03 +0.03 -0.03	-0.35 +0.35 -0.35	+0.08 -0.08 +0.08	-0.35 +0.35 -0.35
(FTAG) VtagSF_B_eigen3 [%]	-0.03 +0.03 -0.03	+0.18 -0.14 +0.14	-0.04 +0.04 -0.04	+0.03 -0.03 +0.03	-0.03 +0.03 -0.03	-0.35 +0.35 -0.35	+0.08 -0.08 +0.08	-0.35 +0.35 -0.35
(FTAG) VtagSF_B_eigen4 [%]	-0.01 +0.01 -0.01	+0.18 -0.14 +0.14	-0.04 +0.04 -0.04	+0.02 -0.02 +0.02	-0.02 +0.02 -0.02	-0.32 +0.32 -0.32	+0.08 -0.08 +0.08	-0.32 +0.32 -0.32
(FTAG) VtagSF_B_eigen5 [%]	-0.01 +0.01 -0.01	+0.18 -0.14 +0.14	-0.04 +0.04 -0.04	+0.02 -0.02 +0.02	-0.02 +0.02 -0.02	-0.32 +0.32 -0.32	+0.08 -0.08 +0.08	-0.32 +0.32 -0.32
(FTAG) VtagSF_C_eigen0 [%]	-0.09 +0.05 -0.05	+0.10 -0.08 +0.08	-0.09 +0.08 -0.08	+0.13 -0.13 +0.13	-0.16 +0.16 -0.16	-0.05 +0.05 -0.05	+0.08 -0.08 +0.08	-0.13 +0.13 -0.13
(FTAG) VtagSF_C_eigen1 [%]	-0.14 +0.05 -0.05	+0.08 -0.06 +0.06	-0.24 +0.24 -0.24	+0.15 -0.15 +0.15	-0.17 +0.17 -0.17	-0.08 +0.08 -0.08	+0.08 -0.08 +0.08	-0.17 +0.17 -0.17
(FTAG) VtagSF_C_eigen2 [%]	-0.18 +0.05 -0.05	+0.08 -0.06 +0.06	-0.24 +0.24 -0.24	+0.17 -0.17 +0.17	-0.17 +0.17 -0.17	-0.08 +0.08 -0.08	+0.08 -0.08 +0.08	-0.17 +0.17 -0.17
(FTAG) VtagSF_C_eigen3 [%]	-0.09 +0.05 -0.05	+0.08 -0.06 +0.06	-0.24 +0.24 -0.24	+0.13 -0.13 +0.13	-0.04 +0.04 -0.04	-0.04 +0.04 -0.04	+0.08 -0.08 +0.08	-0.10 +0.10 -0.10
(FTAG) VtagSF_C_eigen4 [%]	-0.01 +0.01 -0.01	+0.08 -0.06 +0.06	-0.24 +0.24 -0.24	+0.13 -0.13 +0.13	-0.02 +0.02 -0.02	-0.02 +0.02 -0.02	+0.08 -0.08 +0.08	-0.10 +0.10 -0.10
(FTAG) VtagSF_C_eigen5 [%]	-0.01 +0.01 -0.01	+0.08 -0.06 +0.06	-0.24 +0.24 -0.24	+0.13 -0.13 +0.13	-0.02 +0.02 -0.02	-0.02 +0.02 -0.02	+0.08 -0.08 +0.08	-0.10 +0.10 -0.10
(FTAG) $\text{VtagSF_Light_eigen0}$ [%]	-0.09 +0.05 -0.05	+0.10 -0.08 +0.08	-0.24 +0.24 -0.24	+0.13 -0.13 +0.13	-0.05 +0.05 -0.05	-0.05 +0.05 -0.05	+0.08 -0.08 +0.08	-0.13 +0.13 -0.13
(FTAG) $\text{VtagSF_Light_eigen1}$ [%]	-0.03 +0.03 -0.03	+0.08 -0.06 +0.06	-0.24 +0.24 -0.24	+0.13 -0.13 +0.13	-0.05 +0.05 -0.05	-0.05 +0.05 -0.05	+0.08 -0.08 +0.08	-0.13 +0.13 -0.13
(FTAG) $\text{VtagSF_Light_eigen2}$ [%]	-0.03 +0.03 -0.03	+0.08 -0.06 +0.06	-0.24 +0.24 -0.24	+0.13 -0.13 +0.13	-0.05 +0.05 -0.05	-0.05 +0.05 -0.05	+0.08 -0.08 +0.08	-0.13 +0.13 -0.13
(FTAG) $\text{VtagSF_Light_eigen3}$ [%]	-0.03 +0.03 -0.03	+0.08 -0.06 +0.06	-0.24 +0.24 -0.24	+0.13 -0.13 +0.13	-0.05 +0.05 -0.05	-0.05 +0.05 -0.05	+0.08 -0.08 +0.08	-0.13 +0.13 -0.13
(FTAG) $\text{VtagSF_Light_eigen4}$ [%]	-0.02 +0.02 -0.02	+0.08 -0.06 +0.06	-0.24 +0.24 -0.24	+0.13 -0.13 +0.13	-0.02 +0.02 -0.02	-0.02 +0.02 -0.02	+0.08 -0.08 +0.08	-0.13 +0.13 -0.13
(FTAG) $\text{VtagSF_Light_eigen5}$ [%]	-0.02 +0.02 -0.02	+0.08 -0.06 +0.06	-0.24 +0.24 -0.24	+0.13 -0.13 +0.13	-0.02 +0.02 -0.02	-0.02 +0.02 -0.02	+0.08 -0.08 +0.08	-0.13 +0.13 -0.13
(FTAG) $\text{VtagSF_Light_eigen6}$ [%]	-0.02 +0.02 -0.02	+0.08 -0.06 +0.06	-0.24 +0.24 -0.24	+0.13 -0.13 +0.13	-0.02 +0.02 -0.02	-0.02 +0.02 -0.02	+0.08 -0.08 +0.08	-0.13 +0.13 -0.13
(FTAG) $\text{VtagSF_Light_eigen7}$ [%]	-0.03 +0.03 -0.03	+0.08 -0.06 +0.06	-0.24 +0.24 -0.24	+0.13 -0.13 +0.13	-0.05 +0.05 -0.05	-0.05 +0.05 -0.05	+0.08 -0.08 +0.08	-0.13 +0.13 -0.13
(FTAG) $\text{VtagSF_Light_eigen8}$ [%]	-0.03 +0.03 -0.03	+0.08 -0.06 +0.06	-0.24 +0.24 -0.24	+0.13 -0.13 +0.13	-0.05 +0.05 -0.05	-0.05 +0.05 -0.05	+0.08 -0.08 +0.08	-0.13 +0.13 -0.13
(FTAG) $\text{VtagSF_Light_eigen9}$ [%]	-0.03 +0.03 -0.03	+0.08 -0.06 +0.06	-0.24 +0.24 -0.24	+0.13 -0.13 +0.13	-0.05 +0.05 -0.05	-0.05 +0.05 -0.05	+0.08 -0.08 +0.08	-0.13 +0.13 -0.13
(FTAG) $\text{VtagSF_Light_eigen10}$ [%]	-0.03 +0.03 -0.03	+0.08 -0.06 +0.06	-0.24 +0.24 -0.24	+0.13 -0.13 +0.13	-0.05 +0.05 -0.05	-0.05 +0.05 -0.05	+0.08 -0.08 +0.08	-0.13 +0.13 -0.13
(FTAG) $\text{VtagSF_Light_eigen11}$ [%]	-0.03 +0.03 -0.03	+0.08 -0.06 +0.06	-0.24 +0.24 -0.24	+0.13 -0.13 +0.13	-0.05 +0.05 -0.05	-0.05 +0.05 -0.05	+0.08 -0.08 +0.08	-0.13 +0.13 -0.13
(FTAG) $\text{VtagSF_Light_eigen12}$ [%]	-0.03 +0.03 -0.03	+0.08 -0.06 +0.06	-0.24 +0.24 -0.24	+0.13 -0.13 +0.13	-0.05 +0.05 -0.05	-0.05 +0.05 -0.05	+0.08 -0.08 +0.08	-0.13 +0.13 -0.13
(FTAG) $\text{VtagSF_Light_eigen13}$ [%]	-0.03 +0.03 -0.03	+0.08 -0.06 +0.06	-0.24 +0.24 -0.24	+0.13 -0.13 +0.13	-0.05 +0.05 -0.05	-0.05 +0.05 -0.05	+0.08 -0.08 +0.08	-0.13 +0.13 -0.13
(FTAG) $\text{VtagSF_Light_eigen14}$ [%]	-0.03 +0.03 -0.03	+0.08 -0.06 +0.06	-0.24 +0.24 -0.24	+0.13 -0.13 +0.13	-0.05 +0.05 -0.05	-0.05 +0.05 -0.05	+0.08 -0.08 +0.08	-0.13 +0.13 -0.13
(FTAG) $\text{VtagSF_Light_eigen15}$ [%]	-0.02 +0.02 -0.02	+0.08 -0.06 +0.06	-0.24 +0.24 -0.24	+0.13 -0.13 +0.13	-0.05 +0.05 -0.05	-0.05 +0.05 -0.05	+0.08 -0.08 +0.08	-0.13 +0.13 -0.13
(FTAG) $\text{VtagSF_extrapolation}$ [%]	-0.17 +0.17 -0.17	+0.18 -0.18 +0.18	-0.08 +0.08 -0.08	+0.03 -0.03 +0.03	-0.06 +0.06 -0.06	-0.06 +0.06 -0.06	+0.06 -0.06 +0.06	-0.17 +0.17 -0.17
(FTAG) $\text{VtagSF_extrapolation_from_charm}$ [%]	-0.17 +0.17 -0.17	+0.18 -0.18 +0.18	-0.08 +0.08 -0.08	+0.03 -0.03 +0.03	-0.06 +0.06 -0.06	-0.06 +0.06 -0.06	+0.06 -0.06 +0.06	-0.17 +0.17 -0.17
(METPPU) μ [%]	-0.07 +0.07 -0.07	+0.03 -0.03 +0.03	-0.01 +0.01 -0.01	+0.01 -0.01 +0.01	-0.01 +0.01 -0.01	-0.01 +0.01 -0.01	+0.01 -0.01 +0.01	-0.07 +0.07 -0.07
Luminosity [%]	-0.01 +0.01 -0.01	+0.02 -0.02 +0.02	-0.01 +0.01 -0.01	+0.02 -0.02 +0.02	-0.02 +0.02 -0.02	-0.02 +0.02 -0.02	+0.02 -0.02 +0.02	-0.01 +0.01 -0.01
(BK0) singletop_tchan [%]	-0.04 +0.04 -0.04	+0.02 -0.02 +0.02	-0.03 +0.03 -0.03	+0.01 -0.01 +0.01	-0.02 +0.02 -0.02	-0.02 +0.02 -0.02	+0.02 -0.02 +0.02	-0.04 +0.04 -0.04
(BK0) singletop_Wt [%]	-	-	-	-	-	-	-	-
(BK0) ntW [%]	-	-	-	-	-	-	-	-
(BK0) mH [%]	-	-	-	-	-	-	-	-
(JES) LARGERET_Weak_JET_Rtrk_ModelingTau32WTA [%]	-0.52 +0.52 -0.52	+0.11 -0.11 +0.11	-0.26 +0.26 -0.26	+0.85 -0.85 +0.85	-0.55 +0.55 -0.55	-0.33 +0.33 -0.33	+1.15 -1.15 +1.15	+0.01 -0.01 +0.01
(JES) LARGERET_Weak_JET_Rtrk_Baseline_pT [%]	-0.05 +0.05 -0.05	+0.22 -0.22 +0.22	-0.03 +0.03 -0.03	+0.29 -0.29 +0.29	-0.10 +0.10 -0.10	-0.33 +0.33 -0.33	+0.24 -0.24 +0.24	+0.57 -0.57 +0.57
(JES) LARGERET_Weak_JET_Rtrk_Baseline_Mass [%]	-0.05 +0.05 -0.05	+0.22 -0.22 +0.22	-0.03 +0.03 -0.03	+0.31 -0.31 +0.31	-0.10 +0.10 -0.10	-0.33 +0.33 -0.33	+0.24 -0.24 +0.24	+0.57 -0.57 +0.57
(JES) LARGERET_Weak_JET_Rtrk_Baseline_TotalStat [%]	-0.44 +0.44 -0.44	+0.07 -0.07 +0.07	-0.06 +0.06 -0.06	+0.06 -0.06 +0.06	-0.50 +0.50 -0.50	-0.41 +0.41 -0.41	+0.81 -0.81 +0.81	+1.41 -1.41 +1.41
(JES) JET_21NP_JET_Plmp_OffsetNP_1 [%]	-0.12 +0.12 -0.12	+0.03 -0.03 +0.03	-0.05 +0.05 -0.05	+0.02 -0.02 +0.02	-0.03 +0.03 -0.03	-0.03 +0.03 -0.03	+0.01 -0.01 +0.01	-0.16 +0.16 -0.16
(JES) JET_21NP_JET_Plmp_OffsetNP_2 [%]	-0.14 +0.14 -0.14	+0.03 -0.03 +0.03	-0.05 +0.05 -0.05	+0.02 -0.02 +0.02	-0.03 +0.03 -0.03	-0.03 +0.03 -0.03	+0.01 -0.01 +0.01	-0.15 +0.15 -0.15
(JES) JET_21NP_JET_Plmp_OffsetNP_3 [%]	-0.08 +0.08 -0.08	+0.02 -0.02 +0.02	-0.04 +0.04 -0.04	+0.01 -0.01 +0.01	-0.03 +0.03 -0.03	-0.03 +0.03 -0.03	+0.01 -0.01 +0.01	-0.08 +0.08 -0.08
(JES) JET_21NP_JET_Plmp_OffsetNP_4 [%]	-0.08 +0.08 -0.08	+0.02 -0.02 +0.02	-0.04 +0.04 -0.04	+0.01 -0.01 +0.01	-0.03 +0.03 -0.03	-0.03 +0.03 -0.03	+0.01 -0.01 +0.01	-0.08 +0.08 -0.08
(JES) JET_21NP_JET_Plmp_OffsetRhoTopology [%]	-0.02 +0.02 -0.02	+0.08 -0.08 +0.08	-0.05 +0.05 -0.05	+0.02 -0.02 +0.02	-0.03 +0.03 -0.03	-0.03 +0.03 -0.03	+0.01 -0.01 +0.01	-0.08 +0.08 -0.08
(JES) JET_21NP_JET_Plmp_OffsetTau32WTA [%]	-0.05 +0.05 -0.05	+0.01 -0.01 +0.01	-0.06 +0.06 -0.06	+0.02 -0.02 +0.02	-0.03 +0.03 -0.03	-0.03 +0.03 -0.03	+0.01 -0.01 +0.01	-0.08 +0.08 -0.08
(JES) JET_21NP_JET_Plmp_OffsetTau32WTA_NonClosure [%]	-0.03 +0.03 -0.03	+0.01 -0.01 +0.01	-0.06 +0.06 -0.06	+0.02 -0.02 +0.02	-0.03 +0.03 -0.03	-0.03 +0.03 -0.03	+0.01 -0.01 +0.01	-0.08 +0.08 -0.08
(JES) JET_21NP_JET_Plmp_OffsetTotalStat [%]	-0.02 +0.02 -0.02	+0.01 -0.01 +0.01	-0.05 +0.05 -0.05	+0.02 -0.02 +0.02	-0.03 +0.03 -0.03	-0.03 +0.03 -0.03	+0.01 -0.01 +0.01	-0.08 +0.08 -0.08
(LEP) JET_21NP_JET_Plmp_OffsetM1 [%]	-0.05 +0.05 -0.05	+0.01 -0.01 +0.01	-0.11 +0.11 -0.11	+0.03 -0.03 +0.03	-0.05 +0.05 -0.05	-0.18 +0.18 -0.18	+0.08 -0.08 +0.08	+0.01 -0.01 +0.01
(LEP) JET_21NP_JET_Plmp_OffsetM2 [%]	-0.08 +0.08 -0.08	+0.02 -0.02 +0.02	-0.11 +0.11 -0.11	+0.03 -0.03 +0.03	-0.06 +0.			

Not reviewed, for internal circulation only

Bins [GeV]	[1,1.5]	[1.5,2]	[2,3]	[3,4]	[4,5]	[5,7]	[7,10]
$d\sigma/dX$ [pb/GeV]	$4.11 \cdot 10^{-3}$	$3.1 \cdot 10^{-3}$	$1.63 \cdot 10^{-2}$	$9.43 \cdot 10^{-2}$	$5.9 \cdot 10^{-2}$	$3.37 \cdot 10^{-2}$	$9.02 \cdot 10^{-3}$
Total Uncertainty [%]	± 32.02	± 31.57	± 34.41	± 34.41	± 31.10	± 35.96	± 37.08
Statistics [%]	± 4.42	± 5.47	± 5.12	± 7.17	± 9.95	± 9.28	± 14.63
Systematics [%]	± 36.61	± 28.56	± 34.11	± 29.70	± 31.99	± 31.66	± 32.09
(FTAG) ftagSF_B_eigen0 [%]	± 5.46	± 5.29	± 5.27	± 5.30	± 5.06	± 5.58	± 5.33
(FTAG) ftagSF_B_eigen1 [%]	± 0.45	± 0.45	± 0.49	± 0.49	± 0.37	± 0.58	± 0.53
(FTAG) ftagSF_B_eigen2 [%]	± 5.65	± 5.20	± 4.99	± 5.81	± 5.13	± 5.89	± 5.89
(FTAG) ftagSF_B_eigen3 [%]	± 0.72	± 0.71	± 0.73	± 0.74	± 0.72	± 0.81	± 0.72
(FTAG) ftagSF_B_eigen4 [%]	± 0.54	± 0.51	± 0.59	± 0.59	± 0.42	± 0.58	± 0.51
(FTAG) ftagSF_B_eigen5 [%]	± 0.53	± 0.50	± 0.54	± 0.53	± 0.51	± 0.55	± 0.54
(FTAG) ftagSF_B_eigen6 [%]	± 0.65	± 0.65	± 0.65	± 0.65	± 0.61	± 0.65	± 0.64
(FTAG) ftagSF_C_eigen0 [%]	± 0.25	± 0.25	± 0.25	± 0.25	± 0.25	± 0.25	± 0.25
(FTAG) ftagSF_C_eigen1 [%]	± 1.25	± 1.18	± 1.10	± 1.75	± 1.15	± 1.59	± 1.64
(FTAG) ftagSF_C_eigen2 [%]	± 0.58	± 0.41	± 0.51	± 0.51	± 0.48	± 0.51	± 0.50
(FTAG) ftagSF_C_eigen3 [%]	± 0.78	± 0.74	± 0.73	± 0.74	± 0.72	± 0.81	± 0.79
(FTAG) ftagSF_C_eigen4 [%]	± 0.45	± 0.45	± 0.45	± 0.45	± 0.45	± 0.45	± 0.45
(FTAG) ftagSF_Light_eigen0 [%]	± 0.46	± 0.45	± 0.45	± 0.45	± 0.45	± 0.45	± 0.45
(FTAG) ftagSF_Light_eigen1 [%]	± 0.05	± 0.05	± 0.05	± 0.05	± 0.05	± 0.05	± 0.05
(FTAG) ftagSF_Light_eigen2 [%]	± 0.05	± 0.05	± 0.05	± 0.05	± 0.05	± 0.05	± 0.05
(FTAG) ftagSF_Light_eigen3 [%]	± 0.05	± 0.05	± 0.05	± 0.05	± 0.05	± 0.05	± 0.05
(FTAG) ftagSF_Light_eigen4 [%]	± 0.05	± 0.05	± 0.05	± 0.05	± 0.05	± 0.05	± 0.05
(FTAG) ftagSF_Light_eigen5 [%]	± 0.05	± 0.05	± 0.05	± 0.05	± 0.05	± 0.05	± 0.05
(FTAG) ftagSF_Light_eigen6 [%]	± 0.05	± 0.05	± 0.05	± 0.05	± 0.05	± 0.05	± 0.05
(FTAG) ftagSF_Light_eigen7 [%]	± 0.05	± 0.05	± 0.05	± 0.05	± 0.05	± 0.05	± 0.05
(FTAG) ftagSF_Light_eigen8 [%]	± 0.05	± 0.05	± 0.05	± 0.05	± 0.05	± 0.05	± 0.05
(FTAG) ftagSF_Light_eigen9 [%]	± 0.05	± 0.05	± 0.05	± 0.05	± 0.05	± 0.05	± 0.05
(FTAG) ftagSF_Light_eigen10 [%]	± 0.05	± 0.05	± 0.05	± 0.05	± 0.05	± 0.05	± 0.05
(FTAG) ftagSF_Light_eigen11 [%]	± 0.05	± 0.05	± 0.05	± 0.05	± 0.05	± 0.05	± 0.05
(FTAG) ftagSF_Light_eigen12 [%]	± 0.05	± 0.05	± 0.05	± 0.05	± 0.05	± 0.05	± 0.05
(FTAG) ftagSF_Light_eigen13 [%]	± 0.05	± 0.05	± 0.05	± 0.05	± 0.05	± 0.05	± 0.05
(FTAG) ftagSF_Light_eigen14 [%]	± 0.05	± 0.05	± 0.05	± 0.05	± 0.05	± 0.05	± 0.05
(FTAG) ftagSF_Light_eigen15 [%]	± 0.05	± 0.05	± 0.05	± 0.05	± 0.05	± 0.05	± 0.05
(FTAG) ftagSF_extrapolation [%]	± 0.05	± 0.05	± 0.05	± 0.05	± 0.05	± 0.05	± 0.05
(FTAG) ftagSF_extrapolation_from_charm [%]	± 0.12	± 0.07	± 0.05	± 0.03	± 0.05	± 0.02	± 0.05
(MET/P(U) ivt [%]	± 2.00	± 2.03	± 1.97	± 2.03	± 1.97	± 1.97	± 1.95
Luminosity [%]	± 0.00	± 0.00	± 0.00	± 0.00	± 0.00	± 0.00	± 0.00
(BKG) singleton_ichan [%]	—	—	—	—	—	—	—
(BKG) singleton_Wt [%]	—	—	—	—	—	—	—
(BKG) muon [%]	± 0.04	± 0.04	± 0.05	± 0.05	± 0.05	± 0.05	± 0.05
(BKG) oz [%]	± 0.03	± 0.04	± 0.04	± 0.03	± 0.03	± 0.03	± 0.03
(BKG) zh [%]	± 0.04	± 0.05	± 0.03	± 0.03	± 0.04	± 0.03	± 0.04
(LJES) LARGERET_JET_Weak_JET_Rtrk_Modelling_Tau32WTA [%]	± 0.39	± 0.39	± 0.34	± 11.50	± 10.31	± 10.71	± 11.94
(LJES) LARGERET_JET_Weak_JET_Rtrk_Baseline_pT [%]	± 0.43	± 0.43	± 0.43	± 0.43	± 0.43	± 0.43	± 0.43
(LJES) LARGERET_JET_Weak_JET_Rtrk_Baseline_mass [%]	± 0.33	± 0.33	± 0.50	± 1.78	± 0.83	± 0.81	± 0.98
(LJES) LARGERET_JET_Weak_JET_Rtrk_Baseline_Tau32WTA [%]	± 0.32	± 0.32	± 0.32	± 0.84	± 0.83	± 0.83	± 0.24
(JES) JET_2INP_JET_BJES_Response [%]	± 0.05	± 0.05	± 0.05	± 0.05	± 0.05	± 0.05	± 0.05
(JES) JET_2INP_JET_Pileup_PTRes [%]	± 0.02	± 0.02	± 0.02	± 0.02	± 0.01	± 0.01	± 0.01
(JES) JET_2INP_JET_Pileup_OffsetNPV [%]	± 0.02	± 0.02	± 0.05	± 0.05	± 0.05	± 0.04	± 0.04
(JES) JET_2INP_JET_Pileup_OffsetNPV_SigEfficiency [%]	± 0.08	± 0.08	± 0.13	± 0.08	± 0.03	± 0.29	± 0.02
(LEP) MUON_SAGITTA_RHESIAS [%]	—	—	—	—	—	—	—
(JES) JET_2INP_JET_EffectiveNP_3 [%]	± 0.02	± 0.01	± 0.01	± 0.01	± 0.02	± 0.02	± 0.02
(JES) JET_2INP_JET_EffectiveNP_4 [%]	—	—	—	—	± 0.05	—	± 0.01
(JES) LARGERET_JET_Weak_JET_Rtrk_Tracking_mass [%]	± 0.17	± 0.05	± 0.08	± 0.85	± 0.30	± 0.23	± 0.42
(JES) JET_2INP_JET_Pileup_OffsetMu [%]	± 0.26	± 0.25	± 0.26	± 0.64	± 0.51	± 0.67	± 0.35
(JES) LARGERET_JET_OffsetCalibration_TotalStat [%]	± 0.03	± 0.03	± 0.03	± 0.03	± 0.02	± 0.02	± 0.02
(JES) JET_2INP_JET_OffsetCalibration_NonClosure [%]	± 0.01	± 0.01	± 0.01	± 0.01	± 0.02	± 0.02	± 0.02
(JES) JET_2INP_JET_EtaCalibration_TotalStat [%]	± 0.02	± 0.01	± 0.01	± 0.02	± 0.02	± 0.01	± 0.05
(JES) JET_2INP_JET_Flavor_Response [%]	± 0.02	± 0.01	± 0.07	± 0.04	± 0.02	± 0.04	± 0.03
(JES) JET_2INP_JET_EffectiveNP_6 [%]	± 0.02	± 0.08	± 0.06	± 0.05	± 0.07	± 0.06	± 0.03
(JES) JET_2INP_JET_EffectiveNP_5 [%]	—	—	—	—	—	—	—
(JES) JET_2INP_JET_Flavor_Composition [%]	± 0.01	± 0.27	± 0.28	± 0.01	± 0.27	± 0.36	± 0.30
(JES) JET_2INP_JET_SingleParticle_HighPt [%]	± 2.55	± 2.25	± 2.35	± 2.49	± 2.41	± 2.25	± 2.53
(JES) LARGERET_JET_Modelling_pT [%]	± 0.10	± 0.10	± 0.08	± 0.08	± 0.08	± 0.08	± 0.08
(JES) LARGERET_JET_OffsetCalibration [%]	± 0.04	± 0.04	± 0.05	± 0.05	± 0.05	± 0.05	± 0.05
(JES) JET_2INP_JET_EffectiveNP_7 [%]	± 0.02	± 0.02	± 0.06	± 0.03	± 0.02	± 0.02	± 0.02
(JES) LARGERET_JET_Modelling_mass [%]	± 0.18	± 0.26	± 0.21	± 0.29	± 0.27	± 0.27	± 0.28
(JES) JET_2INP_JET_SingleParticle_NA6 [%]	± 0.02	± 0.29	± 0.21	± 0.21	± 0.26	± 0.26	± 0.25
(JES) LARGERET_JET_Total_Pt [%]	± 0.42	± 0.29	± 0.21	± 0.21	± 0.36	± 0.46	± 0.14
(LEP) MUON_SCALE_ALE [%]	± 0.17	± 0.17	± 0.17	± 0.17	± 0.22	± 0.22	± 0.18
(JES) JET_2INP_JET_EffectiveNP_8 [%]	± 0.02	± 0.02	± 0.06	± 0.06	± 0.05	± 0.05	± 0.05
(JES) JET_2INP_JET_EffectiveNP_9 [%]	± 0.04	± 0.04	± 0.05	± 0.05	± 0.05	± 0.05	± 0.05
(PDF) PDF-LHC1C15_m_30_eigen001 [%]	± 0.03	± 0.05	± 0.05	± 0.07	± 0.07	± 0.08	± 0.09
(PDF) PDF-LHC1C15_m_30_eigen002 [%]	± 0.09	± 0.07	± 0.09	± 0.11	± 0.12	± 0.13	± 0.19
(PDF) PDF-LHC1C15_m_30_eigen012 [%]	± 0.06	± 0.06	± 0.07	± 0.07	± 0.04	± 0.06	± 0.06
(PDF) PDF-LHC1C15_m_30_eigen013 [%]	± 0.02	± 0.02	± 0.04	± 0.03	± 0.03	± 0.04	± 0.04
(PDF) PDF-LHC1C15_m_30_eigen014 [%]	± 0.02	± 0.01	± 0.02	± 0.02	± 0.02	± 0.04	± 0.07
(PDF) PDF-LHC1C15_m_30_eigen016 [%]	± 0.02	± 0.04	± 0.07	± 0.07	± 0.02	± 0.05	± 0.12
(PDF) PDF-LHC1C15_m_30_eigen017 [%]	± 0.07	± 0.07	± 0.09	± 0.09	± 0.13	± 0.14	± 0.21
(PDF) PDF-LHC1C15_m_30_eigen021 [%]	± 0.03	± 0.03	± 0.04	± 0.06	± 0.01	± 0.06	± 0.09
(PDF) PDF-LHC1C15_m_30_eigen022 [%]	± 0.052	± 0.48	± 0.55	± 0.72	± 0.69	± 0.86	± 1.22
(PDF) PDF-LHC1C15_m_30_eigen023 [%]	± 0.02	± 0.01	± 0.01	± 0.01	± 0.01	± 0.02	± 0.02
(PDF) PDF-LHC1C15_m_30_eigen024 [%]	± 0.05	± 0.04	± 0.05	± 0.05	± 0.03	± 0.05	± 0.04
(PDF) PDF-LHC1C15_m_30_eigen025 [%]	± 0.03	± 0.01	± 0.01	± 0.02	± 0.02	± 0.02	± 0.03
(PDF) PDF-LHC1C15_m_30_eigen028 [%]	± 0.15	± 0.13	± 0.12	± 0.16	± 0.11	± 0.14	± 0.13
(PDF) PDF-LHC1C15_m_30_eigen029 [%]	± 0.06	± 0.06	± 0.05	± 0.05	± 0.05	± 0.06	± 0.06
(PDF) PDF-LHC1C15_m_30_eigen030 [%]	—	—	± 0.01	—	± 0.03	± 0.03	$\$

Not reviewed, for internal circulation only

Bins (GeV)	[1,1.5]	[1.5,2]	[2,3]	[3,4]	[4,5]	[5,7]	[7,10]
$1/\sigma d\sigma/dX$ [pb/GeV]	$5.33 \cdot 10^{-4}$	$4.02 \cdot 10^{-4}$	$2.11 \cdot 10^{-4}$	$1.22 \cdot 10^{-4}$	$7.65 \cdot 10^{-5}$	$4.37 \cdot 10^{-5}$	$1.17 \cdot 10^{-5}$
Total Uncertainty [%]	-	-	-	-	-	-	-
Statistics [%]	± 5.1	± 7.1	± 7.05	± 8.88	± 1.97	± 1.97	± 1.90
Syst. [%]	± 4.21	± 4.07	± 4.00	± 4.83	± 0.72	± 0.05	± 14.31
Systematic [%]	-	-	-	-	-	-	-
(FTAG) fTagSF_B eigen0 [%]	-	-	-	-	-	-	-
(FTAG) fTagSF_B eigen1 [%]	± 0.11	± 0.08	± 0.08	± 0.05	± 0.14	± 0.21	± 0.07
(FTAG) fTagSF_B eigen2 [%]	± 0.08	± 0.06	± 0.06	± 0.05	± 0.05	± 0.18	± 0.10
(FTAG) fTagSF_B eigen3 [%]	± 0.05	± 0.02	± 0.02	± 0.02	± 0.04	± 0.09	± 0.04
(FTAG) fTagSF_B eigen4 [%]	± 0.03	-	± 0.02	± 0.01	± 0.02	± 0.02	-
(FTAG) fTagSF_B eigen5 [%]	-	-	-	± 0.01	± 0.02	± 0.02	-
(FTAG) fTagSF_C eigen0 [%]	-	-	-	-	-	-	-
(FTAG) fTagSF_C eigen1 [%]	± 0.11	± 0.13	± 0.08	± 0.12	± 0.23	± 0.45	± 0.51
(FTAG) fTagSF_C eigen2 [%]	± 0.09	± 0.10	± 0.08	± 0.15	± 0.20	± 0.45	± 0.55
(FTAG) fTagSF_C eigen3 [%]	± 0.06	± 0.04	± 0.02	± 0.16	± 0.10	± 0.14	± 0.16
(FTAG) fTagSF_C eigen4 [%]	± 0.05	± 0.04	± 0.02	± 0.07	± 0.03	± 0.07	± 0.09
(FTAG) fTagSF_C eigen5 [%]	-	-	-	-	-	-	-
(FTAG) fTagSF_L Light_eigen0 [%]	± 0.11	± 0.26	± 0.05	± 0.08	± 0.23	± 0.22	± 0.05
(FTAG) fTagSF_L Light_eigen1 [%]	± 0.02	± 0.07	± 0.01	± 0.03	± 0.06	± 0.08	-
(FTAG) fTagSF_L Light_eigen2 [%]	± 0.02	± 0.07	± 0.01	± 0.03	± 0.06	± 0.05	-
(FTAG) fTagSF_L Light_eigen3 [%]	-	-	-	-	-	-	-
(FTAG) fTagSF_L Light_eigen4 [%]	± 0.05	± 0.11	± 0.05	± 0.05	± 0.15	± 0.18	± 0.01
(FTAG) fTagSF_L Light_eigen5 [%]	± 0.04	-	-	-	± 0.03	± 0.03	-
(FTAG) fTagSF_L Light_eigen6 [%]	-	-	-	-	-	-	-
(FTAG) fTagSF_L Light_eigen7 [%]	-	-	-	-	-	-	-
(FTAG) fTagSF_L Light_eigen8 [%]	-	-	-	-	-	-	-
(FTAG) fTagSF_L Light_eigen9 [%]	-	-	-	-	-	-	-
(FTAG) fTagSF_L Light_eigen10 [%]	± 0.02	± 0.01	± 0.01	± 0.02	± 0.02	± 0.06	-
(FTAG) fTagSF_L Light_eigen11 [%]	± 0.02	± 0.05	± 0.01	± 0.02	-	± 0.06	-
(FTAG) fTagSF_L Light_eigen12 [%]	± 0.02	± 0.05	± 0.01	± 0.02	-	± 0.06	-
(FTAG) fTagSF_L Light_eigen13 [%]	± 0.02	± 0.01	± 0.01	± 0.02	-	± 0.06	-
(FTAG) fTagSF_L Light_eigen14 [%]	± 0.05	± 0.07	± 0.01	± 0.02	-	± 0.06	-
(FTAG) fTagSF_L Light_eigen15 [%]	± 0.02	± 0.01	± 0.01	± 0.02	-	± 0.06	-
(FTAG) fTagSF_L extrapolation [%]	± 0.13	-	± 0.05	± 0.19	± 0.23	± 0.26	-
(FTAG) fTagSF_L extrapolation_from_charm [%]	-	-	-	-	-	-	-
(MET/Pt) Jvt [%]	± 0.04	-	± 0.01	± 0.01	± 0.04	± 0.04	± 0.02
Luminosity [%]	-	± 0.02	± 0.04	-	± 0.03	± 0.10	± 0.08
(BKG) singletop_tchan [%]	-	-	-	-	-	-	-
(BKG) singletop_Wt [%]	-	-	-	-	-	-	-
(BKG) tW [%]	-	-	-	-	-	-	-
(BKG) tZ [%]	-	-	-	-	-	-	-
(BKG) tH [%]	-	-	-	-	-	-	-
(LJES) LARGERET, Weak_JET_Rirk, Modelling_Tau32WTA [%]	-	-	-	-	-	-	-
(LJES) LARGERET, Weak_JET_Rirk, Baseline_gPt [%]	± 0.10	± 0.07	± 0.05	± 0.31	± 0.09	± 0.13	± 0.40
(LJES) LARGERET, Weak_JET_Rirk, Baseline_mass [%]	-	-	-	-	-	-	-
(LJES) LARGERET, Weak_JET_Rirk, Baseline_Tau32WTA [%]	-	-	-	-	-	-	-
(JES) JET_2INP_JET_BIes_Response [%]	-	-	-	-	-	-	-
(JES) JET_2INP_JET_Pileup_PTerr [%]	-	-	-	-	-	-	-
(JES) JET_2INP_JET_Pileup_OffsetNPV [%]	-	-	-	-	-	-	-
(JES) JET_2INP_JET_Pileup_RhoTopology [%]	-	± 0.05	± 0.06	± 0.05	± 0.03	± 0.06	± 0.12
(JES) JET_2INP_JET_EffectiveVBF_npTerm [%]	-	± 0.02	± 0.04	± 0.04	± 0.07	± 0.19	± 0.12
(LEP) MUON_ID_Scale [1 %]	-	-	-	-	-	-	-
(JES) JET_2INP_JET_EffectiveNP_3 [%]	-	-	-	-	-	-	-
(JES) JET_2INP_JET_EffectiveNP_4 [%]	-	-	-	-	-	-	-
(JES) LARGERET, Weak_JET_Rirk, Tracking_mass [%]	-	± 0.12	± 0.24	± 0.69	± 0.13	± 0.39	± 0.26
(JES) JET_2INP_JET_Pileup_OffsetMu [%]	± 0.02	± 0.05	± 0.03	± 0.03	-	± 0.02	± 0.05
(JES) JET_2INP_JET_TotalStat_mass [%]	-	± 0.05	± 0.02	± 0.16	± 0.02	± 0.12	± 0.13
(JES) JET_2INP_JET_EtaCalibration_NonClosure [%]	± 0.03	± 0.05	± 0.03	± 0.05	± 0.06	± 0.20	± 0.06
(JES) JET_2INP_JET_EtaCalibration_TotalStat [%]	-	± 0.03	± 0.03	± 0.03	± 0.01	-	± 0.03
(JES) EG_Electrons_ID_Accuracy [%]	-	± 0.03	± 0.03	± 0.02	± 0.21	± 0.03	± 0.02
(JES) JET_2INP_JET_Flavor_Response [%]	± 0.03	± 0.03	± 0.02	-	± 0.04	± 0.20	-
(JES) JET_2INP_JET_EffectiveNP_5 [%]	-	-	-	-	-	-	-
(JES) JET_2INP_JET_Flavor_Composition [%]	-	-	-	-	-	-	-
(JES) JET_2INP_JET_SingleParticle_HighPt [%]	-	-	-	-	-	-	-
(JES) JET_2INP_JET_Weak_Rirk_Modelling_pT [%]	± 0.19	± 0.04	± 0.09	± 0.16	± 0.12	± 0.04	± 0.18
(JES) JET_2INP_JET_SingleParticle_lowPt [%]	± 0.02	± 0.01	-	-	± 0.04	± 0.01	-
(JES) MUON_ID [%]	-	-	-	-	-	-	-
(LEP) MUON_SCALE [1 %]	-	-	-	-	-	-	-
(LEP) EG_SCALE_ALL [%]	-	-	-	-	-	-	-
(JES) JET_2INP_JET_EffectiveNP_7 [%]	± 0.01	± 0.01	± 0.05	± 0.02	-	± 0.01	-
(JES) LARGERET, Weak_JET_Rirk, Modelling_mass [%]	-	-	-	-	-	-	-
(JES) JET_2INP_JET_Flavor_Response [%]	-	-	-	-	-	-	-
(JES) JET_2INP_JET_EffectiveNP_6 [%]	-	-	-	-	-	-	-
(JES) JET_2INP_JET_EffectiveNP_8 [%]	-	-	-	-	-	-	-
(JES) PDF4LHC15_alo_30_eigen01 [%]	± 0.08	± 0.08	± 0.06	± 0.05	± 0.11	± 0.06	-
(JES) PDF4LHC15_alo_30_eigen02 [%]	± 0.17	± 0.17	± 0.18	± 0.20	± 0.17	± 0.21	± 0.33
(JES) PDF4LHC15_alo_30_eigen03 [%]	± 0.12	± 0.07	± 0.10	± 0.12	± 0.10	± 0.14	± 0.22
(JES) PDF4LHC15_alo_30_eigen04 [%]	± 0.05	± 0.04	± 0.04	± 0.19	± 0.05	± 0.31	± 0.39
(JES) PDF4LHC15_alo_30_eigen05 [%]	± 0.46	± 0.42	± 0.48	± 0.47	± 0.37	± 0.51	± 0.69
(JES) PDF4LHC15_alo_30_eigen06 [%]	± 0.19	± 0.18	± 0.25	± 0.26	± 0.31	± 0.36	± 0.46
(JES) PDF4LHC15_alo_30_eigen07 [%]	-	-	-	-	-	-	-
(JES) PDF4LHC15_alo_30_eigen08 [%]	± 0.16	± 0.14	± 0.17	± 0.21	± 0.21	± 0.26	± 0.38
(JES) PDF4LHC15_alo_30_eigen09 [%]	± 0.04	± 0.04	± 0.06	± 0.06	± 0.07	± 0.10	± 0.10
(JES) PDF4LHC15_alo_30_eigen10 [%]	± 0.03	± 0.05	± 0.05	± 0.07	± 0.07	± 0.08	± 0.09
(JES) PDF4LHC15_alo_30_eigen11 [%]	± 0.09	± 0.07	± 0.09	± 0.11	± 0.12	± 0.13	± 0.19
(JES) PDF4LHC15_alo_30_eigen12 [%]	± 0.06	± 0.07	± 0.10	± 0.10	± 0.09	± 0.11	± 0.19
(JES) PDF4LHC15_alo_30_eigen13 [%]	± 0.02	± 0.02	± 0.03	± 0.03	± 0.03	± 0.05	± 0.04
(JES) PDF4LHC15_alo_30_eigen14 [%]	-	± 0.01	± 0.02	± 0.02	± 0.02	± 0.04	± 0.07
(JES) PDF4LHC15_alo_30_eigen15 [%]	± 0.02	± 0.04	± 0.04	± 0.07	± 0.02	± 0.05	± 0.12
(JES) PDF4LHC15_alo_30_eigen16 [%]	-	± 0.04	± 0.03	± 0.02	± 0.01	± 0.03	± 0.06
(JES) PDF4LHC15_alo_30_eigen17 [%]	± 0.07	± 0.07	± 0.09	± 0.11	± 0.13	± 0.14	± 0.21
(JES) PDF4LHC15_alo_30_eigen18 [%]	± 0.05	± 0.07	± 0.09	± 0.10	± 0.15	± 0.19	± 0.25
(JES) PDF4LHC15_alo_30_eigen19 [%]	± 0.07	± 0.01	± 0.02	± 0.05	-	± 0.12	± 0.21
(JES) PDF4LHC15_alo_30_eigen20 [%]	± 0.06	± 0.07	± 0.07	± 0.04	± 0.06	-	± 0.06
(JES) PDF4LHC15_alo_30_eigen21 [%]	± 0.03	± 0.03	± 0.04	± 0.06	± 0.01	± 0.06	± 0.09
(JES) PDF4LHC15_alo_30_eigen22 [%]	± 0.12	± 0.48	± 0.55	± 0.72	± 0.69	± 0.86	± 1.22
(JES) PDF4LHC15_alo_30_eigen23 [%]	-	-	-	-	-	-	-
(JES) PDF4LHC15_alo_30_eigen24 [%]	± 0.05	± 0.04	± 0.05	± 0.05	± 0.03	± 0.05	± 0.04
(JES) PDF4LHC15_alo_30_eigen25 [%]	± 0.03	-	± 0.01	± 0.02	-	± 0.02	± 0.03
(JES) PDF4LHC15_alo_30_eigen26 [%]	± 0.04	± 0.03	± 0.02	± 0.03	-	-	-
(JES) PDF4LHC15_alo_30_eigen27 [%]	± 0.04	± 0.04	± 0.05	± 0.04	± 0.03	± 0.03	± 0.06
(PDF) PDF4LHC15_alo_30_eigen28 [%]	± 0.15	± 0.13	± 0.12	± 0.16	± 0.11	± 0.14	± 0.13
(PDF) PDF4LHC15_alo_30_eigen29 [%]	-	-	-	-	-	± 0.01	-
(PDF) PDF4LHC15_alo_30_eigen30 [%]	-	-	-	-	-	± 0.01	-
(MOD) Alternative cross-sectioning model [%]	± 2.64	± 2.50	± 3.84	± 2.69	± 2.43	± 3.93	± 6.11
(MOD) Alternative parton-shower model [%]	± 0.59	± 2.74	± 3.84	± 2.00	± 0.37	± 1.61	± 5.37
(MOD) ISR/FSR + scale [%]	± 0.02	± 1.46	± 0.9				

Bins [GeV]	[0,0.2]	[0.2,0.4]	[0.4,0.6]	[0.6,0.8]	[0.8,1]	[1,1.3]	[1.3,2]
$d\sigma/dX$ [pb/GeV]	$7.96 \cdot 10^{-3}$	$8.04 \cdot 10^{-3}$	$6.73 \cdot 10^{-3}$	$5.7 \cdot 10^{-3}$	$4.26 \cdot 10^{-3}$	$2.95 \cdot 10^{-3}$	$8.5 \cdot 10^{-3}$
Total Uncertainty [%]	± 3.87	± 3.10	± 3.35	± 30.90	± 33.00	± 37.08	± 33.57
Statistics [%]	± 5.07	± 5.57	± 6.09	± 6.65	± 7.70	± 7.57	± 11.58
Systematics [%]	± 34.01	± 29.70	± 30.03	± 28.80	± 32.05	± 34.12	± 31.36
(FTAG) $t\bar{t}q\bar{q}S^2_B$, eigen0 [%]	± 3.42	± 3.47	± 3.39	± 3.29	± 3.34	± 4.99	± 3.16
(FTAG) $t\bar{t}q\bar{q}S^2_B$, eigen1 [%]	± 3.49	± 3.46	± 3.44	± 3.34	± 3.44	± 4.94	± 3.0
(FTAG) $t\bar{t}q\bar{q}S^2_B$, eigen2 [%]	± 3.09	± 3.09	± 3.35	± 3.01	± 3.36	± 4.53	± 2.9
(FTAG) $t\bar{t}q\bar{q}S^2_B$, eigen3 [%]	± 3.82	± 3.81	± 3.24	± 3.26	± 3.78	± 3.51	± 6.57
(FTAG) $t\bar{t}q\bar{q}S^2_B$, eigen4 [%]	± 3.56	± 3.55	± 3.52	± 3.53	± 3.48	± 4.43	± 4.40
(FTAG) $t\bar{t}q\bar{q}S^2_B$, eigen5 [%]	± 3.53	± 3.53	± 3.21	± 3.24	± 3.73	± 3.53	± 6.51
(FTAG) $t\bar{t}q\bar{q}S^2_B$, eigen6 [%]	± 3.63	± 3.65	± 3.38	± 3.24	± 3.73	± 3.63	± 6.71
(FTAG) $t\bar{t}q\bar{q}S^2_C$, eigen0 [%]	± 3.63	± 3.65	± 3.38	± 3.24	± 3.71	± 3.63	± 6.71
(FTAG) $t\bar{t}q\bar{q}S^2_C$, eigen1 [%]	± 3.69	± 3.66	± 3.35	± 3.21	± 3.66	± 3.57	± 6.10
(FTAG) $t\bar{t}q\bar{q}S^2_C$, eigen2 [%]	± 3.56	± 3.51	± 3.26	± 3.36	± 3.61	± 3.57	± 6.15
(FTAG) $t\bar{t}q\bar{q}S^2_C$, eigen3 [%]	± 3.74	± 3.55	± 3.18	± 3.17	± 3.71	± 3.57	± 6.09
(FTAG) $t\bar{t}q\bar{q}S^2_C$, eigen4 [%]	± 3.61	± 3.79	± 3.15	± 3.17	± 3.71	± 3.57	± 6.17
(FTAG) $t\bar{t}q\bar{q}S^2_C$, eigen5 [%]	± 3.63	± 3.79	± 3.15	± 3.17	± 3.71	± 3.57	± 6.17
(FTAG) $t\bar{t}q\bar{q}S^2_C$, eigen6 [%]	± 3.63	± 3.79	± 3.15	± 3.17	± 3.71	± 3.57	± 6.17
(FTAG) $t\bar{t}q\bar{q}S^2_L$, eigen0 [%]	± 3.63	± 3.65	± 3.38	± 3.24	± 3.71	± 3.63	± 6.71
(FTAG) $t\bar{t}q\bar{q}S^2_L$, eigen1 [%]	± 3.63	± 3.65	± 3.38	± 3.24	± 3.71	± 3.63	± 6.71
(FTAG) $t\bar{t}q\bar{q}S^2_L$, eigen2 [%]	± 3.63	± 3.65	± 3.38	± 3.24	± 3.71	± 3.63	± 6.71
(FTAG) $t\bar{t}q\bar{q}S^2_L$, eigen3 [%]	± 3.63	± 3.65	± 3.38	± 3.24	± 3.71	± 3.63	± 6.71
(FTAG) $t\bar{t}q\bar{q}S^2_L$, eigen4 [%]	± 3.63	± 3.65	± 3.38	± 3.24	± 3.71	± 3.63	± 6.71
(FTAG) $t\bar{t}q\bar{q}S^2_L$, eigen5 [%]	± 3.63	± 3.65	± 3.38	± 3.24	± 3.71	± 3.63	± 6.71
(FTAG) $t\bar{t}q\bar{q}S^2_L$, eigen6 [%]	± 3.63	± 3.65	± 3.38	± 3.24	± 3.71	± 3.63	± 6.71
(FTAG) $t\bar{t}q\bar{q}S^2_L$, eigen7 [%]	± 3.63	± 3.65	± 3.38	± 3.24	± 3.71	± 3.63	± 6.71
(FTAG) $t\bar{t}q\bar{q}S^2_L$, eigen8 [%]	± 3.63	± 3.65	± 3.38	± 3.24	± 3.71	± 3.63	± 6.71
(FTAG) $t\bar{t}q\bar{q}S^2_L$, eigen9 [%]	± 3.63	± 3.65	± 3.38	± 3.24	± 3.71	± 3.63	± 6.71
(FTAG) $t\bar{t}q\bar{q}S^2_L$, eigen10 [%]	± 3.63	± 3.65	± 3.38	± 3.24	± 3.71	± 3.63	± 6.71
(FTAG) $t\bar{t}q\bar{q}S^2_L$, eigen11 [%]	± 3.63	± 3.65	± 3.38	± 3.24	± 3.71	± 3.63	± 6.71
(FTAG) $t\bar{t}q\bar{q}S^2_L$, eigen12 [%]	± 3.63	± 3.65	± 3.38	± 3.24	± 3.71	± 3.63	± 6.71
(FTAG) $t\bar{t}q\bar{q}S^2_L$, eigen13 [%]	± 3.63	± 3.65	± 3.38	± 3.24	± 3.71	± 3.63	± 6.71
(FTAG) $t\bar{t}q\bar{q}S^2_L$, eigen14 [%]	± 3.63	± 3.65	± 3.38	± 3.24	± 3.71	± 3.63	± 6.71
(FTAG) $t\bar{t}q\bar{q}S^2_L$, eigen15 [%]	± 3.63	± 3.65	± 3.38	± 3.24	± 3.71	± 3.63	± 6.71
(FTAG) $t\bar{t}q\bar{q}S^2_L$, extrapolation [%]	± 3.14	± 3.16	± 3.05	± 3.06	± 3.05	± 2.58	± 2.51
(FTAG) $t\bar{t}q\bar{q}S^2_L$, extrapolation_from_charm [%]	± 3.14	± 3.16	± 3.05	± 3.06	± 3.05	± 2.58	± 2.51
(MET/Pt/U) ivt [%]	± 0.00	± 0.11	± 0.96	± 0.07	± 0.09	± 0.14	± 0.07
Luminosity [%]	± 2.93	± 2.05	± 1.98	± 2.00	± 1.97	± 1.98	± 1.96
(BKG) singleton_ichan [%]	-	-	-	-	-	-	-
(BKG) singleton_Wt [%]	-	-	-	-	-	-	-
(BKG) muon [%]	± 0.04	± 0.04	± 0.04	± 0.04	± 0.05	± 0.05	± 0.04
(BKG) oz [%]	± 0.04	± 0.03	± 0.04	± 0.04	± 0.03	± 0.05	± 0.04
(BKG) rho [%]	± 0.03	± 0.04	± 0.04	± 0.04	± 0.03	± 0.04	± 0.03
(LJES) LARGERETET, Weak_JET_Rtrk, Modelling_Tau32WTA [%]	± 0.36	± 1.79	± 0.31	± 0.24	± 0.49	± 0.87	± 1.25
(LJES) LARGERETET, Weak_JET_Rtrk, Baseline_pT [%]	± 0.36	± 1.79	± 0.31	± 0.24	± 0.49	± 0.87	± 1.25
(LJES) LARGERETET, Weak_JET_Rtrk, Baseline_mass [%]	± 0.09	± 0.82	± 0.03	± 0.18	± 0.35	± 0.19	± 0.24
(LJES) LARGERETET, Weak_JET_Rtrk, Baseline_Tau32WTA [%]	± 0.47	± 9.36	± 0.42	± 0.32	± 0.96	± 1.94	± 3.51
(JES) JET_2INP_JET_BJES_Response [%]	-	-	-	-	-	-	-
(JES) JET_2INP_JET_Pileup_PTterm [%]	± 0.01	± 0.08	± 0.04	± 0.02	± 0.02	± 0.02	± 0.06
(JES) JET_2INP_JET_Pileup_OffsetNPV [%]	± 0.02	± 0.08	± 0.04	± 0.02	± 0.02	± 0.02	± 0.07
(JES) JET_2INP_JET_Pileup_OffsetEnergy [%]	± 0.03	± 0.05	± 0.03	± 0.02	± 0.02	± 0.02	± 0.05
(JES) JET_2INP_JET_Pileup_OffsetTerm [%]	± 0.06	± 0.13	± 0.06	± 0.20	± 0.10	± 0.12	± 0.06
(LEP) MUON_SAGITTA_RHESIAS [%]	-	-	-	-	-	-	± 0.03
(JES) JET_2INP_JET_EffectiveNP_3 [%]	± 0.01	± 0.01	± 0.01	± 0.01	± 0.02	± 0.02	± 0.03
(JES) JET_2INP_JET_EffectiveNP_4 [%]	± 0.01	-	-	-	-	-	-
(JES) LARGERETET, Weak_JET_Rtrk, Tracking_mass [%]	± 0.11	± 0.48	± 0.01	± 0.13	± 0.46	± 0.13	± 0.25
(JES) JET_2INP_JET_Pileup_OffsetMu [%]	± 0.05	± 0.16	± 0.02	± 0.27	± 0.07	± 0.13	± 0.02
(JES) LARGERETET, Weak_JET_Rtrk, TotalStat_mass [%]	± 0.10	± 0.11	± 0.06	± 0.26	± 0.07	± 0.20	± 0.20
(JES) JET_2INP_JET_EtaCalibration_NonClosure [%]	± 0.06	± 0.04	± 0.02	± 0.09	-	-	± 0.06
(JES) JET_2INP_JET_EtaCalibration_TotalStat [%]	-	-	-	-	± 0.01	± 0.05	± 0.03
(JES) JET_2INP_JET_EtaResolution_ALL [%]	-	-	-	-	-	-	± 0.04
(JES) JET_2INP_JET_EtaResolution_Offset [%]	± 0.04	± 0.06	± 0.05	± 0.11	± 0.01	± 0.06	± 0.03
(JES) JET_2INP_JET_EtaResolution_Offset6 [%]	± 0.05	± 0.08	± 0.04	± 0.08	± 0.01	± 0.09	± 0.15
(JES) JET_2INP_JET_EtaResolution_Offset5 [%]	± 0.05	-	-	-	-	-	± 0.02
(JES) JET_2INP_JET_EtaResolution_Offset4 [%]	± 0.03	± 0.05	± 0.03	± 0.01	-	-	± 0.02
(JES) JET_2INP_JET_ID [%]	± 0.03	± 0.05	± 0.03	± 0.03	± 0.03	± 0.03	± 0.06
(JES) JET_2INP_JET_SCALE_ALE [%]	-	-	-	-	-	-	± 0.06
(JES) JET_2INP_JET_EtaCalibration_Offset7 [%]	-	-	-	-	-	-	± 0.06
(JES) JET_2INP_JET_Weak_JET_Rtrk, Modelling_mass [%]	± 0.24	± 0.82	± 0.05	± 0.57	± 0.13	± 0.31	± 0.24
(JES) JET_2INP_JET_SingleParticle_HighPt [%]	± 0.35	± 3.11	± 0.24	± 0.46	± 0.27	± 0.17	± 0.58
(JES) LARGERETET, Weak_JET_Rtrk, Modelling_pT [%]	± 2.29	± 2.09	± 2.73	± 2.60	± 2.33	± 2.57	± 3.06
(JES) JET_2INP_JET_EffectiveNP_1 [%]	± 0.08	± 0.10	± 0.08	± 0.08	± 0.08	± 0.08	± 0.08
(JES) MUON_ID [%]	± 0.21	± 0.10	± 0.12	± 0.12	± 0.12	± 0.12	± 0.12
(JES) JET_2INP_JET_SCALE_ALE [%]	-	-	-	-	-	-	± 0.06
(JES) JET_2INP_JET_EtaCalibration_Offset7 [%]	-	-	-	-	-	-	± 0.06
(JES) JET_2INP_JET_SingleParticle_NonClosure [%]	± 0.20	± 0.16	± 0.12	± 0.06	± 0.08	± 0.18	± 0.28
(JES) PDF-LHC1C15_nlo_30_eigen009 [%]	± 0.03	± 0.02	± 0.03	± 0.02	± 0.02	± 0.06	± 0.06
(JES) PDF-LHC1C15_nlo_30_eigen010 [%]	± 0.05	± 0.05	± 0.04	± 0.04	± 0.04	± 0.08	± 0.07
(JES) PDF-LHC1C15_nlo_30_eigen011 [%]	± 0.06	± 0.07	± 0.08	± 0.10	± 0.12	± 0.16	± 0.25
(JES) PDF-LHC1C15_nlo_30_eigen012 [%]	± 0.05	± 0.06	± 0.06	± 0.07	± 0.08	± 0.15	± 0.34
(JES) PDF-LHC1C15_nlo_30_eigen013 [%]	± 0.02	± 0.04	± 0.03	± 0.03	± 0.03	± 0.05	± 0.09
(JES) PDF-LHC1C15_nlo_30_eigen014 [%]	± 0.14	± 0.11	± 0.18	± 0.22	± 0.24	± 0.40	± 0.70
(JES) PDF-LHC1C15_nlo_30_eigen007 [%]	± 0.01	-	-	-	-	-	± 0.08
(JES) PDF-LHC1C15_nlo_30_eigen015 [%]	± 0.09	± 0.11	± 0.14	± 0.18	± 0.18	± 0.30	± 0.56
(JES) PDF-LHC1C15_nlo_30_eigen009 [%]	± 0.05	± 0.04	± 0.05	± 0.06	± 0.06	± 0.09	± 0.11
(JES) PDF-LHC1C15_nlo_30_eigen010 [%]	± 0.05	± 0.05	± 0.04	± 0.04	± 0		

Not reviewed, for internal circulation only

Bins [GeV]	[0,0.2]	[0,2,0.4]	[0,4,0.6]	[0,6,0.8]	[0,8,1]	[1,1,1.3]	[1,3,2]	
$1/\text{order}/\Delta X [\text{pb}/\text{GeV}]$	$9.92 \cdot 10^{-1}$	1	$8.39 \cdot 10^{-1}$	$7.11 \cdot 10^{-1}$	$5.32 \cdot 10^{-1}$	$3.68 \cdot 10^{-1}$	$1.06 \cdot 10^{-1}$	
Total Uncertainty [%]	+7.80 -7.76 +4.61 -5.83	+6.96 -7.24 +5.18 -4.53	+7.26 -7.54 +5.68 -4.51	+8.56 -8.54 +6.25 -4.94	+2.11 -2.14 +7.34 -7.19	+10.22 -10.26 +7.19 -7.19	+16.48 -16.55 +11.23 -11.23	
Statistics [%]	-	-	-	-	-	-	-	
Systematics [%]	-	-	-	-	-	-	-	
(FTAG) fTagSE_B eigen0 [%]	-0.07 +0.19 -0.08 +0.07	-0.12 -0.09 +0.15 -0.05	-0.04 +0.04 +0.08 -0.02	-0.04 +0.03 +0.08 -0.02	+0.01 -0.01 +0.01 -0.01	+0.39 -0.38 +0.38 -0.38	+0.06 -0.05 +0.05 -0.05	
(FTAG) fTagSE_B eigen1 [%]	-0.07 +0.19 -0.08 +0.07	-0.12 -0.09 +0.15 -0.05	-0.04 +0.04 +0.08 -0.02	-0.04 +0.03 +0.08 -0.02	+0.01 -0.01 +0.01 -0.01	+0.39 -0.38 +0.38 -0.38	+0.06 -0.05 +0.05 -0.05	
(FTAG) fTagSE_B eigen2 [%]	-0.07 +0.19 -0.08 +0.07	-0.12 -0.09 +0.15 -0.05	-0.04 +0.04 +0.08 -0.02	-0.04 +0.03 +0.08 -0.02	+0.01 -0.01 +0.01 -0.01	+0.39 -0.38 +0.38 -0.38	+0.06 -0.05 +0.05 -0.05	
(FTAG) fTagSE_B eigen3 [%]	-0.07 +0.19 -0.08 +0.07	-0.12 -0.09 +0.15 -0.05	-0.04 +0.04 +0.08 -0.02	-0.04 +0.03 +0.08 -0.02	+0.01 -0.01 +0.01 -0.01	+0.39 -0.38 +0.38 -0.38	+0.06 -0.05 +0.05 -0.05	
(FTAG) fTagSE_C eigen0 [%]	-0.07 +0.19 -0.08 +0.07	-0.12 -0.09 +0.15 -0.05	-0.04 +0.04 +0.08 -0.02	-0.04 +0.03 +0.08 -0.02	+0.01 -0.01 +0.01 -0.01	+0.39 -0.38 +0.38 -0.38	+0.06 -0.05 +0.05 -0.05	
(FTAG) fTagSE_C eigen1 [%]	-0.07 +0.19 -0.08 +0.07	-0.12 -0.09 +0.15 -0.05	-0.04 +0.04 +0.08 -0.02	-0.04 +0.03 +0.08 -0.02	+0.01 -0.01 +0.01 -0.01	+0.39 -0.38 +0.38 -0.38	+0.06 -0.05 +0.05 -0.05	
(FTAG) fTagSE_C eigen2 [%]	-0.07 +0.19 -0.08 +0.07	-0.12 -0.09 +0.15 -0.05	-0.04 +0.04 +0.08 -0.02	-0.04 +0.03 +0.08 -0.02	+0.01 -0.01 +0.01 -0.01	+0.39 -0.38 +0.38 -0.38	+0.06 -0.05 +0.05 -0.05	
(FTAG) fTagSE_C eigen3 [%]	-0.07 +0.19 -0.08 +0.07	-0.12 -0.09 +0.15 -0.05	-0.04 +0.04 +0.08 -0.02	-0.04 +0.03 +0.08 -0.02	+0.01 -0.01 +0.01 -0.01	+0.39 -0.38 +0.38 -0.38	+0.06 -0.05 +0.05 -0.05	
(FTAG) fTagSE_L eigen0 [%]	-0.17 +0.19 -0.08 +0.07	-0.12 -0.09 +0.15 -0.05	+0.12 -0.13 +0.13 -0.13	-0.01 +0.01 -0.01 +0.01	-0.13 +0.13 -0.13 +0.13	-0.43 +0.43 -0.43 +0.43	-0.09 +0.09 -0.09 +0.09	
(FTAG) fTagSE_L eigen1 [%]	-0.17 +0.19 -0.08 +0.07	-0.12 -0.09 +0.15 -0.05	+0.12 -0.13 +0.13 -0.13	-0.01 +0.01 -0.01 +0.01	-0.13 +0.13 -0.13 +0.13	-0.43 +0.43 -0.43 +0.43	-0.09 +0.09 -0.09 +0.09	
(FTAG) fTagSE_L eigen2 [%]	-0.17 +0.19 -0.08 +0.07	-0.12 -0.09 +0.15 -0.05	+0.12 -0.13 +0.13 -0.13	-0.01 +0.01 -0.01 +0.01	-0.13 +0.13 -0.13 +0.13	-0.43 +0.43 -0.43 +0.43	-0.09 +0.09 -0.09 +0.09	
(FTAG) fTagSE_L eigen3 [%]	-0.17 +0.19 -0.08 +0.07	-0.12 -0.09 +0.15 -0.05	+0.12 -0.13 +0.13 -0.13	-0.01 +0.01 -0.01 +0.01	-0.13 +0.13 -0.13 +0.13	-0.43 +0.43 -0.43 +0.43	-0.09 +0.09 -0.09 +0.09	
(FTAG) fTagSE_L eigen4 [%]	-0.17 +0.19 -0.08 +0.07	-0.12 -0.09 +0.15 -0.05	+0.12 -0.13 +0.13 -0.13	-0.01 +0.01 -0.01 +0.01	-0.13 +0.13 -0.13 +0.13	-0.43 +0.43 -0.43 +0.43	-0.09 +0.09 -0.09 +0.09	
(FTAG) fTagSE_L eigen5 [%]	-0.17 +0.19 -0.08 +0.07	-0.12 -0.09 +0.15 -0.05	+0.12 -0.13 +0.13 -0.13	-0.01 +0.01 -0.01 +0.01	-0.13 +0.13 -0.13 +0.13	-0.43 +0.43 -0.43 +0.43	-0.09 +0.09 -0.09 +0.09	
(FTAG) fTagSE_L eigen6 [%]	-0.17 +0.19 -0.08 +0.07	-0.12 -0.09 +0.15 -0.05	+0.12 -0.13 +0.13 -0.13	-0.01 +0.01 -0.01 +0.01	-0.13 +0.13 -0.13 +0.13	-0.43 +0.43 -0.43 +0.43	-0.09 +0.09 -0.09 +0.09	
(FTAG) fTagSE_L eigen7 [%]	-0.17 +0.19 -0.08 +0.07	-0.12 -0.09 +0.15 -0.05	+0.12 -0.13 +0.13 -0.13	-0.01 +0.01 -0.01 +0.01	-0.13 +0.13 -0.13 +0.13	-0.43 +0.43 -0.43 +0.43	-0.09 +0.09 -0.09 +0.09	
(FTAG) fTagSE_L eigen8 [%]	-0.17 +0.19 -0.08 +0.07	-0.12 -0.09 +0.15 -0.05	+0.12 -0.13 +0.13 -0.13	-0.01 +0.01 -0.01 +0.01	-0.13 +0.13 -0.13 +0.13	-0.43 +0.43 -0.43 +0.43	-0.09 +0.09 -0.09 +0.09	
(FTAG) fTagSE_L eigen9 [%]	-0.17 +0.19 -0.08 +0.07	-0.12 -0.09 +0.15 -0.05	+0.12 -0.13 +0.13 -0.13	-0.01 +0.01 -0.01 +0.01	-0.13 +0.13 -0.13 +0.13	-0.43 +0.43 -0.43 +0.43	-0.09 +0.09 -0.09 +0.09	
(FTAG) fTagSE_L eigen10 [%]	-0.17 +0.19 -0.08 +0.07	-0.12 -0.09 +0.15 -0.05	+0.12 -0.13 +0.13 -0.13	-0.01 +0.01 -0.01 +0.01	-0.13 +0.13 -0.13 +0.13	-0.43 +0.43 -0.43 +0.43	-0.09 +0.09 -0.09 +0.09	
(FTAG) fTagSE_L eigen11 [%]	-0.17 +0.19 -0.08 +0.07	-0.12 -0.09 +0.15 -0.05	+0.12 -0.13 +0.13 -0.13	-0.01 +0.01 -0.01 +0.01	-0.13 +0.13 -0.13 +0.13	-0.43 +0.43 -0.43 +0.43	-0.09 +0.09 -0.09 +0.09	
(FTAG) fTagSE_L eigen12 [%]	-0.17 +0.19 -0.08 +0.07	-0.12 -0.09 +0.15 -0.05	+0.12 -0.13 +0.13 -0.13	-0.01 +0.01 -0.01 +0.01	-0.13 +0.13 -0.13 +0.13	-0.43 +0.43 -0.43 +0.43	-0.09 +0.09 -0.09 +0.09	
(FTAG) fTagSE_L eigen13 [%]	-0.17 +0.19 -0.08 +0.07	-0.12 -0.09 +0.15 -0.05	+0.12 -0.13 +0.13 -0.13	-0.01 +0.01 -0.01 +0.01	-0.13 +0.13 -0.13 +0.13	-0.43 +0.43 -0.43 +0.43	-0.09 +0.09 -0.09 +0.09	
(FTAG) fTagSE_L eigen14 [%]	-0.17 +0.19 -0.08 +0.07	-0.12 -0.09 +0.15 -0.05	+0.12 -0.13 +0.13 -0.13	-0.01 +0.01 -0.01 +0.01	-0.13 +0.13 -0.13 +0.13	-0.43 +0.43 -0.43 +0.43	-0.09 +0.09 -0.09 +0.09	
(FTAG) fTagSE_L eigen15 [%]	-0.17 +0.19 -0.08 +0.07	-0.12 -0.09 +0.15 -0.05	+0.12 -0.13 +0.13 -0.13	-0.01 +0.01 -0.01 +0.01	-0.13 +0.13 -0.13 +0.13	-0.43 +0.43 -0.43 +0.43	-0.09 +0.09 -0.09 +0.09	
(FTAG) fTagSE_L extrapolation [%]	+0.16 -0.17	+0.16 -0.17	+0.09 -0.09	+0.02 -0.02	+0.04 -0.04	+0.12 -0.12	+0.41 -0.41	+0.49 -0.49
(FTAG) fTagSE_L extrapolation_from_charm [%]	-0.03 +0.03	-0.03 +0.03	-0.02 +0.02	-0.06 +0.06	+0.02 -0.02	-0.05 +0.05	-0.07 +0.07	-0.07 +0.07
(MET/P(U)) jvt [%]	-0.03 +0.03	-0.03 +0.03	-0.02 +0.02	-0.06 +0.06	+0.02 -0.02	-0.05 +0.05	-0.07 +0.07	-0.07 +0.07
Luminosity [%]	-0.19 +0.19	-0.19 +0.19	-0.14 +0.14	-0.01 +0.01	-0.01 +0.01	-0.04 +0.04	-0.05 +0.05	-0.05 +0.05
(BKG) singleton_1chan [%]	-	-	-	-	-	-	-	-
(BKG) singleton_Wt [%]	-	-	-	-	-	-	-	-
(BKG) mu [%]	-	-	-	-	-	-	-	-
(BKG) mz [%]	-	-	-	-	-	-	-	-
(BKG) rho [%]	-	-	-	-	-	-	-	-
(LJES) LARGERJET_Weak_JET_Rtrk_Modelling_Tau32WTA [%]	+0.52 -0.53	-0.17 +0.18	+0.28 -0.29	+0.53 -0.54	-0.62 +0.62	-0.82 +0.82	-0.75 +0.75	
(LJES) LARGERJET_Weak_JET_Rtrk_Baseline_pT [%]	+0.10 -0.10	+0.28 -0.29	-0.79 +0.80	+0.12 -0.13	+0.32 -0.33	+0.28 -0.29	+1.33 -1.33	
(LJES) LARGERJET_Weak_JET_Rtrk_Baseline_mass [%]	-	-	-	-	-	-	-	-
(LJES) LARGERJET_Weak_JET_Rtrk_Baseline_Tau32WTA [%]	+0.09 -0.09	+0.24 -0.24	+0.17 -0.17	+0.17 -0.17	+0.14 -0.14	-0.50 +0.50	-0.31 +0.31	
(JES) JET_2INP_JET_BJES_Response [%]	-	-	-	-	-	-	-	-
(JES) JET_2INP_JET_Pileup_PTterm [%]	-	-	-	-	-	-	-	-
(JES) JET_2INP_JET_Pileup_OffsetNPV [%]	-0.03 +0.03	+0.04 -0.04	-0.05 +0.05	-0.05 +0.05	-0.05 +0.05	-0.05 +0.05	-0.05 +0.05	+0.05 -0.05
(JES) JET_2INP_JET_Pileup_OffsetNPV_SigTerm [%]	-0.03 +0.03	+0.03 -0.03	+0.02 -0.02	+0.02 -0.02	-0.01 +0.01	-0.01 +0.01	-0.01 +0.01	+0.02 -0.02
(LEP) MUON_SAGITTA_RHISIAS [%]	-	-	-	-	-	-	-	-
(JES) JET_2INP_JET_EffectiveNP_3 [%]	-	-	-	-	-	-	-	-
(JES) JET_2INP_JET_EffectiveNP_4 [%]	-	-	-	-	-	-	-	-
(JES) LARGERJET_Weak_JET_Rtrk_Tracking_mass [%]	-	-	-	-	-	-	-	-
(JES) JET_2INP_JET_Pileup_OffsetMu [%]	-0.04 +0.04	+0.07 -0.07	-0.04 +0.04	-0.04 +0.04	-0.04 +0.04	-0.02 +0.02	-0.02 +0.02	+0.02 -0.02
(JES) JET_2INP_JET_TotalStat_TotalStat_pT [%]	-0.03 +0.03	-0.03 +0.03	-0.03 +0.03	+0.08 -0.08	-0.01 +0.01	-0.06 +0.06	-0.06 +0.06	+0.14 -0.14
(JES) JET_2INP_JET_TRACKING [%]	-	-	-	-	-	-	-	-
(JES) JET_2INP_JET_EffectiveNP_7 [%]	-	-	-	-	-	-	-	-
(JES) LARGERJET_Weak_JET_Rtrk_Modelling_mass [%]	-	-	-	-	-	-	-	-
(JES) LEP_MUON_MS [%]	-	-	-	-	-	-	-	+0.01
(JES) JET_2INP_JET_PunchThrough_MC15 [%]	-	-	-	-	-	-	-	-
(JES) JET_2INP_JET_EtaCalibration_Modelling [%]	-0.02 +0.02	-0.05 +0.05	-0.04 +0.04	-0.04 +0.04	-0.04 +0.04	-0.03 +0.03	-0.03 +0.03	+0.01 -0.01
(JES) JET_2INP_JET_EffectiveNP_2 [%]	-0.07 +0.07	-0.08 +0.08	-0.08 +0.08	-0.08 +0.08	-0.08 +0.08	-0.08 +0.08	-0.08 +0.08	+0.03 -0.03
(JES) JET_2INP_JET_Tracking_Tau32WTA [%]	+0.07 -0.07	-0.05 +0.05	-0.05 +0.05	-0.05 +0.05	-0.05 +0.05	-0.05 +0.05	-0.05 +0.05	+0.03 -0.03
(JES) JET_2INP_JET_EffectiveNP_10 [%]	-0.27 +0.27	-0.42 +0.42	-0.05 +0.05	-0.05 +0.05	-0.34 +0.34	-0.62 +0.62	-1.66 +1.66	
(JES) JET_2INP_JET_EffectiveNP_11 [%]	-0.21 +0.21	-0.40 +0.40	-0.05 +0.05	-0.05 +0.05	-0.34 +0.34	-0.60 +0.60	-1.66 +1.66	
(JES) JET_2INP_JET_EffectiveNP_12 [%]	-0.05 +0.05	-0.06 +0.06	-0.06 +0.06	-0.06 +0.06	-0.05 +0.05	-0.05 +0.05	-0.05 +0.05	+0.05 -0.05
(JES) JET_2INP_JET_EffectiveNP_13 [%]	-0.02 +0.02	-0.04 +0.04	-0.06 +0.06	-0.06 +0.06	-0.02 +0.02	-0.02 +0.02	-0.02 +0.02	+0.05 -0.05
(JES) PDF-LHC1C5_nlo_30_eigen05 [%]	+0.40 -0.40	+0.38 -0.38	+0.43 -0.43	+0.48 -0.48	+0.57 -0.57	+0.65 -0.65	+0.95 -0.95	
(JES) PDF-LHC1C5_nlo_30_eigen06 [%]	+0.14 -0.14	+0.11 -0.11	+0.16 -0.16	+0.22 -0.22	+0.24 -0.24	+0.24 -0.24	+0.10 -0.10	+0.07 -0.07
(JES) PDF-LHC1C5_nlo_30_eigen07 [%]	-0.01 +0.01	-0.03 +0.03	-0.06 +0.06	-0.06 +0.06	-0.01 +0.01	-0.05 +0.05	-0.05 +0.05	-0.05 +0.05
(JES) PDF-LHC1C5_nlo_30_eigen08 [%]	-0.09 +0.09	-0.11 +0.11	-0.14 +0.14	-0.18 +0.18	-0.18 +0.18	-0.30 +0.30	-0.56 +0.56	
(JES) PDF-LHC1C5_nlo_30_eigen09 [%]	-0.05 +0.05	-0.04 +0.04	-0.05 +0.05	-0.06 +0.06	-0.07 +0.07	-0.09		

Not reviewed, for internal circulation only

Bins [GeV]	[0,20]	[20,40]	[40,60]	[60,100]	[100,200]	[200,300]	[300,600]
$d\sigma/dX$ [pb/GeV]	$1.17 \cdot 10^{-2}$	$7.38 \cdot 10^{-3}$	$4.71 \cdot 10^{-3}$	$3.02 \cdot 10^{-3}$	$1.1 \cdot 10^{-3}$	$4.7 \cdot 10^{-4}$	$1.6 \cdot 10^{-4}$
Total Uncertainty [%]	+27.63	+31.29	+31.30	+37.12	+31.65	+33.35	+45.94
Statistics [%]	+4.39	+4.83	+6.76	+7.35	+7.69	+12.97	+17.71
Systematics [%]	+27.19	+31.27	+31.66	+33.06	+31.57	+32.72	+45.53
(FTAG) $b\bar{b}q\bar{q}S^0$ B_eigen0 [%]	+5.84	+5.83	+5.34	+5.34	+5.36	+5.42	+5.03
(FTAG) $b\bar{b}q\bar{q}S^0$ B_eigen1 [%]	+5.03	+5.96	+4.90	+4.95	+4.82	+4.89	+4.92
(FTAG) $b\bar{b}q\bar{q}S^0$ B_eigen2 [%]	+8.83	+8.29	+8.21	+8.33	+8.08	+9.95	+8.33
(FTAG) $b\bar{b}q\bar{q}S^0$ B_eigen3 [%]	+0.53	+0.53	+0.51	+0.51	+0.47	+0.52	+0.53
(FTAG) $b\bar{b}q\bar{q}S^0$ B_eigen4 [%]	+0.54	+0.55	+0.54	+0.54	+0.54	+0.54	+0.54
(FTAG) $b\bar{b}q\bar{q}S^0$ B_eigen5 [%]	+0.04	+0.05	+0.05	+0.04	+0.05	+0.04	+0.04
(FTAG) $b\bar{b}q\bar{q}S^0$ C_eigen0 [%]	+1.94	+1.94	+1.91	+2.06	+1.93	+2.05	+2.06
(FTAG) $b\bar{b}q\bar{q}S^0$ C_eigen1 [%]	+1.78	+3.24	+0.73	+1.38	+1.28	+1.92	+2.02
(FTAG) $b\bar{b}q\bar{q}S^0$ C_eigen2 [%]	+0.16	+0.19	+0.10	+0.13	+0.19	+0.20	+0.20
(FTAG) $b\bar{b}q\bar{q}S^0$ C_eigen3 [%]	+0.13	+0.27	+0.21	+0.61	+0.10	+0.63	+0.42
(FTAG) $b\bar{b}q\bar{q}S^0$ C_eigen4 [%]	+0.13	+0.24	+0.10	+0.23	+0.13	+0.17	+0.19
(FTAG) $b\bar{b}q\bar{q}S^0$ Light_eigen0 [%]	+0.11	+0.19	+0.08	+0.38	+0.12	+0.26	+0.12
(FTAG) $b\bar{b}q\bar{q}S^0$ Light_eigen1 [%]	+0.08	+0.05	+0.05	+0.09	+0.07	+0.07	+0.11
(FTAG) $b\bar{b}q\bar{q}S^0$ Light_eigen2 [%]	+0.11	+0.08	+0.12	+0.09	+0.11	+0.20	+0.08
(FTAG) $b\bar{b}q\bar{q}S^0$ Light_eigen3 [%]	+0.11	+0.09	+0.10	+0.03	+0.11	+0.20	+0.08
(FTAG) $b\bar{b}q\bar{q}S^0$ Light_eigen4 [%]	+0.11	+0.09	+0.10	+0.03	+0.11	+0.20	+0.10
(FTAG) $b\bar{b}q\bar{q}S^0$ Light_eigen5 [%]	+0.01	+0.06	+0.25	+0.02	+0.01	+0.07	+0.10
(FTAG) $b\bar{b}q\bar{q}S^0$ Light_eigen6 [%]	+0.02	+0.02	+0.01	+0.02	+0.02	+0.02	+0.03
(FTAG) $b\bar{b}q\bar{q}S^0$ Light_eigen7 [%]	+0.04	+0.02	+0.08	+0.02	+0.07	+0.15	+0.03
(FTAG) $b\bar{b}q\bar{q}S^0$ Light_eigen8 [%]	+0.07	+0.05	+0.09	+0.03	+0.06	+0.06	+0.03
(FTAG) $b\bar{b}q\bar{q}S^0$ Light_eigen9 [%]	+0.08	+0.05	+0.09	+0.03	+0.04	+0.07	+0.03
(FTAG) $b\bar{b}q\bar{q}S^0$ Light_eigen10 [%]	+0.08	+0.05	+0.09	+0.03	+0.04	+0.07	+0.11
(FTAG) $b\bar{b}q\bar{q}S^0$ Light_eigen11 [%]	+0.08	+0.05	+0.09	+0.03	+0.07	+0.02	+0.11
(FTAG) $b\bar{b}q\bar{q}S^0$ Light_eigen12 [%]	+0.08	+0.05	+0.09	+0.03	+0.07	+0.02	+0.11
(FTAG) $b\bar{b}q\bar{q}S^0$ Light_eigen13 [%]	+0.08	+0.05	+0.09	+0.03	+0.07	+0.02	+0.11
(FTAG) $b\bar{b}q\bar{q}S^0$ Light_eigen14 [%]	+0.08	+0.05	+0.09	+0.03	+0.07	+0.02	+0.11
(FTAG) $b\bar{b}q\bar{q}S^0$ Light_eigen15 [%]	+0.08	+0.05	+0.09	+0.03	+0.07	+0.02	+0.11
(FTAG) $b\bar{b}q\bar{q}S^0$ extrapolation [%]	+0.13	+0.09	+2.96	+3.11	+2.90	+3.01	+3.04
(FTAG) $b\bar{b}q\bar{q}S^0$ extrapolation_from_charm [%]	+3.07	+3.00	+0.01	+0.05	+0.02	+0.02	+0.04
(MET/P(U) jvt [%]	+0.04	+0.09	+0.09	+0.03	+0.12	+0.08	+0.06
Luminosity [%]	+2.01	+2.05	+2.06	+2.03	+1.93	+1.98	+1.76
(BKG) singletop_tchan [%]	+0.00	+2.05	+2.06	+2.05	+1.93	+1.98	+1.77
(BKG) singletop_Wt [%]	+0.02	+0.03	+0.04	+0.06	+0.06	+0.08	+0.07
(BKG) Z [%]	+0.02	+0.03	+0.04	+0.05	+0.07	+0.06	+0.06
(BKG) tH [%]	+0.01	+0.03	+0.04	+0.04	+0.07	+0.08	+0.11
(BKG) tHh [%]	+0.02	+0.03	+0.04	+0.04	+0.07	+0.08	+0.11
(LJES) LARGERETET_Weak_JET_Rtrk_Modelling_Tau32WTA [%]	-8.41	+1.19	+0.72	+1.04	+1.16	+0.97	+0.93
(LJES) LARGERETET_Weak_JET_Rtrk_Baseline_pT [%]	+9.78	+11.26	+10.72	+9.10	+11.46	+10.82	+9.33
(LJES) LARGERETET_Weak_JET_Rtrk_Baseline_mass [%]	+0.61	+0.57	+0.73	+0.11	+0.58	+0.50	+0.10
(LJES) LARGERETET_Weak_JET_Rtrk_Baseline_Tau32WTA [%]	+0.61	+0.57	+0.73	+0.11	+0.58	+0.50	+0.10
(JES) JET_2INP_JET_BJES_Response [%]	+0.08	+0.05	+0.05	+0.05	+0.05	+0.05	+0.03
(JES) JET_2INP_JET_Pileup_PtTerm [%]	-0.01	+0.01	+0.01	+0.01	+0.01	+0.01	+0.05
(JES) JET_2INP_JET_Pileup_OffsetNPV [%]	+0.02	+0.02	+0.02	+0.01	+0.02	+0.04	+0.16
(JES) JET_2INP_JET_Pileup_OffsetNPV_Energy [%]	-0.03	+0.13	+0.12	+0.19	+0.22	+0.12	+0.36
(JES) JET_2INP_JET_OffsetNPV_SecfTerm [%]	-0.06	+0.03	+0.13	+0.29	+0.22	+0.33	+0.09
(LEP) MUON_SAGITTA_RHISIAS [%]	-	-	-	-	-	-	-
(JES) JET_2INP_JET_EffectiveNP_3 [%]	+0.02	-	-	-	+0.03	+0.03	-
(JES) JET_2INP_JET_EffectiveNP_4 [%]	-	-	-	+0.02	-	-	-
(JES) LARGERETET_Weak_JET_Rtrk_Tracking_mass [%]	+0.23	+0.20	+0.38	+0.29	+0.08	+0.49	+0.32
(JES) JET_2INP_JET_Pileup_OffsetMu [%]	+0.01	+0.05	+0.05	+0.05	+0.02	+0.02	+0.03
(JES) LARGERETET_Weak_JET_Rtrk_TotalStat_mass [%]	-	-	-	-	-	-	-
(JES) JET_2INP_JET_EtaCalibration_NonClosure [%]	+0.02	-	-	+0.02	+0.03	+0.03	+0.03
(JES) JET_2INP_JET_EtaCalibration_TotalStat [%]	+0.01	-	-	+0.02	+0.03	+0.03	+0.03
(LEP) EG_RESOLUTION_ALL [%]	-	-	-	+0.11	-	-	-
(JES) JET_2INP_JET_EffectiveNP_6 [%]	+0.04	+0.03	+0.01	+0.03	+0.03	+0.16	-
(JES) JET_2INP_JET_EffectiveNP_5 [%]	-0.01	-	-	+0.01	-	-	-0.01
(JES) JET_2INP_JET_Flavor_Composition [%]	+0.13	+0.24	+0.25	+0.26	+0.10	+0.46	+0.65
(JES) JET_2INP_JET_SingleParticle_HighPt [%]	-0.08	+0.06	-0.17	+0.43	+0.19	+0.43	+0.09
(JES) JET_2INP_JET_Modelling_pT [%]	+2.10	+2.69	+2.04	+1.99	+3.40	+1.98	+5.23
(JES) JET_2INP_JET_Modelling_eta [%]	+0.62	+0.15	+0.53	+0.52	+0.40	+0.46	+0.61
(JES) JET_2INP_JET_Modelling_phi [%]	+0.09	+0.01	+0.04	+0.08	+0.12	+0.40	+0.24
(JES) JET_2INP_JET_OffsetMu [%]	-0.01	-0.01	+0.07	+0.18	+0.02	+0.17	-
(JES) JET_2INP_JET_OffsetNPV [%]	-	-	-	-	-	-	-0.05
(JES) JET_2INP_JET_OffsetNPV_All [%]	-	-	-	+0.11	-	-	-
(JES) JET_2INP_JET_OffsetNPV_7 [%]	-	-	-	+0.11	-	-	+0.01
(JES) LARGERETET_Weak_JET_Rtrk_Modelling_mass [%]	+0.76	+0.71	+0.79	+0.89	+0.08	+0.49	+0.31
(JES) JET_2INP_JET_SingleParticle_Net [%]	-0.67	+0.72	+0.65	+0.26	+0.37	+0.28	+0.35
(LEP) MUON_MS [%]	-	-	-	-	-	-	-0.02
(LEP) MUON_SAGITTA_RHO [%]	-	-	-	-	-	-	-
(JES) JET_2INP_JET_PunchThrough_MC1 [%]	-	-	-	-	-	-	-
(JES) JET_2INP_JET_EtaCalibration_Modelling [%]	+0.03	-	+0.02	+0.03	+0.06	+0.05	+0.17
(JES) JET_2INP_JET_EffectiveNP_2 [%]	-0.02	+0.03	-0.03	+0.15	+0.03	+0.02	+0.05
(JES) LARGERETET_Weak_JET_Rtrk_Tracking_Tau32WTA [%]	-0.10	+0.38	+0.02	+0.55	+0.05	+0.45	+0.11
(JES) LARGERETET_Weak_JET_Rtrk_Tracking_pT [%]	+4.13	+5.43	+4.08	+5.38	+4.01	+6.14	+5.11
(JES) LARGERETET_Weak_JET_Rtrk_TotalStat_Tau32WTA [%]	+0.12	+0.73	+0.71	+0.57	+0.12	+0.49	+0.50
(JES) LARGERETET_Weak_JET_Rtrk_TotalStat [%]	+0.12	+0.18	+0.19	+0.25	+0.25	+0.03	+0.13
(JES) JET_2INP_JET_SingleParticle_Net [%]	+0.03	+0.22	+0.29	+0.09	+0.15	+0.05	+0.02
(JES) LARGERETET_Weak_JET_Rtrk_Wt_jtau_mus_resMass [%]	+0.10	+1.14	+0.10	+1.73	+0.10	+1.25	+1.25
(PDF) PDFLHC1C1_nlo_30_eigen001 [%]	+0.03	+0.07	+0.01	+0.02	+0.13	+0.15	+0.22
(PDF) PDFLHC1C1_nlo_30_eigen002 [%]	+0.21	+0.19	+0.16	+0.16	+0.20	+0.30	+0.07
(PDF) PDFLHC1C1_nlo_30_eigen003 [%]	+0.08	+0.10	+0.09	+0.09	+0.07	+0.07	+1.81
(PDF) PDFLHC1C1_nlo_30_eigen004 [%]	+0.12	+0.20	+0.15	+0.14	+0.19	+0.26	+0.02
(PDF) PDFLHC1C1_nlo_30_eigen005 [%]	+0.34	+0.46	+0.48	+0.49	+0.49	+0.74	+0.88
(PDF) PDFLHC1C1_nlo_30_eigen006 [%]	+0.17	+0.26	+0.21	+0.21	+0.36	+0.39	+0.40
(PDF) PDFLHC1C1_nlo_30_eigen007 [%]	+0.01	+0.01	+0.01	+0.02	+0.02	+0.05	+0.13
(PDF) PDFLHC1C1_nlo_30_eigen008 [%]	+0.15	+0.19	+0.19	+0.19	+0.21	+0.29	+0.39
(PDF) PDFLHC1C1_nlo_30_eigen009 [%]	+0.04	+0.06	+0.06	+0.06	+0.07	+0.08	+0.08
(PDF) PDFLHC1C1_nlo_30_eigen010 [%]	+0.05	+0.06	+0.06	+0.06	+0.11	+0.11	+0.11
(PDF) PDFLHC1C1_nlo_30_eigen011 [%]	+0.07	+0.12	+0.10	+0.09	+0.14	+0.16	+0.17
(PDF) PDFLHC1C1_nlo_30_eigen012 [%]	+0.05	+0.11	+0.11	+0.08	+0.14	+0.11	+0.21
(PDF) PDFLHC1C1_nlo_30_eigen013 [%]	+0.02	+0.04	+0.04	+0.03	+0.07	+0.09	+0.09
(PDF) PDFLHC1C1_nlo_30_eigen014 [%]	+0.03	+0.02	+0.02	+0.03	+0.01	+0.01	+0.04
(PDF) PDFLHC1C1_nlo_30_eigen015 [%]	+0.03	+0.04	+0.07	+0.05	+0.05	+0.03	+0.03
(PDF) PDFLHC1C1_nlo_30_eigen016 [%]	+0.02	-	+0.01	-	+0.05	+0.04	+0.12
(PDF) PDFLHC1C1_nlo_30_eigen017 [%]	+0.06	+0.11	+0.09	+0.08	+0.13	+0.16	+0.12
(PDF) PDFLHC1C1_nlo_30_eigen018 [%]	+0.07	+0.12	+0.09	+0.09	+0.10	+0.13	+0.17
(PDF) PDFLHC1C1_nlo_30_eigen019 [%]	+0.03	+0.00	+0.00	+0.00	+0.00	+0.00	+0.07
(PDF) PDFLHC1C1_nlo_30_eigen020 [%]	+0.07	+0.04	+0.07	+0.07	+0.06	+0.07	+0.06
(PDF) PDFLHC1C1_nlo_30_eigen021 [%]	+0.04	+0.06	+0.04	+0.03	+0.03	+0.08	+0.08
(PDF) PDFLHC1C1_nlo_30_eigen022 [%]	+0.46	+0.63	+0.64	+0.63	+0.74	+0.98	+1.03
(PDF) PDFLHC1C1_nlo_30_eigen023 [%]	-	-	-	-	+0.01	-	+0.07
(PDF) PDFLHC1C1_nlo_30_eigen024 [%]	+0.06	+0.03	+0.02	+0.02	+0.06	+0.08	+0.03
(PDF) PDFLHC1C1_nlo_30_eigen025 [%]	+0.04	+0.03	+0.07	+0.07	+0.06	+0.05	+0.07
(PDF) PDFLHC1C1_nlo_30_eigen026 [%]	+0.01	+0.01	+0.03	+0.03	+0.04	+0.05	+0.06
(PDF) PDFLHC1C1_nlo_30_eigen027 [%]	+0.04	+0.03	+0.07	+0.07	+0.06	+0.04	+0.08
(PDF) PDFLHC1C1_nlo_30_eigen028 [%]	+0.09	+0.10	+0.15	+0.15	+0.17	+0.26	+0.30
(PDF) PDFLHC1C1_nlo_30_eigen029 [%]	-	-	-	-	-	+0.01	-
(PDF) PDFLHC1C1_nlo_30_eigen030 [%]	-	-	-	+0.02	+0.01	+0.02	+0.04
(MOD) Alternative hard-scattering model [%]	+6.28	+12.05	+11.11	+13.01	+7.15	+10.18	+11.75
(MOD) Alternative parton-shower mode [%]	+18.83	+19.63	+18.63	+23.52	+19.63	+15.48	+13.81
(MOD) ISR/FSR + scale [%]	+0.61	+0.10	+0.14	+1.86	+2.39	+8.75	+2.53
(MOD) Monte Carlo sample statistics [%]	+2.11	+2.55	+4.10	+4.54	+5.23	+7.77	+12.42

Table 150: The individual systematic uncertainties in the parton level fiducial phase-space absolute differential cross-sections for the $p_{out}^{\tilde{t}\bar{t}}$ calculated as a percentage of the cross-section.

Not reviewed, for internal circulation only

Bins (GeV)	[0,20]	[20,40]	[40,60]	[60,100]	[100,200]	[200,200]	[300,600]	Σ
$ t\bar{t}(\sigma) /X$ [pb/GeV]	1.46 ± 0.19	9.23 ± 1.0	3.88 ± 10^{-3}	3.78 ± 10^{-3}	1.37 ± 10^{-4}	5.87 ± 10^{-4}	2 ± 10^{-4}	
Total Uncertainty [%]	± 6.12	± 7.08	± 8.64	± 11.13	± 9.69	± 8.36	± 7.91	± 3.96
Statistics [%]	± 2.97	± 4.58	± 4.50	± 4.75	± 4.24	± 4.24	± 4.77	± 3.16
Systematics [%]	± 4.13	± 4.96	± 4.34	± 4.46	± 4.12	± 4.12	± 4.27	± 2.79
(FTAG) ftagSF_B_eigen0 [%]	-	-	-	-	-	-	-	-
(FTAG) ftagSF_B_eigen1 [%]	-	-	-	-	-	-	-	-
(FTAG) ftagSF_B_eigen2 [%]	-	-	-	-	-	-	-	-
(FTAG) ftagSF_C_eigen1 [%]	-	-	-	-	-	-	-	-
(FTAG) ftagSF_Light_eigen0 [%]	-	-	-	-	-	-	-	-
(FTAG) ftagSF_Light_eigen1 [%]	-	-	-	-	-	-	-	-
(FTAG) ftagSF_Light_eigen2 [%]	-	-	-	-	-	-	-	-
(FTAG) ftagSF_Light_eigen3 [%]	-	-	-	-	-	-	-	-
(FTAG) ftagSF_Light_eigen4 [%]	-	-	-	-	-	-	-	-
(FTAG) ftagSF_Light_eigen5 [%]	-	-	-	-	-	-	-	-
(FTAG) ftagSF_Light_eigen6 [%]	-	-	-	-	-	-	-	-
(FTAG) ftagSF_Light_eigen7 [%]	-	-	-	-	-	-	-	-
(FTAG) ftagSF_Light_eigen8 [%]	-	-	-	-	-	-	-	-
(FTAG) ftagSF_Light_eigen9 [%]	-	-	-	-	-	-	-	-
(FTAG) ftagSF_Light_eigen10 [%]	-	-	-	-	-	-	-	-
(FTAG) ftagSF_Light_eigen11 [%]	-	-	-	-	-	-	-	-
(FTAG) ftagSF_Light_eigen12 [%]	-	-	-	-	-	-	-	-
(FTAG) ftagSF_Light_eigen13 [%]	-	-	-	-	-	-	-	-
(FTAG) ftagSF_Light_eigen14 [%]	-	-	-	-	-	-	-	-
(FTAG) ftagSF_extrapolation [%]	-	-	-	-	-	-	-	-
(FTAG) ftagSF_extrapolation_from_charm [%]	-	-	-	-	-	-	-	-
(METTPU) jvt [%]	-	-	-	-	-	-	-	-
Luminosity [%]	-	-	-	-	-	-	-	-
(BKG) singletop_tchan [%]	-	-	-	-	-	-	-	-
(BKG) singletop_Wt [%]	-	-	-	-	-	-	-	-
(BKG) tW [%]	-	-	-	-	-	-	-	-
(BKG) tZ [%]	-	-	-	-	-	-	-	-
(BKG) ttW [%]	-	-	-	-	-	-	-	-
(LJES) LARGERET_Weak_JET_Rtrk_Modelling_Tau32WTA [%]	± 0.93	± 0.93	± 0.18	± 1.22	± 0.02	± 0.24	± 0.98	± 0.98
(LJES) LARGERET_Weak_JET_Rtrk_Baseline_pT [%]	± 0.36	± 0.37	± 0.26	± 1.18	± 0.03	± 1.03	± 0.34	± 0.34
(LJES) LARGERET_Weak_JET_Rtrk_Baseline_mass [%]	± 0.66	± 0.64	± 0.24	± 1.02	± 0.09	± 0.09	± 2.54	± 1.14
(LJES) LARGERET_Weak_JET_Rtrk_Baseline_Tau32WTA [%]	± 0.84	± 0.81	± 0.50	± 1.21	± 0.17	± 0.17	± 1.65	± 0.15
(LJES) JET_2NP_JET_Weak_JET_Rtrk_Baseline_Tau32WTA [%]	± 0.35	-	± 0.25	± 1.26	± 0.02	± 0.02	± 0.06	± 0.06
(JES) JET_2NP_JET_BJES_Response [%]	-	-	-	-	-	-	-	-
(JES) JET_2NP_JET_Pileup_PtTerm [%]	-	-	-	-	-	-	-	-
(JES) JET_2NP_JET_Pileup_OffsetNPV [%]	-	-	-	-	-	-	-	-
(JES) JET_2NP_JET_Pileup_RhoNPV [%]	-	-	-	-	-	-	-	-
(JES) JET_2NP_JET_Pileup_OffsetMu [%]	-	-	-	-	-	-	-	-
(LEP) MUON_SAGITTA_RHOMAS [%]	-	-	-	-	-	-	-	-
(JES) JET_2NP_JET_EffectiveNP_3 [%]	-	-	-	-	-	-	-	-
(JES) JET_2NP_JET_EffectiveNP_4 [%]	-	-	-	-	-	-	-	-
(JES) LARGERET_Weak_JET_Rtrk_Tracking_mass [%]	± 0.12	± 0.09	± 0.27	± 0.40	± 0.19	± 0.38	± 0.43	± 0.08
(JES) JET_2NP_JET_Pileup_OffsetMu [%]	± 0.02	-	± 0.09	± 0.09	± 0.03	± 0.03	± 0.06	± 0.06
(JES) LARGERET_Weak_JET_Rtrk_TotalStat_mass [%]	± 0.02	-	± 0.02	± 0.02	± 0.02	± 0.02	± 0.07	± 0.07
(JES) JET_2NP_JET_EtaCalibration_NonClosure [%]	± 0.03	-	± 0.04	± 0.09	± 0.03	± 0.31	± 0.07	± 0.07
(JES) JET_2NP_JET_EtaCalibration_TotalStat [%]	± 0.03	-	± 0.07	± 0.02	± 0.02	± 0.02	± 0.07	± 0.07
(JES) EG_Electrons_Electrons_Accuracy [%]	± 0.02	-	± 0.02	± 0.09	± 0.02	± 0.02	± 0.02	± 0.02
(JES) JET_2NP_JET_Flavor_Response [%]	± 0.06	± 0.03	± 0.08	± 0.08	± 0.04	± 0.34	± 0.02	± 0.02
(JES) JET_2NP_JET_EffectiveNP_6 [%]	-	-	± 0.02	-	± 0.02	± 0.02	± 0.03	± 0.03
(JES) JET_2NP_JET_EffectiveNP_5 [%]	-	-	-	-	-	-	-	-
(JES) JET_2NP_JET_Flavor_Composition [%]	± 0.08	± 0.03	± 0.03	± 0.03	± 0.02	± 0.20	± 0.39	± 0.08
(JES) JET_2NP_JET_SingleParticle_HighPt [%]	-	± 0.09	± 0.11	-	-	± 0.02	± 0.26	± 0.08
(JES) JET_2NP_JET_EffectiveNP_7 [%]	-	-	-	-	-	-	-	-
(JES) LARGERET_Weak_JET_Rtrk_Tracking_pT [%]	± 0.02	± 0.02	-	± 0.09	± 0.02	± 0.02	± 0.02	± 0.07
(JES) LARGERET_Weak_JET_Rtrk_Tracking_p1 [%]	± 0.03	± 0.03	± 0.05	± 0.05	± 0.03	± 0.03	± 0.03	± 0.03
(JES) LARGERET_Weak_JET_Rtrk_Tracking_pTau [%]	± 0.18	± 0.09	± 0.04	± 1.93	± 0.10	± 0.10	± 2.59	± 1.12
(JES) JET_2NP_JET_Tau32WTA [%]	± 0.01	± 0.01	± 0.01	± 0.01	± 0.01	± 0.01	± 0.15	± 0.15
(JES) JET_JER_SINGLE_NP [%]	± 0.12	± 0.07	± 0.14	± 0.24	± 0.05	± 0.10	± 0.99	± 0.01
(JES) JET_2NP_JET_PunchThrough_MC15 [%]	-	-	-	-	-	-	-	-
(JES) JET_2NP_JET_EtaCalibration_Modelling [%]	± 0.01	± 0.01	-	± 0.01	± 0.01	± 0.01	± 0.14	± 0.14
(JES) JET_2NP_JET_EffectiveNP_2 [%]	-	-	-	-	-	-	± 0.02	± 0.02
(JES) LARGERET_Weak_JET_Rtrk_Tracking_Tau32WTA [%]	± 0.11	-	± 0.05	± 0.05	± 0.01	± 0.01	± 0.07	± 0.07
(JES) LARGERET_Weak_JET_Rtrk_Tracking_pTau [%]	± 0.03	± 0.03	± 0.05	± 0.05	± 0.01	± 0.01	± 0.03	± 0.03
(JES) LARGERET_Weak_JET_Rtrk_Tracking_p1 [%]	± 0.18	± 0.09	± 0.04	± 1.93	± 0.10	± 0.10	± 2.59	± 1.12
(JES) JET_2NP_JET_Tau32WTA [%]	± 0.01	± 0.01	± 0.01	± 0.01	± 0.01	± 0.01	± 0.15	± 0.15
(JES) JET_JER_SINGLE_NP [%]	-	-	-	-	-	-	-	-
(PDF) PDF-LHC15_nlo_30_eigen01 [%]	± 0.03	± 0.07	± 0.01	± 0.13	± 0.15	± 0.15	± 0.22	± 0.22
(PDF) PDF-LHC15_nlo_30_eigen02 [%]	± 0.21	± 0.19	± 0.16	± 0.20	± 0.30	± 0.07	-	-
(PDF) PDF-LHC15_nlo_30_eigen03 [%]	± 0.03	± 0.10	± 0.09	± 0.09	± 0.02	± 0.02	± 0.07	± 0.07
(PDF) PDF-LHC15_nlo_30_eigen04 [%]	± 0.12	± 0.20	± 0.15	± 0.14	± 0.19	± 0.26	± 0.02	± 0.02
(PDF) PDF-LHC15_nlo_30_eigen05 [%]	± 0.34	± 0.06	± 0.06	± 0.06	± 0.04	± 0.74	± 0.08	± 0.08
(PDF) PDF-LHC15_nlo_30_eigen06 [%]	± 0.17	± 0.26	± 0.21	± 0.21	± 0.56	± 0.09	± 0.40	± 0.40
(PDF) PDF-LHC15_nlo_30_eigen07 [%]	± 0.15	± 0.19	± 0.19	± 0.19	± 0.21	± 0.29	± 0.08	± 0.08
(PDF) PDF-LHC15_nlo_30_eigen08 [%]	± 0.05	± 0.06	± 0.06	± 0.06	± 0.02	± 0.02	± 0.05	± 0.13
(PDF) PDF-LHC15_nlo_30_eigen09 [%]	± 0.03	± 0.09	± 0.05	± 0.04	± 0.04	± 0.07	± 0.10	± 0.08
(PDF) PDF-LHC15_nlo_30_eigen10 [%]	± 0.07	± 0.12	± 0.11	± 0.11	± 0.14	± 0.11	± 0.21	± 0.17
(PDF) PDF-LHC15_nlo_30_eigen11 [%]	± 0.05	± 0.11	± 0.11	± 0.11	± 0.14	± 0.11	± 0.21	± 0.17
(PDF) PDF-LHC15_nlo_30_eigen12 [%]	± 0.05	± 0.11	± 0.11	± 0.11	± 0.14	± 0.11	± 0.21	± 0.17
(PDF) PDF-LHC15_nlo_30_eigen13 [%]	± 0.02	± 0.09	± 0.04	± 0.04	± 0.07	± 0.07	± 0.09	± 0.09
(PDF) PDF-LHC15_nlo_30_eigen14 [%]	± 0.03	± 0.08	± 0.02	± 0.02	± 0.02	± 0.01	± 0.04	± 0.04
(PDF) PDF-LHC15_nlo_30_eigen15 [%]	± 0.02	± 0.07	± 0.01	± 0.01	± 0.01	± 0.01	± 0.04	± 0.04
(PDF) PDF-LHC15_nlo_30_eigen16 [%]	± 0.06	± 0.11	± 0.09	± 0.08	± 0.13	± 0.16	± 0.15	± 0.15
(PDF) PDF-LHC15_nlo_30_eigen17 [%]	± 0.06	± 0.07	± 0.07	± 0.07	± 0.01	± 0.01	± 0.07	± 0.07
(PDF) PDF-LHC15_nlo_30_eigen18 [%]	± 0.07	± 0.12	± 0.09	± 0.10	± 0.13	± 0.16	± 0.12	± 0.12
(PDF) PDF-LHC15_nlo_30_eigen19 [%]	± 0.04	± 0.01	± 0.01	± 0.01	± 0.09	± 0.04	± 0.17	± 0.17
(PDF) PDF-LHC15_nlo_30_eigen20 [%]	± 0.07	± 0.04	± 0.07	± 0.07	± 0.06	± 0.07	± 0.06	± 0.06
(PDF) PDF-LHC15_nlo_30_eigen21 [%]	± 0.04	± 0.06	± 0.04	± 0.03	± 0.03	± 0.03	± 0.08	-
(PDF) PDF-LHC15_nlo_30_eigen22 [%]	± 0.46	± 0.63	± 0.64	± 0.63	± 0.74	± 0.98	± 1.03	± 1.03
(PDF) PDF-LHC15_nlo_30_eigen23 [%]	-	-	-	-	-	± 0.01	-	-
(PDF) PDF-LHC15_nlo_30_eigen24 [%]	± 0.06	± 0.03	± 0.02	± 0.02	± 0.16	± 0.08	± 0.05	± 0.05
(PDF) PDF-LHC15_nlo_30_eigen25 [%]	± 0.01	± 0.01	-	-	-	± 0.02	± 0.05	± 0.07
(PDF) PDF-LHC15_nlo_30_eigen26 [%]	± 0.01	± 0.01	± 0.03	± 0.03	± 0.04	± 0.05	± 0.06	± 0.06
(PDF) PDF-LHC15_nlo_30_eigen27 [%]	± 0.04	± 0.03	± 0.07	± 0.07	± 0.06	± 0.06	± 0.04	± 0.04
(PDF) PDF-LHC15_nlo_30_eigen28 [%]	± 0.09	± 0.10	± 0.15	± 0.15	± 0.17	± 0.26	± 0.30	± 0.30
(PDF) PDF-LHC15_nlo_30_eigen29 [%]	-	-	-	-	-	± 0.01	-	-
(PDF) PDF-LHC15_nlo_30_eigen30 [%]	-							

Table 152: The individual systematic uncertainties in the parton level fiducial phase-space absolute differential cross-sections for the $H_T^{\tau\tau}$ calculated as a percentage of the cross-section.

Table 153: The individual systematic uncertainties in the parton level fiducial phase-space relative differential cross-sections for the H_T^{fit} calculated as a percentage of the cross-section.

Bins [GeV]	[0,2.5]	[2.5,2.75]	[2.75,3]	[3,3.15]
$d\sigma/dX$ [pb/GeV]	$3.26 \cdot 10^{-3}$	$1.91 \cdot 10^{-1}$	$7.12 \cdot 10^{-1}$	3.32
Total Uncertainty [%]	+7.8 -70.93	+33.54 -34.70	+34.79 -30.15	+31.79 -30.15
Statistics [%]	+15.05	± 11.31	± 5.85	± 2.79
Systematics [%]	+67.99 -67.77	+35.36 -30.70	+33.55 -34.00	+31.64 -30.00
(FTAG) bTagSF_B_eigen0 [%]	+4.68 +4.99 -4.35	+5.36 -4.35	+5.40 -4.83	+5.32 -4.38
(FTAG) bTagSF_B_eigen1 [%]	+0.46 +0.57 -0.67	+0.60 -0.60	+0.69 -0.69	+0.69 -0.69
(FTAG) bTagSF_B_eigen2 [%]	+0.38 +0.38 -0.38	+0.43 -0.43	+0.49 -0.49	+0.43 -0.43
(FTAG) bTagSF_B_eigen3 [%]	+0.38 +0.38 -0.38	+0.45 -0.45	+0.49 -0.49	+0.33 -0.33
(FTAG) bTagSF_B_eigen4 [%]	+0.19 +0.19 -0.19	+0.21 -0.21	+0.23 -0.23	+0.25 -0.25
(FTAG) bTagSF_B_eigen5 [%]	+0.03 +0.03 -0.03	+0.04 -0.04	+0.04 -0.04	+0.05 -0.05
(FTAG) bTagSF_C_eigen0 [%]	+7.19 +7.19 -7.19	+7.35 -7.35	+7.37 -7.37	+7.34 -7.34
(FTAG) bTagSF_C_eigen1 [%]	+0.53 +0.50 -0.50	+1.43 -0.43	+1.58 -1.58	+1.65 -1.65
(FTAG) bTagSF_C_eigen2 [%]	+0.30 +0.30 -0.30	+0.45 -0.45	+0.54 -0.54	+0.30 -0.30
(FTAG) bTagSF_C_eigen3 [%]	+0.24 +0.24 -0.24	+0.31 -0.31	+0.22 -0.22	+0.14 -0.14
(FTAG) bTagSF_Light_eigen0 [%]	+0.08 +0.08 -0.08	+0.08 -0.08	+0.08 -0.08	+0.08 -0.08
(FTAG) bTagSF_Light_eigen1 [%]	+0.63 +0.63 -0.63	+0.48 -0.48	+0.26 -0.26	+0.23 -0.23
(FTAG) bTagSF_Light_eigen2 [%]	+0.30 +0.30 -0.30	+0.10 -0.10	+0.10 -0.10	+0.15 -0.15
(FTAG) bTagSF_Light_eigen3 [%]	-0.78 +0.19 -0.19	-0.19 +0.21	-0.03 +0.03	-0.15 +0.10
(FTAG) bTagSF_Light_eigen4 [%]	-0.02 +0.02 -0.02	-0.02 +0.03	-0.03 +0.03	+0.08 +0.08
(FTAG) bTagSF_Light_eigen5 [%]	+0.75 +0.75 -0.75	-	+0.03 -0.01	-
(FTAG) bTagSF_Light_eigen6 [%]	+0.19 +0.19 -0.19	-0.06 +0.06	-0.01 +0.01	-0.01 +0.01
(FTAG) bTagSF_Light_eigen7 [%]	-0.30 +0.71 -0.71	-0.09 +0.07	-0.03 +0.05	-0.01 +0.01
(FTAG) bTagSF_Light_eigen8 [%]	+0.11 +0.11 -0.11	-0.04 +0.06	-0.04 +0.02	-0.02 +0.02
(FTAG) bTagSF_Light_eigen9 [%]	-0.04 -0.04 +0.04	-0.06 +0.06	-0.02 +0.02	-0.05 +0.05
(FTAG) bTagSF_Light_eigen10 [%]	-	-0.08 +0.08	-0.02 +0.02	-0.05 +0.05
(FTAG) bTagSF_Light_eigen11 [%]	-	-0.08 +0.08	-0.02 +0.02	-0.05 +0.05
(FTAG) bTagSF_Light_eigen12 [%]	-	-0.08 +0.08	-0.02 +0.02	-0.05 +0.05
(FTAG) bTagSF_Light_eigen13 [%]	-	-0.08 +0.08	-0.02 +0.02	-0.05 +0.05
(FTAG) bTagSF_Light_eigen14 [%]	-	-0.08 +0.08	-0.02 +0.02	-0.05 +0.05
(FTAG) bTagSF_Light_eigen15 [%]	-	-0.08 +0.08	-0.02 +0.02	-0.05 +0.05
(FTAG) bTagSF_extrapolation [%]	+2.50 +2.50 -2.50	+2.58 -2.58	+2.91 -2.88	+3.16 -3.00
(FTAG) bTagSF_extrapolation_from_charm [%]	+0.03 +0.03 -0.03	-0.04 +0.04	+0.02 -0.02	-0.01 +0.01
(MET/PU) jvt [%]	-	-	-	-
Luminosity [%]	+1.89 -1.89	+1.38 -1.88	+0.02 -2.01	+0.01 -2.03
(BKG) singletop_tchan [%]	-	-	-	-
(BKG) singletop_Wt [%]	-	-	-	-
(BKG) nW [%]	+0.07 +0.07 -0.07	+0.08 -0.08	+0.06 -0.06	+0.03 -0.03
(BKG) ttZ [%]	+0.10 +0.10 -0.10	-0.10 +0.10	+0.03 -0.03	+0.02 -0.02
(BKG) tH [%]	-0.09 -0.09 +0.09	-0.09 +0.09	-0.06 +0.06	-0.02 +0.02
(LJES) LARGERJET_Weak_JET_Rtrk_Modelling_Tau32WTA [%]	-3.44 +3.16 -3.16	+11.13 +4.79 -4.79	+9.92 +2.93 -2.93	+10.53 +2.02 -2.02
(LJES) LARGERJET_Weak_JET_Baseline_pT [%]	+3.09 +3.09 -3.09	+11.13 +4.79 -4.79	+9.92 +2.93 -2.93	+10.53 +2.02 -2.02
(LJES) LARGERJET_Weak_JET_Rtrk_Baseline_mass [%]	-1.10 +0.43 -0.43	+0.38 +0.43 -0.43	+0.37 +0.37 -0.37	+0.34 +0.34 -0.34
(LJES) LARGERJET_Weak_JET_Rtrk_Baseline_Tau32WTA [%]	+7.13 +7.13 -7.13	+8.63 -8.63 +7.21	+8.25 -8.25 +8.25	+8.00 -8.00 +8.00
(JES) JET_21NP_JET_BJES_Response [%]	+0.01 +0.01 -0.01	+0.03 -0.03	-	-
(JES) JET_21NP_JET_Pileup_pTTerm [%]	-	-	-	-0.01
(JES) JET_21NP_JET_Pileup_OffsetNPV [%]	+0.27 +0.27 -0.27	+0.10 -0.10	+0.02 -0.02	+0.01 +0.02
(JES) JET_21NP_JET_Pileup_RhoTopology [%]	+0.77 +0.69 -0.69	+0.23 +0.05	+0.16 -0.16	+0.18 -0.08
(JES) JET_21NP_JET_EffectiveNP_8stTerm [%]	-0.01 -0.01 +0.01	-	-	-
(LEP) MUON_SAGITTA_RESBIAS [%]	-	-	-	-
(JES) JET_21NP_JET_EffectiveNP_3 [%]	+0.01 +0.01 -0.01	+0.02 -0.01	+0.02 -0.01	-
(JES) JET_21NP_JET_EffectiveNP_4 [%]	-	-	-	-
(LJES) LARGERJET_Weak_JET_Rtrk_Tracking_mass [%]	-0.23 +0.70 -0.70	+1.06 +0.04	-0.16 -0.01	+0.18 +0.03
(JES) JET_21NP_JET_Pileup_OffsetMu [%]	-	-	-	-
(LJES) LARGERJET_Weak_JET_Rtrk_TotalStat_mass [%]	-0.59 +0.59 -0.59	+0.06 -0.06	-0.08 +0.08	-
(JES) JET_21NP_JET_EtaIntercalibration_NonClosure [%]	+0.11 +0.11 -0.03	+0.07 +0.04	-0.08 +0.03	+0.01 +0.02
(JES) JET_21NP_JET_EtaIntercalibration_TotalStat [%]	-	-	+0.03 +0.03	+0.02 +0.02
(LEP) EG_RESOLUTION_ALL [%]	-	-	+0.07	-
(JES) JET_21NP_JET_Flavor_Response [%]	-0.71 +0.42 -0.42	+0.03 +0.14 -0.02	-0.10 +0.08 +0.02	-
(JES) JET_21NP_JET_EffectiveNP_6 [%]	-	-	-	-
(JES) JET_21NP_JET_EffectiveNP_5 [%]	-	-	-	-
(JES) JET_21NP_JET_EffectiveNP_4 [%]	+1.08 +0.96 -0.96	+0.16 -0.07	+0.01 +0.25 -0.39	+0.23 +0.23 -0.40
(JES) JET_21NP_JET_SingleParticle_HighPt [%]	-	-	-	-
(LJES) LARGERJET_Weak_JET_Rtrk_Modelling_pT [%]	+2.03 +2.26 -2.26	+4.81 -3.13	+2.31 -2.30	+2.30 -1.95 -1.95
(JES) JET_21NP_JET_EffectiveNP_1 [%]	-0.63 +0.63 -0.63	+0.09 -0.09	-0.12 +0.12	-0.03 +0.03
(LEP) MUON_ID [%]	-	-	-	-
(LJES) LARGERJET_Weak_JET_Rtrk_TotalStat_pT [%]	+0.26 -0.35	+0.61 -0.18	+0.37 -0.29	+0.29 -0.24
(LEP) MUON_SCALE [%]	-	-	-	-
(LEP) EG_SCALE_ALL [%]	-	-	-0.07	-
(JES) JET_21NP_JET_EffectiveNP_7 [%]	+0.01 -0.04	+0.01 +0.09	-0.08 +0.35	-
(LJES) LARGERJET_Weak_JET_Rtrk_Modelling_mass [%]	+0.28 +0.28	+1.32	-0.52	-0.62
(LEP) MUON_MS [%]	-	-	-	-
(LEP) MUON_SAGITTA_RHO [%]	-	-	-	-
(JES) JET_21NP_JET_PunchThrough_MC15 [%]	-	-	-	-
(JES) JET_21NP_JET_EtaIntercalibration_Modelling [%]	+0.17 +0.07	+0.12 +0.06	+0.02 -0.08	+0.02 +0.04
(JES) JET_21NP_JET_EffectiveNP_2 [%]	-	-	-	-
(LJES) LARGERJET_Weak_JET_Rtrk_Tracking_Tau32WTA [%]	-0.25 +3.31	-0.61 +3.38	-0.40 +3.31	-0.40 +3.39
(LJES) LARGERJET_Weak_JET_Rtrk_Tracking_pT [%]	+0.03 +0.03	-0.13	-0.01	-0.08
(LJES) LARGERJET_Weak_JET_Rtrk_TotalStat_Tau32WTA [%]	-	-	-	-
(JES) JET_JER_SINGLE_NP [%]	+0.38 +0.38 -0.38	+0.19 -0.19	+0.09 -0.09	+0.12 -0.12
(LJES) LARGERJET_Weak_JET_Top_massRes_mass [%]	+0.42 +0.42 -0.42	+0.80 -0.80	+1.75 -1.75	+1.38 -1.38
(PDF) PDF4LHC15_nlo_30_eigen001 [%]	+0.38 +0.38 -0.38	+0.09 -0.09	+0.02 -0.02	+0.03 -0.03
(PDF) PDF4LHC15_nlo_30_eigen002 [%]	+0.34 +0.34 -0.34	+0.18 -0.18	+0.15 -0.15	+0.19 -0.19
(PDF) PDF4LHC15_nlo_30_eigen003 [%]	+1.32 +1.32 -1.32	+0.05 -0.05	+0.08 -0.08	+0.09 -0.09
(PDF) PDF4LHC15_nlo_30_eigen004 [%]	+0.19 +0.19 -0.19	+0.13 -0.13	+0.14 -0.14	+0.16 -0.16
(PDF) PDF4LHC15_nlo_30_eigen005 [%]	+1.13 +1.13 -1.13	+0.57 -0.57	+0.50 -0.50	+0.41 -0.41
(PDF) PDF4LHC15_nlo_30_eigen006 [%]	+0.64 +0.64 -0.64	+0.27 -0.27	+0.23 -0.23	+0.21 -0.21
(PDF) PDF4LHC15_nlo_30_eigen007 [%]	+0.12 +0.12 -0.12	+0.04 -0.04	+0.02 -0.02	-
(PDF) PDF4LHC15_nlo_30_eigen008 [%]	+0.47 +0.47 -0.47	+0.20 -0.20	+0.18 -0.18	+0.17 -0.17
(PDF) PDF4LHC15_nlo_30_eigen009 [%]	+0.12 +0.12 -0.12	+0.06 -0.06	+0.05 -0.05	+0.05 -0.05
(PDF) PDF4LHC15_nlo_30_eigen010 [%]	+0.06 +0.06 -0.06	+0.08 -0.08	+0.06 -0.06	+0.05 -0.05
(PDF) PDF4LHC15_nlo_30_eigen011 [%]	+0.28 +0.28 -0.28	+0.11 -0.11	+0.10 -0.10	+0.09 -0.09
(PDF) PDF4LHC15_nlo_30_eigen012 [%]	+0.30 +0.30 -0.30	+0.07 -0.07	+0.10 -0.10	+0.09 -0.09
(PDF) PDF4LHC15_nlo_30_eigen013 [%]	+0.09 +0.09 -0.09	+0.04 -0.04	+0.02 -0.02	+0.03 -0.03
(PDF) PDF4LHC15_nlo_30_eigen014 [%]	+0.04 +0.04 -0.04	-	+0.02 -0.02	+0.02 -0.02
(PDF) PDF4LHC15_nlo_30_eigen015 [%]	-	+0.03	+0.06 -0.06	+0.04 -0.04
(PDF) PDF4LHC15_nlo_30_eigen016 [%]	+0.14 +0.14 -0.14	-	-	-
(PDF) PDF4LHC15_nlo_30_eigen017 [%]	+0.22 +0.22 -0.22	+0.10 -0.10	+0.09 -0.09	+0.08 -0.08
(PDF) PDF4LHC15_nlo_30_eigen018 [%]	+0.24 +0.24 -0.24	+0.10 -0.10	+0.10 -0.10	+0.09 -0.09
(PDF) PDF4LHC15_nlo_30_eigen019 [%]	+0.20 +0.20 -0.20	+0.08 -0.08	+0.07 -0.07	+0.06 -0.06
(PDF) PDF4LHC15_nlo_30_eigen020 [%]	+0.07 +0.07 -0.07	+0.05 -0.05	+0.07 -0.07	+0.06 -0.06
(PDF) PDF4LHC15_nlo_30_eigen021 [%]	+0.08 +0.08 -0.08	+0.04 -0.04	+0.03 -0.03	+0.04 -0.04
(PDF) PDF4LHC15_nlo_30_eigen022 [%]	+1.54 +1.54 -1.54	+0.60 -0.60	+0.58 -0.58	+0.55 -0.55
(PDF) PDF4LHC15_nlo_30_eigen023 [%]	+0.09 +0.09 -0.09	+0.01 -0.01	-	-
(PDF) PDF4LHC15_nlo_30_eigen024 [%]	+0.10 +0.10 -0.10	+0.04 -0.04	-	+0.04 -0.04
(PDF) PDF4LHC15_nlo_30_eigen025 [%]	+0.10 +0.10 -0.10	-	-	+0.01 -0.01
(PDF) PDF4LHC15_nlo_30_eigen026 [%]	+0.10 +0.10 -0.10	+0.04 -0.04	+0.03 -0.03	+0.01 -0.01
(PDF) PDF4LHC15_nlo_30_eigen027 [%]	+0.08 +0.08 -0.08	+0.04 -0.04	+0.07 -0.07	+0.04 -0.04
(PDF) PDF4LHC15_nlo_30_eigen028 [%]	+0.37 +0.37 -0.37	+0.16 -0.16	+0.15 -0.15	+0.10 -0.10
(PDF) PDF4LHC15_nlo_30_eigen029 [%]	+0.01 +0.01 -0.01	-	-	-
(PDF) PDF4LHC15_nlo_30_eigen030 [%]	+0.02 +0.02 -0.02	-	+0.02 -0.02	-
(MOD) Alternative hard-scattering model [%]	+57.07 +51.08 +51.08	+19.74 +11.80 +11.80	+11.35 +22.96 +19.16	+11.38 +0.68 +0.68
(MOD) Alternative parton-shower mode [%]	+1.49 +1.49 +1.49	+3.59 -3.59	+0.78 -0.78	+0.68 -0.68
(MOD) ISR/FSR + scale [%]	+8.68 +8.68 +8.68	+7.36 -7.36	+3.71 -3.71	+1.26 -1.26

Bins [GeV]	[0,2.5]	[2.5,2.75]	[2.75,3]	[3.3,15]
$1/\sigma dr/dx$ [pb/GeV]	$4.05 \cdot 10^{-2}$	$2.37 \cdot 10^{-1}$	$8.84 \cdot 10^{-1}$	4.12
Total Uncertainty [%]	+0.29 -59.35	+0.02 -23.69	+0.03 -10.01	+7.18 -7.26
Statistics [%]	± 13.99	± 11.23	± 5.41	± 2.16
Systematics [%]	+67.41 -67.44	+20.20 -19.56	+7.36 -7.73	+6.73 -6.83
(FTAG) bTagSF_B_eigen0 [%]	+0.14 -0.33	+0.02 +0.29	+0.07 -0.03	+0.02 -0.05
(FTAG) bTagSF_B_eigen1 [%]	+0.12 -0.28	+0.07 -0.27	+0.03 -0.03	+0.05 -0.05
(FTAG) bTagSF_B_eigen2 [%]	+0.17 -0.13	+0.14 -0.05	+0.03 -0.02	+0.05 -0.03
(FTAG) bTagSF_B_eigen3 [%]	+0.13 -0.13	+0.05 -0.05	+0.02 -0.02	+0.03 -0.03
(FTAG) bTagSF_B_eigen4 [%]	+0.05 -0.05	+0.03 -0.03	- -	+0.01 +0.01
(FTAG) bTagSF_B_eigen5 [%]	- -0.59	- -0.69	- -0.39	- +0.26
(FTAG) bTagSF_C_eigen0 [%]	+0.40 -0.59	+0.73 -0.69	+0.35 -0.35	+0.22 -0.22
(FTAG) bTagSF_C_eigen1 [%]	- -0.13	- -0.08	- -0.17	- +0.08
(FTAG) bTagSF_C_eigen2 [%]	+0.12 -0.12	+0.08 -0.04	+0.16 -0.05	-0.08 -0.03
(FTAG) bTagSF_C_eigen3 [%]	+0.07 -0.11	+0.04 -0.21	+0.05 -0.04	+0.04 -0.05
(FTAG) bTagSF_Light_eigen0 [%]	+0.35 -0.05	+0.19 -0.04	+0.02 -0.02	+0.04 -0.05
(FTAG) bTagSF_Light_eigen1 [%]	+0.05 -0.17	+0.05 -0.03	+0.02 -0.03	+0.03 -0.03
(FTAG) bTagSF_Light_eigen2 [%]	+0.17 -0.16	+0.03 -0.03	+0.03 -0.03	- -
(FTAG) bTagSF_Light_eigen3 [%]	+0.06 -0.06	+0.03 -0.03	+0.03 -0.03	- -
(FTAG) bTagSF_Light_eigen4 [%]	+0.09 -0.05	+0.12 -0.04	-0.07 +0.08	+0.03 +0.03
(FTAG) bTagSF_Light_eigen5 [%]	+0.63 +0.63	-0.12 -0.12	-0.09 -	-0.04 +0.01
(FTAG) bTagSF_Light_eigen6 [%]	+0.15 -0.15	+0.02 -0.02	- -	- -
(FTAG) bTagSF_Light_eigen7 [%]	-0.16 -0.15	+0.08 +0.03	- -	+0.03 +0.01
(FTAG) bTagSF_Light_eigen8 [%]	+0.12 +0.12	+0.03 +0.03	- -	-0.02 -0.02
(FTAG) bTagSF_Light_eigen9 [%]	+0.03 -0.03	+0.03 -0.03	- -	- -
(FTAG) bTagSF_Light_eigen10 [%]	+0.05 -0.05	+0.04 -0.04	+0.02 -0.02	- -
(FTAG) bTagSF_Light_eigen11 [%]	+0.05 -0.05	+0.04 -0.04	+0.02 -0.02	- -
(FTAG) bTagSF_Light_eigen12 [%]	+0.05 -0.05	+0.04 -0.04	+0.02 -0.02	- -
(FTAG) bTagSF_Light_eigen13 [%]	+0.05 -0.05	+0.04 -0.04	+0.02 -0.02	- -
(FTAG) bTagSF_Light_eigen14 [%]	+0.05 -0.05	+0.04 -0.04	+0.02 -0.02	- -
(FTAG) bTagSF_Light_eigen15 [%]	+0.05 -0.05	+0.04 -0.04	+0.02 -0.02	- -
(FTAG) bTagSF_extrapolation [%]	-0.51 +0.53	-0.42 -0.43	-0.11 +0.11	+0.13 -0.14
(FTAG) bTagSF_extrapolation_from_charm [%]	+0.03 -0.03	+0.04 -0.04	+0.02 -0.02	- -
(MET/PU) jvt [%]	+0.07 -0.07	-0.10 +0.11	-0.02 +0.07	- +0.02
Luminosity [%]	+0.12 -0.11	+0.12 -0.12	- -	-0.02 -0.02
(BKG) singletop_tchan [%]	- -	- -	- -	- -
(BKG) singletop_Wt [%]	- -	- -	- -	- -
(BKG) tW [%]	+0.03 -0.03	+0.04 -0.04	+0.02 -0.02	-0.01 +0.01
(BKG) ttZ [%]	+0.06 -0.07	+0.04 -0.08	- -	+0.02 +0.02
(BKG) tH [%]	-0.06 -0.06	+0.02 -0.03	-0.02 -0.02	+0.02 +0.02
(LJES) LARGERJET_Weak_JET_Rtrk_Modelling_Tau32WTA [%]	- +1.64	- +1.50	- +0.59	- +0.15
(LJES) LARGERJET_Weak_JET_Rtrk_Baseline_pT [%]	-0.56 -0.56	+0.31 +0.56	-0.10 +0.17	+0.08 -0.21
(LJES) LARGERJET_Weak_JET_Rtrk_Baseline_mass [%]	+0.87 +0.87	+0.56 +0.56	- -	- -
(LJES) LARGERJET_Weak_JET_Rtrk_BaselineTau32WTA [%]	- -0.53	- -0.53	- -	- -
(JES) JET_21NP_JET_BJES_Response [%]	+0.01 -0.01	+0.05 -0.05	- -	- -
(JES) JET_21NP_JET_Pileup_pTTerm [%]	+0.01 -0.01	+0.03 -0.02	- -	- -
(JES) JET_21NP_JET_OffsetNPV [%]	+0.22 +0.26	+0.05 +0.04	+0.02 +0.02	-0.03 +0.05
(JES) JET_21NP_JET_Pileup_RhoTopology [%]	+0.34 +0.35	+0.04 +0.19	+0.02 -0.02	+0.06 +0.06
(JES) JET_21NP_JET_EffectiveNP_8restTerm [%]	-0.01 -0.01	- -	- -	- -
(LEP) MUON_SAGITTA_RESBIAS [%]	- -	- -	- -	- -
(JES) JET_21NP_JET_EffectiveNP_3 [%]	- -	- -	- -	- -
(JES) JET_21NP_JET_EffectiveNP_4 [%]	- -	- -	- -	- -
(LJES) LARGERJET_Weak_JET_Rtrk_Tracking_mass [%]	-0.35 +0.75	+0.95 +1.03	-0.28 +0.26	+0.06 +0.03
(JES) JET_21NP_JET_Pileup_OffsetMu [%]	- -0.03	- -0.03	- -	- -
(LJES) LARGERJET_Weak_JET_Rtrk_TotalStat_mass [%]	-0.52 -0.52	+0.06 +0.08	-0.01 -0.01	+0.06 +0.06
(JES) JET_21NP_JET_EtaIntercalibration_NonClosure [%]	+0.09 +0.03	+0.05 +0.04	-0.03 +0.03	+0.02 +0.02
(JES) JET_21NP_JET_EtaIntercalibration_TotalStat [%]	+0.03 +0.01	+0.04 +0.02	+0.03 +0.03	+0.02 +0.02
(LEP) EG_RESOLUTION_ALL [%]	-0.01 -0.01	-0.02 -0.02	+0.06 +0.06	-0.02 -0.02
(JES) JET_21NP_JET_Flavor_Response [%]	-0.63 +0.34	+0.12 +0.05	-0.02 +0.01	+0.08 -0.05
(JES) JET_21NP_JET_EffectiveNP_6 [%]	- -	- -	- -	- -
(JES) JET_21NP_JET_EffectiveNP_5 [%]	- -	- -	- -	- -
(JES) JET_21NP_JET_EffectiveNP_4 [%]	+0.77 -0.55	-0.14 +0.28	-0.05 -0.19	-0.07 +0.11
(JES) JET_21NP_JET_SingleParticle_HighPt [%]	- -	- -	- -	- -
(LJES) LARGERJET_Weak_JET_Rtrk_Modelling_pT [%]	- -	- +	- -	- -
(JES) JET_21NP_JET_EffectiveNP_1 [%]	+0.52 -0.54	+0.06 +0.18	-0.05 -0.02	+0.06 +0.06
(LEP) MUON_ID [%]	- -	- -	- -	- -
(LJES) LARGERJET_Weak_JET_Rtrk_TotalStat_pT [%]	- -	- +0.10	- -	- -
(LEP) MUON_SCALE [%]	- -	- -	- -	- -
(LEP) EG_SCALE_ALL [%]	- -	- -	- -	- -
(JES) JET_21NP_JET_EffectiveNP_7 [%]	+0.02 -0.26	+0.02 -0.16	-0.00 +0.16	+0.01 +0.26
(LJES) LARGERJET_Weak_JET_Rtrk_Modelling_mass [%]	+0.71 -0.71	+1.75 -1.75	-0.09 -0.20	- -
(LEP) MUON_MS [%]	- -	- -	- -	- -
(LEP) MUON_SAGITTA_RHO [%]	- -	- -	- -	- -
(JES) JET_21NP_JET_PunchThrough_MC15 [%]	- -	- -	- -	- -
(JES) JET_21NP_JET_EtaIntercalibration_Modelling [%]	+0.13 +0.07	+0.08 +0.08	-0.02 -0.07	-0.02 +0.04
(JES) JET_21NP_JET_EffectiveNP_2 [%]	- -	- -	- -	- -
(LJES) LARGERJET_Weak_JET_Rtrk_Tracking_Tau32WTA [%]	+0.15 -0.15	-0.21 -0.21	- -	- -
(LJES) LARGERJET_Weak_JET_Rtrk_pT [%]	+3.48 +3.48	+3.08 +3.08	+0.26 +0.26	+0.14 +0.14
(JES) LARGERJET_Weak_JET_Rtrk_TotalStat_Tau32WTA [%]	+0.20 -0.12	-0.17 +0.17	-0.04 +0.05	- -
(JES) JET_JER_SINGLE_NP [%]	+0.23 -0.23	+0.05 +0.05	+0.05 +0.05	± 0.02
(LJES) LARGERJET_Weak_JET_Top_massRes_mass [%]	+1.64 -1.64	+2.02 +2.02	± 0.57	± 0.18
(PDF) PDF4LHC15_nlo_30_eigen001 [%]	+0.38 -0.38	± 0.09	± 0.02	± 0.03
(PDF) PDF4LHC15_nlo_30_eigen002 [%]	+0.34 -0.34	± 0.18	± 0.15	± 0.19
(PDF) PDF4LHC15_nlo_30_eigen003 [%]	+1.32 -1.32	± 0.05	± 0.08	± 0.09
(PDF) PDF4LHC15_nlo_30_eigen004 [%]	+0.19 -0.19	± 0.13	± 0.14	± 0.16
(PDF) PDF4LHC15_nlo_30_eigen005 [%]	+1.13 -1.13	± 0.57	± 0.50	± 0.41
(PDF) PDF4LHC15_nlo_30_eigen006 [%]	+0.64 -0.64	± 0.27	± 0.23	± 0.21
(PDF) PDF4LHC15_nlo_30_eigen007 [%]	+0.12 -0.12	± 0.04	± 0.02	-
(PDF) PDF4LHC15_nlo_30_eigen008 [%]	+0.47 -0.47	± 0.20	± 0.18	± 0.17
(PDF) PDF4LHC15_nlo_30_eigen009 [%]	+0.12 -0.12	± 0.06	± 0.05	± 0.05
(PDF) PDF4LHC15_nlo_30_eigen010 [%]	+0.06 -0.06	± 0.08	± 0.06	± 0.05
(PDF) PDF4LHC15_nlo_30_eigen011 [%]	+0.28 -0.28	± 0.11	± 0.10	± 0.09
(PDF) PDF4LHC15_nlo_30_eigen012 [%]	+0.30 -0.30	± 0.07	± 0.10	± 0.09
(PDF) PDF4LHC15_nlo_30_eigen013 [%]	+0.09 -0.09	± 0.04	± 0.02	± 0.03
(PDF) PDF4LHC15_nlo_30_eigen014 [%]	+0.04 -0.04	-	± 0.02	± 0.02
(PDF) PDF4LHC15_nlo_30_eigen015 [%]	- -	± 0.03	± 0.06	± 0.04
(PDF) PDF4LHC15_nlo_30_eigen016 [%]	+0.14 -0.14	-	-	-
(PDF) PDF4LHC15_nlo_30_eigen017 [%]	+0.22 -0.22	± 0.10	± 0.09	± 0.08
(PDF) PDF4LHC15_nlo_30_eigen018 [%]	+0.24 -0.24	± 0.10	± 0.10	± 0.09
(PDF) PDF4LHC15_nlo_30_eigen019 [%]	+0.20 -0.20	± 0.08	± 0.02	± 0.01
(PDF) PDF4LHC15_nlo_30_eigen020 [%]	+0.07 -0.07	± 0.05	± 0.07	± 0.06
(PDF) PDF4LHC15_nlo_30_eigen021 [%]	+0.08 -0.08	± 0.04	± 0.03	± 0.04
(PDF) PDF4LHC15_nlo_30_eigen022 [%]	+1.54 -1.54	± 0.60	± 0.58	± 0.55
(PDF) PDF4LHC15_nlo_30_eigen023 [%]	+0.09 -0.09	± 0.01	-	-
(PDF) PDF4LHC15_nlo_30_eigen024 [%]	+0.10 -0.10	± 0.04	-	± 0.04
(PDF) PDF4LHC15_nlo_30_eigen025 [%]	+0.10 -0.10	-	-	± 0.01
(PDF) PDF4LHC15_nlo_30_eigen026 [%]	+0.10 -0.10	± 0.04	± 0.03	± 0.01
(PDF) PDF4LHC15_nlo_30_eigen027 [%]	+0.08 -0.08	± 0.04	± 0.07	± 0.04
(PDF) PDF4LHC15_nlo_30_eigen028 [%]	+0.37 -0.37	± 0.16	± 0.15	± 0.10
(PDF) PDF4LHC15_nlo_30_eigen029 [%]	+0.01 -0.01	-	-	-
(PDF) PDF4LHC15_nlo_30_eigen030 [%]	+0.02 -0.02	-	± 0.02	-
(MOD) Alternative hard-scattering model [%]	+65.92 -65.92	± 15.22	± 6.35	± 6.38
(MOD) Alternative parton-shower mode [%]	+13.20 -13.20	± 11.08	± 2.97	± 1.82
(MOD) ISR/FSR + scale [%]	+0.69 -0.69	± 2.81	± 1.60	± 0.13
(MOD) Monte Carlo sample statistics [%]	+8.04 -8.04	± 7.25	± 3.34	± 1.23

Not reviewed, for internal circulation only

Bins [GeV]	[0,0.2]	[0.2,0.4]	[0.4,0.6]	[0.6,0.7]	[0.7,0.8]	[0.8,1]
$d\sigma/dX$ [pb/GeV]	1.09	1.08	9.68... +32.64	$8.89 \cdot 10^{-1}$ +33.27	$5.05 \cdot 10^{-1}$ +33.47	$1.19 \cdot 10^{-1}$ +34.58
Total Uncertainty [%]	+31.31	+31.61	+37.88 +34.43	+34.17 +34.60	+34.17 +34.32	+33.81 +32.32
Statistics [%]	+4.43	+4.60	+2.06	+2.06	+1.72	+1.75
Systematics [%]	+31.15	+30.69	+31.14	+31.34	+31.38	+38.89
(FTAG) bTagSF_B_eigen0 [%]	-	-	-	-	-	-
(FTAG) bTagSF_B_eigen1 [%]	-	-	-	-	-	-
(FTAG) bTagSF_B_eigen2 [%]	-	-	-	-	-	-
(FTAG) bTagSF_B_eigen3 [%]	-	-	-	-	-	-
(FTAG) bTagSF_B_eigen4 [%]	-	-	-	-	-	-
(FTAG) bTagSF_B_eigen5 [%]	-	-	-	-	-	-
(FTAG) bTagSF_C_eigen0 [%]	-	-	-	-	-	-
(FTAG) bTagSF_C_eigen1 [%]	-	-	-	-	-	-
(FTAG) bTagSF_C_eigen2 [%]	-	-	-	-	-	-
(FTAG) bTagSF_C_eigen3 [%]	-	-	-	-	-	-
(FTAG) bTagSF_Light_eigen0 [%]	-	-	-	-	-	-
(FTAG) bTagSF_Light_eigen1 [%]	-	-	-	-	-	-
(FTAG) bTagSF_Light_eigen2 [%]	-	-	-	-	-	-
(FTAG) bTagSF_Light_eigen3 [%]	-	-	-	-	-	-
(FTAG) bTagSF_Light_eigen4 [%]	-	-	-	-	-	-
(FTAG) bTagSF_Light_eigen5 [%]	-	-	-	-	-	-
(FTAG) bTagSF_Light_eigen6 [%]	-	-	-	-	-	-
(FTAG) bTagSF_Light_eigen7 [%]	-	-	-	-	-	-
(FTAG) bTagSF_Light_eigen8 [%]	-	-	-	-	-	-
(FTAG) bTagSF_Light_eigen9 [%]	-	-	-	-	-	-
(FTAG) bTagSF_Light_eigen10 [%]	-	-	-	-	-	-
(FTAG) bTagSF_Light_eigen11 [%]	-	-	-	-	-	-
(FTAG) bTagSF_Light_eigen12 [%]	-	-	-	-	-	-
(FTAG) bTagSF_Light_eigen13 [%]	-	-	-	-	-	-
(FTAG) bTagSF_Light_eigen14 [%]	-	-	-	-	-	-
(FTAG) bTagSF_Light_eigen15 [%]	-	-	-	-	-	-
(FTAG) bTagSF_extrapolation [%]	-	-	-	-	-	-
(FTAG) bTagSF_extrapolation_from_charm [%]	-	-	-	-	-	-
(MET/PU) jvt [%]	+0.13	+0.05	+0.02	-0.03	-0.03	+0.16
Luminosity [%]	+0.16	+0.09	+0.99	-0.98	-	-0.20
(BKG) singletop_tchan [%]	-2.02	+1.98	+1.98	+2.06	+2.01	+1.90
(BKG) singletop_Wt [%]	-	-	-	-	-	-
(BKG) rW [%]	-0.04	+0.04	+0.04	+0.02	+0.02	+0.02
(BKG) tZ [%]	-0.04	+0.04	+0.04	+0.02	+0.02	+0.02
(BKG) tH [%]	-0.04	+0.04	+0.04	+0.02	+0.02	+0.02
(LJES) LARGERJET_Weak_JET_Rtrk_Modelling_Tau32WTA [%]	+0.34	+0.20	+0.20	+0.42	+0.89	+13.47
(LJES) LARGERJET_Weak_JET_Rtrk_Baseline_pT [%]	-0.33	+0.21	+0.23	+0.35	+0.38	+0.37
(LJES) LARGERJET_Weak_JET_Rtrk_Baseline_mass [%]	-0.05	+0.07	+0.03	+2.80	+3.11	+2.83
(LJES) LARGERJET_Weak_JET_Rtrk_Baseline_Tau32WTA [%]	-3.14	-3.04	-2.80	-3.01	-3.03	-2.73
(JES) JET_21NP_JET_BJES_Response [%]	-	-	-	-	-	-
(JES) JET_21NP_JET_Pileup_PTerm [%]	+0.02	-0.02	+0.02	+0.03	+0.05	+0.08
(JES) JET_21NP_JET_Pileup_OffsetNPV [%]	+0.05	+0.03	+0.03	+0.05	+0.05	+0.08
(JES) JET_21NP_JET_Pileup_RhoTopology [%]	+0.22	+0.19	+0.19	+0.10	+0.25	+0.04
(JES) JET_21NP_JET_EffectiveNP_SrestTerm [%]	-0.09	-0.11	-0.05	-0.24	-0.09	-0.10
(LEP) MUON_SAGITTA_RESBIA [%]	-	-	-	-	-	-
(JES) JET_21NP_JET_EffectiveNP_3 [%]	+0.02	+0.01	-	+0.01	+0.01	+0.01
(JES) JET_21NP_JET_EffectiveNP_4 [%]	-	-	-0.03	-0.02	-0.01	-
(LJES) LARGERJET_Weak_JET_Rtrk_Tracking_mass [%]	+0.14	-0.05	+0.42	+0.06	-0.12	+0.46
(JES) JET_21NP_JET_Pileup_OffsetMu [%]	-0.22	+0.04	+0.09	+0.18	+0.15	+0.86
(LJES) LARGERJET_Weak_JET_Rtrk_TotalStat_mass [%]	-0.03	-0.06	-0.15	+0.02	+0.03	-0.16
(JES) JET_21NP_JET_EtaInCalibration_NonClosure [%]	+0.04	+0.06	+0.18	-0.19	+0.16	-
(JES) JET_21NP_JET_EtaInCalibration_TotalStat [%]	+0.01	-	+0.02	+0.01	+0.02	-
(LEP) EG_RESOLUTION_ALL [%]	-0.02	-	-0.01	-0.01	-0.01	-0.02
(JES) JET_21NP_JET_Flavor_Response [%]	-0.01	-0.05	-0.06	-0.20	-0.05	-0.07
(JES) JET_21NP_JET_EffectiveNP_6 [%]	+0.08	+0.07	+0.05	+0.04	+0.10	+0.02
(JES) JET_21NP_JET_EffectiveNP_5 [%]	-	-	-	-0.02	-	-
(JES) JET_21NP_JET_Flavor_Composition [%]	+0.35	+0.19	+0.29	+0.26	+0.35	+0.15
(JES) JET_21NP_JET_SingleParticle_HighPt [%]	-0.19	-0.19	-0.08	-0.28	-0.15	-
(LJES) LARGERJET_Weak_JET_Rtrk_Modelling_pT [%]	+2.39	+0.52	+0.23	+2.87	+1.95	+2.04
(JES) JET_21NP_JET_EffectiveNP_1 [%]	+0.12	+0.07	+0.07	+0.07	+0.10	-0.09
(LEP) MUON_ID [%]	-0.02	-0.10	-0.17	-0.17	-0.03	-0.08
(LJES) LARGERJET_Weak_JET_Rtrk_TotalStat_pT [%]	+0.40	+0.30	+0.17	+0.57	+0.11	+0.51
(LEP) MUON_SCALE [%]	-0.14	-0.29	-0.38	-0.10	-0.32	-0.20
(LEP) EG_SCALE_ALL [%]	-	-	-	-	-	-
(JES) JET_21NP_JET_EffectiveNP_7 [%]	+0.01	-0.04	+0.05	-	-0.01	-
(LJES) LARGERJET_Weak_JET_Rtrk_Modelling_mass [%]	+0.03	+0.15	+1.01	+0.04	+0.49	-0.20
(LEP) MUON_MS [%]	-0.73	-0.90	-0.30	+0.12	+1.04	+0.14
(LEP) MUON_SAGITTA_rho [%]	-	-	-	-	-	-
(JES) JET_21NP_JET_PtThrough_MC15 [%]	-0.05	+0.02	+0.05	-	-	-0.05
(JES) JET_21NP_JET_EtaInCalibration_Modelling [%]	-0.02	-0.03	-0.05	-0.04	+0.02	-0.03
(JES) JET_21NP_JET_EffectiveNP_2 [%]	-0.03	-0.04	-0.05	-0.04	-0.07	-0.05
(LJES) LARGERJET_Weak_JET_Rtrk_Tracking [%]	-0.03	-0.40	-0.32	-0.32	-0.42	-0.10
(LJES) LARGERJET_Weak_JET_Rtrk_Tracking_Tau32WTA [%]	+0.47	+0.49	+0.29	-0.29	+0.20	+0.83
(LJES) LARGERJET_Weak_JET_Rtrk_Tracking_pT [%]	+5.30	+3.14	+5.01	+5.07	+4.09	+5.83
(JES) JET_21NP_JET_EffectiveNP_3 [%]	-0.17	-0.18	-0.14	-0.13	-0.15	-0.10
(JES) JET_JER_SINGLE_NP [%]	+0.23	+0.08	+0.31	+0.03	+0.08	+0.08
(LJES) LARGERJET_Weak_JET_Rtrk_Top_maxRes_mass [%]	+1.55	+1.08	+0.81	+1.68	+1.85	+3.45
(PDF) PDF4LHC15_nlo_30_eigen001 [%]	+0.09	+0.08	+0.01	+0.10	-	-
(PDF) PDF4LHC15_nlo_30_eigen002 [%]	+0.17	+0.17	+0.21	+0.18	+0.28	+0.53
(PDF) PDF4LHC15_nlo_30_eigen003 [%]	+0.12	+0.08	+0.11	+0.11	+0.19	+0.29
(PDF) PDF4LHC15_nlo_30_eigen004 [%]	+0.06	+0.13	+0.17	+0.29	+0.37	+0.92
(PDF) PDF4LHC15_nlo_30_eigen005 [%]	+0.49	+0.47	+0.48	+0.52	+0.58	+0.96
(PDF) PDF4LHC15_nlo_30_eigen006 [%]	+0.20	+0.21	+0.26	+0.34	+0.38	+0.76
(PDF) PDF4LHC15_nlo_30_eigen007 [%]	-	+0.02	+0.02	+0.05	+0.05	+0.12
(PDF) PDF4LHC15_nlo_30_eigen008 [%]	+0.16	+0.16	+0.19	+0.22	+0.33	+0.55
(PDF) PDF4LHC15_nlo_30_eigen009 [%]	+0.05	+0.05	+0.05	+0.07	+0.07	+0.15
(PDF) PDF4LHC15_nlo_30_eigen010 [%]	+0.03	+0.05	+0.06	+0.07	+0.09	+0.11
(PDF) PDF4LHC15_nlo_30_eigen011 [%]	+0.09	+0.09	+0.10	+0.12	+0.16	+0.30
(PDF) PDF4LHC15_nlo_30_eigen012 [%]	+0.06	+0.07	+0.09	+0.10	+0.16	+0.27
(PDF) PDF4LHC15_nlo_30_eigen013 [%]	+0.02	+0.03	+0.03	+0.04	+0.05	+0.08
(PDF) PDF4LHC15_nlo_30_eigen014 [%]	-	+0.01	+0.02	+0.03	+0.05	+0.13
(PDF) PDF4LHC15_nlo_30_eigen015 [%]	+0.02	+0.03	+0.05	+0.02	+0.10	+0.12
(PDF) PDF4LHC15_nlo_30_eigen016 [%]	+0.04	+0.02	-	+0.02	+0.03	+0.18
(PDF) PDF4LHC15_nlo_30_eigen017 [%]	+0.07	+0.09	+0.10	+0.13	+0.16	+0.33
(PDF) PDF4LHC15_nlo_30_eigen018 [%]	+0.06	+0.07	+0.10	+0.16	+0.21	+0.47
(PDF) PDF4LHC15_nlo_30_eigen019 [%]	+0.06	+0.04	+0.04	+0.03	+0.05	+0.46
(PDF) PDF4LHC15_nlo_30_eigen020 [%]	+0.06	+0.07	+0.06	+0.06	+0.07	+0.05
(PDF) PDF4LHC15_nlo_30_eigen021 [%]	+0.03	+0.03	+0.05	+0.03	+0.08	+0.17
(PDF) PDF4LHC15_nlo_30_eigen022 [%]	+0.54	+0.52	+0.63	+0.75	+1.03	+1.86
(PDF) PDF4LHC15_nlo_30_eigen023 [%]	+0.02	-	-	-	+0.01	+0.04
(PDF) PDF4LHC15_nlo_30_eigen024 [%]	+0.06	+0.04	+0.05	+0.04	+0.05	+0.07
(PDF) PDF4LHC15_nlo_30_eigen025 [%]	+0.03	-	+0.02	+0.02	+0.03	+0.02
(PDF) PDF4LHC15_nlo_30_eigen026 [%]	+0.04	+0.02	+0.02	-	-	+0.05
(PDF) PDF4LHC15_nlo_30_eigen027 [%]	+0.04	+0.04	+0.04	+0.03	+0.05	+0.04
(PDF) PDF4LHC15_nlo_30_eigen028 [%]	+0.15	+0.14	+0.13	+0.14	+0.13	+0.09
(PDF) PDF4LHC15_nlo_30_eigen029 [%]	-	-	-	+0.02	-	-
(PDF) PDF4LHC15_nlo_30_eigen030 [%]	-	+0.01	-	+0.04	+0.02	+0.06
(MOD) Alternative hard-scattering model [%]	+9.80	+11.01	+13.50	+13.07	+15.31	+24.23
(MOD) Alternative parton-shower mode [%]	+20.87	+18.55	+20.53	+18.70	+19.34	+21.33
(MOD) ISR/FSR + scale [%]	+2.34	+1.12	+1.49	+0.74	+1.12	+0.29
(MOD) Monte Carlo sample statistics [%]	+2.26	+2.36	+2.39	+5.15	+6.22	+9.92

Table 156: The individual systematic uncertainties in the parton level fiducial phase-space absolute differential cross-sections for the $|\cos \theta^*|$ calculated as a percentage of the cross-section.

Not reviewed, for internal circulation only

Bins [GeV]	[0,0.2]	[0.2,0.4]	[0.4,0.6]	[0.6,0.7]	[0.7,0.8]	[0.8,1]
$1/\text{order}/dX$ [pb/GeV]	1.38	1.37	1.22	$6.38 \cdot 10^{-1}$	$1.51 \cdot 10^{-1}$	
Total Uncertainty [%]	+5.30 -5.30	+5.18 -5.25	+5.66 -5.51	+10.23 -10.28	+13.45 -13.53	+24.88 -24.77
Statistics [%]	± 3.71	± 4.05	± 4.41	± 4.28	± 11.07	± 17.30
Systematics [%]	+3.22 -3.28	+2.46 -2.60	+2.73 -2.43	+3.51 -3.50	+4.61 -4.85	+4.99 -4.81
(FTAG) bTagSF_B_eigen0 [%]	-0.13	-	-0.13	+0.09	-0.13	-
(FTAG) bTagSF_B_eigen1 [%]	-0.08	-	-0.15	-0.03	+0.14	+0.02
(FTAG) bTagSF_B_eigen2 [%]	-0.03	-	-0.11	-0.10	+0.05	+0.04
(FTAG) bTagSF_B_eigen3 [%]	-0.03	-	-0.05	-0.04	-0.03	+0.03
(FTAG) bTagSF_B_eigen4 [%]	-0.04	-	-0.04	-0.01	-	+0.03
(FTAG) bTagSF_B_eigen5 [%]	-0.01	-	-0.04	+0.01	-0.01	+0.03
(FTAG) bTagSF_C_eigen0 [%]	-0.13	-0.35	+0.68	-0.85	+0.83	+0.05
(FTAG) bTagSF_C_eigen1 [%]	-0.08	-0.26	+0.41	-0.49	+0.50	-0.09
(FTAG) bTagSF_C_eigen2 [%]	-0.01	-0.05	+0.13	-0.25	+0.19	-0.10
(FTAG) bTagSF_C_eigen3 [%]	-0.01	-0.01	-0.03	-0.09	-0.07	-0.02
(FTAG) bTagSF_Light_eigen0 [%]	-0.03	+0.01	-0.05	+0.09	+0.04	+0.05
(FTAG) bTagSF_Light_eigen1 [%]	+0.07	-0.01	-0.02	+0.03	-0.05	+0.04
(FTAG) bTagSF_Light_eigen2 [%]	+0.03	-0.02	-0.04	+0.03	-0.02	-0.07
(FTAG) bTagSF_Light_eigen3 [%]	+0.02	+0.05	-0.03	-0.04	-0.02	+0.05
(FTAG) bTagSF_Light_eigen4 [%]	+0.05	-0.07	-0.03	-0.15	-0.03	-0.03
(FTAG) bTagSF_Light_eigen5 [%]	-0.02	-0.02	-0.04	-0.03	-0.03	-0.04
(FTAG) bTagSF_Light_eigen6 [%]	-	-	-0.05	-	-0.01	+0.05
(FTAG) bTagSF_Light_eigen7 [%]	-0.02	-0.02	-	-0.05	-0.01	+0.02
(FTAG) bTagSF_Light_eigen8 [%]	-0.02	-0.02	-0.03	-0.04	-0.02	+0.05
(FTAG) bTagSF_Light_eigen9 [%]	-0.04	+0.02	-	+0.04	-0.02	+0.03
(FTAG) bTagSF_Light_eigen10 [%]	-	-0.03	+0.02	+0.05	-	-0.03
(FTAG) bTagSF_Light_eigen11 [%]	-	-0.03	-0.03	-0.05	-	+0.03
(FTAG) bTagSF_Light_eigen12 [%]	-	-0.03	-0.03	-0.05	-	+0.03
(FTAG) bTagSF_Light_eigen13 [%]	-	-0.03	-0.02	-0.05	-	+0.03
(FTAG) bTagSF_Light_eigen14 [%]	-	-0.03	-0.02	-0.05	-	+0.03
(FTAG) bTagSF_Light_eigen15 [%]	-	-0.03	-0.02	-0.05	-	+0.03
(FTAG) bTagSF_extrapolation [%]	+0.15	+0.04	-0.20	+0.10	-0.17	-0.27
(FTAG) bTagSF_extrapolation_from_charm [%]	-	-0.15	-0.14	-0.21	-0.14	+0.27
(MET/PU) jvt [%]	-0.05 +0.02 -0.02	-0.02 +0.02 -0.02	-0.03 -0.02 -0.02	-0.04 -0.02 -0.06	-0.07 -0.05 -0.01	+0.09 -0.09 -0.01
Luminosity [%]	-	-	-	-	-	-
(BKG) singletop_tchan [%]	-	-	-	-	-	-
(BKG) singletop_Wt [%]	-	-	-	-	-	-
(BKG) tW [%]	-	-	-	-0.02	-0.02	-0.02
(BKG) tZ [%]	-	-	-	-0.01	+0.01	+0.01
(BKG) tH [%]	-	-	-	-0.01	-	-
(LJES) LARGERJET_Weak_JET_Rtrk_Modelling_Tau32WTA [%]	-	-	-	-0.01	-	-
(LJES) LARGERJET_Weak_JET_Rtrk_Baseline_pT [%]	+0.12	+0.16	+0.05	+0.14	-0.41	-0.25
(LJES) LARGERJET_Weak_JET_Rtrk_Baseline_mass [%]	-	-	-	-	-	-
(LJES) LARGERJET_Weak_JET_Rtrk_Baseline_Tau32WTA [%]	+0.03	-0.63	+0.83	-0.72	+1.17	-1.35
(JES) JET_21NP_JET_BJES_Response [%]	-0.51	+0.59	-0.42	-0.18	-0.60	+1.78
(JES) JET_21NP_JET_Pileup_PtTerm [%]	-	-0.02	-	-0.02	-	+0.01
(JES) JET_21NP_JET_Pileup_OffsetNPV [%]	+0.02	-	-	-0.07	+0.05	+0.01
(JES) JET_21NP_JET_Pileup_RhoTopology [%]	-0.03	-0.04	-	-0.14	-0.03	-0.04
(JES) JET_21NP_JET_EffectiveN3stTerm [%]	-	-	-	-	-	-
(LEP) MUON_SAGITTA_RESBIAS [%]	-	-	-	-	-	-
(JES) JET_21NP_JET_EffectiveN3 [%]	-	-	-	-	-	-
(JES) JET_21NP_JET_EffectiveN4 [%]	-	-	-	-	-	-
(LJES) LARGERJET_Weak_JET_Rtrk_Tracking_mass [%]	+0.01 -0.25	-0.15 -0.01	+0.30 +0.09	-0.06 -0.15	-0.24 +0.44	-0.58 +0.83
(JES) JET_21NP_JET_Pileup_OffsetMu [%]	-0.01	+0.01	-0.01	+0.01	-0.01	-0.01
(LJES) LARGERJET_Weak_JET_Rtrk_TotalStat_mass [%]	-0.03	-0.03	-0.12	-0.14	+0.09	-0.07
(JES) JET_21NP_JET_Extralocalibration_NonClosure [%]	+0.03	-0.02	+0.02	-0.13	+0.03	+0.04
(JES) JET_21NP_JET_Extralocalibration_TotalStat [%]	-	-	-	-0.01	-	-0.06
(LEP) EG_RESOLUTION_ALL [%]	-0.01	-0.02	+0.01	-0.02	-0.01	-0.01
(JES) JET_21NP_JET_Flavor_Response [%]	+0.02	-	-0.02	-0.07	-	-
(JES) JET_21NP_JET_EffectiveN6 [%]	-	-	-	-	-	-
(JES) JET_21NP_JET_EffectiveNP_5 [%]	-	-	-	-0.01	-	-
(JES) JET_21NP_JET_Flavor_Composition [%]	-0.05	+0.04	+0.04	+0.01	+0.10	-0.13
(JES) JET_21NP_JET_SingleParticle_HighPt [%]	-0.02	-0.09	-0.13	-0.02	+0.02	+0.02
(LJES) LARGERJET_Weak_JET_Rtrk_Modelling_pT [%]	-0.02 +0.03	+0.14 -0.26	-0.20 -0.48	+0.45 -0.03	-0.45 +0.03	-0.35 +0.05
(JES) JET_21NP_JET_EffectiveN1 [%]	-	-	-	-0.01	-	-
(LEP) MUON_ID [%]	-0.01	-	-	-	-	-
(LJES) LARGERJET_Weak_JET_Rtrk_TotalStat_pT [%]	+0.09	+0.05	-0.02	+0.18	-0.05	+0.15
(LEP) MUON_SCALE [%]	-	-	-	-	-	-
(JES) EG_SCALE_ALL [%]	-	-	-0.04	-	-	-
(JES) JET_21NP_JET_EffectiveNP_7 [%]	+0.02	-0.04	+0.02	-	+0.01	-
(JES) LARGERJET_Weak_JET_Rtrk_Modelling_mass [%]	-	-	-0.01	-	-	-
(LEP) MUON_MS [%]	-	-	-	-	-	-
(LEP) MUON_SAGITTA_RHO [%]	-	-	-	-	-	-
(JES) JET_21NP_JET_PunchThrough_MC15 [%]	-	-	-	-	-	-
(JES) JET_21NP_JET_Extralocalibration_Modelling [%]	+0.01	-0.01	+0.02	-0.03	-0.02	-0.08
(JES) JET_21NP_JET_EffectiveP2 [%]	-0.01	-0.01	+0.03	-	+0.03	+0.05
(LJES) LARGERJET_Weak_JET_Rtrk_Tracking_Tau32WTA [%]	-0.13	-	+0.09	+0.09	-	+0.31
(JES) LARGERJET_Weak_JET_Rtrk_Tracking_pT [%]	-0.03	+0.03	-0.08	+0.14	-0.97	-0.69
(JES) LARGERJET_Weak_JET_Rtrk_TotalStat_Tau32WTA [%]	-0.01	-0.08	+0.11	+0.05	-0.40	+0.70
(JES) JET_JER_SINGLE_NP [%]	+0.12	+0.20	+0.19	+0.15	+0.19	+0.04
(LJES) LARGERJET_Weak_JET_Top_massRes_mass [%]	+0.23	+0.24	+0.52	+0.37	+0.54	+2.16
(PDF) PDF4LHC15_nlo_30_eigen001 [%]	+0.09	+0.08	+0.05	+0.10	-	-
(PDF) PDF4LHC15_nlo_30_eigen002 [%]	+0.17	+0.17	+0.21	+0.18	+0.28	+0.53
(PDF) PDF4LHC15_nlo_30_eigen003 [%]	+0.12	+0.08	+0.11	+0.11	+0.19	+0.29
(PDF) PDF4LHC15_nlo_30_eigen004 [%]	+0.06	+0.13	+0.17	+0.29	+0.37	+0.92
(PDF) PDF4LHC15_nlo_30_eigen005 [%]	+0.49	+0.47	+0.48	+0.52	+0.58	+0.96
(PDF) PDF4LHC15_nlo_30_eigen006 [%]	+0.20	+0.21	+0.26	+0.34	+0.38	+0.76
(PDF) PDF4LHC15_nlo_30_eigen007 [%]	-	+0.02	+0.02	+0.05	+0.05	+0.12
(PDF) PDF4LHC15_nlo_30_eigen008 [%]	+0.16	+0.16	+0.19	+0.22	+0.33	+0.55
(PDF) PDF4LHC15_nlo_30_eigen009 [%]	+0.05	+0.05	+0.05	+0.07	+0.07	+0.15
(PDF) PDF4LHC15_nlo_30_eigen010 [%]	+0.03	+0.05	+0.06	+0.07	+0.09	+0.11
(PDF) PDF4LHC15_nlo_30_eigen011 [%]	+0.09	+0.09	+0.10	+0.12	+0.16	+0.30
(PDF) PDF4LHC15_nlo_30_eigen012 [%]	+0.06	+0.07	+0.09	+0.10	+0.16	+0.27
(PDF) PDF4LHC15_nlo_30_eigen013 [%]	+0.02	+0.03	+0.03	+0.04	+0.05	+0.08
(PDF) PDF4LHC15_nlo_30_eigen014 [%]	-	+0.01	+0.02	+0.03	+0.05	+0.13
(PDF) PDF4LHC15_nlo_30_eigen015 [%]	+0.02	+0.03	+0.05	+0.02	+0.10	+0.12
(PDF) PDF4LHC15_nlo_30_eigen016 [%]	+0.04	+0.02	-	+0.03	+0.03	+0.18
(PDF) PDF4LHC15_nlo_30_eigen017 [%]	+0.07	+0.09	+0.10	+0.13	+0.16	+0.23
(PDF) PDF4LHC15_nlo_30_eigen018 [%]	+0.06	+0.07	+0.10	+0.16	+0.21	+0.47
(PDF) PDF4LHC15_nlo_30_eigen019 [%]	+0.06	+0.04	+0.01	+0.05	+0.16	+0.46
(PDF) PDF4LHC15_nlo_30_eigen020 [%]	+0.06	+0.07	+0.06	+0.06	+0.07	+0.05
(PDF) PDF4LHC15_nlo_30_eigen021 [%]	+0.03	+0.03	+0.05	+0.03	+0.08	+0.17
(PDF) PDF4LHC15_nlo_30_eigen022 [%]	+0.54	+0.52	+0.63	+0.75	+1.03	+1.86
(PDF) PDF4LHC15_nlo_30_eigen023 [%]	+0.02	-	-	-	+0.01	+0.04
(PDF) PDF4LHC15_nlo_30_eigen024 [%]	+0.06	+0.04	+0.05	+0.04	+0.05	+0.07
(PDF) PDF4LHC15_nlo_30_eigen025 [%]	+0.03	-	+0.02	+0.02	+0.03	+0.02
(PDF) PDF4LHC15_nlo_30_eigen026 [%]	+0.04	+0.02	+0.02	-	-	+0.05
(PDF) PDF4LHC15_nlo_30_eigen027 [%]	+0.04	+0.04	+0.04	+0.03	+0.05	+0.04
(PDF) PDF4LHC15_nlo_30_eigen028 [%]	+0.15	+0.14	+0.13	+0.14	+0.13	+0.09
(PDF) PDF4LHC15_nlo_30_eigen029 [%]	-	-	-	+0.02	-	-
(PDF) PDF4LHC15_nlo_30_eigen030 [%]	-	+0.01	-	+0.04	+0.02	+0.06
(MOD) Alternative hard-scattering model [%]	+2.60	+1.22	+1.60	+1.12	+3.67	+13.81
(MOD) Alternative parton-shower mode [%]	+1.26	+1.63	+0.83	+1.46	+0.65	+1.82
(MOD) ISR/FSR & scale [%]	+0.98	+0.25	+0.10	+2.17	+0.26	+1.63
(MOD) Monte Carlo sample statistics [%]	+1.90	+2.09	+2.23	+4.97	+6.08	+9.75

Table 157: The individual systematic uncertainties in the parton level fiducial phase-space relative differential cross-sections for the $|\cos\theta^*|$ calculated as a percentage of the cross-section.

956 H. Uncertainties at detector level

957 H.1. Detector fractional uncertainties

958 To show visually the impact of the systematics for each observable, we grouped the systematics in broad
 959 groups and plotted their relative impact compared to the nominal prediction. The groups are defined as
 960 follows:

961 **Large- R Jet Energy Scale** Baseline mass and pT calibration, modelling mass and pT calibration, track-
 962 ing mass and pT calibration, total statistics mass and pT calibration;

963 **Large- R Jet Tagging** Baseline sub-jettiness ratio τ_3/τ_2 calibration, modelling sub-jettiness ratio τ_3/τ_2
 964 calibration, tracking sub-jettiness ratio τ_3/τ_2 calibration, total statistics sub-jettiness ratio τ_3/τ_2
 965 calibration;

966 **Narrow Jet Energy Scale** b-Tagged jet energy scale, η intercalibration model, Flavor composition, Fla-
 967 vor response, Effective detector, Effective mixed, Effective model, Effective stat., Jet energy resol-
 968 ution, Punch-through, Single particle high- p_T , Pile-up offset ρ topology, Pile-up offset p_T ;

969 **Pileup** E_T^{miss} Soft Jet Scale, E_T^{miss} Soft Jet Resolution, Jet reconstruction efficiency, Jet vertex fraction,
 970 Pile-up offset μ , Pile-up offset N_{PV} ;

971 **Flavour tagging** b -Tagging efficiency, c -tagging efficiency, light-flavors tagging efficiency;

972 **Leptons** Muon (ID) momentum resolution, Muon momentum scale, Muon (MS) momentum resolution,
 973 Electron energy scale, Electron energy resolution.

974 **H.2. Tables of detector systematic uncertainties**

[Not reviewed, for internal circulation only]

Bins	-0.5–0.5
Statistics [%]	± 0.6
Systematics [%]	± 12.0
Total Uncertainty [%]	± 12.7
(LJES) Large- R jet Modelling τ_{32} [%]	± 7.03 $+7.97$
Light-jet tagging efficiency (eigenvector 10) [%]	-
Light-jet tagging efficiency (eigenvector 13) [%]	-
Light-jet tagging efficiency (eigenvector 12) [%]	-
Single top t -channel treatment [%]	± 0.19
Light-jet tagging efficiency (eigenvector 0) [%]	-0.20 $+0.20$
(JES) Flavour response [%]	-
b -Quark tagging extrapolation [%]	± 2.28 -2.24
Electron energy resolution [%]	-
b -Quark tagging efficiency (eigenvector 0) [%]	-3.87 $+3.97$
QCD data-driven background shape [%]	-
Pile-up [%]	-0.41 $+0.44$
E_T^{miss} Soft jet resolution para [%]	-
(JES) η intercalibration non-closure [%]	-
b -Quark tagging efficiency (eigenvector 1) [%]	-3.60 $+3.68$
Muon (MS) momentum resolution [%]	-
b -Quark tagging efficiency (eigenvector 4) [%]	-0.18 $+0.18$
(JES) b -Tagged jet energy scale [%]	-
Single top Wt cross-section [%]	-
E_T^{miss} Soft jet scale [%]	-
(JES) η intercalibration model [%]	-
Electron energy scale [%]	-
(JES) Effective detector NP set 7 [%]	-
Jet vertex tagging [%]	-
Light-jet tagging efficiency (eigenvector 9) [%]	-0.19
Light-jet tagging efficiency (eigenvector 8) [%]	-0.19
(LJES) Large- R jet top-quark mass resolution [%]	∓ 1.00
(JES) Effective detector NP set 8 (restTerm) [%]	-
Light-jet tagging efficiency (eigenvector 1) [%]	-
(LJES) Large- R jet Baseline p_T [%]	$+1.88$ -1.66
Light-jet tagging efficiency (eigenvector 3) [%]	-
Light-jet tagging efficiency (eigenvector 2) [%]	-
(JES) Effective detector NP set 6 [%]	-
(LJES) Large- R jet TotalStat p_T [%]	$+0.25$ -0.19
Light-jet tagging efficiency (eigenvector 7) [%]	-
Muon sagitta ho [%]	-
(JES) Pile-up offset N_{PV} [%]	-
c -Quark tagging efficiency (eigenvector 2) [%]	-0.45
c -Quark tagging efficiency (eigenvector 3) [%]	-0.35
c -Quark tagging efficiency (eigenvector 0) [%]	-1.32 $+1.54$
c -Quark tagging efficiency (eigenvector 1) [%]	-1.06 $+0.89$ -0.92
(LJES) Large- R jet TotalStat τ_{32} [%]	± 0.13
b -Quark tagging efficiency (eigenvector 3) [%]	-0.38 $+0.39$
E_T^{miss} Soft jet resolution perp [%]	-
(JES) Effective detector NP set 2 [%]	-
b -Quark tagging extrapolation from c -Quark [%]	-
(LJES) Large- R jet Tracking p_T [%]	$+3.94$ -3.72
(JES) Effective detector NP set 3 [%]	-
(LJES) Large- R jet TotalStat mass [%]	-
(JES) Effective detector NP set 5 [%]	-
(LJES) Large- R jet Baseline mass [%]	$+0.39$ -0.39
Muon energy scale [%]	-
(JES) Pile-up offset p_T [%]	-
(LJES) Large- R jet Modelling mass [%]	$+0.30$ -0.39
(JES) Effective detector NP set 1 [%]	-
(LJES) Large- R jet Baseline τ_{32} [%]	-5.64 $+6.21$
(JES) Single particle high- p_T [%]	-
Light-jet tagging efficiency (eigenvector 5) [%]	-
(JES) Pile-up offset ρ topology [%]	$+0.15$
(LJES) Large- R jet Modelling p_T [%]	$+1.87$ -1.63
(JES) η intercalibration total stat [%]	-
Light-jet tagging efficiency (eigenvector 4) [%]	-
Muon (ID) momentum resolution [%]	-
(JES) Flavour composition [%]	$+0.19$ -0.13
(JES) Effective detector NP set 4 [%]	-
Light-jet tagging efficiency (eigenvector 11) [%]	-
(LJES) Large- R jet Tracking τ_{32} [%]	-0.30 $+0.28$
(LJES) Large- R jet Tracking mass [%]	-
Light-jet tagging efficiency (eigenvector 6) [%]	-
(JES) Pile-up offset μ [%]	-
b -Quark tagging efficiency (eigenvector 2) [%]	-0.56 $+0.57$
(JES) Punch-through [%]	-
Muon sagitta resolution bias [%]	-

Not reviewed, for internal circulation only

Table 158: The individual systematic uncertainties in the inclusive cross-section measurement calculated as a percentage. Dashes are used when the estimated relative systematic uncertainty for that bin is below 0.1%.

Not reviewed, for internal circulation only

Bins [GeV]	500.0–550.0	550.0–600.0	600.0–650.0	650.0–700.0	700.0–750.0	750.0–800.0	800.0–1000.0	1000.0–1200.0
Statistics [%]	+1.0	+1.2	+1.30	+2.0	+2.6	+3.7	+2.7	+8.9
Systematics [%]	+10.3	+11.9	+13.0	+14.3	+16.3	+13.8	+20.7	+21.9
Total Uncertainty [%]	+11.1	+12.3	+13.4	+14.1	+17.3	+12.8	+21.1	+23.8
(JES) Large- R jet Modelling τ_{32} [%]	-11.2	+12.8	+13.5	+14.1	+17.5	+18.2	+21.2	+25.4
Light-jet tagging efficiency (eigenvector 10) [%]	-0.72	+0.74	+0.76	+0.76	+0.76	+0.76	+0.76	+0.76
Light-jet tagging efficiency (eigenvector 13) [%]	-	-	-	-	-	-	-	-
Light-jet tagging efficiency (eigenvector 12) [%]	-	-	-	-	-	-	-	-
Single top t -channel treatment [%]	+0.25	+0.12	+0.20	+0.12	+0.17	-	+0.36	+0.45
Light-jet tagging efficiency (eigenvector 0) [%]	+0.24	-	+0.11	+0.36	+0.33	-	-	+0.74
(JES) Flavour response [%]	-	-	-	-	-	-	-	-
b -Quark tagging extrapolation [%]	+1.66	+2.10	+2.63	+1.02	+5.40	+4.10	+5.27	+6.71
Electron energy resolution [%]	-1.64	-2.07	-2.59	-2.97	-3.33	-3.99	-5.10	-6.36
QCD data-driven background shape [%]	+3.81	+4.02	+4.07	+4.09	+4.08	+4.33	+4.33	+4.33
Pile-up [%]	-0.57	-0.13	+0.44	+0.45	+0.45	+1.84	+1.71	+1.71
E_T^{miss} Soft jet resolution para [%]	+0.56	+0.29	+0.57	+0.30	+0.93	-0.78	-0.35	+5.91
(JES) η intercalibration non-cllosure [%]	-	-	-	-	-	-	-	-
b -Quark tagging efficiency (eigenvector 1) [%]	+3.46	+3.63	+3.72	+3.74	+3.72	+3.78	+3.77	+3.62
Muon (MS) momentum resolution [%]	+3.54	+3.71	+3.80	+3.82	+3.81	+3.88	+3.87	+3.72
b -Quark tagging efficiency (eigenvector 4) [%]	+0.15	+0.18	+0.20	+0.21	+0.23	+0.26	+0.30	+0.34
(JES) b -Tagged jet energy scale [%]	-	-	-	-	-	-	-	-
Single top W cross-section [%]	-	-	-	-	-	-	-	-
E_T^{miss} Soft scale [%]	-	-	-	-	-	-	-	-
(JES) η intercalibration model [%]	-	-	-	-	-	-	-	-
Electron energy scale [%]	-	-	-	-	-	+0.32	-	-
(JES) Effective detector NP set 7 [%]	-	-	-	-	-	-	-	-
Jet vertex tagging [%]	-	-	-	-0.12	-	-	-	+0.15
Light-jet tagging efficiency (eigenvector 9) [%]	-0.19	-0.21	-	-	-	-0.30	-	-
Light-jet tagging efficiency (eigenvector 8) [%]	-0.19	-0.21	-	-	-	-0.30	-	-
(JES) Large- R jet top-quark mass resolution [%]	+0.05	+1.46	+1.54	+0.44	+0.83	+0.33	+0.11	+2.74
(JES) Effective detector NP set 8 (restTerm) [%]	-	-	-	-	-	-	-	-
Light-jet tagging efficiency (eigenvector 1) [%]	-	-	-	-	-	-	-	+0.32
(JES) Large- R jet Baseline p_T [%]	+1.69	+0.95	+1.35	+2.35	+4.06	+1.75	+9.36	+3.39
Light-jet tagging efficiency (eigenvector 3) [%]	-1.64	-0.79	-1.63	-1.58	-3.74	-0.11	-7.97	-6.30
Light-jet tagging efficiency (eigenvector 2) [%]	-	-	+0.10	-	-	-	-	-
Light-jet tagging efficiency (eigenvector 4) [%]	-	-	-	+0.14	+0.16	+0.10	-	-0.36
(JES) Effective detector NP set 6 [%]	-	-	-	-0.14	-0.16	-0.10	-	+0.36
(JES) Large- R jet TotalStat τ_{32} [%]	+0.24	+0.31	+0.19	-	+0.16	+0.67	+0.12	-0.63
(JES) Light-jet tagging efficiency (eigenvector 7) [%]	-0.33	-0.23	-0.20	-0.23	-0.11	-0.19	-0.24	-0.13
Muon sagitta $h\sigma$ [%]	-	-	-	-	+0.11	-	-	+0.13
(JES) Pile-up offset N_{PV} [%]	-	-	-	-	-	-	-	-
c-Quark tagging efficiency (eigenvector 2) [%]	-0.40	-0.48	-0.45	-0.49	-0.49	-0.57	-0.44	-0.28
c-Quark tagging efficiency (eigenvector 3) [%]	-0.30	-0.36	-0.36	-0.36	-0.43	-0.45	-0.47	-0.38
c-Quark tagging efficiency (eigenvector 0) [%]	-1.43	-1.46	-1.40	-1.39	-1.71	-1.74	-1.62	-0.98
c-Quark tagging efficiency (eigenvector 1) [%]	+0.79	+0.98	+0.92	+0.96	+0.92	+1.34	+0.62	+0.42
(JES) Large- R jet TotalStat τ_{32} [%]	+0.15	+0.11	-0.11	-0.15	-0.15	-0.19	-0.25	-0.36
b-Quark tagging efficiency (eigenvector 3) [%]	-0.31	-0.38	-0.43	-0.46	-0.50	-0.58	-0.73	-0.38
E_T^{miss} Soft jet resolution perp [%]	+0.31	+0.38	+0.44	+0.46	+0.50	+0.58	+0.73	+0.89
(JES) Effective detector NP set 2 [%]	-	-	-	-	-	-	-	-
b -Quark tagging extrapolation from c-Quark [%]	-	-	-	-	-	-	-	-
(JES) Large- R jet Tracking p_T [%]	-3.04	+3.33	+3.57	+4.57	+4.85	+5.66	+2.76	+8.96
(JES) Effective detector NP set 3 [%]	-	-	-	-	-	-	-	-
(JES) Large- R jet TotalStat mass [%]	-	-	-	-	-	-0.37	-	+2.36
(JES) Effective detector NP set 5 [%]	-	-	-	-	-	-	-	-
(JES) Large- R jet Baseline mass [%]	+0.34	+0.29	+0.27	+0.47	+0.44	+0.34	+0.88	+0.14
Muon energy scale [%]	-	-	-	-	-	-0.23	-	-
(JES) Pile-up offset p_T [%]	-	-	-	-	-	-	-	-
(JES) Large- R jet Modelling mass [%]	-0.53	+0.12	-0.15	-1.03	-0.51	-1.05	-0.41	+3.17
(JES) Effective detector NP set 1 [%]	-0.30	-0.15	-0.15	-0.15	-0.15	-0.15	-	-
(JES) Large- R jet Baseline τ_{32} [%]	+5.37	+5.98	+6.16	+7.07	+9.25	+8.59	+10.9	+12.5
(JES) Single particle high- η [%]	-	-	-	-	-	-	-	-0.19
Light-jet tagging efficiency (eigenvector 5) [%]	-	-	-	-	-	-	-	+0.42
(JES) Pile-up offset ρ topology [%]	-2.19	+1.95	+1.57	+6.22	+1.51	-0.23	-0.29	-0.23
(JES) Large- R jet Modelling p_T [%]	-1.93	-1.41	+1.54	-1.30	-0.48	-6.84	-8.93	-10.2
(JES) η intercalibration total stat [%]	-	-	-	-	-	-	-	-1.52
Light-jet tagging efficiency (eigenvector 4) [%]	-	-	-	-	-0.20	-	-	-0.45
Mass (ID) momentum resolution [%]	-0.14	+0.26	+0.25	+0.16	+0.15	+0.14	+0.24	-0.23
(JES) Flavour composition [%]	-	-	-0.16	-0.25	-0.30	-0.14	-0.15	-
(JES) Effective detector NP set 4 [%]	-	-	-	-	-	-	-	-
Light-jet tagging efficiency (eigenvector 11) [%]	-	-	-	-	-	-	-	-
(JES) Large- R jet Tracking τ_{32} [%]	-0.23	-0.26	-0.26	-0.26	-0.04	-0.27	-0.38	-0.53
(JES) Large- R jet Tracking mass [%]	+0.27	+0.26	+0.23	+0.30	+0.29	+0.49	+0.29	+0.35
Light-jet tagging efficiency (eigenvector 6) [%]	-	-	-0.46	-	-	-	-	+0.18
(JES) Pile-up offset μ [%]	-	-	-	-	-	-	-	-0.18
b-Quark tagging efficiency (eigenvector 2) [%]	-0.48	+0.57	+0.63	-0.65	-0.72	-0.78	-0.87	-0.92
(JES) Punch-through [%]	-	-	-	-	-	-	-	-
Muon sagitta resolution bias [%]	-	-	-	-	-	-	-	-

Table 159: The individual systematic uncertainties in the leading top-quark transverse momentum calculated as a percentage of the leading top-quark transverse momentum in each bin. Dashes are used when the estimated relative systematic uncertainty for that bin is below 0.1%.

Bins	0.0–0.3	0.3–0.6	0.6–0.9	0.9–1.2	1.2–1.5	1.5–2.0
Statistics [%]	± 1.2	± 1.2	± 1.3	± 1.7	± 2.0	± 2.4
Systematics [%]	$+11.6$	$+12.0$	$+12.3$	$+12.6$	$+12.5$	$+10.9$
Total Uncertainty [%]	-13.3	$+12.4$	$+12.7$	$+13.4$	$+12.8$	$+10.8$
(LJES) Large- R jet Modelling τ_{32} [%]	-6.73	-7.03	-7.17	-7.58	-7.40	-6.45
Light-jet tagging efficiency (eigenvector 10) [%]	+8.50	+7.57	+7.94	+8.30	+8.15	+6.58
Light-jet tagging efficiency (eigenvector 13) [%]	-	-	-	-	-	-
Light-jet tagging efficiency (eigenvector 12) [%]	-	-	-	-	-	-
Single top t -channel treatment [%]	± 0.25	± 0.21	± 0.12	± 0.21	± 0.21	-
Light-jet tagging efficiency (eigenvector 0) [%]	-0.16	-	-0.16	-0.19	-0.51	-0.35
(JES) Flavour response [%]	-	-	+0.16	+0.19	+0.51	+0.38
b -Quark tagging extrapolation [%]	+2.41	+2.32	+2.34	+2.31	+2.09	+1.68
Electron energy resolution [%]	-2.37	-2.28	-2.30	-2.28	-2.06	-1.65
b -Quark tagging efficiency (eigenvector 0) [%]	-3.91	-3.86	-3.96	-4.06	-3.85	-3.21
QCD data-driven background shape [%]	+4.01	+3.96	+4.06	+4.16	+3.94	+3.29
Pile-up [%]	∓ 0.36	± 0.14	-0.13	-	± 0.40	-
E_T^{miss} Soft jet resolution para [%]	-0.46	-0.57	-0.30	-	-1.17	+0.16
E_T^{miss} Soft jet resolution perp [%]	+0.76	+0.41	+0.20	+0.41	+0.85	-0.35
(JES) η intercalibration non-closure [%]	-	-	-	-	-	-
b -Quark tagging efficiency (eigenvector 1) [%]	-3.65	-3.59	-3.72	-3.74	-3.47	-2.99
Muon (MS) momentum resolution [%]	+3.73	+3.68	+3.81	+3.83	+3.55	+3.07
b -Quark tagging efficiency (eigenvector 4) [%]	-0.19	-0.18	-0.18	-0.18	-0.17	-0.14
(JES) b -Tagged jet energy scale [%]	+0.19	+0.18	+0.18	+0.18	+0.17	+0.14
Single top Wt cross-section [%]	-	-	-	-	-	-
E_T^{miss} Soft jet scale [%]	-	-	-	-	-	-
(JES) η intercalibration model [%]	-	-	-	-	-	-
Electron energy scale [%]	-	-	-	-	-	-
(JES) Effective detector NP set 7 [%]	-	-	-	-	-	-
Jet vertex tagging [%]	-	-	-	-	+0.10	-
Light-jet tagging efficiency (eigenvector 9) [%]	-0.22	-0.20	-	-0.22	-	-
Light-jet tagging efficiency (eigenvector 8) [%]	-0.22	-0.19	-	-	-0.22	-
(LJES) Large- R jet top-quark mass resolution [%]	∓ 0.84	∓ 0.76	∓ 1.23	∓ 1.54	∓ 0.81	∓ 1.10
(JES) Effective detector NP set 8 (restTerm) [%]	-	-	-	-	-	-
Light-jet tagging efficiency (eigenvector 1) [%]	-	-	-	-	-	-
(LJES) Large- R jet Baseline p_T [%]	+1.79	+2.14	+1.86	+1.75	+2.04	+1.43
Light-jet tagging efficiency (eigenvector 3) [%]	-1.32	-2.04	-1.65	-1.78	-1.53	-1.63
Light-jet tagging efficiency (eigenvector 2) [%]	-	-	-	-	-0.10	-1.11
(JES) Effective detector NP set 6 [%]	-	-	-	-	-	-
(LJES) Large- R jet TotalStat p_T [%]	+0.29	+0.24	+0.21	+0.23	+0.28	+0.19
Light-jet tagging efficiency (eigenvector 7) [%]	-0.13	-0.31	-0.17	-0.21	-0.16	-0.13
Muon sagitta ho [%]	-	-	-	-	-	-
(JES) Pile-up offset N_{PV} [%]	-	-	-	-	-	-
c -Quark tagging efficiency (eigenvector 2) [%]	-0.54	-0.46	-0.37	-0.48	-0.35	-0.44
c -Quark tagging efficiency (eigenvector 3) [%]	+0.13	-	-	-	-	+0.16
c -Quark tagging efficiency (eigenvector 0) [%]	-0.3	-1.0	-1.40	-0.6	-1.8	-0.33
c -Quark tagging efficiency (eigenvector 1) [%]	-1.21	-1.02	-0.94	-1.15	-0.86	-1.16
(LJES) Large- R jet TotalStat τ_{32} [%]	+0.18	+0.82	+0.07	+0.98	+0.09	+1.00
b -Quark tagging efficiency (eigenvector 3) [%]	-0.41	-0.39	-0.40	-0.38	+0.10	+0.21
E_T^{miss} Soft jet resolution perp [%]	+0.41	+0.39	+0.40	+0.38	+0.38	+0.26
(JES) Effective detector NP set 2 [%]	-	-	-	-	-	-
b -Quark tagging extrapolation from c -Quark [%]	-	-	-	-	-	-
(LJES) Large- R jet Tracking p_T [%]	+3.67	+4.21	+3.94	+3.78	+4.37	+3.93
(JES) Effective detector NP set 3 [%]	-3.56	-3.85	-3.60	-3.67	-4.31	-3.51
(LJES) Large- R jet TotalStat mass [%]	-	-	-0.14	-	-	-
(JES) Effective detector NP set 5 [%]	-	-	+0.12	-	-	-
(LJES) Large- R jet Baseline mass [%]	+0.41	+0.56	-	+0.70	+0.25	+0.22
Muon energy scale [%]	-0.47	-0.58	-0.42	-0.42	-	-
(JES) Pile-up offset p_T [%]	-	-	-	-	-	-
(LJES) Large- R jet Modelling mass [%]	+0.51	+0.42	-	+0.62	-0.20	+0.61
(JES) Effective detector NP set 1 [%]	-0.83	-0.41	-0.40	-0.31	-	-
(LJES) Large- R jet Baseline τ_{32} [%]	-5.37	-5.53	-5.90	-6.00	-5.95	-5.44
(JES) Single particle high p_T [%]	+6.67	+5.98	+6.09	+6.67	+5.90	+5.28
Light-jet tagging efficiency (eigenvector 5) [%]	-	-	-	-	-	-
(JES) Pile-up offset ρ topology [%]	+0.16	+0.14	+0.19	-	-	-
(LJES) Large- R jet Modelling p_T [%]	+1.65	+1.92	+2.10	+1.72	+2.33	+1.58
(JES) η intercalibration total stat [%]	-1.40	-1.84	-1.62	-1.78	-1.72	-1.41
Light-jet tagging efficiency (eigenvector 4) [%]	-	-	-	-	-0.27	-0.14
Muon (ID) momentum resolution [%]	-	-	-	-	-	-
(JES) Flavour composition [%]	+0.19	+0.20	+0.26	+0.13	+0.13	+0.12
(JES) Effective detector NP set 4 [%]	-	-0.15	-0.13	-0.11	-0.11	-0.28
Light-jet tagging efficiency (eigenvector 11) [%]	-	-	-	-	-	-
(LJES) Large- R jet Tracking τ_{32} [%]	-0.36	-0.22	-0.40	-0.18	-0.21	-0.47
(LJES) Large- R jet Tracking mass [%]	+0.35	+0.28	+0.26	+0.22	+0.20	+0.24
b -Quark tagging efficiency (eigenvector 2) [%]	-0.23	-	-0.33	-	+0.35	+0.48
(JES) Pile-up offset μ [%]	-	-	-	-	-	-
(JES) Punch-through [%]	-0.59	-0.58	-0.60	-0.56	-0.51	-0.41
Muon sagitta resolution bias [%]	-	-	-	-	-	-

Table 160: The individual systematic uncertainties in the leading top-quark absolute value of the rapidity calculated as a percentage of the leading top-quark rapidity in each bin. Dashes are used when the estimated relative systematic uncertainty for that bin is below 0.1%.

Bins [GeV]	350.0–400.0	400.0–450.0	450.0–500.0	500.0–550.0	550.0–600.0	600.0–800.0	800.0–1200.0
Statistics [%]	+2.5	+1.8	+1.2	+1.1	+1.5	+1.3	+4.3
Systematics [%]	+9.94	+11.1	+11.7	+11.7	+13.8	+15.5	+21.0
Total Uncertainty [%]	+10.3	+11.9	+12.0	+12.8	+14.6	+15.4	+21.6
(LJES) Large- R jet Modelling τ_{32} [%]	-5.51	-6.0	-6.25	-5.46	-8.65	-10.88	-11.8
Light-jet tagging efficiency (eigenvector 10) [%]	-	-	-	-	-	-	-
Light-jet tagging efficiency (eigenvector 13) [%]	-	-	-	-	-	-	-
Light-jet tagging efficiency (eigenvector 12) [%]	-	-	-	-	-	-	-
Single top t -channel treatment [%]	+0.19	+0.25	+0.15	+0.26	+0.10	+0.15	+0.12
Light-jet tagging efficiency (eigenvector 0) [%]	-0.13	-0.33	-0.16	-0.15	-0.17	-0.23	-0.19
(JES) Flavour response [%]	+0.13	+0.33	+0.17	+0.15	+0.17	+0.23	+0.20
b -Quark tagging extrapolation [%]	+1.28	+1.58	+2.02	+2.34	+3.02	+4.03	+6.68
Electron energy resolution [%]	-1.27	-1.56	-2.00	-2.31	-2.97	-3.93	-6.38
b -Quark tagging efficiency (eigenvector 0) [%]	-3.38	-3.58	-3.89	-4.00	-4.19	-4.22	-4.33
QCD data-driven background shape [%]	+0.46	+3.67	+3.98	+4.10	+0.80	+0.86	+4.47
Pile-up [%]	-0.49	+0.47	+0.19	+0.24	+0.81	-0.46	+0.52
E_T^{miss} Soft jet resolution para [%]	+0.38	+0.31	+0.65	+0.23	+0.60	+0.71	+0.45
(JES) η intercalibration non-closure [%]	-	-	-	-	-	-	-
b -Quark tagging efficiency (eigenvector 1) [%]	-3.10	-3.32	-3.62	-3.72	-3.93	-3.96	-3.75
Muon (MS) momentum resolution [%]	+3.17	+3.40	+3.70	+3.81	+4.03	+4.06	+3.85
b -Quark tagging efficiency (eigenvector 4) [%]	-0.11	-0.15	-0.18	-0.19	-0.22	-0.26	-0.35
(JES) b -Tagged jet energy scale [%]	+0.11	+0.15	+0.18	+0.19	+0.22	+0.26	+0.35
Single top Wt cross-section [%]	-	-	-	-	-	-	-
E_T^{miss} Soft jet scale [%]	-	-	-	-	-	-	-
(JES) η intercalibration model [%]	-	-	-	-	-	-	-
Electron energy scale [%]	-	-	-	-	-	-	-
(JES) Effective detector NP set 7 [%]	-	-	-	-	-	-	-
Jet vertex tagging [%]	-	+0.13	-	-	-	-	-
Light-jet tagging efficiency (eigenvector 9) [%]	-0.28	-0.27	-	-	-	-	-
Light-jet tagging efficiency (eigenvector 8) [%]	-0.28	-0.30	-	-	-	-	+0.12
(JES) Large- R jet top-quark mass resolution [%]	+3.51	+0.18	+1.29	+0.68	+0.82	-	+2.04
(JES) Effective detector NP set 8 (restTerm) [%]	-	-	-	-	-	-	-
Light-jet tagging efficiency (eigenvector 1) [%]	-	-	-	-	-	-	-0.15
(LJES) Large- R jet Baseline p_T [%]	+2.05	+2.86	+1.68	+0.91	+0.78	+2.19	+0.62
Light-jet tagging efficiency (eigenvector 3) [%]	-2.41	-2.33	-1.24	-0.61	-1.03	-2.33	-7.42
Light-jet tagging efficiency (eigenvector 2) [%]	-	-	-	-	-	+0.12	+0.17
(JES) Effective detector NP set 6 (%)	-	-	+0.17	-	-	-0.10	-
(LJES) Large- R jet TotalStat p_T [%]	+0.29	+0.42	-0.24	+0.29	+0.20	+0.27	-0.37
Light-jet tagging efficiency (eigenvector 7) [%]	-	-	-	-	-	-	+0.10
Muon sagitta $h\sigma$ [%]	-	-	-	-	-	-	-
(JES) Pile-up offset N_{PV} [%]	-	-	-	-	-	-	-
c -Quark tagging efficiency (eigenvector 2) [%]	-0.52	-0.39	+0.17	+0.17	+0.18	+0.14	+0.13
c -Quark tagging efficiency (eigenvector 3) [%]	-0.35	-0.30	-0.36	+0.37	-	-0.32	-
c -Quark tagging efficiency (eigenvector 0) [%]	-1.59	-1.26	-1.64	-1.81	-1.42	-1.35	-1.07
c -Quark tagging efficiency (eigenvector 1) [%]	-1.08	-0.88	+1.94	+1.74	+0.97	+0.91	+0.55
(LJES) Large- R jet TotalStat τ_{32} [%]	-0.78	-0.65	+0.98	+0.95	+0.83	+0.89	+0.49
b -Quark tagging efficiency (eigenvector 3) [%]	+0.12	+0.11	+0.15	+0.11	+0.14	+0.14	+0.41
E_T^{miss} Soft jet resolution perp [%]	+0.20	+0.31	+0.38	+0.41	+0.49	+0.38	+0.85
(JES) Effective detector NP set 2 [%]	-	-	-	-	-	-	-
b -Quark tagging extrapolation from c -Quark [%]	-	-	-	-	-	-	-
(LJES) Large- R jet Tracking p_T [%]	+2.62	+4.03	+3.82	+3.75	+4.42	+5.15	+6.69
(JES) Effective detector NP set 3 [%]	-2.87	-3.47	-3.73	-3.37	-4.43	-4.98	-6.61
(LJES) Large- R jet TotalStat mass [%]	-	-	-	-	-	-	-0.62
(JES) Effective detector NP set 5 [%]	-	+0.23	-	-	-	-	-
(LJES) Large- R jet Baseline mass [%]	+0.83	+0.35	+0.42	+0.18	+0.22	+0.14	+0.58
Muon energy scale [%]	-1.17	-0.42	-0.42	-0.19	-0.23	-0.12	-
(JES) Pile-up offset p_T [%]	-	-	-	-	-	-	-
(LJES) Large- R jet Modelling mass [%]	+0.48	+0.68	+0.39	-	-	-0.23	+0.36
(JES) Effective detector NP set 1 [%]	-1.26	-0.18	-0.52	-	-	-	+0.33
(LJES) Large- R jet Baseline τ_{32} [%]	-4.30	-5.10	-5.50	-5.47	-6.58	-7.56	-10.3
(JES) Single particle high- p_T [%]	+5.19	+5.21	+5.64	+6.35	+7.36	+8.91	+9.62
Light-jet tagging efficiency (eigenvector 5) [%]	-	-	-	-	-	-	-
(JES) Pile-up offset ρ topology [%]	-0.18	-	+0.12	-	-0.17	+0.12	+0.42
(LJES) Large- R jet Modelling p_T [%]	-0.12	-0.18	-0.20	+2.05	+1.84	+1.16	+1.57
(JES) η intercalibration total stat [%]	-1.40	-1.17	-2.10	-1.64	-1.90	-1.25	-1.89
Light-jet tagging efficiency (eigenvector 4) [%]	-	-0.16	-	-	-	-	-
(JES) Pile-up offset μ topology [%]	-0.18	-0.16	-	-	-	-	-
(LJES) Large- R jet Tracking τ_{32} [%]	-0.22	-0.29	-0.27	-0.24	-0.37	-0.42	-1.39
(JES) Large- R jet Tracking mass [%]	+0.10	+0.18	+0.40	+0.23	+0.32	+0.35	+0.49
Light-jet tagging efficiency (eigenvector 6) [%]	-0.89	-	-	+0.28	-	+0.20	+0.45
(JES) Pile-up offset μ [%]	-	-	-	-	-	-	-
b -Quark tagging efficiency (eigenvector 2) [%]	-0.37	-0.46	-0.55	-0.60	-0.71	-0.78	-0.93
(JES) Punch-through [%]	-0.37	+0.46	+0.56	+0.60	+0.71	+0.78	+0.94
Muon sagitta resolution bias [%]	-	-	-	-	-	-	-

Table 161: The individual systematic uncertainties in the 2nd leading top-quark transverse momentum calculated as a percentage of the 2nd leading top-quark transverse momentum in each bin. Dashes are used when the estimated relative systematic uncertainty for that bin is below 0.1%.

Bins	0.0–0.3	0.3–0.6	0.6–0.9	0.9–1.2	1.2–1.5	1.5–2.0
Statistics [%]	± 1.2	± 1.3	± 1.3	± 1.7	± 1.9	± 2.0
Systematics [%]	$+12.3$	$+11.7$	$+12.1$	$+11.8$	$+13.1$	$+11.4$
Total Uncertainty [%]	$+13.0$	$+12.4$	$+12.3$	$+13.6$	$+13.2$	$+12.5$
(LJES) Large- R jet Modelling τ_{32} [%]	-7.28 +8.06	-6.74 +7.73	-7.19 +7.47	-6.76 +8.95	-7.76 +8.47	-6.68 +7.74
Light-jet tagging efficiency (eigenvector 10) [%]	-	-	-	-	-	-
Light-jet tagging efficiency (eigenvector 13) [%]	-	-	-	-	-	-
Light-jet tagging efficiency (eigenvector 12) [%]	-	-	-	-	-	-
Single top t -channel treatment [%]	± 0.23	± 0.16	± 0.23	± 0.13	± 0.34	-
Light-jet tagging efficiency (eigenvector 0) [%]	-0.17 +0.18	-0.13 +0.14	-0.12 +0.12	-0.51 +0.50	-0.13 +0.13	-0.21 +0.21
(JES) Flavour response [%]	-	-	-	-	-	-
b -Quark tagging extrapolation [%]	$+2.37$ -2.33	$+2.37$ -2.34	$+2.34$ -2.30	$+2.18$ -2.15	$+2.16$ -2.13	$+1.87$ -1.85
Electron energy resolution [%]	-	-	-	-	-	-
b -Quark tagging efficiency (eigenvector 0) [%]	-3.98 +4.08	-3.90 +4.00	-3.90 +4.00	-3.85 +3.95	-3.77 +3.86	-3.64 +3.74
QCD data-driven background shape [%]	$+0.45$	± 0.27	± 0.11	-	-	-
Pile-up [%]	-0.45 +0.45	-0.12 +0.29	-0.50 +0.38	-0.26 +0.35	-0.14 +0.83	-1.29 +0.76
E_T^{miss} Soft jet resolution para [%]	-	-	-	-	-	-
(JES) η intercalibration non-closure [%]	-	-	-	-	-	-
b -Quark tagging efficiency (eigenvector 1) [%]	-3.69 +3.77	-3.65 +3.73	-3.65 +3.73	-3.49 +3.57	-3.54 +3.62	-3.40 +3.48
Muon (MS) momentum resolution [%]	-	-	-	-	-	-
b -Quark tagging efficiency (eigenvector 4) [%]	-0.19 +0.19	-0.18 +0.18	-0.19 +0.19	-0.18 +0.18	-0.18 +0.18	-0.15 +0.15
(JES) b -Tagged jet energy scale [%]	-	-	-	-	-	-
Single top Wt cross-section [%]	-	-	-	-	-	-
E_T^{miss} Soft jet scale [%]	-	-	-	-	-	-
(JES) η intercalibration model [%]	-	-	-	-	-	-
Electron energy scale [%]	-	-	-	-	-	-
(JES) Effective detector NP set 7 [%]	-	-	-	-	-	-
Jet vertex tagging [%]	-	-	-	-0.12	-	-0.12
Light-jet tagging efficiency (eigenvector 9) [%]	-0.20	-0.21	-	-0.21	-	-
Light-jet tagging efficiency (eigenvector 8) [%]	-	-0.20	-	-0.26	-	-
(LJES) Large- R jet top-quark mass resolution [%]	∓ 1.31	∓ 0.89	∓ 0.45	∓ 1.67	∓ 0.65	∓ 1.25
(JES) Effective detector NP set 8 (restTerm) [%]	-	-	-	-	-	-
Light-jet tagging efficiency (eigenvector 1) [%]	-	-	-	-	-	-
(LJES) Large- R jet Baseline p_T [%]	$+1.76$ -1.51	$+1.69$ -1.52	$+1.86$ -2.11	$+2.14$ -1.84	$+2.51$ -1.32	$+1.81$ -1.60
Light-jet tagging efficiency (eigenvector 3) [%]	-	-	-	-	-	-
Light-jet tagging efficiency (eigenvector 2) [%]	-	-	-	+0.20	+0.12	+0.12
(JES) Effective detector NP set 6 [%]	-	-	-	-0.20	-0.12	-0.12
(LJES) Large- R jet TotalStat p_T [%]	$+0.26$ -0.14	$+0.21$ -0.20	$+0.27$ -0.21	$+0.27$ -0.29	$+0.29$ -0.25	$+0.19$ -
Light-jet tagging efficiency (eigenvector 7) [%]	-	-	-	-	-	-
Muon sagitta ho [%]	-	-	-	-	-	-
(JES) Pile-up offset N_{PV} [%]	-	-	-	-	-	-
c -Quark tagging efficiency (eigenvector 2) [%]	-0.43	-0.56	-0.44	-0.45	-0.41	-0.35
c -Quark tagging efficiency (eigenvector 3) [%]	-	+0.17	-	-	-	-
c -Quark tagging efficiency (eigenvector 0) [%]	-0.34 +1.58	-0.40 +1.69	-0.35 +1.40	-0.31 +1.30	-0.35 +1.55	-0.28 +1.85
c -Quark tagging efficiency (eigenvector 1) [%]	-1.02 +0.86	-1.24 +1.08	-0.99 +0.81	-0.98 +0.78	-1.08 +0.89	-1.03 +0.87
(LJES) Large- R jet TotalStat τ_{32} [%]	± 0.13 +0.13	± 0.17 -0.39	± 0.12 +0.40	± 0.13 -0.39	-	± 0.12 +0.30
b -Quark tagging efficiency (eigenvector 3) [%]	-0.41	-0.39	-0.40	-0.39	-0.36	-0.30
E_T^{miss} Soft jet resolution perp [%]	-	-	-	-	-	-
(JES) Effective detector NP set 2 [%]	-	-	-	-	-	-
b -Quark tagging extrapolation from c -Quark [%]	-	-	-	-	-	-
(LJES) Large- R jet Tracking p_T [%]	$+3.77$ -3.79	$+3.83$ -3.37	$+3.89$ -3.81	$+4.18$ -3.84	$+4.65$ -3.97	$+4.01$ -4.04
(JES) Effective detector NP set 3 [%]	-	-	-	-	-	-
(LJES) Large- R jet TotalStat mass [%]	-	-	-	-	-	-
(JES) Effective detector NP set 5 [%]	-	-	-	-	-	-
(LJES) Large- R jet Baseline mass [%]	$+0.49$ -0.62	$+0.32$ -0.44	$+0.36$ -0.46	$+0.33$ -0.26	$+0.66$ -	-
Muon energy scale [%]	-	-	-	-	-	-
(JES) Pile-up offset p_T [%]	-	-	-	-	-	-
(LJES) Large- R jet Modelling mass [%]	$+0.53$ -0.99	$+0.22$ -0.53	$+0.22$ -0.15	-	$+0.74$ -	-0.26 +0.43
(JES) Effective detector NP set 1 [%]	-	-	-	-	-	-
(LJES) Large- R jet Baseline τ_{32} [%]	-5.90 +6.33	-5.44 +6.06	-5.77 +5.94	-5.40 +6.62	-6.27 +6.65	-5.06 +6.10
(JES) Single particle high p_T [%]	-	-	-	-	-	-
Light-jet tagging efficiency (eigenvector 5) [%]	-	-	-	-	-	-
(JES) Pile-up offset ρ topology [%]	-	± 0.21	± 0.14	-	-	± 0.20
(LJES) Large- R jet Modelling p_T [%]	$+1.86$ -1.68	$+1.76$ -1.52	$+1.85$ -1.77	$+1.92$ -1.58	$+2.37$ -1.40	$+1.77$ -1.87
(JES) η intercalibration total stat [%]	-	-	-	-	-	-
Light-jet tagging efficiency (eigenvector 4) [%]	-	-	-	-0.19	-	-
Muon (ID) momentum resolution [%]	-	-	-	-	-	-
(JES) Flavour composition [%]	$+0.18$ -0.13	$+0.22$ -0.14	$+0.16$ -0.14	$+0.23$ -	$+0.11$ -0.16	$+0.21$ -
(JES) Effective detector NP set 4 [%]	-	-	-	-	-	-
Light-jet tagging efficiency (eigenvector 11) [%]	-	-	-	-	-	-
(LJES) Large- R jet Tracking τ_{32} [%]	-0.31 +0.29	-0.33 -0.28	-0.21 +0.26	-0.35 +0.23	-0.42 +0.35	-0.24 -0.37
(LJES) Large- R jet Tracking mass [%]	-	-	-	-	-	± 0.24
Light-jet tagging efficiency (eigenvector 6) [%]	-	-	-	-	-	-
(JES) Pile-up offset μ [%]	-	-	-	-	-	-
b -Quark tagging efficiency (eigenvector 2) [%]	-0.59 +0.59	-0.59 +0.59	-0.59 +0.59	-0.52 +0.53	-0.52 +0.52	-0.50 +0.50
(JES) Punch-through [%]	-	-	-	-	-	-
Muon sagitta resolution bias [%]	-	-	-	-	-	-

Table 162: The individual systematic uncertainties in the 2nd leading top-quark absolute value of the rapidity calculated as a percentage of the 2nd leading top-quark rapidity in each bin. Dashes are used when the estimated relative systematic uncertainty for that bin is below 0.1%.

Bins [TeV]	1.0–1.1	1.1–1.2	1.2–1.3	1.3–1.4	1.4–1.5	1.5–1.7	1.7–1.9	1.9–2.1	2.1–2.3	2.3–3.0
Statistics [%]	+1.6	+1.3	+1.5	+1.7	+2.0	+1.7	+2.4	+3.5	+5.0	+5.0
Systematics [%]	+11.2	+11.6	+12.1	+12.6	+13.0	+12.9	+13.9	+12.7	+18.4	+13.0
Total Uncertainty [%]	+11.4	+11.9	+13.2	+13.5	+14.8	+13.6	+16.3	+15.1	+16.3	+17.1
(JES) Large- R jet Modelling τ_{32} [%]	-6.15	-6.85	-7.33	-7.69	-7.63	-7.97	-8.34	-7.03	-11.3	-6.53
Light-jet tagging efficiency (eigenvector 10) [%]	+6.68	+7.56	+8.19	+8.59	+9.24	+8.97	+10.2	+9.58	+11.1	+10.3
Light-jet tagging efficiency (eigenvector 13) [%]	-	-	-	-	-	-	-	-	-	-
Light-jet tagging efficiency (eigenvector 12) [%]	-	-	-	-	-	-	-	-	-	-
Single top t -channel treatment [%]	+0.14	+0.24	+0.23	+0.21	+0.14	-	+0.15	+0.41	+0.15	-
Light jet tagging efficiency (eigenvector 0) [%]	-0.31	-0.11	-0.18	-0.23	-0.18	-0.20	-0.23	-0.25	-0.19	-
(JES) Flavour response [%]	+0.31	+0.11	+0.18	+0.23	+0.18	+0.23	+0.23	+0.24	+0.19	-
b -Quark tagging extrapolation [%]	+1.68	+2.00	+2.33	+2.53	+2.78	+2.91	+3.14	+3.56	+3.17	+3.66
Electron energy resolution [%]	-1.67	-1.98	-2.29	-2.50	-2.73	-2.84	-3.06	-3.46	-3.08	-3.49
b -Quark tagging efficiency (eigenvector 0) [%]	-3.73	-3.88	-3.98	-3.91	-3.87	-3.82	-3.75	+0.46	-3.71	-3.27
QCD data-driven background shape [%]	+0.59	+0.12	+0.20	+0.26	+0.76	+0.52	-0.13	+1.12	+0.50	+0.30
Pile-up [%]	-1.00	-0.39	-0.38	-0.38	-0.38	-0.36	-0.31	-0.31	-0.39	-0.30
E_T^{miss} Soft jet resolution para [%]	-	-	-	-	-	+0.44	+0.51	+0.80	+1.78	+0.88
(JES) η intercalibration non-closure [%]	-	-	-	-	-	-	-	-	-	-
b -Quark tagging efficiency (eigenvector 1) [%]	-3.44	-3.61	-3.71	-3.70	-3.66	-3.54	-3.50	-3.38	-3.32	-2.91
Muon (MS) momentum resolution [%]	+3.52	+3.70	+3.80	+3.78	+3.75	+3.62	+3.59	+3.46	+3.41	+2.99
b -Quark tagging efficiency (eigenvector 4) [%]	-0.15	-0.17	+0.19	+0.19	+0.20	+0.20	+0.21	+0.23	+0.21	+0.20
(JES) b -Tagged jet energy scale [%]	+0.16	+0.17	+0.19	+0.19	+0.20	+0.20	+0.21	+0.23	+0.21	+0.20
Single top Wt cross-section [%]	-	-	-	-	-	-	-	-	-	-
E_T^{miss} Soft jet scale [%]	-	-	-	-	-	-	-	-	-	-
(JES) η intercalibration model [%]	-	-	-	-	-	-	-	-	-	-
Electron energy scale [%]	-	-	-	-	-	-	+0.46	-	-	-
(JES) Effective detector NP set 7 [%]	-	-	-	-	-	-	-	-	-	-
Jet vertex tagging [%]	-0.13	-	-	-	-	-	-	-	-0.12	-
Light-jet tagging efficiency (eigenvector 9) [%]	-0.22	-	-	-	-0.19	-	-	-	-	-
Light-jet tagging efficiency (eigenvector 8) [%]	-0.24	-	-	-	-	-	-	-	-	-
(JES) Large- R jet top-quark mass resolution [%]	+0.64	+0.53	+0.80	+1.40	+0.14	+0.84	+0.59	+1.60	+1.45	+3.63
(JES) Effective detector NP set 8 (restTerm) [%]	-	-	-	-	-	-	-	-	-	-
Light-jet tagging efficiency (eigenvector 1) [%]	-	-	-	-	-	-	-	-	-	-
(JES) Large- R jet Baseline p_T [%]	+1.97	+1.54	+1.50	+0.85	+2.79	+1.84	+2.63	+3.38	+4.42	+3.64
(JES) Large- R jet Baseline τ_{32} [%]	-1.97	-0.55	-1.37	-1.28	-2.98	-1.63	-3.63	-3.07	-1.48	-4.15
Light-jet tagging efficiency (eigenvector 3) [%]	-	-	-0.11	-0.11	-	+0.11	+0.11	-	-	-
Light-jet tagging efficiency (eigenvector 2) [%]	+0.16	-	-	-	+0.11	-	+0.11	-	-	-
(JES) Effective detector NP set 6 [%]	-0.16	-	-	-	-0.11	-	-0.11	-	-	-
(JES) Large- R jet TotalStat p_T [%]	+0.32	+0.13	+0.28	+0.16	+0.42	-	+0.15	+0.55	-	+0.36
Light-jet tagging efficiency (eigenvector 7) [%]	-0.12	-0.18	-0.12	-0.72	-	-0.19	-0.23	-0.17	-0.27	-0.45
Muon sagitta ho [%]	-	-	-	-	-	-	-	-	-	-
(JES) Pile-up offset N_{PV} [%]	-	-	-	-	-	-	-	-	-	-
c-Quark tagging efficiency (eigenvector 2) [%]	-0.42	-0.49	-0.38	-0.46	-0.46	-0.44	-0.38	-0.45	-0.26	-
c-Quark tagging efficiency (eigenvector 3) [%]	-	+0.19	-	+0.15	-	+0.15	+0.15	+0.11	+0.28	-
c-Quark tagging efficiency (eigenvector 0) [%]	-0.35	-0.35	-0.33	-0.37	-0.33	-0.33	-0.29	-	-	-0.24
c-Quark tagging efficiency (eigenvector 1) [%]	+1.51	+2.00	+1.35	+1.47	+1.14	+1.56	+1.34	+1.69	+0.90	+0.29
c-Quark tagging efficiency (eigenvector 2) [%]	-1.05	-1.30	-0.87	-1.00	-0.89	-1.03	-0.94	-1.22	-0.61	-0.13
(JES) Large- R jet TotalStat τ_{32} [%]	+0.87	+0.15	+0.69	+0.69	+0.74	+0.74	+0.90	+0.19	+1.14	+0.17
b-Quark tagging efficiency (eigenvector 3) [%]	+0.31	+0.36	+0.42	+0.40	+0.46	+0.44	+0.48	+0.50	+0.49	+0.51
E_T^{miss} Soft jet resolution perp [%]	-	-	-	-	-	-	-	-	-	-
(JES) Effective detector NP set 2 [%]	-	-	-	-	-	-	-	-	-	-
b-Quark tagging extrapolation from c-Quark [%]	-	-	-	-	-	-	-	-	-	-
(JES) Large- R jet Tracking p_T [%]	+4.36	+3.12	+3.61	+4.03	+4.83	+4.07	+5.24	+3.15	+6.50	+5.69
(JES) Effective detector NP set 3 [%]	-3.03	-2.25	-4.74	-3.37	-3.56	-3.24	-6.16	-4.09	-1.97	-4.96
(JES) Large- R jet TotalStat mass [%]	-	-	+0.19	-	-	-	-	-	-	-0.92
(JES) Effective detector NP set 5 [%]	-	-	-	-	-	-	-	-	-	+0.15
(JES) Large- R jet Baseline mass [%]	+0.26	+0.55	+0.46	+0.94	+0.37	+0.42	-	+1.24	-	-0.67
Muon energy scale [%]	-0.33	-0.64	-0.40	-0.73	-	-0.21	-0.38	-	-0.21	-
(JES) File-up offset p_T [%]	-	-	-	-	-	-	-	-	-	-
(JES) Large- R jet Modelling mass [%]	-0.30	-0.60	-0.63	-0.72	-0.78	-0.19	+0.17	+1.05	-0.29	-0.52
(JES) Effective detector NP set 1 [%]	-	-	-	-	-	+0.10	-	-	-	-0.21
(JES) Large- R jet Baseline τ_{32} [%]	-4.90	-5.69	-5.72	-6.10	-6.30	-6.30	-6.87	-5.74	-9.98	-5.23
(JES) Single particle high- p_T [%]	+1.18	+0.90	+0.40	+0.87	+0.30	+0.88	+0.93	+0.79	+0.30	+0.24
Light-jet tagging efficiency (eigenvector 5) [%]	-	-	-	-	-	-	-	-	-	-
(JES) File-up offset topology [%]	-	+0.16	-	+0.13	+0.14	+0.13	-	+0.14	+0.16	+0.26
(JES) Large- R jet Modelling p_T [%]	+2.55	+1.81	+2.01	+1.17	+1.73	+1.51	+1.60	+1.55	+2.20	+1.26
(JES) Large- R jet Baseline τ_{32} [%]	-1.94	-1.73	-1.87	-1.87	-1.64	-1.72	-0.03	-1.91	-0.36	-1.74
(JES) η intercalibration total stat [%]	-	-	-	-	-	-	-	-	-	-
Light-jet tagging efficiency (eigenvector 4) [%]	-0.14	-	-	-	-	-0.12	-	-0.10	-	-
Muon (ID) momentum resolution [%]	+0.12	-0.11	-0.10	-0.18	-0.10	-0.22	-	-	-	-
(JES) Flavour composition [%]	+0.16	+0.17	+0.21	+0.15	+0.24	+0.20	-	+0.15	+0.16	+0.17
(JES) Effective detector NP set 4 [%]	-	-	-	-	-	-	-	-	-0.25	-
Light-jet tagging efficiency (eigenvector 11) [%]	-	-	-	-	-	-	-	-	-	-
(JES) Large- R jet Tracking τ_{32} [%]	-0.26	-0.35	-0.19	-0.42	-0.19	-0.25	-0.46	-0.26	-1.19	-0.43
(JES) Large- R jet Tracking mass [%]	+0.23	+0.31	+0.28	+0.26	+0.49	+0.18	+0.34	+0.52	+0.35	+0.31
Light-jet tagging efficiency (eigenvector 6) [%]	-	-	-	-	-0.27	-	-	-	-	+0.59
(JES) Pile-up offset μ [%]	-0.47	-0.53	-0.61	-0.59	-0.69	-0.63	-0.64	-0.62	-0.65	-0.66
b-Quark tagging efficiency (eigenvector 2) [%]	+0.47	+0.53	+0.61	+0.60	+0.70	+0.63	+0.64	+0.62	+0.65	+0.66
(JES) Punch-through [%]	-	-	-	-	-	-	-	-	-	-
Muon sagitta resolution bias [%]	-	-	-	-	-	-	-	-	-	-

Table 163: The individual systematic uncertainties in the top quark-antiquark system invariant mass calculated as a percentage of the invariant mass in each bin. Dashes are used when the estimated relative systematic uncertainty for that bin is below 0.1%.

Not reviewed, for internal circulation only

Bins [TeV]	1.0–1.1	1.1–1.2	1.2–1.3	1.3–1.4	1.4–1.5	1.5–1.7	1.7–1.9	1.9–2.1	2.1–2.3	2.3–3.0
Statistics [%]	+1.6	+1.3	+1.5	+1.7	+2.0	+1.7	+2.4	+3.5	+5.0	+5.0
Systematics [%]	+11.2	+11.6	+12.1	+12.6	+13.0	+12.9	+13.9	+12.7	+18.4	+13.0
Total Uncertainty [%]	+11.4	+11.9	+13.2	+13.5	+14.8	+13.6	+16.3	+15.1	+16.3	+17.1
(JES) Large- R jet Modelling τ_{32} [%]	-6.15	-6.85	-7.33	-7.69	-7.63	-7.97	-8.34	-7.03	-11.3	-6.53
Light-jet tagging efficiency (eigenvector 10) [%]	+6.68	+7.56	+8.19	+8.59	+9.24	+8.97	+10.2	+9.58	+11.1	+10.3
Light-jet tagging efficiency (eigenvector 13) [%]	-	-	-	-	-	-	-	-	-	-
Light-jet tagging efficiency (eigenvector 12) [%]	-	-	-	-	-	-	-	-	-	-
Single top t -channel treatment [%]	+0.14	+0.24	+0.23	+0.21	+0.14	-	+0.15	+0.41	+0.15	-
Light jet tagging efficiency (eigenvector 0) [%]	-0.31	-0.11	-0.18	-0.23	-0.18	-0.20	-0.23	-0.25	-0.19	-
(JES) Flavour response [%]	+0.31	+0.11	+0.18	+0.23	+0.18	+0.23	+0.23	+0.24	+0.19	-
b -Quark tagging extrapolation [%]	+1.68	+2.00	+2.33	+2.53	+2.78	+2.91	+3.14	+3.56	+3.17	+3.66
Electron energy resolution [%]	-1.67	-1.98	-2.29	-2.50	-2.73	-2.84	-3.06	-3.46	-3.08	-3.49
b -Quark tagging efficiency (eigenvector 0) [%]	-3.73	-3.88	-3.98	-3.91	-3.87	-3.82	-3.75	+0.46	-3.71	-3.27
QCD data-driven background shape [%]	+0.59	+0.12	+0.20	+0.76	+0.52	-	-0.13	-1.43	+1.12	+0.50
Pile-up [%]	-1.00	-0.39	-0.38	-0.38	-0.36	-0.36	-0.51	-0.80	-1.78	+0.88
E_T^{miss} Soft jet resolution para [%]	-	-	-	-	-	-	-	-	-	-
(JES) η intercalibration non-closure [%]	-	-	-	-	-	-	-	-	-	-
b -Quark tagging efficiency (eigenvector 1) [%]	-3.44	-3.61	-3.71	-3.70	-3.66	-3.54	-3.50	-3.38	-3.32	-2.91
Muon (MS) momentum resolution [%]	+3.52	+3.70	+3.80	+3.78	+3.75	+3.62	+3.59	+3.46	+3.41	+2.99
b -Quark tagging efficiency (eigenvector 4) [%]	-0.15	-0.17	+0.19	+0.19	+0.20	+0.20	+0.21	+0.23	+0.21	+0.20
(JES) b -Tagged jet energy scale [%]	+0.16	+0.17	+0.19	+0.19	+0.20	+0.20	+0.21	+0.23	+0.21	+0.20
Single top Wt cross-section [%]	-	-	-	-	-	-	-	-	-	-
E_T^{miss} Soft jet scale [%]	-	-	-	-	-	-	-	-	-	-
(JES) η intercalibration model [%]	-	-	-	-	-	-	-	-	-	-
Electron energy scale [%]	-	-	-	-	-	-	+0.46	-	-	-
(JES) Effective detector NP set 7 [%]	-	-	-	-	-	-	-	-	-	-
Jet vertex tagging [%]	-0.13	-	-	-	-	-	-	-	-0.12	-
Light-jet tagging efficiency (eigenvector 9) [%]	-0.22	-	-	-	-0.19	-	-	-	-	-
Light-jet tagging efficiency (eigenvector 8) [%]	-0.24	-	-	-	-	-	-	-	-	-
(JES) Large- R jet top-quark mass resolution [%]	+0.64	+0.53	+0.80	+1.40	+0.14	+0.84	+0.59	+1.60	+1.45	+3.63
(JES) Effective detector NP set 8 (restTerm) [%]	-	-	-	-	-	-	-	-	-	-
Light-jet tagging efficiency (eigenvector 1) [%]	-	-	-	-	-	-	-	-	-	-
(JES) Large- R jet Baseline p_T [%]	+1.97	+1.54	+1.50	+0.85	+2.79	+1.84	+2.63	+3.38	+4.42	+3.64
(JES) Large- R jet Baseline τ_{32} [%]	-1.97	-0.55	-1.37	-1.28	-2.98	-1.63	-3.63	-3.07	-1.48	-4.15
Light-jet tagging efficiency (eigenvector 3) [%]	-	-	-	+0.11	-	-	+0.11	-	-	-
Light-jet tagging efficiency (eigenvector 2) [%]	+0.16	-	-	-	+0.11	-	+0.11	-	-	-
(JES) Effective detector NP set 6 [%]	-0.16	-	-	-	-0.11	-	-0.11	-	-	-
(LJES) Large- R jet TotalStat p_T [%]	+0.32	+0.13	+0.28	+0.16	+0.42	-	+0.15	+0.55	-	+0.36
Light-jet tagging efficiency (eigenvector 7) [%]	-0.12	-0.18	-0.12	-0.72	-	-0.19	-0.23	-0.17	-0.27	-0.45
Muon sagitta ho [%]	-	-	-	-	-	-	-	-	-	-
(JES) Pile-up offset N_{PV} [%]	-0.42	-0.49	-0.38	-0.46	-0.46	-0.44	-0.38	-0.45	-0.26	-
c-Quark tagging efficiency (eigenvector 2) [%]	-0.42	-0.19	-0.15	-0.15	-	+0.15	+0.11	+0.38	-	-
c-Quark tagging efficiency (eigenvector 3) [%]	-0.35	-0.35	-0.33	-0.37	-0.33	-0.33	-0.29	-	-	-
c-Quark tagging efficiency (eigenvector 0) [%]	+1.51	+2.00	+1.35	+1.47	+1.14	+1.56	+1.34	+1.69	+0.90	+0.29
c-Quark tagging efficiency (eigenvector 1) [%]	-1.05	-1.30	-0.87	-1.00	-0.89	-1.03	-0.94	-1.22	-0.61	-0.13
(LJES) Large- R jet TotalStat τ_{32} [%]	+0.87	+0.15	+0.69	+0.69	+0.74	+0.74	+0.90	+0.19	+1.14	+0.17
b-Quark tagging efficiency (eigenvector 3) [%]	+0.31	+0.36	+0.15	+0.40	-0.46	-0.44	-0.48	+0.37	+0.38	+0.31
E_T^{miss} Soft jet resolution perp [%]	-	-	-	-	-	-	-	-	-	-
(JES) Effective detector NP set 2 [%]	-	-	-	-	-	-	-	-	-	-
b-Quark tagging extrapolation from c-Quark [%]	-	-	-	-	-	-	-	-	-	-
(LJES) Large- R jet Tracking p_T [%]	+4.36	+3.12	+3.61	+4.03	+4.83	+4.07	+5.24	+3.15	+6.50	+5.69
(JES) Effective detector NP set 3 [%]	-3.03	-2.25	-4.74	-3.37	-3.56	-3.24	-6.16	-4.09	-1.97	-4.96
(LJES) Large- R jet TotalStat mass [%]	-	-	+0.19	-	-	-	-	-	-	-0.92
(JES) Effective detector NP set 5 [%]	-	-	-	-	-	-	-	-	-	+0.15
(LJES) Large- R jet Baseline mass [%]	+0.26	+0.55	+0.46	+0.94	+0.37	+0.42	-	+1.24	-	-0.67
Muon energy scale [%]	-0.33	-0.64	-0.40	-0.73	-	-0.21	-0.38	-	-0.21	-
(JES) File-up offset p_T [%]	-	-	-	-	-	-	-	-	-	-
(LJES) Large- R jet Modelling mass [%]	-0.30	-0.60	-0.63	-0.72	-0.78	-0.78	-0.10	-	-0.29	+0.21
(JES) Effective detector NP set 1 [%]	-	-	-	-	-	-	-0.14	-	-0.21	-
(LJES) Large- R jet Baseline τ_{32} [%]	-4.90	-5.69	-5.72	-6.10	-6.30	-6.30	-5.87	-5.74	-5.98	-5.23
(JES) Single particle high- p_T [%]	+1.18	+0.90	+0.40	+0.87	+0.30	+0.88	+0.93	+0.79	+0.70	+0.24
Light-jet tagging efficiency (eigenvector 5) [%]	-	-	-	-	-	-	-	-	-	-
(JES) File-up offset topology [%]	-	+0.16	-	+0.13	+0.14	+0.13	-	+0.14	+0.16	+0.26
(LJES) Large- R jet Modelling p_T [%]	+2.55	+1.81	+2.01	+1.17	+1.73	+1.51	+1.60	+1.55	+2.20	+1.26
(JES) Pile-up offset μ [%]	-1.94	-1.73	-1.87	-1.87	-1.64	-1.72	-0.03	-1.91	-0.36	-1.74
(JES) η intercalibration total stat [%]	-	-	-	-	-	-	-	-	-	-
Light-jet tagging efficiency (eigenvector 4) [%]	-0.14	-	-	-	-	-0.12	-	-0.10	-	-
Muon (ID) momentum resolution [%]	-	-	-	-	-	+0.14	-	+0.10	-	-
(JES) Flavour composition [%]	+0.16	+0.17	+0.21	+0.15	+0.24	+0.20	-	+0.15	+0.16	+0.17
(JES) Effective detector NP set 4 [%]	-0.12	-0.11	-0.10	-0.18	-0.10	-0.22	-	-	-0.25	-
Light-jet tagging efficiency (eigenvector 11) [%]	-	-	-	-	-	-	-	-	-	-
(LJES) Large- R jet Tracking τ_{32} [%]	-0.26	-0.35	-0.19	-0.42	-0.19	-0.25	-0.46	-0.26	-1.19	-0.43
(LJES) Large- R jet Tracking mass [%]	+0.23	+0.31	+0.28	+0.26	+0.40	+0.18	+0.34	+0.52	+0.35	+0.31
Light-jet tagging efficiency (eigenvector 6) [%]	-	-	-	-0.27	-	-	-	-	-	+0.59
(JES) Pile-up offset μ [%]	-	-	-	-	-	-	-	-	-	-
b-Quark tagging efficiency (eigenvector 2) [%]	-0.47	-0.53	-0.61	-0.59	-0.69	-0.63	-0.64	-0.62	-0.65	-0.66
(JES) Punch-through [%]	-	-	-	-	-	-	-	-	-	+0.66
Muon sagitta resolution bias [%]	-	-	-	-	-	-	-	-	-	-

Table 164: The individual systematic uncertainties in the top quark-antiquark system transverse momentum calculated as a percentage of the transverse momentum in each bin. Dashes are used when the estimated relative systematic uncertainty for that bin is below 0.1%.

Bins	0.0–0.3	0.3–0.6	0.6–0.9	0.9–1.2	1.2–1.5	1.5–2.0
Statistics [%]	± 1.0	± 1.1	± 1.4	± 1.9	± 2.3	± 5.0
Systematics [%]	$+11.7$	$+11.9$	$+12.0$	$+12.6$	$+14.2$	$+10.7$
Total Uncertainty [%]	$+13.0$	$+12.5$	$+12.7$	$+13.0$	$+12.2$	$+13.0$
(LJES) Large- R jet Modelling τ_{32} [%]	-6.75 +8.22	-7.00 +7.70	-6.85 +7.91	-7.70 +8.28	-8.99 +7.36	-4.50 +7.99
Light-jet tagging efficiency (eigenvector 10) [%]	-	-	-	-	-	-
Light-jet tagging efficiency (eigenvector 13) [%]	-	-	-	-	-	-
Light-jet tagging efficiency (eigenvector 12) [%]	-	-	-	-	-	-
Single top t -channel treatment [%]	± 0.22	± 0.18	± 0.30	-	± 0.14	± 0.13
Light-jet tagging efficiency (eigenvector 0) [%]	-0.12 +0.12	-0.13 +0.13	-0.21 +0.23	-0.52 +0.51	-0.30 +0.29	-0.19 +0.19
(JES) Flavour response [%]	-	-	-	-	-	-
b -Quark tagging extrapolation [%]	$+2.39$ -2.35	$+2.35$ -2.31	$+2.24$ -2.21	$+1.99$ -1.97	$+2.08$ -2.05	$+1.63$ -1.61
Electron energy resolution [%]	-	-	-	-	-	-
b -Quark tagging efficiency (eigenvector 0) [%]	-3.91 +4.01 +0.55	-3.94 +4.04 -0.55	-3.83 +3.92 -0.22	-3.73 +3.82 -0.02	-3.91 +4.00 -0.58	-3.74 +3.84 +1.77
QCD data-driven background shape [%]	-0.25 -0.61	-0.17 -0.39	-0.22 -0.48	-0.21 -0.21	-0.16 -0.62	-0.17 +1.77
Pile-up [%]	+0.36	-	+0.59	+0.60	+0.52	-1.79
E_T^{miss} Soft jet resolution para [%]	-	-	-	-	-	-
(JES) η intercalibration non-closure [%]	-	-	-	-	-	-
b -Quark tagging efficiency (eigenvector 1) [%]	-3.65 +3.73	-3.66 +3.74	-3.56 +3.64	-3.45 +3.52	-3.63 +3.71	-3.35 +3.43
Muon (MS) momentum resolution [%]	-	-	-	-	-	-
b -Quark tagging efficiency (eigenvector 4) [%]	-0.19 +0.19	-0.19 +0.19	-0.18 +0.18	∓ 0.17	-0.17 +0.17	-0.14 +0.14
(JES) b -Tagged jet energy scale [%]	-	-	-	-	-	-
Single top Wt cross-section [%]	-	-	-	-	-	-
E_T^{miss} Soft jet scale [%]	-	-	-	-	-	-
(JES) η intercalibration model [%]	-	-	-	-	-	-
Electron energy scale [%]	-	-	-	-	-	-
(JES) Effective detector NP set 7 [%]	-	-	-	-	-	-
Jet vertex tagging [%]	-	-	-	-0.12	-	-
Light-jet tagging efficiency (eigenvector 9) [%]	-0.20	-0.21	-0.20	-	-	-
Light-jet tagging efficiency (eigenvector 8) [%]	-	-0.20	-	-0.22	-	-
(LJES) Large- R jet top-quark mass resolution [%]	∓ 1.31	∓ 0.52	∓ 0.95	∓ 2.01	∓ 0.54	∓ 1.12
(JES) Effective detector NP set 8 (restTerm) [%]	-	-	-	-	-	-
Light-jet tagging efficiency (eigenvector 1) [%]	-	-	-	-	-	-
(LJES) Large- R jet Baseline p_T [%]	+1.77 -1.48	+1.82 -1.96	+2.08 -1.57	+1.88 -1.58	+2.18 -1.74	+1.82 -1.52
Light-jet tagging efficiency (eigenvector 3) [%]	-	-	-	-	-	-
Light-jet tagging efficiency (eigenvector 2) [%]	-	-	+0.12	+0.11 +0.22	+0.16	+0.14
(JES) Effective detector NP set 6 [%]	-	-	-0.12	-0.22	-0.16	-0.14
(LJES) Large- R jet TotalStat p_T [%]	+0.29 -0.21	+0.17 -0.23	+0.30 -0.12	+0.16 -0.19	+0.36 -0.15	+0.12 -0.14
Light-jet tagging efficiency (eigenvector 7) [%]	-	-	-	-	-	-
Muon sagitta ho [%]	-	-	-	-	-	-
(JES) Pile-up offset N_{PV} [%]	-	-	-	-	-	-
c -Quark tagging efficiency (eigenvector 2) [%]	-0.45	-0.48	-0.51	-0.34	-0.46	-
c -Quark tagging efficiency (eigenvector 3) [%]	-	-	+0.13	-	-	-
c -Quark tagging efficiency (eigenvector 0) [%]	-0.33 +1.54 +0.78	-0.34 +1.33 -0.88	-0.36 +1.79 -0.87	-0.38 +1.43 -0.87	-0.43 +1.97 -1.21	-1.69 +1.75 -0.85
c -Quark tagging efficiency (eigenvector 1) [%]	-0.10 +0.78	-1.07 -0.88	-1.21 +1.02	-0.87 +0.72	-1.21 +0.90	-1.21 +0.72 -0.10
(LJES) Large- R jet TotalStat τ_{32} [%]	+0.14 -0.41	+0.11 -0.40	+0.13 -0.37	+0.12 -0.33	+0.16 +0.34	+0.18 +0.26
b -Quark tagging efficiency (eigenvector 3) [%]	+0.41	+0.40	+0.38	+0.33	+0.34	+0.26
E_T^{miss} Soft jet resolution perp [%]	-	-	-	-	-	-
(JES) Effective detector NP set 2 [%]	-	-	-	-	-	-
b -Quark tagging extrapolation from c -Quark [%]	-	-	-	-	-	-
(LJES) Large- R jet Tracking p_T [%]	+3.78 -3.41	+3.79 -3.73	+4.17 -3.95	+4.04 -4.01	+4.58 -4.21	+5.93 -3.93
(JES) Effective detector NP set 3 [%]	-	-	-	-	-	-
(LJES) Large- R jet TotalStat mass [%]	-	-	-	-	-	-
(JES) Effective detector NP set 5 [%]	-	-	-	-	-	-
(LJES) Large- R jet Baseline mass [%]	+0.41 -0.68	+0.39 -0.40	+0.37 -0.25	+0.38 -0.17	+0.47 -0.27	-0.22 +0.25
Muon energy scale [%]	-	-	-	-	-	-
(JES) Pile-up offset p_T [%]	-	-	-	-	-	-
(LJES) Large- R jet Modelling mass [%]	+0.44 -0.91	+0.16 -0.27	+0.44 -0.19	+0.28 -0.21	+0.38 -0.21	-0.72 +0.85
(JES) Effective detector NP set 1 [%]	-	-	-	-	-	-
(LJES) Large- R jet Baseline τ_{32} [%]	-5.39 +6.39	-5.70 +6.07	-5.52 +6.19	-6.13 +6.40	-6.95 +5.39	-3.72 +6.48
(JES) Single particle high p_T [%]	-	-	-	-	-	-
Light-jet tagging efficiency (eigenvector 5) [%]	-	-	-	-	-	-
(JES) Pile-up offset ρ topology [%]	+0.18	+0.14	+0.11	-	+0.17	+0.42
(LJES) Large- R jet Modelling p_T [%]	+1.74 -1.61	+1.82 -1.61	+2.18 -1.67	+1.74 -1.58	+2.15 -1.79	+2.11 -1.82
(JES) η intercalibration total stat [%]	-	-	-	-	-	-
Light-jet tagging efficiency (eigenvector 4) [%]	-	-	-	-0.17	-	-
Muon (ID) momentum resolution [%]	-	-	-	-	-	-
(JES) Flavour composition [%]	+0.24	+0.19	+0.14	-	+0.17	+0.43
(JES) Effective detector NP set 4 [%]	-	-0.13	-0.16	-0.17	-0.15	-
Light-jet tagging efficiency (eigenvector 11) [%]	-	-	-	-	-	-
(LJES) Large- R jet Tracking τ_{32} [%]	-0.27 +0.31	-0.28 +0.24	-0.26 +0.30	-0.40 +0.24	-0.60 +0.30	-0.14 +0.24
(LJES) Large- R jet Tracking mass [%]	-0.21	-	-	-	+0.21	+0.96
Light-jet tagging efficiency (eigenvector 6) [%]	-	-	-	-	-	-
(JES) Pile-up offset μ [%]	-	-	-	-	-	-
b -Quark tagging efficiency (eigenvector 2) [%]	-0.60 +0.61	-0.58 +0.58	-0.55 +0.55	-0.47 +0.48	-0.53 +0.53	-0.42 +0.42
(JES) Punch-through [%]	-	-	-	-	-	-
Muon sagitta resolution bias [%]	-	-	-	-	-	-

Table 165: The individual systematic uncertainties in the top quark-antiquark system absolute value of the rapidity calculated as a percentage of the rapidity in each bin. Dashes are used when the estimated relative systematic uncertainty for that bin is below 0.1%.

Bins [GeV]	0.0–20.0	20.0–40.0	40.0–60.0	60.0–100.0	100.0–200.0	200.0–300.0	300.0–600.0
Statistics [%]	± 0.9	± 1.2	± 1.8	± 1.6	± 1.9	± 3.4	± 5.1
Systematics [%]	± 11.9	± 12.4	± 11.3	± 12.1	± 12.0	± 12.4	± 12.9
Total Uncertainty [%]	± 12.7	± 13.4	± 12.9	± 12.3	± 11.9	± 12.9	± 13.0
(LJES) Large- R jet Modelling τ_{32} [%]	-6.95 +7.92	-7.25 +8.65	-7.54 +7.54	-7.27 +7.59	-7.00 +7.79	-6.43 +7.98	-7.37 +8.10
Light-jet tagging efficiency (eigenvector 10) [%]	-	-	-	-	-	-	-
Light-jet tagging efficiency (eigenvector 13) [%]	-	-	-	-	-	-	-
Light-jet tagging efficiency (eigenvector 12) [%]	-	-	-	-	-	-	-
Single top t -channel treatment [%]	± 0.21	± 0.16	-	± 0.27	± 0.28	± 0.11	± 0.13
Light-jet tagging efficiency (eigenvector 0) [%]	-0.14 +0.13	-	-0.45 +0.45	-0.21 +0.22	-0.17 +0.17	-0.55 +0.61	+0.22 -0.22
(JES) Flavour response [%]	-	-	-	-	-	-0.26	-
b -Quark tagging extrapolation [%]	+2.47 -2.43	+2.36 -2.32	+2.15 -2.12	+2.18 -2.15	+1.97 -1.94	+2.11 -2.19	+2.73 -2.13
Electron energy resolution [%]	-	-	-	-	-	-	-
b -Quark tagging efficiency (eigenvector 0) [%]	-4.14 +4.25	-4.01 +4.11	-3.75 +3.84	-3.64 +3.73	-3.51 +3.59	-3.86 +4.20	-3.52 +3.60
QCD data-driven background shape [%]	-	-	-	-	± 0.13	-0.20	+0.21
Pile-up [%]	-0.65 +0.41	-0.15 +0.37	-0.47 +0.54	+0.29 +0.33	-0.63 +0.71	-1.11 +0.16	+0.33 +0.16
E_T^{miss} Soft jet resolution para [%]	-	-	-	-	-	-	-
(JES) η intercalibration non-closure [%]	-	-	-	-	-	-0.22	-
b -Quark tagging efficiency (eigenvector 1) [%]	-3.89 +3.98	-3.75 +3.83	-3.46 +3.54	-3.37 +3.45	-3.21 +3.28	-3.45 +3.53	-3.20 +3.27
Muon (MS) momentum resolution [%]	-	-	-	-	-	-	-
b -Quark tagging efficiency (eigenvector 4) [%]	-0.19 +0.19	-0.19 +0.19	-0.18 +0.18	-0.17 +0.17	-0.15 +0.15	-0.17 +0.17	-0.16 +0.16
(JES) b -Tagged jet energy scale [%]	-	-	-	-	-	-	-
Single top Wt cross-section [%]	-	-	-	-	-	-	-
E_T^{miss} Soft jet scale [%]	-	-	-	-	-	-	-
(JES) η intercalibration model [%]	-	-	-	-	-	-	-
Electron energy scale [%]	-	-	-	-	-	-	-
(JES) Effective detector NP set 7 [%]	-	-	-	-	-	-	-
Jet vertex tagging [%]	-	-	-	-	+0.11	-	+0.16
Light-jet tagging efficiency (eigenvector 9) [%]	-	-	-0.20	-0.25	-0.35	-0.43	-0.54
Light-jet tagging efficiency (eigenvector 8) [%]	-	-	-0.26	-0.25	-0.33	-0.34	-0.57
(LJES) Large- R jet top-quark mass resolution [%]	± 1.26	± 0.97	± 0.72	± 1.28	± 1.20	± 0.91	± 0.58
(JES) Effective detector NP set 8 (restTerm) [%]	-	-	-	-	-	-	-
Light-jet tagging efficiency (eigenvector 1) [%]	-	-	-	-	-	-	-
(LJES) Large- R jet Baseline p_T [%]	+1.39 -1.32	+1.94 -1.54	+1.39 -1.74	+1.86 -2.12	+2.80 -1.61	+3.50 -3.04	+1.92 -1.06
Light-jet tagging efficiency (eigenvector 3) [%]	-	-	-	-	-	+0.16	-
Light-jet tagging efficiency (eigenvector 2) [%]	-	-	+0.17	-	-	+0.14	-
(JES) Effective detector NP set 6 (%)	-	-	-	-	-	-	-
(LJES) Large- R jet TotalStat p_T [%]	+0.18 -0.19	+0.28 -0.14	+0.21 -0.25	+0.26 -0.18	+0.30 -0.17	+0.39 -0.29	+0.31 -0.44
Light-jet tagging efficiency (eigenvector 7) [%]	-	-	-	-	-	+0.10	-
Muon sagitta ho [%]	-	-	-	-	-	-	-
(JES) Pile-up offset N_{PV} [%]	-	-	-	-	-	-0.23	-
c -Quark tagging efficiency (eigenvector 2) [%]	-0.33 +0.18	-0.36 +0.11	-0.35 -0.35	-0.64 -0.58	-	-0.84	-0.90
c -Quark tagging efficiency (eigenvector 3) [%]	-0.35 -0.35	-0.33 -0.35	-0.28 -0.28	-0.46 -0.46	-0.44 -0.44	-0.62 -0.57	-
c -Quark tagging efficiency (eigenvector 0) [%]	-1.55 +1.55	-1.45 +1.45	-0.93 +0.94	-0.92 +0.94	-1.35 +1.35	-2.23 +2.23	-0.57 +1.70
c -Quark tagging efficiency (eigenvector 1) [%]	+0.97 +0.97	+0.90 +0.90	+0.76 +0.76	+2.07 +2.07	+1.15 +1.15	+1.73 +1.73	+1.70 +0.72
(LJES) Large- R jet TotalStat τ_{32} [%]	+0.10 +0.10	+0.16 +0.16	+0.55 +0.55	+1.72 +1.72	+0.84 +0.84	+0.23 +0.23	+0.72 +0.72
b -Quark tagging efficiency (eigenvector 3) [%]	+0.42 +0.42	+0.40 +0.40	+0.37 +0.37	+0.36 +0.36	+0.33 +0.33	+0.39 +0.39	+0.37 +0.37
E_T^{miss} Soft jet resolution perp [%]	-	-	-	-	-	-	-
(JES) Effective detector NP set 2 (%)	-	-	-	-	-	-	-
b -Quark tagging extrapolation from c -Quark [%]	-	-	-	-	-	-	-
(LJES) Large- R jet Tracking p_T [%]	+3.60 -3.22	+4.33 -4.07	+3.50 -3.44	+3.91 -4.57	+4.23 -2.99	+4.37 -5.31	+5.22 -4.76
(JES) Effective detector NP set 3 (%)	-	-	-	-	-	-	-
(LJES) Large- R jet TotalStat mass [%]	-	-	-	-	-	+0.43	-
(JES) Effective detector NP set 5 (%)	-	-	-	-	-	-	-
(LJES) Large- R jet Baseline mass [%]	+0.50 -0.53	+0.44 -0.64	+0.58 -0.32	-0.26 -0.42	+0.30 +1.29	+1.29 -0.21	-
Muon energy scale [%]	-	-	-	-	-	-	-
(JES) Pile-up offset p_T [%]	-	-	-	-	-	-	-
(LJES) Large- R jet Modelling mass [%]	+0.63 -0.61	+0.45 -0.58	+0.63 -0.42	-0.52 -0.40	-	+1.81 +0.13	-0.32 +0.13
(JES) Effective detector NP set 1 (%)	-	-	-	-	-	+0.27	-
(LJES) Large- R jet Baseline τ_{32} [%]	-5.53 +6.22	-5.68 +6.79	-5.66 +5.82	-5.90 +5.90	-5.61 +5.90	-5.24 +6.55	-5.81 +5.53
(JES) Single particle high- p_T [%]	-	-	-	-	-	-	-
Light-jet tagging efficiency (eigenvector 5) [%]	-	-	-	-	-	-	-
(JES) Pile-up offset ρ topology [%]	-	-	+0.16	+0.13	-	+0.29	+0.24
(LJES) Large- R jet Modelling p_T [%]	+1.69 -1.42	+2.12 -1.71	+1.49 -1.73	+1.60 -1.87	+2.36 -1.37	+1.92 -2.22	+3.40 -1.96
(JES) η intercalibration total stat [%]	-	-	-	-	-	-	-
Light-jet tagging efficiency (eigenvector 4) [%]	-	-	-0.18	-	-	-0.24	-
Muon (ID) momentum resolution [%]	-	-	+0.18	-	-	+0.29	-
(JES) Flavour composition [%]	+0.16 -0.16	+0.19 -0.14	+0.17 -0.14	+0.18 -0.25	+0.20 -0.14	+0.35 -0.30	+0.45 -0.45
(JES) Effective detector NP set 4 (%)	-	-	-	-	-	-	-
Light-jet tagging efficiency (eigenvector 11) [%]	-	-	-	-	-	-	-
(LJES) Large- R jet Tracking τ_{32} [%]	-0.26 +0.19	-0.29 +0.14	-0.33 +0.36	-0.37 +0.30	-0.30 +0.22	-0.33 +1.49	-0.21 +0.25
(LJES) Large- R jet Tracking mass [%]	-	-	-	-0.31	-	-	+0.75
Light-jet tagging efficiency (eigenvector 6) [%]	-	-	-	-	-	-	-
(JES) Pile-up offset μ [%]	-	-	-	-	-	-	-
b -Quark tagging efficiency (eigenvector 2) [%]	-0.64 +0.64	-0.60 +0.61	-0.52 +0.52	-0.52 +0.52	-0.47 +0.47	-0.49 +0.49	-0.50 +0.50
(JES) Punch-through [%]	-	-	-	-	-	-	-
Muon sagitta resolution bias [%]	-	-	-	-	-	-	-

Table 166: The individual systematic uncertainties in the top quark-antiquark system out-of-plane momentum $|p_{\text{out}}^{t\bar{t}}|$, calculated as a percentage of the out-of-plane momentum in each bin. Dashes are used when the estimated relative systematic uncertainty for that bin is below 0.1%.

Bins [rad]	0.0–2.5	2.5–2.75	2.75–3.0	3.0–3.14
Statistics [%]	±4.7	±3.0	±1.4	±0.7
Systematics [%]	+13.0 -1.9 +13.8 -12.8	+12.1 -13.2 +12.5 -13.5	+11.5 -12.0 +11.5 -12.1	+12.1 -13.0
Total Uncertainty [%]	-	-	-	-
(LJES) Large- R jet Modelling τ_{32} [%]	-7.90 +7.04	-5.92 +7.81	-6.81 +7.52	-7.15 +8.17
Light-jet tagging efficiency (eigenvector 10) [%]	-	-	-	-
Light-jet tagging efficiency (eigenvector 13) [%]	-	-	-	-
Light-jet tagging efficiency (eigenvector 12) [%]	-	-	-	-
Single top t -channel treatment [%]	±0.18	-	±0.24	±0.19
Light-jet tagging efficiency (eigenvector 0) [%]	+0.48 -0.48 +0.29 +1.78 -1.76	+0.31 +0.31 -0.29 +1.85 -1.83	+0.18 +0.18 -0.18 +1.98 -1.94	+0.18 +0.18 -0.18 +2.41 -2.37
b -Quark tagging extrapolation [%]	-	-	-	-
Electron energy resolution [%]	-	-	-	-
b -Quark tagging efficiency (eigenvector 0) [%]	-3.55 -3.63 -0.73 +0.75 -0.39 +0.86	-3.70 +3.80 +1.12 -1.12 -0.35 +0.36	-3.51 -3.60 -0.45 +0.45 -0.14 +0.40	-4.00 +4.10 - -
QCD data-driven background shape [%]	-	-	-	-
Pile-up [%]	-	-	-	-
E_T^{miss} Soft jet resolution para [%]	-	-	-	-
(JES) η intercalibration non-closure [%]	-0.42	-	-	-
b -Quark tagging efficiency (eigenvector 1) [%]	-3.30 +3.37	-3.26 +3.33	-3.25 +3.32	-3.74 +3.83
Muon (MS) momentum resolution [%]	-	-	-	-
b -Quark tagging efficiency (eigenvector 4) [%]	-0.13 +0.13	-0.15 +0.15	-0.16 +0.16	-0.19 +0.19
(JES) b -Tagged jet energy scale [%]	-	-	-	-
Single top Wt cross-section [%]	-	-	-	-
E_T^{miss} Soft jet scale [%]	-	-	-	-
(JES) η intercalibration model [%]	-	-	-	-
Electron energy scale [%]	-	-	-	-
(JES) Effective detector NP set 7 [%]	-	-	-	-
Jet vertex tagging [%]	-	+0.14 -0.17	-	-
Light-jet tagging efficiency (eigenvector 9) [%]	-0.61	-0.38	-0.31	-
Light-jet tagging efficiency (eigenvector 8) [%]	-0.50	-0.36	-0.30	-
(LJES) Large- R jet top-quark mass resolution [%]	±0.95	-	±1.14	±1.15
(JES) Effective detector NP set 8 (restTerm) [%]	-	-	-	-
Light-jet tagging efficiency (eigenvector 1) [%]	-	-	-	-
(LJES) Large- R jet Baseline p_T [%]	+4.03 -1.11	+3.36 -2.84	+2.03 -1.91	+1.63 -1.46
Light-jet tagging efficiency (eigenvector 3) [%]	+0.15	-0.13	-	-
Light-jet tagging efficiency (eigenvector 2) [%]	+0.20	-	-	-
(JES) Effective detector NP set 6 [%]	-	-	-	-
(LJES) Large- R jet TotalStat p_T [%]	+0.18 -0.25	+0.42 -0.12	+0.25 -0.20	+0.23 -0.20
Light-jet tagging efficiency (eigenvector 7) [%]	-0.14 +0.15	-	-	-
Muon sagitta ho [%]	-	-	-	-
(JES) Pile-up offset N_{PV} [%]	+0.19 -0.34	-	-	-
c -Quark tagging efficiency (eigenvector 2) [%]	-0.68	-0.63	-0.35	-
c -Quark tagging efficiency (eigenvector 3) [%]	-0.98	-	-	+0.11
c -Quark tagging efficiency (eigenvector 0) [%]	-2.10 +2.08	-1.90 +1.95	-1.59 +1.59	-1.42 +0.45
c -Quark tagging efficiency (eigenvector 1) [%]	+1.53 +0.97	+1.36 +0.10	+1.31 +0.03	+0.91 +0.80
(LJES) Large- R jet TotalStat τ_{32} [%]	-	+0.19	+0.11	-0.12
b -Quark tagging efficiency (eigenvector 3) [%]	-0.26 +0.26	-0.32 +0.32	-0.34 +0.34	-0.41 +0.41
E_T^{miss} Soft jet resolution perp [%]	-	-	-	-
(JES) Effective detector NP set 2 [%]	-	-	-	-
b -Quark tagging extrapolation from c -Quark [%]	-	-	-	-
(LJES) Large- R jet Tracking p_T [%]	+2.79 -3.61	+5.60 -4.91	+3.74 -3.69	+3.92 -3.63
(JES) Effective detector NP set 3 [%]	-	-	-	-
(LJES) Large- R jet TotalStat mass [%]	-	+0.39	-	-
(JES) Effective detector NP set 5 [%]	-	-	-	-
(LJES) Large- R jet Baseline mass [%]	-	+0.41	+0.25	+0.44
Muon energy scale [%]	-	-	-	-
(JES) Pile-up offset p_T [%]	-	-	-	-
(LJES) Large- R jet Modelling mass [%]	-	+0.85	-0.37	+0.46 -0.51
(JES) Effective detector NP set 1 [%]	+0.44	-	-	-
(LJES) Large- R jet Baseline τ_{32} [%]	-6.50 +5.99	-4.66 +6.32	-5.50 +5.72	-5.73 +6.38
(JES) Single particle high- p_T [%]	-	-	-	-
Light-jet tagging efficiency (eigenvector 5) [%]	+0.12 -0.11	-	-	-
(JES) Pile-up offset ρ topology [%]	+0.01 -0.47	-	+0.11 +0.10	+0.14 -0.51
(LJES) Large- R jet Modelling p_T [%]	+1.76 -1.77	+3.26 -2.20	+1.72 -1.59	+1.82 -1.59
(JES) η intercalibration total stat [%]	-	-	-	-
Light-jet tagging efficiency (eigenvector 4) [%]	-0.44 +0.54	-	-	-
Muon (ID) momentum resolution [%]	-	-	-	-
(JES) Flavour composition [%]	+0.77	-	+0.16	+0.18
(JES) Effective detector NP set 4 [%]	-0.52	-	-0.22	-
Light-jet tagging efficiency (eigenvector 11) [%]	-	-	-	-
(LJES) Large- R jet Tracking τ_{32} [%]	-0.15 +0.16	-0.40 +0.26	-0.26 +0.22	-0.31 +0.30
(LJES) Large- R jet Tracking mass [%]	-0.13 +0.42	+0.75	-	-
Light-jet tagging efficiency (eigenvector 6) [%]	-	-	-	-
(JES) Pile-up offset μ [%]	-	-	-	-
b -Quark tagging efficiency (eigenvector 2) [%]	-0.40 +0.40	-0.43 +0.43	-0.48 +0.48	-0.61 +0.61
(JES) Punch-through [%]	-	-	-	-
Muon sagitta resolution bias [%]	-	-	-	-

Table 167: The individual systematic uncertainties in the top quark-antiquark system aperture angle $\Delta\phi^{t\bar{t}}$, calculated as a percentage of the aperture angle in each bin. Dashes are used when the estimated relative systematic uncertainty for that bin is below 0.1%.

Bins [GeV]	1000.0–1100.0	1100.0–1200.0	1200.0–1300.0	1300.0–1400.0	1400.0–1600.0	1600.0–1800.0	1800.0–2200.0
Statistics [%]	±1.1	±1.3	±1.7	±2.4	±2.1	±3.8	±6.6
Systematics [%]	±1.4	±1.6	±1.2	±1.6	±0.7	±2.2	±2.2
Total Uncertainty [%]	±1.9	±1.5	±1.4	±1.6	±0.3	±2.2	±2.2
(JES) Large- R jet Modelling $r\tau\tau$ [%]	-6.6	-8.34	-8.78	-9.00	-10.4	-11.7	-12.5
Light-jet tagging efficiency (eigenvector 10) [%]	+0.03	+8.68	+0.05	+0.05	+13.2	+44.3	+12.1
Light-jet tagging efficiency (eigenvector 13) [%]	-	-	-	-	-	-	-
Light-jet tagging efficiency (eigenvector 12) [%]	-	-	-	-	-	-	-
Single top t -channel treatment [%]	±0.23	±0.12	±0.22	±0.15	-	±0.12	±0.20
Light-jet tagging efficiency (eigenvector 0) [%]	-0.21	-0.19	-0.22	-0.21	-	-0.23	-0.54
(JES) Flavour response [%]	+0.20	+0.20	+0.22	+0.22	-	+0.23	+0.55
b -Quark tagging extrapolation [%]	-2.01	+2.63	+3.25	+3.70	+4.50	+6.00	+6.31
Electron energy resolution [%]	-1.99	-2.59	-3.18	-3.62	-4.37	-5.77	-6.03
E_T^{miss} Soft jet resolution para [%]	-	-	-	-	-	-	-
(JES) η intercalibration non-closure [%]	-	-	-	-	-	-	-
b -Quark tagging efficiency (eigenvector 1) [%]	-3.59	-3.80	-3.88	-3.86	-3.88	-3.89	-3.39
Muon (MS) momentum resolution [%]	-3.57	-3.89	-3.97	-3.96	-3.98	-3.99	-3.48
b -Quark tagging efficiency (eigenvector 4) [%]	-0.17	-0.20	-0.23	-0.25	-0.27	-0.34	-0.32
(JES) b -Tagged jet energy scale [%]	-	-	-	-	+0.27	+0.34	+0.32
Single top Wt cross-section [%]	-	-	-	-	-	-	-
E_T^{miss} Soft jet scale [%]	-	-	-	-	-	-	-
(JES) η intercalibration model [%]	-	-	-	-	-	-	-
Electron energy scale [%]	-	-	-	-	+0.26	-	-
(JES) Effective detector NP set 7 [%]	-	-	-	-	-	-	-
Jet vertex tagging [%]	-	-	-	-0.11	-	-	-
Light-jet tagging efficiency (eigenvector 9) [%]	-	-	-	-0.20	-	-	-
Light-jet tagging efficiency (eigenvector 8) [%]	-	-	-	-0.20	-0.18	-0.28	-
(JES) Large- R jet top-quark mass resolution [%]	±1.07	±0.84	±1.12	-	±0.68	±0.49	±4.72
(JES) Effective detector NP set 8 (restTerm) [%]	-	-	-	-	-	-	-
Light-jet tagging efficiency (eigenvector 1) [%]	-	-	-	-	-	-0.18	+0.17
(JES) Large- R jet Baseline p_T [%]	+1.33	+0.63	+1.91	+2.58	+4.74	+9.18	+9.17
Light-jet tagging efficiency (eigenvector 3) [%]	-0.35	-0.72	-0.42	-3.07	-5.55	+7.82	-6.73
Light-jet tagging efficiency (eigenvector 2) [%]	-	-	-0.14	-	-	-0.20	-
Light-jet tagging efficiency (eigenvector 4) [%]	-	-	-0.14	-	-	-0.20	-0.21
(JES) Effective detector NP set 6 [%]	-	-	-0.10	-0.12	-	-	+0.21
(JES) Large- R jet TotalStat p_T [%]	+0.23	+0.32	+0.21	+0.26	-	+0.80	+0.48
Light-jet tagging efficiency (eigenvector 7) [%]	-0.12	-0.30	-	-0.51	-0.33	-	-0.12
Muon sagitta $h\sigma$ [%]	-	-	-	-	-	-	+0.12
(JES) Pile-up offset N_{PV} [%]	-	-	-	-	-	-	-
c -Quark tagging efficiency (eigenvector 2) [%]	-0.45	-0.53	-0.40	-	-0.45	-0.43	-0.29
c -Quark tagging efficiency (eigenvector 3) [%]	-0.14	+0.21	+0.10	-0.36	+0.17	+0.13	+0.19
c -Quark tagging efficiency (eigenvector 0) [%]	-0.33	-0.39	-0.49	-0.32	-0.47	-0.39	-1.29
c -Quark tagging efficiency (eigenvector 1) [%]	+1.68	+2.38	+1.38	+1.44	+1.63	+4.43	+1.25
(JES) Large- R jet TotalStat p_T [%]	-0.99	-1.05	+0.75	+0.56	+0.99	+9.12	+0.62
b -Quark tagging efficiency (eigenvector 3) [%]	-0.16	+0.13	-0.52	-0.15	-0.14	+0.20	+0.44
(JES) Soft jet resolution perp [%]	-0.36	+0.44	+0.52	+0.55	+0.62	+0.82	+0.79
(JES) Effective detector NP set 2 [%]	-	-	-	-	-	-	-
b -Quark tagging extrapolation from c -Quark [%]	-	-	-	-	-	-	-
(JES) Large- R jet Tracking p_T [%]	+3.34	+4.22	+4.75	+5.31	+6.56	+7.65	+7.62
(JES) Effective detector NP set 3 [%]	-3.85	-3.95	-3.22	-5.66	-6.53	-4.43	-6.21
(JES) Large- R jet TotalStat mass [%]	-	-	-	-	+0.28	-	-
(JES) Effective detector NP set 5 [%]	-	-	-	-	-	-	-
(JES) Large- R jet Baseline mass [%]	+0.27	+0.36	+0.45	-	+0.20	-	+2.29
Muon energy scale [%]	-0.32	-0.17	-0.50	-	-	-	-
(JES) Pile-up offset p_T [%]	-	-	-	-	-	-	-
(JES) Large- R jet Modelling mass [%]	-0.15	+0.21	+0.21	-0.18	+0.68	-	+1.85
(JES) Effective detector NP set 1 [%]	-0.29	-	-0.94	-	-0.10	-	+0.27
(JES) Large- R jet Baseline t_2 [%]	+5.65	+6.50	+8.15	+8.54	+10.2	+10.3	+10.1
(JES) Single particle high- p_T [%]	-	-	-	-	-	-	-
Light-jet tagging efficiency (eigenvector 5) [%]	-	-	-	-	-	-	+0.16
(JES) Pile-up offset ρ topology [%]	+0.15	+0.20	+0.13	-	+0.17	+0.20	+0.42
(JES) Large- R jet Modelling p_T [%]	+1.97	+1.61	+1.82	+0.74	+1.56	+1.92	+1.80
(JES) η intercalibration total stat [%]	-0.95	-1.32	-0.92	-1.69	-1.39	-0.13	-2.94
Light-jet tagging efficiency (eigenvector 4) [%]	-	-	-	-	-	+0.10	-0.30
Muon (ID) momentum resolution [%]	-	-	-	-	-	-	+0.30
(JES) Flavour composition [%]	+0.25	+0.24	+0.15	-	+0.13	-	-
(JES) Effective detector NP set 4 [%]	-0.14	-	-0.22	-	-0.13	-	-
Light-jet tagging efficiency (eigenvector 11) [%]	-	-	-	-	-	-	-
(JES) Large- R jet Tracking t_2 [%]	-0.23	-0.42	-0.40	-0.36	-0.49	-0.34	-2.72
(JES) Large- R jet Tracking mass [%]	+0.33	+0.27	+0.32	+0.38	+0.38	+0.29	+0.44
Light-jet tagging efficiency (eigenvector 6) [%]	-	-	-0.30	-	+0.42	-	+0.12
(JES) Pile-up offset μ [%]	-	-	-	-	-	-	-0.12
b -Quark tagging efficiency (eigenvector 2) [%]	+0.54	+0.62	+0.71	+0.78	+0.82	+0.94	+0.83
(JES) Punch-through [%]	-	-	-	-	-	-	-
Muon sagitta resolution bias [%]	-	-	-	-	-	-	-

Table 168: The individual systematic uncertainties in the top-quark and antiquark transverse momenta $H_T^{t\bar{t}}$, calculated as a percentage of the transverse momentum $H_T^{t\bar{t}}$ in each bin. Dashes are used when the estimated relative systematic uncertainty for that bin is below 0.1%.

Bins	0.0–0.3	0.3–0.6	0.6–0.8	0.8–1.0	1.0–1.2	1.2–1.4	1.4–2.0
Statistics [%]	± 1.1	± 1.1	± 1.7	± 1.8	± 2.7	± 2.6	± 3.6
Systematics [%]	$+11.7$	$+11.8$	$+11.9$	$+12.2$	$+13.0$	$+13.9$	$+12.7$
Total Uncertainty [%]	$+11.7$	$+12.7$	$+12.8$	$+12.5$	$+13.2$	$+12.9$	$+12.7$
(LJES) Large- R jet Modelling τ_{32} [%]	-6.83 +8.09	-6.84 +7.89	-6.84 +7.81	-7.41 +7.82	-7.80 +8.62	-8.56 +8.00	-7.14 +7.02
Light-jet tagging efficiency (eigenvector 10) [%]	-	-	-	-	-	-	-
Light-jet tagging efficiency (eigenvector 13) [%]	-	-	-	-	-	-	-
Light-jet tagging efficiency (eigenvector 12) [%]	-	-	-	-	-	-	-
Single top t -channel treatment [%]	± 0.22	± 0.14	± 0.28	± 0.29	-	± 0.18	-
Light-jet tagging efficiency (eigenvector 0) [%]	-0.13	-0.11	-0.21	-0.30	-0.62	-0.25	-0.30
(JES) Flavour response [%]	-	-	-	-	-	-	-
b -Quark tagging extrapolation [%]	$+2.41$ -2.36	$+2.32$ -2.28	$+2.27$ -2.23	$+2.13$ -2.10	$+2.00$ -1.98	$+2.10$ -2.07	$+1.83$ -1.80
Electron energy resolution [%]	-	-	-	-	-	-	-
b -Quark tagging efficiency (eigenvector 0) [%]	-3.94 $+4.04$	-3.88 $+3.98$	-3.88 $+3.97$	-3.79 $+3.88$	-3.67 $+3.75$	-3.96 $+4.06$	-3.87 $+3.96$
QCD data-driven background shape [%]	$+0.23$ -0.22	$+0.13$ $+0.46$	$+0.38$ $+0.38$	-	-0.47 $+0.34$	± 0.49 $+0.42$	∓ 0.86 -
Pile-up [%]	$+0.22$	$+0.50$	$+0.77$	-	$+1.17$	$+0.72$	-1.16
E_T^{miss} Soft jet resolution para [%]	-	-	-	-	-	-	-
(JES) η intercalibration non-closure [%]	-	-	-	-	-	-	-
b -Quark tagging efficiency (eigenvector 1) [%]	-3.68 $+3.76$	-3.61 $+3.69$	-3.59 $+3.68$	-3.52 $+3.60$	-3.38 $+3.45$	-3.69 $+3.77$	-3.50 $+3.58$
Muon (MS) momentum resolution [%]	-	-	-	-	-	-	-
b -Quark tagging efficiency (eigenvector 4) [%]	-0.19 $+0.19$	-0.18 $+0.18$	-0.18 $+0.18$	-0.17 $+0.17$	-0.17 $+0.17$	-0.17 $+0.17$	-0.15 $+0.15$
(JES) b -Tagged jet energy scale [%]	-	-	-	-	-	-	-
Single top Wt cross-section [%]	-	-	-	-	-	-	-
E_T^{miss} Soft jet scale [%]	-	-	-	-	-	-	-
(JES) η intercalibration model [%]	-	-	-	-	-	-	-
Electron energy scale [%]	-	-	-	-	-	-	-
(JES) Effective detector NP set 7 [%]	-	-	-	-	-	-	-
Jet vertex tagging [%]	-	-	-	-	$+0.12$	-	-
Light-jet tagging efficiency (eigenvector 9) [%]	-0.20	-0.20	-0.21	-	-	-0.21	-
Light-jet tagging efficiency (eigenvector 8) [%]	-	-0.20	-0.20	-	$+0.11$	-0.29	-0.21
(LJES) Large- R jet top-quark mass resolution [%]	∓ 1.10	∓ 0.64	∓ 1.65	∓ 1.07	∓ 1.14	-	∓ 0.89
(JES) Effective detector NP set 8 (restTerm) [%]	-	-	-	-	-	-	-
Light-jet tagging efficiency (eigenvector 1) [%]	-	-	-	-	-	-	-
(LJES) Large- R jet Baseline p_T [%]	$+1.77$ -1.57	$+1.82$ -1.91	$+2.06$ -1.55	$+1.64$ -1.41	$+2.45$ -1.49	$+1.89$ -2.05	$+2.41$ -1.51
Light-jet tagging efficiency (eigenvector 3) [%]	-	-	-	-	-0.22	-	-
Light-jet tagging efficiency (eigenvector 2) [%]	-	-	$+0.12$	$+0.12$	$+0.29$	$+0.15$	$+0.20$
(JES) Effective detector NP set 6 [%]	-	-	-0.12	-0.12	-0.29	-0.15	-0.20
(LJES) Large- R jet TotalStat p_T [%]	$+0.29$ -0.21	$+0.17$ -0.20	$+0.33$ -0.19	$+0.21$ -0.23	$+0.15$ -	$+0.25$ -0.20	$+0.40$ -
Light-jet tagging efficiency (eigenvector 7) [%]	-	-	-	-	± 0.16	-	-
Muon sagitta ho [%]	-	-	-	-	-	-	-
(JES) Pile-up offset N_{PV} [%]	-	-	-	-	-	-	-
c -Quark tagging efficiency (eigenvector 2) [%]	-0.42	-0.53	-0.47	-0.41	-0.41	-0.57	-
c -Quark tagging efficiency (eigenvector 3) [%]	-	$+0.15$	-	$+0.11$	-	$+0.14$	-
c -Quark tagging efficiency (eigenvector 0) [%]	-0.32 $+0.39$	-0.36 ± 1.52	-0.36 ± 1.70	-0.32 ± 1.55	-0.42 ± 1.56	-0.43 ± 1.06	-0.37 ± 1.76
c -Quark tagging efficiency (eigenvector 1) [%]	-0.93 $+0.15$	-0.18 $+0.10$	-0.18 $+0.91$	-0.18 $+0.86$	-0.27 $+0.88$	-0.27 $+0.90$	-0.27 $+0.64$
(LJES) Large- R jet TotalStat τ_{32} [%]	$+0.15$ -0.42	-0.12 $+0.39$	-0.12 $+0.39$	-0.35 $+0.35$	-0.13 $+0.33$	$+0.12$ $+0.34$	$+0.17$ $+0.30$
b -Quark tagging efficiency (eigenvector 3) [%]	$+0.14$ -0.42	$+0.11$ $+0.39$	$+0.13$ $+0.39$	-0.35 $+0.35$	-0.13 $+0.33$	$+0.12$ $+0.34$	$+0.17$ $+0.30$
E_T^{miss} Soft jet resolution perp [%]	-	-	-	-	-	-	-
(JES) Effective detector NP set 2 [%]	-	-	-	-	-	-	-
b -Quark tagging extrapolation from c -Quark [%]	-	-	-	-	-	-	-
(LJES) Large- R jet Tracking p_T [%]	$+3.67$ -3.48	$+3.96$ -3.58	$+3.93$ -4.22	$+3.77$ -3.76	$+4.97$ -4.04	$+4.26$ -3.80	$+5.60$ -4.81
(JES) Effective detector NP set 3 [%]	-	-	-	-	-	-	-
(LJES) Large- R jet TotalStat mass [%]	-	-	-	-	$+0.17$	-	-
(JES) Effective detector NP set 5 [%]	-	-	-	-	-	-	-
(LJES) Large- R jet Baseline mass [%]	$+0.45$ -0.69	$+0.33$ -0.34	$+0.20$ -0.35	$+0.63$ -	$+0.28$ -0.22	$+1.04$ -0.34	-0.51 $+0.41$
Muon energy scale [%]	-	-	-	-	-	-	-
(JES) Pile-up offset p_T [%]	-	-	-	-	-	-	-
(LJES) Large- R jet Modelling mass [%]	$+0.44$ -0.89	$+0.19$ -0.24	$+0.44$ -0.38	$+0.35$ -	$+0.33$ -0.31	$+0.63$ -0.23	-1.07 $+0.91$
(JES) Effective detector NP set 1 [%]	-	-	-	-	-	-	-
(LJES) Large- R jet Baseline τ_{32} [%]	-5.46 $+6.31$	-5.54 $+6.23$	-5.55 $+6.04$	-5.96 $+6.20$	-6.09 $+6.45$	-6.93 $+6.00$	-5.19 $+5.49$
(JES) Single particle high- p_T [%]	-	-	-	-	-	-	-
Light-jet tagging efficiency (eigenvector 5) [%]	-	-	-	-	-	-	-
(JES) Pile-up offset ρ topology [%]	$+0.18$	-	$+0.13$	-	$+0.14$	$+0.14$	$+0.29$
(LJES) Large- R jet Modelling p_T [%]	$+1.74$ -1.63	$+1.86$ -1.64	$+0.14$ -1.66	$+1.82$ -1.55	$+2.22$ -1.53	$+1.95$ -1.85	$+2.57$ -1.80
(JES) η intercalibration total stat [%]	-	-	-	-	-	-	-
Light-jet tagging efficiency (eigenvector 4) [%]	-	-	-	-	-0.30	-	-
Muon (ID) momentum resolution [%]	-	-	-	-	$+0.29$	-	-
(JES) Flavour composition [%]	$+0.25$ -0.10	$+0.18$ -0.11	$+0.17$ -0.20	-	$+0.19$ -0.24	$+0.16$ -	$+0.28$ -0.11
(JES) Effective detector NP set 4 [%]	-	-	-	-	-	-	-
Light-jet tagging efficiency (eigenvector 11) [%]	-	-	-	-	-	-	-
(LJES) Large- R jet Tracking τ_{32} [%]	-0.29 $+0.31$	-0.27 -0.24	-0.26 $+0.32$	-0.40 $+0.21$	-0.25 $+0.30$	-0.37 $+0.26$	-0.77 $+0.26$
(LJES) Large- R jet Tracking mass [%]	-0.14 -	-	-	$+0.27$	-	$+0.25$	-0.60 $+0.65$
Light-jet tagging efficiency (eigenvector 6) [%]	-	-	-	-	-	-	-
(JES) Pile-up offset μ [%]	-	-	-	-	-	-	-
b -Quark tagging efficiency (eigenvector 2) [%]	-0.61 $+0.61$	-0.56 $+0.56$	-0.56 $+0.56$	-0.55 $+0.55$	-0.43 $+0.43$	-0.54 $+0.54$	-0.46 $+0.46$
(JES) Punch-through [%]	-	-	-	-	-	-	-
Muon sagitta resolution bias [%]	-	-	-	-	-	-	-

Table 169: The individual systematic uncertainties in the top quark-antiquark system longitudinal boost y_B^{tf} , calculated as a percentage of the longitudinal boost in each bin. Dashes are used when the estimated relative systematic uncertainty for that bin is below 0.1%.

Not reviewed, for internal circulation only

Bins	1.0–1.5	1.5–2.0	2.0–3.0	3.0–4.0	4.0–5.0	5.0–7.0	7.0–10.0
Statistics [%]	± 1.1	± 1.4	± 1.3	± 1.9	± 2.5	± 2.3	± 3.1
Systematics [%]	$+12.3$	$+12.4$	$+12.6$	$+11.0$	$+11.5$	$+11.5$	$+9.75$
Total Uncertainty [%]	$+13.4$	$+13.3$	$+12.3$	$+11.3$	$+11.3$	$+11.2$	$+10.5$
(LJES) Large- R jet Modelling τ_{32} [%]	-7.17	-7.30	-7.62	-6.19	-6.80	-6.83	-5.50
(LJES) Large- R jet Modelling τ_{32} [%]	$+7.90$	$+8.34$	$+7.41$	$+8.69$	$+8.94$	$+7.66$	$+7.71$
Light-jet tagging efficiency (eigenvector 10) [%]	-	-	-	-	-	-	-
Light-jet tagging efficiency (eigenvector 13) [%]	-	-	-	-	-	-	-
Light-jet tagging efficiency (eigenvector 12) [%]	-	-	-	-	-	-	-
Single top t -channel treatment [%]	± 0.23	± 0.19	± 0.14	± 0.12	± 0.30	± 0.30	-
Light-jet tagging efficiency (eigenvector 0) [%]	-0.13	-0.38	-0.17	-0.15	-	-0.29	-0.19
(JES) Flavour response [%]	-	-	-	-	-	$+0.33$	$+0.19$
b-Quark tagging extrapolation [%]	$+2.39$	$+2.34$	$+2.33$	$+2.13$	$+2.01$	$+2.25$	$+1.81$
Electron energy resolution [%]	-2.36	-2.31	-2.29	-2.10	-1.98	-2.22	-1.78
b-Quark tagging efficiency (eigenvector 0) [%]	-3.98	-3.96	-3.93	-3.84	-3.55	-3.74	-3.36
b-Quark tagging efficiency (eigenvector 0) [%]	$+4.08$	$+4.05$	$+4.03$	$+3.94$	$+3.64$	$+3.83$	$+3.45$
QCD data-driven background shape [%]	$+0.27$	$+0.26$	$+0.41$	$+0.49$	-	-0.67	$+0.17$
Pile-up [%]	$+0.85$	-0.81	-0.12	$+0.89$	$+1.05$	$+0.66$	-0.17
E_T^{miss} Soft jet resolution para [%]	-	-	-	-	-	-	-
(JES) η intercalibration non-closure [%]	-	-	-	-	-	-	-
b-Quark tagging efficiency (eigenvector 1) [%]	-3.70	-3.67	-3.66	-3.56	-3.35	-3.46	-3.08
Muon (MS) momentum resolution [%]	$+3.78$	$+3.75$	$+3.75$	$+3.65$	$+3.43$	$+3.54$	$+3.15$
b-Quark tagging efficiency (eigenvector 4) [%]	-0.19	-0.19	-0.18	-0.17	-0.15	-0.18	-0.16
(JES) b-Tagged jet energy scale [%]	$+0.19$	$+0.19$	$+0.18$	$+0.17$	$+0.15$	$+0.18$	$+0.16$
Single top W cross-section [%]	-	-	-	-	-	-	-
E_T^{miss} Soft jet scale [%]	-	-	-	-	-	-	-
(JES) η intercalibration model [%]	-	-	-	-	-	-	-
Electron energy scale [%]	-	-	-	-	-	-	-
(JES) Effective detector NP set 7 [%]	-	-	-	-	-	-	-
Jet vertex tagging [%]	-	-	-	-	-	-	-
Light-jet tagging efficiency (eigenvector 9) [%]	-0.12	-	-	-	-	-	-
Light-jet tagging efficiency (eigenvector 8) [%]	-0.22	-0.25	-	-0.20	-	-	-
(LJES) Large- R jet top-quark mass resolution [%]	± 1.28	± 0.36	± 0.97	± 0.77	± 0.96	± 1.12	± 1.91
(JES) Effective detector NP set 8 (restTerm) [%]	-	-	-	-	-	-	-
Light-jet tagging efficiency (eigenvector 1) [%]	-	-	-	-	-	-	-
(LJES) Large- R jet Baseline p_T [%]	$+1.95$	$+1.86$	$+1.91$	$+2.13$	$+1.69$	$+1.78$	$+0.98$
Light-jet tagging efficiency (eigenvector 3) [%]	-1.56	-1.48	-1.94	-1.61	-2.03	-1.78	-0.89
Light-jet tagging efficiency (eigenvector 2) [%]	-	-	-	-	-	-	-
(JES) Effective detector NP set 6 [%]	-	-	-	-	-	-	-
(LJES) Large- R jet TotalStat p_T [%]	$+0.33$	$+0.23$	$+0.19$	$+0.16$	$+0.26$	$+0.33$	-
Light-jet tagging efficiency (eigenvector 7) [%]	-	-	-	-	-	-	-
Muon sagitta ho [%]	-	-	-	-	-	-	-
(JES) Pile-up offset N_{PV} [%]	-	-	-	-	-	-	-
c-Quark tagging efficiency (eigenvector 2) [%]	-0.49	-0.51	-0.42	-	-0.48	-0.51	-
c-Quark tagging efficiency (eigenvector 3) [%]	-	$+0.13$	-0.35	-	$+0.11$	$+0.23$	-0.30
c-Quark tagging efficiency (eigenvector 0) [%]	-1.65	-0.37	-0.38	-0.25	-0.43	-1.79	-0.98
c-Quark tagging efficiency (eigenvector 1) [%]	$+1.74$	$+1.69$	$+1.68$	$+1.04$	$+1.39$	$+1.83$	$+0.94$
(LJES) Large- R jet TotalStat τ_{32} [%]	$+0.95$	$+1.04$	$+0.87$	$+0.56$	$+0.86$	$+1.14$	$+0.59$
b-Quark tagging efficiency (eigenvector 3) [%]	$+0.12$	$+0.18$	$+0.14$	-	-0.17	-	$+0.11$
E_T^{miss} Soft jet resolution perp [%]	-	-	-	-	-	-	-
(JES) Effective detector NP set 2 [%]	-	-	-	-	-	-	-
b-Quark tagging extrapolation from c-Quark [%]	-	-	-	-	-	-	-
(LJES) Large- R jet Tracking p_T [%]	$+4.14$	$+4.25$	$+3.73$	$+3.97$	$+3.81$	$+3.42$	$+2.96$
(JES) Effective detector NP set 3 [%]	-3.88	-3.68	-3.61	-3.80	-3.63	-4.10	-2.70
(JES) Effective detector NP set 1 [%]	-	-	-	-	-	-	-
(LJES) Large- R jet TotalStat mass [%]	-	-	-	-0.18	-	-	-
(JES) Effective detector NP set 5 [%]	-	-	-	-	-	-	-
(LJES) Large- R jet Baseline mass [%]	$+0.36$	$+0.37$	$+0.27$	$+0.81$	$+0.57$	$+0.50$	$+0.33$
Muon energy scale [%]	-0.54	-0.33	-0.58	-	-0.20	-0.56	-
(JES) Pile-up offset p_T [%]	-	-	-	-	-	-	-
(LJES) Large- R jet Modelling mass [%]	$+0.25$	$+0.23$	$+0.13$	$+0.96$	$+0.54$	$+0.34$	-0.10
(JES) Effective detector NP set 1 [%]	-0.58	-0.45	-0.81	-0.10	-	-	$+1.01$
(LJES) Large- R jet τ_{32} [%]	-	-	-	-	-	-	-
(JES) Single particle high- p_T [%]	-	-	-	-	-	-	-
Light-jet tagging efficiency (eigenvector 5) [%]	-	-	-	-	-	-	-
(JES) Pile-up offset ρ topology [%]	$+0.16$	$+0.22$	$+0.12$	-	-	$+0.10$	-
(LJES) Large- R jet Modelling p_T [%]	$+2.02$	$+1.81$	$+1.90$	$+1.86$	$+1.76$	$+1.66$	$+1.66$
(JES) η intercalibration total stat [%]	-	-	-	-	-	-	-0.90
Light-jet tagging efficiency (eigenvector 4) [%]	-	$+0.13$	-	-	-	-0.16	-
Muon (ID) momentum resolution [%]	-	-	-	-	-	-	-
(JES) Flavour composition [%]	$+0.18$	$+0.21$	$+0.22$	-	$+0.17$	$+0.25$	$+0.19$
(JES) Effective detector NP set 4 [%]	-0.15	-	-0.17	-	-0.10	-0.23	-
Light-jet tagging efficiency (eigenvector 11) [%]	-	-	-	-	-	-	-
(LJES) Large- R jet Tracking τ_{32} [%]	-0.35	-0.45	-0.24	-0.20	-0.26	-0.21	-0.21
(LJES) Large- R jet Tracking mass [%]	$+0.13$	-	$+0.24$	$+0.23$	$+0.30$	$+0.27$	$+0.40$
Light-jet tagging efficiency (eigenvector 6) [%]	-	-	-	-0.21	-	-	-
(JES) Pile-up offset μ [%]	-	-	-	-	-	-	-
b-Quark tagging efficiency (eigenvector 2) [%]	-0.59	-0.57	-0.57	-0.55	-0.52	-0.57	-0.47
(JES) Punch-through [%]	-	-	-	-	-	-	-
Muon sagitta resolution bias [%]	-	-	-	-	-	-	-

Table 170: The individual systematic uncertainties in the top quark-antiquark system $\chi^{\bar{t}t}$, calculated as a percentage of the $\chi^{\bar{t}t}$ in each bin. Dashes are used when the estimated relative systematic uncertainty for that bin is below 0.1%.

Not reviewed, for internal circulation only

Bins	0.0–0.2	0.2–0.4	0.4–0.6	0.6–0.7	0.7–0.8	0.8–1.0
Statistics [%]	± 1.2	± 1.1	± 1.2	± 2.2	± 2.3	± 3.4
Systematics [%]	± 12.3	± 12.7	± 11.5	± 11.6	± 10.4	± 10.4
Total Uncertainty [%]	± 12.3	± 12.8	± 11.5	± 11.8	± 10.4	± 10.9
(LJES) Large- R jet Modelling τ_{32} [%]	-7.19 +7.91	-7.61 +8.21	-6.72 +7.94	-6.68 +8.32	-5.96 +6.92	-5.91 +8.03
Light-jet tagging efficiency (eigenvector 10) [%]	-	-	-	-	-	-
Light-jet tagging efficiency (eigenvector 13) [%]	-	-	-	-	-	-
Light-jet tagging efficiency (eigenvector 12) [%]	-	-	-	-	-	-
Single top t -channel treatment [%]	± 0.25	± 0.14	± 0.15	± 0.33	-	± 0.19
Light-jet tagging efficiency (eigenvector 0) [%]	-0.25 +0.25	-0.15 +0.15	-0.19 +0.19	-0.19 +0.21	-0.14 +0.14	-0.18 +0.17
(JES) Flavour response [%]	-	-	-	-	-	-
b -Quark tagging extrapolation [%]	+2.39 -2.35	+2.36 -2.32	+2.18 -2.14	+2.22 -2.19	+1.90 -1.87	+1.68 -1.66
Electron energy resolution [%]	-	-	-	-	-	-
b -Quark tagging efficiency (eigenvector 0) [%]	-3.97 +4.07	-3.97 +4.07	-3.83 +3.92	-3.65 +3.63	-3.53 +3.53	-3.07 +3.15
QCD data-driven background shape [%]	∓ 0.18	∓ 0.11	± 0.46	± 0.32	∓ 0.32	∓ 0.27
Pile-up [%]	-0.84 +0.75	-0.42 +0.45	+0.26 -	+0.30 -0.61	-1.53 +1.42	-1.27 -0.63
E_T^{miss} Soft jet resolution para [%]	-	-	-	-	-	-
(JES) η intercalibration non-closure [%]	-	-	-	-	-	-
b -Quark tagging efficiency (eigenvector 1) [%]	-3.67 +3.76	-3.67 +3.76	-3.59 +3.68	-3.44 +3.52	-3.24 +3.32	-2.85 +2.92
Muon (MS) momentum resolution [%]	-	-	-	-	-	-
b -Quark tagging efficiency (eigenvector 4) [%]	-0.19 +0.19	-0.18 +0.18	-0.18 +0.18	-0.16 +0.16	-0.16 +0.16	-0.13 +0.13
(JES) b -Tagged jet energy scale [%]	-	-	-	-	-	-
Single top Wt cross-section [%]	-	-	-	-	-	-
E_T^{miss} Soft jet scale [%]	-	-	-	-	-	-
(JES) η intercalibration model [%]	-	-	-	-	-	-
Electron energy scale [%]	-	-	-	-	-	-
(JES) Effective detector NP set 7 [%]	-	-	-	-	-	-
Jet vertex tagging [%]	-0.12	-	-	-	-	± 0.11
Light-jet tagging efficiency (eigenvector 9) [%]	-0.23	-	-	-	-	-0.13
Light-jet tagging efficiency (eigenvector 8) [%]	-0.25	-	-	-	-	-
(LJES) Large- R jet top-quark mass resolution [%]	∓ 1.14	∓ 0.93	∓ 0.54	∓ 1.22	∓ 1.53	∓ 2.30
(JES) Effective detector NP set 8 (restTerm) [%]	-	-	-	-	-	-
Light-jet tagging efficiency (eigenvector 1) [%]	-	-	-	-	-	-
(LJES) Large- R jet Baseline p_T [%]	+1.98 -1.58	+2.02 -1.83	+1.80 -1.76	+1.89 -1.21	+1.14 -1.67	+1.01 -1.00
Light-jet tagging efficiency (eigenvector 3) [%]	-	-	-	-	-	-
Light-jet tagging efficiency (eigenvector 2) [%]	+0.12	-	-	-	-	+0.11
(JES) Effective detector NP set 6 [%]	-	-	-	-	-	-0.11
(LJES) Large- R jet TotalStat p_T [%]	+0.30 -0.12	+0.24 -0.22	+0.15 -0.28	+0.38 -	+0.11 -0.22	+0.28 -0.17
Light-jet tagging efficiency (eigenvector 7) [%]	-	-	-	-	-	-
Muon sagitta ho [%]	-	-	-	-	-	-
(JES) Pile-up offset N_{PV} [%]	-	-	-	-	-	-
c -Quark tagging efficiency (eigenvector 2) [%]	-0.49	-0.50	-0.37	-0.52	-	-0.36
c -Quark tagging efficiency (eigenvector 3) [%]	-	+0.12	-	+0.29	-0.31	+0.15
c -Quark tagging efficiency (eigenvector 0) [%]	-0.40	-0.40	-0.29	-1.87	-0.86	-1.10
c -Quark tagging efficiency (eigenvector 1) [%]	-1.61 +1.64	-1.79 +1.81	-1.13 +1.80	-1.87 +1.88	+0.82 +0.86	+0.03 +0.83
(LJES) Large- R jet TotalStat τ_{32} [%]	+0.95 -0.13	+1.04 -0.14	+0.62 -0.11	+1.20 +0.13	+0.49 -0.34	+0.70 -0.29
b -Quark tagging efficiency (eigenvector 3) [%]	+0.44 +0.41	+0.45 +0.39	+0.31 +0.37	+0.37 +0.37	-0.34 +0.34	+0.29 +0.29
E_T^{miss} Soft jet resolution perp [%]	-	-	-	-	-	-
(JES) Effective detector NP set 2 [%]	-	-	-	-	-	-
b -Quark tagging extrapolation from c -Quark [%]	-	-	-	-	-	-
(LJES) Large- R jet Tracking p_T [%]	+4.11 -3.79	+4.09 -3.86	+3.91 -3.66	+3.66 -3.41	+2.86 -3.53	+3.38 -2.97
(JES) Effective detector NP set 3 [%]	-	-	-	-	-	-
(LJES) Large- R jet TotalStat mass [%]	-	-	-0.11	-	-	-
(JES) Effective detector NP set 5 [%]	-	-	+0.12	-	-	-
(LJES) Large- R jet Baseline mass [%]	+0.34 -0.50	+0.33 -0.37	+0.60 -0.42	+0.34 -0.38	+0.26 -	-0.30 +0.13
Muon energy scale [%]	-	-	-	-	-	-
(JES) Pile-up offset p_T [%]	-	-	-	-	-	-
(LJES) Large- R jet Modelling mass [%]	+0.12 -0.49	+0.24 -0.71	+0.66 -0.31	-	+0.56 -	-0.15 +0.11
(JES) Effective detector NP set 1 [%]	-	-	-	-	-	-
(LJES) Large- R jet Baseline τ_{32} [%]	-5.69 +6.11	-6.16 +6.59	-5.36 +6.00	-5.51 +6.72	-4.62 +5.32	-5.37 +6.05
(JES) Single particle high- p_T [%]	-	-	-	-	-	-
Light-jet tagging efficiency (eigenvector 5) [%]	+0.17	+0.15	+0.16	-0.16	+0.13	-
(JES) Pile-up offset ρ topology [%]	-	-	-	-	-	-
(LJES) Large- R jet Modelling p_T [%]	+1.90 -1.37	+2.01 -1.86	+1.76 -1.74	+2.07 -1.27	+1.34 -2.06	+1.19 -1.09
(JES) η intercalibration total stat [%]	-	-	-	-	-	-
Light-jet tagging efficiency (eigenvector 4) [%]	-	-	-	-0.12	-	-
Muon (ID) momentum resolution [%]	-	-	-	+0.14	-	-
(JES) Flavour composition [%]	+0.19 -0.15	+0.16 -0.14	+0.23 -	+0.18 -0.20	+0.22 -0.11	-
(JES) Effective detector NP set 4 [%]	-	-	-	-	-	-
Light-jet tagging efficiency (eigenvector 11) [%]	-	-	-	-	-	-
(LJES) Large- R jet Tracking τ_{32} [%]	-0.40 +0.31	-0.31 +0.29	-0.24 +0.24	-0.20 +0.33	-0.26 +0.16	-0.12 +0.26
(LJES) Large- R jet Tracking mass [%]	-	-	-	-	+0.28	+0.47
Light-jet tagging efficiency (eigenvector 6) [%]	-	-	-	-	-	-
(JES) Pile-up offset μ [%]	-	-	-	-	-	-
b -Quark tagging efficiency (eigenvector 2) [%]	-0.59 +0.59	-0.57 +0.57	-0.54 +0.54	-0.60 +0.60	-0.49 +0.49	-0.43 +0.44
(JES) Punch-through [%]	-	-	-	-	-	-
Muon sagitta resolution bias [%]	-	-	-	-	-	-

Table 171: The individual systematic uncertainties in the top quark-antiquark system $\cos \theta^*$, calculated as a percentage of the $\cos \theta^*$ in each bin. Dashes are used when the estimated relative systematic uncertainty for that bin is below 0.1%.

975 I. Particle-level unfolding validation

976 In order to validate the accuracy of the unfolding methods, closure and stress tests have been performed.

977 I.1. Closure test

978 The nominal signal sample is used to demonstrate that the unfolding (using inputs from nominal sample)
 979 can recover the truth spectrum given the reconstructed spectrum as input. In this case, exactly the same
 980 events were used for the unfolding machinery and for the input spectrum from the nominal signal sample.
 981 An exact closure is observed in Figures 105 and 106 for all unfolding methods considered.

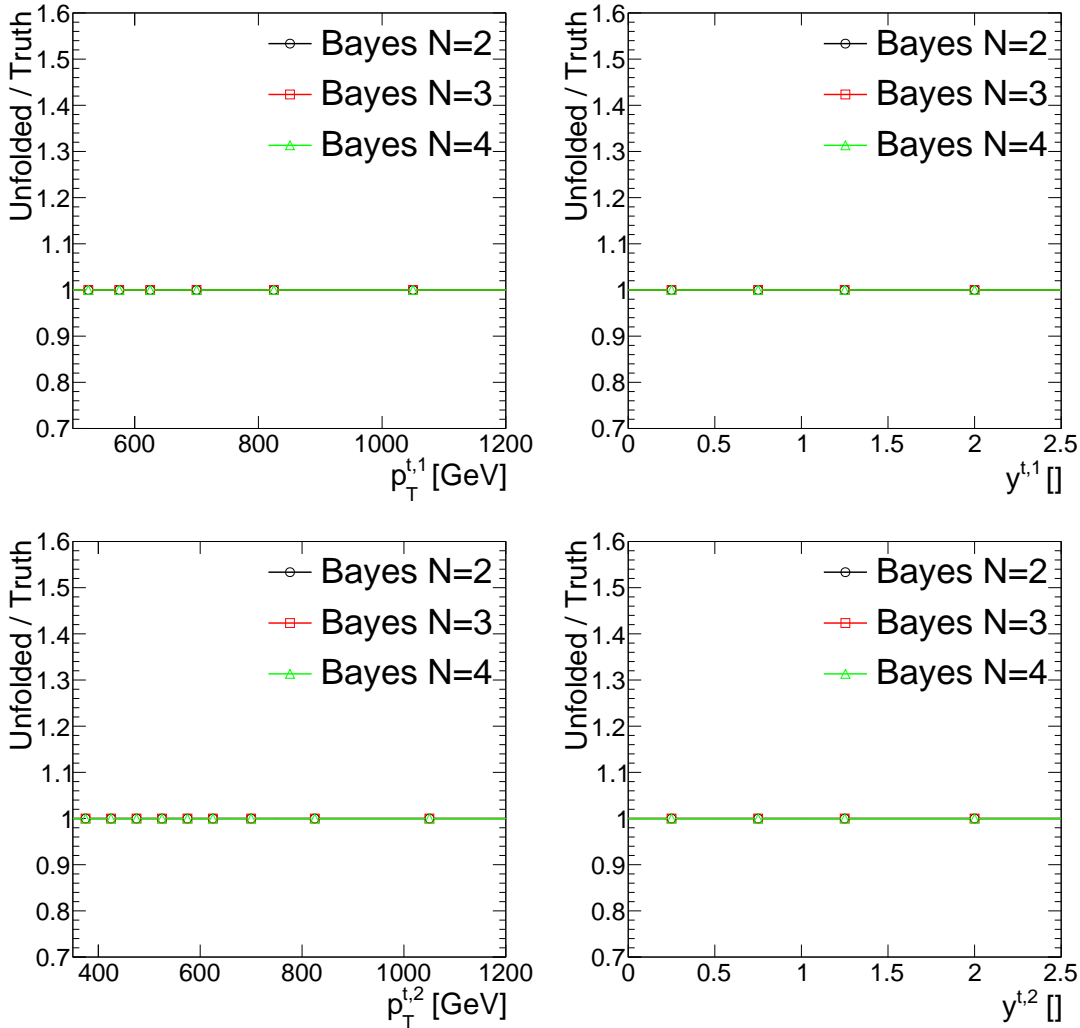


Figure 105: Closure test for the leading and subleading top-jet candidate p_T and rapidity at particle-level.

Not reviewed, for internal circulation only

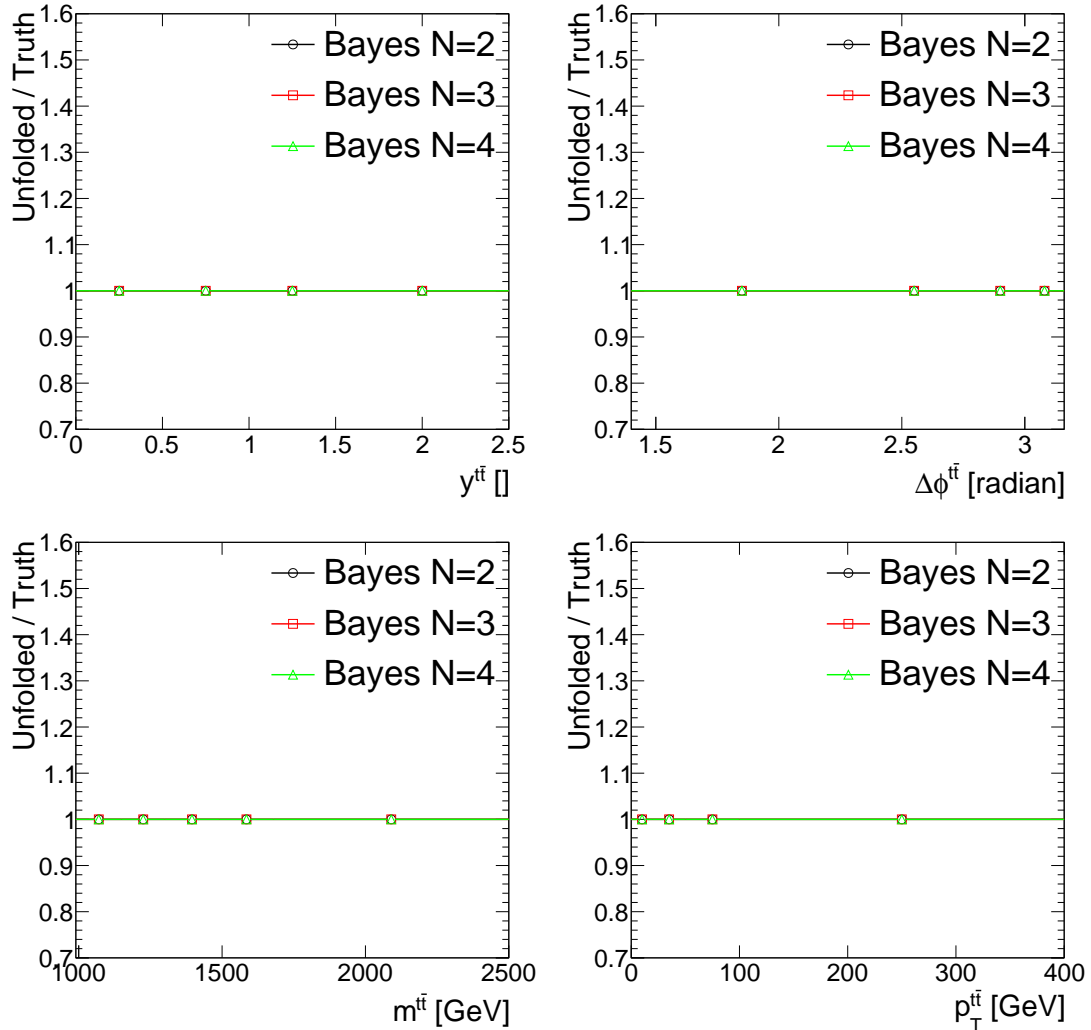


Figure 106: Closure test for the $t\bar{t}$ system observables at particle-level.

982 I.2. Stress test

983 Due to the possible imperfect agreement of the Monte Carlo prediction of the signal, it is also necessary
 984 to check whether the unfolding procedures will still recover the correct distributions, or to set a limit on
 985 any possible bias that could arise. This was explored by reweighting the nominal MC sample in various
 986 ways and then unfolded each reweighted sample to measure the potential bias associated with a given
 987 choice of reweighting.

988 Different reweighting models were tested by applying additional event weights to the nominal signal
 989 sample. The additional event weights depend on truth top quark kinematics. These distributions are
 990 referred to as the reweighted distributions. We adopted the approach used in $t\bar{t}$ lepton+jets differential
 991 measurement. We derive a reweighting function based on data-MC disagreement at reco-level and use it
 992 to perform the stress tests.

993 In Fig. 107-108 we show the (data-bckg)/signal ratio at the reconstructed level as a function of all kin-
 994 ematic variables which we do unfold. We use the linear fits to these ratios as a reweighting functions in
 995 the stress tests below.

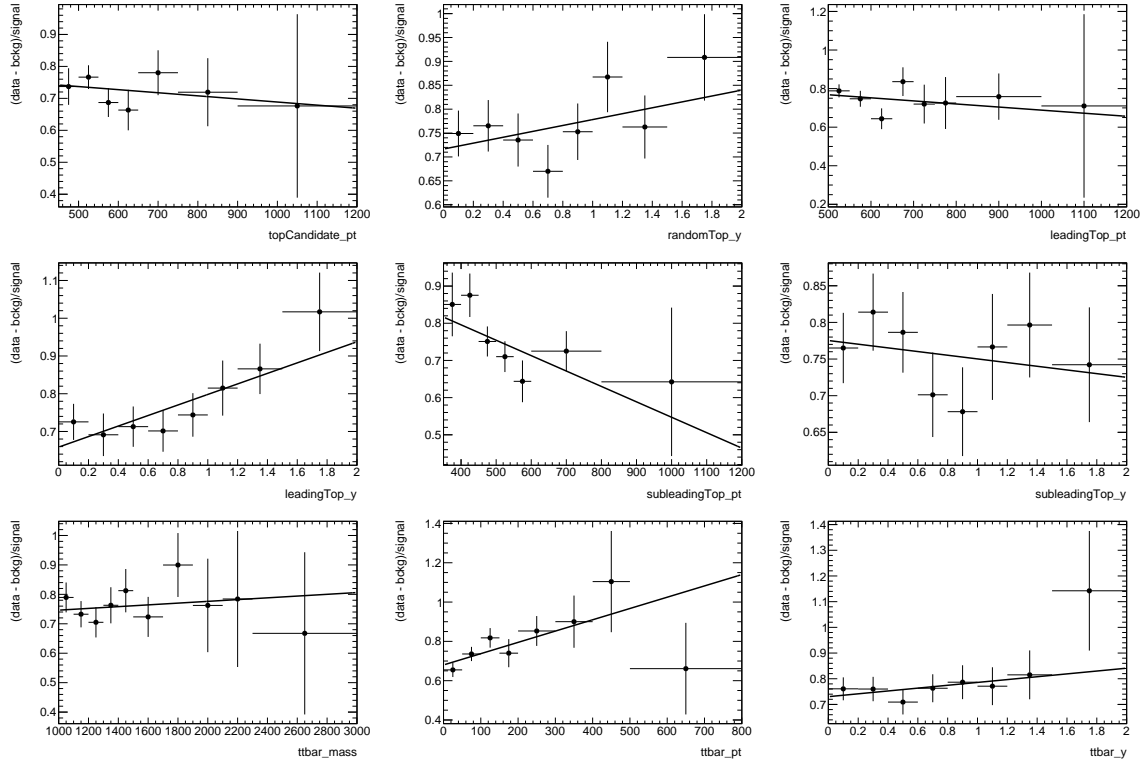


Figure 107: The $(\text{data}-\text{bckg})/\text{signal}$ ratio at the reconstructed level as a function of various kinematic variables.

996 The reweighted detector level distribution is unfolded with nominal unfolding inputs and compared to the
 997 reweighted truth distribution.

998 Figures 109-111 show the results of the stress tests for the top kinematic variables which we do unfold.
 999 The stress tests did not uncover any instability in the unfolding procedure.

Not reviewed, for internal circulation only

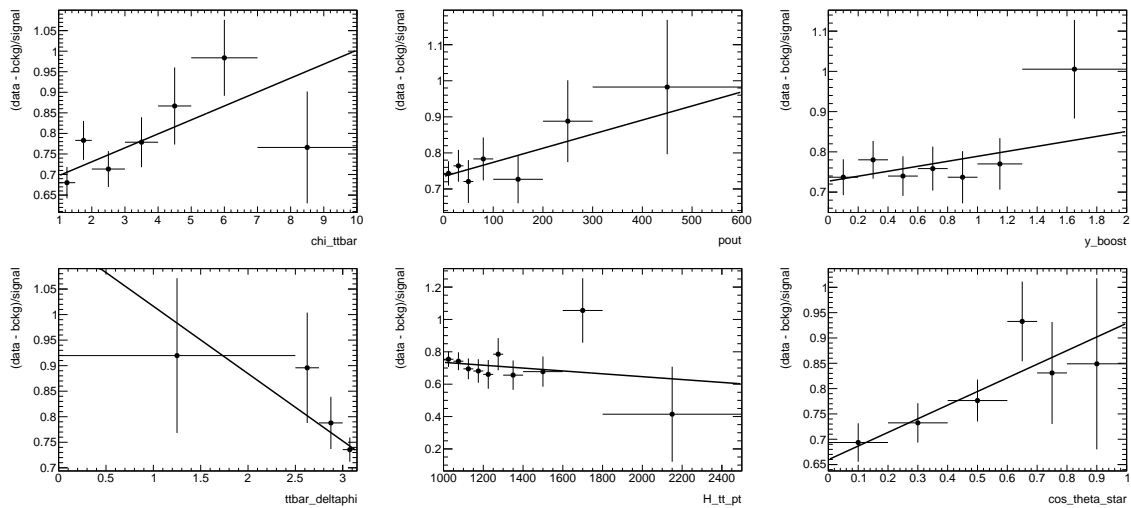


Figure 108: The $(\text{data} - \text{bckg})/\text{signal}$ ratio at the reconstructed level as a function of another kinematic variables.

Not reviewed, for internal circulation only

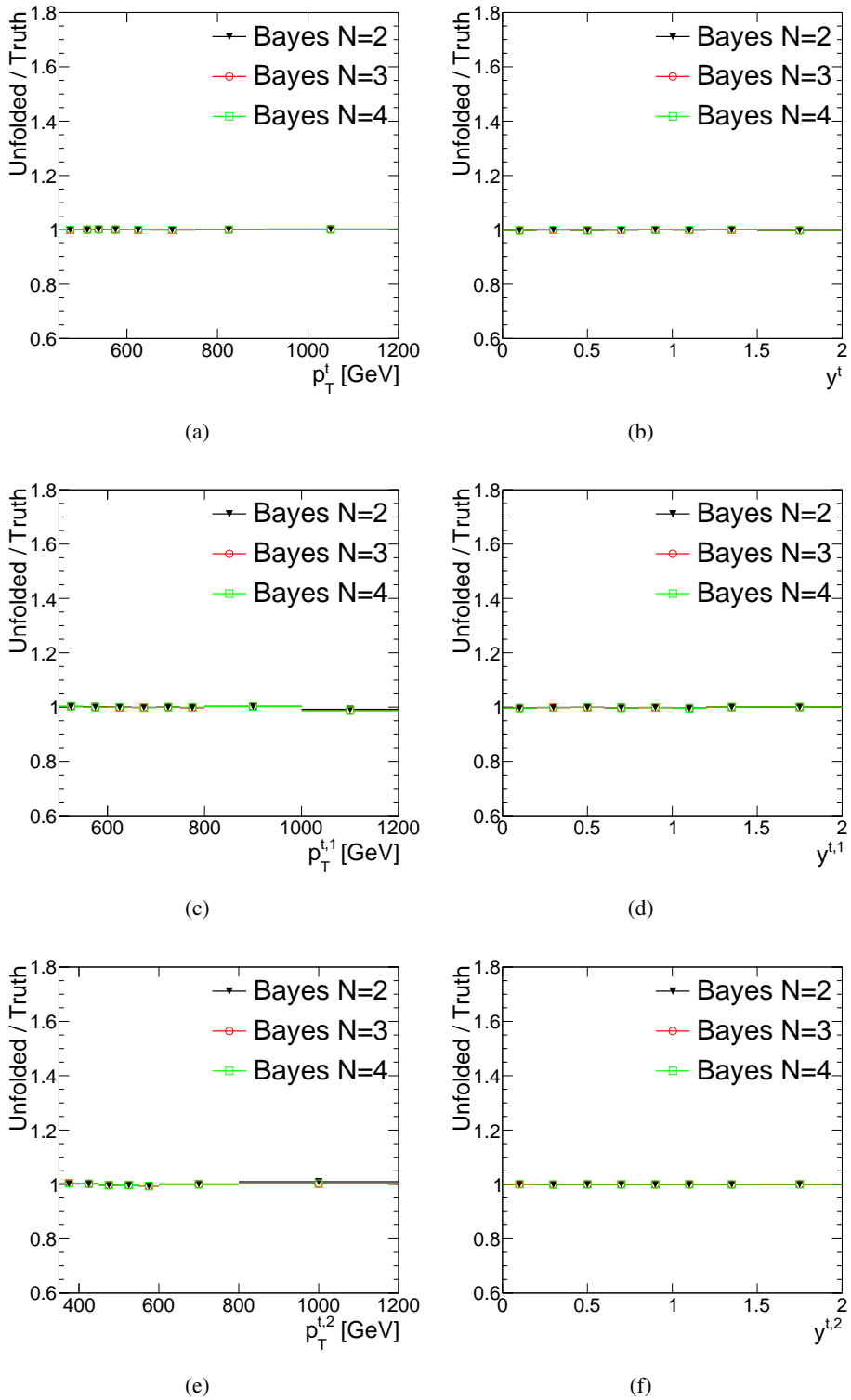


Figure 109: Stress test results for random top, leading top, and subleading top p_T and $|y|$ distributions. The figures show the ratios between unfolded reweighted and truth reweighted distributions for the particle-level fiducial phase space.

Not reviewed, for internal circulation only

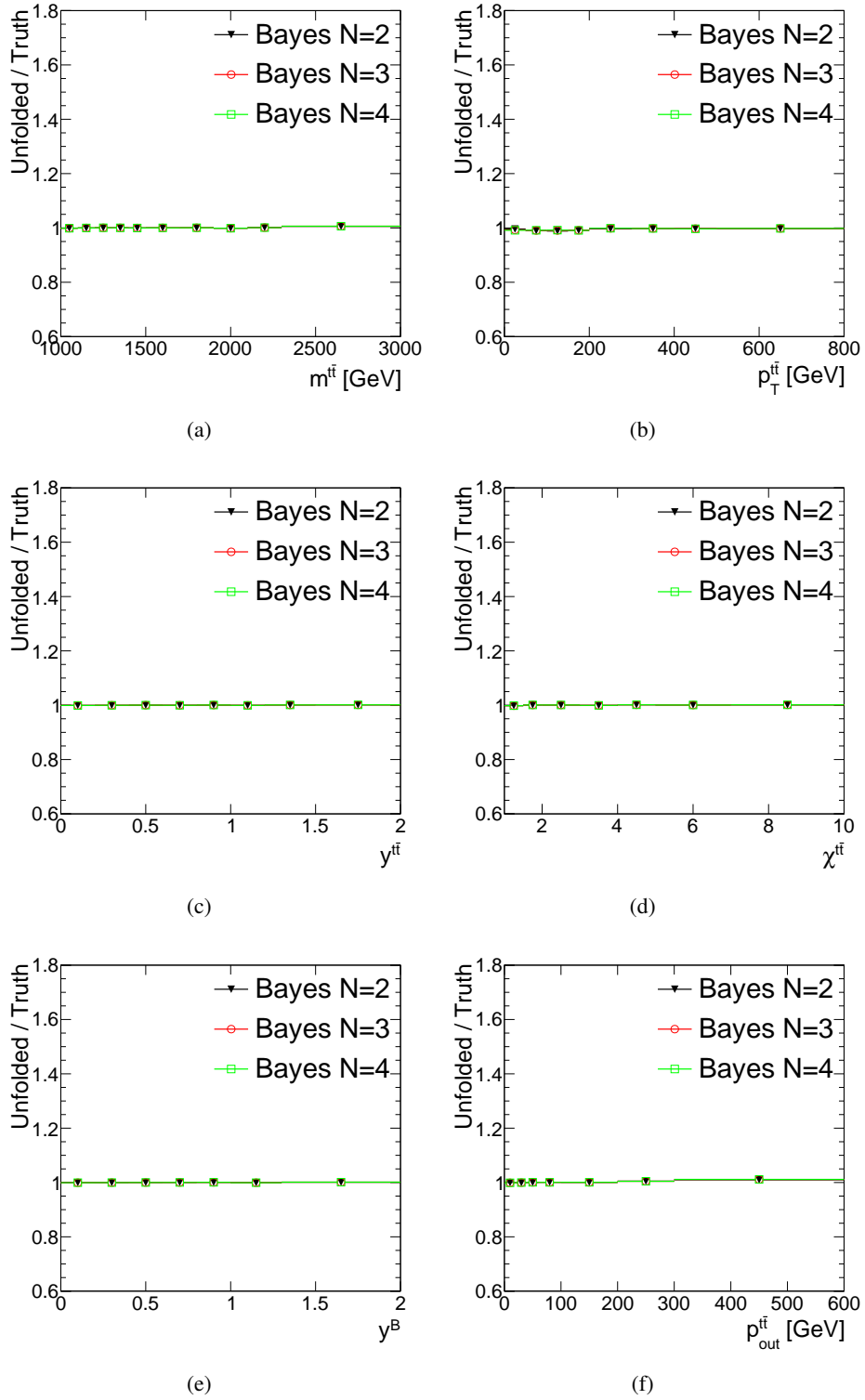


Figure 110: Stress test results for various $t\bar{t}$ distributions. The figures show the ratios between unfolded reweighted and truth reweighted distributions for the particle-level fiducial phase space.

Not reviewed, for internal circulation only

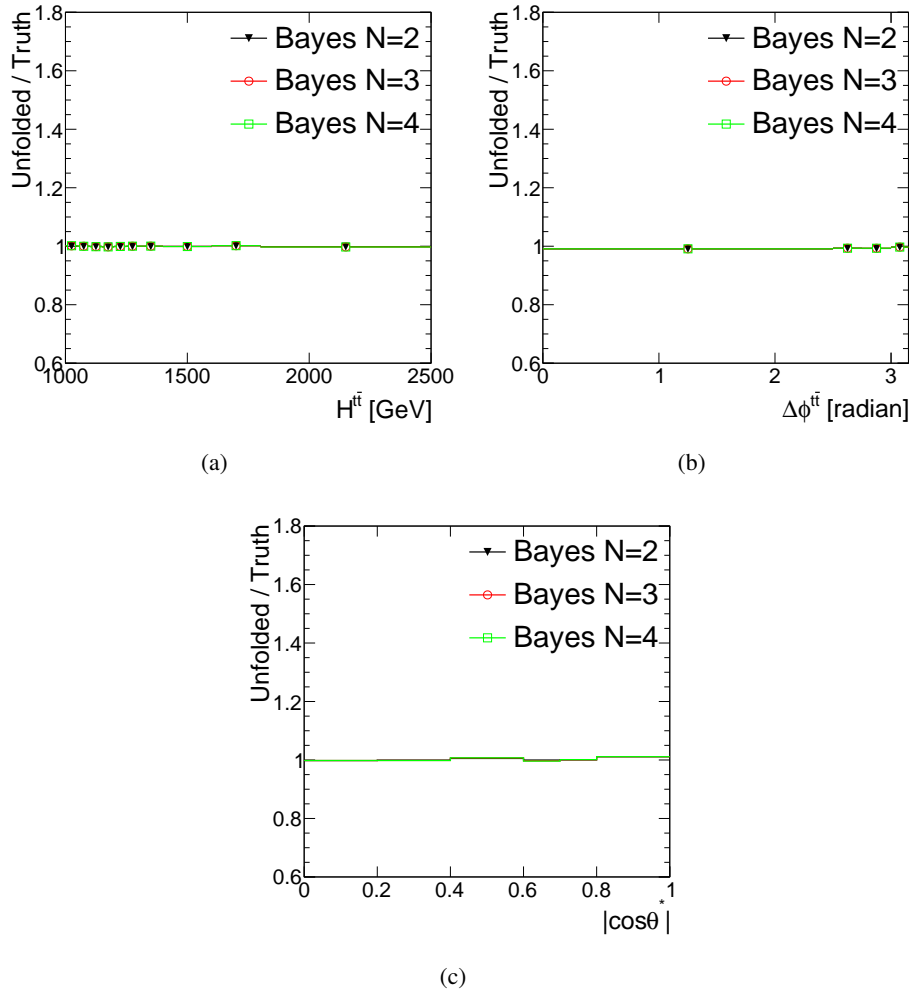


Figure 111: Stress test results for $t\bar{t} H_T$, $\Delta\phi$ and $\cos\theta^*$ distribution. The figures show the ratios between unfolded reweighted and truth reweighted distributions for the particle-level fiducial phase space.

I.3. An additional closure test using smeared MC distributions

1001 A further test to determine the stability of the unfolding procedure is performed by taking the predicted
1002 reconstructed distributions (MC signal + background) for the various kinematic variables, fluctuating
1003 each bin using a Gaussian with a width equal to the expected relative statistical uncertainty of the data,
1004 and creating pseudo-experiments. Each pseudo experiment is passed through background subtraction
1005 and the full unfolding procedure. The mean and root mean square of each bin are calculated for 1 000
1006 pseudo-experiments and compared with the MC truth distributions.

1007 The means of the pseudo-experiment results divided by the nominal truth are shown in Figures 112 and
1008 113 for various iterations of the unfolding algorithm for both the Bayes unfolding techniques.

1009 We see generally very good “closure”, with means consistent with unity, except the subleading jet p_T
1010 distribution. One concern is the relative modest MC samples, and the effect that fluctuations on the truth
1011 distributions may have on the results of this procedure.

1012 The standard deviation of the pseudo-experiment results divided by mean of the pseudo-experiment res-
1013 ults are shown in Figures 114 and 115 for various iterations of the unfolding algorithm for both the Bayes
1014 unfolding techniques.

Not reviewed, for internal circulation only

Not reviewed, for internal circulation only

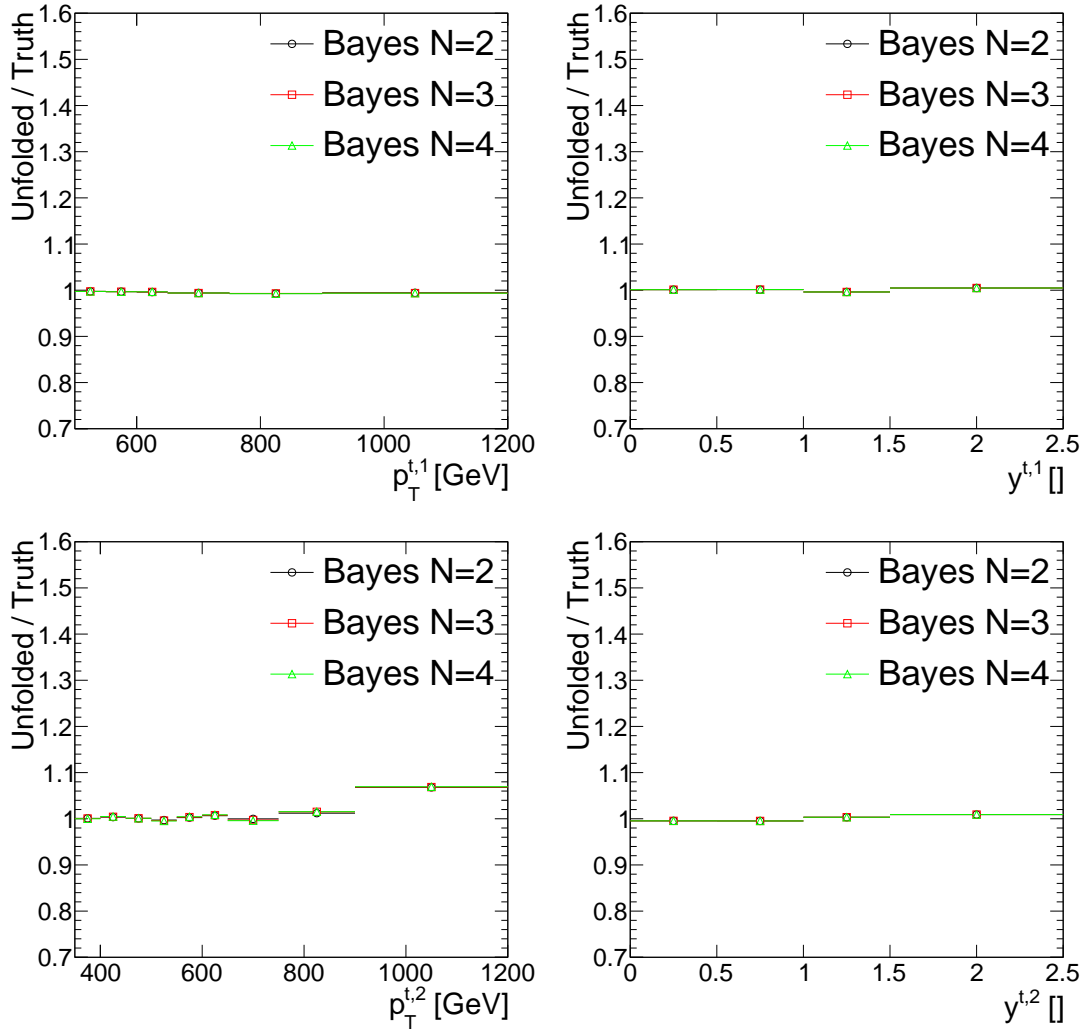


Figure 112: The mean of the pseudo-experiment results divided by the nominal truth for the leading and subleading top-jet candidate p_T and rapidity.

Not reviewed, for internal circulation only

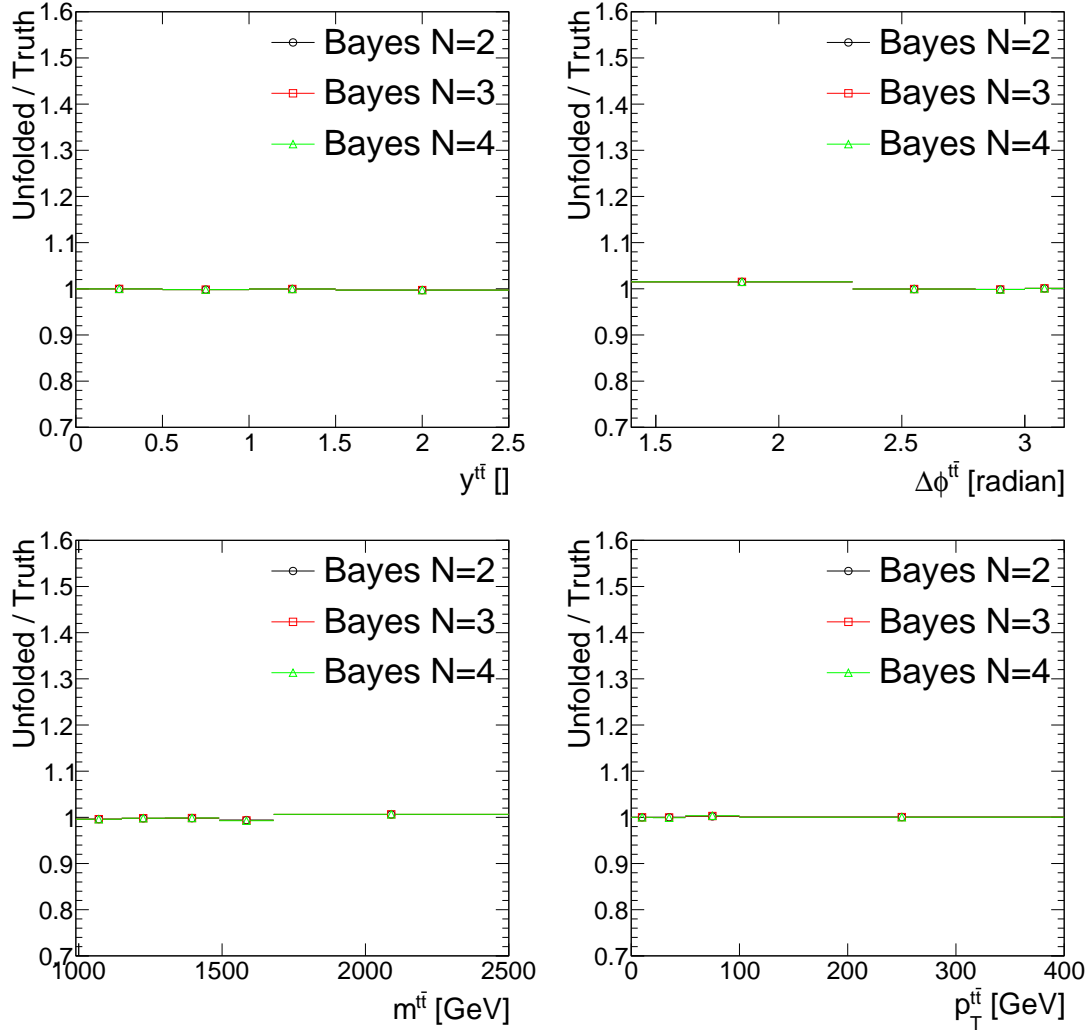


Figure 113: The mean of the pseudo-experiment results divided by the nominal truth for the $t\bar{t}$ system observables.

Not reviewed, for internal circulation only

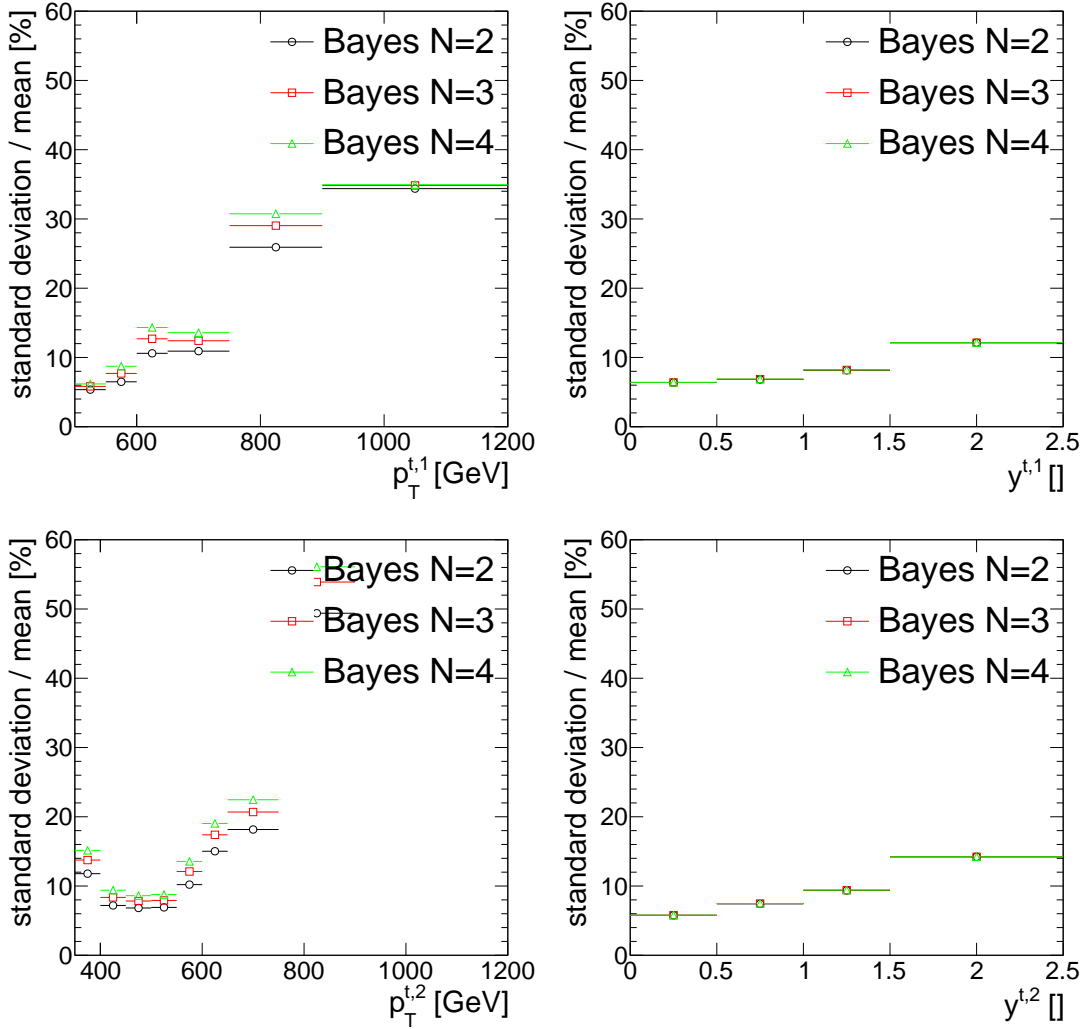


Figure 114: The relative spread of the pseudo-experiment results for the leading and subleading top-jet candidate p_T and rapidity.

Not reviewed, for internal circulation only

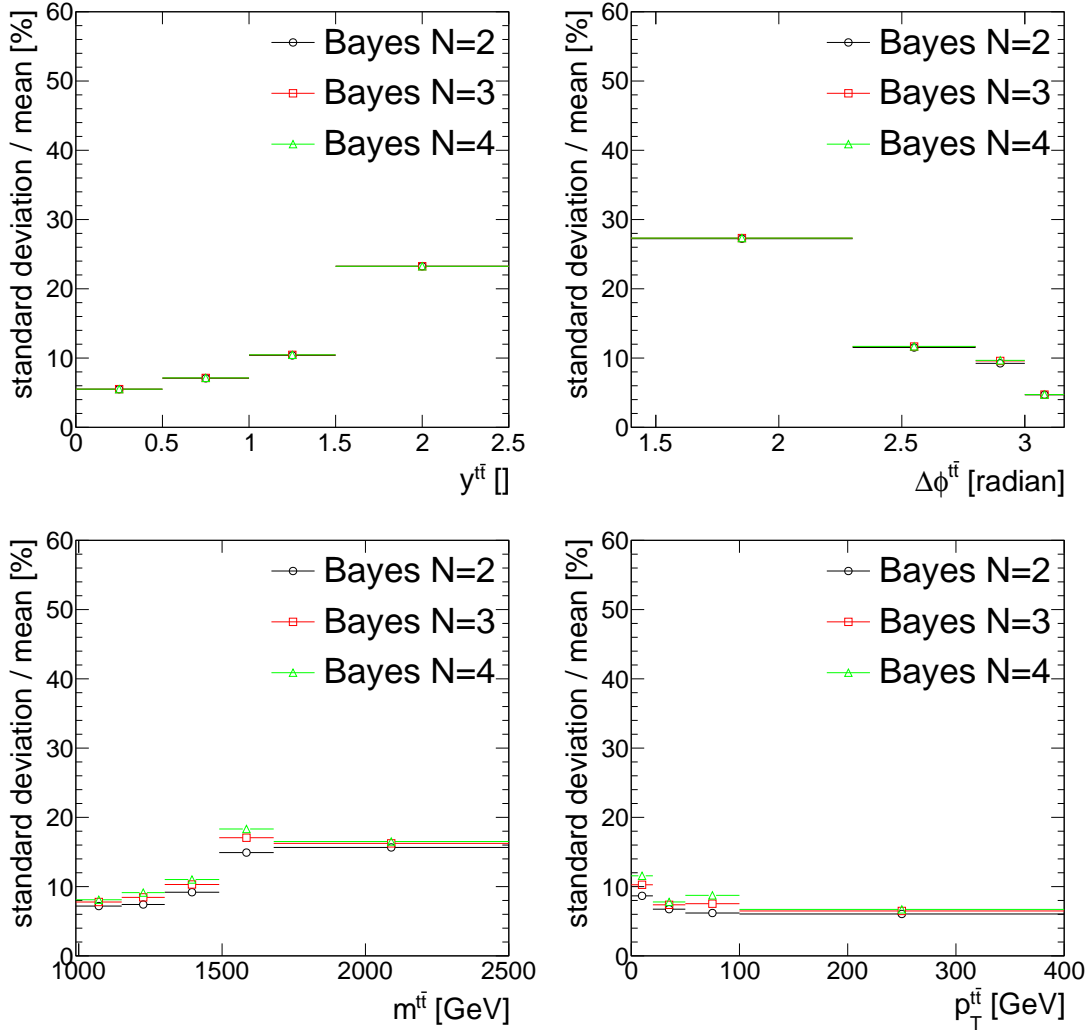


Figure 115: The relative spread of the pseudo-experiment results for the $t\bar{t}$ system observables.

1015 **I.4. Pull test**

The stability of the unfolding method with respect to the statistical fluctuations in data is checked by performing pull tests. The same pseudo-experiments are used as constructed in Appendix I.3. Again, each pseudo experiment is passed through background subtraction and the full unfolding procedure and the pull for bin j is calculated for each pseudo-experiment i :

$$P_i^j = \frac{s_i^j - s_{\text{truth}}^j}{\sigma_i^j}, \quad (9)$$

1016 where s_i^j is the cross-section measured in bin j for pseudo-experiment i , s_{truth}^j is the truth cross-section in
1017 bin j , and σ_i^j is the statistical uncertainty of the unfolded cross-section in bin j . The means and standard
1018 deviations (widths) of the pull distributions are shown in Figures 116, 117, 118, and 119. The means
1019 are found to be consistent with zero and the widths with one, which proves the stability of the unfolding
1020 method.

Not reviewed, for internal circulation only

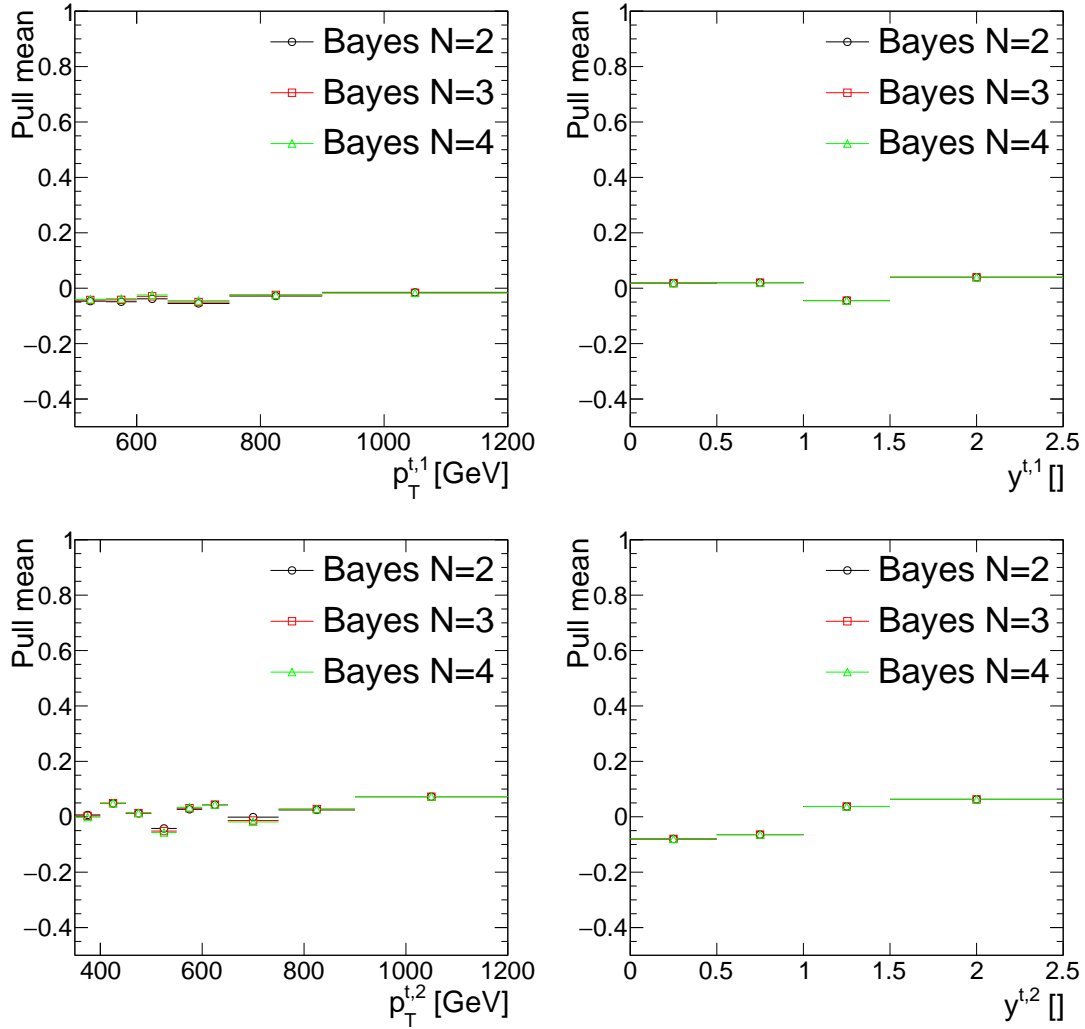


Figure 116: The mean of the pull from the pseudo-experiments for the leading and subleading top-jet candidate p_T and rapidity.

Not reviewed, for internal circulation only

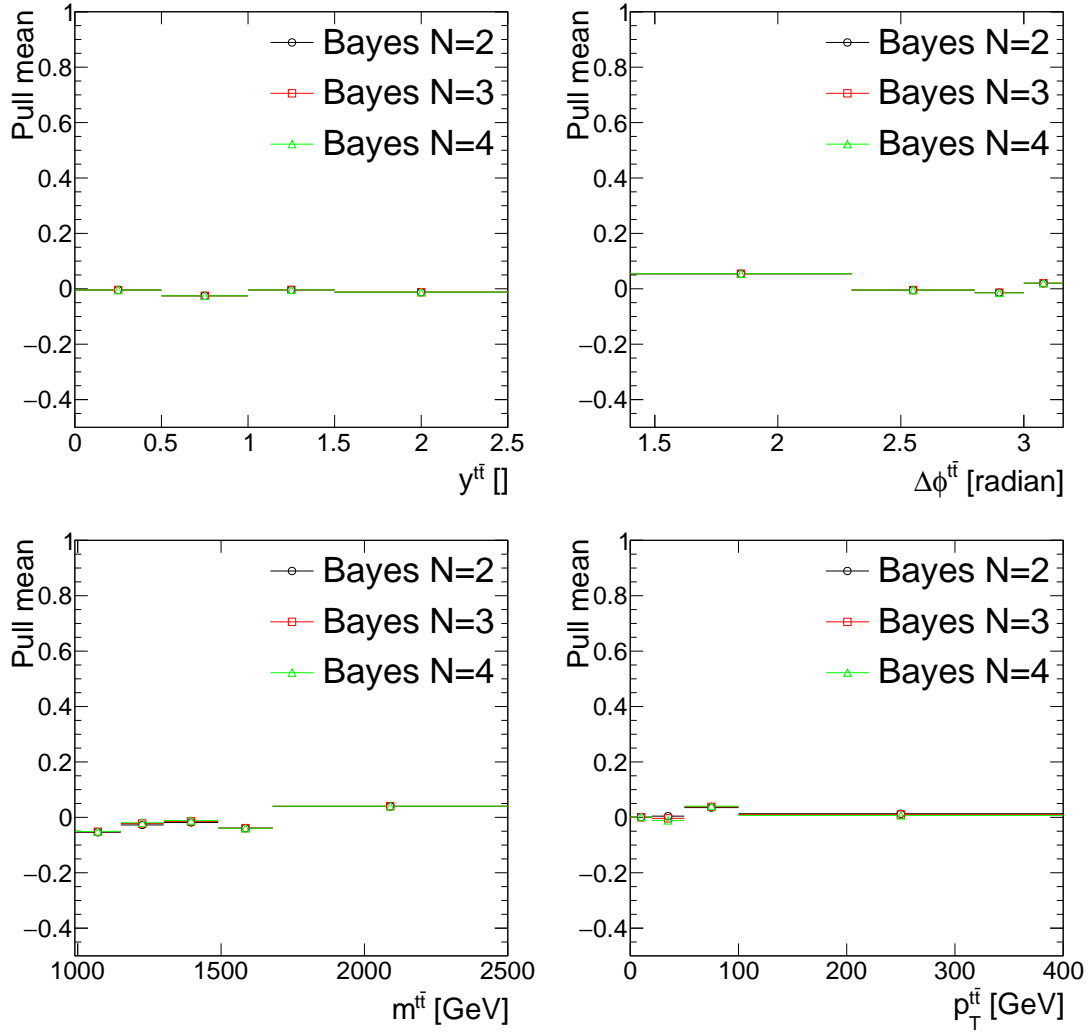


Figure 117: The mean of pull from pseudo-experiments for the $t\bar{t}$ system observables.

Not reviewed, for internal circulation only

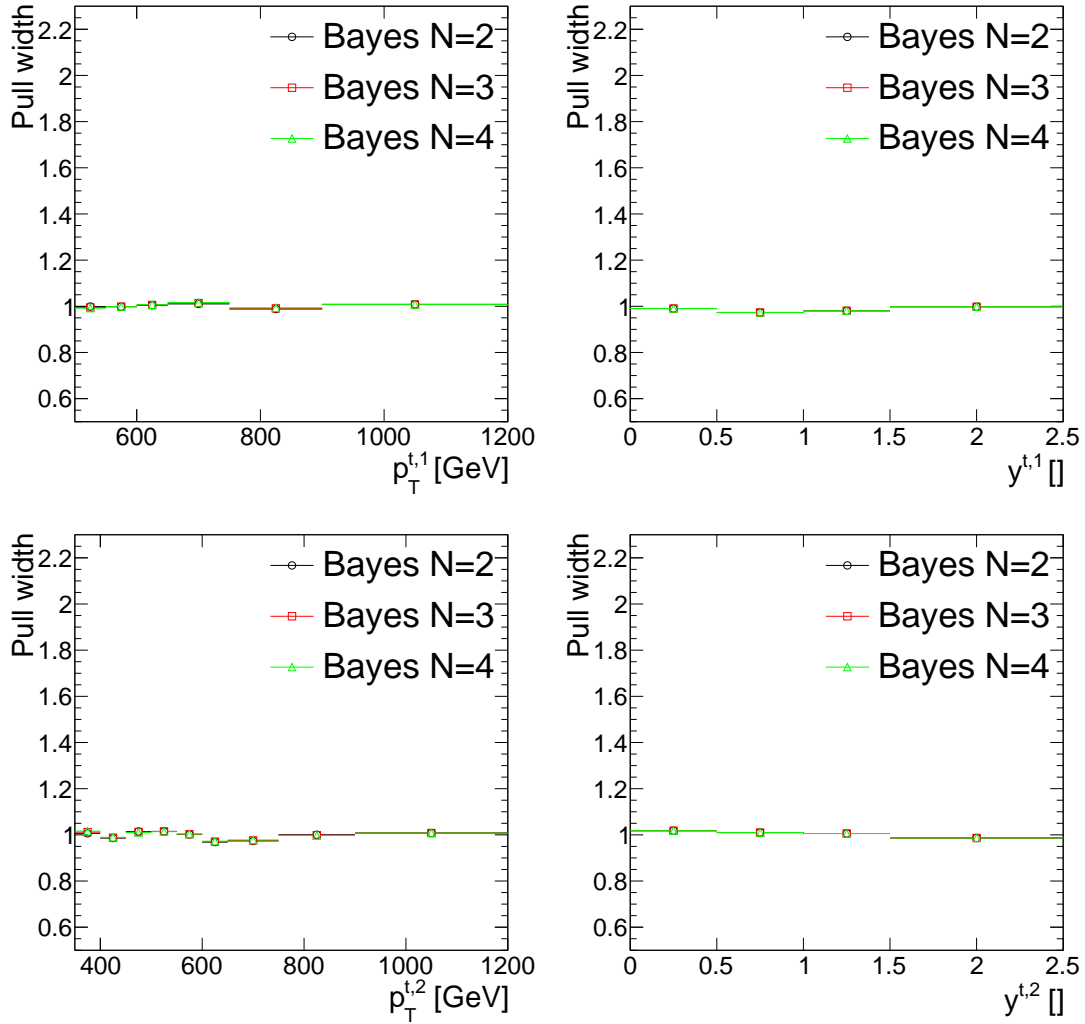


Figure 118: The width of the pull from the pseudo-experiments for the leading and subleading top-jet candidate p_T and rapidity.

Not reviewed, for internal circulation only

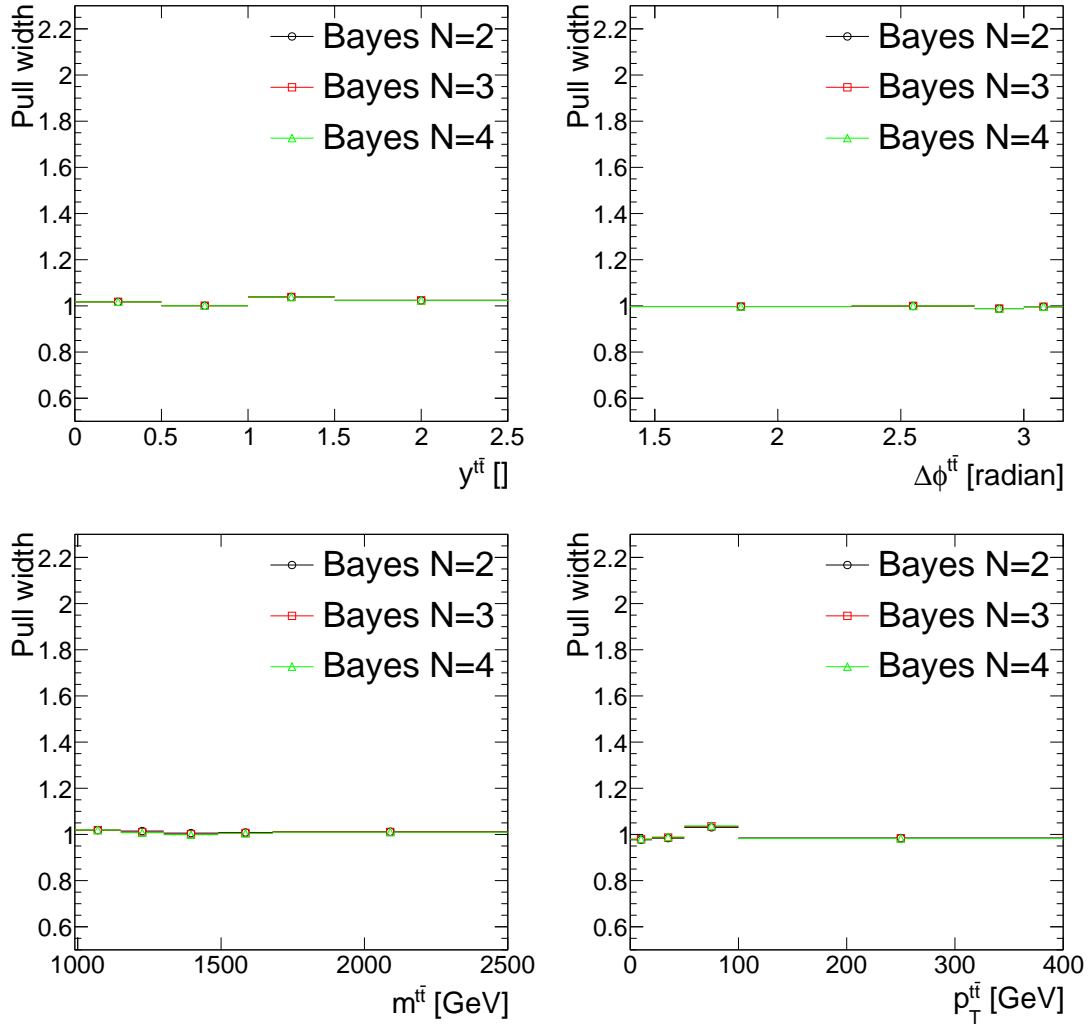


Figure 119: The width of pull from pseudo-experiments for the $t\bar{t}$ system observables.

1021 **I.5. Stress test of τ_{32} variable**

1022 In this section, we test the dependency of the shape of the unfolded particle variables on the τ_{32} variable.
 1023 We discovered that τ_{32} distribution is strongly signal modelling dependent. Therefore, it is needed to test
 1024 how the shapes of variables can be affected by mismodelling of this variable.

We performed the test by stressing of the leading particle level large-R jet τ_{32} using the following formula:

$$\text{weight}_{\text{REWEIGHTED}} = \text{weight}_{\text{NOMINAL}} \cdot (0.714 \cdot (\text{particle level leading large-R jet } \tau_{32}) + 0.493) \quad (10)$$

1025 Figures 120-122 show the results of the stress tests for the top kinematic variables which we do unfold.
 1026 The stress tests uncover instability in the normalization. This was expected because stressing of the τ_{32}
 1027 variable changes efficiency of the detector level cuts. However, the shapes of variables appears to be well
 1028 preserved for all variables. Small slope is seen for the leading top p_T , $t\bar{t} p_T$ and $t\bar{t} H_T$ variables. Shape of
 1029 other variables appears to be almost intact.

Not reviewed, for internal circulation only

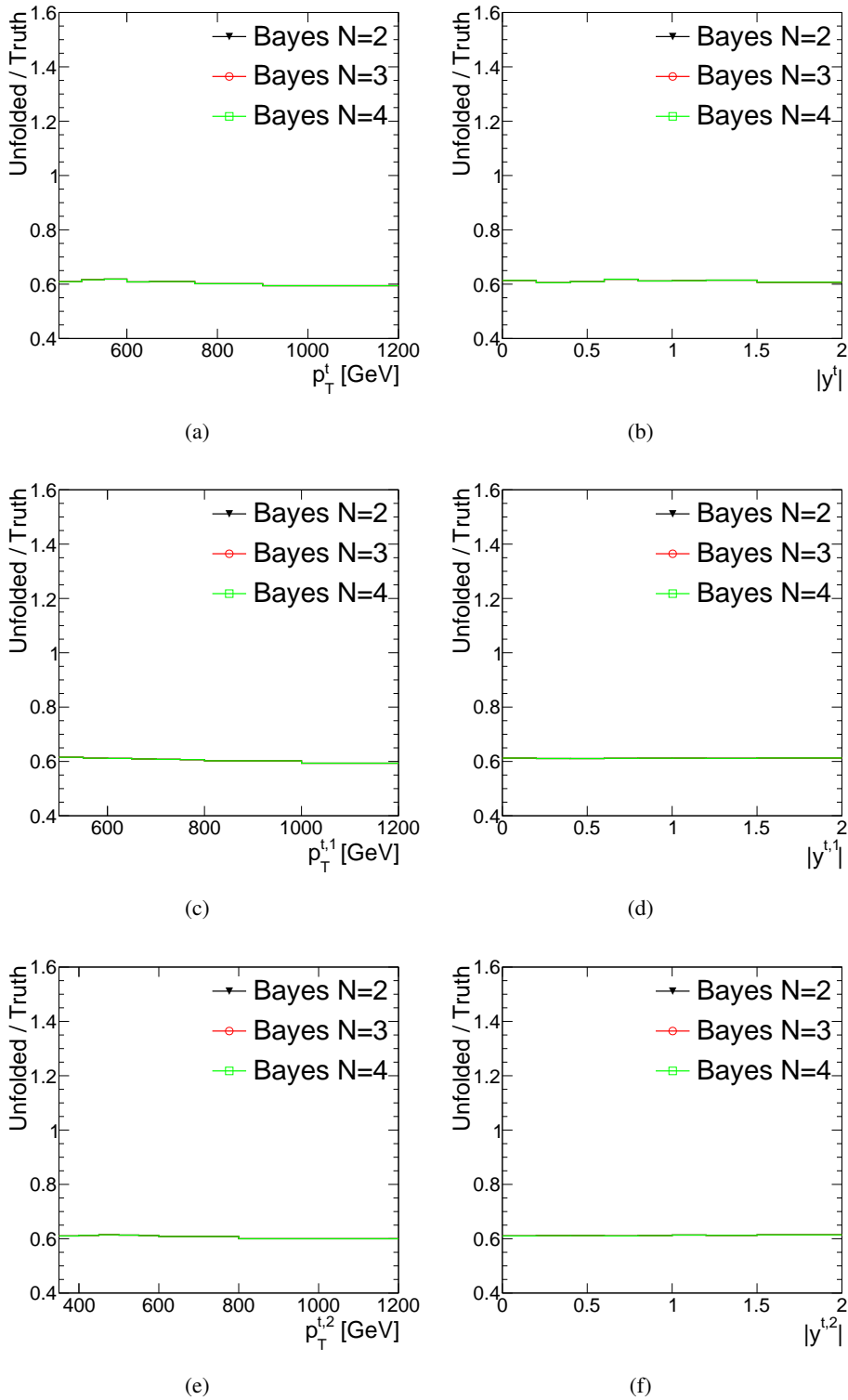


Figure 120: Stress test results for random top, leading top, and subleading top p_T and $|y|$ distributions. The figures show the ratios between unfolded reweighted and truth reweighted distributions for the particle-level fiducial phase space.

Not reviewed, for internal circulation only

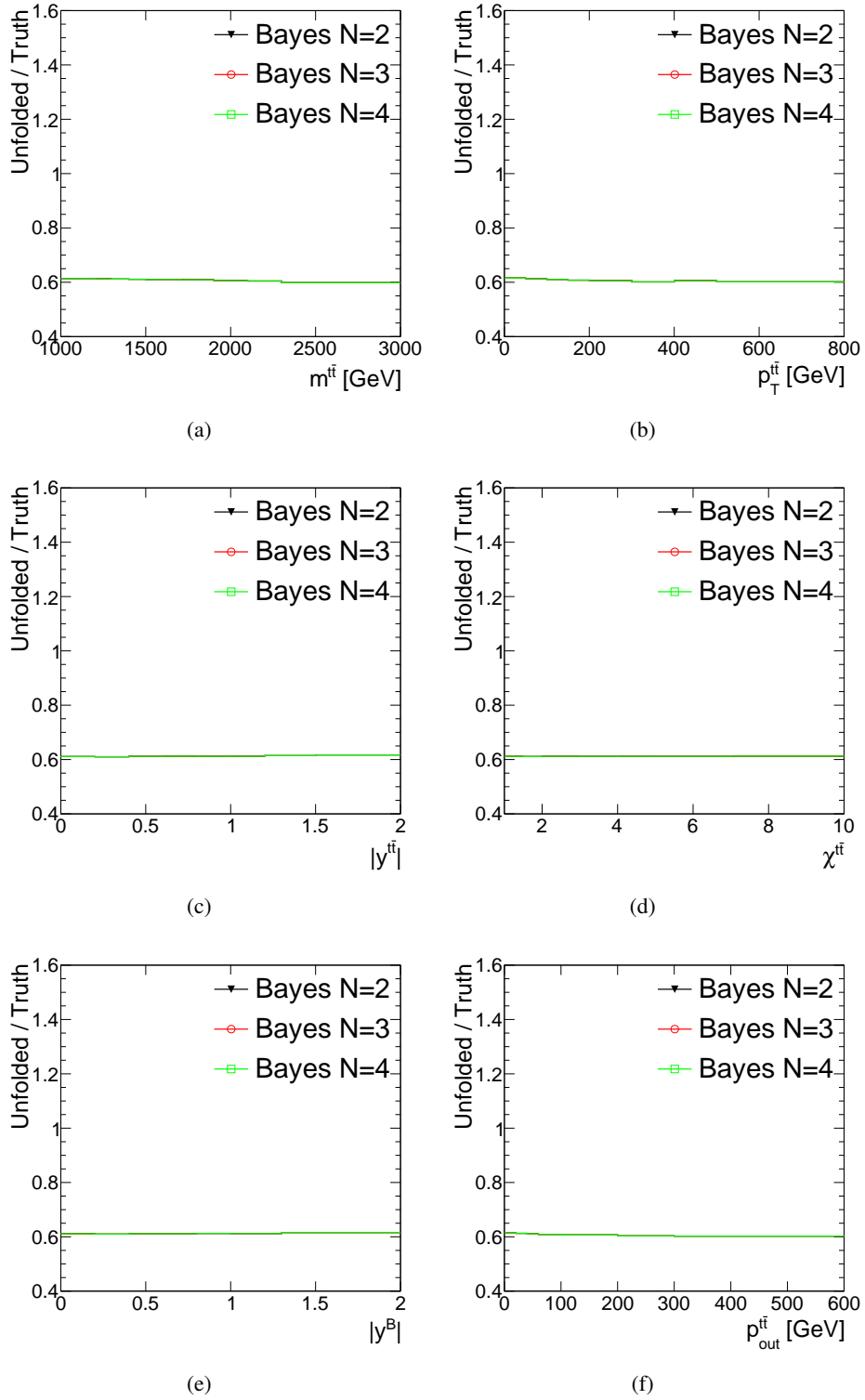


Figure 121: Stress test results for various $t\bar{t}$ distributions. The figures show the ratios between unfolded reweighted and truth reweighted distributions for the particle-level fiducial phase space.

Not reviewed, for internal circulation only

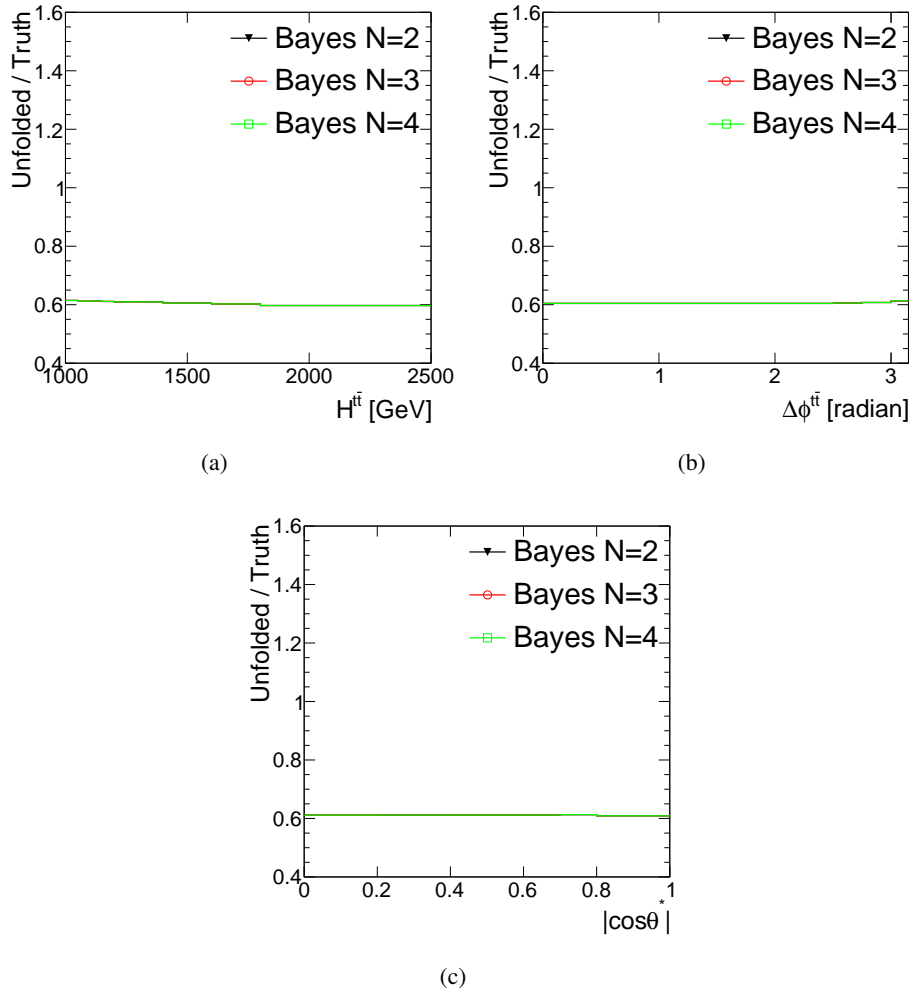


Figure 122: Stress test results for $t\bar{t} H_T$, $\Delta\phi$ and $\cos\theta^*$ distribution. The figures show the ratios between unfolded reweighted and truth reweighted distributions for the particle-level fiducial phase space.

1030 J. Stress tests at parton-level

1031 J.1. Parton-level phase-space stress tests

1032 In the stress test, the modified distributions at detector level are unfolded to the parton-level using the
 1033 nominal migration matrices and corrections for the detector-level and truth-level cuts. Afterwards, such
 1034 unfolded distributions are compared to the reweighted truth-level distributions. The method passes the
 1035 test if there is good agreement in the ratio of the unfolded and reweighted truth-level distributions.

1036 The modified distributions are obtained from the nominal sample. The same set of events is used to create
 1037 modified distribution but with the event weights multiplied by scale factor which depends on truth top p_T ,
 1038 $m_{t\bar{t}}$, or $p_T^{t\bar{t}}$, respectively. These distributions are referred to as the reweighted distributions. We adopted
 1039 the approach used in $t\bar{t}$ lepton+jets differential measurement. We derive a weighting function based on
 1040 data-MC disagreement at reco-level and use it to perform the stress tests.

1041 In Fig. 123 and Fig. 124 we show the (data-bckg)/signal ratio at the reconstructed level as a function of
 1042 the kinematic variable we are unfolding. We use the linear fits to these ratios as a reweighting functions
 1043 in the stress tests below.

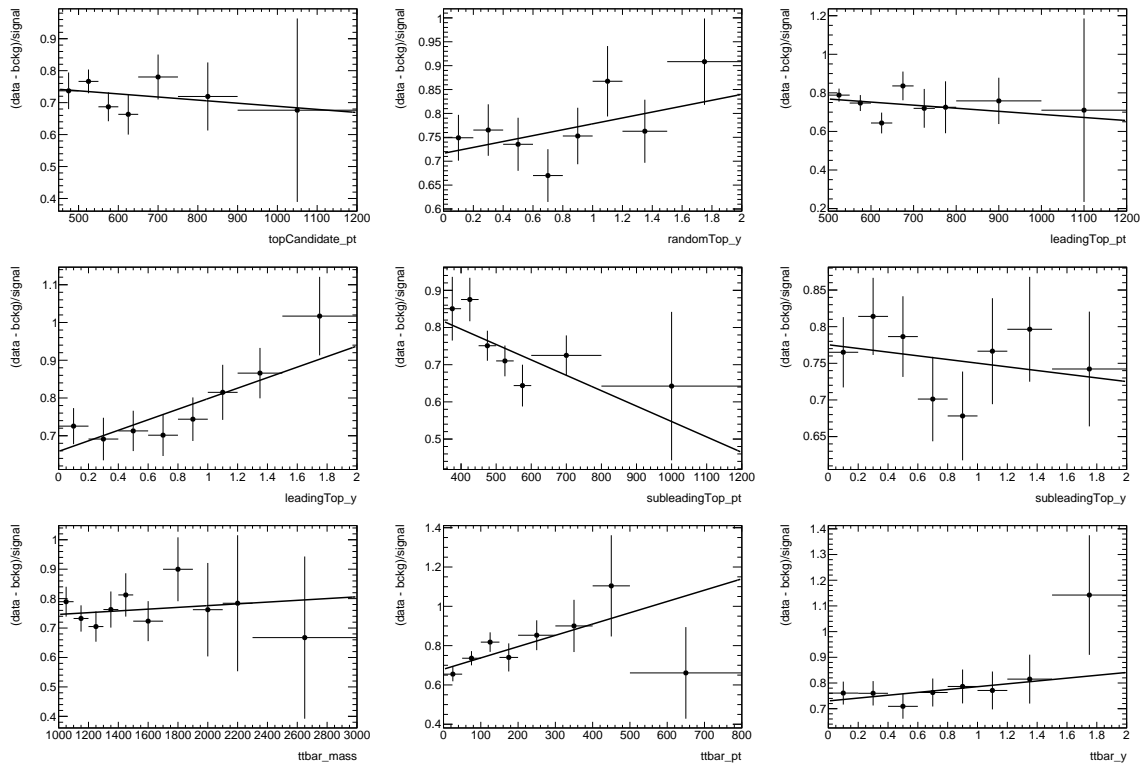


Figure 123: The (data-bckg)/signal ratio at the reconstructed level as a function of various kinematic variables.

1044 The stress tests documented here employ the parton-level phase-space used in the analysis. Stress tests
 1045 using the full phase space at parton-level had shown instability in the unfolded distributions. This in-
 1046 stability is avoided by using a phase-space at the parton-level which is closer to the phase-space at the
 1047 detector level.

Not reviewed, for internal circulation only

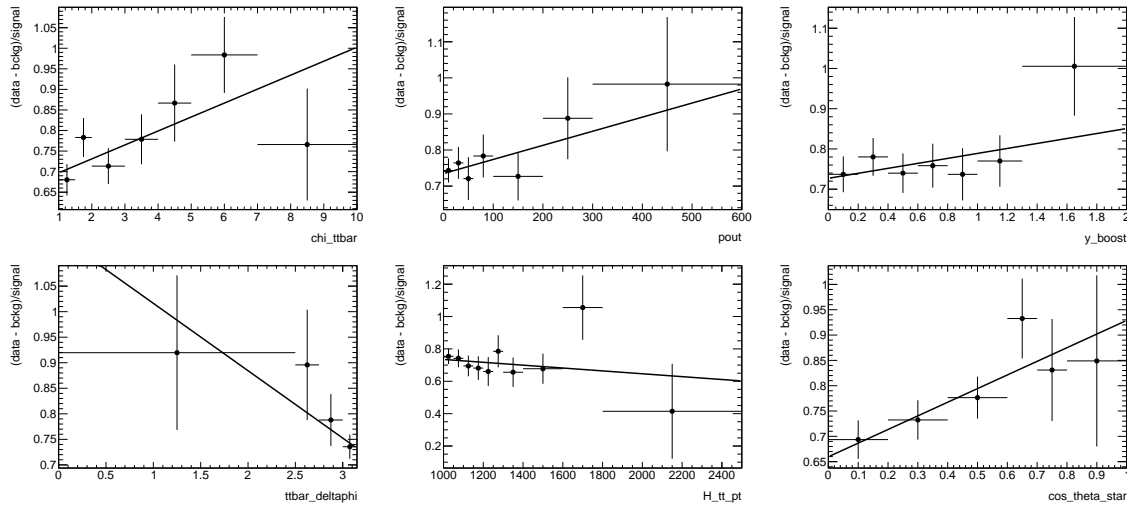


Figure 124: The $(\text{data} - \text{bckg})/\text{signal}$ ratio at the reconstructed level as a function of another kinematic variables.

1048 J.1.1. Parton-level phase-space selection

1049 The phase-space at the parton-level is chosen as large as possible.

1050 Since we are using a selection on the second leading top-jet $p_T > 350$ GeV at the detector level, it was
1051 seen as beneficial to use this cut also at parton level. So, at the parton level, we defined the phase-space
1052 by the combination of cuts

- 1053 • leading top $p_T > 500$ GeV
- 1054 • 2nd leading top $p_T > 350$ GeV.

1055 In the following section, the stress tests show that with this selection, the unfolding procedure is stable.

1056 J.1.2. Stress test results in parton level phase-space

1057 In this section, results of the stress test in parton level phase-space are presented.

1058 Figures 125-127 show the results of the stress tests for the top kinematic variables which we do unfold.
1059 Most of the stress tests did not uncover instability in the unfolding procedure. There is very slight trend
1060 in the stress test for leading top $|y|$. Also, the lowest bin in $\Delta\phi$ spectrum pass the stress test only at about
1061 10% level . However, there is very low statistics in this bin and we have 80% total uncertainty in this bin
1062 in the unfolded distribution.

Not reviewed, for internal circulation only

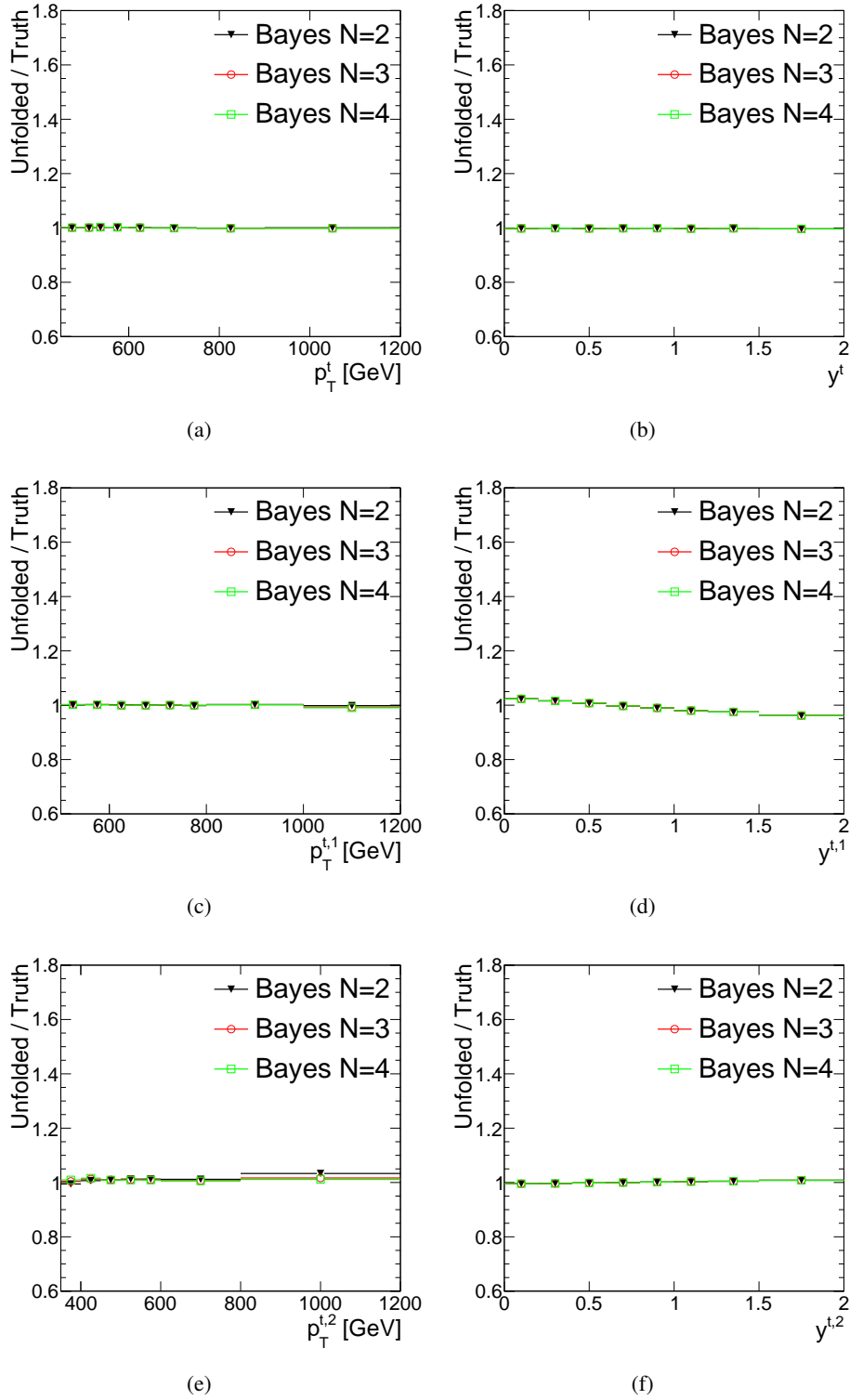


Figure 125: Stress test results for random top, leading top, and subleading top p_T and $|y|$ distributions. The figures show the ratios between unfolded reweighted and truth reweighted distributions at fiducial phase-space parton-level.

Not reviewed, for internal circulation only

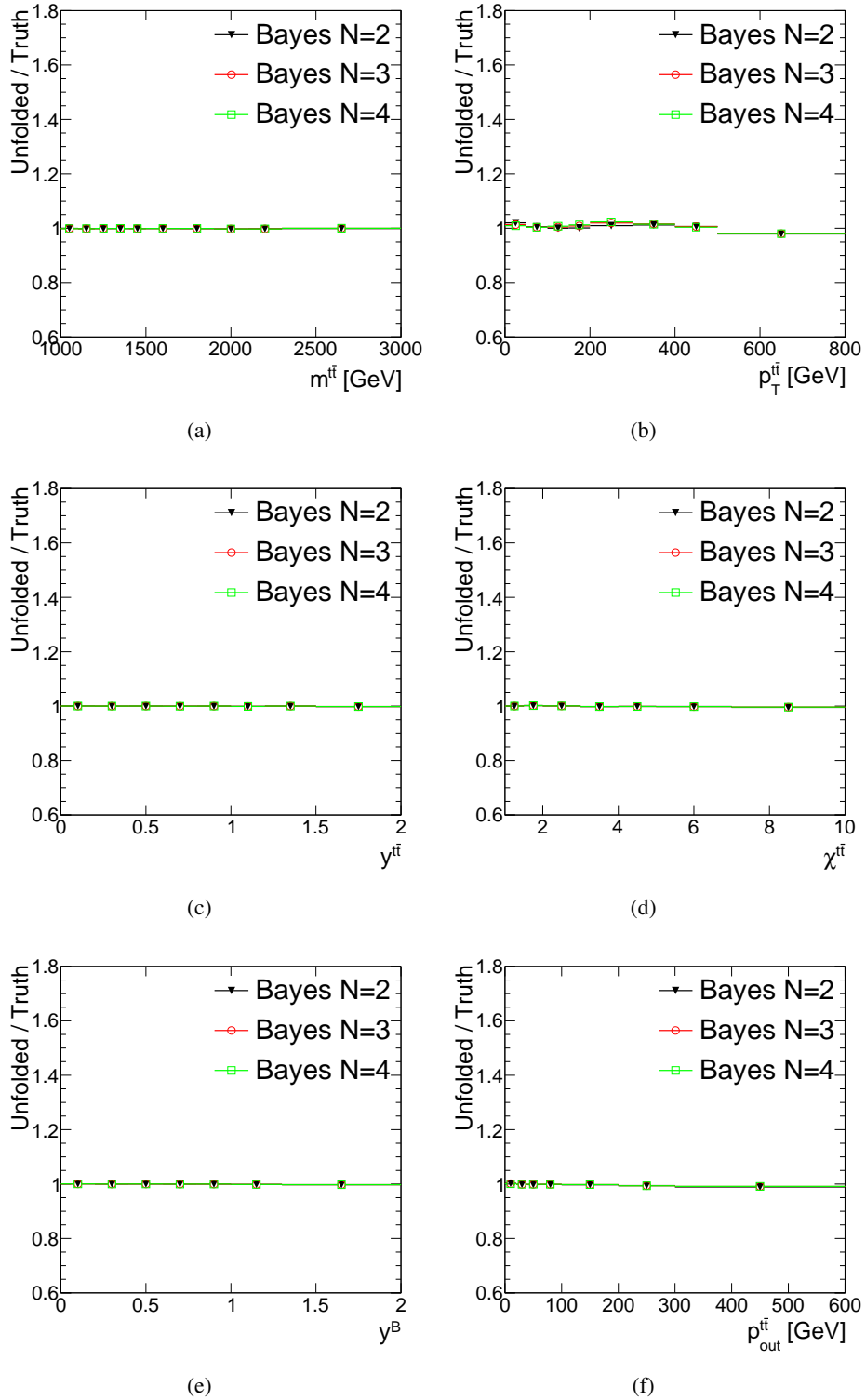


Figure 126: Stress test results for various $t\bar{t}$ distributions. The figures show the ratios between unfolded reweighted and truth reweighted distributions at parton-level.

Not reviewed, for internal circulation only

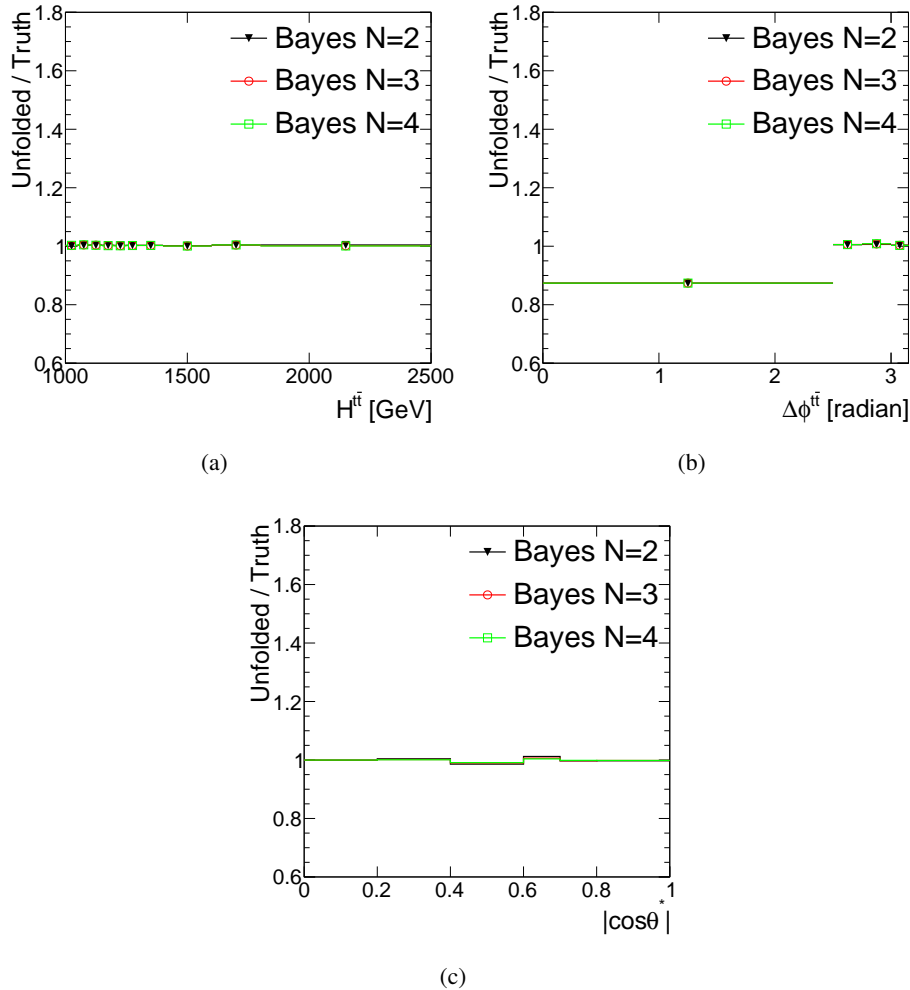


Figure 127: Stress test results for $t\bar{t} H_T$, $\Delta\phi$ and $\cos\theta^*$ distribution. The figures the ratios between unfolded reweighted and truth reweighted distributions at parton-level.

1063 J.1.3. Stress test results with single bump in the distributions

1064 In this section, the unfolding is stressed with reweighting functions from the previous which are increased
1065 by factor of 1.15 in the single bin of the parton level histogram. Figures 128, 129 and 130 show results
1066 of the stress. The information about peak is completely lost for most variables. Information is lost due to
1067 big migrations between the bins.

Not reviewed, for internal circulation only

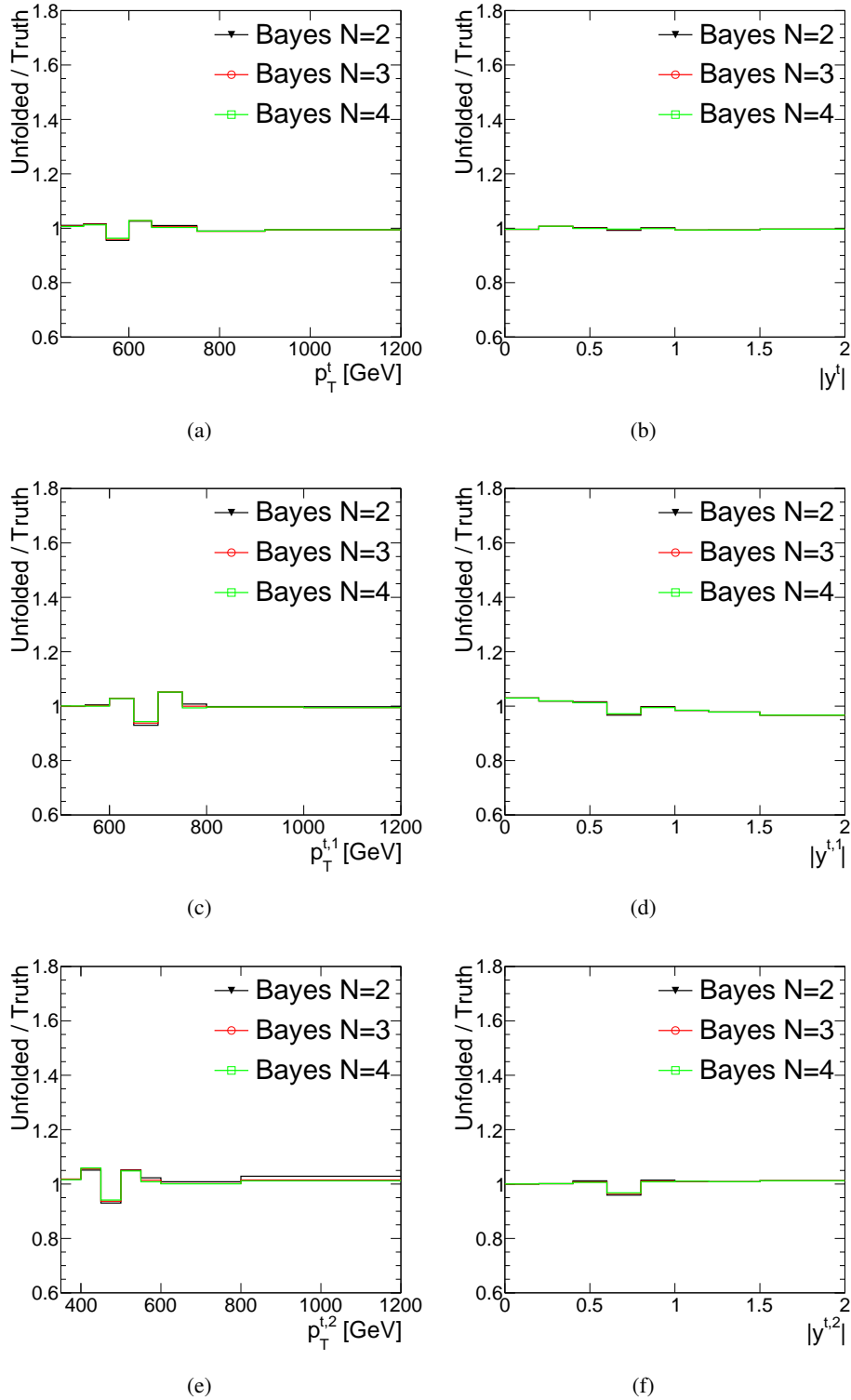


Figure 128: Stress test results for random top, leading top, and subleading top p_T and $|y|$ distributions. The figures show the ratios between unfolded reweighted and truth reweighted distributions at fiducial phase-space parton-level.

Not reviewed, for internal circulation only

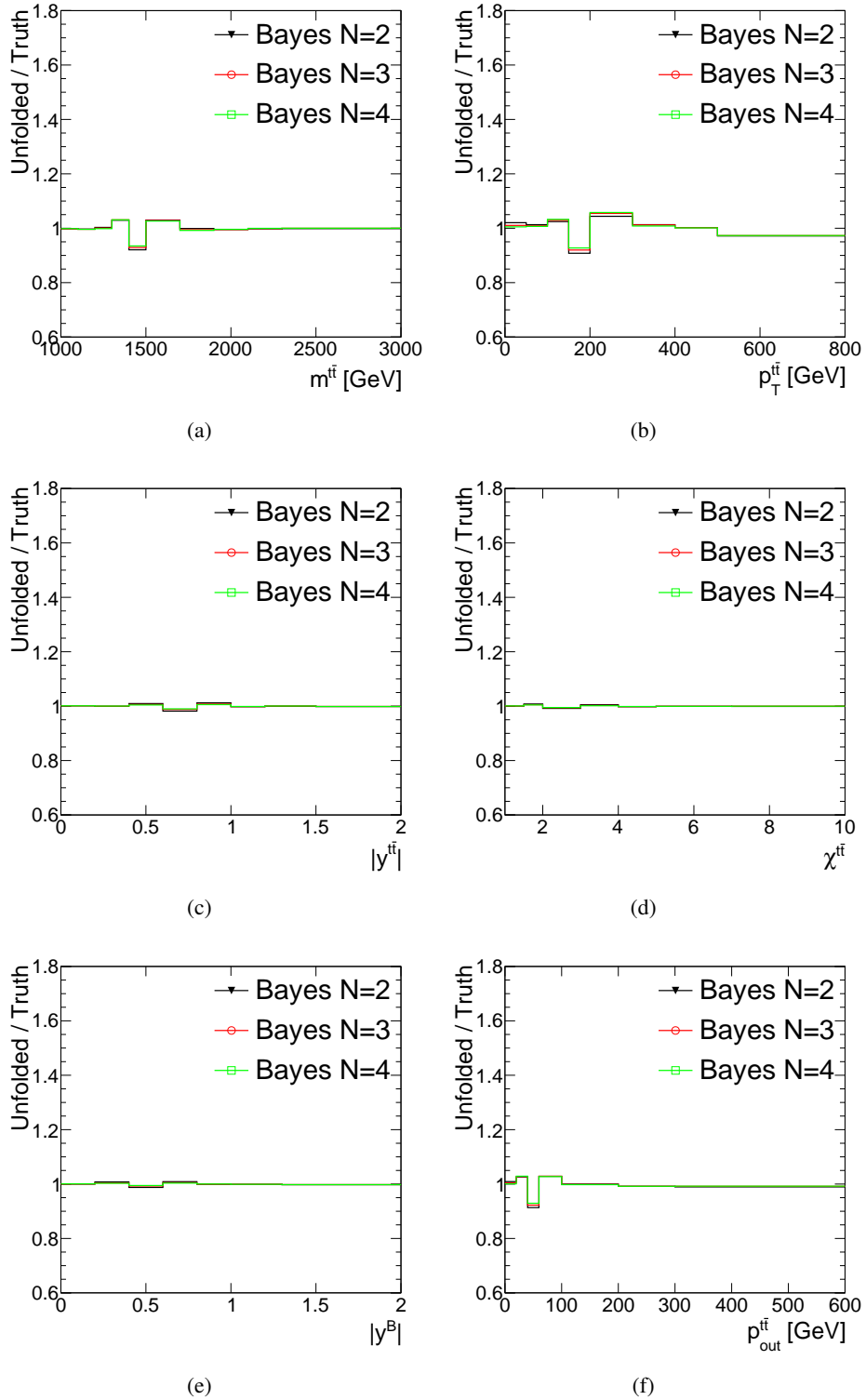


Figure 129: Stress test results for various $t\bar{t}$ distributions. The figures show the ratios between unfolded/reweighted and truth distributions at parton-level.

Not reviewed, for internal circulation only

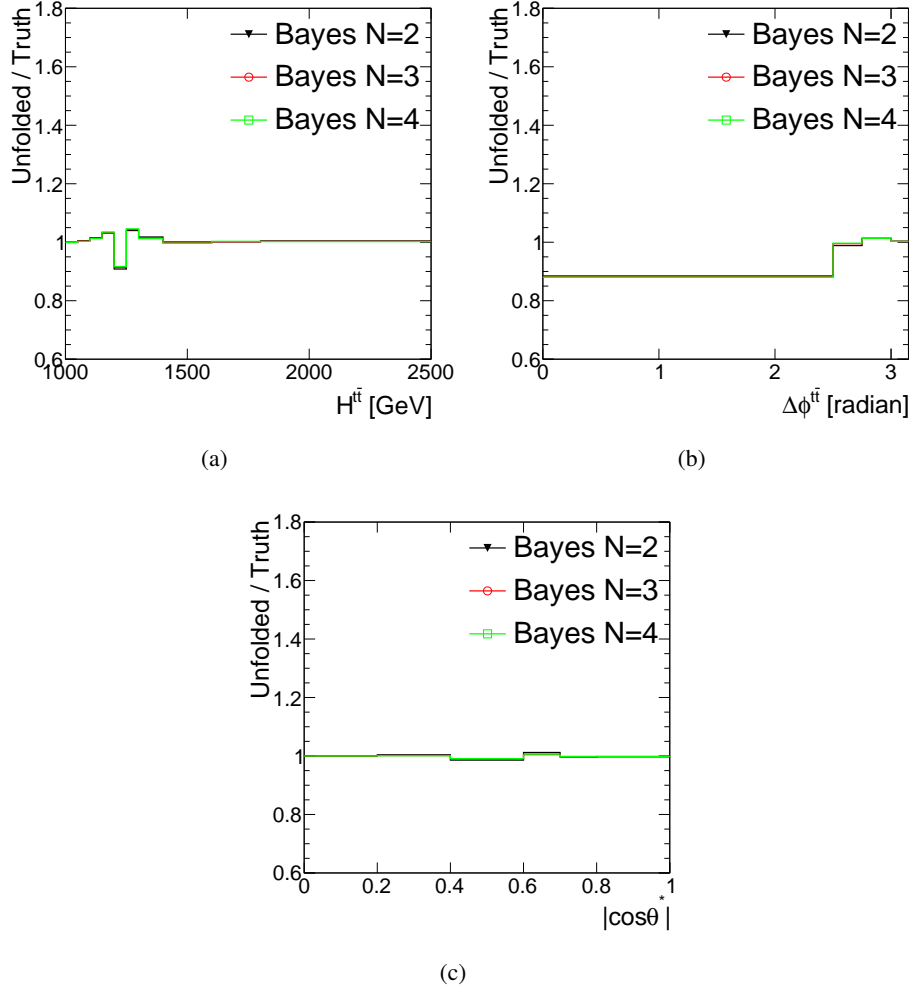


Figure 130: Stress test results for $t\bar{t} H_T$, $\Delta\phi$ and $\cos\theta^*$ distribution. The figures the ratios between unfolded reweighted and truth reweighted distributions at parton-level.

1068 K. Stress test for full parton-level phase space

1069 K.1. Reweighted distributions

1070 In the stress test, the modified distributions at detector level are unfolded using nominal migration matrix
 1071 and corrections of reco and truth level cuts. Afterwards, such unfolded distributions are compared to
 1072 reweighted truth-level distributions.

1073 The modified distributions are obtained from the nominal sample. The same set of events is used to create
 1074 modified distribution but with event weights multiplied by truth top p_T dependent scale factor. These
 1075 distributions are referred to as the reweighted distributions.

1076 For each variable, two reweighted distributions are defined. The reweighted weights are defined using the
 1077 following formulas:

$$\text{weight}_{\text{REWEIGHTED } 1} = \text{weight}_{\text{NOMINAL}} \cdot (-0.0008 \cdot (\text{truth top } p_T [\text{GeV}] \cdot 0.9 + 1.1)) \quad (11)$$

$$\text{weight}_{\text{REWEIGHTED } 2} = \text{weight}_{\text{NOMINAL}} \cdot (0.0008 \cdot (\text{truth top } p_T [\text{GeV}] \cdot 0.9 + 0.9)) \quad (12)$$

1078 and are plotted in Fig. 131. The distribution obtained from this reweighting is called 'reweighted 1' and
 1079 'reweighted 2' distribution, respectively.

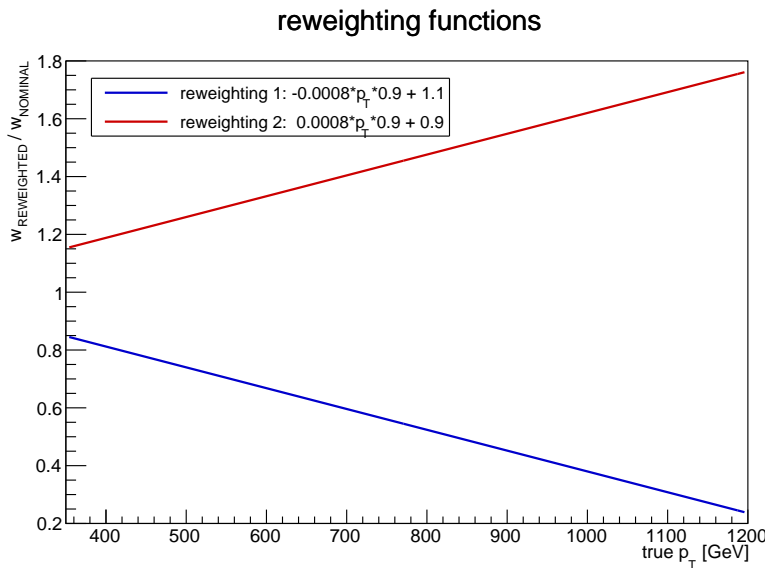


Figure 131: The functions used for reweighting as a function of parton level top quark p_T .

1080 Figures 132-137 show the comparison between reweighted and nominal distributions at the detector and
 1081 the full phase-space parton level for random top p_T , leading top p_T , 2nd leading top p_T , $t\bar{t}$ mass, $t\bar{t}$ p_T and
 1082 the absolute value of $t\bar{t}$ rapidity. For some of the variables (mostly top quark pair variables), the ratios
 1083 between reco level distributions and ratios between truth level distributions are different. This is the first
 1084 indication that it will be problematic to unfold reweighted distributions using nominal efficiencies.

Not reviewed, for internal circulation only

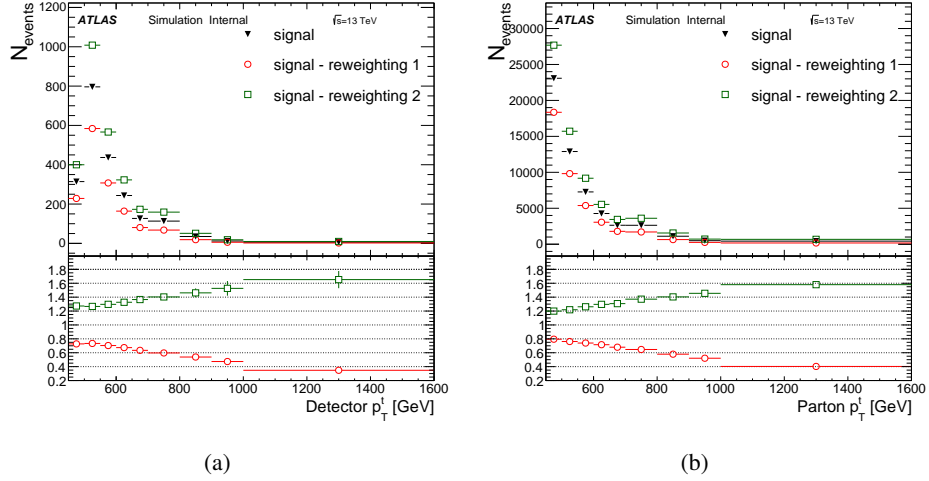


Figure 132: The comparison between reweighted and nominal distributions for random top p_T . Figure (a) shows reco level comparison and figure (b) truth level comparison between distributions.

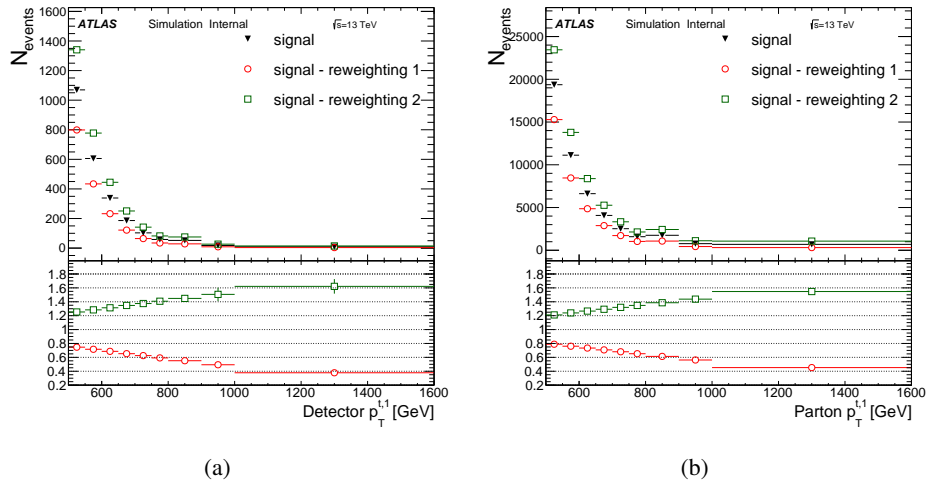


Figure 133: The comparison between reweighted and nominal distributions for leading top p_T . Figure (a) shows reco level comparison and figure (b) truth level comparison between distributions.

Not reviewed, for internal circulation only

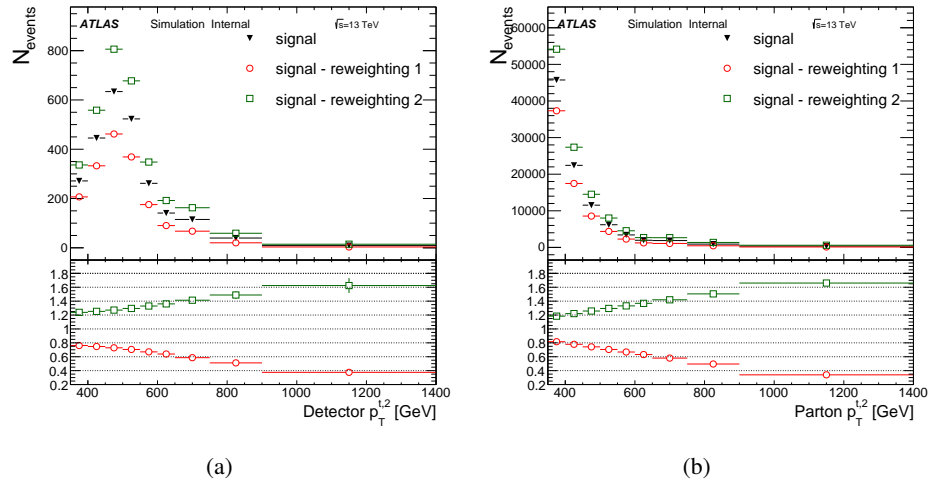


Figure 134: The comparison between reweighted and nominal distributions for 2nd leading top p_T . Figure (a) shows reco level comparison and figure (b) truth level comparison between distributions.

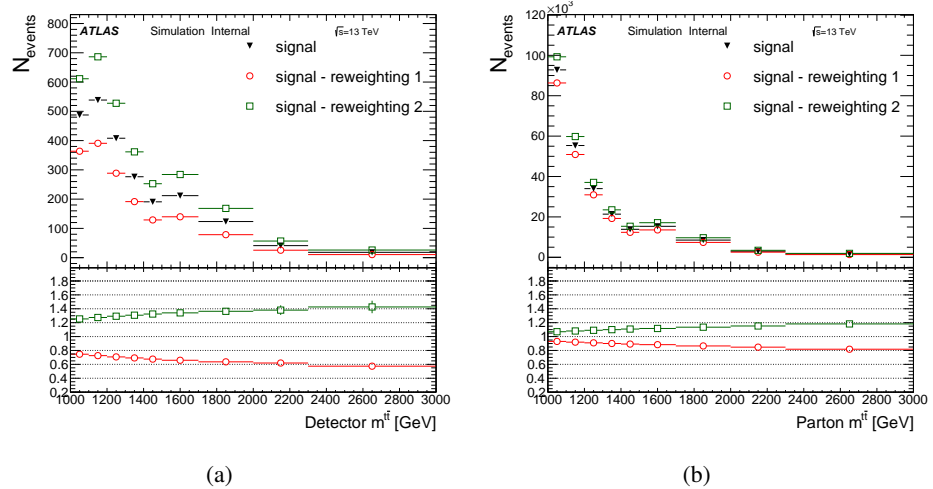


Figure 135: The comparison between reweighted and nominal distributions for $t\bar{t}$ mass. Figure (a) shows reco level comparison and figure (b) truth level comparison between distributions.

Not reviewed, for internal circulation only

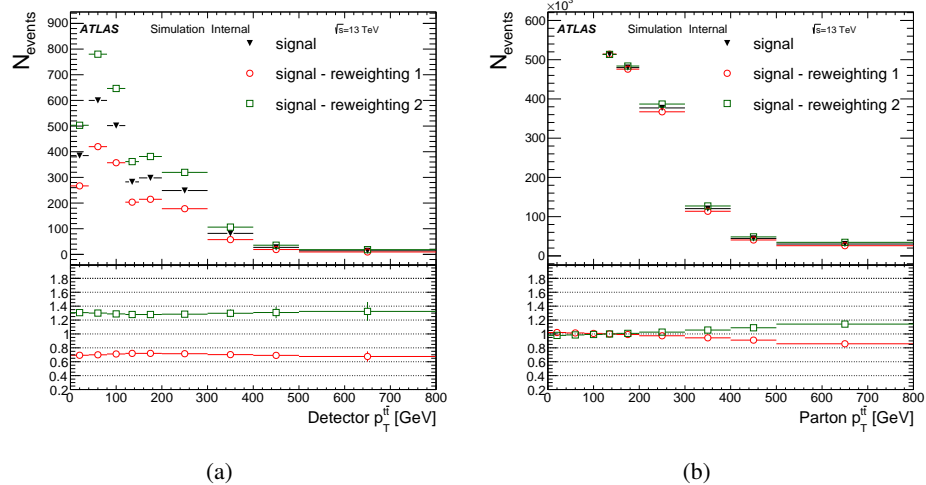


Figure 136: The comparison between reweighted and nominal distributions for $t\bar{t}$ p_T . Figure (a) shows reco level comparison and figure (b) truth level comparison between distributions.

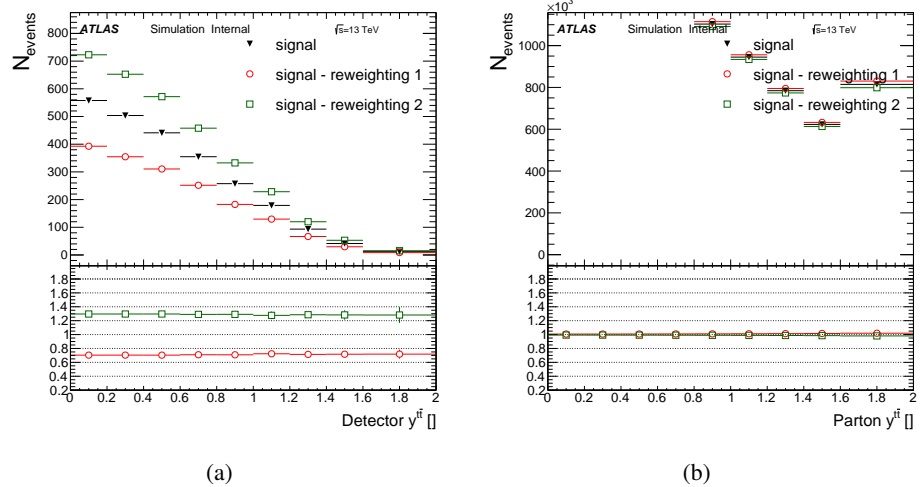


Figure 137: The comparison between reweighted and nominal distributions for absolute value of $t\bar{t}$ rapidity. Figure (a) shows reco level comparison and figure (b) truth level comparison between distributions.

1085 **K.2. Stress test results at full phase space**

1086 This subsection contains results of stress tests applied on the reweighted variables presented in the previous
 1087 section. For all variables, the unfolding procedure did not pass the stress test. The unfolded distributions
 1088 for reweighted variables are biased from the reweighted truth distributions. However, the results of
 1089 the stress test are different for different variables. The results are presented as a ratio plot between unfol-
 1090 ded and truth level reweighted distribution. In all the following plots, the results are shown for the iterative
 1091 Bayesian unfolding method performed with three different number of iterations (2,3,4 iterations).

1092 Figure 138 shows results of the stress test for the random top p_T . The difference between unfolded and
 1093 truth distributions is about 10%. The shape of distribution is also affected.

1094 Figure 139 shows results of the stress test for the leading top p_T . Result is similar to random top p_T
 1095 result.

1096 Figure 140 shows results of the stress test for the 2nd leading top p_T . For this variable, there is the best
 1097 agreement between unfolded and truth level distributions. The difference is only in bins with $p_T < 500$
 1098 GeV.

1099 Figure 141 shows results of the stress test for the $t\bar{t}$ mass. The result of the stress test is worse than
 1100 previous results. Difference in the ratio plots is about 20% and shape is also affected.

1101 Figure 142 shows results of the stress test for the $t\bar{t} p_T$. The result is even worse than for the $t\bar{t}$ mass.
 1102 Relative difference is about 30% and the shape is strongly affected.

1103 Figure 143 shows results of the stress test for the $t\bar{t}$ rapidity. The relative difference is about 30%. But it
 1104 seems that the shape is not affected.

1105 The different results of stress test are caused by different size of the phase space at parton level. No
 1106 parton level cuts are applied but the phase space is determined by the limits of histograms. The phase
 1107 space is completely full only for $t\bar{t} p_T$ and $t\bar{t}$ rapidity. For the $t\bar{t}$ mass and variables related with top quark,
 1108 the parton phase space is smaller and it is 'closer' to the phase space at detector level. In the case of
 1109 2nd leading top p_T , it seems that phase spaces for $p_T > 500$ GeV are close enough to perform unfolding
 1110 procedure.

1111 **K.3. Stress test of individual steps of unfolding**

1112 Since the stress test shown that unfolding procedure is unstable, it is important to investigate which step
 1113 of unfolding cause the problem. Basically, unfolding procedure can be divided into three steps. The first
 1114 step is bin-by-bin correction of truth level cuts after reco level cuts are applied (f_{acc}^j). This correction is
 1115 applied on reco level distribution before migration matrix can be used. The second step is transformation
 1116 using a migration matrix (\mathcal{M}_{ij}). And the third step is inverse correction of reco level cuts after truth level
 1117 cuts (ϵ_{eff}^i). In this subsection, the stress test is applied on each step of the unfolding separately.

Not reviewed, for internal circulation only

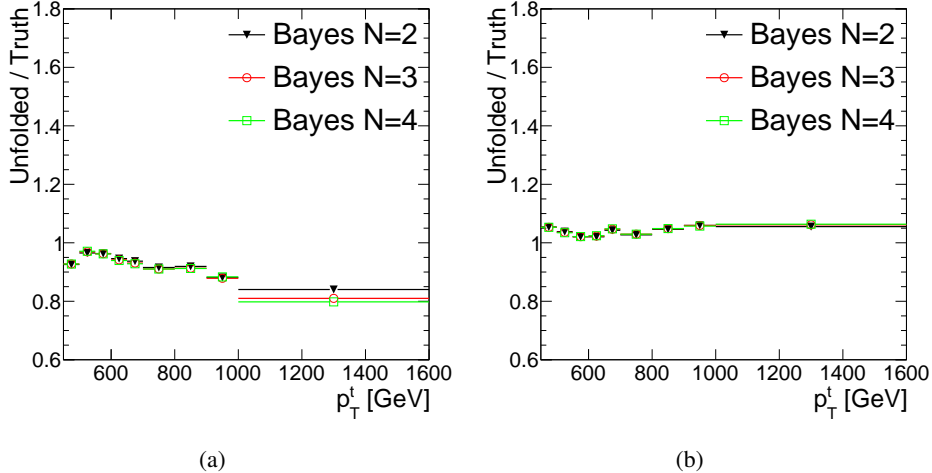


Figure 138: Stress test results for random top p_T distribution. Figure shows ratios between unfolded reweighted and truth reweighted distributions at full phase space parton level for (a) reweighted 1 and (b) reweighted 2 distributions.

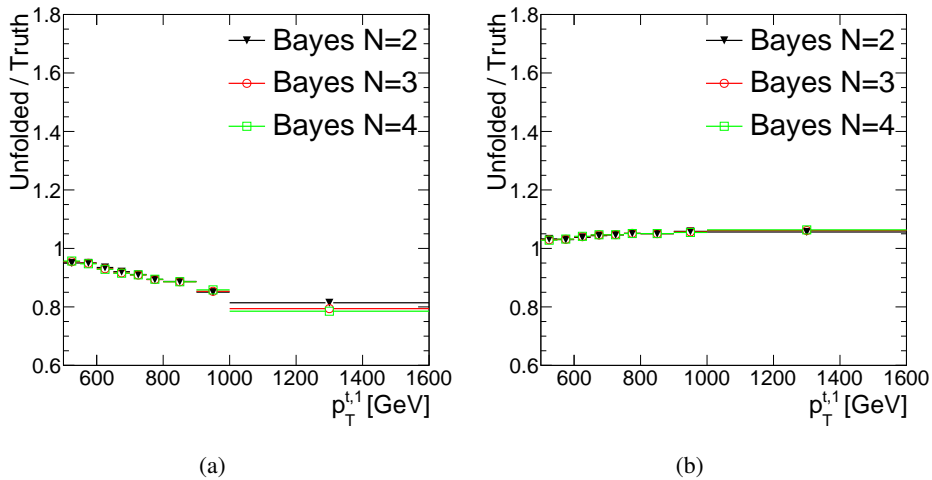


Figure 139: Stress test results for leading top p_T distribution. Figure shows ratios between unfolded reweighted and truth reweighted distributions at full phase space parton level for (a) reweighted 1 and (b) reweighted 2 distributions.

Not reviewed, for internal circulation only

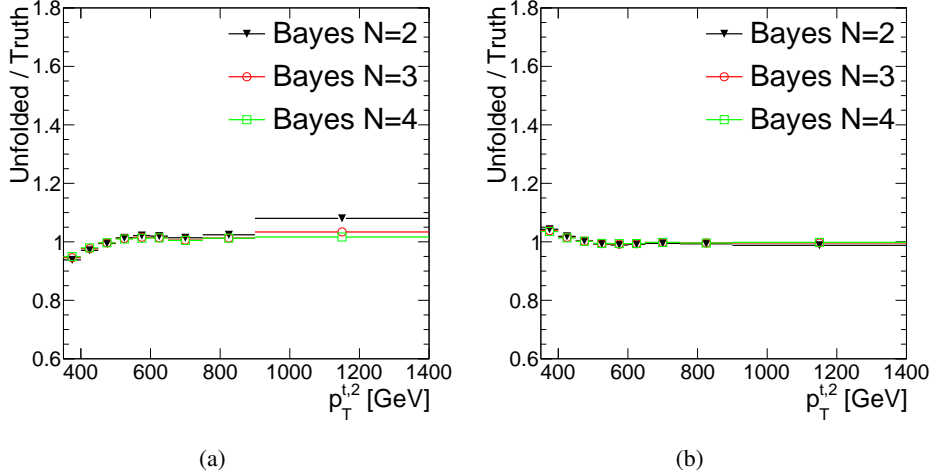


Figure 140: Stress test results for 2nd leading top p_T distribution. Figure shows ratios between unfolded reweighted and truth reweighted distributions at full phase space parton level for (a) reweighted 1 and (b) reweighted 2 distributions.

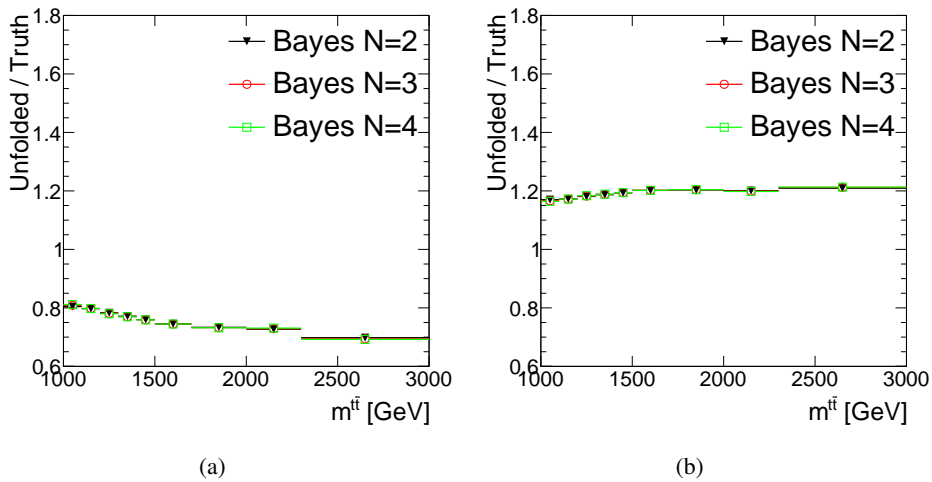


Figure 141: Stress test results for $t\bar{t}$ mass distribution. Figure shows ratios between unfolded reweighted and truth reweighted distributions at full phase space parton level for (a) reweighted 1 and (b) reweighted 2 distributions.

Not reviewed, for internal circulation only

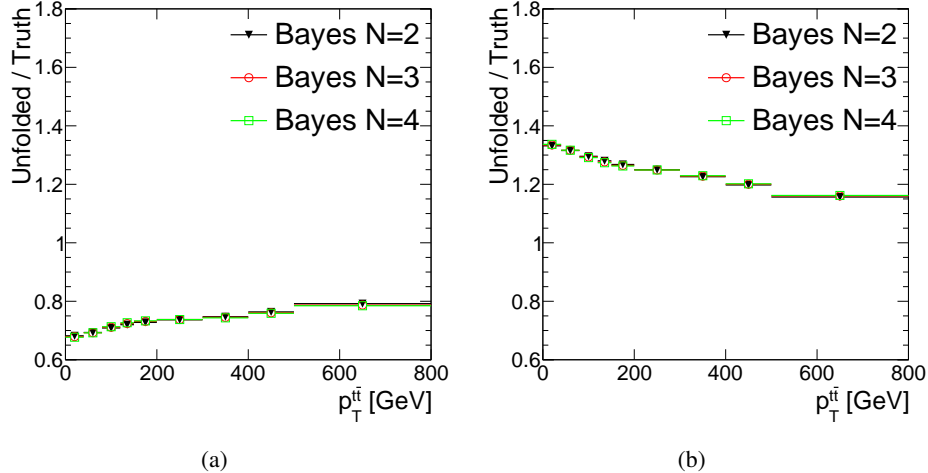


Figure 142: Stress test results for $t\bar{t}$ p_T distribution. Figure shows ratios between unfolded reweighted and truth reweighted distributions at full phase space parton level for (a) reweighted 1 and (b) reweighted 2 distributions.

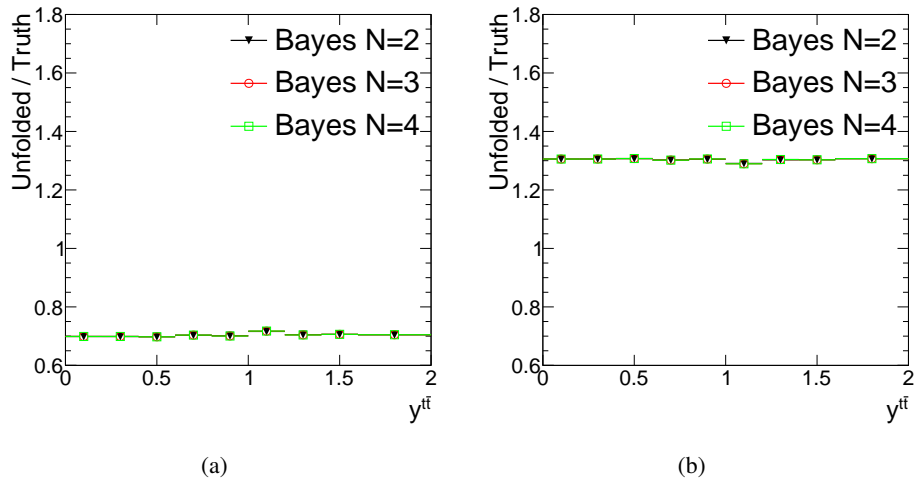


Figure 143: Stress test results for $t\bar{t}$ $|y|$ distribution. Figure shows ratios between unfolded reweighted and truth reweighted distributions at full phase space parton level for (a) reweighted 1 and (b) reweighted 2 distributions.

1118 Migration matrix

1119 The stability of the migration matrix is tested in the similar way as the stability of the full unfolding
 1120 procedure. In this test, reweighted distribution at detector level is corrected using the correction of truth
 1121 level cuts which is also reweighted. Then, the nominal migration is used to transform distribution from
 1122 detector to parton level. The last step is correction of reco level cuts which is again calculated from the
 1123 reweighted sample. So, only the migration matrix is from nominal sample.

1124 The unfolded distribution obtained from this procedure is compared with reweighted truth distribution.
1125 Only the migration matrix can make difference between these variables, so migration matrix is stable only
1126 if ratio between distributions is unity.

1127 The results of this test are shown in figures 144-149. Ratios between unfolded and truth distributions are
1128 close to unity for all variables. Hence, the migration matrices are stable.

Not reviewed, for internal circulation only

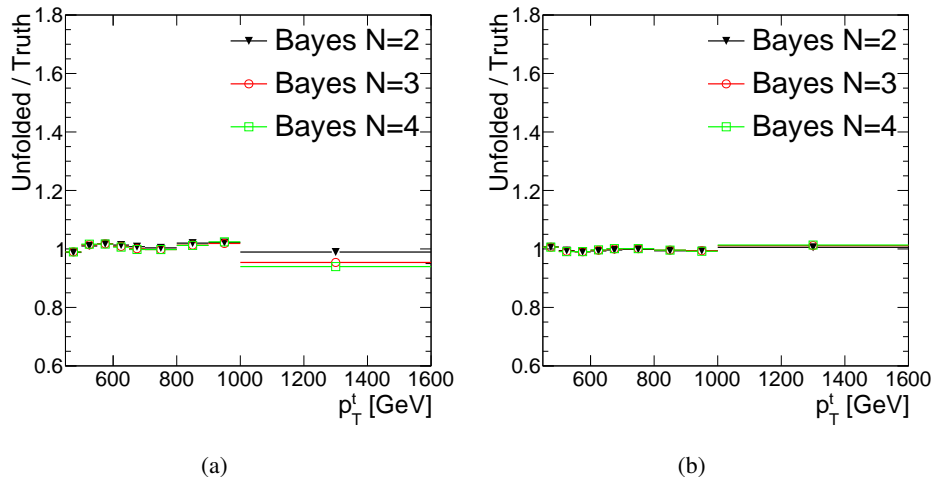


Figure 144: Test of stability of migration matrix for random top p_T distribution. Figure shows ratios between unfolded reweighted and truth reweighted distributions at full phase space parton level for (a) reweighted 1 and (b) reweighted 2 distributions.

1129 Correction of truth level cuts

1130 Instability in unfolding procedure can be caused by instability in corrections of truth or reco level cuts.
1131 This paragraph contains comparison of efficiencies of truth level cuts after reco level cuts.

1132 Plots 150-155 show that these corrections are also stable.

1133 Correction of reco level cuts

Since migration matrices and corrections of truth level cuts are stable, the source of instability has to be in corrections of reco level cuts. Indeed, plots 156-161 show instability of these corrections. Effect of this instability is similar as the effect observed in the full stress test (figures 138-143).

Not reviewed, for internal circulation only

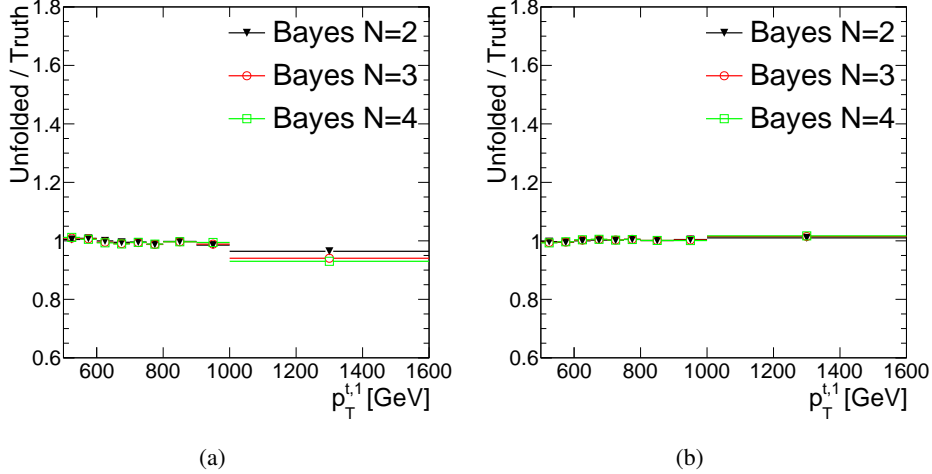


Figure 145: Test of stability of migration matrix for leading top p_T distribution. Figure shows ratios between unfolded reweighted and truth reweighted distributions at full phase space parton level for (a) reweighted 1 and (b) reweighted 2 distributions.

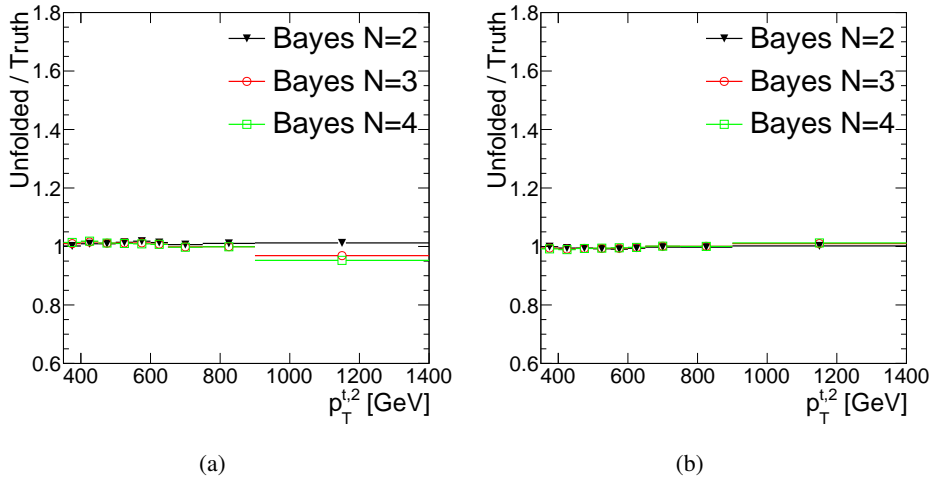


Figure 146: Test of stability of migration matrix for 2nd leading top p_T distribution. Figure shows ratios between unfolded reweighted and truth reweighted distributions at full phase space parton level for (a) reweighted 1 and (b) reweighted 2 distributions.

Not reviewed, for internal circulation only

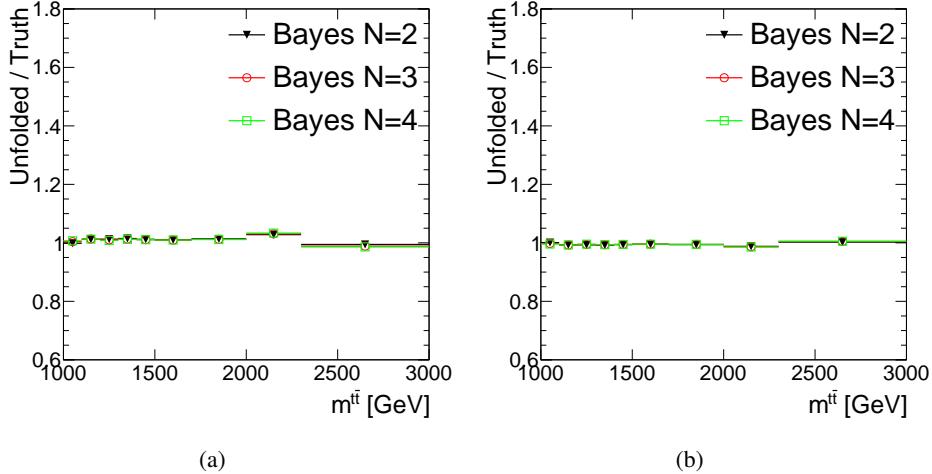


Figure 147: Test of stability of migration matrix for $t\bar{t}$ mass distribution. Figure shows ratios between unfolded reweighted and truth reweighted distributions at full phase space parton level for (a) reweighted 1 and (b) reweighted 2 distributions.

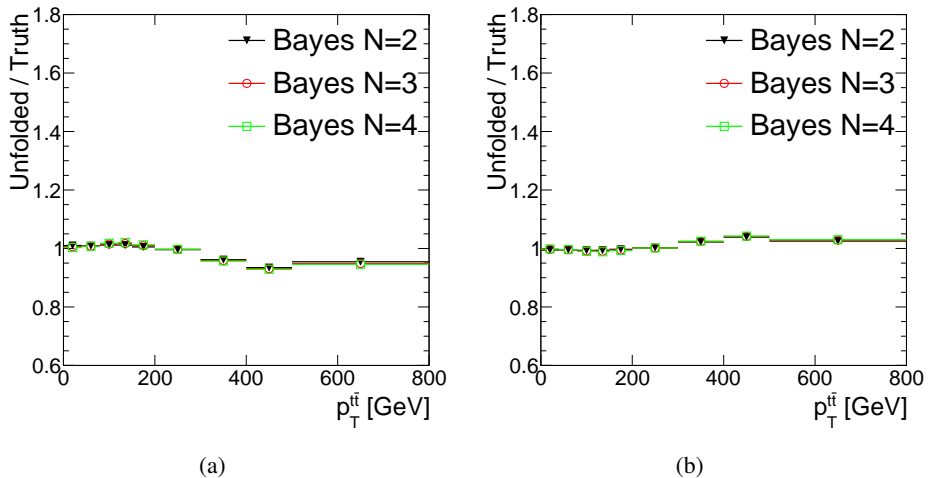


Figure 148: Test of stability of migration matrix for $t\bar{t}$ p_T distribution. Figure shows ratios between unfolded reweighted and truth reweighted distributions at full phase space parton level for (a) reweighted 1 and (b) reweighted 2 distributions.

Not reviewed, for internal circulation only

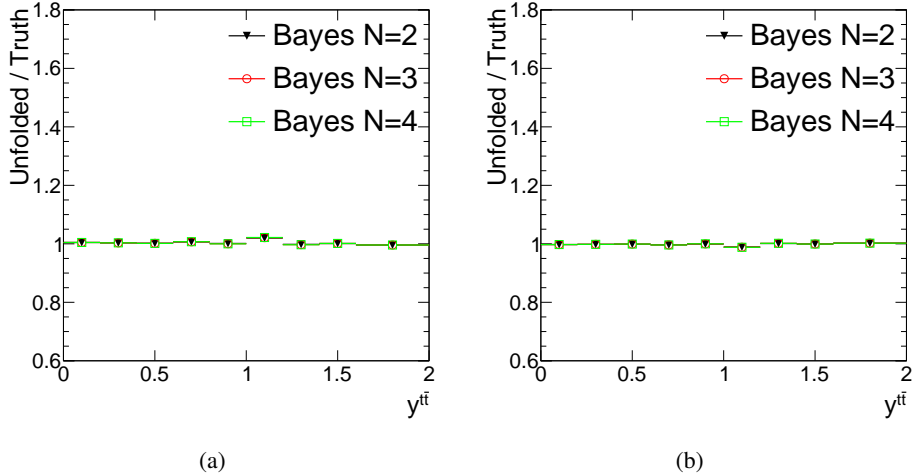


Figure 149: Test of stability of migration matrix for $t\bar{t} |y|$ distribution. Figure shows ratios between unfolded reweighted and truth reweighted distributions at full phase space parton level for (a) reweighted 1 and (b) reweighted 2 distributions.

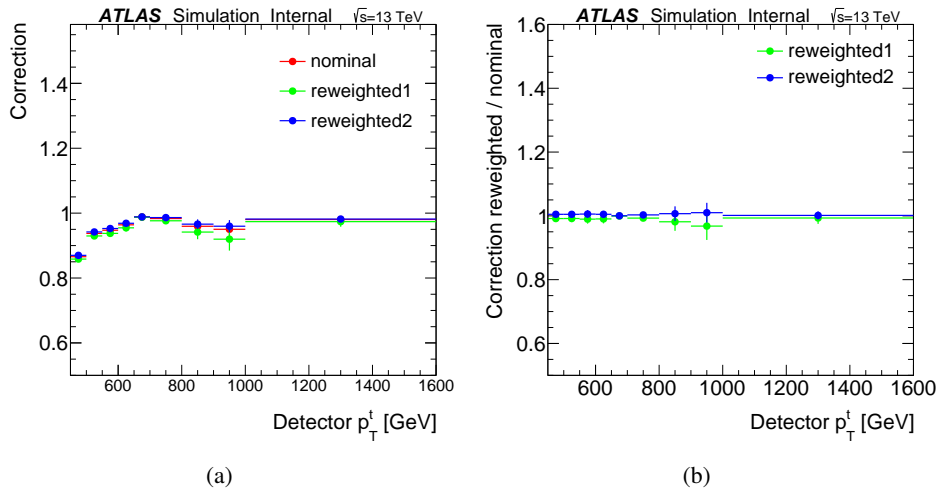


Figure 150: Test of stability of efficiency of truth level cuts for random top p_T distribution. Figure (a) shows nominal and reweighted efficiencies of truth level cuts and (b) ratio between reweighted and nominal efficiencies.

Not reviewed, for internal circulation only

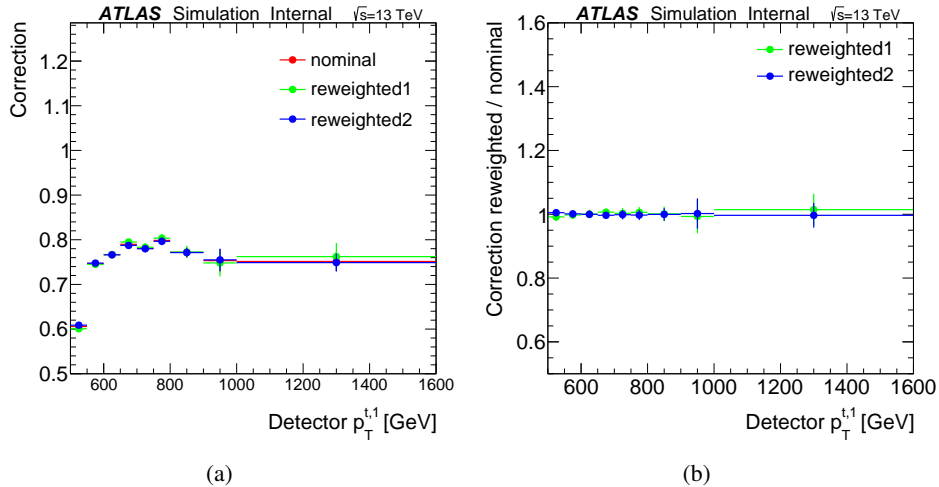


Figure 151: Test of stability of efficiency of truth level cuts for leading top p_T distribution. Figure (a) shows nominal and reweighted efficiencies of truth level cuts and (b) ratio between reweighted and nominal efficiencies.

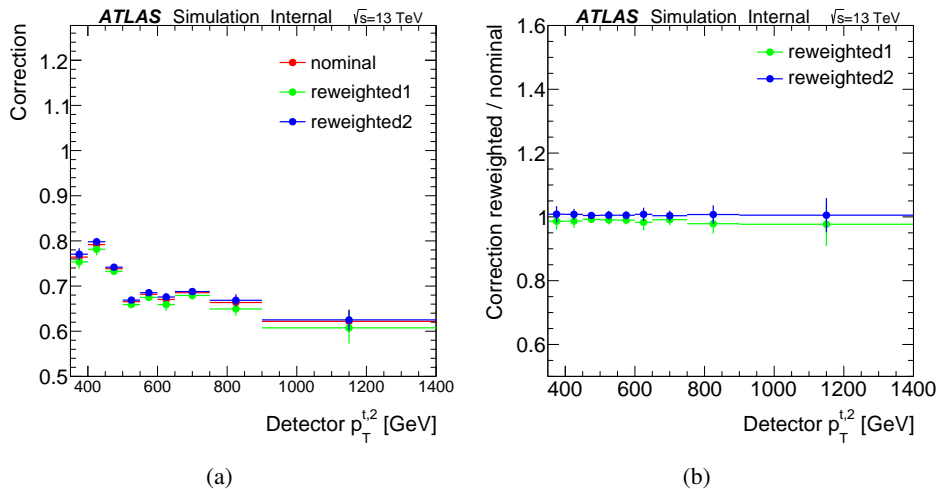


Figure 152: Test of stability of efficiency of truth level cuts for 2nd leading top p_T distribution. Figure (a) shows nominal and reweighted efficiencies of truth level cuts and (b) ratio between reweighted and nominal efficiencies.

Not reviewed, for internal circulation only

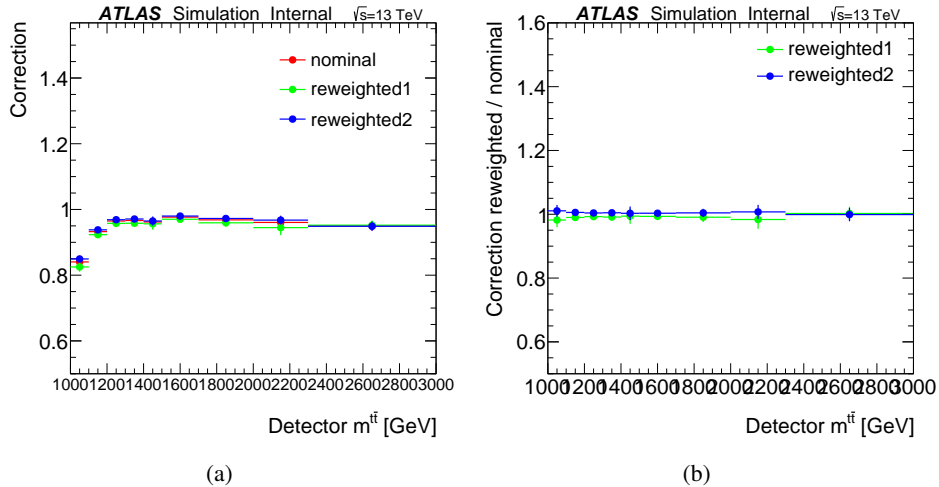


Figure 153: Test of stability of efficiency of truth level cuts for $t\bar{t}$ mass distribution. Figure (a) shows nominal and reweighted efficiencies of truth level cuts and (b) ratio between reweighted and nominal efficiencies.

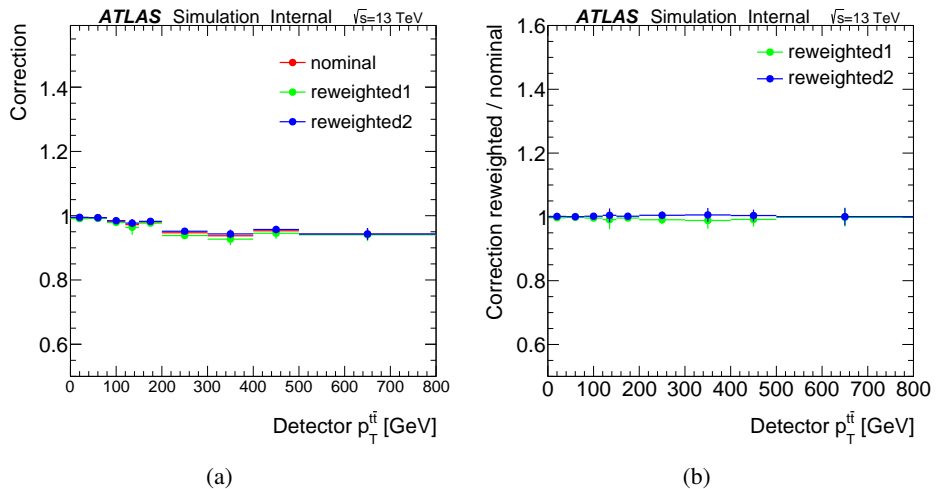


Figure 154: Test of stability of efficiency of truth level cuts for $t\bar{t}$ p_T distribution. Figure (a) shows nominal and reweighted efficiencies of truth level cuts and (b) ratio between reweighted and nominal efficiencies.

Not reviewed, for internal circulation only

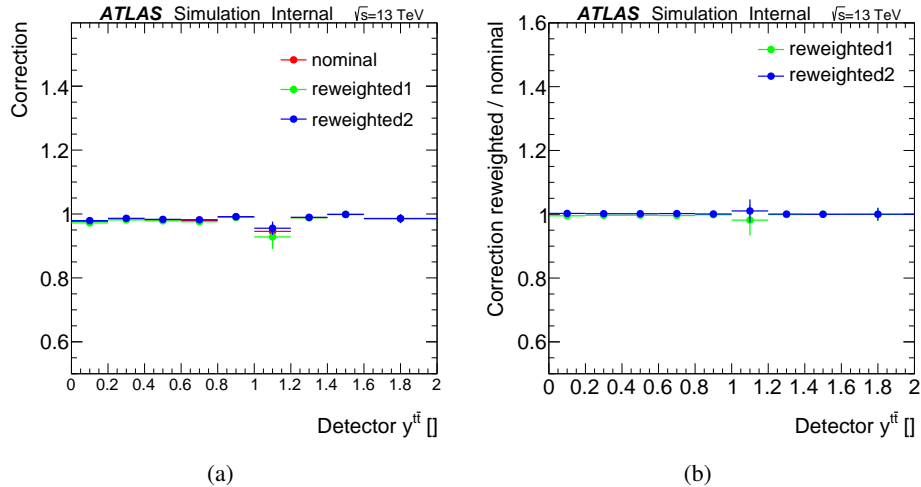


Figure 155: Test of stability of efficiency of truth level cuts for $t\bar{t} |y|$ distribution. Figure (a) shows nominal and reweighted efficiencies of truth level cuts and (b) ratio between reweighted and nominal efficiencies.

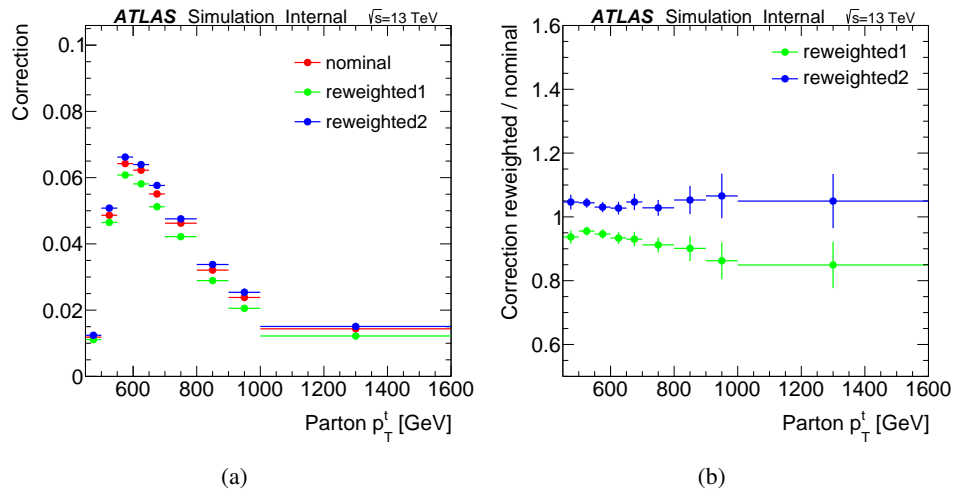


Figure 156: Test of stability of efficiency of reco level cuts for random top p_T distribution. Figure (a) shows nominal and reweighted efficiencies of reco level cuts and (b) ratio between reweighted and nominal efficiencies.

Not reviewed, for internal circulation only

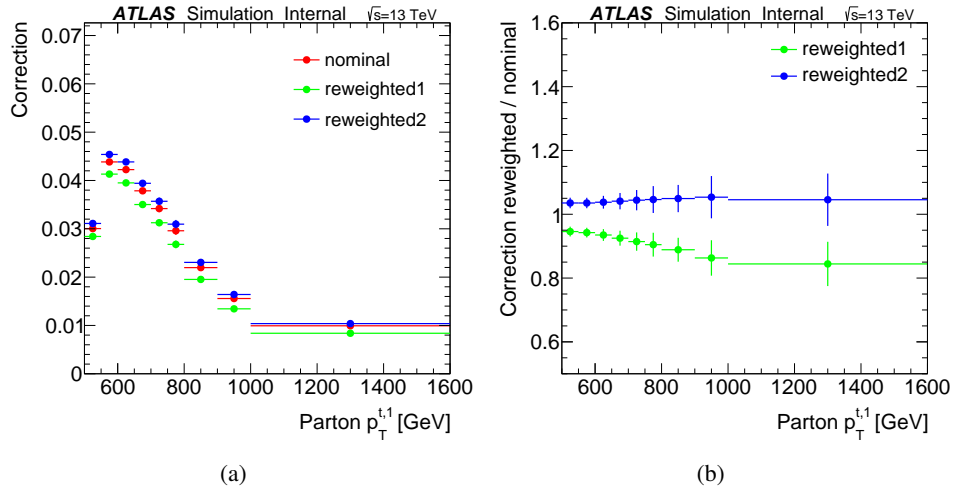


Figure 157: Test of stability of efficiency of reco level cuts for leading top p_T distribution. Figure (a) shows nominal and reweighted efficiencies of reco level cuts and (b) ratio between reweighted and nominal efficiencies.

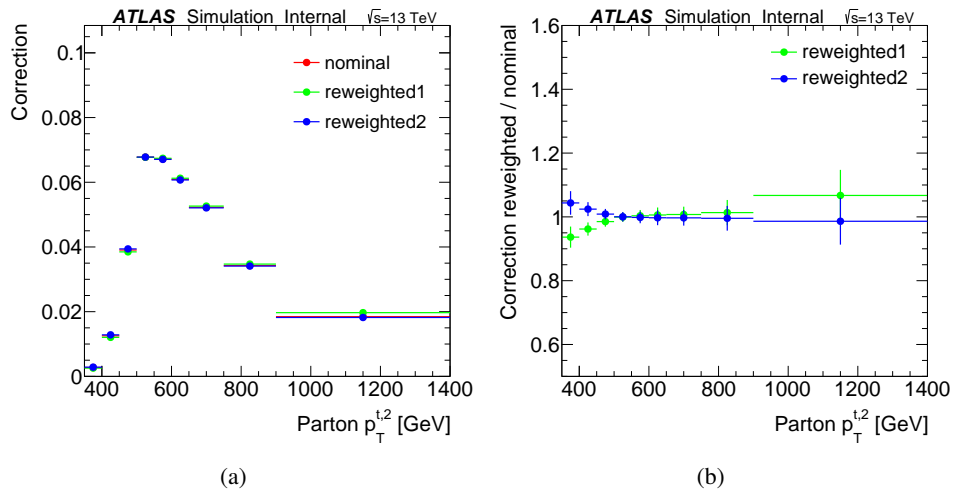


Figure 158: Test of stability of efficiency of reco level cuts for 2nd leading top p_T distribution. Figure (a) shows nominal and reweighted efficiencies of reco level cuts and (b) ratio between reweighted and nominal efficiencies.

Not reviewed, for internal circulation only

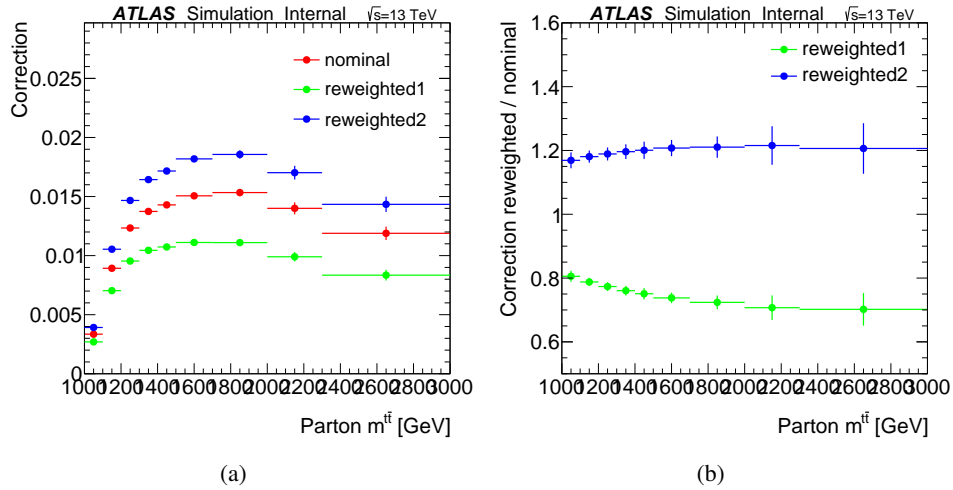


Figure 159: Test of stability of efficiency of reco level cuts for $t\bar{t}$ mass distribution. Figure (a) shows nominal and reweighted efficiencies of reco level cuts and (b) ratio between reweighted and nominal efficiencies.

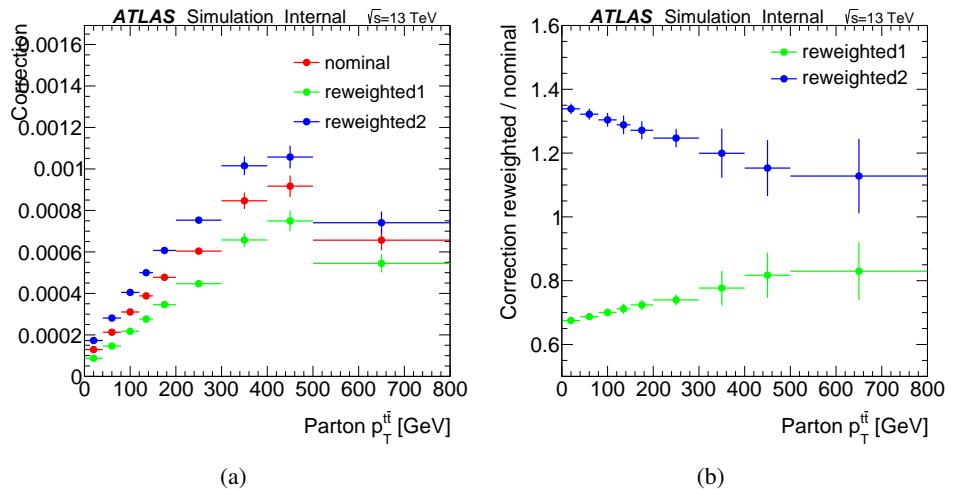


Figure 160: Test of stability of efficiency of reco level cuts for $t\bar{t}$ p_{T} distribution. Figure (a) shows nominal and reweighted efficiencies of reco level cuts and (b) ratio between reweighted and nominal efficiencies.

Not reviewed, for internal circulation only

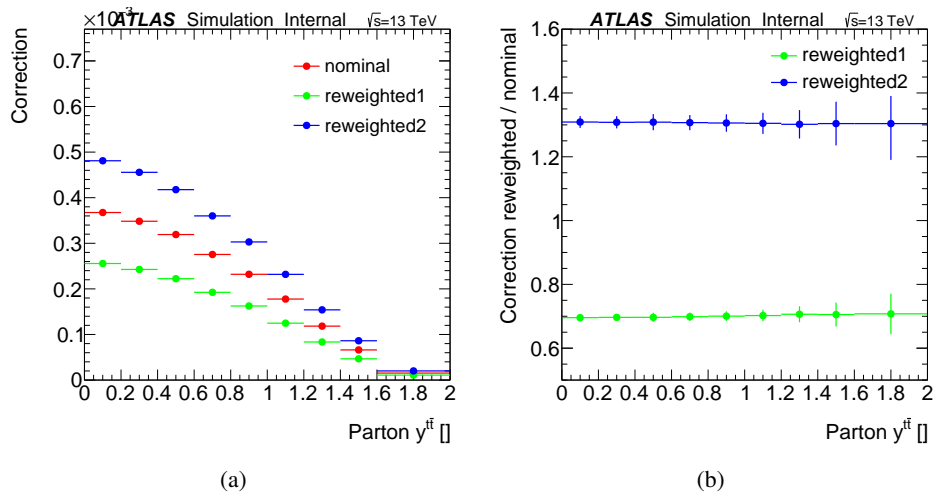


Figure 161: Test of stability of efficiency of reco level cuts for $t\bar{t}$ y distribution. Figure (a) shows nominal and reweighted efficiencies of reco level cuts and (b) ratio between reweighted and nominal efficiencies.

1137 L. The ABCD background estimation method

1138 L.1. General principles

1139 We outline the assumptions behind the ABCD background estimation technique and how it is applied in
 1140 this analysis. The ABCD technique has a long history, with the first account of using it in hadron-hadron
 1141 collisions in a W boson cross section measurement [55]. The general idea of the method is to divide the
 1142 data into four regions A, B, C and D, according to values of two parameters $i, j \in \{0, 1\}$, as it is shown in
 table 172.

	$j = 0$	$j = 1$
$i = 0$	A	B
$i = 1$	C	D

Table 172: Four regions classified according to properties i and j .

1143

1144 The goal of the ABCD method is to estimate a distribution of variable x arising from background sources
 1145 in region D from known data distributions in regions A, B and C. In this context, D is often considered
 1146 the “signal” region, while the other three regions are dominated by background sources. Hence, it is
 1147 independent of theoretical predictions and is considered “data-driven.”

1148 There are two possible approaches to estimate the distribution in region D.

1149 The first approach is based on two assumptions:

- 1150 1. The parameters i, j are statistically independent variables.
- 1151 2. The variable x has to be identically distributed in regions B and D, i.e. parameter i has no effect on
 1152 the shape of distribution x .

The first assumption is used for estimation of the total number of events in region D. Under this assumption, the total number of events in region D can be estimated by the formula

$$D = \frac{B}{A}C, \quad (13)$$

1153 where A, B, C and D denote the numbers of events in regions A, B, C and D, respectively.

1154 The second assumption is used for an estimation of a differential distribution of the variable x in region
 1155 D.

If the differential distribution in region B is estimated by a histogram and $B[k]$ denotes the number of events stored in the k^{th} bin of the histogram then the number of events in the k^{th} bin of the histogram in the region D can be estimated by the formula

$$D[k] = \frac{C}{A}B[k]. \quad (14)$$

The second approach is based on the idea of applying the formula (13) bin-by-bin. Using this approach the ABCD estimate for the k^{th} bin in the signal region is obtained using formula

$$D[k] = \frac{C[k]}{A[k]} B[k]. \quad (15)$$

1156 The “bin-by-bin” method has the following assumptions:

- 1157 1. The parameters i, j are independent statistical variables in all regions defined by bins of the histo-
- 1158 gram.
- 1159 2. The distribution of variable x has the same shape in all the regions.

1160 In the following, we will focus on the second “bin-by-bin” approach.

1161 Note that the following section describes the 9-region approach to the multijet background calculation.

1162 It was used for a preliminary measurement, but has been superseded by the 16-region approach described

1163 in the next Appendix.

1164 L.2. ABCD method using 9 regions

1165 In this analysis, the ABCD technique is extended by decomposing the event sample into 9 regions (see

1166 section L.1 for general description of the ABCD method). Events which pass the preselection criteria are

1167 classified into 9 regions according to the results of top-tagging and b-matching applied on the leading and

1168 recoil large jet. Two parameters are used: N_t and N_b . Parameter $N_t \in \{0, 1, 2\}$ denotes the number of

1169 top-tags and parameter $N_b \in \{0, 1, 2\}$ denotes the number of b-matches. Regions are labeled by letters A,

1170 B, C, D, E, F, G, H and S, as summarized in Table 173.

	0t	1t	2t
0b	A	D	G
1b	B	E	H
2b	C	F	S

Table 173: The ABCD method employing 9 regions for the multijet background determination.

1171 The method is used for estimation of the multijet background estimate in signal region S. In the other

1172 regions, the multijet event yield is estimated by subtraction of the MC $t\bar{t}$ signal process, the $t\bar{t}$ non-

1173 allhadronic process and the Wt single-top process:

$$N_{\text{multijet}} = N_{\text{data}} - N_{\text{MC signal}} - N_{\text{MC } t\bar{t} \text{ nonallhad}} - N_{\text{MC } Wt \text{ single-top}}. \quad (16)$$

1174 There are several possible calculations to determine the multijet background in region S:

$$\begin{aligned} S_1 &= \frac{G}{D} F \\ S_2 &= \frac{H}{E} F \\ S_3 &= \frac{G}{A} C \\ S_4 &= \frac{H}{B} C \end{aligned} \quad (17)$$

1175 Since region F is expected to have high purity, the multijet estimate in region F using formula (16) depends
 1176 on the MC $t\bar{t}$ signal prediction. Therefore, estimates S_1, S_2 from equation (17) are also dependent on this
 1177 MC prediction. Therefore, these estimates are not used for the multijet background estimate.

The multijet background estimate in the region S is estimated as an average of estimates S_3, S_4 , i.e.

$$S^{\text{ABCD}} = \left(\frac{G}{A} + \frac{H}{B} \right) \frac{C}{2} \quad (18)$$

1178 Regions used in this formula are labeled by yellow color in the table 173.

1179 We close this section by summarizing the assumptions that are used to obtain the multijet background
 1180 estimate in Eq. 18: Let x be the variable of interest, i.e. the goal is to estimate the multijet background
 1181 distribution of variable x in the signal region S. The assumptions are:

- 1182 1. The number of top-tags (N_t) and number of b-matches (N_b) are independent statistical variables for
 1183 all bins of the histogram for the background process.
- 1184 2. The range of variable x in the regions ABCDEGH is the same as in the signal region S.

1185 L.3. Correlation factor between N_t and N_b

1186 The correlation factor between number of top-tags, N_t , and number of b-matches, N_b , is calculated for
 1187 each of the 9 regions. Its elements are filled by multijet estimates from Eq. 16. The estimated value of
 1188 the correlation factor between N_t and N_b is 0.0081. Figure 162 shows correlation plots between N_t and
 1189 N_b . The correlation between N_t and N_b appears to be negligible.

1190 The table 174 shows two ABCD multi-jet estimates and their average which is used for multijet back-
 1191 ground prediction in the signal region. Difference between two estimates is about 7%.

Regions and sidebands	Predicted events
$S = D \times C / A$	697.5 ± 14.74
$S = E \times C / B$	777.9 ± 18.54
Average	737.7 ± 15.9

Table 174: ABCD multijet background estimates in the signal region. The table contains predicted number of events in the signal region calculated using several methods. The uncertainties are statistical.

1192 The table 175 contains results of cross-checks of ABCD method. ABCD multijet estimates in the side-
 1193 band regions are compared with observed multijet background. These cross-checks are used for testing of

Not reviewed, for internal circulation only

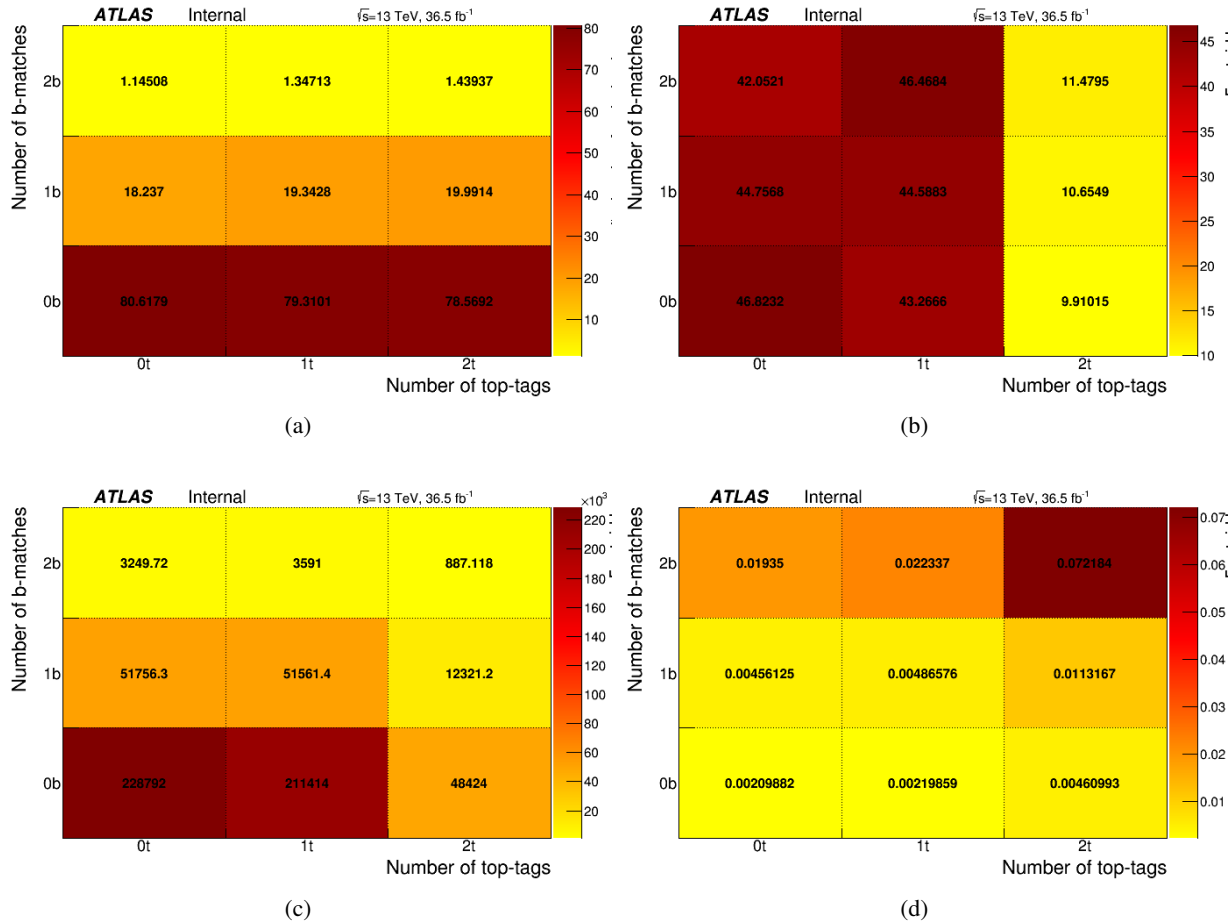


Figure 162: Number of b-matches (y-axis) versus number of top-tags (x-axis): (a) histogram with normalized columns, (b) histogram with normalized rows, (c) not normalized histogram and (d) relative MC \oplus data statistical errors in the bins of the histogram. Event yields are calculated using formula 16.

1194 effect of possible correlation between N_t and N_b . The table shows that this correlation has small but not
 1195 completely negligible effect. Differences between observed and predicted events yields are not always
 1196 within statistical errors but they are always under 10%.

1197 Figures 163, 164, 165 and 166 contains similar comparisons between predicted and observed large R
 1198 jet kinematic distributions in the sidebands regions. The figures show comparisons in regions E, F and
 1199 H. Effect of the correlation is very small but not negligible. For example, predicted distributions in
 1200 figures 163(a) and 163(b) are shifted down slightly from the observed distribution.

1201 L.4. Data \oplus MC statistical uncertainties

1202 This section describes the algorithm for calculating the data statistical uncertainties \oplus the MC statistical
 1203 uncertainties for the ABCD multijet estimate from Eq. 18. The ABCD estimate is calculated from
 1204 histograms from sideband regions. These histograms have the same binning. Let us denote $N_{ij}^{(k)}$ number

Region	Predicted events	Observed events	Predicted / Observed
E = B*D/A	47952 ± 263.59	51561 ± 250.89	0.93 ± 0.0068273
F = C*D/A	3021.1 ± 59.358	3591 ± 80.212	0.84131 ± 0.025028
F = C*E/B	3249.8 ± 66.764	3591 ± 80.212	0.90497 ± 0.027464
H = B*G/A	11025 ± 75.835	12321 ± 139.43	0.89478 ± 0.01185
H = E*G/D	11855 ± 84.05	12321 ± 139.43	0.96216 ± 0.012849

Table 175: Comparison between observed multijet background and ABCD estimates in sideband regions. Observed multijet background is calculated using formula 16. The uncertainties are statistical.

of events in the k^{th} bin of the histogram in the region with i b-matches and j top-tags. Similarly, let us denote $\sigma_{ij}^{(k)}$ data statistical uncertainty \oplus the MC statistical uncertainty in the k^{th} bin of the histogram.

The uncertainties of the ABCD estimate are determined from an ensemble of 10 000 pseudo-experiments. In each pseudo-experiment, for each bin and for all regions, pseudo-random numbers $N_{ij,\text{random}}^{(k)}$ are drawn using normal distribution with mean $N_{ij}^{(k)}$ and sigma $\sigma_{ij}^{(k)}$. The ABCD estimate is determined for each pseudo-experiment individually and uncertainties of the ABCD estimate are the RMS of the results of ABCD method.

The ABCD estimates, data \oplus MC uncertainties, relative uncertainties and mean values of pseudo-experiments for the leading top-jet p_{T} histogram are shown in Table 176. Relative uncertainties are increasing with bin number from 6% to 20%. Mean values of pseudo-experiments are statistically equivalent to the ABCD estimates.

Bin number	1	2	3	4	5	6	7	8	9
Bin range [GeV]	500-550	550-600	600-650	650-700	700-750	750-800	800-900	900-1000	1000-1600
Estimates	341.7	152.2	89.37	51.38	28.04	16.32	16.33	7.318	4.817
Uncertainties	12.72	6.996	4.664	3.416	2.799	2.431	1.709	1.074	0.913
Relative uncertainties	0.03721	0.04596	0.05218	0.06648	0.09982	0.149	0.1046	0.1467	0.1895
Means	341.7	152.3	89.31	51.48	28.04	16.43	16.32	7.273	4.826

Table 176: The ABCD background estimates, data \oplus MC uncertainties, relative uncertainties and mean values of pseudo-experiments for the leading top-jet p_{T} histogram.

Not reviewed, for internal circulation only

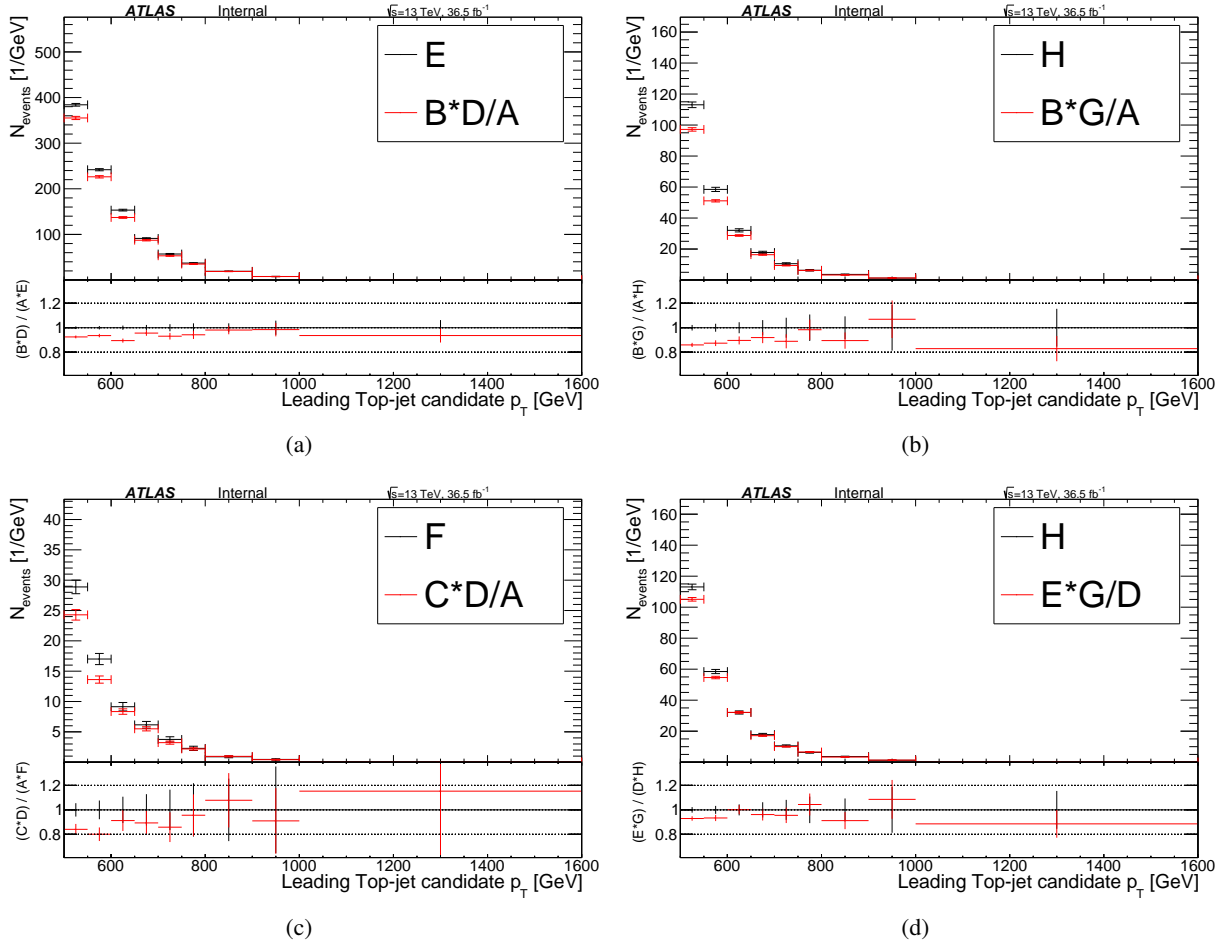


Figure 163: Comparison between observed multijet background distributions and ABCD estimates in sideband regions. The figure contains leading top-jet p_T distributions in sideband regions. Observed distributions are calculated using formula 16. The uncertainties are statistical.

Not reviewed, for internal circulation only

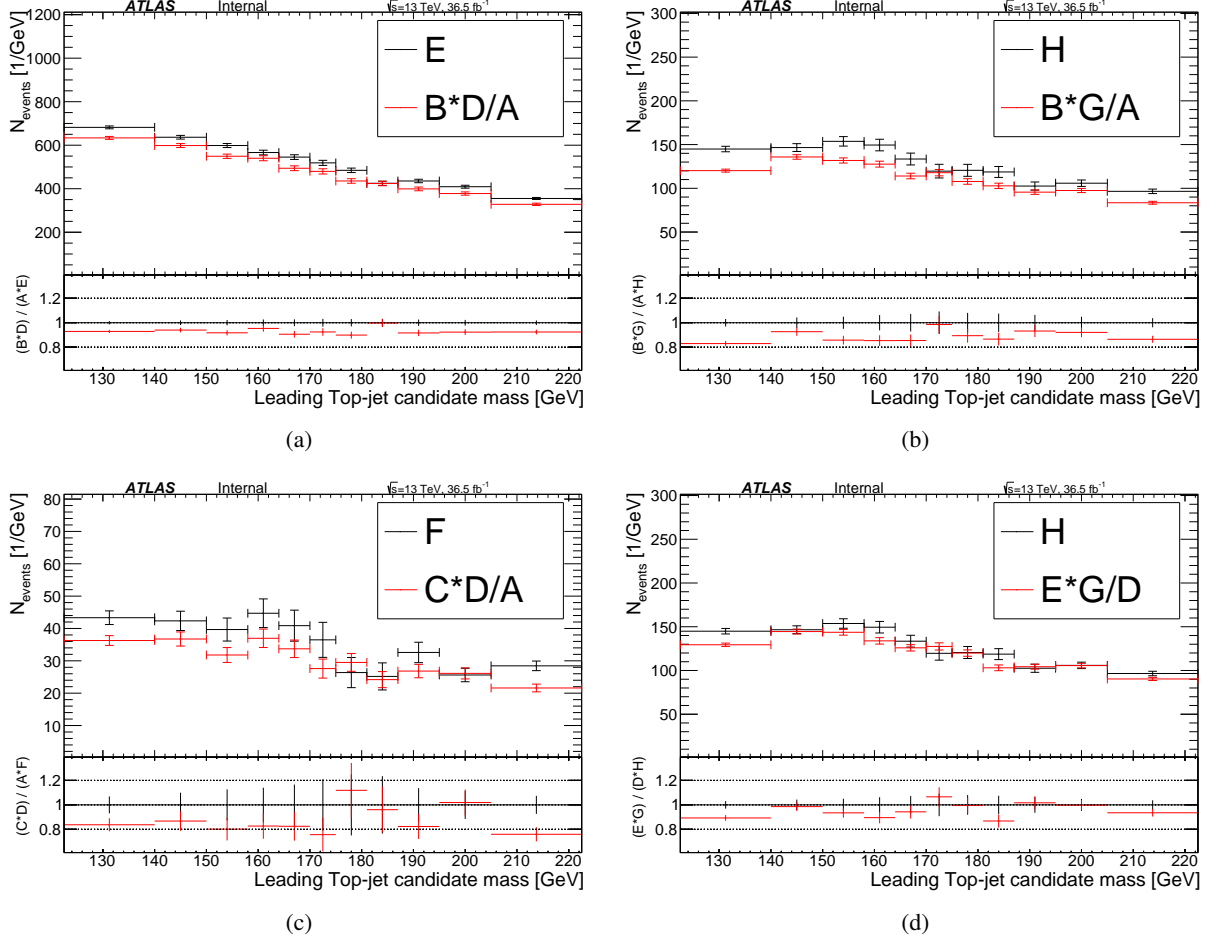


Figure 164: Comparison between observed multijet background and ABCD estimates in sideband regions. The figure contains leading top-jet mass distributions in sideband regions. Observed distributions are calculated using formula 16. The uncertainties are statistical.

Not reviewed, for internal circulation only

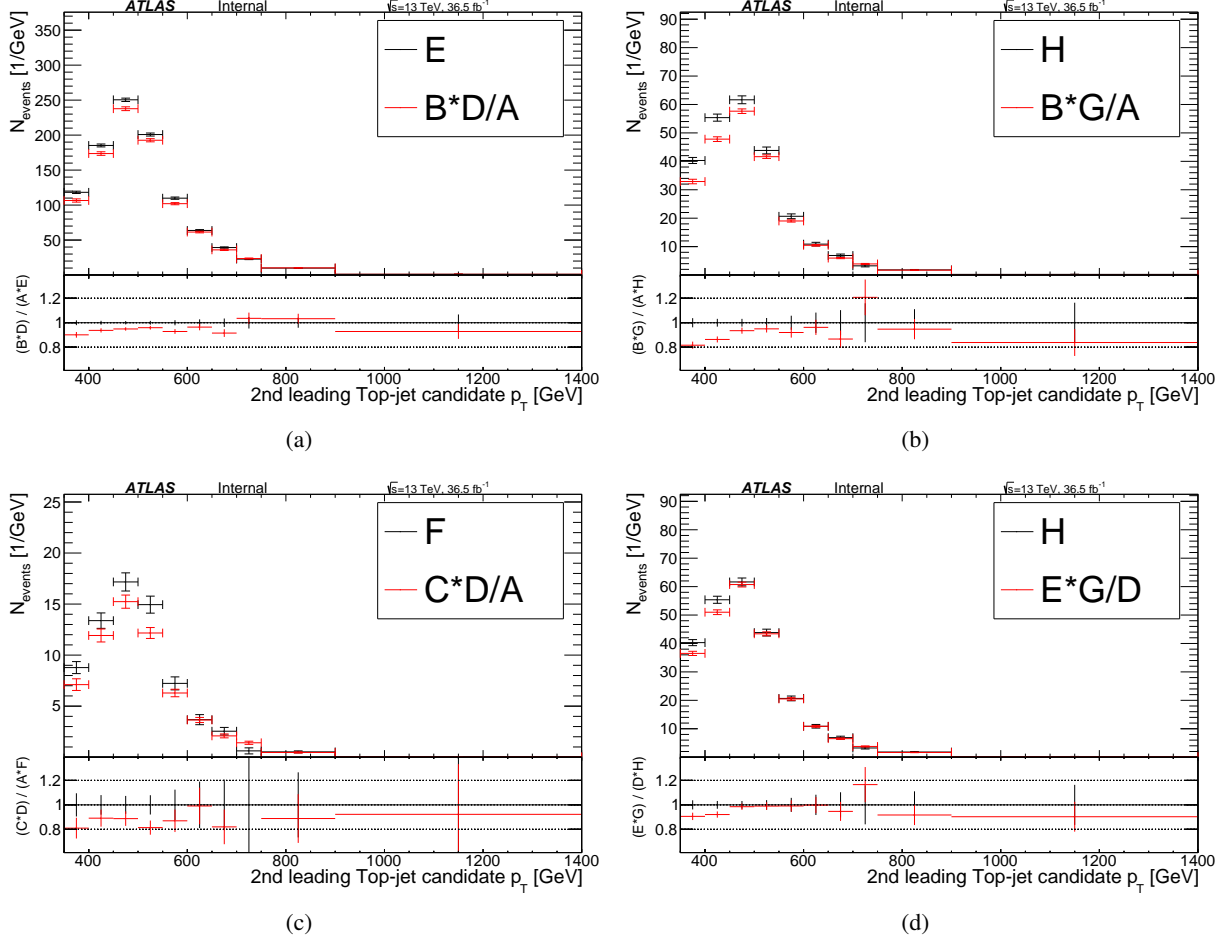


Figure 165: Comparison between observed multijet background and ABCD estimates in sideband regions. The figure contains 2nd leading top-jet p_T distributions in sideband regions. Observed distributions are calculated using formula 16. The uncertainties are statistical.

Not reviewed, for internal circulation only

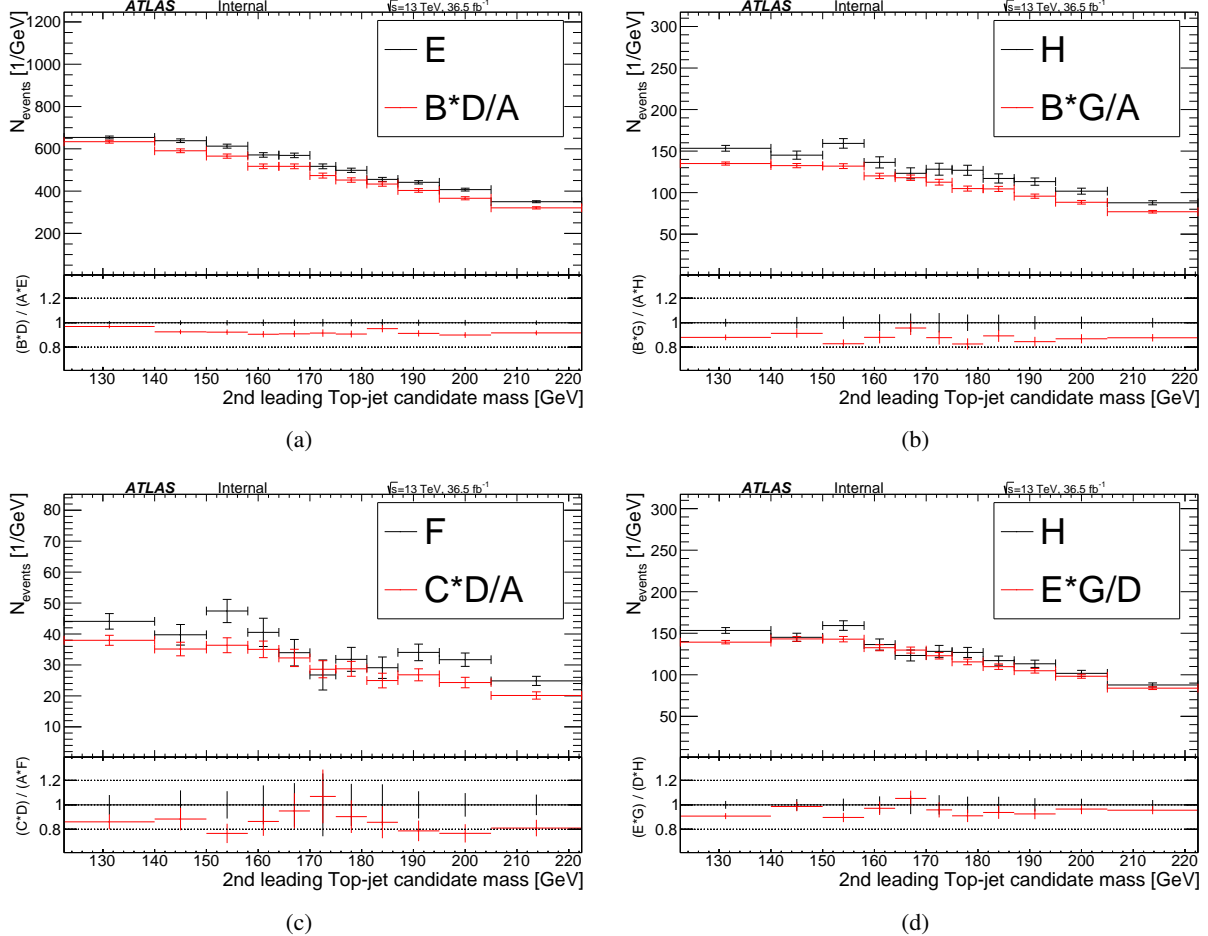


Figure 166: Comparison between observed multijet background and ABCD estimates in sideband regions. The figure contains 2nd leading top-jet mass distributions in sideband regions. Observed distributions are calculated using formula 16. The uncertainties are statistical.

1216 M. Comparison of the old ABCD9 and Monte Carlo QCD multijet 1217 background estimates

1218 In this appendix, we compare the ABCD multijet background estimates with the multijet prediction us-
 1219 ing NLO matrix element calculations coupled with parton shower and hadronization models, the latter
 1220 computed using the PYTHIA 8 generator.

1221 Comparisons of the calculations are shown in Figure 167. There is reasonable agreement between the two
 1222 estimates of multijet background, although the statistical uncertainties on the MC estimates are large.

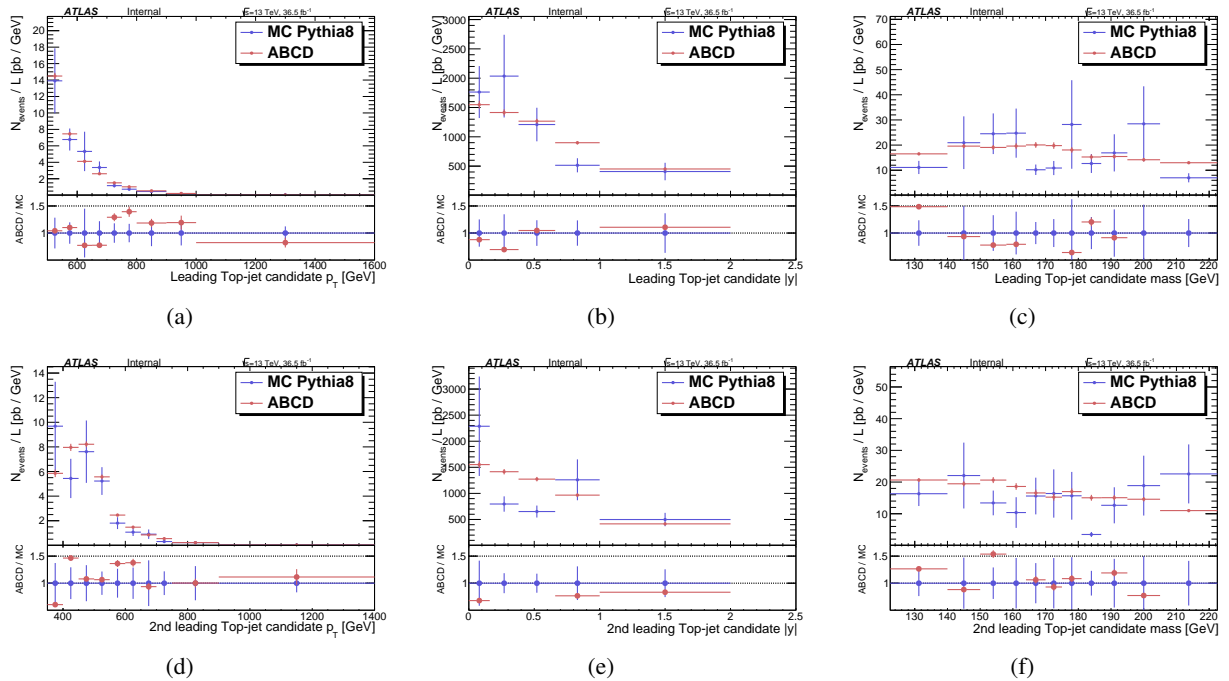


Figure 167: Comparison between the ABCD and PYTHIA 8 multijet background estimates in the signal region (S): (a) p_T , (b) absolute value of the rapidity and (c) mass of the leading top, and (d) transverse momentum, (e) absolute value of the rapidity and (f) of the second leading top. The uncertainties in the ABCD estimates include both data \oplus MC statistical uncertainties. In the case of the PYTHIA 8 calculation, the uncertainties reflect MC statistical uncertainties only.

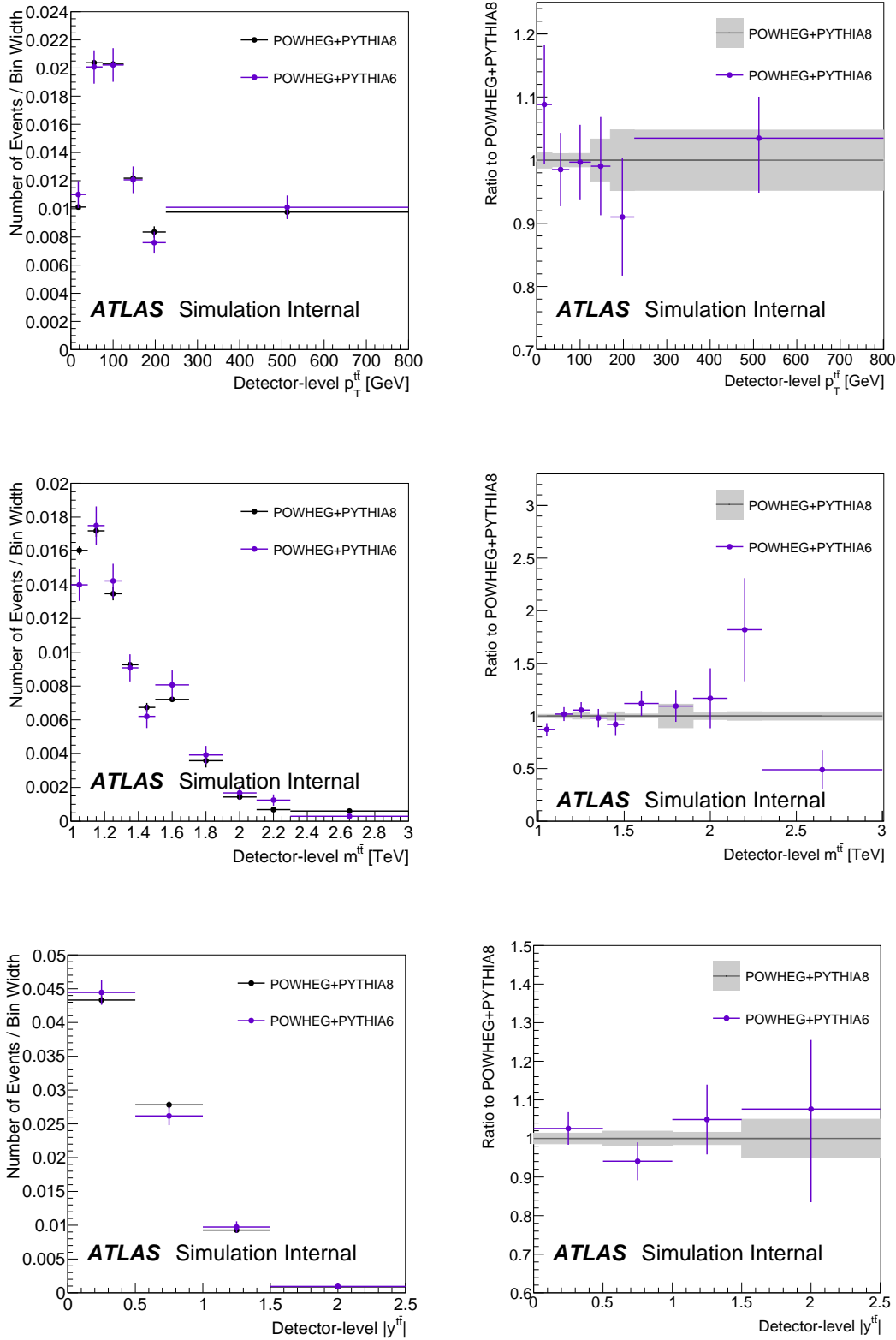
Not reviewed, for internal circulation only

N. Comparison of Monte Carlo Generators

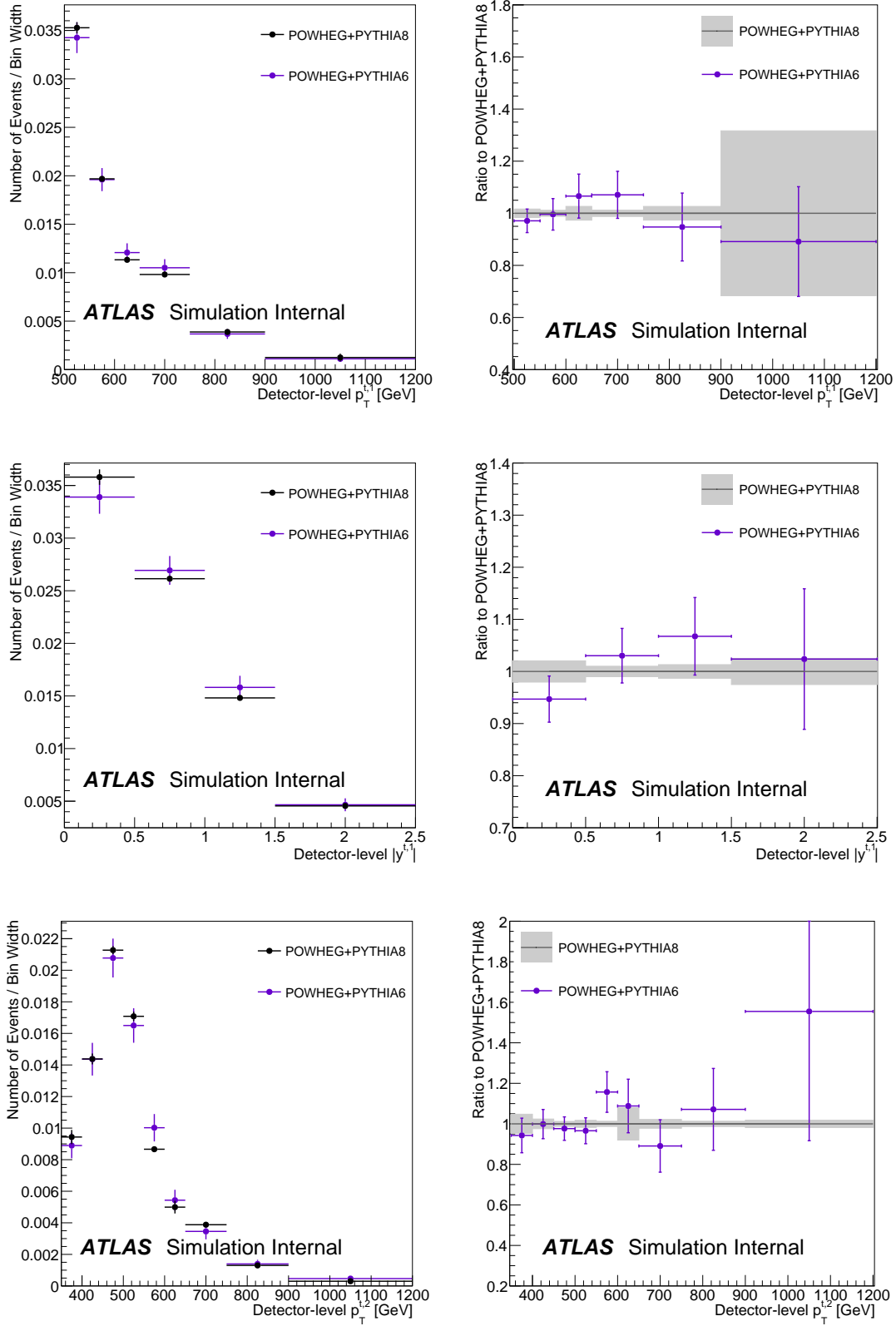
1223 While the Monte Carlo generator used for the nominal sample in this analysis is PowHEG+PYTHIA6, a $t\bar{t}$
1224 all-hadronic boosted sample made with Born-level suppression factor was also considered. The sample
1225 is generated with PowHEG+PYTHIA8 , and so its agreement with the PYTHIA6 sample must be validated. In
1226 order to perform this validation, the distributions of final state observables made by the two generators,
1227 normalized to the same area, are shown in Figures N–168. Because PYTHIA6 is tuned to the 8 TeV data,
1228 and PYTHIA8 is not yet tuned completely, we expect some differences between the distributions. Indeed,
1229 minor differences are observed, however most of the points agree within error.

1230 As a second comparison, the ratio of both normalized PowHEG+PYTHIA6 and PowHEG+PYTHIA8 distributions
1231 to the PowHEG+PYTHIA8 distributions are plotted. To compare the uncertainties between the two
1232 samples, we divided the error in each bin for both samples by the central value of the PowHEG+PYTHIA8 dis-
1233 tribution for that bin. The plots show a substantial decrease in statistical uncertainty for the PowHEG+PYTHIA8 sample
1234 with the exception of a few bins, which is consistent with the larger sample size. The ratio plots agree
1235 with the comparison of the distributions, showing ratios close to one. Deviations can be justified again
1236 considering the differences in the tuning of the two samples.

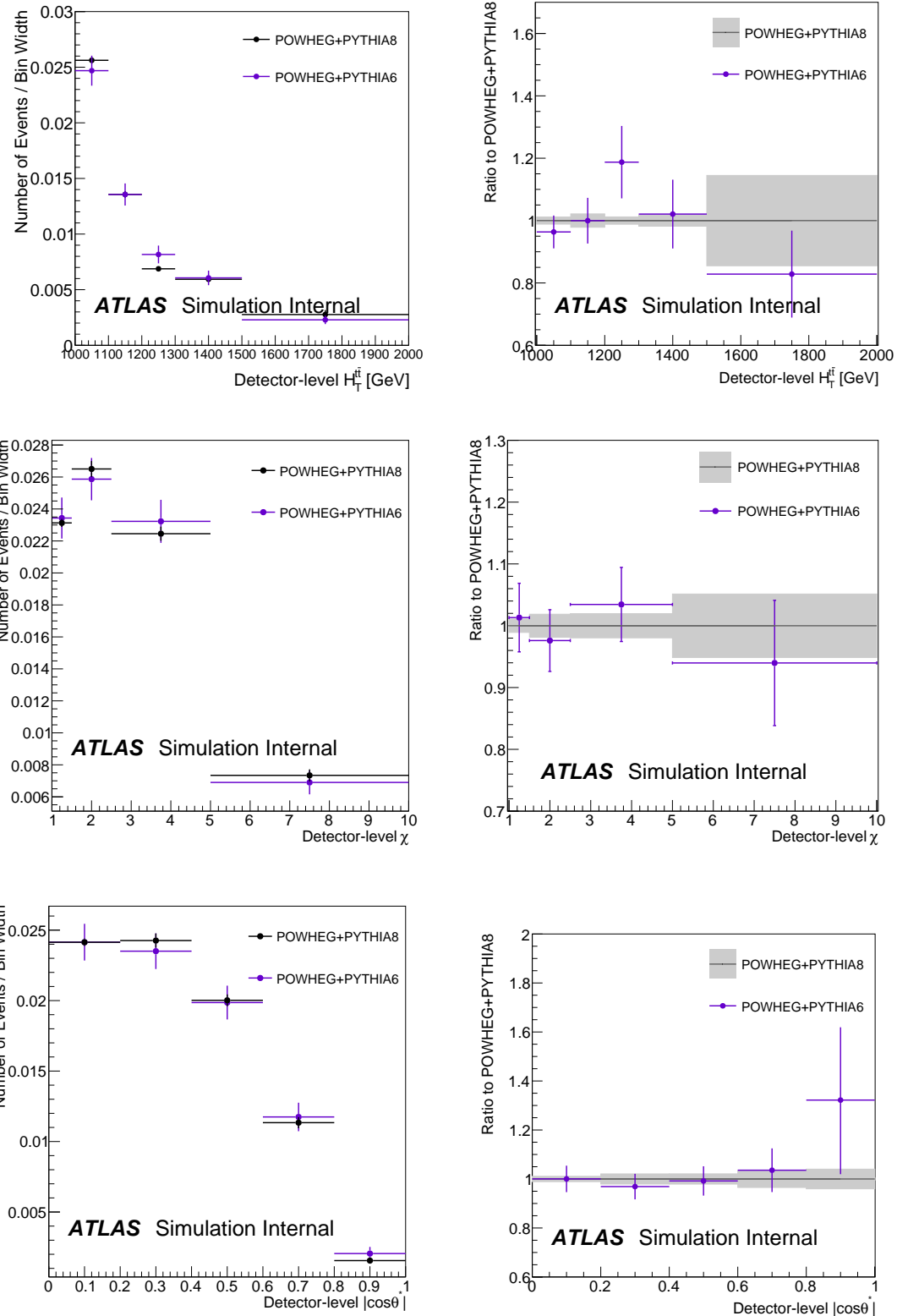
Not reviewed, for internal circulation only



Not reviewed, for internal circulation only



Not reviewed, for internal circulation only



Not reviewed, for internal circulation only

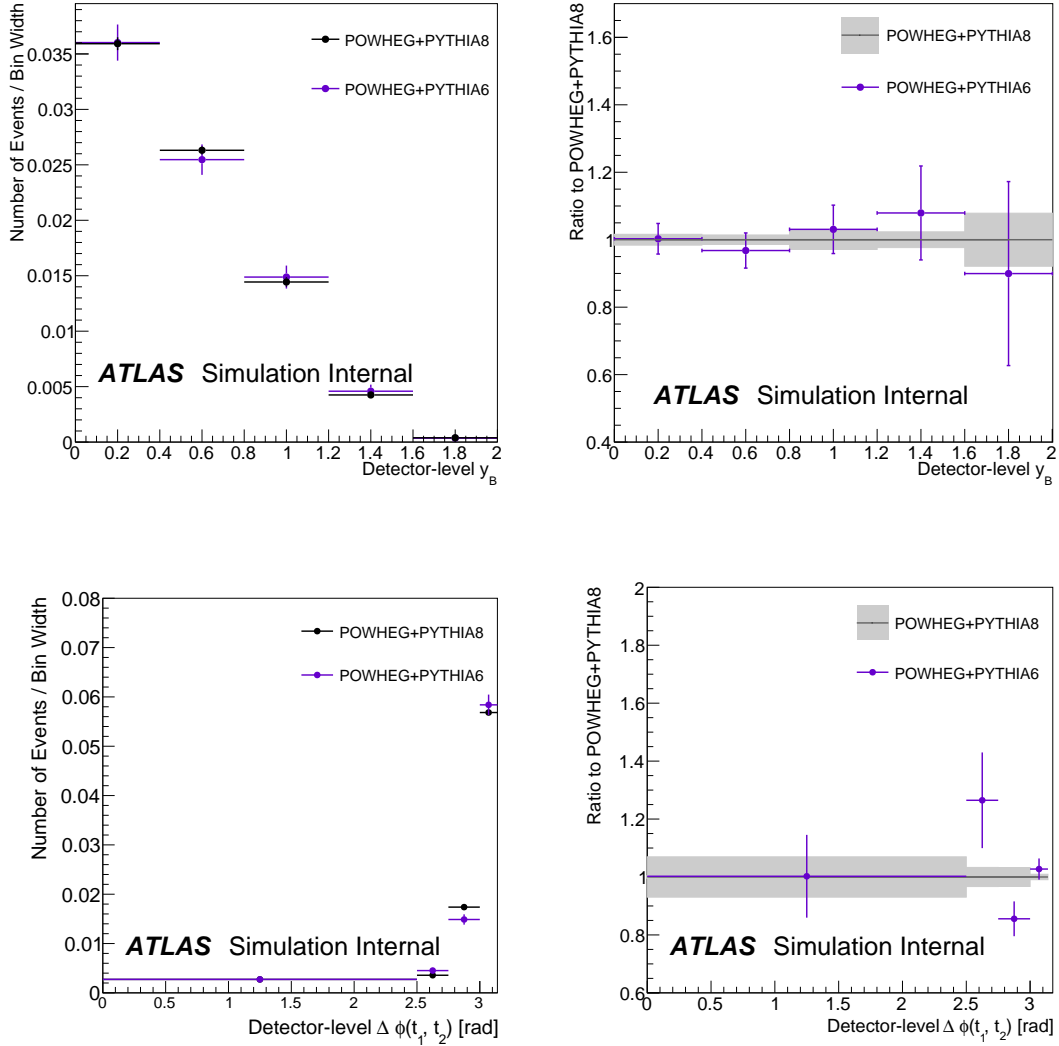


Figure 168: Distributions and ratio plots of final state observables using the Powheg+Pythia6 and Powheg+Pythia8 samples.

1238 O. ABCD method using 16 regions

1239 This section describes how we use the ABCD method for multijet background estimates in the signal re-
 1240 gion using a 16-region approach. Studies in this section are based on full 2015+2016 dataset of 36.5 fb^{-1} ,
 1241 and this is the technique used for the current analysis.

1242 **O.1. Classification of events into 16 regions**

1243 In this analysis, two large R jets are used for reconstruction of the $t\bar{t}$ event. In order to suppress back-
 1244 ground, top tagging and b-matching are applied on both large R jets. Events are classified into 16 regions
 1245 according to results of these algorithms. Let us denote

- 1246 • t_1 ... result of the leading large R jet top tagging
- 1247 • b_1 ... result of the leading large R jet B-matching
- 1248 • t_2 ... result of the 2nd leading large R jet top-tagging
- 1249 • b_2 ... result of the 2nd leading large R jet B-matching

1250 These parameters are equal to 1 if the corresponding object is top-tagged (B-matched), otherwise they
 1251 are equal to 0. The 16 regions are labeled according to table 177. The table also contains signal purities
 1252 (MC signal to data) in each region. The signal region 'S' is colored by the red color. Only green regions
 1253 are used for ABCD multijet estimates. The blue regions K,L,M,N contain larger fraction of signal and
 1254 ABCD estimates based on these regions will have high systematic uncertainties. Therefore, these regions
 1255 are not used.

2nd large-R jet	1t1b	J (7.57%)	K (21.3%)	L (41.6%)	S
0t1b	B (2.19%)	D (5.76%)	H (13.4%)	N (47.2%)	
1t0b	E (0.723%)	F (2.39%)	G (6.44%)	M (30.2%)	
0t0b	A (0.228%)	C (0.763%)	I (2.23%)	O (10.7%)	
	0t0b	1t0b	0t1b	1t1b	

1st large-R jet

Table 177: Classification into 16 regions according to results of top-tagging and b-matching applied on the leading and the 2nd leading large-R jet. The numbers in parentheses give the purity of the sample, *i.e.*, the expected number of events predicted by $t\bar{t}$ all-hadronic Monte Carlo simulation divided by the number of observed events in that region.

1256 **O.2. Correlations between parameters**

1257 The ABCD method requires an independence between the parameters. Therefore, it is needed to study
 1258 the correlations between parameters t_1 , b_1 , t_2 and b_2 and their effects on an ABCD multijet background
 1259 estimate.

1260 There are six possible correlations between these parameters:

- 1261 1. t_1 vs. b_1

- 1262 2. t_2 vs. b_2
 1263 3. t_1 vs. b_2
 1264 4. t_2 vs. b_1
 1265 5. t_1 vs. t_2
 1266 6. b_1 vs. b_2

1267 Figure 169 shows tables concerning event yields in 16 regions. Possible correlations between leading and
 1268 2nd leading large-R jet properties could be observed in tables with normalized rows and columns. These
 1269 tables show that these properties are not highly correlated. However, more detailed studies are needed to
 1270 estimate the effect of correlations. This is done in the following sections.

Not reviewed, for internal circulation only

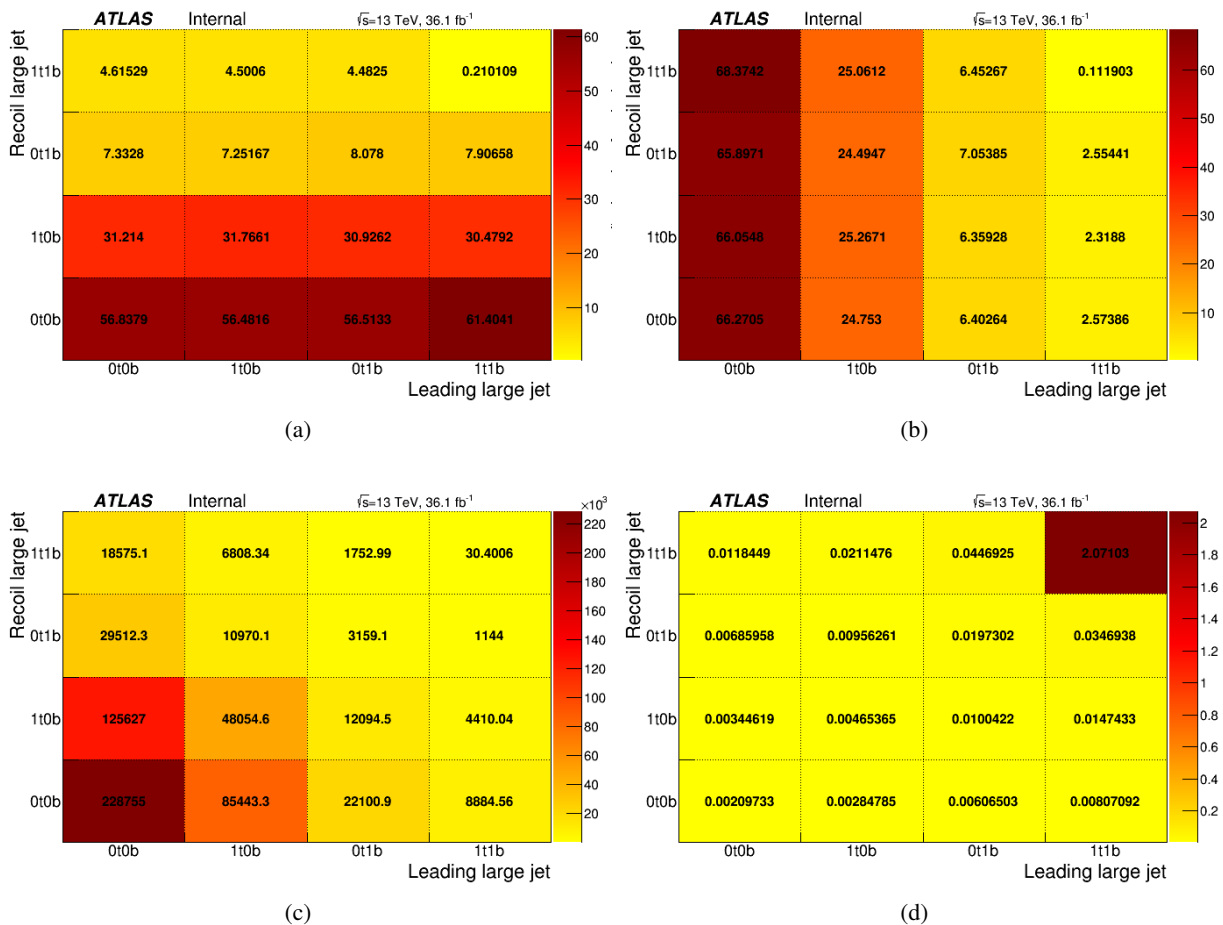


Figure 169: Leading large jet tagging (y-axis) vs. 2nd leading large R jet (x-axis): (a) table with normalized columns, (b) table with normalized rows, (c) with multijet event yields and (d) relative MC \oplus data statistical errors in the table. Event yields are calculated using formula 16.

1271 **O.2.1. Measurement of the effect of correlations on the ABCD multijet background estimate**

The effect of correlations on ABCD multijet background estimates can be measured in the green regions which are multijet background enriched. Let us start with correlations between t_1 and b_1 . Effect of the correlations can be expressed using coefficient k_{t_1,b_1} defined in the following formula

$$C \times I/A = k_{t_1,b_1} \cdot O \quad (19)$$

1272 If parameters t_1 and b_1 are independent then coefficient k_{t_1,b_1} is equal to 1. Otherwise, k_{t_1,b_1} is not equal
1273 to 1. This coefficient can be a constant or it can depend on some variables related with large R jets.

1274 The effect of other correlations is expressed in a similar way using the following formulas.

$$B \times E/A = k_{t_2,b_2} \cdot J \quad (20)$$

$$B \times C/A = k_{t_1,b_2} \cdot D \quad (21)$$

$$E \times I/A = k_{t_2,b_1} \cdot G \quad (22)$$

$$E \times C/A = k_{t_1,t_2} \cdot F \quad (23)$$

$$B \times I/A = k_{b_1,b_2} \cdot H \quad (24)$$

1275 Coefficients k_{t_1,b_1} , k_{t_2,b_2} , k_{t_1,b_2} , k_{t_2,b_1} , k_{t_1,t_2} and k_{b_1,b_2} are affected also by systematic errors. Therefore,
1276 systematic errors should be taken into account during measurement of these coefficients.

1277 Measured global values of coefficients k_{t_1,b_1} , k_{t_2,b_2} , k_{t_1,b_2} , k_{t_2,b_1} , k_{t_1,t_2} and k_{b_1,b_2} are listed in table 178. The
1278 global coefficients are calculated from a ratio of predicted and measured event yields in the region. Statistical
1279 errors are calculated using pseudo-experiments. The algorithm is same as it is used for calculation
1280 of the statistical errors of ABCD estimates. All systematic uncertainties are accounted except of signal,
1281 background modeling and PDF uncertainties. The largest measured difference of 13% between predicted
1282 and observed corresponds to correlation between t_2 and b_2 . Correlations between t_1 and b_1 has also sig-
1283 nificant effect. Correlations t_1 vs. t_2 and b_1 vs. b_2 have small effect and correlations t_1 vs. b_2 and t_2 vs.
1284 b_1 appear to be negligible.

Observed	Predicted	Kind of correlation	Measured coefficient (Pred./Obs.)
O	$C \times I/A$	t_1 vs. b_1	$k_{t_1,b_1} = 0.94278 \pm 0.013522 + 0.006268 - 0.008238$
J	$B \times E/A$	t_2 vs. b_2	$k_{t_2,b_2} = 0.8725 \pm 0.0093343 + 0.004723 - 0.004426$
D	$B \times C/A$	t_1 vs. b_2	$k_{t_1,b_2} = 1.0059 \pm 0.012543 + 0.007305 - 0.004431$
G	$E \times I/A$	t_2 vs. b_1	$k_{t_2,b_1} = 1.0028 \pm 0.012326 + 0.003124 - 0.003687$
F	$E \times C/A$	t_1 vs. t_2	$k_{t_1,t_2} = 0.97464 \pm 0.0066455 + 0.00556 - 0.003945$
H	$B \times I/A$	b_1 vs. b_2	$k_{b_1,b_2} = 0.90284 \pm 0.019735 + 0.04075 - 0.03607$

Table 178: The global coefficients describing the effect of correlations on ABCD estimates. The column 'Observed' lists the regions with measured distributions. The column 'predicted' contains formulas used for calculation of predicted distribution. Measured coefficients are ratios of predicted and observed event yields in the regions. Measured numbers are in the form: nominal \pm (stat. \oplus MC stat. error) + systematic error up – systematic error down.

1285 Figure 170 shows a comparison of predicted and observed leading large R jet pt distributions in sideband
1286 regions. This comparison can be used for measurement of local values of coefficients k_{t_1,b_1} , k_{t_2,b_2} , k_{t_1,b_2} ,
1287 k_{t_2,b_1} , k_{t_1,t_2} and k_{b_1,b_2} . Effects of correlations in bins are similar to global effects observed in table 178.

Not reviewed, for internal circulation only

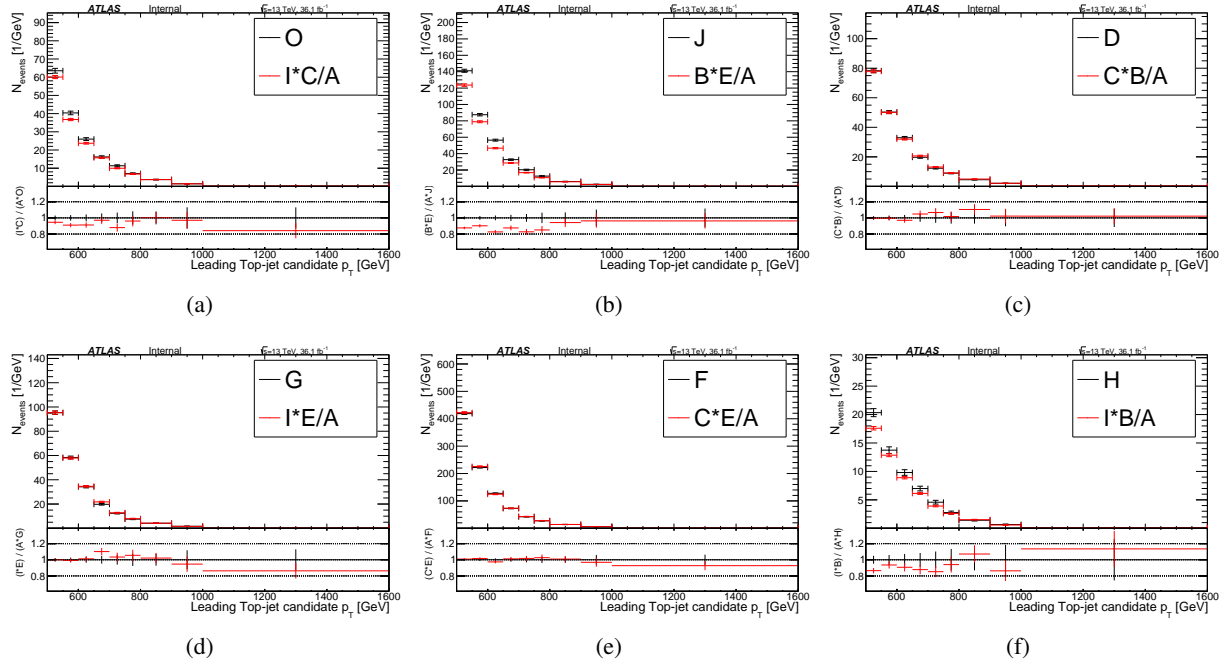


Figure 170: Measurement of effects of correlations on the ABCD estimates. Distributions predicted by ABCD estimates are compared with observed distributions.

1288 O.3. Effect of correlations in 9 regions

1289 Appendix L describes ABCD method using decomposition of events into 9 regions. All these regions can
 1290 be expressed using 16 regions. Therefore, all ABCD estimates from the 9 regions can be expressed using
 1291 terms from 16 regions. It is also possible to determine impact of correlations found in the 16 regions onto
 1292 ABCD estimates in 9 regions.

1293 O.3.1. Transformation from 16 to 9 regions

1294 The transformation from 16 to 9 regions is given by the following formulas:

$$\begin{aligned}
 A^{(9)} &= A \\
 B^{(9)} &= B + I \\
 C^{(9)} &= H \\
 D^{(9)} &= E + C \\
 E^{(9)} &= J + D + G + O \\
 F^{(9)} &= L + N \\
 G^{(9)} &= F \\
 H^{(9)} &= K + M \\
 S^{(9)} &= S,
 \end{aligned} \tag{25}$$

1295 where regions with superscript '(9)' are from 9 regions and regions without superscript are from 16
 1296 regions.

1297 **O.3.2. Theoretical description of impact of correlation**

1298 The goal of this section is to estimate how much the estimates from the 9 regions are affected by observed
 1299 correlations. The following derivations will be based on this assumption:

- 1300 • Effect of correlations between two parameters does not depend on fixed values of other two para-
 1301 meters (e.g. $\frac{BC}{AD} = \frac{JF}{EK} = k_{t_1,b_2}, \dots$)

It is not possible to test this assumption in data because 'blue' regions from the table 177 are needed for that. These regions contain lot of signal and observed multijet background obtained from formula

$$\text{Multijet background} = \text{Data} - (\text{MC signal} + \text{MC } t\bar{t} \text{ nonalhad} + \text{MC Wt single-top}) \quad (26)$$

1302 is not precise enough in these regions. However, this assumption can be tested in MC dijet samples.

1303 Let us assume that the assumption is satisfied. In the following derivation, capital letters denotes exact
 1304 multijet background distribution in corresponding region and $k_{t_1,b_1}, k_{t_2,b_2}, k_{t_1,b_2}, k_{t_2,b_1}, k_{t_1,t_2}, k_{b_1,b_2}$ denotes
 1305 exact values of coefficients corresponding to correlations.

$$\begin{aligned} E^{(9)} \sim \frac{B^{(9)}D^{(9)}}{A^{(9)}} &= \frac{(B+I)(E+C)}{A} = \frac{BE}{A} + \frac{IC}{A} + \frac{BC}{A} + \frac{EI}{A} = k_{t_1,b_1} \cdot O + k_{t_2,b_2} \cdot J + k_{t_1,b_2} \cdot D + k_{t_2,b_1} \cdot G \\ H^{(9)} \sim \frac{G^{(9)}B^{(9)}}{A^{(9)}} &= \frac{FB}{A} + \frac{FI}{A} = \frac{FJEB}{EJA} + \frac{FOCI}{COA} = k_{t_1,b_2} \cdot k_{t_2,b_2} \cdot K + k_{t_2,b_1} \cdot k_{t_1,b_1} \cdot M \\ F^{(9)} \sim \frac{C^{(9)}D^{(9)}}{A^{(9)}} &= \frac{HE}{A} + \frac{HC}{A} = \frac{HJEB}{BJA} + \frac{HO CI}{IOA} = k_{t_2,b_1} \cdot k_{t_2,b_2} \cdot L + k_{t_1,b_2} \cdot k_{t_1,b_1} \cdot N \\ S^{(9)} \sim \frac{C^{(9)}G^{(9)}}{A^{(9)}} &= \frac{HF}{A} = \frac{FJ}{KE} \frac{KE}{J} \frac{HO}{NI} \frac{NI}{O} \frac{1}{A} = k_{t_1,b_2} \frac{KE}{J} k_{t_1,b_2} \frac{NI}{O} \frac{1}{A} = k_{t_1,b_2}^2 \frac{KN}{DS} \frac{DA}{BC} \frac{BE}{AJ} \frac{CI}{AO} S \\ &= k_{t_1,b_2}^2 k_{t_2,b_1} \frac{1}{k_{t_1,b_2}} k_{t_2,b_2} k_{t_1,b_1} \cdot S = k_{t_1,b_1} \cdot k_{t_2,b_2} \cdot k_{t_2,b_1} \cdot k_{t_1,b_2} \cdot S \end{aligned} \quad (27)$$

1306 ABCD estimates from 9 regions were transformed into 16 regions using Eq 25. After that, these estimates
 1307 were expressed as a function of coefficients corresponding to correlations.

1308 Only the last estimate predicts multijet background in the signal region. Other estimates predict multijet
 1309 background in the sideband regions. One can see that effects of correlations are different for each estimate.
 1310 $\frac{C^{(9)}G^{(9)}}{A^{(9)}}$ estimate is affected by correlations more than other estimates. Therefore, even small difference
 1311 between $E^{(9)}$ and $\frac{B^{(9)}D^{(9)}}{A^{(9)}}$ can lead to the large difference between S and $\frac{C^{(9)}G^{(9)}}{A^{(9)}}$.

1312 **O.3.3. Measured effect of correlations**

1313 In the previous section, the effect of correlations on four ABCD estimates from 9 regions is described
 1314 theoretically using formulas in Eq. 27. This section contains results of measurement of the effect of
 1315 the correlations on these four estimates. In this section, we use again distributions from Eq. 26 as the
 1316 'observed' multijet background in the regions.

Let us begin with $\frac{B^{(9)}D^{(9)}}{A^{(9)}}$ estimate. This estimate predicts multijet background distribution in region $E^{(9)}$. This region is also multijet background enriched. Therefore, formula from Eq. 26 gives a good multijet background estimate in the region $E^{(9)}$. The measured ratio between predicted and observed yields is $0.9426 \pm 0.006787 + 0.004352 - 0.004263$.

The estimate $\frac{G^{(9)}B^{(9)}}{A^{(9)}}$ predicts multijet background distribution in region $H^{(9)}$. Regions used for ABCD estimate are multijet enriched but this is not completely true for region $H^{(9)}$. The signal purity in the region $H^{(9)}$ is 22.3%. Therefore, formula from Eq. 26 gives us inaccurate multijet background estimate in this region. Therefore, alternative possibilities, how to estimate effect of correlations, are also tested. Three different methods are used for estimation of an effect of correlations.

1. The first method simply ignores the fact that there is high signal purity in the region $H^{(9)}$ and effect of correlation is estimated from a ratio predicted/observed. The measured ratio is $0.9665 \pm 0.01345 + 0.05803 - 0.05509$.
2. The second method does not use formula from Eq. 26 as a multijet background distribution in region $H^{(9)}$. Distribution in region $H^{(9)}$ is estimated from ABCD estimates from 16 regions as it is show in the following equation:

$$H^{(9)} = K + M = \frac{1}{k_{t_1,b_2}} \cdot \frac{JF}{E} + \frac{1}{k_{t_2,b_1}} \cdot \frac{FO}{C} = \frac{DA}{BC} \frac{JF}{E} + \frac{GA}{EI} \frac{FO}{C} \quad (28)$$

The used ABCD estimates relies only on correlations t_1 vs. b_2 and t_2 vs. b_1 . Effect of these correlations was already proven to be negligible. However, effects of these correlations was corrected using factors $\frac{DA}{BC}$ and $\frac{GA}{EI}$. Measured ratio between the predicted and $H^{(9)}$ distributions is $0.8998 \pm 0.01288 + 0.008525 - 0.008289$.

3. The third method uses formula

$$\frac{G^{(9)}B^{(9)}}{A^{(9)}} = k_{t_1,b_2} \cdot k_{t_2,b_2} \cdot K + k_{t_2,b_1} \cdot k_{t_1,b_1} \cdot M \quad (29)$$

derived in Eq. 27 as a numerator and $H^{(9)} = K + M$ as a denominator. Multijet estimates in regions K and M are obtained from Eq. 26. Coefficients are determined from Eq. 19-22. The measured ratio is $0.8986 \pm 0.01288 + 0.008317 - 0.00796$.

The three methods gives us consistent results. Predicted distribution is shifted about 10% down.

Let us continue with $\frac{C^{(9)}D^{(9)}}{A^{(9)}}$ estimate which predicts multijet background distribution in the region $F^{(9)}$. The situation is similar as in the previous case. Therefore, three methods are also used for an estimation of an effect of the correlations.

1. The first method uses a ratio between predicted and observed distributions. The measured ratio is $1.006 \pm 0.03417 + 0.09657 - 0.09229$.
2. Distribution in region $F^{(9)}$ is estimated from the following formula

$$F^{(9)} = L + N = \frac{1}{k_{t_2,b_1}} \cdot \frac{JH}{B} + \frac{1}{k_{t_1,b_2}} \cdot \frac{HO}{I} = \frac{GA}{EI} \frac{JH}{B} + \frac{DA}{BC} \frac{HO}{I} \quad (30)$$

The used ABCD estimates relies also only on correlations t_1 vs. b_2 and t_2 vs. b_1 . Effect of these correlations is also corrected using the factors $\frac{DA}{BC}$ and $\frac{GA}{EI}$. The measured ratio between the predicted and $F^{(9)}$ distributions is $0.8982 \pm 0.01307 + 0.008064 - 0.0081$.

3. The third method uses formula

$$\frac{C^{(9)}D^{(9)}}{A^{(9)}} = k_{t_2,b_1} \cdot k_{t_2,b_2} \cdot L + k_{t_1,b_2} \cdot k_{t_1,b_1} \cdot N \quad (31)$$

1345 derived in Eq. 27 as a numerator and $F^{(9)} = L + N$ as a denominator. The measured ratio is $0.8985 \pm 0.01307 + 0.007955 - 0.008097$.

1347 The second and the third methods are in a good agreement. But the first approach returns slightly different
1348 result but it is within uncertainties. Big systematic uncertainty for the first method is caused by very high
1349 signal purity in the region $F^{(9)}$ (45%). Therefore, observed distribution from Eq. 26 is imprecise.

1350 Finally, the estimate $\frac{C^{(9)}G^{(9)}}{A^{(9)}}$ predicts multijet background distribution in the signal region $S^{(9)}$. Two
1351 methods are tested:

1352 1. The first method is a measurement of the ratio between ABCD estimate and observed distribution
1353 in the region S . The measured ratio is $21.83 \pm 1701 + 159.2 - 132.5$.

2. The effect of correlation is estimated using the following formula

$$\frac{C^{(9)}G^{(9)}}{A^{(9)}S^{(9)}} = k_{t_1,b_1} \cdot k_{t_2,b_2} \cdot k_{t_2,b_1} \cdot k_{t_1,b_2} = \frac{CI}{AO} \cdot \frac{BE}{JA} \cdot \frac{BC}{DA} \cdot \frac{EI}{AG} \quad (32)$$

1354 which is derived from the last line of the Eq. 27. The measured effect of correlations is $0.8175 \pm 0.02372 + 0.01523 - 0.01538$.

1356 The first method is very imprecise because the signal region has very high signal purity (about 92%). The
1357 second method gives us better information about impact of correlation on ABCD estimate.

1358 All results are listed in table 179. The predicted distribution in the signal region is shifted about 18% down
1359 due to correlation effects from the correct distribution. ABCD techniques using 9 regions systematically
1360 underestimate multijet background.

Observed	Predicted	Method of measurement	Measured effect
$E^{(9)}$	$B^{(9)} \times D^{(9)}/A^{(9)}$		$0.9426 \pm 0.006787 + 0.004352 - 0.004263$
$H^{(9)}$	$G^{(9)} \times B^{(9)}/A^{(9)}$	First method	$0.9665 \pm 0.01345 + 0.05803 - 0.05509$
$H^{(9)}$	$G^{(9)} \times B^{(9)}/A^{(9)}$	Second method	$0.8998 \pm 0.01288 + 0.008525 - 0.008289$
$H^{(9)}$	$G^{(9)} \times B^{(9)}/A^{(9)}$	Third method	$0.8986 \pm 0.01288 + 0.008317 - 0.00796$
$F^{(9)}$	$C^{(9)} \times D^{(9)}/A^{(9)}$	First method	$1.006 \pm 0.03417 + 0.09657 - 0.09229$
$F^{(9)}$	$C^{(9)} \times D^{(9)}/A^{(9)}$	Second method	$0.8982 \pm 0.01307 + 0.008064 - 0.0081$
$F^{(9)}$	$C^{(9)} \times D^{(9)}/A^{(9)}$	Third method	$0.8985 \pm 0.01307 + 0.007955 - 0.008097$
$S^{(9)}$	$C^{(9)} \times G^{(9)}/A^{(9)}$	First method	$21.83 \pm 1701 + 159.2 - 132.5$
$S^{(9)}$	$C^{(9)} \times G^{(9)}/A^{(9)}$	Second method	$0.8175 \pm 0.02372 + 0.01523 - 0.01538$

Table 179: Measured effect of the correlations on ABCD estimates in 9 regions. Measured numbers are in the form: nominal \pm (stat. \oplus MC stat. error) + systematic error up – systematic error down.

1361 O.4. ABCD estimates from the 16 regions

1362 Decomposition into the 16 regions can be used for ABCD multijet background estimate in the signal re-
1363 gion. Estimate should be made from the multijet background enriched regions which are colored by green

1364 color in the table 177. There are many possibilities how to make an ABCD estimate from the "green"
 1365 regions. These estimates can be affected by the correlation in a different way. Effects of correlations can
 1366 be corrected using the factors shown in the table 180. Actually, it seems that all possible estimates from
 1367 the green regions can be derived from the one fixed estimate. Other estimates can be derived from this
 1368 estimate using the correction factors from the table.

Let us choose estimate $S_0 = \frac{JO}{A}$. This estimate is made from the regions in the corners of the table 177.
 At first, let us estimate effect of correlations:

$$\frac{JO}{A} = \frac{JF}{EK} \frac{FO}{CM} \frac{EKMC}{F^2 A} = \frac{JF}{EK} \frac{FO}{CM} \frac{KM}{FS} \frac{CE}{FA} \cdot S = k_{t_1,b_2} \cdot k_{t_2,b_1} \cdot k_{b_1,b_2} \cdot k_{t_1,t_2} \cdot S. \quad (33)$$

1369 So, S_0 estimate is affected by the four sources of correlations.

1370 Other estimates can be calculated from the S_0 estimate and correction factors. Some of these estimates
 1371 are listed in the table 181. For example, $S_1 = S_0 \cdot \frac{FA}{CE} = S_0/k_{t_1,t_2}$. Therefore, correlation effect between t_1
 1372 and t_2 is corrected.

1373 The most interesting estimates are S_2 , S_3 and S_9 . S_2 and S_3 estimates are interesting because they are
 1374 not affected by correlations between t_1 and t_2 and between b_1 and b_2 . They are affected only by the
 1375 correlations t_1 vs. b_2 and t_2 vs. b_1 . According to table 178, these correlations have negligible effect.
 1376 These are the most simple estimates (based on 7 regions only) which have this property. Estimate S_9 is
 1377 interesting because all effects of correlations are corrected. On the other hand, this estimate has larger
 1378 statistical errors than other estimates. All "yellow" estimates are affected by the correlation between b_1
 1379 and b_2 and "blue" estimates are affected by the correlation between t_1 and t_2 .

1380 As was already written, all sources of correlation are corrected in the S_9 estimate. The estimate is derived
 1381 in the following equation:

$$S_9 = S_0 \cdot \frac{1}{k_{t_1,b_2}} \cdot \frac{1}{k_{t_2,b_1}} \cdot \frac{1}{k_{t_1,t_2}} \cdot \frac{1}{k_{b_1,b_2}} = \frac{JO}{A} \cdot \frac{DA}{BC} \cdot \frac{GA}{EI} \cdot \frac{FA}{EC} \cdot \frac{HA}{BI} = \frac{J \cdot O \cdot H \cdot F \cdot D \cdot G \cdot A^3}{(B \cdot E \cdot C \cdot I)^2} \quad (34)$$

1382 All four sources of correlations are corrected using correction factors from the table 180. S_9 is expressed
 1383 in very symmetric form. It is the only one possible estimate which is formed from the green regions and
 1384 which has all correlation corrected. It has also one other important property with respect to correlations.
 1385 Effects of correlations are measured and they are affected by errors. It can possibly introduce systematic
 1386 errors to ABCD estimate. However, all effects of correlations are taken into account in the estimate S_9 .
 1387 Therefore, uncertainties in measured effects of correlation are taken into account when uncertainties of
 1388 the estimate are calculated using pseudo-experiments. In other words, uncertainties of measured effects
 1389 of correlations are included in the statistical and systematic uncertainties of the ABCD estimate.
 1390 And finally, since this estimate has no alternatives there is no systematic uncertainty related with the
 1391 choice of the method.

1392 Because of these reasons, estimate S_9 is chosen for the multijet background estimation.

1393 Table 182 lists predicted multijet background event yields in the signal region using ABCD estimates from
 1394 9 and 16 regions estimates. ABCD estimate from 9 regions called 'ABCD4' is an average of estimates
 1395 'ABCD4 b0' and 'ABCD4 b1'. Estimates based on the 16 regions with similar level of correlations
 1396 between the tagging rates are consistent.

Factor	$\frac{DA}{BC}$	$\frac{GA}{EI}$	$\frac{FA}{EC}$	$\frac{HA}{BI}$	$\frac{OA}{CI}$	$\frac{JA}{BE}$
Effect of correlation	$\frac{1}{k_{t1,b2}}$	$\frac{1}{k_{t2,b1}}$	$\frac{1}{k_{t1,t2}}$	$\frac{1}{k_{b1,b2}}$	$\frac{1}{k_{t1,b1}}$	$\frac{1}{k_{t2,b2}}$

Table 180: Correction factors

	Estimate	Correlation effect
S ₀	J × O/A	$k_{t1,b2} \cdot k_{t2,b1} \cdot k_{t1,t2} \cdot k_{b1,b2}$
S ₁	F × J × O / (C × E)	$k_{t1,b2} \cdot k_{t2,b1} \cdot k_{b1,b2}$
S ₂	F × J × O × H / (E × I × D)	$k_{t1,b2}^2 \cdot k_{t2,b1}$
S ₃	F × J × O × H / (B × C × G)	$k_{t1,b2} \cdot k_{t2,b1}^2$
S ₄	F × J × O × I / (A × C × G)	$k_{t1,b2}^2 \cdot k_{t2,b1} \cdot k_{b1,b2}$
S ₅	F × J × O × B / (A × E × D)	$k_{t1,b2} \cdot k_{t2,b1}^2 \cdot k_{b1,b2}$
S ₆	H × J × O / (I × B)	$k_{t1,b2} \cdot k_{t2,b1} \cdot k_{t1,t2}$
S ₇	H × J × O × C / (D × I × A)	$k_{t2,b1}^2 \cdot k_{t1,b2} \cdot k_{t1,t2}$
S ₈	H × J × O × E / (B × A × G)	$k_{t2,b1} \cdot k_{t1,b2}^2 \cdot k_{t1,t2}$
S ₉	J × O × H × F × D × G × A ³ / (B × E × C × I) ²	1

Table 181: ABCD estimates from the 16 regions. Table lists formulas used for ABCD estimates and expected effect of correlations on estimates.

	Estimate	Predicted event yields
S ₀	J × O/A	722.8 ± 10.2
S ₁	F × J × O / (C × E)	740.5 ± 11.46
S ₂	F × J × O × H / (E × I × D)	827.3 ± 23.69
S ₃	F × J × O × H / (B × C × G)	824.5 ± 23
S ₄	F × J × O × I / (A × C × G)	744.9 ± 14.56
S ₅	F × J × O × B / (A × E × D)	746.6 ± 14.37
S ₆	H × J × O / (I × B)	801 ± 21.52
S ₇	H × J × O × C / (D × I × A)	807.6 ± 22.95
S ₈	H × J × O × E / (B × A × G)	805 ± 22.21
S ₉	J × O × H × F × D × G × A ³ / (B × E × C × I) ²	811.9 ± 29.6
ABCD4 b0	G × C/A	672.6 ± 14.2
ABCD4 b1	H × C/B	688.8 ± 16.67
ABCD4	$0.5 \times (G/A + H/B) \times C$	680.7 ± 14.7

Table 182: ABCD estimates from the 16 and 9 regions. Table lists predicted number of multijet events in the signal region.

¹³⁹⁷ In the 16 regions, it is possible to correct (reduce) effect of correlations between parameters. Therefore, estimates from the use of the 16 region decomposition are less affected by these correlations.

1399 **O.5. Results from MC dijet samples**

1400 All properties required by ABCD methods can be tested using MC simulated events. Of course, if some
 1401 property is valid for MC it does not mean that it is valid for real data. But, if methods works for MC, one
 1402 can hope that it works also for data. Pythia8 JZXW dijet samples (DSID=3610**) are used.

1403 **O.5.1. Measured effect of correlations on simple ABCD estimates**

1404 Table 183 lists global coefficients measured from simulated events. This table is analogical to the
 1405 table 179 from section O.2.1. MC samples have poor statistics in the regions. Therefore, statistical
 1406 errors are high. However, correlations can be seen also in this table. Effect of correlations is for most
 1407 sources of correlations consistent with the table 178 but in the case of correlation between t_2 and b_2 the
 effect is significantly stronger.

Observed	Predicted	Type of correlation	Predicted / Observed
O	$C \times I/A$	t_1 vs. b_1	0.86224 ± 0.065197
J	$B \times E/A$	t_2 vs. b_2	0.67547 ± 0.04792
D	$B \times C/A$	t_1 vs. b_2	1.094 ± 0.076313
G	$E \times I/A$	t_2 vs. b_1	0.98836 ± 0.065803
F	$E \times C/A$	t_1 vs. t_2	0.98991 ± 0.039515
H	$B \times I/A$	b_1 vs. b_2	0.80909 ± 0.094777

Table 183: The global coefficients describing the effect of correlations on ABCD estimates. The column 'Observed' lists the regions with measured distributions. The column 'predicted' contains formulas used for calculation of predicted distribution. Coefficients are ratios of predicted and observed event yields in the regions. Numbers are obtained from MC dijet simulation. The errors are statistical.

1408

1409 **O.5.2. Effect of correlations in 9 regions**

1410 In this section, algorithms described in section O.3.3 are applied on MC simulated events. Effect of
 1411 correlations is measured for four estimates from 9 regions. Results are listed in table 184. The methods
 1412 are same as are used for data. Different methods applied on the same estimate are in good agreement for
 1413 all four estimates. The effect of correlations is much stronger than in the data.

1414 **O.5.3. Comparison of ABCD estimates**

1415 In this section, ABCD methods described in section O.4 are applied on simulated dijet events. The ABCD
 1416 predicted event yields from these estimates are listed in table 185. Number of MC multijet events in the
 1417 signal region is 857.5 ± 181.8 . One can see, that some ABCD methods from 16 regions (green and blue)
 1418 are affected less by correlations and they are closer to correct distribution.

Not reviewed, for internal circulation only

Observed	Predicted	Method of measurement	Effect of correlations
$E^{(9)}$	$B^{(9)} \times D^{(9)}/A^{(9)}$		0.8491 ± 0.03592
$H^{(9)}$	$G^{(9)} \times B^{(9)}/A^{(9)}$	First method	0.7242 ± 0.05927
$H^{(9)}$	$G^{(9)} \times B^{(9)}/A^{(9)}$	Second method	0.7741 ± 0.06393
$H^{(9)}$	$G^{(9)} \times B^{(9)}/A^{(9)}$	Third method	0.7762 ± 0.06418
$F^{(9)}$	$C^{(9)} \times D^{(9)}/A^{(9)}$	First method	0.7046 ± 0.1167
$F^{(9)}$	$C^{(9)} \times D^{(9)}/A^{(9)}$	Second method	0.7515 ± 0.06268
$F^{(9)}$	$C^{(9)} \times D^{(9)}/A^{(9)}$	Third method	0.7679 ± 0.06445
$S^{(9)}$	$C^{(9)} \times G^{(9)}/A^{(9)}$	First method	0.4147 ± 0.1135
$S^{(9)}$	$C^{(9)} \times G^{(9)}/A^{(9)}$	Second method	0.6129 ± 0.1022

Table 184: Effect of the correlations on ABCD estimates in 9 regions. Numbers are obtained from MC dijet simulation.

Estimate		Predicted event yields
S_0	$J \times O/A$	504.8 ± 48.21
S_1	$F \times J \times O / (C \times E)$	511.9 ± 53.94
S_2	$F \times J \times O \times H / (E \times I \times D)$	704.2 ± 126.2
S_3	$F \times J \times O \times H / (B \times C \times G)$	637.8 ± 117.3
S_4	$F \times J \times O \times I / (A \times C \times G)$	507 ± 74.5
S_5	$F \times J \times O \times B / (A \times E \times D)$	576.9 ± 76.02
S_6	$H \times J \times O / (I \times B)$	636.7 ± 101.1
S_7	$H \times J \times O \times C / (D \times I \times A)$	701.6 ± 127
S_8	$H \times J \times O \times E / (B \times A \times G)$	640.4 ± 118.1
S_9	$J \times O \times H \times F \times D \times G \times A^3 / (B \times E \times C \times I)^2$	651.7 ± 168.8
ABCD4 b0	$G \times C/A$	355.4 ± 41.76
ABCD4 b1	$H \times C/B$	471 ± 58.65
ABCD4	$0.5 \times (G/A + H/B) \times C$	413.2 ± 47.08
Truth value	S	857.5 ± 181.8

Table 185: ABCD estimates from the 16 and 9 regions. Table lists predicted number of multijet events in the signal region. Numbers are obtained from MC dijet simulation.

1419 **O.6. The ABCD Method with Matrix Operations**

1420 The ABCD16 tableau can be interpreted as a 4x4 matrix, upon which matrix operators are applied in
1421 order to get the background estimation.

$$\mathcal{M} = \begin{pmatrix} J & K & L & S \\ B & D & H & N \\ E & F & G & M \\ A & C & I & O \end{pmatrix} = \begin{pmatrix} \mathcal{M}_{0011} & \mathcal{M}_{1011} & \mathcal{M}_{0111} & \mathcal{M}_{1111} \\ \mathcal{M}_{0001} & \mathcal{M}_{1001} & \mathcal{M}_{0101} & \mathcal{M}_{1101} \\ \mathcal{M}_{0010} & \mathcal{M}_{1010} & \mathcal{M}_{0110} & \mathcal{M}_{1110} \\ \mathcal{M}_{0000} & \mathcal{M}_{1000} & \mathcal{M}_{0100} & \mathcal{M}_{1100} \end{pmatrix}$$

1422 In order to estimate the background contribution in region S , one wants to extract first the 4 elements of
1423 M which will be used for the computation. For example, $SKMF$ is obtained by defining the following
1424 projection operators P and Q :

$$P = \begin{pmatrix} 0 & 1 & 0 & 0 \\ 0 & 0 & 0 & 1 \end{pmatrix}$$

$$Q = \begin{pmatrix} 1 & 0 & 0 & 0 \\ 0 & 0 & 1 & 0 \end{pmatrix}$$

1425 So that

$$A = Q \cdot \mathcal{M} \cdot P^T = \begin{pmatrix} \mathcal{M}_{1011} & \mathcal{M}_{1111} \\ \mathcal{M}_{1010} & \mathcal{M}_{1110} \end{pmatrix} = \begin{pmatrix} K & S \\ F & M \end{pmatrix}$$

Thus:

$$\det[A] = KM - SF = 0 \Rightarrow S = \frac{KM}{F}$$

1426 Alternatively, the scalar value S can be obtained by making use of the following matrices:

$$U_1 = \begin{pmatrix} 1 & 0 \\ 0 & 0 \end{pmatrix}$$

$$U_2 = \begin{pmatrix} 0 & 0 \\ 0 & 1 \end{pmatrix}$$

$$V_1 = \begin{pmatrix} 1 & 0 \end{pmatrix}$$

$$V_2 = \begin{pmatrix} 0 & 1 \end{pmatrix}$$

1427 So that

$$(V_1 U_1 A^T U_2 V_2^T)^{-1} \cdot \det[U_1 A U_1^T + U_2 A \cdot U_2^T] = \frac{\mathcal{M}_{1011} \mathcal{M}_{1110}}{\mathcal{M}_{1010}} = \frac{KM}{F}$$

¹⁴²⁸ As regions K and M are heavily contaminated by the $t\bar{t}$ signal, one wants to iterate the procedure to have
¹⁴²⁹ an estimate of their contributions, based on other control regions.

Region K' can be estimated using regions $KJEF$:

$$\det \left[\begin{pmatrix} 1 & 0 & 0 & 0 \\ 0 & 0 & 1 & 0 \end{pmatrix} \cdot \mathcal{M} \cdot \begin{pmatrix} 1 & 0 \\ 0 & 1 \\ 0 & 0 \\ 0 & 0 \end{pmatrix} \right] = \det \begin{pmatrix} \mathcal{M}_{0011} & \mathcal{M}_{1011} \\ \mathcal{M}_{0010} & \mathcal{M}_{1010} \end{pmatrix} = \det \begin{pmatrix} J & K \\ E & F \end{pmatrix} = JF - KE = 0 \Rightarrow K' = \frac{JF}{E}$$

Region M' can be estimated using regions $MFCO$:

$$\det \left[\begin{pmatrix} 0 & 0 & 1 & 0 \\ 0 & 0 & 0 & 1 \end{pmatrix} \cdot \mathcal{M} \cdot \begin{pmatrix} 0 & 0 \\ 1 & 0 \\ 0 & 0 \\ 0 & 1 \end{pmatrix} \right] = \det \begin{pmatrix} \mathcal{M}_{1010} & \mathcal{M}_{1110} \\ \mathcal{M}_{1000} & \mathcal{M}_{1100} \end{pmatrix} = \det \begin{pmatrix} F & M \\ C & O \end{pmatrix} = FO - MC = 0 \Rightarrow M' = \frac{FO}{C}$$

$$S_1 = \frac{K' \times M'}{F} = \frac{1}{F} \times \frac{JF}{E} \times \frac{FO}{C} = \frac{F \times J \times O}{C \times E}$$

¹⁴³⁰ The method described so far assumes that there are no correlations among the elements of the matrix \mathcal{M} .
¹⁴³¹ In order to introduce correlations, first we want to build the matrix itself from two vectors representing
¹⁴³² the b - and t -tagging state of the leading jets, i.e.:

$$\begin{aligned} j^1 &= (j_{00}^1 \quad j_{10}^1 \quad j_{01}^1 \quad j_{11}^1) \\ j^2 &= (j_{00}^2 \quad j_{10}^2 \quad j_{01}^2 \quad j_{11}^2) \end{aligned}$$

¹⁴³³ where j_{tb}^n represent the t - and b -tagging state of jet n .

¹⁴³⁴ These vectors can be transformed into diagonal matrices by the following procedure: first, one defines a
¹⁴³⁵ set of matrices $e(i)$ with all elements zero except the one on the diagonal corresponding to the i -th element
¹⁴³⁶ of the vector, e.g.:

Not reviewed, for internal circulation only

$$\begin{aligned}
 j^1 e(1) &= (j_{00}^1 \ j_{10}^1 \ j_{01}^1 \ j_{11}^1) \begin{pmatrix} 1 & 0 & 0 & 0 \\ 0 & 0 & 0 & 0 \\ 0 & 0 & 0 & 0 \\ 0 & 0 & 0 & 0 \end{pmatrix} = \begin{pmatrix} j_{00}^1 & 0 & 0 & 0 \\ 0 & 0 & 0 & 0 \\ 0 & 0 & 0 & 0 \\ 0 & 0 & 0 & 0 \end{pmatrix} \\
 j^1 e(2) &= (j_{00}^1 \ j_{10}^1 \ j_{01}^1 \ j_{11}^1) \begin{pmatrix} 0 & 0 & 0 & 0 \\ 0 & 1 & 0 & 0 \\ 0 & 0 & 0 & 0 \\ 0 & 0 & 0 & 0 \end{pmatrix} = \begin{pmatrix} 0 & 0 & 0 & 0 \\ 0 & j_{10}^1 & 0 & 0 \\ 0 & 0 & 0 & 0 \\ 0 & 0 & 0 & 0 \end{pmatrix} \\
 j^1 e(3) &= (j_{00}^1 \ j_{10}^1 \ j_{01}^1 \ j_{11}^1) \begin{pmatrix} 0 & 0 & 0 & 0 \\ 0 & 0 & 0 & 0 \\ 0 & 0 & 1 & 0 \\ 0 & 0 & 0 & 0 \end{pmatrix} = \begin{pmatrix} 0 & 0 & 0 & 0 \\ 0 & 0 & 0 & 0 \\ 0 & 0 & j_{01}^1 & 0 \\ 0 & 0 & 0 & 0 \end{pmatrix} \\
 j^1 e(4) &= (j_{00}^1 \ j_{10}^1 \ j_{01}^1 \ j_{11}^1) \begin{pmatrix} 0 & 0 & 0 & 0 \\ 0 & 0 & 0 & 0 \\ 0 & 0 & 0 & 0 \\ 0 & 0 & 0 & 1 \end{pmatrix} = \begin{pmatrix} 0 & 0 & 0 & 0 \\ 0 & 0 & 0 & 0 \\ 0 & 0 & 0 & 0 \\ 0 & 0 & 0 & j_{11}^1 \end{pmatrix}
 \end{aligned}$$

¹⁴³⁷ So that:

$$\begin{aligned}
 J^1 &= \sum_{i=1}^4 j^1 e(i) = \begin{pmatrix} j_{00}^1 & 0 & 0 & 0 \\ 0 & j_{10}^1 & 0 & 0 \\ 0 & 0 & j_{01}^1 & 0 \\ 0 & 0 & 0 & j_{11}^1 \end{pmatrix} \\
 J^2 &= \sum_{i=1}^4 j^2 e(i) = \begin{pmatrix} j_{00}^2 & 0 & 0 & 0 \\ 0 & j_{10}^2 & 0 & 0 \\ 0 & 0 & j_{01}^2 & 0 \\ 0 & 0 & 0 & j_{11}^2 \end{pmatrix}
 \end{aligned}$$

¹⁴³⁸ If we define the following matrices:

$$\begin{aligned}
 C &= \begin{pmatrix} 1 & 1 & 1 & 1 \\ 1 & 1 & 1 & 1 \\ 1 & 1 & 1 & 1 \\ 1 & 1 & 1 & 1 \end{pmatrix} \\
 X &= \begin{pmatrix} 0 & 0 & 0 & 1 \\ 0 & 0 & 1 & 0 \\ 0 & 1 & 0 & 0 \\ 1 & 0 & 0 & 0 \end{pmatrix}
 \end{aligned}$$

¹⁴³⁹ Then we get:

$$XJ^2CJ^1 = \begin{pmatrix} 0 & 0 & 0 & 1 \\ 0 & 0 & 1 & 0 \\ 0 & 1 & 0 & 0 \\ 1 & 0 & 0 & 0 \end{pmatrix} \begin{pmatrix} j_{00}^2 & 0 & 0 & 0 \\ 0 & j_{10}^2 & 0 & 0 \\ 0 & 0 & j_{01}^2 & 0 \\ 0 & 0 & 0 & j_{11}^2 \end{pmatrix} \begin{pmatrix} 1 & 1 & 1 & 1 \\ 1 & 1 & 1 & 1 \\ 1 & 1 & 1 & 1 \\ 1 & 1 & 1 & 1 \end{pmatrix} \begin{pmatrix} j_{00}^1 & 0 & 0 & 0 \\ 0 & j_{10}^1 & 0 & 0 \\ 0 & 0 & j_{01}^1 & 0 \\ 0 & 0 & 0 & j_{11}^1 \end{pmatrix} = \begin{pmatrix} j_{00}^1 j_{11}^2 & j_{10}^1 j_{11}^2 & j_{01}^1 j_{11}^2 & j_{11}^1 j_{11}^2 \\ j_{01}^1 j_{01}^2 & j_{10}^1 j_{01}^2 & j_{01}^1 j_{01}^2 & j_{11}^1 j_{01}^2 \\ j_{00}^1 j_{10}^2 & j_{10}^1 j_{10}^2 & j_{01}^1 j_{10}^2 & j_{11}^1 j_{10}^2 \\ j_{00}^1 j_{00}^2 & j_{10}^1 j_{00}^2 & j_{01}^1 j_{00}^2 & j_{11}^1 j_{00}^2 \end{pmatrix}$$

¹⁴⁴⁰ We recognize that:

$$\begin{pmatrix} j_{00}^1 j_{11}^2 & j_{10}^1 j_{11}^2 & j_{01}^1 j_{11}^2 & j_{11}^1 j_{11}^2 \\ j_{01}^1 j_{01}^2 & j_{10}^1 j_{01}^2 & j_{01}^1 j_{01}^2 & j_{11}^1 j_{01}^2 \\ j_{00}^1 j_{10}^2 & j_{10}^1 j_{10}^2 & j_{01}^1 j_{10}^2 & j_{11}^1 j_{10}^2 \\ j_{00}^1 j_{00}^2 & j_{10}^1 j_{00}^2 & j_{01}^1 j_{00}^2 & j_{11}^1 j_{00}^2 \end{pmatrix} = \begin{pmatrix} \mathcal{M}_{0011} & \mathcal{M}_{1011} & \mathcal{M}_{0111} & \mathcal{M}_{1111} \\ \mathcal{M}_{0001} & \mathcal{M}_{1001} & \mathcal{M}_{0101} & \mathcal{M}_{1101} \\ \mathcal{M}_{0010} & \mathcal{M}_{1010} & \mathcal{M}_{0110} & \mathcal{M}_{1110} \\ \mathcal{M}_{0000} & \mathcal{M}_{1000} & \mathcal{M}_{0100} & \mathcal{M}_{1100} \end{pmatrix} = \begin{pmatrix} J & K & L & S \\ B & D & H & N \\ E & F & G & M \\ A & C & I & O \end{pmatrix} = \mathcal{M}$$

¹⁴⁴¹ Finally, the purpose of the matrix C is to introduce correlations among the element of \mathcal{M} . A correlation
¹⁴⁴² between two elements appears whenever the corresponding element of C is different from 1. To give a
¹⁴⁴³ practical example, let's say that

$$C = \begin{pmatrix} 1 & 1 & 1 & 1 \\ 1 & 1 & 1 & 1 \\ 1 & 1 & 1 & 1 \\ 1 & w & 1 & 1 \end{pmatrix}$$

Then

$$\mathcal{M}' = XJ^2CJ^1 = \begin{pmatrix} \mathcal{M}_{0011} & w \cdot \mathcal{M}_{1011} & \mathcal{M}_{0111} & \mathcal{M}_{1111} \\ \mathcal{M}_{0001} & \mathcal{M}_{1001} & \mathcal{M}_{0101} & \mathcal{M}_{1101} \\ \mathcal{M}_{0010} & \mathcal{M}_{1010} & \mathcal{M}_{0110} & \mathcal{M}_{1110} \\ \mathcal{M}_{0000} & \mathcal{M}_{1000} & \mathcal{M}_{0100} & \mathcal{M}_{1100} \end{pmatrix}$$

$$A' = Q \cdot \mathcal{M}' \cdot P^T = \begin{pmatrix} w \cdot \mathcal{M}_{1011} & \mathcal{M}_{1111} \\ \mathcal{M}_{1010} & \mathcal{M}_{1110} \end{pmatrix} = \begin{pmatrix} w \cdot K & S \\ F & M \end{pmatrix}$$

Thus:

$$\det[A'] = w \cdot KM - SF = 0 \Rightarrow S = \frac{w \cdot KM}{F}$$

1444 P. Optimization of B-Tagging Working Points

1445 The analysis was originally performed using a b -tagging workpoint point with nominal efficiency of 70%.
 1446 With this choice of working point, the signal-over-background for the full sample is approximately 2.4.
 1447 Although we expect that the signal-to-background would drop if we relaxed the b -tagging working point,
 1448 it was not clear that we had optimized the analysis to obtain the smallest possible uncertainties. We
 1449 therefore chose as our figure-of-merit the uncertainty on the background subtracted-signal yield, taking
 1450 into account both statistical and systematic uncertainties on this measure.

1451 We note that this assumes that the signal and background are distributed in the same way across the
 1452 distributions we are measuring. This is approximately the case for most of the kinematic variables, and in
 1453 particular the top-quark p_T and rapidity.

1454 We therefore performed the analysis with a working point of 77% and compared the results with the
 1455 nominal selection, in particular estimating the uncertainty on the background-subtracted yield.

1456 The results are summarized in Table 186. Although there is an increase in the background-subtracted
 1457 signal by 27%, the S/B ratio goes from 2.4 to 1.6. More importantly, the uncertainty on the background-
 1458 subtracted yield increases from 3.6% to 4.5%. This increase in uncertainty comes from the increase in
 1459 90% of the estimated multijet background and its associated uncertainty. The latter is dominated by the
 1460 systematic uncertainty on this estimate.

1461 We conclude that relaxing the b -tagging working point of 70% does not improve the analysis.

Source	70% Working Point		77% Working Point	
	Events	Uncertainty	Events	Uncertainty
Predicted all-hadronic $t\bar{t}$	2,486	510	3,104	637
Non-all-hadronic $t\bar{t}$	116	29	152	38
Single top-quark	23	13	35	19
$t\bar{t} + X$	32			
Multijet	883	58	1,753	115
Events observed	3,512		5,058	
Observed-Background	2,458	89 (3.6%)	3,118	142 (4.5%)
Signal-to-Background	2.42		1.59	

Table 186: A comparison of the backgrounds and event yields with two different b-tagging working points. The uncertainties quoted include the statistical uncertainties and the uncertainties associated with the detector-level sources. No modelling uncertainties are included.

1462 Q. Optimization of Signal Scale Factor

1463 **NB: no signal scale factor is applied for the analysis. Control regions show good data/MC nor-**
 1464 **malization, and the QCD background estimate is only somewhat sensitive to signal normalization**
 1465 **due to the small signal contamination used for the QCD estimation. This appendix was written to**
 1466 **investigate the possibility of using a scale factor, but it is not applied in the analysis. Nonetheless**
 1467 **these studies were useful in understanding the dependence of signal normalization on modelling.**

1468 The data/prediction ratio does not appear to be optimal for the nominal sample Powheg+Pythia8 if the
 1469 NNLO+NNLL cross-section of 380.1 pb is applied. An iterative procedure is applied in order to find the
 1470 best-fit scale factor yielding the optimal χ^2/NDF for a certain observable for which the shapes of signal
 1471 and background are significantly different. Such an observable has been identified as the mass of the
 1472 anti- k_T R=0.4 jet with highest p_T among the ones geometrically matched to the leading anti- k_T R=1.0
 1473 jet.

1474 The procedure is as follows:

- 1475 1. Start with a scale factor $f = 1.0$. Run the ABCD16 method to estimate the background;
- 1476 2. Keeping the background fixed, perform a scan in the range $f = 0.5 - 2.0$. Find the best value \hat{f}
 1477 corresponding to the minimum χ^2/NDF ;
- 1478 3. Set $f = \hat{f}$. Run the ABCD16 method to estimate the background;
- 1479 4. Repeat until convergence, i.e. the best-fit value of \hat{f} become stable.

1480 The convergence is reached after 2 iterations. The procedure has been repeated for different Monte Carlo
 1481 signal samples as shown in Tab. 187. An example is given in Fig. 171 for Powheg+Herwig 7. Figures
 1482 172–178 show the detector-level observables compared to the Powheg+Pythia8 prediction scaled by a
 1483 factor 0.75.

Sample (DSID)	Cross-section [pb]	Scale Factor	Data/Prediction	χ^2/NDF
Powheg+Pythia8 (410506)	380.11	0.75	0.99	–
Powheg+Herwig 7 (410530)	285.05	1.30	1.00	1.1418
Powheg+Pythia6 (410007)	380.11	0.85	0.99	0.9399
MADGRAPH5_AMC@NLO+Pythia8 (410160)	379.19	0.85	1.00	0.9566

Table 187: Signal scale factor to be applied in order to minimize the χ^2/NDF .

Not reviewed, for internal circulation only

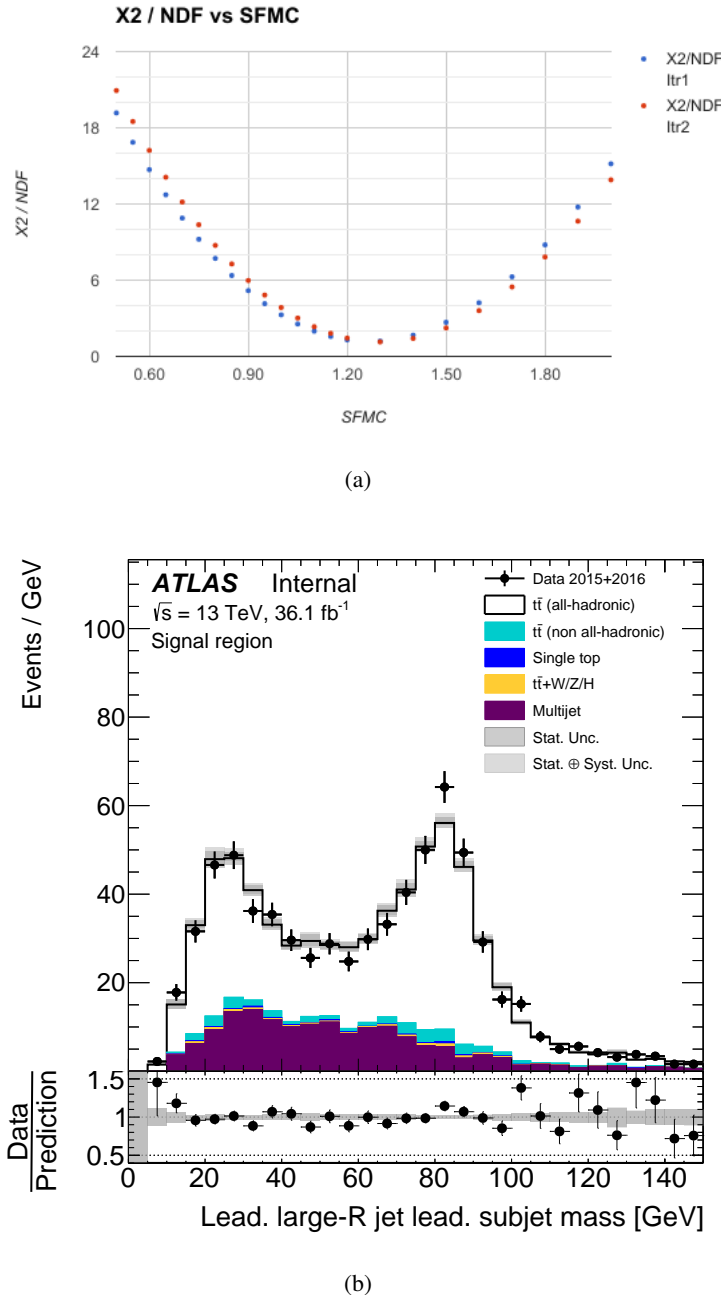


Figure 171: Scale factor optimization: (a) χ^2/NDF as a function of the data/prediction ratio for the Powheg +HERWIG 7 sample and (b) the resulting distribution of the leading sub-jet mass.

Not reviewed, for internal circulation only

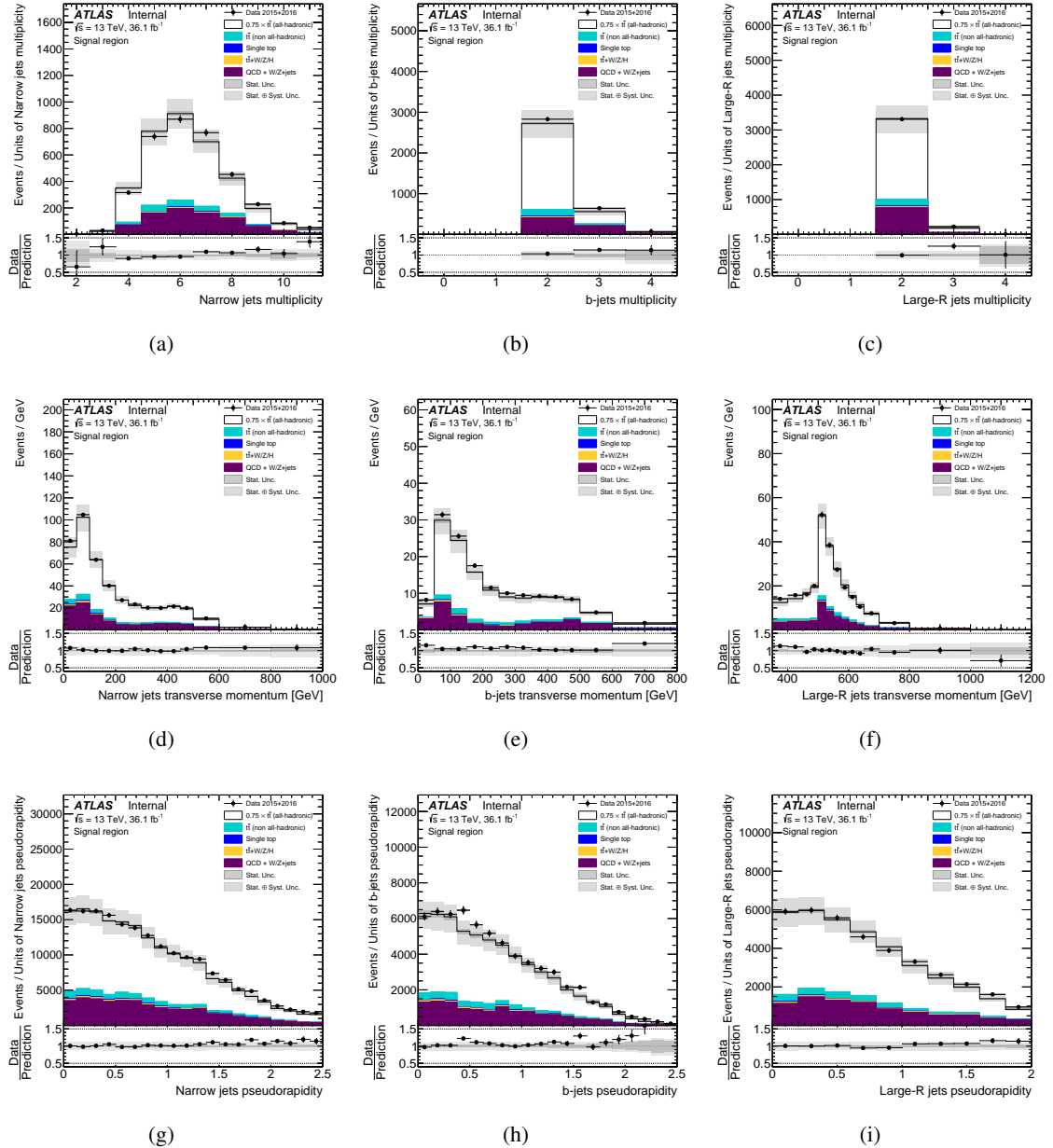


Figure 172: Kinematic distributions of jets in the signal region (S): (a) multiplicity, (d) transverse momentum and (g) rapidity of anti- k_t R=0.4 jets, (b) multiplicity, (e) transverse momentum and (h) rapidity of anti- k_t R=0.4 b-tagged jets, (c) multiplicity, (f) transverse momentum and (i) rapidity of anti- k_t R=1.0 jets. Data distributions are compared to predictions using PowHEG+PYTHIA8 as the $t\bar{t}$ signal model scaled by a factor 0.75. The hashed area indicates the combined statistical and systematic uncertainties on the total prediction, excluding systematic uncertainties related to the modelling of the $t\bar{t}$ system.

Not reviewed, for internal circulation only

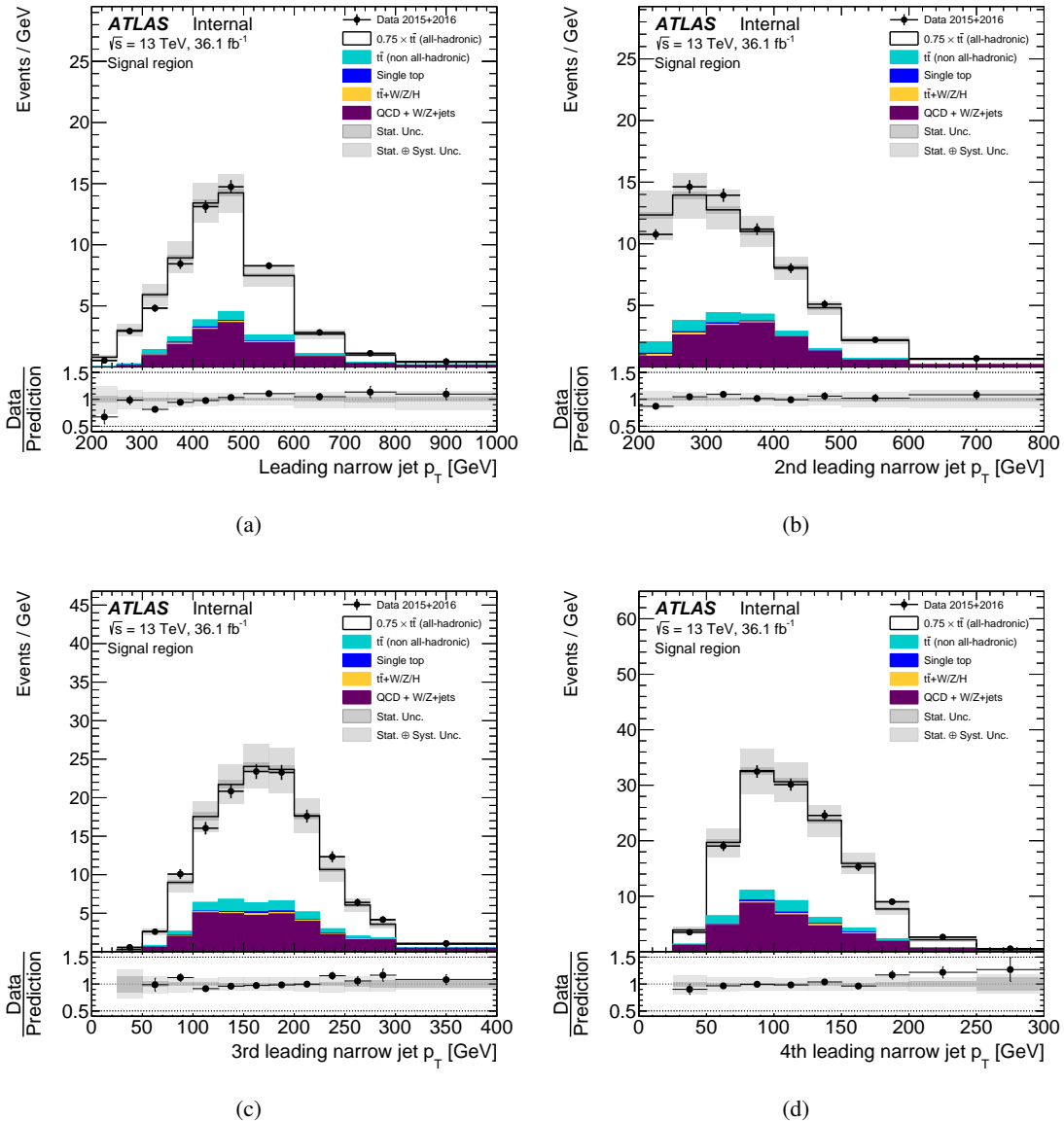


Figure 173: Kinematic distributions of the four leading small- R jets in the signal region (S): (a) leading jet transverse momentum, (b) second-leading jet transverse momentum, (c) third-leading jet transverse momentum and (d) fourth-leading jet transverse momentum. Data distributions are compared to predictions using PowHEG+PYTHIA8 as the $t\bar{t}$ signal model scaled by a factor 0.75. The hashed area indicates the combined statistical and systematic uncertainties on the total prediction, excluding systematic uncertainties related to the modelling of the $t\bar{t}$ system.

Not reviewed, for internal circulation only

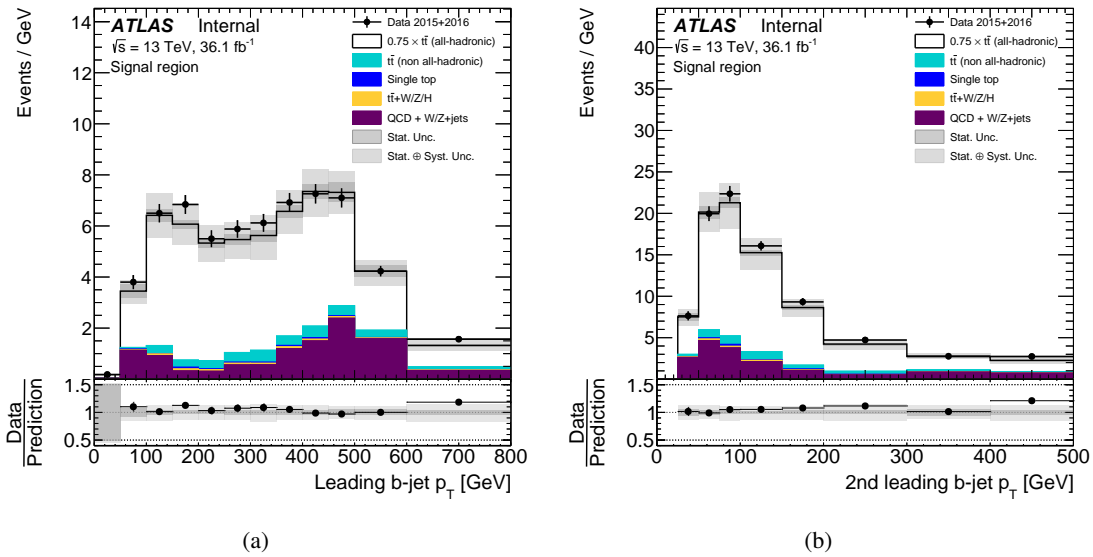


Figure 174: Kinematic distributions of b -tagged jets in the signal region (S): (a) leading b -tagged and (b) second-leading b -tagged jet transverse momenta. Data distributions are compared to predictions using PowHEG+PYTHIA8 as the $t\bar{t}$ signal model scaled by a factor 0.75. The hashed area indicates the combined statistical and systematic uncertainties on the total prediction, excluding systematic uncertainties related to the modelling of the $t\bar{t}$ system.

Not reviewed, for internal circulation only

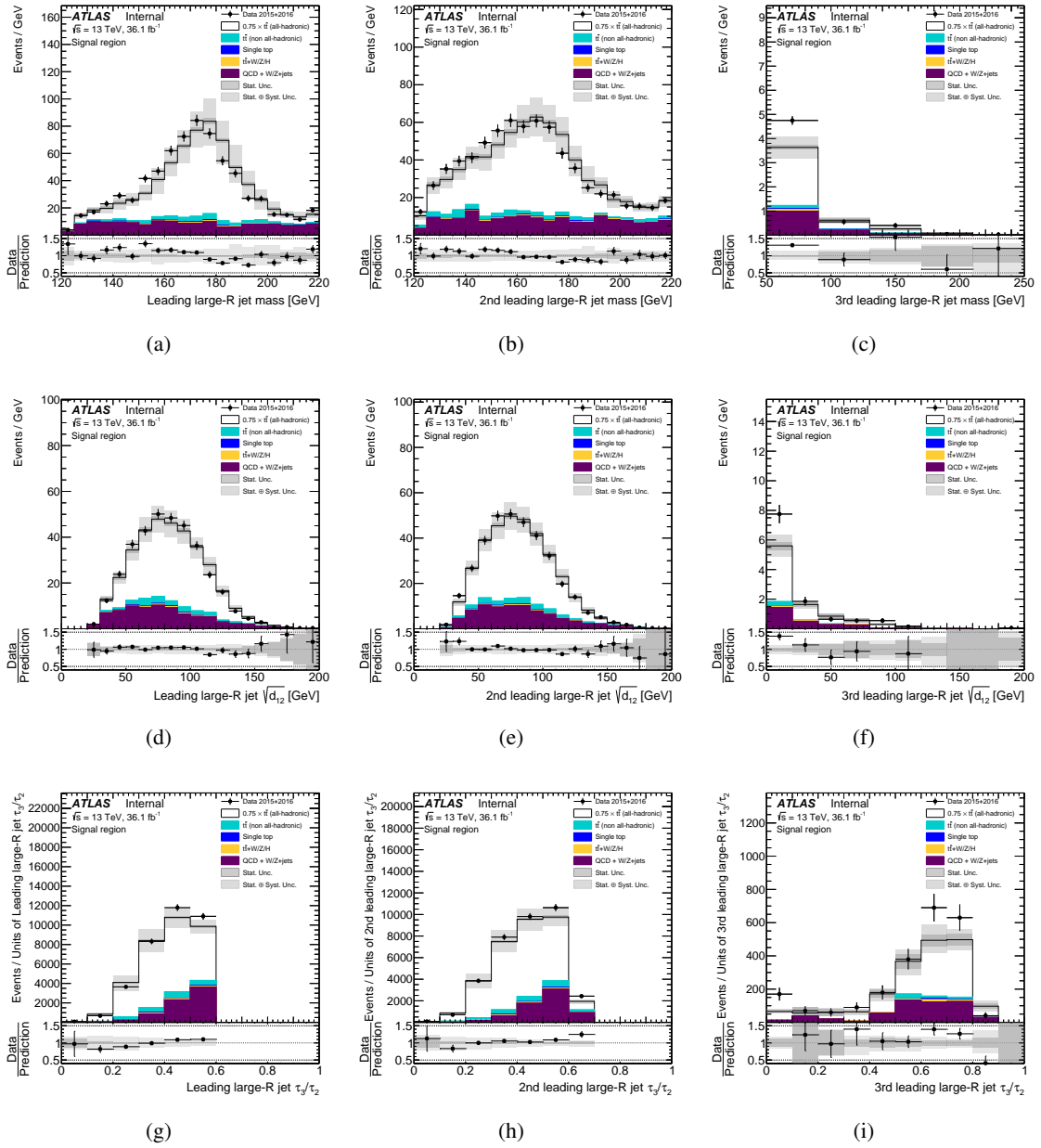


Figure 175: Kinematic distributions of large- R jets in the signal region (S): (a) mass, (d) splitting scale and (g) N-subjettiness of the leading anti- k_t R=1.0 trimmed jet, (b) mass, (e) splitting scale and (h) N-subjettiness of the second leading large- R jet and (c) mass, (f) splitting scale and (i) N-subjettiness of the third leading large- R jet. Data distributions are compared to predictions using PowHEG+PYTHIA8 as the $t\bar{t}$ signal model scaled by a factor 0.75. The hashed area indicates the combined statistical and systematic uncertainties on the total prediction, excluding systematic uncertainties related to the modelling of the $t\bar{t}$ system.

Not reviewed, for internal circulation only

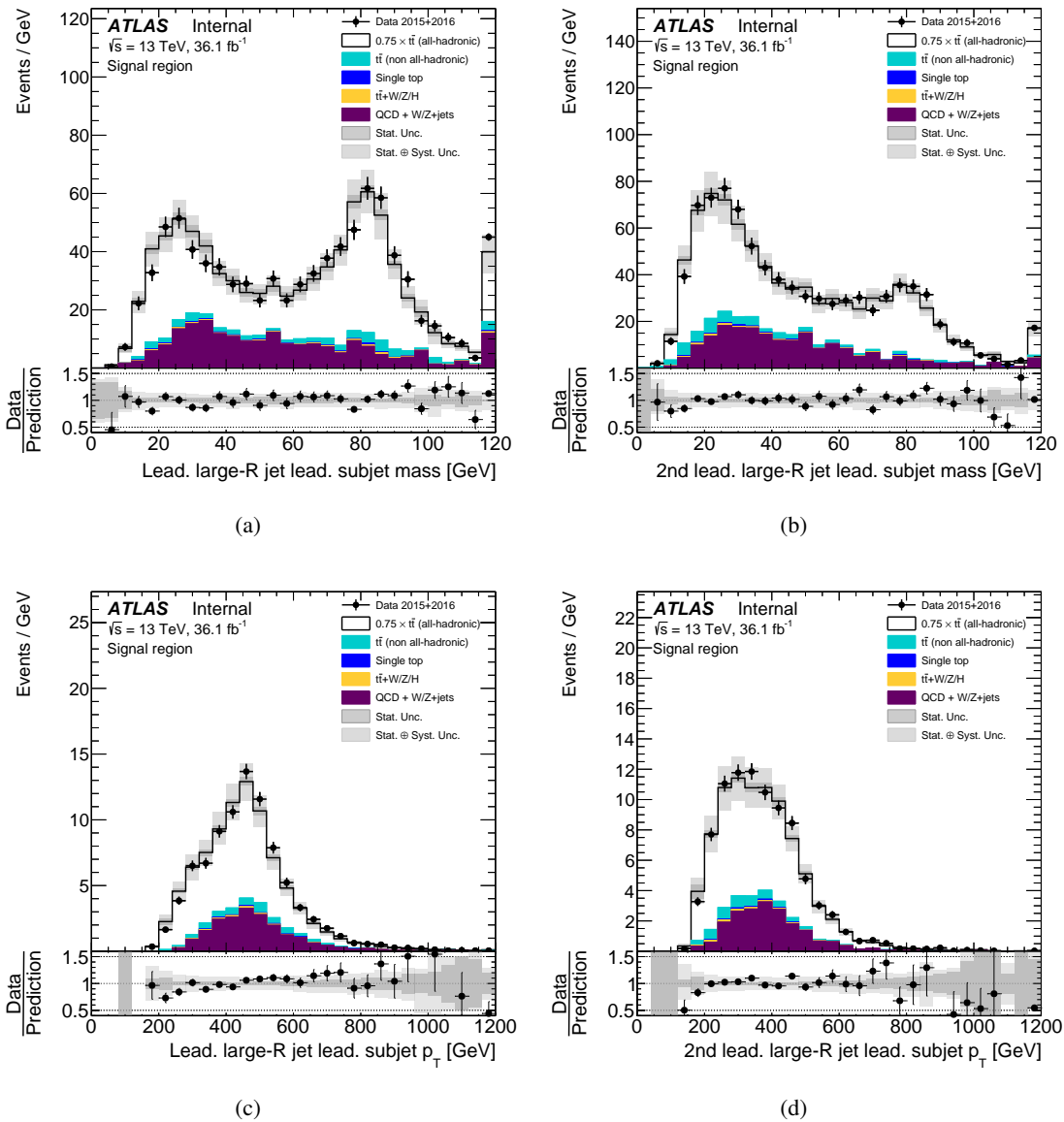


Figure 176: Kinematic distributions of the leading small- R jet embedded in a large- R jet in the signal region (S): (a) mass and (c) transverse momentum of the leading small- R jet embedded in the leading large- R jet, and (b) mass and (d) transverse momentum of the leading small- R jet embedded in the second-leading large- R jet. Data distributions are compared to predictions using PowHEG+PYTHIA8 as the $t\bar{t}$ signal model scaled by a factor 0.75. The hashed area indicates the combined statistical and systematic uncertainties on the total prediction, excluding systematic uncertainties related to the modelling of the $t\bar{t}$ system.

Not reviewed, for internal circulation only

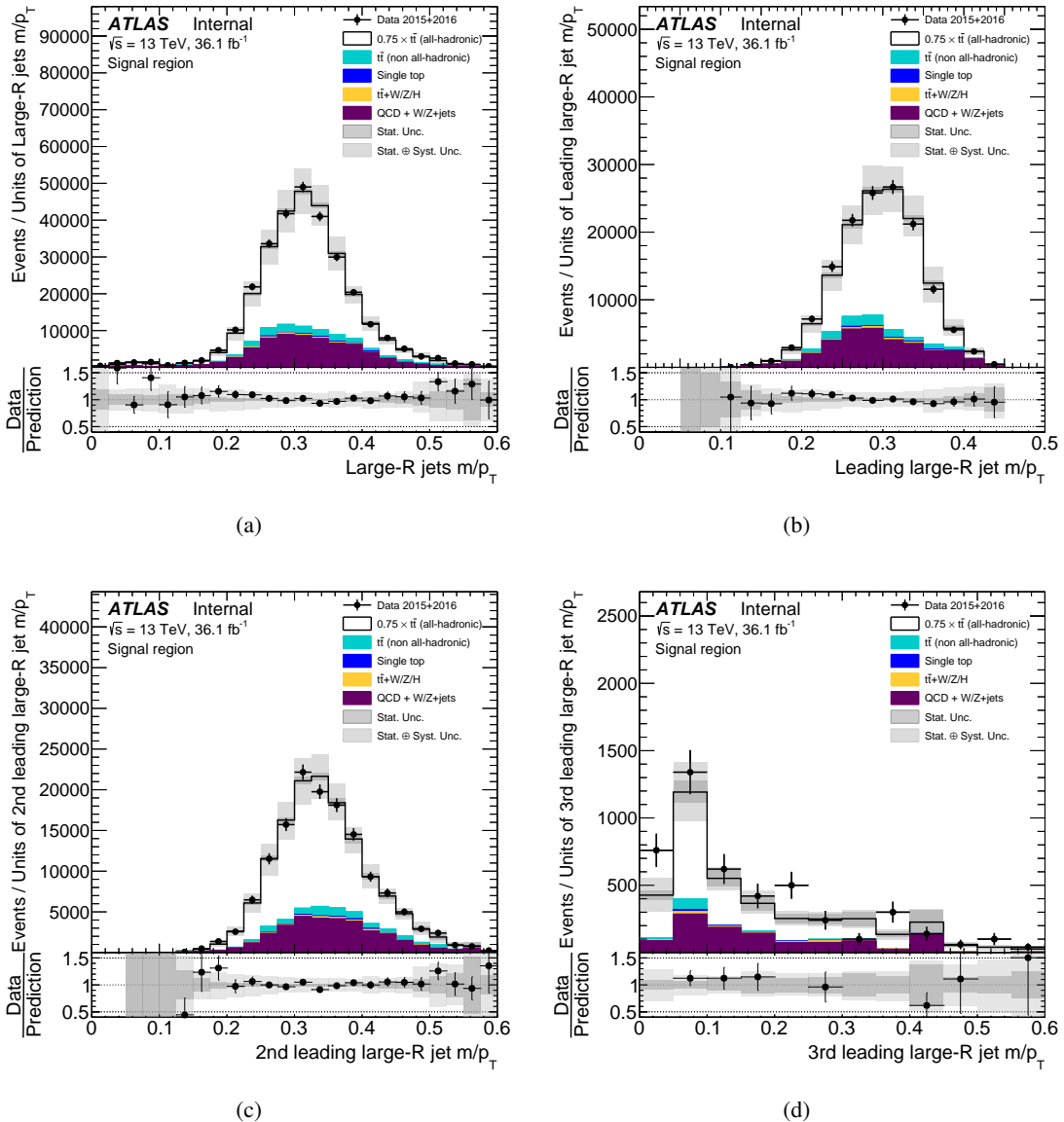


Figure 177: Kinematic distributions of mass-over-transverse-momentum of (a) all large- R jets, (b) the leading large- R jet, (c) the second-leading large- R jet and (d) the third-leading large- R jet. Data distributions are compared to predictions using PowHEG+PYTHIA8 as the $t\bar{t}$ signal model scaled by a factor 0.75. The hashed area indicates the combined statistical and systematic uncertainties on the total prediction, excluding systematic uncertainties related to the modelling of the $t\bar{t}$ system.

Not reviewed, for internal circulation only

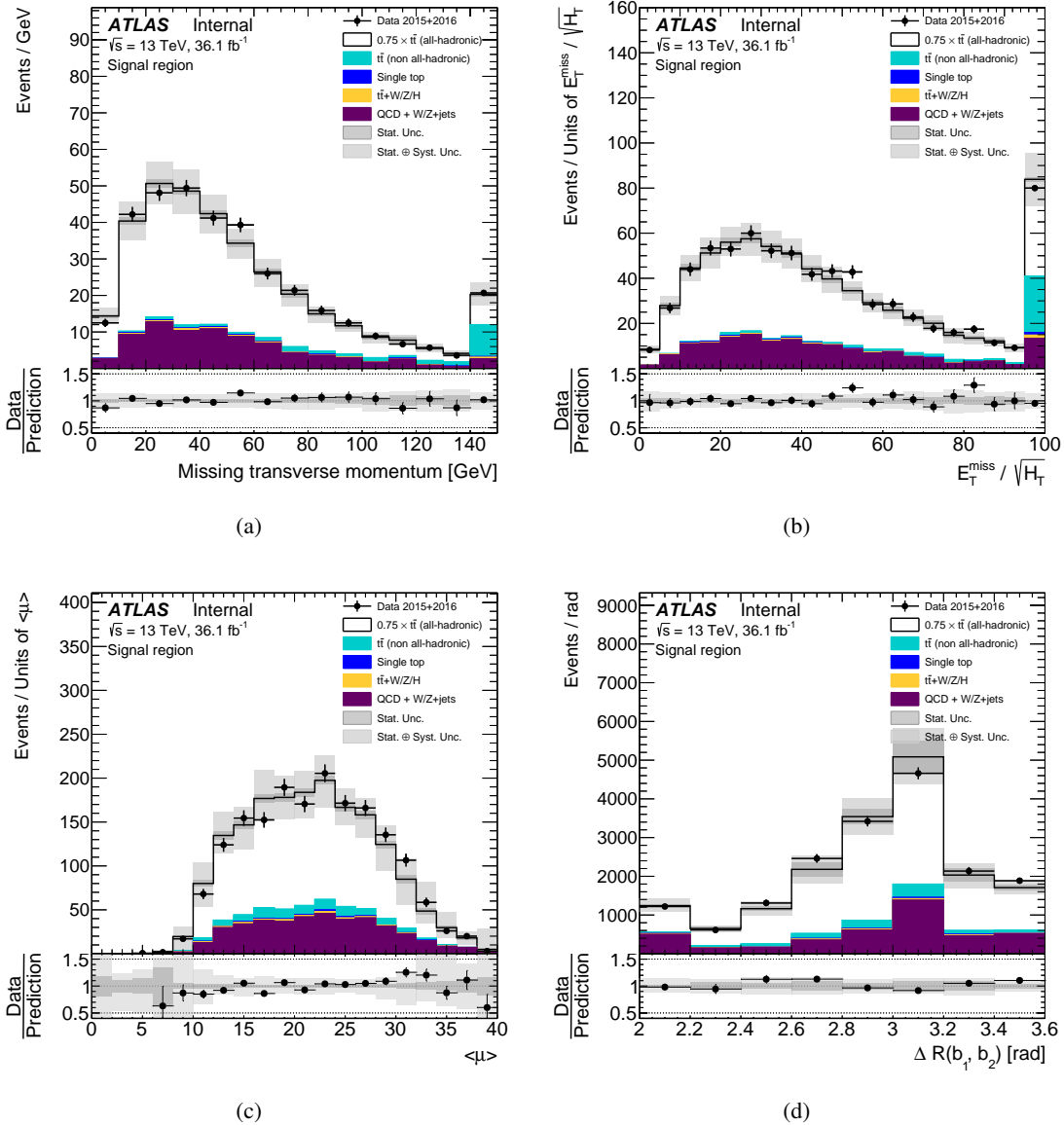


Figure 178: Event-wise variables in the signal region (S): (a) E_T^{miss} , (b) E_T^{miss} significance, (c) average number of interactions per bunch crossing ($\langle\mu\rangle$), and (d) ΔR between two b -tagged jets matched to large- R jets. Data distributions are compared to predictions using PowHEG+Pythia8 as the $t\bar{t}$ signal model scaled by a factor 0.75. The hashed area indicates the combined statistical and systematic uncertainties on the total prediction, excluding systematic uncertainties related to the modelling of the $t\bar{t}$ system. N.B. The average number of interactions per bunch in the data has been prescaled by the factor of 1/1.09 and pileup reweighting has been done to propagate any pileup-dependent effects into the MC event selection.

1484 R. Comparison against different Powheg +Pythia8 tunings

1485 R.1. Initial- and final-state radiation

1486 The unfolded cross-sections are compared against two different initial- and final-state radiation models
 1487 used in the estimation of the IFSR systematic uncertainty. These Powheg +Pythia8 samples have been
 1488 tuned in order to be compatible with data in the low- p_T regime of the $t\bar{t}$ production.

Not reviewed, for internal circulation only

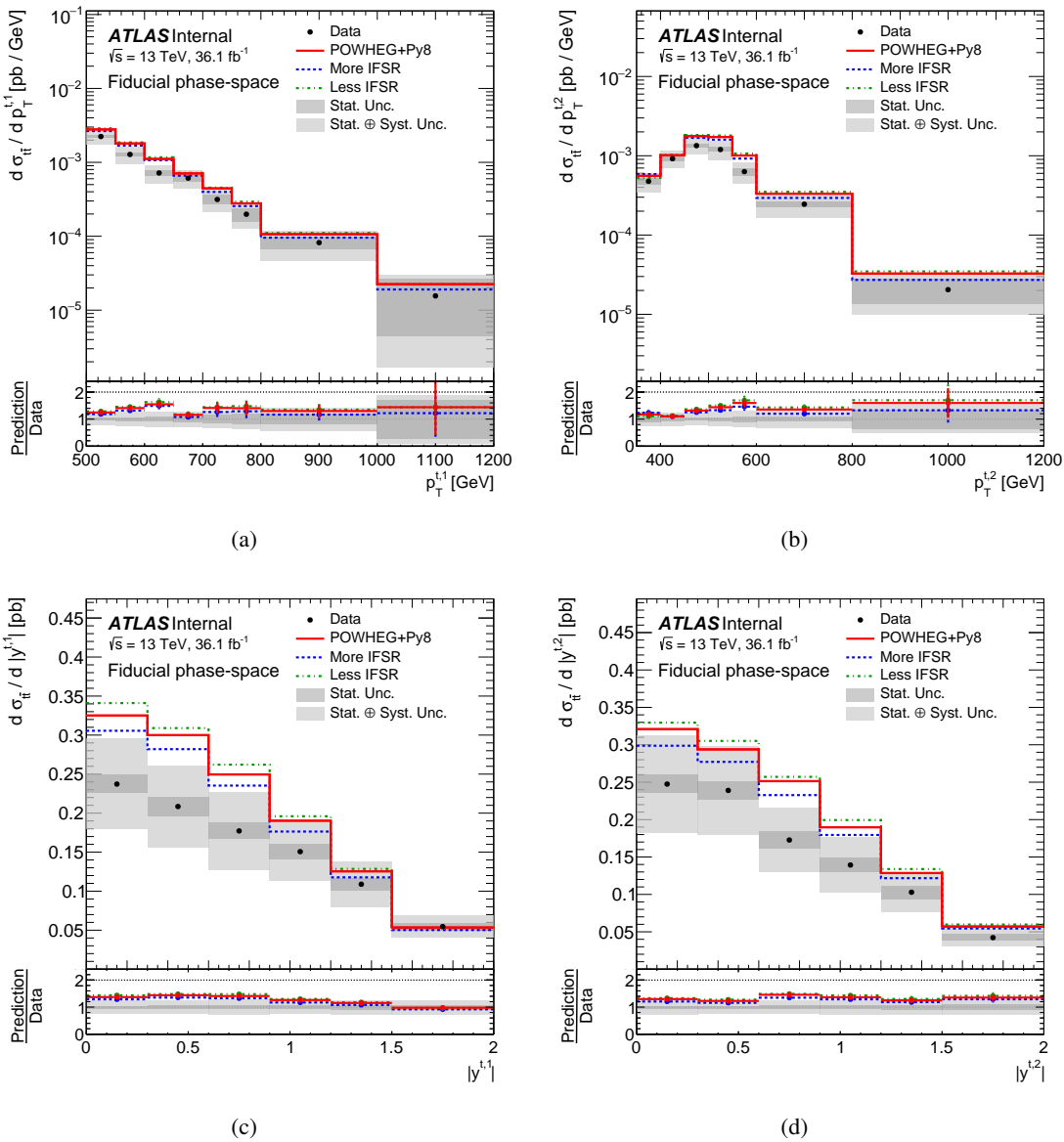


Figure 179: Fiducial phase-space absolute differential cross-sections as a function of (a) transverse momentum and (c) absolute value of the rapidity of the leading top-quark, and (b) transverse momentum and (d) absolute value of the rapidity of the second-leading top-quark. The gray bands indicate the total uncertainty on the data in each bin. The Powheg+Pythia8 generator is used as the nominal prediction to correct for detector effects.

Not reviewed, for internal circulation only

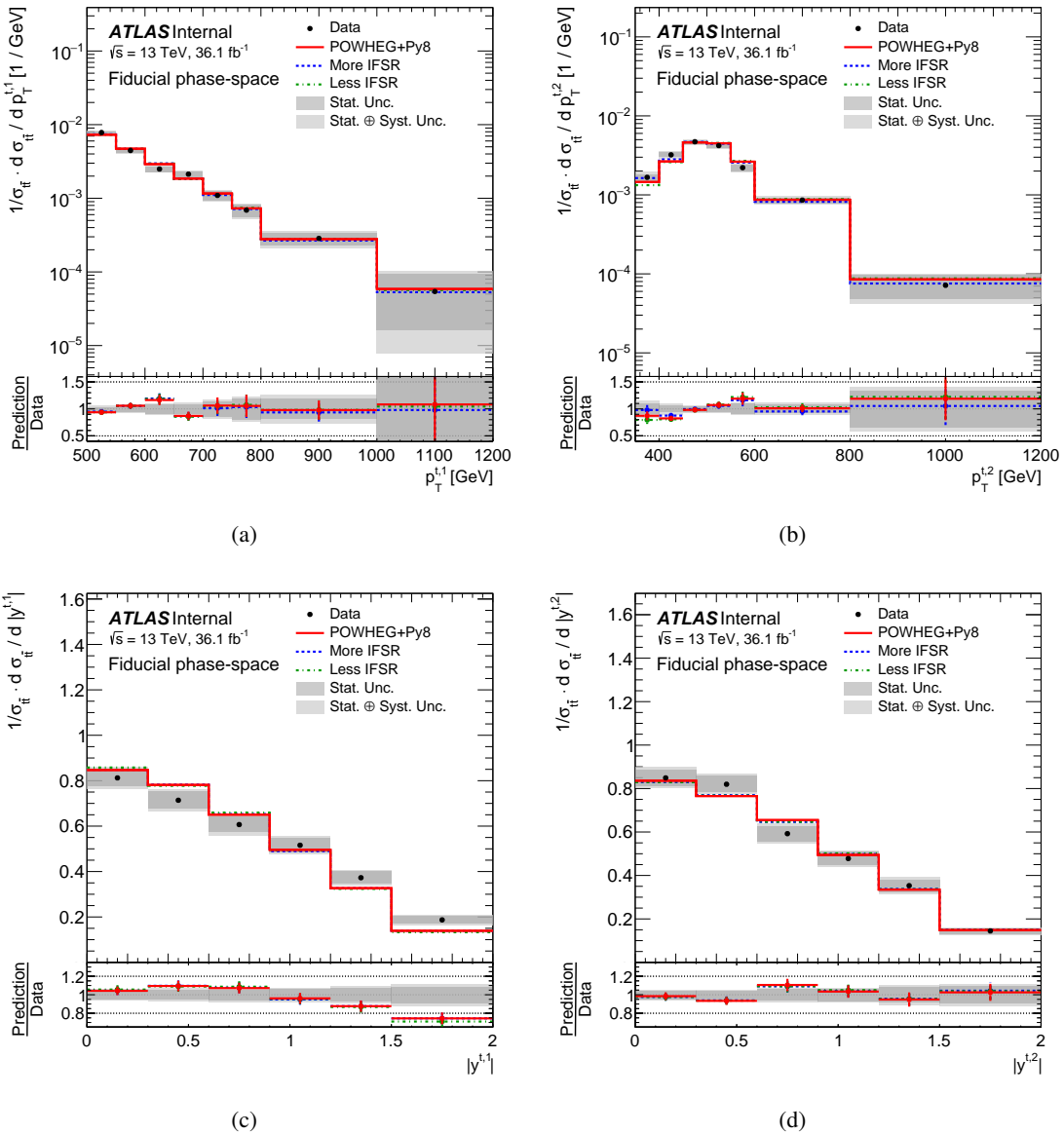


Figure 180: Fiducial phase-space normalized differential cross-sections as a function of (a) transverse momentum and (c) absolute value of the rapidity of the leading top-quark, and (b) transverse momentum and (d) absolute value of the rapidity of the second-leading top-quark. The gray bands indicate the total uncertainty on the data in each bin. The Powheg+Pythia8 generator is used as the nominal prediction to correct for detector effects.

Not reviewed, for internal circulation only

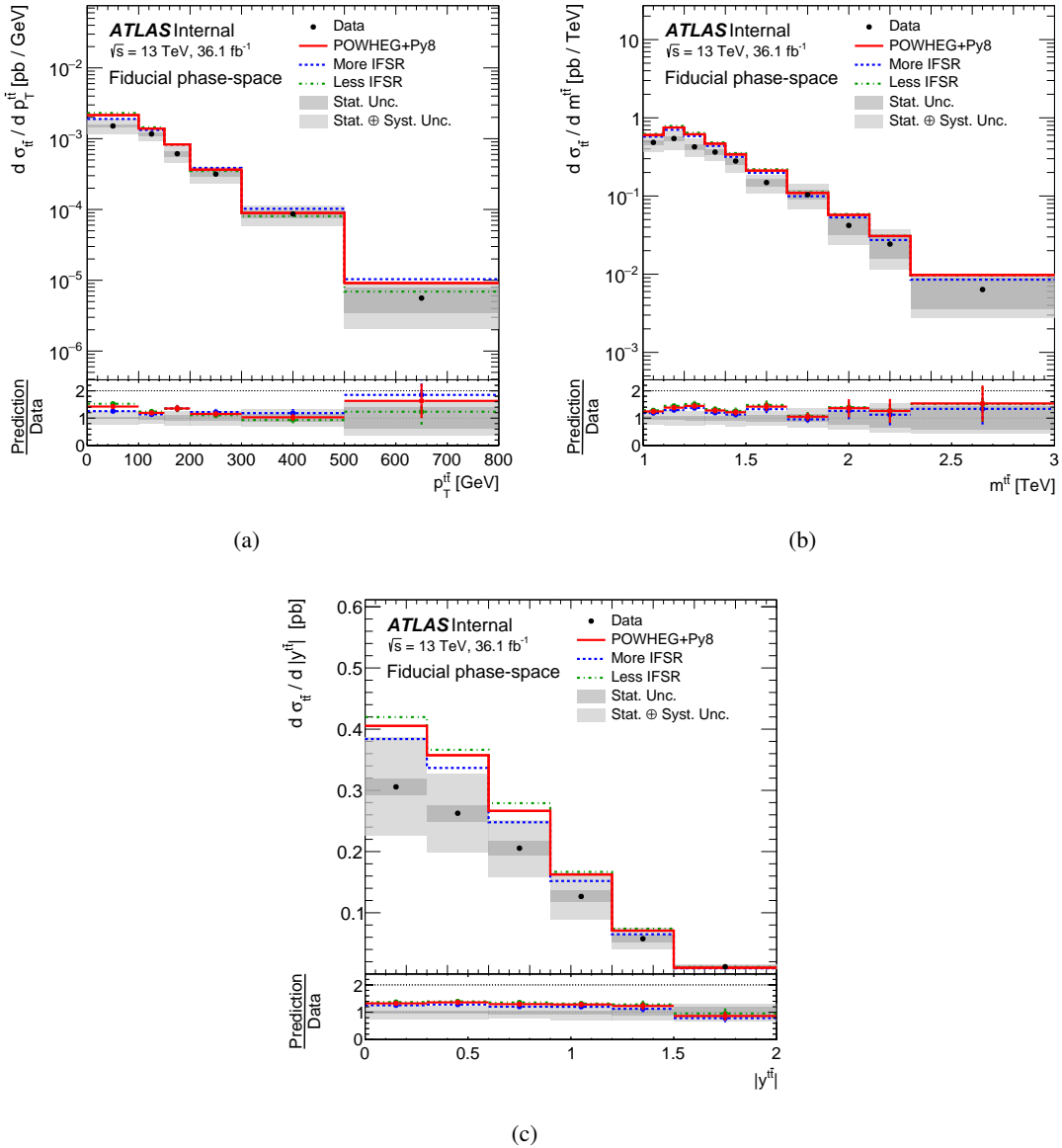


Figure 181: Fiducial phase-space absolute differential cross-sections as a function of (a) transverse momentum, (b) invariant mass and (c) absolute value of the rapidity of the $t\bar{t}$ system. The gray bands indicate the total uncertainty on the data in each bin. The Powheg+Pythia8 generator is used as the nominal prediction to correct for detector effects.

Not reviewed, for internal circulation only

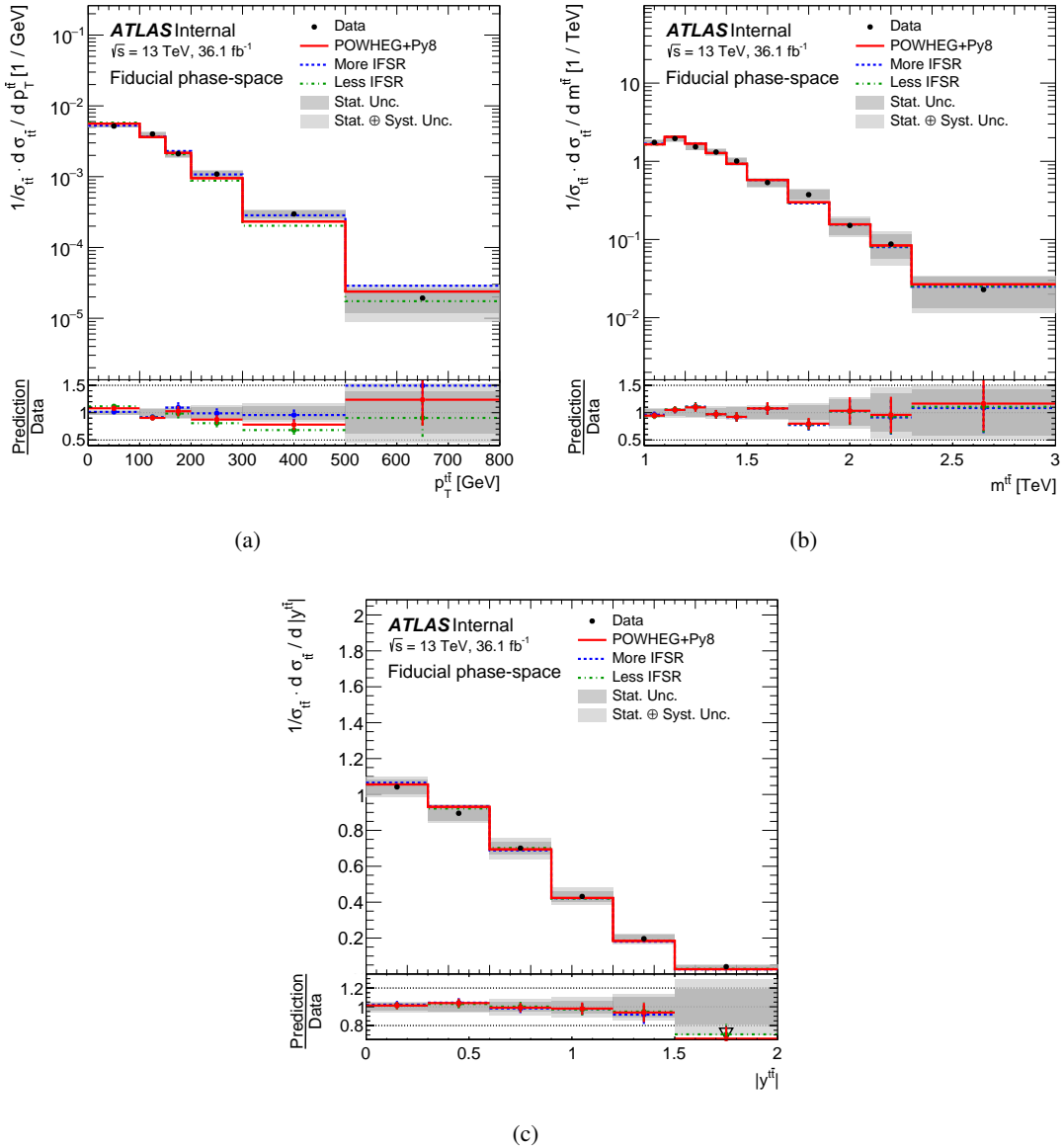


Figure 182: Fiducial phase-space normalized differential cross-sections as a function of (a) transverse momentum, (b) invariant mass and (c) absolute value of the rapidity of the $t\bar{t}$ system. The gray bands indicate the total uncertainty on the data in each bin. The Powheg+Pythia8 generator is used as the nominal prediction to correct for detector effects.

Not reviewed, for internal circulation only

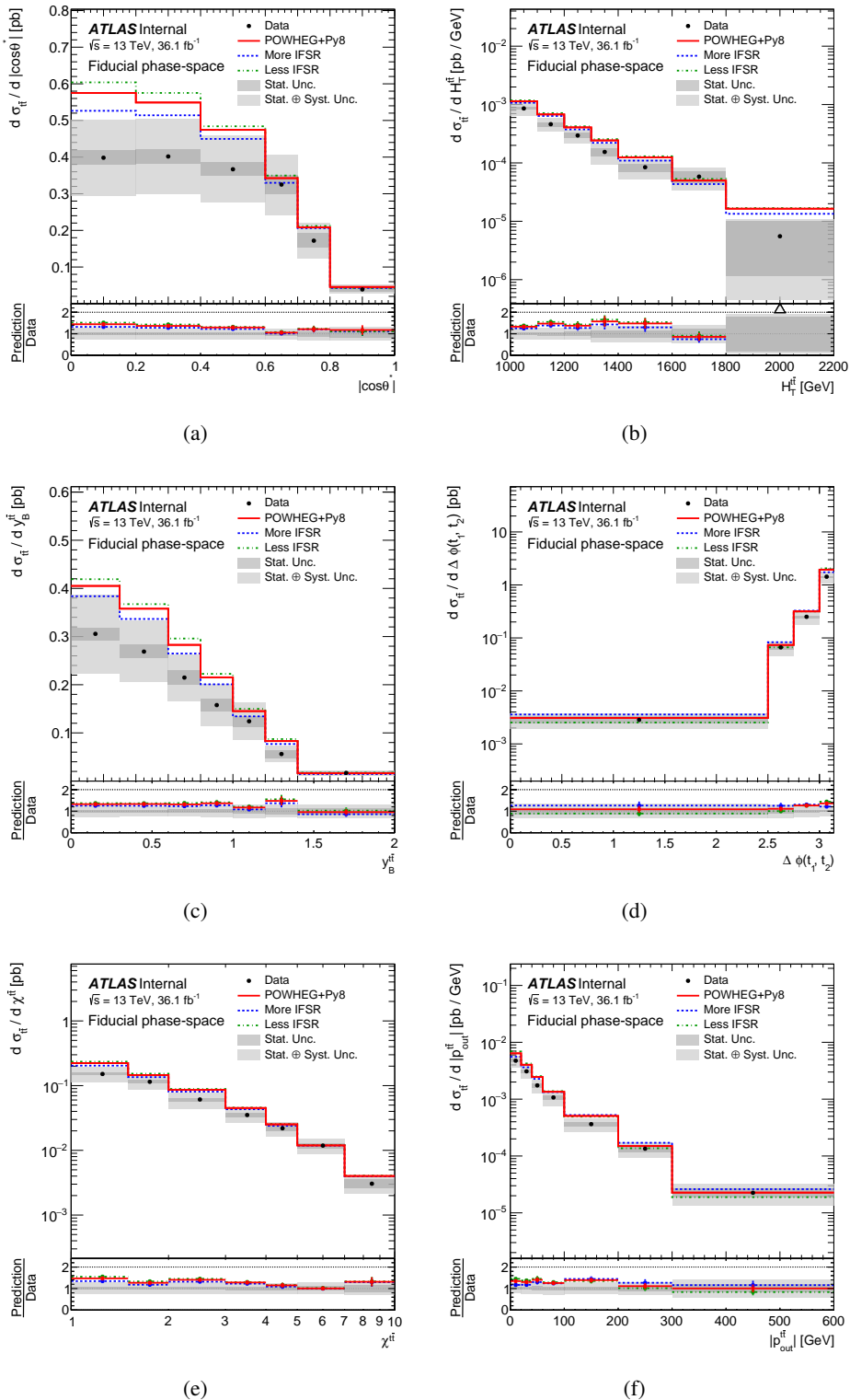


Figure 183: Fiducial phase-space absolute differential cross-sections as a function of (a) production angle in the Collins-Soper reference frame, (b) scalar sum of the two top-quarks' transverse momenta, (c) longitudinal boost $y_B^{\bar{t}\bar{t}}$, (d) azimuthal angle between the two top-quarks $\Delta\phi_{t\bar{t}}$, (e) production angle $\chi^{\bar{t}\bar{t}}$ and (f) absolute value of the out-of-plane momentum $p_{\text{out}}^{\bar{t}\bar{t}}$. The gray bands indicate the total uncertainty on the data in each bin. The Powheg+Pythia8 generator is used as the nominal prediction to correct for detector effects.

Not reviewed, for internal circulation only

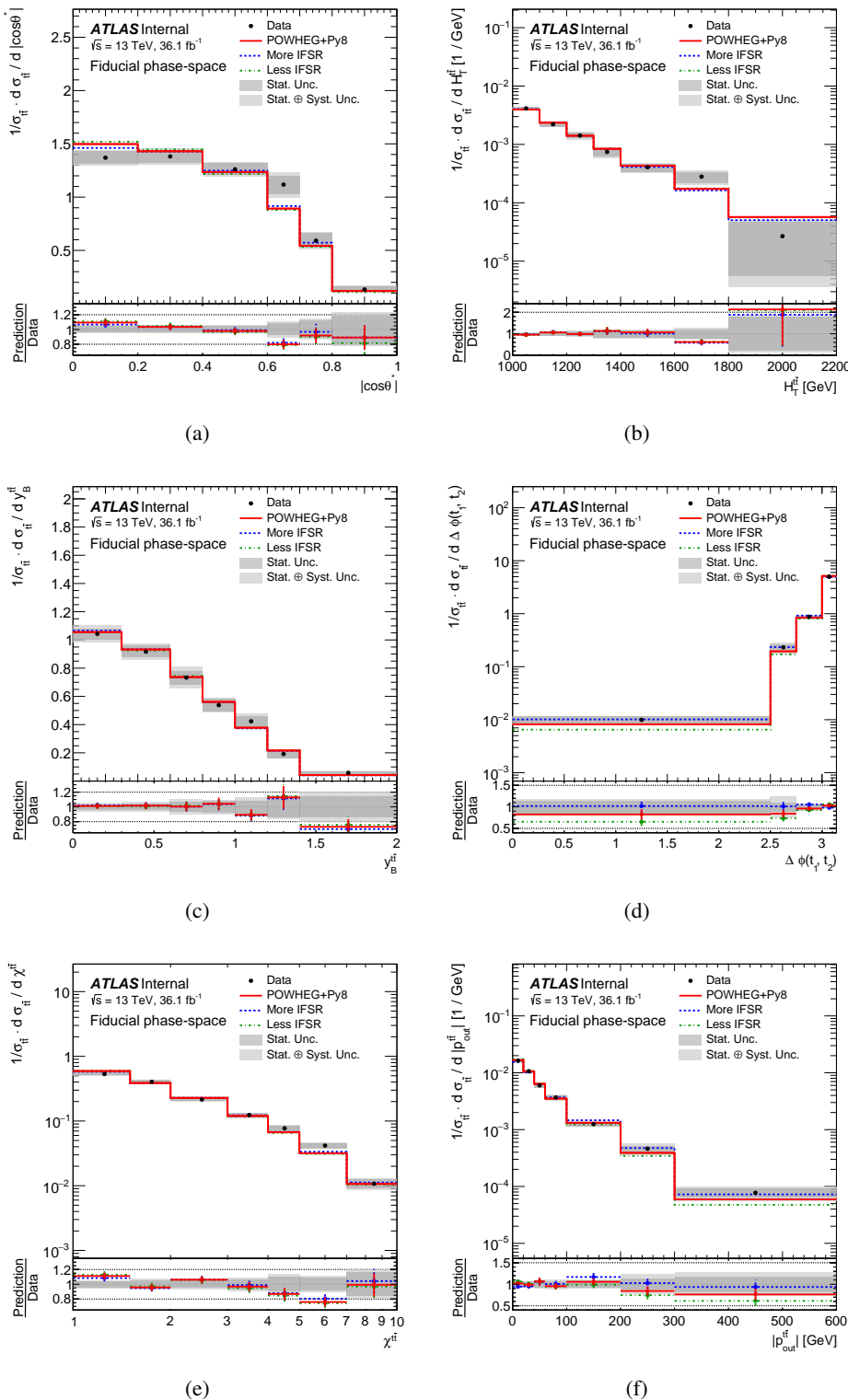


Figure 184: Fiducial phase-space normalized differential cross-sections as a function of (a) production angle in the Collins-Soper reference frame, (b) scalar sum of the two top-quarks' transverse momenta, (c) longitudinal boost $y_B^{t\bar{t}}$, (d) azimuthal angle between the two top-quarks $\Delta\phi_{t\bar{t}}$, (e) production angle $\chi^{t\bar{t}}$ and (f) absolute value of the out-of-plane momentum $p_{out}^{t\bar{t}}$. The gray bands indicate the total uncertainty on the data in each bin. The Powheg+Pythia8 generator is used as the nominal prediction to correct for detector effects.

1489 R.1.1. Parton level comparison

Not reviewed, for internal circulation only

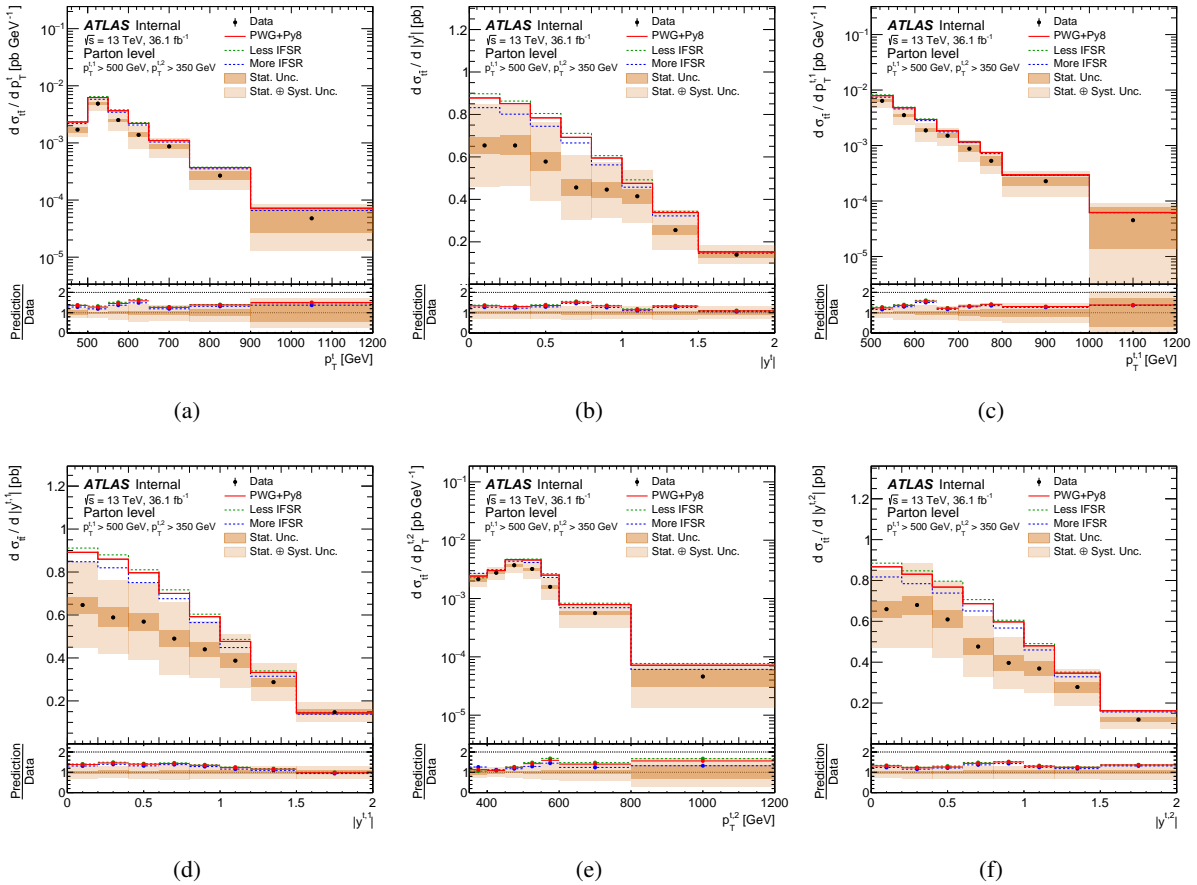


Figure 185: The unfolded parton-level absolute differential cross-sections are shown for (a) the transverse momentum of the top quark, (b) the absolute value of the rapidity of the top quark, (c) the transverse momentum of the leading top quark, (d) the absolute value of the rapidity of the leading top quark, (e) the transverse momentum of the subleading top quark, and (f) the the absolute value of the rapidity of the subleading top quark.

Not reviewed, for internal circulation only

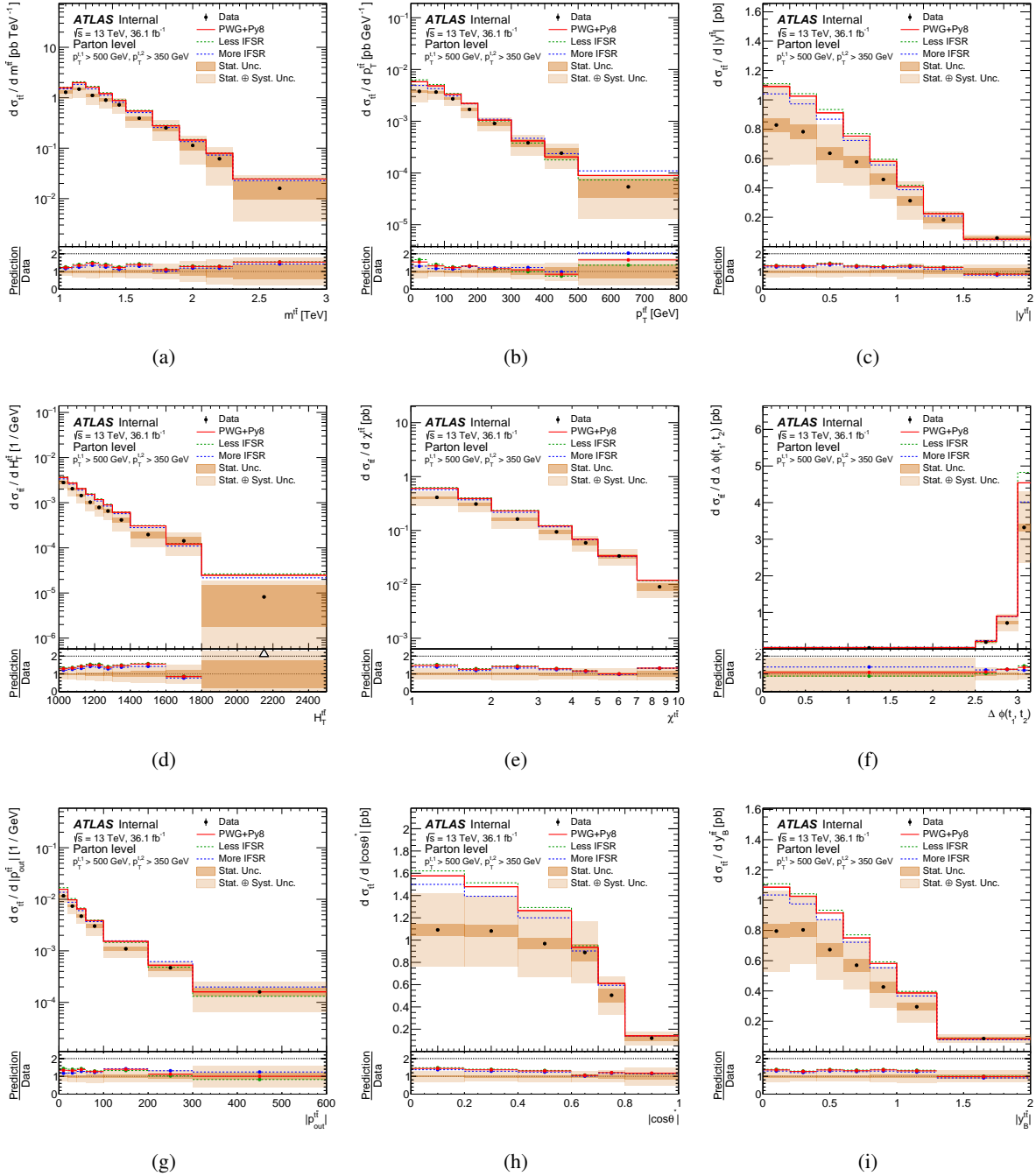


Figure 186: The unfolded parton-level absolute differential cross-sections are shown for (a) the $t\bar{t}$ invariant mass, (b) the $t\bar{t}$ p_T , (c) the absolute value of $t\bar{t}$ rapidity, (d) the $H^{t\bar{t}}$, (e) $\chi^{t\bar{t}}$, and (f) the $\Delta\phi(t_1, t_2)$, (g) the $p_{t\bar{t}}^{\text{out}}$, (h) the $\cos\theta^*$, and (i) the $y_B^{t\bar{t}}$.

Not reviewed, for internal circulation only

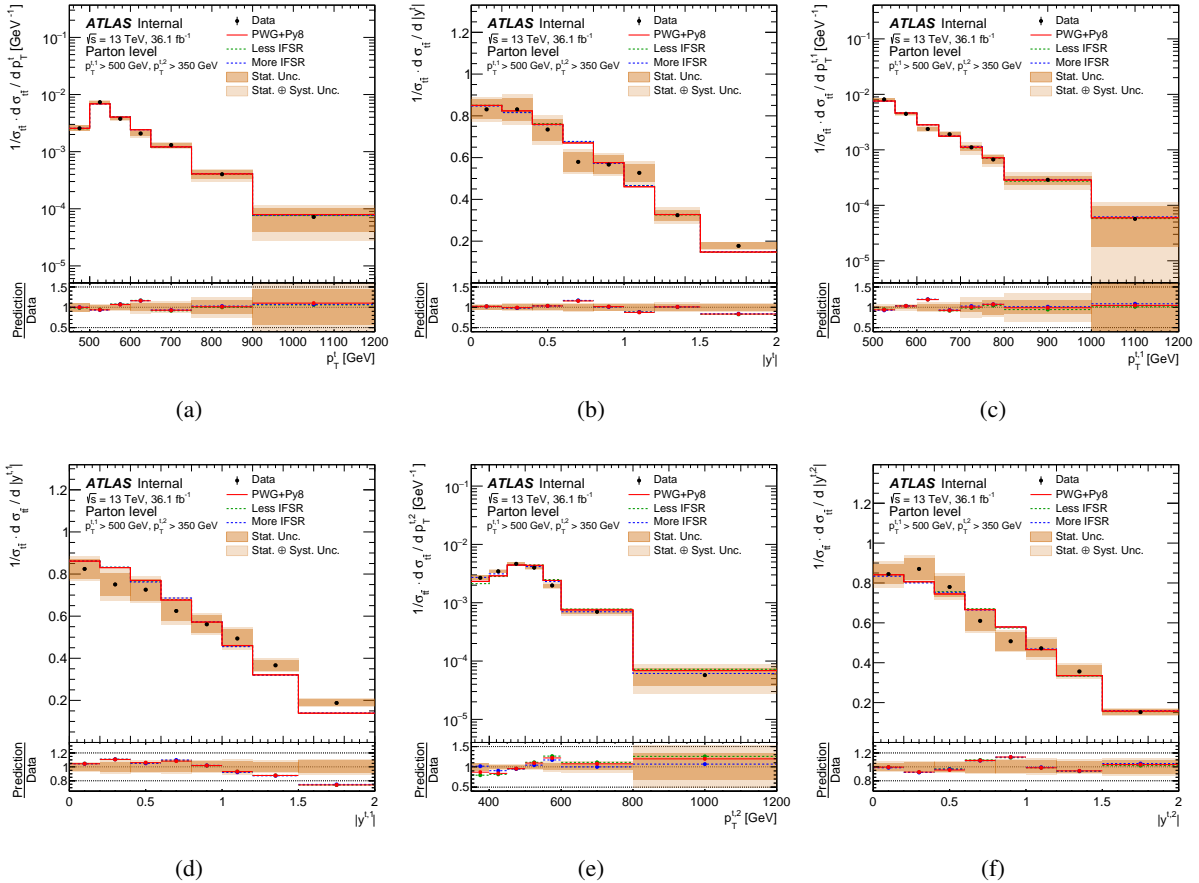


Figure 187: The unfolded parton-level relative differential cross-sections are shown for (a) the transverse momentum of the top quark, (b) the relolute value of the rapidity of the top quark, (c) the transverse momentum of the leading top quark, (d) the relolute value of the rapidity of the leading top quark, (e) the transverse momentum of the subleading top quark, and (f) the the relolute value of the rapidity of the subleading top quark.

Not reviewed, for internal circulation only

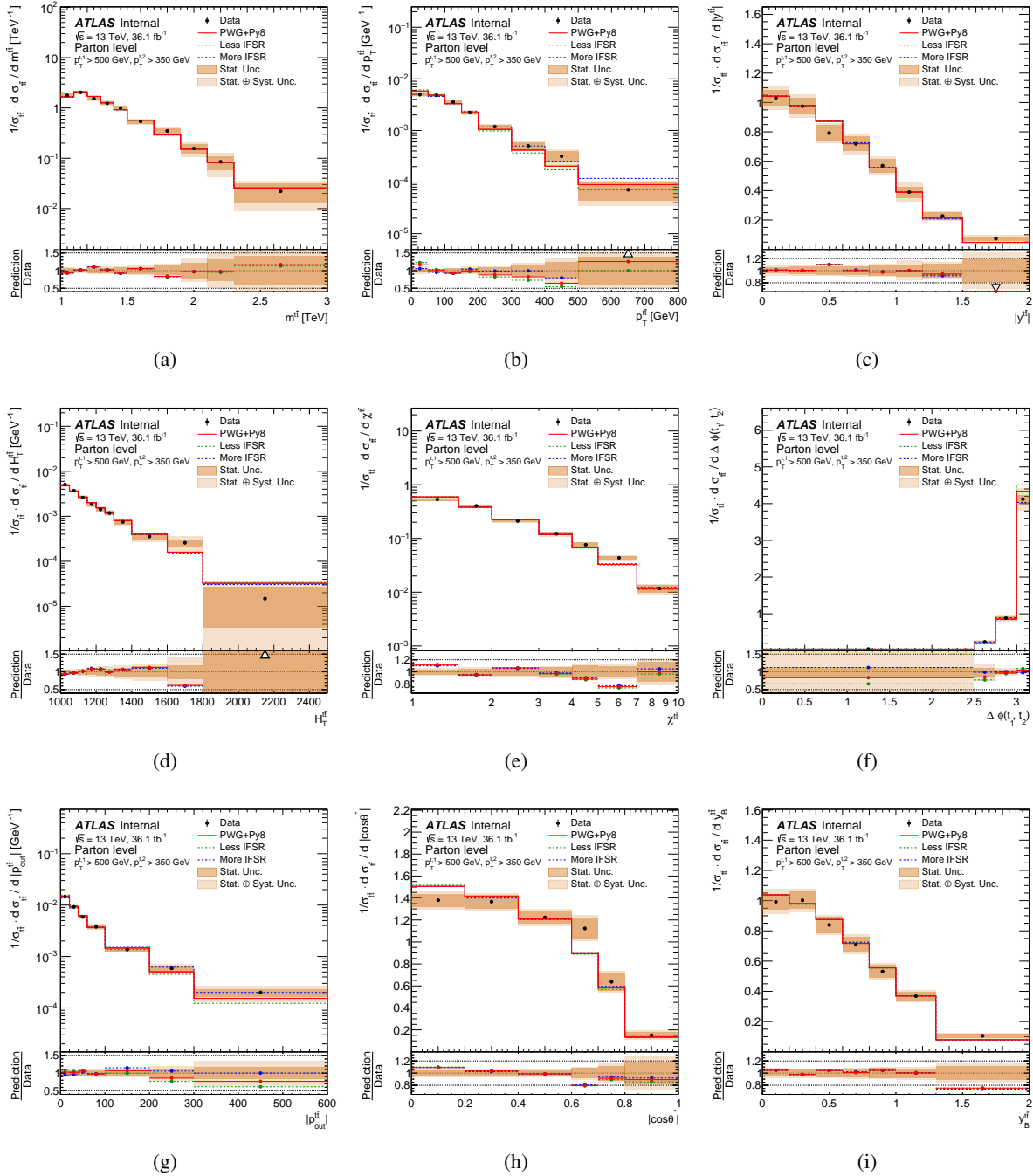


Figure 188: The unfolded parton-level relative differential cross-sections are shown for (a) the $t\bar{t}$ invariant mass, (b) the $t\bar{t}$ p_T , (c) the absolute value of $t\bar{t}$ rapidity, (d) the $H^{t\bar{t}}$, (e) $\chi^{t\bar{t}}$, and (f) the $\Delta\phi(t_1, t_2)$, (g) the $p_{\text{out}}^{t\bar{t}}$, (h) the $\cos\theta^*$, and (i) the $y_B^{t\bar{t}}$.

1490 R.2. Parton distribution functions

1491 The unfolded cross-sections are compared against the nominal Powheg +Pythia8 sample, reweighted
 1492 using different parton distribution functions. The PDF sets under consideration are: NNPDF 3.0 NLO
 1493 (nominal) [56], MMTH2014 [57], CT14 [58], PDF4LHC15 [59]. The difference between the nominal
 1494 and alternative samples is too small to discriminate among different PDF sets.

Not reviewed, for internal circulation only

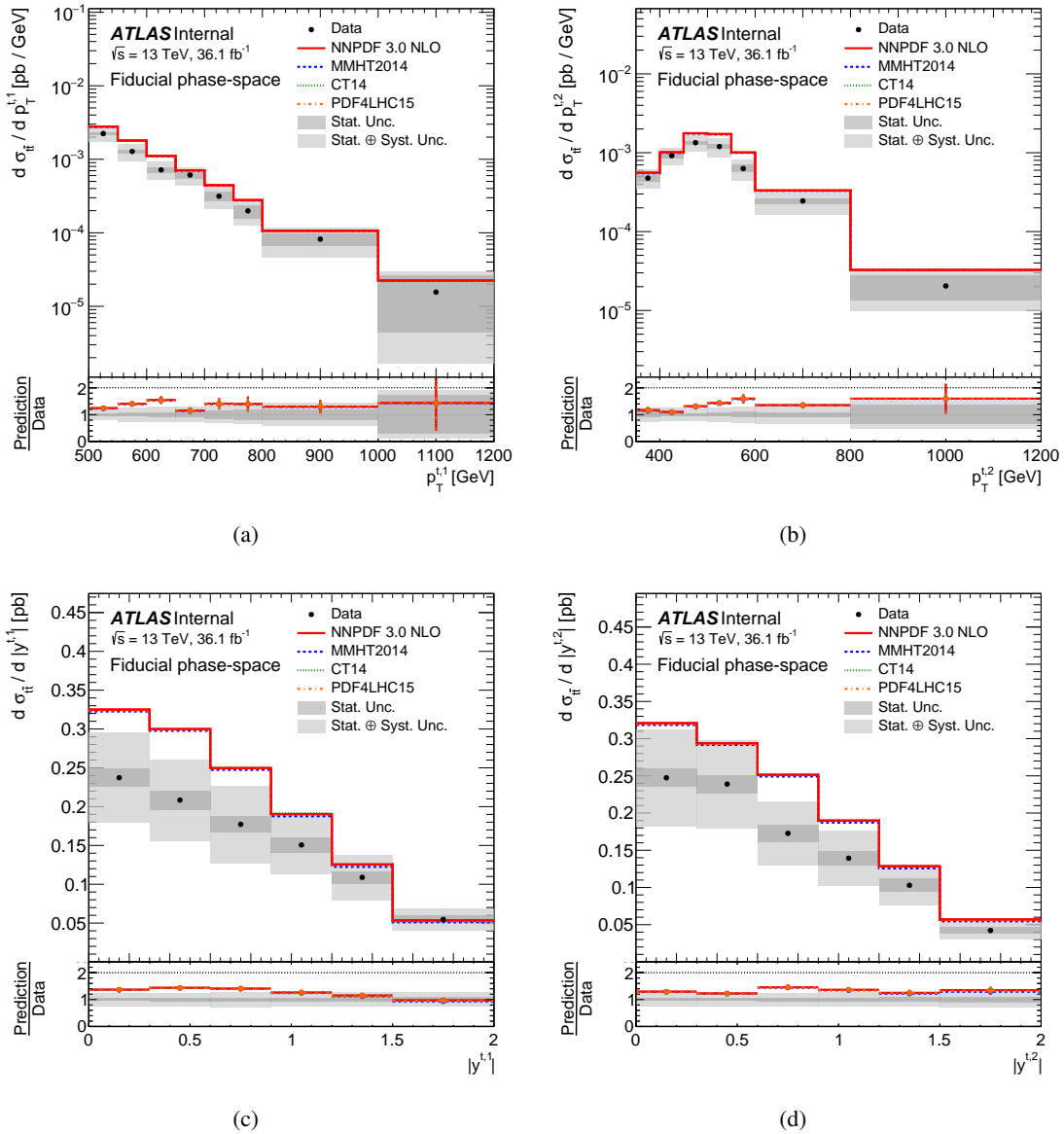


Figure 189: Fiducial phase-space absolute differential cross-sections as a function of (a) transverse momentum and (c) absolute value of the rapidity of the leading top-quark, and (b) transverse momentum and (d) absolute value of the rapidity of the second-leading top-quark. The gray bands indicate the total uncertainty on the data in each bin. The Powheg+Pythia8 generator is used as the nominal prediction to correct for detector effects.

Not reviewed, for internal circulation only

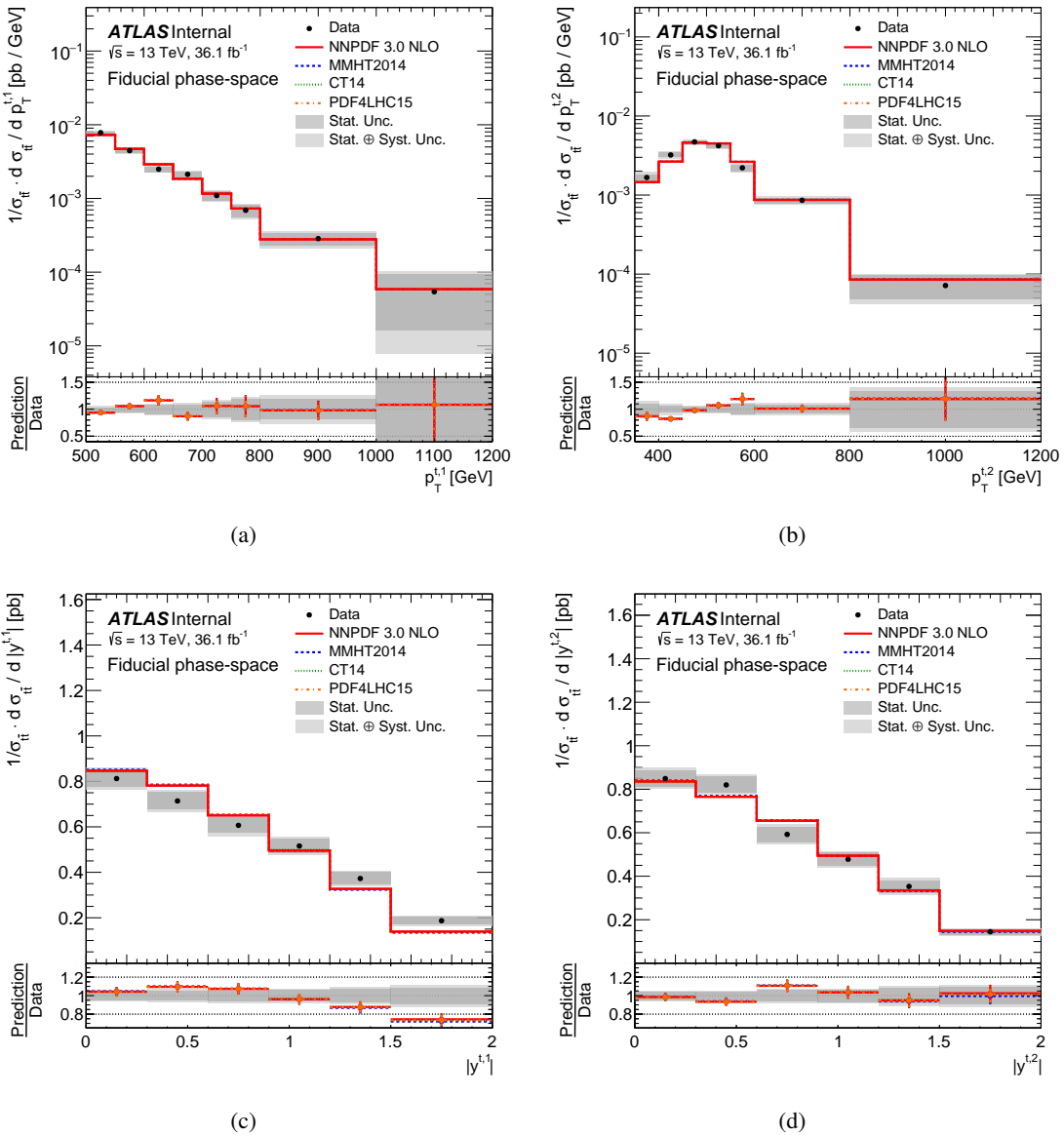


Figure 190: Fiducial phase-space normalized differential cross-sections as a function of (a) transverse momentum and (c) absolute value of the rapidity of the leading top-quark, and (b) transverse momentum and (d) absolute value of the rapidity of the second-leading top-quark. The gray bands indicate the total uncertainty on the data in each bin. The Powheg+Pythia8 generator is used as the nominal prediction to correct for detector effects.

Not reviewed, for internal circulation only

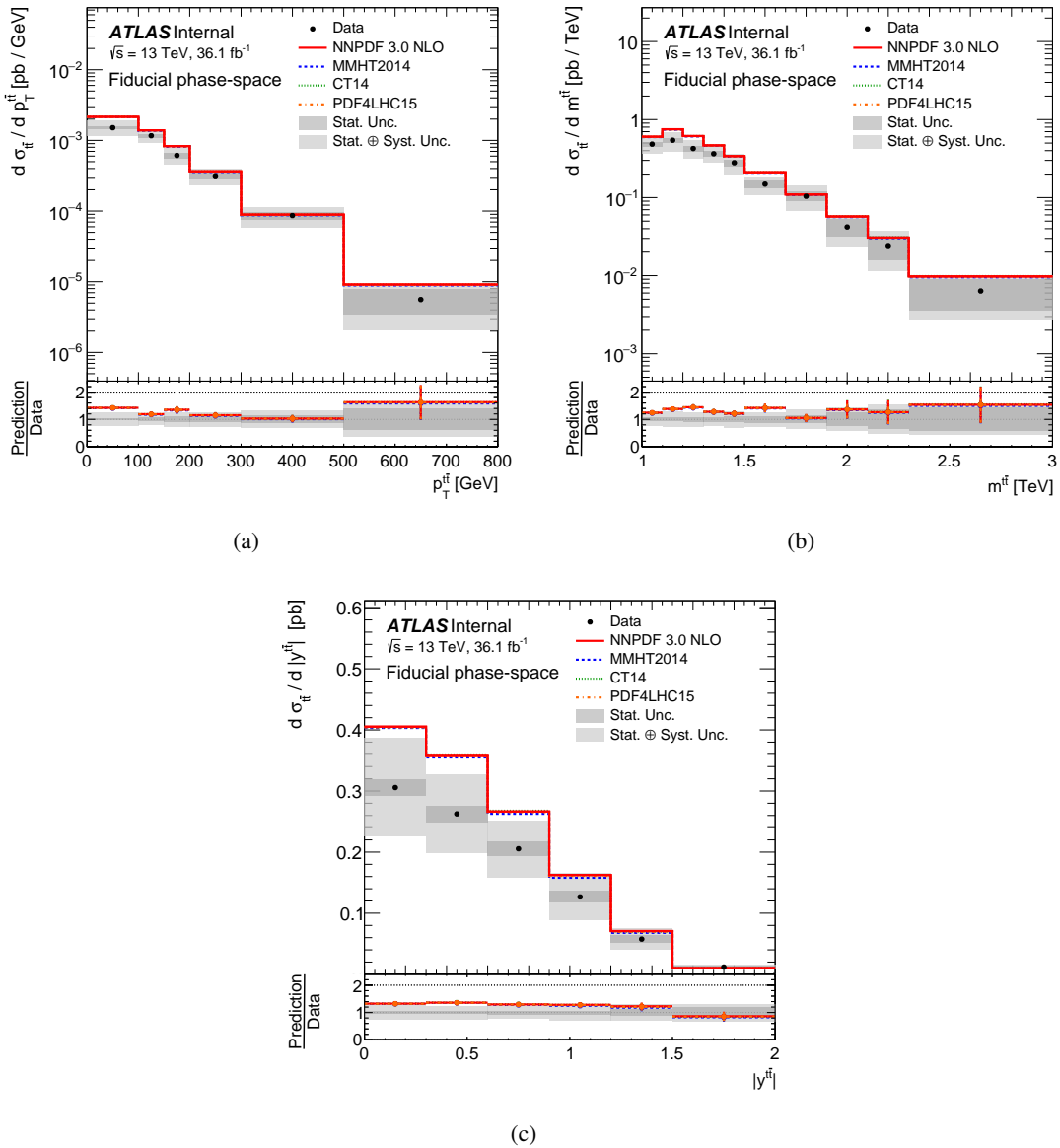


Figure 191: Fiducial phase-space absolute differential cross-sections as a function of (a) transverse momentum, (b) invariant mass and (c) absolute value of the rapidity of the $t\bar{t}$ system. The gray bands indicate the total uncertainty on the data in each bin. The PowHEG+PYTHIA8 generator is used as the nominal prediction to correct for detector effects.

Not reviewed, for internal circulation only

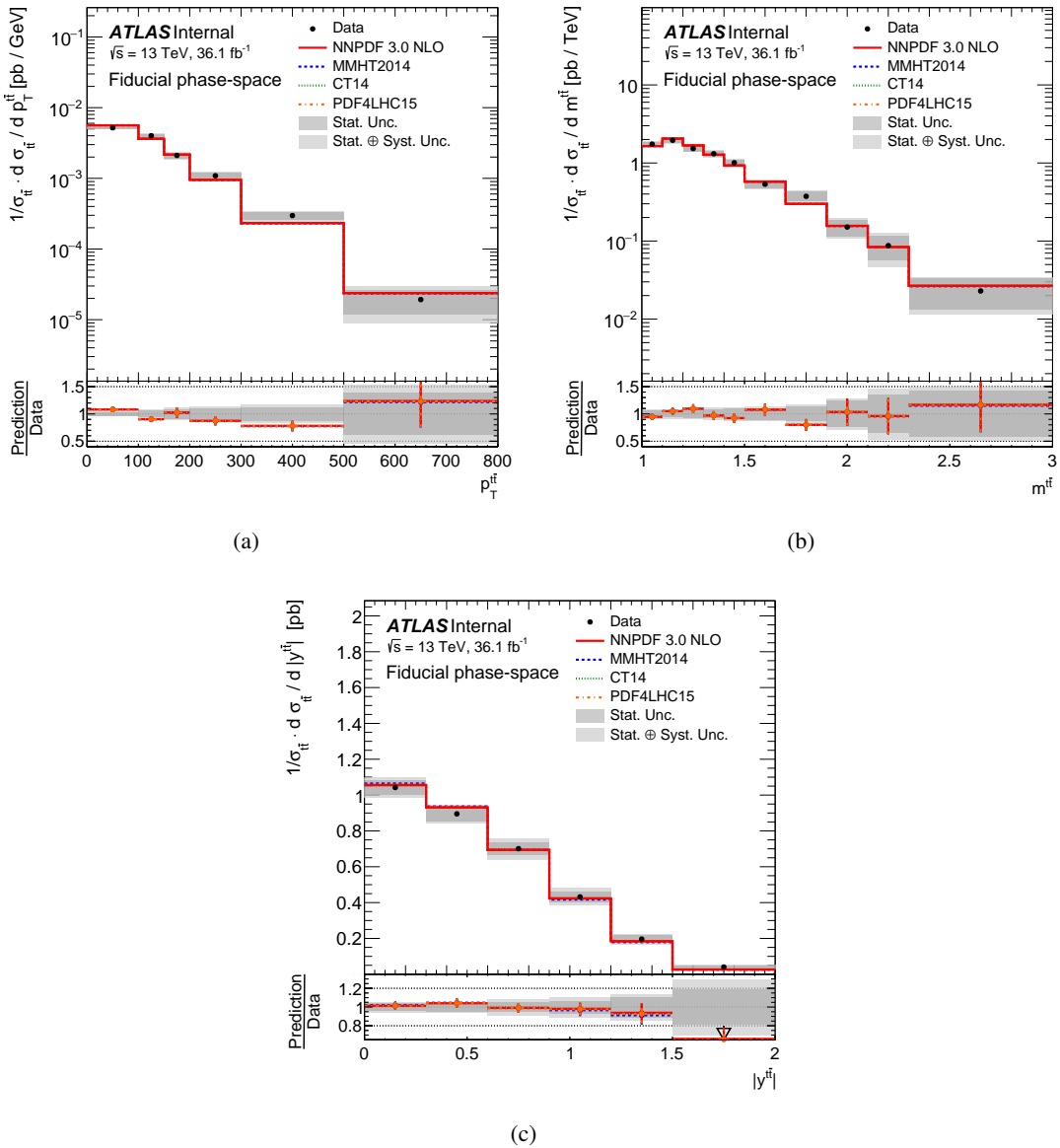


Figure 192: Fiducial phase-space normalized differential cross-sections as a function of (a) transverse momentum, (b) invariant mass and (c) absolute value of the rapidity of the $t\bar{t}$ system. The gray bands indicate the total uncertainty on the data in each bin. The Powheg+Pythia8 generator is used as the nominal prediction to correct for detector effects.

Not reviewed, for internal circulation only

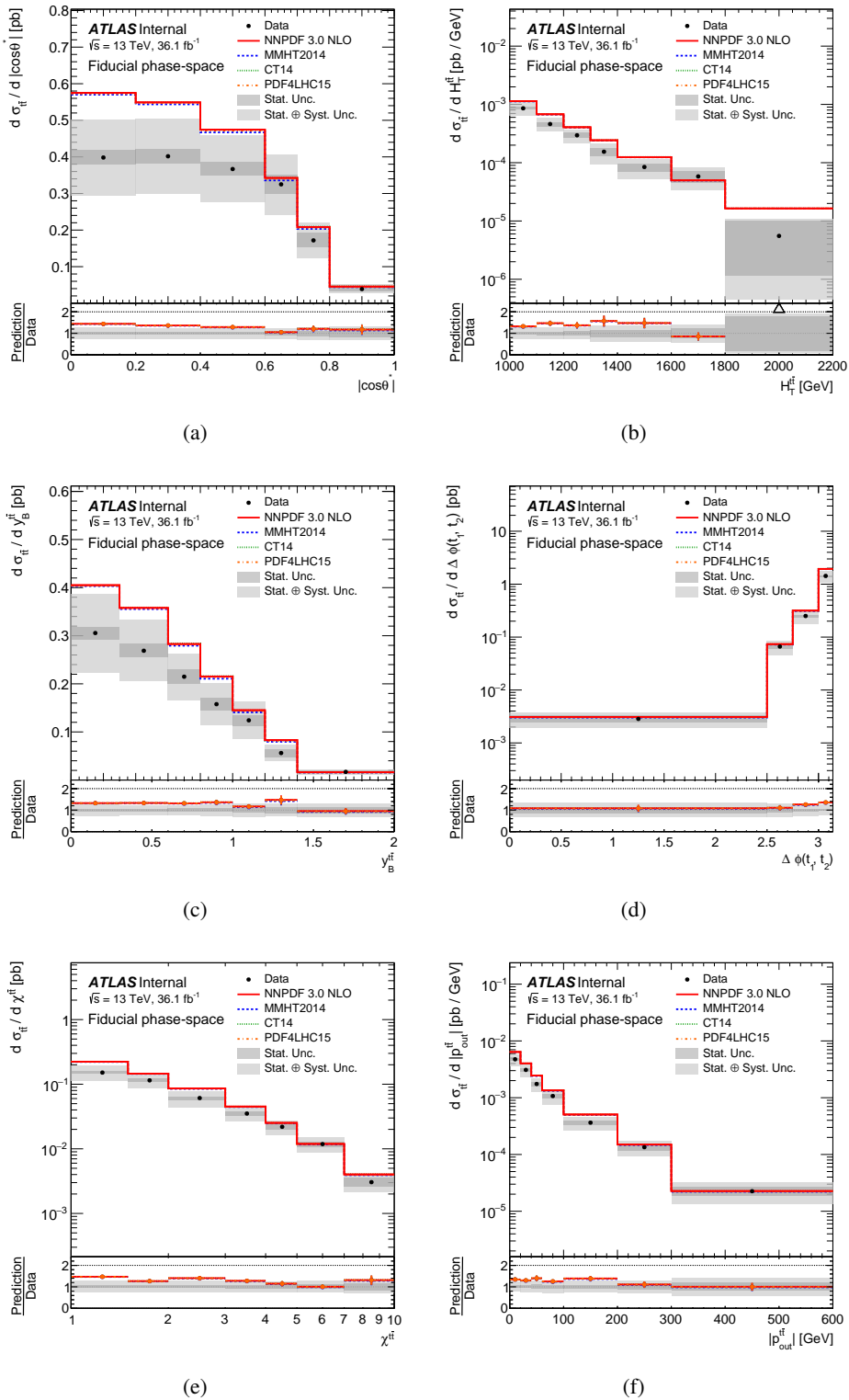


Figure 193: Fiducial phase-space absolute differential cross-sections as a function of (a) production angle in the Collins-Soper reference frame, (b) scalar sum of the two top-quarks' transverse momenta, (c) longitudinal boost $y_B^{t\bar{t}}$, (d) azimuthal angle between the two top-quarks $\Delta\phi_{t\bar{t}}$, (e) production angle $\chi^{t\bar{t}}$ and (f) absolute value of the out-of-plane momentum $p_{out}^{t\bar{t}}$. The gray bands indicate the total uncertainty on the data in each bin. The PowHEG+PYTHIA8 generator is used as the nominal prediction to correct for detector effects.

Not reviewed, for internal circulation only

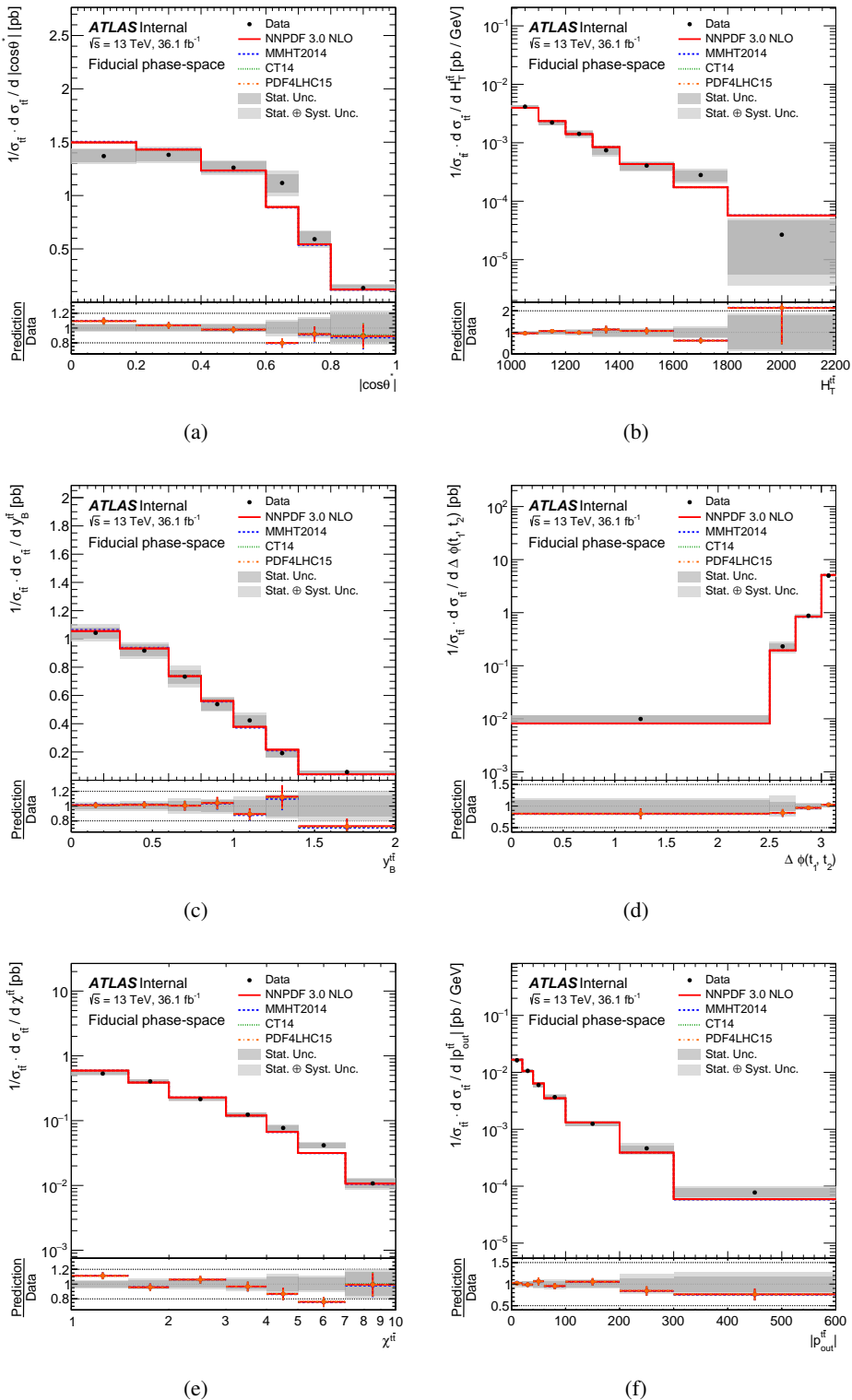


Figure 194: Fiducial phase-space normalized differential cross-sections as a function of (a) production angle in the Collins-Soper reference frame, (b) scalar sum of the two top-quarks' transverse momenta, (c) longitudinal boost $y_B^{\bar{t}t}$, (d) azimuthal angle between the two top-quarks $\Delta\phi_{\bar{t}t}$, (e) production angle $\chi_{\bar{t}t}^f$ and (f) absolute value of the out-of-plane momentum $p_{\text{out}}^{\bar{t}t}$. The gray bands indicate the total uncertainty on the data in each bin. The PowHEG+PYTHIA8 generator is used as the nominal prediction to correct for detector effects.

1495 S. Checks on data yield dependence on data-taking periods

1496 In this appendix, the event yield i.e. the number of events per integrated luminosity was investigated. A
 1497 small drop of the yield by about 6% was observed in the data towards the end of the data-taking period
 1498 in 2016. The reason was investigated by looking at the yield dependence on μ for both the data and
 1499 simulated signal events.

1500 S.1. Data yield vs data set periods

1501 Fig. 195 shows the average number of yields per 1 pb^{-1} as a function of the data taking period: the entire
 1502 2015 period and 2016 period A – L. The yield for 2016 after period E was dropped by about 6% with
 1503 respect to period A - D. In order to identify the cuts causing the drop, the yields were also obtained for
 1504 each step of the cut flow and shown in Fig. 196. The drop was apparent in b-tagging and top-tagging
 1505 steps.

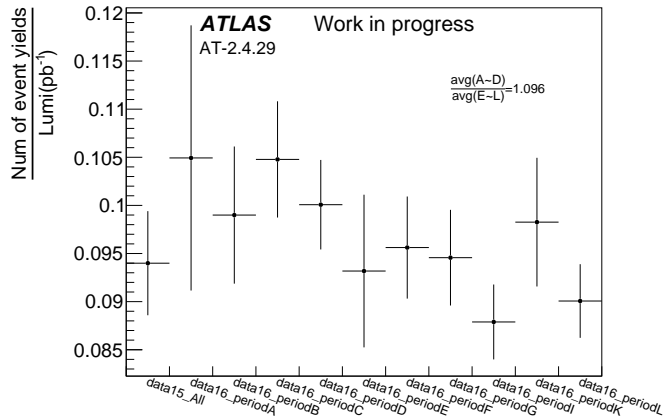


Figure 195: Event yield after the final event selection as a function of data periods for 2015–2016 data.

1506 The drop may come from increased activities caused by pile-up. The luminosity and the μ value were
 1507 increased significantly around the period E. The yields were plotted as a function of μ for both data and
 1508 MC sample Powheg +Pythia8 to see if such effect exists. Fig. 197 shows the ratio, R_b , of events with and
 1509 without the b -matching for the events passing the top jet p_T and mass criteria:

$$R_b = \frac{\text{events passing top-tag and } b\text{-tag criteria}}{\text{events passing top-tag criteria}}$$

1510 To study the pile-up dependence on top taggers, similarly the ratio R_t was calculated, which is the ratio
 1511 with and without top tagging but the b -tag criteria:

$$R_t = \frac{\text{events passing top-tag and } b\text{-tag criteria}}{\text{events passing } b\text{-tag criteria}}$$

1512 and is shown in Fig. 198.

Not reviewed, for internal circulation only

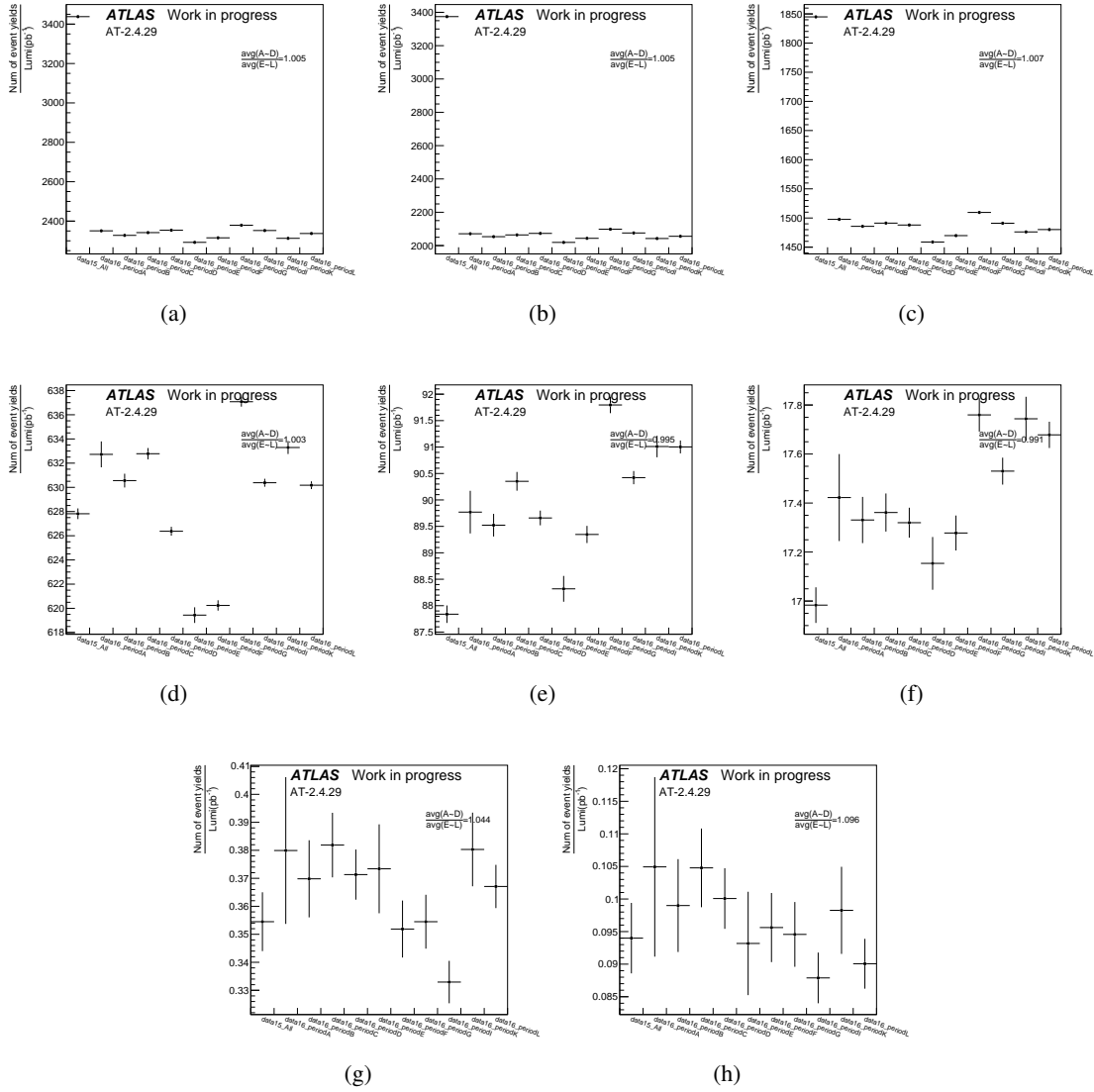


Figure 196: Event yield vs data periods for each step of event selection. **(a)** after preselection. **(b)** after Trigger(2015: HLT_j360_a10r_L1J100, 2016: HLT_j420_a10r_L1J100). **(c)** after selecting two large jets $p_T > 350 \text{ GeV}$. **(d)** after selecting Leading large jets $p_T > 500 \text{ GeV}$. **(e)** after requiring the mass of the Leading large jets within 50 GeV of the top quark mass. **(f)** after requiring the mass of the 2nd Leading large jets within 50 GeV of the top quark mass. **(g)** after requiring both jets to be b -tagged. **(h)** after requiring 2 leading large jets to be top-tagged. Cuts are applied sequentially.

Not reviewed, for internal circulation only

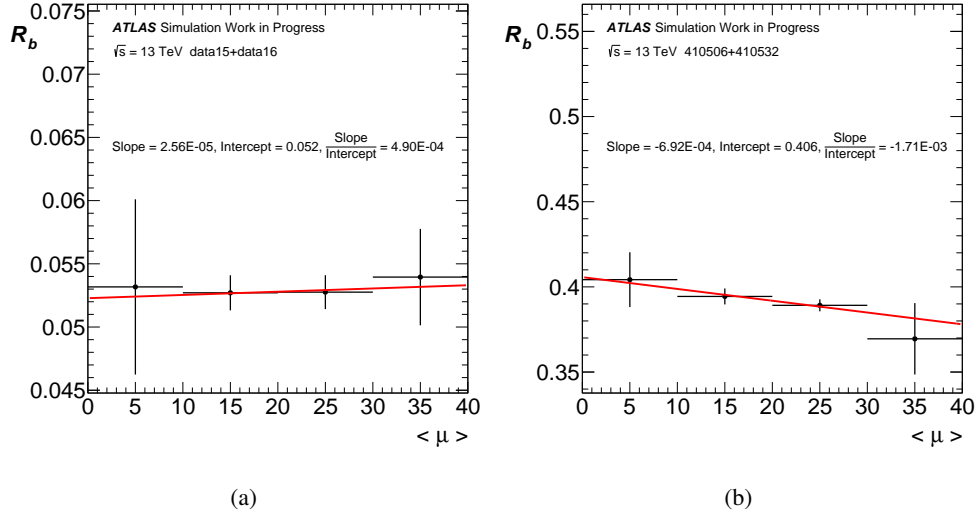


Figure 197: Fraction of events passing the b -tag criteria vs μ . (a) data15+16 (b) POWHEG +PYTHIA8

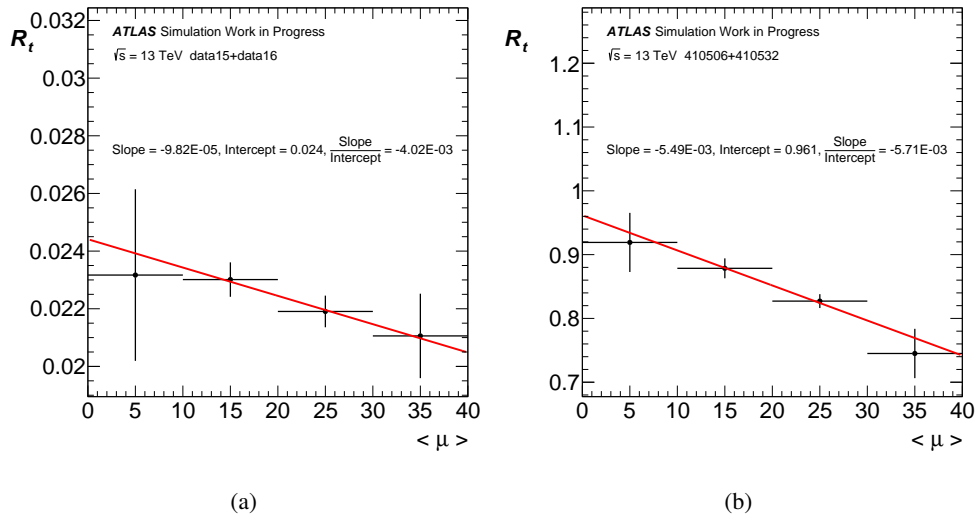


Figure 198: Fraction of events passing the top tagging criteria vs μ . (a) data15+16 (b) POWHEG +PYTHIA8

1513 The same ratio are also calculated for the $t\bar{t}$ MC sample. Since the data contain large fraction of back-
1514 ground from dijets, the value R_b and R_t cannot directly be compared. Instead the slopes in μ are obtained
1515 by fitting the ratio with straight lines for qualitative understanding. Negative slopes are observed in R_t for
1516 both data and MC, while the sign of the R_b slope is positive for the data while it is negative for the MC.
1517 This means that the top tagging algorithm may decrease in its efficiency with increasing event activity,
1518 while there is no clear evidence if the b -tagging efficiency has been decreasing with increasing μ .

Not reviewed, for internal circulation only

T. Comparsion of Powheg +Pythia8 with Powheg +Herwig7

1519 There observed difference that the cross sections for Powheg +Pythia8 was about 25% higher than the
1520 data and also Powheg +Herwig7. This difference was observed after all the detector-level level cuts, while
1521 in validation regions such difference was no prominent. In order to understand this problem, the variables
1522 used in the top selection i.e. τ_{32} and the large jet mass distributions, are studied for these two models in
1523 this section. The study was done by comparing the two models in each step of the event selection.

1524 Figures 199 and 200 show the detector-level distributions for the leading and sub-leading jet respect-
1525 ively. Fig. 201 shows the efficiency and acceptance corrections as a function of the transverse mo-
1526 mentum and absolute value of the rapidity for the leading and sub-leading top-quark candidates. Fi-
1527 nally, Fig. 202 shows a comparison of the unfolded absolute differential cross-sections when using either
1528 Powheg+Pythia8 or Powheg+Herwig7. The difference around 13% in the overall efficiency correction
1529 results in a slightly higher inclusive cross-section when using Powheg+Herwig7, which improves the
1530 agreement between the Monte Carlo predictions and the unfolded data.
1531

Not reviewed, for internal circulation only

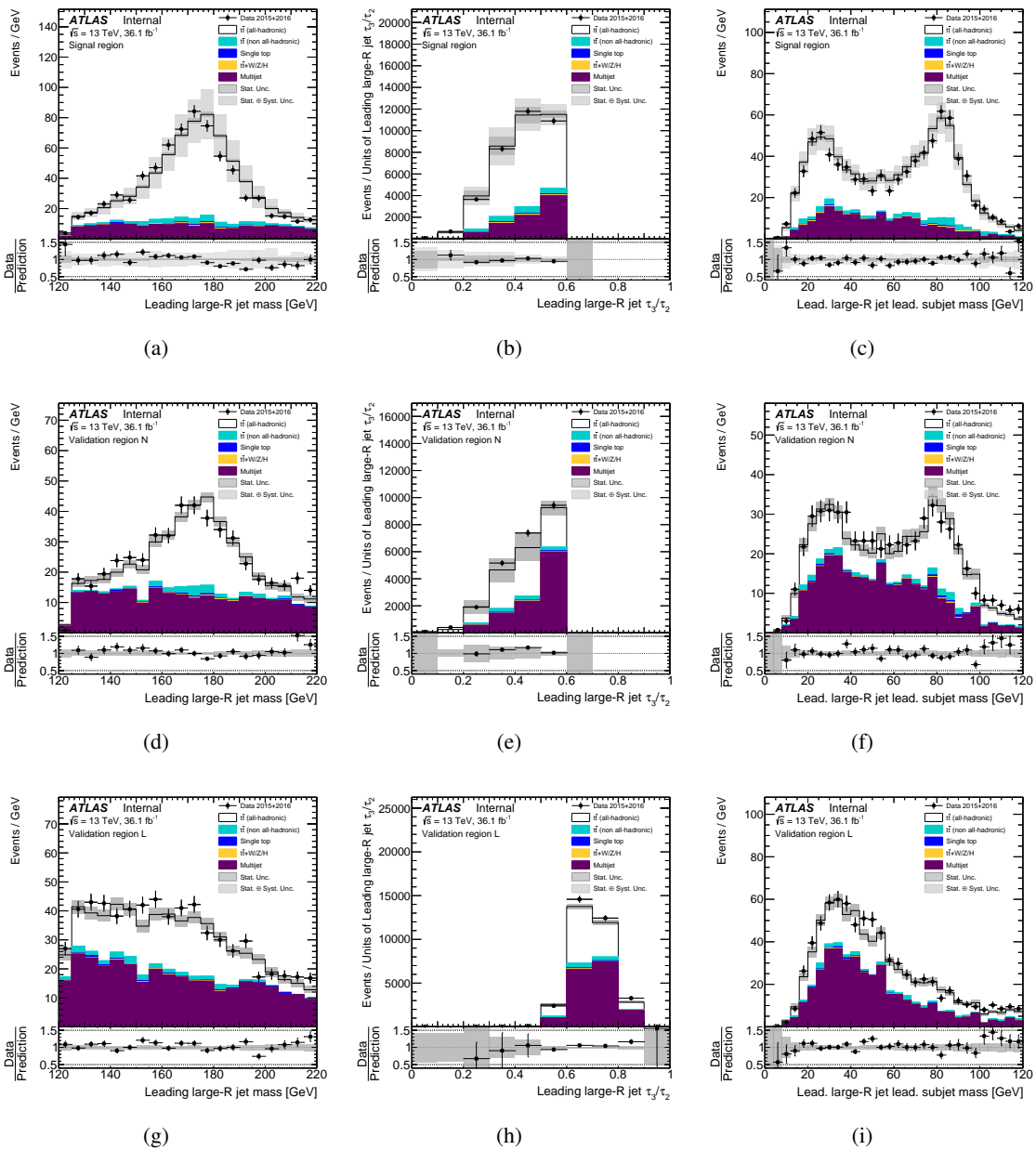


Figure 199: Kinematic distributions of large- R jets in the signal and control regions N and L: mass, 3/2-subjettiness ratio and leading subjet mass of the leading jet.

Not reviewed, for internal circulation only

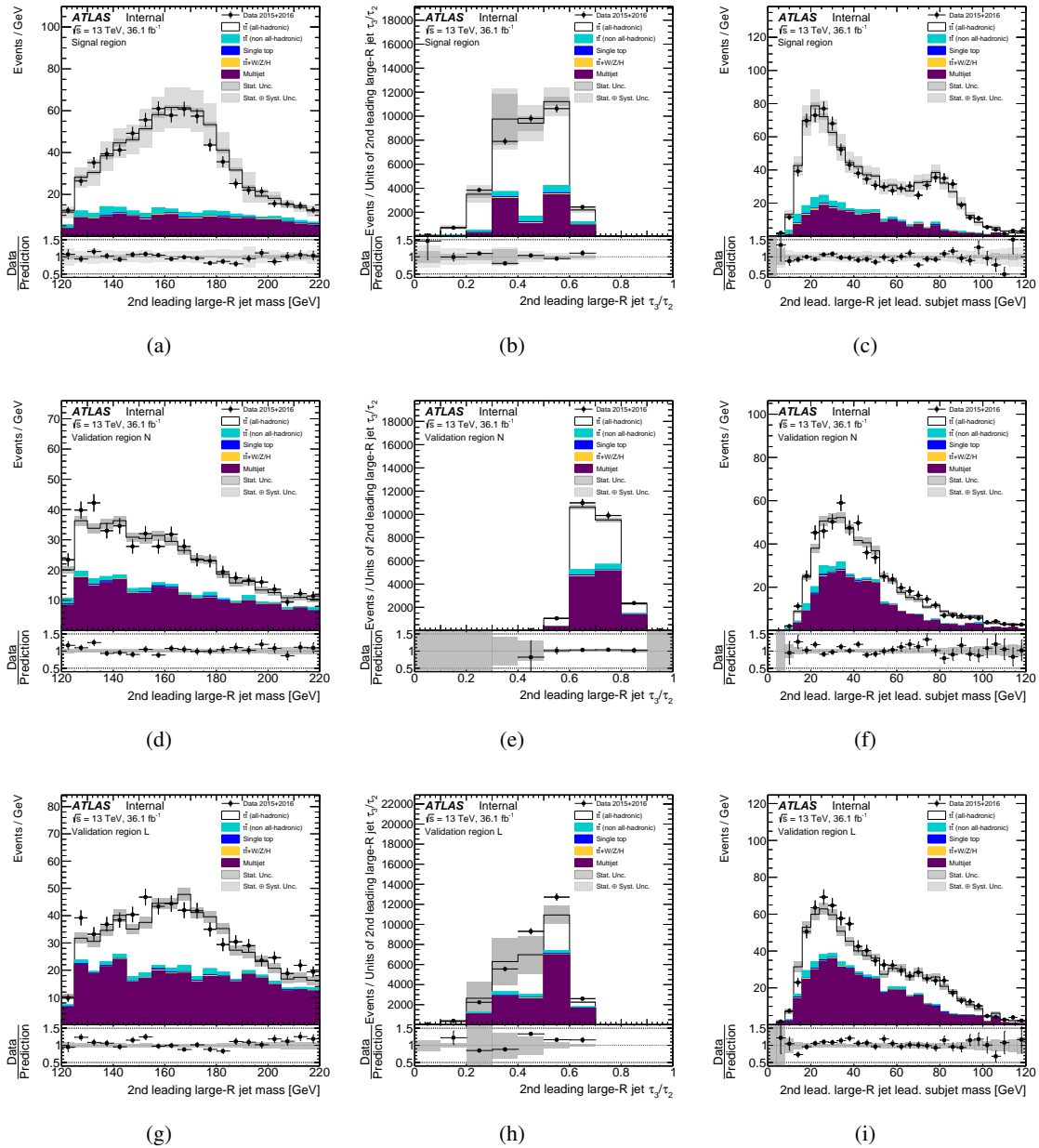


Figure 200: Kinematic distributions of large- R jets in the signal and control regions N and L: mass, N-subjettiness ratio and leading subjet mass of the sub-leading jet.

Not reviewed, for internal circulation only

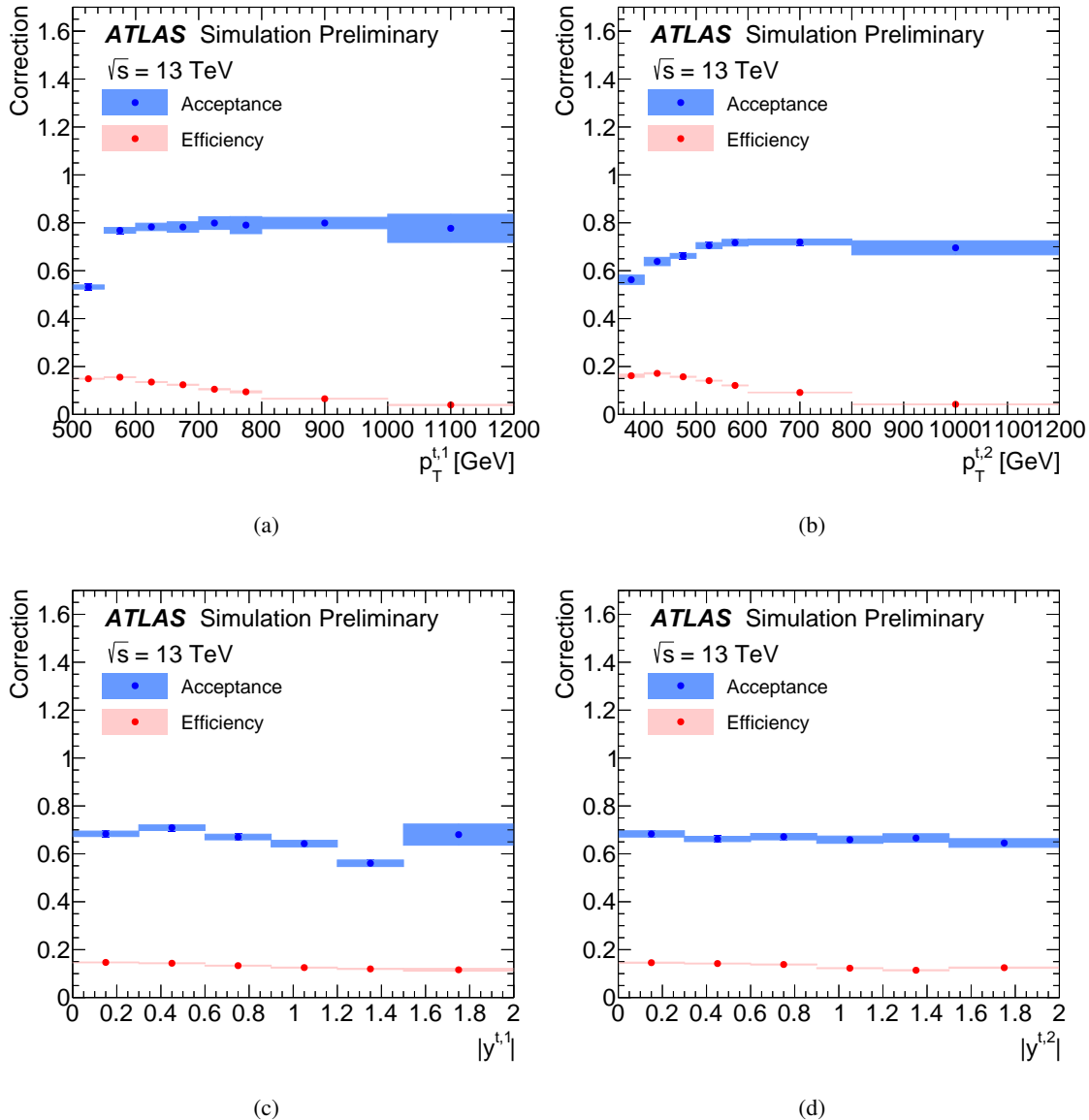


Figure 201: Fiducial phase-space acceptance and efficiency corrections as a function of (a) transverse momentum and (c) absolute value of the rapidity of the leading top-quark, and (b) transverse momentum and (d) absolute value of the rapidity of the second-leading top-quark. The blue and red bands indicate the statistical uncertainty on the signal Monte Carlo in each bin. The PowHEG+HERWIG7 generator is used as the nominal prediction to correct for detector effects. Uncertainties are estimated using standard binomial statistics.

Not reviewed, for internal circulation only

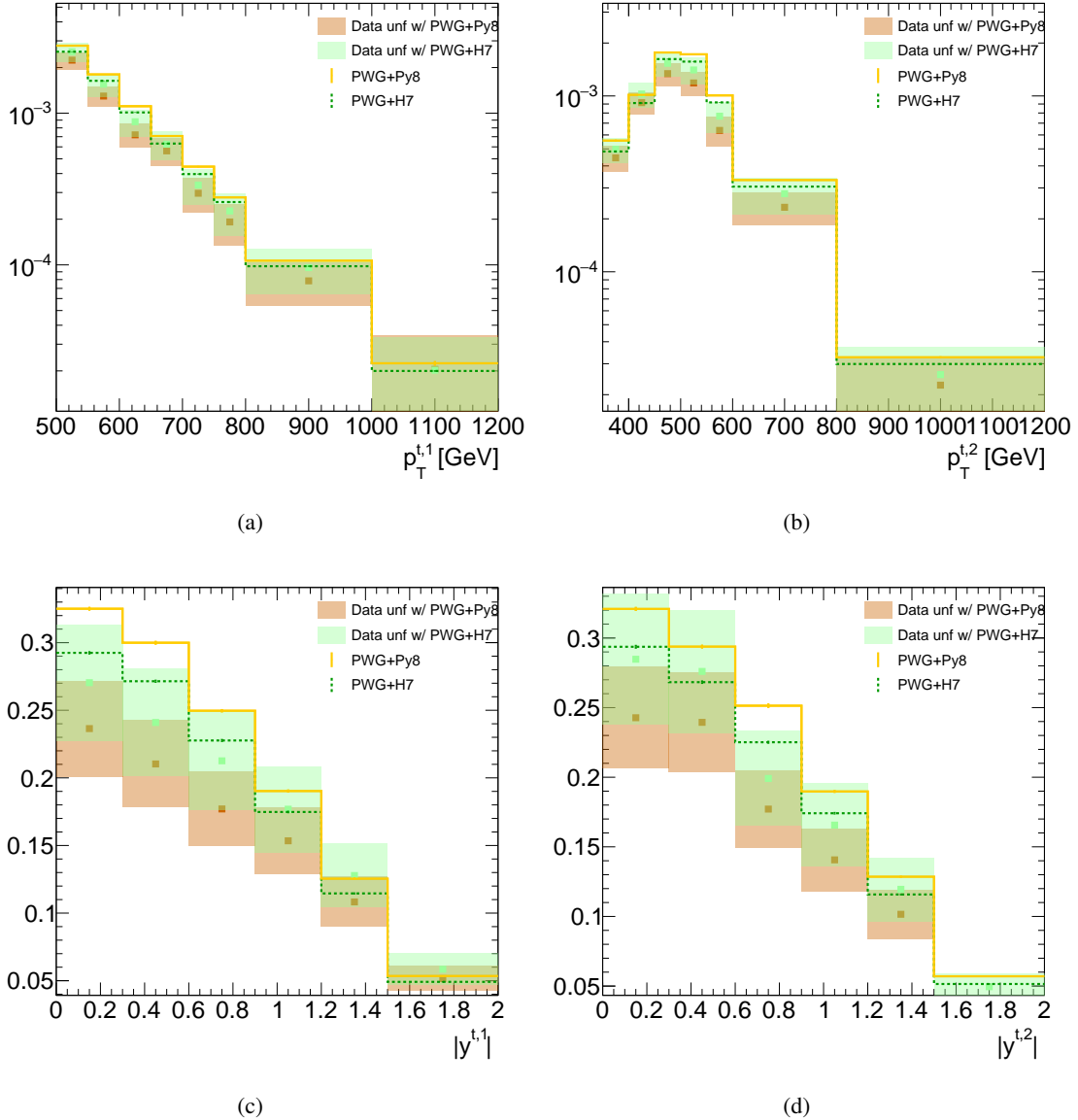


Figure 202: Comparison between Monte Carlo predictions and unfolded data in the fiducial phase-space: The difference around 13% in the overall efficiency correction results in a slightly higher inclusive cross-section when using PowHEG+HERWIG7, which improves the agreement between the Monte Carlo predictions and the unfolded data. The coloured bands represent detector uncertainties.

1532 T.1. Comparison with τ_{32} at each step in the RECO level

1533 Fig. 203 shows the τ_{32} distributions for each cut step in RECO level. The clear difference appeared in
1534 the ratio of Powheg +Herwig7 to Powheg +Pythia8 after the mass cut($|\Delta m| < 50\text{GeV}$) step. In order
1535 to investigate the cause of the difference at the mass cut step, the mass distributions themselves are also
1536 investigated. They are shown in Fig.204. Powheg +Herwig7 gives more events in the low mass region
1537 than Powheg +Pythia8, while the top mass peak is more prominent in Powheg +Pythia8. This would
1538 result in larger decrease in the number of events after the mass cut. The reason why this also changes the
1539 shape of the τ_{32} is not clear.

Not reviewed, for internal circulation only

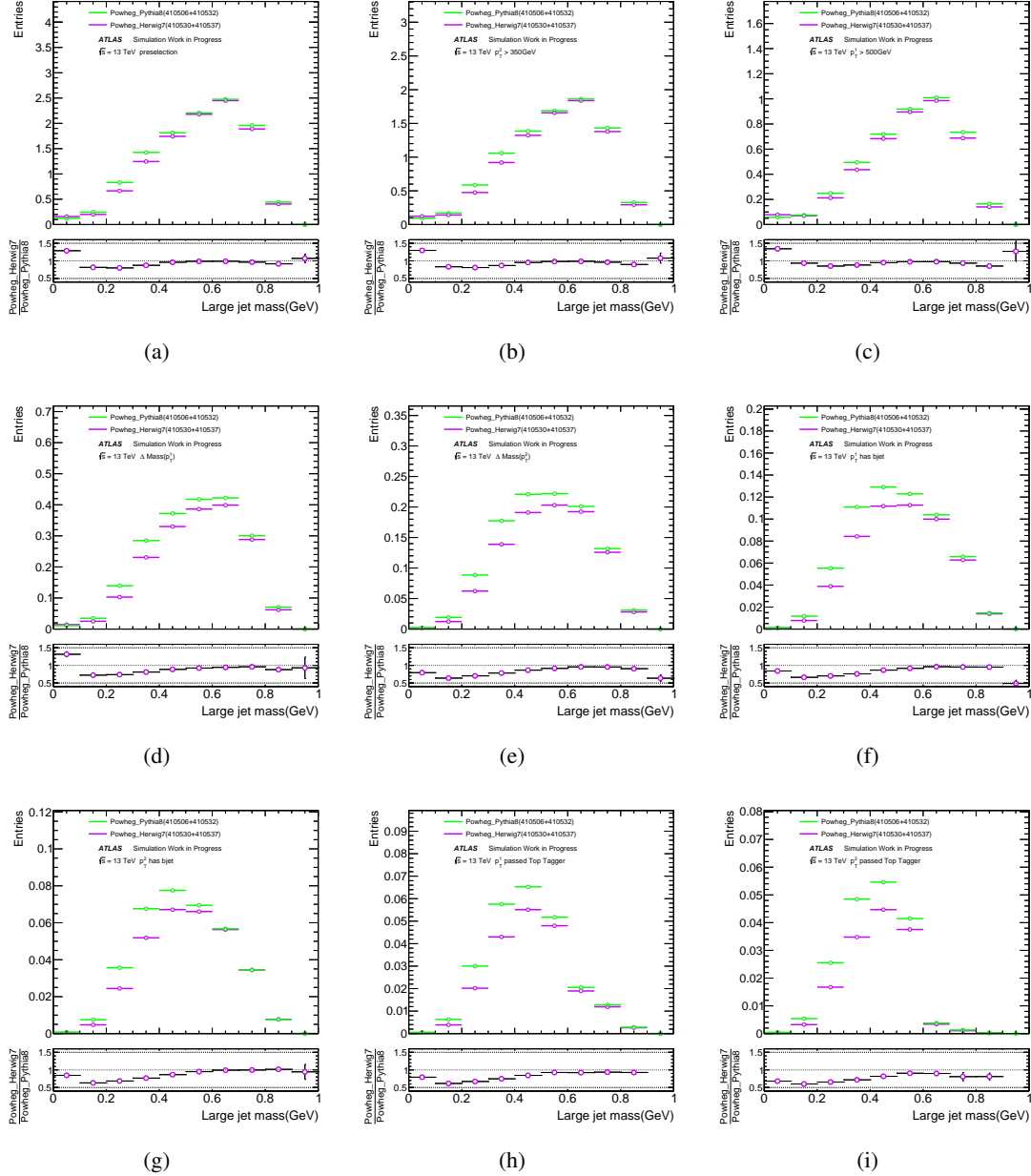


Figure 203: τ_{32} for each step of event selection at the reco level. (a) after preselection and trigger . (b) after selecting two large jets $p_T > 350 \text{ GeV}$. (c) after selecting Leading large jets $p_T > 500 \text{ GeV}$. (d) after requiring the mass of the Leading large jets within 50 GeV of the top quark mass. (e) after requiring the mass of the 2nd Leading large jets within 50 GeV of the top quark mass. (f) after requiring b -tag in the Leading large jet. (g) after requiring b -tag in the 2nd Leading large jet. (h) after requiring Leading large jet to be top-tagged. (i) after requiring 2nd Leading large jet to be top-tagged. Cuts are applied sequentially.

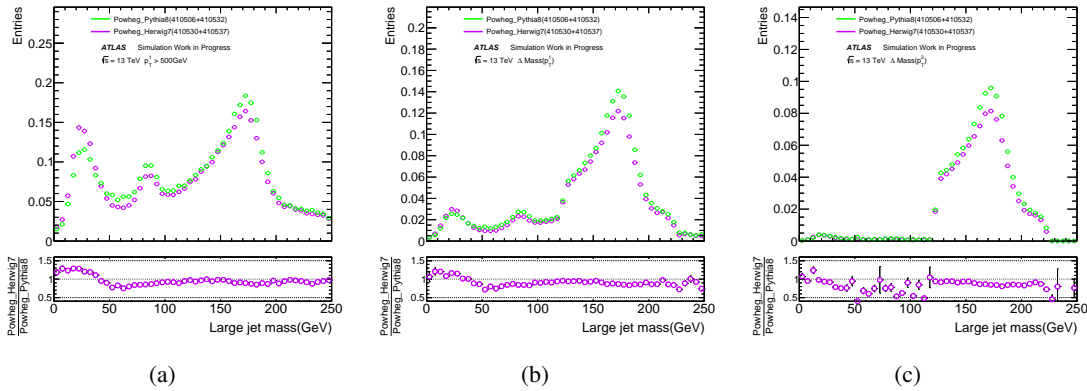


Figure 204: before and after mass cut at RECO level. (a) after selecting Leading large jets $p_T > 500$ GeV. (b) after requiring the mass of the Leading large jets within 50 GeV of the top quark mass. (c) after requiring the mass of the 2nd Leading large jets within 50 GeV of the top quark mass.

1540 T.2. Comparison with τ_{32} at each step in the particle level

1541 The behaviours of the τ_{32} distribution were also investigated in the particle level. Fig. 205 shows the τ_{32}
1542 distributions at the particle level.

1543 No significant difference between the two models was found before the mass cut. Similar behavior ob-
1544 served in the RECO level, however, was observed in the particle level in the τ_{32} ratio after the mass cuts.
1545 The mass distributions at the particle level was also investigated and shown in Fig. 206. There again sim-
1546 ilar tendency was observed in the particle level. These indicate that the observed difference between the
1547 two models in the RECO level in fact comes from the different particle distributions, i.e. originated from
1548 the model difference.

1549 For quantitative understanding, two kinds of values are estimated. One is integrating the cross section in
1550 a mass range of 125GeV and 220GeV for RECO and particle level. The values are listed in the Tab. 188.
1551 PowHEG +HERWIG7 showed 12.4% lower than PowHEG +PYTHIA8 at reco level, while 9.1% lower at particle
level. The other one is integrating the cross section in the τ_{32} range of 0 and 0.6, the values are listed in

	POWHEG +HERWIG7	POWHEG +PYTHIA8	$1 - \frac{\text{POWHEG+HERWIG7}}{\text{POWHEG+PYTHIA8}}$
Reco level(125~220GeV)	0.92	1.05	12.4%
Particle level(125~220GeV)	0.70	0.77	9.1%

Table 188: Comparsion of intergrated mass distribtuion around the top mass with PowHEG +HERWIG7 and PowHEG +PYTHIA8 in the RECO and particle level

1552 the Tab. 189. PowHEG +HERWIG7 showed 19.2% lower than PowHEG +PYTHIA8 in reco level, while 12.9%
1553 lower in particle level. From the above values about mass and τ_{32} , similar behaviors appear in both reco
1554 and particle level, although the difference is less pronounced in the particle level than the RECO level.
1555 This would mean that the difference of reco with different MC signal samples is not completely from
1556 detector effect, mostly from particle level effect.

Not reviewed, for internal circulation only

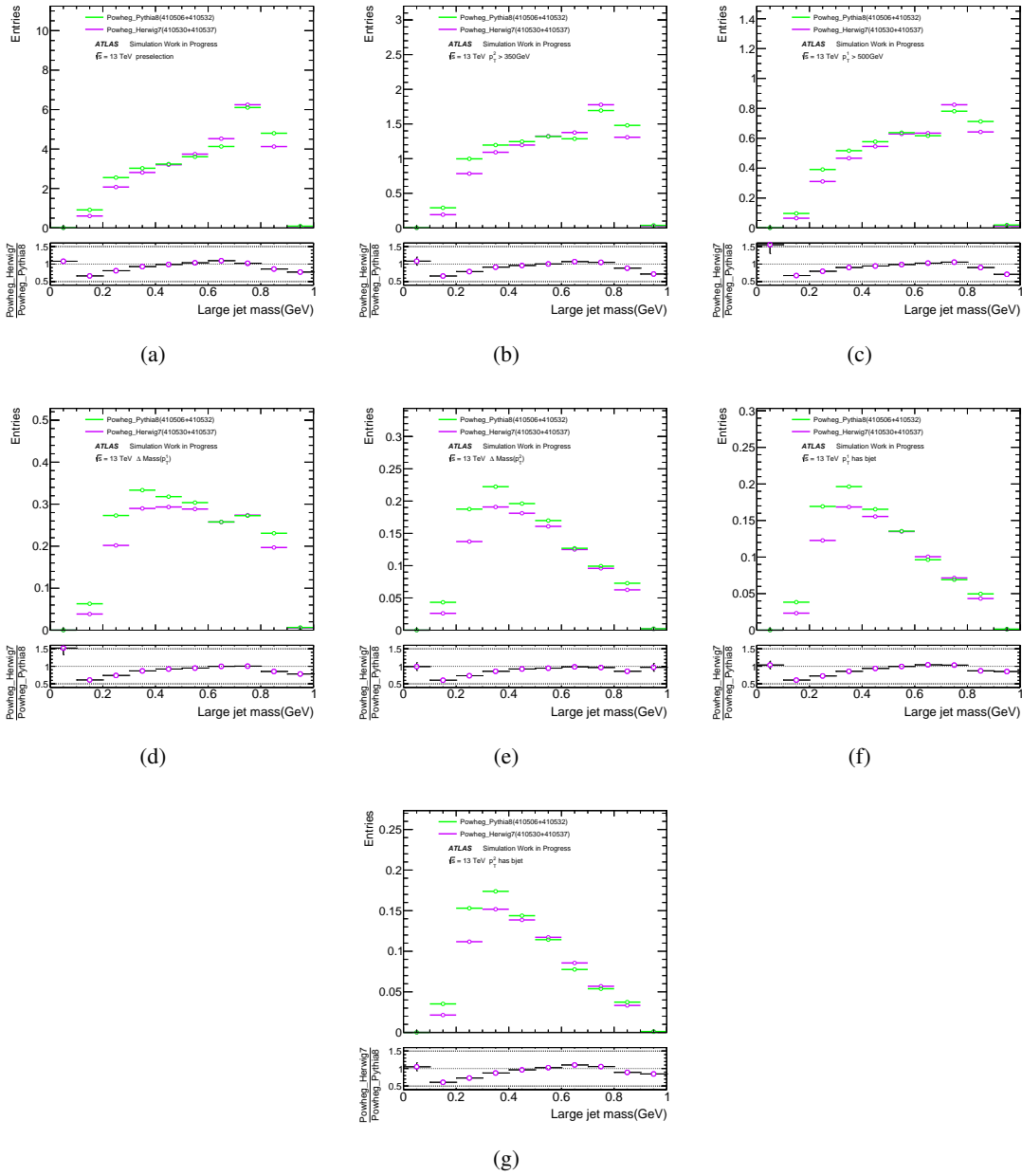


Figure 205: τ_{32} distribution for each cut step at the particle level. (a) after preselection and trigger. (b) after selecting two large jets $p_T > 350$ GeV. (c) after selecting Leading large jets $p_T > 500$ GeV. (d) after requiring the mass of the Leading large jets within 50 GeV of the top quark mass. (e) after requiring the mass of the 2nd Leading large jets within 50 GeV of the top quark mass. (f) after requiring b -tag in the Leading large jet. (g) after requiring b -tag in the 2nd Leading large jet. Cuts are applied sequentially.

Not reviewed, for internal circulation only

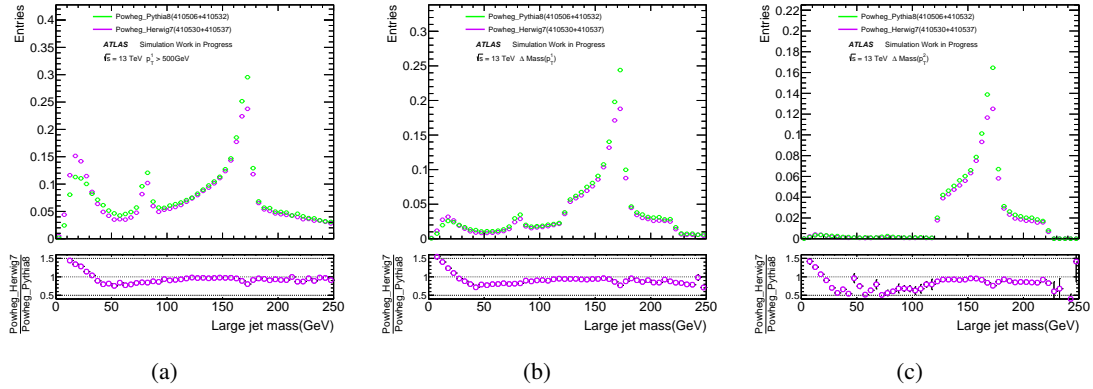


Figure 206: before and after mass cut at the particle level. (a) after selecting Leading large jets $p_T > 500 \text{ GeV}$. (b) after requiring the mass of the Leading large jets within 50 GeV of the top quark mass. (c) after requiring the mass of the 2nd Leading large jets within 50 GeV of the top quark mass.

	POWHEG +HERWIG7	POWHEG +PYTHIA8	$1 - \frac{\text{POWHEG+HERWIG7}}{\text{POWHEG+PYTHIA8}}$
Reco level($\tau_{32} < 0.6$)	0.21	0.26	19.2%
Particle level($\tau_{32} < 0.6$)	0.54	0.62	12.9%

Table 189: Comparsion of intergrating τ_{32} from 0 to 0.6 with POWHEG +HERWIG7 and POWHEG +PYTHIA8 in the RECO and particle level

U. 2D distributions

1558 A number of two-dimensional kinematic distributions have been obtained for significant pairs of observ-
1560 ables. Such distributions put the signal models to a more stringent test and represent a first step towards
1561 double-differential cross-sections. A Kolmogorov-Smirnov test is run between data and prediction in
1562 each sub-plot (1 meaning perfect agreement, 0 total disagreement),

1563 Figures 207–209 show the agreement between data and prediction when the Powheg+Pythia8 generator
1564 is used as signal model. Similar plots are presented for Powheg+Herwig7 in figs. 210–212.

Not reviewed, for internal circulation only

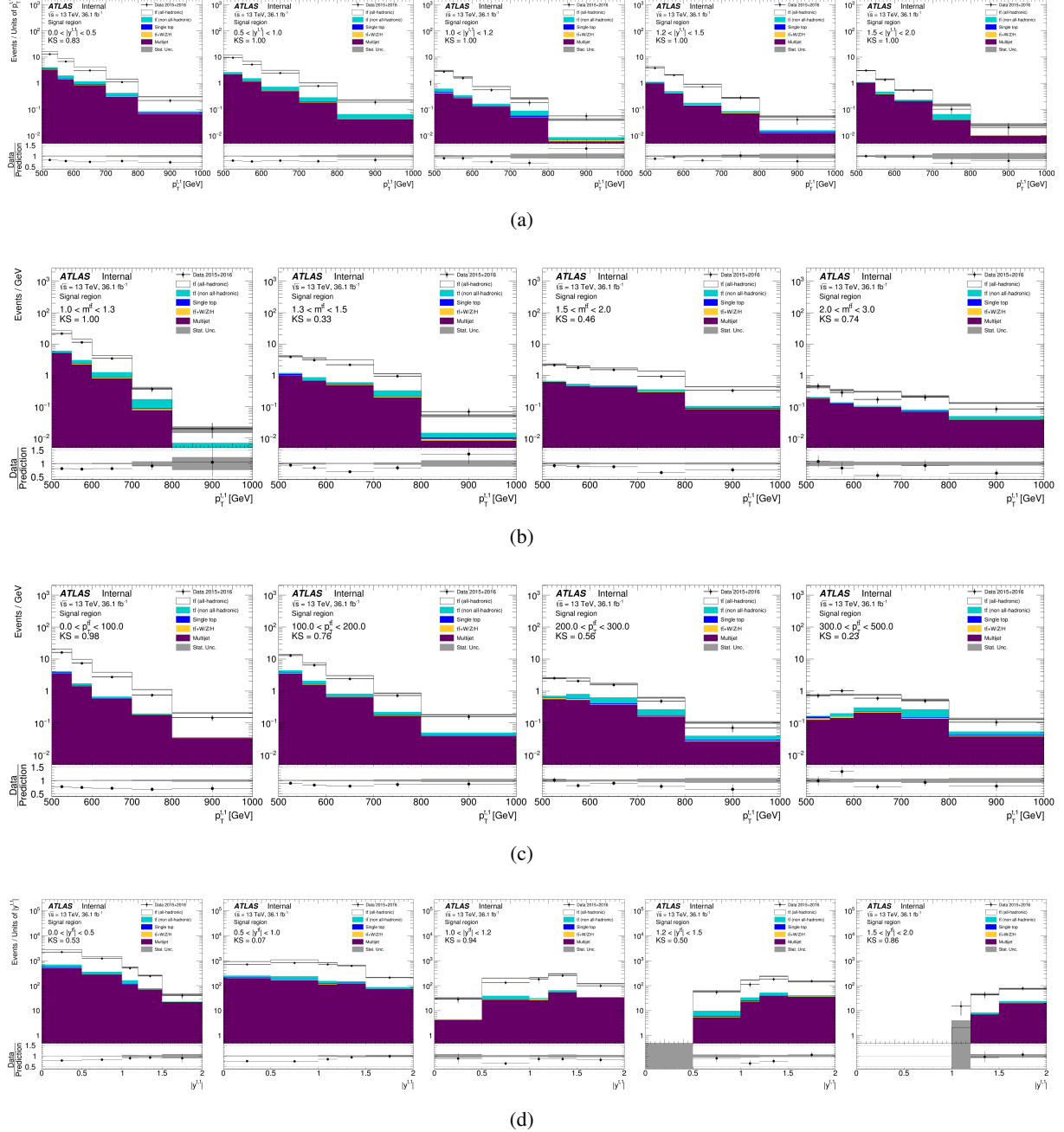


Figure 207: Kinematic distributions of the leading top-quark in the signal region (S): (a) p_T^t vs $|y^t|$, (b) p_T^t vs $m^{t\bar{t}}$, (c) p_T^t vs $p_T^{t\bar{t}}$, (d) $|y^t|$ vs $|y^{t\bar{t}}|$. The PowHEG+PYTHIA8 generator is used as signal model.

Not reviewed, for internal circulation only

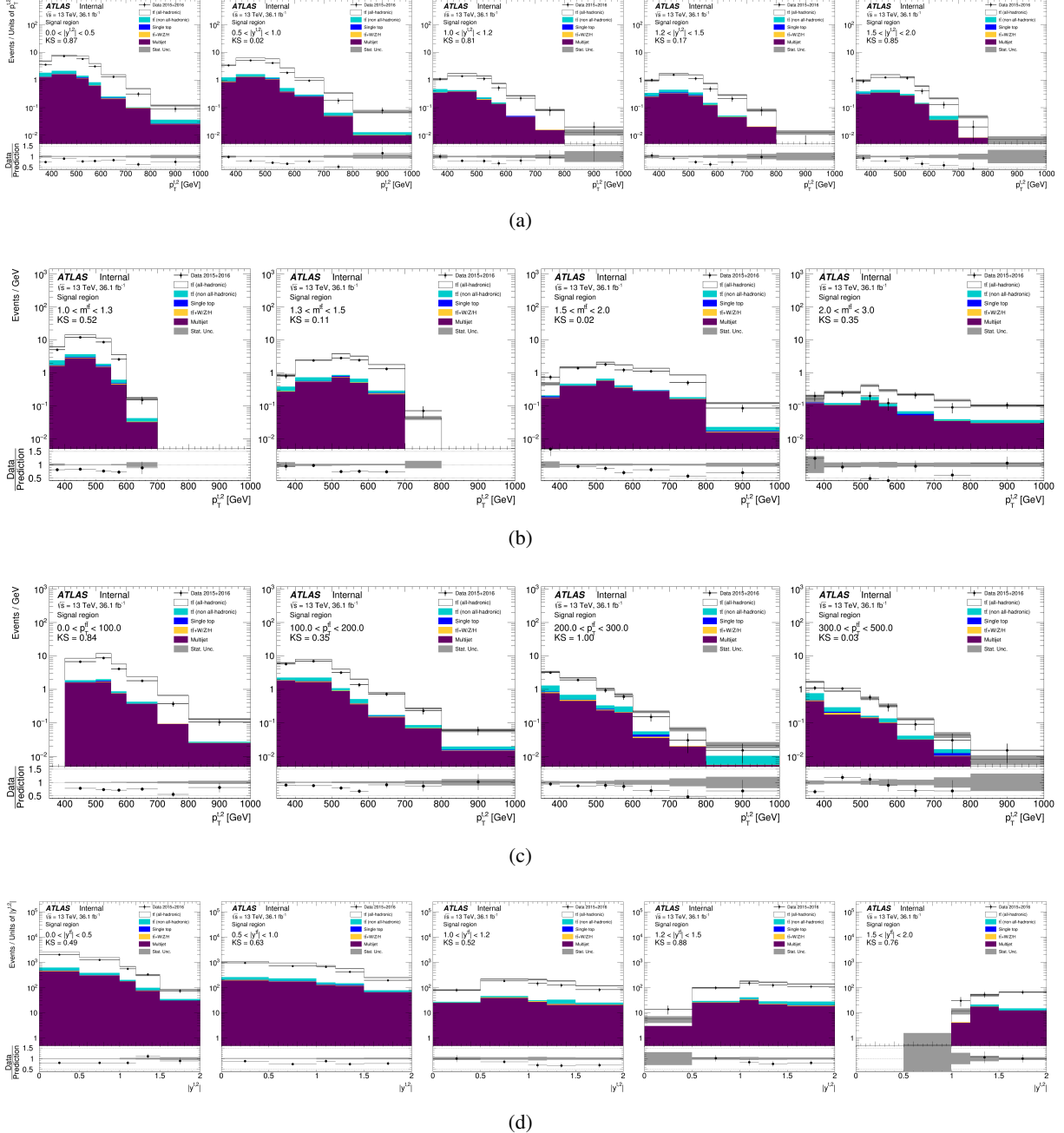


Figure 208: Kinematic distributions of the second-leading top-quark in the signal region (S): (a) p_T^t vs $|y^t|$, (b) p_T^t vs $m_{t\bar{t}}$, (c) p_T^t vs $p_T^{t\bar{t}}$, (d) $|y^t|$ vs $|y^{t\bar{t}}|$. The PowHEG+PYTHIA8 generator is used as signal model.

Not reviewed, for internal circulation only

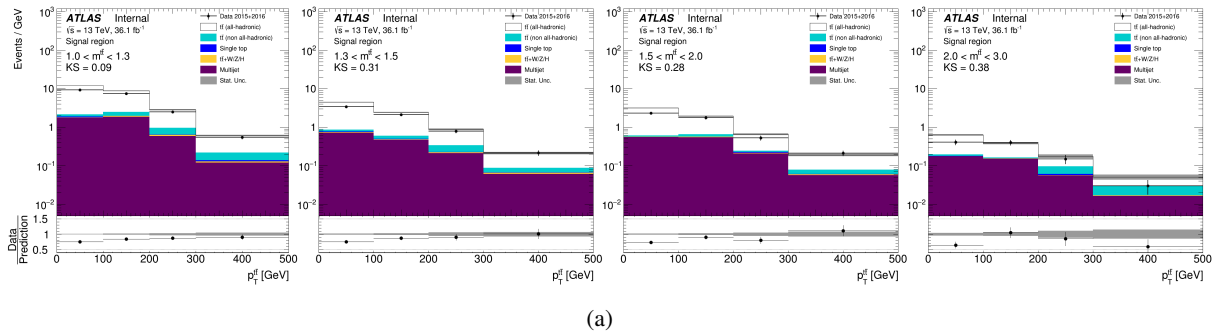


Figure 209: Kinematic distributions of the $t\bar{t}$ pair: (a) $p_T^{t\bar{t}}$ vs $m^{t\bar{t}}$. The Powheg+Pythia8 generator is used as signal model.

Not reviewed, for internal circulation only

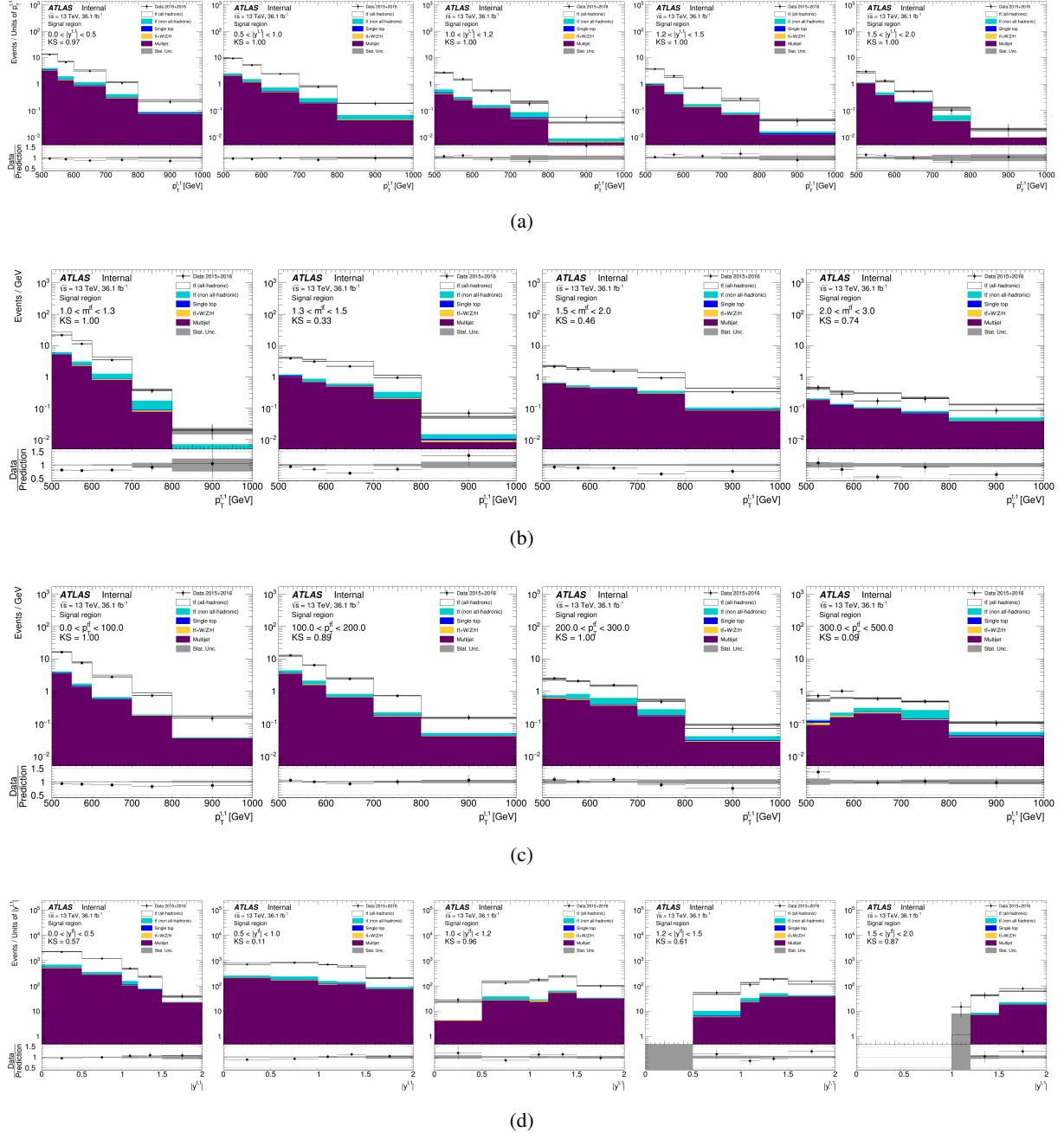


Figure 210: Kinematic distributions of the leading top-quark in the signal region (S): (a) p_T^t vs $|y^t|$, (b) p_T^t vs $m^{t\bar{t}}$, (c) p_T^t vs $p_T^{t\bar{t}}$, (d) $|y^t|$ vs $|y^{t\bar{t}}|$. The PowHEG+HERWIG7 generator is used as signal model.

Not reviewed, for internal circulation only

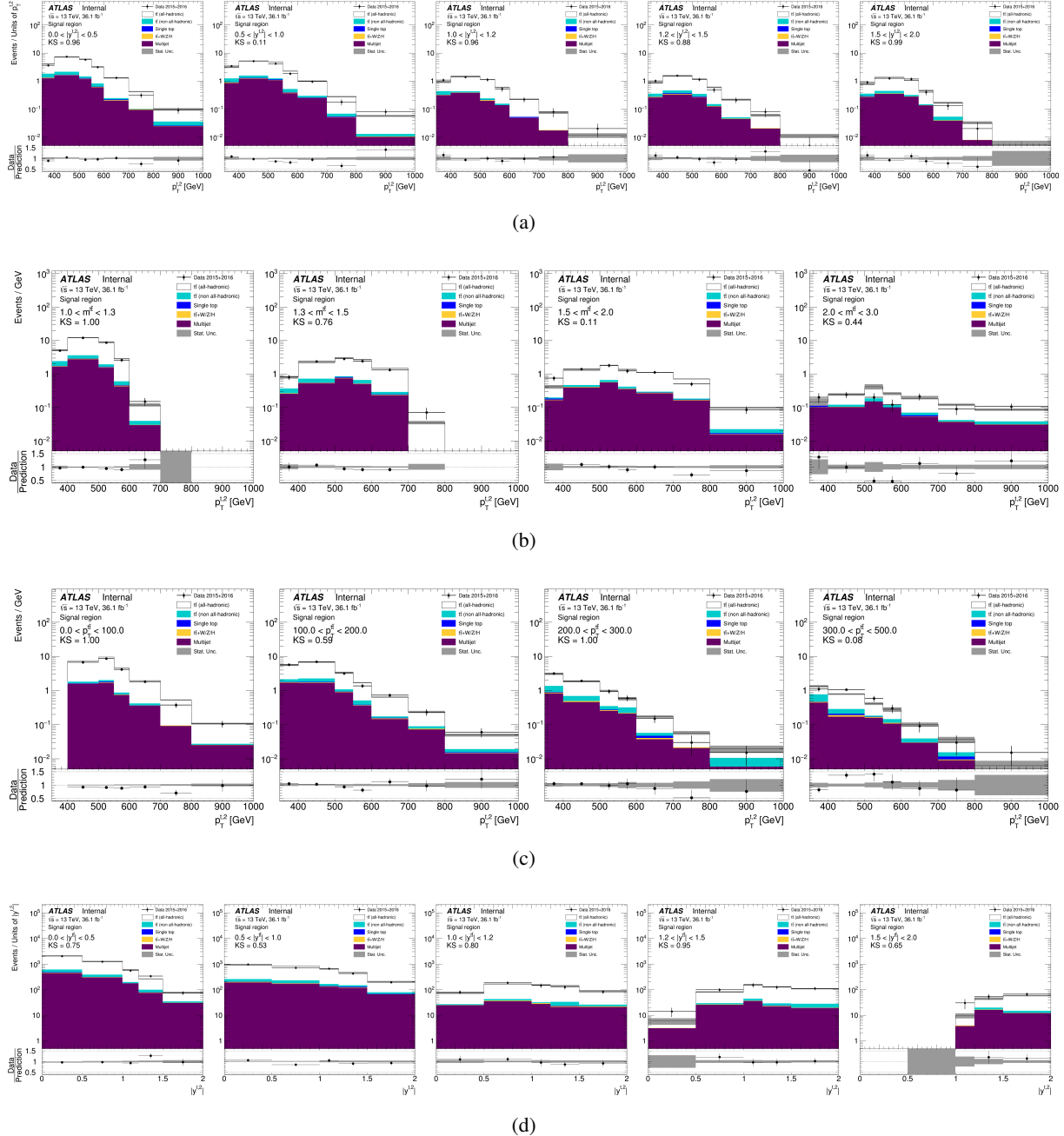


Figure 211: Kinematic distributions of the second-leading top-quark in the signal region (S): (a) p_T^t vs $|y^t|$, (b) p_T^t vs m_t^2 , (c) p_T^t vs $p_T^{t\bar{t}}$, (d) $|y^{t\bar{t}}|$ vs $|y^t|$. The PowHEG+HERWIG7 generator is used as signal model.

Not reviewed, for internal circulation only

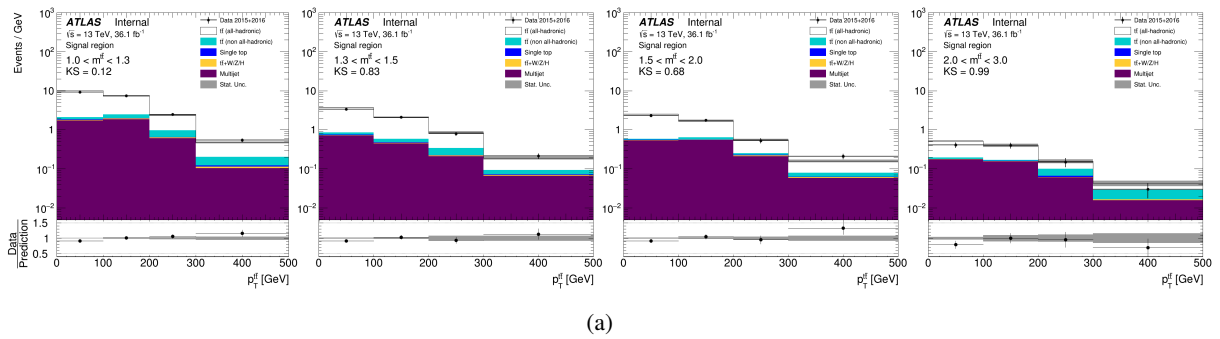


Figure 212: Kinematic distributions of the $t\bar{t}$ pair: (a) p_T^t vs m^t . The PowHEG+HERWIG7 generator is used as signal model.

V. Statistical correlations among variable using bootstrapping methods

1565 Correlation among variables can be studied using the Monte Carlo signal simulation. However, one wants
1566 to compare the theoretical model to what is observed in real data. To do so, in principle one has to unfold
1567 a large number of double-differential cross-sections. Alternatively, a simplified approach was put forward
1568 in past publications [3] which relies only on single-differential distributions.

1570 Statistical correlations among the variables are evaluated by unfolding statistically coupled (co-varied)
1571 1000 replicas of individual spectra in data using the bootstrap method [60]. The result is obtained by
1572 concatenating the differential cross-sections for each pseudo-experiment.

1573 The result is presented in Fig. 213 for absolute cross-sections and 214 for relative cross-sections at the
1574 particle level, and in Fig. 215–216 at the parton level.

Not reviewed, for internal circulation only

ATLAS Internal $\sqrt{s} = 13 \text{ TeV}$, Ldt = 36.1 fb^{-1}

Fiducial phase-space statistical correlations

Absolute cross-sections

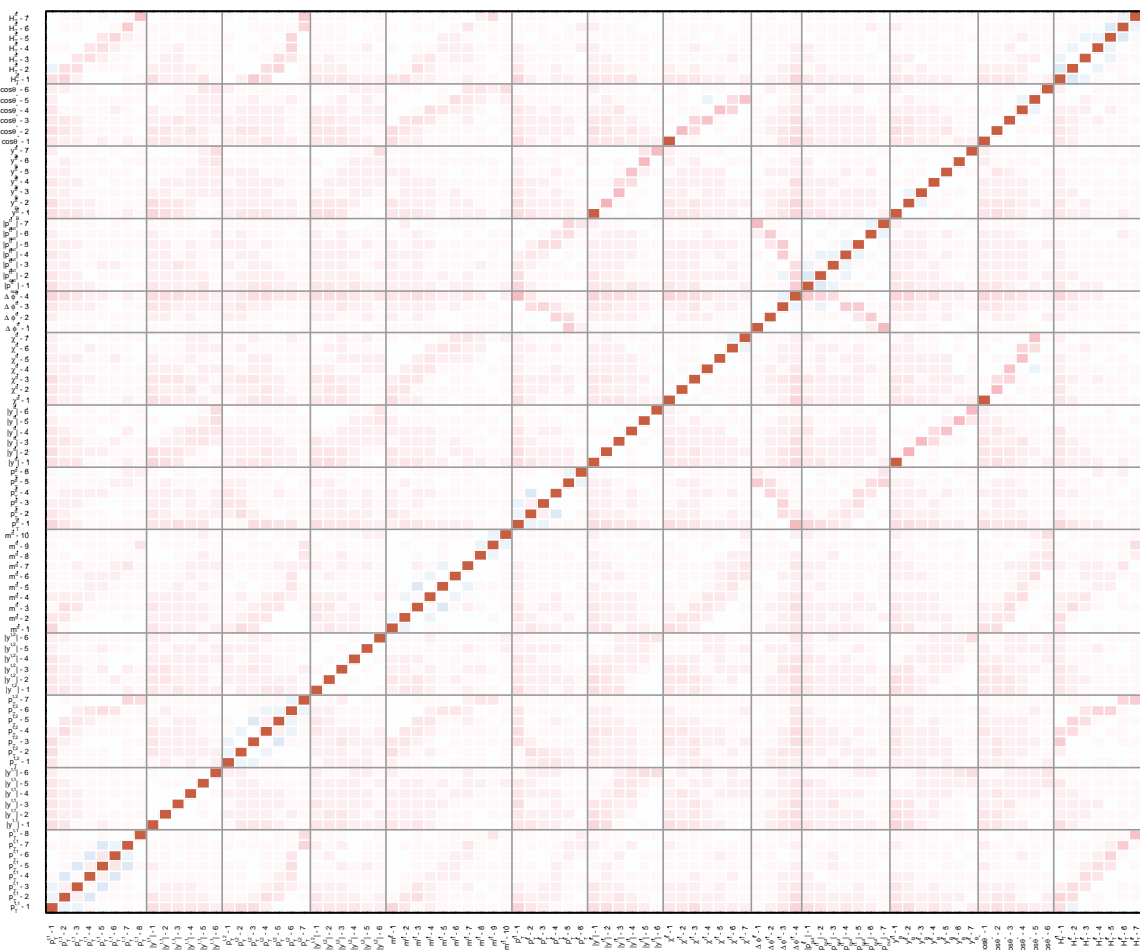


Figure 213: Statistical correlations among absolute fiducial phase-space differential cross-sections at the particle level. The covariance is evaluated by unfolding statistically coupled (co-varied) replicas of individual spectra in data using the bootstrap method [60].

Not reviewed, for internal circulation only

ATLAS Internal $\sqrt{s} = 13 \text{ TeV}$, Ldt = 36.1 fb^{-1}

Fiducial phase-space statistical correlations

Relative cross-sections

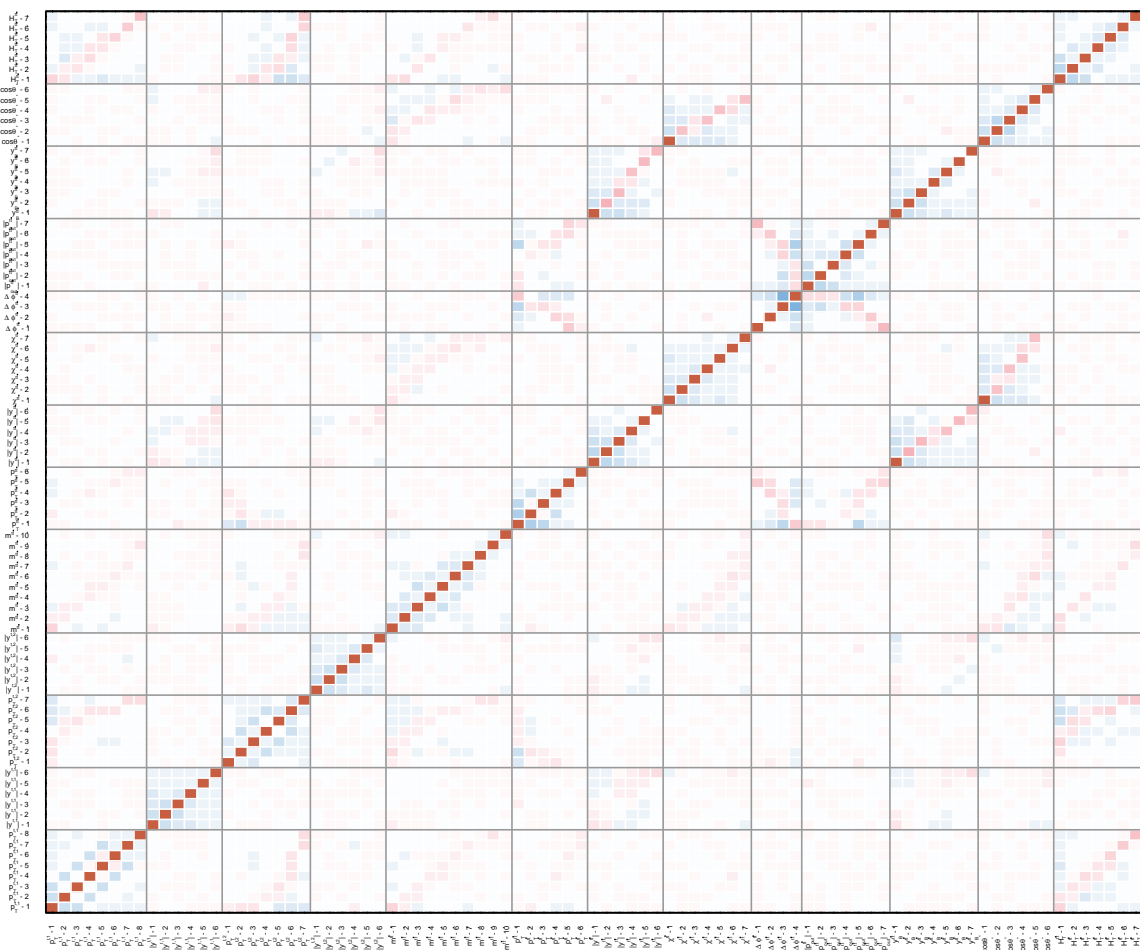


Figure 214: Statistical correlations among relative fiducial phase-space differential cross-sections at the particle level. The covariance is evaluated by unfolding statistically coupled (co-varied) replicas of individual spectra in data using the bootstrap method [60].

Not reviewed, for internal circulation only

ATLAS Internal $\sqrt{s} = 13 \text{ TeV}$, $L = 36.1 \text{ fb}^{-1}$

Fiducial phase-space statistical correlations

Absolute cross-sections, parton level

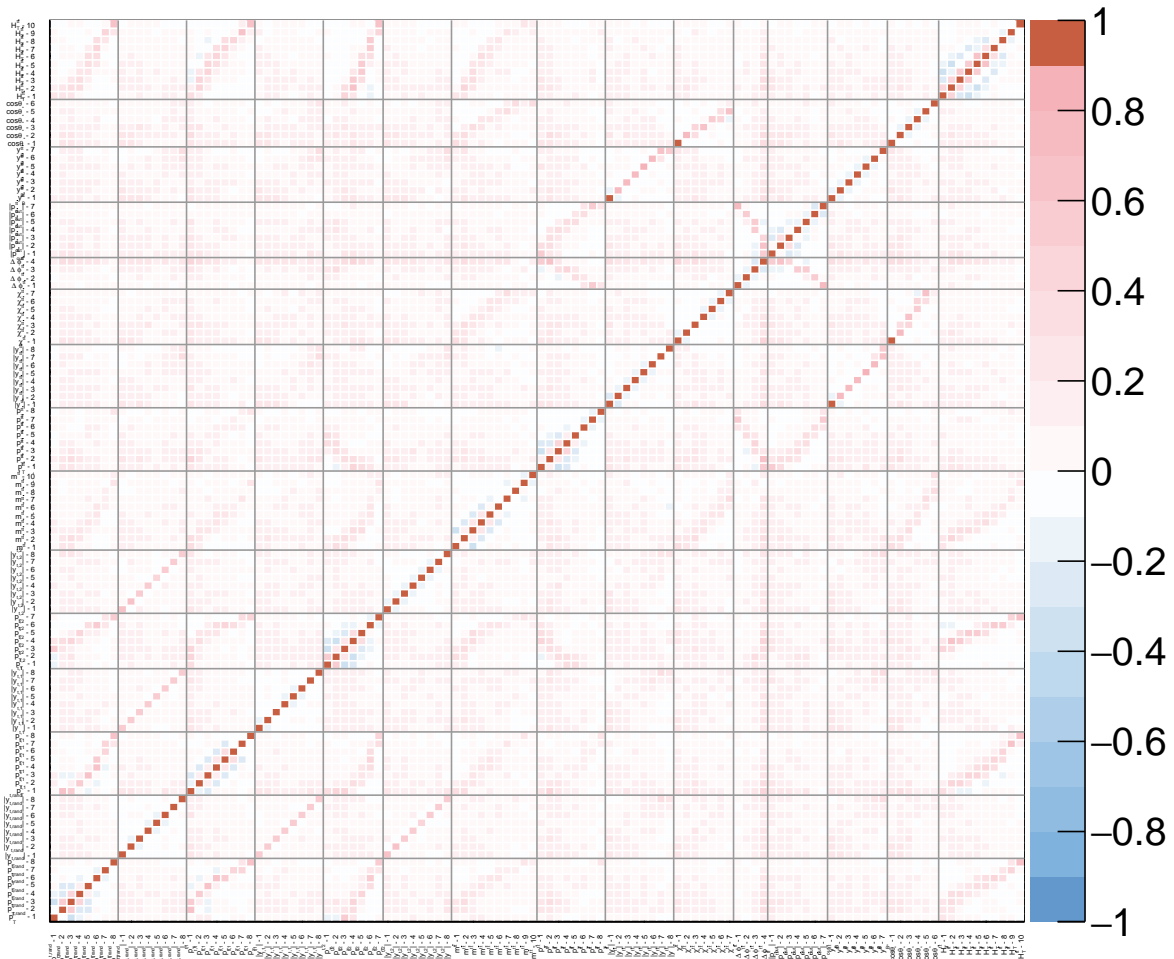


Figure 215: Statistical correlations among absolute fiducial phase-space differential cross-sections at the parton level. The covariance is evaluated by unfolding statistically coupled (co-varied) replicas of individual spectra in data using the bootstrap method [60].

Not reviewed, for internal circulation only

ATLAS Internal $\sqrt{s} = 13 \text{ TeV}$, $L = 36.1 \text{ fb}^{-1}$

Fiducial phase-space statistical correlations

Relative cross-sections, parton level

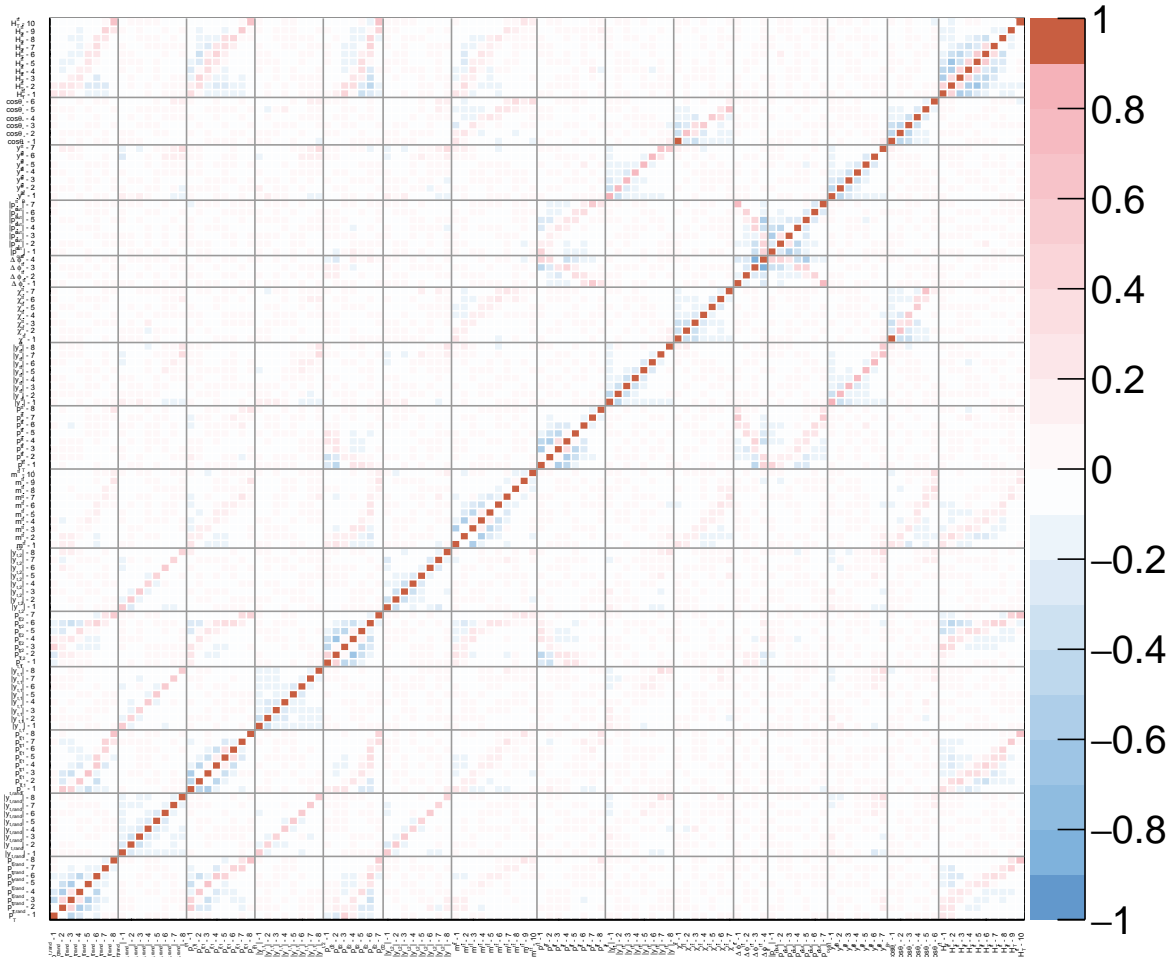


Figure 216: Statistical correlations among relative fiducial phase-space differential cross-sections at the parton level. The covariance is evaluated by unfolding statistically coupled (co-varied) replicas of individual spectra in data using the bootstrap method [60].

1575 W. Evaluation of covariance matrices

1576 A bin-to-bin covariance matrix is computed for each differential cross section measurement, both absolute
 1577 and relative. It is evaluated by using a pseudo-experiments method that allows to include all the contribu-
 1578 tions of both statistical and experimental systematic uncertainties and their correlations (see Section 8)
 1579 and all the correlations introduced by the unfolding procedure.

1580 The pseudo-experiment method is the same as the one used in the most recent ATLAS papers on $t\bar{t}$
 1581 differential cross-sections using $ell + jets$ events. They are : the published measurement of $t\bar{t}$ differential
 1582 cross section for highly boosted top quarks as a function of their transverse momentum at $\sqrt{s} = 8$ TeV [61]
 1583 and the approved measurement of $t\bar{t}$ differential cross section for both resolved and highly boosted top
 1584 quarks as a function of a variety of kinematic variables at $\sqrt{s} = 13$ TeV [62]. The method is described in
 1585 detail in Appendix J of the internal documentation of the first paper using highly boosted top quarks [63].
 1586 A summary is given here, including the main differences with respect to the detailed discussion.

1587 The analysis software is presently integrated with the unfolding package in a publicly accessible ATLAS
 1588 SVN ³. The most updated version will be saved there once a few additional changes that make it more
 1589 flexible are included.

1590 For each variable, a covariance matrix is obtained by summing two covariance matrices.

1591 The first covariance matrix incorporates uncertainties from statistical effects, detector-related sources,
 1592 background modelling and limited size of the simulated samples. The procedure used to derive this first
 1593 matrix is called “pre-unfolding” scheme because the systematic effects are injected before the unfolding
 1594 procedure so as to take into account all the correlations introduced by unfolding and their connection with
 1595 statistical fluctuations.

1596 The procedure to calculate the first covariance matrix is as follows:

- 1597 • The estimate is obtained by performing 10k pseudo-experiments. In each pseudo-experiment, each
 1598 bin of the selected data distribution dN/dX is varied independently following a Poisson distribution
 1599 to take into account statistical uncertainties.
- 1600 • For each systematic uncertainty effect related to detector effects (see Section 8) Gaussian-distributed
 1601 shifts are then coherently included by scaling each Poisson-fluctuated bin content with the expec-
 1602 ted relative bin-content variation from the associated systematic uncertainty effect and adding the
 1603 Gaussian-weighted result to the initial Poisson-fluctuated bin content.
- 1604 • The relative bin-content variation in each bin j accounting for the i -th systematics type $\Delta_j^{\text{syst } i}$ is
 1605 defined as the difference of the varied and nominal signal+background events (pseudo-data) count
 1606 in each bin, normalized to the expected nominal yield:

$$\Delta_j^{\text{syst } i} \equiv \frac{\mathcal{S}_j^{\text{syst } i} + \mathcal{B}_j^{\text{syst } i} - \mathcal{S}_j^{\text{nominal } i} - \mathcal{B}_j^{\text{nominal } i}}{\mathcal{S}_j^{\text{nominal } i} + \mathcal{B}_j^{\text{nominal } i}}.$$

1604 The positively (negatively) varied pseudo-data distribution for a given systematic effect results
 1605 from changing the systematic source of interest by one standard deviation in the “up” (down) or
 1606 “positive” (negative) direction and building the resulting signal+background prediction. In the case

³ The code is in the 0-0-0 branch in <https://svnweb.cern.ch/trac/atlasinst/browser/Institutes/Bologna/TTbarUnfold?order=name>

1607 of a one-sided systematic uncertainty, positively and negatively varied distributions are obtained by
 1608 symmetrizing the contribution with respect to the nominal prediction.

- In each pseudo-experiment, a random number $\lambda_i \sim \mathcal{N}(0, 1)$ (Gaussian distribution of a unit width and centered at zero) is drawn for each systematics source, common to all bins. When λ_i is positive (negative), for each bin the “up” (“down”) relative pseudo-data variation is multiplied with $|\lambda_i|$ and the Poisson-fluctuated bin content to build the associated systematic shift. The value of bin content j in the k -th pseudo-experiment is thus constructed as

$$\text{toy}_j^k \equiv \mathcal{P}(D_j) \left[1 + \sum_{\text{syst } i} |\lambda_{\text{syst } i}| \Delta_j^{\text{syst } i} \right]$$

1609 where $\mathcal{P}(D_j)$ is the Poisson-fluctuated data content.

- Notice that the uncertainty sources are considered independent, but within a systematic source, all the bins are taken as fully coherent (i.e. fully correlated): this is why the Gaussian fluctuations have independent random numbers with respect to each other, while there is a unique random number for all the shifts corresponding to a given uncertainty. If the number of events in a given bin of the distribution becomes negative, due to the effect of the combined systematic shifts, the value in this bin is set to zero. A detailed discussion of this choice is given in Appendix N.1 of the internal documentation for the $t\bar{t}$ differential cross section measurement using highly boosted top quark events at the $\sqrt{s}= 13$ TeV [64]. Finally, differential cross-sections are obtained by unfolding each varied distribution with the nominal background and unfolding corrections as described in Sections 6 and 7. The results are used to compute a covariance matrix following the standard formula:

$$\text{Cov}(i, j) = \langle (\text{d}\sigma_i - \langle \text{d}\sigma_i \rangle) \cdot (\text{d}\sigma_j - \langle \text{d}\sigma_j \rangle) \rangle_N \quad (35)$$

where i, j are the i -th and j -th bins of the variable of interest and the averages are performed over the N pseudo-experiments. The corresponding correlation matrices are evaluated as

$$\text{Corr}(i, j) = \text{Cov}(i, j) / \sqrt{\text{Cov}(i, i) \text{Cov}(j, j)}, \quad (36)$$

- The effects of the limited Monte Carlo sample size and of the multi-jet background uncertainty (see Section 5 are included by adding independent Gaussian-distributed shifts to each bin of the pseudo-data distribution. For each bin the shift is extracted from a Gaussian distribution whose width is represented by the statistical uncertainty on the total prediction resulting from the bin content. This takes into account both the size of the Monte Carlo samples and the background uncertainty.
- The second covariance matrix is obtained by summing four separate covariance matrices corresponding to the effects of $t\bar{t}$ generator, parton shower and hadronisation, ISR/FSR and PDF uncertainties. This procedure is called “post-unfolding” scheme because systematic effects are obtained by quantities that are obtained by unfolding the initial distributions: this is necessary because signal modelling uncertainties effects cannot be represented by a variation at the detector level and so they cannot be included in the “pre-unfolding” pseudo-experiment formalism used to derive the first covariance matrix. In this scheme the standard deviations of the covariance matrices are derived by scaling each measured cross-section with the appropriate relative systematic uncertainty. The relative uncertainty is derived by unfolding the background-subtracted differential distribution produced by a given model with the corrections

Observable	PWG+PY8		MG5_AMC@NLO+Py8		PWG+H7		PWG+PY8 (more IFSR)		PWG+PY8 (less IFSR)		SHERPA 2.2.1	
	χ^2/NDF	$p\text{-value}$										
$p_T^{t,1}$	7.6/8	0.48	8.9/8	0.35	6.1/8	0.63	9.7/8	0.29	7.5/8	0.49	9.8/8	0.28
$ y^{t,1} $	16.7/6	0.01	27.3/6	<0.01	12.6/6	0.05	21.9/6	<0.01	15.1/6	0.02	12.1/6	0.06
$p_T^{t,2}$	10.7/7	0.15	6.6/7	0.47	10.4/7	0.17	15.9/7	0.03	6.2/7	0.52	8.5/7	0.29
$ y^{t,2} $	5.7/6	0.45	7.8/6	0.25	3.5/6	0.74	6.3/6	0.40	4.2/6	0.65	5.3/6	0.51
$m^{t\bar{t}}$	8.6/10	0.57	11.9/10	0.29	5.6/10	0.85	11.0/10	0.36	7.9/10	0.64	15.0/10	0.13
$p_{\text{out}}^{t\bar{t}}$	8.8/6	0.19	26.8/6	<0.01	10.2/6	0.12	17.3/6	<0.01	2.7/6	0.84	3.4/6	0.76
$\Delta\phi^{t\bar{t}}$	5.6/6	0.47	8.2/6	0.23	3.7/6	0.72	5.5/6	0.48	5.3/6	0.50	3.4/6	0.76
$H_T^{t\bar{t}}$	16.2/7	0.02	16.1/7	0.02	13.1/7	0.07	21.3/7	<0.01	9.8/7	0.20	22.7/7	<0.01
$y_B^{t\bar{t}}$	8.4/7	0.30	11.0/7	0.14	5.6/7	0.59	9.1/7	0.25	7.7/7	0.36	6.0/7	0.54
$ p_{\text{out}}^{t\bar{t}} $	5.8/7	0.56	59.6/7	<0.01	5.3/7	0.63	11.9/7	0.10	5.2/7	0.64	8.9/7	0.26
$\Delta\phi^{t\bar{t}}$	5.1/4	0.28	49.2/4	<0.01	6.2/4	0.19	13.2/4	0.01	1.4/4	0.84	3.6/4	0.47
$H_T^{t\bar{t}}$	8.8/7	0.27	9.8/7	0.20	6.0/7	0.54	10.3/7	0.17	7.6/7	0.37	6.0/7	0.54
$\cos\theta^*$	11.7/6	0.07	14.4/6	0.03	9.3/6	0.16	16.6/6	0.01	6.8/6	0.34	21.6/6	<0.01

Table 190: Comparison between the absolute particle-level fiducial differential cross-sections and the predictions from several MC generators. For each variable and prediction, a χ^2 and a p -value are calculated using the covariance matrix described in the text, which includes all sources of uncertainty. The number of degrees of freedom (NDF) is equal to N_b , where N_b is the number of bins in the distribution.

Observable	PWG+PY8		MG5_AMC@NLO+Py8		PWG+H7		PWG+PY8 (more IFSR)		PWG+PY8 (less IFSR)		SHERPA 2.2.1	
	χ^2/NDF	$p\text{-value}$										
$p_T^{t,1}$	7.7/7	0.36	8.2/7	0.32	8.0/7	0.33	9.1/7	0.24	8.7/7	0.27	9.3/7	0.23
$ y^{t,1} $	7.5/5	0.18	12.2/5	0.03	6.8/5	0.24	8.8/5	0.12	8.1/5	0.15	4.0/5	0.55
$p_T^{t,2}$	8.6/6	0.20	2.6/6	0.86	9.9/6	0.13	12.2/6	0.06	5.0/6	0.54	5.0/6	0.55
$ y^{t,2} $	3.7/5	0.59	4.6/5	0.46	3.1/5	0.68	3.5/5	0.63	3.2/5	0.67	2.9/5	0.72
$m^{t\bar{t}}$	4.5/9	0.88	4.7/9	0.86	4.0/9	0.91	5.3/9	0.81	5.2/9	0.82	10.0/9	0.35
$p_T^{t\bar{t}}$	7.8/5	0.17	20.9/5	<0.01	12.6/5	0.03	15.0/5	0.01	1.9/5	0.86	1.9/5	0.87
$ y^{t\bar{t}} $	1.1/5	0.95	2.2/5	0.83	0.9/5	0.97	0.8/5	0.98	1.8/5	0.88	1.7/5	0.89
$\chi^{t\bar{t}}$	14.2/6	0.03	12.7/6	0.05	13.6/6	0.03	16.9/6	<0.01	10.1/6	0.12	18.5/6	<0.01
$y_B^{t\bar{t}}$	2.5/6	0.87	3.3/6	0.77	2.2/6	0.90	2.6/6	0.86	2.8/6	0.84	3.0/6	0.81
$ p_{\text{out}}^{t\bar{t}} $	1.9/6	0.93	53.1/6	<0.01	3.1/6	0.80	4.2/6	0.64	4.8/6	0.57	5.9/6	0.44
$\Delta\phi^{t\bar{t}}$	0.9/3	0.84	16.3/3	<0.01	2.0/3	0.58	3.0/3	0.40	0.6/3	0.89	3.4/3	0.33
$H_T^{t\bar{t}}$	4.8/6	0.57	5.2/6	0.52	4.5/6	0.61	5.0/6	0.54	5.0/6	0.55	3.1/6	0.80
$\cos\theta^*$	9.9/5	0.08	10.5/5	0.06	9.3/5	0.10	12.8/5	0.03	6.5/5	0.26	18.7/5	<0.01

Table 191: Comparison between the normalized particle-level fiducial differential cross-sections and the predictions from several MC generators. For each variable and prediction, a χ^2 and a p -value are calculated using the covariance matrix described in the text, which includes all sources of uncertainty. The number of degrees of freedom (NDF) is equal to $N_b - 1$, where N_b is the number of bins in the distribution.

1635 (acceptance, efficiency and response matrix) derived from a different model, taking the bin-by-bin dif-
 1636 ference between the unfolded distribution and the generated (“truth”) distribution at particle or parton
 1637 level and dividing such difference for the generated (“truth”) distribution at particle or parton level on
 1638 a bin-by-bin basis. The generation of relative uncertainties based on simulated events is described in
 1639 section [app:systematics]. The bin-to-bin correlation value is set to unity since their contributions are
 1640 determined by pairs of dedicated samples.

1641 The tables 190, 191, 192 and 193 provide the χ^2 and p -values resulting from the comparisons of the
 1642 differential cross-sections with predictions for particle and parton-level results.

1643 Subsections W.1 and W.2 give the covariance and correlation matrices for all the differential cross section
 1644 results.

Observable	PWG+PY8		MG5_AMC@NLO+Py8		PWG+H7		PWG+PY8 (more IFSR)		PWG+PY8 (less IFSR)		SHERPA 2.2.1	
	χ^2/NDF	$p\text{-value}$										
p_T^t	5.2/7	0.63	4.8/7	0.68	5.4/7	0.61	4.5/7	0.72	6.2/7	0.52	6.2/7	0.51
$ y^t $	12.2/8	0.14	8.9/8	0.35	10.3/8	0.24	10.7/8	0.22	13.3/8	0.10	13.1/8	0.11
$p_T^{t,1}$	10.6/8	0.23	11.5/8	0.18	10.2/8	0.25	10.6/8	0.23	11.6/8	0.17	15.9/8	0.04
$p_T^{t,2}$	19.8/8	0.01	22.5/8	<0.01	17.6/8	0.02	18.0/8	0.02	21.0/8	<0.01	17.0/8	0.03
y_{central}	9.8/7	0.20	4.3/7	0.75	10.2/7	0.18	7.2/7	0.40	13.4/7	0.06	12.0/7	0.10
y_{central}	8.6/8	0.37	8.4/8	0.40	7.6/8	0.47	7.5/8	0.48	8.9/8	0.35	13.5/8	0.10
y_{central}	9.4/10	0.49	7.2/10	0.70	8.5/10	0.58	7.5/10	0.68	11.4/10	0.33	11.6/10	0.31
y_{central}	10.7/8	0.22	11.4/8	0.18	11.8/8	0.16	7.6/8	0.47	15.1/8	0.06	55.3/8	<0.01
y_{central}	6.9/8	0.54	8.0/8	0.43	6.7/8	0.57	6.8/8	0.56	7.4/8	0.49	11.3/8	0.18
y_{central}	14.3/7	0.05	8.3/7	0.31	12.9/7	0.07	10.7/7	0.15	17.0/7	0.02	16.7/7	0.02
$ p_{\text{out}}^{\tau\bar{\tau}} $	6.7/7	0.46	7.3/7	0.40	6.2/7	0.51	6.8/7	0.45	7.2/7	0.40	8.2/7	0.31
$ p_{\text{out}}^{\tau\bar{\tau}} $	5.7/7	0.57	35.1/7	<0.01	3.9/7	0.79	5.4/7	0.61	8.3/7	0.31	12.9/7	0.08
$\Delta\Phi^{\tau\bar{\tau}}$	2.6/4	0.62	31.2/4	<0.01	3.0/4	0.56	0.6/4	0.96	5.8/4	0.22	4.0/4	0.40
$H_T^{\tau\bar{\tau}}$	14.6/10	0.15	11.6/10	0.31	13.7/10	0.19	11.3/10	0.33	16.4/10	0.09	19.4/10	0.04
$\cos\theta^*$	10.4/6	0.11	5.3/6	0.50	9.5/6	0.15	8.3/6	0.22	12.2/6	0.06	16.5/6	0.01

Not reviewed

Table 192: Comparison between the absolute parton-level differential cross-sections and the predictions from several MC generators. For each variable and prediction, a χ^2 and a p -value are calculated using the covariance matrix described in the text, which includes all sources of uncertainty. The number of degrees of freedom (NDF) is equal to N_b , where N_b is the number of bins in the distribution.

Observable	PWG+PY8		MG5_AMC@NLO+Py8		PWG+H7		PWG+PY8 (more IFSR)		PWG+PY8 (less IFSR)		SHERPA 2.2.1	
	χ^2/NDF	$p\text{-value}$										
p_T^t	3.7/6	0.72	4.5/6	0.61	4.0/6	0.67	3.9/6	0.69	4.0/6	0.68	4.3/6	0.64
$ y^t $	4.3/7	0.75	4.1/7	0.77	4.0/7	0.78	4.4/7	0.73	4.3/7	0.74	5.3/7	0.62
$p_T^{t,1}$	5.9/7	0.55	7.0/7	0.43	5.9/7	0.55	6.4/7	0.50	6.2/7	0.52	7.6/7	0.37
$ y^{t,1} $	5.5/7	0.60	8.3/7	0.31	5.1/7	0.65	5.9/7	0.55	5.5/7	0.60	4.7/7	0.70
$p_T^{t,2}$	5.7/6	0.46	2.8/6	0.83	6.1/6	0.41	4.6/6	0.60	7.4/6	0.29	7.0/6	0.32
$ y^{t,2} $	4.4/7	0.73	5.1/7	0.65	4.2/7	0.76	4.4/7	0.73	4.3/7	0.74	5.9/7	0.55
$m^{\tau\bar{\tau}}$	4.0/9	0.91	3.7/9	0.93	3.9/9	0.92	3.9/9	0.92	4.3/9	0.89	4.6/9	0.86
$p_T^{\tau\bar{\tau}}$	5.1/7	0.65	7.0/7	0.42	6.2/7	0.52	3.7/7	0.81	6.8/7	0.45	30.1/7	<0.01
$y^{\tau\bar{\tau}}$	1.8/7	0.97	2.9/7	0.90	2.0/7	0.96	2.0/7	0.96	1.9/7	0.97	4.2/7	0.76
$\chi^{\tau\bar{\tau}}$	7.9/6	0.24	5.0/6	0.55	7.3/6	0.29	6.4/6	0.38	9.0/6	0.17	7.6/6	0.27
$y_B^{\tau\bar{\tau}}$	1.0/6	0.99	1.4/6	0.96	1.0/6	0.98	1.1/6	0.98	1.0/6	0.99	1.0/6	0.99
$ p_{\text{out}}^{\tau\bar{\tau}} $	1.7/6	0.94	16.9/6	<0.01	1.2/6	0.98	1.9/6	0.93	2.7/6	0.84	3.9/6	0.69
$\Delta\Phi^{\tau\bar{\tau}}$	0.5/3	0.93	13.1/3	<0.01	0.7/3	0.87	0.1/3	1.00	1.1/3	0.78	0.2/3	0.98
$H_T^{\tau\bar{\tau}}$	5.2/9	0.81	5.7/9	0.77	7.4/9	0.60	6.9/9	0.64	5.6/9	0.78	5.9/9	0.75
$\cos\theta^*$	5.5/5	0.35	3.2/5	0.66	5.3/5	0.38	5.0/5	0.42	6.2/5	0.29	7.8/5	0.17

Table 193: Comparison between the normalized parton-level differential cross-sections and the predictions from several MC generators. For each variable and prediction, a χ^2 and a p -value are calculated using the covariance matrix described in the text, which includes all sources of uncertainty. The number of degrees of freedom (NDF) is equal to $N_b - 1$, where N_b is the number of bins in the distribution.

1645 W.1. Particle level covariances and correlations

bin [GeV]	500-550	550-600	600-650	650-700	700-750	750-800	800-1000	1000-1200
500-550	2.60e-07	1.72e-07	1.00e-07	8.19e-08	4.89e-08	3.07e-08	1.59e-08	2.83e-09
550-600	1.72e-07	1.32e-07	7.25e-08	5.51e-08	3.36e-08	2.16e-08	1.09e-08	1.83e-09
600-650	1.00e-07	7.25e-08	4.82e-08	3.38e-08	1.93e-08	1.29e-08	6.71e-09	1.21e-09
650-700	8.19e-08	5.51e-08	3.38e-08	3.35e-08	1.76e-08	9.70e-09	5.60e-09	1.06e-09
700-750	4.89e-08	3.36e-08	1.93e-08	1.76e-08	1.54e-08	7.20e-09	3.24e-09	7.74e-10
750-800	3.07e-08	2.16e-08	1.29e-08	9.70e-09	7.20e-09	6.66e-09	2.12e-09	3.29e-10
800-1000	1.59e-08	1.09e-08	6.71e-09	5.60e-09	3.24e-09	2.12e-09	1.65e-09	1.84e-10
1000-1200	2.83e-09	1.83e-09	1.21e-09	1.06e-09	7.74e-10	3.29e-10	1.84e-10	3.79e-10

Table 194: Covariance matrix for the absolute particle-level fiducial phase-space differential cross-section as a function of the transverse momentum of the leading top-quark jet , accounting for the statistical and systematic uncertainties.

bin [GeV]	500-550	550-600	600-650	650-700	700-750	750-800	800-1000	1000-1200
500-550	1.00	0.93	0.90	0.88	0.77	0.74	0.77	0.28
550-600	0.93	1.00	0.91	0.83	0.75	0.73	0.74	0.26
600-650	0.90	0.91	1.00	0.84	0.71	0.72	0.75	0.28
650-700	0.88	0.83	0.84	1.00	0.78	0.65	0.75	0.30
700-750	0.77	0.75	0.71	0.78	1.00	0.71	0.64	0.32
750-800	0.74	0.73	0.72	0.65	0.71	1.00	0.64	0.21
800-1000	0.77	0.74	0.75	0.75	0.64	0.64	1.00	0.23
1000-1200	0.28	0.26	0.28	0.30	0.32	0.21	0.23	1.00

Table 195: Correlation matrix for the absolute particle-level fiducial phase-space differential cross-section as a function of the transverse momentum of the leading top-quark jet , accounting for the statistical and systematic uncertainties.

bin [GeV]	350-400	400-450	450-500	500-550	550-600	600-800	800-1200
350-400	1.75e-08	2.32e-08	3.44e-08	3.56e-08	2.04e-08	8.86e-09	9.38e-10
400-450	2.32e-08	5.20e-08	6.65e-08	6.56e-08	3.89e-08	1.68e-08	1.77e-09
450-500	3.44e-08	6.65e-08	1.08e-07	1.02e-07	5.75e-08	2.52e-08	2.56e-09
500-550	3.56e-08	6.56e-08	1.02e-07	1.11e-07	5.97e-08	2.53e-08	2.47e-09
550-600	2.04e-08	3.89e-08	5.75e-08	5.97e-08	3.96e-08	1.45e-08	1.48e-09
600-800	8.86e-09	1.68e-08	2.52e-08	2.53e-08	1.45e-08	7.01e-09	6.50e-10
800-1200	9.38e-10	1.77e-09	2.56e-09	2.47e-09	1.48e-09	6.50e-10	1.51e-10

Table 196: Covariance matrix for the absolute particle-level fiducial phase-space differential cross-section as a function of the transverse momentum of the second-leading top-quark jet , accounting for the statistical and systematic uncertainties.

bin [GeV]	350-400	400-450	450-500	500-550	550-600	600-800	800-1200
350-400	1.00	0.77	0.79	0.81	0.77	0.80	0.58
400-450	0.77	1.00	0.89	0.86	0.86	0.88	0.63
450-500	0.79	0.89	1.00	0.93	0.88	0.91	0.63
500-550	0.81	0.86	0.93	1.00	0.90	0.91	0.60
550-600	0.77	0.86	0.88	0.90	1.00	0.87	0.61
600-800	0.80	0.88	0.91	0.91	0.87	1.00	0.63
800-1200	0.58	0.63	0.63	0.60	0.61	0.63	1.00

Table 197: Correlation matrix for the absolute particle-level fiducial phase-space differential cross-section as a function of the transverse momentum of the second-leading top-quark jet , accounting for the statistical and systematic uncertainties.

bin [GeV]	0.00-0.30	0.30-0.60	0.60-0.90	0.90-1.20	1.20-1.50	1.50-2.00
0.00-0.30	3.60e-03	3.04e-03	2.85e-03	2.07e-03	1.55e-03	7.26e-04
0.30-0.60	3.04e-03	3.02e-03	2.58e-03	1.88e-03	1.42e-03	6.61e-04
0.60-0.90	2.85e-03	2.58e-03	2.64e-03	1.77e-03	1.35e-03	6.17e-04
0.90-1.20	2.07e-03	1.88e-03	1.77e-03	1.44e-03	9.67e-04	4.49e-04
1.20-1.50	1.55e-03	1.42e-03	1.35e-03	9.67e-04	8.43e-04	3.34e-04
1.50-2.00	7.26e-04	6.61e-04	6.17e-04	4.49e-04	3.34e-04	1.97e-04

Table 198: Covariance matrix for the absolute particle-level fiducial phase-space differential cross-section as a function of absolute value of the rapidity of the leading top-quark jet , accounting for the statistical and systematic uncertainties.

bin [GeV]	0.00-0.30	0.30-0.60	0.60-0.90	0.90-1.20	1.20-1.50	1.50-2.00
0.00-0.30	1.00	0.92	0.92	0.91	0.89	0.86
0.30-0.60	0.92	1.00	0.91	0.90	0.89	0.86
0.60-0.90	0.92	0.91	1.00	0.91	0.90	0.86
0.90-1.20	0.91	0.90	0.91	1.00	0.88	0.84
1.20-1.50	0.89	0.89	0.90	0.88	1.00	0.82
1.50-2.00	0.86	0.86	0.86	0.84	0.82	1.00

Table 199: Correlation matrix for the absolute particle-level fiducial phase-space differential cross-section as a function of absolute value of the rapidity of the leading top-quark jet , accounting for the statistical and systematic uncertainties.

bin [GeV]	0.00-0.30	0.30-0.60	0.60-0.90	0.90-1.20	1.20-1.50	1.50-2.00
0.00-0.30	4.43e-03	3.76e-03	2.77e-03	2.36e-03	1.58e-03	7.37e-04
0.30-0.60	3.76e-03	3.65e-03	2.46e-03	2.13e-03	1.44e-03	6.65e-04
0.60-0.90	2.77e-03	2.46e-03	2.07e-03	1.55e-03	1.04e-03	4.86e-04
0.90-1.20	2.36e-03	2.13e-03	1.55e-03	1.49e-03	8.81e-04	4.18e-04
1.20-1.50	1.58e-03	1.44e-03	1.04e-03	8.81e-04	7.44e-04	2.75e-04
1.50-2.00	7.37e-04	6.65e-04	4.86e-04	4.18e-04	2.75e-04	1.55e-04

Table 200: Covariance matrix for the absolute particle-level fiducial phase-space differential cross-section as a function of absolute value of the rapidity of the second-leading top-quark jet , accounting for the statistical and systematic uncertainties.

bin [GeV]	0.00-0.30	0.30-0.60	0.60-0.90	0.90-1.20	1.20-1.50	1.50-2.00
0.00-0.30	1.00	0.94	0.92	0.92	0.87	0.89
0.30-0.60	0.94	1.00	0.90	0.91	0.87	0.88
0.60-0.90	0.92	0.90	1.00	0.88	0.84	0.86
0.90-1.20	0.92	0.91	0.88	1.00	0.84	0.87
1.20-1.50	0.87	0.87	0.84	0.84	1.00	0.81
1.50-2.00	0.89	0.88	0.86	0.87	0.81	1.00

Table 201: Correlation matrix for the absolute particle-level fiducial phase-space differential cross-section as a function of absolute value of the rapidity of the second-leading top-quark jet , accounting for the statistical and systematic uncertainties.

bin [GeV]	0-100	100-150	150-200	200-300	300-500	500-800
0-100	1.54e-07	9.41e-08	6.04e-08	2.94e-08	9.69e-09	9.85e-10
100-150	9.41e-08	7.30e-08	4.11e-08	1.86e-08	6.59e-09	5.79e-10
150-200	6.04e-08	4.11e-08	3.21e-08	1.28e-08	4.14e-09	4.07e-10
200-300	2.94e-08	1.86e-08	1.28e-08	8.22e-09	1.97e-09	2.08e-10
300-500	9.69e-09	6.59e-09	4.14e-09	1.97e-09	1.02e-09	6.04e-11
500-800	9.85e-10	5.79e-10	4.07e-10	2.08e-10	6.04e-11	2.40e-11

Table 202: Covariance matrix for the absolute particle-level fiducial phase-space differential cross-section as a function of transverse momentum of the $t\bar{t}$ system , accounting for the statistical and systematic uncertainties.

bin [GeV]	0-100	100-150	150-200	200-300	300-500	500-800
0-100	1.00	0.89	0.86	0.83	0.77	0.51
100-150	0.89	1.00	0.85	0.76	0.76	0.44
150-200	0.86	0.85	1.00	0.79	0.72	0.46
200-300	0.83	0.76	0.79	1.00	0.68	0.47
300-500	0.77	0.76	0.72	0.68	1.00	0.39
500-800	0.51	0.44	0.46	0.47	0.39	1.00

Table 203: Correlation matrix for the absolute particle-level fiducial phase-space differential cross-section as a function of transverse momentum of the $t\bar{t}$ system , accounting for the statistical and systematic uncertainties.

Not reviewed, for internal circulation only

bin [GeV]	1.00-1.10	1.10-1.20	1.20-1.30	1.30-1.40	1.40-1.50	1.50-1.70	1.70-1.90	1.90-2.10	2.10-2.30	2.30-3.00
1.00-1.10	1.41e-02	1.65e-02	1.24e-02	9.05e-03	8.81e-03	4.19e-03	3.70e-03	1.59e-03	9.58e-04	2.34e-04
1.10-1.20	1.65e-02	2.54e-02	1.69e-02	1.19e-02	1.20e-02	5.64e-03	5.00e-03	2.21e-03	1.26e-03	2.96e-04
1.20-1.30	1.24e-02	1.69e-02	1.44e-02	9.20e-03	8.66e-03	4.26e-03	3.73e-03	1.61e-03	9.66e-04	2.37e-04
1.30-1.40	9.05e-03	1.19e-02	9.20e-03	8.12e-03	6.36e-03	2.98e-03	2.69e-03	1.15e-03	7.45e-04	1.83e-04
1.40-1.50	8.81e-03	1.20e-02	8.66e-03	6.36e-03	7.41e-03	2.85e-03	2.60e-03	1.12e-03	6.60e-04	1.67e-04
1.50-1.70	4.19e-03	5.64e-03	4.26e-03	2.98e-03	2.85e-03	1.91e-03	1.18e-03	5.31e-04	3.21e-04	8.05e-05
1.70-1.90	3.70e-03	5.00e-03	3.73e-03	2.69e-03	2.60e-03	1.18e-03	1.42e-03	4.54e-04	2.66e-04	7.19e-05
1.90-2.10	1.59e-03	2.21e-03	1.61e-03	1.15e-03	1.12e-03	5.31e-04	4.54e-04	3.73e-04	1.09e-04	2.80e-05
2.10-2.30	9.58e-04	1.26e-03	9.66e-04	7.45e-04	6.60e-04	3.21e-04	2.66e-04	1.09e-04	2.09e-04	1.70e-05
2.30-3.00	2.34e-04	2.96e-04	2.37e-04	1.83e-04	1.67e-04	8.05e-05	7.19e-05	2.80e-05	1.70e-05	1.52e-05

Table 204: Covariance matrix for the absolute particle-level fiducial phase-space differential cross-section as a function of invariant mass of the $t\bar{t}$ system , accounting for the statistical and systematic uncertainties.

bin [GeV]	1.00-1.10	1.10-1.20	1.20-1.30	1.30-1.40	1.40-1.50	1.50-1.70	1.70-1.90	1.90-2.10	2.10-2.30	2.30-3.00
1.00-1.10	1.00	0.87	0.87	0.85	0.86	0.81	0.83	0.69	0.56	0.51
1.10-1.20	0.87	1.00	0.89	0.83	0.87	0.81	0.83	0.72	0.55	0.48
1.20-1.30	0.87	0.89	1.00	0.85	0.84	0.81	0.83	0.70	0.56	0.51
1.30-1.40	0.85	0.83	0.85	1.00	0.82	0.76	0.79	0.66	0.57	0.52
1.40-1.50	0.86	0.87	0.84	0.82	1.00	0.76	0.80	0.67	0.53	0.50
1.50-1.70	0.81	0.81	0.81	0.76	0.76	1.00	0.72	0.63	0.51	0.47
1.70-1.90	0.83	0.83	0.83	0.79	0.80	0.72	1.00	0.62	0.49	0.49
1.90-2.10	0.69	0.72	0.70	0.66	0.67	0.63	0.62	1.00	0.39	0.37
2.10-2.30	0.56	0.55	0.56	0.57	0.53	0.51	0.49	0.39	1.00	0.30
2.30-3.00	0.51	0.48	0.51	0.52	0.50	0.47	0.49	0.37	0.30	1.00

Table 205: Correlation matrix for the absolute particle-level fiducial phase-space differential cross-section as a function of invariant mass of the $t\bar{t}$ system , accounting for the statistical and systematic uncertainties.

Not reviewed, for internal circulation only

bin [GeV]	0.00-0.30	0.30-0.60	0.60-0.90	0.90-1.20	1.20-1.50	1.50-2.00
0.00-0.30	6.83e-03	5.20e-03	3.67e-03	3.00e-03	1.22e-03	1.56e-04
0.30-0.60	5.20e-03	4.51e-03	2.98e-03	2.38e-03	9.84e-04	1.27e-04
0.60-0.90	3.67e-03	2.98e-03	2.40e-03	1.66e-03	7.00e-04	9.88e-05
0.90-1.20	3.00e-03	2.38e-03	1.66e-03	1.53e-03	5.59e-04	7.15e-05
1.20-1.50	1.22e-03	9.84e-04	7.00e-04	5.59e-04	2.90e-04	2.96e-05
1.50-2.00	1.56e-04	1.27e-04	9.88e-05	7.15e-05	2.96e-05	1.16e-05

Table 206: Covariance matrix for the absolute particle-level fiducial phase-space differential cross-section as a function of absolute value of the rapidity of the $t\bar{t}$ system , accounting for the statistical and systematic uncertainties.

bin [GeV]	0.00-0.30	0.30-0.60	0.60-0.90	0.90-1.20	1.20-1.50	1.50-2.00
0.00-0.30	1.00	0.94	0.91	0.93	0.87	0.55
0.30-0.60	0.94	1.00	0.90	0.91	0.86	0.55
0.60-0.90	0.91	0.90	1.00	0.87	0.84	0.59
0.90-1.20	0.93	0.91	0.87	1.00	0.84	0.54
1.20-1.50	0.87	0.86	0.84	0.84	1.00	0.51
1.50-2.00	0.55	0.55	0.59	0.54	0.51	1.00

Table 207: Correlation matrix for the absolute particle-level fiducial phase-space differential cross-section as a function of absolute value of the rapidity of the $t\bar{t}$ system , accounting for the statistical and systematic uncertainties.

bin [GeV]	0.00-0.20	0.20-0.40	0.40-0.60	0.60-0.70	0.70-0.80	0.80-1.00
0.00-0.20	1.18e-02	1.08e-02	9.45e-03	7.87e-03	4.50e-03	9.01e-04
0.20-0.40	1.08e-02	1.13e-02	9.15e-03	7.66e-03	4.40e-03	8.83e-04
0.40-0.60	9.45e-03	9.15e-03	8.54e-03	6.60e-03	3.80e-03	7.59e-04
0.60-0.70	7.87e-03	7.66e-03	6.60e-03	6.73e-03	3.05e-03	6.41e-04
0.70-0.80	4.50e-03	4.40e-03	3.80e-03	3.05e-03	2.41e-03	3.46e-04
0.80-1.00	9.01e-04	8.83e-04	7.59e-04	6.41e-04	3.46e-04	1.57e-04

Table 208: Covariance matrix for the absolute particle-level fiducial phase-space differential cross-section as a function of production angle in the Collins-Soper reference frame , accounting for the statistical and systematic uncertainties.

bin [GeV]	0.00-0.20	0.20-0.40	0.40-0.60	0.60-0.70	0.70-0.80	0.80-1.00
0.00-0.20	1.00	0.94	0.94	0.88	0.85	0.66
0.20-0.40	0.94	1.00	0.93	0.88	0.85	0.66
0.40-0.60	0.94	0.93	1.00	0.87	0.84	0.65
0.60-0.70	0.88	0.88	0.87	1.00	0.76	0.62
0.70-0.80	0.85	0.85	0.84	0.76	1.00	0.56
0.80-1.00	0.66	0.66	0.65	0.62	0.56	1.00

Table 209: Correlation matrix for the absolute particle-level fiducial phase-space differential cross-section as a function of production angle in the Collins-Soper reference frame , accounting for the statistical and systematic uncertainties.

bin [GeV]	1000-1100	1100-1200	1200-1300	1300-1400	1400-1600	1600-1800	1800-2200
1000-1100	5.61e-08	2.77e-08	1.60e-08	1.25e-08	6.87e-09	4.21e-09	6.28e-10
1100-1200	2.77e-08	1.72e-08	8.64e-09	6.81e-09	3.74e-09	2.33e-09	3.72e-10
1200-1300	1.60e-08	8.64e-09	6.97e-09	3.79e-09	2.15e-09	1.40e-09	2.48e-10
1300-1400	1.25e-08	6.81e-09	3.79e-09	4.30e-09	1.65e-09	1.10e-09	1.86e-10
1400-1600	6.87e-09	3.74e-09	2.15e-09	1.65e-09	1.30e-09	5.60e-10	9.81e-11
1600-1800	4.21e-09	2.33e-09	1.40e-09	1.10e-09	5.60e-10	6.24e-10	5.37e-11
1800-2200	6.28e-10	3.72e-10	2.48e-10	1.86e-10	9.81e-11	5.37e-11	7.28e-11

Table 210: Covariance matrix for the absolute particle-level fiducial phase-space differential cross-section as a function of scalar sum of the transverse momenta of the two top-quark jets , accounting for the statistical and systematic uncertainties.

bin [GeV]	1000-1100	1100-1200	1200-1300	1300-1400	1400-1600	1600-1800	1800-2200
1000-1100	1.00	0.89	0.81	0.81	0.80	0.71	0.31
1100-1200	0.89	1.00	0.79	0.79	0.79	0.71	0.33
1200-1300	0.81	0.79	1.00	0.69	0.71	0.67	0.35
1300-1400	0.81	0.79	0.69	1.00	0.70	0.67	0.33
1400-1600	0.80	0.79	0.71	0.70	1.00	0.62	0.32
1600-1800	0.71	0.71	0.67	0.67	0.62	1.00	0.25
1800-2200	0.31	0.33	0.35	0.33	0.32	0.25	1.00

Table 211: Correlation matrix for the absolute particle-level fiducial phase-space differential cross-section as a function of scalar sum of the transverse momenta of the two top-quark jets , accounting for the statistical and systematic uncertainties.

bin [GeV]	0.00-0.30	0.30-0.60	0.60-0.80	0.80-1.00	1.00-1.20	1.20-1.40	1.40-2.00
0.00-0.30	7.10e-03	5.23e-03	3.75e-03	3.46e-03	3.05e-03	1.18e-03	3.43e-04
0.30-0.60	5.23e-03	4.41e-03	2.93e-03	2.68e-03	2.31e-03	9.18e-04	2.60e-04
0.60-0.80	3.75e-03	2.93e-03	2.52e-03	1.91e-03	1.64e-03	6.73e-04	1.93e-04
0.80-1.00	3.46e-03	2.68e-03	1.91e-03	2.06e-03	1.52e-03	6.06e-04	1.77e-04
1.00-1.20	3.05e-03	2.31e-03	1.64e-03	1.52e-03	1.57e-03	5.10e-04	1.55e-04
1.20-1.40	1.18e-03	9.18e-04	6.73e-04	6.06e-04	5.10e-04	2.95e-04	5.85e-05
1.40-2.00	3.43e-04	2.60e-04	1.93e-04	1.77e-04	1.55e-04	5.85e-05	2.61e-05

Table 212: Covariance matrix for the absolute particle-level fiducial phase-space differential cross-section as a function of longitudinal boost y_B^{tt} , accounting for the statistical and systematic uncertainties.

bin [GeV]	0.00-0.30	0.30-0.60	0.60-0.80	0.80-1.00	1.00-1.20	1.20-1.40	1.40-2.00
0.00-0.30	1.00	0.93	0.89	0.91	0.91	0.81	0.80
0.30-0.60	0.93	1.00	0.88	0.89	0.88	0.80	0.77
0.60-0.80	0.89	0.88	1.00	0.84	0.82	0.78	0.75
0.80-1.00	0.91	0.89	0.84	1.00	0.85	0.78	0.76
1.00-1.20	0.91	0.88	0.82	0.85	1.00	0.75	0.77
1.20-1.40	0.81	0.80	0.78	0.78	0.75	1.00	0.67
1.40-2.00	0.80	0.77	0.75	0.76	0.77	0.67	1.00

Table 213: Correlation matrix for the absolute particle-level fiducial phase-space differential cross-section as a function of longitudinal boost y_B^{tt} , accounting for the statistical and systematic uncertainties.

bin [GeV]	0.00-2.50	2.50-2.75	2.75-3.00	3.00-3.14
0.00-2.50	1.23e-06	1.33e-05	5.54e-05	2.80e-04
2.50-2.75	1.33e-05	4.80e-04	9.68e-04	5.28e-03
2.75-3.00	5.54e-05	9.68e-04	5.21e-03	2.45e-02
3.00-3.14	2.80e-04	5.28e-03	2.45e-02	1.30e-01

Table 214: Covariance matrix for the absolute particle-level fiducial phase-space differential cross-section as a function of azimuthal angle between the two top-quark jets $\Delta\phi_{t\bar{t}}$, accounting for the statistical and systematic uncertainties.

bin [GeV]	0.00-2.50	2.50-2.75	2.75-3.00	3.00-3.14
0.00-2.50	1.00	0.55	0.69	0.70
2.50-2.75	0.55	1.00	0.61	0.67
2.75-3.00	0.69	0.61	1.00	0.94
3.00-3.14	0.70	0.67	0.94	1.00

Table 215: Correlation matrix for the absolute particle-level fiducial phase-space differential cross-section as a function of azimuthal angle between the two top-quark jets $\Delta\phi_{t\bar{t}}$, accounting for the statistical and systematic uncertainties.

bin [GeV]	1.00-1.50	1.50-2.00	2-3	3-4	4-5	5-7	7-10
1.00-1.50	1.72e-03	1.10e-03	6.87e-04	3.41e-04	1.97e-04	1.19e-04	2.86e-05
1.50-2.00	1.10e-03	8.24e-04	4.63e-04	2.33e-04	1.33e-04	8.09e-05	1.98e-05
2-3	6.87e-04	4.63e-04	3.09e-04	1.43e-04	8.29e-05	4.99e-05	1.20e-05
3-4	3.41e-04	2.33e-04	1.43e-04	8.26e-05	4.11e-05	2.50e-05	5.99e-06
4-5	1.97e-04	1.33e-04	8.29e-05	4.11e-05	3.28e-05	1.40e-05	3.45e-06
5-7	1.19e-04	8.09e-05	4.99e-05	2.50e-05	1.40e-05	1.03e-05	2.05e-06
7-10	2.86e-05	1.98e-05	1.20e-05	5.99e-06	3.45e-06	2.05e-06	8.34e-07

Table 216: Covariance matrix for the absolute particle-level fiducial phase-space differential cross-section as a function of production angle $\chi^{t\bar{t}}$, accounting for the statistical and systematic uncertainties.

bin [GeV]	1.00-1.50	1.50-2.00	2-3	3-4	4-5	5-7	7-10
1.00-1.50	1.00	0.93	0.94	0.91	0.83	0.89	0.76
1.50-2.00	0.93	1.00	0.92	0.89	0.81	0.88	0.75
2-3	0.94	0.92	1.00	0.90	0.82	0.88	0.75
3-4	0.91	0.89	0.90	1.00	0.79	0.85	0.72
4-5	0.83	0.81	0.82	0.79	1.00	0.76	0.66
5-7	0.89	0.88	0.88	0.85	0.76	1.00	0.70
7-10	0.76	0.75	0.75	0.72	0.66	0.70	1.00

Table 217: Correlation matrix for the absolute particle-level fiducial phase-space differential cross-section as a function of production angle $\chi^{t\bar{t}}$, accounting for the statistical and systematic uncertainties.

bin [GeV]	0-20	20-40	40-60	60-100	100-200	200-300	300-600
0-20	1.19e-06	8.35e-07	4.65e-07	3.19e-07	9.97e-08	2.93e-08	7.52e-09
20-40	8.35e-07	7.01e-07	3.58e-07	2.40e-07	7.64e-08	2.27e-08	5.89e-09
40-60	4.65e-07	3.58e-07	2.37e-07	1.32e-07	4.22e-08	1.34e-08	3.35e-09
60-100	3.19e-07	2.40e-07	1.32e-07	1.04e-07	2.78e-08	8.78e-09	2.29e-09
100-200	9.97e-08	7.64e-08	4.22e-08	2.78e-08	1.12e-08	2.79e-09	7.23e-10
200-300	2.93e-08	2.27e-08	1.34e-08	8.78e-09	2.79e-09	1.84e-09	2.28e-10
300-600	7.52e-09	5.89e-09	3.35e-09	2.29e-09	7.23e-10	2.28e-10	1.21e-10

Table 218: Covariance matrix for the absolute particle-level fiducial phase-space differential cross-section as a function of absolute value of the out-of-plane momentum $p_{out}^{t\bar{t}}$, accounting for the statistical and systematic uncertainties.

bin [GeV]	0-20	20-40	40-60	60-100	100-200	200-300	300-600
0-20	1.00	0.92	0.88	0.91	0.86	0.63	0.63
20-40	0.92	1.00	0.88	0.89	0.86	0.63	0.64
40-60	0.88	0.88	1.00	0.84	0.82	0.64	0.63
60-100	0.91	0.89	0.84	1.00	0.81	0.64	0.65
100-200	0.86	0.86	0.82	0.81	1.00	0.61	0.62
200-300	0.63	0.63	0.64	0.64	0.61	1.00	0.48
300-600	0.63	0.64	0.63	0.65	0.62	0.48	1.00

Table 219: Correlation matrix for the absolute particle-level fiducial phase-space differential cross-section as a function of absolute value of the out-of-plane momentum $p_{out}^{t\bar{t}}$, accounting for the statistical and systematic uncertainties.

bin [GeV]	500-550	550-600	600-650	650-700	700-750	750-800	800-1000	1000-1200
500-550	1.87e-07	1.74e-08	-1.40e-08	5.80e-09	-1.05e-08	-1.09e-08	-6.48e-09	-2.68e-09
550-600	1.74e-08	9.89e-08	1.45e-08	-6.03e-09	-3.83e-09	-3.14e-09	-3.40e-09	-9.95e-10
600-650	-1.40e-08	1.45e-08	5.70e-08	1.67e-08	-6.14e-09	1.08e-09	1.98e-09	6.48e-10
650-700	5.80e-09	-6.03e-09	1.67e-08	5.55e-08	8.35e-09	-6.67e-09	3.20e-09	1.15e-09
700-750	-1.05e-08	-3.83e-09	-6.14e-09	8.35e-09	4.08e-08	5.92e-09	-3.65e-10	1.04e-09
750-800	-1.09e-08	-3.14e-09	1.08e-09	-6.67e-09	5.92e-09	2.22e-08	6.60e-10	-5.72e-10
800-1000	-6.48e-09	-3.40e-09	1.98e-09	3.20e-09	-3.65e-10	6.60e-10	5.20e-09	-1.42e-11
1000-1200	-2.68e-09	-9.95e-10	6.48e-10	1.15e-09	1.04e-09	-5.72e-10	-1.42e-11	2.77e-09

Table 220: Covariance matrix for the normalized particle-level fiducial phase-space differential cross-section as a function of the transverse momentum of the leading top-quark jet , accounting for the statistical and systematic uncertainties.

bin [GeV]	500-550	550-600	600-650	650-700	700-750	750-800	800-1000	1000-1200
500-550	1.00	0.13	-0.14	0.06	-0.12	-0.17	-0.21	-0.12
550-600	0.13	1.00	0.19	-0.08	-0.06	-0.07	-0.15	-0.06
600-650	-0.14	0.19	1.00	0.30	-0.13	0.03	0.12	0.05
650-700	0.06	-0.08	0.30	1.00	0.18	-0.19	0.19	0.09
700-750	-0.12	-0.06	-0.13	0.18	1.00	0.20	-0.03	0.10
750-800	-0.17	-0.07	0.03	-0.19	0.20	1.00	0.06	-0.07
800-1000	-0.21	-0.15	0.12	0.19	-0.03	0.06	1.00	-0.00
1000-1200	-0.12	-0.06	0.05	0.09	0.10	-0.07	-0.00	1.00

Table 221: Correlation matrix for the normalized particle-level fiducial phase-space differential cross-section as a function of the transverse momentum of the leading top-quark jet , accounting for the statistical and systematic uncertainties.

bin [GeV]	350-400	400-450	450-500	500-550	550-600	600-800	800-1200
350-400	5.11e-08	7.28e-09	-7.19e-10	6.14e-09	7.52e-10	-1.50e-10	-4.91e-10
400-450	7.28e-09	9.31e-08	1.95e-08	-3.95e-09	-1.09e-09	7.94e-10	-1.21e-09
450-500	-7.19e-10	1.95e-08	9.68e-08	1.21e-08	-1.34e-08	3.53e-09	-1.01e-09
500-550	6.14e-09	-3.95e-09	1.21e-08	7.12e-08	2.79e-09	-2.66e-09	-1.50e-09
550-600	7.52e-10	-1.09e-09	-1.34e-08	2.79e-09	5.06e-08	1.17e-10	1.87e-10
600-800	-1.50e-10	7.94e-10	3.53e-09	-2.66e-09	1.17e-10	7.33e-09	2.97e-10
800-1200	-4.91e-10	-1.21e-09	-1.01e-09	-1.50e-09	1.87e-10	2.97e-10	7.95e-10

Table 222: Covariance matrix for the normalized particle-level fiducial phase-space differential cross-section as a function of the transverse momentum of the second-leading top-quark jet , accounting for the statistical and systematic uncertainties.

bin [GeV]	350-400	400-450	450-500	500-550	550-600	600-800	800-1200
350-400	1.00	0.11	-0.01	0.10	0.01	-0.01	-0.08
400-450	0.11	1.00	0.20	-0.05	-0.02	0.03	-0.14
450-500	-0.01	0.20	1.00	0.15	-0.19	0.13	-0.12
500-550	0.10	-0.05	0.15	1.00	0.05	-0.12	-0.20
550-600	0.01	-0.02	-0.19	0.05	1.00	0.01	0.03
600-800	-0.01	0.03	0.13	-0.12	0.01	1.00	0.12
800-1200	-0.08	-0.14	-0.12	-0.20	0.03	0.12	1.00

Table 223: Correlation matrix for the normalized particle-level fiducial phase-space differential cross-section as a function of the transverse momentum of the second-leading top-quark jet , accounting for the statistical and systematic uncertainties.

bin [GeV]	0.00-0.30	0.30-0.60	0.60-0.90	0.90-1.20	1.20-1.50	1.50-2.00
0.00-0.30	1.84e-03	-2.98e-04	1.41e-04	-1.87e-04	-9.07e-06	-4.15e-05
0.30-0.60	-2.98e-04	2.03e-03	9.54e-05	-2.42e-05	9.62e-05	-6.32e-05
0.60-0.90	1.41e-04	9.54e-05	2.04e-03	-1.01e-06	2.51e-04	7.47e-05
0.90-1.20	-1.87e-04	-2.42e-05	-1.01e-06	1.24e-03	-4.09e-05	-3.69e-05
1.20-1.50	-9.07e-06	9.62e-05	2.51e-04	-4.09e-05	9.21e-04	-6.96e-06
1.50-2.00	-4.15e-05	-6.32e-05	7.47e-05	-3.69e-05	-6.96e-06	3.30e-04

Table 224: Covariance matrix for the normalized particle-level fiducial phase-space differential cross-section as a function of absolute value of the rapidity of the leading top-quark jet , accounting for the statistical and systematic uncertainties.

bin [GeV]	0.00-0.30	0.30-0.60	0.60-0.90	0.90-1.20	1.20-1.50	1.50-2.00
0.00-0.30	1.00	-0.15	0.07	-0.12	-0.01	-0.05
0.30-0.60	-0.15	1.00	0.05	-0.02	0.07	-0.08
0.60-0.90	0.07	0.05	1.00	-0.00	0.18	0.09
0.90-1.20	-0.12	-0.02	-0.00	1.00	-0.04	-0.06
1.20-1.50	-0.01	0.07	0.18	-0.04	1.00	-0.01
1.50-2.00	-0.05	-0.08	0.09	-0.06	-0.01	1.00

Table 225: Correlation matrix for the normalized particle-level fiducial phase-space differential cross-section as a function of absolute value of the rapidity of the leading top-quark jet , accounting for the statistical and systematic uncertainties.

bin [GeV]	0.00-0.30	0.30-0.60	0.60-0.90	0.90-1.20	1.20-1.50	1.50-2.00
0.00-0.30	1.71e-03	-2.95e-04	-9.71e-05	-1.69e-04	1.27e-04	-2.11e-05
0.30-0.60	-2.95e-04	1.74e-03	-2.33e-04	-1.19e-04	9.33e-06	-2.33e-05
0.60-0.90	-9.71e-05	-2.33e-04	2.12e-03	-5.78e-05	3.54e-05	5.44e-05
0.90-1.20	-1.69e-04	-1.19e-04	-5.78e-05	1.31e-03	-1.12e-04	3.80e-06
1.20-1.50	1.27e-04	9.33e-06	3.54e-05	-1.12e-04	1.30e-03	-1.38e-05
1.50-2.00	-2.11e-05	-2.33e-05	5.44e-05	3.80e-06	-1.38e-05	2.13e-04

Table 226: Covariance matrix for the normalized particle-level fiducial phase-space differential cross-section as a function of absolute value of the rapidity of the second-leading top-quark jet , accounting for the statistical and systematic uncertainties.

bin [GeV]	0.00-0.30	0.30-0.60	0.60-0.90	0.90-1.20	1.20-1.50	1.50-2.00
0.00-0.30	1.00	-0.17	-0.05	-0.11	0.09	-0.03
0.30-0.60	-0.17	1.00	-0.12	-0.08	0.01	-0.04
0.60-0.90	-0.05	-0.12	1.00	-0.03	0.02	0.08
0.90-1.20	-0.11	-0.08	-0.03	1.00	-0.09	0.01
1.20-1.50	0.09	0.01	0.02	-0.09	1.00	-0.03
1.50-2.00	-0.03	-0.04	0.08	0.01	-0.03	1.00

Table 227: Correlation matrix for the normalized particle-level fiducial phase-space differential cross-section as a function of absolute value of the rapidity of the second-leading top-quark jet , accounting for the statistical and systematic uncertainties.

bin [GeV]	0-100	100-150	150-200	200-300	300-500	500-800
0-100	4.23e-08	-1.22e-08	-8.36e-09	6.38e-09	-2.67e-09	1.20e-10
100-150	-1.22e-08	1.16e-07	3.29e-09	-1.53e-10	1.13e-09	1.64e-09
150-200	-8.36e-09	3.29e-09	5.46e-08	4.71e-09	-9.24e-10	1.37e-10
200-300	6.38e-09	-1.53e-10	4.71e-09	2.13e-08	-6.65e-10	2.80e-10
300-500	-2.67e-09	1.13e-09	-9.24e-10	-6.65e-10	2.96e-09	2.89e-11
500-800	1.20e-10	1.64e-09	1.37e-10	2.80e-10	2.89e-11	1.78e-10

Table 228: Covariance matrix for the normalized particle-level fiducial phase-space differential cross-section as a function of transverse momentum of the $t\bar{t}$ system , accounting for the statistical and systematic uncertainties.

bin [GeV]	0-100	100-150	150-200	200-300	300-500	500-800
0-100	1.00	-0.17	-0.17	0.21	-0.24	0.04
100-150	-0.17	1.00	0.04	-0.00	0.06	0.36
150-200	-0.17	0.04	1.00	0.14	-0.07	0.04
200-300	0.21	-0.00	0.14	1.00	-0.08	0.14
300-500	-0.24	0.06	-0.07	-0.08	1.00	0.04
500-800	0.04	0.36	0.04	0.14	0.04	1.00

Table 229: Correlation matrix for the normalized particle-level fiducial phase-space differential cross-section as a function of transverse momentum of the $t\bar{t}$ system , accounting for the statistical and systematic uncertainties.

bin [GeV]	1.00-1.10	1.10-1.20	1.20-1.30	1.30-1.40	1.40-1.50	1.50-1.70	1.70-1.90	1.90-2.10	2.10-2.30	2.30-3.00
1.00-1.10	1.91e-02	1.09e-03	-2.83e-03	1.50e-03	5.59e-04	9.08e-04	-7.00e-05	-1.55e-05	4.52e-04	-1.40e-04
1.10-1.20	1.09e-03	2.72e-02	-1.33e-03	5.46e-03	2.55e-03	2.06e-03	1.09e-03	1.18e-03	1.95e-03	3.76e-05
1.20-1.30	-2.83e-03	-1.33e-03	1.42e-02	-3.34e-04	-2.35e-03	-2.30e-04	-2.74e-04	-1.57e-04	-9.35e-05	-6.73e-05
1.30-1.40	1.50e-03	5.46e-03	-3.34e-04	1.83e-02	2.02e-03	-1.74e-04	1.85e-03	1.04e-03	1.91e-03	2.00e-04
1.40-1.50	5.59e-04	2.55e-03	-2.35e-03	2.02e-03	1.13e-02	-4.52e-04	4.55e-04	3.33e-04	6.49e-04	8.44e-05
1.50-1.70	9.08e-04	2.06e-03	-2.30e-04	-1.74e-04	-4.52e-04	5.03e-03	-4.94e-04	1.18e-04	4.37e-04	1.04e-05
1.70-1.90	-7.00e-05	1.09e-03	-2.74e-04	1.85e-03	4.55e-04	-4.94e-04	3.36e-03	8.60e-05	4.29e-04	1.01e-04
1.90-2.10	-1.55e-05	1.18e-03	-1.57e-04	1.04e-03	3.33e-04	1.18e-04	8.60e-05	1.69e-03	2.11e-04	2.74e-05
2.10-2.30	4.52e-04	1.95e-03	-9.35e-05	1.91e-03	6.49e-04	4.37e-04	4.29e-04	2.11e-04	1.64e-03	3.66e-05
2.30-3.00	-1.40e-04	3.76e-05	-6.73e-05	2.00e-04	8.44e-05	1.04e-05	1.01e-04	2.74e-05	3.66e-05	1.02e-04

Table 230: Covariance matrix for the normalized particle-level fiducial phase-space differential cross-section as a function of invariant mass of the $t\bar{t}$ system , accounting for the statistical and systematic uncertainties.

bin [GeV]	1.00-1.10	1.10-1.20	1.20-1.30	1.30-1.40	1.40-1.50	1.50-1.70	1.70-1.90	1.90-2.10	2.10-2.30	2.30-3.00
1.00-1.10	1.00	0.05	-0.17	0.08	0.04	0.09	-0.01	-0.00	0.08	-0.10
1.10-1.20	0.05	1.00	-0.07	0.24	0.15	0.18	0.11	0.17	0.29	0.02
1.20-1.30	-0.17	-0.07	1.00	-0.02	-0.19	-0.03	-0.04	-0.03	-0.02	-0.06
1.30-1.40	0.08	0.24	-0.02	1.00	0.14	-0.02	0.24	0.19	0.35	0.15
1.40-1.50	0.04	0.15	-0.19	0.14	1.00	-0.06	0.07	0.08	0.15	0.08
1.50-1.70	0.09	0.18	-0.03	-0.02	-0.06	1.00	-0.12	0.04	0.15	0.01
1.70-1.90	-0.01	0.11	-0.04	0.24	0.07	-0.12	1.00	0.04	0.18	0.17
1.90-2.10	-0.00	0.17	-0.03	0.19	0.08	0.04	0.04	1.00	0.13	0.07
2.10-2.30	0.08	0.29	-0.02	0.35	0.15	0.15	0.18	0.13	1.00	0.09
2.30-3.00	-0.10	0.02	-0.06	0.15	0.08	0.01	0.17	0.07	0.09	1.00

Table 231: Correlation matrix for the normalized particle-level fiducial phase-space differential cross-section as a function of invariant mass of the $t\bar{t}$ system , accounting for the statistical and systematic uncertainties.

Not reviewed, for internal circulation only

bin [GeV]	0.00-0.30	0.30-0.60	0.60-0.90	0.90-1.20	1.20-1.50	1.50-2.00
0.00-0.30	2.45e-03	-6.06e-04	5.68e-04	3.11e-04	-1.12e-04	1.06e-04
0.30-0.60	-6.06e-04	2.48e-03	-1.73e-04	3.07e-04	-2.94e-05	4.31e-05
0.60-0.90	5.68e-04	-1.73e-04	3.07e-03	7.29e-04	4.71e-05	1.88e-04
0.90-1.20	3.11e-04	3.07e-04	7.29e-04	1.96e-03	9.34e-06	1.25e-04
1.20-1.50	-1.12e-04	-2.94e-05	4.71e-05	9.34e-06	4.97e-04	1.19e-06
1.50-2.00	1.06e-04	4.31e-05	1.88e-04	1.25e-04	1.19e-06	8.43e-05

Table 232: Covariance matrix for the normalized particle-level fiducial phase-space differential cross-section as a function of absolute value of the rapidity of the $t\bar{t}$ system , accounting for the statistical and systematic uncertainties.

bin [GeV]	0.00-0.30	0.30-0.60	0.60-0.90	0.90-1.20	1.20-1.50	1.50-2.00
0.00-0.30	1.00	-0.25	0.21	0.14	-0.10	0.23
0.30-0.60	-0.25	1.00	-0.06	0.14	-0.03	0.09
0.60-0.90	0.21	-0.06	1.00	0.30	0.04	0.37
0.90-1.20	0.14	0.14	0.30	1.00	0.01	0.31
1.20-1.50	-0.10	-0.03	0.04	0.01	1.00	0.01
1.50-2.00	0.23	0.09	0.37	0.31	0.01	1.00

Table 233: Correlation matrix for the normalized particle-level fiducial phase-space differential cross-section as a function of absolute value of the rapidity of the $t\bar{t}$ system , accounting for the statistical and systematic uncertainties.

bin [GeV]	0.00-0.20	0.20-0.40	0.40-0.60	0.60-0.70	0.70-0.80	0.80-1.00
0.00-0.20	4.18e-03	-8.58e-04	-8.91e-04	-5.85e-04	-3.26e-04	7.42e-06
0.20-0.40	-8.58e-04	5.02e-03	-1.02e-03	4.24e-04	-4.91e-05	1.73e-05
0.40-0.60	-8.91e-04	-1.02e-03	4.28e-03	-7.55e-04	-2.64e-04	-7.48e-05
0.60-0.70	-5.85e-04	4.24e-04	-7.55e-04	1.08e-02	-9.31e-04	1.02e-04
0.70-0.80	-3.26e-04	-4.91e-05	-2.64e-04	-9.31e-04	4.94e-03	-1.85e-04
0.80-1.00	7.42e-06	1.73e-05	-7.48e-05	1.02e-04	-1.85e-04	7.36e-04

Table 234: Covariance matrix for the normalized particle-level fiducial phase-space differential cross-section as a function of production angle in the Collins-Soper reference frame , accounting for the statistical and systematic uncertainties.

bin [GeV]	0.00-0.20	0.20-0.40	0.40-0.60	0.60-0.70	0.70-0.80	0.80-1.00
0.00-0.20	1.00	-0.19	-0.21	-0.09	-0.07	0.00
0.20-0.40	-0.19	1.00	-0.22	0.06	-0.01	0.01
0.40-0.60	-0.21	-0.22	1.00	-0.11	-0.06	-0.04
0.60-0.70	-0.09	0.06	-0.11	1.00	-0.13	0.04
0.70-0.80	-0.07	-0.01	-0.06	-0.13	1.00	-0.10
0.80-1.00	0.00	0.01	-0.04	0.04	-0.10	1.00

Table 235: Correlation matrix for the normalized particle-level fiducial phase-space differential cross-section as a function of production angle in the Collins-Soper reference frame , accounting for the statistical and systematic uncertainties.

bin [GeV]	1000-1100	1100-1200	1200-1300	1300-1400	1400-1600	1600-1800	1800-2200
1000-1100	6.51e-08	-1.47e-09	3.69e-09	1.28e-09	-6.99e-10	-2.07e-09	-1.62e-09
1100-1200	-1.47e-09	3.28e-08	5.09e-10	-2.70e-09	-6.65e-10	-1.01e-09	-6.59e-10
1200-1300	3.69e-09	5.09e-10	3.78e-08	8.82e-09	6.17e-10	1.53e-09	-1.91e-10
1300-1400	1.28e-09	-2.70e-09	8.82e-09	2.36e-08	1.68e-10	1.09e-09	6.89e-11
1400-1600	-6.99e-10	-6.65e-10	6.17e-10	1.68e-10	6.10e-09	-2.53e-10	-3.64e-11
1600-1800	-2.07e-09	-1.01e-09	1.53e-09	1.09e-09	-2.53e-10	4.27e-09	-1.23e-10
1800-2200	-1.62e-09	-6.59e-10	-1.91e-10	6.89e-11	-3.64e-11	-1.23e-10	9.69e-10

Table 236: Covariance matrix for the normalized particle-level fiducial phase-space differential cross-section as a function of scalar sum of the transverse momenta of the two top-quark jets , accounting for the statistical and systematic uncertainties.

bin [GeV]	1000-1100	1100-1200	1200-1300	1300-1400	1400-1600	1600-1800	1800-2200
1000-1100	1.00	-0.03	0.07	0.03	-0.04	-0.12	-0.20
1100-1200	-0.03	1.00	0.01	-0.10	-0.05	-0.09	-0.12
1200-1300	0.07	0.01	1.00	0.29	0.04	0.12	-0.03
1300-1400	0.03	-0.10	0.29	1.00	0.01	0.11	0.01
1400-1600	-0.04	-0.05	0.04	0.01	1.00	-0.05	-0.01
1600-1800	-0.12	-0.09	0.12	0.11	-0.05	1.00	-0.06
1800-2200	-0.20	-0.12	-0.03	0.01	-0.01	-0.06	1.00

Table 237: Correlation matrix for the normalized particle-level fiducial phase-space differential cross-section as a function of scalar sum of the transverse momenta of the two top-quark jets , accounting for the statistical and systematic uncertainties.

bin [GeV]	0.00-0.30	0.30-0.60	0.60-0.80	0.80-1.00	1.00-1.20	1.20-1.40	1.40-2.00
0.00-0.30	2.77e-03	1.24e-04	1.12e-03	-6.03e-05	7.60e-04	2.87e-06	7.12e-05
0.30-0.60	1.24e-04	3.01e-03	2.10e-04	1.68e-04	6.44e-04	-6.52e-05	7.25e-05
0.60-0.80	1.12e-03	2.10e-04	4.75e-03	-1.43e-04	1.27e-03	1.49e-04	1.20e-04
0.80-1.00	-6.03e-05	1.68e-04	-1.43e-04	2.29e-03	2.20e-05	-5.14e-05	2.38e-05
1.00-1.20	7.60e-04	6.44e-04	1.27e-03	2.20e-05	2.52e-03	-4.21e-05	1.02e-04
1.20-1.40	2.87e-06	-6.52e-05	1.49e-04	-5.14e-05	-4.21e-05	7.43e-04	-5.94e-06
1.40-2.00	7.12e-05	7.25e-05	1.20e-04	2.38e-05	1.02e-04	-5.94e-06	7.76e-05

Table 238: Covariance matrix for the normalized particle-level fiducial phase-space differential cross-section as a function of longitudinal boost $y_B^{t\bar{t}}$, accounting for the statistical and systematic uncertainties.

bin [GeV]	0.00-0.30	0.30-0.60	0.60-0.80	0.80-1.00	1.00-1.20	1.20-1.40	1.40-2.00
0.00-0.30	1.00	0.04	0.31	-0.02	0.29	0.00	0.15
0.30-0.60	0.04	1.00	0.06	0.06	0.23	-0.04	0.15
0.60-0.80	0.31	0.06	1.00	-0.04	0.37	0.08	0.20
0.80-1.00	-0.02	0.06	-0.04	1.00	0.01	-0.04	0.06
1.00-1.20	0.29	0.23	0.37	0.01	1.00	-0.03	0.23
1.20-1.40	0.00	-0.04	0.08	-0.04	-0.03	1.00	-0.02
1.40-2.00	0.15	0.15	0.20	0.06	0.23	-0.02	1.00

Table 239: Correlation matrix for the normalized particle-level fiducial phase-space differential cross-section as a function of longitudinal boost $y_B^{t\bar{t}}$, accounting for the statistical and systematic uncertainties.

bin [GeV]	0.00-2.50	2.50-2.75	2.75-3.00	3.00-3.14
0.00-2.50	6.21e-06	2.85e-05	1.28e-05	-6.83e-05
2.50-2.75	2.85e-05	3.22e-03	1.40e-03	-1.76e-04
2.75-3.00	1.28e-05	1.40e-03	4.12e-03	-3.77e-03
3.00-3.14	-6.83e-05	-1.76e-04	-3.77e-03	1.61e-02

Table 240: Covariance matrix for the normalized particle-level fiducial phase-space differential cross-section as a function of azimuthal angle between the two top-quark jets $\Delta\phi_{t\bar{t}}$, accounting for the statistical and systematic uncertainties.

bin [GeV]	0.00-2.50	2.50-2.75	2.75-3.00	3.00-3.14
0.00-2.50	1.00	0.20	0.08	-0.22
2.50-2.75	0.20	1.00	0.38	-0.02
2.75-3.00	0.08	0.38	1.00	-0.46
3.00-3.14	-0.22	-0.02	-0.46	1.00

Table 241: Correlation matrix for the normalized particle-level fiducial phase-space differential cross-section as a function of azimuthal angle between the two top-quark jets $\Delta\phi_{t\bar{t}}$, accounting for the statistical and systematic uncertainties.

bin [GeV]	1.00-1.50	1.50-2.00	2-3	3-4	4-5	5-7	7-10
1.00-1.50	6.20e-04	-6.47e-05	-2.21e-05	-2.20e-05	-2.08e-05	-6.57e-06	-1.02e-06
1.50-2.00	-6.47e-05	6.65e-04	4.13e-05	2.79e-05	-7.54e-06	6.23e-06	3.05e-06
2-3	-2.21e-05	4.13e-05	2.00e-04	1.65e-05	2.00e-05	3.10e-06	1.28e-06
3-4	-2.20e-05	2.79e-05	1.65e-05	1.26e-04	1.40e-06	7.28e-06	-2.38e-07
4-5	-2.08e-05	-7.54e-06	2.00e-05	1.40e-06	9.34e-05	-2.53e-06	6.26e-08
5-7	-6.57e-06	6.23e-06	3.10e-06	7.28e-06	-2.53e-06	1.65e-05	-2.64e-07
7-10	-1.02e-06	3.05e-06	1.28e-06	-2.38e-07	6.26e-08	-2.64e-07	2.99e-06

Table 242: Covariance matrix for the normalized particle-level fiducial phase-space differential cross-section as a function of production angle $\chi^{\tilde{t}^*}$, accounting for the statistical and systematic uncertainties.

bin [GeV]	1.00-1.50	1.50-2.00	2-3	3-4	4-5	5-7	7-10
1.00-1.50	1.00	-0.10	-0.06	-0.08	-0.09	-0.06	-0.02
1.50-2.00	-0.10	1.00	0.11	0.10	-0.03	0.06	0.07
2-3	-0.06	0.11	1.00	0.10	0.15	0.05	0.05
3-4	-0.08	0.10	0.10	1.00	0.01	0.16	-0.01
4-5	-0.09	-0.03	0.15	0.01	1.00	-0.06	0.00
5-7	-0.06	0.06	0.05	0.16	-0.06	1.00	-0.04
7-10	-0.02	0.07	0.05	-0.01	0.00	-0.04	1.00

Table 243: Correlation matrix for the normalized particle-level fiducial phase-space differential cross-section as a function of production angle $\chi^{\tilde{t}^*}$, accounting for the statistical and systematic uncertainties.

bin [GeV]	0-20	20-40	40-60	60-100	100-200	200-300	300-600
0-20	9.79e-07	-1.28e-07	1.08e-08	7.39e-08	-2.97e-09	3.24e-08	3.41e-09
20-40	-1.28e-07	4.36e-07	-2.06e-08	-1.32e-08	-1.35e-08	3.25e-09	-1.50e-09
40-60	1.08e-08	-2.06e-08	3.02e-07	-1.75e-08	-8.25e-09	3.32e-09	-2.91e-10
60-100	7.39e-08	-1.32e-08	-1.75e-08	1.30e-07	-7.59e-09	1.52e-08	6.27e-10
100-200	-2.97e-09	-1.35e-08	-8.25e-09	-7.59e-09	1.66e-08	1.06e-09	4.17e-10
200-300	3.24e-08	3.25e-09	3.32e-09	1.52e-08	1.06e-09	1.13e-08	5.48e-10
300-600	3.41e-09	-1.50e-09	-2.91e-10	6.27e-10	4.17e-10	5.48e-10	6.93e-10

Table 244: Covariance matrix for the normalized particle-level fiducial phase-space differential cross-section as a function of absolute value of the out-of-plane momentum $p_{out}^{t\bar{t}}$, accounting for the statistical and systematic uncertainties.

bin [GeV]	0-20	20-40	40-60	60-100	100-200	200-300	300-600
0-20	1.00	-0.20	0.02	0.21	-0.02	0.31	0.13
20-40	-0.20	1.00	-0.06	-0.06	-0.16	0.05	-0.09
40-60	0.02	-0.06	1.00	-0.09	-0.12	0.06	-0.02
60-100	0.21	-0.06	-0.09	1.00	-0.16	0.40	0.07
100-200	-0.02	-0.16	-0.12	-0.16	1.00	0.08	0.12
200-300	0.31	0.05	0.06	0.40	0.08	1.00	0.20
300-600	0.13	-0.09	-0.02	0.07	0.12	0.20	1.00

Table 245: Correlation matrix for the normalized particle-level fiducial phase-space differential cross-section as a function of absolute value of the out-of-plane momentum $p_{out}^{t\bar{t}}$, accounting for the statistical and systematic uncertainties.

1646 **W.2. Parton level covariances and correlations**

bin [GeV]	450-500	500-550	550-600	600-650	650-750	750-900	900-1200
450-500	2.36e-07	5.17e-07	3.35e-07	2.05e-07	1.23e-07	3.90e-08	8.26e-09
500-550	5.17e-07	1.61e-06	1.02e-06	6.00e-07	3.53e-07	1.11e-07	2.24e-08
550-600	3.35e-07	1.02e-06	7.18e-07	4.21e-07	2.35e-07	7.31e-08	1.46e-08
600-650	2.05e-07	6.00e-07	4.21e-07	2.72e-07	1.45e-07	4.38e-08	8.84e-09
650-750	1.23e-07	3.53e-07	2.35e-07	1.45e-07	9.45e-08	2.67e-08	5.67e-09
750-900	3.90e-08	1.11e-07	7.31e-08	4.38e-08	2.67e-08	1.15e-08	1.78e-09
900-1200	8.26e-09	2.24e-08	1.46e-08	8.84e-09	5.67e-09	1.78e-09	1.07e-09

Table 246: Covariance matrix for the absolute parton-level phase-space differential cross-section as a function of the transverse momentum of the top quark, accounting for the statistical and systematic uncertainties.

bin [GeV]	450-500	500-550	550-600	600-650	650-750	750-900	900-1200
450-500	1.00	0.84	0.81	0.81	0.82	0.75	0.52
500-550	0.84	1.00	0.95	0.91	0.91	0.82	0.54
550-600	0.81	0.95	1.00	0.95	0.90	0.81	0.53
600-650	0.81	0.91	0.95	1.00	0.90	0.78	0.52
650-750	0.82	0.91	0.90	0.90	1.00	0.81	0.56
750-900	0.75	0.82	0.81	0.78	0.81	1.00	0.51
900-1200	0.52	0.54	0.53	0.52	0.56	0.51	1.00

Table 247: Correlation matrix for the absolute parton-level phase-space differential cross-section as a function of the transverse momentum of the top quark, accounting for the statistical and systematic uncertainties.

Not reviewed, for internal circulation only

bin [GeV]	0.00-0.20	0.20-0.40	0.40-0.60	0.60-0.80	0.80-1.00	1.00-1.20	1.20-1.50	1.50-2.00
0.00-0.20	3.87e-02	3.46e-02	3.35e-02	2.82e-02	2.38e-02	2.18e-02	1.64e-02	7.98e-03
0.20-0.40	3.46e-02	3.63e-02	3.13e-02	2.69e-02	2.26e-02	2.08e-02	1.56e-02	7.58e-03
0.40-0.60	3.35e-02	3.13e-02	3.38e-02	2.57e-02	2.19e-02	2.00e-02	1.52e-02	7.40e-03
0.60-0.80	2.82e-02	2.69e-02	2.57e-02	2.37e-02	1.81e-02	1.69e-02	1.28e-02	6.20e-03
0.80-1.00	2.38e-02	2.26e-02	2.19e-02	1.81e-02	1.71e-02	1.40e-02	1.07e-02	5.20e-03
1.00-1.20	2.18e-02	2.08e-02	2.00e-02	1.69e-02	1.40e-02	1.47e-02	9.78e-03	4.79e-03
1.20-1.50	1.64e-02	1.56e-02	1.52e-02	1.28e-02	1.07e-02	9.78e-03	8.17e-03	3.61e-03
1.50-2.00	7.98e-03	7.58e-03	7.40e-03	6.20e-03	5.20e-03	4.79e-03	3.61e-03	1.97e-03

Table 248: Covariance matrix for the absolute parton-level phase-space differential cross-section as a function of the rapidity of the top quark, accounting for the statistical and systematic uncertainties.

bin [GeV]	0.00-0.20	0.20-0.40	0.40-0.60	0.60-0.80	0.80-1.00	1.00-1.20	1.20-1.50	1.50-2.00
0.00-0.20	1.00	0.92	0.93	0.93	0.93	0.92	0.92	0.91
0.20-0.40	0.92	1.00	0.90	0.92	0.91	0.90	0.91	0.90
0.40-0.60	0.93	0.90	1.00	0.91	0.91	0.90	0.91	0.91
0.60-0.80	0.93	0.92	0.91	1.00	0.90	0.90	0.92	0.91
0.80-1.00	0.93	0.91	0.91	0.90	1.00	0.89	0.91	0.89
1.00-1.20	0.92	0.90	0.90	0.90	0.89	1.00	0.89	0.89
1.20-1.50	0.92	0.91	0.91	0.92	0.91	0.89	1.00	0.90
1.50-2.00	0.91	0.90	0.91	0.91	0.89	0.89	0.90	1.00

Table 249: Correlation matrix for the absolute parton-level phase-space differential cross-section as a function of the rapidity of the top quark, accounting for the statistical and systematic uncertainties.

bin [GeV]	500-550	550-600	600-650	650-700	700-750	750-800	800-1000	1000-1200
500-550	2.77e-06	1.77e-06	9.85e-07	7.64e-07	4.96e-07	2.92e-07	1.48e-07	2.16e-08
550-600	1.77e-06	1.25e-06	6.76e-07	5.13e-07	3.34e-07	1.95e-07	9.86e-08	1.40e-08
600-650	9.85e-07	6.76e-07	4.04e-07	2.95e-07	1.83e-07	1.09e-07	5.64e-08	8.35e-09
650-700	7.64e-07	5.13e-07	2.95e-07	2.52e-07	1.55e-07	8.31e-08	4.52e-08	7.04e-09
700-750	4.96e-07	3.34e-07	1.83e-07	1.55e-07	1.18e-07	6.42e-08	3.02e-08	5.66e-09
750-800	2.92e-07	1.95e-07	1.09e-07	8.31e-08	6.42e-08	4.75e-08	1.83e-08	3.29e-09
800-1000	1.48e-07	9.86e-08	5.64e-08	4.52e-08	3.02e-08	1.83e-08	1.19e-08	1.55e-09
1000-1200	2.16e-08	1.40e-08	8.35e-09	7.04e-09	5.66e-09	3.29e-09	1.55e-09	1.88e-09

Table 250: Covariance matrix for the absolute parton-level phase-space differential cross-section as a function of the transverse momentum of the leading top quark, accounting for the statistical and systematic uncertainties.

bin [GeV]	500-550	550-600	600-650	650-700	700-750	750-800	800-1000	1000-1200
500-550	1.00	0.95	0.93	0.92	0.87	0.81	0.81	0.30
550-600	0.95	1.00	0.95	0.91	0.87	0.80	0.81	0.29
600-650	0.93	0.95	1.00	0.92	0.84	0.78	0.81	0.30
650-700	0.92	0.91	0.92	1.00	0.90	0.76	0.82	0.32
700-750	0.87	0.87	0.84	0.90	1.00	0.86	0.80	0.38
750-800	0.81	0.80	0.78	0.76	0.86	1.00	0.77	0.35
800-1000	0.81	0.81	0.81	0.82	0.80	0.77	1.00	0.33
1000-1200	0.30	0.29	0.30	0.32	0.38	0.35	0.33	1.00

Table 251: Correlation matrix for the absolute parton-level phase-space differential cross-section as a function of the transverse momentum of the leading top quark, accounting for the statistical and systematic uncertainties.

bin [GeV]	350-400	400-450	450-500	500-550	550-600	600-800	800-1200
350-400	4.40e-07	4.64e-07	5.25e-07	4.89e-07	2.86e-07	1.13e-07	1.08e-08
400-450	4.64e-07	5.76e-07	7.00e-07	6.30e-07	3.65e-07	1.45e-07	1.40e-08
450-500	5.25e-07	7.00e-07	9.81e-07	9.01e-07	5.01e-07	1.96e-07	1.90e-08
500-550	4.89e-07	6.30e-07	9.01e-07	8.92e-07	4.96e-07	1.87e-07	1.76e-08
550-600	2.86e-07	3.65e-07	5.01e-07	4.96e-07	2.99e-07	1.09e-07	1.01e-08
600-800	1.13e-07	1.45e-07	1.96e-07	1.87e-07	1.09e-07	4.51e-08	4.11e-09
800-1200	1.08e-08	1.40e-08	1.90e-08	1.76e-08	1.01e-08	4.11e-09	7.32e-10

Table 252: Covariance matrix for the absolute parton-level phase-space differential cross-section as a function of the transverse momentum of the second-leading top quark, accounting for the statistical and systematic uncertainties.

bin [GeV]	350-400	400-450	450-500	500-550	550-600	600-800	800-1200
350-400	1.00	0.92	0.80	0.78	0.79	0.81	0.60
400-450	0.92	1.00	0.93	0.88	0.88	0.90	0.68
450-500	0.80	0.93	1.00	0.96	0.92	0.93	0.71
500-550	0.78	0.88	0.96	1.00	0.96	0.93	0.69
550-600	0.79	0.88	0.92	0.96	1.00	0.94	0.68
600-800	0.81	0.90	0.93	0.93	0.94	1.00	0.72
800-1200	0.60	0.68	0.71	0.69	0.68	0.72	1.00

Table 253: Correlation matrix for the absolute parton-level phase-space differential cross-section as a function of the transverse momentum of the second-leading top quark, accounting for the statistical and systematic uncertainties.

bin [GeV]	0.00-0.20	0.20-0.40	0.40-0.60	0.60-0.80	0.80-1.00	1.00-1.20	1.20-1.50	1.50-2.00
0.00-0.20	4.13e-02	3.14e-02	3.37e-02	3.29e-02	2.51e-02	2.29e-02	1.67e-02	8.31e-03
0.20-0.40	3.14e-02	2.90e-02	2.68e-02	2.63e-02	2.02e-02	1.84e-02	1.34e-02	6.65e-03
0.40-0.60	3.37e-02	2.68e-02	3.16e-02	2.78e-02	2.17e-02	1.97e-02	1.45e-02	7.19e-03
0.60-0.80	3.29e-02	2.63e-02	2.78e-02	2.94e-02	2.07e-02	1.92e-02	1.40e-02	6.92e-03
0.80-1.00	2.51e-02	2.02e-02	2.17e-02	2.07e-02	1.75e-02	1.44e-02	1.07e-02	5.33e-03
1.00-1.20	2.29e-02	1.84e-02	1.97e-02	1.92e-02	1.44e-02	1.49e-02	9.77e-03	4.83e-03
1.20-1.50	1.67e-02	1.34e-02	1.45e-02	1.40e-02	1.07e-02	9.77e-03	7.83e-03	3.52e-03
1.50-2.00	8.31e-03	6.65e-03	7.19e-03	6.92e-03	5.33e-03	4.83e-03	3.52e-03	2.05e-03

Table 254: Covariance matrix for the absolute parton-level phase-space differential cross-section as a function of the absolute value of the rapidity of the leading top quark, accounting for the statistical and systematic uncertainties.

bin [GeV]	0.00-0.20	0.20-0.40	0.40-0.60	0.60-0.80	0.80-1.00	1.00-1.20	1.20-1.50	1.50-2.00
0.00-0.20	1.00	0.91	0.93	0.94	0.93	0.92	0.93	0.90
0.20-0.40	0.91	1.00	0.89	0.90	0.90	0.88	0.89	0.86
0.40-0.60	0.93	0.89	1.00	0.91	0.92	0.91	0.92	0.89
0.60-0.80	0.94	0.90	0.91	1.00	0.91	0.92	0.92	0.89
0.80-1.00	0.93	0.90	0.92	0.91	1.00	0.89	0.92	0.89
1.00-1.20	0.92	0.88	0.91	0.92	0.89	1.00	0.90	0.87
1.20-1.50	0.93	0.89	0.92	0.92	0.92	0.90	1.00	0.88
1.50-2.00	0.90	0.86	0.89	0.89	0.89	0.87	0.88	1.00

Table 255: Correlation matrix for the absolute parton-level phase-space differential cross-section as a function of the absolute value of the rapidity of the leading top quark, accounting for the statistical and systematic uncertainties.

bin [GeV]	0.00-0.20	0.20-0.40	0.40-0.60	0.60-0.80	0.80-1.00	1.00-1.20	1.20-1.50	1.50-2.00
0.00-0.20	3.62e-02	3.68e-02	3.37e-02	2.57e-02	2.23e-02	1.97e-02	1.52e-02	7.11e-03
0.20-0.40	3.68e-02	4.35e-02	3.67e-02	2.83e-02	2.45e-02	2.16e-02	1.66e-02	7.88e-03
0.40-0.60	3.37e-02	3.67e-02	3.75e-02	2.57e-02	2.26e-02	1.97e-02	1.49e-02	7.25e-03
0.60-0.80	2.57e-02	2.83e-02	2.57e-02	2.20e-02	1.69e-02	1.51e-02	1.14e-02	5.49e-03
0.80-1.00	2.23e-02	2.45e-02	2.26e-02	1.69e-02	1.66e-02	1.27e-02	9.95e-03	4.74e-03
1.00-1.20	1.97e-02	2.16e-02	1.97e-02	1.51e-02	1.27e-02	1.31e-02	8.60e-03	4.17e-03
1.20-1.50	1.52e-02	1.66e-02	1.49e-02	1.14e-02	9.95e-03	8.60e-03	7.54e-03	3.13e-03
1.50-2.00	7.11e-03	7.88e-03	7.25e-03	5.49e-03	4.74e-03	4.17e-03	3.13e-03	1.73e-03

Table 256: Covariance matrix for the absolute parton-level phase-space differential cross-section as a function of the absolute value of the rapidity of the second-leading top quark, accounting for the statistical and systematic uncertainties.

bin [GeV]	0.00-0.20	0.20-0.40	0.40-0.60	0.60-0.80	0.80-1.00	1.00-1.20	1.20-1.50	1.50-2.00
0.00-0.20	1.00	0.93	0.91	0.91	0.91	0.90	0.92	0.90
0.20-0.40	0.93	1.00	0.91	0.92	0.91	0.90	0.91	0.91
0.40-0.60	0.91	0.91	1.00	0.89	0.90	0.89	0.89	0.90
0.60-0.80	0.91	0.92	0.89	1.00	0.88	0.89	0.89	0.89
0.80-1.00	0.91	0.91	0.90	0.88	1.00	0.86	0.89	0.89
1.00-1.20	0.90	0.90	0.89	0.89	0.86	1.00	0.86	0.88
1.20-1.50	0.92	0.91	0.89	0.89	0.89	0.86	1.00	0.87
1.50-2.00	0.90	0.91	0.90	0.89	0.89	0.88	0.87	1.00

Table 257: Correlation matrix for the absolute parton-level phase-space differential cross-section as a function of the absolute value of the rapidity of the second-leading top quark, accounting for the statistical and systematic uncertainties.

bin [GeV]	0-50	50-100	100-150	150-200	200-300	300-400	400-500	500-800
0-50	1.36e-06	1.20e-06	7.81e-07	4.98e-07	2.43e-07	1.26e-07	7.14e-08	2.12e-08
50-100	1.20e-06	1.17e-06	7.98e-07	5.16e-07	2.48e-07	1.27e-07	7.26e-08	2.27e-08
100-150	7.81e-07	7.98e-07	5.90e-07	3.92e-07	1.78e-07	9.04e-08	5.31e-08	1.64e-08
150-200	4.98e-07	5.16e-07	3.92e-07	2.94e-07	1.34e-07	6.41e-08	4.14e-08	1.21e-08
200-300	2.43e-07	2.48e-07	1.78e-07	1.34e-07	8.04e-08	3.58e-08	2.20e-08	6.52e-09
300-400	1.26e-07	1.27e-07	9.04e-08	6.41e-08	3.58e-08	2.59e-08	1.07e-08	3.76e-09
400-500	7.14e-08	7.26e-08	5.31e-08	4.14e-08	2.20e-08	1.07e-08	1.57e-08	1.69e-09
500-800	2.12e-08	2.27e-08	1.64e-08	1.21e-08	6.52e-09	3.76e-09	1.69e-09	1.29e-09

Table 258: Covariance matrix for the absolute parton-level phase-space differential cross-section as a function of the $t\bar{t} p_T$, accounting for the statistical and systematic uncertainties.

bin [GeV]	0-50	50-100	100-150	150-200	200-300	300-400	400-500	500-800
0-50	1.00	0.95	0.87	0.79	0.73	0.67	0.49	0.50
50-100	0.95	1.00	0.96	0.88	0.81	0.73	0.54	0.58
100-150	0.87	0.96	1.00	0.94	0.82	0.73	0.55	0.59
150-200	0.79	0.88	0.94	1.00	0.87	0.73	0.61	0.62
200-300	0.73	0.81	0.82	0.87	1.00	0.78	0.62	0.64
300-400	0.67	0.73	0.73	0.73	0.78	1.00	0.53	0.65
400-500	0.49	0.54	0.55	0.61	0.62	0.53	1.00	0.38
500-800	0.50	0.58	0.59	0.62	0.64	0.65	0.38	1.00

Table 259: Correlation matrix for the absolute parton-level phase-space differential cross-section as a function of the $t\bar{t} p_T$, accounting for the statistical and systematic uncertainties.

bin [GeV]	1000-1100	1100-1200	1200-1300	1300-1400	1400-1500	1500-1700	1700-1900	1900-2100	2100-2300	2300-3000
1000-1100	1.28e-07	1.57e-07	1.21e-07	8.53e-08	7.41e-08	4.07e-08	3.20e-08	1.64e-08	7.29e-09	
1100-1200	1.57e-07	2.24e-07	1.72e-07	1.14e-07	9.97e-08	5.56e-08	4.36e-08	2.26e-08	9.46e-09	
1200-1300	1.21e-07	1.72e-07	1.41e-07	9.37e-08	7.81e-08	4.37e-08	3.47e-08	1.78e-08	7.79e-09	
1300-1400	8.53e-08	1.14e-07	9.37e-08	7.01e-08	5.65e-08	2.97e-08	2.38e-08	1.22e-08	5.70e-09	
1400-1500	7.41e-08	9.97e-08	7.81e-08	5.65e-08	5.23e-08	2.63e-08	2.03e-08	1.06e-08	4.76e-09	
1500-1700	4.07e-08	5.56e-08	4.37e-08	2.97e-08	2.63e-08	1.65e-08	1.12e-08	5.66e-09	2.51e-09	
1700-1900	3.20e-08	4.36e-08	3.47e-08	2.38e-08	2.03e-08	1.12e-08	1.02e-08	4.66e-09	1.98e-09	
1900-2100	1.64e-08	2.26e-08	1.78e-08	1.22e-08	1.06e-08	5.66e-09	4.66e-09	3.26e-09	1.08e-09	
2100-2300	7.29e-09	9.46e-09	7.79e-09	5.70e-09	4.76e-09	2.51e-09	1.98e-09	1.08e-09	1.10e-09	
2300-3000	2.16e-09	2.79e-09	2.27e-09	1.63e-09	1.40e-09	7.54e-10	6.15e-10	2.90e-10	1.49e-10	

Table 260: Covariance matrix for the absolute parton-level phase-space differential cross-section as a function of the $t\bar{t}$ invariant mass, accounting for the statistical and systematic uncertainties.

bin [GeV]	1000-1100	1100-1200	1200-1300	1300-1400	1400-1500	1500-1700	1700-1900	1900-2100	2100-2300	2300-3000
1000-1100	1.00	0.93	0.90	0.90	0.91	0.89	0.88	0.80	0.61	
1100-1200	0.93	1.00	0.97	0.91	0.92	0.91	0.91	0.83	0.60	
1200-1300	0.90	0.97	1.00	0.94	0.91	0.91	0.91	0.83	0.63	
1300-1400	0.90	0.91	0.94	1.00	0.93	0.88	0.89	0.80	0.65	
1400-1500	0.91	0.92	0.91	0.93	1.00	0.90	0.88	0.81	0.63	
1500-1700	0.89	0.91	0.91	0.88	0.90	1.00	0.86	0.77	0.59	
1700-1900	0.88	0.91	0.91	0.89	0.88	0.86	1.00	0.81	0.59	
1900-2100	0.80	0.83	0.83	0.80	0.81	0.77	0.81	1.00	0.57	
2100-2300	0.61	0.60	0.63	0.65	0.63	0.59	0.59	0.57	1.00	
2300-3000	0.61	0.59	0.61	0.62	0.62	0.59	0.61	0.51	0.45	

Table 261: Correlation matrix for the absolute parton-level phase-space differential cross-section as a function of the $t\bar{t}$ invariant mass, accounting for the statistical and systematic uncertainties.

Not reviewed, for internal circulation only

bin [GeV]	0.00-0.20	0.20-0.40	0.40-0.60	0.60-0.80	0.80-1.00	1.00-1.20	1.20-1.50	1.50-2.00
0.00-0.20	7.91e-02	5.73e-02	5.37e-02	4.18e-02	3.41e-02	3.32e-02	1.54e-02	3.35e-03
0.20-0.40	5.73e-02	4.82e-02	4.11e-02	3.27e-02	2.68e-02	2.44e-02	1.19e-02	2.64e-03
0.40-0.60	5.37e-02	4.11e-02	4.10e-02	2.96e-02	2.45e-02	2.29e-02	1.10e-02	2.40e-03
0.60-0.80	4.18e-02	3.27e-02	2.96e-02	2.62e-02	1.93e-02	1.78e-02	8.70e-03	1.96e-03
0.80-1.00	3.41e-02	2.68e-02	2.45e-02	1.93e-02	1.79e-02	1.42e-02	7.15e-03	1.60e-03
1.00-1.20	3.32e-02	2.44e-02	2.29e-02	1.78e-02	1.42e-02	1.58e-02	6.46e-03	1.42e-03
1.20-1.50	1.54e-02	1.19e-02	1.10e-02	8.70e-03	7.15e-03	6.46e-03	3.75e-03	6.98e-04
1.50-2.00	3.35e-03	2.64e-03	2.40e-03	1.96e-03	1.60e-03	1.42e-03	6.98e-04	3.38e-04

Table 262: Covariance matrix for the absolute parton-level phase-space differential cross-section as a function of the absolute value of $t\bar{t}$ rapidity, accounting for the statistical and systematic uncertainties.

bin [GeV]	0.00-0.20	0.20-0.40	0.40-0.60	0.60-0.80	0.80-1.00	1.00-1.20	1.20-1.50	1.50-2.00
0.00-0.20	1.00	0.93	0.94	0.92	0.90	0.94	0.89	0.65
0.20-0.40	0.93	1.00	0.92	0.92	0.91	0.89	0.89	0.65
0.40-0.60	0.94	0.92	1.00	0.90	0.90	0.90	0.88	0.65
0.60-0.80	0.92	0.92	0.90	1.00	0.89	0.88	0.88	0.66
0.80-1.00	0.90	0.91	0.90	0.89	1.00	0.84	0.87	0.65
1.00-1.20	0.94	0.89	0.90	0.88	0.84	1.00	0.84	0.61
1.20-1.50	0.89	0.89	0.88	0.88	0.87	0.84	1.00	0.62
1.50-2.00	0.65	0.65	0.65	0.66	0.65	0.61	0.62	1.00

Table 263: Correlation matrix for the absolute parton-level phase-space differential cross-section as a function of the absolute value of $t\bar{t}$ rapidity, accounting for the statistical and systematic uncertainties.

bin [GeV]	0.00-2.50	2.50-2.75	2.75-3.00	3.00-3.15
0.00-2.50	5.41e-04	1.15e-03	3.85e-03	1.49e-02
2.50-2.75	1.15e-03	3.98e-03	1.09e-02	4.51e-02
2.75-3.00	3.85e-03	1.09e-02	5.24e-02	2.05e-01
3.00-3.15	1.49e-02	4.51e-02	2.05e-01	9.70e-01

Table 264: Covariance matrix for the absolute parton-level phase-space differential cross-section as a function of $\Delta\phi(t_1, t_2)$, accounting for the statistical and systematic uncertainties.

bin [GeV]	0.00-2.50	2.50-2.75	2.75-3.00	3.00-3.15
0.00-2.50	1.00	0.78	0.72	0.65
2.50-2.75	0.78	1.00	0.76	0.73
2.75-3.00	0.72	0.76	1.00	0.91
3.00-3.15	0.65	0.73	0.91	1.00

Table 265: Correlation matrix for the absolute parton-level phase-space differential cross-section as a function of $\Delta\phi(t_1, t_2)$, accounting for the statistical and systematic uncertainties.

bin [GeV]	0-20	20-40	40-60	60-100	100-200	200-300	300-600
0-20	1.05e-05	7.06e-06	4.17e-06	2.92e-06	9.14e-07	3.31e-07	1.43e-07
20-40	7.06e-06	5.28e-06	3.15e-06	2.13e-06	6.61e-07	2.52e-07	1.10e-07
40-60	4.17e-06	3.15e-06	2.04e-06	1.33e-06	4.07e-07	1.61e-07	7.04e-08
60-100	2.92e-06	2.13e-06	1.33e-06	1.04e-06	2.97e-07	1.17e-07	5.74e-08
100-200	9.14e-07	6.61e-07	4.07e-07	2.97e-07	1.13e-07	3.66e-08	1.87e-08
200-300	3.31e-07	2.52e-07	1.61e-07	1.17e-07	3.66e-08	2.15e-08	7.01e-09
300-600	1.43e-07	1.10e-07	7.04e-08	5.74e-08	1.87e-08	7.01e-09	5.63e-09

Table 266: Covariance matrix for the absolute parton-level phase-space differential cross-section as a function of $p_{out}^{\bar{t}\bar{t}}$, accounting for the statistical and systematic uncertainties.

bin [GeV]	0-20	20-40	40-60	60-100	100-200	200-300	300-600
0-20	1.00	0.95	0.90	0.88	0.84	0.70	0.59
20-40	0.95	1.00	0.96	0.91	0.85	0.75	0.64
40-60	0.90	0.96	1.00	0.91	0.85	0.77	0.66
60-100	0.88	0.91	0.91	1.00	0.86	0.78	0.75
100-200	0.84	0.85	0.85	0.86	1.00	0.74	0.74
200-300	0.70	0.75	0.77	0.78	0.74	1.00	0.64
300-600	0.59	0.64	0.66	0.75	0.74	0.64	1.00

Table 267: Correlation matrix for the absolute parton-level phase-space differential cross-section as a function of $p_{out}^{\bar{t}\bar{t}}$, accounting for the statistical and systematic uncertainties.

bin [GeV]	0.00-0.20	0.20-0.40	0.40-0.60	0.60-0.80	0.80-1.00	1.00-1.30	1.30-2.00
0.00-0.20	7.27e-02	5.71e-02	5.13e-02	3.99e-02	3.38e-02	2.66e-02	5.82e-03
0.20-0.40	5.71e-02	5.16e-02	4.25e-02	3.36e-02	2.83e-02	2.15e-02	4.96e-03
0.40-0.60	5.13e-02	4.25e-02	4.06e-02	2.95e-02	2.51e-02	1.93e-02	4.37e-03
0.60-0.80	3.99e-02	3.36e-02	2.95e-02	2.55e-02	1.95e-02	1.52e-02	3.51e-03
0.80-1.00	3.38e-02	2.83e-02	2.51e-02	1.95e-02	1.83e-02	1.27e-02	2.96e-03
1.00-1.30	2.66e-02	2.15e-02	1.93e-02	1.52e-02	1.27e-02	1.09e-02	2.19e-03
1.30-2.00	5.82e-03	4.96e-03	4.37e-03	3.51e-03	2.96e-03	2.19e-03	6.80e-04

Table 268: Covariance matrix for the absolute parton-level phase-space differential cross-section as a function of $y_B^{\bar{t}\bar{t}}$, accounting for the statistical and systematic uncertainties.

bin [GeV]	0.00-0.20	0.20-0.40	0.40-0.60	0.60-0.80	0.80-1.00	1.00-1.30	1.30-2.00
0.00-0.20	1.00	0.93	0.95	0.93	0.93	0.94	0.83
0.20-0.40	0.93	1.00	0.93	0.93	0.92	0.90	0.84
0.40-0.60	0.95	0.93	1.00	0.92	0.92	0.92	0.83
0.60-0.80	0.93	0.93	0.92	1.00	0.90	0.91	0.84
0.80-1.00	0.93	0.92	0.92	0.90	1.00	0.90	0.84
1.00-1.30	0.94	0.90	0.92	0.91	0.90	1.00	0.80
1.30-2.00	0.83	0.84	0.83	0.84	0.84	0.80	1.00

Table 269: Correlation matrix for the absolute parton-level phase-space differential cross-section as a function of $y_B^{\bar{t}\bar{t}}$, accounting for the statistical and systematic uncertainties.

bin [GeV]	450-500	500-550	550-600	600-650	650-750	750-900	900-1200
450-500	1.97e-07	4.85e-08	3.22e-08	3.69e-08	1.21e-09	-1.93e-09	-1.12e-10
500-550	4.85e-08	3.31e-07	8.00e-08	1.11e-08	-2.50e-08	-1.35e-08	-5.72e-09
550-600	3.22e-08	8.00e-08	1.21e-07	5.54e-08	-3.81e-09	-6.31e-10	-7.85e-10
600-650	3.69e-08	1.11e-08	5.54e-08	8.73e-08	1.01e-08	1.86e-09	7.18e-10
650-750	1.21e-09	-2.50e-08	-3.81e-09	1.01e-08	2.60e-08	1.97e-09	8.01e-10
750-900	-1.93e-09	-1.35e-08	-6.31e-10	1.86e-09	1.97e-09	7.85e-09	3.15e-10
900-1200	-1.12e-10	-5.72e-09	-7.85e-10	7.18e-10	8.01e-10	3.15e-10	1.64e-09

Table 270: Covariance matrix for the normalized parton-level phase-space differential cross-section as a function of the transverse momentum of the top quark, accounting for the statistical and systematic uncertainties.

bin [GeV]	450-500	500-550	550-600	600-650	650-750	750-900	900-1200
450-500	1.00	0.19	0.21	0.28	0.02	-0.05	-0.01
500-550	0.19	1.00	0.40	0.07	-0.27	-0.27	-0.25
550-600	0.21	0.40	1.00	0.54	-0.07	-0.02	-0.06
600-650	0.28	0.07	0.54	1.00	0.21	0.07	0.06
650-750	0.02	-0.27	-0.07	0.21	1.00	0.14	0.12
750-900	-0.05	-0.27	-0.02	0.07	0.14	1.00	0.09
900-1200	-0.01	-0.25	-0.06	0.06	0.12	0.09	1.00

Table 271: Correlation matrix for the normalized parton-level phase-space differential cross-section as a function of the transverse momentum of the top quark, accounting for the statistical and systematic uncertainties.

bin [GeV]	0.00-0.20	0.20-0.40	0.40-0.60	0.60-0.80	0.80-1.00	1.00-1.20	1.20-1.50	1.50-2.00
0.00-0.20	3.21e-03	-6.71e-04	-8.85e-05	7.36e-05	-1.31e-04	-2.24e-04	8.92e-05	-1.06e-04
0.20-0.40	-6.71e-04	5.99e-03	3.28e-07	6.65e-04	3.48e-04	4.05e-04	3.12e-04	-4.30e-05
0.40-0.60	-8.85e-05	3.28e-07	4.72e-03	-2.79e-04	1.75e-04	3.82e-04	2.19e-04	-2.32e-05
0.60-0.80	7.36e-05	6.65e-04	-2.79e-04	3.97e-03	-9.84e-05	1.90e-04	3.48e-04	-4.04e-05
0.80-1.00	-1.31e-04	3.48e-04	1.75e-04	-9.84e-05	3.00e-03	-6.10e-05	2.25e-04	-3.74e-05
1.00-1.20	-2.24e-04	4.05e-04	3.82e-04	1.90e-04	-6.10e-05	2.93e-03	-1.58e-05	1.99e-05
1.20-1.50	8.92e-05	3.12e-04	2.19e-04	3.48e-04	2.25e-04	-1.58e-05	1.52e-03	-2.72e-05
1.50-2.00	-1.06e-04	-4.30e-05	-2.32e-05	-4.04e-05	-3.74e-05	1.99e-05	-2.72e-05	3.47e-04

Table 272: Covariance matrix for the normalized parton-level phase-space differential cross-section as a function of the rapidity of the top quark, accounting for the statistical and systematic uncertainties.

bin [GeV]	0.00-0.20	0.20-0.40	0.40-0.60	0.60-0.80	0.80-1.00	1.00-1.20	1.20-1.50	1.50-2.00
0.00-0.20	1.00	-0.15	-0.02	0.02	-0.04	-0.07	0.04	-0.10
0.20-0.40	-0.15	1.00	0.00	0.14	0.08	0.10	0.10	-0.03
0.40-0.60	-0.02	0.00	1.00	-0.06	0.05	0.10	0.08	-0.02
0.60-0.80	0.02	0.14	-0.06	1.00	-0.03	0.06	0.14	-0.03
0.80-1.00	-0.04	0.08	0.05	-0.03	1.00	-0.02	0.11	-0.04
1.00-1.20	-0.07	0.10	0.10	0.06	-0.02	1.00	-0.01	0.02
1.20-1.50	0.04	0.10	0.08	0.14	0.11	-0.01	1.00	-0.04
1.50-2.00	-0.10	-0.03	-0.02	-0.03	-0.04	0.02	-0.04	1.00

Table 273: Correlation matrix for the normalized parton-level phase-space differential cross-section as a function of the rapidity of the top quark, accounting for the statistical and systematic uncertainties.

bin [GeV]	500-550	550-600	600-650	650-700	700-750	750-800	800-1000	1000-1200
500-550	3.92e-07	5.65e-08	-2.91e-08	-1.22e-08	-2.34e-08	-2.52e-08	-1.61e-08	-3.60e-09
550-600	5.65e-08	1.03e-07	1.79e-08	-8.10e-09	-3.04e-09	-4.14e-09	-4.57e-09	-4.38e-10
600-650	-2.91e-08	1.79e-08	5.62e-08	1.21e-08	-1.77e-09	1.10e-09	2.13e-09	1.30e-09
650-700	-1.22e-08	-8.10e-09	1.21e-08	4.24e-08	1.46e-08	-4.43e-09	2.96e-09	1.03e-09
700-750	-2.34e-08	-3.04e-09	-1.77e-09	1.46e-08	3.91e-08	1.47e-08	4.44e-09	2.28e-09
750-800	-2.52e-08	-4.14e-09	1.10e-09	-4.43e-09	1.47e-08	2.51e-08	3.68e-09	1.04e-09
800-1000	-1.61e-08	-4.57e-09	2.13e-09	2.96e-09	4.44e-09	3.68e-09	6.54e-09	5.99e-10
1000-1200	-3.60e-09	-4.38e-10	1.30e-09	1.03e-09	2.28e-09	1.04e-09	5.99e-10	2.65e-09

Table 274: Covariance matrix for the normalized parton-level phase-space differential cross-section as a function of the transverse momentum of the leading top quark, accounting for the statistical and systematic uncertainties.

bin [GeV]	500-550	550-600	600-650	650-700	700-750	750-800	800-1000	1000-1200
500-550	1.00	0.28	-0.20	-0.09	-0.19	-0.25	-0.32	-0.11
550-600	0.28	1.00	0.24	-0.12	-0.05	-0.08	-0.18	-0.03
600-650	-0.20	0.24	1.00	0.25	-0.04	0.03	0.11	0.11
650-700	-0.09	-0.12	0.25	1.00	0.36	-0.14	0.18	0.10
700-750	-0.19	-0.05	-0.04	0.36	1.00	0.47	0.28	0.22
750-800	-0.25	-0.08	0.03	-0.14	0.47	1.00	0.29	0.13
800-1000	-0.32	-0.18	0.11	0.18	0.28	0.29	1.00	0.14
1000-1200	-0.11	-0.03	0.11	0.10	0.22	0.13	0.14	1.00

Table 275: Correlation matrix for the normalized parton-level phase-space differential cross-section as a function of the transverse momentum of the leading top quark, accounting for the statistical and systematic uncertainties.

bin [GeV]	350-400	400-450	450-500	500-550	550-600	600-800	800-1200
350-400	1.86e-07	8.01e-08	-3.15e-08	-5.53e-08	-3.19e-08	-1.08e-08	-1.97e-09
400-450	8.01e-08	9.25e-08	2.13e-08	-4.18e-08	-2.58e-08	-9.02e-09	-1.96e-09
450-500	-3.15e-08	2.13e-08	1.01e-07	3.97e-08	3.35e-09	3.01e-09	-9.12e-10
500-550	-5.53e-08	-4.18e-08	3.97e-08	9.27e-08	3.67e-08	3.25e-09	-7.59e-10
550-600	-3.19e-08	-2.58e-08	3.35e-09	3.67e-08	5.23e-08	9.63e-09	5.54e-10
600-800	-1.08e-08	-9.02e-09	3.01e-09	3.25e-09	9.63e-09	9.36e-09	7.48e-10
800-1200	-1.97e-09	-1.96e-09	-9.12e-10	-7.59e-10	5.54e-10	7.48e-10	6.29e-10

Table 276: Covariance matrix for the normalized parton-level phase-space differential cross-section as a function of the transverse momentum of the second-leading top quark, accounting for the statistical and systematic uncertainties.

bin [GeV]	350-400	400-450	450-500	500-550	550-600	600-800	800-1200
350-400	1.00	0.61	-0.23	-0.42	-0.32	-0.26	-0.18
400-450	0.61	1.00	0.22	-0.45	-0.37	-0.31	-0.26
450-500	-0.23	0.22	1.00	0.41	0.05	0.10	-0.11
500-550	-0.42	-0.45	0.41	1.00	0.53	0.11	-0.10
550-600	-0.32	-0.37	0.05	0.53	1.00	0.44	0.10
600-800	-0.26	-0.31	0.10	0.11	0.44	1.00	0.31
800-1200	-0.18	-0.26	-0.11	-0.10	0.10	0.31	1.00

Table 277: Correlation matrix for the normalized parton-level phase-space differential cross-section as a function of the transverse momentum of the second-leading top quark, accounting for the statistical and systematic uncertainties.

bin [GeV]	0.00-0.20	0.20-0.40	0.40-0.60	0.60-0.80	0.80-1.00	1.00-1.20	1.20-1.50	1.50-2.00
0.00-0.20	3.93e-03	-2.42e-04	-2.52e-04	6.89e-04	-1.57e-04	2.63e-04	-1.37e-04	1.05e-06
0.20-0.40	-2.42e-04	6.68e-03	-5.30e-04	1.21e-03	3.15e-04	4.47e-04	1.54e-04	1.85e-04
0.40-0.60	-2.52e-04	-5.30e-04	4.00e-03	-6.58e-04	-3.38e-05	-2.05e-05	-1.24e-05	6.27e-05
0.60-0.80	6.89e-04	1.21e-03	-6.58e-04	4.54e-03	-1.30e-04	5.21e-04	9.43e-05	1.43e-04
0.80-1.00	-1.57e-04	3.15e-04	-3.38e-05	-1.30e-04	2.44e-03	-1.29e-04	7.12e-05	4.50e-05
1.00-1.20	2.63e-04	4.47e-04	-2.05e-05	5.21e-04	-1.29e-04	2.66e-03	-5.20e-05	1.46e-04
1.20-1.50	-1.37e-04	1.54e-04	-1.24e-05	9.43e-05	7.12e-05	-5.20e-05	1.04e-03	1.99e-05
1.50-2.00	1.05e-06	1.85e-04	6.27e-05	1.43e-04	4.50e-05	1.46e-04	1.99e-05	5.06e-04

Table 278: Covariance matrix for the normalized parton-level phase-space differential cross-section as a function of the absolute value of the rapidity of the leading top quark, accounting for the statistical and systematic uncertainties.

bin [GeV]	0.00-0.20	0.20-0.40	0.40-0.60	0.60-0.80	0.80-1.00	1.00-1.20	1.20-1.50	1.50-2.00
0.00-0.20	1.00	-0.05	-0.06	0.16	-0.05	0.08	-0.07	0.00
0.20-0.40	-0.05	1.00	-0.10	0.22	0.08	0.11	0.06	0.10
0.40-0.60	-0.06	-0.10	1.00	-0.15	-0.01	-0.01	-0.01	0.04
0.60-0.80	0.16	0.22	-0.15	1.00	-0.04	0.15	0.04	0.09
0.80-1.00	-0.05	0.08	-0.01	-0.04	1.00	-0.05	0.04	0.04
1.00-1.20	0.08	0.11	-0.01	0.15	-0.05	1.00	-0.03	0.13
1.20-1.50	-0.07	0.06	-0.01	0.04	0.04	-0.03	1.00	0.03
1.50-2.00	0.00	0.10	0.04	0.09	0.04	0.13	0.03	1.00

Table 279: Correlation matrix for the normalized parton-level phase-space differential cross-section as a function of the absolute value of the rapidity of the leading top quark, accounting for the statistical and systematic uncertainties.

bin [GeV]	0.00-0.20	0.20-0.40	0.40-0.60	0.60-0.80	0.80-1.00	1.00-1.20	1.20-1.50	1.50-2.00
0.00-0.20	4.10e-03	-9.20e-04	5.46e-04	2.95e-05	-1.57e-04	-2.47e-04	2.25e-04	1.82e-04
0.20-0.40	-9.20e-04	4.22e-03	-6.88e-04	-1.68e-04	-2.75e-04	-1.92e-04	-1.46e-04	1.34e-06
0.40-0.60	5.46e-04	-6.88e-04	5.22e-03	-4.48e-04	-1.63e-05	-1.02e-04	5.25e-05	9.03e-05
0.60-0.80	2.95e-05	-1.68e-04	-4.48e-04	3.64e-03	-5.00e-04	-4.16e-05	2.90e-05	7.53e-05
0.80-1.00	-1.57e-04	-2.75e-04	-1.63e-05	-5.00e-04	2.91e-03	-6.42e-04	-6.87e-06	-3.32e-05
1.00-1.20	-2.47e-04	-1.92e-04	-1.02e-04	-4.16e-05	-6.42e-04	2.73e-03	-3.58e-04	2.71e-08
1.20-1.50	2.25e-04	-1.46e-04	5.25e-05	2.90e-05	-6.87e-06	-3.58e-04	1.38e-03	3.65e-05
1.50-2.00	1.82e-04	1.34e-06	9.03e-05	7.53e-05	-3.32e-05	2.71e-08	3.65e-05	3.81e-04

Table 280: Covariance matrix for the normalized parton-level phase-space differential cross-section as a function of the absolute value of the rapidity of the second-leading top quark, accounting for the statistical and systematic uncertainties.

bin [GeV]	0.00-0.20	0.20-0.40	0.40-0.60	0.60-0.80	0.80-1.00	1.00-1.20	1.20-1.50	1.50-2.00
0.00-0.20	1.00	-0.22	0.12	0.01	-0.05	-0.07	0.09	0.15
0.20-0.40	-0.22	1.00	-0.15	-0.04	-0.08	-0.06	-0.06	0.00
0.40-0.60	0.12	-0.15	1.00	-0.10	-0.00	-0.03	0.02	0.06
0.60-0.80	0.01	-0.04	-0.10	1.00	-0.15	-0.01	0.01	0.06
0.80-1.00	-0.05	-0.08	-0.00	-0.15	1.00	-0.23	-0.00	-0.03
1.00-1.20	-0.07	-0.06	-0.03	-0.01	-0.23	1.00	-0.19	0.00
1.20-1.50	0.09	-0.06	0.02	0.01	-0.00	-0.19	1.00	0.05
1.50-2.00	0.15	0.00	0.06	0.06	-0.03	0.00	0.05	1.00

Table 281: Correlation matrix for the normalized parton-level phase-space differential cross-section as a function of the absolute value of the rapidity of the second-leading top quark, accounting for the statistical and systematic uncertainties.

Not reviewed, for internal circulation only

bin [GeV]	0-50	50-100	100-150	150-200	200-300	300-400	400-500	500-800
0-50	3.69e-07	1.09e-07	2.54e-08	-1.62e-08	-4.87e-08	-2.54e-08	-1.91e-08	-1.57e-09
50-100	1.09e-07	9.44e-08	1.82e-08	-3.90e-08	-3.48e-08	-1.77e-08	-1.47e-08	-3.48e-09
100-150	2.54e-08	1.82e-08	7.74e-08	3.50e-08	-9.46e-09	2.22e-09	2.61e-10	2.02e-09
150-200	-1.62e-08	-3.90e-08	3.50e-08	7.85e-08	1.76e-08	8.04e-09	1.11e-08	3.50e-09
200-300	-4.87e-08	-3.48e-08	-9.46e-09	1.76e-08	3.49e-08	1.12e-08	6.89e-09	2.65e-09
300-400	-2.54e-08	-1.77e-08	2.22e-09	8.04e-09	1.12e-08	1.98e-08	4.26e-09	2.30e-09
400-500	-1.91e-08	-1.47e-08	2.61e-10	1.11e-08	6.89e-09	4.26e-09	1.86e-08	9.01e-10
500-800	-1.57e-09	-3.48e-09	2.02e-09	3.50e-09	2.65e-09	2.30e-09	9.01e-10	1.61e-09

Table 282: Covariance matrix for the normalized parton-level phase-space differential cross-section as a function of the $t\bar{t} p_T$, accounting for the statistical and systematic uncertainties.

bin [GeV]	0-50	50-100	100-150	150-200	200-300	300-400	400-500	500-800
0-50	1.00	0.58	0.15	-0.10	-0.43	-0.30	-0.23	-0.06
50-100	0.58	1.00	0.21	-0.45	-0.61	-0.41	-0.35	-0.28
100-150	0.15	0.21	1.00	0.45	-0.18	0.06	0.01	0.18
150-200	-0.10	-0.45	0.45	1.00	0.34	0.20	0.29	0.31
200-300	-0.43	-0.61	-0.18	0.34	1.00	0.43	0.27	0.35
300-400	-0.30	-0.41	0.06	0.20	0.43	1.00	0.22	0.41
400-500	-0.23	-0.35	0.01	0.29	0.27	0.22	1.00	0.16
500-800	-0.06	-0.28	0.18	0.31	0.35	0.41	0.16	1.00

Table 283: Correlation matrix for the normalized parton-level phase-space differential cross-section as a function of the $t\bar{t} p_T$, accounting for the statistical and systematic uncertainties.

Not reviewed, for internal circulation only

bin [GeV]	1000-1100	1100-1200	1200-1300	1300-1400	1400-1500	1500-1700	1700-1900	1900-2100	2100-2300	2300-3000
1000-1100	3.39e-08	4.21e-09	-6.09e-09	6.24e-10	-2.10e-10	4.34e-10	1.14e-10	8.63e-10	3.63e-10	
1100-1200	4.21e-09	2.17e-08	5.26e-09	-8.86e-10	-1.68e-09	-8.91e-11	-9.82e-11	7.07e-10	3.25e-10	
1200-1300	-6.09e-09	5.26e-09	1.51e-08	5.09e-09	-2.84e-09	-2.83e-11	1.11e-09	9.24e-10	8.19e-10	
1300-1400	6.24e-10	-8.86e-10	5.09e-09	1.38e-08	3.07e-09	-6.38e-10	1.19e-09	1.19e-09	1.01e-09	
1400-1500	-2.10e-10	-1.68e-09	-2.84e-09	3.07e-09	9.93e-09	4.57e-10	-4.12e-10	4.40e-10	1.82e-10	
1500-1700	4.34e-10	-8.91e-11	-2.83e-11	-6.38e-10	4.57e-10	4.19e-09	2.93e-10	3.19e-10	4.31e-10	
1700-1900	1.14e-10	-9.82e-11	1.11e-09	1.19e-09	-4.12e-10	2.93e-10	3.35e-09	7.59e-10	4.83e-10	
1900-2100	8.63e-10	7.07e-10	9.24e-10	1.19e-09	4.40e-10	3.19e-10	7.59e-10	2.29e-09	5.52e-10	
2100-2300	3.63e-10	3.25e-10	8.19e-10	1.01e-09	1.82e-10	4.31e-10	4.83e-10	5.52e-10	1.36e-09	
2300-3000	-9.42e-11	-1.70e-10	3.92e-11	6.47e-11	9.51e-12	5.98e-11	1.39e-10	4.99e-11	5.01e-11	

Table 284: Covariance matrix for the normalized parton-level phase-space differential cross-section as a function of the $t\bar{t}$ invariant mass, accounting for the statistical and systematic uncertainties.

bin [GeV]	1000-1100	1100-1200	1200-1300	1300-1400	1400-1500	1500-1700	1700-1900	1900-2100	2100-2300	2300-3000
1000-1100	1.00	0.16	-0.27	0.03	-0.01	0.04	0.01	0.10	0.05	
1100-1200	0.16	1.00	0.29	-0.05	-0.11	-0.01	-0.01	0.10	0.06	
1200-1300	-0.27	0.29	1.00	0.35	-0.23	-0.00	0.16	0.16	0.18	
1300-1400	0.03	-0.05	0.35	1.00	0.26	-0.08	0.17	0.21	0.23	
1400-1500	-0.01	-0.11	-0.23	0.26	1.00	0.07	-0.07	0.09	0.05	
1500-1700	0.04	-0.01	-0.00	-0.08	0.07	1.00	0.08	0.10	0.18	
1700-1900	0.01	-0.01	0.16	0.17	-0.07	0.08	1.00	0.27	0.23	
1900-2100	0.10	0.10	0.16	0.21	0.09	0.10	0.27	1.00	0.31	
2100-2300	0.05	0.06	0.18	0.23	0.05	0.18	0.23	0.31	1.00	
2300-3000	-0.05	-0.11	0.03	0.05	0.01	0.08	0.22	0.10	0.12	

Table 285: Correlation matrix for the normalized parton-level phase-space differential cross-section as a function of the $t\bar{t}$ invariant mass, accounting for the statistical and systematic uncertainties.

Not reviewed, for internal circulation only

bin [GeV]	0.00-0.20	0.20-0.40	0.40-0.60	0.60-0.80	0.80-1.00	1.00-1.20	1.20-1.50	1.50-2.00
0.00-0.20	7.06e-03	7.65e-04	4.80e-04	1.38e-03	1.06e-03	2.78e-03	5.08e-04	6.19e-04
0.20-0.40	7.65e-04	6.38e-03	-3.12e-04	8.84e-04	5.65e-04	1.87e-03	2.07e-04	3.44e-04
0.40-0.60	4.80e-04	-3.12e-04	4.50e-03	-2.28e-04	1.84e-04	5.40e-04	1.05e-04	2.00e-04
0.60-0.80	1.38e-03	8.84e-04	-2.28e-04	4.87e-03	2.08e-04	1.52e-03	9.83e-05	5.09e-04
0.80-1.00	1.06e-03	5.65e-04	1.84e-04	2.08e-04	3.65e-03	9.01e-04	2.25e-04	2.99e-04
1.00-1.20	2.78e-03	1.87e-03	5.40e-04	1.52e-03	9.01e-04	4.60e-03	3.97e-04	5.88e-04
1.20-1.50	5.08e-04	2.07e-04	1.05e-04	9.83e-05	2.25e-04	3.97e-04	9.91e-04	5.79e-05
1.50-2.00	6.19e-04	3.44e-04	2.00e-04	5.09e-04	2.99e-04	5.88e-04	5.79e-05	5.19e-04

Table 286: Covariance matrix for the normalized parton-level phase-space differential cross-section as a function of the absolute value of $t\bar{t}$ rapidity, accounting for the statistical and systematic uncertainties.

bin [GeV]	0.00-0.20	0.20-0.40	0.40-0.60	0.60-0.80	0.80-1.00	1.00-1.20	1.20-1.50	1.50-2.00
0.00-0.20	1.00	0.11	0.09	0.24	0.21	0.49	0.19	0.32
0.20-0.40	0.11	1.00	-0.06	0.16	0.12	0.35	0.08	0.19
0.40-0.60	0.09	-0.06	1.00	-0.05	0.05	0.12	0.05	0.13
0.60-0.80	0.24	0.16	-0.05	1.00	0.05	0.32	0.04	0.32
0.80-1.00	0.21	0.12	0.05	0.05	1.00	0.22	0.12	0.22
1.00-1.20	0.49	0.35	0.12	0.32	0.22	1.00	0.19	0.38
1.20-1.50	0.19	0.08	0.05	0.04	0.12	0.19	1.00	0.08
1.50-2.00	0.32	0.19	0.13	0.32	0.22	0.38	0.08	1.00

Table 287: Correlation matrix for the normalized parton-level phase-space differential cross-section as a function of the absolute value of $t\bar{t}$ rapidity, accounting for the statistical and systematic uncertainties.

bin [GeV]	0.00-2.50	2.50-2.75	2.75-3.00	3.00-3.15
0.00-2.50	1.15e-03	9.96e-04	5.14e-04	-2.35e-03
2.50-2.75	9.96e-04	2.87e-03	1.43e-03	-5.21e-03
2.75-3.00	5.14e-04	1.43e-03	7.02e-03	-1.22e-02
3.00-3.15	-2.35e-03	-5.21e-03	-1.22e-02	7.57e-02

Table 288: Covariance matrix for the normalized parton-level phase-space differential cross-section as a function of $\Delta\phi(t_1, t_2)$, accounting for the statistical and systematic uncertainties.

bin [GeV]	0.00-2.50	2.50-2.75	2.75-3.00	3.00-3.15
0.00-2.50	1.00	0.55	0.18	-0.25
2.50-2.75	0.55	1.00	0.32	-0.35
2.75-3.00	0.18	0.32	1.00	-0.53
3.00-3.15	-0.25	-0.35	-0.53	1.00

Table 289: Correlation matrix for the normalized parton-level phase-space differential cross-section as a function of $\Delta\phi(t_1, t_2)$, accounting for the statistical and systematic uncertainties.

bin [GeV]	0-20	20-40	40-60	60-100	100-200	200-300	300-600
0-20	1.83e-06	5.00e-07	6.29e-08	-4.68e-08	-6.47e-08	-2.72e-08	-2.16e-08
20-40	5.00e-07	5.47e-07	1.87e-07	-6.09e-08	-4.12e-08	-1.89e-08	-1.32e-08
40-60	6.29e-08	1.87e-07	2.97e-07	2.22e-08	-1.62e-08	1.33e-09	-2.89e-09
60-100	-4.68e-08	-6.09e-08	2.22e-08	1.90e-07	4.75e-09	1.20e-08	1.56e-08
100-200	-6.47e-08	-4.12e-08	-1.62e-08	4.75e-09	3.53e-08	4.62e-09	5.41e-09
200-300	-2.72e-08	-1.89e-08	1.33e-09	1.20e-08	4.62e-09	1.46e-08	2.45e-09
300-600	-2.16e-08	-1.32e-08	-2.89e-09	1.56e-08	5.41e-09	2.45e-09	7.18e-09

Table 290: Covariance matrix for the normalized parton-level phase-space differential cross-section as a function of $p_{out}^{\bar{t}\bar{t}}$, accounting for the statistical and systematic uncertainties.

bin [GeV]	0-20	20-40	40-60	60-100	100-200	200-300	300-600
0-20	1.00	0.50	0.09	-0.08	-0.26	-0.17	-0.19
20-40	0.50	1.00	0.46	-0.19	-0.30	-0.21	-0.21
40-60	0.09	0.46	1.00	0.09	-0.16	0.02	-0.06
60-100	-0.08	-0.19	0.09	1.00	0.06	0.23	0.42
100-200	-0.26	-0.30	-0.16	0.06	1.00	0.20	0.34
200-300	-0.17	-0.21	0.02	0.23	0.20	1.00	0.24
300-600	-0.19	-0.21	-0.06	0.42	0.34	0.24	1.00

Table 291: Correlation matrix for the normalized parton-level phase-space differential cross-section as a function of $p_{out}^{\bar{t}\bar{t}}$, accounting for the statistical and systematic uncertainties.

bin [GeV]	0.00-0.20	0.20-0.40	0.40-0.60	0.60-0.80	0.80-1.00	1.00-1.30	1.30-2.00
0.00-0.20	6.71e-03	2.70e-04	2.34e-05	1.30e-03	4.71e-05	1.23e-03	4.07e-04
0.20-0.40	2.70e-04	5.79e-03	-5.48e-04	6.59e-04	5.20e-05	3.41e-04	1.89e-04
0.40-0.60	2.34e-05	-5.48e-04	4.13e-03	-5.62e-04	-1.62e-04	1.90e-04	3.38e-06
0.60-0.80	1.30e-03	6.59e-04	-5.62e-04	4.06e-03	-3.50e-04	4.84e-04	2.69e-04
0.80-1.00	4.71e-05	5.20e-05	-1.62e-04	-3.50e-04	2.58e-03	-6.81e-05	3.85e-05
1.00-1.30	1.23e-03	3.41e-04	1.90e-04	4.84e-04	-6.81e-05	1.85e-03	1.23e-04
1.30-2.00	4.07e-04	1.89e-04	3.38e-06	2.69e-04	3.85e-05	1.23e-04	3.06e-04

Table 292: Covariance matrix for the normalized parton-level phase-space differential cross-section as a function of $y_B^{t\bar{t}}$, accounting for the statistical and systematic uncertainties.

bin [GeV]	0.00-0.20	0.20-0.40	0.40-0.60	0.60-0.80	0.80-1.00	1.00-1.30	1.30-2.00
0.00-0.20	1.00	0.04	0.00	0.25	0.01	0.35	0.28
0.20-0.40	0.04	1.00	-0.11	0.14	0.01	0.10	0.14
0.40-0.60	0.00	-0.11	1.00	-0.14	-0.05	0.07	0.00
0.60-0.80	0.25	0.14	-0.14	1.00	-0.11	0.18	0.24
0.80-1.00	0.01	0.01	-0.05	-0.11	1.00	-0.03	0.04
1.00-1.30	0.35	0.10	0.07	0.18	-0.03	1.00	0.16
1.30-2.00	0.28	0.14	0.00	0.24	0.04	0.16	1.00

Table 293: Correlation matrix for the normalized parton-level phase-space differential cross-section as a function of $y_B^{t\bar{t}}$, accounting for the statistical and systematic uncertainties.

1647 X. Studies to investigate global χ^2 calculation

1648 Studies were made to determine the robustness of calculating a “global χ^2 ,” where the 1-dimensional
 1649 information obtained from the measurements of the 13 differential cross-sections and the comparison
 1650 with specific predictions are combined into a single figure-of-merit that could be used to assist in sorting
 1651 models that best agree with the observations, for MC tuning and for PDF fitting.

1652 Two approaches to performing this global calculation were investigated. They use different ways to
 1653 defined an extended covariance matrix which is then used as input for the χ^2 calculation defined in Sec-
 1654 tion 9. This covariance matrix is then inverted and used to calculate the χ^2 associated with each set of
 1655 predictions.

1656 They are called “full post-unfolding” and “hybrid pre-unfolding”. In the post-unfolding scheme the cal-
 1657 culation was carried out for both the absolute and the normalized differential cross-section measurements.
 1658 The “hybrid pre-unfolding” scheme was implemented only partially, as the inclusion of data and MC
 1659 statistical uncertainties requires additional work and validation.

1660 Finally, a study was made of an alternative approach to combining χ^2 's and p -values.

1661 X.1. Determination of covariance matrices

1662 X.1.1. Calculation of post-unfolding covariance matrix

1663 The first approach is to use a so-called “post-unfolding” χ^2 calculation. In this approach the “post-
 1664 unfolding” scheme described in Appendix W to derive the signal modelling covariance matrix for a single
 1665 distribution is extended to all distributions and all systematic effects to build an extended systematic cov-
 1666 ariance matrix. This is then summed with the statistical covariance matrix determined using the bootstrap
 1667 technique documented in Appendix V.

1668 Operatively the “post-unfolding” extended covariance matrix is built by taking the following steps:

- 1669 1. For each systematic uncertainty an extended $\sum_{j=1}^N n_j$ covariance matrix $CovSys$ is derived where $j \in$
 1670 $1, \dots, N$, N is the number of distributions to be unfolded and n_j is the number of bins of the j^{th}
 1671 distribution defined as

$$1672 CovSys(m_k, n_p, s) = \rho(m_k, n_p, s) * \sigma(m_k, s) * \sigma(n_p, s), \quad (37)$$

1673 where $\sigma(n_k)$ ($\sigma(m_p)$) is the “post-unfolding” standard deviation associated to the s^{th} systematic
 1674 effect derived from simulated signal events for the n^{th} (m^{th}) bin of the k^{th} (p^{th}) distribution and
 1675 $\rho(m_k, n_p)$ is the correlation assumed between the m^{th} bin of the k^{th} distribution and the m^{th} bin of
 1676 the n^{th} of the p^{th} distribution.

- 1677 2. The extended covariance matrices obtained for the different systematic uncertainties are summed to
 1678 obtain the total systematic covariance matrix $CovSys$:

$$1679 CovSys(m_k, n_p) = \sum_s CovSys(m_k, n_p, s). \quad (38)$$

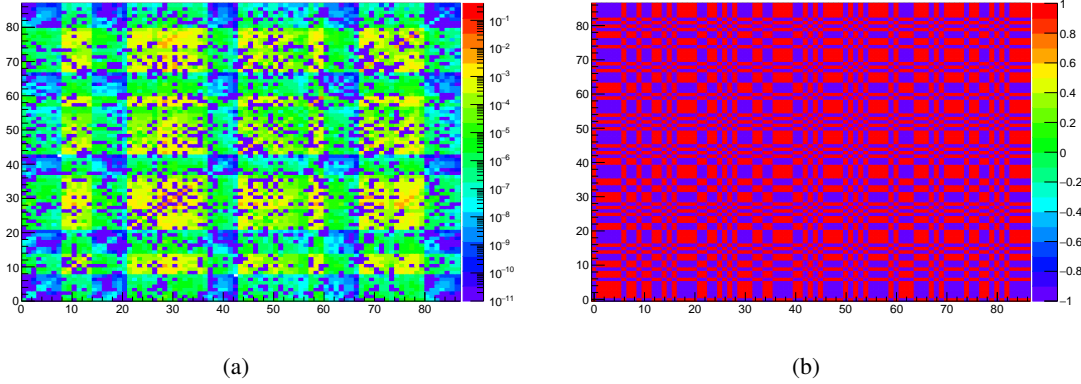


Figure 217: The covariance (a) and correlation (b) matrices for the systematic uncertainty on the integrated luminosity resulting from the calculations for the relative differential cross-section measurements employing the “best-guess” correlation assumption.

- 1675 3. The final total extended “post-unfolding” covariance matrix Cov is obtained by summing the sys-
 1676 tematic covariance matrix $CovSys$ and the extended statistical covariance matrix $CovStat$ derived
 1677 using the bootstrap technique (see Appendix V):

$$Cov(m_k, n_p) = CovSys(m_k, n_p) + CovStat(m_k, n_p). \quad (39)$$

1678 The correlation model for the s^{th} systematic uncertainty represented by $\rho(m_k, n_p, s)$ needs an extended set
 1679 of assumption with respect to the one-dimensional case: in addition to the correlation between different
 1680 bins of the same variable (“intra-variable” correlations), one needs to have a model for the correlation
 1681 between different bins of different variables (“inter-variable” correlations). Three models for correlations
 1682 were investigated:

- 1683 • $\rho(m_k, n_p, s) = 0$ if $k \neq p$ and = 1 otherwise. No inter-variable correlations are included.
- 1684 • $\rho(m_k, n_p, s) = 1$ if the products of the “up” and “minus” shifts associated to the m^{th} and n^{th} bin
 1685 are both positive, $\rho(m_k, n_p, s) = -1$ if the products of the “up” and “minus” shifts associated to the
 1686 m^{th} and n^{th} bin are both negative, $\rho(m_k, n_p, s) = 0$ if the products of the “up” and “minus” shifts
 1687 associated to the m^{th} and n^{th} bin have different signs. This model is called “best-guess” correlation
 1688 model.
- 1689 • $\rho(m_k, n_p, s) = 1$

1690 The advantage of using these models for defining the correlations is that they are relatively straightfor-
 1691 ward, using the estimates of systematic uncertainties on the 1-dimensional variables. However, they are
 1692 assumptions that have not been extensively validated and the variation in χ^2 values gives some sense of
 1693 the sensitivity of the results.

1694 An example of the resulting covariance and correlation matrices is shown in Fig. 217, using the “best-
 1695 guess” correlation assumption for one source of uncertainty (the integrated luminosity in this case).

1696 X.1.2. Calculation of hybrid pre-unfolding covariance matrix

1697 The second approach to calculating the covariance matrix is in an extension of the “pre-unfolding” ap-
 1698 proach outlined in Appendix W to estimate an extended covariance matrix incorporating data statistical
 1699 uncertainties and systematic effects from detector, background modelling and Monte Carlo sample size.
 1700 This covariance matrix is added to a “post-unfolding” extended matrix associated the remaining model-
 1701 ling uncertainties.

1702 In operative terms this is built by taking the following steps

- 1703 1. An extended $\sum_{j=1}^N n_j$ covariance matrix *CovNoModel* is derived where N is the number of distri-
 1704 butions to be unfolded and n_j is the number of bins of the j^{th} distribution. This matrix is defined
 1705 by running pseudoexperiments using the “pre-unfolding” scheme defined in Appendix W, which
 1706 determines a different set of Gaussian-distributed systematic shifts to be added to each bin of each
 1707 distribution. For each pseudo-experiment the coherent injection of Gaussian-distributed systematic
 1708 shifts is extended to all variables i.e. a unique Gaussian random number is used to determine
 1709 all the shifts corresponding to a given uncertainty for all the bins of all the distributions ⁴. The
 1710 current implementation treats the statistical uncertainties associated with the data sample size and
 1711 the size of the simulated sample in an approximate manner. The fluctuations in all the bins of all
 1712 the distributions are considered independent, while correlations are expected between bins
 1713 of two different distributions because the same data and Monte carlo events are used to derive the
 1714 results for each distribution. The current implementation incorporates the statistical uncertainties
 1715 as independent shifts of each bin so it does not take into account the statistical correlations arising
 1716 from the fact that all 13 variables are measured using the same events.
- 1717 2. A second “post-unfolding” covariance matrix *CovModel* is defined exactly as in the first approach,
 1718 but including only effects from generator, parton shower and hadronization, IFSR and PDF.
- 1719 3. The total extended “hybrid” covariance matrix is obtained by summing *CovModel* and *CovNoModel*.

1720 In order to account for the data statistical correlations, the statistical shift derived from bootstrap-derived
 1721 histograms could be employed (see Appendix V): this step needs additional coding effort to be included in
 1722 the present software. Very preliminary results suggest that the method results in χ^2 values that are within
 1723 10 to 20% of the results from the post-unfolding methodology applied to the relative measurements (30
 1724 to 40% for the absolute measurements). The reasons for the differences are not fully understood.

1725 X.2. Limitations of the approaches studied

1726 X.2.1. Limitations in data statistical covariance matrix

1727 The covariance matrix that incorporates the statistical correlations between the 13 variables (and form-
 1728 ally each range that is measured and reported as a bin) is determined using a bootstrap technique. This
 1729 technique uses the signal events employing a bootstrap calculation to determine each correlation coef-
 1730 ficient. This covariance matrix is provided in the auxiliary materials in Appendix. V. This is employed
 1731 in the post-unfolding calculation, while data statistical uncertainties are currently (incorrectly) treated as
 1732 independent for each bin in the pre-unfolding technique.

⁴ For instance if the random Gaussian number extracted for JES systematic uncertainty for pseudo-experiment number N is 0.4, all bins of all variables will use a JES shift corresponding to 0.4σ for the given bin.

- 1733 Although this bootstrapped matrix is free of modelling uncertainties, it is based on a limited number
 1734 of events (pair-wise correlations are calculated using 1000 data events drawn from the signal sample of
 1735 approximately 3500 events). The uncertainties associated with this covariance matrix are not incorporated
 1736 in the χ^2 calculation. We also note that this calculation has not been validated for use in this context; it
 1737 was calculated and provided in response to requests from external parties.
- 1738 The MC statistical uncertainty is estimated in the current calculation by using the bootstrapped data
 1739 correlation matrix as a proxy. The actual correlation matrix from the MC sample should be employed
 1740 (but not implemented for the calculations described here).
- 1741 In addition we note that the current pre-unfolding calculation is taking data and MC statistical uncertain-
 1742 ties in an incorrect way.

1743 X.2.2. Limits of pre-unfolding and hybrid post-unfolding schemes

1744 In the course of these studies, several difficulties were encountered, several of them common to both
 1745 approaches:

- 1746 1. The use of post-unfolding instead of pre-unfolding to propagate the systematic uncertainties results
 1747 in different χ^2 calculations from the results presented for the individual variables. Although the res-
 1748 ults show a similar trend, differences of up to 30-40% are seen when comparing the pre-unfolding
 1749 and post-unfolding χ^2 calculations for a single variable.
- 1750 2. Although the post-unfolding procedure allows for an efficient calculation of the covariance matrices,
 1751 it does not take into account the effect of unfolding, which effectively decorrelates the effect of the
 1752 systematic uncertainties. Assumptions regarding how strongly correlated the systematic effects are
 1753 across all the measured values have to be made for the post-unfolding calculation. Reasonable
 1754 choices of correlation result in different χ^2 values and interpretations. The hybrid post-unfolding
 1755 scheme takes into account these effects in a more consistent manner.
- 1756 3. Neither technique as implemented accounts correctly for the statistical correlations between vari-
 1757 ables in the global χ^2 . This is best approximated in the post-unfolding treatment, but requires
 1758 further development.
- 1759 4. The 13 variables are strongly correlated. In principle, the final state is characterized by two four-
 1760 vectors, or eight variables all told. This should reduce the number of degrees of freedom. However,
 1761 no natural solution to the determination of the total number of degrees of freedom has been found.
 1762 This makes calculation of a p -value associated with the global χ^2 problematic.

1763 These issues are discussed in more detail below.

1764 X.2.3. Difference between post-unfolding and pre-unfolding calculations

1765 The assumption that the post-unfolding approach is robust was tested by doing a direct comparison of the
 1766 results of post-unfolding and pre-unfolding calculations for the individual distributions. These are shown
 1767 in Table 294 for the predictions of the PowHEG+PYTHIA8 predictions for the normalized particle-level
 1768 fiducial differential cross-sections.

Observable	Pre-unfolding		Post-unfolding	
	χ^2/NDF	p-value	χ^2/NDF	p-value
$p_T^{t,1}$	7.7/7	0.36	5.0/7	0.66
$ y^{t,1} $	7.5/5	0.18	6.0/5	0.31
$p_T^{t,2}$	8.6/6	0.20	6.5/6	0.37
$ y^{t,2} $	3.7/5	0.59	3.2/5	0.66
$m^{t\bar{t}}$	4.5/9	0.88	4.9/9	0.84
$pT^{t\bar{t}}$	7.8/5	0.17	6.8/5	0.24
$ y^{t\bar{t}} $	1.1/5	0.95	0.8/5	0.98
$\chi^{t\bar{t}}$	14.2/6	0.03	10.7/6	0.10
$y_B^{t\bar{t}}$	2.5/6	0.87	1.8/6	0.93
$ p_{out}^{t\bar{t}} $	1.9/6	0.93	1.6/6	0.95
$\Delta\phi^{t\bar{t}}$	0.9/3	0.84	1.9/3	0.59
$H_T^{t\bar{t}}$	4.8/6	0.57	4.4/6	0.62
$\cos\theta^*$	9.9/5	0.08	8.1/5	0.15

Table 294: Comparison between the normalized particle-level fiducial differential cross-sections and the POWHEG+PYTHIA8 predictions using the pre-unfolding and post-unfolding covariance matrix calculations.

1769 There is a systematic reduction in the χ^2 when using the post-unfolding covariance matrices for this
 1770 example. Interestingly, the same comparison using the absolute differential cross-section measurements
 1771 results in the opposite trend, with the post-unfolding χ^2 calculations being about 25% higher.

1772 These are significant differences, and imply that the post-unfolding results have to be treated as less-
 1773 reliable than the ones obtained taking into account how unfolding affects the propagation of systematic
 1774 uncertainties and their correlations.

1775 X.2.4. Correlations of systematic uncertainties across variables

1776 The comparison of pre-unfolding and post-unfolding χ^2 values for single variables implies that the naive
 1777 assumption that all systematic uncertainties are 100% correlated is incorrect. It is of note that even in the
 1778 cases of a single variable, the effects of a systematic uncertainty may reverse itself across the bins that the
 1779 variable is measured over. In those cases, the relative correlation flips from being positive to negative and
 1780 is taken into account by reversing the sign of the term.

1781 Various tests of the sensitivity of the resulting χ^2 values to what assumptions were made regarding the
 1782 correlations of the systematic uncertainties between variables, including 0% 50%, 100% and our “best-
 1783 guess” as described earlier.

1784 A comparison of the results are shown in Table 295 for various comparisons of the relative differen-
 1785 tial cross-section measurements (“best-guess” here refers to the calculation where 0% correlations are
 1786 assumed between variables). One sees changes in the χ^2 values that range from 64.4 to 85.3 for the
 1787 POWHEG+PYTHIA8 predictions, and 135.0 to 199.0 for the MADGRAPH5_AMC@NLO +PYTHIA8 predictions.
 1788 The variation in the global χ^2 results for the absolute differential cross-section measurements show even
 1789 greater variation.

1790 We make no claim that any of these calculations are correct. The point here is to note that the resulting
 1791 χ^2 values are sensitive to the choice of correlation assumption.

1792 We note that the assumption of levels of correlation other than $\pm 100\%$ or 0% create a further challenge
 1793 of maintaining the coherence of all the correlations internally. For example, if variable i and j are 80%

Correlation Assumption	PWG+PY8		MG5_AMC@NLO+Py8		PWG+H7	
	χ^2/NDF	$p\text{-value}$	χ^2/NDF	$p\text{-value}$	χ^2/NDF	$p\text{-value}$
No Inter-variable correlations	64.4/74	0.78	136.0/74	< 0.01	68.3/74	0.67
“Best-guess” correlations	68.6/74	0.66	176.0/74	< 0.01	69.2/74	0.64
50% correlations	68.1/74	0.67	135.0/74	< 0.01	74.3/74	0.47
100% correlations	71.9/74	0.55	199.0/74	< 0.01	73.4/74	0.50

Table 295: Comparison between the χ^2 calculations under different assumptions of the correlations between the systematic uncertainties between variables for the relative differential cross-section measurements.

correlated, then this correlation should be reflected in the correlations with a third variable k . Ensuring this coherence places even more constraints on the calculation. From experience, a naive assignment of correlations can result in a covariance matrix which is no longer positive-definite and can result in negative χ^2 values. More sophisticated approaches that respect the coherence of the correlations require further development.

X.2.5. Number of degrees of freedom

The total number of measured values in the analysis is 87. However, there are strong correlations between the variables (e.g., $p_T^{t,1}$, $p_T^{t,2}$ and $m^{t\bar{t}}$). We therefore expect the effective number of degrees of freedom to be substantially smaller than the total number of bins.

A standard technique for assessing this is to perform an eigenvalue decomposition of the covariance matrix, and examine the change in the eigenvalues, having sorted them in order of value. One would expect to see a significant drop in eigenvalues when one exceeds the effective number of degrees of freedom. This is tested against the data statistical covariance matrix for the relative differential cross-section measurements, and one sees that there are only 74 sizeable eigenvalues, with the remaining 13 being an order of magnitude or smaller.

Such a test on the total covariance matrix determined by the post-unfolding procedure does not provide a clear “break” in the eigenvalues. They tend to fall by a factor of 2 to 3 when comparing one eigenvalue to the next, suggesting that the resulting matrix has maximal rank. Nor is there a significant change in this pattern when we go from the absolute measurements to the normalized measurements (where we would expect at least a reduction of 13 in the number of degrees of freedom).

This makes the calculation of a p -value (and then the resulting interpretation regarding goodness-of-fit) from the χ^2 problematic. No solution for this has been identified. What are presented are p -value calculations assuming maximal rank.

X.3. Alternate Approach: Combining p -values using the Brown/Kost method

To combine statistically a series of measurements with known NDF, χ^2 and p -values, but when the details of how these have been calculated are not available or irrelevant (“meta-analysis”), a method devised by Brown [65] and later refined by Kost [66] can be applied. A classical solution was derived by Fisher, but it is valid only in the simple case where no correlation among the measurements are present. The latter method addresses this problem.

1823 If X is a tuple of n uncorrelated values distributed as a gaussian, then the sum of their sum is distributed
1824 as a χ^2 distribution with n degrees of freedom:

$$\chi_n^2 = \sum_i^n G_i \quad (40)$$

$$E[\chi_n^2] = n \quad (41)$$

$$Var[\chi_n^2] = 2n \quad (42)$$

1825 If all the values of X are scaled by the same multiplicative factor c , the scaled χ^2 looks like:

$$c\chi_n^2 = \sum_i^n cG_i = c \sum_i^n G_i \quad (43)$$

$$E[c\chi_n^2] = cn \quad (44)$$

$$Var[c\chi_n^2] = 2c^2n \quad (45)$$

1826 Assuming no correlations among the elements of X , one can combine the p -values by the application of
1827 the Fisher formula:

$$\Psi_f = \sum_i^n (-2 \log p_i) \sim \chi_{2n}^2 \quad (46)$$

1828 Which is distributed as a χ^2 distribution with $2n$ degrees of freedom. In fact, the negative log of uniform
1829 random variables follows an exponential distribution. When scaled by 2 these follow a chi-squared dis-
1830 tribution with 2 degrees of freedom, and a sum of chi-squared distributions is also chi-squared with the
1831 degrees of freedom summed.

1832 If there are correlations, the combination is performed by an approximated multivariate normal distribu-
1833 tion Ψ_f (i.e. a scaled $\chi^2 \rightarrow c\chi^2$) such that the true and the approximate distributions have the same first
1834 two moments (mean and variance):

$$E[\Psi_f] = cf \quad (47)$$

$$Var[\Psi_f] = 2c^2f \quad (48)$$

1835 By inverting the relationship:

$$f = \frac{2E[\Psi_f]^2}{Var[\Psi_f]} \quad (49)$$

$$c = \frac{Var[\Psi_f]}{2E[\Psi_f]} \quad (50)$$

1836 The first two momenta of Ψ_f can be thus expressed by:

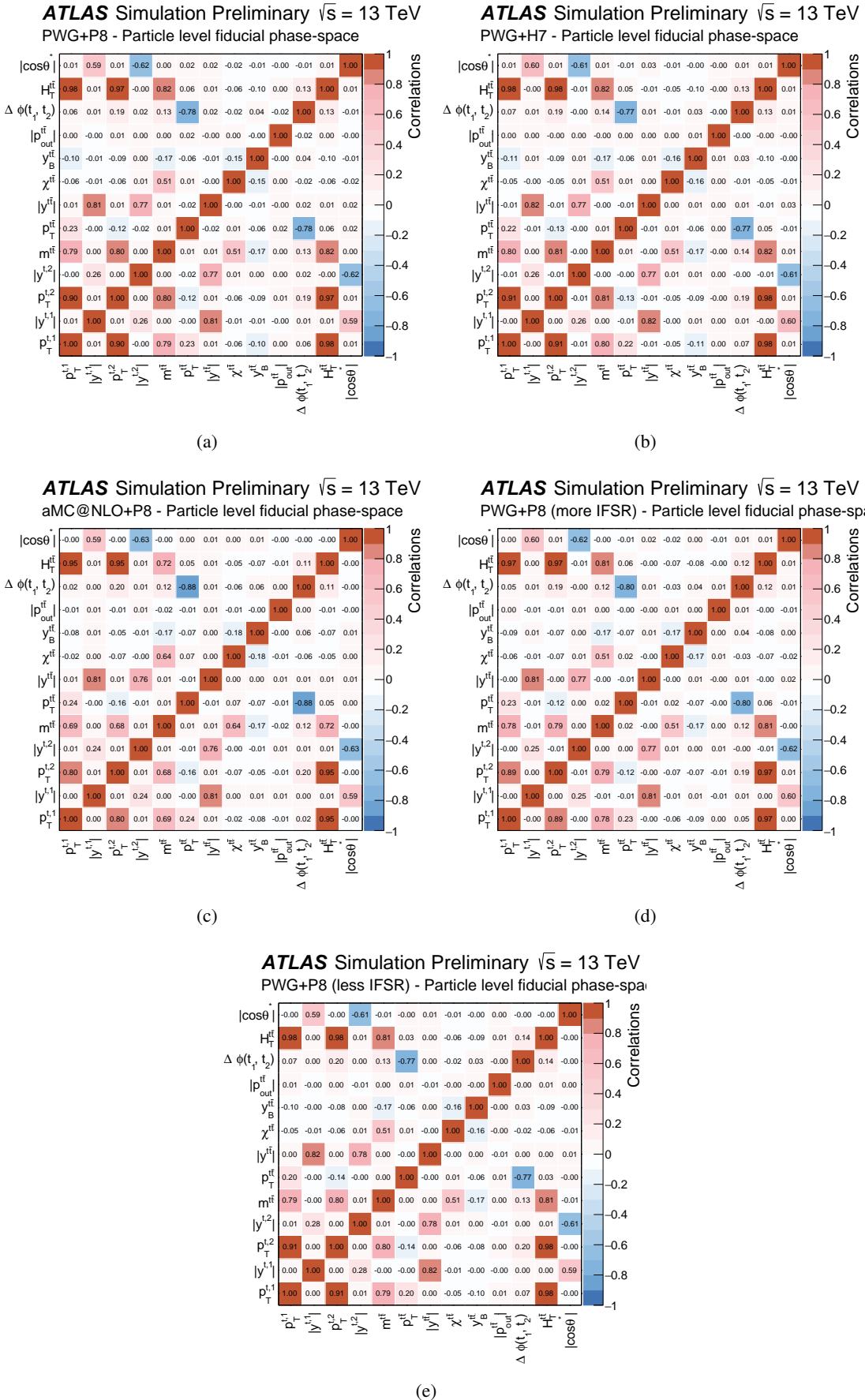
$$E[\Psi_f] = 2n \quad (51)$$

$$Var[\Psi_f] = \sum_{i,j}^n cov(-2 \log p_i, -2 \log p_j) \sim 3.263\rho_{ij} + 0.710\rho_{ij}^2 + 0.027\rho_{ij}^3 \quad (52)$$

1837 In this case, the correlations factors ρ_{ij} were derived from the Monte Carlo simulation of the $t\bar{t}$ process
 1838 at particle level in the signal region. The covariance among p -values was estimated using the Kost poly-
 1839 nominal approximation, obtained by numerical integration, as a function of the correlation coefficients ρ_{ij} .
 1840 The correlation factors are generally consistent among the generators under consideration. Interestingly,
 1841 as shown in Fig.218, the MADGRAPH5_AMC@NLO+PYTHIA8 generator predicts stronger correlations for
 1842 $(\Delta\phi^{t\bar{t}}, p_T^{t\bar{t}})$ and stronger correlations for $(p_T^{t\bar{t}}, m^{t\bar{t}})$ for both the leading and subleading top quark, and $(H_T^{t\bar{t}},$
 1843 $m^{t\bar{t}})$.

1844 Table 219 shows the intermediate steps of the calculation for the particle-level normalized distributions.
 1845 Table 220 shows a comparison with respect to the methods presented before, where correlations among
 1846 bins are taken into account. As a result, the MADGRAPH5_AMC@NLO+PYTHIA8 sample is always dis-
 1847 favored by the Brown/Kost method. The Powheg+PYTHIA8 sample with more IFSR settings is accepted
 1848 or disfavored by the post-unfolding depending on assumptions about correlations, and disfavored by the
 1849 Brown/Kost method. The other samples are compatible with the observed data.

Not reviewed, for internal circulation only



14th October 2017 – 15:48

427

Figure 218: Fiducial phase-space correlations among observables for the (a) Powheg+Pythia8, (b) Powheg+Herwig7, (c) MadGraph5_AMC@NLO+Pythia8, and Powheg+Pythia8 with (d) more and (e) less IFSR radiation.

	PWG+P8	aMC@NLO+P8	PWG+H7	PWG+P8 (more IFSR)	PWG+P8 (less IFSR)
Global χ^2 (no corr)	75.1/74 p = 0.442	156.5/74 p<0.01	80.0/74 p = 0.296	99.2/74 p=0.027	63.7/74 p=0.798
Fisher χ^2_{2n} (no corr)	27.6/26 p=0.38	112.8/26 p<0.01	31.5/26 p=0.21	76.0/26 p<0.01	19.2/26 p=0.83
$E[\Psi]$	26	26	26	26	26
$\sigma[\Psi]$	58.4	58.0	60.8	58.1	56.9
f	23	23	22	23	23
c	1.12	1.11	1.17	1.12	1.09
Brown/Kost Ψ_i (w/ corr)	24.6/23 p=0.374	101.2/23 p<0.01	27.0/22 p=0.213	68.1/23 p<0.01	17.6/23 p=0.780

Figure 219: Application of the Brown/Kost method to fiducial phase-space normalized distributions.

	PWG+P8	aMC@NLO+P8	PWG+H7	PWG+P8 (more IFSR)	PWG+P8 (less IFSR)
Sum of chi2	75.1/74 p = 0.44	156.5/74 p<0.01	80.0/74 p = 0.30	99.2/74 p=0.03	63.7/74 p=0.80
Fisher χ^2_{2n} (no corr)	27.6/26 p=0.38	112.8/26 p<0.01	31.5/26 p=0.21	76.0/26 p<0.01	19.2/26 p=0.83
Brown/Kost Ψ_i (w/ correlations)	24.6/23 p=0.38	101.2/23 p<0.01	27.0/22 p=0.21	68.1/23 p<0.01	17.6/23 p=0.78
Best guess No correlations	64.4/74 p=0.78	130.0/74 p<0.01	68.3/74 p=0.67	85.4/74 p=0.17	54.0/74 p=0.96
Best guess (w/ correlations)	68.6/74 p=0.66	176.0/74 p<0.01	69.2/74 p=0.64	84.8/74 p=0.18	66.0/74 p=0.73
100% correlations No inter-variable	85.3/74 p=0.17	185.0/74 p<0.01	93.6/74 p=0.06	117.0/74 p<0.01	68.7/74 p=0.65
100% correlations w/ inter-variable	71.9/74 p=0.55	199.0/74 p<0.01	73.4/74 p=0.50	89.3/74 p=0.11	69.3/74 p=0.63

Figure 220: Comparison of the Brown/Kost method to other methods for fiducial phase-space normalized distributions.

1850 X.4. Conclusions

1851 We come to the following conclusions regarding the current effort to calculate a “global χ^2 ” using the
 1852 1-dimensional results:

- 1853 1. The post-unfolding method has several flaws and we suggest abandoning such a calculation. The
 1854 key issues are that a) it is incoherent with the pre-unfolding calculations that are used in the paper
 1855 for each variable, b) there is unreasonable sensitivity to the assumed correlations of systematic
 1856 uncertainties and c) there is difficulty in determining the number of degrees of freedom.
- 1857 2. The pre-unfolding method avoids having to make assumptions regarding correlations, but needs
 1858 further validation and development. In particular, the incorporation of an appropriate model for
 1859 the data and MC statistical correlations requires further coding and validation. Efforts to this have
 1860 started, but the timeline for completion of this study is uncertain and several conceptual issues have
 1861 yet to be fully resolved.

1862 This highlights the importance that correlations play in any effort to combine these measurements. We
 1863 recommend that these general observations be communicated to those that use the auxiliary information
 1864 for additional interpretation. As we currently understand, these data are not used in this way.

1865 References

- Not reviewed, for internal circulation only
- [1] R. Frederix and F. Maltoni, *Top pair invariant mass distribution: a window on new physics*, JHEP **01** (2009) 047, arXiv: [0712.2355 \[hep-ph\]](#).
 - [2] ATLAS Collaboration, *Measurements of top quark pair relative differential cross-sections with ATLAS in pp collisions at $\sqrt{s} = 7$ TeV*, Eur. Phys. J. C **73** (2013) 2261, arXiv: [1207.5644 \[hep-ex\]](#).
 - [3] ATLAS Collaboration, *Measurements of normalized differential cross-sections for ttbar production in pp collisions at $\sqrt{s} = 7$ TeV using the ATLAS detector*, Phys. Rev. D **90** (2014) 072004, arXiv: [1407.0371 \[hep-ex\]](#).
 - [4] ATLAS Collaboration, *Differential top-antitop cross-section measurements as a function of observables constructed from final-state particles using pp collisions at $\sqrt{s} = 7$ TeV in the ATLAS detector*, JHEP **06** (2015) 100, arXiv: [1502.05923 \[hep-ex\]](#).
 - [5] ATLAS Collaboration, *Measurements of top-quark pair differential cross-sections in the lepton+jets channel in pp collisions at $\sqrt{s} = 8$ TeV using the ATLAS detector* (2015), arXiv: [1511.04716 \[hep-ex\]](#).
 - [6] CMS Collaboration, *Measurement of differential top-quark-pair production cross sections in pp collisions at $\sqrt{s} = 7$ TeV*, Eur. Phys. J. C **73** (2013) 2339, arXiv: [1211.2220 \[hep-ex\]](#).
 - [7] CMS Collaboration, *Measurement of the differential cross section for top quark pair production in pp collisions at $\sqrt{s} = 8$ TeV*, Submitted to Eur. Phys. J. C (2015), arXiv: [1505.04480 \[hep-ex\]](#).
 - [8] ATLAS Collaboration, *Search for resonances decaying into top-quark pairs using fully hadronic decays in pp collisions with ATLAS at $\sqrt{s} = 7$ TeV*, JHEP **01** (2013) 116, arXiv: [1211.2202 \[hep-ex\]](#).
 - [9] ATLAS Collaboration, *Measurements of $t\bar{t}$ differential cross-sections in the all-hadronic channel with the ATLAS detector using highly boosted top quarks in pp collisions at $\sqrt{s} = 13$ TeV*, ATLAS-CONF-2016-100, 2016, URL: <http://cdsweb.cern.ch/record/2217231>.
 - [10] ATLAS Collaboration, *Search for New Phenomena in Dijet Angular Distributions in Proton-Proton Collisions at $\sqrt{s} = 8$ TeV Measured with the ATLAS Detector*, Phys. Rev. Lett. **114** (2015) 221802, arXiv: [1504.00357 \[hep-ex\]](#).
 - [11] L. Apanasevich et al., *Evidence for Parton k_T Effects in High- p_T Particle Production*, Phys. Rev. Lett. **81** (1998) 2642–2645.
 - [12] C. Degrande et al., *Non-resonant New Physics in Top Pair Production at Hadron Colliders*, JHEP **03** (2011) 125, arXiv: [1010.6304 \[hep-ph\]](#).
 - [13] A. Denner et al., *NLO QCD corrections to WWbb production at hadron colliders*, Phys. Rev. Lett. **106** (2011) 052001, arXiv: [1012.3975 \[hep-ph\]](#).
 - [14] G. Bevilacqua et al., *Complete off-shell effects in top quark pair hadroproduction with leptonic decay at next-to-leading order*, JHEP **02** (2011) 083, arXiv: [1012.4230 \[hep-ph\]](#).
 - [15] T. Sjostrand, S. Mrenna and P. Z. Skands, *A Brief Introduction to PYTHIA 8.1*, Comput. Phys. Commun. **178** (2008) 852, arXiv: [0710.3820 \[hep-ph\]](#).
 - [16] ATLAS Collaboration, *Further ATLAS tunes of PYTHIA 6 and Pythia 8*, ATL-PHYS-PUB-2011-014, 2011, URL: <http://cds.cern.ch/record/1400677>.

- 1905 [17] A. Martin et al., *Parton distributions for the LHC*, *Eur. Phys. J. C* **63** (2009) 189, arXiv: [0901.0002](#) [hep-ph].
- 1906
- 1907 [18] S. Agostinelli et al., *GEANT4: a simulation toolkit*, *Nucl. Instrum. Methods Phys. A* **506** (2003) 250, [CERN-IT-2002-003](#).
- 1908
- 1909 [19] S. Frixione, P. Nason and G. Ridolfi, *A positive-weight next-to-leading-order Monte Carlo for*
1910 *heavy flavour hadroproduction*, *JHEP* **09** (2007) 126, arXiv: [0707.3088](#) [hep-ph].
- 1911 [20] R. D. Ball et al., *Parton distributions with LHC data*, *Nucl. Phys.* **B867** (2013) 244–289, arXiv:
1912 [1207.1303](#) [hep-ph].
- 1913 [21] ATLAS Collaboration, *ATLAS Run 1 Pythia8 tunes*, ATL-PHYS-PUB-2014-021, <https://cds.cern.ch/record/1966419> (2014).
- 1914
- 1915 [22] M. Czakon, P. Fiedler and A. Mitov, *Total Top-Quark Pair-Production Cross Section at Hadron*
1916 *Colliders Through $O(\alpha_S^4)$* , *Phys. Rev. Lett.* **110** (2013) 252004, arXiv: [1303.6254](#) [hep-ph].
- 1917 [23] P. Artoisenet et al., *Automatic spin-entangled decays of heavy resonances in Monte Carlo simulations*, *JHEP* **1303** (2013) 015, arXiv: [1212.3460](#) [hep-ph].
- 1918
- 1919 [24] T. Sjöstrand, S. Mrenna and P.Z. Skands, *PYTHIA 6.4 physics and manual*, *JHEP* **05** (2006) 026,
1920 arXiv: [hep-ph/0603175](#) [hep-ph].
- 1921 [25] P. Z. Skands, *Tuning Monte Carlo Generators: The Perugia Tunes*, *Phys. Rev.* **D82** (2010) 074018,
1922 arXiv: [1005.3457](#) [hep-ph].
- 1923 [26] N. Kidonakis, *Top quark production* (2013), arXiv: [1311.0283](#) [hep-ph].
- 1924 [27] S. Frixione, P. Nason and B. R. Webber, *Matching NLO QCD and parton showers in heavy flavor*
1925 *production*, *JHEP* **08** (2003) 007, arXiv: [hep-ph/0305252](#) [hep-ph].
- 1926 [28] D. J. Lange, *The EvtGen particle decay simulation package*, *Nucl. Instrum. Meth.* **A462** (2001) 152.
- 1927 [29] ATLAS Collaboration, *Jet Calibration and Systematic Uncertainties for Jets Reconstructed in the*
1928 *ATLAS Detector at $\sqrt{s} = 13$ TeV*, ATL-PHYS-PUB-2015-015, 2015, url: <https://cds.cern.ch/record/2037613>.
- 1929
- 1930 [30] ATLAS Collaboration, *Optimization of the ATLAS b-tagging performance for the 2016 LHC run*,
1931 *ATLAS-CONF-2016-012*, <https://atlas.web.cern.ch/Atlas/GROUPS/PHYSICS/PUBNOTES/ATL-PHYS-PUB-2016-012/> () .
- 1931
- 1932
- 1933 [31] D. Krohn, J. Thaler and L.-T. Wang, *Jet Trimming*, *JHEP* **02** (2010) 084, arXiv: [0912.1342](#) [hep-ph].
- 1934
- 1935 [32] Caudron, J. et al., *Boosted hadronic top identification at ATLAS for early 13 TeV data*, ATL-COM-
1936 *PHYS-2015-755*, <https://cds.cern.ch/record/2036200> (2015).
- 1937 [33] ATLAS Collaboration, *Electron efficiency measurements with the ATLAS detector using the 2015*
1938 *LHC proton-proton collision data*, ATL-CONF-2016-024 (), url: <https://cds.cern.ch/record/2157687>.
- 1939
- 1940 [34] ATLAS Collaboration, *Muon reconstruction performance of the ATLAS detector in proton–proton*
1941 *collision data at $\sqrt{s} = 13$ TeV* (2016), arXiv: [1603.05598](#) [hep-ex].
- 1941
- 1942 [35] M. Czakon, D. Heymes and A. Mitov, *Dynamical scales for multi-TeV top-pair production at the*
1943 *LHC* (2016), arXiv: [1606.03350](#) [hep-ph].
- 1943
- 1944 [36] G. D’Agostini, *A Multidimensional unfolding method based on Bayes’ theorem*, *Nucl. Instrum. Meth.*
1945 *A362* (1995) 487–498.
- 1945

- 1946 [37] H. B. Prosper and L. Lyons, *Proceedings, PHYSTAT 2011 Workshop on Statistical Issues Related*
 1947 *to Discovery Claims in Search Experiments and Unfolding* (p. 313-318), CERN (2011).
- 1948 [38] M. Cacciari, G. P. Salam and G. Soyez, *The Catchment Area of Jets*, JHEP 04 (2008) 005, arXiv:
 1949 [0802.1188 \[hep-ph\]](https://arxiv.org/abs/0802.1188).
- 1950 [39] ATLAS Collaboration, *Expected performance of the ATLAS b-tagging algorithms in Run-2*, ATLAS-
 1951 CONF-2015-022, <https://atlas.web.cern.ch/Atlas/GROUPS/PHYSICS/PUBNOTES/ATL-PHYS-PUB-2015-022/> () .
- 1953 [40] ATLAS Collaboration, *Jet energy measurement and its systematic uncertainty in proton-proton*
 1954 *collisions at $\sqrt{s} = 7 \text{ TeV}$ with the ATLAS detector*, Eur. Phys. J. C75 (2015) 17, arXiv: [1406.0076](https://arxiv.org/abs/1406.0076)
 1955 [hep-ex].
- 1956 [41] ATLAS Collaboration, *Jet energy measurement with the ATLAS detector in proton-proton collisions*
 1957 *at $\sqrt{s} = 7 \text{ TeV}$* , Eur. Phys. J. C 73 (2013) 2304, arXiv: [1112.6426 \[hep-ex\]](https://arxiv.org/abs/1112.6426).
- 1958 [42] ATLAS Collaboration, *Single hadron response measurement and calorimeter jet energy scale un-*
 1959 *certainty with the ATLAS detector at the LHC*, Eur. Phys. J. C73 (2013) 2305, arXiv: [1203.1302](https://arxiv.org/abs/1203.1302)
 1960 [hep-ex].
- 1961 [43] ATLAS Collaboration, *Jet energy resolution in proton-proton collisions at $\sqrt{s} = 7 \text{ TeV}$ recorded*
 1962 *in 2010 with the ATLAS detector*, Eur. Phys. J. C 73 (2013) 2306, arXiv: [1210.6210 \[hep-ex\]](https://arxiv.org/abs/1210.6210).
- 1963 [44] ATLAS Collaboration, *Calibration of b-tagging using dileptonic top pair events in a combinatorial*
 1964 *likelihood approach with the ATLAS experiment*, ATLAS-CONF-2014-004, 2014, URL: <http://cdsweb.cern.ch/record/1664335>.
- 1966 [45] ATLAS Collaboration, *Measurement of the b-tag Efficiency in a Sample of Jets Containing Muons*
 1967 *with 5 fb^{-1} of Data from the ATLAS Detector*, ATLAS-CONF-2012-043, <https://cds.cern.ch/record/1435197> (2012).
- 1969 [46] ATLAS Collaboration, *Measurement of the Mistag Rate of b-tagging algorithms with 5 fb^{-1} of*
 1970 *Data Collected by the ATLAS Detector*, ATLAS-CONF-2012-040, <https://cds.cern.ch/record/1435194> (2012).
- 1972 [47] ATLAS Collaboration, *Electron performance measurements with the ATLAS detector using the*
 1973 *2010 LHC proton-proton collision data*, Eur. Phys. J. C 72 (2012) 1909, arXiv: [1110.3174](https://arxiv.org/abs/1110.3174)
 1974 [hep-ex].
- 1975 [48] ATLAS Collaboration, *Electron efficiency measurements with the ATLAS detector using the 2015*
 1976 *LHC proton-proton collision data*, ATLAS-CONF-2016-024, 2016, URL: <http://cdsweb.cern.ch/record/2157687>.
- 1978 [49] ATLAS Collaboration, *Measurement of the muon reconstruction performance of the ATLAS de-*
 1979 *tector using 2011 and 2012 LHC proton–proton collision data*, Eur. Phys. J. C74 (2014) 3130,
 1980 arXiv: [1407.3935 \[hep-ex\]](https://arxiv.org/abs/1407.3935).
- 1981 [50] J. Butterworth et al., *PDF4LHC recommendations for LHC Run II*, Journal of Physics G: Nuclear
 1982 and Particle Physics <http://stacks.iop.org/0954-3899/43/i=2/a=023001> 43.2
 1983 (2016) 023001.
- 1984 [51] ATLAS Collaboration, *Luminosity Determination in pp Collisions at $\sqrt{s} = 8 \text{ TeV}$ using the ATLAS*
 1985 *Detector at the LHC*, Submitted to Eur. Phys. J. C (2016), arXiv: [1608.03953 \[hep-ex\]](https://arxiv.org/abs/1608.03953).
- 1986 [52] ATLAS Collaboration, *Search for the associated production of a Higgs boson and a top quark*
 1987 *pair in multi lepton final states with the ATLAS detector*, ATLAS-CONF-2016-058, 2016, URL:
 1988 <http://cdsweb.cern.ch/record/2205153>.

- 1989 [53] ATLAS Collaboration, *Measurement of the differential cross-section of highly boosted top quarks*
 1990 *as a function of their transverse momentum in $\sqrt{s} = 8$ TeV proton-proton collisions using the*
 1991 *ATLAS detector*, Phys. Rev. **D93.3** (2016) 032009, arXiv: [1510.03818](https://arxiv.org/abs/1510.03818) [hep-ex].
- 1992 [54] ATLAS Collaboration, *Measurements of top-quark pair differential cross-sections in the lepton+jets*
 1993 *channel in pp collisions at $\sqrt{s}=13$ TeV using the ATLAS detector*, submitted for publication to
 1994 JHEP (2017), arXiv: [1708.00727](https://arxiv.org/abs/1708.00727) [hep-ex].
- 1995 [55] F. Abe et al., *Measurement of W-boson production in 1.8-TeV p \bar{p} collisions*, Phys. Rev. Lett. **62** (9
 1996 1989) 1005–1008.
- 1997 [56] R. D. Ball et al., *Parton distributions for the LHC Run II*, JHEP **04** (2015) 040, arXiv: [1410.8849](https://arxiv.org/abs/1410.8849)
 1998 [hep-ph].
- 1999 [57] L. A. Harland-Lang et al., *Parton distributions in the LHC era: MMHT 2014 PDFs*, Eur. Phys. J.
 2000 **C75** (2015) 204, arXiv: [1412.3989](https://arxiv.org/abs/1412.3989) [hep-ph].
- 2001 [58] S. Dulat et al., *The CT14 Global Analysis of Quantum Chromodynamics* (2015), arXiv: [1506.07443](https://arxiv.org/abs/1506.07443) [hep-ph].
- 2003 [59] J. Rojo et al., *The PDF4LHC report on PDFs and LHC data: Results from Run I and preparation*
 2004 *for Run II* (2015), arXiv: [1507.00556](https://arxiv.org/abs/1507.00556) [hep-ph].
- 2005 [60] G. Bohm and G. Zech, *Introduction to statistics and data analysis for physicists*, http://www-library.desy.de/preparch/books/vstatmp_engl.pdf, Hamburg: Verl. Dt. Elektronen-Synchrotron, 2010 336,
 2006 ISBN: 978-3-935702-41-6.
- 2008 [61] G. Aad et al., *Measurements of top-quark pair differential cross-sections in the lepton+jets channel*
 2009 *in pp collisions at $\sqrt{s} = 8$ TeV using the ATLAS detector*, Eur. Phys. J. **C76.10** (2016) 538, arXiv:
 2010 [1511.04716](https://arxiv.org/abs/1511.04716) [hep-ex].
- 2011 [62] Bellagamba, L. et al., *Measurements of top-quark pair differential cross-sections in the lepton+jets*
 2012 *channel in pp collisions at $\sqrt{s} = 13$ TeV using the ATLAS detector*, ATL-COM-PHYS-2015-1577,
 2013 <https://cds.cern.ch/record/2117626> (2017).
- 2014 [63] Arguin, J. F. et al., *Measurement of the top-antitop pair differential fiducial cross-section as a*
 2015 *function of the top quark pT in the boosted topology*, ATL-COM-PHYS-2013-1093 () .
- 2016 [64] Bellagamba, L. et al., *Measurements of top-quark pair differential cross-sections of highly-boosted*
 2017 *top quarks in the lepton+jets channel in pp collisions at $\sqrt{s} = 13$ TeV using the ATLAS detector*,
 2018 ATL-COM-PHYS-2015-1578 () .
- 2019 [65] M. B. Brown, *400: A Method for Combining Non-Independent, One-Sided Tests of Significance*,
 2020 Biometrics **31.4** (1975) 987–992, ISSN: 0006341X, 15410420, URL: <http://www.jstor.org/stable/2529826>.
- 2022 [66] J. T. Kost and M. P. McDermott, *Combining dependent P-values*, Statistics and Probability Letters
 2023 **60.2** (2002) 183 –190, ISSN: 0167-7152, URL: <http://www.sciencedirect.com/science/article/pii/S0167715202003103>.

2025 List of contributions

Peter Berta	Monte Carlo background evaluation, unfolding, closure and stress tests.
Ye Chen	Ntuple generation, covariance calculations, data validation.
Kyle Cormier	Data-driven background estimation, Monte Carlo samples, rivet routine, INT note editor.
Riccardo Di Sipio	Analysis strategy, data-driven background estimation, unfolding, statistical interpretation, paper contact editor.
Robin Hayes	Hadronic trigger studies, closure tests.
Petr Jačka	Monte Carlo and data-driven background evaluation, unfolding, stress tests, correlations.
Roman Lysák	Supervisor, unfolding, stress tests, event displays.
Jiří Kvita	Supervisor, binning optimization, correlation across observables.
Rupert Leitner	Supervisor.
Cassandra Miller	Hadronic trigger studies, closure tests.
Shima Shimizu Noda	Supervisor.
Jan Palicka	Bin optimization, correlation across observables.
Marino Romano	Unfolding program.
Pekka Sinervo	Supervisor, data-driven background estimation, statistical interpretation, paper contact editor.
Francesco Spanó	Systematic uncertainties, covariance calculations, coordination with studies using other channels, paper contact editor.
Federica Fabbri	Ntuple functionality.
Yuji Yamazaki	Supervisor.

2026

Not reviewed, for internal circulation only